THE STRENGTH AND STIFFNESS OF SOILS ASSOCIATED WITH EXCAVATIONS

A thesis submitted to the University of London (Imperial College of Science and Technology) for the degree of Doctor of Philosophy in the Faculty of Engineering and for the Diploma of Membership of the Imperial College

by

Jan Eise Hellings

December 1988

ABSTRACT

The stress changes which a soil undergoes in the vicinity of an excavation are discussed.

Attempts are made in the laboratory to model stress conditions in the active and passive zones around retained excavations.

The behaviour of both a silica sand and high quality undisturbed samples of London clay from a borehole specially drilled at Bell Common is examined following a comprehensive laboratory test programme using the most up to date equipment and testing techniques.

Strength and stiffness parameters are compared for a state of stress relief with those for other states. Conventional triaxial apparatuses were used together with stress path cells controlled both manually and by computer. New local strain measurement devices were used to obtain a better estimate of stiffness.

A new machine for testing specimens in plane strain compression or extension has been developed and a test on a specimen of London clay is described.

Theoretical and laboratory studies were undertaken of the influence of membrane confinement in laboratory tests. Currently used methods for correcting for these effects are reviewed.

ACKNOWLEDGEMENTS

The research described in this thesis was sponsored initially by consultants Maunsell and Ove Arup and contractor Cementation, whose generosity enabled the programme to commence. The Science and Engineering Research Council invested considerable funds enabling a large proportion of the work to be completed. The Transport and Road Research Laboratory also contributed substantial funds for the work on London clay and the construction of the plane strain apparatus. The author is extremely grateful to all these organisations.

Professor J.B. Burland supervised the research and was responsible for instigating the programme and arranging the funding, the author is most grateful to him for having the opportunity to carry out the research and for his guidance, inspiration, encouragement and enthusiasm throughout. He was also responsible for reading and commenting on the manuscript.

The other members of academic staff at the Soil Mechanics Section of Imperial College are also thanked for their ideas and encouragement - the author is privileged to have worked with them: Professors Skempton, Vaughan and Hutchinson and Dr. Chandler, and Dr. Skinner (who also bravely attempted to improve the author's golf game), Drs. Potts and Jardine deserve special thanks for their many ideas and constructive criticism. Thanks are due to Dr. Hight of G.C.G for his valuable assistance, particularly with the membrane correction study.

The technical staff of the Soil Mechanics Section were responsible for the very impressive array of instrumentation and equipment described in this thesis, Messrs. Steven Ackerley, Graham Keefe, Lou Spall, Roger Hare, Allan Bolsher and Mrs. Eileen Gibbs. The author is greatly indebted to each of them for their many ideas and constant encouragement, as well as for the expert manufacture and assembly of the equipment which is a great credit to them.

Special thanks are due to Sectional Secretary Kathy Evans for her help and to Library staff Kay Crooks and Jessica Underhill.

Departmental photographers Richard Packer and Andrew Chipling were responsible for the excellent photographs.

Thanks are due to Alison Davis for skilfully producing many of the drawings and to Frances Donnelly for the excellent typing.

The author is indebted to Professor I.F. Symons of T.R.R.L. whose suggestions and encouragement were a great help.

Dr. E. Bromhead of Kingston Polytechnic kindly provided the drilling rig and operators; thanks are due to him and his staff.

I will always value the help and friendship of past and present members of the IC Soil Mechanics Research Group: A. Addis, A. Bond, L. Bressani, M. Crilley, R. Day, G. Dounias, A. Fourie, D. French, S. Haeri, M. Leddra, Teta and Ioannis Lefas, L. Lemos, M. Maccarini, M. Mahmoud, J. Maswoswe, C. Menkiti, N. Ninis (assistance with several of the clay tests), D. Nyaoro, E. Ovando-Shelley, D. Schreiner, S. Shibuya, P. Smith, Theodora Tika-Vassilikos and Najwa Yassir. Their assistance in many ways contributed greatly to the research programme. Particular thanks are due to Dr. David Toll whose great skill with computers enabled so many tests to be performed.

In carrying out the research and writing the thesis I remember with respect the late Professor Jere Jennings, my first teacher of Soil Mechanics. I wish to remember my late mother and to thank my father for his continuous encouragement and assistance.

Finally I would like to dedicate this thesis to my wife Dee and to my children Simon and Lucy.

CONTENTS

VOLUME 1

		Page
ABSTRACT		i
ACKNOWLEDGEMENTS		ii
CHAPTER 1	INTRODUCTION	1
1.1.	REQUIREMENT FOR STRENGTH AND STIFFNESS OF SOILS	
1.2.	METHODS OF OBTAINING STRENGTH AND STIFFNESS OF SOILS IN EXCAVATIONS	
1.3.	SCOPE OF THESIS	
CHAPTER 2	STRESS CHANGES IN THE VICINITY OF AN EXCAVATION	5
2.1.	INTRODUCTION	
2.2.	METHODS OF MEASURING IN SITU STRESSES	
	2.2.1. Laboratory techniques	
	2.2.2. Field measurement techniques	
	2.2.3. Indirect measurement from back analyses	
2.3.	STRESSES ON AN ELEMENT OF SOIL IN THE VICINITY OF AN EXCAVATION	
2.4.	SUMMARY	
CHAPTER 3	LABORATORY TESTING PROGRAMME: APPARATUS EMPLOYED, SAMPLE ACQUISITION, SPECIMEN PREPARATION AND SET-UP AND TESTING PROCEDURES.	11
3.1.	INTRODUCTION	
3.2.	DESCRIPTION OF THE APPARATUS EMPLOYED	

3.2.1. Introduction
3.2.2. The conventional triaxial apparatus
3.2.3. The stress path cells
3.2.4. The computer controlled system
3.3. INSTRUMENTATION USED WITH THE APPARATUS
3.3.1. Introduction
3.3.2. Load cells
3.3.3. Pressure transducers
3.3.4. External strain transducers
3.3.5. Local strain measurement
3.3.6. Radial strains
3.3.7. Volume gauges
3.3.8. Data retrieval systems
3.3.9. Microcomputer control systems
3.4. SAMPLE ACQUISITION, PREPARATION AND SPECIMEN SET-UP
3.4.1. Introduction
3.4.2. The sand samples
3.4.2.1. Sample preparation
3.4.2.2. Specimen set-up
3.4.2.3. Shaped specimens
3.4.2.4. Lubricated ends
3.4.3 The clay samples
3.4.3.1 Soil sampling
3.4.3.1.1 Introduction
3.4.3.1.2 Drilling rig and sampling tubes
3.4.3.1.3 Drilling and sampling procedures
3.4.3.2. Specimen preparation
3.4.3.3. Specimen set-up
3.4.3.4. Lubricated ends
3.5. TESTING PROCEDURES
3.5.1. Introduction
3.5.2. Triaxial testing of sand specimens using the conventional apparatus
3.5.3. Testing of sand specimens in the stress path cells
3.5.3.1. Compression and extension tests
3.5.3.2. Passive stress relief tests

3.5.3.3. Active stress increase tests
3.5.3.4. Data logging and reduction
3.5.4. Testing of clay specimens in the stress path cells
3.5.4.1. Manually controlled tests
3.5.4.2. Computer controlled tests
3.5.4.3. Measurement of suction
3.5.4.4. Reduction of triaxial test results
3.5.5. Other tests

CHAPTER 4 THE NEW PLANE STRAIN APPARATUS 44

4.1. INTRODUCTION
4.2. A BRIEF REVIEW OF SOME PREVIOUS AND EXISTING PLANE STRAIN APPARATUS
4.2.1. The Wood (1958) device
4.2.2. The Green (1969) device
4.2.3. The Atkinson (1973) device
4.2.4. Some other notable devices
4.2.4.1. The MIT (Wykeham Farrance) device by Dickey et al. (1968).
4.2.4.2. The University of Tokyo - Institute of Industrial Science-device (Tatsuoka et al., 1986).
4.3 THE NEW IMPERIAL COLLEGE PLANE STRAIN DEVICE
4.3.1. Introduction
4.3.2. The specimen dimensions
4.3.3. The rubber membrane
4.3.4. The vertical loading assembly
4.3.5. The horizontal loading assembly
4.3.6. The stress path cell
4.3.7. Instrumentation

4.4. A PLANE STRAIN TEST ON AN UNDISTURBED SPECIMEN OF LONDON CLAY
4.4.1. Introduction
4.4.2. Specimen set-up
4.4.3. Test procedure
4.5. ERRORS AND CORRECTIONS
4.5.1. Side friction
4.5.2. End platen movement
4.5.3. Membrane effects
4.6. SUGGESTED IMPROVEMENTS TO THE IMPERIAL COLLEGE DEVICE

CHAPTER 5 TESTS ON A SILTY SAND 66
5.1. INTRODUCTION
5.2. MAXIMUM AND MINIMUM DENSITY AND ANGLE OF REPOSE
5.3. TRIAXIAL COMPRESSION AND EXTENSION TESTS
5.3.1. Drained tests
5.3.2. Undrained tests
5.4. STATE BOUNDARY SURFACE
5.4.1. Introduction
5.4.2. Critical state framework
5.4.3. The effect of dilation
5.4.4. Bolton's (1986) model
5.5. PASSIVE STRESS RELIEF TESTS
5.6. ACTIVE STRESS INCREASE TESTS
5.7. STIFFNESS

CHAPTER 6 TESTS ON CLAY FROM BELL COMMON 79
6.1. INTRODUCTION
6.2. THE GROUND PROFILE
6.2.1. Borehole profile
6.2.2. Classification profile
6.2.3. Undrained strength profile
6.2.4. In situ stresses
6.2.4.1. Stresses from in situ instrumentation and suction measurements

6.2.4.2. The filter paper technique of suction measurement

6.2.4.3. In situ stress paths during and subsequent to excavation

6.3. EFFECTIVE STRENGTH AND STIFFNESS - LONDON CLAY AND CLAYGATE BEDS

6.3.1. Effective strength envelopes - London clay

6.3.1.1. Undrained extension tests

6.3.1.2. Constant q dissipation tests

6.3.1.3. Passive stress relief tests

6.3.1.4. Plane strain passive stress relief test

6.3.1.5. Triaxial compression tests

6.3.1.6. Comparison between triaxial extension and compression failure envelopes

6.3.1.7. Results plotted in terms of critical state axes

6.3.1.8. Reasons for high mobilised strength under passive stress relief conditions

6.3.2. Effective strength envelope - Claygate Beds

6.3.2.1. Results plotted in terms of critical state axes

6.3.3. Undrained stiffness - London clay

6.3.3.1. Undrained extension from initial isotropic stress

6.3.3.2. Undrained extension from initial K_o stresses

6.3.3.3. Undrained compression from initial K_o stresses

6.3.4. Stiffness - Claygate Beds

6.3.5. Volumetric strains - London clay

6.3.5.1. Swelling from high initial effective stress

6.3.5.2. Swelling at constant q

6.3.5.3. Swelling to initial K_o stresses

6.3.5.4. Drained tests

6.4. DESIGN PARAMETERS
6.4.1. Effective strength - Claygate Beds
6.4.2. Effective strength - London clay
6.4.3. Initial vertical and horizontal effective stresses
6.4.4. The undrained stiffness properties of London clay and Claygate Beds
6.4.5. Compressibility of the London clay and Claygate Beds
6.5 PUBLISHED DATA
6.5.1. Effective strength
6.5.2. Stiffness

CHAPTER 7 SUMMARY AND CONCLUSION 103
7.1. GENERAL
7.2. TESTS IN TRIAXIAL AND STRESS PATH CELLS
7.2.1. Strengths
7.2.2. Stiffness
7.3. PLANE STRAIN APPARATUS
7.4. SOME SPECIAL COMMENTS WITH REGARD TO THE TESTING
7.4.1. Cross sectional area correction for extension tests
7.4.2. Calibration of measuring equipment
7.4.3. End effects
7.4.4. Membrane restraint
7.5. THE FILTER PAPER TECHNIQUE OF SUCTION MEASUREMENT
7.6. SUGGESTIONS FOR FUTURE RESEARCH

REFERENCES 111

APPENDICES

APPENDIX A1 CALIBRATION OF INSTRUMENTATION 121

A1.1. INTRODUCTION

A1.2. LOAD CELLS

A1.2.1. Calibratin for load

A1.2.2. Calibration for deflections of load cell

A1.3. PRESSURE TRANSDUCERS

A1.4. DISPLACEMENT TRANSDUCERS

A1.5. VOLUME GAUGES

APPENDIX A2 LOCAL STRAIN MEASUREMENT 127

A2.1. INTRODUCTION

A2.2. THE NEW PENDULUM LOCAL STRAIN DEVICE

A2.3. EFFECT ON LOCAL STRAIN READINGS OF ROTATION OF SUPPORT PADS

A2.4. LOCAL STRAIN DEVICE SUPPORT PAD DESIGN

APPENDIX A3 THE EFFECT OF A CONFINING RUBBER MEMBRANE ON A TRIAXIAL SPECIMEN 136

A3.1. INTRODUCTION

A3.2. THE HENKEL AND GILBERT (1952) THEORY FOR MEMBRANE CORRECTIONS

A3.2.1. Laboratory tests on remoulded London clay specimens

A3.2.2. Theoretical considerations

A3.2.3. Tests on strips of membranes

A3.2.4. Theory compared with experimental results

A3.3. THE DUNCAN AND SEED (1965) THEORY FOR MEMBRANE CORRECTION

A3.3.1. Theory derivation

A3.3.2. Numerical comparison of Duncan and Seed's and Henkel and Gilbert's theories

A3.3.3. Use of the Duncan and Seed method

A3.4. FINITE ELEMENT ANALYSIS
A3.4.1. Mesh
A3.4.2. Description of analyses
A3.4.3. Results
A3.5. YOUNG'S MODULUS OF LATEX RUBBER MEMBRANE
A3.5.1. Laboratory tests on strips of membrane
A3.5.2. Laboratory tests on the whole membrane
A3.5.3. Test results
A3.5.4. Effect of soaking on membranes
A3.5.5. Discussion
A3.6. LABORATORY TESTS ON RUBBER SPECIMENS
A3.6.1. Introduction
A3.6.2. Tests without a membrane
A3.6.3. Tests with membrane enclosed specimens
A3.6.3.1. Extension tests
A3.6.3.2. Compression tests
A3.6.4. Effect of initial wrinkles in membrane
A3.6.5. Finite element simulation of rubber dummy tests
A3.7. BUCKLING OF MEMBRANES DURING COMPRESSION TESTS
A3.8. FORMATION OF SLIP PLANES IN SPECIMENS
A3.9. SUMMARY AND CONCLUSIONS

APPENDIX A4 DETAILED SAND TEST RESULTS 162

APPENDIX A5 DETAILED LONDON CLAY TEST RESULTS 163

APPENDIX A6 CONSTRUCTION DRAWINGS FOR THE NEW PLANE STRAIN DEVICE 164

APPENDIX A7 NOTATION EMPLOYED 165

VOLUME 2: TABLES AND FIGURES 168

CHAPTER 2 169

CHAPTER 3 172

CHAPTER 4 186

CHAPTER 5 199

CHAPTER 6 235

APPENDIX A1 285

APPENDIX A2 294

APPENDIX A3 322

APPENDIX A4 386

APPENDIX A5 475

APPENDIX A6 550

CHAPTER 1

INTRODUCTION

CHAPTER 1

INTRODUCTION

1.1. REQUIREMENT FOR STRENGTH AND STIFFNESS OF SOILS

Knowledge of the strength or stiffness of soil is fundamental to most calculations in soil mechanics such as those for bearing capacity, settlement and slope stability.

In particular, modern methods using numerical analyses such as the finite element technique for the design or analysis of excavation supports and prediction of movements rely very heavily on the parameters of strength and stiffness.

Traditionally, excavations have been designed using empirical or semi-empirical methods derived from field observations. For example methods recommended by Terzaghi and Peck (1967) are often used along with guidance from the Code of Practice for Earth Retaining Structures CP2 for design of load support systems and estimation of movements associated with excavations. While these have been quite adequate for traditional support systems and moderately sized excavations, the proliferation of newer support systems such as the diaphragm retaining wall and larger and deeper excavations in the midst of city centres have necessitated more sophisticasted methods of design and highlighted inconsistencies in CP2. (Hubbard et al., 1984).

The rapidly increasing sophistication and diminishing cost of computers and the more widespread availability of computer programs are enabling techniques such as the finite element method to be used much more commonly than was previously possible. Additionally, many engineers have had the foresight to instal monitoring systems within and around the excavations to enable not only the behaviour of the excavation and its support system to be monitored, but also to enable a back analysis to be done as a check on the original design methods and parameters. Notable examples of these from the early 1970s onwards have been excavations at Britannic House (Cole and Burland, 1972), the Central

London YMCA (St. John, 1975) and the Palace of Westminster (Burland and Hancock, 1977).

More recently the design and construction of a diaphragm retaining wall for the cut and cover tunnel for the M25 motorway at Bell Common have enabled the most up to date techniques of analysis to be used (Potts and Burland, 1983 and Hubbard et al, 1983). In addition, a very comprehensive field monitoring programme is being conducted at the tunnel as part of a joint BRE and TRRL programme (Tedd et al, 1984). The importance of strength and stiffness parameters used in the analysis was highlighted and as a result the research programme described in this thesis was instigated.

1.2. METHODS OF OBTAINING STRENGTH AND STIFFNESS OF SOILS IN EXCAVATIONS

Traditionally, drained triaxial compression testing (Bishop and Henkel, 1962) has yielded friction angles used in analyses for strength calculations. These are usually conducted at stress levels approximately equal to the overburden pressure at the foundation level prior to excavation. The change of strength parameters of London clay with stress level was highlighted by Bishop et al. (1965). The advent of the stress path cell (Bishop and Wesley, 1975) enabled triaxial specimens to be tested, modelling an in situ stress path. These are now widely used, especially in research establishments. As a result of strength testing it is now well known that strength and stiffness parameters can be very different from those obtained by traditional triaxial compression testing (see for example Hight et al., 1985).

It has long been recognised that stiffness obtained from laboratory testing of specimens using external strain measurements yields stiffnesses far smaller than those of the in situ material. This was evident from in situ plate load testing conducted by Marsland (1971). In addition, back analyses for the excavations mentioned previously have shown stiffnesses to be much greater than those obtained from laboratory tests. This prompted the development of methods and instruments to more accurately assess the stiffness of specimens tested in the laboratory (Burland and Symes, 1982).

1.3. SCOPE OF THESIS

In this thesis the behaviour of both sand and high quality undisturbed samples of London clay from boreholes specially drilled at Bell Common is examined in the light of a comprehensive laboratory test programme using the most up to date equipment and techniques. Strength and stiffness parameters under conditions of stress relief common for excavations are compared with those in other situations. Conventional triaxial apparatus were used as well as stress path cells, controlled both manually and by computer. New local strain measurement devices were designed and constructed in order to obtain a better estimate of stiffness.

A new apparatus for testing specimens in plane strain in either extension or compression within a stress path cell was designed and constructed and was used for a test on a specimen of London clay.

The procedures which were used for very accurate calibration of devices for measuring loads, stresses and strains when testing at low stress levels are described.

The effect of membrane restraint on specimens is examined in detail.

CHAPTER 2

STRESS CHANGES IN THE VICINITY OF AN EXCAVATION

CHAPTER 2.

STRESS CHANGES IN THE VICINITY OF AN EXCAVATION

2.1. INTRODUCTION

In order to examine the strength and stiffness of soils associated with excavations, a knowledge of stress changes which the soil undergoes is important. The significance of the stress path followed is now well known (for example, Hight et al., 1985), with soil behaviour very much dependent on it.

Although in situ stresses are notoriously difficult to measure, nevertheless a combination of in situ measurement, laboratory testing techniques and back analyses of instrumented excavation support systems have enabled researchers to make a good assessment of these stresses.

The techniques and the stresses measured are discussed in the following sections.

2.2. METHODS OF MEASURING IN SITU STRESSES

2.2.1. Laboratory techniques

One of the earliest assessments of in situ stresses was that of Skempton (1961) for the overconsolidated London clay at Bradwell, on the east coast of England, as part of investigations of a short term slip in an excavation. Skempton related K_o to the capillary pressure P_K in an undisturbed sample, finding P_K directly from suction measurements (discussed in more detail in Chapter 3) and indirectly by swelling tests and strength tests. Very high values of K_o, up to about 3, were obtained for samples near the ground surface and decreasing with depth.

Atkinson (1973) quotes similarly high values of K_o for London clay at other locations, such as Ashford Common, High Ongar and in London at Swiss Cottage, the Barbican and Oxford Circus.

Clearly, the high horizontal stresses are a result of stress relief due to erosion of the one-time thick deposits of London clay. It is apparent that, for these high stresses, the material will be at, or close to, a condition of passive failure.

Some researchers have deduced in situ horizontal stresses in sedimentary deposits by the assumption that strain in the horizontal plane is zero during deposition and erosion. Singh et al., (1973) used an instrumented oedometer to reconstruct the geological history of an overconsolidated reconstituted clay, allowing it to consolidate and to swell. Findings of note from this experiment were: the passive failure line was reached in unloading, the rate of volumetric strain increased as stresses decreased and at very low stresses neither pore water pressures nor volumetric strains stabilised in a 'reasonable' time.

Som (1968) used an instrumented oedometer to measure horizontal stresses from loading and unloading on an undisturbed specimen of London clay. During unloading, the stress path was found to curve towards the passive failure line and then change direction, travelling along the line towards the origin.

2.2.2. Field measurement techniques

Many attempts have been made to measure in situ stresses directly by insertion of pressure cells such as the spade cells described by Tedd and Charles (1983). However, insertion will disturb the in situ stresses and in the case of a stiff overconsolidated clay, tend to increase them. Corrections have then to be applied (for example Tedd and Charles, 1983).

Development of instrumented probes such as the camkometer (Hughes, 1973) and more recently the self boring pressuremeter described in some detail by Wroth (1984) and Windle and Wroth (1977) have also enabled measurements to be made of in situ stresses. However, as with the pressure cells, care has to be exercised with interpretation of the results.

2.2.3. Indirect measurement from back anlysis

Instrumentation for measuring forces and moments in support systems in excavations enables a back analysis to be performed as a check on assumed or measured stress distributions in the supported ground. Several deep basements in London have been thus instrumented and analysed and are described in the literature (for example St. John, 1975).

2.3. STRESSES ON AN ELEMENT OF SOIL IN THE VICINITY OF AN EXCAVATION

St. John (1975) illustrates stresses on an element of soil behind an excavation and also beneath an excavation, for the case of rapid excavation in an overconsolidated clay. His illustrations are reproduced as Figure 2.1. In the case of an element at the side of an excavation (Element A) total vertical stresses are assumed to remain constant during excavation, while the total horizontal stress decreases to m due to yielding of the excavation side.

In terms of effective stresses the initial stresses represented by n' moves to m' towards the active failure envelope, resulting in a decrease in pore water pressure. With time, the pore pressure will gradually increase and, depending on the amount of side movement, the active stress state may become fully mobilised and point o' will move down the failure line toward the origin.

For an element beneath the base of an excavation (Element B) the point representing original stresses prior to excavation n, n' moves to m, m'. During equalisation of pore water pressures m' will move to o', on the passive failure envelope and towards the origin.

Burland and Fourie (1985) demonstrate the stress path for an element in front of an embedded cantilever retaining wall during drained excavation (Figure 2.2). The initial in situ stresses acting on an element of soil A is represented by point 0 ($K_o \searrow 1$). For initial excavation stresses will decrease to point 1. On further excavation to 2, the stress path will curve towards a passive failure line reaching a state

of limiting equilibrium. The stress path for the element will move down a passive failure line towards the origin as excavation proceeds from 2 to 3. Shear strains and dilatency will develop in the soil as stresses move down the passive failure line .

Burland and Fourie note that the location of path 2-3 cannot be assumed to be unique but that it may be dictated by the swelling and dilatency. They term the stress path of the type 0-3 in Figure 2.2 a passive stress relief path since stress reduction causes the soil element to move into a state of passive failure.

It should be noted that stresses in the passive stress relief region are much lower than are normally adopted in laboratory testing.

Attempts were made by Burland and Fourie to model such a stress path by testing a specimen of soil in a stress path apparatus. The testing arrangement will be described in more detail in Chapter 3, and involves decreasing the vertical stress on a specimen by shearing it in extension and simultaneously allowing the horizontal stress to decrease. Although their results will be considered in more detail later, it is worth noting that, as expected, specimens in the passive stress relief region showed very high dilatency, with a rate increasing as the effective stress decreased. It is interesting to note that for specimens under K_o swelling (such as those in oedometers) for constant axial straining, the dilatency rate will remain constant throughout the test, directly proportional to the axial strain rate. It would thus appear that passive stress relief may involve soil straining radially as well as axially.

2.4. SUMMARY

Accurate measurement of stresses in the vicinity of excavations are extremely difficult to make and should involve a combination of several methods, both by in situ and laboratory testing techniques. Such techniques have been employed at the Bell Common Tunnel (Potts and Burland, 1983) and are described in Chapter 6.

As soil properties such as strength and stiffness are very often highly stress path dependent, it follows that caution should be exercised in adopting such properties determined from conventional triaxial tests. In addition, these conventional tests are usually carried out at stress levels far in excess of those generally encountered in situations of stress relief.

CHAPTER 3

LABORATORY TEST PROGRAMME: APPARATUS EMPLOYED, SAMPLE ACQUISITION, SPECIMEN PREPARATION AND SET-UP AND TESTING PROCEDURES

CHAPTER 3.

LABORATORY TEST PROGRAMME: APPARATUS EMPLOYED, SAMPLE ACQUISITION, SPECIMEN PREPARATION AND SET-UP AND TESTING PROCEDURES

3.1. INTRODUCTION

A testing programme was undertaken in an attempt to model the stress changes in soil in the vicinity of an excavation, particularly the passive zone at the foot of the excavation. These stress changes were discussed in some detail in Chapter 2.

A silt-sand mixture was tested first as this was thought to be a rapid way of establishing testing procedures due to the speed with which the freely draining sand could be tested. This was followed by a series of tests on high quality undisturbed samples of clay from a borehole which was drilled at Bell Common.

A description of the apparatus and instrumentation used is given in the following sections along with methods of specimen setting up and testing procedures.

3.2. DESCRIPTION OF THE APPARATUS EMPLOYED

3.2.1. Introduction

This section is devoted to a description of the triaxial apparatus used, namely a conventional compression device of the type described by Bishop and Henkel (1962) and 2 set-ups which included stress path cells (hydraulic triaxial cells) as described by Bishop and Wesley (1975). All 3 accommodated 76mm high, 38mm diameter specimens. No mention is made of the more standard testing apparatus used, for the determination of Atterberg limits, particle size distribution and specific gravity, nor is the standard 76mm diameter rear loading oedometer described. All this apparatus conformed to BS 1377 (1975) and a fuller description can be found in texts such as Head (1982).

The new plane strain apparatus is described in Chapter 4.

All the testing was carried out in the research laboratories of the Imperial College Soil Mechanics Section (IC). The laboratories were temperature controlled to 20°C ± 1°C although the temperature control system broke down on 2 or 3 occasions while testing was in progress.

3.2.2. The Conventional triaxial apparatus

A general arrangement of the conventional compression triaxial apparatus used is shown in Figure 3.1. The triaxial cell was a standard Wykeham Farrance Engineering (WFE) cell for 38mm diameter specimens. Pressure was provided by compressed air (to a maximum pressure of about 820kPa) through air-water interfaces. The cell pressure interface was a bladder type, supplied by Wykeham Farrance Engineering (WFE). The back pressure air-water interface was one of the standard 'Bellofram' type rolling seal units manufactured and marketed by the IC workshop. The loading system consisted of a screw jack operated by an electric motor and WFE gear box. The reaction was provided by a yoke in which a screw for height adjustment to the top of the internal load cell was housed.

The back pressure lead could be opened either to an open burette or under pressure to a 100ml automatic volume gauge or to a hand operated screw-control. Air pressure (both cell pressure and back pressure) was adjusted by hand through Watson and Smith type 10-B manostat control valves. The cell pressure was measured by a 1000kPa Bell and Howell transducer and the back pressure measured at the base by a 700kPa Bell and Howell transducer (both models 4-306-0131). A connection between back pressure and cell pressure was provided to enable both to be increased simultaneously for the tests involving loose sand specimens. The apparatus was provided with a conventional dial gauge for measurement of vertical displacement.

3.2.3. The stress path cells

Two stress path cells were used. Both were originally attached to a conventional 'Christmas tree' plumbing arrangement with pressure applied from a double mercury tube system (1000 kPa maximum) with self-compensating control (Bishop and Henkel 1962). The general arrangement

is shown in Figure 3.2 and a photograph of the system in the top part of Figure 3.3. Each cell had 3 pressure transducers, one each to measure cell, porewater and ram pressure. During the latter part of the testing programme each of the ram pressure transducers were taken off to be used in place of cell and pore pressure transducers which were accidentally damaged. Transducers in one of the cells were Bell and Howell 0-1000 kPa range and on the other cell Senso-metrics 0-2000 kPa range.

Porewater drainage was through Saran tubing which is extremely stiff, yielding at less than 10^{-7} cm^3/metre for a 1 kPa change in pressure (Gens, 1982). There was concern at one stage of the testing due to the difficulty in obtaining sufficiently high B values for saturation tests on samples, that even this yield may not have been sufficiently low enough. For this reason the Saran tubing was stripped from one of the cells and replaced with fine bore stainless steel tubing. However, a very slow leak from one of the connections was later found to be the cause of the low B-values. Following replacement of the connections, the Saran tubing behaved perfectly satisfactorily and no difference was found in its performance compared to the stainless steel tubing.

The pore water volume changes were recorded by 50cc IC automatic volume gauge, one for each cell.

In addition to the transducers, a 450 kg capacity IC internal load cell was fitted to each cell. A set of electrolevel local strain measuring devices was fitted to one of the cells and for the latter part of the test programme a set of the new pendulum type local strain measuring devices were used with the other cell. (See Section 3.3.5).

A Druck pressure transducer probe was used with each cell for measuring mid-height pore water pressures in the clay specimens. Specimen displacements were recorded externally by displacement transducers. Displacements could also be observed on externally mounted dial gauges.

Constant rate of strain testing was achieved by driving the screw contol cylinder connected to the lower pressure chamber of the cell at a

constant rate. This was done using a motor driving through a Kopp variator and multi-output spindle gearbox.

During the latter stages of the test programme, a computer controlled pressure system was developed (Toll, 1988) and one of the hydraulic triaxial cells was connected into the system. Several tests with more complex stress paths were carried out on clay samples with this system. Development and refinement of the system continued as the testing proceeded.

3.2.4. The Computer controlled system

A diagrammatic arrangement of the system is shown in Figure 3.4 with a photograph in the bottom part of Figure 3.3. The control system comprised a BBC microcomputer, an analogue to digital (A/D) converter and 3 air valve controllers. Later on a ram pump controller was also commissioned.

Each air valve controller was connected to an air-water interface which in turn was connected to a valve control board. IC type interfaces were used for the cell and ram pressures. The volume transducer, itself an interface, was used for the pore water pressure control. The control board replaced the old 'Christmas trees' and was specifically designed for pressurisation by compressed air, rather then by the old mercury column system.

For extension tests with the stress path cells one of 2 top cap arrangements could be used: either a bayonet type fitting which acts as a hook between load cell and top cap, or a suction cap fitting. When connecting specimen to top cap great care must be taken not to stress the specimen unduly. Both arrangements are shown in Figure 3.5.

3.3. INSTRUMENTATION USED WITH THE APPARATUS

3.3.1. Introduction

The instruments used with the apparatus will be described in more detail in the following paragraphs. For a much fuller treatment of the

subject, the reader is referred to an internal report by Jardine (1986). The instrumentation used for logging of data will also be described. Calibration of the instruments is discussed in Appendix A1. This had to be performed with great care due to the low stress levels used in several of the tests.

3.3.2. Load cells

The load cells used were of the type designed by Dr Angus Skinner of IC. Since the early 1970's several hundred have been manufactured at the College and have been successfully used in Britain and the rest of the world. The principles of their design have been described in detail by El-Ruwayih (1975). The sensing element is a strain gauged steel triangle whose deflection is related to the applied load and is insensitive to temperature effects, horizontal forces or eccentricity of loading. The triangle is supported at its corners in a groove cut in the body of the load cell and within limits can move in the groove so as to overcome temperature effects. It is important for the support corners to be as smooth as possible as irregularities can lead to non-linear load-deflection characteristics at the lower stress levels. This was found to be the case at the start of the test programme and the cells were stripped and the corners honed down leading to a remarkable improvement.

The cavity in which the sensing element is housed is filled with Diala oil and sealed with a cover. For the early manufactured cells the cover was made of rubber, but recent cells, including those used for the testing programme are made of metal.

At one point in the programme problems were encountered with drift of readings at zero load, up to 0.5N per day either increasing or decreasing at a regular rate. This was found to be due to moisture entering the oil-filled cavity through a faulty seal and affecting the strain gauges. The seals were replaced and no further problems were encountered.

A disadvantage of the loose fitting triangle is encountered in running a test from, say, compression to extension. For example, in a strain controlled test there will be an interruption to the loading while the triangle corners move through the gaps.

3.3.3. Pressure transducers

As noted in Section 3.2 two types of pressure transducers were used for the triaxial testing, Bell and Howell 0-1000kPa and Senso-metric 0-2000kPa.

The Bell and Howell transducers use unbonded strain gauges connected to a pressure sensing diaphragm. The Senso-metrics transducer is a semi-conductor diaphragm transducer. All the transducers performed well throughout the test programme. The drift over a month was typically 1-2 kPa at the most. There were problems originally with 2 of the new Shape transducers: one was found unusually to have a second order calibration and the other was found to be very sensitive to temperature changes. Both were discarded.

The transducers were deaired prior to installation by flushing with deaired water through a length of fine polythene tubing and keeping the transducers pressurised subsequently. The transducers were left open to a sufficient volume of water so that the pressure did not fluctuate unduly due to temperature changes. (This could have destroyed a transducer).

Surface mounted Druck piezometer probes described by Hight (1983) were used for all the clay testing. The probe is 6.5mm in diameter and incorporates a small silicon diaphragm into which is diffused a full semi-conductor strain gauge bridge. The very small gap between the ceramic stone and the diaphragm results in very small compliance. The probe has a highly linear calibration and was found to be indespensable for adjusting stress and strain rates, particularly for the tests with more complicated stress paths. It was, however, found to drift more and be more temperature dependent than the other pressure transducers. The gauges were calibrated (and deaired) in a pressurised triaxial cell

with no specimen and when not in use were kept submerged in a beaker of water.

The major problem encountered with some of the probes was a tendency for the apparent recorded pressure to change as the cell pressure changed, even when the specimen pore water pressure remained constant. This was eventually traced to the ceramic stone pushing back onto the diaphragm. The fault was apparently fairly common in probes manufactured in the early 1980's. In more recently manufactured probes the gap between stone and diaphragm has been increased. It is recommended that where the performance of the probe is not known to be satisfactory, a test is performed installing the probe on a dummy saturated stone specimen in the usual way. With the back pressure drainage open, the cell pressure is increased. If the probe is defective, the recorded pressure will change.

3.3.4. External strain transducers

Transducers used to measure strain externally were supplied by Minster Precision Engineering. Axial movement of the plunger displaces a tapered wedge which deflects a pair of cantilevered arms. Foil gauges attached to the stem of the cantilevers develop strains related to the displacement. Maximum travel of the plunger was 25mm. The gauges worked quite satisfactorily for all the tests.

The dial gauges used were manufactured by John Bull with a resolution of either .025mm or .0025mm. For both types the travel was 12mm.

3.3.5. Local strain measurement

Measurements of local strains were made with a pair of electrolevel gauges attached to diametrically opposite sides of the specimen. More recently, a new form of the gauge, a pendulum gauge, has been developed. Local strains were used for the initial part of a test when external strain readings included specimen bedding and compliance of the machine. The subject of local strain measurement including the development of the new devices are discussed further in Appendix A2.

3.3.6. Radial strains

Measurements of radial strains were made with a device developed by Maswoswe (1985) (Figure 3.6). The device is a belt in the form of a rectangular frame of 2 brass plates and 2 hollow stainless steel rods.

One of the plates has a hollow brass extension tube in which a displacement transducer is secured. A footing pad of thin brass sheeting to which is attached an armature rod rests opposite the transducer on the specimen. The other plate holds a second footing pad. The frame and attachments are very light, weighing only 30g.

The transducer is a submersible miniature LVDT (linear variable differential transformer) supplied by RDP Electronics Ltd. The model used was a D5/40W unit. It could withstand external pressures of up to 1700kPa and had a working range of about ±3mm, with the central ±1mm having a linear calibration. The energising supply is 5rms at 5kHz and the sensitivity is 2mV/V/.025mm The LVDT was extremely stable. Problems were encountered on occasion with the armature sticking, probably due to the footing pad (and thus the armature) not sitting square to the LVDT.

3.3.7. Volume gauges

For measurement of changes of pore water volumes the IC volume change apparatus was used.

Water flowing to or from a specimen vertically displaces a cylinder, isolated by Belloframs, by an amount proportional to the volume change. An MPE transducer (Section 3.3.4) is fixed to the outer casing of the apparatus and the plunger rests on an arm which is attached to the inner moving cylinder. Maswoswe (1985) describes the device in some detail.

It is important to deair the gauges fully otherwise there will be fluctuations in the readings due to changes of pressure.

Bellofram friction causes a drop of pressure of around 5kPa from one side of the gauge to the other. This pressure drop fluctuates 1 to 2 kPa with a change in the rate of dilation or contraction of the specimen. For tests at higher effective stresses this is not a problem, but at lower effective stresses the back pressure has to be monitored frequently and adjusted. With the computer control system this is done automatically.

A paraffin/water volume gauge as described by Bishop and Henkel (1962) was used for one triaxial test on sand and for calibrating the automatic volume gauge; the gauge had a capacity of 25ml and an accuracy of .05ml. (See Appendix A1 for calibration details).

3.3.8. Data retrieval systems

Three data retrieval systems were used:

- Data read off analogue to digital converter boxes for the tests with the conventional triaxial cell.
- A Solartron Data Transfer Unit (DTU) for triaxial tests with hydraulic cells during the early part of the test programme which was replaced later on by the
- Solartron Orion system connected to a Prime computer.

Analogue to digital boxes used with the conventional triaxial tests were Shape model TDI-1000/ID units with digital display. The voltage range (gain) is adustable to suit the range of the transducer and the zero can be adjusted.

The Solartron data transfer unit consists of a d.c. power supply, a digital voltmeter, an analogue scanner and a data transfer unit. Readings of up to 50 channels can be taken at intervals from 1 second up to 4 hours. Data is continuously printed out. The units were reliable, but the printers were troublesome. The Solartron units were replaced by a computer based data acquisition and reduction system (Toll, 1988). The system is shown diagrammatically in Figure 3.7. At the centre of the system is a Prime 250 computer having 2Mbytes of core

memory and 576Mbytes of disc space. A Solartron 3530 Orion-A unit logs the data. Each measurement by the analogue/digital converter (adc) is a continuous integration of 150 readings per second. This leads to increased sensitivity and better interference rejection. The adc has five measurement ranges. During the first scan the range for each channel is automatically established and stored. In subsequent scans the respective range for each channel is adopted. Should an input be out of range, then the adc moves to a new range. This leads to a very high sensitivity.

The transducers are linked to the Orion by a work station. Each station contains its own power supply and 2 signal conditioning cards. The power supply is a model MPSU1 by Constant Electronics Ltd, capable of providing +5V output at 1Amp. The signal conditioning cards are Sangamo carrier amplifier (Series C-A) cards for use with transducers needing an a.c. excitation voltage and giving an a.c. output: the electrolevel local strain measuring devices were connected to these cards.

The Orion is connected to the Prime computer using 2 lines: one line for sending commands to the Orion, the other for outputting all logged data. There is a movable terminal which can be plugged into the work station.

A pen plotter, line printer and magnetic tape drive are also accessible through the Prime computer, as are a graphics terminal and printer.

3.3.9. Microcomputer control systems

Several triaxial tests on clay specimens were performed in stress path cells linked to a microcomputer control system. The control system comprises a microcomputer, an adc and two types of controller (air valve or ram pump) driven by a stepper motor drive unit.

The microcomputer is a BBC Master 128 with twin floppy disc drives and a green screen monitor.

The adc is a 16 channel unit manufactured by CIL Electronics Ltd. Unlike the Orion unit, the CIL unit does not have the facility for

adjusting the voltage range. However, 12 channels are fixed at 100mV which is suitable for most strain gauged devices while the remaining 4 channels are for 10V range, suitable for transducers using modulator-demodulator signal conditioning such as LVDTs and electrolevel gauges. Each reading taken is the average of 1000 consecutive readings in 0.17 seconds so as to reduce scatter.

There are 3 air valve controllers labelled 'Box 1', 'Box 2' and 'Box 3', one each for the pore water, cell and ram pressures (see Fig. 3.4). The controllers are stepper motor driven manostat air regulators by Watson and Smith Type 10-B with a pressure range 10-820kPa, adjustable in increments of .07kPa.

A constant rate of strain or 'ram' pump was manufactured in the IC workshop and successfully used with one of the clay tests. The pump which is also stepper motor driven from the computer has a capacity of 100ml and the volume could be adjusted in steps of .0002ml. In Figure 3.4 the pump is labelled 'Box 4'. Oscillator circuits provide pulses of 0.07kPa at a controllable rate of between 50 pulses per second and 1 pulse per 1000 seconds.

3.4. SAMPLE ACQUISITION, PREPARATION AND SPECIMEN SET-UP

3.4.1. Introduction

Some details of the soil tested follow and a description is given of the preparation and setting up of the specimens.

3.4.2. The sand samples

The sand used in the test programme was a mixture of two grades of industrial silica silt and sand. The sand fraction was a washed uniformly sized medium-fine graded sand (Lower Greensand) type D52/100 provided by the David Ball Company, Cambridge. The sand consisted of at least 97% SiO_2. The silt fraction was crushed silica type HPF4 provided by British Industrial Sand consisting of 98.5% SiO_2.

3.4.2.1. Sample preparation

The dry silt and sand in proportions of 1 part silt to 9 parts sand by weight was thoroughly mixed with a teaspoon. Specimens with 4 different densities were required - these were given labels A, B, C and D. Table 3.1 shows the proportions of sand and distilled water used for each specimen type. The proportions were arrived at initially by trial and error. The more water present, the quicker the specimen would saturate under a back pressure. However, with too much water, the specimen would slump.

3.4.2.2. Specimen set-up

The mixture was carefully spooned into a split former lined with a rubber membrane and held against the former by vacuum. (See Figure 3.8). The sand was distributed as uniformly as possible. After each set of 3 spoonfuls had been placed the specimen formed thus far was compacted by rodding. Three types of rod were used 3mm, 8mm, and 23mm diameter. The fine rod was used for both types C and D (the loosest) with the least rodding effort directed at D. The intermediate rod was used for mix B and the thickest rod for the densest mix, type A. With experience it was possible to get a specimen within about 1% of the required porosity. Pluviation of the mix through water would have been an alternative method of specimen formation but there would have been the possibility of the silt fraction separating from the sand fraction as it passed through the water resulting in a non uniform specimen.

When all the mix had been spooned into the former the top cap was placed on the specimen and the membrane was turned over the cap and sealed against it with 3 rubber O-rings. The former was then removed and the dimensions of the specimen taken. Both diameter and height were measured using a brass dummy specimen with known dimensions as a reference. Purpose built dial gauge indicators were used to obtain height and diameter readings firstly for the dummy and then for the specimen. For each of the soil types it was found that the specimen would stand up quite satisfactorily without any suction having to be applied to the specimen.

Where used, instruments for measuring local strains and radial strains were then attached. For local strains electrolevel devices were used and for radial strains the belt used by Maswoswe (1985) was employed. Fixing pads were cleaned by scraping off old adhesive and degreasing with Butanone. During the early part of the test programme pads were fixed with a 2 part adhesive called 'M-Bond 200'. Catalyst was brushed onto the membrane and a drop of glue spread on each footing which was then pressed against the specimen. Later in the programme 'Loctite Superglue' was used instead and found to be equally effective. In the case of the local strain devices great care had to be taken not to glue the hinges. For looser specimens which could easily be damaged, after fixing to the specimen sides the instruments were suspended from threads hanging from L-shaped rods which were screwed into base plugs of the stress path cell. The arrangement was such that when the pedestal with the specimen was raised, on completion of saturation and following application of a positive effective stress, the threads became slack and the specimen alone supported the instruments.

As a precaution against getting any sand down the sides of the pedestal and to the upper bellofram, a square of rubber membrane with a hole cut in the centre was always placed around the pedestal before setting up the specimen. Otherwise some sharp edged grains of sand would have resulted in a punctured bellofram during the test while the pedestal was moving.

The specimen enclosing membrane was sometimes found to puncture during manufacture of the densest specimens. Another membrane was therefore placed over this membrane to minimise the possibility of leakage.

The perspex cell was put into position over the specimen and attached to the base. It was most important before screwing the stainless steel units onto the stainless steel pillars that the threads were clean and well oiled as any dirt would tend to fuse the threads together. The cell was then filled with deaired water. The valves isolating the connection between cell and back pressure supply lines were opened and an increasing pressure slowly applied simultaneously to cell and back pressure. The back pressure was increased to about 415kPa with the

cell pressure being left about 2kPa more than the back pressure. The specimen was then left 2 to 3 days to saturate until the B value was found to be above 0.95. The cell pressure was then set to the required value for the test and the specimen was left to consolidate. On completion of consolidation the test commenced. Care had to be taken for the extension tests for the pedestal to be sufficiently high at the start of the test to allow the required extension strain to take place during the test.

The process of saturation could probably have been speeded up by percolating water through the specimen rather than by relying on dissolving of air in the voids under a high back pressure. However, it was felt that, as with pluviation, the fine silt fraction might have migrated through the specimen.

3.4.2.3. Shaped specimens

In an attempt to dictate the position of necking in a dense specimen during an extension test and get the specimen to contract under the radial strain belt some sand specimens were formed with the centre third portion of the sample inset slightly with a diameter about 1.3mm less than that of the remainder of the sample. The inset was formed by placing a strip of self adhesive tape around the middle third of the inside of the splitformer. The former was clamped to the pedestal around the membrane and the sample formed in the usual way. Slightly less sand was required due to the reduced volume.

3.4.2.4. Lubricated ends

As a check on possible end effects in sand tests a few specimens were set up with lubricated ends. A metal disc with a 6mm hole in the centre was set on top of the pedestal in place of the porous stone. Two discs of rubber membrane with holes in the centre and with slits cut radially from the edge to just short of the centre hole were greased top and bottom with a thin smear of silicon grease and placed on top of the metal disc. The specimen was formed in the usual way. Then a further 2 greased membrane discs similar to the lower discs but without holes

placed on top of the specimen. The top cap was set and the rest of the preparation proceeded as usual.

3.4.3. The Clay samples

3.4.3.1. Soil sampling

3.4.3.1.1. Introduction.

A borehole was drilled to a depth of 21m at the Bell Common Tunnel on the M25 motorway. The borehole was located about halfway along the tunnel, 40m to the north side, to the rear of Wensley House. Figure 3.9 shows the location of the borehole along with those of other boreholes which were drilled as part of the site investigation programmes conducted at Bell Common during 1972 (the first) and 1977-78 (the second).

This Section describes how the borehole was drilled and samples taken.

3.4.3.1.2. Drilling rig and sampling tubes.

A Pilcon Wayfairer Mark 1 rig belonging to Kingston Polytechnic was used to drill the new borehole. The rig was normally used for rotary drilling and the recovery of U100 samples, so an adaptor was made (at IC) to screw in one side to the NWY drill rods and on the other side to the sampling tubes.

The rig was operated by Kingston Polytechnic assisted by personnel from IC.

The thin wall steel sampling tubes were borrowed from the Building Research Establishment. They were nominally 100mm diameter by 700mm long, although often they were shorter. The wall thickness of 1.6mm was less than the maximum recommended by Hvorslev for a satisfactory area ratio of the cutting head.

3.4.3.1.3. Drilling and sampling procedures.

Concrete anchors were cast in holes which had been excavated near the rig and the rig was tied down to the anchors.

Generally, the drilling procedure was first to take a sample by pushing the sampling tube in a continuous motion into the soil. On completion the rods were twisted, the tube withdrawn, detached and labelled and the ends waxed. The borehole was then augered out to the bottom and the sampling process repeated.

At the end of each day the samples were transported to Imperial College and stored in the Constant Temperature Store until used.

Considerable problems were encountered in attempting to sample between depths of 3m and 8m due to alternating layers of gravel, sand and clay below the water table which is between 3m and 4m deep. Over these depths it was possible to take only disturbed bag samples.

In order to overcome the problem of collapse and to seal off the water, casing was driven initially to 8m then further to 8.75m, and finally to 9.01m.

There was also some difficulty in extracting slurry from the base of the borehole at the start of some of the drill runs. Efforts to remove this with an auger were not always successful and often there was some slurry in the top of the sampling tube. As much as possible was removed, but some was found to have remained on reopening the tubes in the laboratory.

It would have been useful to have had a special device for removing this slurry from the boreholes, such as a cleaning 'bucket' with slots in the bottom which could be attached to the drill rods and rotated at the bottom of the hole.

Altogether 31 samples were taken, 3 of them bag samples and the rest tube samples.

A drilling record is shown in Table 3.2 recording the sample depths, hydraulic 'push' pressure during sampling and the sample number. The triaxial and plane strain tests carried out on clay specimens are described in some detail in subsequent sections and are also listed against the core lengths in Table 3.2.

3.4.3.2. Specimen preparation

When a sample was required the core was extracted from a tube using a vertical hydraulic jack sampling extractor, pushing in a direction from bottom of tube to top of tube i.e. continuing the sample in the same direction of travel relative to the sample tube as during sampling. The initial portion of sample was rejected in each tube, a piece cut off for the specimen and the remaining soil in the tube was then rewaxed for later use.

A triaxial specimen was trimmed using a sharp knife initially and then finally a wire saw and frame, similar to that suggested by Bishop and Henkel (1962). Three sets of trimmings were taken and weighed for moisture content determination. When the long sides of the specimen were complete it was placed on its side in a split former and the ends cut square. The dimensions of the specimen were then ascertained using Vernier callipers and the specimen was weighed.

3.4.3.3. Specimen set-up

Drainage lines were flushed and the specimen installed in the triaxial apparatus. Saturated porous stones together with a soaked filter paper disc between stone and specimen were used top and bottom of the specimen. In addition, a small coil of fuse wire as recommended by Burland and Maswoswe (1982) was used on each end of the specimen to separate it initially from the saturated porous stones and prevent the high suction present in the London Clay from drawing water into the specimen. This would not only have caused the suction to decrease but also it could have caused cavitation in the pore pressure measuring tubes. On application of the cell pressure, the wire coils would embed themselves into the specimen ends.

A rubber membrane was checked for holes visually and then inflated and submerged in water as a further check. A rubber grommet for housing a pore water pressure probe was fitted at the midheight of the membrane and sealed with 3 coats of liquid latex. The membrane was placed over the specimen and the sides were smoothed to evacuate air. A coil of fuse wire, a filter paper disc and a porous stone, both saturated, and a top cap were set on the specimen. The membrane was turned over the top cap and sealed with 3 O-rings at the top and 3 O-rings at the bottom. The mid-height pore water pressure probe was installed in the grommet: the ceramic face of the probe was first coated with some kaolin slurry in an attempt to initially prevent the high negative suction transmitting to the probe and then pushed into the grommet to touch the specimen side. Two O-rings were placed over the grommet, clamping it to the probe. The whole was then coated with 3 layers of a latex solution.

Devices for measuring local strains were then attached in the manner described previously. For some of the tests electrolevel gauges were used while for others the new pendulum type gauges were used. For one of the tests the radial strain belt was used in addition to the pore pressure probe and the local strain devices. The belt support pads were first attached through holes to the inside of the membrane. Layers of latex rubber were painted around the holes to seal the pads to the membrane. The membrane was then set over the specimen using a special former. This left the pads bearing directly against the sides of the specimen. The remainder of the belt was then set around the specimen and attached to the pads. It is believed that this was the first occasion at IC that all 3 instruments had been used on a 38mm specimen. Figure 3.10 shows a photograph of the set up.

The cell surround was then lowered over the specimen and fixed. The cell was filled with deaired water and pressurised with drainage shut. A high pressure was used, usually 700kPa in order to saturate the specimen and measure the initial effective stress.

3.4.3.4. Lubricated ends

In order to check for the effects of end restraint one test was performed on a clay specimen with lubricated ends. A metal disc and 2

discs of lightly greased membrane were inserted in place of the porous stone in a similar manner as for the lubricated end sand specimen. (See section 3.4.2.4). The remainder of the set-up was then as described above.

3.5. TESTING PROCEDURES

3.5.1. Introduction

The procedures will be described in a sequence similar to that adopted for the test programme, namely:

- drained and undrained compression testing of sand specimens using the conventional triaxial apparatus;
- drained and undrained compression and extension testing of sand specimens in the stress path cell;
- drained and undrained compression and extension testing of clay specimens in the stress path cell.

3.5.2. Triaxial testing of sand specimens using the conventional apparatus

A series of drained and undrained compression tests were carried out on the sand mixture over the range of densities A to D at initial effective stresses between 10 and 50kPa in the conventional triaxial apparatus. The drained tests were labelled TXDRLY where X was either A, B, C or D depending on the initial mix density and Y was the approximate initial effective stress in the specimen. The undrained tests were labelled TXUNLY.

Transducer readings were displayed in volts on analogue to digital convertor boxes, one each for cell pressure, pore water pressure, load cell and automatic volume gauge. The 'zero' reading on the boxes was adjusted (this was checked before and after a test) together with the gain control so as to maximise the accuracy of the reading over the anticipated voltage range.

The gear box was set to run the tests at a constant rate of strain of 5% per hour. This speed was found to be convenient for taking a sufficient number of readings, initially at about 0.2% strain intervals (2.5 minutes) and after 1% strain at 0.5% strain intervals. As the material was freely draining, consolidation times were extremely short. A consolidation test was performed on a triaxial specimen with lubricated ends. The porous stone normally used at the lower end of the specimen was replaced by a metal disc with a small hole in the centre (as described in 3.4.2.4). A C_v of 400cm^2/min was found which gave a required time to the first reading of 0.8 minutes according to Bishop and Henkel's (1962) method. For triaxial tests with porous stones C_v would be even greater and the testing rate sufficiently slow as not to allow the build up of excess pore water pressures.

The 90kg load cell was lowered until it just touched the top of the specimen, the drainage valve was shut for undrained tests and shearing commenced. Deflection readings were read off a dial gauge to an accuracy of .025mm.

The tests were run until the axial strain was about 20%. However, in the case of the undrained test, especially for the denser mixes, the test had to be terminated much earlier, generally at about 6% strain due to the continually increasing deviator load exceeding the load cell capacity. An adequate portion of the stress-strain curve was nevertheless defined.

During the drained tests a close watch had to be kept on the back pressure as this tended to change. It was found that friction in the bellofram seals of the volume gauges tended to affect the back pressure. Although there was usually a decrease in pressure across the volume gauge of about 5kPa, this could vary with the varying contraction or dilation of the specimen. Although this phenomenon was not significant at the normal stress level at which tests are run in the laboratory the effect at effective stresses of below 50kPa and certainly below 10kPa had to be carefully monitored and checked by adjustment in the back pressure.

At the end of the test the load was taken off the specimen and the load cell and transducer zeros taken and checked against initial zeros. There were no problems with apparatus or instrumentation during this series of tests.

Test results were reduced with the help of a program which was written for an HP 41CV hand-held calculator. After completion of this test programme, software for storing, reducing and plotting triaxial test data was written for the PRIME computer by Toll (1988) and use was then made of the computer and software package for storage and reduction of the data. For this reduction the specimen was assumed to remain cylindrical.

Correction for the effects of the membrane were made to the applied stresses by the use of the Duncan and Seed (1967) expression for membrane correction. Additional horizontal stresses due to the initial diameter of the membrane being less than the diameter of the specimen were also accounted for. The influence of membranes is extensively dealt with in Appendix A3.

3.5.3. Testing of sand specimens in the stress path cells

3.5.3.1. Compression and extension tests

Drained and undrained compression and extension testing of the sand mixture was also carried out in 2 stress path cells. The compression tests were labelled as detailed in Section 3.5.2. The extension tests were labelled for drained tests TXDRULY and for undrained tests TXUNULY with X and Y as before the material type and the initial effective stress respectively.

Pressure was applied through a self-compensating mercury system. Volumetric strain was recorded through an automatic volume gauge although a paraffin-water burette was used for one test. Axial deformations were recorded from an external displacement transducer; in addition it was useful to have a dial gauge for use during top cap connection and setting of the pedestal. Internal load cells of 450kg

capacity were used. Electrolevel type small strain measuring devices were employed for some of the tests. The radial strain belt was used in a few of the extension tests. There were pressure transducers for measuring cell and pore water pressure. There was also a pressure transducer at the lower cell chamber for use if required as a back up to the deviator stress measured by the load cell, by translating the pressure into a force on the underside of the pedestal, taking into account the effective belloform area.

For tests in the stress path cells one of 3 top caps were used:

Either:

(a) a flat surfaced cap for compression tests,

or (b) a suction cap arrangement for extension tests,

or (c) a bayonet fitting for extension tests.

Arrangements (b) and (c) are illustrated in Figure 3.5.

The suction cap arrangement were used for tests where deviator stresses went from extension to compression or vice versa. The height of the groove in the top cap was somewhat greater then the diameter of the bayonet. In travelling from extension to compression this play would cause a discontinuity in loading. However, all the sand mixture tests were either extension or compression tests, so there was a choice as to which top cap arrangement should be used for the extension tests. The bayonet fitting was far simpler to work with compared to the suction cap and was preferred.

With the bayonet fitting which had 2 prongs it was possible for the top cap to rotate about the axis of the prongs during shearing of the specimen, whereas the rigidity of the suction cap arrangement kept the top of the specimen horizontal. However, there did not appear to be any noticeable difference in test results between the two methods nor in failure modes of the specimens.

Prior to connecting the top cap to the specimen in the case of the extension test or prior to commencement of shearing in the case of the

compression test, the cell pedestal was adjusted manually through the screw control cylinder. For extension tests the pedestal was raised to the top of its travel so there was more than adequate travel available for the anticipated total axial strain. For compression tests the pedestal was set at its lowest position.

For the undrained tests the pore water pressure valve was shut after isotropic consolidation and prior to shearing, whereas the valve remained open for the drained tests.

A constant rate of strain increase or decrease was effected by coupling the screw control cylinder to a motor and gearbox. The cylinder in turn was connected through to the chamber beneath the pedestal. As with the sand tests done in the conventional triaxial apparatus a strain rate of 5% per hour was used.

Extension and compression tests were performed from initial isotropic effective stresses ranging from 0.5kPa to about 500kPa and a back pressure of 415kPa. In order to improve the definition of the compressive failure envelopes in the low stress region, some additional drained compression tests were done where an attempt was made to decrease the cell pressure during shear so as to keep the mean effective stress s' constant. The cell pressure was decreased by manually winding down the mercury column in steps. The tests were labelled TXDRUCY, with X and Y as before.

For tests particularly at the lower effective stresses care had to be taken to ensure that the cell and pore water pressure transducer calibrations had not changed during the test. The plumbing arrangment was such that pore water pressure transducers could be easily interconnected and readings were checked against each other before and after every test. The transucers were found to be extremely stable.

Load cell readings were taken before and after each test: no significant variation was found. However, as mentioned in Section 3.3.2, there were problems during the test programme with moisture getting into the oil in load cells through defective seals and affecting the strain gauges.

These cells had to be stripped down, refilled with oil and resealed.

As was the case for the conventional triaxial apparatus test programme, for drainage tests at effective stresses below about 50kPa, a close watch had to be kept on the back pressure as the friction in the bellofram of the automatic volume gauges caused a varying pressure drop across the gauge as the volumetric strain rate changed.

Drained tests were generally continued to a few percent beyond the point of maximum deviator stress for the denser specimens and to 20% axial strain for the looser specimens. Undrained tests were continued to 20% strain except for the denser specimens where the tests were terminated when the deviator load approached the load cell capacities.

3.5.3.2. Passive stress relief tests

A series of 7 passive stress relief tests were performed on medium dense to loose sand specimens. These were labelled SPS1 to SPS7. An additional series of 9 tests were done on dense specimens of sand. These were labelled SPS/A/1 to 8 and SPS/B/1. Tests were conducted generally following the method described by Fourie (1984) and Burland and Fourie (1985). The specimens were isotropically consolidated to an effective stress of 100kPa and then sheared drained in extension at a constant rate of axial strain to about 80% of the estimated failure deviator stress. The cell pressure was then switched from the compensating mercury line to a non-compensating mercury line with no reservoir pot at the top of it. Thus, as the pedestal in the cell dropped, so water would continue to be drawn into the cell. This in turn would lead to the mercury dropping and a reduction in the cell pressure.

Three different tube sizes were tried for the mercury line: tubes of cross-sectional area 1.98mm^2, 7.92mm^2 and 31.7mm^2 (termed 'thin' to 'thick' respectively).

The tests were continued until the cell pressure had dropped to about the same value as the pore water pressure. The axial strain to achieve

this varied, depending on the particular tube used for the cell pressure line. For the thickest tube, the test went to about 20% strain, whilst for the thinnest tube the test terminated at about 5% strain.

3.5.3.3. Active stress increase tests

A series of 3 active stress increase tests were performed on the sand. These were labelled SASI1 to 3. As for the passive stress relief tests the specimens were isotropically consolidated to 100kPa. They were then sheared in drained compression to 80% of the estimated failure deviatior stress at a constant rate of strain. The cell pressure was then switched from the compensating mercury line to the non-compensating mercury line resulting in a gradually increasing cell pressure as shearing continued.

3.5.3.4. Data logging and reduction

Readings were recorded every minute (i.e. about every 0.1% axial strain) to 1 hour (5% strain) and thereafter every 10 minutes (0.8% strain) to the end of the test.

Initially data was logged automatically by the Solartron DTU and voltages printed out at the required intervals. This data was then processed in the same way as the data obtained from the conventional triaxial apparatus. Later in the programme the Solartron was replaced by the Orion data logging system which in combination with the Prime mainframe computer meant that data could be stored, retrieved and analysed very quickly compared to the methods used previously. Transducer readings could be logged at either 3 or 10 second, 1, 10, 30, 60 or 120 minute intervals. Readings at intervals smaller than 3 seconds could also be taken using a special magnetic tape facility, but it was not necessary to use it for the testing programme.

Monitoring of up to 4 channels of current readings were possible simultaneously with converted values of pressures, displacement volumes or loads being displayed on a screen at 1 second intervals.

Reduction of the test data was done along the lines previously described in Section 3.5.2 using the software package in conjunction with the Prime computer.

3.5.4. Testing of clay specimens in the stress path cells

A series of triaxial tests were performed on specimens from undisturbed samples from Bell Common in the 2 stress path cells used previously for the sand testing programme. For the initial part of the programme both cells remained connected to the mercury systems described previously for provision of pressure. However, one cell was eventually connected up to a new computer controlled system and several tests with more complex stress paths were performed through this system.

3.5.4.1. Manually controlled tests

Specimens were initially subjected to a high cell pressure with the pore water drainage valve shut in order both to saturate the specimen and also to measure the initial effective stress (suction) in the specimens. A cell pressure of 700kPa was usually applied. However, for some of the specimens which were to be sheared unconsolidated undrained from the isotropic stress state the B value was found to be less than 0.95. For these specimens the cell pressures were then increased to 850kPa which was generally found to be sufficient for enough air in the specimen to go into solution and give B greater than 0.95. For 2 tests, however, the B value was still too low and water was percolated from bottom to top of specimens with a pressure gradient of 10kPa over several days until the specimens were saturated.

Although there was no visible leak in the pore water lines leading to the external pore water pressure transducer, it was nevertheless decided to dismantle and renew the line. For subsequent tests there were no further problems with low B values.

After about 24 hours the pore water pressures as recorded by the probe and the base pore water pressure transducer had generally stablised. This pressure was then taken for the suction measurement.

As with the sand tests, bayonet or suction top cap fittings were used and the pedestal was set either near the top of its run or near the bottom depending on whether the sample was to be sheared in compression or extension. The load cell was not connected to the specimen top cap until isotropic swelling or consolidation (if required) was complete.

For tests with the mercury column system providing the pressures where a constant rate of axial strain increase or decrease was required, the motor and gearbox coupled to the screw cylinder was used in a manner described previously for the sand tests. Strain rates were chosen using those employed for London clay testing by Jardine (1985) and Fourie (1984) as guidelines, namely about 0.5% per day for drained tests and about 5% per day for undrained tests. As a mid-height probe was used for each test it was possible to readily control the rates so as to avoid undue pore pressure gradients in the specimen. Generally the differences were kept to below 5kPa.

A pair of local strain measuring devices, either the older electrolitic type, or the newly developed pendulum type (see Appendix A2), were used for each test.

Transducer readings were recorded with the Orion system. Readings at very frequent intervals were taken during the initial stage of shearing for each test for calculation of stiffness at small strains, for strains of .0005%, .001%, .002%, .005%, .01%, .05%, 0.1% and 0.5% following Jardine (1985). Thereafter it was sufficient to have readings at 0.5% intervals.

The following types of tests were carried out, listing the terminology:

TX -- Y: T denotes triaxial, X the material: L for London clay, C for Claygate Beds. Y is the test number and -- the type of test as follows:

UU: Unconsolidated undrained extension tests from the initial isotropic effective stress.

CU: Specimens consolidated/swelled isotropically, and sheared undrained in extension.

D: Specimens swelled back isotropically, and sheared drained in extension.

In order to return some of the specimens to in situ stress conditions, they were allowed to swell or consolidate from the initial isotropic stress state to the estimated in situ stress conditions (K_o). The following five types of test were then carried out:

DRUL: Swelling under decreasing axial stress and zero lateral strain conditions.

SU: Undrained shear to failure in extension.

A: Sheared in compression with the vertical stress constant and lateral stress reducing to simulate active conditions.

SUD: Undrained shear in extension to almost 80% estimated failure stress. The pore pressure was then increased at constant deviator stress until failure achieved.

PS: Passive stress relief tests. The specimens were sheared undrained in extension to about 80% failure stress. The cell pressure line was then switched to the mercury standpipe and a passive stress relief test carried out drained as described by Burland and Fourie (1985). One mercury tube of 7.92mm^2 area was used for the passive stress relief tests. Two of the passive stress relief tests, TLPS4 and 5, were carried out using computer control. For these two tests a constant rate of axial extension was applied and the cell pressure was set to reduce in a fixed proportion to the axial strain. For the former, a rate of 100 kPa/% strain and for the later 200 kPa/% strain was used.

All the extension tests were performed by decreasing the axial stress rather than increasing the radial stress.

3.5.4.2. Computer controlled tests

The testing described in the previous section was augmented by a further series of tests on specimens following similar stress paths but controlled by a BBC microcomputer. Each test was divided into a number of stages.

- Stage 1: isotropic swelling. The cell pressure and back pressure were held at constant values until the difference between probe and base pore water transducer readings was less than 5kPa.

  The control then proceeded to

- Stage 2: anisotropic swelling to K_o (except for those samples where K_o was estimated to be unity). The deviator stress control (box 3) was set so as to decrease the deviator stress at a rate of 1kPa per hour. The cell pressure control (box 2) then decreased the cell pressure according to the equation of the swelling line.

  Control then proceeded to

- Stage 3: For tests except the active stress tests, undrained shear to about 80% estimated failure deviator stress. Generally the shearing was stress controlled with Box 3 set to decrease t at the rate of 2kPa/hour. However, one test was performed under strain control with Box 3 set to decrease the ram pressure so that the axial strain decreased at a fixed rate (0.2%/hr).

- Stage 3(a): For active tests the ram pressure was increased while the cell pressure decreased keeping the vertical stress on the sample constant. Generally the ram pressure was set to increase t at a constant rate of 0.4kPa/hr., though for one test the cell pressure was set to decrease at 2kPa/hr whilst the ram pressure was set to alter so as to maintain a constant

value of vertical stress. For the undrained active tests the cell pressure was increased when necessary during shearing so as to keep the pore water pressure from dropping below 50kPa as the specimen dilated.

- Stage 3(b): An attempt was made to run the test at a constant rate of strain as the sample approached failure by requiring Box 3 to adjust the ram pressure accordingly. However, the computer could not control the particular interaction between ram and cell pressures. A computer controlled screw control cylinder or 'constant rate of strain pump' was developed and used in the latter stage of a drained active test.

- Stage 4: For tests other than the active tests the specimens were subjected either to:

  (a) Pore pressure dissipation. Ram pressure was set to maintain a constant vertical stress on the specimen while the pore pressure increased at a rate of 1kPa/hour until the specimen failed.

  or

  (b) Imposed passive stress relief. Box 3 was set to decrease the ram pressure in such a way that the specimen extended at a constant strain rate of around 0.2% per day. Box 2 was set to decrease the cell pressure at a constant rate in relation to the change in axial strain.

A copy of a typical control sheet is shown in Figure 3.11 for the K_o swelling stage of a test. The 'Hold Value' of the control equation is an initial value of the control equation to which the increment is added. The 'Maximum Pulses' number is the maximum number of pulses of 0.07kPa given at a particular time. The computer scans the boxes continuously in rotation in the order of 1, 2, 3 and 4 and pulses as necessary. It is important to find the correct balance of pulses between boxes 2 and 3 as the ram and cell pressures are interrelated

for the hydraulic cell: a change in pressure in one will affect the other. The alarms can be used to pause the control either indefinitely or for a period of time while, for example, excess pore pressures dissipate. They can also be used to transfer control automatically from one stage to the next.

Note that it was not vital to choose the correct strain rate for the various computer controlled tests. An allowable difference between the mid-height pore pressure as registered on the probe and the base pore pressure was set. If this was exceeded during the tests then all action ceased and stresses were maintained for a defined duration, usually 5 minutes. This was the first time that tests had been run in this way at IC.

A pore pressure difference of 5kPa was defined for several of the earlier computer controlled tests. However, as the probe reading was found to fluctuate by up to 3kPa (due to zero drift) the difference was increased to 8kPa so as not to slow down the test unduly.

At the end of each test the specimen was removed from the cell and weighed. It was then placed in an oven for 24 hours for determination of the dry weight.

3.5.4.3. Measurement of suction

An exercise was performed to augment the data presented by Chandler and Guttierrez (1986) concerning measurement of suction by the filter paper technique. Several specimens at known suctions were carefully split longitudinally down the middle after removal from the triaxial cell. A small rectangle of Whatman's No. 42 filter paper 25mm by 50mm was inserted between the two halves of the specimen. The specimen was then wrapped in plastic film and waxed. After 5 days the filter paper was removed and both it and the specimen weighed. Both were then put into an oven for 24 hours for dry weight determination.

Concurrent with this exercise, during setting up of a specimen, a length of core usually about 80mm long was split diametrically at 2 points and

a 76mm disc of Whatman's No. 42 filter paper inserted at each of the 2 splits. The core was then put together again, wrapped in plastic film and waxed. After 5 days the discs were removed and their wet and dry weights determined.

3.5.4.4. Reduction of triaxial test results

Triaxial test results were reduced using the computer as for the sand tests and account was taken of the effects of the confining membrane. (Appendix A3).

3.5.5. Other tests

Other tests including index tests such as liquid and plastic limits, grading tests, specific gravity tests and an oedometer test were performed. A detailed description of procedures for these tests will not be given here. Generally the guidelines in BS1377 (1975) were followed with further guidance in the case of the oedometer test from Head (1982); the reader's attention is drawn to these publications.

With regard to the specific gravity test procedure one significant departure from BS1377 is worthy of note. Following the standard procedure of applying a vacuum to deair the slurry in the specific gravity bottle, a specific gravity of 2.64 was found. This was thought to be too low in comparison to the specific gravity of other silica sands, such as Ham River sand which is 2.66. It was felt by Skinner (1986) that the vacuum method may not remove all the air and that the slurry should be gently heated.

A further set of specific gravity tests were then done, but before applying a vacuum the slurry was carefully heated over a bunsen burner and left to simmer for about 30 minutes to evacuate the air bubbles. The remainder of the precedure was as before. A significantly higher specified gravity of 2.66 was then found.

A specific gravity of 2.74 was found for the London clay.

CHAPTER 4

THE NEW PLANE STRAIN APPARATUS

CHAPTER 4

THE NEW PLANE STRAIN APPARATUS

4.1. INTRODUCTION

Although the triaxial shear test is now the standard method employed to find strength parameters of a soil, in reality in many field situations, such as cuttings and embankments, the soil behaviour is one of plane strain, with little or no displacement in the long direction and with the 3 principal stresses being unequal. This is quite different from the stress and strain situation existing in a triaxial test where the conditions are axi-symmetric with 2 of the 3 principal stresses always equal and with the specimen usually straining in all three principal stress directions.

The reason for the triaxial test's popularity is the relative simplicity of the apparatus and the ease of doing a test compared to the complexity of the apparatus which have been used in attempts to model the plane strain situation. Another reason is the uncertainty of the influence of the apparatus on the specimen as to whether the specimen stresses and strains actually represent the field situation. Nevertheless, with the development of new apparatus, such as the stress path cell, and new instrumentation such as the internal load cells and data logging systems, the task of plane strain testing is becoming easier and the modelling itself more accurate.

4.2. A BRIEF REVIEW OF SOME PREVIOUS AND EXISTING PLANE STRAIN APPARATUS

The earliest attempts to test rectangular prismatic specimens in plane strain or in generalised 3-dimensional stress emerged in the late 1940's and early 1950's. The apparatus and loading systems, usually a system of lever arms and weights, were fairly crude and little attention was paid to factors such as friction on specimen sides, now recognised as being important.

Hambly and Roscoe (1969) discuss the requirements of a general soils testing machine: interchangibility of principal stress directions, suitable range of available strain and simplicity of operation. Atkinson (1973) recognised the difficulty of constructing an apparatus to satisfy all these requirements and suggested that it was better to have a machine to test a particular soil under a rather narrow set of loading conditions at the expense of versatility.

Many apparatus for testing prismatic specimens under plane strain conditions developed in the last 30 years or so have comprised 2 pairs of rigid loading platens - one pair to apply the vertical load and one pair to restrict the specimen in one horizontal direction - and 1 pair of flexible platens, usually the rubber membrane which confines the specimen, and through which the load is applied using a fluid pressure.

While some apparatus have no facility for measuring the intermediate principal stress, for example Duncan and Seed (1966) at Berkeley, and Powrie (1986) at Cambridge, most incorporate some stress measuring device in, or as part of, the rigid plane strain platen.

At IC, the first plane strain apparatus was designed by Bishop and Wood, and the construction details were presented by Wood (1958). The machine was used for testing specimens of compacted Glacial Till. The apparatus was later used by Cornforth (1964) for testing sand.

Green (1969) designed and built a new machine which again was used for testing sand. This machine was used by Reades (1972) also to test sand. The Delft Soil Mechanics Laboratory still use the apparatus for plane strain testing (Van Leussen and Niewenhuis, 1984).

Atkinson (1973) designed and constructed a third IC plane strain apparatus which he used for testing specimens of London clay. This apparatus was modified by Wesley (1975) and used for testing specimens of very soft estuarine clay. Gens (1982) used the apparatus for testing specimens of reconstituted Glacial Till.

Successive Imperial College apparatus have been adapted to suit the particular testing requirements and have incorporated some of the better features of the previously built apparatus and adopted state-of-the-art instrumentation.

A brief description of the main features of each of the devices follows.

4.2.1. The Wood (1958) device

The specimens tested are 406mm long, 102mm high and 51mm wide. The specimen, together with upper and lower platens, is enclosed in a rubber membrane. Specimen drainage is from the bottom plate only. Sections through the apparatus enclosing a specimen are illustrated in Figure 4.1. The specimen is loaded via 2 pistons passing through the top of the cell and bearing onto a stiff plate. The cell pressure and vertical deviator stress are applied in an identical manner to the conventional triaxial test. An end clamp is placed in contact with the ends of the specimen and prevents changes in length of the specimen during shear by means of 2 facing plates connected through 4 symmetrically placed tie bars. The end of the clamp incorporates a pressure cell with a rubber diaphragm on the side facing the specimen. A metal disc which bears against the facing plate at this end is attached to the diaphragm such that the rubber forms a slightly flexible annulus. The annulus, filled with water, is connected to a null indicator. The pressure in the annulus is adjusted to keep the null indicator mercury thread at a fixed position. This balancing pressure is converted to end stress. The ends are lubricated with silicon grease.

4.2.2. The Green (1969) device

Green tested specimens of Ham River Sand 84mm long, 81mm high and 53mm wide. As with the Wood apparatus, general stress conditions are imposed by means of two stresses applied through two pairs of rigid platens in the axial and one lateral direction, together with the third stress applied by means of a hydraulic pressure on the rubber membrane which encloses the specimen. A small loading frame is suspended around the specimen incorporating a hydraulic ram at one end and a load cell (belt

proving ring) at the other. The displacement of these lateral platens is controlled by the supply of oil to the hydraulic ram. Green designated this loading frame as the 'Independent Stress Control' (ISC) belt.

The apparatus is shown in Figure 4.2. The device is housed in a specially constructed large version of the conventional triaxial cell with a perspex cylinder 22mm thick, 336mm inner diameter and 432mm high. The cell was so constructed that it is possible to completely assemble the specimen and frame and axial loading mechanism in place, and thereafter lower the cylinder over the cell top and onto the base.

A notable feature of the device is the suspension of the loading frame or belt on 4 fine brass wires so that as the axial loading ram moves a certain vertical distance, the belt moves exactly half this distance, maintaining the line of action of the lateral belt load through the centre of the specimen. This arrangement also minimises the frictional forces acting on the end platens.

It is possible only to perform vertical compression tests (i.e. specimen straining in compression or not at all in the vertical direction) with this device.

4.2.3. The Atkinson (1973) device

The Imperial College internal load cells were being produced since the early 1970's. Atkinson was able to take advantage of these to do away with the relatively bulky internal proving rings which Green used. Consequently, he was able to dramatically increase the length of the specimen from 84mm to 203mm and still fit the apparatus inside Green's cell. In addition, Atkinson was able to utilise the Bellofram rolling seal as a loading device (this had been used in creep tests at IC by Lovenbury, 1969) and construct a new loading device with the specimen mounted on top of the loading ram. This was a forerunner of the Bishop and Wesley stress path cell, with the pedestal mounted at the top of the loading ram, at the bottom end of which is a piston and pressure chamber.

The specimen size is 203mm long, 76mm high and 38mm wide. A specially fabricated rubber membrane encloses the specimen as well as a top platen and a bottom platen (similar to Wood's device) in which ceramic drainage strips are set. Top and bottom platens seal the membrane. Loading platens above and below these connect through to a load cell and pedestal respectively.

Atkinson was obliged to manufacture a support gland for the stem of the vertical load cell due to the great distance which existed from the top of Green's cell to the top of Atkinson's device. This distance was previously required to house the proving ring and Green's large top loading platen.

A loading frame with platens at either end similar in principle to that of Wood and Green provides restraint in the horizontal direction.

The arrangement is shown in Figure 4.3.

At one end the platen is adjustable, with a travel of 2.5mm. This adjustment is provided by a stainless steel wedge actuated by a small piston connected to the axial screw ram pressure system.

The second end platen contains an electrical resistance load cell spanning between the platen face and the plate to which the tie rods are fastened.

Green's idea of the loading frame moving half the rate that the specimen vertical loading pedestal moves so as to maintain the line of action of the lateral load through the centre of the specimen was adopted by Atkinson. Instead of the frame being suspended, it rests on a system of support rods and levers (rails) which are attached to the cell base and pedestal. However, this system created frictional forces which caused the horizontal loads to be undermeasured. Wesley (1975) modified the end platen mountings, redesigning the level supports and introducing a small roller bearing (wheel) at each of the 4 corners of the frame.

As with the Wood and Green devices, the Atkinson device cannot be used for extension tests.

4.2.4. Some other notable devices

4.2.4.1. The MIT (Wykeham Farrance) device by Dickey et al., (1968)

The device is currently marketed by Wykeham Farrance (Catalogue No. WF24490). The specimen size is 89mm long, 89mm high and 36mm wide.

The device, which is shown in Figure 4.4, is capable of loading a specimen with the major principal stress in either the vertical or the horizontal direction, unlike any of the devices described previously.

Unlike any of the IC devices, the absence of the facility to be able to move the end platens horizontally a small distance, requires that the specimen has to be initially anisotropically consolidated: if tests are run from an isotropic state, there is a danger of separation between sample end and end platen. Even shearing from an anisotropic state, Dickey et al. highlight problems due to seating effects.

Even though the platens are greased, they have strong reservations about the accuracy of the measured stresses due to frictional forces between platens and specimen.

4.2.4.2. The University of Tokyo - Institute of Industrial Science- device (Tatsuoka et al., 1986)

This device is similar to the IC devices in that 2 of the principal stresses are transmitted through 2 pairs of rigid platens. The third principal stress is transmitted through the rubber membrane jacketed sides of the sample, applied by the pressure of the water in the cell in which the apparatus is housed (See Figure 4.5). Two specimen sizes were used:

a) 80mm long, 80mm high and 43mm wide
b) 101mm long, 103mm high and 55mm wide

As with the IC devices horizontal restraint is provided through a loading frame comprising 2 stainless steel platens joined together by 4

symmetrically arranged tie rods. A load cell is located at one of the platens. There is, however, no facility for moving one of the plane strain platens with the ends of the specimen during isotropic compression.

The load cells supporting the end platens (LC3 and LC4 in Figure 4.5) are used to assess side friction on the end platens for tests at low stresses. At higher stresses these load cells are replaced by springs in an effort to keep the line of action of the horizontal stresses between sample and end platens in one place. All the loads are measured by strain gauged phosphor bronze load cells.

4.3. THE NEW IMPERIAL COLLEGE PLANE STRAIN DEVICE

4.3.1. Introduction

A new plane strain device has been designed by the writer and constructed in the IC Soil Mechanics Workshop. Working drawings from which the machine was built are enclosed at the back of the thesis in Appendix A6 (sheets p/1 to p/4). Note that for the most part Imperial units of length were used. This was to facilitate the workshop's task as their machine controls are in Imperial units. It was also necessitated by metal plating being manufactured to Imperial units.

The apparatus is shown in section in Figure 4.6. Figure 4.7 shows the apparatus set up in the stress path cell. Photographs of the apparatus are reproduced in Figures 4.8 and 4.9.

As a framework for the design, the main requirements for the machine were:

(a) that it should be possible to have the major principal stress acting either vertically or horizontally (i.e. either compression or extension testing)
and
(b) that it should be possible to test a prismatic sample cut from a nominal 100mm diameter tube sample of London clay.

The previous IC apparatus were used as a basis for the design of the new apparatus: the device has rigid platens top and bottom providing the axial loading. A loading frame with rigid platens either end connects with the rods providing the horizontal, or plane strain loading.

The rubber jacketed specimen, located within the loading frame and bounded top and bottom by the rigid platens, is enclosed within a large stress path cell, similar to that used by Atkinson (1973). The cell hydraulic pressure provides the third principal stress.

4.3.2. The specimen dimensions

The sampling tubes were nominally 100mm diameter. The loading frame has been designed for specimens with a length between 80mm and 85mm. A vertical cross-section of 76mm high by 38mm wide is used, similar to the standard triaxial specimen, and the same as that used by Atkinson (1973). A horizontal section through the specimen is therefore a rectangle 38mm wide by a maximum 85mm long. The length of the diagonal between opposite corners of the rectangle is then 93mm which is 7mm less than the nominal tube diameter, sufficient to take into account variations in the tube diameter.

4.3.3. The rubber membrane

The latex rubber membranes for the plane strain tests are specially manufactured by Wykeham Farrance (item No. 24491A01) to the writer's specification. A former 85mm long, 38mm wide and 114mm high (38mm over and above the specimen height to allow for the top and bottom platens which are included within the membrane) was made. The former widens at each end to 180mm high by 120mm wide, splaying at an angle of about 15°. The membrane is therefore open at either end, with 'flaps' which are attached to the platens at each end of the specimen. The purpose of the splay is twofold:

(i) the former has to be so shaped as to stop liquid latex accumulating at corners during the dipping process during manufacture

and

(ii) the platens at either end of the specimen have raised polished central bearing areas and the splay in the membrane contours the flaps over the step.

The membrane is nominally 0.30mm thick except for one of the flaps which is 0.60mm thick. This is inevitable due to the way the former is dipped, with the latex running to one of the splays.

4.3.4. The vertical loading assembly

Enclosed within the membrane with the specimen are the top and bottom platens, (4) and (5) on Figure 4.6. Each platen is made of stainless steel with the faces adjacent to the specimen ground and polished to a mirror finish. Set in each of these faces is a bauxite drainage rod, about 5mm square section, along the long axis. Each end of the rods is connected to 'Enot' fittings which in turn connect to fine bore stainless steel tubing (27). An O-ring runs round the top side of the top platen and the bottom side of the bottom platen near the edges.

Top and bottom membrane sealing platens ((3) and (6)) push against these O-rings and so seal the top and bottom portions of the membrane. The bottom platen (5) is connected through the bottom sealing platen (6) to the bottom loading head (7). This in turn is connected through a bottom spacer cylinder (shown in Figure 4.7) to the pedestal of the stress path cell.

At the top of the specimen, the top membrane sealing platen houses a bolt (2) which connects through a spacer (1) to the load cell.

4.3.5. The horizontal loading assembly

As mentioned previously the specimen is enclosed within a horizontal 'frame' with platens on either side connected through the rods (20).

At one end of the specimen is a load cell (9) faced with a make-up platen (10). The load cell is the Imperial College 0-45kg cell used previously for measurement of horizontal loads in the Atkinson

apparatus but with a new electrical lead and lead sealing piece. The cell is connected through this piece to the back up platen (8). The tie rods attach to this platen at each corner. There is a clearance around the tie rods in the holes in the make-up platens so that all the horizontal load is transmitted to the load cell.

On the opposite side, the specimen bears against an adjustable platen (11). Both this platen and the make-up platens are made of stainless steel. The faces adjacent to the specimen are raised proud of the remainder of the plate and are ground and polished to a mirror finish. A membrane sealing ring screwed down onto an O-ring set into the faces of each of these platens seals the membrane on the specimen sides.

The adjustable platen (11) is connected to an end platen (12) through a screw shaft (13). A stud (16) prevents the threaded screw shaft from turning. A gear (15) connected to a spacer or support piece (14) is turned through the control rod (18) and gear (17) supported by plate (19) when adjustment of the platen (11) is required. For example, for isotropic consolidation, when the platen will move as the specimen compresses, the screw shaft is set forward. The slot in the shaft through which stud (16) passes is sufficiently wide to take up the adjustable platen movement. Prior to the start of plane strain shearing, the screw shaft is turned back away from the sample until it just catches the stud.

The horizontal loading frame rests through 4 wheels (25) on support rails (22) and (23). One set of wheels are attached directly to the adjustable platen, while the other is attached to the back platen (8) through supporting plates (24). The rails are hinged on one side to the bottom loading head (7) and on the other to the fixed crossbars (21). The adjustable platen maintains verticality (i) through bearing against the adjustable plate guide (26) and (ii) through a close tolerance for the rod holes through the platen and (iii) a close tolerance between the screw shaft and screw shaft hole in the adjustable platen.

Horizontal strains are measured through an LVDT housed in a purpose made clamp between the load cell make-up plate on one side and the adjustable plate on the other.

4.3.6. The Stress path cell

The stress path cell in which the plane strain apparatus is housed is that used by Maswoswe (1985) for testing 100mm diameter samples. (Figure 4.7). The top portion of the cell, i.e. base, top cover perspex surround and support pillars is essentially the same as for the cell used by Green (1969) and Atkinson (1973). However, the lower chamber has been enlarged so that the effective area of the lower bellofram at 355.41cm^2 is 3.88 times larger than that of the top bellofram (for the normal smaller stress path cell these areas are similar). Further, unlike for the smaller stress path cells, the linear bearing is submerged in oil and thus the ram pressure is oil fed.

The cell used by Atkinson (1973) is similar to the smaller stress path cell in that the linear bearing runs in air (Figure 4.3).

The external strain measurement transducer connects at one end to an arm connected to the ram and at the other to the underside of the cell.

As with Green and Atkinson, the great advantage of this type of cell construction is being able to assemble the plane strain apparatus and specimen entirely and thereafter encase them in the perspex surround.

4.3.7. Instrumentation

Measurement instrumentation for the plane strain device and stress path was generally similar to that used for the triaxial and stress path testing described in Chapter 3.

A notable exception was for pressure measurement, where Shape Instruments model SP10Z0 0-1000kPa transducers were used. These were semi-conducter diaphragm transducers.

Details of instrumentation and calibration can be found in Appendix A1.

4.4 A PLANE STRAIN TEST ON AN UNDISTURBED SPECIMEN OF LONDON CLAY

4.4.1. Introduction

A specimen of undisturbed London clay trimmed from a sample retrieved from the borehole at Bell Common was set up and tested in the new device under conditions of passive stress relief.

4.4.2. Specimen set-up

A membrane was prepared by first visually checking for holes. A rubber grommet for housing a pore pressure probe was installed at the mid-height of the membrane, slightly to one side of the centre line.

It was found to be convenient to first set up the membrane round a dummy steel block of similar dimensions to the specimen. The top and bottom platens were boiled to saturate the porous drainage rods. Two rectangular pieces of membrane with slots cut around the positions of the rods were lubricated with a thin layer of silicon grease and placed one against each platen. The platens were then placed above and below the dummy. The bottom loading head was then attached through the bottom membrane sealing platen to the bottom platen (refer to Figure 4.6). The bottom loading head was then screwed down through the bottom spacer to the stress path cell pedestal. The support rail crossbars and support rails were set in position. The two membrane sealing rings were hung loosely over each end of the specimen.

The horizontal loading frame, previously assembled, was set into position around the specimen. The end flaps of the membrane were held against the end plates with the membrane sealing rings. The hole positions for the group fixing screws were then marked on each flap. The whole assembly was then dismantled. Small holes were punched through the flaps at the marked positions. The dummy specimen and membrane were then once more assembled in the vertical loading assembly as before, except that the lower two drainage leads were attached.

A length of London clay core was then set in a special jig which was used to cut the specimen to dimensions of approximately 38mm wide, 76mm high and 82mm long. The jig was used previously by Atkinson (1973), Wesley (1975) and Gens (1982) for preparing their plane strain specimens. Although their specimens were nearly twice as long, it was nevertheless possible to adjust the sides of the jig to enable a shorter specimen to be cut. Great care was taken to get the specimen sides square. The length of the specimen was made slightly greater than the length of the top and bottom platens to take into account shortening on application of isotropic stress at the start of the test.

Trimmings were taken during the specimen preparation for the purpose of water content determination.

The sample mass and exact dimensions were found.

The dummy specimen was removed from the membrane. The drainage leads were flushed through to evacuate any air. The clay specimen was then inserted in place of the dummy. The membrane sides were smoothed over to remove pockets of air.

Rectangles of greased membrane were placed against the bearing faces of the load cell make-up platen and the adjustable platen ((10) and (11) of Figure 4.6). The horizontal loading frame was then placed around the specimen and the membrane flaps sealed against the platens by the sealing rings. Some kaolin slurry was smeared over the face of a pore water pressure probe and the probe was inserted into the rubber grommet and sealed with O-rings and liquid latex following the procedures recommended by Hight (1983).

A pair of pendulum type local strain measuring devices were attached, one to each side of the specimen at the middle of the face.

The top drainage leads were then attached as was the top membrane sealing platen.

The vertical load cell was then connected to the bolt. The perspex cell surround was lowered and attached to the base. The top cell sealing ring was screwed down and the cell filled with deaired water and pressurised.

The drainage valves remained shut initially during measurement of the initial effective stress of the specimen.

4.4.3. Test procedure

A passive stress relief test was performed on the specimen.

In general, procedures followed were those described previously for the passive stress relief triaxial tests on London clay (Chapter 3).

After isotopic swelling, the specimen was swelled anisotropiclly to the estimated in situ stress state by manually reducing the ram pressure in steps. The side screw mechanism was then turned back until the adjustable platen was locked to the end platen; subsequent shearing would then be under plane strain conditions.

Drained shearing continued to 80% of the estimated failure load at a constant rate of stress decrease. This was achieved by decreasing the ram pressure using a digitally governed stepper motor connected to a monostat air valve. By trial and error, a rate decreasing the ram pressure by 1 pulse (equivalent to about 0.1kPa) every 4 hours was found to shear the sample at a rate which did not lead to unduly low probe pore pressures.

Attempts were made to run the test at a constant rate of strain decrease, as for the tests in the stress path cell. But there were fluctuations in ram pressure due to temperature effects (shown up by the cyclic nature of the loading over 24 hours) which translated into large changes of vertical load over the relatively large lower bellofram area (a change in the ram pressure of 0.1kPa leads to a change of 3.5N in the vertical load on a specimen). This was despite the temperature

fluctuation being at the most ±1°C. The strain control with the ram was abandoned in favour of a manostat valve and a stress controlled operation, with surge of pressure attenuated.

The passive stress relief phase commenced by switching the cell pressure to a non compensating mercury line 31.7mm^2 in section. The decrease of ram pressure was continued at -1 pulse every 4 hours, equivalent to a strain rate of about -.06% per day.

4.5. ERRORS AND CORRECTIONS

Possible errors and ways of correcting for them are now examined.

4.5.1. Side friction

In order to assume that the vertical and horizontal stresses σ_a and σ_p are principal stresses it is necessary to limit any friction between specimen and platens to extremely low values in proportion to the stresses being measured. (The other horizontal stress σ_h will be a principal stress as it acts through a membrane).

The plane strain machine has been designed so that the underside of the specimen will move vertically twice as much as the side platens. This means that, with the top of the specimen fixed, the centre of the specimen will always be coincident with the centre of the side platens. Thus, in compression, shear stress on the specimen sides will vary from zero at the centre to a maximum at the top and bottom, acting in a direction away from the specimen centre. In extension, the shear stress will act towards the centre. Therefore the gross friction over the entire specimen side will be zero.

The shear stresses acting from or to the specimen centre will act in a direction opposite to the applied vertical stress. However, due to the specimen side centres remaining coincident with the side platen centres, these stresses are half what they would have been had the sides been fixed (as they are with the MIT device, for example).

Wood (1958) and Wade (1963) employed an energy balance to estimate theoretically the required vertical deviator stress correction due to shear between end platens and specimen sides. Wood's expression for undrained loading:

$$(\sigma_a)_r = \frac{\mu\sigma H^2}{6LB}\left[\sinh^{-1}\frac{B}{H} + \frac{B^3}{H^3}\sinh^{-1}\frac{H}{B} + \frac{2B}{H}\sqrt{\left(1+\frac{B^2}{H^2}\right)}\right] \quad (4.1)$$

where σ_a is the vertical deviator stress, σ is the normal stress between platens at specimen sides and specimen and L, B and H are specimen length, breadth and height respectively.

$(\mu\sigma)$ is then the shear stress across the soil-platen interface with μ being the coefficient of friction.

Wade's (1963) extension to the above equation for drained loading showed a small difference only.

Inserting the dimensions of the specimen described herein into equation (4.1):

$$(\sigma_a)_r = 0.56(\mu\sigma) \quad (4.2)$$

Alternatively, assuming a linear distribution of shear stress from zero at mid-height of specimen to a maximum of $(\mu\sigma)$ at the top (or bottom) of specimen.

$$(\sigma_a)_r = 0.48\mu\sigma \quad (4.3)$$

This is close to the value in equation (4.1).

Wood's expression is shown graphically in Figure 4.10. Points representing various plane strain and independent stress control apparatus have been added. The advantage of specimens long in relation to their breadth is clear. For Atkinson's longer specimen, the deviator stress correction is about half that given in (4.3) above whereas for a cubic sample, it is double.

The actual value of shear between specimen and side platen ($\mu\sigma$) will depend on the roughnesses of specimen and platen sides and the effect of lubrication (if any) between the two surfaces.

The behaviour of many lubrication systems have been studied and suggested in the past to limit friction, for example, Roscoe (1953), Rowe and Burden (1964), Lee and Seed (1964), Green (1969), Atkinson (1973), Tatsuoka et al. (1984). In the majority of tests, layer(s) of silicon grease and latex membrane(s) have been used. The membrane cushions irregularities on the surface of the specimen and the grease lubricates the surfaces. A balance has to be sought between the increasing shear resistance of a more viscous grease and its longer lasting shear resistance with time.

Various proprietry brands of silicon grease have been used. Often a powdered filler such as polytetrafluoroethylene (PTFE) or molybdenum disulphide have been added. These help to increase the resistance of the grease to squeezing out. However, this process can significantly increase the shear resistance, as Tatsuoka et al. (1984) found.

Atkinson (1973) found that the presence of water increased the shear resistance of the grease. This was a significant finding as tests to find the shear resistance of lubricant against platens have generally been done in air. Further, it is clear that the effectiveness of lubrication systems decreases with time. (Tatsuoka et al. 1984, Atkinson, 1973). Atkinson decided that lubrication was ineffective for tests lasting more than a few days and performed his plane strain tests without lubrication between the latex membrane at the specimen ends and the platens.

He performed a series of friction slider tests and also plane strain tests in a jacketed polystyrene specimen with and without lubrication. He found for shear between latex membrane and polished steel surface that the shear resistance built up gradually to a peak value of 10kPa at around 0.8% strain for all normal loads above 14kPa.

Tatsuoka et al. (1986) used 2 types of lubricants between the membrane and platen for their plane strain tests. For tests with effective normal stresses between specimen ends and platens above 10kPa a thin layer of 'Dow Corning' high vacuum grease and for tests at effective stresses below 10kPa, a less viscous silicon grease 'Shin-etsu KS63G' was used. A shear resistance of 0.4kPa is claimed for these systems.

Substituting these values of shear in Wood's equation (4.2):

- for a maximum shear of 10kPa (no lubrication)

$$(\sigma_A)_r = 0.56 \times 10 = 5.6\text{kPa}$$

- for a maximum shear of 0.4kPa (lubricated)

$$(\sigma_A)_r = 0.56 \times 0.4 = 0.2\text{kPa}$$

For a test with lubricated ends lasting more than a few days it would seem reasonable to assume a correction somewhere between these two values, depending on the circumstances of the test.

Note that for all plane strain tests performed where the membrane enclosing the specimen is not attached to the end platens at the specimen ends (e.g. Atkinson, Green, Tatsuoka etc.) the normal stress between sample end and platen is the horizontal deviator stress. However, for the writer's new plane strain apparatus, the membrane is sealed against the end platens, so the normal stress between platen and specimen will be the intermediate horizontal effective stress. So for example, in a compression test under isotropic stress conditions, the normal stress between specimen and end platen would be zero for Atkinson's apparatus but for the writer's apparatus it would be equal to the value of the isotropic stress.

4.5.2. End platen movement

Although plane strain conditions are assumed, there will always be some deformation of the specimen in the direction of the intermediate stress

axis. This deformation will be due to both bedding effects and also deformation of the assembly comprising the horizontal loading system.

As with specimens for triaxial testing, the effects of bedding can be lessened by cutting the ends of the specimen as square and as flat as possible. Furthermore, the screw mechanism for adjusting one of the end platens enable some of the bedding to be taken up at the start of a test. Such a mechanism is not incorporated into the MIT device which has fixed ends (Figure 4.4) nor does the Japanese device (Figure 4.5) appear to have such a facility.

The largest component of movement of the horizontal loading assembly will be that due to deformation of the load cell measuring the intermediate principal stress. By the nature of load cells, there must always be a deflection for a load to be measured and the magnitude of this deflection will depend on the construction of the particular load cell.

As mentioned before, the load cell incorporated in the new device was that used previously in the Atkinson (1973) plane strain apparatus. Atkinson's load-deflection curve for this load cell in compression is shown in Figure 4.11. For the initial part of the curve, say up to about a 50 lb load, or about 220N, the slope is about 440μm/N; over 400N the slope is 380μm/N.

The 200N Japanese load cell (Tatsuoka 1986) constructed of phosphor bronze yields 463 μm/N.

The MIT (WFE) apparatus (Figure 4.4) has 2 load cells, one in each end plate. Together the deflection is given as 15μm/N, although the cells occupy only a small portion of the end plates. Also, the construction of the MIT device is such that the end platens apply a total load, rather than a deviator load, as is the case with the new IC device and the Japanese device. Hence the loads applied by the MIT cell will be more for an equivalent stress.

A calibration for the horizontal load deflection for the new IC plane strain apparatus is shown in Figure 4.12. This was obtained by setting up the apparatus with a steel dummy block as a specimen (with dimensions similar to a specimen). The horizontal screw device was used to first compress the load cell and then tension it against the block. It was not possible to go to a tension lower than -80N due to the danger of breaking the plastic coupling in the screw control rod (Figure 4.7). Despite the hysteresis it can be seen that (a) in compression, parts of the curve are appreciably steeper than Atkinson's curve, (b) in tension the curve steepens appreciably near the extremity of the calibration, the assembly being perhaps five times softer than for compression.

Horizontal stiffness characteristics quoted by the various authors were for the load cells themselves, rather than for the entire horizontal assembly with a dummy specimen which includes bedding and is more realistic.

The steep tension curve is probably due to the design of the load cell. The rear of the cell is sealed with a rubber membrane which is clamped between two plates. In tension the supported corners of the load cell 'star' bears against the rubber and will deflect.

4.5.3. Membrane effects

As the horizontal cross sectional area of the specimen is large compared to the area of membrane intersected by a horizontal plane, the membrane correction to the vertical stress is small, about 1 kPa at 8% axial strain. Membrane effects horizontally should be negligible due to the membrane being clamped to the end platens.

4.6. SUGGESTED IMPROVEMENTS TO THE IMPERIAL COLLEGE DEVICE

The following modifications are suggested

- the rubber backing at the load cell in the end platen should be removed, to limit horizontal movement.

- the plastic universal coupling in the vertical control rod assembly should be replaced with a more rigid brass coupling.

- the ram assembly and belloframe in the stress path cell should be completely overhauled; extreme care should be taken in reassembling to limit entrapment of air.

CHAPTER 5

TESTS ON A SILTY SAND

CHAPTER 5
TESTS ON A SILTY SAND

5.1. INTRODUCTION

A large number of triaxial tests were performed on specimens of silty sand. Details of the sand specimen preparation, set-up and testing procedures are described in Chapter 3. Specimens were prepared covering a range of densities, from very loose to very dense and were tested at confining pressures from around 1kPa to almost 1000kPa. Compression and extension tests were performed both drained and also undrained.

Results of these tests are presented and an attempt is made to find a state boundary surface which fits the results.

Several passive stress relief tests were performed on dense specimens and also loose specimens of sand. The results are compared with those from the aforementioned extension triaxial tests.

A few active stress increase tests were performed and the results are described.

Finally the stiffness of the sand is examined in the light of measurements of shear modulus through local axial strain measurement.

Detailed plots for all tests are given in Appendix A4.

For all triaxial tests account has been taken of the influence of the confining membrane as detailed in Appendix A3.

5.2. MAXIMUM AND MINIMUM DENSITY AND ANGLE OF REPOSE

The maximum and minimum densities were found by performing tests according to Kolbuszewski's (1948) method and expanded by Cornforth (1973). A maximum density of 2064kg/m^3 and a minimum density of 1865 kg/m^3 corresponding to maximum and minimum void ratios of 0.92 and 0.56 respectively were obtained.

An angle of repose of a dry heap of 33° was obtained, following Cornforth's (1973) recommended method.

These figures are very similar to those for the well documented Ham River sand, also a fine quartz sand but without the silt fraction, with maximum and minimum void ratios of 0.92 and 0.59 (Bishop and Green, 1965). The Ham River Sand is not as dense at minimum void ratio, presumably due to the absence of the silt fraction.

The angle of repose of Ham River sand is also 33°.

5.3. TRIAXIAL COMPRESSION AND EXTENSION TESTS

The results of all triaxial tests on sand are summarised graphically in Appendix 4 and are discussed below. The mobilised friction angle ϕ' is found from the secant modulus for peak q/p'. The ϕ' angles are plotted against p' at the maximum q/p'.

5.3.1. Drained tests

Figure 5.1 shows ϕ' v p' for all the drained compression tests and Figure 5.2 for all the drained extension tests. The points are shown with voids ratio at peak of q/p'. Despite the scatter of points it is clear that ϕ' increases with decreasing p', especially for lower e values. ϕ' remains approximately constant for p' between 100 kPa and 1000 kPa.

The points have been contoured by eye for e values between 0.65 and 0.90. For the dense specimens, there is an increase in ϕ'_m of almost 40% between 100 kPa and 10 kPa. For the loosest specimens, i.e. e = 0.85, the increase is more modest, around 15%. The extension tests give higher friction angles, at the same p' and e, than do the compression tests. This has been found to be generally the case for many of the commonly tested sands (Ladd et al 1977). It is interesting to note a mobilised friction angle of about 60° in extension for e = 0.65.

The ϕ' values are sumarised graphically (Figure 5.3) for various e values for tests at p' = 10 kPa and also for p' = 100 kPa. The differences are tabulated in Table 5.1: at 10 kPa extension tests consistently give ϕ' values about 7^{o} greater than compression tests. At 100 kPa the difference is 4^{o}.

The increasing mobilised strength with decreasing stress levels is well known for sands and has been reported by many researchers. For example

. Ponce and Bell (1971) noted increasing ϕ' values at stress levels less than about 35kPa for a medium grain size clean quartz sand tested in triaxial compression.

. Stroud (1971) found increasing ϕ' values for a coarse quartzitic sand, Leighton Buzzard sand, tested in a simple shear apparatus, at stress levels less than about 70kPa.

. Fukushima and Tatsuoka (1984) performed drained triaxial compression tests on Toyoura sand, a fine quartzitic sand and found only slightly increasing friction angles for stresses less than 50kPa. In plane strain compression (Tatsuoka et al. 1986) ϕ' was found to increase at stress levels less than 500kPa down to about 50kPa and then remain almost constant.

. Vesic and Clough (1968) performed triaxial compression tests on a medium grained quartzitic sand in a stress range from 100kPa to over 100,000 kPa. They found an increase of ϕ' from about 32^{o} at 10,000 kPa to about 44^{o} at 100 kPa for the dense sand.

A feature of the tests was a varying rate of dilatency depending on void ratio and also stress level: the denser the sample the more strongly dilatent the behaviour. Figures 5.4 and 5.5 show the rates of volumetric and axial strains at failure plotted against stress level with e values at q/p' 'maximum' and at the end of the test (q/p' 'ultimate') shown alongside each point. Despite the scatter of data, there is an obvious trend and contours of constant e values have been estimated by eye and drawn in. It is interesting to note that,

for the denser sand, the dilatency for the same stress level and voids ratio, appears to be greater for compression than for extension despite the mobilised friction angles for extension being greater than for compression.

Dilatency will be discussed in some detail in Section 5.4.

5.3.2. Undrained tests

Results of undrained compression and extension triaxial tests are summarised in Figure 5.6 - 5.9.

Figures 5.6 and 5.7 show mobilised friction angles ϕ' (peak q/p') plotted against p' with e values at failure shown next to each point. As expected, ϕ' increases with decreasing e. The data is insufficient to notice any definite trend of decreasing ϕ' with increasing p' for constant e (as for the drained tests). However broken lines have been sketched showing approximate ϕ' values for constant e values. As for the drained tests, it is seen that ϕ' at a particular e is up to 4^{o} less in the stress level range 100 to 1000kPa for compression tests than for extension tests.

Figures 5.8 and 5.9 show the rates of change of pore water pressure at failure to change of axial strain against p'; e values are shown next to each point. Once again it is difficult to contour the data, nevertheless tentative constant e lines have been sketched in.

5.4. STATE BOUNDARY SURFACE

5.4.1. Introduction

Many researchers have attempted to model the behaviour of sands.

Ovando-Shelley (1986) lists factors which determine the behaviour of granular materials: voids ratio; relative density, grading and grain size, particle shape, interparticle friction, fabric, anisotropy and stress history.

5.4.2. Critical state framework

Atkinson and Bransby (1978) attempted to fit the behaviour of sands within the critical state framework proposed by Schofield and Wroth (1968) for clays. However, particular difficulties are the flat slope λ of a virgin compression line making the calculation of p'_e, the equivalent consolidation pressure rather uncertain. The normal consolidation line is difficult to establish, if indeed there is a unique line (Ovando-Shelley, 1986), as tests have to be performed at stress levels much larger than those commonly adopted in the laboratory.

In certain respects the sands behave as overconsolidated clays, with the loose sands equivalent to lightly overconsolidated clays and the dense sands to heavily overconsolidated clays. The critical state line, if such a line exists, will therefore always be approached from the 'dry' side.

Atkinson and Bransby propose a new parameter v_λ, the value of specific volume on a reference section of p' = 1kPa. This parameter is obtained by projecting the point, in v, lnp' space, parallel to the normally consolidated or critical state lines to the reference section p' = 1 kPa.

The Hvorslev surface, it is proposed, should then be established by plotting test results in terms of q/p', v_λ axes. Stroud's (1971) test results plotted thus show a possible Hvorslev surface and critical state line, as do those from Vesic and Clough (1968).

No attempt has been made to put the results of the present testing programme (described in Section 5.3) into a critical state framework. However, the plots of Figures 5.1 and 5.2 define boundary surfaces in terms of q,p' and e for the sand at failure.

5.4.3. The effect of dilation

It is clear from Figures 5.4 and 5.5 that there must exist a relation between mobilised friction angle and dilation rate. Many researchers

have attempted to quantify this relationship, the more notable being Taylor (1948) whose model was modified by Bishop (1954) for use with triaxial testing and Rowe (1962). Atkinson and Bransby (1978) described a relation in terms of the critical state theory.

Three expressions derived from Bishop's, Rowe's and Atkinson and Bransby's expressions are given below for triaxial compression or extension tests. In these expressions q_c represents the shear stress without the dilatency component, q is the measured shear stress and σ'_r the effective horizontal stress.

- Bishop

$$q_c = q + \sigma'_r \frac{d\epsilon_v}{d\epsilon_1} \qquad (5.1)$$

- Rowe

$$q_c = \frac{q + \sigma'_r (1-C)}{C} \qquad (5.2)$$

where $C = 1 - \frac{d\epsilon_v}{d\epsilon_1}$

- Atkinson and Bransby

$$\frac{q'_c}{p'_c} = \frac{q}{p'} + \frac{d\epsilon_v}{d\epsilon_s} \qquad (5.3)$$

Rowe's model apears to be the most commonly used, see for example Ponce and Bell (1971).

5.4.4. Bolton's (1986) model

Bolton (1986) has analysed a large amount of published data from more than a dozen researchers concerning the strength and dilatency of sands.

He has proposed expressions, based on Rowe's (1962) theories, for the friction angle of a sand or the maximum dilatency rate, as a function of relative density I_D, p', and a 'critical' friction angle ϕ'_{crit} such that for triaxial strain

$$\phi'_{max} - \phi'_{crit} = 3I_R \qquad (5.4)$$

and

$$-\left(\frac{d\epsilon_v}{d\epsilon_a}\right)_{max} = 0.3I_R \qquad (5.5)$$

where

$$I_R = I_D\,(10 - \ln p')-1 \qquad (5.6)$$

the 'relative dilatency index'.

The correlations are recommended in the range $0 < I_R < 4$. Bolton proposes that $\phi'_{max} = \phi'_{crit}$ when there is no dilation, i.e. $I_R = 0$. The critical friction angle, Bolton proposes, should be the angle of repose of a dry heap of sand.

For the case of the present research, as noted in Section 5.2, the angle of repose was found to be 33° - this value is noted by Bolton as typical of all quartz sands. However, it is clear from Figures 5.1 and 5.2 that the friction angle at minimum density will be less than 33°, decreasing to less than 28° at 100kPa.

All the results of the compression and extension tests described in Section 5.3 have been reduced according to Bolton's methods and plotted on Figures 5.10 - 5.12. The data have been plotted in terms of ϕ'_{max} and I_R, ignoring ϕ'_{crit} (equation 5.4.) as this is a constant in the equation, so enabling the coefficient '3' to be checked. For

compression it can be seen (Figure 5.10) that most of the results fall below Bolton's line, certainly in the range $0 < I_R < 4$ recommended. Similarly the dilation values also fall well below Bolton's line (slope = 0.3). So for compression, Bolton's prediction of friction angle is almost 5^o too high for lower I_R values.

For the case of extension tests (Figure 5.11) the prediction of friction angle is reasonable for I_R values up to about 2, but underpredicts significantly beyond this. As for the compression tests, the dilation rate is very much less than that predicted by Bolton (Figure 5.12).

In a discussion to Bolton's paper, Tatsuoka (1987) presents plane strain tests results for Toyoura sand and points out that Bolton should have included considerations of anisotropy in strength and deformation.

5.5. PASSIVE STRESS RELIEF TESTS

A series of passive stress relief tests were performed on specimens of sand, seven tests on loose sand (SPS 1-7) and nine on dense sand (SPS/A/1 - 8, SPS/B/1). The method of performing the tests was as described in Chapter 3. The cross sectional area of mercury tubing controlling the rate of decrease of cell pressure was varied between tests from a very fine tube (1.98mm^2 cross sectional area) giving a rapid decrease in cell pressure to a large tube (39.6mm^2) giving a much slower decrease in cell pressure.

The tests performed are listed in Table 5.2(a) and 5.2(b), the initial voids ratio of the specimens are shown together with control tubing cross sectional area and some notes concerning specimen shape during each test.

As explained in Chapter 3, the specimens were sheared in drained extension from an isotropic stress state to around 80% of the estimated shear strength. From this point the specimens were sheared in passive stress relief.

Generally, each test was continued until the vertical stress in the specimen became very small.

The detailed plots for all tests are included in Appendix A4.

The stress paths are given in terms of p', q in Figures 5.13 and 5.14.

As might be expected for tests whose cell pressures are controlled by the thickest mercury tubes, the stress paths move off from the drained line with the flattest trajectories. The paths then rapidly reach a failure envelope before changing direction and travelling up towards the origin of the axes. For those specimens with thinner tubes, or more rapid cell pressure decrease, the stress paths may not reach a failure envelope for some time, or may even miss the extension failure envelope and fail instead in compression.

It appears that regardless of the tube thickness used in these tests, the stress paths meet a failure envelope and travel up along this envelope towards the origin as the stresses continue to be relieved, or meet the envelope and then move inside it due to necking of the specimen at a particular point or points in the specimen, without fully mobilising the strength of the remainder of the specimen.

For the tests, final axial strains in extension varied from about 3% for specimens with the thinnest cell pressure tubes, to over 20% for those with the thickest. Figures 5.15 and 5.16 show q plotted against ϵ_a. These generally show the tests proceeding to higher strains for those with the thickest mercury control tubes and also much flatter slopes of the q - ϵ_a curves for the passive stress relief phases.

A notable feature of the passive stress relief tests was the increasing rate of dilation as the tests progressed. Figures 5.17 and 5.18 show volumetric strain plotted against axial strain and illustrate this feature.

The mobilised shear strength (secant modulus for peak q/p') is shown plotted against p' for the passive stress relief portions of the tests

in Figures 5.19 and 5.20. The resulting curves are superimposed on those from Figure 5.2 (the failure envelopes from the drained extension tests).

The passive stress relief curves are shown with increasing mobilised friction angles up to the point where a limiting envelope is reached for drained failure in extension (for a particular voids ratio). The specimen then fails initially and either collapses with mobilised strength dropping rapidly, or the failure is 'contained' and the strength continues to increase considerably in excess of the shear strength from the extension tests at an equivalent voids ratio.

A feature of the passive stress relief tests was the initial failure or 'neck' in the sample at first failure. From this point the deformation was either reasonably uniform with other 'necks' developing to maintain an approximate right cylinder or failure continued at either one or two points leading to premature collapse of the sample. Tables 5.2a and b give a description of specimen deformation.

In general, where the specimen deformation was more uniform, so the mobilised strengths continued to increase (Figure 5.19 and 5.20).

The reason for the very high mobilised shear strengths in passive stress relief is not known at present. Part of the excess strength would be due to the increasing dilation rate.

Rowe's (1962) correction was applied to test SPS3. The corrected curve is shown in Figure 5.21 along with the drained line for e = 0.7 (from Figure 5.2) and is still well in excess of strengths from the drained extension tests at equivalent e. Although the drained line for e = 0.7 is drawn, those for e = 0.8 and e = 0.9, similar e values to those for SPS3, would give lower ϕ' values, emphasising even more the enhanced strength for SPS3.

Also shown on Figure 5.21 is the envelope for drained extension tests at e = 0.70 along with failure points from the TCDRUL series of drained extension tests (e approximately 0.7) after correction for dilation by

Rowe's method. The points plot close to the e = 0.70 contour from the undrained extension test series, exhibiting the validity, in this case, of Rowe's equation. Detailed plots before and after correction are given in Appendix A4.

5.6. ACTIVE STRESS INCREASE TESTS

As an extension to the passive stress relief test programme, attempts were made to reverse the procedure and perform an 'active stress increase' test. Here the specimen is sheared drained in compression and at a suitable point, the cell pressure control is switched to fixed (non compensating) mercury tubes as for the passive stress relief tests. The cell pressure will therefore increase and the stress path will travel towards the active failure envelope.

Three such tests were performed on moderately loose specimens SASI1, SASI2 and SASI3. Initial voids ratios were .77, .82 and .79 respectively. Figures 5.22, 5.23 and 5.24 summarise the test results. For test 1 a 7.92mm^2 cell pressure mercury tube was used for the initial portion of the test. However it appeared that the stress path (in q - p' space) was too flat to intersect the failure envelope, so control was changed to 31.7mm^2. Even so, the specimen did not appear to be failing. For test 2 a tubing cross section of 39.6mm^2 was used after the initial drained shear at constant cell pressure, but was nevertheless inadequate and was changed to 47.5mm^2 during the latter part of the test. For test 3, 47.5mm^2 tubing was used throughout the test, following the initial drained shear with constant cell pressure. This appeared to be more successful giving the steepest stress path and collapse of the specimen at p' about 200KPa.

Figure 5.25 shows the stress paths plotted in ϕ', p' space superimposed on the failure contours from the drained compression tests. It can be seen that the mobilised strength for tests 1 and 2 increased gradually from about 33^o to about 36^o, a few degrees more than the equivalent drained ϕ'. However for test 3 the mobilised friction angle increases rapidly to around 38^o when the sample collapses. It should be noted that the axial strain at this point was about 28%. The voids ratio at

'failure' was 0.81 making the specimen very much stronger than an equivalent specimen undergoing drained compression (by almost 8^{o} for the same e and p').

5.7. STIFFNESS

Several of the triaxial specimens were instrumented with local strain measuring devices. Figures 5.26 to 5.31 show G/p' plotted against ϵ_a for specimens with a range of densities. Note that all these stiffnesses are for stress paths from an isotropic stress state. Table 5.3 summarises the data. For dense sands at .02% axial strain the normalised stiffness varied between 400 and 800, decreasing to between 200 and 300 at .1% strain. For loose sands the stiffnesses were between 200 and 500 at .02% strain decreasing to 100 to 250 at .1% strain.

CHAPTER 6

TESTS ON CLAY FROM BELL COMMON

CHAPTER 6

TESTS ON CLAY FROM BELL COMMON

6.1. INTRODUCTION

Specimens of Claygate Beds and London clay from the borehole at Bell Common were tested for strength and stiffness according to the procedures outlined in Chapters 3 and 4 and the results are described in the following sections. The results are supplemented with those from the commercial test programme of sampling and testing carried out in 1972 and 1977-78 at Bell Common. In addition, results from Fourie (1984) and Maswoswe (1981) are also given.

An attempt is made to plot the results within a critical state framework.

Methods which have been used to estimate the in situ stresses at Bell Common are described and measurements are given for stresses measured before, during and after construction.

6.2. THE GROUND PROFILE

6.2.1. Borehole profile.

The cores and bag samples are described in Figure 6.1 where the profile is shown. Figure 6.2 is a photograph of core pieces typical of horizons at 1.5m., 2.5m., 4.5m., 14.0m., and 17.6m.

The top 2m comprises a firm yellowish-brown sandy, silty clay being Head material.

From 2m to 8m are the Claygate Beds, a light yellowish brown soft to firm intact clay interbedded with sand and gravel.

The water table was encountered between 3m and 4m.

London Clay forms the remainder of the profile, starting stiff and jointed and becoming very stiff at about 17m. There are, however, silty horizons, in particular one just below 11m and another at 14m. Two types of jointing were apparent: a random small-scale jointing where the joints are clean and often appear slickensided and larger joints passing across the core with a silty covering.

6.2.2. Classification profile.

A profile of moisture content (liquid and plastic limits and natural moisture content), bulk unit weight and clay fraction is shown in Figure 6.3. No analyses were carried out on the soil between 3 and 9m.

As expected, the sandy Claygate material has a relatively low plasticity index, unit weight and a clay fraction less than 40%.

The silty horizons within the London clay are evident from the profiles on Figure 6.3. A typical clay fraction of around 50% or more, drops to 30 or 40 for the less plastic material. The unit weight, usually at least 20kN/m^3, drops to about 19.5kN/m^3 for the silty horizons, and the plasticity index from 50 to only about 25 to 30. Clearly the horizon at around 11m to 12m is less silty than that between 13m and 15m.

In general the natural moisture content was close to the plastic limit, typical of a stiff overconsolidated clay.

A study of the adjacent commercial boreholes (Figure 6.4 are profiles for that) shows that the silty horizons do not appear to be continuous from borehole to borehole. The profiles and also the simple soil properties are similar to those for the new borehole.

6.2.3. Undrained strength profile.

Undrained strengths from triaxial extension tests are plotted against depth in Figure 6.5. Also shown are results of undrained extension tests performed by Fourie (1984) and Maswoswe (1985). Note the exceptionally high strength at a depth of 13m in the silty horizon. No Atterberg limits are available for the soil used by Fourie or Maswoswe.

Figure 6.6 shows the commercial undrained compression test results from all boreholes at Bell Common and also the Hellings/Fourie/Maswoswe undrained extension tests superimposed. In addition those results from the boreholes closest to the new borehole are highlighted.

As would be expected the scatter for results is high due to (a) scale effect due to the use of 38mm samples and (b) the natural variability of the clay.

It is of interest to note that the extension tests fall within the spread of results from the compression tests. Also that the results from boreholes closest to the new borehole are not noticeably different from those of all the boreholes at the Bell Common Tunnel.

6.2.4. In situ stresses.

In situ horizontal stresses have been assessed using both in situ instrumentation and testing and also indirectly from laboratory suction measurements on triaxial samples.

6.2.4.1. Stresses from in situ instrumentation and suction measurements

An oedometer test carried out on a specimen from 15.2m depth indicated that the present ground has been overlain by a maximum of 60m of soil corresponding to an overconsolidation ratio of about 4 at this depth (Figure 6.7) assuming the previous water table at the previous surface and the present water table 3m down. The OCR for other depths are shown in Figure 6.8.

In situ horizontal stresses at Bell Common between 4 and 15m have been measured by the self boring pressuremeter and also by the camkometer self boring load cell (Windle and Wroth, 1977). In addition push-in Glotzl type spade cells were installed at 6m, 9m and 12m depth (Tedd and Charles, 1981). The measurements reduced to effective stresses are shown on Figure 6.9.

Note that the spade cell readings are known to over-read and the given pressures incorporate a correction of half the estimated undrained

shear strength (Tedd et al., 1984). A pore water pressure profile is also shown. The water levels in the London Clay were hydrostatic and varied seasonally between 3 and 4m below the surface (Hubbard et al 1984).

The profile for a water table at 3m has been plotted. The vertical effective stress has also been estimated from bulk density values and is also shown.

Both the self boring pressuremeter and self boring local cell stress values show a wide scatter.

A full line has been drawn through the corrected spade cell readings and has been extrapolated downwards. This line is taken to represent the in-situ values of σ_h'.

Potts and Burland (1983) produced a similar plot except that the data was presented in terms of total stresses.

A profile of K_o versus depth has been deduced from Figure 6.9 and is shown as Figure 6.10. It is interesting to compare this profile with one for Bradwell London clay deduced from suction measurements and presented by Skempton (1961). The profiles are remarkably similar in shape.

Figure 6.11 shows the effective horizontal stress curve of Figure 6.9 plotted to a smaller scale and compared with a normally consolidated horizontal stress distribution of K_o = 0.6 (assumed value). The overconsolidated line presumably curves down to the normally consolidated line at depth.

Suction measurements on triaxial specimens were made after the method of Skempton (1961) and Burland and Maswoswe (1982) and are described in more detail subsequently.

K_o is derived from the expression

$$K_o = \frac{p'_k/\sigma'_v - A_s}{1 - A_s} \qquad (6.1)$$

where p'_k is the capillary pressure, or suction, and A_s is Skempton's A value.

Burland and Maswoswe have plotted 2 points for each of their suction values, one for $A_s = 0.5$ and one for $A_s = 0.3$. London clay typically is known to behave as the former, at least during the initial stages of a test.

K_o and consequently σ_h' are rather insensitive to A_s according to this equation. It is also interesting to note that, according to Atkinson and Bransby (1978), A_s is dependent on the stress path.

The suction values plotted on Figure 6.12 show a wide scatter. Note the very high values in the silty horizon between 13 and 14m. In Figure 6.13 the effective in situ stress (p'_o) has been plotted against p'_k. The p'_o values were estimated from Figure 6.9. The points fall to the right of the 45° line and fall in 2 clusters, one with an average of 100 kPa or greater than the insitu values and another about 350 kPa greater. Most of those in the latter group appear to be from silty samples. Very high values of P'_k could also indicate $A_s < 0$ which may be compatible with silty material (Bishop and Henkel, 1962). It is of interest to note that Jardine (1985) also measured suction value for London clay samples from Canons Park about 100kPa greater than actual in situ effective stresses. He ascribed this mostly to disturbance during sampling operations. It is, however, likely that the high suction values may also be, in part, due to a drying out of the specimens during preparation prior to testing (i.e. during trimming a 38mm specimen from 100mm core).

Four points in Figure 6.12 from Burland and Maswoswe's tests on 100mm samples are all on the lower limit of the scatter, presumably due to the fact that very little specimen preparation was necessary.

It is interesting to compare theoretically p'_k deduced from equation 6.1 with p'_o:

$$p'_k = \sigma'_v \left\{ K_o + A_s(1-K_o) \right\} \qquad (6.2)$$

and

$$p'_o = \frac{\sigma'_v}{3} (1 + 2K_o) \qquad (6.3)$$

It can thus be seen that p'_k and p'_o will be equal only for particular values of K_o and A_s.

K_o values from Skempton's expression have been derived from Burland and Maswoswe's results and the resulting horizontal stresses plotted on Figure 6.9. The values are close to those measured in situ.

6.2.4.2. The Filter paper technique of suction measurement

During the test programme the filter paper method of suction measurement for fine grained soil samples as outlined by Chandler and Gutierrez (1986), was used both for sections of the 100mm core and for 38mm diameter triaxial specimens.

The method involves inserting a piece of filter paper within a soil sample whose suction is required and sealing the whole to prevent evaporation. The filter paper wets up to a water content in equilibrium with the magnitude of the soil suction and measurement of the water content of the filter paper enables the soil suction to be determined from a previously established correlation.

For the sections of core, p'_o was estimated from Figure 6.9 and, for the purposes of this exercise, assumed equal to p'_k. For the triaxial specimens stresses were the all round stresses imposed on the specimen prior to removal from the triaxial apparatus.

The results are shown plotted in Figure 6.14. It can be seen that the results generally fall around Chandler and Gutierrez' correlation line, even at lower stress levels, despite the often significant differences found between p'_o and p'_k for specimens as exhibited in Figure 6.13.

Each length of core was split at several points and a piece of filter paper inserted at each split. For this reason a range of moisture contents are shown for core for a particular stress level.

The siltier samples are shown to have imparted more moisture to the filter paper and so fall to the right of the line.

6.2.4.3. In situ stress paths during and subsequent to excavation

Measurements of in situ stresses at the Bell Common tunnel are described in detail by Tedd et al. (1984). Stresses deduced from gauges at a point 12m below original ground level (about 2.7m below dredge level) and just in front of the wall are plotted in Figure 6.15 in terms of s', t parameters. Also plotted are stresses from a gauge installed near the end of construction just in front of the wall at a depth of 16m below original ground level. No account has been taken of possible wall friction effects on the measured stresses.

6.3. EFFECTIVE STRENGTH AND STIFFNESS - LONDON CLAY AND CLAYGATE BEDS

Table 6.1 is a schedule of triaxial tests on specimens of Claygate Beds and London clay. The results of all the tests are presented in detail in graph form in Appendix A5.

Figure 6.16 depicts the triaxial and plane strain specimen after testing and Figures 6.17 (a) and (b) are photographs following testing of triaxial specimens TLUU1, TLPS2, TLPS6, TLA1, TLDRUL1 and TLDRUL2. A photograph of plane strain sample PLPS1 is shown with part of the testing apparatus on Figure 4.9 (Chapter 4). Strength and stiffness parameters are deduced in the following sections.

Note that for all tests account has been taken of the influence of the confining membrane according to the methods outlined in Appendix A3.

6.3.1. Effective strength envelopes - London clay

6.3.1.1. Undrained extension tests.

Figure 6.18 shows the undrained effective stress paths in q, p' space for the undrained extension tests on London clay. The majority of tests were sheared from initially isotropic stress conditions. Specimens TLCU1 and 2 were allowed to swell isotropically to low stresses prior to undrained shearing. Specimens TLSU1 and 2 were swelled to estimated at rest pressure conditions prior to shearing. It can be seen that during undrained shear p' remains approximately constant and the stress path reaches failure with very little deviation from the pre-failure path.

Figure 6.19 shows the points of maximum shear stress plotted in q,p' space. Most of the points lie on a well defined envelope shown by the thick broken line. It can be seen that the envelope is curved. The chain dotted lines correspond to various values of effective angle of friction ϕ'. At values of p' less than about 100 kN/m^2 the envelope corresponds to $\phi' = 32^o$.

6.3.1.2. Constant q dissipation tests.

Two special extension tests (TLSUD1A and 2B) were carried out in which an attempt was made to simulate the process of undrained unloading followed by pore pressure increase at constant shear stress. Figure 6.20 shows the stress paths for these two tests in q v p' space. The broken line in this figure represents the failure envelope for the undrained extension tests (Figure 6.19). It can be seen that the failure points for the dissipation tests lie close to the undrained failure envelope.

Also shown in Figure 6.20 are the stress paths for the swelling tests in which an attempt was made to maintain conditions of no lateral yield during swelling (tests TLDRUL1 and 2). It can be seen that the stress paths for both tests touch the undrained failure envelope in extension but do not cross it.

Test TLD1 is also shown in Figure 6.20. This specimen was nominally sheared drained in extension, but excess pore water pressures in the

early part of the test caused the stress path to deviate from the normal drained stress path.

6.3.1.3. Passive stress relief tests.

Altogether five passive stress relief tests were carried out such that the strength of the soil was fully mobilised (TLPS1 to 4 and 6). The strengths in TLPS5 was not fully mobilised. The stress paths for each of these tests is plotted in Figure 6.21. The broken line represents the failure envelope for the undrained extension tests (Figure 6.19). Fourie's (1984) passive stress relief test L1 on an intact specimen of London Clay has been added (following correction to stresses due to membrane restraint which he did not do).

It can be seen that the stress paths for the passive stress-relief tests, apart from TLPS5, all cross the undrained failure line giving values of ϕ' well in excess of undrained values. Tests TLPS1 and 4 and L1 give stress paths which move a long way down towards the origin remaining outside the undrained envelope (apart from TLPS4 path at p' of about 120 kPa which moved inside briefly due to a computer malfunction) and then move back inside it or towards it as failure progresses with decreasing values of p' less than 40 kPa. Tests 2, 3 and 6 each moved outside the envelope initially but after failure planes were observed to develop in the specimens at around peak q, necking ensued at the planes and failure was generally confined to localised zones for the remainder of the tests. The similarity in behaviour of TLPS6 which had lubricated ends, to that for other tests with conventional ends can be seen.

The reason for the passive stress relief paths lying outside the undrained failure envelope, when the constant q dissipation tests coincide with it, is not understood at this time. The phenomenon may provide an important element of conservatism in the use of traditional methods for deriving design strength parameters.

It will be recalled from Section 3.5.4.1 that, for all tests apart from TLPS4 and 5, all pressure control mercury tubing of cross sectional

area 7.92mm^2 was used. TLPS4 and 5 were controlled by computer: for 4 the cell pressure (and consequently σ_h' due to u being constant) was set to decrease at the rate of 100 kPa/% axial strain and for 5 at 200 kPa/% axial strain. These were very much higher than those resulting from the mercury tube control which, for the 7.92mm^2 tubing, were around 40 kPa/% axial strain at the start of the passive stress relief phase, decreasing to around 15 near the end. It is apparent from Figure 6.21 that the rate of 200 kPa/% axial strain for TLPS5 was so high that the stress path did not meet a passive failure envelope.

In an interesting exercise Potts (1986) has reanalysed the Bell Common Tunnel by the finite element method using a modified Cam-clay model simulating excavation under fully drained conditions. For an element of soil in front of the retaining wall, a decrease of σ'_h with ϵ_a of 45 kPa/% axial strain decreasing to 23 kPa/% axial strain was predicted. This is similar to rates resulting from mercury tube control to the cell pressure in the passive stress relief tests.

6.3.1.4. Plane strain passive stress relief test.

A single passive stress relief test was carried out in the plane-strain apparatus. The results of the test are plotted in Figure 6.22 in terms of q* v p' where q* is the three-dimensional deviator stress and p' is the mean of the three principle effective stresses. The broken line represents the Mohr Coulomb failure envelope for the undrained triaxial extension tests (Figure 6.19).

It can be seen that, as for the triaxial passive stress relief tests, the stress path moves well outside the failure envelope for the undrained extension tests.

This single test result provides important additional evidence to support the notion that the strength under conditions of passive stress relief is significantly greater than that inferred from conventional extension tests.

6.3.1.5. Triaxial compression tests.

This study has been directed principally towards a study of the soil properties in the passive zone on the excavation side of the wall - hence the emphasis on extension tests. Only three compression tests were carried out - two drained tests following active stress paths with σ_v' constant and σ_h' decreasing (TLA1 and 2A) and an active undrained test TLUA1.

The above data from this study has been supplemented with five consolidated undrained tests carried out by Fourie and three consolidated drained tests by Maswoswe on high quality samples from Bell Common. In addition a number of commercial consolidated drained triaxial compression tests were carried out during the original site investigation.

Figure 6.23 shows the peak values of q against p' for these data. There is good agreement between Fourie's undrained tests and Maswoswe's drained tests. The two active drained tests (TLA1 and 2A) appear to agree with the standard tests but the consolidated undrained test TLUA1 gives a high strength. The commercial tests on samples from nearby boreholes show a significant scatter. No plasticity data is available for Fourie or Maswoswe's tests.

The broken line in Figure 6.23 represents the best estimate of the failure envelope for triaxial compression tests on the London clay at Bell Common.

6.3.1.6. Comparison between triaxial extension and compression failure envelopes

The failure envelopes in Figures 6.19 and 6.23 for extension and compression respectively cannot be directly compared because of the characteristics of a q, p' plot. However they may be superimposed in a plot of t,s'.

Figure 6.24 shows the two failure envelopes transformed to such a plot. It can be seen that for any given average stress $(\sigma_v' + \sigma_h')/2$ the

strength in extension is between 10 kN/m^2 and 20 kN/m^2 weaker than in compression. This difference appears to be due largely to an apparent cohesive intercept on the compression side.

6.3.1.7. Results plotted in terms of critical state axes

Apart from tests TLCU1 and TLCU2 the rate of change of porewater pressures at the end points for the undrained extension tests were very small. In Fig. 6.25 a best fit straight line through the endpoints of the stress paths plotted in terms of p', q axes gives a slope of - 0.69, i.e. $\phi' = 22.9^o$ with a positive intercept on the q axis. The best straight line through the origin gives a slope of -.65, i.e. $\phi' = 21.4^o$. Both of these slopes are very close to the well known critical state ϕ' for London clay in compression, 22.5^o. (Jardine 1985, Parry 1958).

Results of Jardine's (1985) oedometer tests on a London clay slurry are shown in Figure 6.26. The slope of the curve decreases to about 0.16 with increasing pressure.

Parry (1985) gives a slope $\lambda = 0.161$. It is interesting to note that the 'normally consolidated' portion of the oedometer test result of Figure 6.7 gives a slope of 0.19, or $\lambda = 0.08$ in terms of e, ln p' axes. This is much flatter than for the test on the slurry presumably due to ageing and bonding which has taken place in the in situ sample of London clay or that the oedometer curve did not reach the virgin line.

Using $\lambda = 0.16$ and N, the specific volume of isotropically consolidated soil at p' = 1.0 kN/m^2, equal to 2.836, equivalent pressure p'_e values were obtained. Figure 6.27 shows the undrained extension tests normalised with p'_e. A Hvorslev envelope has been drawn using the end points of all the undrained stress paths as guides, slope h = -.651 and intercept with the p'_e axis g = -.015. This gives Γ, the value of specific volume v corresponding to p' = 1.0 kN/m^2 on the critical state line, equal to 2.73 (c.f. Parry, 1958, $\Gamma = 2.759$).

The intercept of the Hvorslev surface with the critical state line gives the critical state point $p'/p'_e = 0.517$ and $q/p'_e = -.352$.

It is interesting to examine Jardine's (1985) undrained triaxial tests on reconstituted London clay (Figure 6.28). The void ratios for all four compression tests were similar, about 0.9, giving a p'_e = 347.2 kPa. Tests LR1 and LR1.5 move to the left to a critical state point, while tests LR7 and LR3 are moving to the right. A critical state point has been drawn between the two groups, at s' = 201, t = 77. For this point therefore p'/p_e = 0.504. This compares reasonably with the critical state point in Figure 6.27 of p'/p'_e = 0.517 which is of course for extension. A critical state point is not as clear for the extension tests as it perhaps is for the compression tests. Stress paths for tests LRE1 and 1.5 do, however, appear to be moving to a point in extension equivalent to the point shown in compression.

The normally consolidated Rendulic surface will curve from the critical state point to the p'/p'_e axis, intercepting at 1.0.

The critical state line and Hvorslev surface are reproduced in Figure 6.29 at lower stress levels. The passive stress relief test results have been normalised with p'_e as have the swelling tests TLSUDIA and TLSUD2B. Fourie's 1984 passive stress relief test L1 corrected for membrane effects is plotted. Test TLD1 is also shown. The plain strain test results are plotted in terms of the octahedral or 3-D deviator stress normalised with p'_e.

It can be seen that all the passive stress relief stress paths, apart from TLPS5 which did not fail, will pass through the Hvorslev surface.

After failure (point denoted 'f') the paths curve towards the origin, sometimes remaining outside the Hvorslev surface (test TLPS1) but usually apparently passing back through the surface. For these cases there was severe necking of the triaxial sample at one point only (Section 6.3.1.3) so the true deviator stress at the neck was actually larger rather than the false deviator stress which was averaged over an assumed right cylindrical sample.

The swelling tests and drained test TLD1 generally failed near the Hvorslev surface.

As an alternative to the usual way of depicting the results in terms of the critical state theory, Atkinsons and Bransby's (1978) method for sand was also used. This method attempts to overcome the problem of the effects of low uncertain λ values in evaluating p'_e values, and also the difficulty of establishing an N value with some accuracy.

Atkinson and Bransby define v_λ as the 'specific volume on the reference section'

$$v_\lambda = v + \lambda \ln p' \qquad (6.4)$$

Here the effect of λ will not be as critical as that of v, the specimen specific volume.

Figure 6.30 shows the undrained tests plotted in terms of v_λ, q/p' axes. Hvorslev and Rendulic surfaces have been sketched in. Passive stress relief tests have been plotted in Figure 6.31. Again, the peaks of the passive stress relief stress paths (apart from TLPS5) can be seen to fall outside the Hvorslev surface.

The Hvorslev surface, drawn independently on Figure 6.27, has been transposed in terms of v_λ, q/p' axes to Figure 6.30. The two surfaces are almost coincident.

The drained compression tests TLA1 and TLA2A and the undrained test TLUA1 have been plotted in terms of critical state axes q/p'_e and p'/p'_e in Figure 6.32. In addition peak failure points from drained commercial compression tests and also those from three tests of Fourie (1984) have been similarly reduced and are also shown on Figure 6.32.

Ignoring TLUA1 a best fit line gives a slope h = .81 and intercept g = .0358 equivalent to a ϕ' of 20.9°. This compares well with the Hvorslev ϕ' of 21.4° for the extension tests.

6.3.1.8. Reason for high mobilised strength under passive stress relief conditions

It is not known at this stage why mobilised strengths under passive stress relief conditions should be comparatively large. A possible explanation might be stress dilatency: a notable feature of the tests has been the large swelling.

It is interesting to apply the stress dilatency theory or energy corrections to the shear strengths which correct q according to the volumetric strain rate (Section 5.4.3).

Although these are more commonly used in the case of silts and sands, Rowe et al. (1963) have applied the Rowe correction to dilatent clays.

The curves of Figure 6.29 for passive stress relief tests TLPS1 and TLPS2 has been corrected for dilatency effects according to the expressions of Rowe (1962), Bishop (1954) and Atkinson and Bransby (1978). The resulting curves are shown in Figure 6.33. The Rowe curves lie within the critical state line/Hvorslev line region while those of Bishop and of Atkinson and Bransby (denoted 'Cambridge') lie some distance beneath the critical state line.

6.3.2. Effective strength envelope - Claygate Beds

Two tests are available from this programme. These results together with some from the commercial tests are plotted in Figures 6.34. An envelope drawn through the results gives $\phi' = 32.7^{o}$ and $c' = 0$.

Passive stress relief test TCPS1 as well as Fourie's (1984) test CG1 corrected for membrane effects are also plotted on Figure 6.34.

As for the London Clay tests, the passive stress relief tests exhibit a higher mobilised strength.

6.3.2.1. Results plotted in terms of critical state axes

There being no data available concerning the critical state parameters for Claygate Beds, λ = 0.16 and N = 2.836 from London Clay were used to plot the two Claygate test results TCUU1 and TCPS1, in terms of p'/p_e, q/p'_e axes. (Figure 6.35). Claygate test CG1 corrected for membrane effects is also included.

As for the London clay tests, the passive stress relief tests exhibit a higher Hvorslev envelope than does the undrained extension test TCUU1.

6.3.3. Undrained stiffness - London clay

The following three types of triaxial undrained test were carried out:

(i) Undrained extension from initial isotropic stress.
(ii) Undrained extension from initial K_o stresses.
(iii) Undrained compression from initial K_o stresses.

The majority of tests were for type (ii) and only one of type (iii).

The results for (i) are presented separately in a plot of normalised secant undrained shear modulus G_u/p' versus log shear strain (Figure 6.36). Stiffness for undrained compression and extension tests from K_o are plotted together in Figure 6.37. Claygate Bed tests are also shown on this plot and the results are discussed in Section 6.3.4.

6.3.3.1. Undrained extension from initial isotropic stress

Figure 6.36 shows a composite plot of G_u/p' versus log shear strain for four of the tests TLUU1, 3, 4 and 5. It can be seen that the results fall into quite a narrow range. The values of G_u/p' at 0.01 per cent strain range from 166 to 97.

6.3.3.2. Undrained extension from initial K_o stresses

Figure 6.37 shows a composite plot of G_u/p' versus log shear strain for the undrained shearing stage of the following tests TLSU1 and 2, TLPS1,

3, 4 and 6 and TLSUD1A and TLSUD2B. Values of G_u/p' at .01% strain range from 130 to about 300. For comparison stiffness ranges for the undrained extension tests from isotropic at 0.1% and 0.01% strain are shown. The stiffness at 0.01% strain for the tests from K_o is about twice that for the tests from an initial isotropic stress.

For comparison the results of the drained phase of test TLPS2 are shown in Figure 6.37. The agreement with the undrained results is very reasonable.

6.3.3.3. Undrained compression from initial K_o stresses

Only one undrained compression test of this type was carried out (TLUA1) and the result is shown in Figure 6.37. The result compares reasonably well with the extension tests but the stiffness in compression reduces less rapidly with increase in strain. This phenomenon reflects the larger changes in shear stress and strain that are required to bring the sample to failure in compression from a K_o value which is greater than one.

For comparison the results of two drained compression tests from K_o conditions (TLA1 and TLA2A) are shown in Figure 6.37. The agreement is seen to be very reasonable.

6.3.4. Stiffness-Claygate Beds

As described previously sampling in Claygate Beds proved very difficult. However, samples were taken from depths of between 1.8m and 2.9m. Three undrained tests were carried out. Test TCUA1 was an undrained active test (compression) carried out from isotropic stress conditions. Test TCUU1 was an undrained extension test carried out from isotropic stress conditions. Test TCPS1 was a passive stress relief test but the initial part of the test was undrained from isotropic stress conditions. The results are plotted on Figure 6.37. It can be seen that the results fall in a narrow range. The values of G_u/p' at .01 per cent strain is about 600. Hence, at this level of strain, the material is two to five times stiffer than London Clay values.

6.3.5. Volumetric Strains - London Clay

The five phases of the various tests that were carried out may be used to study the volumetric behaviour of the London clay:

(i) Swelling from high initial effective stress under approximately one-dimensional conditions.

(ii) Swelling under conditions of constant shear stress.

(iii) Swelling from initial isotropic stress to in situ K_o stresses.

(iv) Drained triaxial tests.

(v) Swelling under passive stress relief.

For most of the phases, sufficient readings are not available from the early portions of the phases to examine the bulk modulus at very low volumetric strains. However data from 7 tests have been plotted in Figure 6.38 against axes of normalised effective secant bulk modulus versus volumetric strain: TLPS1 passive stress relief phase and also anisotropic swelling phase and anisotropic swelling phases from the following tests: TLPS2, 3 and 4, TLSU1, TLDUD1A and TLDRUL2. Although the apparent very high stiffness for some of the tests such as TLPS4 and TLPS2 may be due to incomplete drainage during the early part of the phase and despite the scatter between the tests being high, the results nevertheless show increasing normalised bulk modulus at lower volumetric strains. This is similar to results obtained by Jardine (1987) on triaxial tests on London clay.

The rate of decrease of the effective bulk modulus becomes relatively small at volumetric strains higher than about 0.1 per cent. In order to examine this area in more detail the entire phases (i) to (iv) mentioned above have been examined further. These are discussed separately in the following:

6.3.5.1. Swelling from high initial effective stress

Figures 6.39 and 6.40 show the results of tests TLDRUL 1 and 2 plotted in terms of volumetric strain versus log p' during swelling under K_o conditions from high initial values of p'. It can be seen that for most practical purposes the swelling curves are linear and correspond to values of K'/p' = 78.8 and 61.2 for tests TLDRUL1 and 2 respectively.

Three tests (TLD1, TLCU1 and TLCU2) entailed isotropic swelling from high initial values of p'. No measurements of volumetric strain were made during the swelling process but the equilibrium values were recorded. The associated values of K'/p' were 26.5, 43.6 and 24.8 respectively.

6.3.5.2. Swelling at constant q

The two tests for which swelling took place at constant shear stress were TLSUD1A and TLSUD2B and the associated stress paths are shown in Figure 6.20. The relationships between volumetric strain and log p' are plotted in Figures 6.41 and 6.42. In both cases the relationship is remarkably linear. The values of K'/p' for the two tests are 24.2 and 13.2 respectively.

6.3.5.3. Swelling to initial K_o stresses

A large number of tests were carried out in which the specimens were swelled from initial isotropic stress to K_o conditions prior to carrying out other tests. The swelling characteristics of these tests are given in Table 6.2.

6.3.5.4. Drained tests

Three drained tests were carried out. The initial stages of test TLPS2 were drained prior to passive stress relief testing. Also two active drained tests were carried out from intial K_o conditions (TLA1 and

2A). The swelling characteristics of these latter two tests are plotted in Figures 6.43 and 6.44 in terms of volumetric strain versus log p'. It can be seen that over the initial part of the tests, when the specimens are remote from failure, there is a linear relationship between volumetric strian and log p'. The values of K'/p' from the drained tests are given in Table 6.2.

All the values of K'/p' are plotted against depth in Figure 6.45. It can be seen that most of the values lie between 20 and 40. However in the more silty layer between 13m and 15m depth distinctly higher values of between 60 and 100 were measured.

6.4. DESIGN PARAMETERS

In this Section the results of the test programme together with the results of previous investigations are summarised to provide the best estimates of the soil parameters needed for carrying out a finite element analysis of the Bell Common Tunnel retaining walls. The emphasis of this analysis will be directed towards the deformations and stresses set up during and subsequent to construction.

6.4.1. Effective strength - Claygate Beds

Two tests are available from this programme. These results together with some from the commercial tests are plotted in Figure 6.34 in terms of $(\sigma_1 - \sigma_3)/2$ versus $(\sigma_1' + \sigma_3')/2$. An envelope drawn through the tests gives a value of $\phi' = 32.7^{\circ}$ and $c' = 0$.

6.4.2. Effective strength - London clay

Figure 6.24 shows the effective strength failure envelopes for the London Clay for compression and extension.

6.4.3. Initial vertical and horizontal effective stresses

Figure 6.9 gives the relationships between σ_v' and σ_h' with depth. The pore water pressures are also shown.

6.4.4. The undrained stiffness properties of London clay and Claygate Beds.

Jardine et al. (1986) have shown that a logarithmic function can be fitted to the measured relationship between secant G'_u/p' and shear strain ϵ. The function is written:

$$\frac{G'}{p'} = A + B \cos\left\{\alpha\left(\log \frac{\epsilon}{C}\right)^{\gamma}\right\} \qquad (6.5)$$

The values of constants to give a fit for an above expression are listed in Table 6.3. The resulting curves drawn through the data, are shown in Figure 6.37.

6.4.5. Compressibility of the London clay and Claygate Beds

A mean line drawn through the results of Figure 6.38 is almost exactly coincident with a curve derived by Jardine (1987) for tests on London clay of the form of the logarithmic function given above. The values of the constants for the function are given in Table 6.3. A volumetric strain cut off limit $\epsilon_{v(max)}$ (i.e. elastic limit) of 0.185 per cent has been selected as the point at which the tangent modulus of the normalised bulk modulus equals the mean K'/p' of 30 derived from Figure 6.45.

No measurements of K' were made for the Claygate Beds. With the stiffness for the Claygate around 2.5 times more than that of the London clay it is suggested that a bulk modulus expression equally stiffer than that derived for the London clay be adopted. The constants are given in Table 6.3.

6.5. PUBLISHED DATA

No published data could be found for the strength and stiffness of Claygate beds other than that connected with the Bell Common testing programme. However, there exists a large amount of published data for London clay.

6.5.1. Effective strength

Bishop et al. (1965) describe a comprehensive testing programme on London clay from Ashford Common, north London. They carried out both drained and undrained triaxial compression tests at effective stress levels from 2kPa to about 800kPa. Atterberg limits and clay fractions for this clay were very similar to those obtained for the Bell Common London clay.

A distinctly curved failure envelope was obtained giving higher friction angles at lower stress levels.

At stress levels up to about 700kPa, c' values varying between 0 and 250 kPa and ϕ' values of between 23^{o} and 29^{o} were obtained.

More recently Jardine (1985) from triaxial compression tests on London clay from Canons Park, North London, found ϕ' varying from about 22.5^{o} to 25^{o} with c' varying from 15 kPa to 0 respectively. Effective stress levels for these tests were between 150 and 300kPa.

6.5.2. Stiffness

Cole and Burland (1972) back analysed observed movements of the diaphragm retaining walls at Britannic House and derived the distribution of undrained Young's Modulus with depth corresponding to these movements. Subsequently the distribution has been refined, following other such back analyses, for example that for the Palace of Westminster (Burland and Hancock, 1977). This was the distribution which was used for the Class 'A' prediction for Bell Common by Potts and Burland (1983) and is reproduced as Figure 6.46.

More recently, with the development of local strain measuring devices for laboratory testing of soils, e.g. Burland and Symes (1982), Jardine et al. (1986) and Clayton and Khatrush (1987), it has been possible to derive expressions for stiffnesses of soils in the laboratory. These, unlike for previous testing using external axial strain measurements, approximate much more closely to those obtained from back analysis of excavations.

It is interesting to derive values of G_u (= $E_u/3$) at various depths from the curve of Figure 6.46 and normalise them with p' obtained from Figure 6.9. An average G_u/p' of about 200 is obtained over the 20m depth. This tangent modulus corresponds to a secant modulus of about 300 for the expressions adopted in this thesis for the Bell Common London clay which would be the stiffness at about .01% strain (Figure 6.37).

CHAPTER 7

SUMMARY AND CONCLUSIONS

CHAPTER 7

SUMMARY AND CONCLUSIONS

7.1. GENERAL

Attempts have been made in the laboratory to simulate stress paths associated with excavations with emphasis on the passive stress area beneath excavations and to examine strengths and stiffnesses of specimens under these conditions. In particular strength and stiffness parameters were required for strata at Bell Common to enable a back analysis of the retaining wall to be carried out; these parameters are given in Chapter 6.

A programme of tests was carried out first on a sand in order to refine testing techniques more rapidly than would have been possible with a clay.

A borehole was drilled at Bell Common and high quality samples of Claygate Beds and London clay were obtained and tested in the laboratory.

7.2. TESTS IN TRIAXIAL AND STRESS PATH CELLS

7.2.1. Strengths

Strength showed a dependency on stress level and stress path.

Specimens of dense sand tested in drained compression showed an increase in ϕ' from about 40° at 100kPa to over 50° at 10kPa. In extension, friction angles are about 7° more at 10kPa and 4° more at 100kPa.

The London clay also exhibits a curved failure envelope. At values of p' less than about 100kPa the envelope corresponds to a ϕ' approximately equal to 32° decreasing to between 20° and 25° at a stress level of about 500kPa. The compression envelope is more or less similar in form to the extension envelope with the strength in extension about 10 to 20kPa weaker than in compression.

Under conditions of passive stress relief both sand and clay mobilise extremely high strengths, significantly higher than those mobilised in routine drained and undrained extension, even allowing for moisture content differences. There appears to be a failure envelope, outside the Hvorslev envelope, along which a passive stress path travels. For a loose sand, ϕ' of about 60^{o} was mobilised at stress levels of around 10-20kPa. For London Clay, ϕ' of over 35^{o} was obtained at stress levels of about 100kPa. These high strengths may add an element of conservatism to a design where traditional friction angles have been utilised. The reasons for such high strengths under conditions of passive stress relief are not understood but are thought to be connected with the strongly dilatent behaviour which takes place under these conditions.

7.2.2. Stiffness

For many of the tests local axial strain measuring devices similar to those used by Jardine (1984) were employed. The device was later modified in order to give a more accurate measurement of local strains. Full details of this work are given in the Appendix.

It was possible to measure axial strains locally for only a few of the sand specimens due to the non availability of the small strain devices. However, those measured showed the normalised shear modulus G/p' decreasing with increasing axial strain as follows : for dense sand at .02% axial strain the stiffness varied between 400 and 800, decreasing to between 200 and 300 at .1% strain. For loose sands, the stiffnesses were between 200 and 500 at .02% decreasing to 100 to 250 at .1% strain.

Bulk moduli were not measured for the sand tests.

For the London clay tests, as expected (Jardine 1985), the shear moduli decreased with strain level as did those for the Claygate Beds. For the London clay, stiffnesses were greater in compression than in extension, but the rate of decrease with strain level was greater in extension than in compression. Shear moduli normalised with current effective stress G/p' was found to decrease in compression from about 300 at .01% strain

to about 60 at .1% strain. This relatively rapid rate of decrease of shear modulus in extension was not found by Jardine (1987) for tests conducted on London clay from a central London site. Jardine's stiffer response may have been due to a small recompression which was applied to the specimens following swelling to an estimated highest previously imposed in situ stress: this was to simulate deposition of gravels over the London clay following erosion. Sharply reversing the stress path direction in such a manner prior to shearing would be expected to lead to a stiffer response. (Hight et al., 1985).

For Claygate Beds the normalised shear modulus was about 640 at .01% strain decreasing to 200 at .1% strain.

For the London clay tests, attempts were made to assess the change of bulk modulus with the change of volumetric strain. A wide fluctuation of stiffnesses were measured. However, the mean curve was found to be similar to a distribution quoted by Jardine (1987) for a central London site. Bulk modulus normalised with mean effective stress was found to decrease from about 150 at .05% strain to about 100 at .1% strain.

7.3. PLANE STRAIN APPARATUS

The new plane strain apparatus was found to function satisfactorily despite problems which were encountered with the stress path cell within which it was enclosed. A successful passive stress relief test was completed on an undisturbed specimen of London clay. As far as the author is aware, this was the first plane strain test which had been performed on an undisturbed specimen of London clay in extension.

As for the triaxial passive stress relief tests, high shear strengths were also mobilised during the use of the plane strain test.

It was unfortunately not possible to obtain meaningful small axial strain readings due to a malfunction of equipment during the early stages of the test.

7.4. SOME SPECIAL COMMENTS WITH REGARD TO THE TESTING

7.4.1. Cross sectional area correction for extension tests

Testing in extension is notoriously difficult due to the possibility of specimens narrowing at a particular point of weakness ('necking') and the uncertainty of the calculation of stresses thereafter. However, sufficient data have been gathered from tests before significant necking has been observed and from those tests which have failed with the specimen remaining approximately right cylindrical during the test, to be confident of the findings reported. In any event, where the diameter has reduced significantly at a particular point in the specimen, the stress calculated on the reduced area would be greater and therefore the mobilised strength also.

7.4.2. Calibration of measuring equipment

Very careful attention was paid to calibration.

Load and stress readings were most critical for tests carried out at low stress levels.

For pressure measurement, cell and back pressure transducers were frequently cross checked and the regressions adjusted so that the transducers gave similar readings over the anticipated pressure range for the test; effective stresses were accurate to within no more than ± 0.4kPa., probably less.

Load cell calibrations were adopted such that there was greater accuracy at lower stress levels: generally better than ±0.5N error to ±30N load. Beyond this the error was estimated to have been less than 1.0%.

7.4.3. End Effects

As a check on possible friction effects of the end caps on the specimens, several tests were performed with lubricated ends. No differences which may have been ascribed to friction effects were

noticed between these and tests performed without lubricated ends.

7.4.4. Membrane restraint

From the very earliest extension tests conducted on loose sands at low confining stresses, it became clear, with the mobilised strength increasing at a fairly constant rate up to high strains, that the restraint due to the confining membrane was significant.

An extensive programme of tests was conducted using rubber dummy specimens, with and without membranes. In addition, finite element analyses were performed in an effort to model the interaction between membrane and specimen.

Apart from verifying the restraint offered in extension, restraint was also found to exist in compression tests at effective stresses as low as 2kPa., surprisingly even while the membrane was wrinkling or buckling.

The currently used theories for correction of stresses due to membrane restraint, namely those of Henkel and Gilbert (152) and Duncan and Seed (1965) were studied.

Henkel and Gilbert's equation for correction to vertical stresses is simple and is widely used. It is recommended in both BS1377 and ASTM D2850-82. However an error in their method for calculating the rubber stiffness leads to the correction being significantly underestimated for compression tests but reasonably accurate for extension tests.

Duncan and Seed look at the membrane stresses in terms of simultaneous vertical and horizontal action (plane stress) which is probably closer to reality than Gilbert and Henkel's approach of treating the stresses separately.

They give expressions (complex relative to those of Gilbert and Henkel) for vertical and horizontal stress corrections. The resulting vertical stress correction is very similar using either theory: typically, for an undrained compression on a triaxial specimen 76mm high and 38mm

diameter the vertical stress correction will be about 10kPa at 20% axial strain for a latex rubber membrane about 0.3mm thick. The radial stress correction will be less than 2kPa (including the effect of the initial radial stretching of membrane around specimen). Finite element analyses indicate that this may be somewhat severe and that the actual radial membrane stress may be less than that predicted by Duncan and Seed.

Full details of the investigations into membrane restraint are given in Appendix A3.

7.5. THE FILTER PAPER TECHNIQUE OF SUCTION MEASUREMENT

During the test programme the filter paper method of suction measurement was used with London clay for both sections of 100mm core samples and for triaxial specimens.

The technique was proposed by Chandler and Gutierrez (1986) as a simple method for estimation of the suction in a soil sample and thence also p'_o (and K_o, knowing the vertical effective stress at a point in the ground).

For the triaxial specimens, p'_k was taken to be the average all round stress (p'_o) exerted on the specimen prior to insertion of the filter paper. For the core samples, p'_k was assumed equal to p'_o estimated to exist at the point in the ground where the sample was recovered. It should be remembered though that there is no a priori reason why p'_o should be equal to p'_k. Nevertheless, points do fall fairly evenly about the calibration of Chandler and Gutierrez, though with a wide scatter, especially for siltier samples.

7.6. SUGGESTIONS FOR FUTURE RESEARCH

Although the concept of the passive stress relief stress path has been examined in some detail, it is not clear why such high strengths are mobilised compared with other stress paths in extension. It is

possible that stress dilatency contributes to the enhanced strength. Several researchers have studied stress dilatency for granular materials, but the concept when applied to clays does not appear to have received much attention. Further study is required.

It would be instructive to perform passive stress relief tests on other materials commonly found in Britain, such as Glacial Till.

More tests should be conducted with the plane strain device after modifications recommended in Chapter 4 have been undertaken. A test programme, in the first instance comprising undrained and drained compression and extension tests on undisturbed specimens of London clay would be instructive, followed by further tests with other stress paths, including passive stress relief.

Some additional research into small strain stiffness of London clay in extension could be usefully carried out with the modified local strain gauge devices. In the field, every effort should be made to continue to instrument and monitor stresses and strains in the vicinity of excavations and so enable back analyses to be performed. Only in that way is it possible to check on strengths and stiffnesses such as those reported in this thesis and so obtain a better understanding of the behaviour of soils associated with excavations.

REFERENCES

REFERENCES

A.S.T.M. (1982): Standard test method for unconsolidated undrained compressive strength of cohesive soils in triaxial compression. D2850-82.

Atkinson, J.H. (1973): The deformation of undisturbed London clay. PhD Thesis, University of London.

Atkinson, J.H. and Bransby, P.L. (1978): The mechanics of soils. McGraw-Hill Book Company (UK) Ltd.

B.S. 1377 (1975): British standard methods of test for soils for civil engineering purposes.

Berre, T. (1978): Effect of rubber membranes, side drain and specimen height on results of triaxial tests. N.G.I. internal report; 56103-10.

Berre, T. (1982): Triaxial testing at the N.G.I. A.S.T.M. Geotechnical Testing Journal; 5; 1/2; 3-17.

Bishop, A.W. (1954): Discussion on paper by A.D.M. Penman. Geotechnique 4; 1; 43.

Bishop, A.W. (1965): The influence of end restraint on the compression strength of a cohesionless soil. Geotechnique 15; 3; 243-266.

Bishop, A.W. and Henkel, D.J. (1962): The measurement of soil properties in the triaxial test. Edward Arnold; London.

Bishop, A.W., Webb, D.L. and Lewin, P.I. (1965): Undisturbed samples of London clay from the Ashford Common shaft: Strength-effective stress relationships. Geotechnique 15; 1; 1-31.

Bishop, A.W. and Wesley, L.D. (1975): A hydraulic triaxial apparatus for controlled stress path testing. Geotechnique 25; 1; 657-670.

Bolton, M.D. (1986): The strength and dilatency of sands. Geotehnique 36; 1; 65-78.

Burland, J.B. and Fourie, A.B. (1985): The testing of soils under conditions of passive stress relief. Geotechnique 35; 2; 193-198.

Burland, J.B. and Hancock, R.J.R. (1977): Underground car park at the House of Commons: geotechnical aspects. Structural Engineer 55; 87-100.

Burland, J.B. and Maswoswe, J. (1982): Discussion. Geotechnique 32; 3; 285-286.

Burland, J.B. and Symes, M. (1982): A simple axial displacement gauge for use in the triaxial apparatus. Geotechnique 32; 1; 62-65.

Chandler, R.J. (1966): The Measurement of residual strength in triaxial compression. Geotechnique 16; 3; 181-186.

Chandler, R.J. and Guttierrez, C.I. (1986): The filter paper method of suction measurement. Geotechnique 36; 2; 265-268.

Clayton, C.R.I. and Khatrush, S.A. A new device for measuring local axial strains on triaxial strains. Geotechnique 36; 4; 593-597.

Cole, K.W. and Burland, J.B. (1972): Observations of retaining wall movements associated with a large excavation. Proc. 5th Eur. Conf. Soil Mech. and Found. Engg. 1; 445-453.

Cornforth, D.H. (1964): Some experiments on the influence of strain conditions on the strength of sand. Geotechnique 15; 2; 143-167.

Cornforth, D.H. (1973): Prediction of drained strength of sands from relative density measurements. A.S.T.M. special technical publication 523; 281-303.

De Lory, F.A. (1957): Long term stability of slopes in over consolidated clay. PhD Thesis; University of London.

Dickey, J.W., Ladd, C.C. and Rixner, J.J. (1968): A plane strain device for testing clays. M.I.T. research report R68-3; Soils Publication 237.

Duncan, J.M. and Bolton - Seed H. (1965): Errors in strength tests and recommended corrections. Report TE654-4 for U.S. Army Engineers W.E.S; Dept. of C.E. Inst. of Transportation and Traffic Engineering; University of California, Berkeley.

El-Ruwayih, A.A. (1975): Stress-strain characteristics of a rockfill and of clays under high pore water tension. PhD thesis; University of London.

Fourie, A.B. (1984): The behaviour of retaining walls in stiff clay. PhD thesis; University of London.

Fukushima, S. and Tatsuoka, F. (12984): Strength and deformation characteristics of saturated sand at extremely low pressures. Soils and Foundations 24; 4; 30-48.

Gens, A. (1982): Stress-strains and strength characteristics of a low plasticity clay. PhD thesis; University of London.

Green, G.E. (1969): Strength and compressibility of granular materials under generalised strain conditions. PhD thesis; University of London.

Hambly, E.C. and Roscoe, K.H. (1969): Observations and predictions of stresses and strains of wet clays. Proc. 7th Int. Conf. Soil Mech. and Found. Engg. 1; 173-181.

Head, K.H. (1982): Manual of soil laboratory testing 2; Pentech Press; London.

Henkel, D.J. and Gilbert, G.D. (1952): The effect of the rubber membrane on the measured triaxial strength of clay samples. Geotechnique 3; 1; 20-29.

Hight, D.W. (1983): Laboratory investigations of sea-bed clays. PhD thesis; University of London.

Hight, D.W., Gens, A. and Jardine, R.J. (1985): Evaluation of geotechnical parameters from offshore clay. Advances in underwater technology and offshore engineering 3; 253-268. Published by Graham and Trotman Ltd.

Hubbard, H.W., Potts, D.M., Miller, D. and Burland, J.B. (1984): Design of the retaining walls for the M25 cut and cover tunnel at Bell Common. Geotechnique 34; 4; 495-512.

Hughes, J. (1973): An instrument for the in situ measurement of the properties of soft clays. PhD thesis; University of Cambridge.

Hvorslev, M.J. (1949): Subsurface exploration and sampling of soils for civil engineering purposes.

Jardine, R.J. (1985): Investigations of pile-soil behaviour with special reference to the foundations of offshore structures. PhD thesis; University of London.

Jardine, R.J. (1986): Electrical transducers used in soil mechanics laboratories. Internal report; Imperial College soil mechanics section.

Jardine, R.J. (1987): Personal communication.

Jardine, R.J., Potts, D.M., Fourie, A.B. and Burland, J.B. (1986): Studies of the influence of non linear stress-strain characteristics in soil-structure interaction: Geotechnique 36; 3; 377-396.

Jardine, R.J., Symes, M.J. and Burland, J.B. (1984): The measurement of soil stiffness in the triaxial apparatus. Geotechnique 34; 3; 323-340.

Kolbuszewski, J.J. (1948): An experimental study of the maximum and minimum porosities of sands. Proc. 2nd Int. Conf. Soil Mech. and Found. Engg. 1; 158-165.

Ladd, C.C., Foott, R., Ishihara, K., Schlosser, F. and Poulos, H. (1977): Stress deformation and strength characteristics. Proc. 9th Int. Conf. Soil Mech. and Found. Engg; 2; 421-494.

La Rochelle, P. (1960): The short term stability of slopes in London clay. PhD thesis; University of London.

La Rochelle, P., Leroueil, S., Trak, B., Blais, L. and Tavenas, F. (1986): Obervational approach to membrane and area corrections in triaxial tests. A.S.T.M. specialty conference on triaxial testing; Louisville U.S.A.

Lee, K.L. and Seed, H.B. (1964): Discussion. Jnl. of SMF Div. ASCE 90; SM6; 173-175.

Leroueil, S. (1986): Personal communication.

Lovenbury, H.T. (1969): Creep characteristics of London clay. PhD thesis; University of London.

Marsland, A. (1971): Laboratory and in situ measurements of the deformation moduli of London clay. Proc. symp. on interaction of structure and foundation; Midland Soil Mech. and Found. Engg. Soc. Birmingham UK.

Maswoswe, J. (1981): Bell Common - report on soil testing performed at Imperial College for T.R.R.L.

Maswoswe, J. (1985): Stress paths for a compacted soil during collapse due to wetting. PhD thesis; University of London.

Mayne, P.W. and Kulhawy, F.H. (1982): OCR relationships in soil. Jnl. Geotech. Engg. Div. - A.S.C.E.; GT6; 851-872.

Molenkamp, F. and Lugar, H.J. (1981): Modelling and minimisation of membrane penetration effects in tests on granular soils. Geotechnique 31; 4; 471-486.

Ng, R.M.C. and Lo, K.Y. (1985): The measurement of soil parameters relevant to tunnelling in clays. Can. Geotech. Jul 22; 375-391.

Ovando-Shelley, E. (1986): Stress-strain behaviour of granular soils tested in the triaxial cell. PhD thesis; University of London.

Parry, R.H.G. (1958): Discussion. Geotechnique 8; 183-186.

Peck, R.B. (1969): Deep excavations and tunnelling in soft ground. State of the art report. Proc. 7th Int. Conf. Soil Mech. and Found. Engg.; 225-290.

Ponce, V.M. and Bell, J.M. (1971): Shear strength of sand at extremely low pressures. Incl. of SMF Div. ASCE 97; SM4; 625-638.

Potts, D.M. and Burland, J.B. (1983): A numerical investigation of the retaining walls of the Bell Common tunnel. TRRL supplementary report 783.

Potts, D.M. (1986): Personal communication.

Powrie, W. (1986): The behaviour of diaphragm walls in clay. PhD thesis; University of Cambridge.

Reades, D.W. (1972): Stress-strain characteristics of a sand under 3 dimensional loading. PhD thesis; University of London.

Roscoe, K.H. (1953): An apparatus for the application of simple shear to soil samples. Proc. 3rd Int. Conf. Soil Mech. and Found. Engg. 1; 186-191.

Rowe, P.W. (1962): The stress-dilatency relation for static equilibrium of an assembly of particles in contact. Proc. R. Soc. A. 264; 500-527.

Rowe, P.W. and Barden, L. (1964): Importance of free ends in triaxial testing. Jnl SMF Div. - A.S.C.E. 90; SM1, 1-77.

Rowe, P.W., Oates, D.B. and Skermer, N.A. (1963): The stress dilatency perormance of two clays. A.S.T.M. special tech. publication 361; 134-143.

St. John, H. (1975): Field and theoretical studies of the behaviour of ground around deep excavations in London clay. PhD thesis; University of Cambridge.

Sandrani, S.S. (1977): The strength of London clay in total and effective stress terms. PhD thesis; University of London.

Schofield, A.N. and Wroth, C.P. (1968): Critical state soil mechanics. McGraw-Hill book company, London.

Singh, R., Henkel, D.J. and Sangrey, D.A. (1973): Shear and K_o swelling of overconsolidated clay. Proc. 8th Int. Conf. Soil Mech. and Found. Engg. 1; 367-376.

Skempton, A.W. (1961): Horizontal stresses in an overconsolidated London clay. 5th Int. Conf. Soil Mech. and Found. Engg. 1; 351-357.

Skempton, A.W. and Henkel, D.J. (1957): Tests on London clay from deep borings at Paddington, Victoria and the South Bank. Proc. 4th Int. Conf. Soil Mech. and Found. Engg. 1; 100-106.

Skinner, A.S. (1985): Personal communication.

Som, N. (1968): The effect of stress path in the deformation and consolidation of London clay. PhD thesis; University of London.

Stroud, M.A. (1971): Sand at low stress levels in the S.S.A. PhD thesis University of Cambridge.

Symons, I.F. (1967): Discussion. Proc. Geotech. Conf. Oslo 2; 175-177.

Tatsuoka, F., Sakamoto, M., Kawamura, T. and Fukushima, S. (1986): Strength and deformation characteristics of sand in plane strain compression at extremely low pressures. Soils and Foundations 26; 1; 65-84.

Tatsuoka, F., Molenkamp, F., Torii, T. and Hino, T. (1984): Behaviour of lubrication layers of platens in element tests. Soils and Foundations 24; 1; 113-128.

Tatsuoka, F. (1987): Discussion. Geotechnique 37; 2; 219-226.

Taylor, D.W. (1948): Fundamentals of soil mechanics. Wiley, New York.

Tedd, P., Chard, B.M., Charles, J.A. and Symons, I.F. (1984): Behaviour of a propped embedded retaining wall in stiff clay at Bell Common tunnel. Geotechnique 34; 4; 513-632.

Tedd, P. and Charles, J.A. (1983): Evaluation of push-in pressure cells in stiff clay, Int. Symp. on in situ testing, Paris.

Tedd, P. and Charles, J.A. (1985): The strength of London clay in relation to the design of embedded retaining walls. Geotechnique 35; 2; 199-204.

Terzaghi, K. and Peck, R.B. (1967): Soil mechanics in engineering practice. Wiley, New York.

Toll, D.G. (1988): The behaviour of unsaturated compacted naturally occurring gravel. PhD thesis, University of London.

Van Leussen, W. and Miewenhuis, J.D. (1984): Soil mechanics aspects of dredging: Geotechnique 34; 3; 359-381.

Vesic, A.S. and Clough, G.W. (1968): Behaviour of granular materials under high stress. Jnl of SMF Div. ASCE 94; SM3; 661-688.

Wade, N.H. (1963): Plane strain failure characteristics of a saturated clay. PhD thesis; University of London.

Wesley, L.D. (1975): Influence of stress path and anisotropy on the behaviour of soft alluvial clay. PhD thesis; University of London.

Windle, D. and Wroth, C.P. (1977): The use of a self boring pressuremeter to determine the undrained properties of clays. Ground engineering 10; 6; 37-48.

Wood, C.C. (1958): Shear strength and volume change characteristics of compacted soils under conditions of plume strain. PhD thesis; University of London.

Wroth, C.P. (1984): The interpretation of in situ tests. Geotechnique 34; 4; 449-489.

APPENDIX A1

CALIBRATION OF INSTRUMENTATION

APPENDIX A1

CALIBRATION OF INSTRUMENTATION

A1.1. INTRODUCTION

All test results depend directly on the calibration of the instrumentation. Any inaccurate calibrating would lead to inaccurate results regardless of the care with which tests were performed. Many tests described in this thesis were carried out at low effective stresses, often on weak specimens. The accuracy of the calibration was thus even more important than might usually be the case.

A description of the methods used to calibrate the instruments follows, and the calibrations are presented in Table A1.1 together with an estimate of errors.

In order to check for any change of calibration with time, instruments were recalibrated at 12-18 month intervals with no significant change encountered.

A1.2. LOAD CELLS

A1.2.1. Calibration for load

Load cells were calibrated for compressive loads greater than 108N using a Budenberg dead weight calibrator. Prior to calibration the load was cycled 5 times from zero to 90% of maximum cell rating so as to minimise hysteresis. For new load cells the load was cycled 10 times. The reading of the load cell under no load was noted at the start of each cycle as a check on the adequacy of the cycling: this generally stabilised after 2 or 3 cycles at the most.

The load cells were calibrated through 3 cycles of loading and unloading.

For compressive loads between 0 and 108N, the load cell was screwed down on a smooth level steel pad. Weights were then stacked on a purpose

made platform which fitted on the top of the stem. As before, the cell was calibrated through 3 cycles.

For tension calibration the load cell was suspended in a heavy duty steel frame. An aluminium hanger was screwed to the underside of the cell. Weights were then stacked on the hanger and the cell calibrated through 3 cycles generally to -300N. For the plain strain machine load cells the calibrations were taken to -900N.

A straight line was fitted to the calibration results. The slope of the line was greater in tension than in compression, varying from one cell to another, between 3% and 10%. This is because the support, or pivot point for the corners of the load cell star is nearer to the centre on the upper side than on the lower side, giving a shorter lever arm in tension. Also, the slope increases slightly as the load increases in compression, or decreases in tension. Nevertheless, in tension the mean error from the best fitting straight line is only at the most ±1N down to -300N. In compression, the slope increase, which varied from cell to cell, was at best a 1.5% increase for the whole range 0-4200N compared to ± 0.5N for the low range 0-114N, and at worst 6.9%.

As most compression tests were done at lower stress levels (and it is at these levels where it is especially important for errors to be minimised) with deviatoric loads rarely above 1000N and usually below 100N, the slope for the 0 to 114N calibration was adopted and is given in Table A1.1. The error for this range is less than ±0.5N, but usually even better at ±0.1N. For greater compressive loads up to 1000N, using the low compression regression, the best straight line loads are less than the actual loads by a maximum of 10%. The exception is the vertical load cell in the plane strain machine, which has a larger error. No compressive tests were, however, carried out with this machine.

A1.2.2. Calibration for deflection of load cell

Although local strain measuring devices were used for many of the tests, each load cell was nevertheless calibrated for its load-deflection

characteristics so that the externally measured deflections could be corrected. A brass dummy specimen was used in the stress path cells and a steel dummy in the plain strain cell. In addition in an effort to calibrate out some of the bedding effects between top cap or pedestal and specimen, porous stones were incorporated and the rubber suction cap or bayonet fitting used, as appropriate.

Results are shown in Figure A1.1 and Figure A1.2. The group of curves in compression are similar to each other, as are the curves in extension. At -300N, the deflection is about 0.3mm which represents 0.4% axial strain for a 76mm high specimen.

The deflection of the 1000N cell (labelled '1' on Figure A1.1) with a star of 'EN57' steel is appreciably less than that of the others which are for 4500N cells with stars of the softer 'Maragin' steel.

A1.3. PRESSURE TRANSDUCERS

For calibrating the pressure transducers, the stress path cells were filled with water with transducers in place (the mid height pore water pressure probe was left exposed inside the cell) and connected to the Burdenberg dead weight calibrator.

The transducers were then calibrated simultaneously through 3 cycles of pressure between 0 and 1000kPa.

A straight line fitted to the results deviates most at the lower stresses (up to around 150kPa pressure) where the slope of the actual pressure-voltage curve is steeper than that for the remainder of the readings. Nevertheless, the mean error from the best straight line is at the most ±1.5kPa but usually less than ±1kPa for the Bell and Howell and Shape transducers and only ±0.4kPa for the Senso-metric transducers and ±0.5 to ±0.7kPa for the Druck probes.

In an effort to increase further the accuracy of the pressure readings, the lower stress ranges were generally avoided. Also, both cell and

back pressure transducers were frequently cross checked and the regressions adjusted so that the transducers gave similar readings over the anticipated test pressure range. In this way the pressures recorded were accurate to within no more than ±0.4kPa, probably less.

A1.4. DISPLACEMENT TRANSDUCERS

MPE displacement transducers were calibrated using a Vernier Calibrator with a resolution of .01mm through 1 cycle of the 25mm range. The calibrating apparatus has an inherent 'backlash' of just under 0.1mm. So, in calibrating the reverse leg of a cycle, the apparatus should be wound beyond each of the required calibration points by at least 0.1mm (say 0.15mm to be safe) and then wound back in the same direction as the original cycle.

The mean error from the best straight line fitted through the calibration points was around ± .007mm.

A similar procedure was followed for calibrating the LVDTs from the radial strain belt used with some of the passive stress relief sand specimens and the horizontal displacement gauge of the plane strain apparatus. A 3rd order polynomial curve was fitted to the former calibration (mean error ±.006mm) and a straight line to the latter (mean error ±.003mm).

Devices for measuring local strains on specimens (electrolevel and pendulum type gauges) were also calibrated using the vernier calibrator in a similar fashion. The calibrations are discussed in Appendix A2.

A1.5. VOLUME GAUGES

The volume gauges were calibrated against a burette through one cycle of the 50ml (or 100ml in the case of the conventional triaxial) apparatus .

Generally the gauges were calibrated through a closed burette against a back pressure. However, some calibrations were also done through an open burette as a comparison. No significant difference was found in the calibration.

The mean error from the best straight line through the calibrated points was around ±.05ml.

APPENDIX A2

LOCAL STRAIN MEASUREMENT

APPENDIX A2

LOCAL STRAIN MEASUREMENT

A2.1. INTRODUCTION

It is now well established that for accurate stiffness measurements specimen strains should be measured locally during the initial stages of a triaxial test in order to overcome bedding and compliance effects (Burland and Symes, 1982, and Jardine et al., 1984).

Jardine et al. (1984) mounted 2 devices diametrically opposite each other on a 38mm triaxial sample. The heart of the device is a glass capsule of electrolytic fluid (see Figure A2.1). Co-planar electrodes protrude into the capsule and are partially immersed in the electrolyte. The impedance between the central electrode and the outer ones vary as the capsule is tilted. The capsule is housed in a metal tube which is attached through 2 hinged legs and bearing pads to the sample. The hinges are made of PTFE.

The devices are manufactured at IC and have been in use in the Laboratory for several years. With the Orion logging system currently in operation the incoming mains supply of 220/240 volts AC is transformed to DC ± 15 volts frequency 2kHz. The current passes through a modulator/demodulator circuit to the electrolevel device to give an output of ± 10 volts DC for ± 50 degrees of tilt.

Whereas Burland and Symes (1982) report scatters of ± 2mV during monitoring it has been noticed that electrolevel gauges currently in use at IC give typical scatters of ± 4mV, or worse, over several hours. This would be equivalent to about ± .005% strain. As we are looking at axial strains as small as .001 to .002% this gives cause for concern and makes interpretation extremely difficult. (See Figure A2.2 for a typical calibration and Figure A2.3 for a plot of a continuous monitoring over 16 hours of a 5 year old electrolevel gauge with legs clamped).

It is known that the electrolytic fluid breaks down at a rate depending on the amount and level of excitation. The capsule manufacturers, IFO International (UK) Ltd, state that the fluid remains "within output specification for 10000 hours (just over a year) of continuous excitation at a level of 25-1000 Hz."

Since installation of the Orion system in August 1984 the gauges have been continuously energised. With the Solatron DTU system previously employed the gauges were energised only when readings were required.

A2.2. THE NEW PENDULUM LOCAL STRAIN DEVICE

Whereas no deterioration in the scatter of the readings has been noticed in the last 2 years it was nevertheless decided to proceed with the design of a new type of local strain device. This embraced the general geometry of the existing device, though with a shorter span between support pads. Instead of an electrolytic capsule the device has a strain gauged pendulum type arrangement similar to the larger 'tiltmeter' currently manufactured and the borehole inclinometer previously manufactured at IC.

A heavy weight or bob made of mallory hangs on the end of a strip of spring steel 5 thousandths of an inch thick. The strips are strain gauged with 4 x 350 Ω strain gauges connected in a full bridge configuration. As the device tilts, so the steel strip bends and the strain gauge resistance changes. Because of the extremely small scale (the capsule in which the arrangement must hang is only 12mm diameter by 35mm long) there are several potential problems: flexibility and creep of the steel strip, the very small size of strain gauges and limited space for the bob. The prototype device constructed is shown in diagrammatic form in Figure A2.4 and is photographed in Figure A2.5 with the outer casing dismantled.

A typical calibration over several cycles is shown on Figure A2.6. It can be seen that the regression is not quite linear, averaging about

1500mm/volt. With the strain gauge device the input is direct current thus obviating the need for the expensive modulating/ demodulating equipment.

A stability check over 60 hours is shown in Figure A2.7. The scatter is about $\pm 3 \times 10^{7}$ volts, or ± .0005mm, equivalent to .001% axial strain.

Although the stability may vary with time, due, for example to any temperature fluctuations (though none have been apparent) the very small strain readings will be required only for a limited time. For example, at the typical London Clay drained triaxial test strain rate of 0.5% per day, .01% strain will be reached in about half an hour. For undrained tests at an external axial strain rate of 4.5% axial strain per day, .01% would be reached in 3 minutes, though due to bedding, this would normally be somewhat longer, perhaps 30 minutes.

As a direct comparison between new and old type gauges, triaxial test TLUU3 was carried out with both types of gauges together on the one specimen. The diametrical axis of one pair of gauges was at 90° to the other pair. Stiffness-axial strain relationship and deviator stress-axial strain relationships are shown in Figures A2.8 and A2.9. It can be seen that results for the 2 gauge types plot very close to each other, although the old gauge type plot shows a higher stiffness in the very small strain region (< .002%). A possible reason for this is discussed later. Due to the different levels of scatter, interpretation of the electrolevel type gauge was more difficult than that for the pendulum type, though it is comforting to note that, in general, the 2 plots are almost coincident. There is the possibility that the sample stiffness varied in each of the directions and that a difference in the gauges compensated for this. This does, however, seem unlikely.

A2.3. EFFECT ON LOCAL STRAIN READINGS OF ROTATION OF SUPPORT PADS

It was noticed in the early stages of the triaxial testing programme that, where there was marked barrelling of the specimen in compression

tests or necking in extension tests, the fixing pads would rotate about their hinges. It can be seen from Figure A2.10 that any rotation of the hinges, which would normally be in mutually opposite directions, would lead to an error in the recorded strain.

For specimens in extension and prone to necking, hinge rotation would underestimate the extension. For compression tests, the compression would also be underestimated. Thus, for both tests, the specimen would appear stiffer than was actually the case.

Fourie (1984), in describing results of passive stress relief extension tests, noted that the internal or local strain rate, according to the electrolevel gauge readings, varied continuously during his passive stress relief extension tests on London clay. In fact, near the end of the tests, the portion of the specimen between the gauge pads was shown by the gauges to apparently be in compression.

In order to investigate this further, marks were drawn at equal spacing down the side of the membrane of two triaxial passive stress relief specimens: on a medium dense sand SPS6 and SPS7 and one on a dense specimen of sand SPS/A/6.

For SPS6, apart from recording, as usual, the internal and external strain readings, a Vernier telescope was used to record vertical movement of the marks, and also vertical movement of the pads. These are recorded in Figure A2.11. In Figure 2.12 locally and externally measured strains are compared.

In the case of SPS7 (material similar to SPS6) and also for the denser specimen SPS/A/6, the specimen was photographed from a fixed position at frequent intervals during the test. Relative movement of the marks on the membrane were found from the scale rule set up inside the cell adjacent to the specimen. (See photographs Figures A2.13 and A2.14). Vertical deformation within the specimen scaled off the photographs is plotted on Figures A2.15 and A2.16 for SPS7 and the local and external strains are compared in Figure A2.17. For test SPS/A/6 local deformations are plotted in Figure A2.18 and A2.19 and strains compared in Figure A2.20.

It can be seen that the specimens generally deformed fairly uniformly in the vertical direction for the duration of the tests: marks nearer the fixed specimen top moved least and those closer to the base moved most. This is contrary to what is indicated by the electrolevel gauges. These show lower strain in the early stages of the test than that recorded externally (due to bedding). However, the apparent local strain then increases beyond that recorded externally (perhaps due to the change of volumetric strain rate affecting the pad rotation).

Near the end of the tests the gauges indicate very little local straining, or even compression (as claimed by Fourie, 1984). The fluctuating apparent local strain rate is presumably due to pad rotation.

A2.4. LOCAL STRAIN DEVICE SUPPORT PAD DESIGN

The amount of pad rotation will depend on the level of necking or barrelling of the specimen. Usually this specimen distortion becomes visible after around 2% axial strain, if at all, and is generally more pronounced in softer clays or looser sands. Therefore, it may be tempting to suggest that pad rotation is neglibible up to this point and that local strain measurements would be unaffected. This may well be true in certain cases, but 2% axial strain is only 1.5mm for a 76mm high specimen and it is doubtful if it is possible to notice by eye any radial strain effects associated with such a small vertical deflection.

A series of compression tests were performed on a neoprene rubber specimen with dimensions 75mm high by 37.4mm diameter. Electrolevel gauges were mounted on the sides ('level' with the specimen sides) of the specimen in the usual way for one of the tests. For another the gauge pad supports were inset into small holes in the specimen so that the centres of the hinges were approximately level with the specimen sides.

Two tests were done with ends bearing against dry porous stones. (Tests RLR1, ends 'rough', pads level and RIR1, ends 'rough', pads inset).

The tests were repeated, but with specimen ends greased and bearing against smooth surfaces. (Tests RLS1, pads level and RIS1, pads inset). Figure A2.21 shows photographs of the 4 tests, each at an axial strain of about 16%.

Figures A2.22 and A2.23 show locally measured axial strain, plotted against externally measured axial strain. The tests with greased ends could not be taken to high strains, as the specimen tended to slip out sideways. Nevertheless, the following emerges:

(i) Where the pad hinge points are level with the specimen sides (ie pads inset) locally measured strain nearly coincides with externally measured strain after bedding effects have been overcome, for both rough and smooth ended samples.

(ii) Where pads are level with specimen sides the internally and externally measured strain differences gradually increase as the tests progress. Note that, unlike a soil specimen, the sides of the rubber specimen tended to remain vertical, with distortion very close to the end points only. Hence, pad rotation may not have been as severe as might have occurred in a soft clay or loose sand specimen with rough ends and at similar strains.

An attempt has been made to estimate theoretically the effect of pad rotation *on* a local strain device measurement at small strain extension for an undrained test. An assumption has to be made regarding the deformed shape of a specimen. For simplicity, the sides were assumed to deform linearly from zero at the ends to a maximum of y_m at the centre following an idea by Leroueil (1986).

Figure A2.24 shows a derivation of the relationships between α, r_o, H_o and ϵ_a (offset from vertical of deformed specimen side, initial specimen radius and initial specimen height, and axial strain respectively).

$$\text{Sin } \alpha = \frac{2r_o}{H_o} \cdot \frac{\epsilon_a}{(1-\epsilon_a)^2} \qquad \text{(A2.1)}$$

So, for any particular strain, it is possible to find sin α and also the distance between the pad hinge points, b'.

From Figure A2.10 the effect of pad tilting on the inclination of the lower leg of the device can be seen. It is the tilt θ of this leg which determines the device reading. From the trigonometry of the triangle formed by the device legs, it can be shown that:

$$\theta = \sin^{-1} \left\{ \frac{(b')^2 + c^2 - a^2}{2c(b')} \right\} \qquad \text{(A2.2)}$$

Note that θ can be either positive or negative depending on the magnitude of b'.

Two differently configured devices are currently in use at IC for use with 38mm diameter specimens:

(1) 'Old' type: a = 52, c = 15, h = 3mm
range about 45-55mm between pads (b).

and

(2) 'New' type: a = 43, c = 17, h = 3mm
range about 35-45mm between pads (b).

From equation A2.2 it can be shown that over these ranges, for each additional degree of inclination or declination (ie change in θ), the distance between the pads (b') will change approximately 0.28mm for the 'old' type and 0.25mm for the 'new' type.

For any particular specimen axial strain it is then possible to find the difference in θ due to pad rotation and consequently a theoretical error in the strain reading.

Table A2.1 shows the percentage error at .002, 1 and 5% axial strains where the initial gap between pads is 50mm and 40mm for the larger configuration ('old' type) and 40mm for the smaller configuration ('new' type). It can be seen that the error varies and is greatest (15%) for the smaller pad gap, ie when the lower device leg is more inclined, down to 6% at the larger gap. This leads to a greater change in θ for a

particular strain. Consideration of the length of the shorter of the two legs is thus important for minimising error due to pad tilt - the shorter the leg, the larger will be the error (due again to a greater change in θ for a particular strain). Also to minimise errors, the device should be operated with the lower leg as level as possible.

Over and above the general consideration of small strain device configuration for minimising errors is the distance from the pad hinge to the side of the specimen. The closer the hinge is to the side of the specimen, the smaller will be the error. The pad currently in use at IC has been modified so that the hinge is 0.5mm from the specimen side. (See Figure A2.5). Employing the same technique as before, a theoretical error of 1% is obtained at a strain of 0.002% with the initial gap between pads of 40mm for a 'new' configuration gauge. This is a considerable improvement on the 6% which was calculated for the case of the existing pads. For the 'old' type device configuration, for an initial gap of 40mm at an axial strain of .002%, with 'old' type pads, the error, as mentioned previously, was 15%. With the 'new' pads (0.5mm hinge to sample distance) the error is now 3%.

Three unconfined compression tests were performed with a pair of the new configuration devices with 'new' pads attached to the rubber specimen mentioned previously. These tests were then repeated twice with the same devices but with 'old' pads attached. Figure A2.25 shows the results plotted on a graph of local versus external strain. Although a marked improvement of 'new' pads over 'old', even the curve of results of the 'new' pad tests deviates noticeably from the 45° line at higher strains.

APPENDIX A3

THE EFFECT OF A CONFINING RUBBER MEMBRANE ON A TRIAXIAL SPECIMEN

APPENDIX A3

THE EFFECT OF A CONFINING RUBBER MEMBRANE ON A TRIAXIAL SPECIMEN

A3.1. INTRODUCTION

From the results of the triaxial testing of sand at low effective stresses described in Chapter 5 it was suspected that a confining membrane enhanced the strength of a specimen: for tests on loose to medium dense specimens, where the decrease in strength beyond peak shear stress was not large, the apparent mobilised strength continued to increase to an axial strain of 20% and beyond.

Several attempts have been made in the past to obtain theoretical corrections to axial and radial stresses due to a confining membrane around a specimen. Some researchers have assumed that a specimen which fails by bulging deforms as a right cylinder. Others have derived theories for corrections to stresses on a specimen where it fails along a slip plane.

Notable of the bulging corrections are those of Henkel and Gilbert (1952) and the later attempt at refinement by Duncan and Seed (1965).

These theories are reviewed in Sections A3.2 and A3.3 and the results of elastic finite element analyses on a specimen with a confining membrane are presented in A3.4, where an attempt is made to assess the effect of various relative stiffnesses of specimen and membrane and Poisson's ratios of specimen, on the interaction between membrane and specimen.

Section A3.5 describes tests to find the stiffness of membranes while a series of tests on rubber specimens with and without membranes are described in A3.6.

An assessment of the effect of buckling of a membrane during a compression test is made in section A3.7 and in A3.8 the effect of slip planes on membrane corrections is discussed briefly.

A3.2. THE HENKEL AND GILBERT (1952) THEORY FOR MEMBRANE CORRECTION

A3.2.1. Laboratory tests on remoulded London clay specimens

Henkel and Gilbert prepared almost 200 remoulded triaxial specimens 76mm high, 38mm diameter of London clay at various moisture contents. These were then tested undrained to an axial strain of 20% either unconfined or with a confining membrane but with zero cell pressure ('rubber only') or with a confining membrane but at cell pressures of between 35 and 350kPa ('triaxial'). The tests were performed for 3 different thicknesses of latex rubber membrane: 0.10, 0.20 and 0.50mm.

For each particular membrane thickness the compressive strength was greater for the 'triaxial' than for the 'rubber only', which in turn was greater than for the 'unconfined' tests. Whilst the compressive strength of the clay generally increased with decreasing water content, the differences in the compressive strength between the 3 types of test for a particular membrane thickness at a particular strain remained the same regardless of moisture content. The membrane effect increased with increasing membrane thickness. For the 'triaxial' tests there was no difference between tests conducted at different cell pressures.

In the following, HG denotes Henkel and Gilbert.

A3.2.2. Theoretical considerations

HG derived two theoretical expressions, one for the vertical component of membrane stress (axial) and one for the horizontal component (radial).

The vertical component was derived assuming that the membrane acts as a compression shell. The resultant load taken by the membrane divided by the specimen cross sectional area, or the vertical rubber correction is

$$\Delta\sigma_a = \frac{\pi D_0 M \epsilon_a (1-\epsilon_a)}{A_0 (1-\epsilon_v)} \qquad \text{(A3.1)}$$

where D_0 and A_0 are the original specimen diameter and cross sectional area,

ϵ_a is the axial strain

ϵ_v is the volumetric strain (negative for dilation) and

M is the compression modulus of the rubber membrane with units load per original length of membrane per strain.

The horizontal component was derived for the case of the membrane buckling as the specimen compresses, with the increasing diameter inducing a hoop tension in the rubber which would appear as an increase in the minor principal stress.

$$\Delta\sigma_r = \frac{2M}{D_o} \quad \frac{\sqrt{(1-\epsilon_v)} - \sqrt{(1-\epsilon_a)}}{(1-\epsilon_a)\sqrt{(1-\epsilon_v)}} \qquad \text{(A3.2)}$$

A3.2.3. Tests on strips of membranes

Extension tests were performed by HG on 25mm wide strips of rubber membrane to find the 'extension modulus' for each of the thicknesses of membranes they used. Results of these tests are reproduced in Figure A3.1. This shows tensile load on the membrane strip plotted against strain in the rubber. The broken lines are those of HG.

As would be expected, due to decreasing membrane thickness with increasing strain, M decreases as the membrane extends (ie the curves curve upwards). As it is not possible to perform a similar test to find the compression modulus of the membrane, HG make the assumption that moduli in extension and compression would be equal (ie $M_c = M_e$). For their compression tests on London clay, which were sheared to 20% axial strain, HG used the secant modulus at 10% strain as as an average M value for the test.

A3.2.4. Theory compared with experimental results

The theoretical axial and radial corrections obtained from Eq A3.1 and A3.2 for failure which occurred at 15% axial strain together with the actual measured corrections are reproduced in figure A3.2. Note that HG plotted the horizontal stress corrections as corrections to vertical

compressive strength presumably justified by the tests being undrained on saturated specimens. (Φ_{uu} = 0 so the Mohr circle diameter remains constant but displaces to the right on a τ-σ plot, with horizontal and vertical stress increments being equal).

The compression shell theory results appear to underpredict the required corrections by about 20% ('triaxial' tests). Stresses for the 'rubber only' test line are about 40% higher than those predicted by the hoop stress theory. Each of these theories will now be considered.

HG make the assumption that the compression modulus is equal to the extension modulus. (It is the latter which is actually measured in the modulus test). It will be recalled from Figure A3.1 that the extension modulus decreases with increasing extension, due to the decrease in membrane thickness. Conversely, if it were possible to perform the test in compression, the compression modulus would increase with compression due to the increasing thickness of membrane. If one uses Young's modulus for the membrane, E_m, rather than M, for a specimen compressed to a strain ϵ_a, equating loads carried by the membrane at the strain ϵ_a:

$$\pi D_o M \epsilon_a = \pi D t E_m \epsilon_a \qquad \text{(A3.3)}$$

or $$M = D/D_o . t . E_m$$

where D_o, M are as defined for Eq. A3.1 and D and t are the current specimen diameter and current membrane thickness respectively.

Now assuming both specimen and membrane remain a right cylinder during straining and the volume of the membrane remains constant,

$$\frac{D.t}{D_o} = \frac{t_o}{1-\epsilon_a}$$

So, Eq. A3.3 becomes:

$$M = \frac{t_o \, E_m}{1-\epsilon_a} \qquad \text{(A3.4)}$$

where t_o is the initial membrane thickness.

While the assumption of E_m remaining the same in compression and extension is probably justified , it can be seen why M decreases in extension testing (ϵ_a negative and decreasing). On the other hand, M must increase in compression (ϵ_a positive and increasing).

HG's curves for the membrane modulus in extension (Figure A3.1) can then be corrected for compression M_c by multiplying the extension M_e values by

$$\left[\frac{1+\epsilon_a}{1-\epsilon_a}\right]$$

The curves for compression thus obtained are shown in Figure A3.1. Equation A3.1 also becomes

$$\Delta\sigma_a = \frac{4t_o}{D_o} E_m \frac{\epsilon_a}{1-\epsilon_v} \qquad (A3.5)$$

Taking the secant modulus, as before at 10% strain, HG's M values are increased by the ratio 1.1/0.9 = 1.22 and the theoretical correction shown in Figure A3.2 also increases by 22%. The theoretical points now coincide exactly with the experimental values.

Many other researchers have made the error of using extension moduli for compression tests and found corrections much smaller than anticipated, putting the results down to a deficiency in the HG theory, for example, La Rochelle et al. (1986) and Wade (1963). The HG Eq. A3.1 has been widely used and is recommended by Bishop and Henkel (1962) and Head (1982) and also in ASTM D2850-82 and BS1377.

As regards HG's 'rubber only' tests, ie tests with membrane, but no cell pressure, as mentioned before, the theoretical stress correction used (Eq. A3.2 - hoop stress correction) was around 40% less than those required. Obviously the membrane does not behave as postulated. Even though the specimen and membrane are unconfined, there may well have been, in addition to the horizontal contribution to strength (if any), a vertical contribution in the form of a proportion of Eq. A3.1.

The action of membranes when they enclose specimens in compression in tests at very low effective stress will be discussed later.

A3.3. THE DUNCAN AND SEED (1965) THEORY FOR MEMBRANE CORRECTION

A3.3.1. Theory derivation

Duncan and Seed derived expressions for stresses in a membrane from the equations of elasticity for an element of the membrane in plane stress assuming Poisson's ratio to be 0.5.

$$E_m \epsilon_z = [\sigma_z - \tfrac{1}{2} (\sigma_p + \sigma_n)] \qquad \text{(A3.6)}$$

$$E_m \epsilon_p = [\sigma_p - \tfrac{1}{2} (\sigma_n + \sigma_z)] \qquad \text{(A3.7)}$$

$$E_m \epsilon_n = [\sigma_n - \tfrac{1}{2} (\sigma_p + \sigma_z)] \qquad \text{(A3.8)}$$

where ϵ_z, ϵ_p and ϵ_n are the vertical, perimetric and normal strains in the membrane respectively
and σ_z, σ_p and σ_n the vertical, normal and perimetric stresses in the membrane.
E_m is Young's Modulus for the membrane.

If σ_n is assumed to have no effect (ie the membrane is not carrying any load in the σ_n direction which would otherwise be carried by the specimen and is taken as zero, and the specimen (and membrane) is assumed to deform as a right cylinder, then equations A3.6 and A3.7 reduce to:

$$\sigma_z = \frac{2E_m}{3} \left[2\epsilon_a + 1 - \sqrt{\frac{1-\epsilon_v}{1-\epsilon_a}} \right] \qquad \text{(A3.9)}$$

and

$$\sigma_p = \frac{2E_m}{3} \left[2 - 2\sqrt{\frac{1-\epsilon_v}{1-\epsilon_a}} + \epsilon_a \right] \qquad \text{(A3.10)}$$

(compressive stresses taken as positive)
Correcting for the vertical and horizontal stresses on a specimen:

$$\Delta\sigma_a = -\frac{8}{3} \frac{E_m t_o}{D_o} \left[2 \epsilon_a + 1 - \sqrt{\frac{1-\epsilon_v}{1-\epsilon_a}} \right] \frac{1}{1-\epsilon_v}$$

the vertical stress correction

and

$$\Delta\sigma_r = -\frac{4}{3} \frac{E_m t_o}{D_o} \left[2 - 2\sqrt{\frac{1-\epsilon_v}{1-\epsilon_a}} + \epsilon_a \right] \frac{1}{1-\epsilon_v}$$

the horizontal (or radial) stress correction

The equations can also be expressed in terms of the radial and axial strains ϵ_r and ϵ_a. (ϵ_a is positive for vertical compression, while ϵ_r defined as negative for bulging).

$$\Delta\sigma_a = -\frac{8}{3}\frac{E_m t_o}{D_o}(2\epsilon_a + \epsilon_r)\frac{1}{(1-\epsilon_r)^2(1-\epsilon_a)} \qquad \text{(A3.11)}$$

$$\Delta\sigma_r = -\frac{4}{3}\frac{E_m t_o}{D_o}(\epsilon_a + 2\epsilon_r)\frac{1}{(1-\epsilon_r)^2(1-\epsilon_a)} \qquad \text{(A3.12)}$$

where $\epsilon_r = \frac{\sqrt{(1-\epsilon_v)}}{\sqrt{(1-\epsilon_a)}} - 1$

assuming the specimen remains right cylindrical.

A3.3.2. Numerical comparison of Duncan and Seed's and Henkel and Gilbert's Theories

For HG's method for correction to stress on a specimen due to a membrane (Equations A3.1 and A3.2) it is possible to express membrane stresses in terms of E_m:

$$\sigma_z = E_m \epsilon_a \qquad \text{(A3.13)}$$

vertical stress

and $$\sigma_p = E_m \left[\frac{\sqrt{(1-\epsilon_v)}}{\sqrt{(1-\epsilon_a)}} - 1 \right] \qquad \text{(A3.14)}$$

horizontal stress

In order to compare the relative magnitudes of HG's and DS's stress corrections, the ratios of the stress magnitudes have been plotted in Figure A3.3 for compression tests (ie ϵ_a positive). The two methods give similar results for axial stresses, HG being about 6% higher than DS at 20% axial strain.

However, the two methods are obviously quite different for the calculation of horizontal, or hoop stresses in the membrane. The HG

method gives stresses up to 60 times those of DS at low strains, although at higher strains this decreases to about 3.

In the case of extension tests (ie negative axial strain) the ratio of magnitudes of axial and radial stresses for Henkel and Gilbert and Duncan and Seed have been plotted in Figure A3.3(b). Unlike for the case of compression the ratio for axial stresses is slightly less than unity: for ϵ_a = 20%, HG give an axial stress about 4% less than DS. However, for hoop stresses the two methods again give quite different results: HG predict compressive hoop stresses whereas DS predict tensile hoop stresses. It can be seen comparing Figs A3.3(a) and A3.3(b) (hoop stresses) that the ratio HG/DS is similar for both compression and extension tests, but for the latter the ratio is negative implying extremely large compressive hoop stresses.

For the DS method, we might feel it would be more logical for stresses in the membrane to be equal in magnitude but opposite in sign for the cases of tests with equal but opposite vertical compression and extension strains. In fact, axial stresses for compression are slightly less than for extension (but opposite in sign). Hoop stresses on the other hand are tensile for both extension and compression tests, but for extension tests, the hoop tensions are not as large as for the compression tests: about 30% less at 20% axial strain to only about 1% less at 2% strain.

The reason for the disparity between compression and extension tests lies in the assumption that the specimen will remain a right cylinder. For a particular strain in extension which is equal but opposite to that in compression, it can be seen from Figure A3.3(c) that the magnitude of the radial strain for the compression test will be greater than the radial strain for the extension test.

A3.3.3. Use of the Duncan and Seed method

The Duncan and Seed method has been used by Ponce and Bell (1971) at the University of Colorado, by Fukushima and Tutsuoka (1984) at the University of Tokyo, by Molenkamp and Luger (1981) at Delft and by Berre (1982) at the NGI. All the tests were in compression.

A3.4. FINITE ELEMENT ANALYSIS

A3.4.1. Mesh

A series of finite element analyses was performed on a specimen 38mm high (half a specimen height only, due to symmetry) and 38mm diameter. A membrane 0.30mm thick jacketed the specimen and top cap which was 7mm thick and 38mm diameter. As the specimen was symmetrical around a vertical axis through the centre it was necessary only to divide one half the 38 x 38 specimen plus top cap and membrane into elements. A mesh of 96 elements was used (see Figure A3.4). Smaller elements were used adjacent to the membrane and top cap. The membrane was assumed to be attached rigidly to the specimen and top cap and the top cap also attached rigidly to the specimen.

The analyses were performed using the ICFEP program written by Dr D M Potts of IC. The program is displacement based so that the displacement at the nodes are the basic unknowns. Then, according to the chosen element shapes, a shape function is formed to relate global displacements with nodal displacements. The elements used are 8 noded isoparametric rectangular. The displacement at all points are evaluated using the condition of compatibility. Strains are found at integration points within each element. Stresses are then found from an assumption of a constitutive law. In general 2 x 2 reduced integration was used.

A3.4.2. Description of analyses

10 computer runs were performed. A point load was applied at the centre of the top cap of such a magnitude that the axial strain of the specimen was between 1% and 2% for the specimen and membrane properties chosen. The parameters used in the computer runs are tabulated in Table A3.1. Note that run 7 is not listed: this was identical to run 1 except that a more complex system of integration points (3 x 3) within each element was used. However, the resultant stresses and strains were almost identical to those of run 1. It was not necessary to ascribe units to the load and stiffnesses as ratios only were required for comparisons to be made between the various runs. No units are therefore shown on Figures relating to this Section.

A3.4.3. Results

The vertical and lateral displacements of the membrane are plotted in Figures A3.5 to A3.13. The vertical compressive stress distribution in the membrane is plotted on Figures A3.14 to A3.19. Fig A3.20 shows the vertical compressive stress along the bottom elements from specimen centre line to membrane for run 1 and run 8 (as for run 1 but in effect no membrane). The difference represents the stress carried by the membrane.

Although the relevant figures have not been reproduced here, as expected due to the high relative stiffness of the top cap, the analyses showed no differences between a run with a point load and one with an equivalent uniformly distributed load. Also compression and extension loading gave equal but opposite signed results.

As would be expected due to the greatly differing stiffness between membrane, specimen and top cap, the compressive stresses in the top portion of the membrane are very much influenced by the top cap. However, in the lower half of the specimen the stresses in the membrane are fairly uniform. The ratio of vertical stress in the membrane from the DS method assuming an average strain down the membrane to stresses in the lower element of the membrane from the finite element (FE) method versus ratio of specimen to membrane stiffness is plotted in Figure A3.21. It can be seen that vertical membrane stresses predicted from the DS method are close to those of the FE analysis. For most triaxial tests, where the specimen will be very much stiffer than the membrane, the ratio DS/FE appears to tend to about 0.92 in compression. It will be recalled from Figure A3.3 that the HG compressive vertical stresses will then be slightly greater.

It should be noted that for a specimen with Poisson's ratio $\nu_1 = 0.3$ (run 4) the vertical membrane stress in compression appears slightly higher than for $\nu_1 = 0.5$ with DS/FE = 0.87 at $E_s/E_m = 2$, compared with .92 for $\nu_1 = 0.5$.

Hoop stresses for the membrane near the mid height of the specimen are plotted in Figure A3.22 as a ratio DS/FE versus E_s/E_m for Poisson's ratio for both sample and membrane $\nu_1 = \nu_2 = 0.5$. It can be seen that for $E_s \gg E_m$, the ratio DS/FE tends to about 1.8. For run 4 with $\nu_1 = 0.3$, a compresive hoop stress in the membrane was actually predicted by the FE method (even though the specimen bulged in compression) with DS/FE = -.04 at $E_s/E_m = 2$.

Radial stresses between specimen and membrane, derived from the DS hoop stresses, are plotted in Figure A3.23. These decrease with an increasingly stiffer specimen. The radial stresses from the FE analysis showed great fluctuation within each element, and from elements to element, however, the general trend was for the stresses to decrease with increasing specimen stiffness.

A3.5. YOUNG'S MODULUS OF LATEX RUBBER MEMBRANE

A3.5.1. Laboratory tests on strips of membrane

Tests were performed on strips of membrane 25mm wide according to the Henkel and Gilbert (1952) (denoted HG as before) testing procedure to find the membrane modulus. Instead of using glass rods top and bottom to support the membrane strip and a Vernier to take readings of strain, polished steel rods were used, 4.7mm diameter each, pointed at one end and facing a graduated rule according to Head's (1982) idea. This method was found to be more convenient and gave more reproducible results than that of HG.

Nevertheless, the test is fairly crude. There were difficulties due to oscillation of the pointers due to movement of the membrane, especially at the lower loads.

Although powder was used between membrane and rod, for the early loads, very little strain was observed: this was probably due to friction effects. A silicon grease lubricant was also tried, but results were much the same as for the powder.

A3.5.2. Laboratory tests on the whole membrane

A set of 4 comparative tests (M1, M2, M3, M5) were done using the whole membrane in a dry stress path cell. The membrane was attached to the top and bottom platens with several O-rings (no specimen inside). An extension test was then performed.

A3.5.3. Test results

Load versus strain readings for all the tests are plotted in Figure A3.24. There is a great scatter of results using the HG type test. Results from the 4 whole-membrane tests converted to load on a double 25mm strip fall very close to each other and roughly within the band of results from the HG tests.

There were problems with slippage of membranes past the O-rings at higher strains in the full membrane tests. This would show as an apparently lower stiffness at higher strains. Figure A3.25 is a plot of E versus membrane strain. This shows an apparent decrease in stiffness with increasing strain, from around 1400kPa at 10% strain to 1100kPa at 20% strain. Also indicated on Figure A3.25 are values of E for latex rubber membranes (values were either quoted or deduced from Modulus values) quoted by or deduced from other researchers in their membrane correction routines. These vary from about 1200kPa to 1500kPa.

A3.5.4. Effect of soaking on membranes

In order to examine the effect of soaking on the membrane stiffness, modulus tests were performed on 25mm strips following completion of the triaxial test. Figure A3.26 shows values of E at 10 and 20% strains plotted against duration of soaking. It would appear that for about the first month E remains largely unaffected at about 1400kPa at the 10% strain level. After this there is a decrease in stiffness of about 300kPa to 1100kPa over the following 6 weeks. The stiffness seems to remain reasonably constant thereafter. Another feature of the soaking was a slightly increased membrane thickness in some cases of up to 10% and also an increase in membrane circumference, up to 7% for some membranes.

A3.5.5. Discussion

It is difficult to envisage a decrease of stiffness with strain level for latex rubber. This apparent decrease may be due to the method of experimentation: in the case of whole membrane tests, slippage of the membrane past the O-rings and in the case of the tests on strips friction effects at the support rods leading to varying membrane thicknesses. A value of Young's Modulus of 1400kPa has been used for membrane corrections for tests of up to 4 week's duration. Beyond this 1100kPa has been used.

A3.6. LABORATORY TESTS ON RUBBER SPECIMENS

A3.6.1. Introduction

A series of triaxial tests were performed on 2 rubber dummy specimens, with and without an enclosing membrane. One specimen was made of neoprene rubber with dimensions 37.64mm diameter by 75.00mm height. The other specimen with dimensions 37.03mm diameter by 73.48mm height was made of a softer silicon rubber solution. Unlike the neoprene specimen, the silicon specimen had many small voids in it: these were due to air bubbles which were trapped during the manufacture of the sample.

The specimens were tested in a stress path cell, in extension at a cell pressure of 200kPa (high enough to attain an axial strain of around -20% for the negative deviator stress) and in compression at cell pressures of 2kPa and 50kPa. The specimen stood between the steel pedestal at the bottom and a perspex top cap.

A3.6.2. Tests without a membrane

A series of extension and compression tests were first carried out on the rubber specimens without membranes. For the extension tests a strip of membrane, about 25mm wide was placed at the top of the specimen, half on the specimen and half on the pedestal. The reason for using the strips was to prevent cell water from entering between the cap or pedestal and the specimen which would have prevented

the application of a negative deviator stress to the top of the specimen. The strips were pleated at their midheight so as to minimise their restraint to the specimen as the specimen contracted radially at its extremities. The specimens were strained at a rate of 5% per hour.

Stress-strain curves are shown in Figures A3.27 to A3.32. Note that for these plots, the first letter 'R' denotes rubber specimen, 'H' denotes the 'hard', or neoprene specimen and 'S' the 'soft', or silicon specimen. 'L' denotes loading in compression and 'UL' unloading in extension. The number after each test label is the cell pressure in kPa at which the test was conducted.

E for the H specimen is less in extension than in compression whereas for the S specimen the stress-strain curves are similar in both compression and extension. Also, while the stress strain curves are almost linear for the H specimen, the S specimen stiffens with strain, probably due to the voids in the specimen closing. For each group of similar tests the effect of bedding is evident in the low strain region (below about 3% axial strain). Measurements of local strains were not made. For the 'H' specimen there appears to be no effect of pressure on the stress-strain curve, ie E at both 2kPa and 50kPa cell pressures are similar, about 900-950kPa. For the 'S' specimen, the stiffness increases with increasing cell pressure. E is about 800kPa over the range 0-20% strain.

A3.6.3. Tests with membrane enclosed specimens

The extension and compression tests were repeated, but with a membrane round the rubber specimens.

A3.6.3.1. Extension tests

Stress strain curves from 2 extension tests on the H specimen are shown plotted in Figure A3.33 (test designations prefixed with 'M' for test with membrane) along with the extension tests on the rubber specimens

alone for comparison. The effect of the membrane is then the difference between the two groups of tests. At -15% axial strain the difference is about -13kPa. The tests have been corrected for effects of the membrane according to the DS method; Figure A3.34 shows the corrected curves. The initial membrane thickness and diameter are also shown in Figure A3.34 (t_o and D_o respectively in mm). It can be seen that a correction of about -7kPa remains to be applied, over and above the DS correction which is about -6kPa at -15% strain.

In order to assess the effects of possible friction between the membrane and specimen, a further extension test was performed on a jacketed specimen, but with a thin layer of silicon grease as lubrication between membrane and specimen. The results are shown in Figure A3.35 with the test designated 'MHULL200' (the second 'L' denoting lubrication). The corrected curves (DS method) are plotted in Figure A3.36. There appears to be a slight decrease in shear stress due to lubrication.

A series of extension tests similar to those described above were repeated on the soft specimen. The stress-strain curves were corrected as before. The results are plotted on Figures A3.37 to A3.40. Once again the DS correction is only about half that actually required. The grease seems to have had little effect on the specimen behaviour (Figure A3.40).

For all the extension tests the deformed shape remained perfectly right cylindrical. At the extremities of the specimen, therefore, the membrane was stretched more severely than for the rest of the specimen. In order to assess these end effects a special extension test (RHUL200) was carried out without a membrane, but with strips of membrane sealing the specimen extremities. Unlike the strips used previously the strips were not pleated at their mid height. The resulting stress-strain curve is shown in Figure A3.41 together with the corrected extension test curves for the jacketed sample described previously. Comparing this with Figure A3.34 it can be seen that the gap between unjacketed and jacketed (corrected) stress- strain curves is now much smaller, about -4kPa compared to -7kPa previously obtained. Perhaps the end effect is the reason for the apparent additional correction required above that predicted by theory.

A3.6.3.2. Compression tests

A series of compression tests on Hard and Soft rubber specimens with membranes were carried out in a stress path cell at both 2kPa and 50kPa cell pressures. The series included a test with the specimen sides lubricated with grease. As before the stress strain curves are shown both uncorrected and corrected. Figures A3.42 to A3.49 show results of tests on the Hard specimen and Figures A3.50 to A3.57 show results of tests on the Soft specimen.

The DS correction applied to the compression test results appears to hold reasonably well, especially at the low cell pressure. For the 50kPa cell pressure test, however, there may be some under correction at the lower strains (Figs. A3.45 and A3.53). However, this may be partly due to bedding effects. Note though that La Rochelle et al. (1986) in their tests on rubber specimen found a similar phenomenon.

The principal stress ratios are plotted for tests at 50kPa cell pressure on the soft rubber specimen in Figure A3.58. The importance of including both axial and radial stress corrections can be seen.

Buckling, or wrinkling of the membrane occurred in tests MSL2 and MSL50 from the start of the test, but this became more pronounced from about 7% axial strain. No buckling at all was noticed during the Hard rubber tests MHL2 and MHL50.

In compression, both Hard and Soft specimens barrelled near their extremities due to frictional restraint, but sides remained vertical over the rest of the specimen.

Compression tests with greased specimen sides (Figs A3.46-49 - Hard specimen and A3.54-57 - Soft specimen) show conflicting results. For the Hard specimen which has very smooth sides, the grease has caused the membrane to loose all its influence on the specimen in compression. For the soft specimen, on the other hand, the grease actually caused the membrane effect to increase the shear stress over and above that for the case of no grease between membrane and specimen. This effect was most

likely produced by the interaction between the silicon grease and sides of silicon rubber specimen which were rougher than those of the Hard specimen.

A3.6.4. Effect of initial wrinkles in membrane

As a final exercise, an extension test was performed on a Hard specimen with a membrane with initial wrinkles, one near either extremity and one at the middle, in an attempt to ascertain the effect of these on the membrane restraint (Test MHULW200). The stress-strain curve is shown in Figure A3.59 from which it appears that the initial wrinkles have no effect.

A3.6.5. Finite element simulation of rubber dummy tests

An FE analysis was performed simulating the compression test on the hard rubber specimen, both without and with a membrane, using specimen dimensions and membrane thickness described previously in A3.4 (ie specimens 76 x 38mm, membrane 0.3mm thick) An E for the specimen of 950kPa was used.

The top cap was made to displace by a fixed amount, representing a 7% axial strain in each case. The load on the top cap necessary to cause this strain divided by the corrected specimen cross-sectional area assuming right cylindrical deformation is shown ploted against axial strain in Figure A3.60. The curves will be linear due to the sample being elastic. The difference in vertical stress at E_a = 7% is identical to that predicted by the DS method.

The actual rubber dummy test results with and without a membrane (from Fig. A3.42) have been superimposed. The FE corrections are greater because a membrane of thickness 0.26mm was actually used for the test compared with 0.30mm in the FE analysis.

A3.7. BUCKLING OF MEMBRANES DURING COMPRESSION TESTS

It may seem reasonable to assume that buckling of the membrane during a compression test would have the effect of reducing its stiffness and thus the vertical load which the membrane carries and that the level of buckling would depend on the pressure at which the membrane is held against the specimen (ie the horizontal effective stress). However, in the case of the compression tests on the rubber specimens, apart from the apparently slightly higher stresses at lower strain levels for the tests at 50kPa pressure, there appears to be little difference in the membrane resistance between the 2kPa and 50kPa tests, regardless of buckling of the membrane for tests on the Soft specimen, and no buckling for tests on the Hard specimen.

As described in A3.2, HG carried out a series of compression tests on jacketed specimens of remoulded London clay unconfined, ie at zero cell pressure. They found that resistance offered by the membrane to be about half that offered in the case of undrained triaxial tests with cell pressures in the range 35kPa to 350kPa. Within this range, however, there was no difference in the membrane resistance regardless of cell pressure.

Similarly La Rochelle et al. (1986) in their triaxial compression tests on a jacketed rubber specimen at zero cell pressure found the membrane resistance to be about half that offered by the membrane for triaxial tests at a cell pressure of 100kPa.

It would seem that from zero cell pressure the membrane resistance increases rapidly with increasing cell pressure: from about half resistance at zero cell pressure to almost full resistance at 2kPa effective horizontal stress. Wade (1963) corrects his test data for membrane restraint only up to the point where first buckling of the membrane is noticed. Thereafter the correction remains at a constant value. It would appear, however, from the compression tests on rubber specimens that this procedure is not correct as the magnitude of the restraint can continue to increase after onset of membrane buckling.

Figure A3.61 shows stress-strain curves for a series of 6 drained triaxial compression tests on a very loose silty sand with similar initial void ratios. The deviator stresses have been normalised by dividing by the horizontal effective stress (from 1kPa to 400kPa).

The curves have been corrected over their entire range for membrane restraint using the DS method. It would be expected that all the normalised stress-strain curves be approximately coincident. It is clear, however, that this is incorrect for the test at 1kPa effective stress but approximately correct for the test at 5kPa initial effective stress. Note that for the latter test onset of membrane buckling was at 3% axial strain. For the 1kPa test the membrane buckled from the start.

The required correction for the test at 1kPa effective stress is thus somewhat less than the full DS correction.

Thus, regardless of membrane buckling, it would appear that the membrane retains considerable vertical stiffness: beyond about 2kPa effective horizontal stress buckling of the membrane appears to have no effect on the stiffness.

A3.8. FORMATION OF SLIP PLANES IN SPECIMENS

Although discussion regarding contribution of membrane restraint to apparent triaxial strength has related only to a bulging type failure of the specimen, in a stiff overconsoldiated clay and also in dense sands slip planes are often observed to form during a triaxial test. Movement along these planes by one part of a specimen relative to another can lead to a local distortion of the membrane.

Several researchers modelled the effect of this membrane distortion on a sample. For example De Lory (1957), La Rochelle (1960), Chandler (1966) and Symons (1967). Usually cylinders of plexiglass with preformed lubricated slip planes were used as specimens.

La Rochelle et al. (1986) describes a correction to the deviator stress for a triaxial specimen which was formulated following a series of such tests:

$$\frac{1.5\Pi \; do\sqrt{(M \; f \; d_o \; \delta)}}{a_c}$$

where

d_o is the initial specimen diameter

a_c is the current cross-sectional area of the specimen,

δ is the axial strain due to movement along the slip plane,

f is the shear stress between membrane and specimen (dependent on effective horizontal stress and friction angles of the soil),

and M is the extension modulus of the membrane.

The problem with this approach is that very often bulging (or necking) continues throughout a test, regardless of the formation of a slip plane. Also it is very common for several parallel and/or conjugate slip planes to appear within the sample. The edges of the slip planes often deform under pressure of the membrane.

La Rochelle et al (1986) calculate that membrane correction for a test on a specimen of Saint-Alban clay which failed along a slip plane. The correction is the same order of magnitude as that which is obtained from the modified Henkel and Gilbert axial stress correction for a bulging failure (see Figure A3.62).

Some researchers may have been encouraged in their work on membrane effect of slip plane formation by their use of erroneously low axial stress corrections in compression tests from the HG theory, as discussed previously in A3.2. Nevertheless the deformed shape of the membrane due to severe distortion along a slip plane is quite different from that of the bulging failure and it would then seem reasonable to apply corrections modelling this specific mode of failure.

A3.9. SUMMARY AND CONCLUSIONS

It is clear from results of the triaxial tests on sand and on rubber dummy specimens at low effective stresses where the deviator stress continued to increase with strain, that restraint of the membrane has to be taken into account in the calculation of stresses on the specimens.

The interaction of the membrane with top cap, bottom pedestal and specimen is very complex, depending on the elastic properties of the membrane, specimen shape (which continuously changes during a test), surface friction properties on specimen sides, E and ν of the specimen. Very often the membrane will buckle, or wrinkle during compression tests.

Henkel and Gilbert (1952) produced expressions for the vertical and horizontal stresses exerted by a membrane on a specimen, the vertical correction to be used for cases of no membrane buckling, ie when the membrane acted as a 'compression shell', and the horizontal component (which they translated to a vertical correction for their undrained tests) for the case when the membrane buckled (ie as a 'hoop' shell). Their theory did not fit the results of their extensive compression test programme data on remoulded London clay samples at all well: the required corrections were higher than those predicted by theory. However, their vertical correction method is in error for compression tests due to the use of the membrane extension modulus M_e in compression rather than a compression modulus M_c and when this is corrected, their required vertical corrections exactly fit their theory.

$$\text{ie} \qquad M_c = M_e \cdot \left[\frac{1+\epsilon_a}{1-\epsilon_a} \right] \qquad \text{(A3.15)}$$

In order to avoid confusion with the use of these muduli (which depend on membrane thickness and which vary during a test) it is better to use Young's Modulus E_m for the membrane. Henkel and Gilbert's expression for vertical stress correction has been suitably modified for a triaxial specimen: equation A3.5 refers.

The test suggested by Henkel and Gilbert to find the extension modulus of a membrane is very simple, but does produce quite a scatter of results. From this test there is an apparent decrease of E with strain, though in reality this is hard to believe. The average E is about 1400 kPa and this compares well with that quoted for latex rubber membranes by other reseachers. Where membranes are soaked E appears to start decreasing rapidly after membranes have been in water about a month to around 1100kPa.

Duncan and Seed (1965) attempted to refine Henkel and Gilbert's theory by assuming an element of the membrane to be in a condition of plane stress. Vertical and horizontal stresses were linked using elasticity considerations and equations were produced for both axial and radial stress corrections (Equations A3.11, A3.12).

The equations for stress correction from both theories have been compared. The axial stress corrections are in fact very similar for both equations. In compression HG is about 6% greater than DS at 20% axial strain while in extension DS is slightly greater than HG. For hoop stress, however (and therefore radial stresses) the HG stress is up to 50 times that predicted by the DS theory in compression; the high HG value is not evident in the tests on rubber specimens. The DS radial stress correction worked well in the case of the test on the rubber specimens (Fig A3.58). Hoop stresses appear to decrease with increasing specimen stiffness and with decreasing Poisson's ratio. In fact the FE analysis predicts a compressive hoop stress for Poisson's ratio of specimen of 0.3 in a compression test.

The finite element analyses gave axial stress corrections which are broadly in line with those of the theories: DS being around 0.9 times that in the FE analysis. The relative values of Young's Moduli of specimen to membrane are not significant for practical values of the ratio (ie $E_s \gg E_m$). For ν of the specimen of 0.3 the required axial stress correction is shown to be slightly more than for $\nu = 0.5$, about 16% more than that forecast by DS. With regard to radial stress corrections, DS appears to overestimate compared to the FEA: DS/FE $\approx$ 1.6 for $\nu = 0.5$. However, for $\nu = 0.3$, the FEA predicts compressive hoop stresses, which is not possible in practice.

The series of triaxial tests on rubber specimens shows corrections required for compression tests to be similar to those predicted by the theories. Below 2kPa effective horizontal stress however, the required correction is less than half that forecast by theory. Figure A3.58 sand tests and Figure A3.61 Henkel and Gilbert London clay tests refer. In the extension test the correction required was about double that from the theories. It is likely, however, that the special end effects present for tests on the jacketed rubber specimens, with the step at the end cap and pedestal due to specimen sides remaining vertical, would cause additional stretching of the membrane. In the FE analysis rough ends were assumed, and in the extension tests on sands and clays, the diameter of the ends of the specimen remained generally constant.

For compression tests the frictional characteristics of the sides do affect the behaviour of the membrane. If the specimen sides are particularly greasy then there may be no axial restraint by the membrane. However, it is felt that for most sands and clays tested the sides are sufficiently rough to prevent slip between specimen and membrane. Putting wrinkles in the membrane prior to testing does not appear to affect its restraint.

Slip plane failures are usually accompanied by some bulging or necking as well. Theories derived for membrane correction due to slip planes appear to give a similar correction to DS or HG theories, certainly at lower effective stresses where the corrections are important. Caution should be exercised in the case of post slip plane formation correction where membrane distortion due to the slip plane is excessive.

To get an idea of the magnitudes of corrections involved using the DS theory consider the following examples:

(a) passive stress relief extension test TLPS1:

E_m = 1100kPa (long duration test)

With t_o = 0.30mm, D_o = 38.26mm, initial membrane circumferences 113mm, ϵ_a = -0.16 and ϵ_v = .09.

$\Delta\sigma_a$ = 6.5kPa and $\Delta\sigma_r$ = 1.0kPa

To this radial correction should be added the effects of the initial membrane diameter being less than that of the specimen:

$\Delta\sigma_r$ becomes 2.1kPa.

(b) An undrained compression test with the usual IC membrane ie t_o = 0.30mm and circumference = 114mm, D_o = 38mm, ϵ_a = 0.20

Then, by DS theory
Inital radial membrane strain:
ϵ_r = .047
Total final ϵ_r = .165

$\Delta\sigma_r$ = 1.7kPa
and $\Delta\sigma_a$ = -7.8kPa

For an undrained extension test with
ϵ_a = -0.20 and the same membrane as for the compression test:
Initial membrane radial strain
ϵ_r = .047
Total final ϵ_r = -.040

so $\Delta\sigma_r$ = 1.6kPa
and $\Delta\sigma_a$ = 9.6kPa

Although the Henkel and Gilbert and Duncan and Seed theories give very similar axial corrections, the Henkel and Gilbert radial correction does not seem to be relevant. Therefore it is recommended that the Duncan and Seed equations be used, taking into account initial radial strain of the membrane. All triaxial and plane strain test data described in this thesis have been so corrected.

All the corrections are directly proportional to Young's Modulus and thickness of the membrane. For this reason as thin as possible membranes should be used made of a rubber with the least stiffness. Berre (1978) at the NGI describes triaxial tests with neoprene rubber membranes with

E = 131kPa. If this is quoted correctly it is 10 times less than that for the latex membranes. The larger the specimen cross sectional area to membrane cross sectional area the less important will be the membrane effects.

The thicknesses of the membranes used in the triaxial tests have been measured by placing the membranes over a brass dummy specimen and then measuring the overall diameter at several points with callipers. The average reading is then subtracted for the diameter of the dummy and halved to find the membrane thickness. As the membrane is stretched going onto the dummy, the thickness will decrease slightly: this is corrected for.

Measurement with a micrometer on the membrane alone is difficult due to deformation of the membrane.

Ponce and Bell (1971) suggest finding the density of the membrane material, then for any strip of membrane, by careful weighing and measurement of the surface area, an average thickness can be found. The method has been checked by the author for 2 membranes and found to work well. However, one has to assume that the density will remain constant.

APPENDIX A4

DETAILED SAND TEST RESULTS

The reader is referred to Volume 2 for detailed plots of all the sand test triaxial results. Table A4.1 is a schedule of the sand tests.

APPENDIX A5

DETAILED LONDON CLAY TEST RESULTS

Detailed plots of all the London clay and Claygate Beds triaxial and plane strain tests described in Chapter 6 are given in Volume 2. Table A5.1 is a schedule of these tests.

APPENDIX A6

CONSTRUCTION DRAWINGS FOR THE NEW PLANE STRAIN DEVICE

Four construction drawings for the new plane strain device (P/1 to P/4) are enclosed in Volume 2.

APPENDIX A7

NOTATION EMPLOYED

A, B, C	Constants for non-linear stiffness-strain equation.
A, B	Skempton's pore pressure parameters.
C_v	Coefficient of consolidation
C_α	Rate of secondary compression
D, D_o	Diameter
E, E', E_u	Young's modulus (the latter two being drained and undrained respectively)
G, G', G_u	Shear modulus (the latter two being drained and undrained respectively)
H	Height
I_R	Relative dilatency index
K'	Bulk modulus
K_o	Coefficient of earth pressure at rest
L	Length
M	Slope of critical state line when it is projected on to a constant volume plane
M_c	Value of M for triaxial compresion tests

M_e	Value of M for triaxial extension tests
N	Specific volume of isotropically normally consolidated soil at p' = 1.0kPa
OCR	Overconsolidation ratio
PI	Plasticity index
S_u	Undrained shear strength
V	Volume
b	Intermediate principal stress parameter $(\sigma_2 - \sigma_3)/(\sigma_1 + \sigma_3)$
e	Voids ratio
g, h	Soil constants defining the Hvorslev surface
p'	$(\sigma_1' + \sigma_2' + \sigma_3')/3$, special cases P'_o, p'_f: initial and final p'.
p'_e	Equivalent pressure: value of p' at the point on the normal consolidation line at the same specific volume.
p_k, p'_k	Soil suction
q	$(\sigma_1 - \sigma_3)$
q*	$(1/\sqrt{2})[(\sigma'_h - \sigma'_p)^2 + (\sigma'_p - \sigma'_a)^2 + (\sigma'_a - \sigma'_h)^2]^{\frac{1}{2}}$
s	$(\sigma_1 + \sigma_3)/2$
s'	$(\sigma'_1 + \sigma'_3)/2$
t	thickness of membrane or $(\sigma_1 - \sigma_3)/2$.

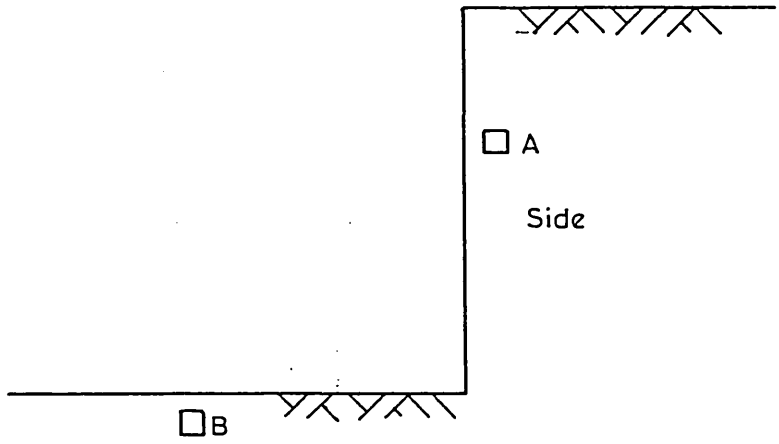
u	Pore water pressure
v	Specific volume
v_λ	Specific volume on a reference section
α, γ	Constants for non-linear stiffness-strain equation
ϵ	Strain, subscripts a axial, r radial etc.
ϵ_v	Volumetric strain (negative for dilation).
Γ	Specific volume of soil at critical state with p'=1.0kPa.
λ	Slope of normal consolidation line.
ν, ν', ν_u	Poisson's ratio.
ϕ'	Effective angle of friction.
σ	Normal stress (σ_1, σ_2, σ_3, σ_a, σ_r etc.).
σ'	Effective normal stress.
σ_a, σ_p, σ_h.	Normal stresses for plane strain device.
τ	Shear stress

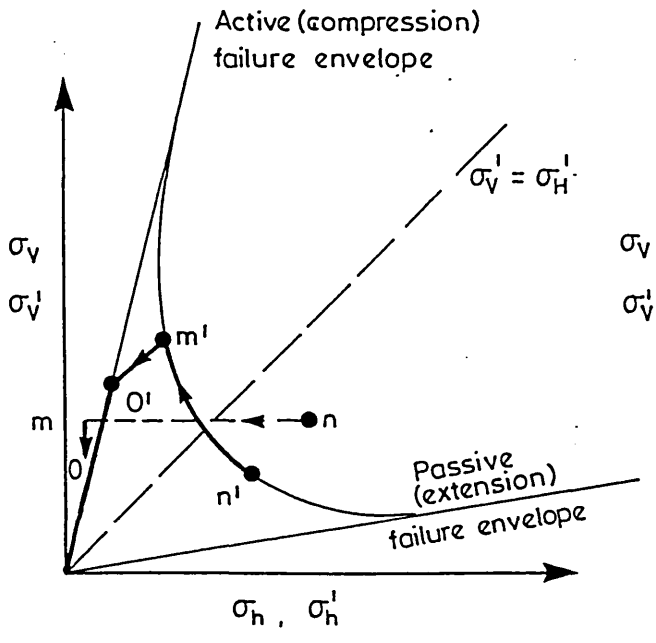
VOLUME 2

TABLES AND FIGURES

CHAPTER 2

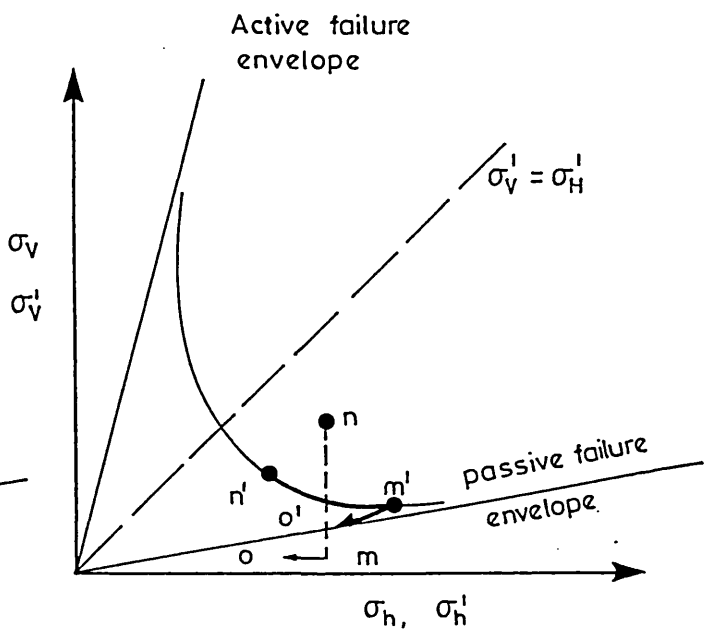
FIGURES





Excavation: side

Element A.



Excavation: base

Element B.

Figure 2.1. Stress paths around excavations: undrained shear followed by pore water pressure increase.

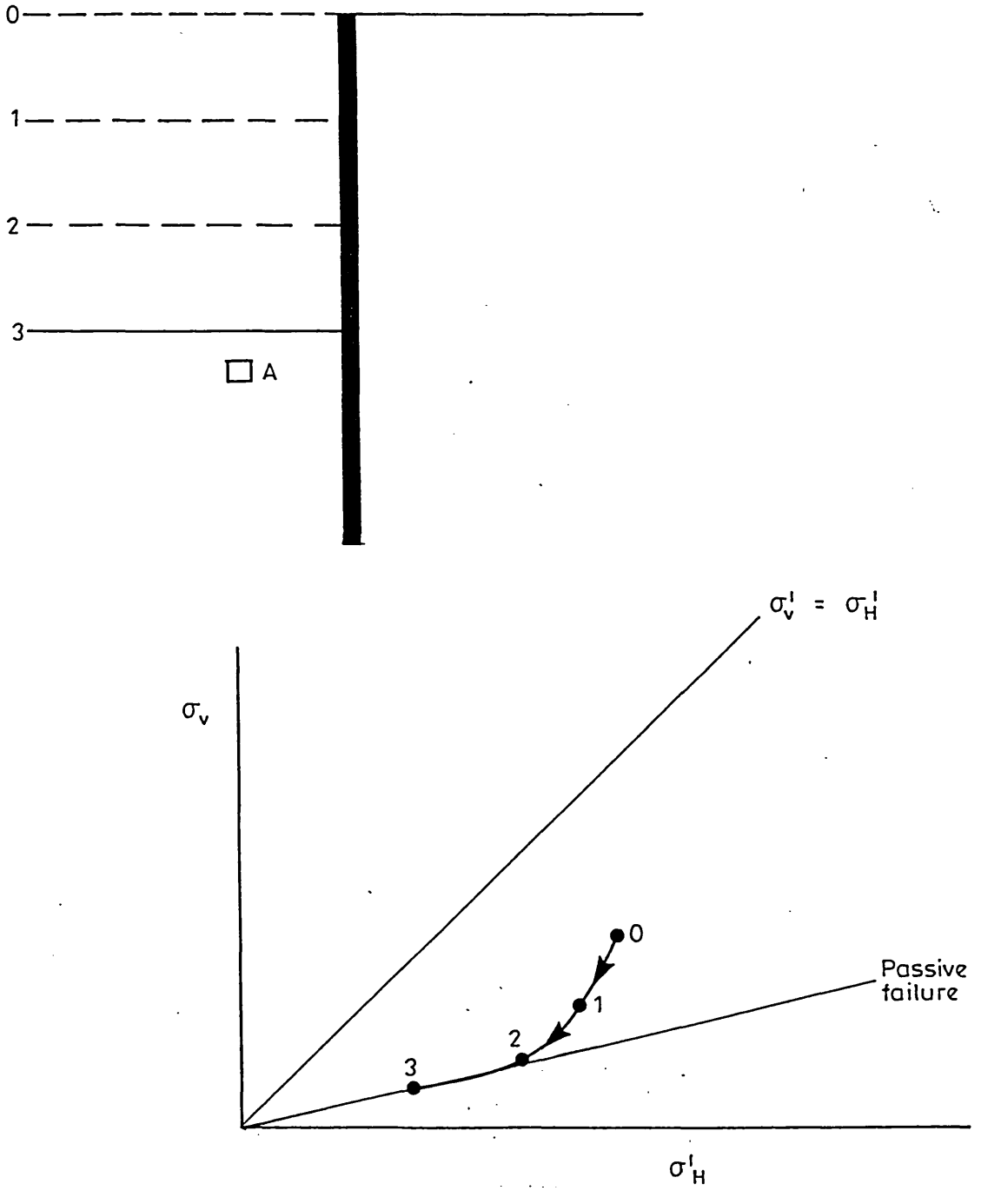


Figure 2.2. Stress path associated with drained excavation in front of an embedded cantilever retaining wall (After Burland and Fourie, 1985).

CHAPTER 3

TABLES AND FIGURES

Table 3.1

Details of sand mix used for programme of tests on sand specimens

Specimen Type		A	B	C	D
Target initial porosity	%	37	39	42	47
Target initial voids ratio		.59	.64	.72	.89
Mass dry sand	g	132.8	128.6	122.5	114.6
Mass water	g	23.5	24.4	24.5	22.9
Initial moisture content	%	17.7	19.0	20.0	20.0
Approximate initial specimen saturation ratio	%	80	75	70	60

Table 3.2

Drilling Record for New Borehole at Bell Common
(NOTE: All tube samples unless otherwise stated)

Date	Depth(m) from	to	Hydraulic pressure ($lbs/inch^2$)	Comments	Sample no.	Test specimens from this core length
19.8.85	0	0.6	700	Topsoil, roots.	1	-
	0.6	1.2	1000	Sandy clay.	2	-
	1.2	1.8	1600	Obstruction (stones?)	3	-
	1.8	2.3	1000	Claygate.	4	TCUU1, TCPS1
	2.3	2.93	2400	Obstruction (stones) near bottom.	5	TCUA1
	2.93	4.0	2400	Auger thru' gravel. Bag sample. Water at about 4m.	6	-
	4.0	4.5	2400	Mostly gravel, clay matrix.	7	-
	5.0	8.0	-	Tube sample not possible: sand and stones. Bag sample from auger.	8	-
	8.0	8.6	1200	Tube sample taken: Sand clay mixture (disturbed). Borehole caving badly. Move 0.5m, redrill at larger diameter to 8m and case hole.	9	-
21.8.85	8.16	8.66	1400	Core sample from 8.16m: again mostly sand and stones.	10	-
22.8.85	8.8	9.3	1400	Casing driven further to 8.75m. London clay.	11	TLA2 (test spoiled)
	9.3	10.2	1500	London clay.	12	TLA2A, TLSU2
	10.2	10.88	1000	London clay.	13	TLPS5, TLUU4, TLSUD2B
	10.7	11.52	1200	London clay.	14	TLCU1
	11.52	11.85	2400	Claystone obstruction: Auger to 12.48m.	15	TLCU2
	11.9	12.5		Claystone/London clay: bag sample.	16	
	12.5	13.05	2400	London clay	17	TLUU5
	13.1	13.67	1600	London clay	18	TLPS2, TLDRUL2
	13.67	14.24	1800	London clay	19	TLDRUL1, TLUU1
	14.24	14.83	2100	London clay	20	TLPS1
	14.83	15.35	2300	London clay	21	TLA1, TLUU2
27.8.85	16.21	16.61	2400	Sample tube full of silt/ sand. Deepen casing to 9.0m.	22	-
	16.7	17.14	2200	London clay.	23	TLPS4, TLD1
	17.2	17.67	2200	London clay.	24	TLSU1
	17.45	17.93	2000	London clay.	25	PLPS1
	17.93	18.53	2200	London clay.	26	TLSUD1, TLSUD1A
28.8.85	18.59	18.94	2400	London clay.	27	TLUU3
	18.94	19.35	2200	London clay: the core is dry due to poor waxing.	28	-
	19.55	20.00	2100	London clay.	29	TLUA1
	20.11	20.54	2400	London clay.	30	TLPS3, TLPS6
	20.69	21.02	2300	London clay: dry core (poor waxing). End of borehole.	31	-

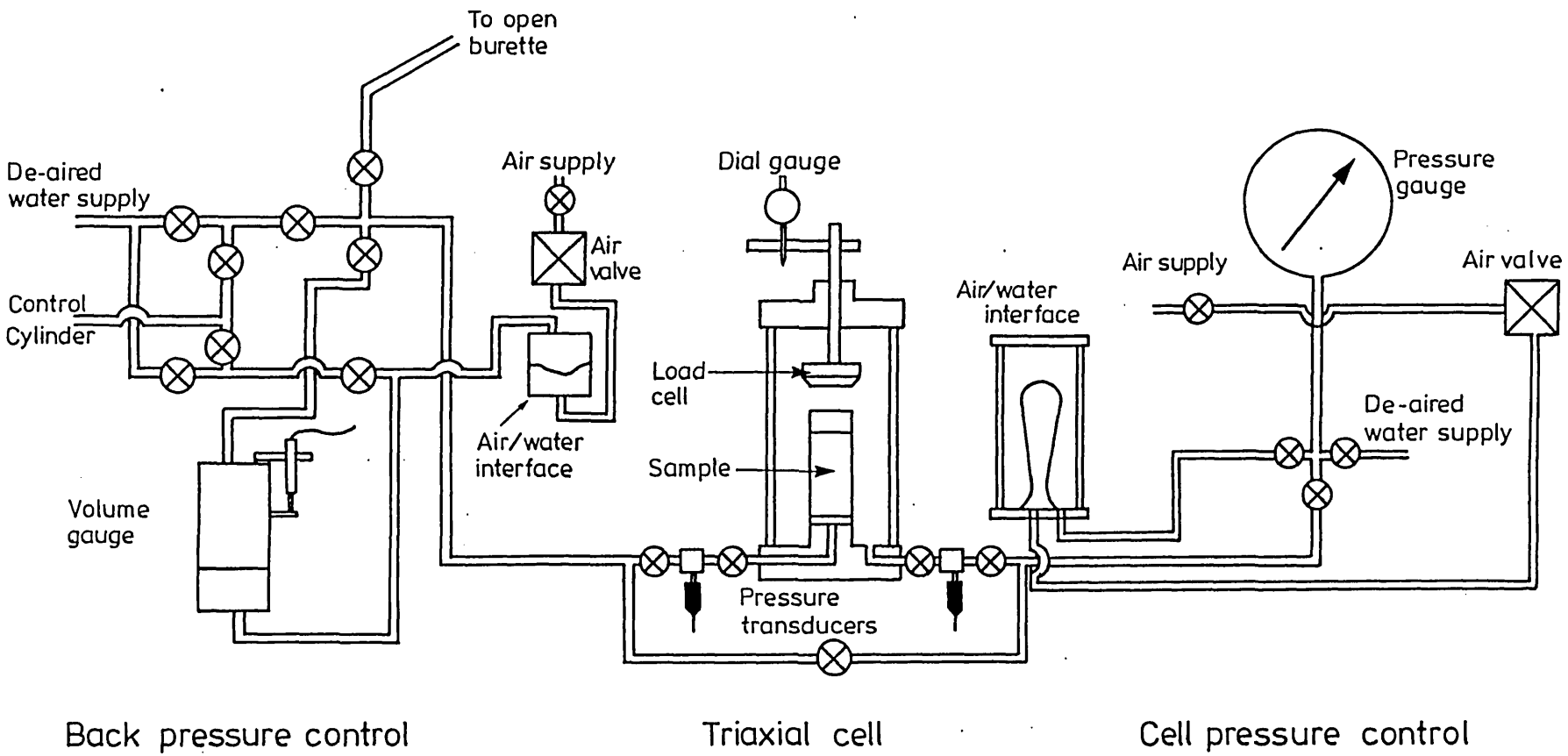


Figure 3.1. General arrangement of conventional compression triaxial apparatus.

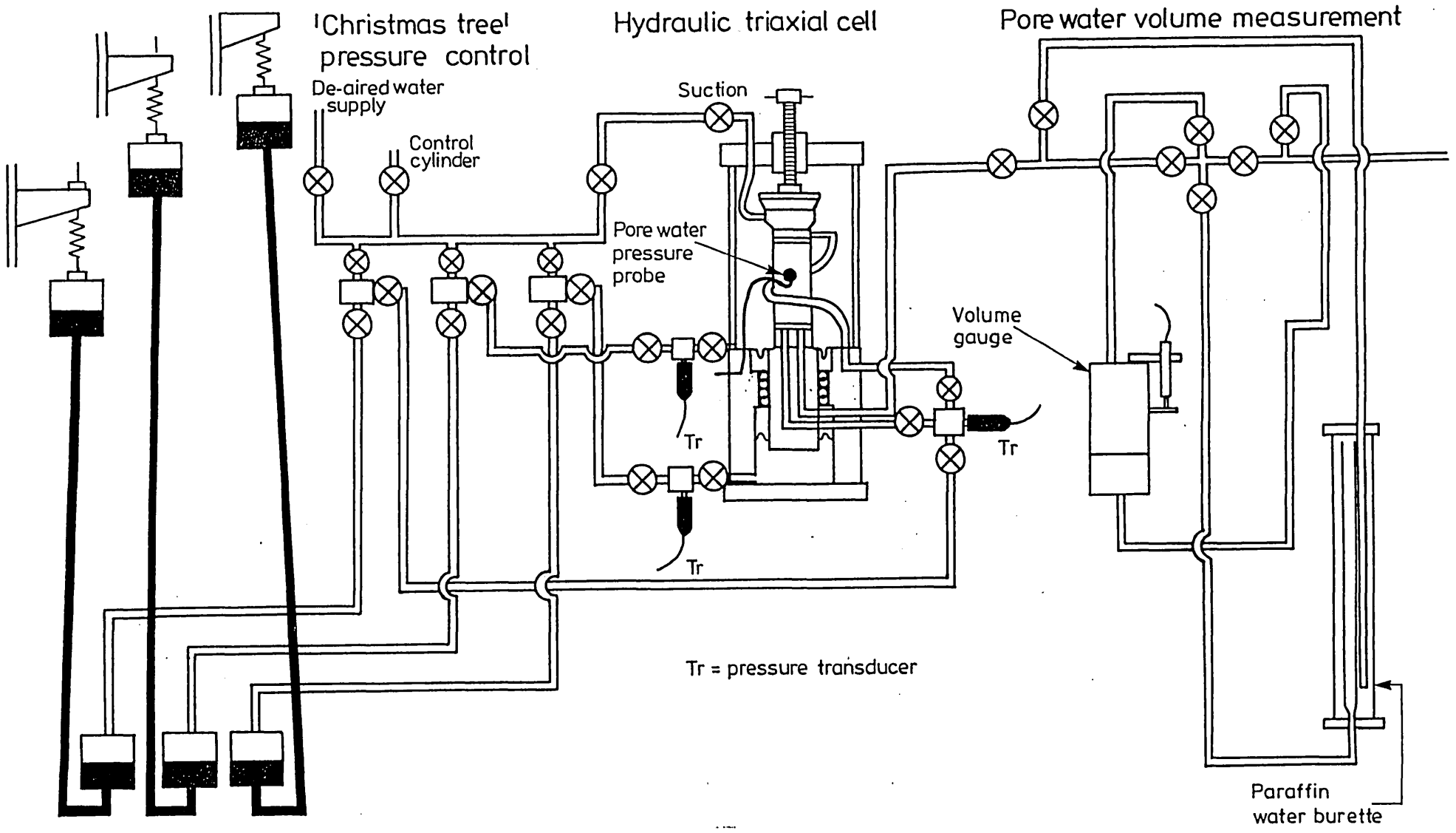
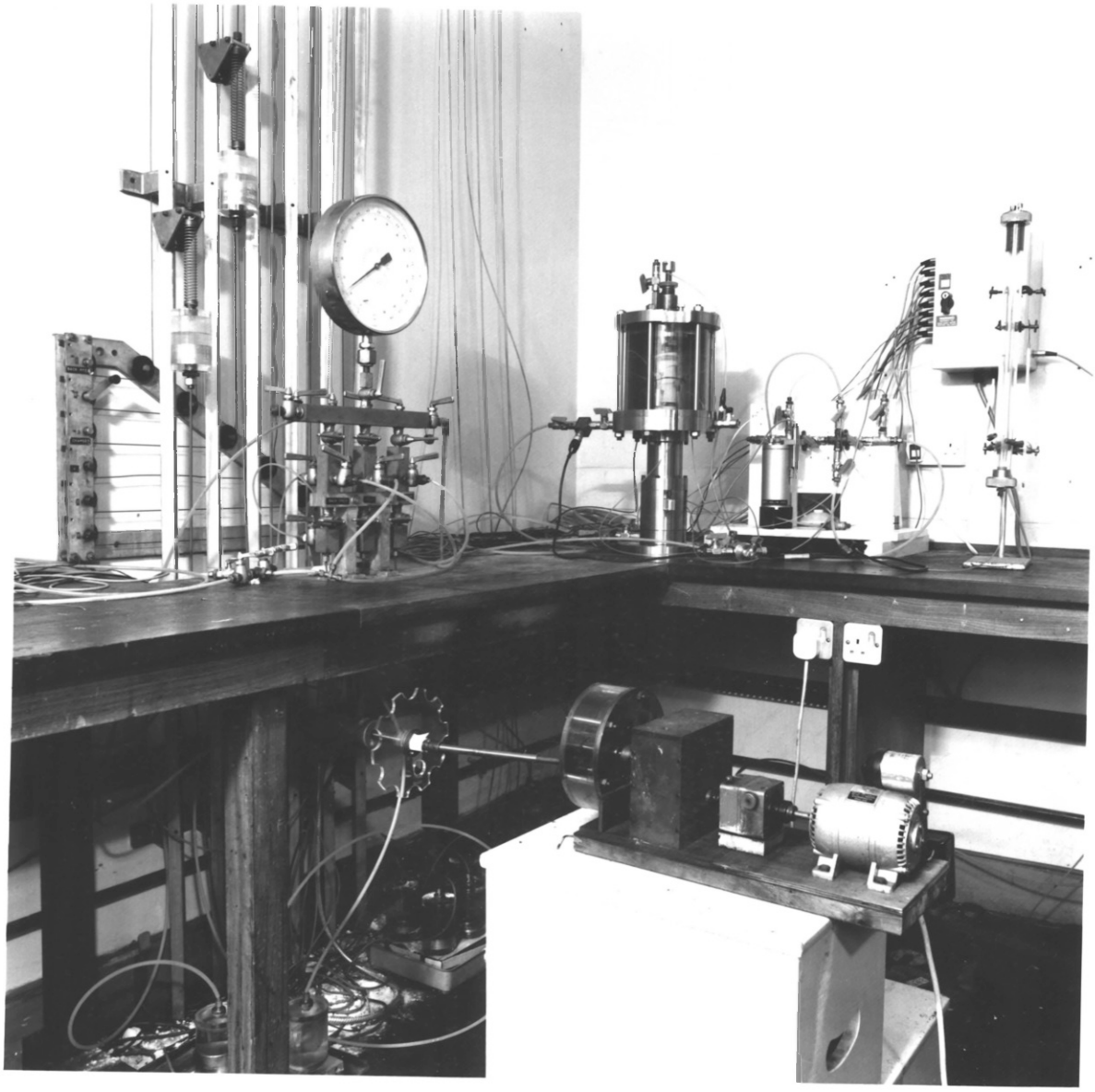
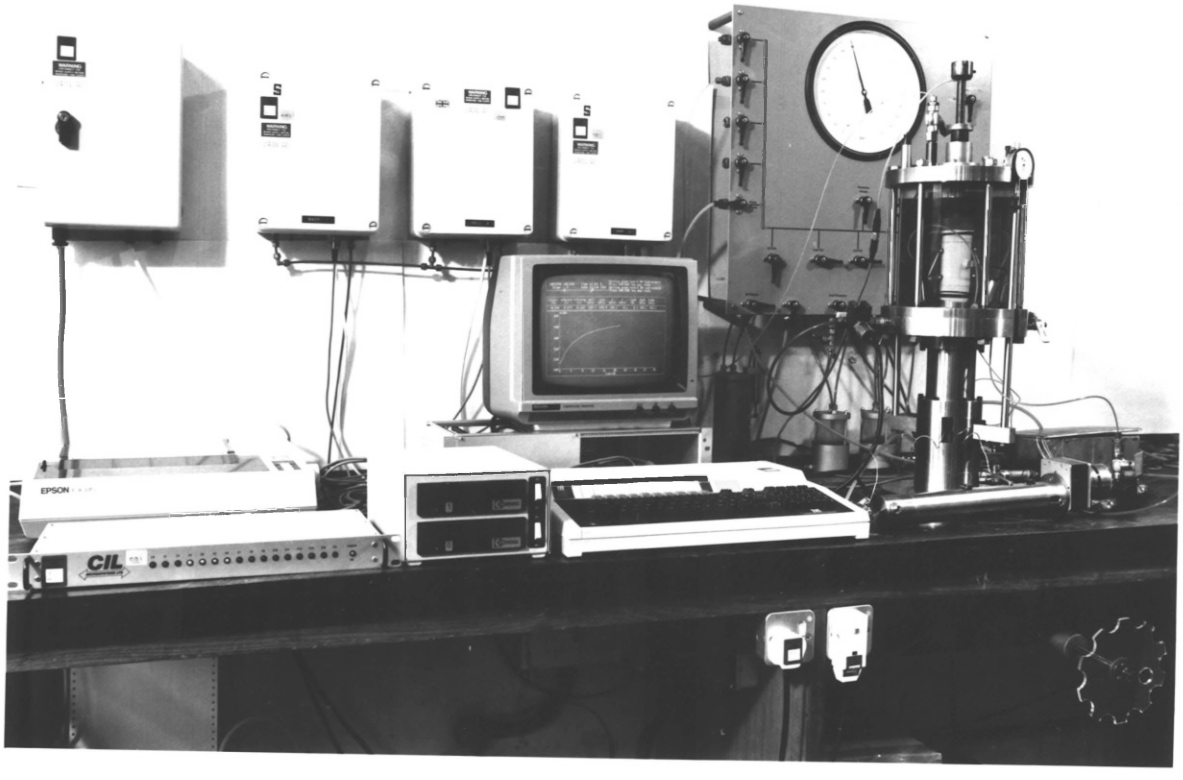


Figure 3.2. General arrangement of the Bishop and Wesley stress path cell connected to a self compensating mercury control.

Figure 3.3

Photograph of stress path cells with a self compensating mercury system (top) and a computer controlled system (bottom).




EPSON
CIL

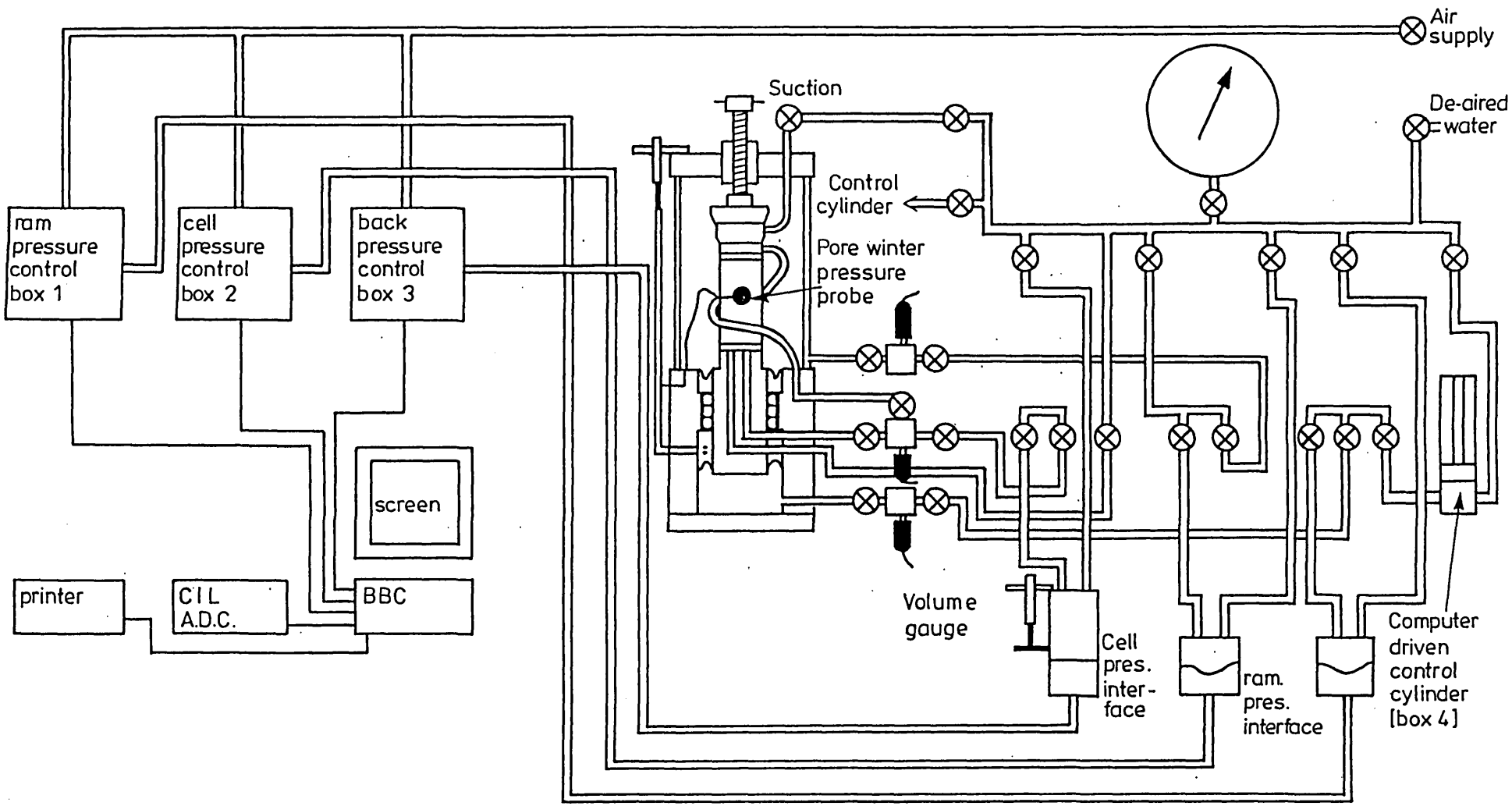


Figure 3.4. General arrangement of the new microcomputer control system driving a stress path cell.

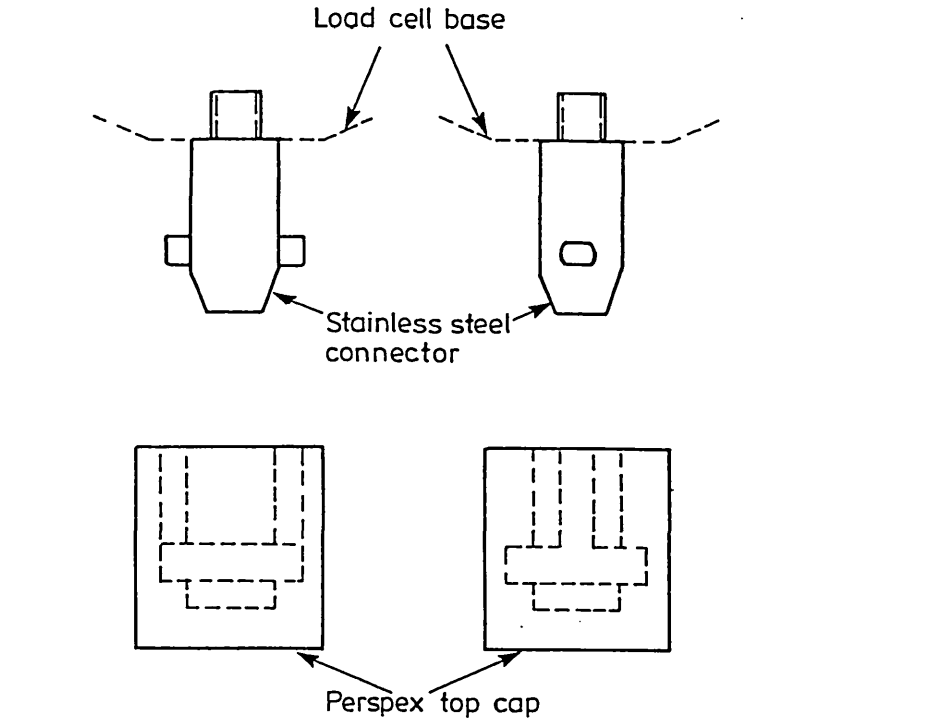


Figure 3.5. Methods of connecting the top cap to the load cell for extension tests.

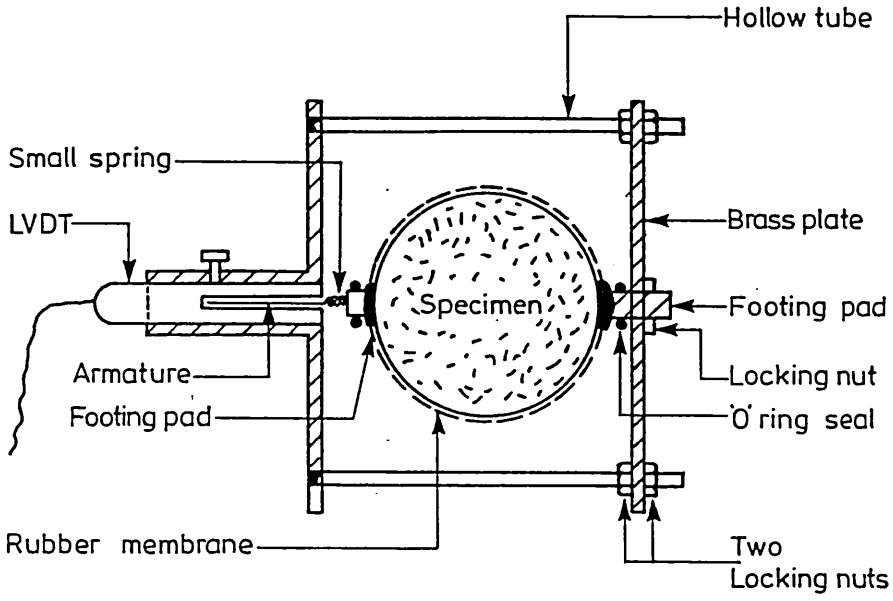


Figure 3.6. The radial strain belt.

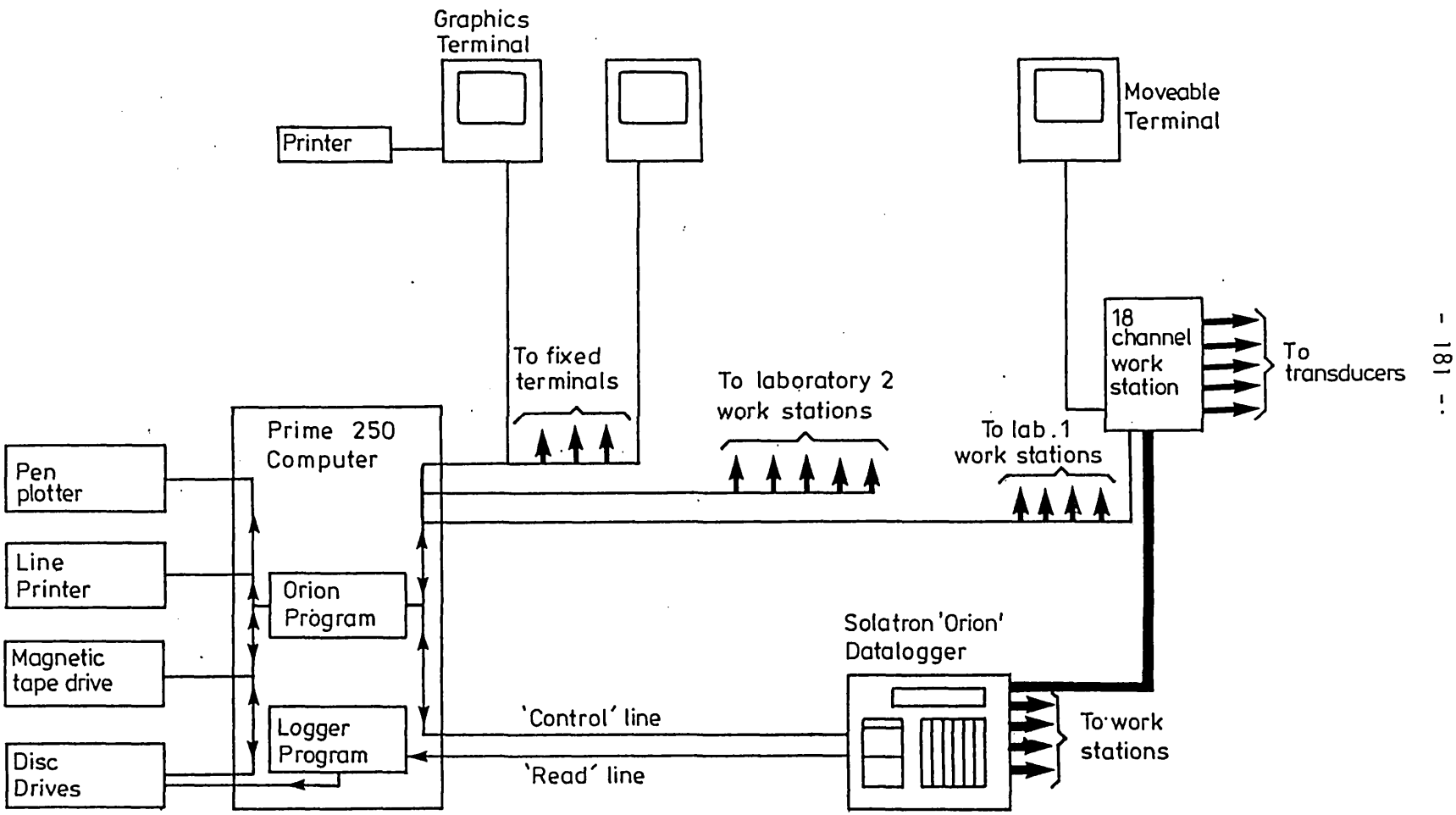


Figure 3.7. The ORION data logging system (After Toll 1988).

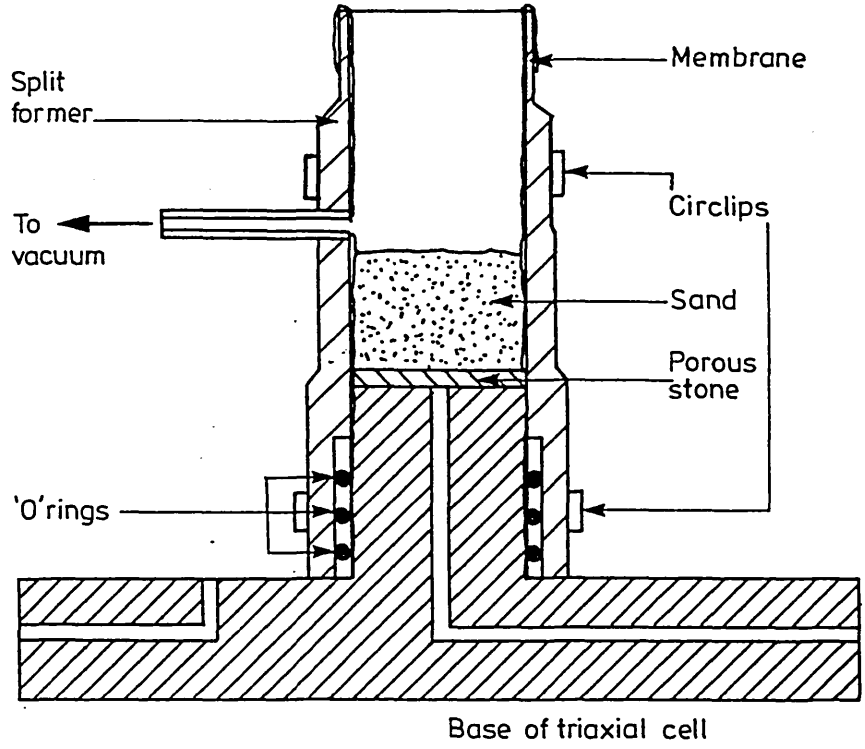


Figure 3.8. Arrangement for forming a sand specimen for triaxial testing.

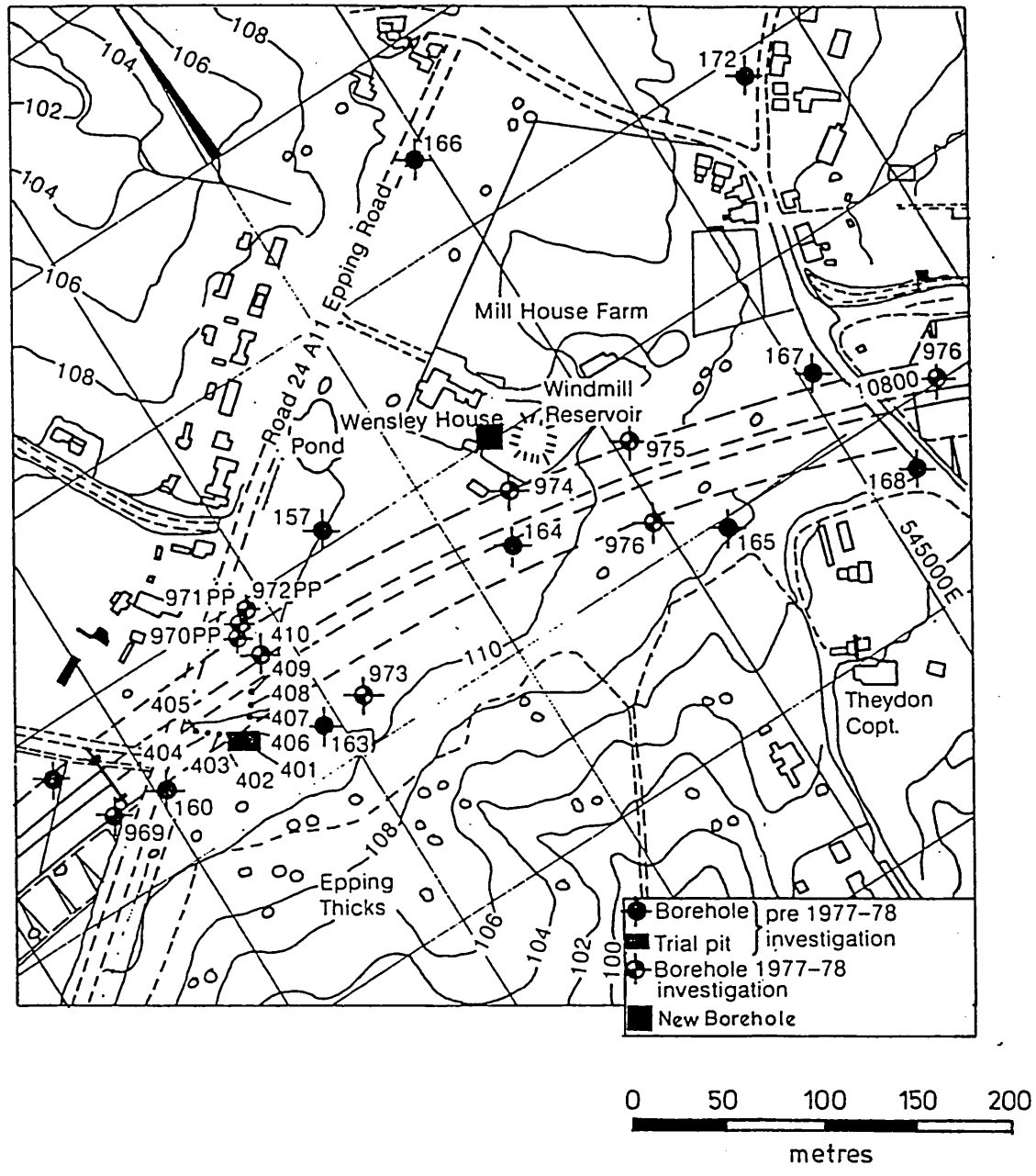
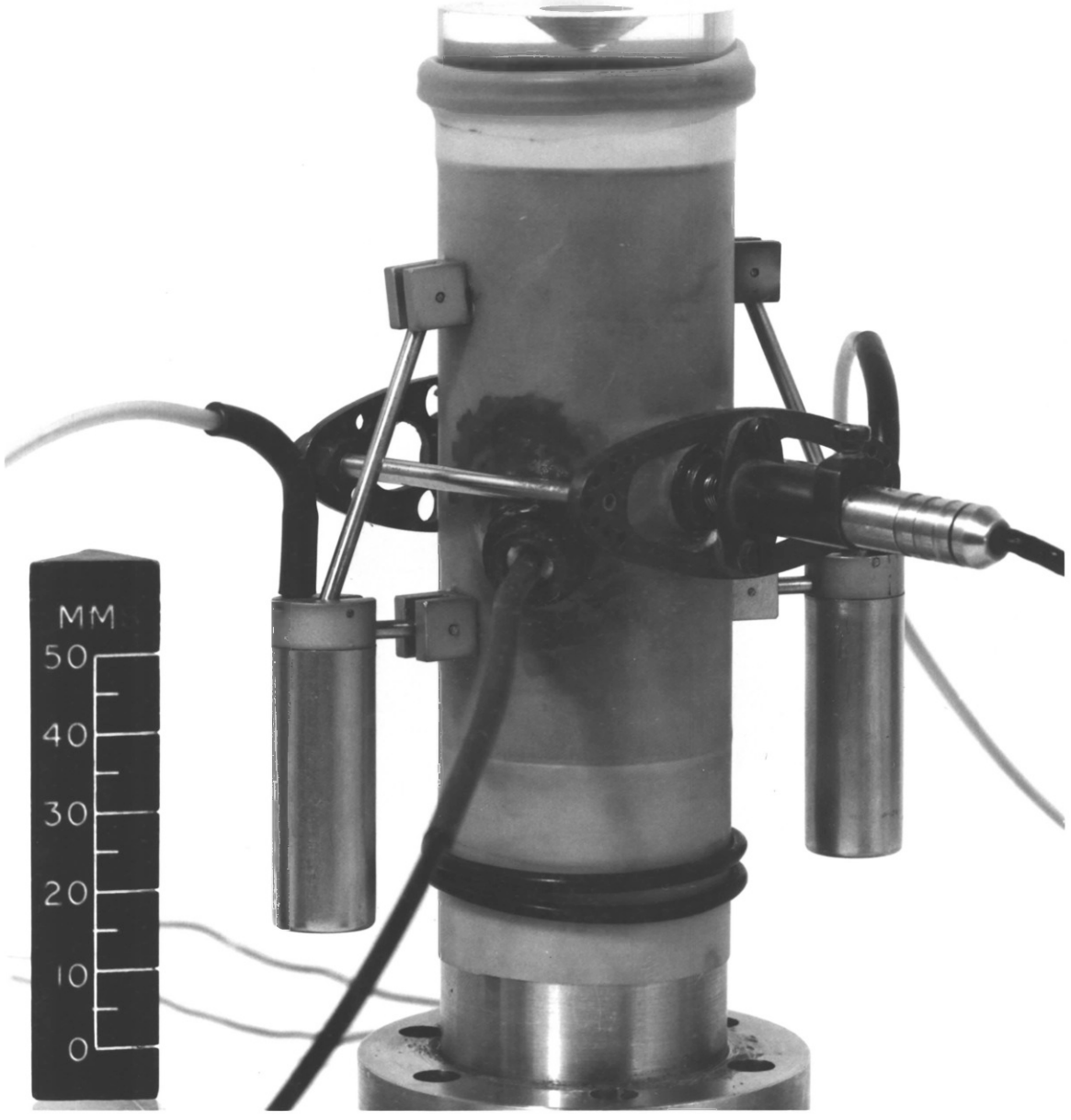


Figure 3.9. Location plan for new borehole at Bell Common.

Figure 3.10

Photograph of a 38mm triaxial specimen with local strain devices, pore water pressure probe and radial strain belt.


MM
50
40
30
20
10
0

STAGE 2

Stage description: KO SWELLING

Triggers to start Stage 2		
Stage 1	probe-back<5 AND back-probe<5	CONT

Box	1	2	3	4
Status	on	on	on	off
Control equation	back	.43*(s'-280)-t	t	
Hold value	450	0	-8	
Tolerance	0.5	0.5	0.5	
Increment	0	0	-1	
Maximum pulses	20	20	5	

Alarm 1	t<=-21 OR s'<231	WAIT 0:1:0 2
Alarm 2	probe-back>5 OR back-probe>5	WAIT 0:5:0 2
Alarm 3	t<-21 AND s'<231	WAIT
Alarm 4	Undefined	

Figure 3.11. Typical control sheet from one of the stages of a computer controlled test (Test TLPS4).

CHAPTER 4

FIGURES

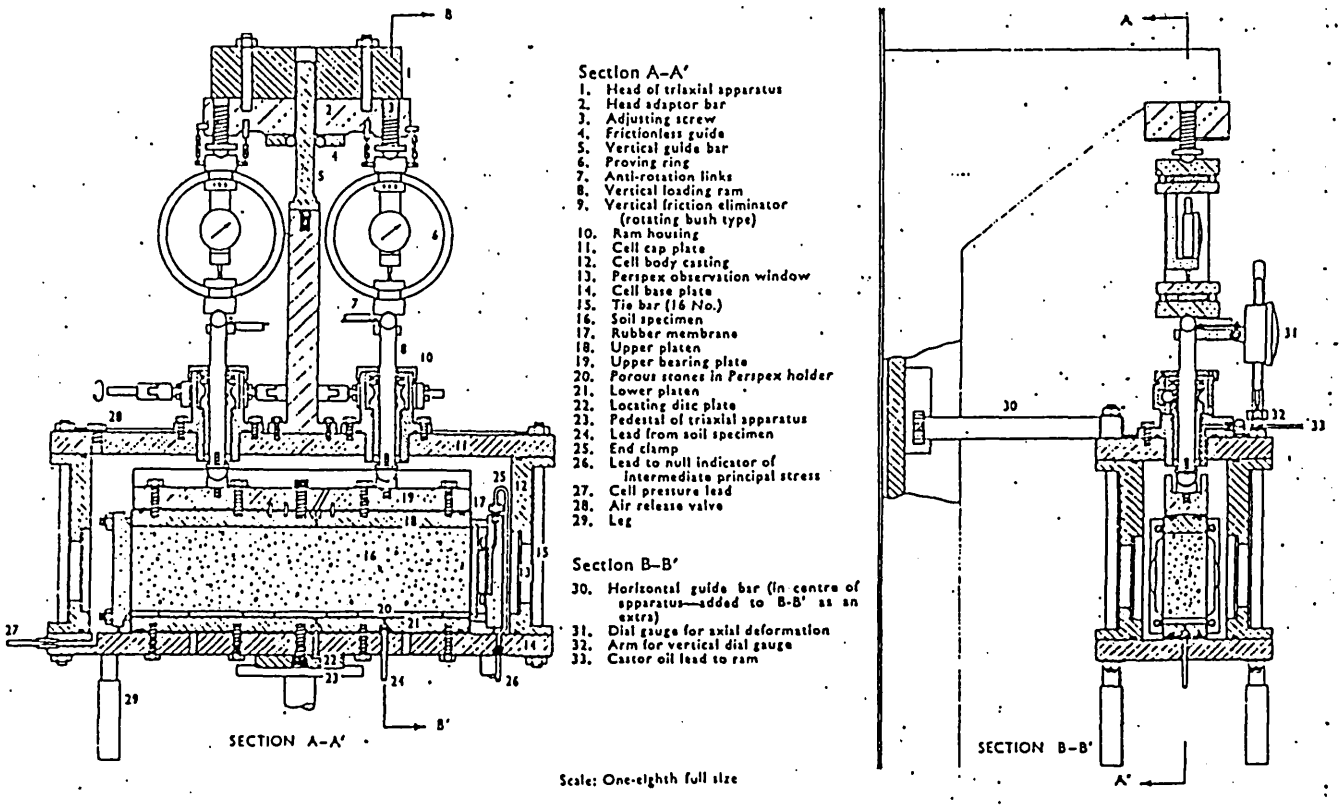


Figure 4.1. The Wood (1958) Imperial College plane strain apparatus.

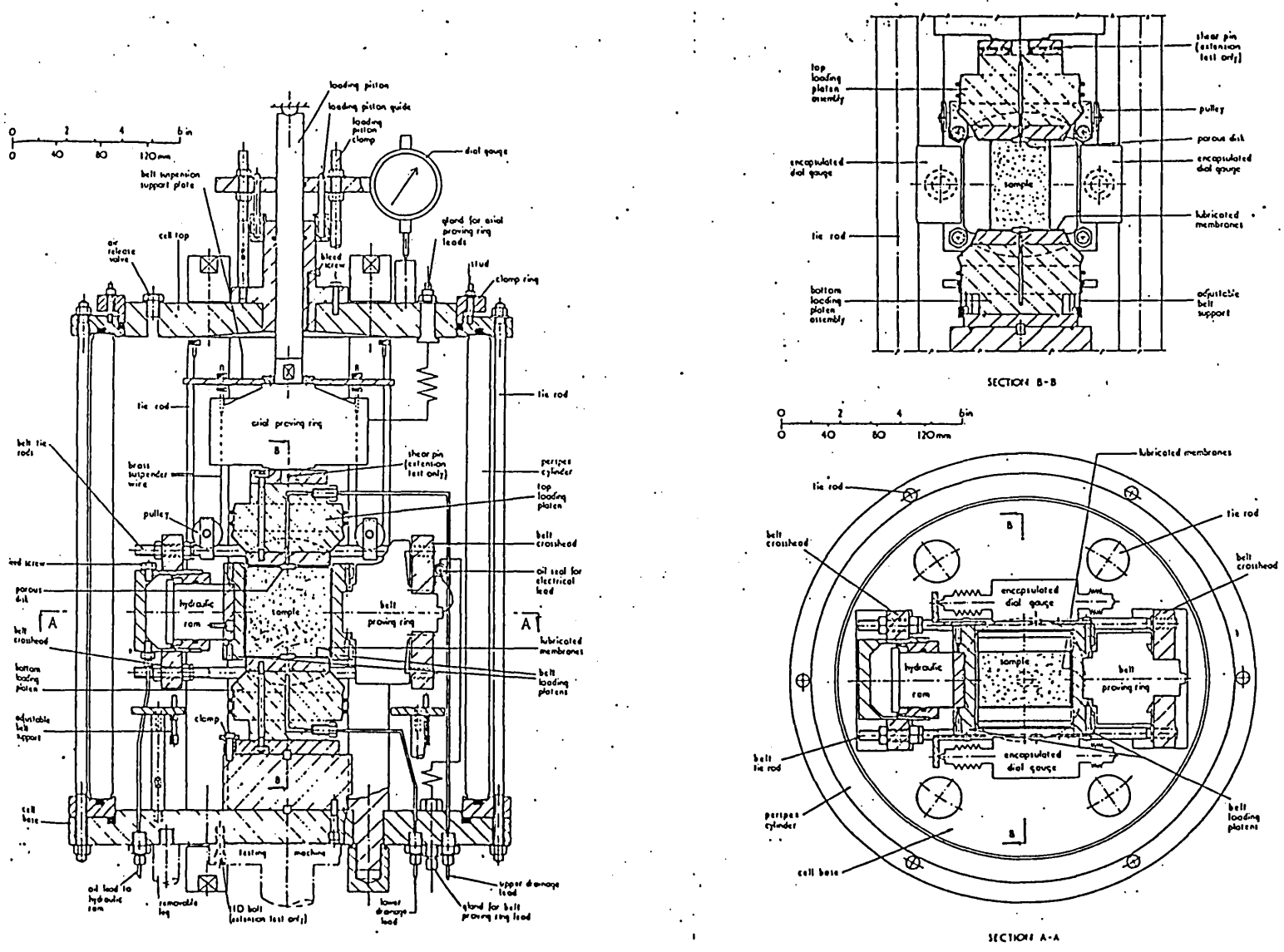


Figure 4.2. Green's (1969) independent stress control machine.

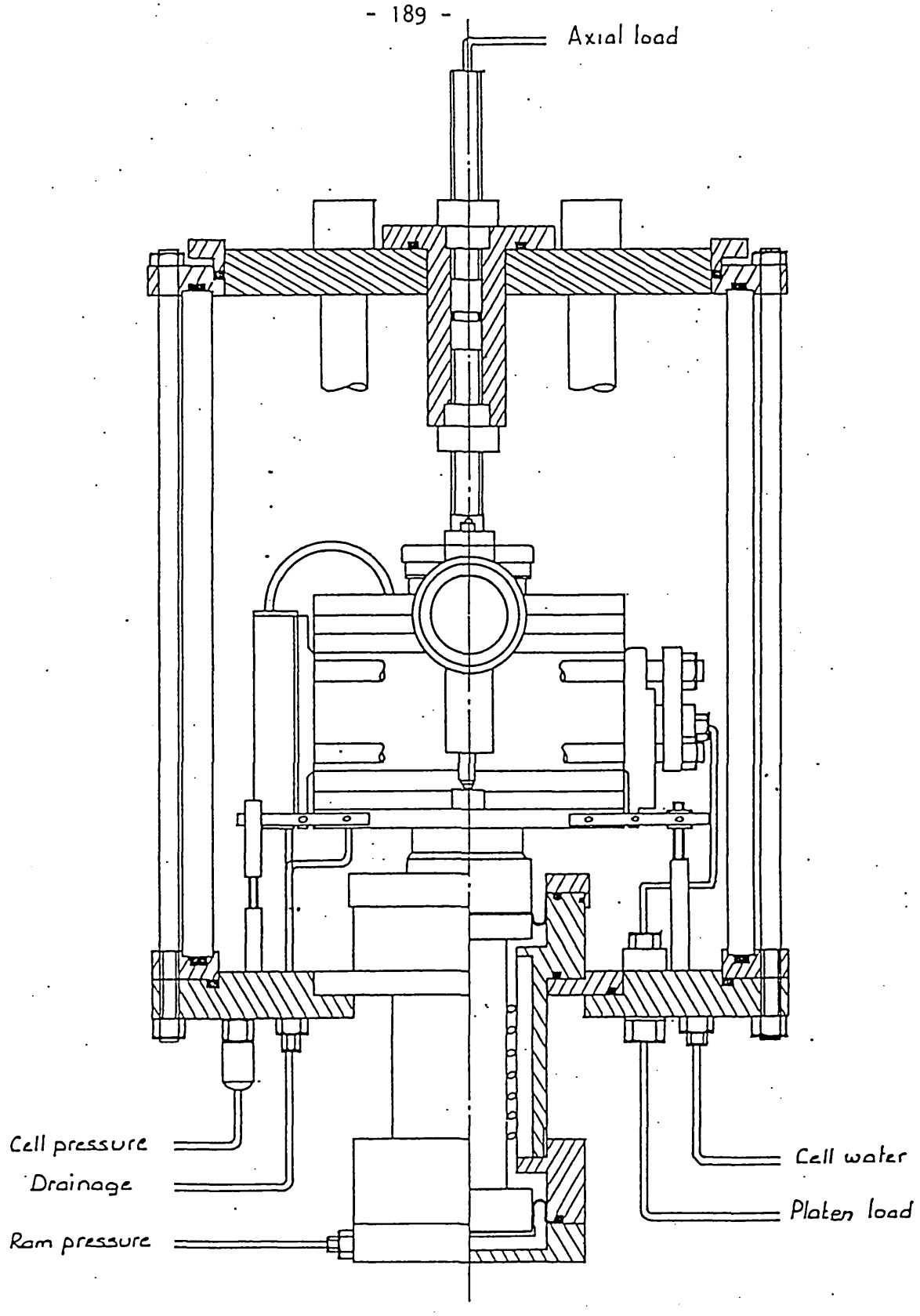


Figure 4.3. The Atkinson (1973) plane strain machine.

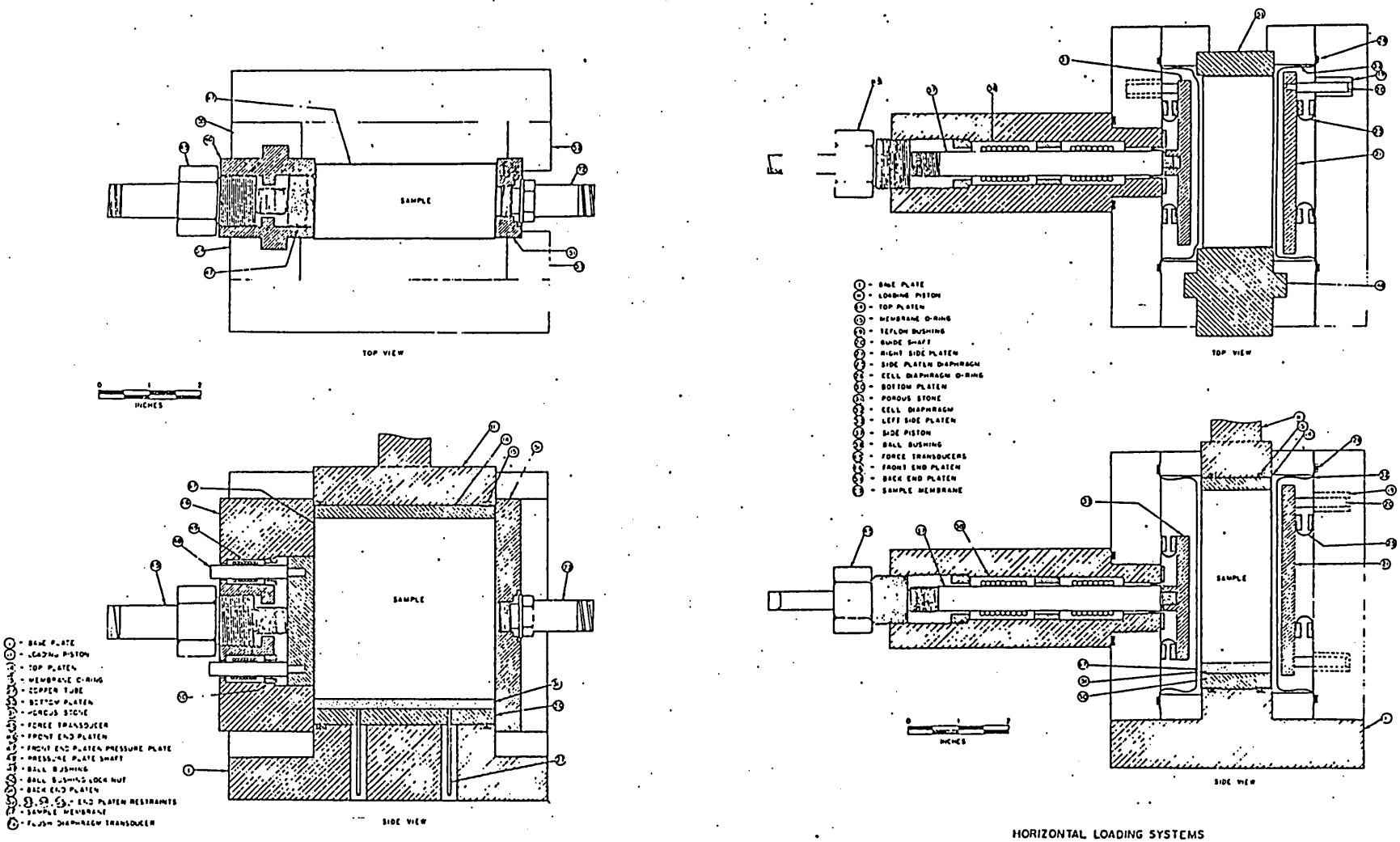
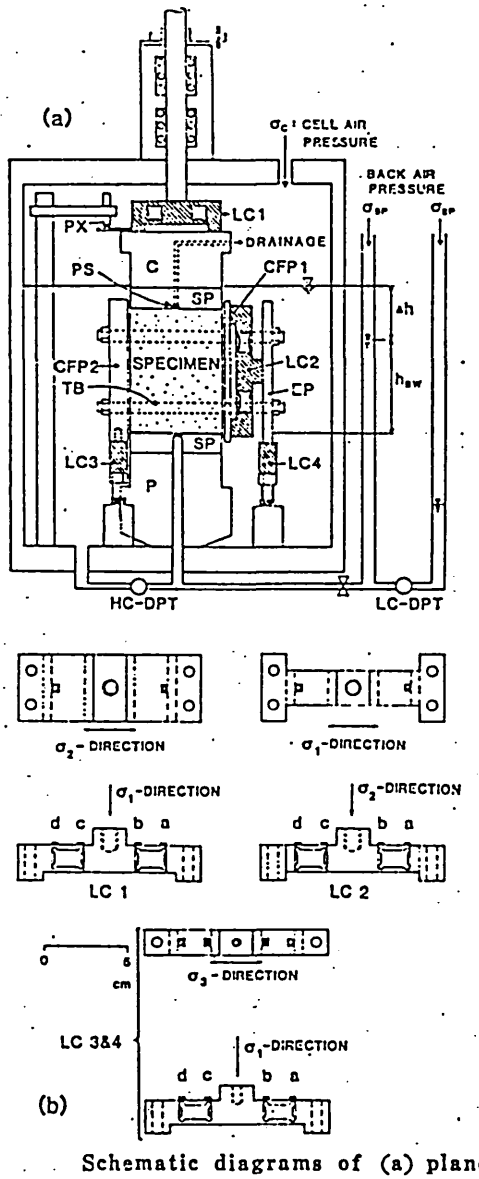
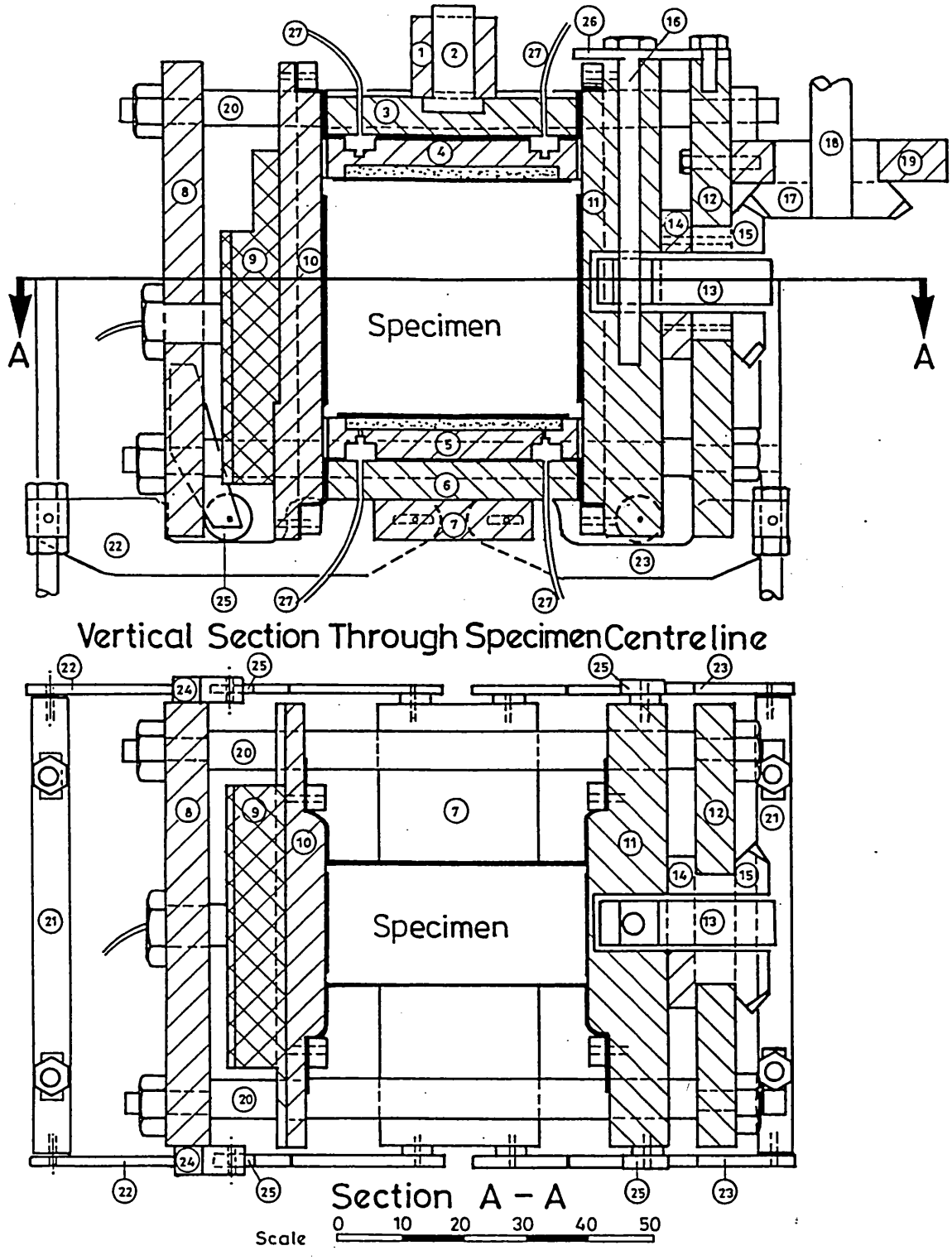


Figure 4.4. The M.I.T. (Dickey et al, 1968) apparatus.



Schematic diagrams of (a) plane strain compression apparatus and (b) load cells used in tests at σ_3'=0.05 and 0.1kgf/cm²(HC-DPT ; high-capacity differential pressure transducer to measure σ_c' and LC-DPT ; low capacity differential pressure transducer to measure volume change) (1kgf/cm²= 98kN/m²)

Figure 4.5. The University of Tokyo (Institute of Industrial Science) plane strain apparatus.



1 Top spacer
2 Bolt
3 Top membrane sealing platen
4 Top platen
5 Bottom platen
6 Bottom membrane sealing platen
7 Bottom loading head
8 Back-up platen
9 Load cell
10 Make-up platen
11 Adjustable platen
12 End plate
13 Screw shaft
14 Gear support piece
15 Gears
16 Stud
17 Gears
18 Screw control rod
19 Support plate
20 End platen tie rods
21 Support rail crossbars
22 Support rails
23 Support rails
24 Supporting plate
25 Wheels
26 Adjustable plate guide
27 Drainage

Figure 4.6. The new plane strain apparatus.

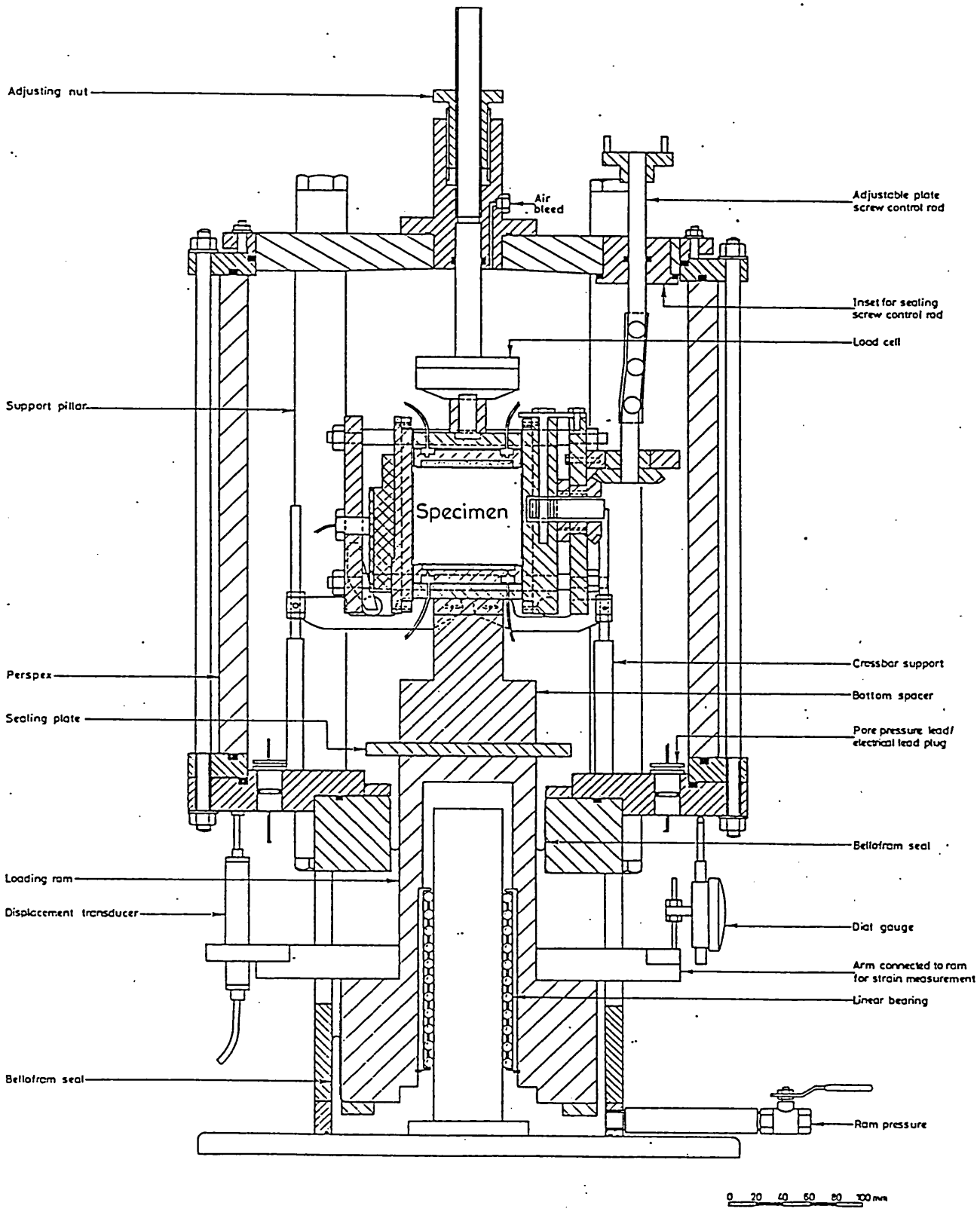
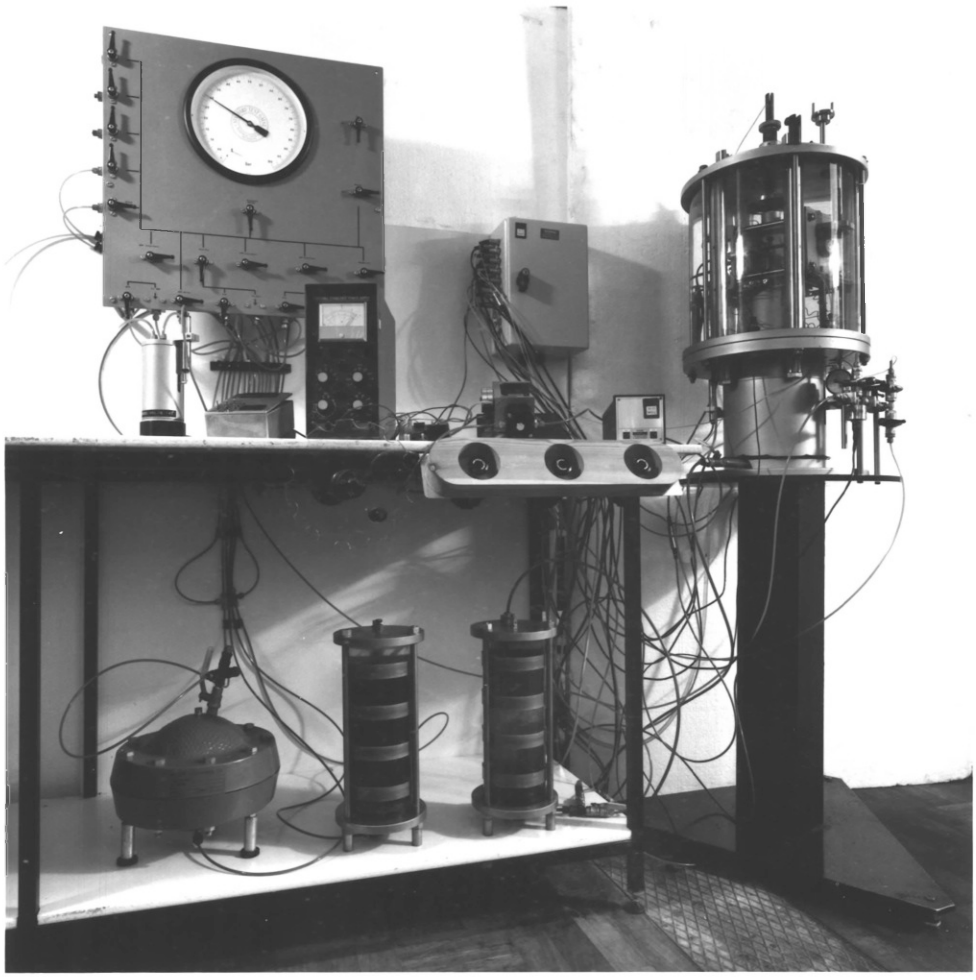


Figure 4.7. The new plane strain machine set up in a stress path cell.

Figure 4.8

Photograph of general view of stress path cell and plane strain apparatus with control equipment (top) and the plane strain apparatus with specimen (bottom)



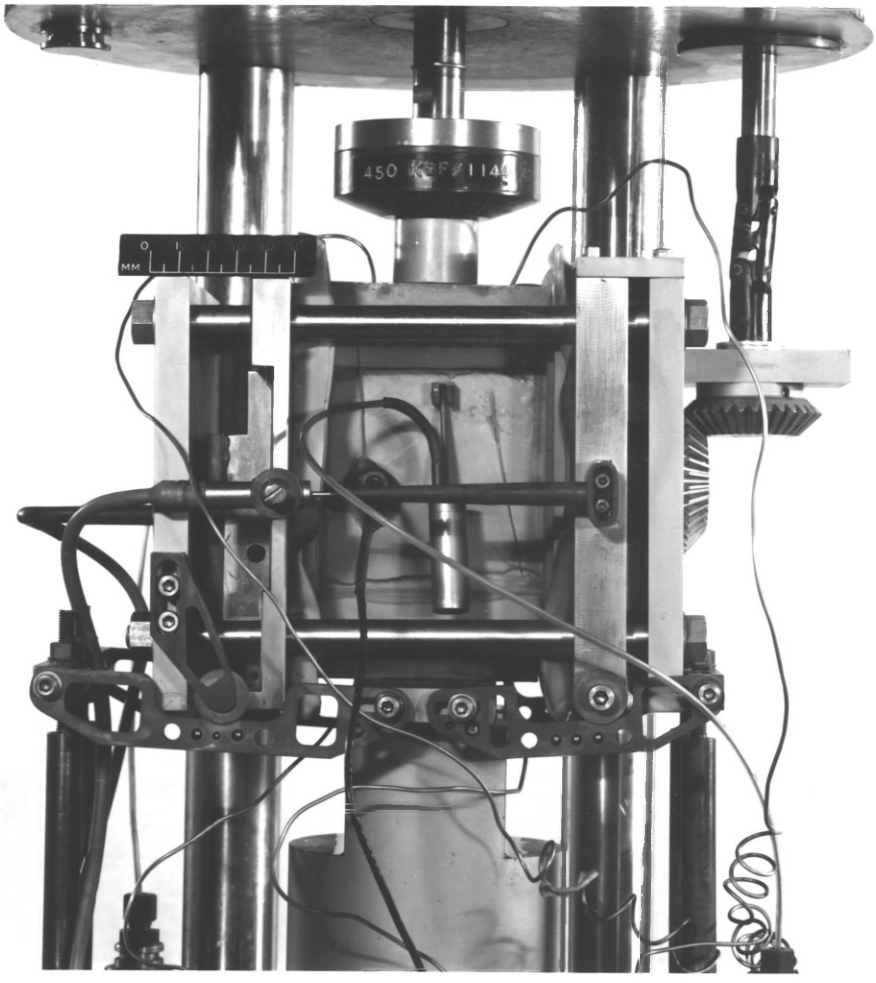
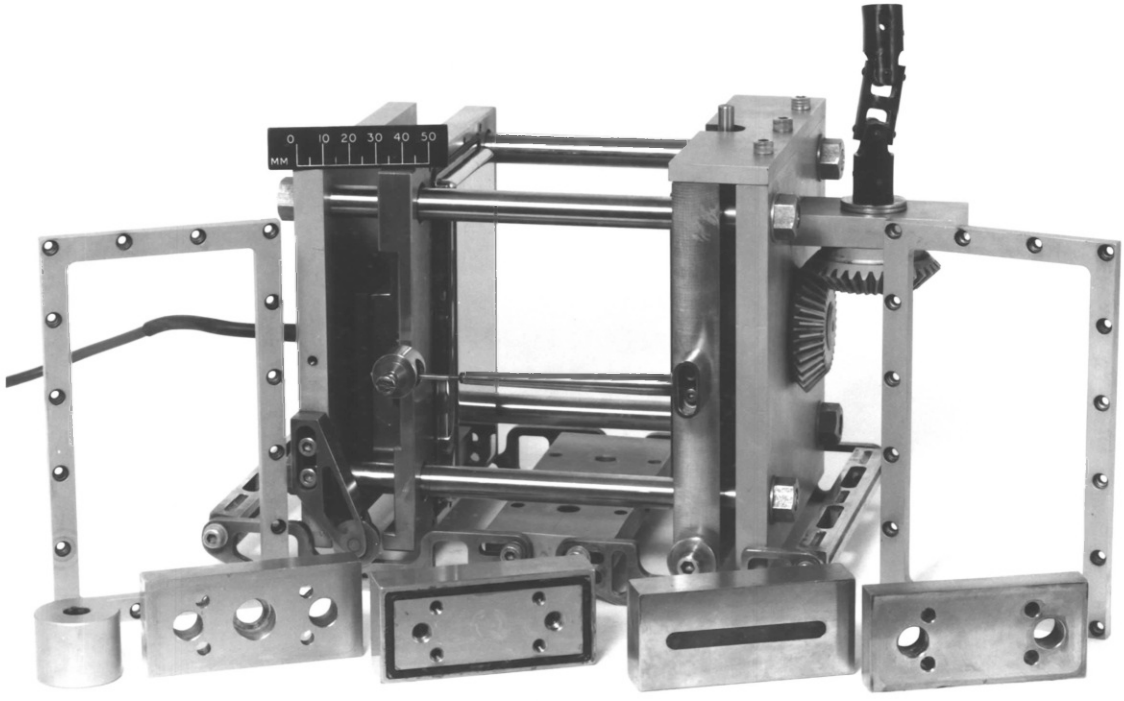
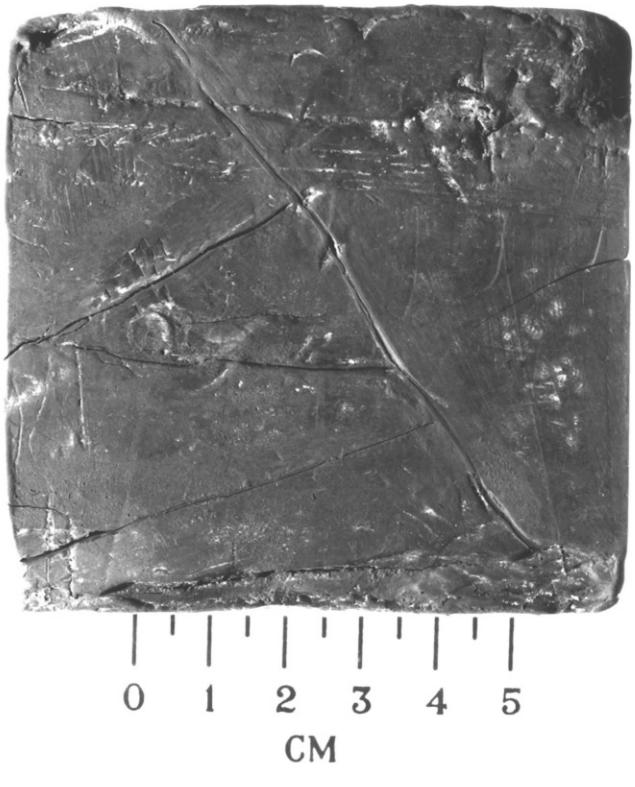

450 KGF/114
0
MM

Figure 4.9

Photograph of components of the plane strain apparatus (top) and specimen of London clay after testing in plane strain-test PLPS1 (bottom).


0 10 20 30 40 50
MM


0 1 2 3 4 5
CM

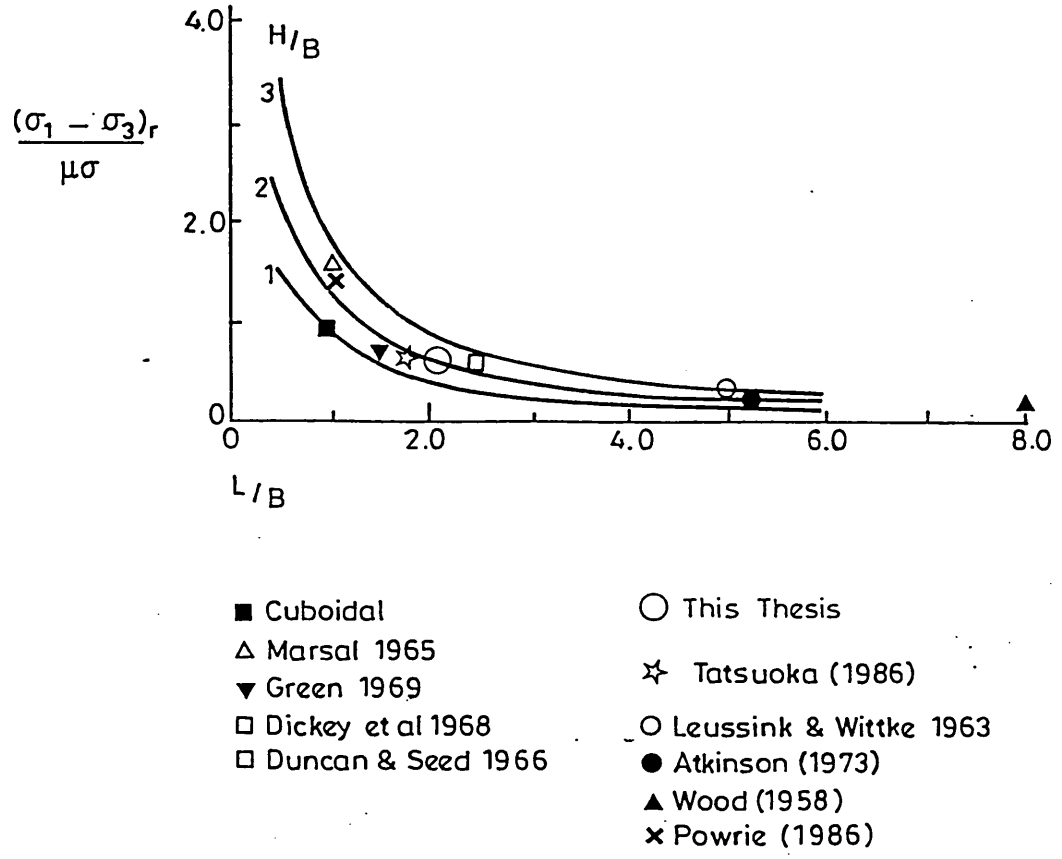


Figure 4.10. The influence of specimen size on the end platen friction correction for plane strain tests.

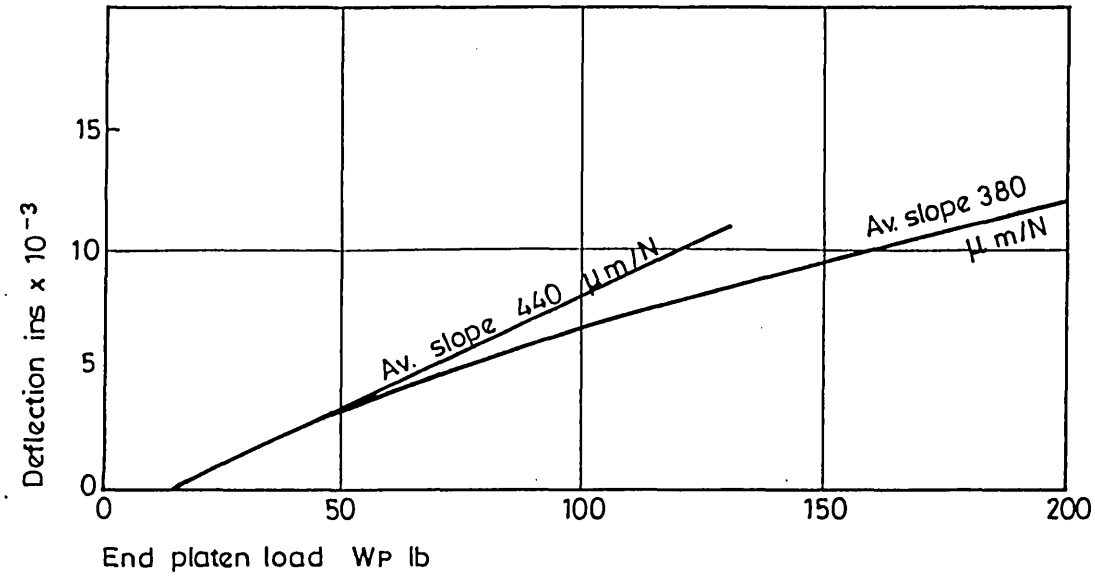


Figure 4.11. Calibration (By Atkinson, 1973) of the load cell deflection characteristics used in the new plane strain device to measure end platen stresses.

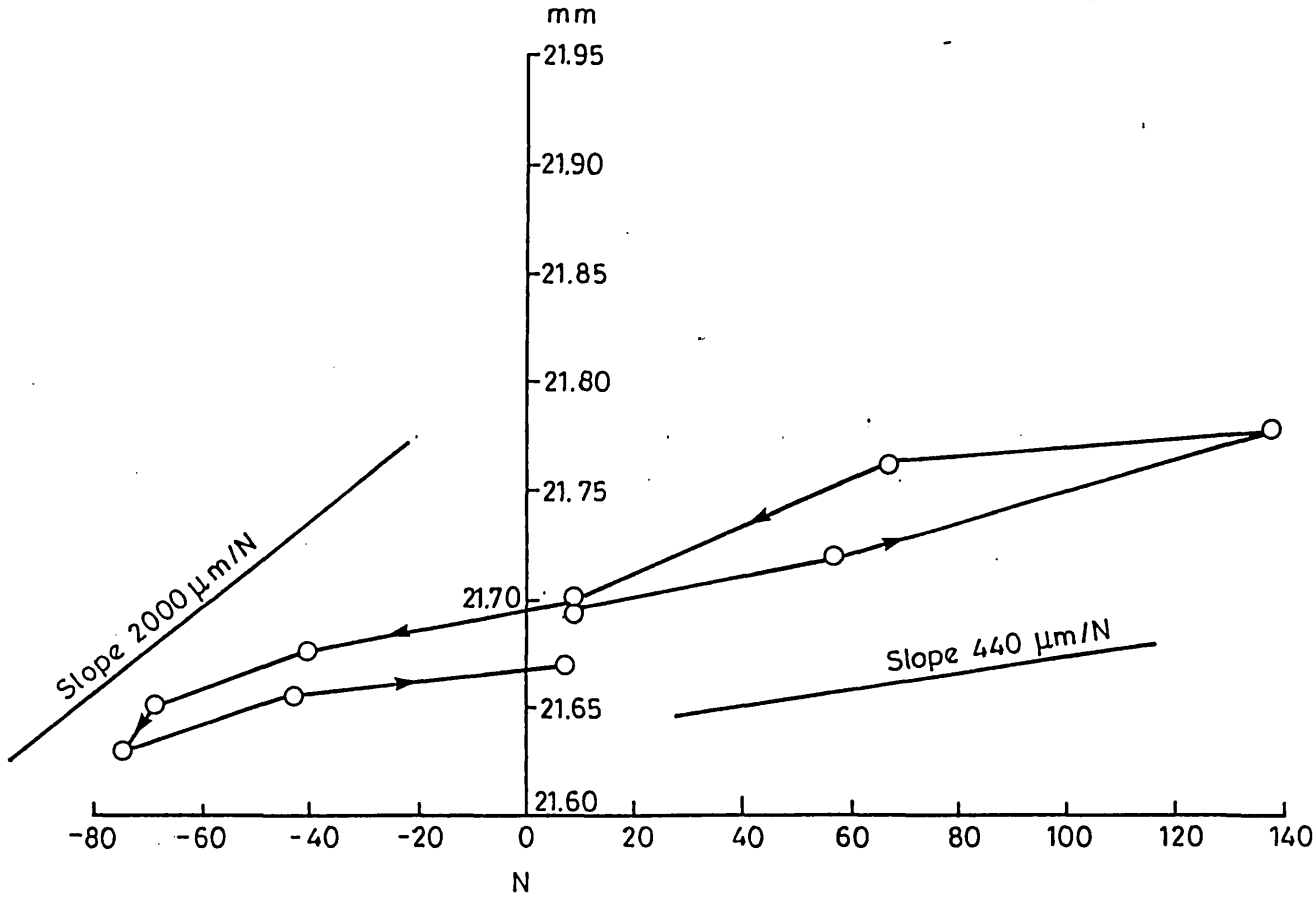


Figure 4.12. Stiffness of the plane strain horizontal loading assembly.

CHAPTER 5

TABLES AND FIGURES

Table 5.1

Mobilised friction angles at peak strength for compression and extension tests on sand: drained and undrained tests

	drained tests						undrained tests at p' = 100kPa tension		undrained tests at p'= 100kPa compression	
	p' = 10kPa			p' = 100kPa						
e	Φ'_e	Φ'_c	$\Delta\Phi_{e-c}$	Φ'_e	Φ'_c	$\Delta\Phi_{e-c}$	Φ'_e	$\Delta\Phi_{d-u}$	Φ'_c	$\Delta\Phi_{d-u}$
.90	34°	-	-	29°	-	-	-	-		
.85	37°	29°	8°	31°	27°	4°	-	-		
.80	41°	34°	7°	34°	30°	4°	32°	2°		
.75	46°	39°	7°	37°	33°	4°	-	-		
.70	53°	46°	7°	41°	37°	4°	36°	5°	35°	2°
.65	60°	52°	8°	45°	41°	4°	-	-		
.60	-	-	-	-	-	-	42°	-	38°	
	Average difference = 7°			Average difference = 4°						

Φ'_e, Φ'_c Friction angles extension, compression triaxial tests respectively.

$\Delta\Phi'_{e-c}$ Difference between extension and compression friction angles.

$\Delta\Phi'_{d-u}$ Difference between drained and undrained friction angles.

Table 5.2(a)

Passive Stress Relief Tests on Loose Sand

Test No.	Initial Voids Ratio	Cross sectional area of cell pressure mercury control tubes (mm^2)	Specimen shape during test
SPS1	0.80	7.92	Uniform deformation then necking at specimen extremities
SPS2	0.76	7.92	Necking at specimen extremities
SPS3	0.84	39.6	Necking at centre then at extremities
SPS4	0.70	39.6	Necking at extremities
SPS5	0.76	1.98	Necking at centre then uniform deformation
SPS6	0.79	31.7	Necking at centre then at extremities
SPS7	0.78	31.7	Ditto

Table 5.2(b)

Passive Stress Relief Tests on Dense Sand

Test No.	Initial Voids Ratio	Cross sectional area of cell pressure mercury control tubes (mm^2)	Specimen shape during test
SPS/A/1	0.66	7.92	Necking mainly top and bottom of specimen with some at centre
SPS/A/Z	0.61	7.92	Ditto
SPS/A/3	0.60	1.98	Necking at top of specimen
SPS/A/4	0.61	7.92	Specimen formed with initial narrowing over centre. Necking at centre.
SP5/A/5	0.59	7.92	Specimen formed with initial narrowing over centre. Slight necking at top but generally uniform deformation throughout.
SPS/A/6	0.62	31.7	Specimen formed with initial narrowing over centre. Uniform deformation throughout, then necking top and bottom.
SPS/A/7	0.62	31.7	Necking at top of specimen, then uniform deformation.
SPS/A/8	0.62	7.92	Necking at centre of specimen and at top. (NB Lubricated ends used).
SPS/B/1	0.65	31.7	Necking at the top.

Table 5.3

Secant normalised shear modulus (G/p') for sand specimens (ref. Figs. 5.26 - 5.31).

Extension tests

	Dense		Loose	
Axial Strain	.02%	.1%	.02%	.1%
Undrained	400 - 800	200 - 300	-	-
Drained	600 - 800	200	200 - 400	120

Compression Tests

	Dense		Loose	
Axial Strain	.02%	.1%	.02%	.1%
Undrained	600	200	400	120
Drained	-	300	200 - 500	100 - 250

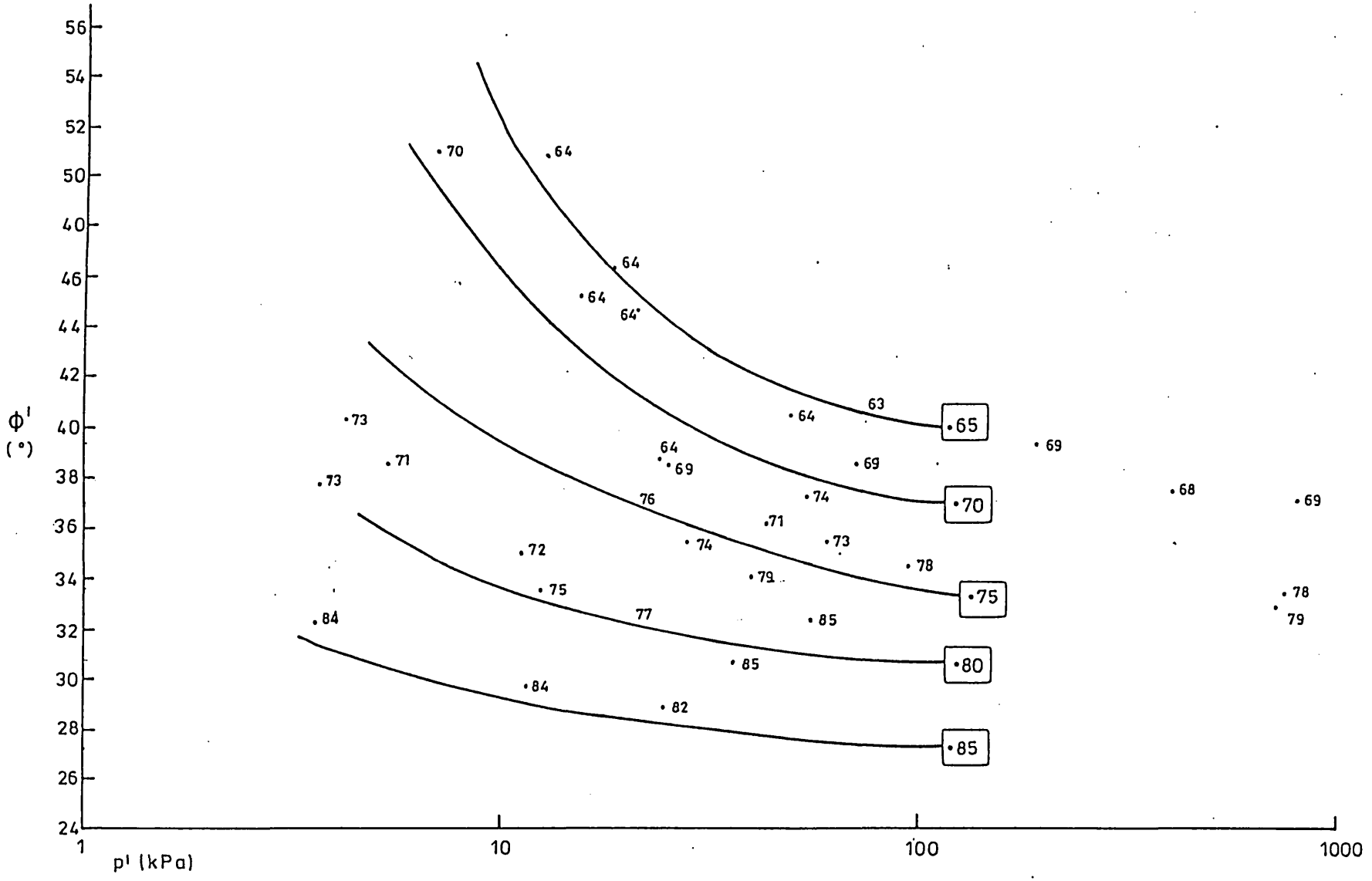


Figure 5.1. Sand: drained compression tests. ϕ'_m versus p' at peak (q/p').

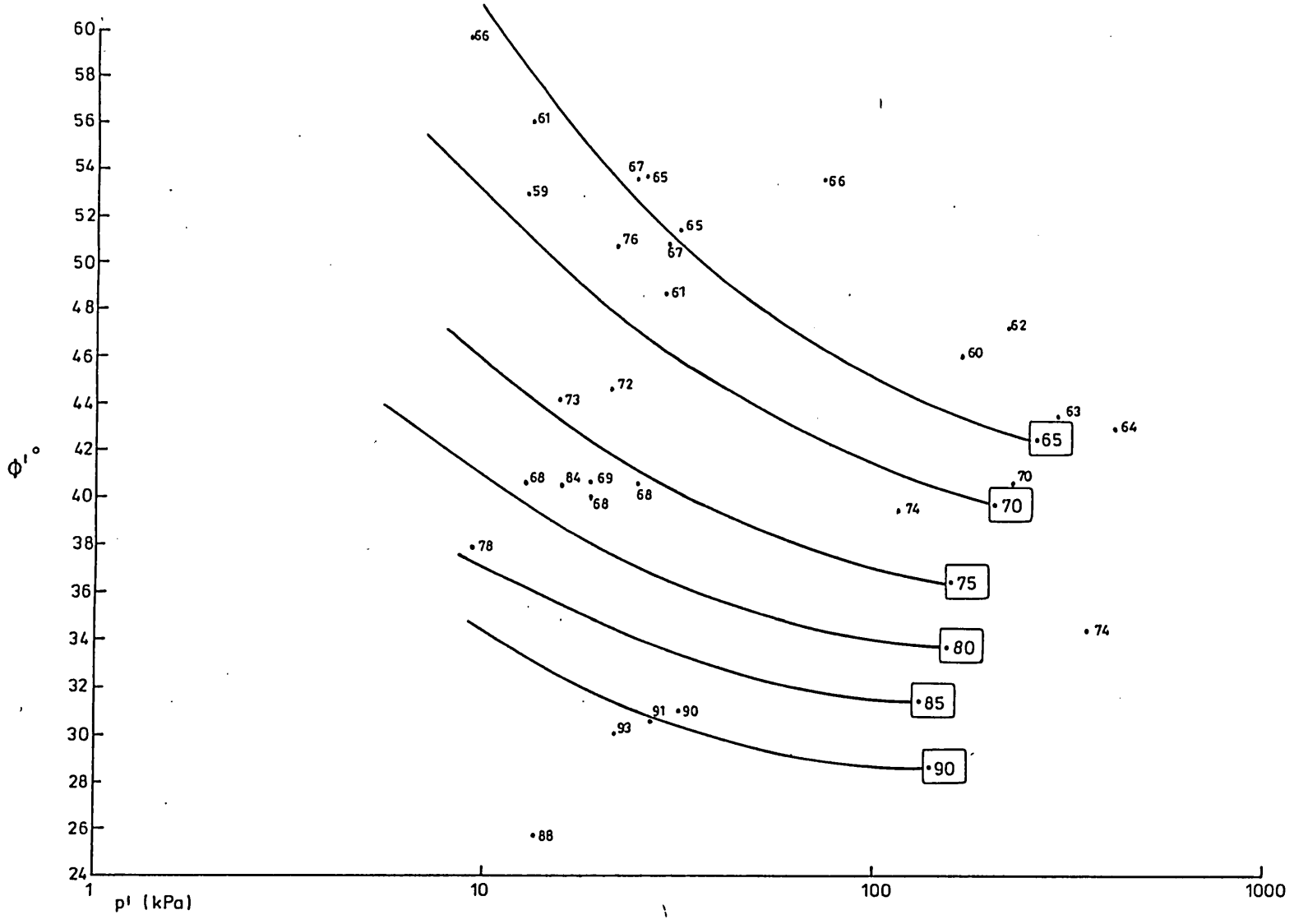


Figure 5.2. Sand: drained extension tests. ϕ'_m versus p' at peak (q/p').

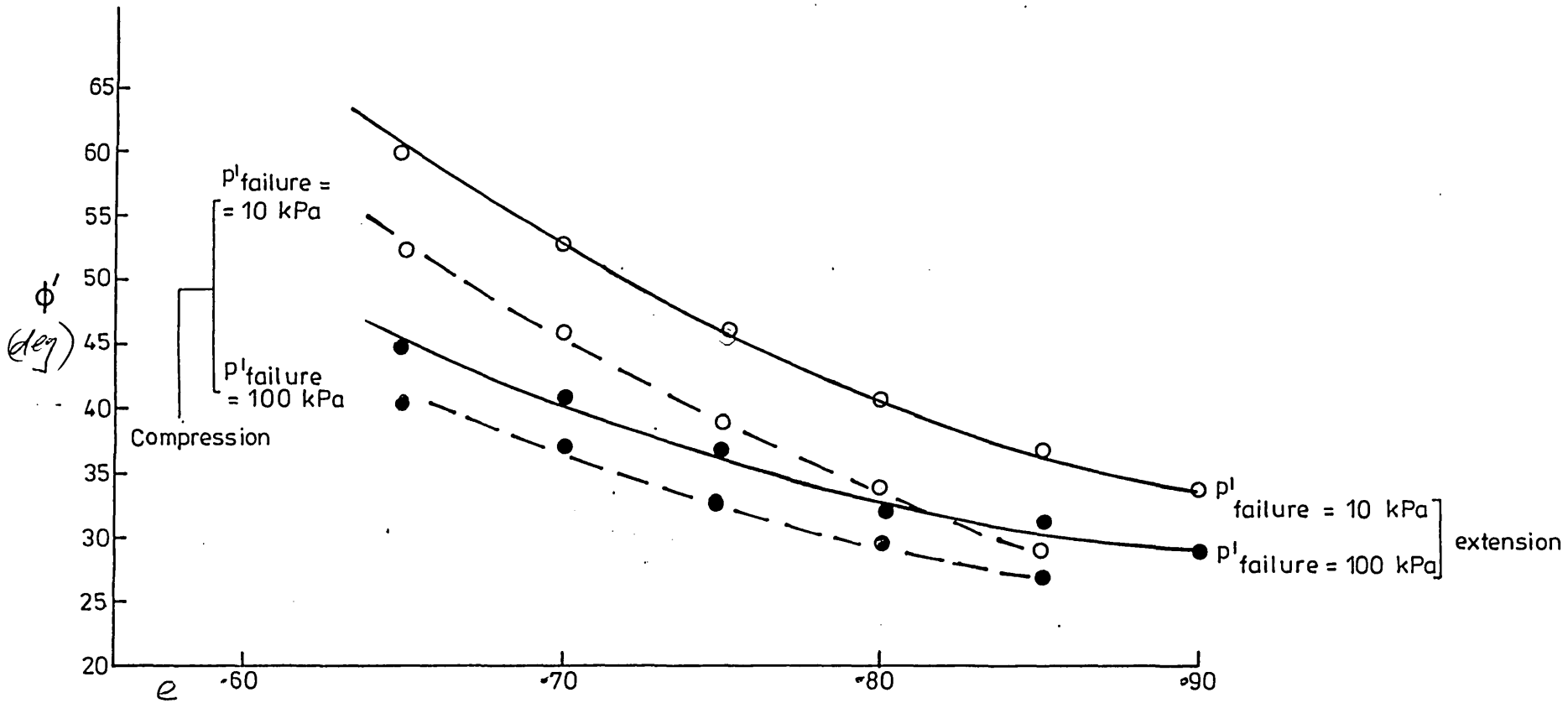


Figure 5.3. Sand: ϕ' versus e at both p' = 10 kPa and at p' = 100kPa (for maximum q/p').

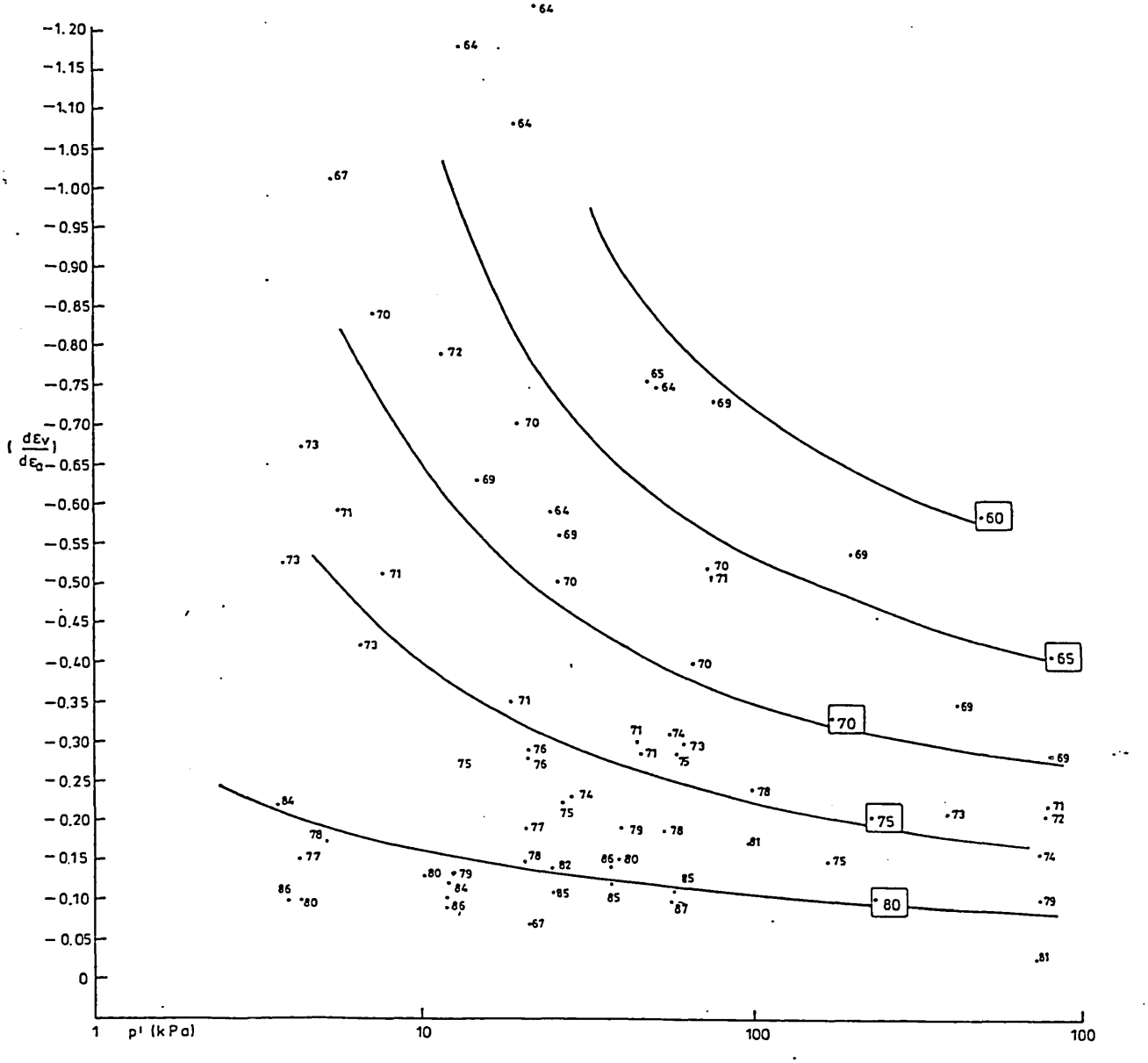


Figure 5.4. Sand: drained compression tests. $d\epsilon_v/d\epsilon_a$ versus p' at both q/p' peak and also q/p' ultimate.

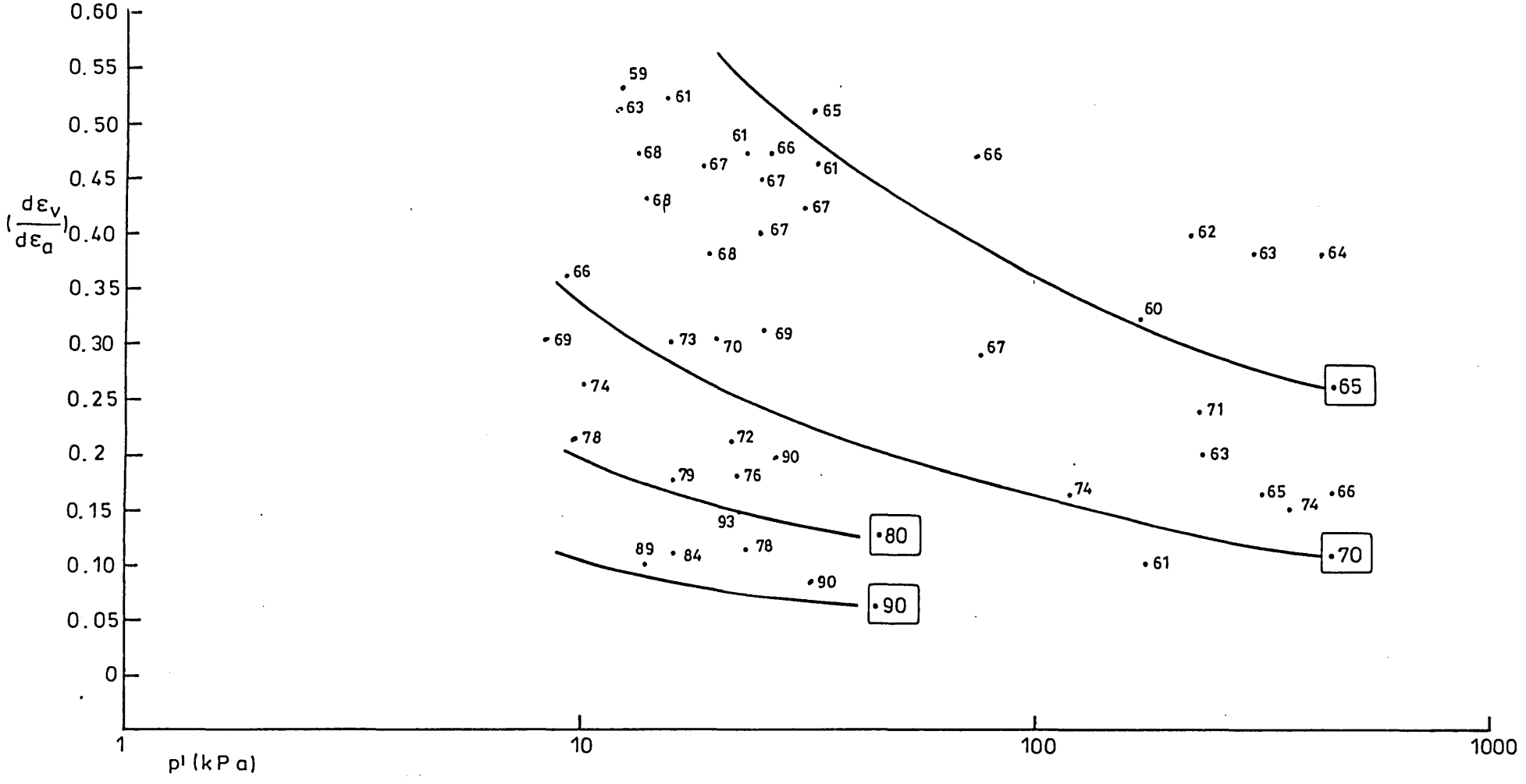


Figure 5.5. Sand: drained extension tests. $d\varepsilon_v/d\varepsilon_a$ versus p' at both q/p' maximum and also q/p' ultimate.

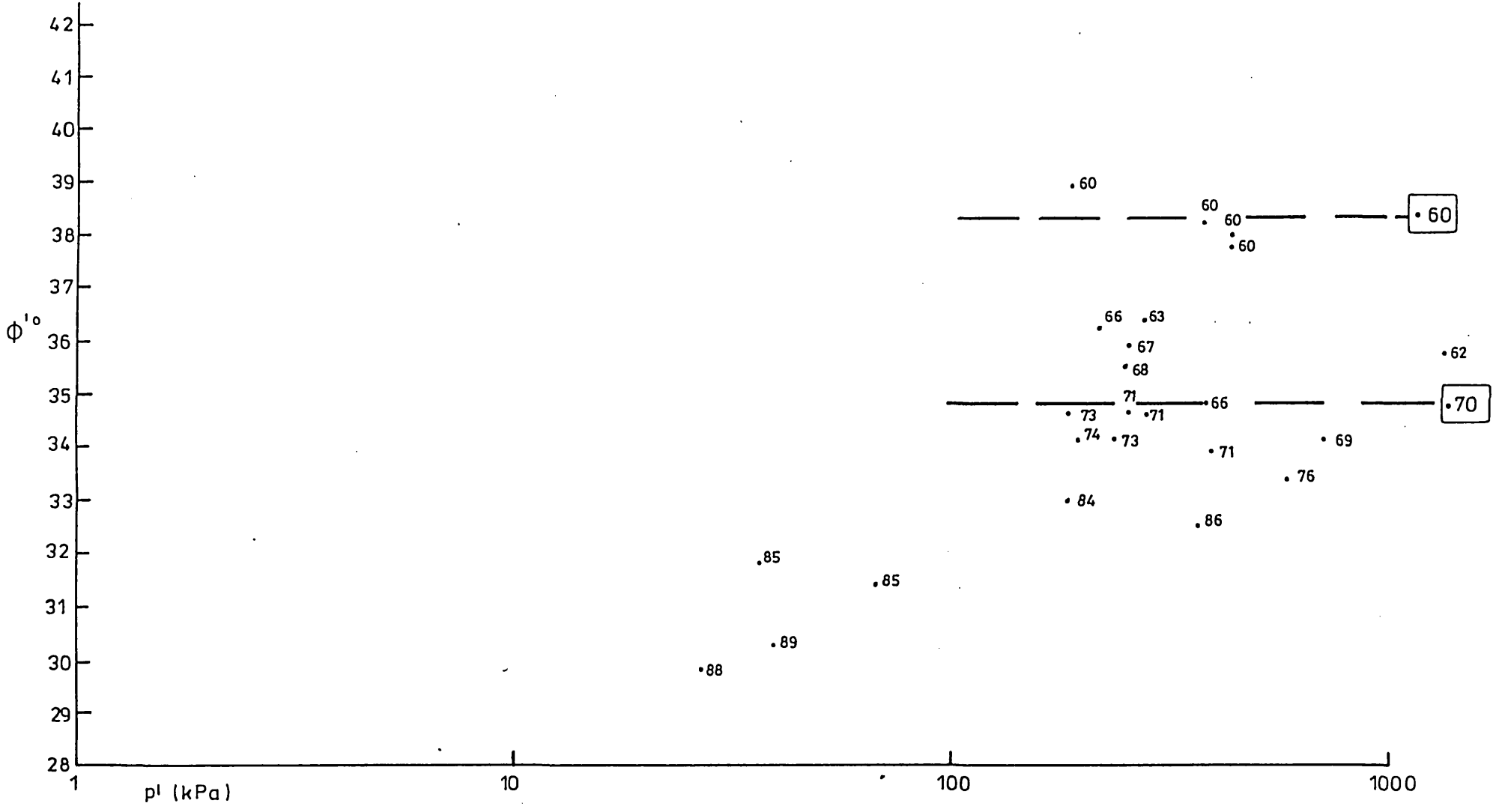


Figure 5.6. Sand: undrained compression tests. φ' versus p' at peak (q/p').

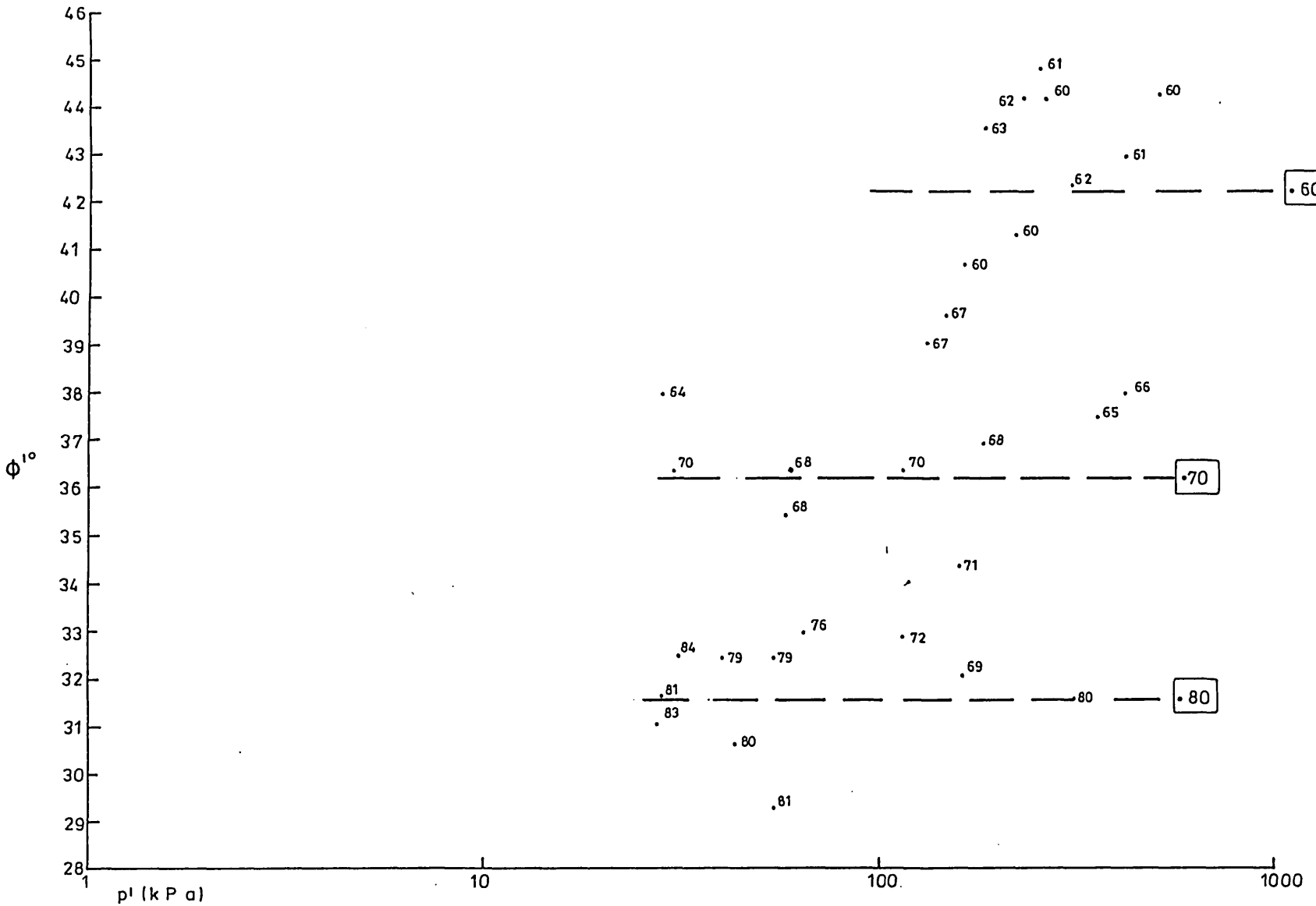


Figure 5.7. Sand: undrained extension tests. φ' versus p' at peak q/p'.

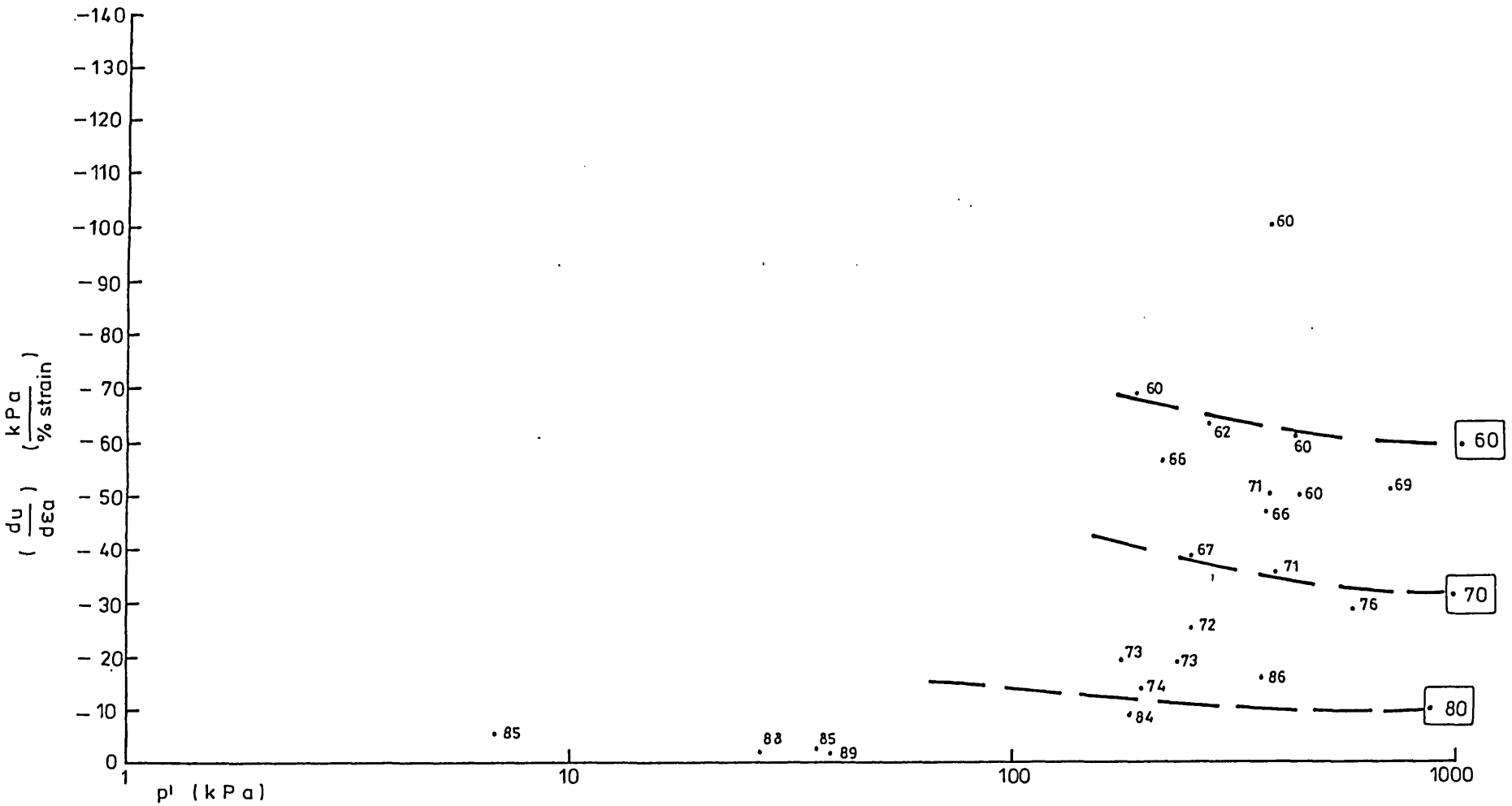


Figure 5.8. Sand: undrained compression tests. $du/d\varepsilon_a$ versus p' at peak q/p'.

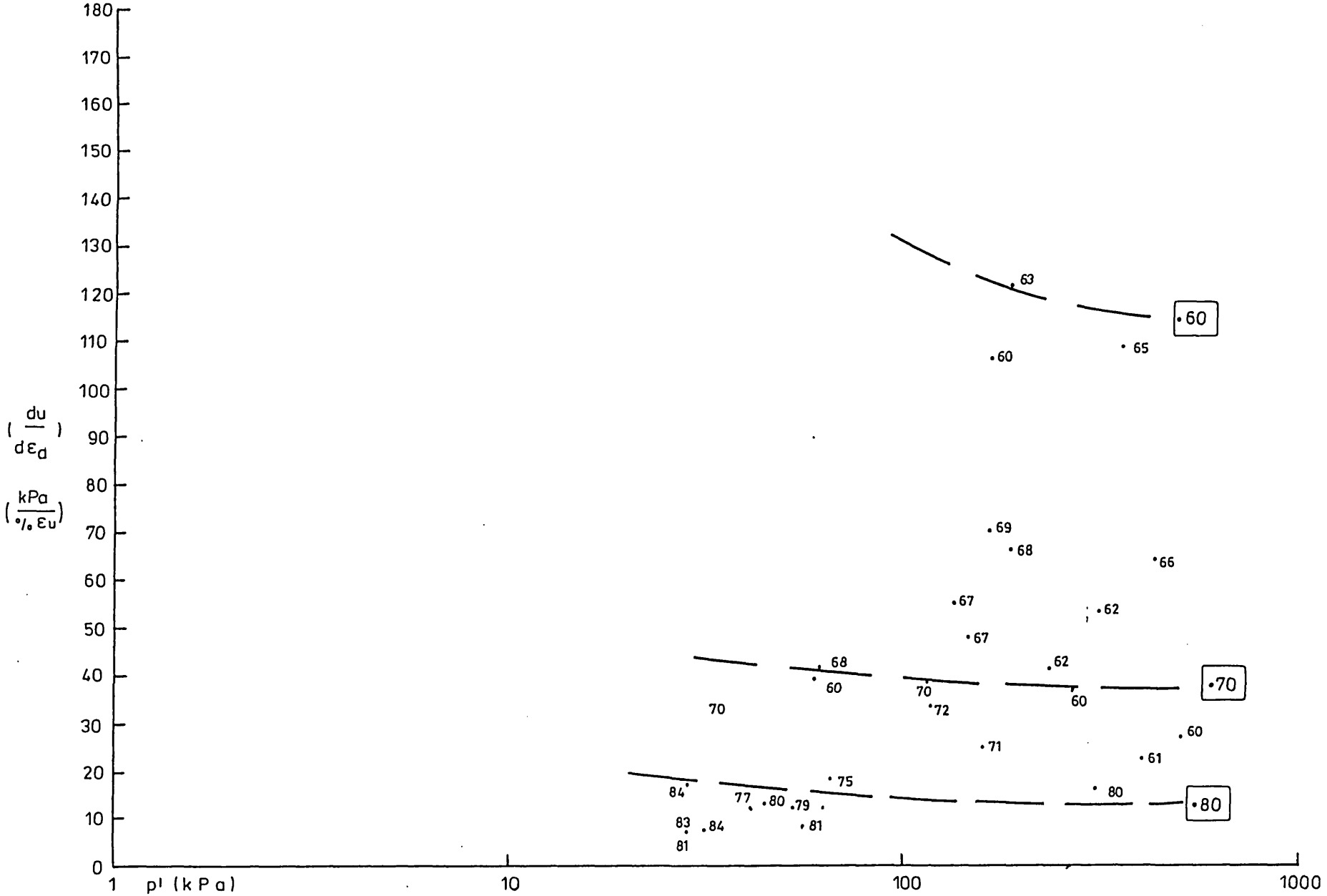


Figure 5.9. Sand: undrained extension tests. $du/d\varepsilon_a$ versus p' at peak q/p'.

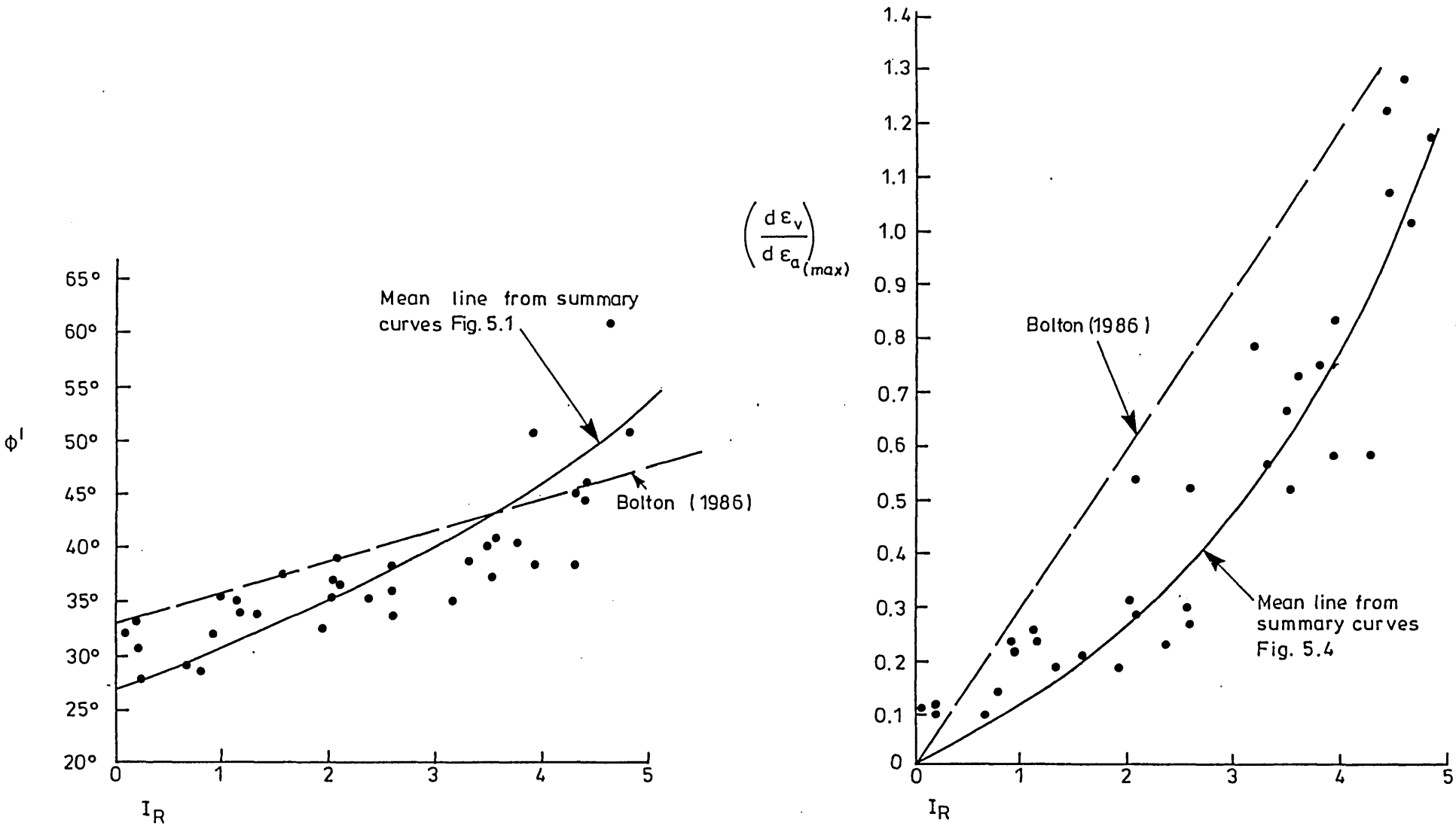


Figure 5.10. Sand: drained compression tests. ϕ', $d\varepsilon_v/d\varepsilon_a$ versus I_R: comparision with Bolton's (1986) correlation.

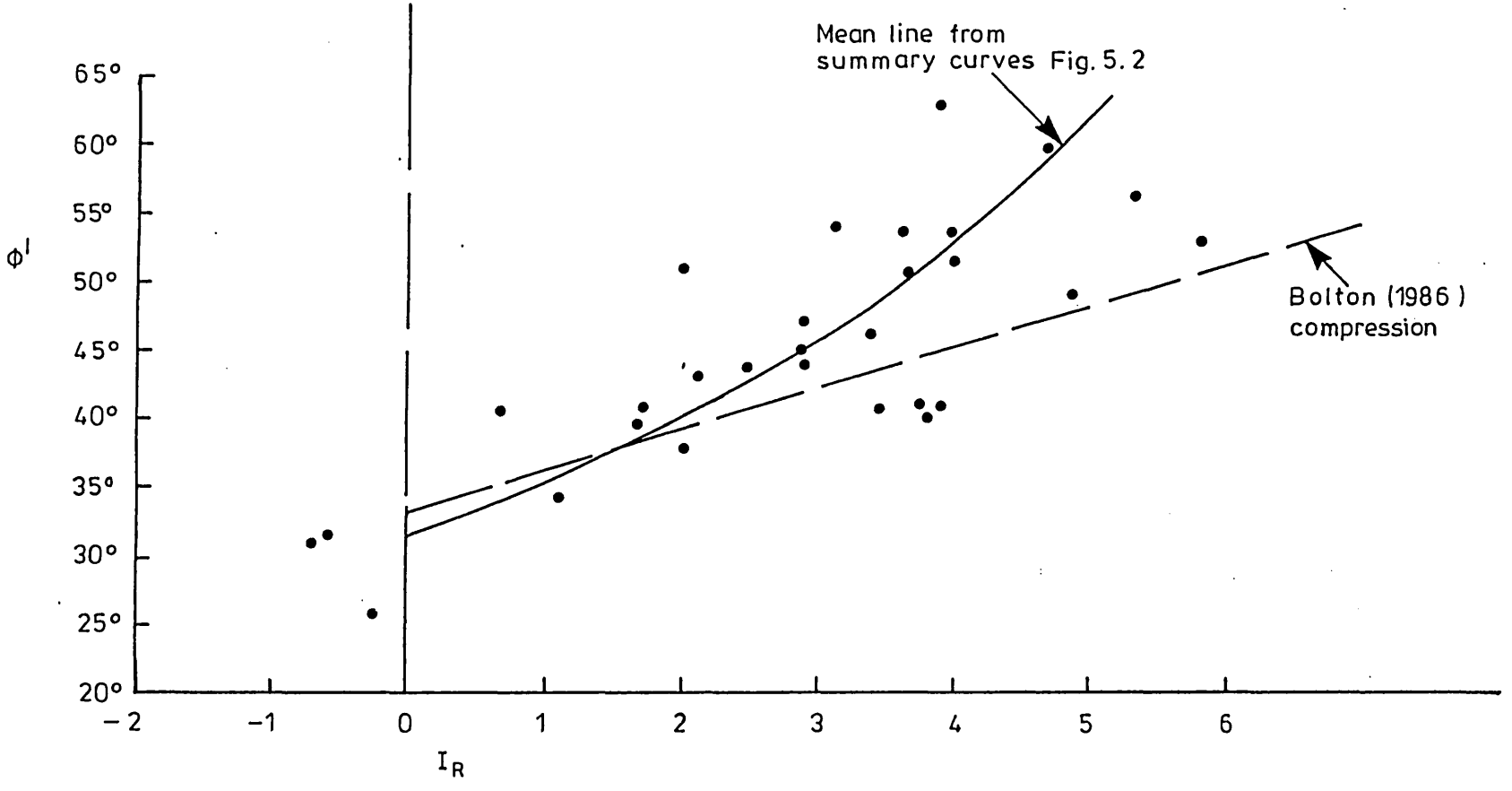


Figure 5.11. Sand: drained extension tests. ϕ' versus I_R: comparison with Bolton's (1986) correlation.

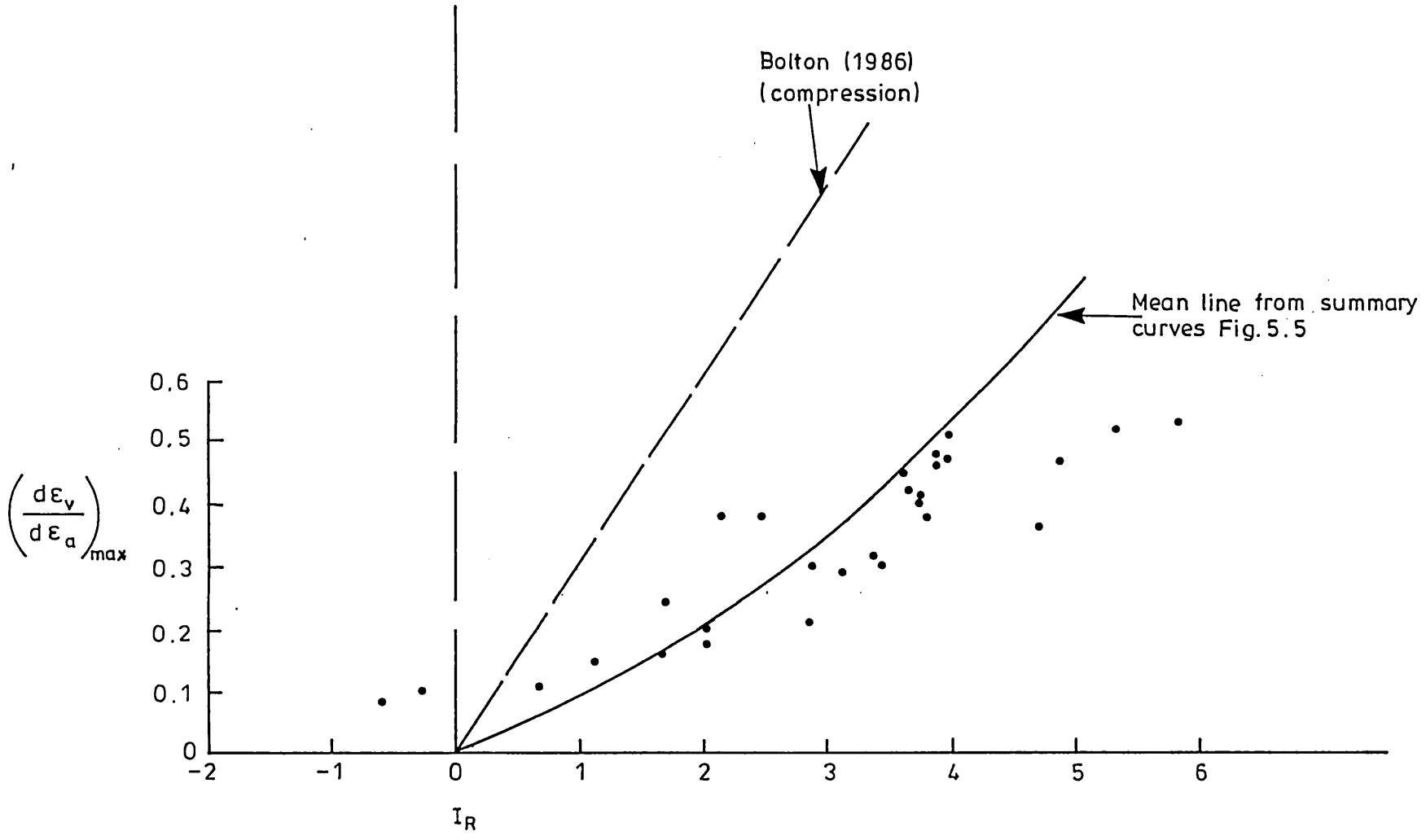


Figure 5.12. Sand: drained extension tests. $d\epsilon_v/d\epsilon_a$ versus I_R: comparison with Bolton's (1986) correlation.

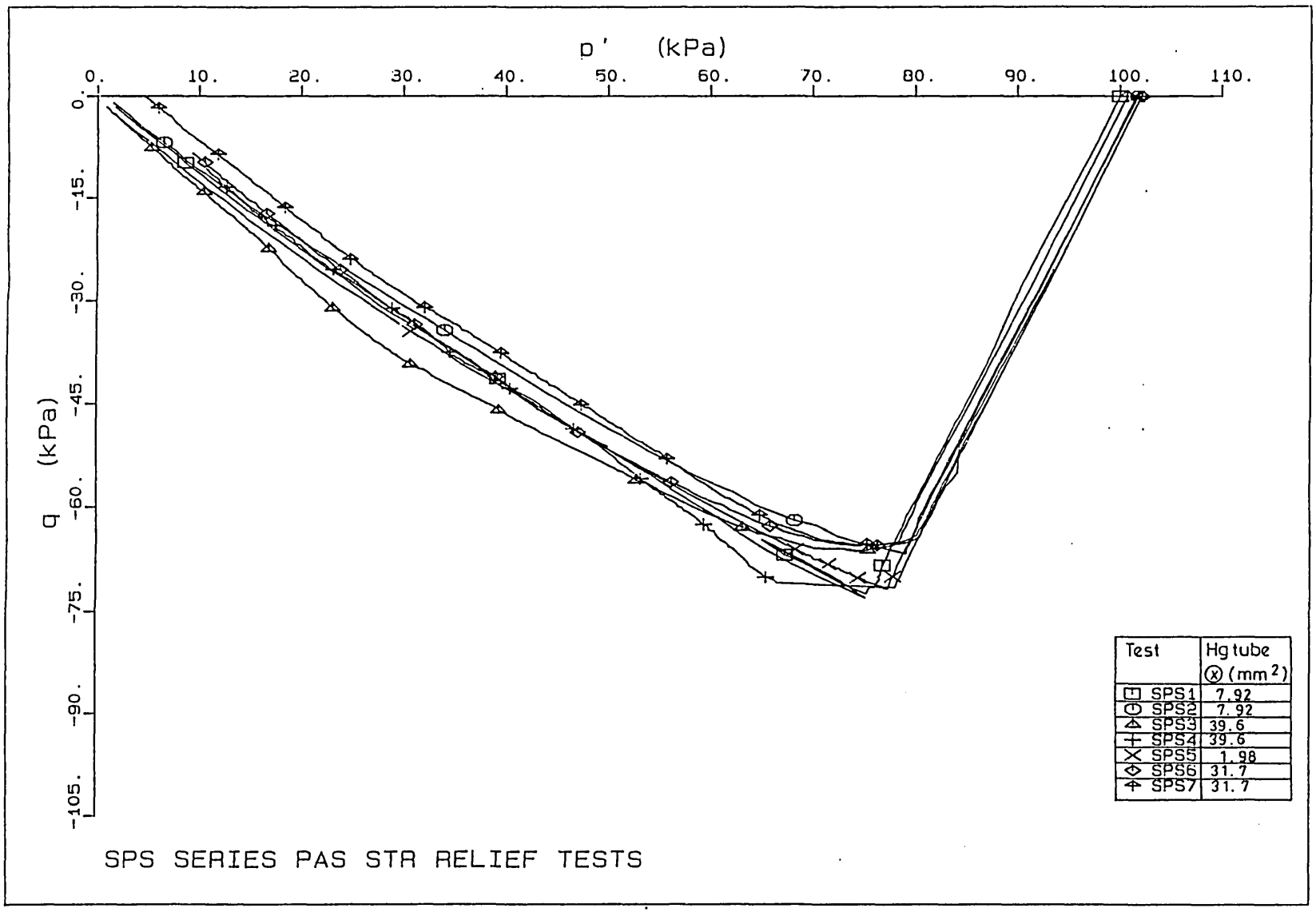


Figure 5.13. Stress paths for passive stress relief tests on loose sand specimens.

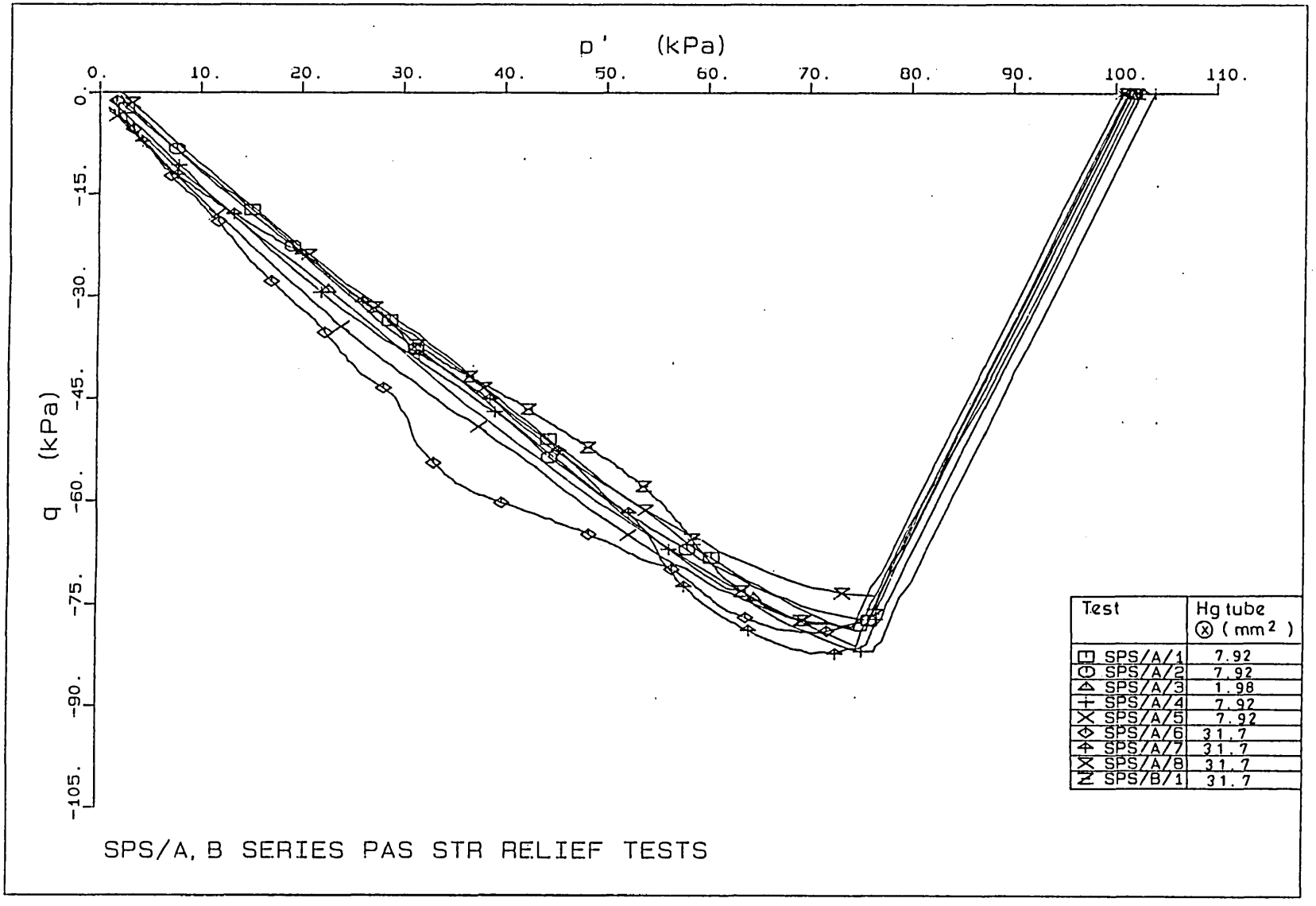


Figure 5.14. Stress paths for passive stress relief tests on dense sand specimens.

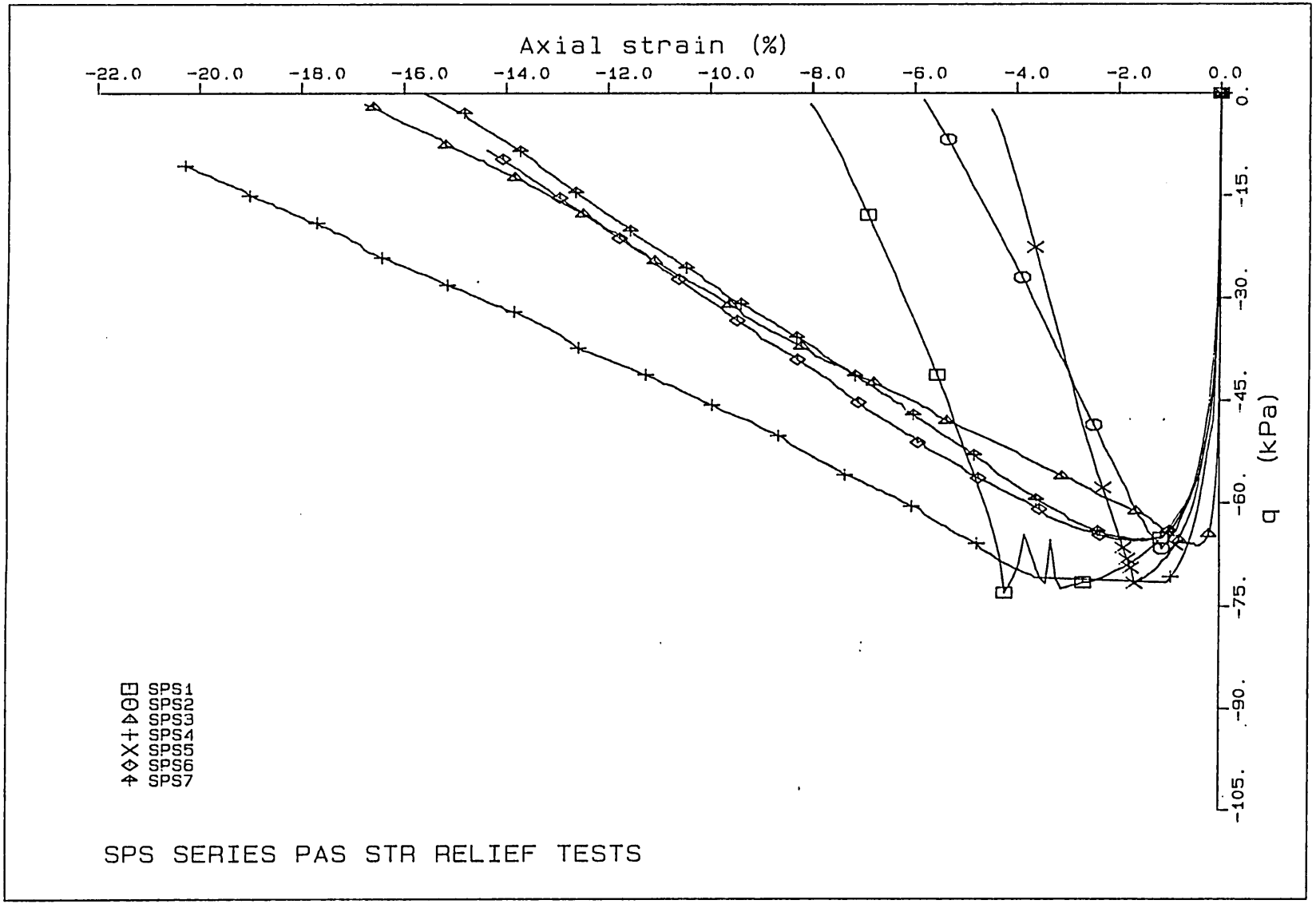


Figure 5.15. Passive stress relief tests on loose sand: q versus ϵ_a.

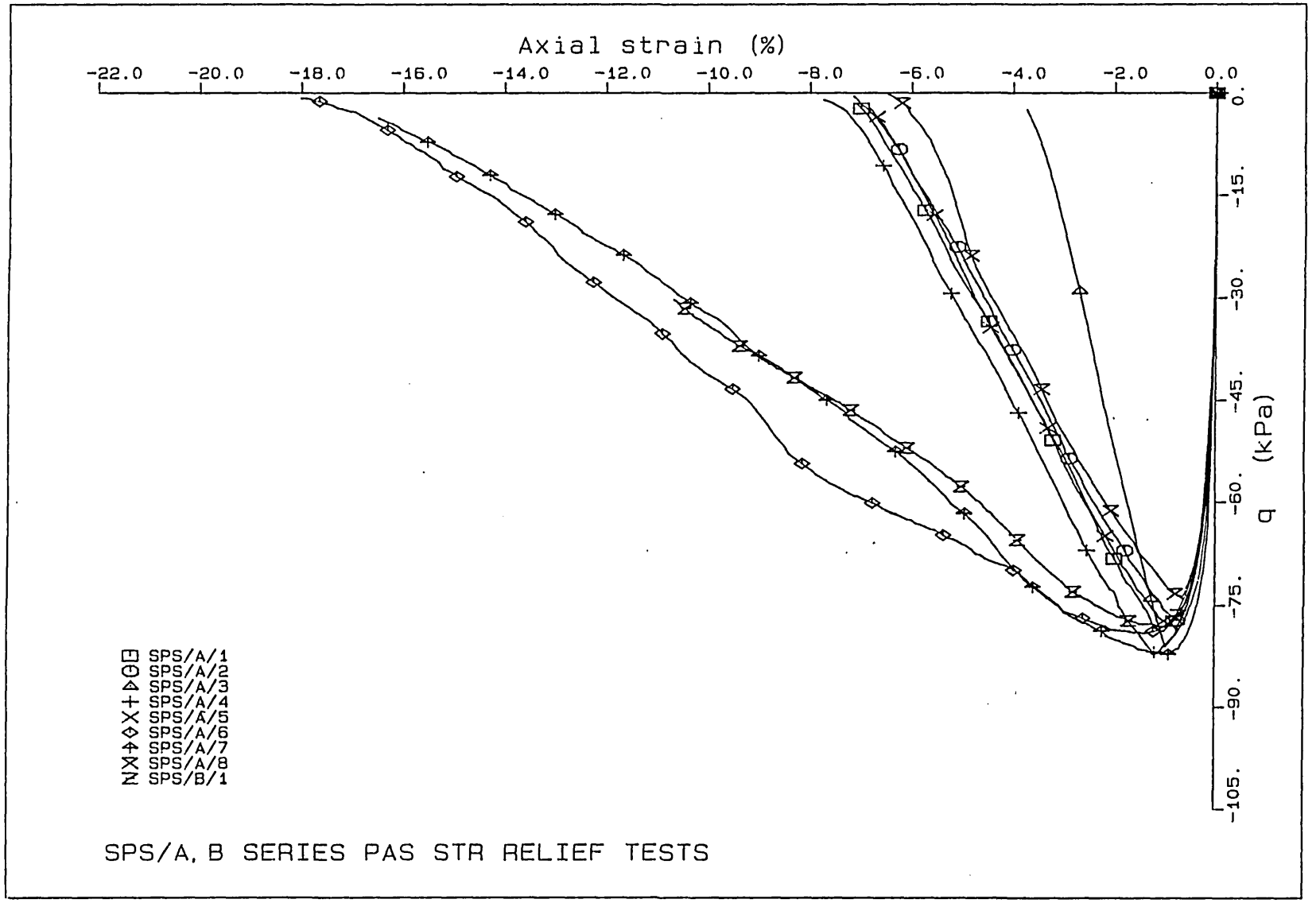


Figure 5.16. Passive stress relief tests on dense sand: q versus ϵ_a.

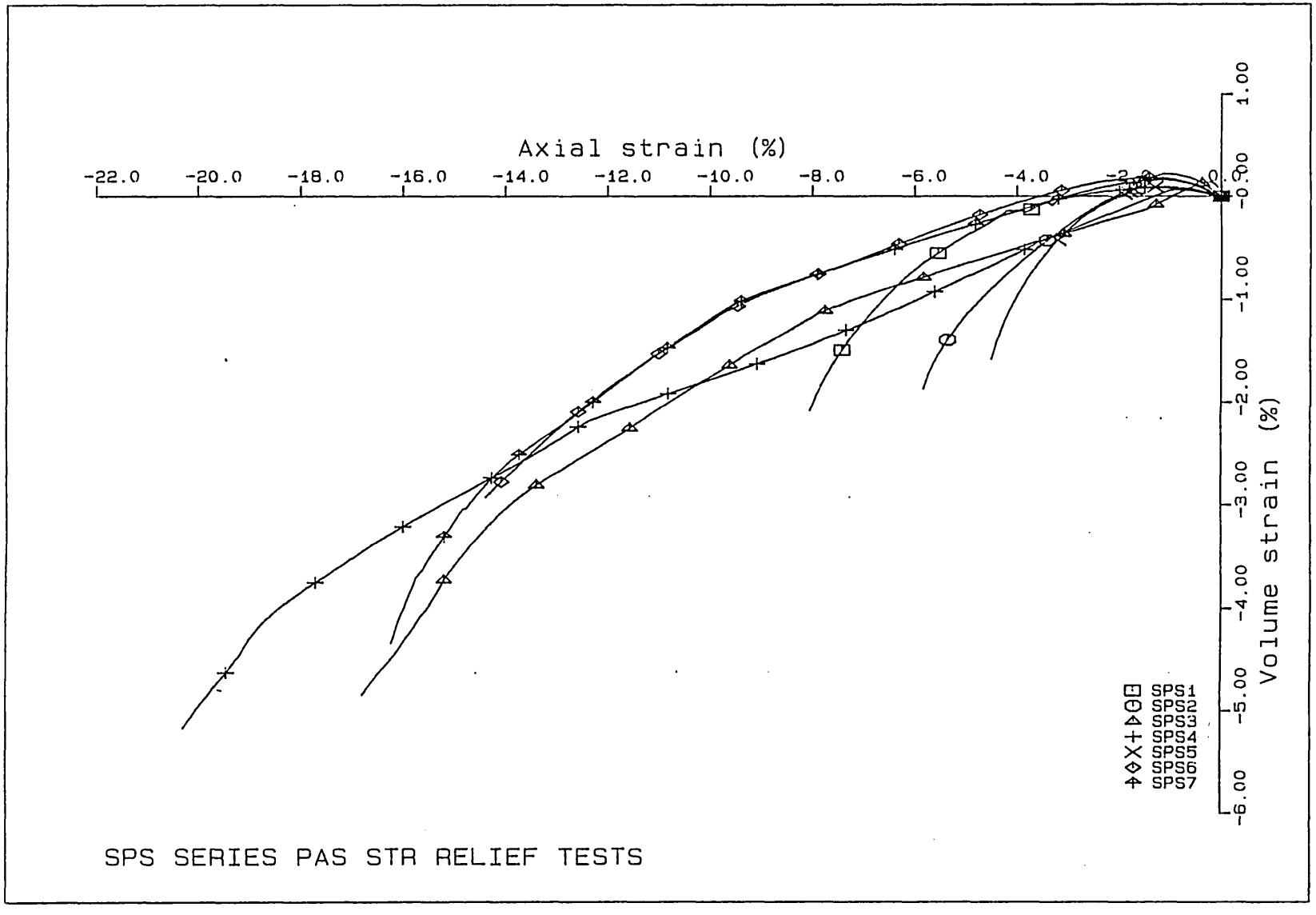


Figure 5.17. Passive stress relief tests on loose sand: ϵ_v versus ϵ_a.

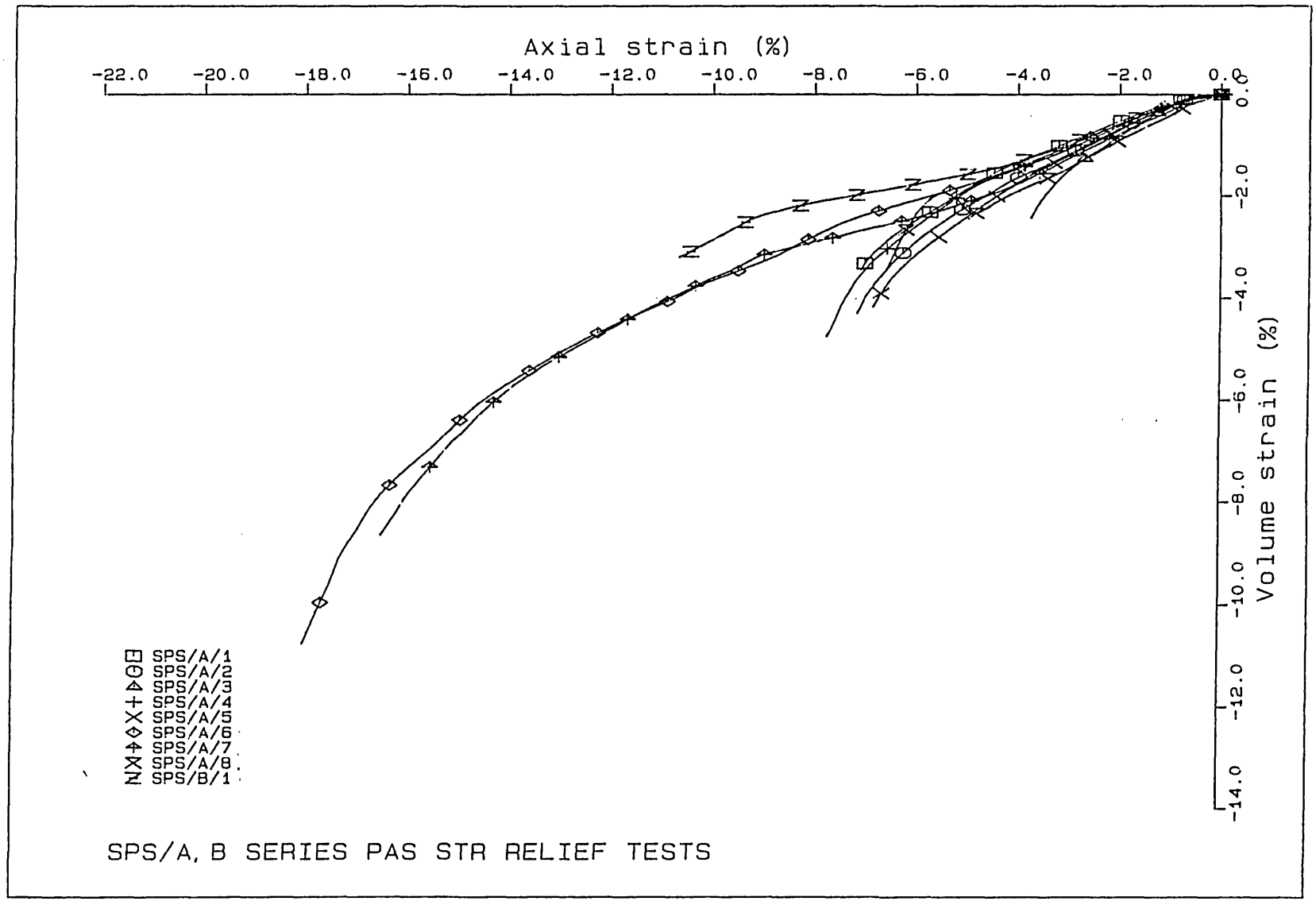


Figure 5.18. Passive stress relief tests on dense sand: ϵ_v versus ϵ_a.

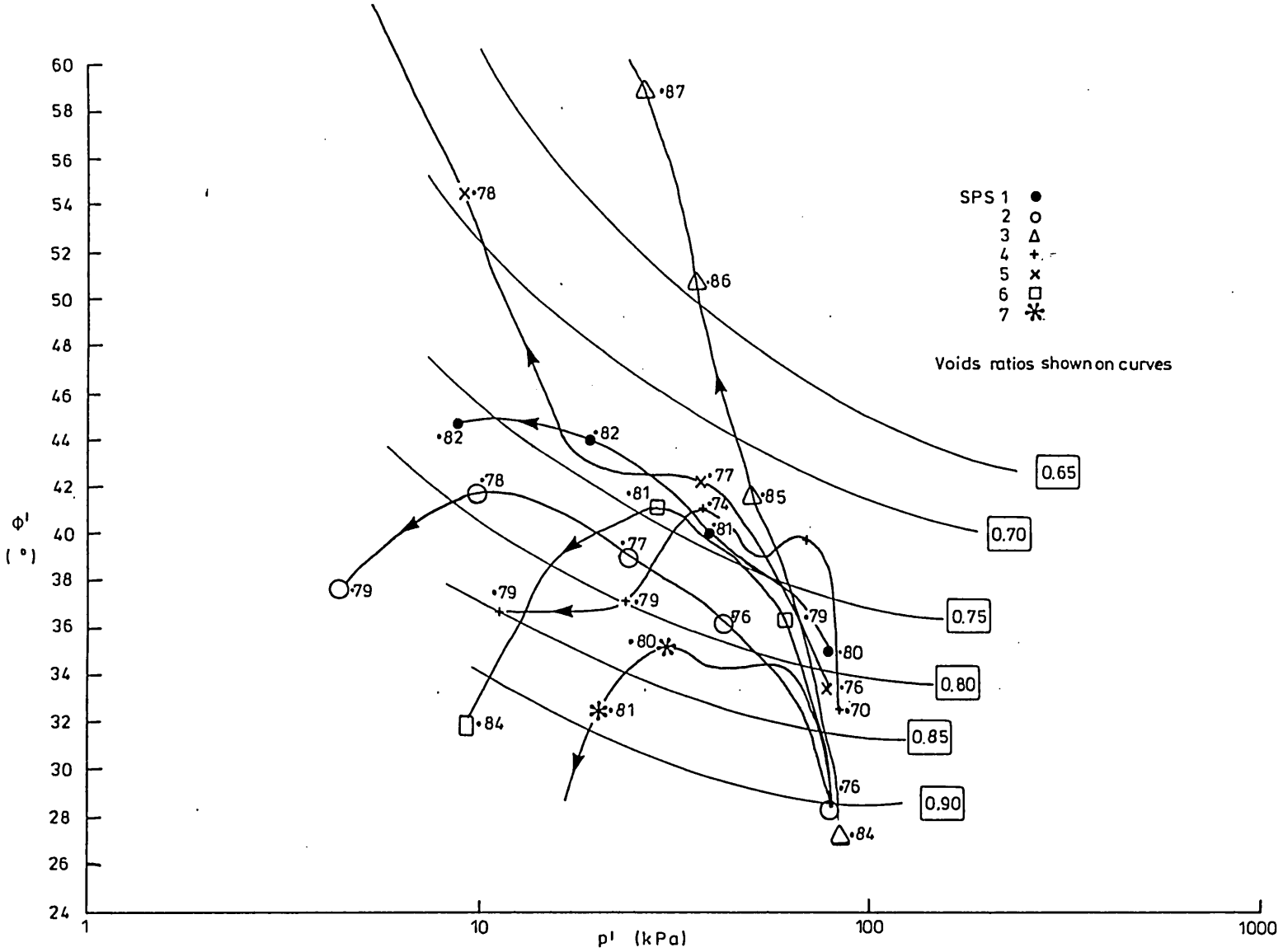


Figure 5.19. Passive stress relief stress paths for loose sand specimens: ϕ' versus p'.

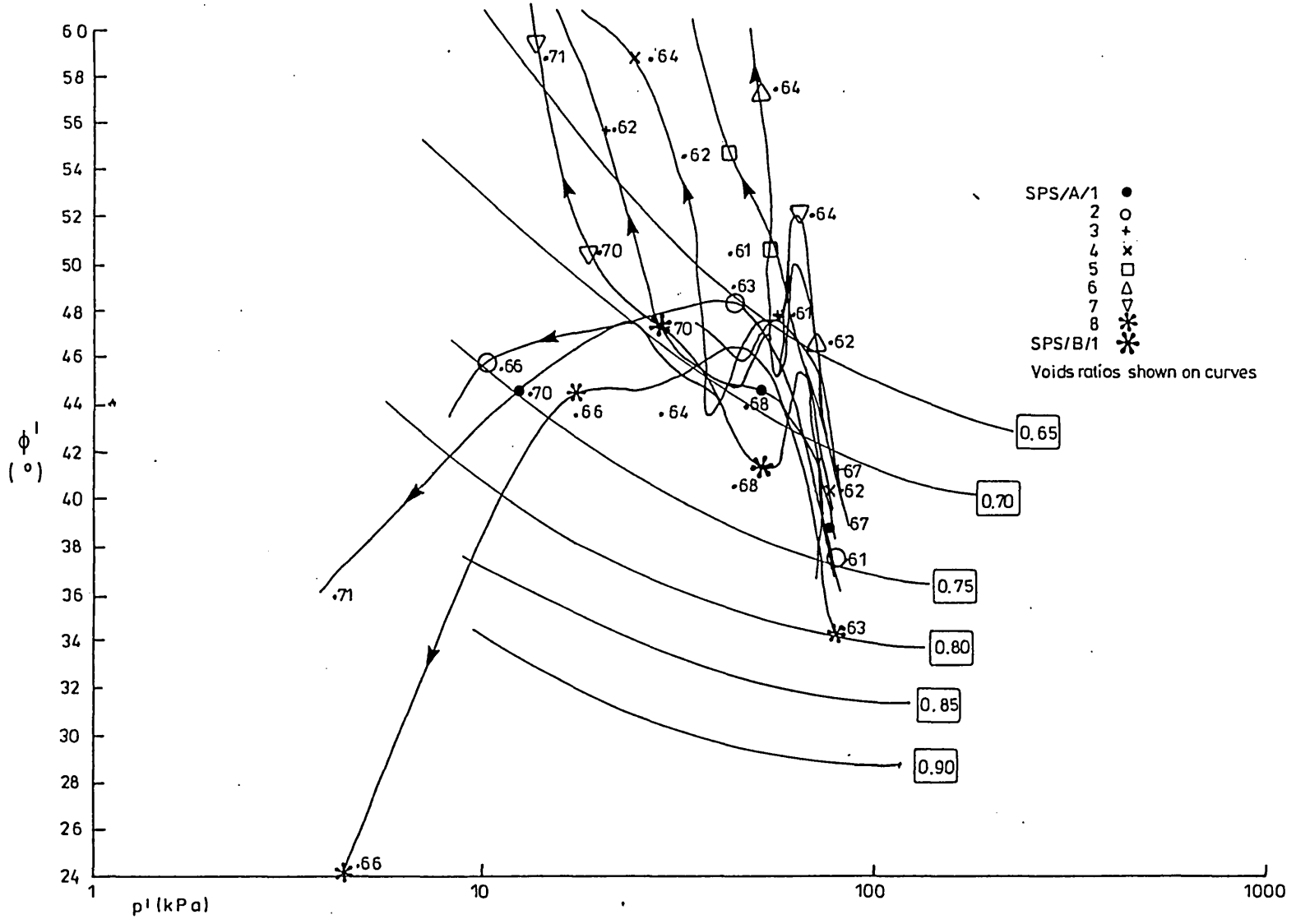


Figure 5.20. Passive stress relief stress paths for dense sand specimens: ϕ' versus p'.

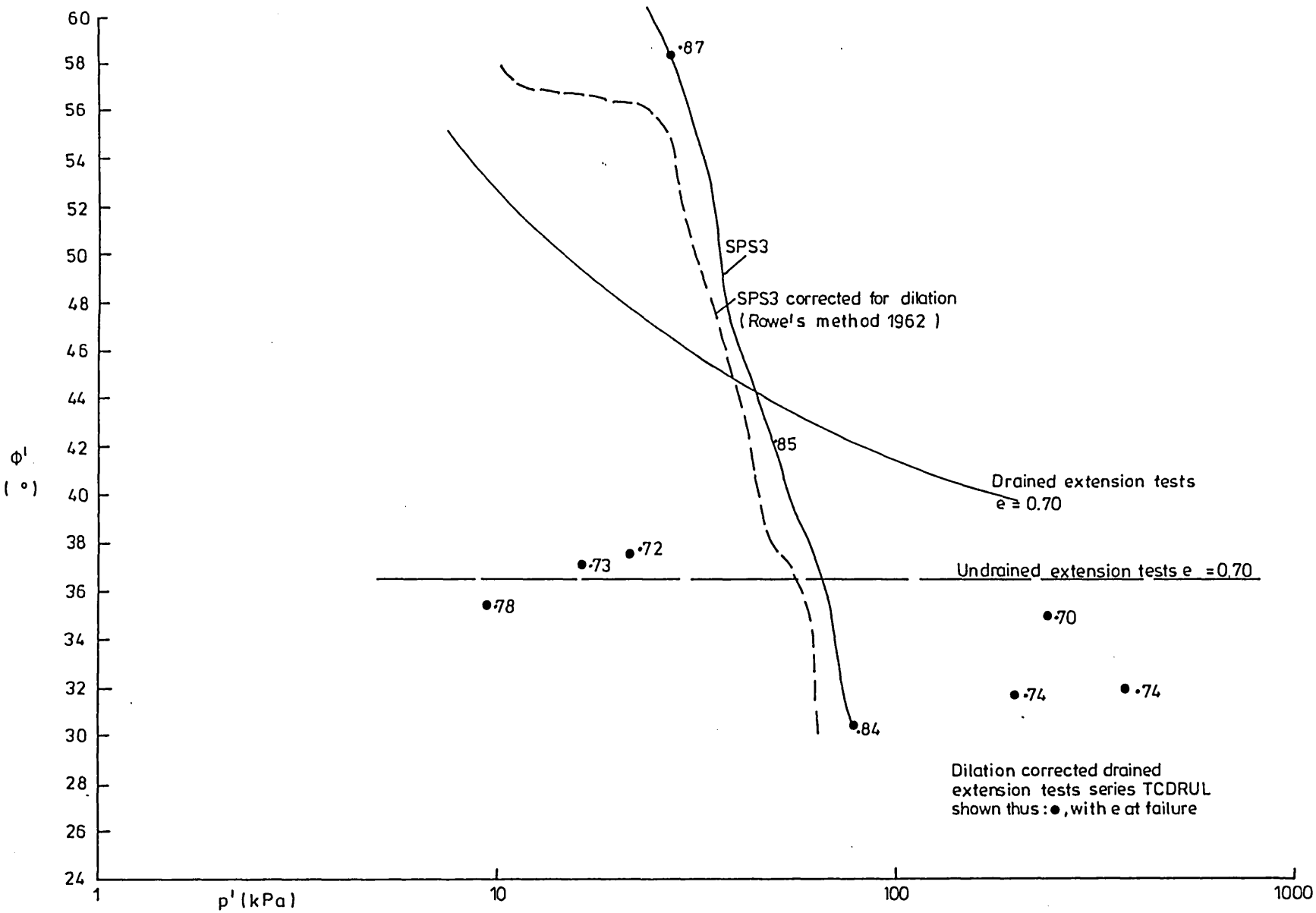


Figure 5.21. Sand tests: correction for dilation during shearing in passive stress relief tests SPS3 and drained extension tests TCDRUL.

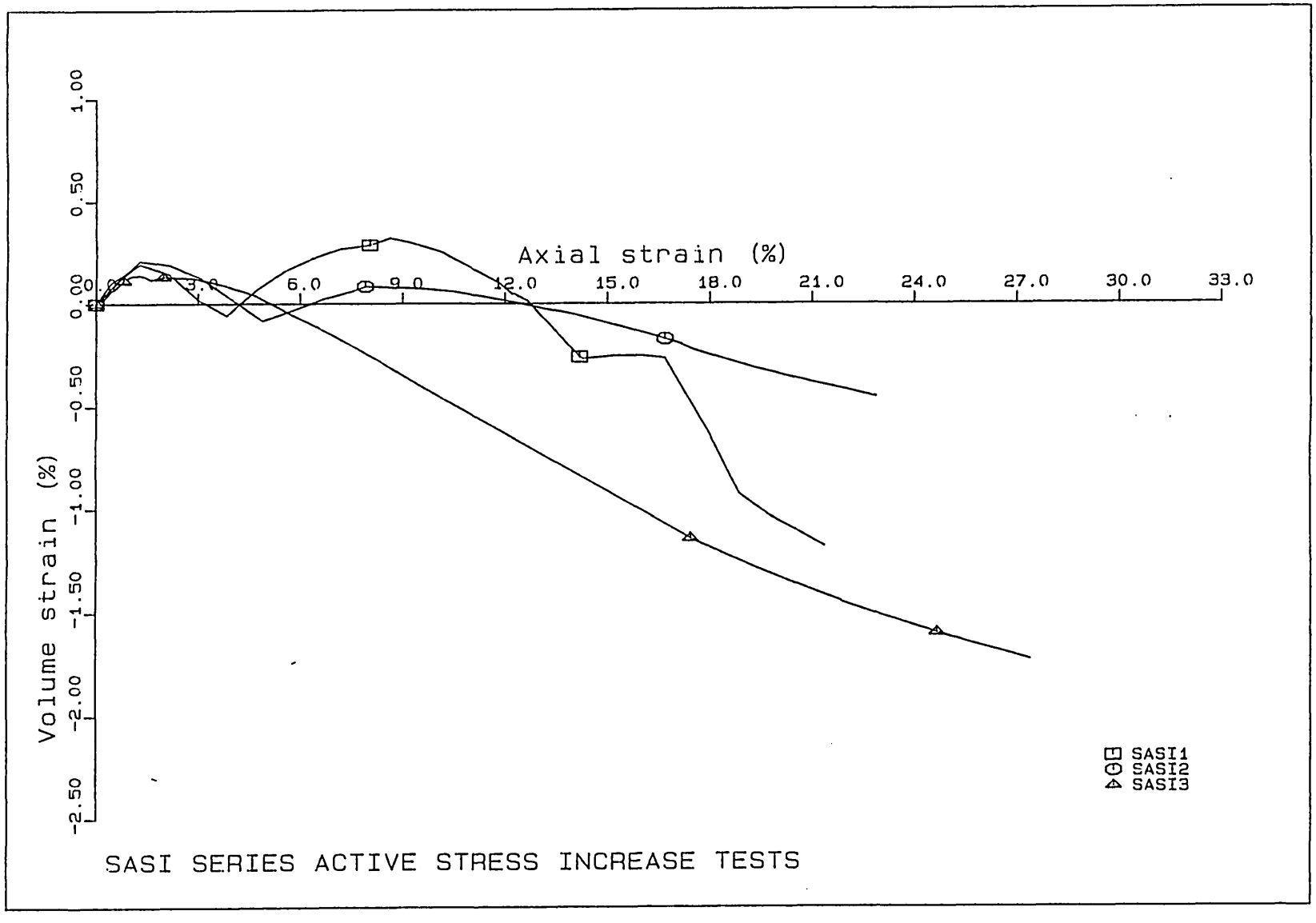


Figure 5.22. Active stress increase tests in sand: ϵ_v versus ϵ_a.

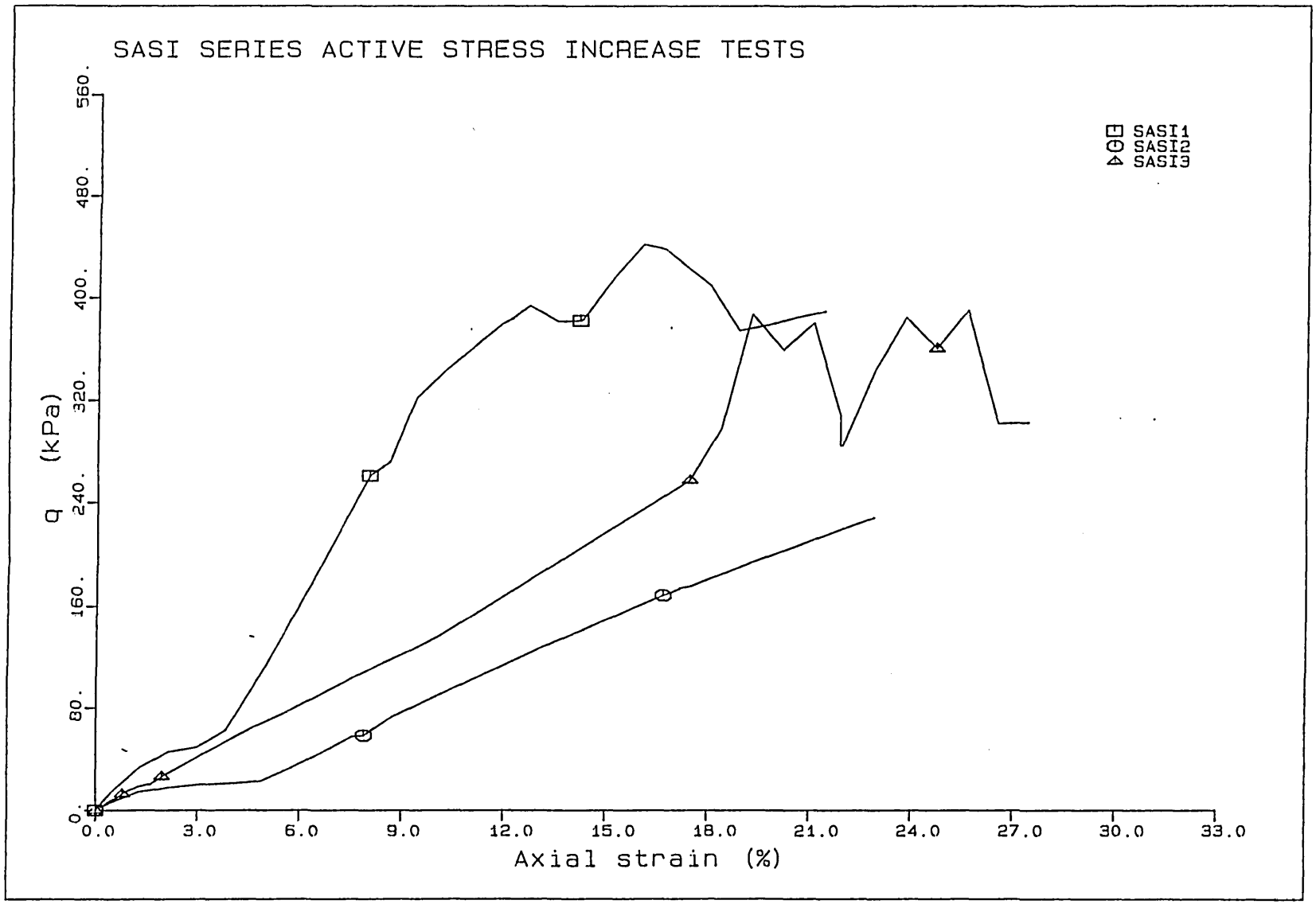


Figure 5.23. Active stress increase tests on sand: q versus ϵ_a.

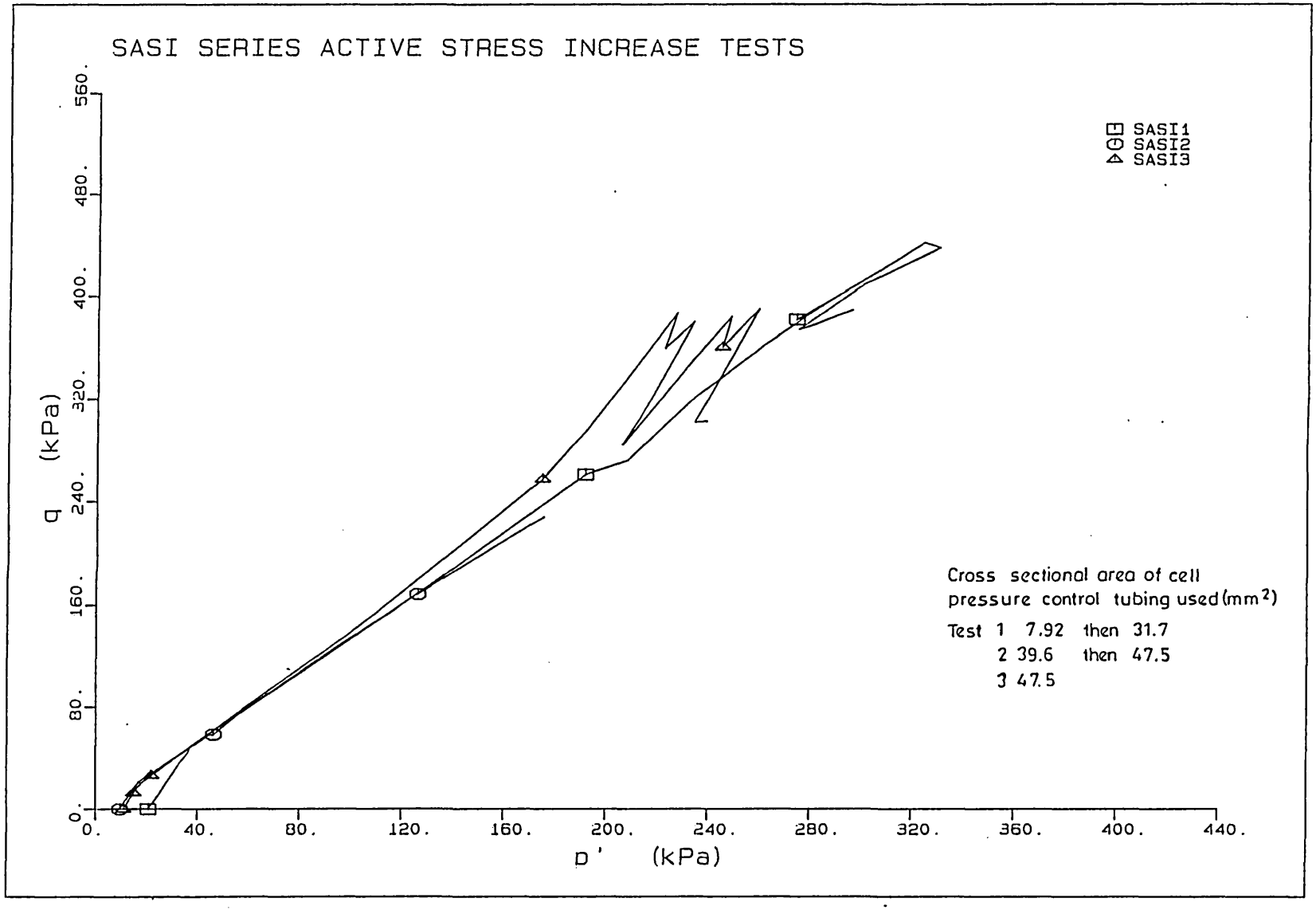


Figure 5.24. Active stress increase tests on sand: q versus p'.

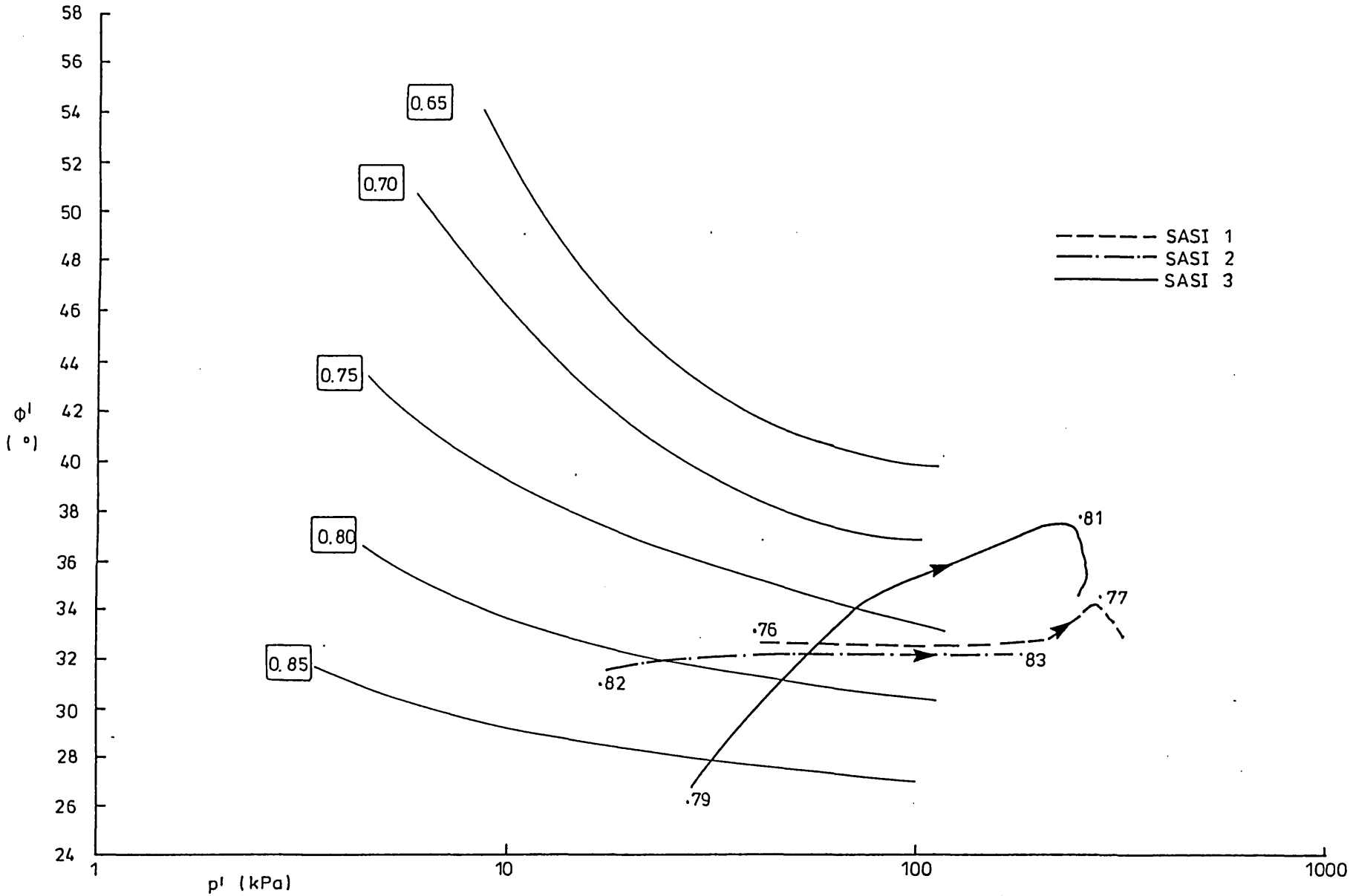


Figure 5.25. Active stress increase tests on sand: φ' versus p'.

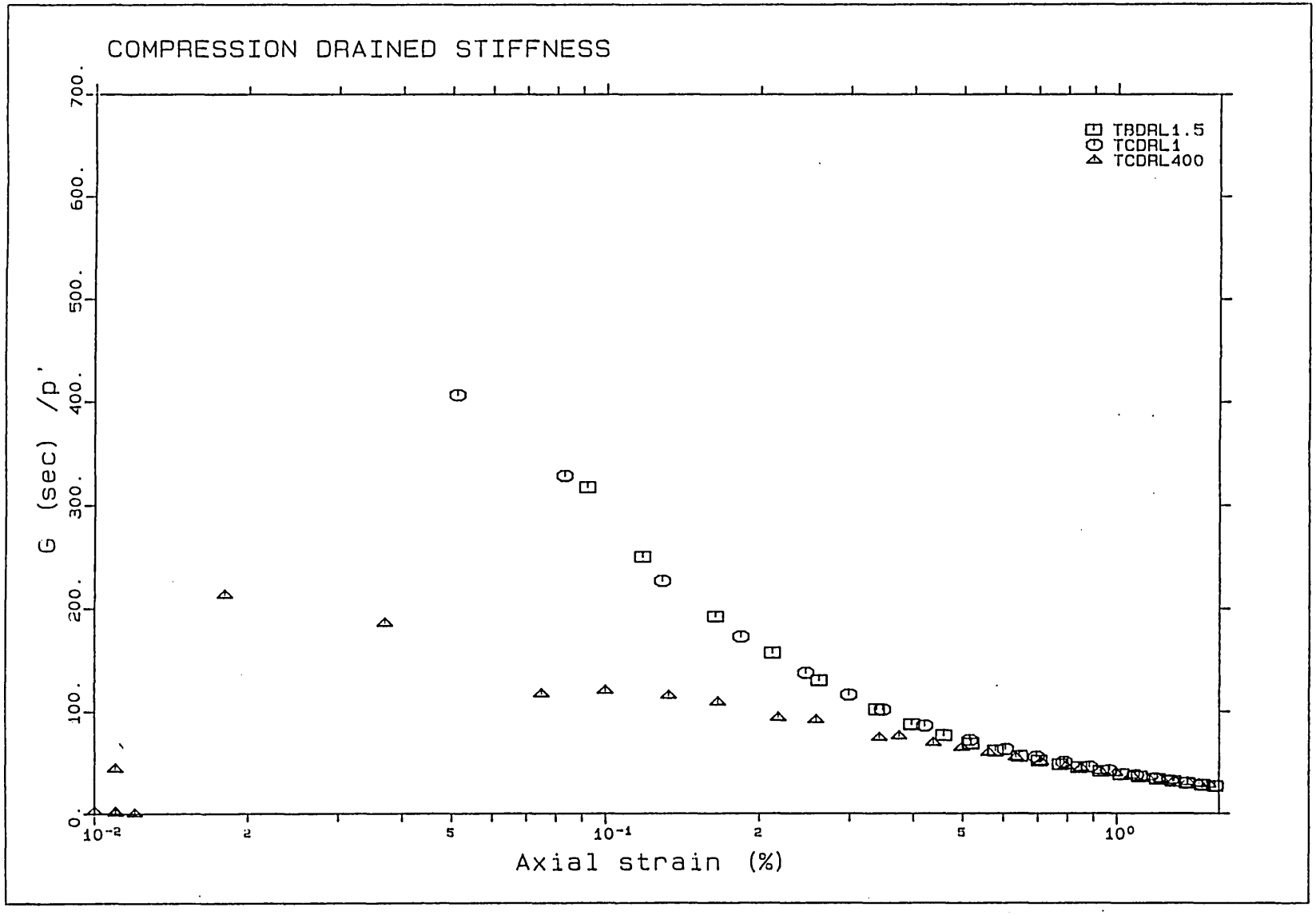


Figure 5.26. Dense and loose sand: compression drained shear modulus.

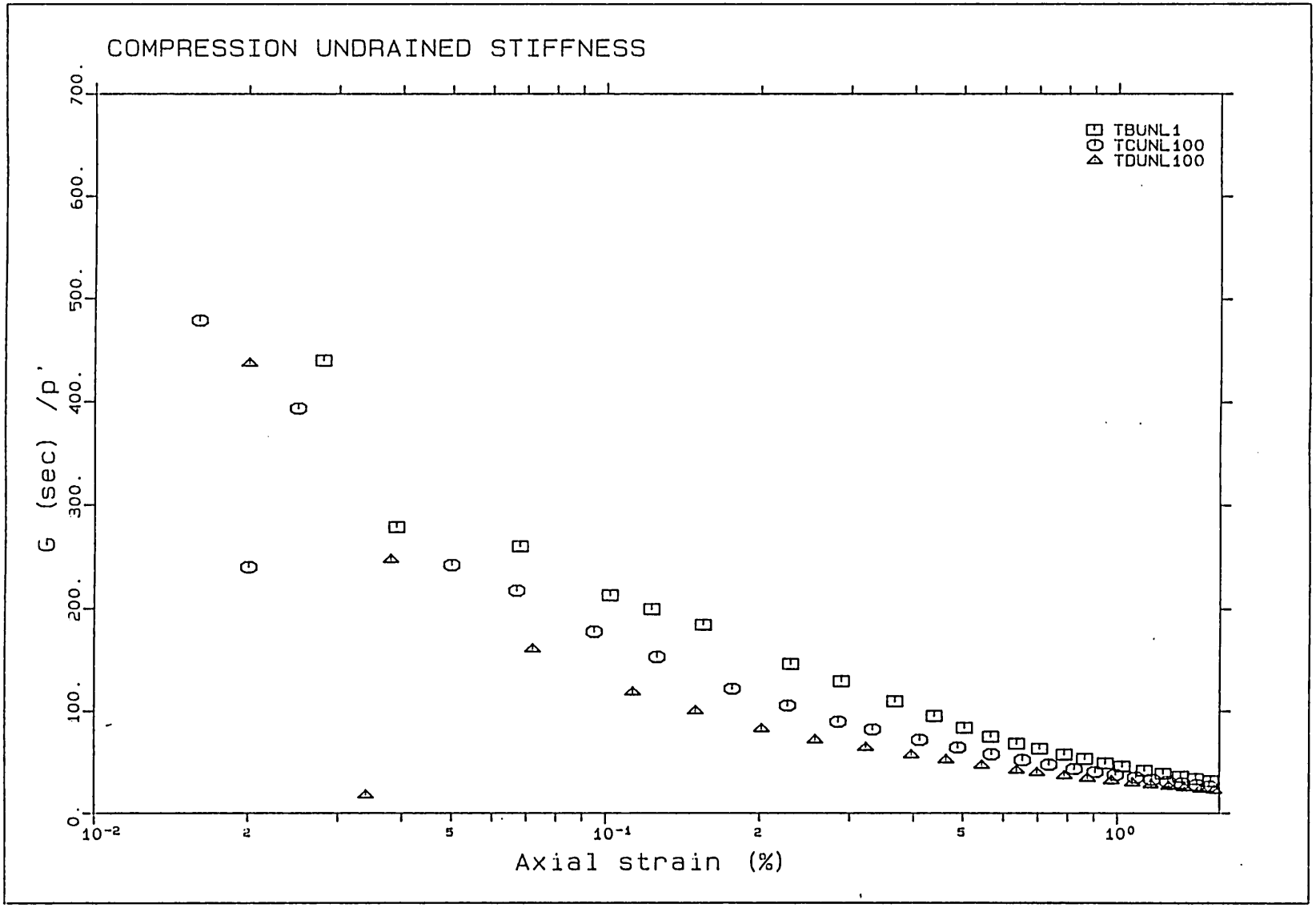


Figure 5.27. Dense and loose sand: compression drained shear modulus.

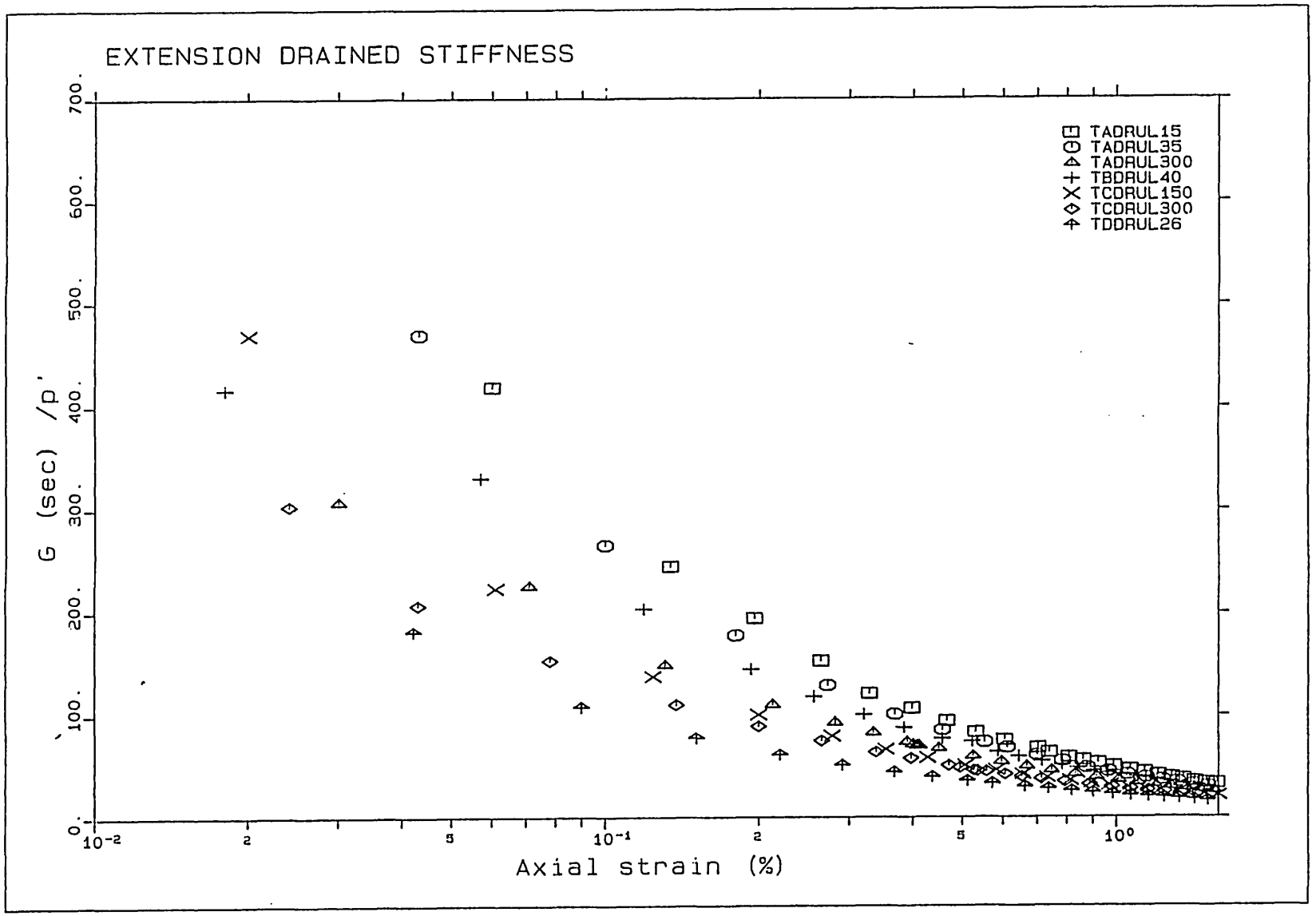


Figure 5.28. Dense and loose sand: extension drained shear modulus.

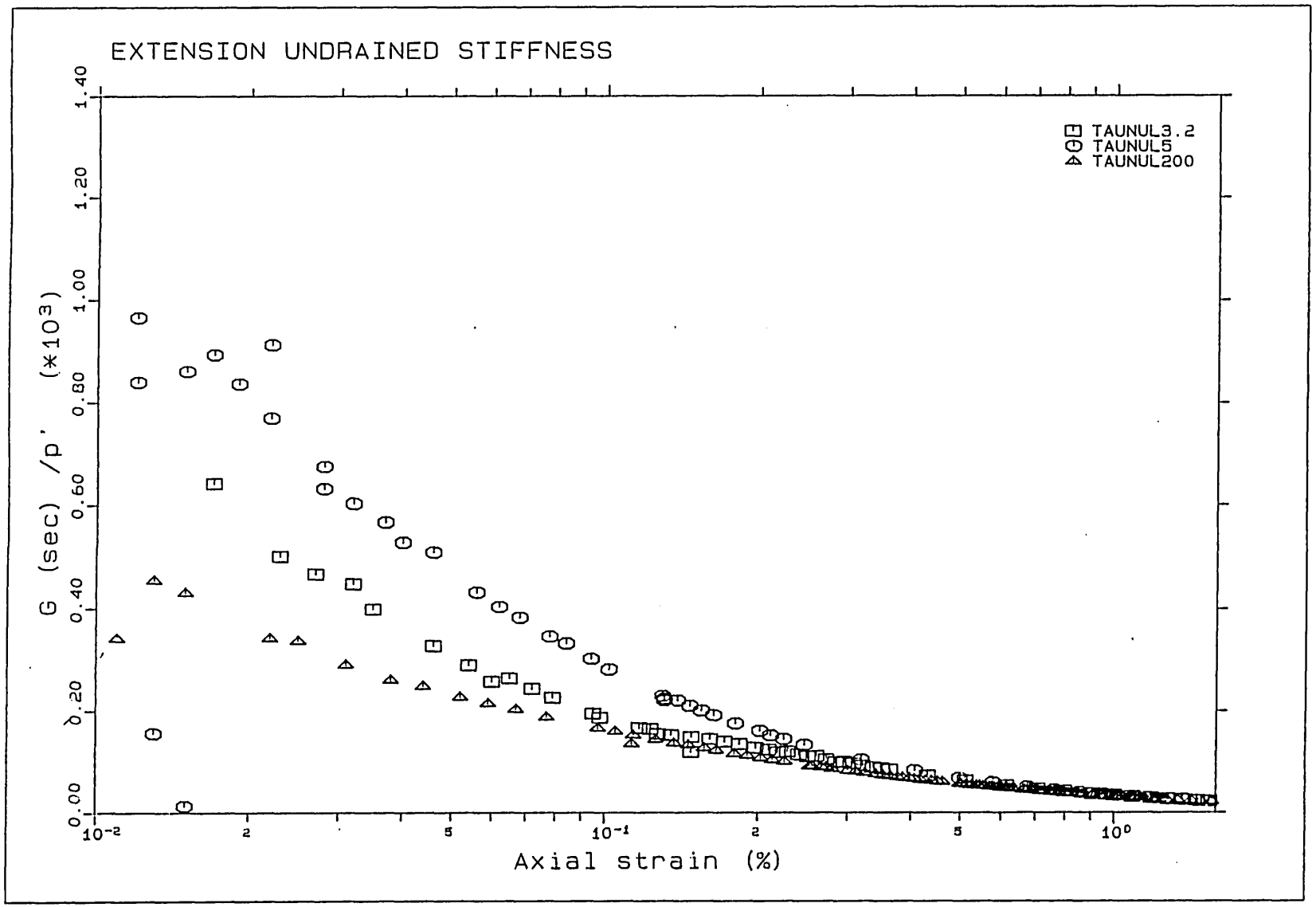


Figure 5.29. Dense sand: extension undrained shear modulus.

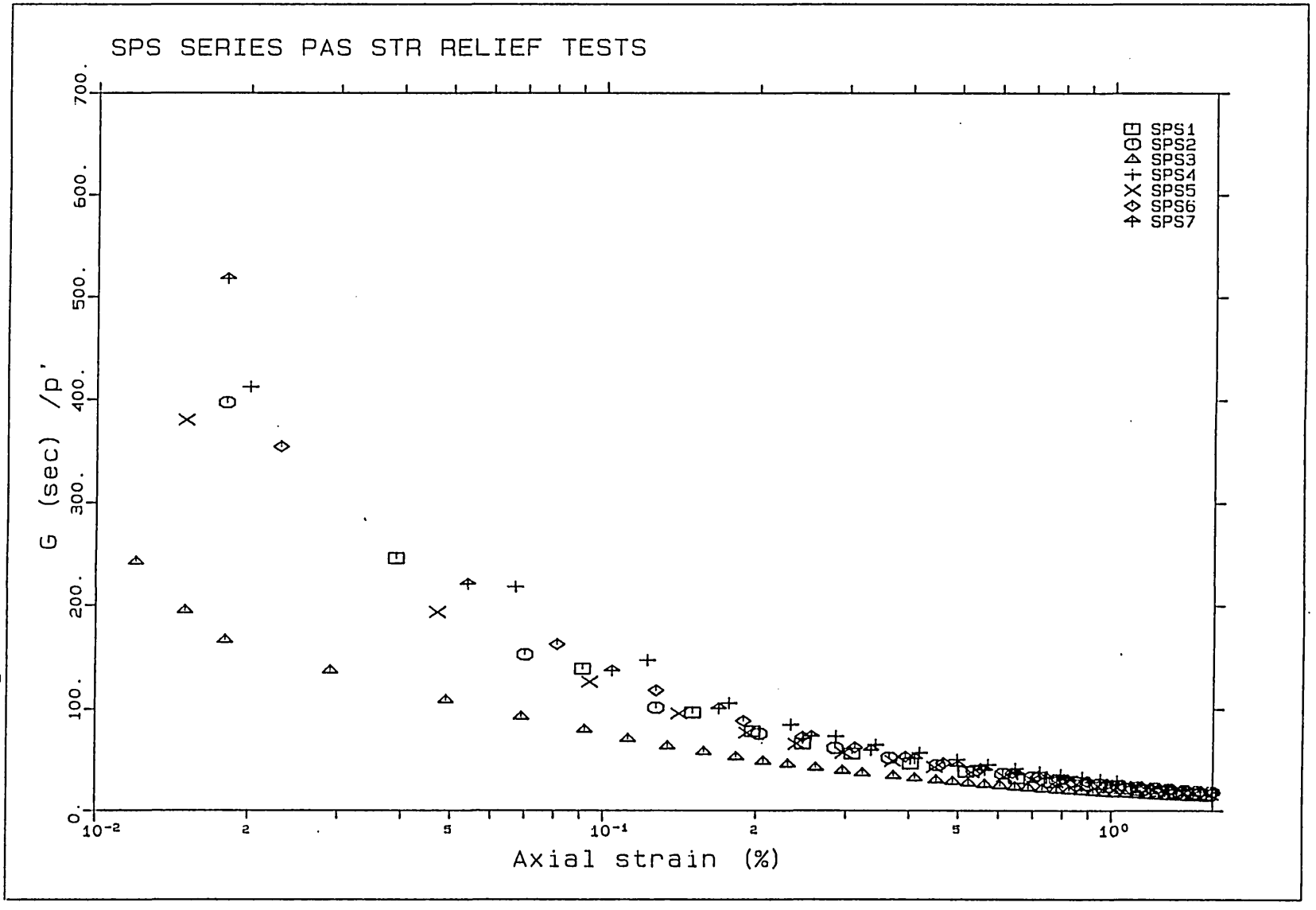


Figure 5.30. Loose sand: extension drained shear modulus.

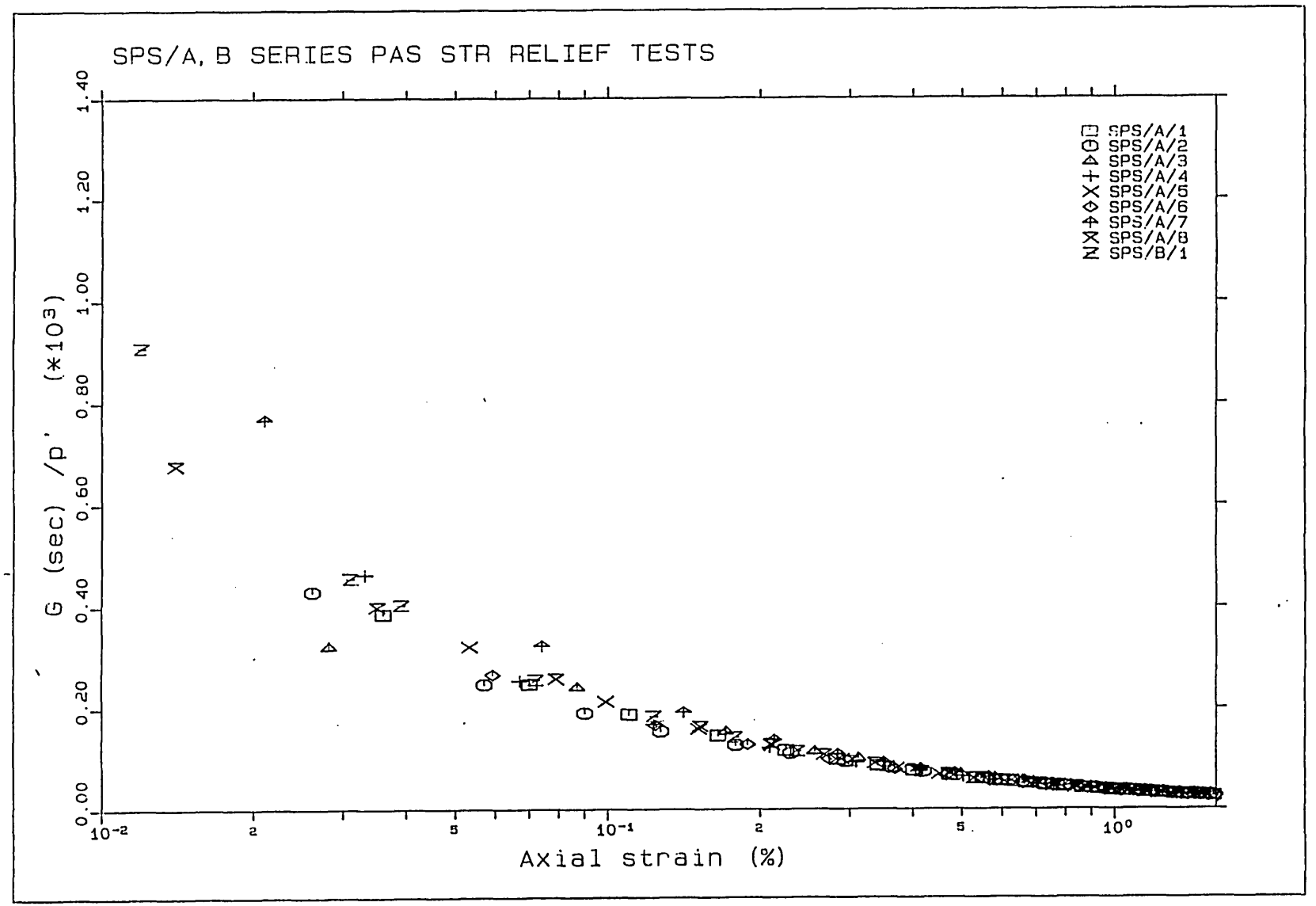


Figure 5.31. Dense sand: extension drained shear modulus.

CHAPTER 6

TABLES AND FIGURES

Table 6.1

Schedule of triaxial tests and plane strain tests on specimens of Claygate beds and London clay. (All tests are extension unless otherwise noted).

Label	Depth (m) (plasticity index)	Description of testing procedure	Initial p'	p' after isotropic swell or consolidation	K_o Stresses p'	K_o Stresses q	Stress after partial shear stage p'	Stress after partial shear stage q	Appendix
TCUU1	1.9 (26)	Undrained shear to failure from isotropic stress	19	42					A5.A1
TLUU1	14.2 (28)	" " " "	326	356					A5.A2
TLUU2	15.3 (35)	" " " "	371	380					A5.A3
TLUU3	18.9 (47)	" " " "	520	598					A5.A4
TLUU4	10.6 (39)	" " " "	310	303					A5.A5
TLUU5	13.0 (37)	" " " "	652	787					A5.A6
TLSU1	17.5 (42)	Swell to K_o. Undrained shear to failure.	340	331	251	- 33			A5.B1
TLSU2	9.4 (31)	" " " "	250	280	206	- 76			A5.B2
TLCU1	11.4 (37)	Swell to low p'. Undrained shear to failure.	371	105					A5.C1
TLCU2	11.6 (37)	" " " "	388	55					A5.C2
TCPS1	2.2 (27)	Swell to K_o. Undrained shear. Passive stress relief.	193	44	44	- 0	65	-57	A5.D1
TLPS1	14.8 (26)	" " " "	220	338	232	- 66	232	-132	A5.D2
TLPS2	13.4 (22)	Swell to K_o. Drained shear. Passive stress relief.	576	401	223	- 69	205	-125	A5.D3
TLPS3	20.4 (37)	Swell to K_o. Undrained shear. Passive stress relief.	300	350	280	- 37	312	-163	A5.D4
TLPS4	16.3 (39)	Swell to K_o. Undrained shear. Passive stress relief (computer control).	246	267	242	- 45	288	-182	A5.D5
TLPS5	10.3 (39)	Swell to K_o. Undrained shear. Passive stress relief (computer control).	223	247	204	- 85	213	-112	A5.D6
TLPS6	20.5 (37)	Swell to K_o. Undrained shear. Passive stress relief (Lubricated ends).	350	353	283	- 46	331	-153	A5.D7
TLDRUL1	13.8 (30)	K_o swell from high initial p'.	380	409					A5.E1
TLDRUL2	13.6 (26)	" " " "	620	400					A5.E2
TLD1	17.1 (39)	Isotropic swell. Undrained/ drained shear. (Incomplete pore water pressure dissipation during early part of test).	620	81					A5.F1
TLSUD1A	18.5 (43)	Swell to K_o. Undrained shear. Swell with q const.	289	317	259	-46	314	-183	A5.G1
TLSUD2B	10.7 (39)	" " " "	543	264	246	-42	231	-126	A5.G2
TCUA1	2.5 (26)	Undrained compression σ_v constant, σ_h decreasing.	512	50	50	-0			A5.H1
TLUA1	19.9 (31)	Swell to K_o. Undrained compression σ_v constant, σ_h decreasing.	586	350	280	-41			A5.I1
TLA1	15.2 (33)	Swell to K_o. Drained compression σ_v constant, σ_h decreasing.	300	338	223	-39			A5.J1
TLA2A	9.8 (36)	" " " "	310	245	197	-77			A5.J2
PLPS1	17.9 (49)	Swell to K_o. Drained shear. Passive stress relief.	390	269	250	-45	217	-111	A5.K1

Table 6.2

Swelling characteristics of London Clay

Swelling Characteristics to Initial K_o Conditions

Depth (m)	Test	P_o' (kN/m^2)	P_f' (kN/m^2)	Δv (per cent)	K' (MN/m^2)	K'/p'
14.8	TLPS1	338	231	- 0.39	27.4	96
13.4	TLPS2	401	223	- 0.84	21.2	68
20.4	TLPS3	350	280	- 0.73	9.6	30
10.3	TLPS5	247	205	- 0.81	5.2	23
20.5	TLPS6	353	283	- 1.28	5.5	17
17.5	TLSU1	331	251	- 1.05	7.6	26
9.4	TLSU2	280	207	- 1.60	4.6	19
10.7	TLSUD2B	255	212	- 0.92	4.6	20
18.5	TLSUD1A	317	259	- 0.55	10.5	37
19.9	TLUA1	350	281	- 0.33	20.9	66
15.2	TLA1	338	234	- 0.91	11.4	40
9.8	TLA2A	245	197	- 0.66	7.3	33

Swelling Characteristics during Drained Tests

15.2	TLA1	223	130	- 1.11	8.5	48
9.8	TLA2A	197	115	- 0.96	8.5	56
13.4	TLPS2	223	205	- 0.14	12.9	60

Table 6.3

Non-Linear undrained stiffness and effective bulk modulus stiffness parameters

Undrained stiffness parameters
(G_u/p' versus ϵ_s)

Description	A	B	C (%)	α	γ	ϵ(min) (%)	ϵ(max) (%)
London Clay - Compression	570	557	0.00007	1.47	0.453	0.0003	2.0
London Clay - Extension	317	350	0.000105	1.22	0.61	0.0005	0.11
Claygate Beds	633	647	0.0005	1.36	0.62	0.0007	0.1

Effective bulk modulus stiffness parameters
(K'/p' versus ϵ_v)

London Clay	520	495	0.0006	1.8	0.44	0.0007	0.185
Claygate Beds	1300	1238	0.0006	1.8	0.44	0.0007	0.185

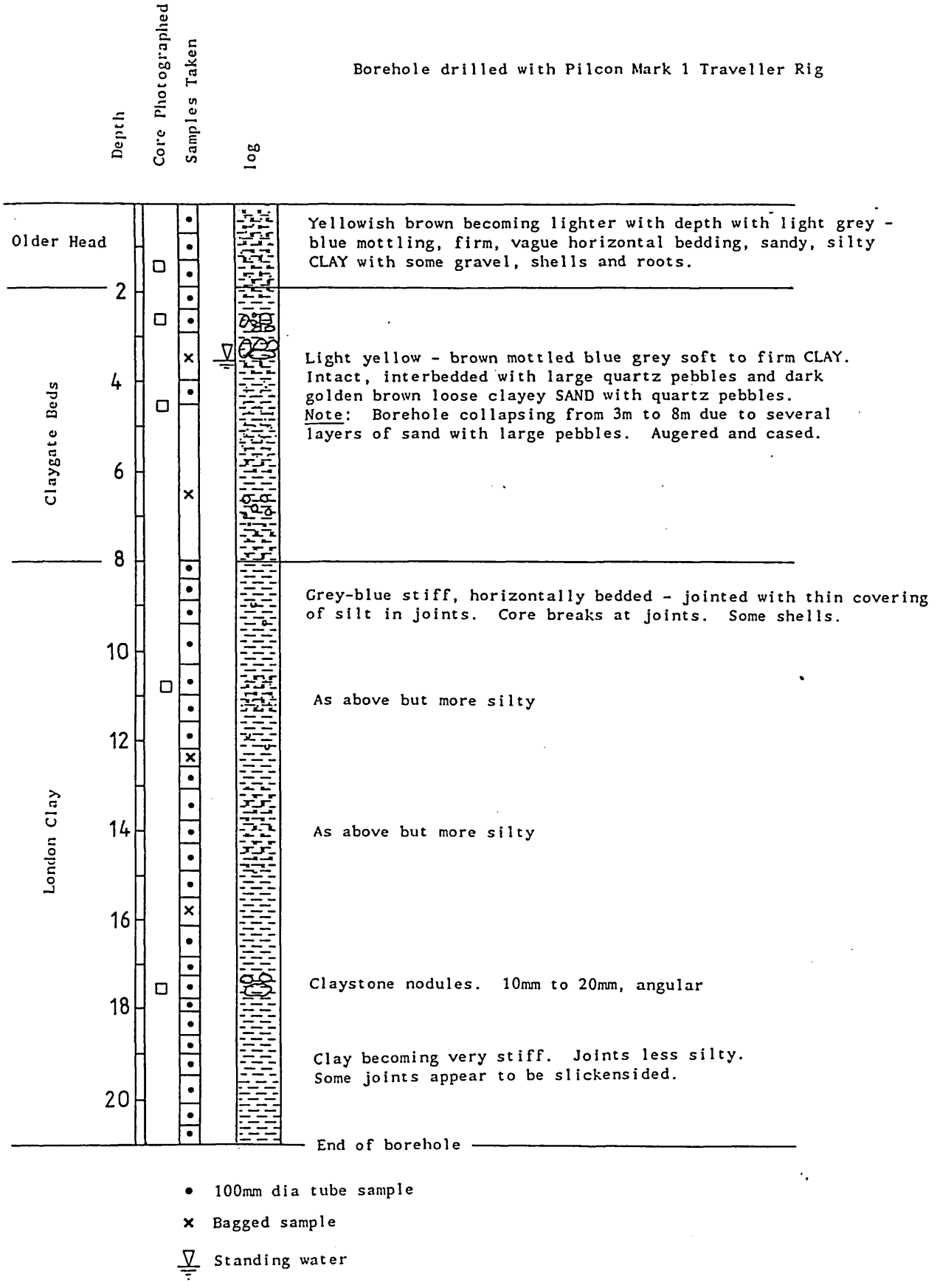
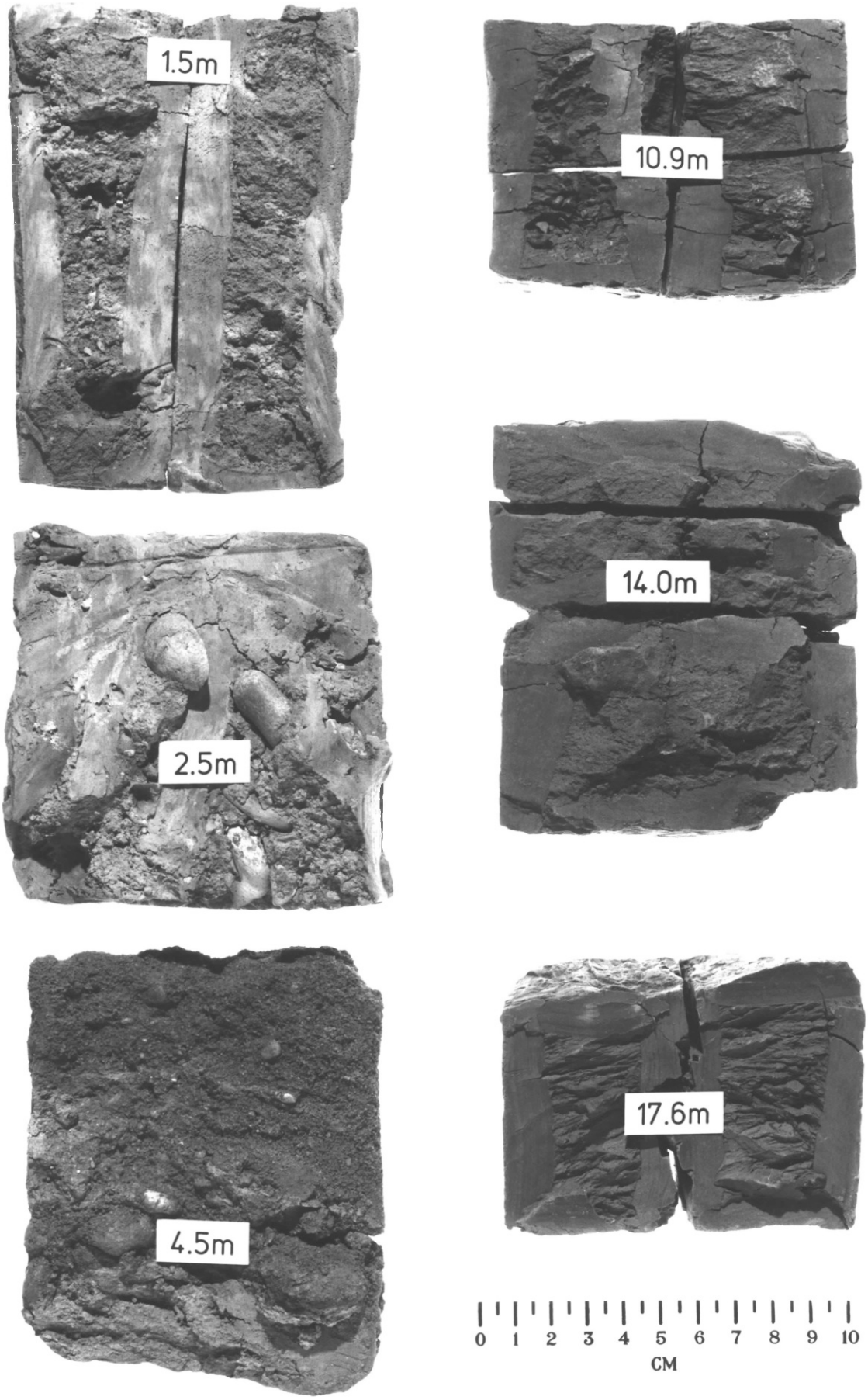


Figure 6.1. Log of borehole drilled at Bell Common.

Figure 6.2

Photographs of split samples from various depths.


1.5m
10.9m
14.0m
2.5m
4.5m
17.6m
0 1 2 3 4 5 6 7 8 9 10
CM

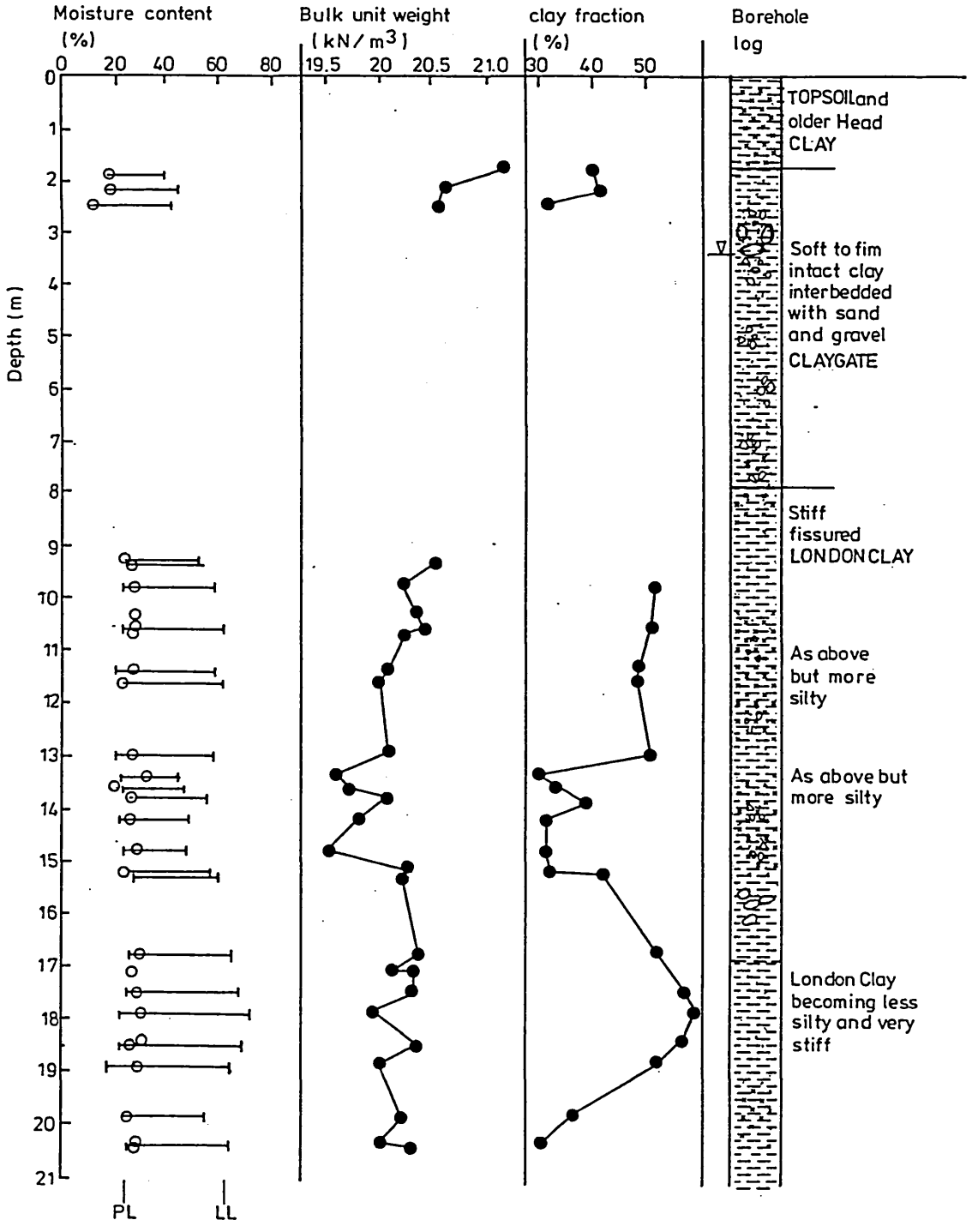


Figure 6.3. New borehole: profile of index properties.

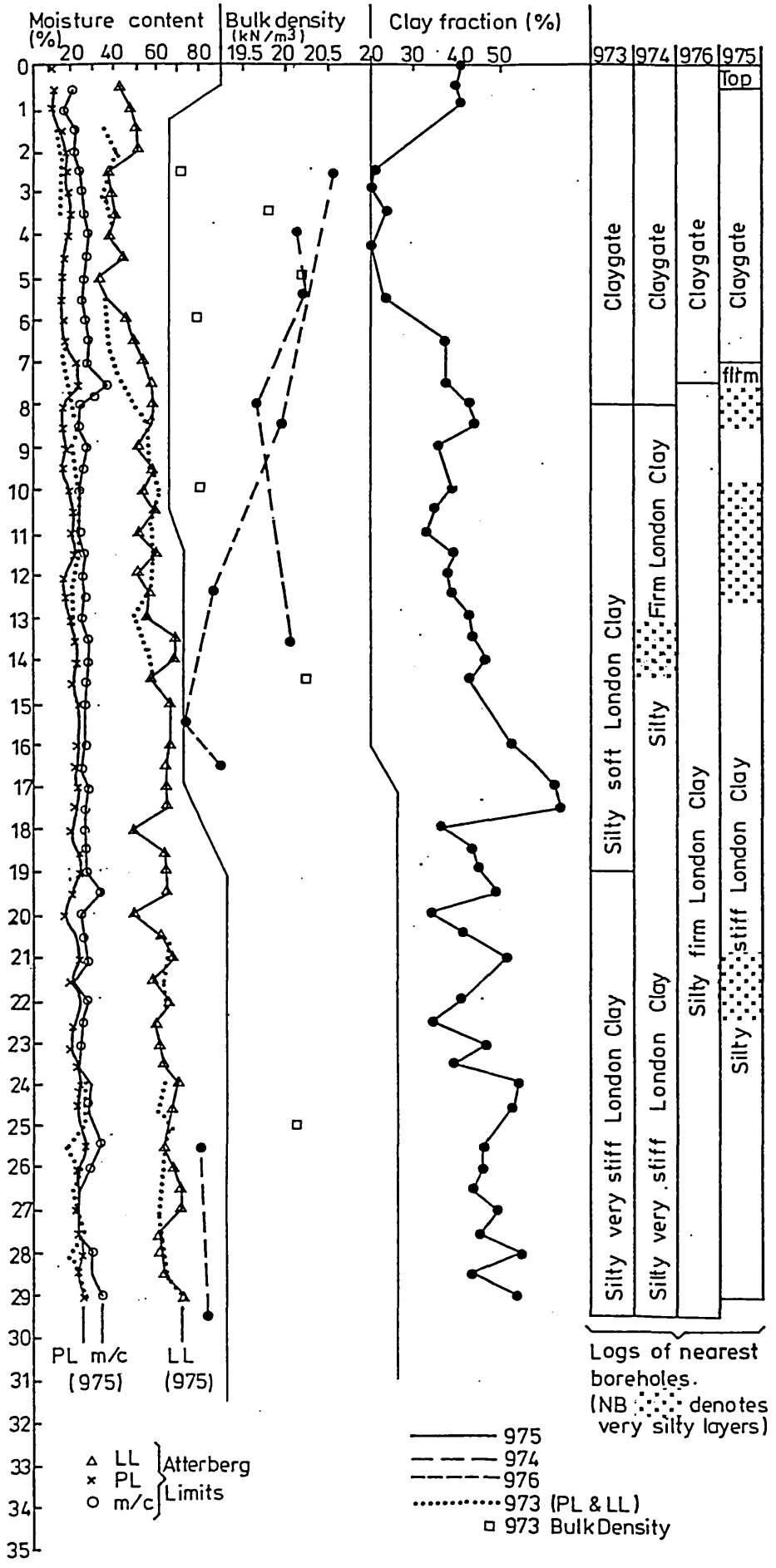


Figure 6.4. Profile of index properties: previous boreholes.

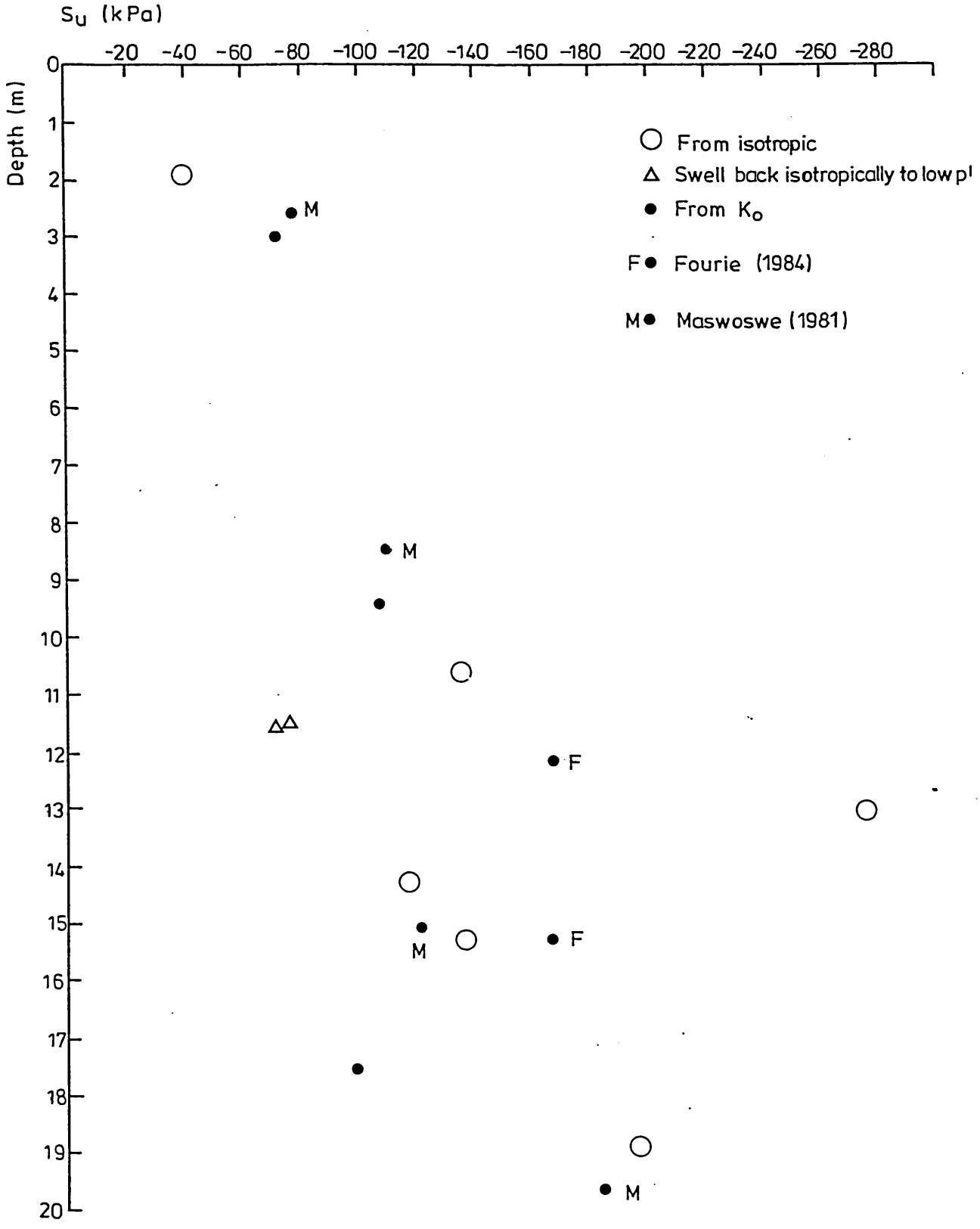


Figure 6.5. Undrained strength versus depth from triaxial extension tests.

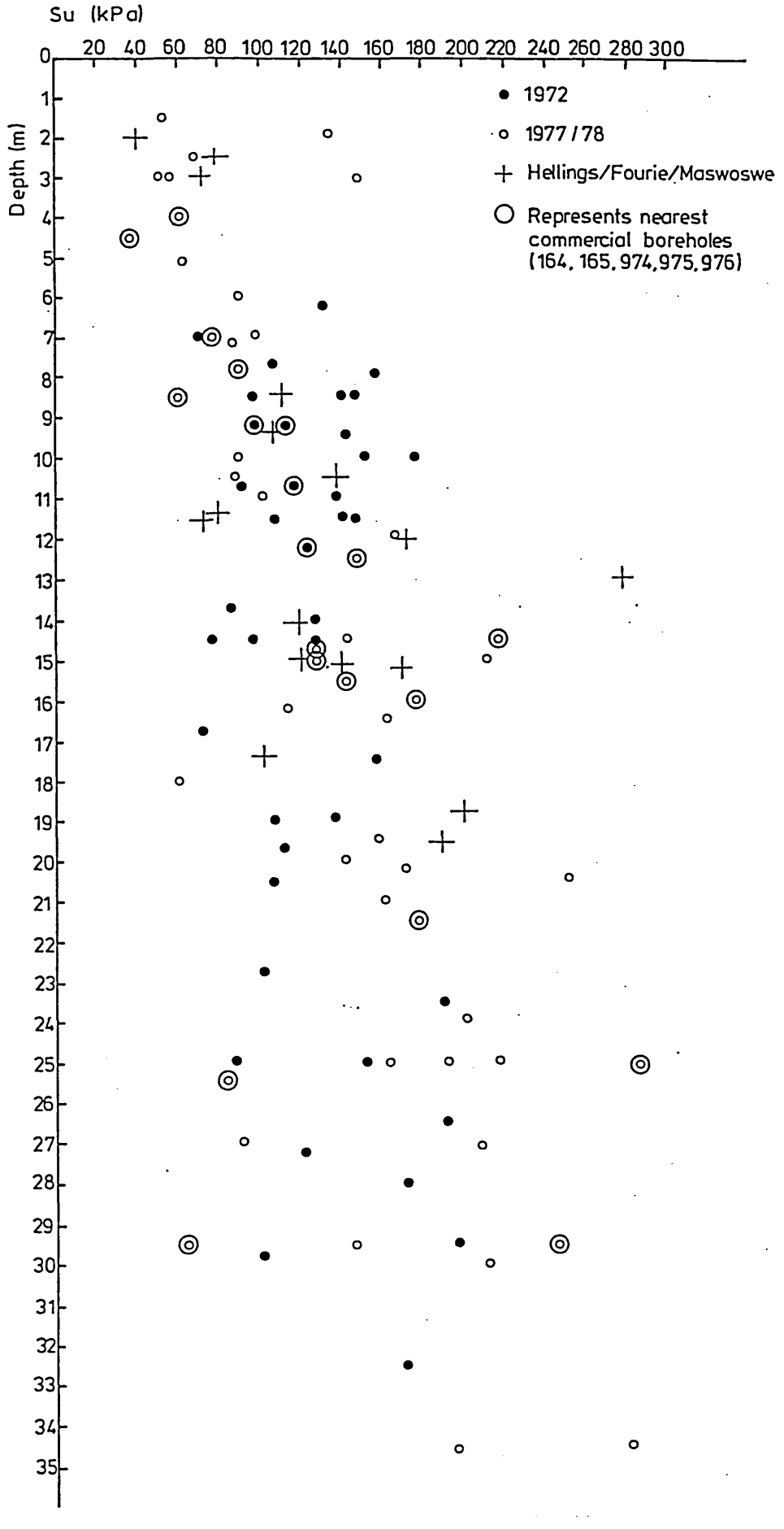
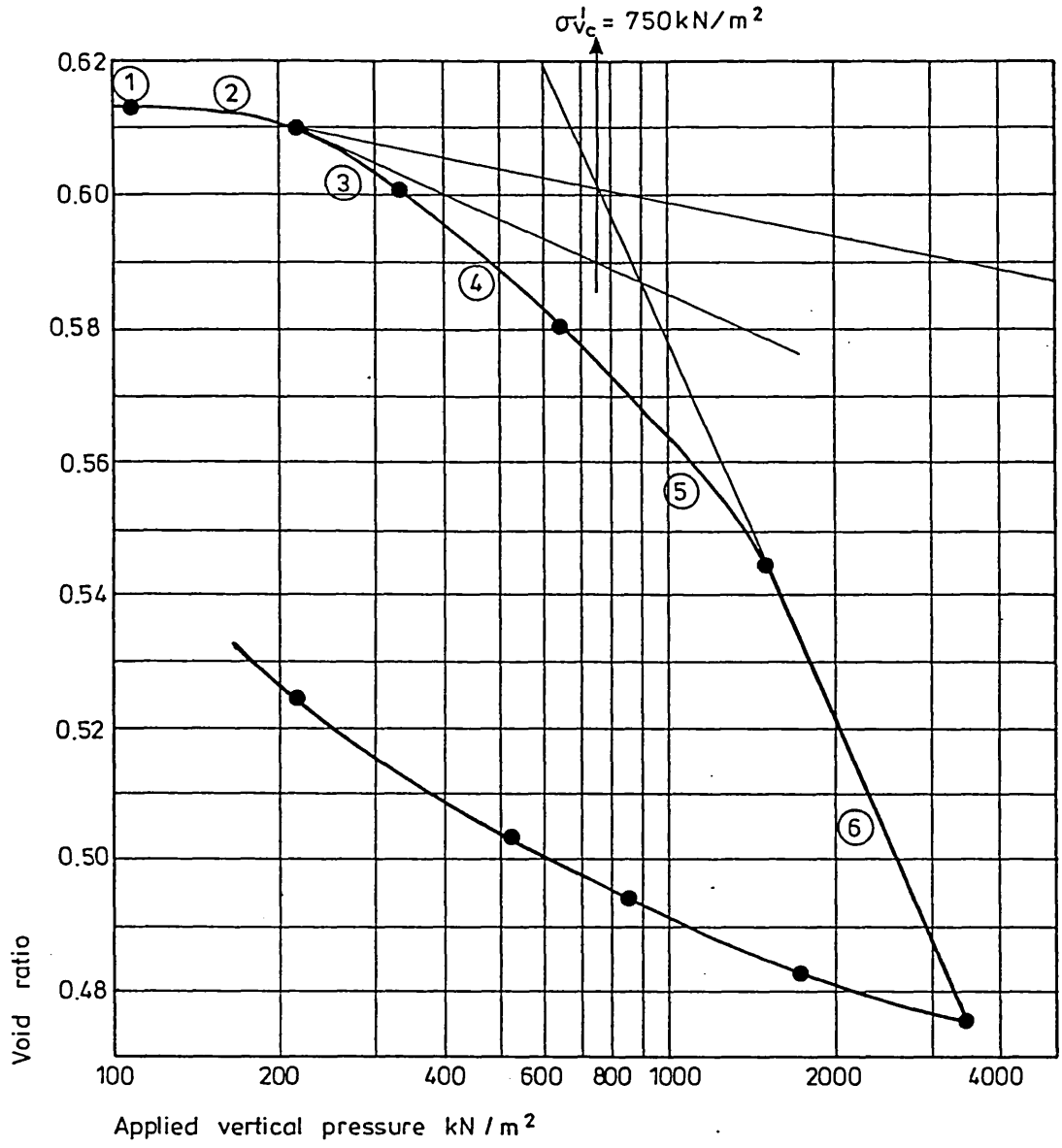


Figure 6.6. Undrained compression and extension strength versus depth: all boreholes.



Pressure range	C_α rate of secondary compression	C_v coeff. of consolidation (m^2/yr)
②	0.0004	2.6
③	0.0003	4.4
④	0.0005	6.4
⑤	0.0026	8.2
⑥	0.0054	2.8

Figure 6.7. Oedometer test on London clay specimen from 15.2m depth (silty clay).

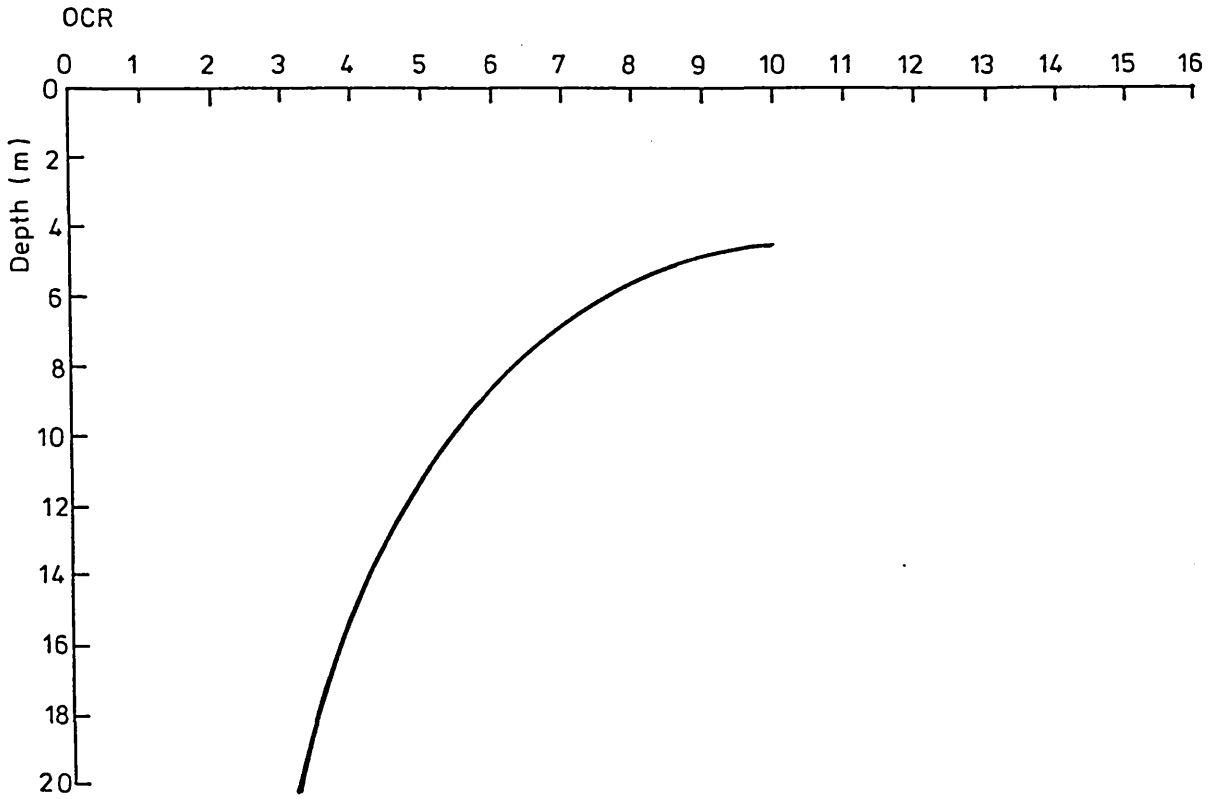


Figure 6.8. Overconsolidation ratio (OCR) versus depth (maximum previous groundwater level taken to be at previous ground surface).

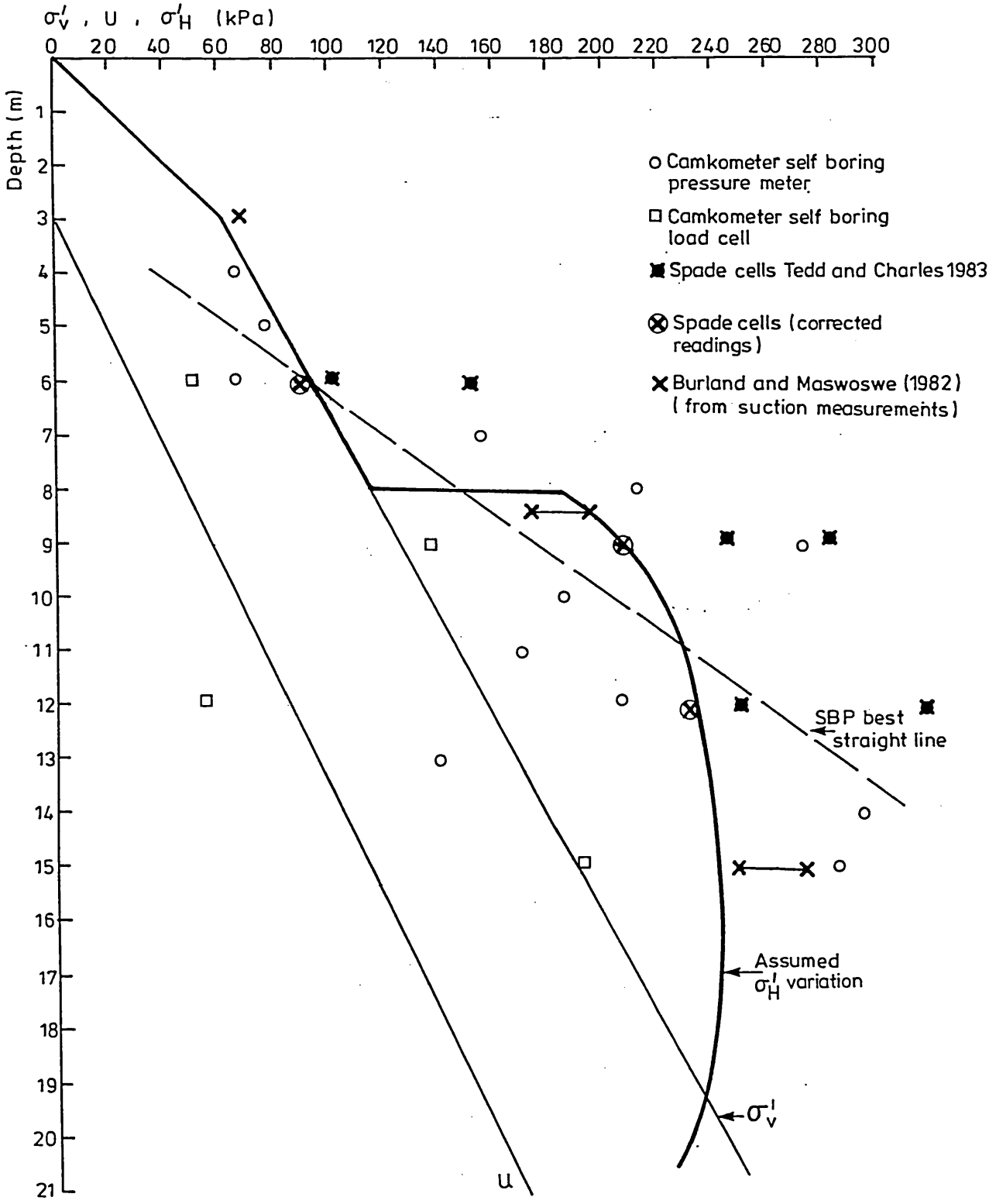


Figure 6.9. Assumed variation of horizontal and vertical effective stresses and porewater pressure with depth.

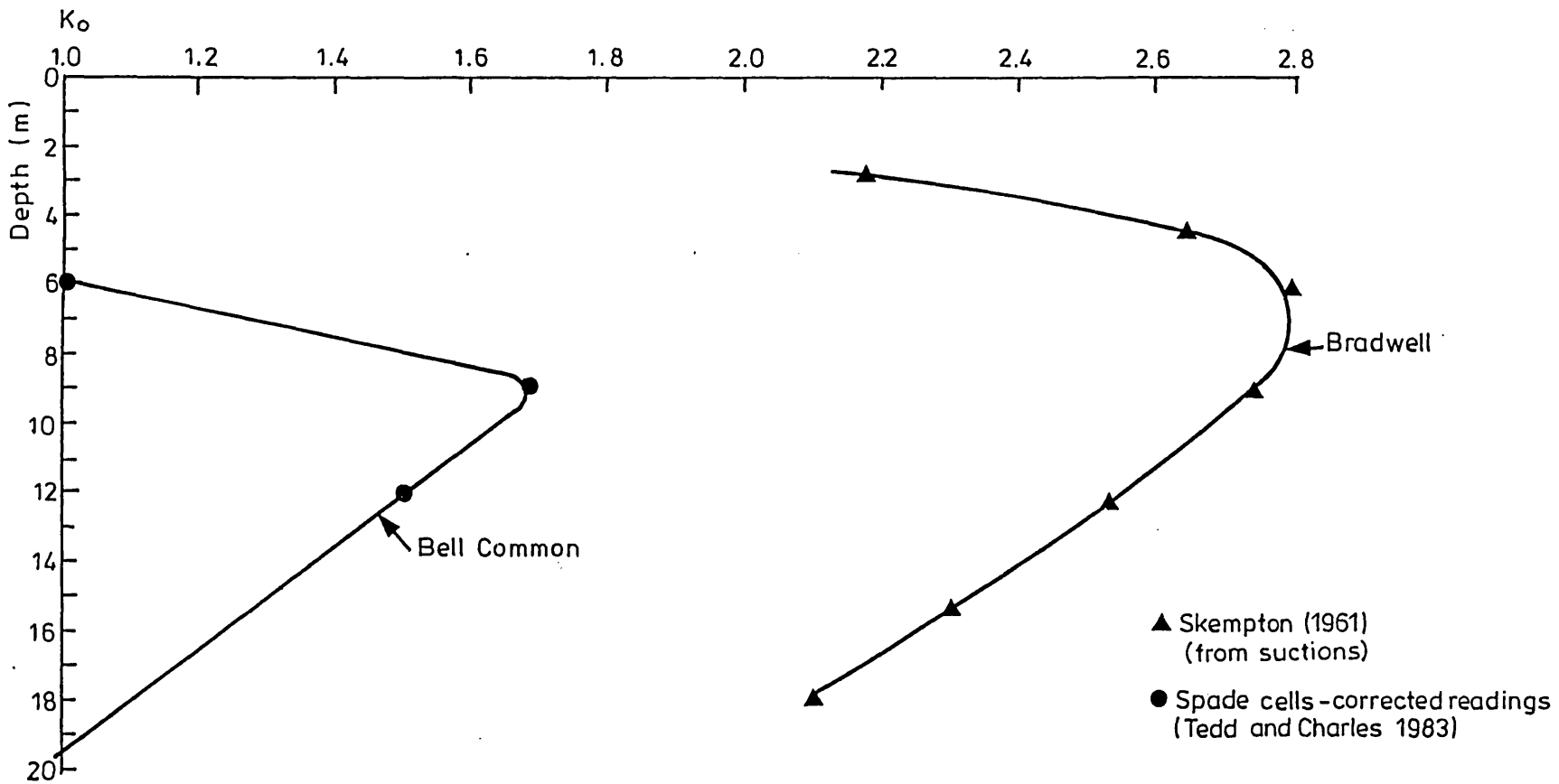


Figure 6.10. Variation of K_o with depth: Bell Common and Bradwell.

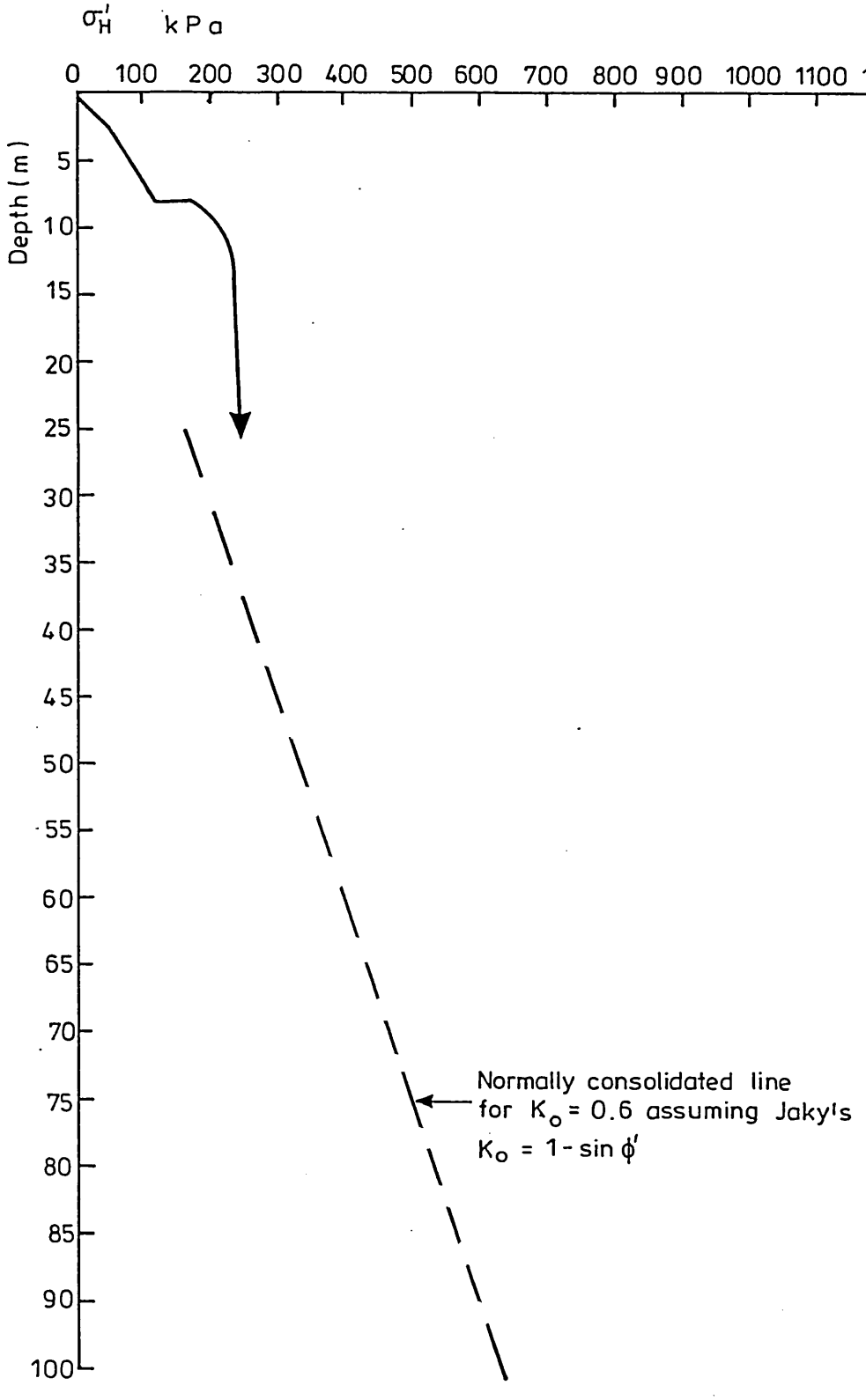


Figure 6.11. Assumed horizontal effective stress variation with depth.

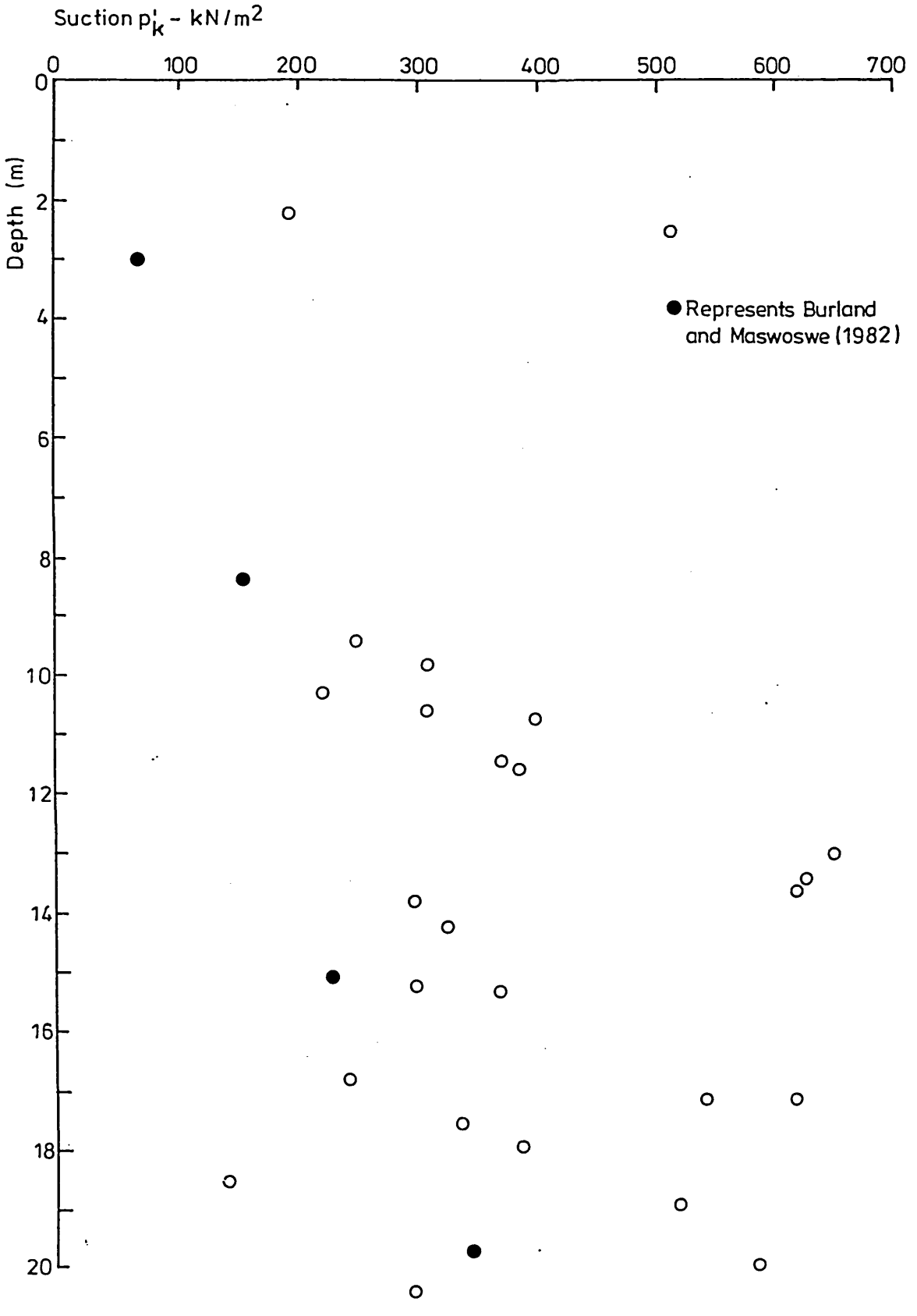


Figure 6.12. Variation of p'_k with depth.

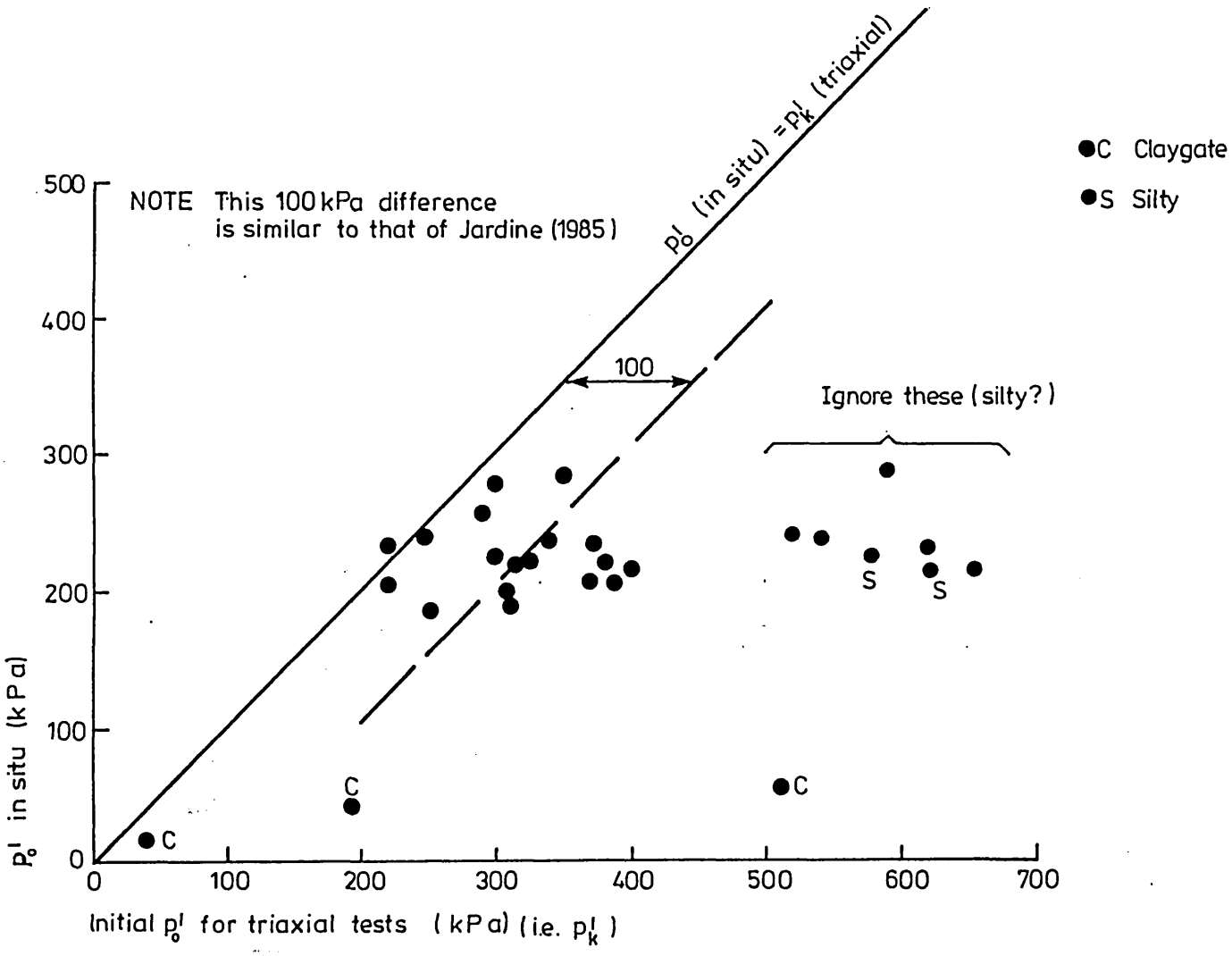


Figure 6.13. Comparison between p_k' and p_o'.

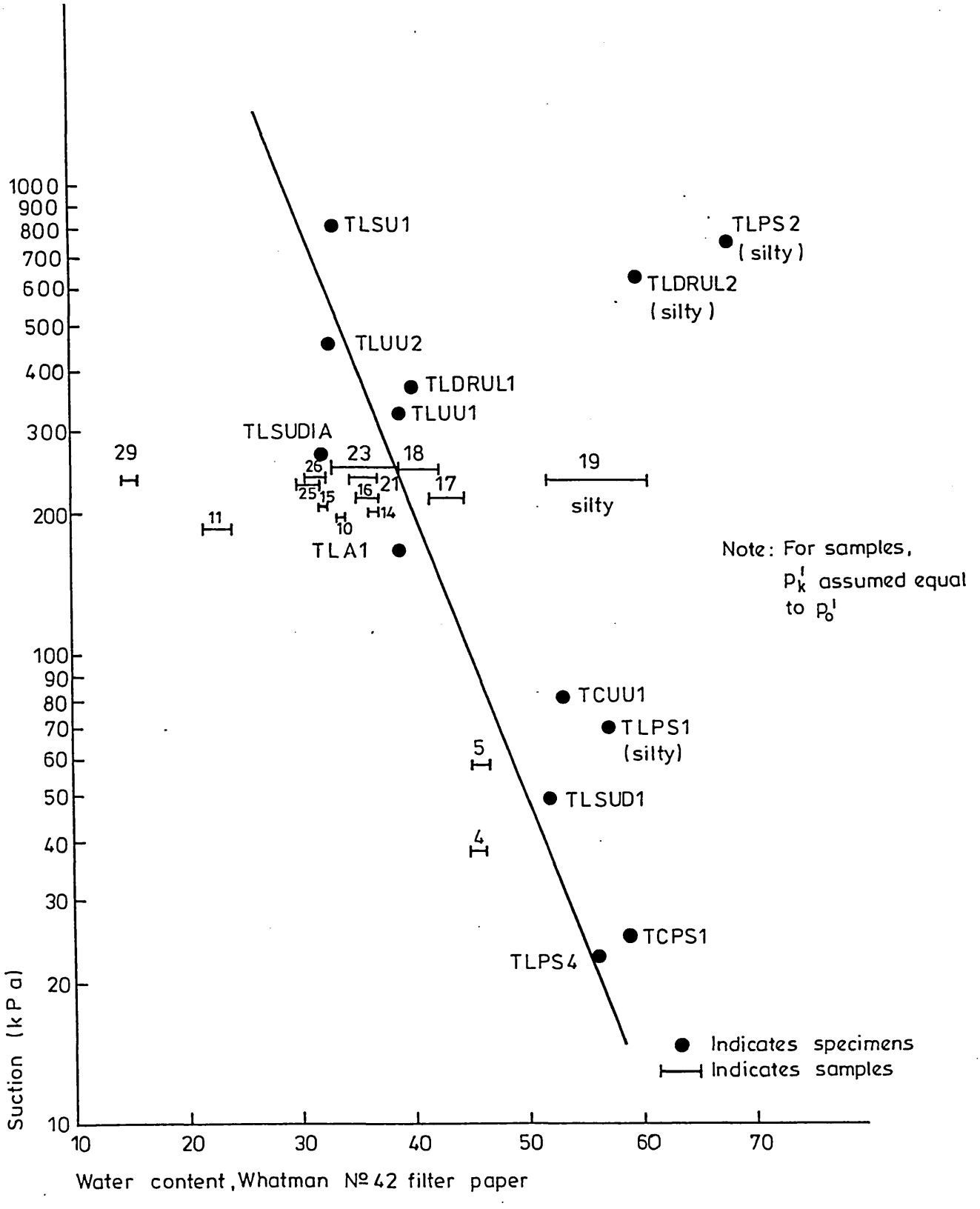
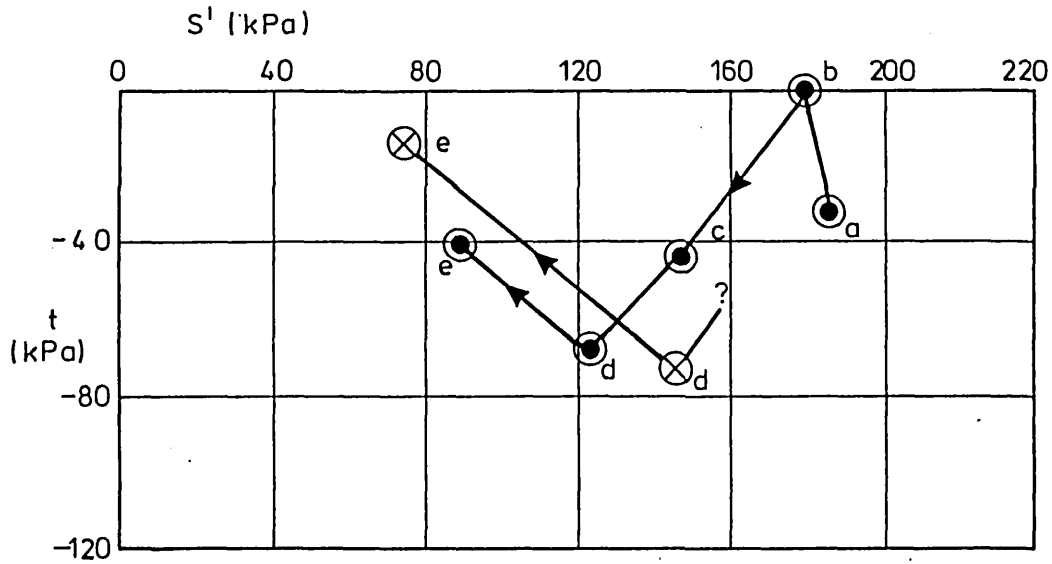


Figure 6.14. Chandler and Gutierrez' (1986) filter paper technique for estimating in situ effective stresses.



gauge 12m depth
gauge 16m depth
} in front of wall

Sequence of major events

a April 1982

b May 1982

c July 1982

d February 1983

a→b excavation for diaphragm wall

b→c excavation to 5m

c→d excavation to 8m

d→e dissipation:-horizontal stresses decrease, porewater pressures increase.

Figure 6.15. Stresses monitored in front of the wall at Bell Common.

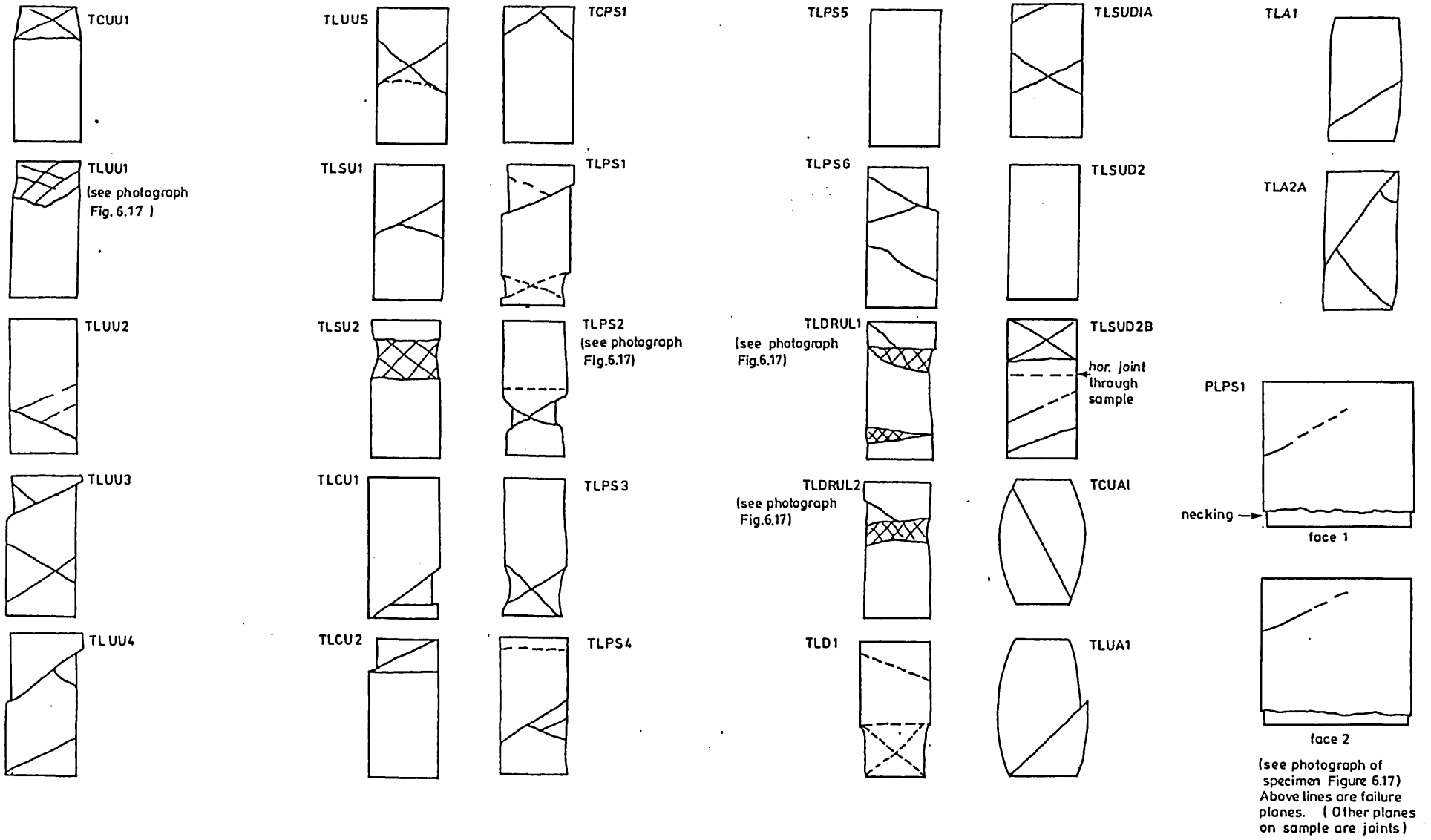
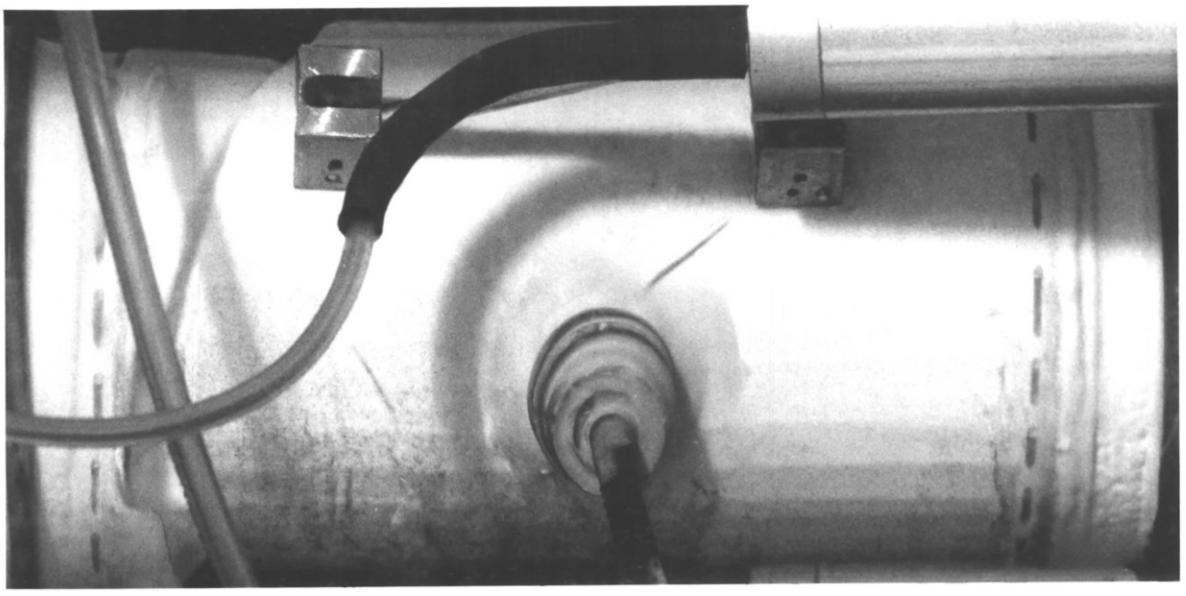


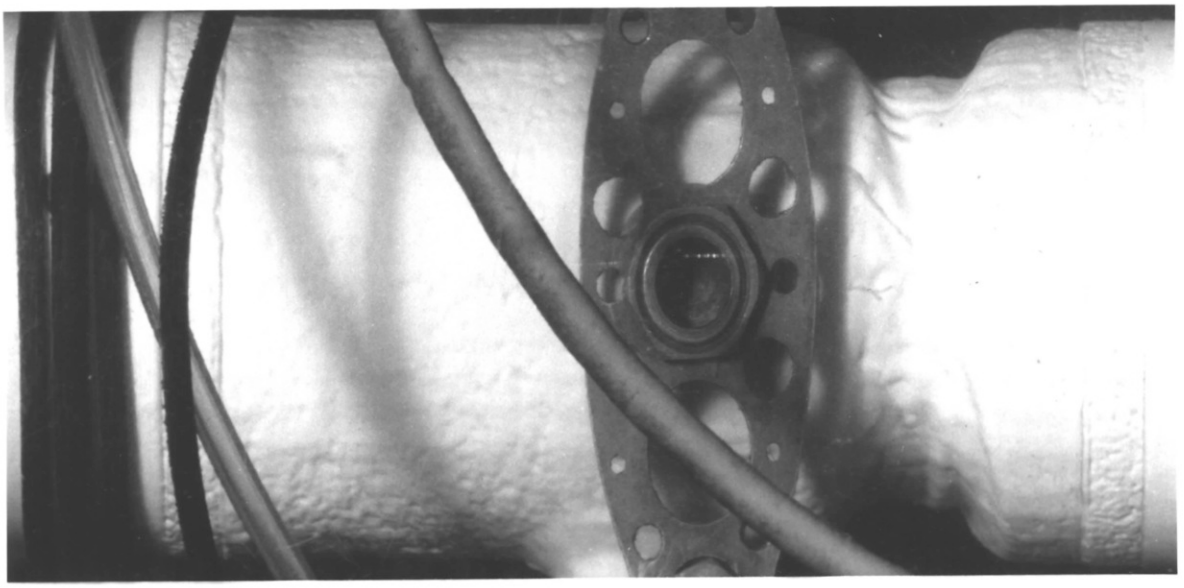
Figure 6.16. Failure modes of clay specimens.

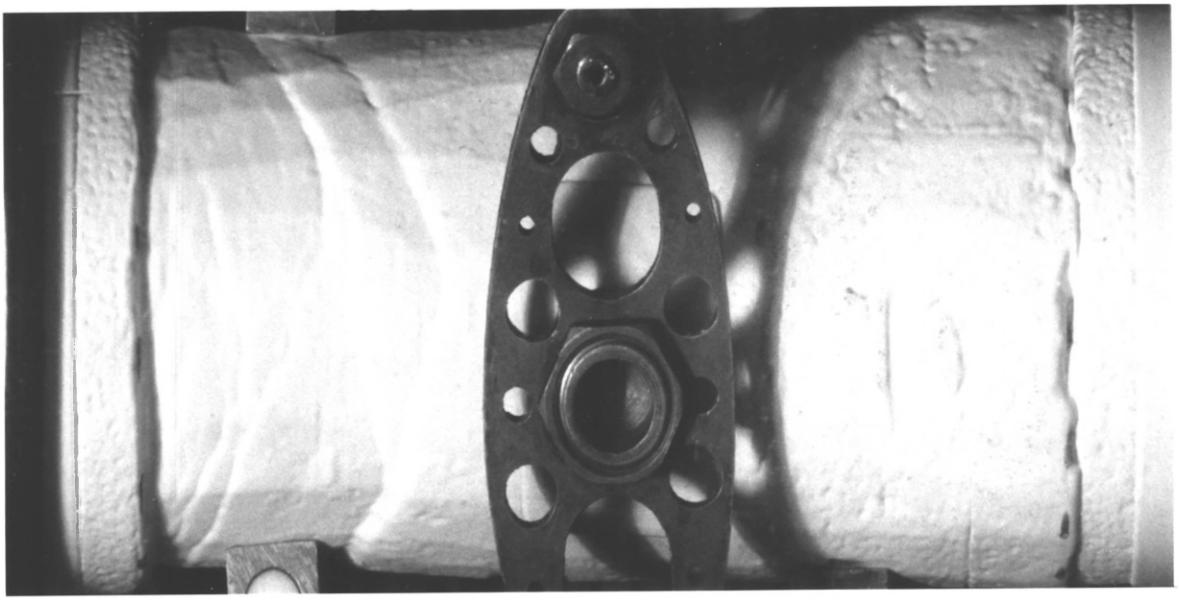
Figure 6.17

Photographs of some triaxial specimens after testing -

Sheet 1 left to right: TLUU1, TLPS2, TLPS6.
Sheet 2 left to right: TLA1, TLDRUL1, TLDRUL2.

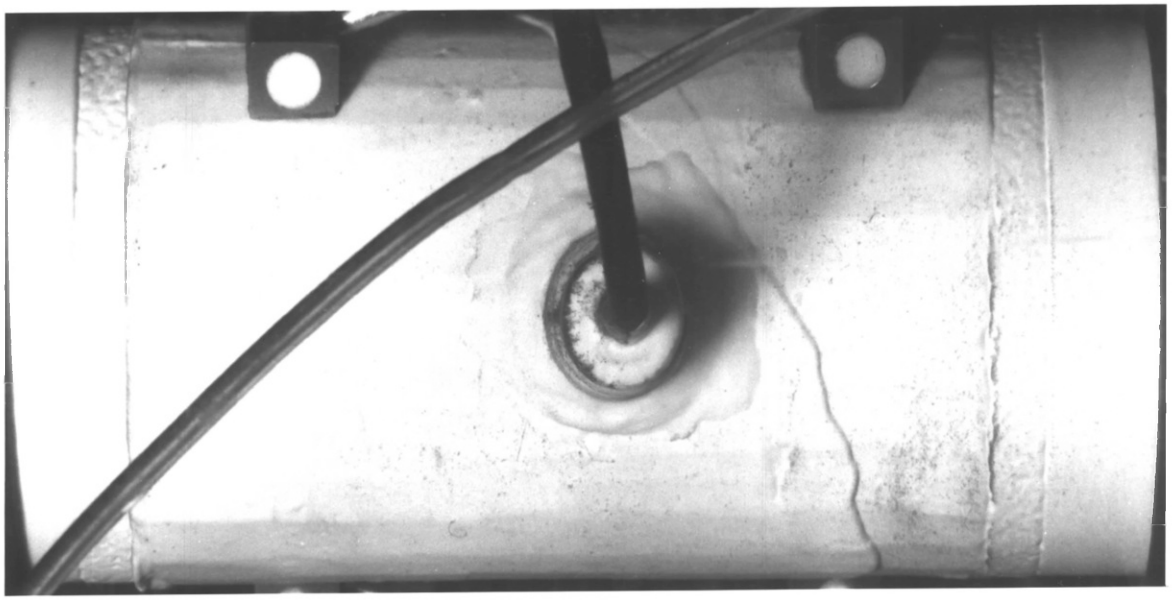












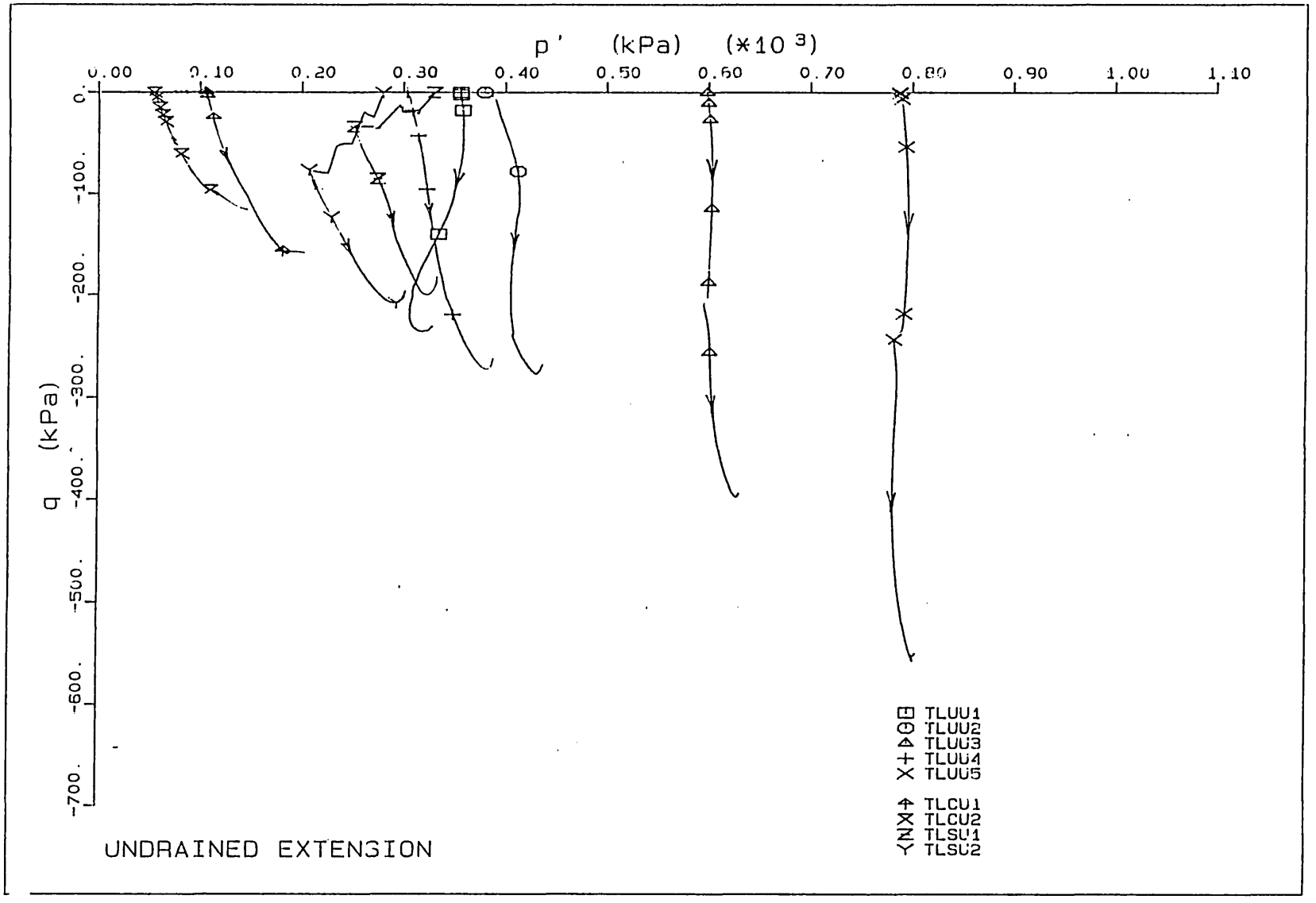


Figure 6.18. Results of undrained triaxial extension tests on London clay: p' versus q.

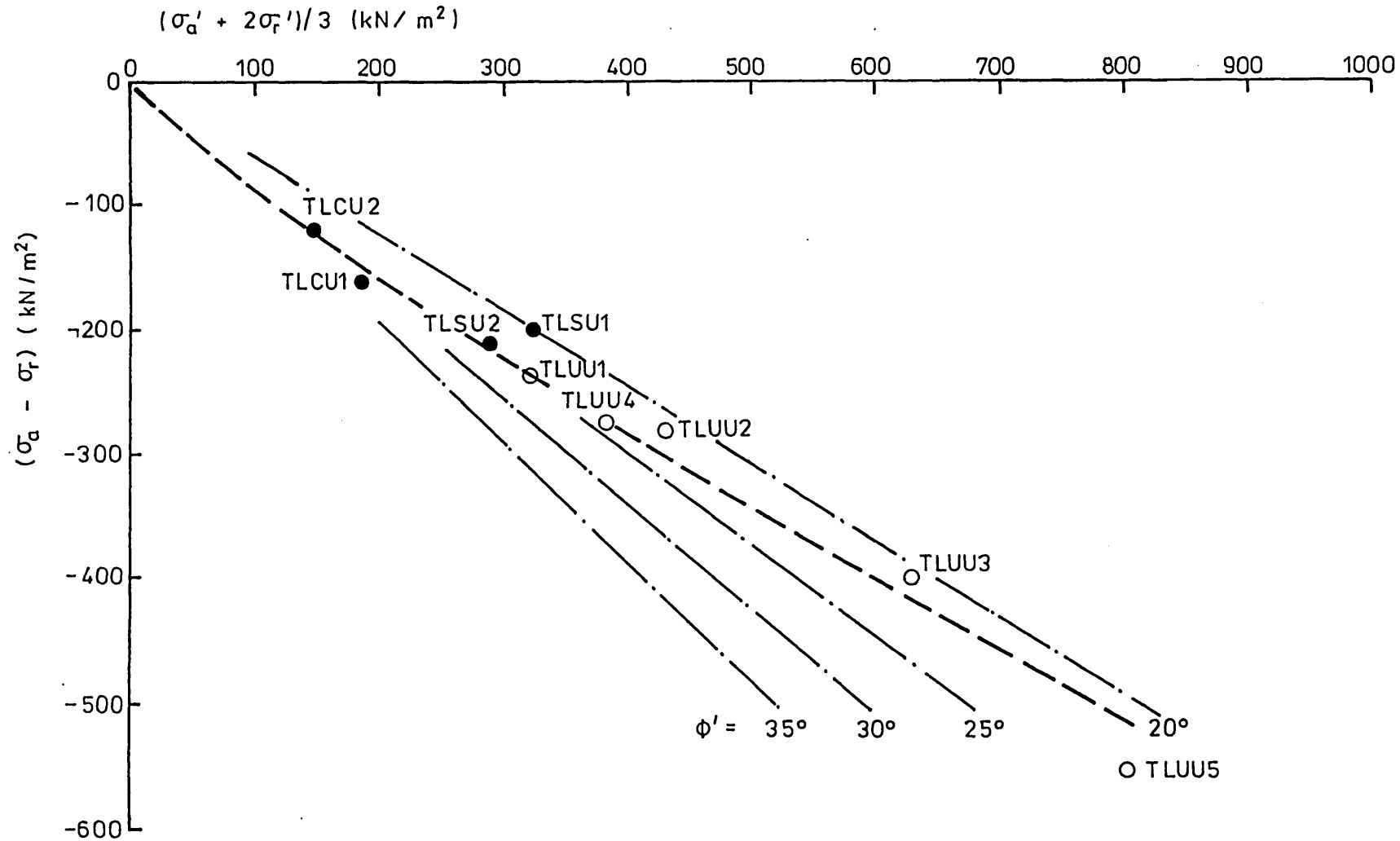


Figure 6.19. Peak strengths from undrained triaxial extension tests on London clay.

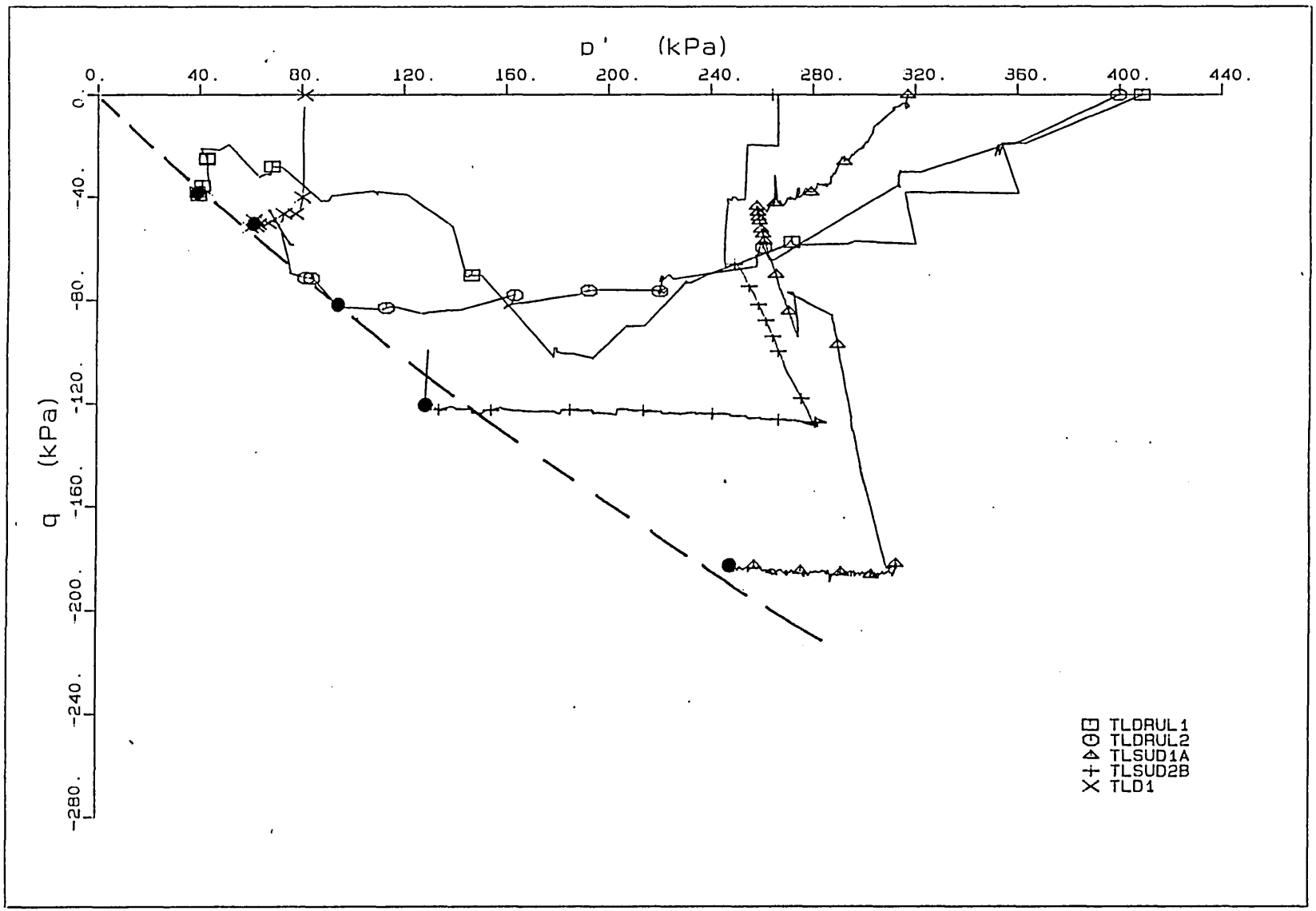


Figure 6.20. Stress paths for constant q swelling tests, K_o swelling tests and an undrained/drained extension test on London clay.

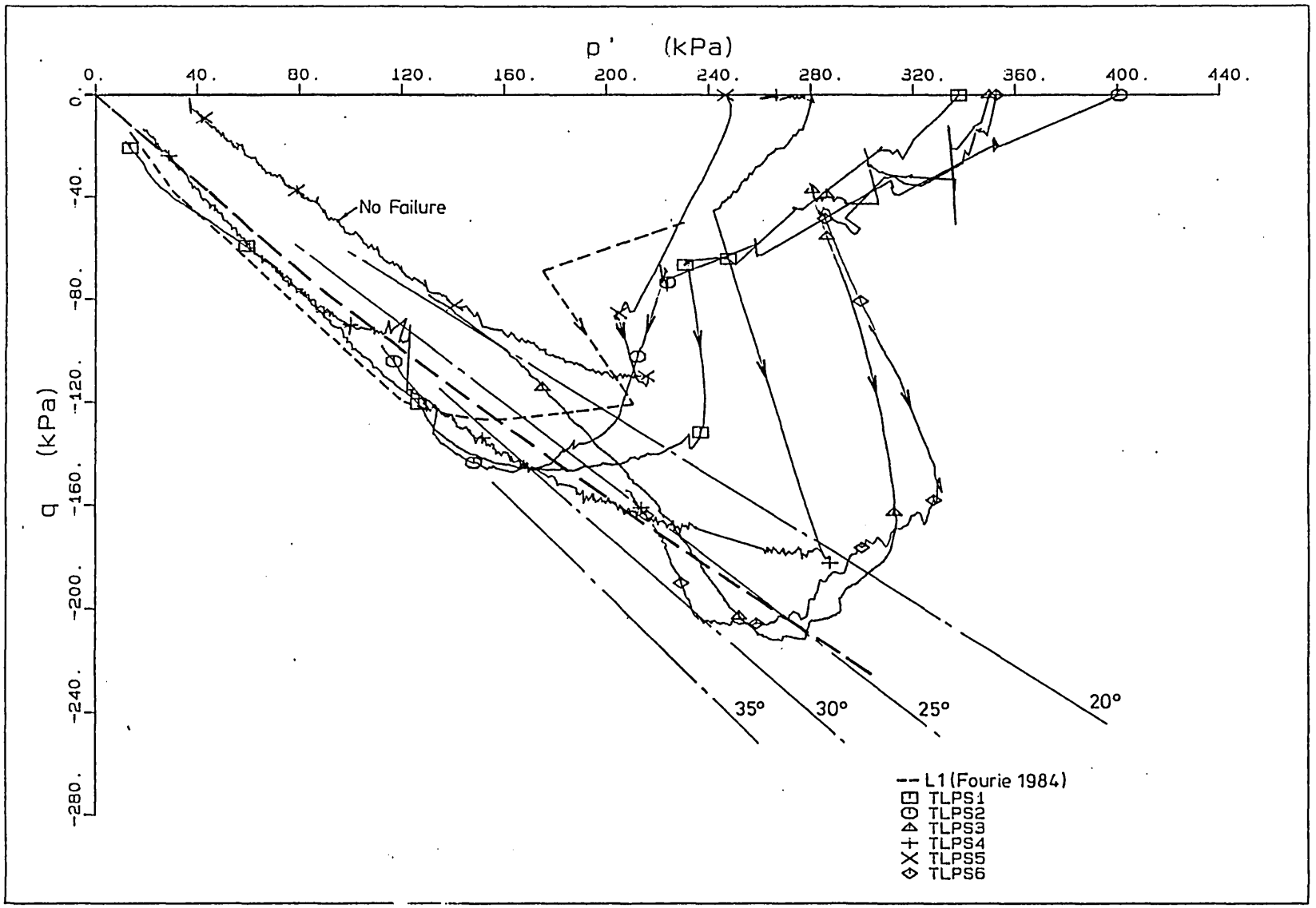


Figure 6.21. Stress paths for triaxial passive stress relief tests on London clay: p' versus q.

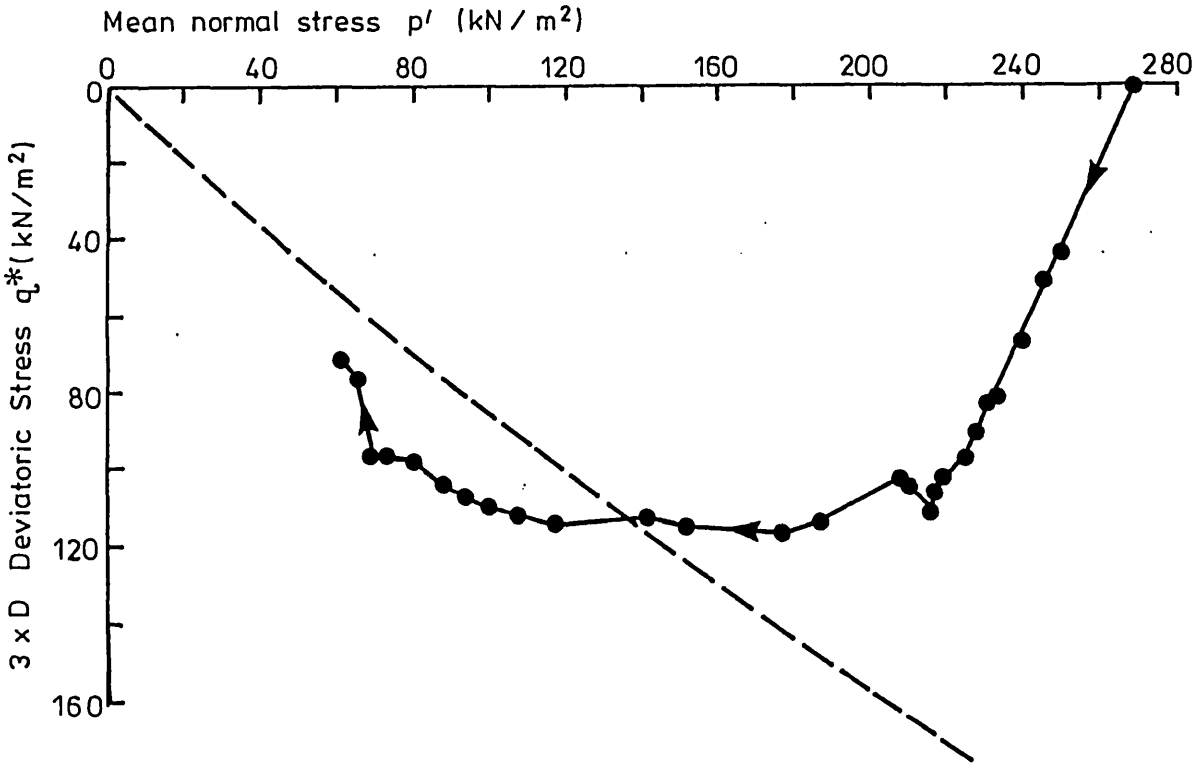


Figure 6.22. Stress path for plane strain passive stress relief test PLPS1.

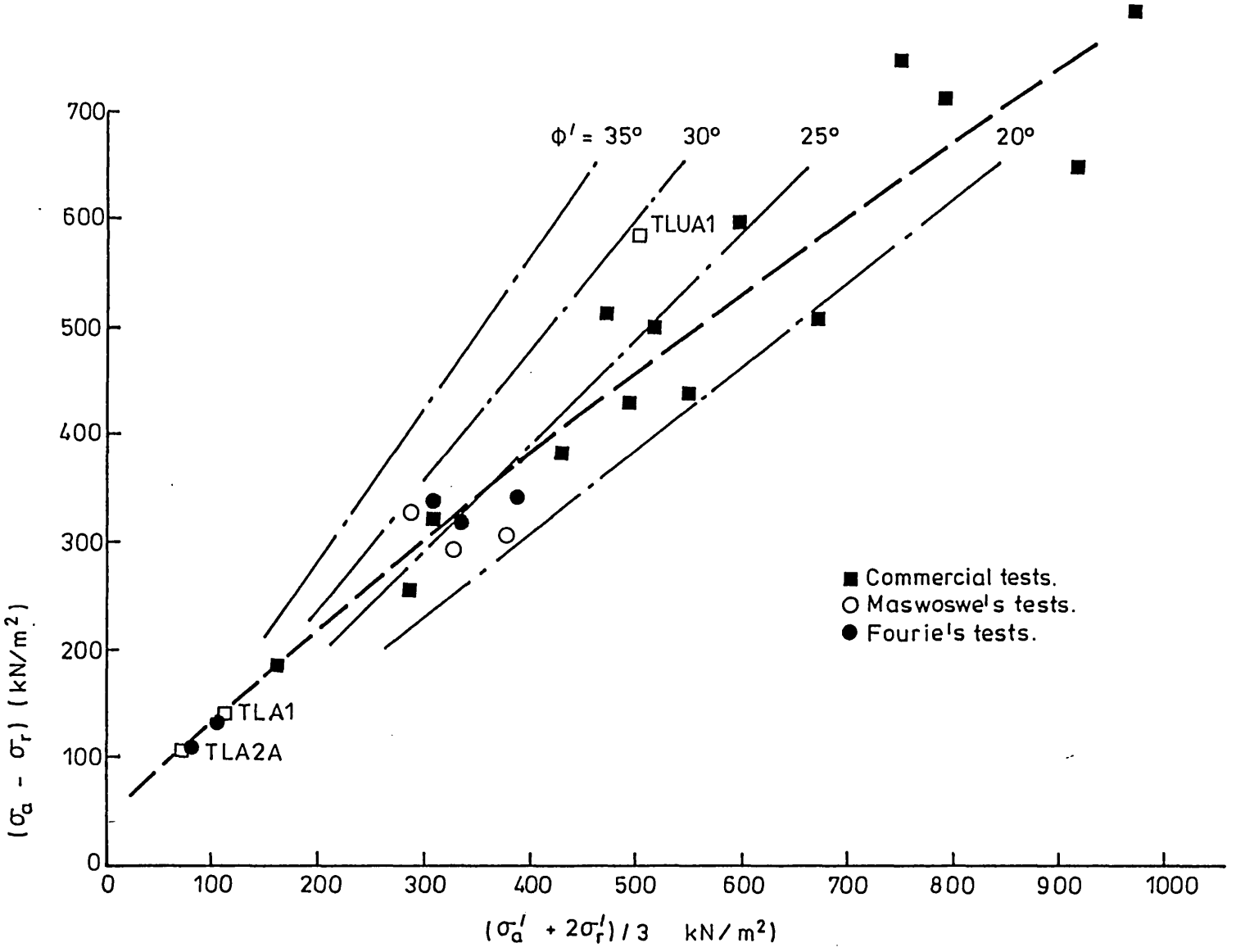


Figure 6.23. Peak strengths from drained and undrained triaxial compression tests on London clay.

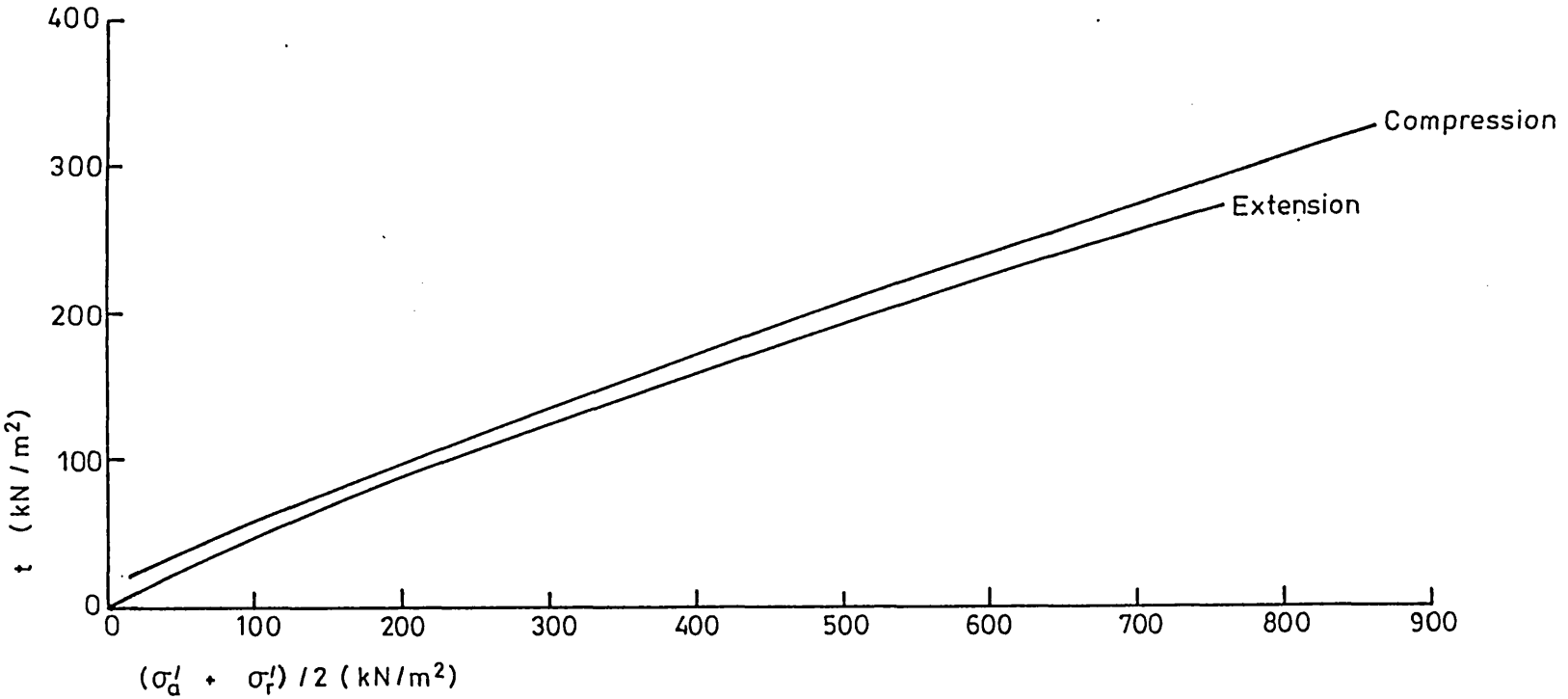


Figure 6.24 Comparison of failure envelopes from triaxial compression and extension tests on London clay.

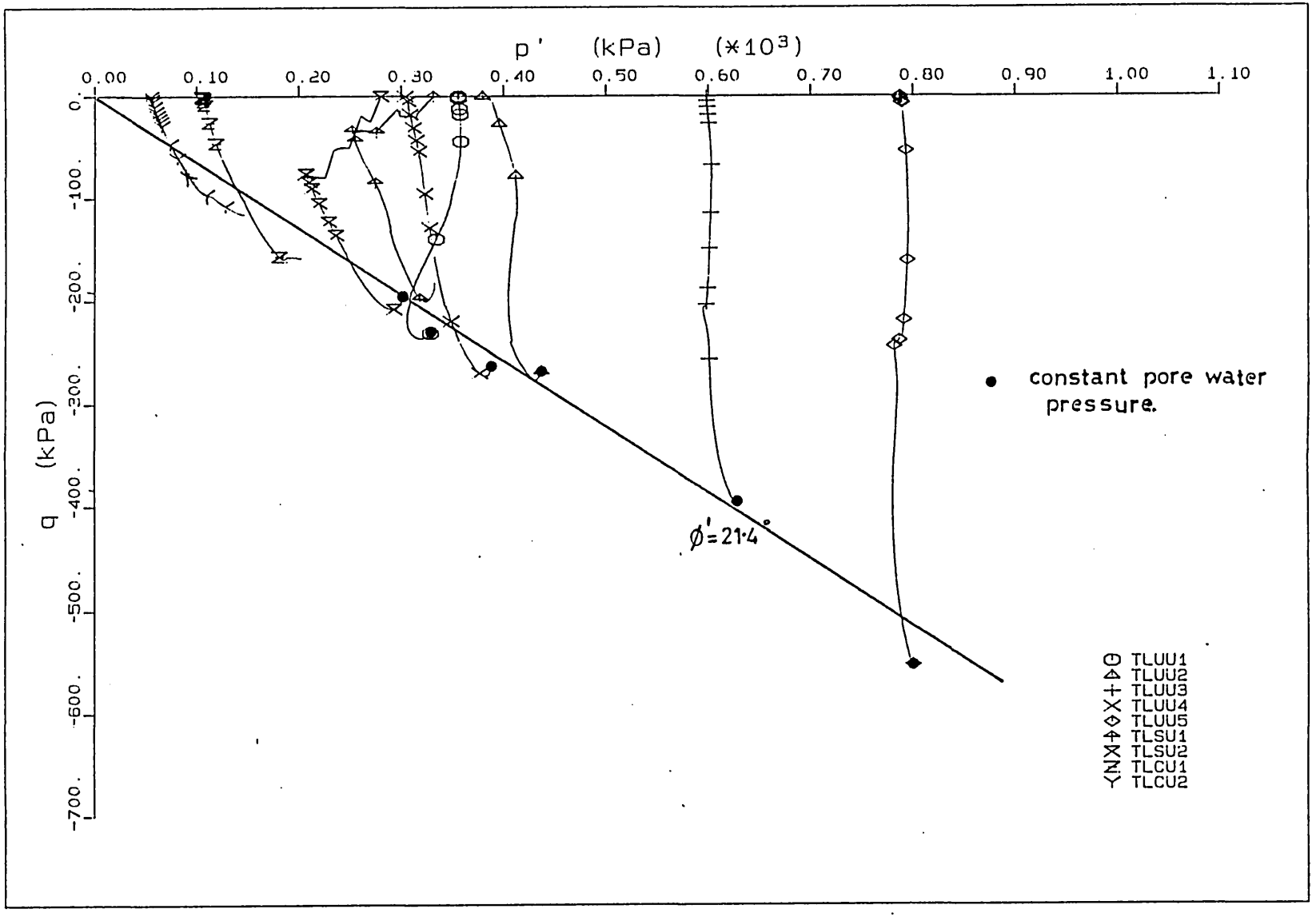


Figure 6.25. Undrained extension tests on London clay: constant pore water pressure points.

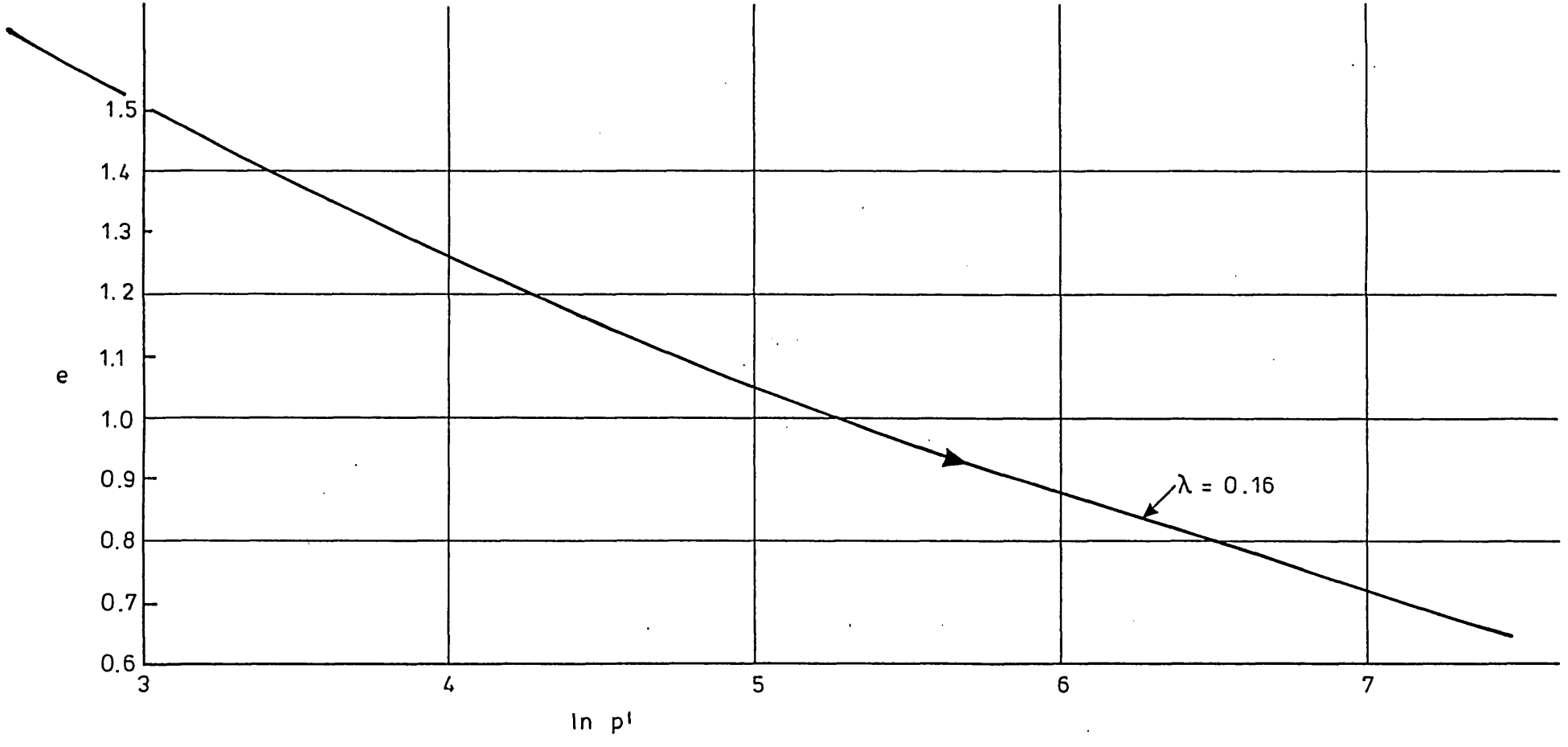


Figure 6.26. Jardine's (1985) London clay slurry oedometer test (converted from σ_v' to p' by p' = .733 σ_v' assuming K_o = 0.6).

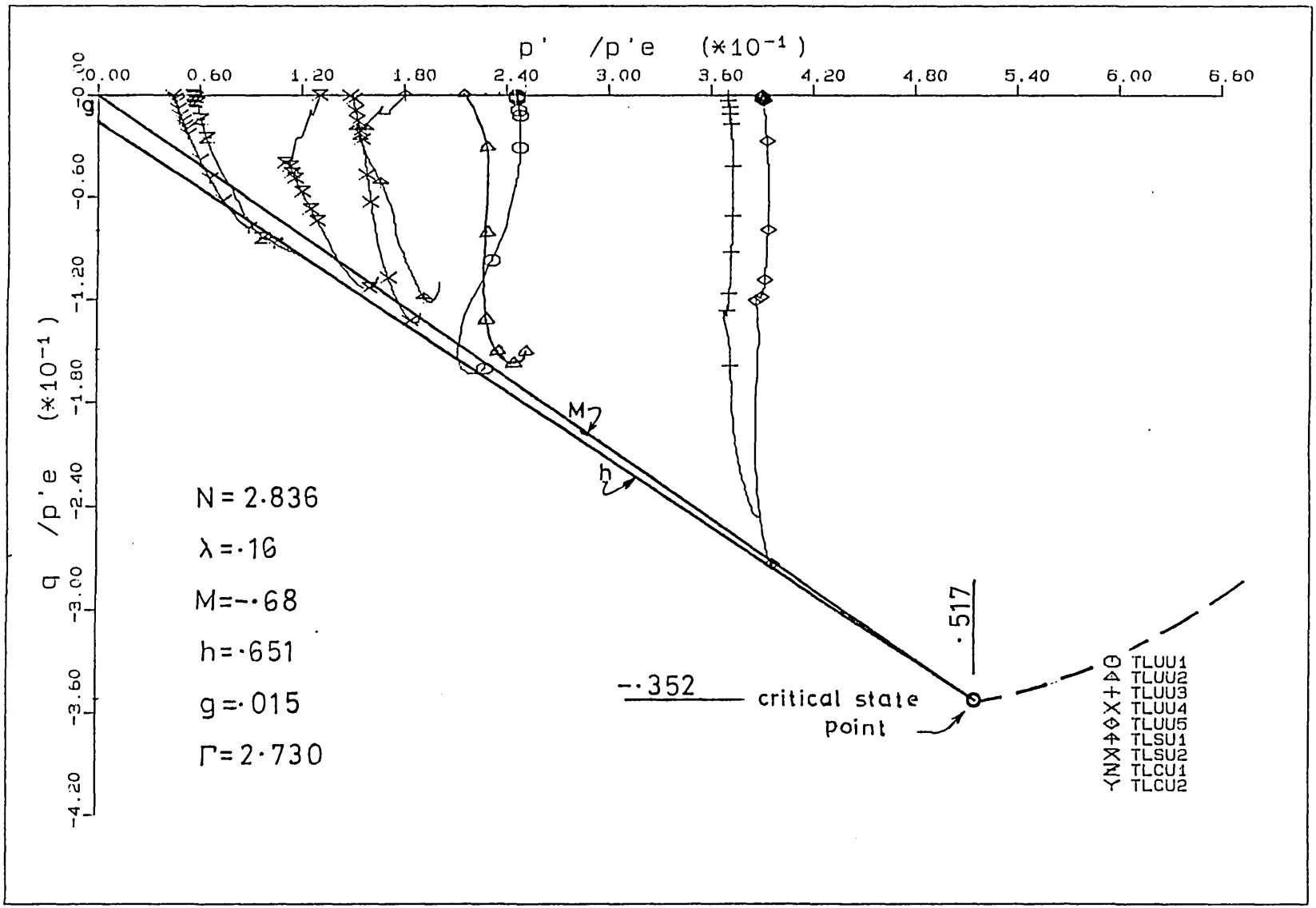


Figure 6.27. Critical state surface and Hvorslev surface for London clay extension tests.

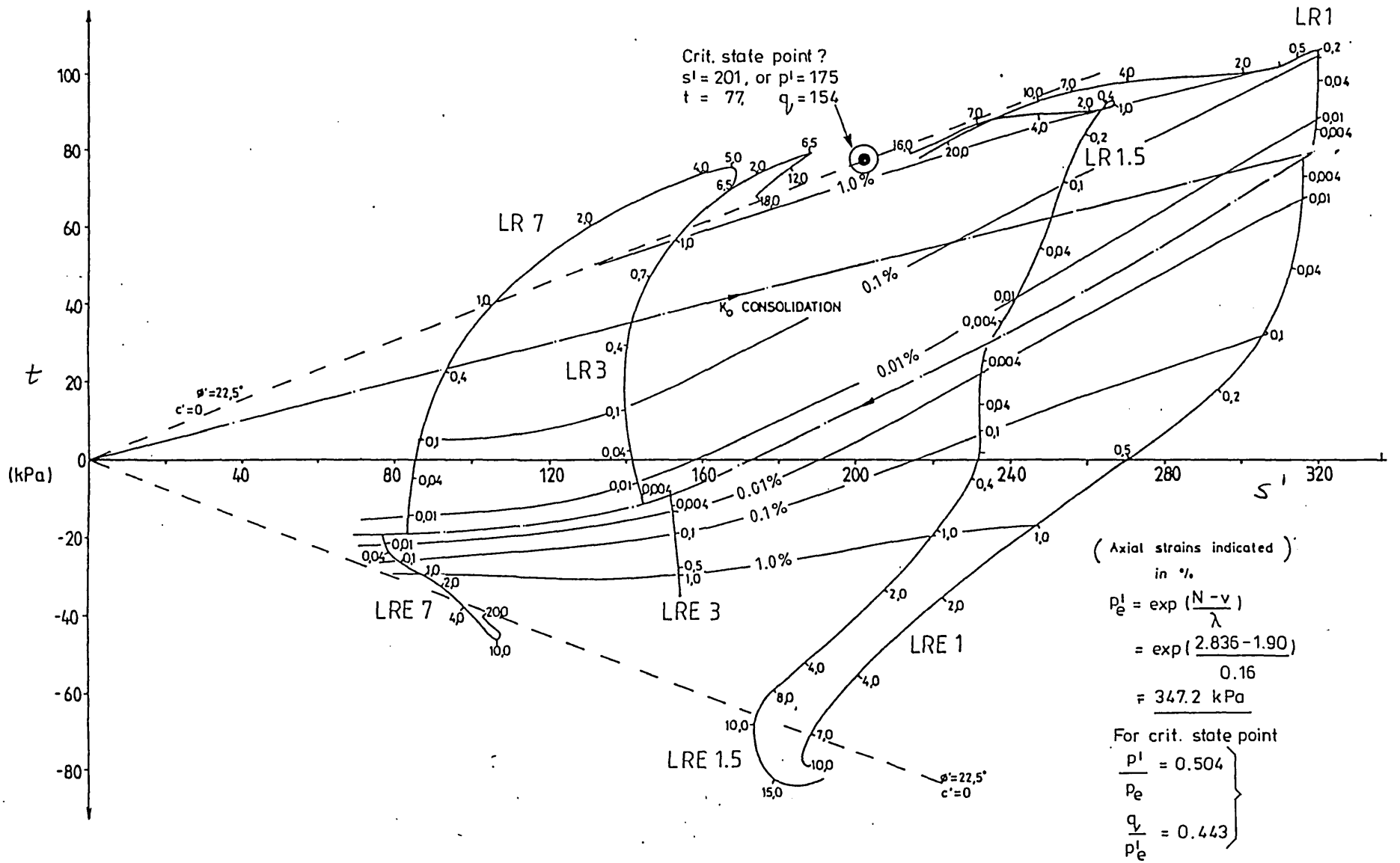


Figure 6.28. Effective stress paths for undrained tests on reconstituted London clay (after Jardine, 1985).

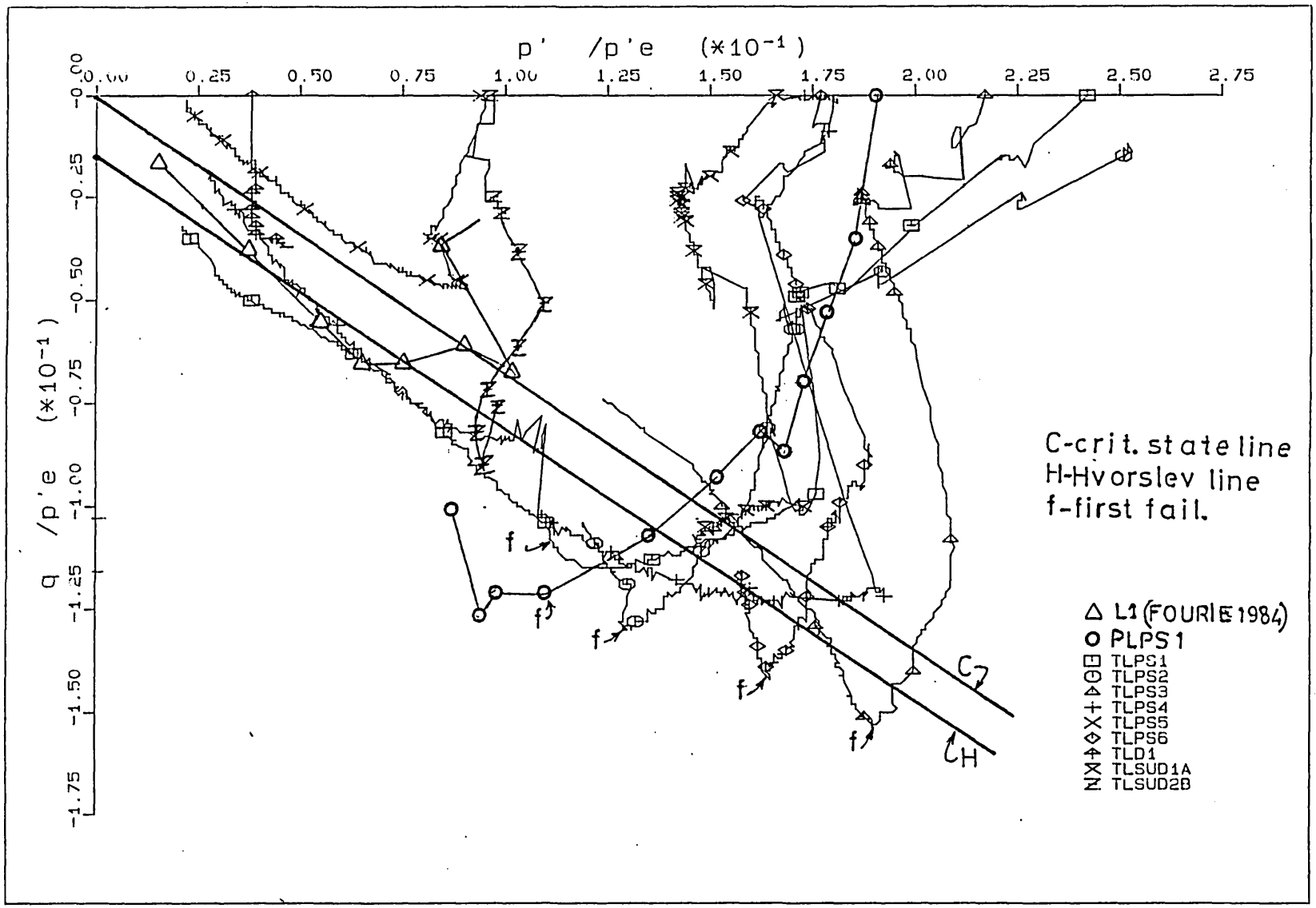


Figure 6.29. Stress paths from London clay triaxial passive stress relief tests, constant q swelling tests, undrained/drained test and plane strain passive stress relief test plotted in terms of critical state parameters.

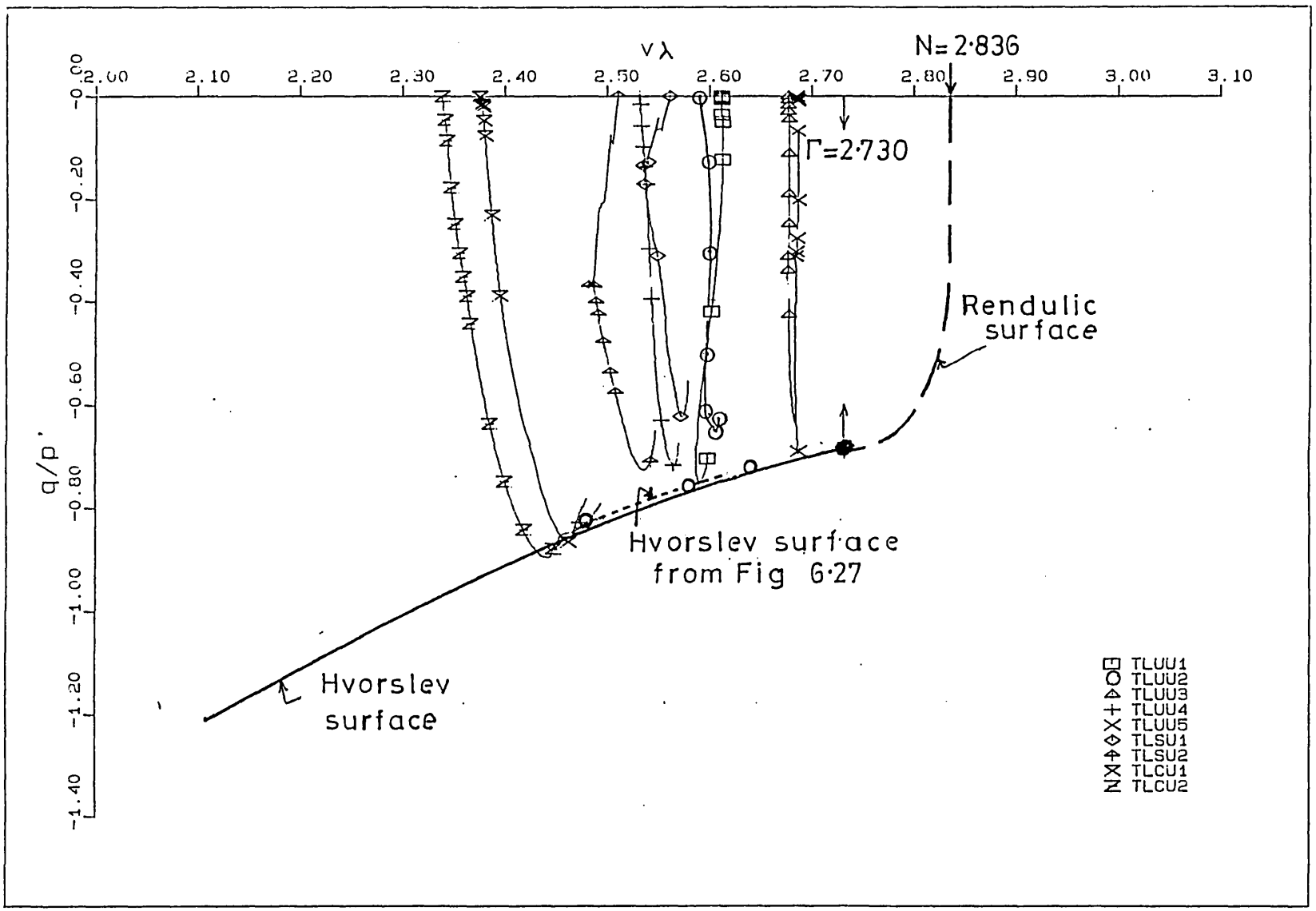


Figure 6.30. London clay undrained extension tests plotted in terms of v_λ, q/p'.

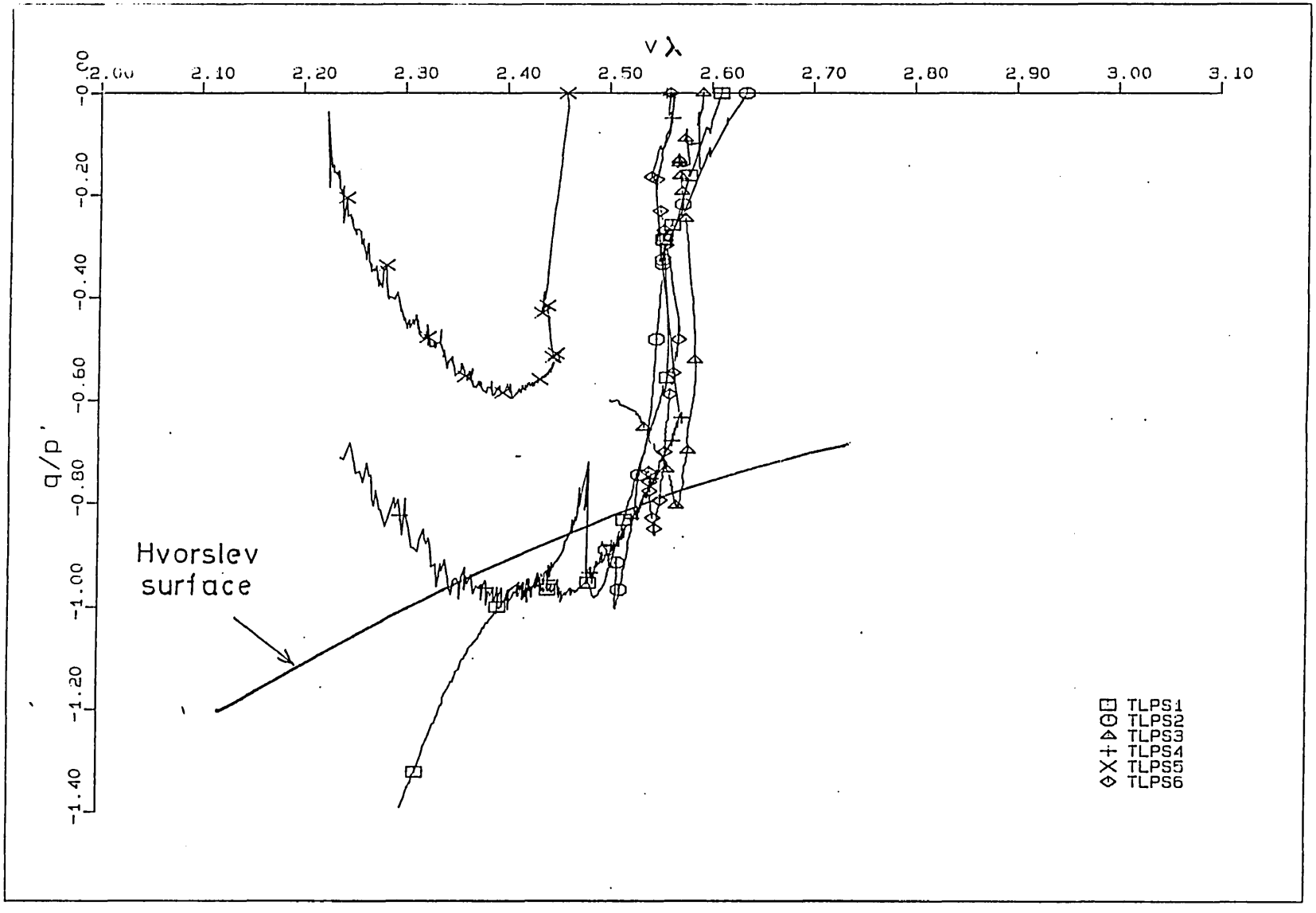


Figure 6.31. London clay passive stress relief tests plotted in terms of v_λ, q/p'.

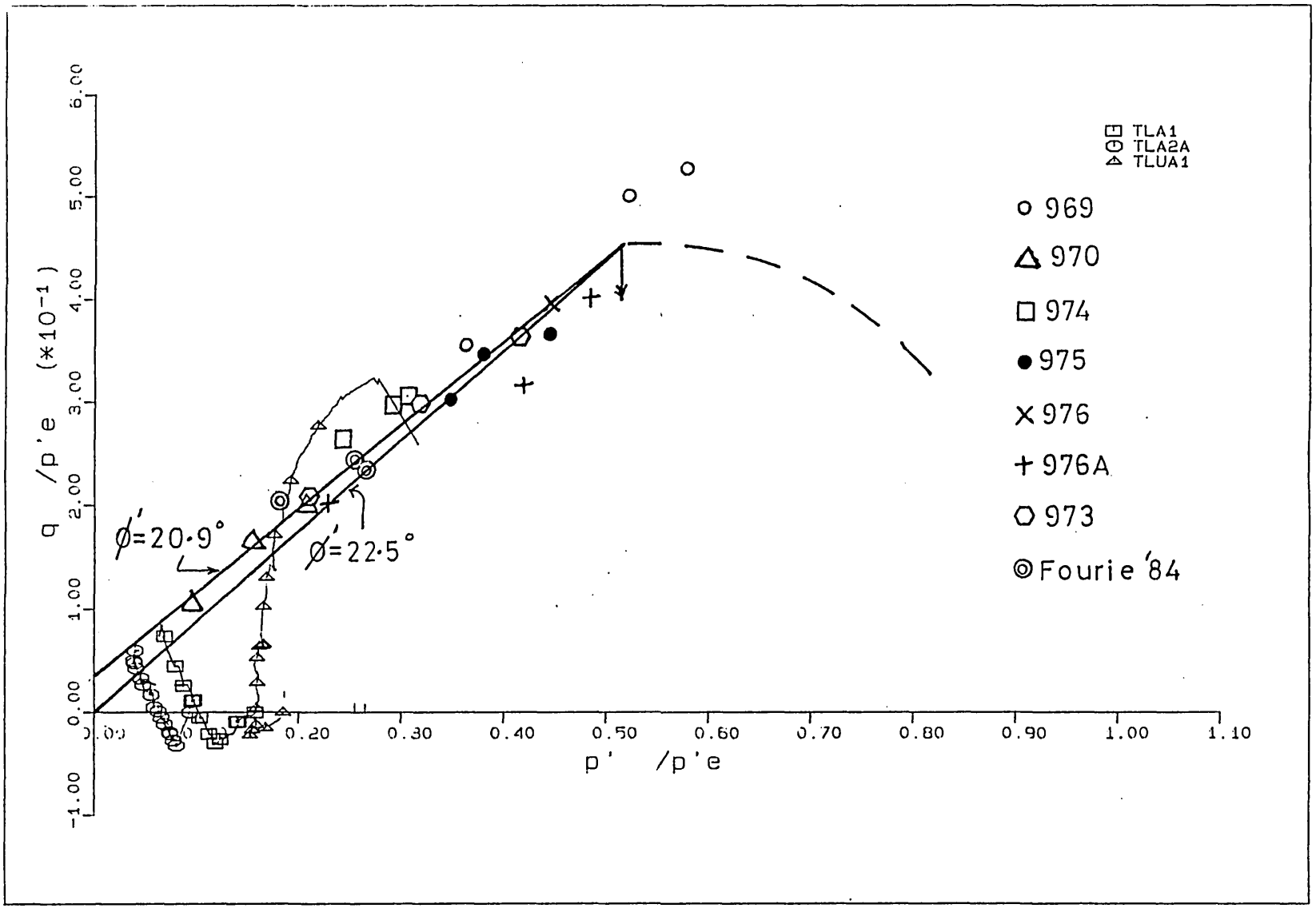


Figure 6.32. London clay compression tests plotted in terms of critical state parameters.

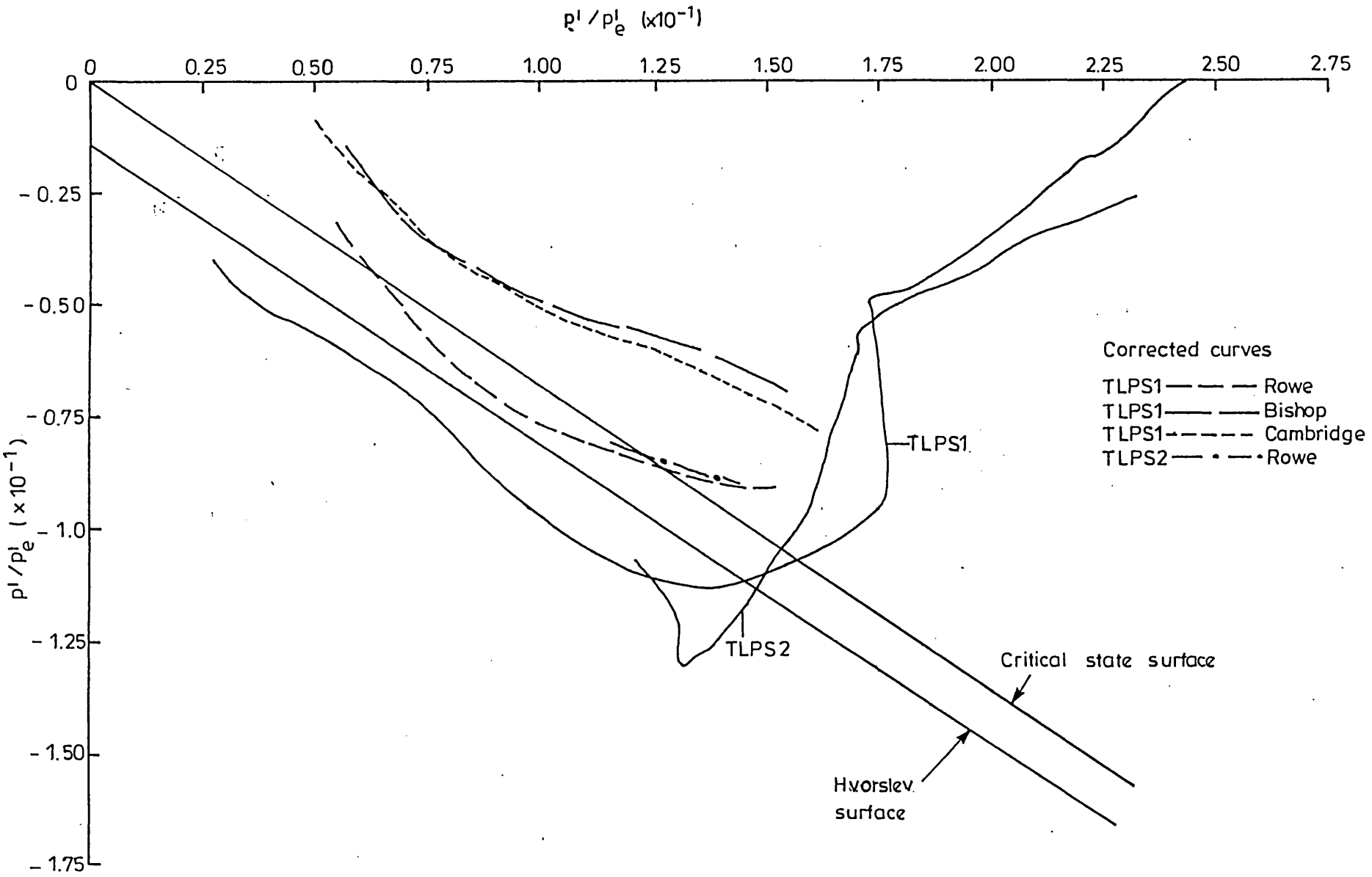


Figure 6.33. Stress paths for London clay passive stress relief tests plotted in terms of p'/p'_e versus q/p'_e; corrections for dilatency effects shown.

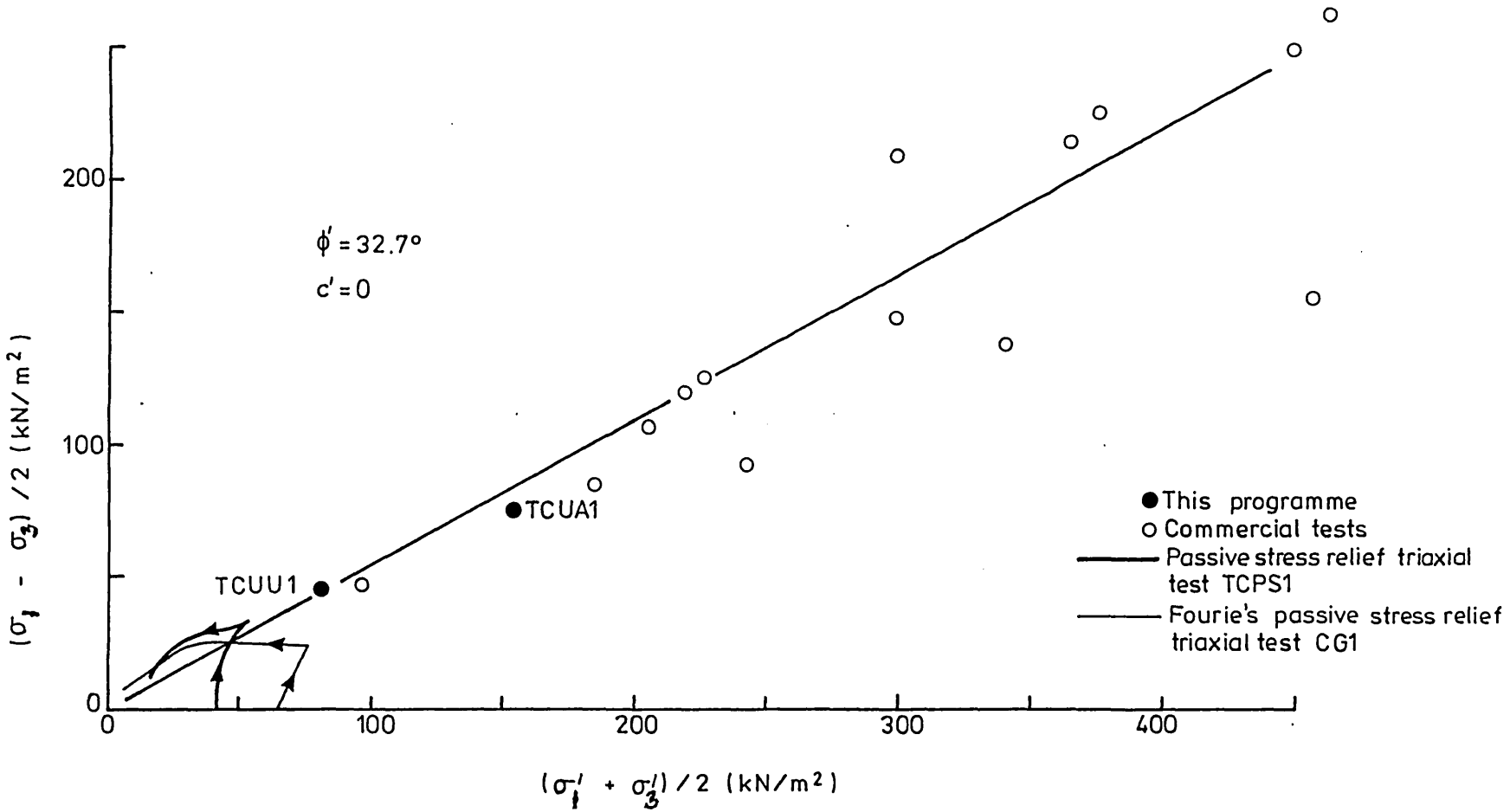


Figure 6.34. Undrained and passive stress relief tests on Claygate Beds - compression and extension tests.

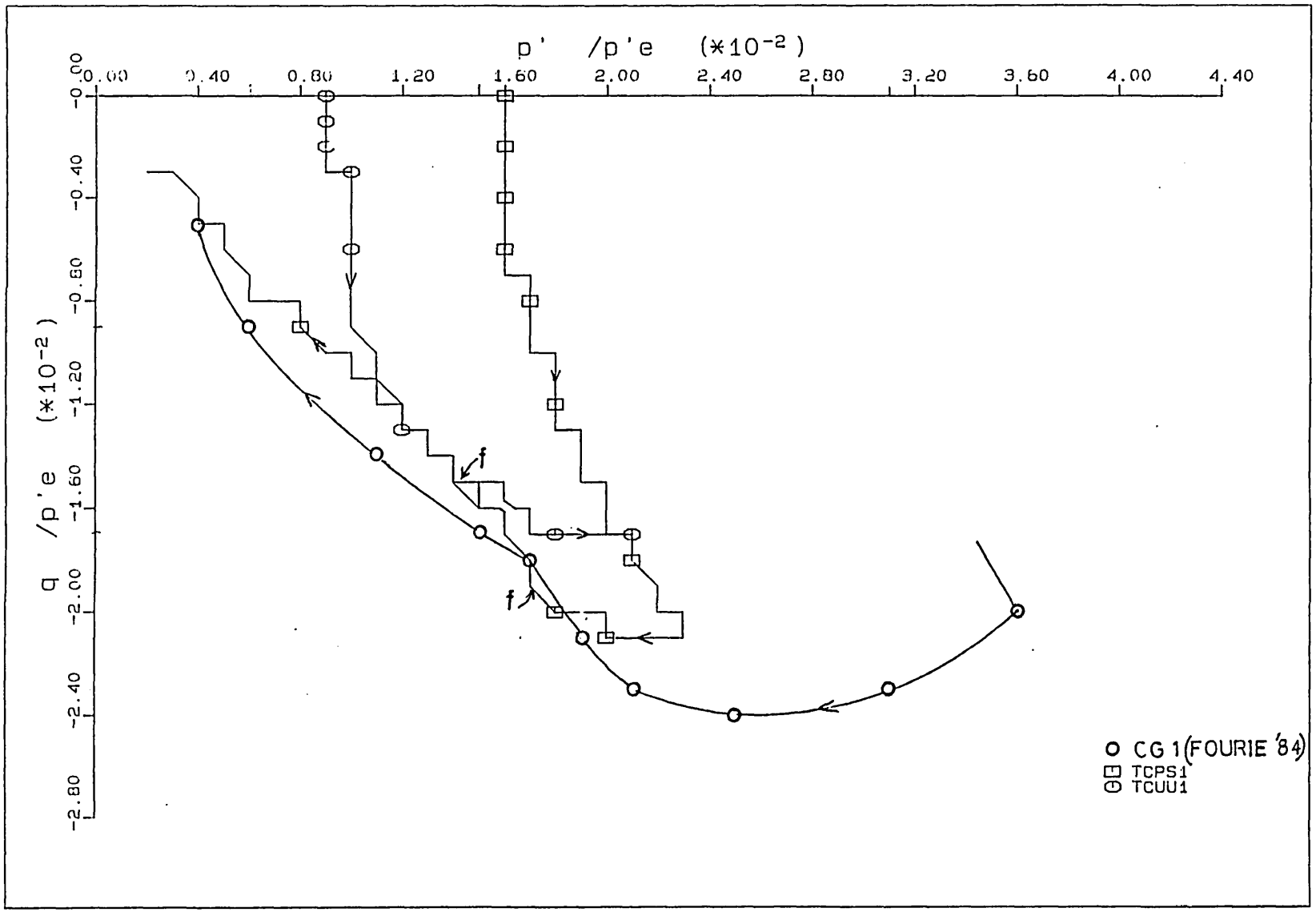


Figure 6.35. Claygate Beds: undrained extension and passive stress relief tests plotted in terms of critical state parameters.

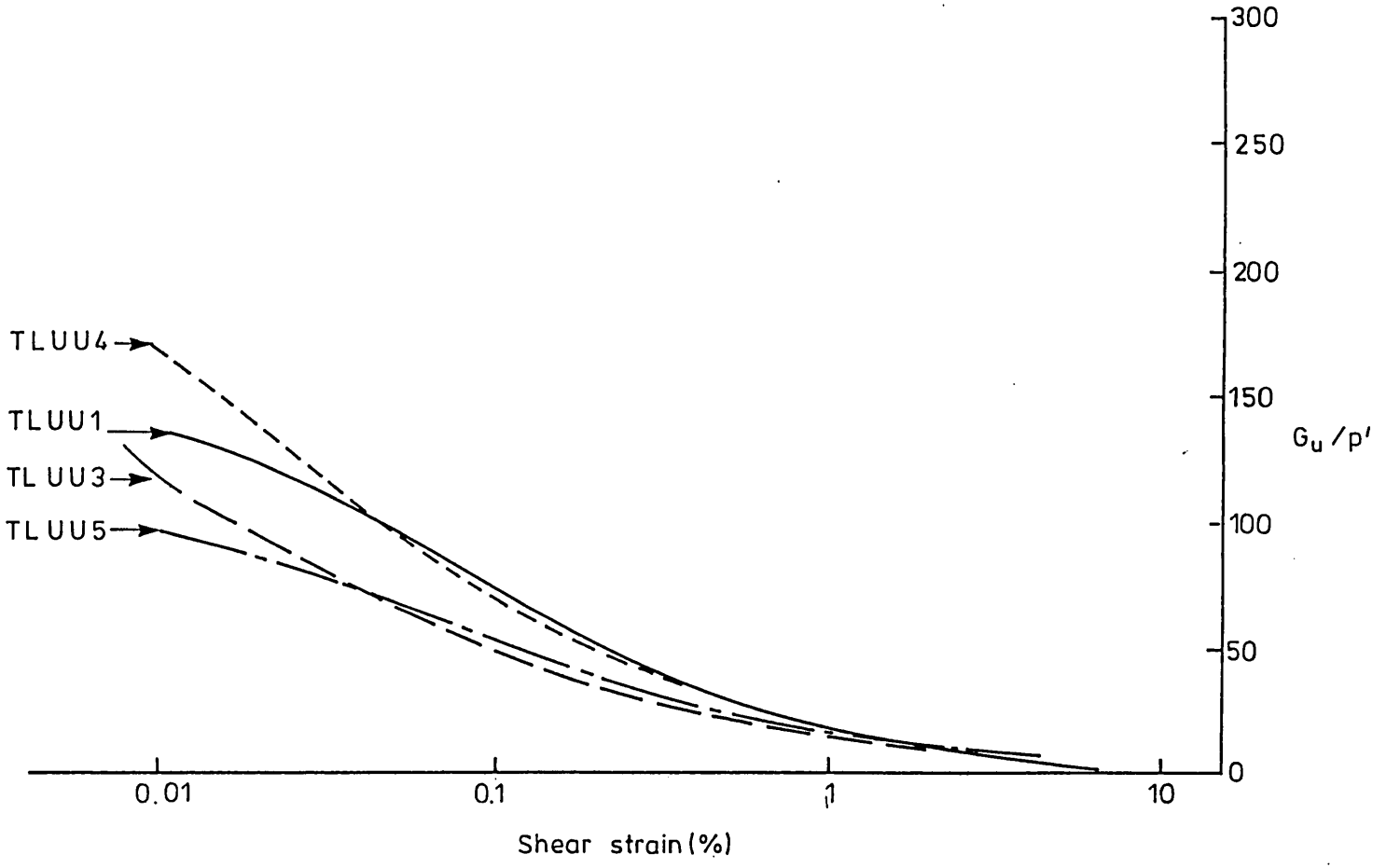


Figure 6.36. G_u/p' versus shear strain for undrained extension tests from initial isotropic stress: London clay.

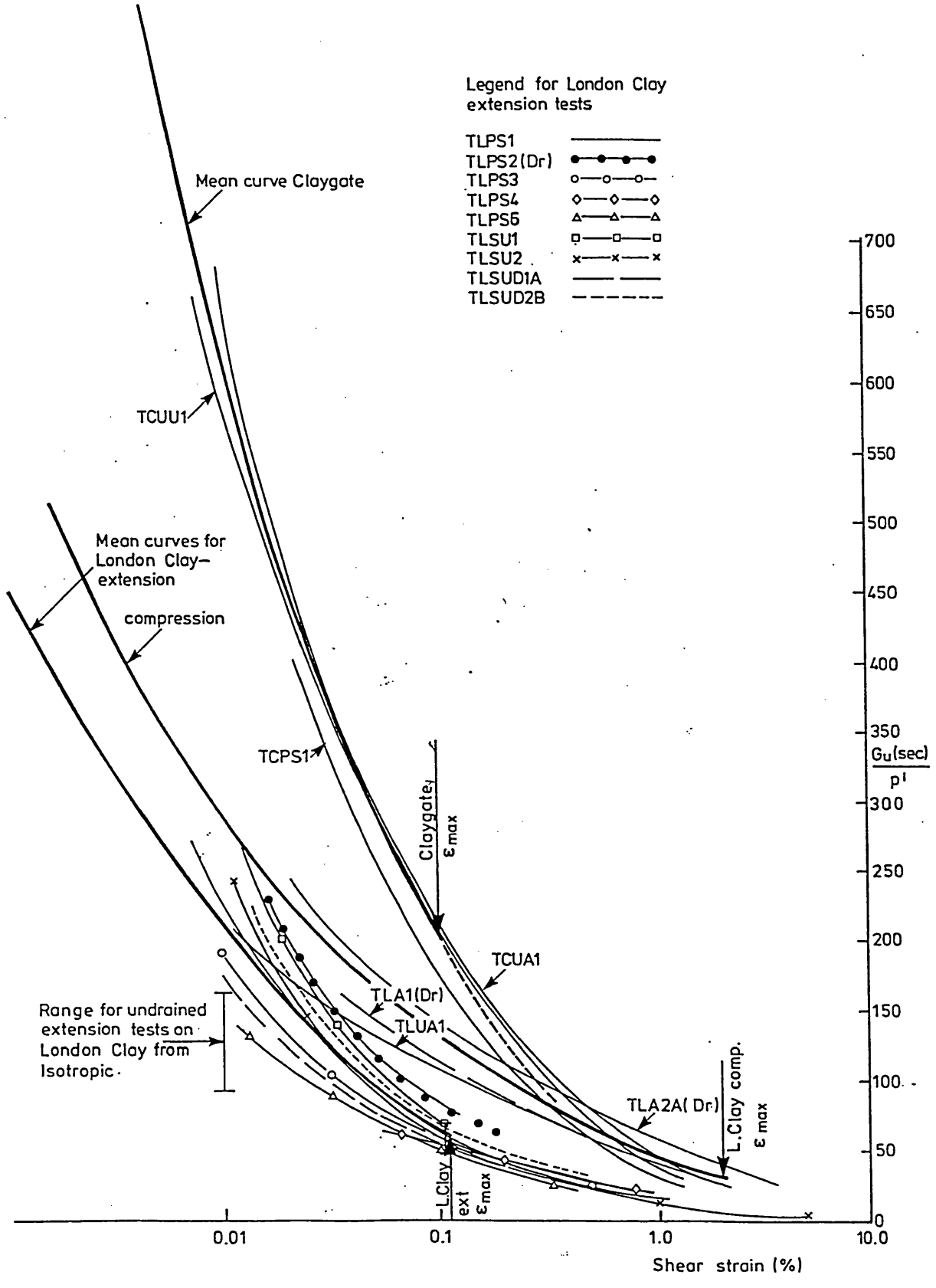


Figure 6.37. London clay and Claygate Beds: Gu/p' versus shear strain for undrained extension and compression tests from K_o.

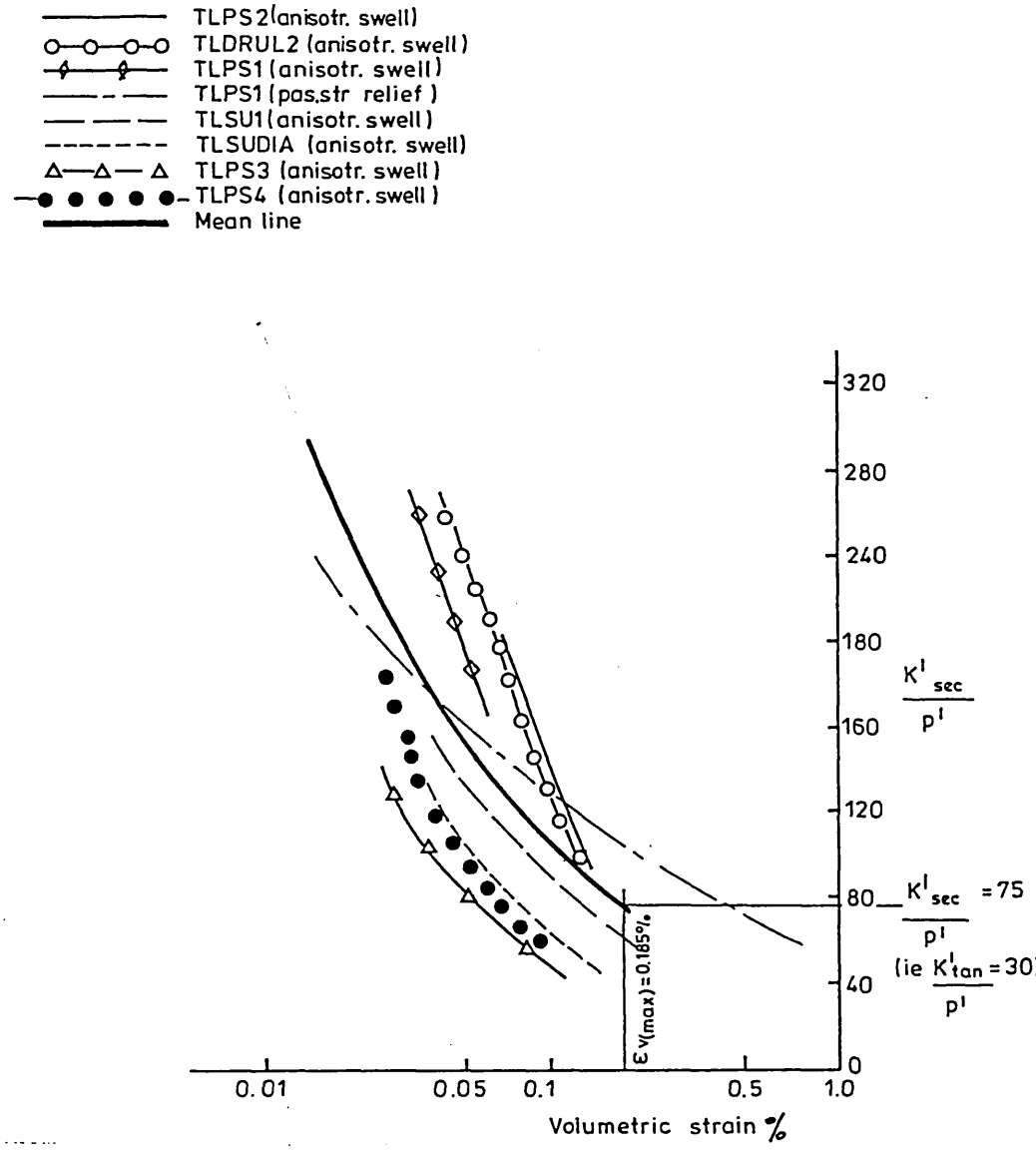


Figure 6.38. K'_{sec}/p' versus volumetric strain for swelling phases of extension tests on London clay.

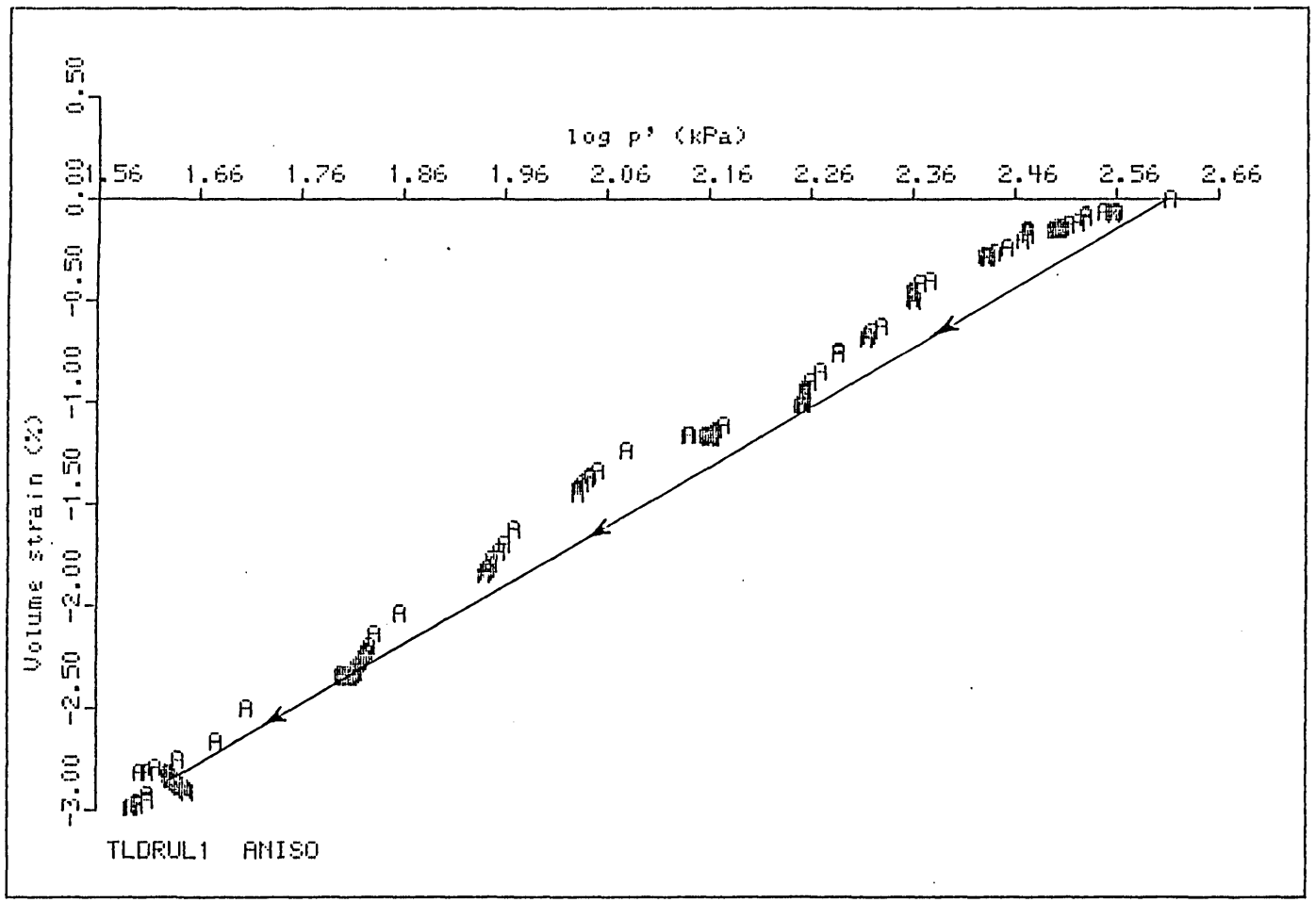


Figure 6.39. Relationship between volumetric strain and log p' for K_o swelling test TLDRUL1.

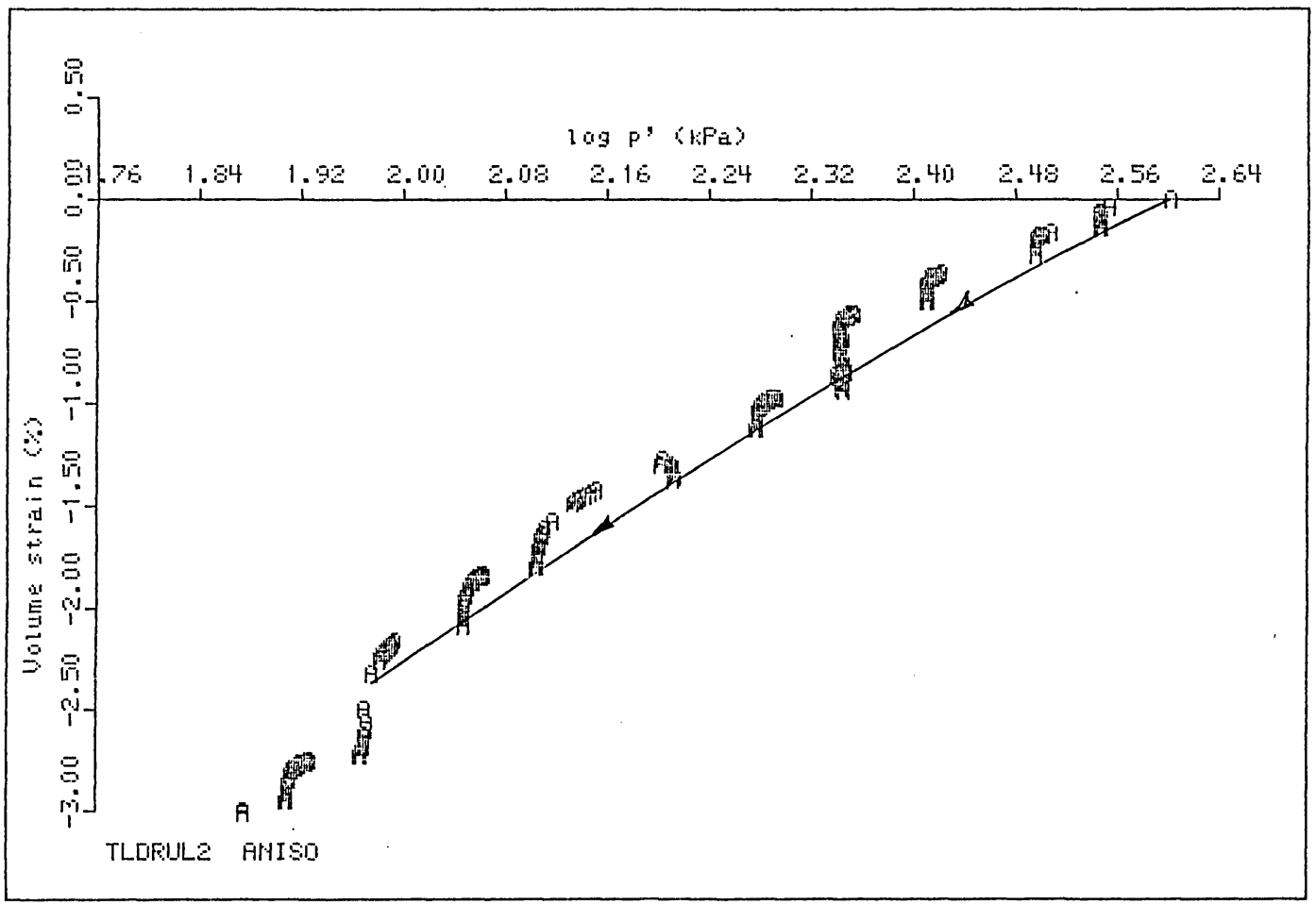


Figure 6.40. Relationship between volumetric strain and log p' for K_o swelling test TLDRUL2.

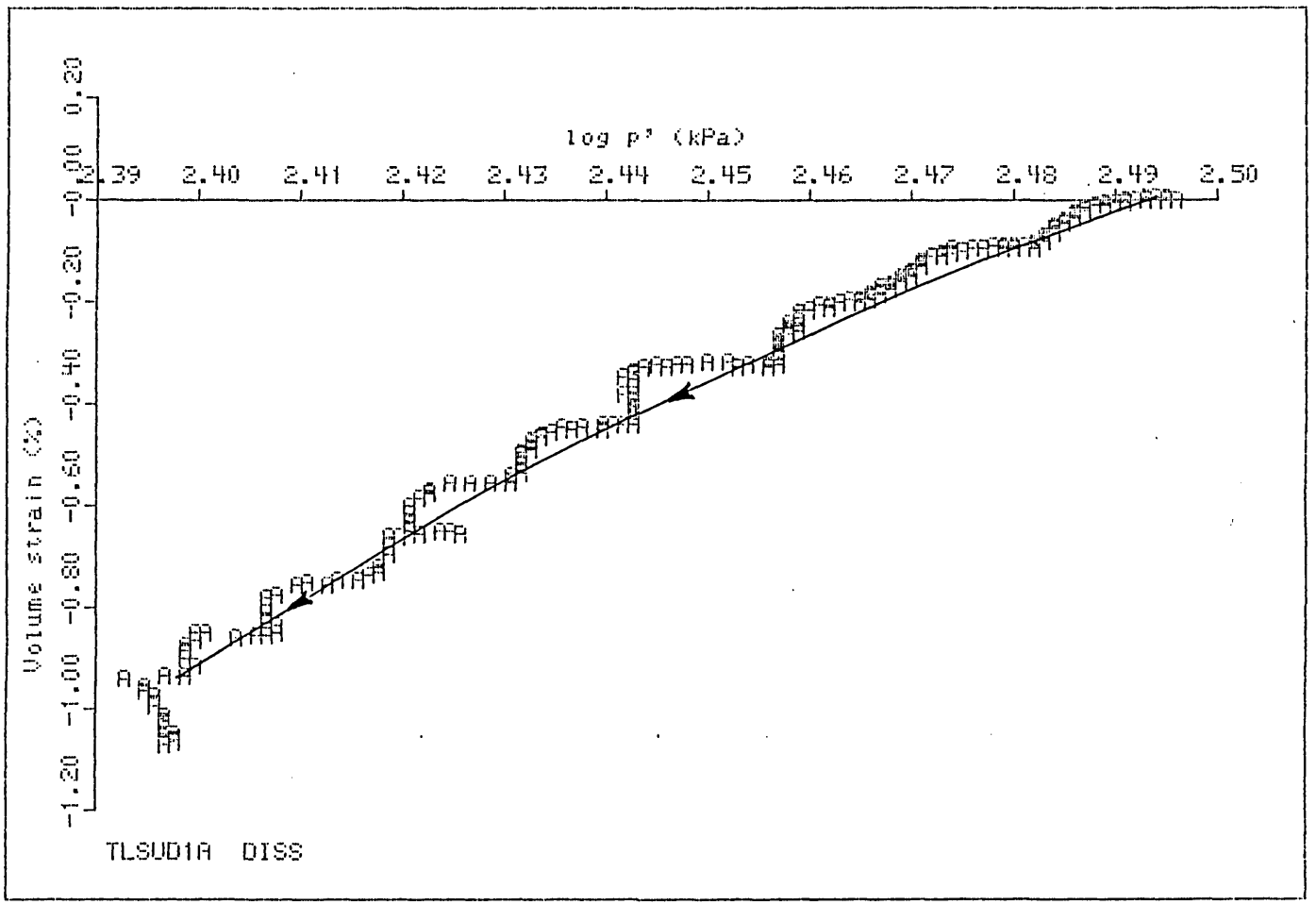


Figure 6.41. Relationship between volumetric strain and log p' for constant q swelling test TSLUD1A.

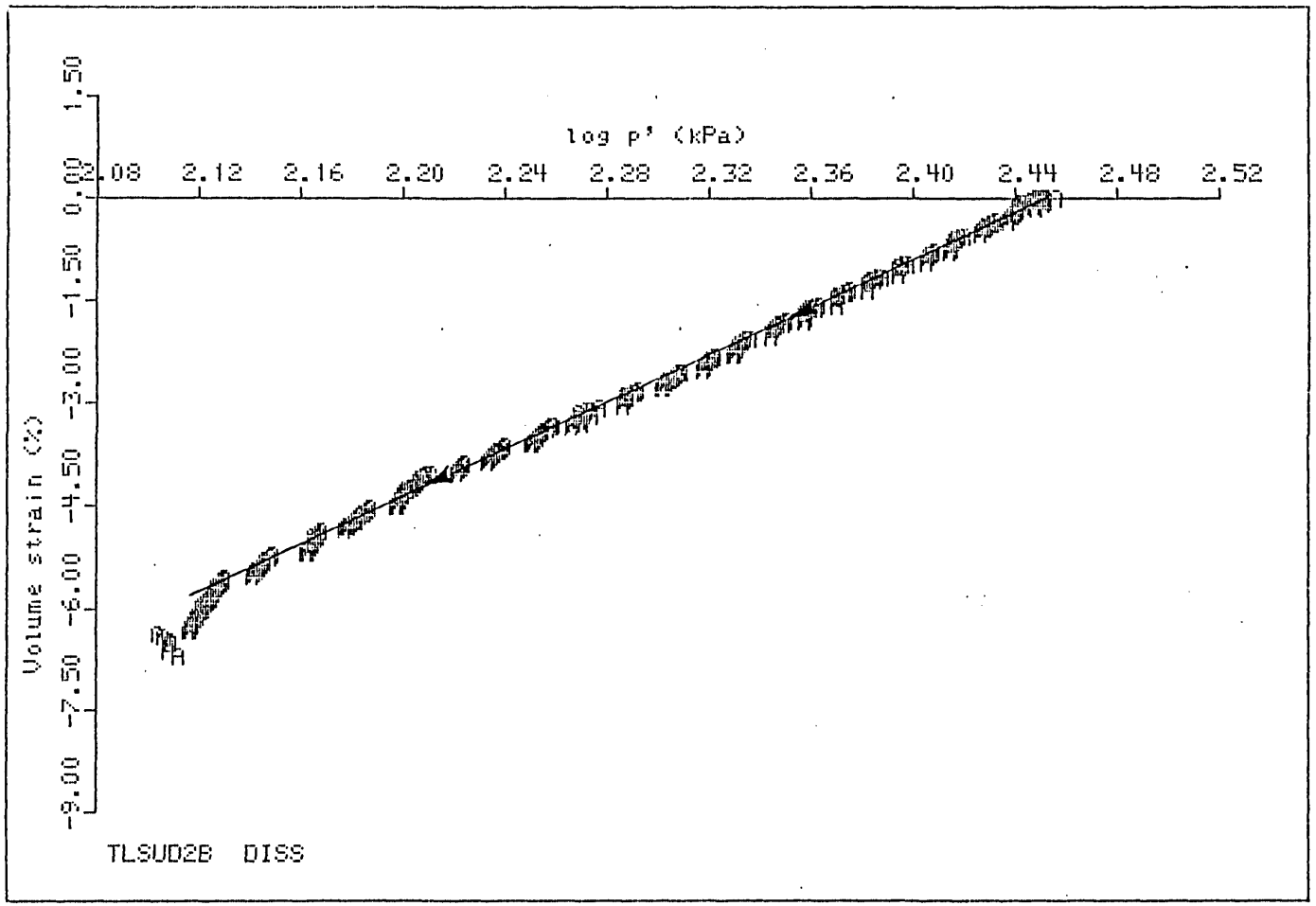


Figure 6.42. Relationship between volumetric strain and log p' for constant q swelling test TLSUD2B.

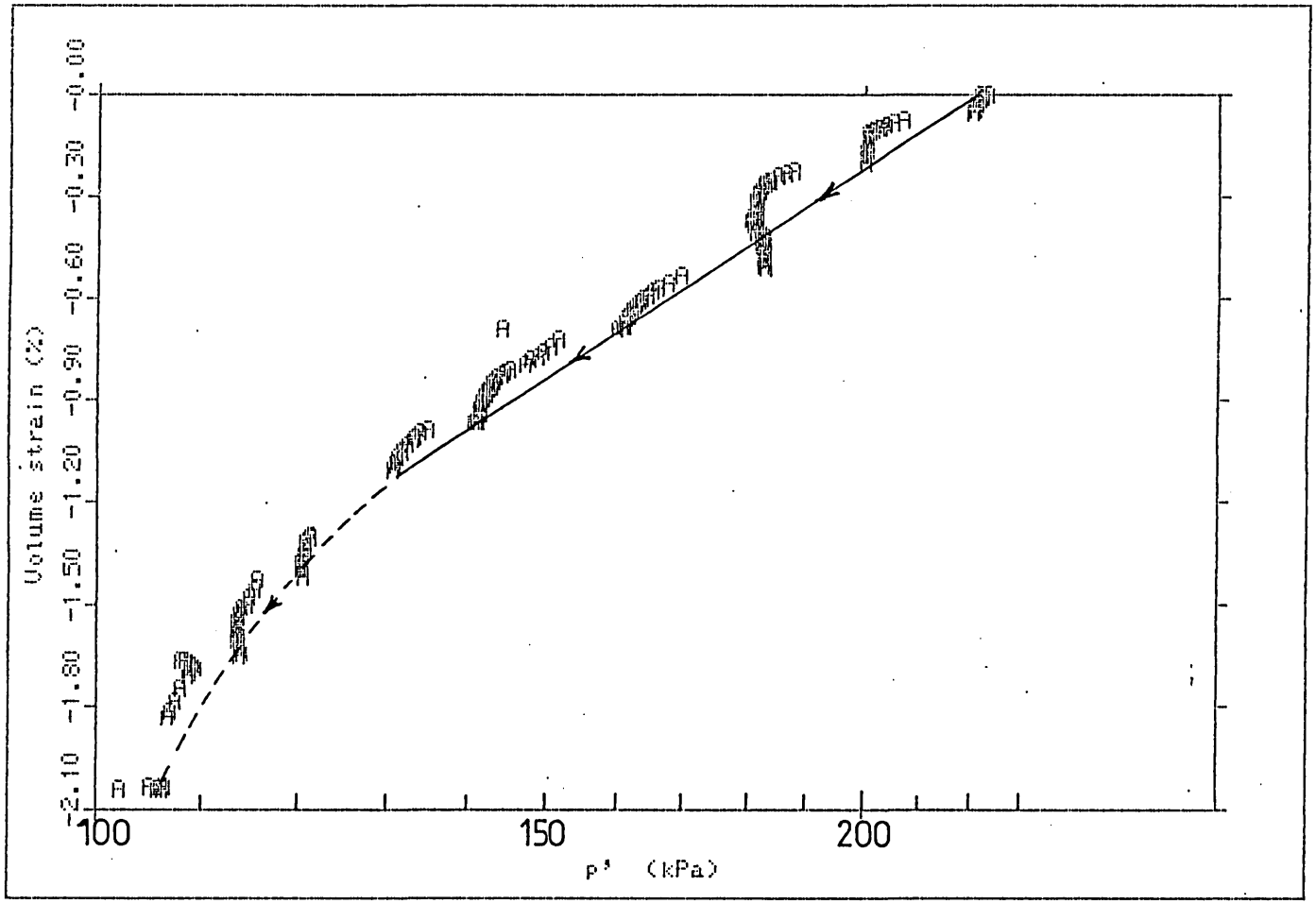


Figure 6.43. Relationship between volumetric strain and log p' for drained active test TLA1.

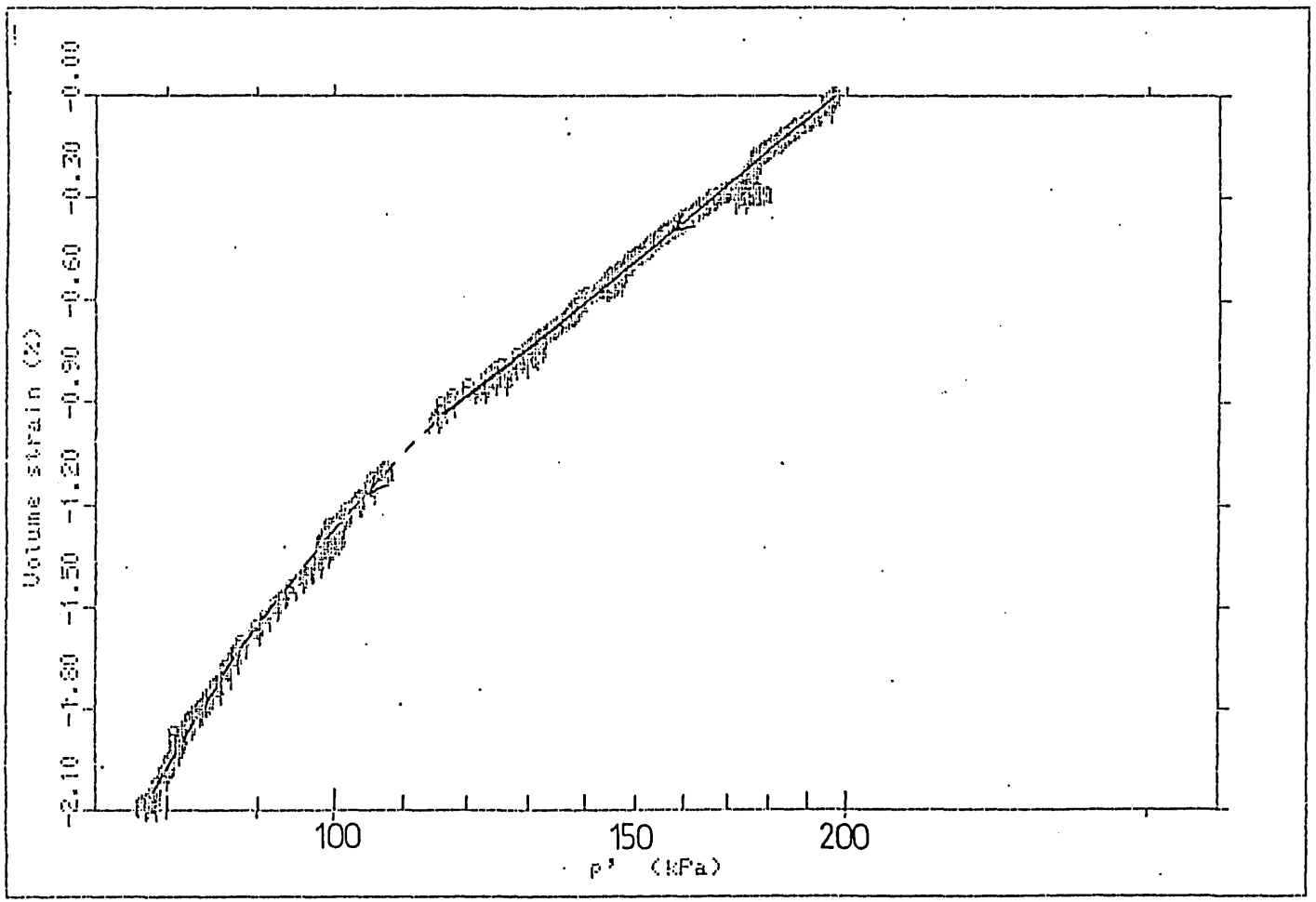


Figure 6.44. Relationship between volumetric strain and log p' for drained active test TLA2A.

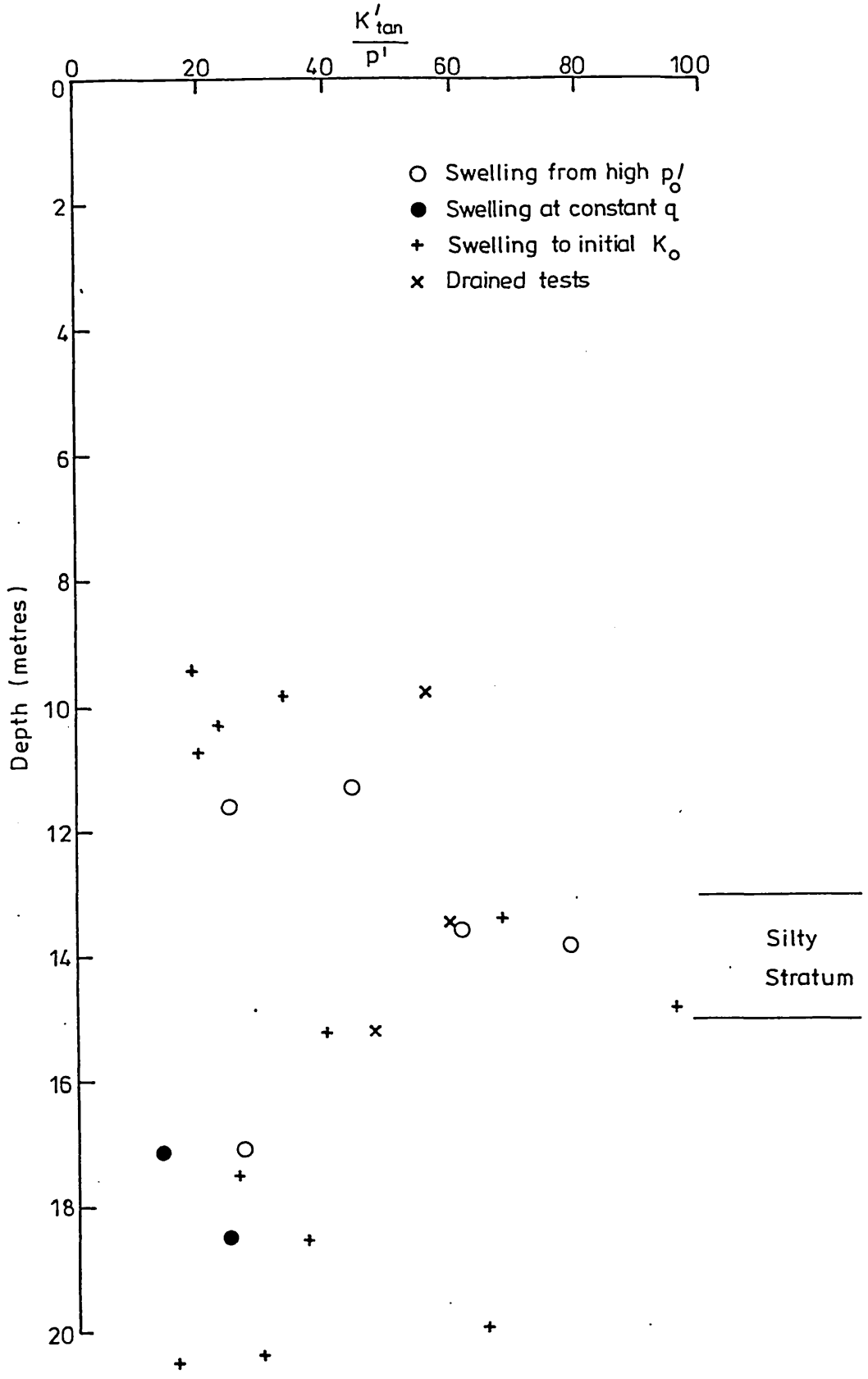


Figure 6.45. Values of K'/p' plotted against depth.

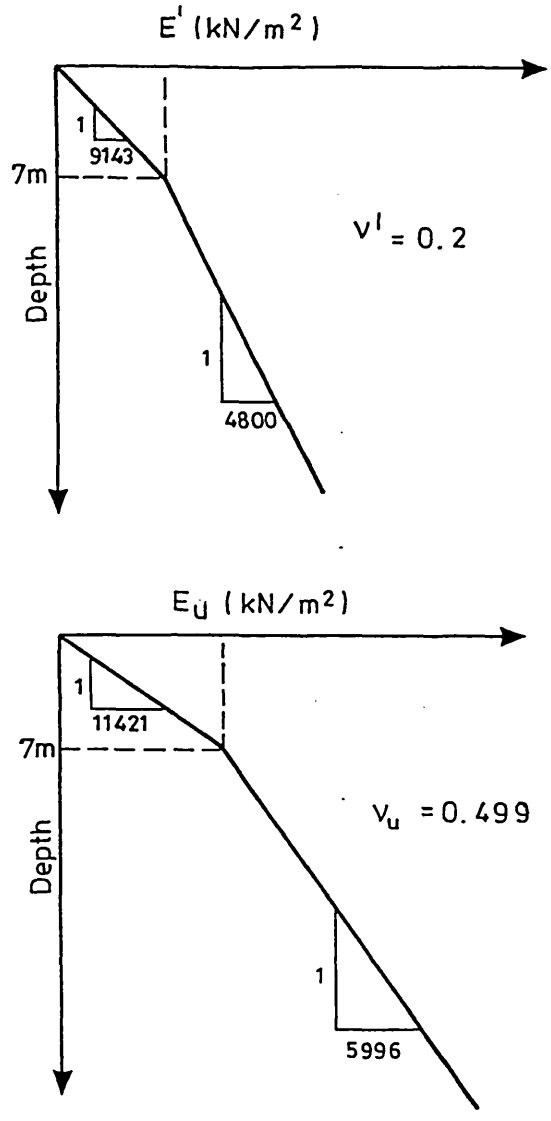


Figure 6.46. Variation of E_u, E' with depth. After Potts and Burland (1983).

APPENDIX A1

TABLES AND FIGURES

Table A1.1

Calibrations of instruments used with the triaxial, stress path and plane strain cells

(5 sheets)

Conventional triaxial cell calibrations
May - July 1984

Transducer	Model	Range	Sensitivity	Resolution	Mean error from best st. line	Coefft. of correlation of best st. line	Remarks
Cell Pressure	Bell & Howell	0-700kPa	257.0kPa/mV	0.3kPa	±1.5kPa	0.99996	with conventional triaxial May 1984
Back Pressure	Bell & Howell	0-700kPa	282.0kPa/mV	0.3kPa	±0.5kPa	0.99999	
Load Cell	IC	Compression 0-1000N	494.3N/mV*	0.5N	±0.4N*	0.99995	*for range 0-15N. For rest of compr. range error will be -2% max
Vol Gauge	IC	0-100ml	72ml/mV	0.07ml	±0.04	0.99999	

Stress path Cell 1 May - July 1984

Cell Pressure	Bell & Howell	0-1000kPa	87.11kPa/mV	0.09kPa	±1.0kPa	0.99999	
Back Pressure	Bell & Howell	0-1000kPa	84.20kPa/mV	0.08kPa	±1.4kPa	0.99998	Stress path cell 1: Solartron DTU, May - July 1984
Ram Pressure	Bell & Howell	0-1000kPa	89.19kPa/mV	0.09kPa	±0.6kPa	1.00000	
Load Cell	IC	tension -4500N-0	158.7N/mV* (tension)	0.2N	±0.4N	0.99998	*Extension tests only
Vol Gauge	IC	0-50ml	2.39ml/mV	0.002ml	±.03ml	1.00000	
Displ	MPE	0-25mm	4.76mm/mV	0.005mm	±.006mm	0.99998	

Stress path cell calibrations: Cell 1

Transducer	Model	Range	Sensitivity	Resolution	Mean error from best st. line	Coefft. of correlation of best st. line	Remarks
		September 1984					
Ram Pressure	Bell & Howell (4-306-0131)	0-1000kPa	51.67kPa/mV	.01kPa	±0.6kPa	0.99999	Recalibration of Cell 1 with Orion September 1984
Back Pressure	Bell & Howell (4-306-0131)	0-1000kPa	51.65kPa/mV	.01kPa	±1.5kPa	1.00000	
Cell Pressure	Bell & Howell (4-306-0131)	0-1000kPa	50.78kPa/mV	.01kPa	±1.0kPa	1.00000	
Disp. Trans.	MPE	0-25mm	1.06mm/mV	.005mm	±.007mm	0.99998	
Vol Gauge	IC	0-50ml	1.34ml/mV	.002ml	±.03ml	1.00000	
Load Cell	IC	compression 0-4500N	80.2N/mV* (compression)	0.1N	±.1N*	1.00000	*for range 0-114N. Beyond this, error will be -0.3% max
		tension -4500-0	83.4N/mV (tension)	0.1N	±1.3N	0.99980	0-300N
		February 1986					
Ram Pressure	Bell & Howell (4-306-0131)	0-1000kPa	51.71kPa/mV	.01kPa	±0.5kPa	1.00000	Stress path Cell 1 recalibration with new load cell Feb 1986
Back Pressure	Bell & Howell (4-306-0131)	0-1000kPa	52.42kPa/mV	.01kPa	±0.7kPa	1.00000	
Cell Pressure	Bell & Howell (4-306-0131)	0-1000kPa	51.11kPa/mV	.01kPa	±0.6kPa	1.00000	
Disp. Trans.	MPE	0-25mm	1.065mm/mV	.005mm	±.007	0.99999	
Vol Gauge	IC	0-50ml	1.354ml/mV***	.002ml	±.05ml***	1.00000	***Against a back pressure
Load Cell	IC	compression 0-4500N	73.9N/mV (compression)	0.1N	±.1N**	0.99998	**For loads 0-114N. Beyond this error will increase to -1% max
		tension -4500-0	77.8N/mV (tension)	0.1N	±1.0N*	0.99993	*For loads 0-300N (-.5N error to -30N)
Pore pres. Probe	Druck PDCR81 No 3209(CH68)	0-1400kPa	17.17kPa/mV	.01kPa	±.5kPa	1.00000	

Stress path cell calibrations: Cell 2

Transducer	Model	Range	Sensitivity	Resolution	Mean error from best st. line	Coefft. of correlation of best st. line	Remarks
		September 1984					
Ram Pressure	Senso-Metric (SP91-KES)	0-2000kPa	20.41kPa/mV	.01kPa	±0.2kPa	1.00000	Stress path Cell 2 Orion September 1984
Back Pressure	Senso-Metric (SP91-KES)	0-2000kPa	20.39kPa/mV	.01kPa	±0.2kPa	1.00000	
Cell Pressure	Senso-Metric (SP91-KES)	0-2000kPa	20.43kPa/mV	.01kPa	±0.2kPa	1.00000	
Disp. Trans.	MPE	0-25mm	0.976mm/mV	.005mm	±.007mm	0.99999	
Vol Gauge	IC	0-50ml	1.862ml/mV**	.002ml	±.04ml**	0.99996**	**against open burette
Load Cell	IC	compression 0-4500N	77.70N/mV (compression)	0.1N	±0.2N*	0.99997	*for range 0-114N. Beyond this, error will be up to +1%
		tension -4500-0	85.04N/mV (tension)	0.1N	±0.4N	0.99995	0 to -300N
		September 1985					
Ram Pressure	Senso-Metric (SP91-KES)	0-2000kPa	20.42kPa/mV	.01kPa	±0.4kPa	0.99999	Stress path Cell 2 Orion recalibration September 1985
Back Pressure	Senso-Metric (SP91-KES)	0-2000kPa	20.39kPa/mV	.01kPa	±0.4kPa	0.99999	
Cell Pressure	Senso-Metric (SP91-KES)	0-2000kPa	20.43kPa/mV	.01kPa	±0.4kPa	0.99999	
Disp. Trans.	MPE	0-25mm	0.978mm/mV	.005mm	±.007mm	0.99999	
Vol Gauge	IC	0-50ml	1.866ml/mV*	.002ml	±.05ml*	0.99997*	*Against a back pressure
Load Cell	IC	compression 0-4500N	77.97N/mV (compression)	0.1N	±.1N**	1.00000	**For range 0-114N. Beyond this error will increase to -1% max
		tension -4500-0	85.46N/mV (tension)	0.1N	±1.0N*	0.99991	*For loads 0-300N (±.2N error to -30N)
Pore pres. Probe	Druck PDCR81 No 2421(CH67)	0-1400kPa	17.71kPa/mV	.01kPa	±.7kPa	1.00000	

Stress path cell load cell calibrations
April 1986 and LVDT calibrations

Transducer	Model	Range	Sensitivity	Resolution	Mean error from best st. line	Coefft.of correlation of best st. line	Remarks	
Load Cell	IC	compression 0-4500N	74.58N/mV* (compression)	0.1N	± .1N*	1.00000	*For loads 0 to 140N. Beyond this error will be -.5%	Stress path Cell 1 ld cell regauged April 1986
		tension -4500-0N	77.80mV** (tension)	0.1N	±.5N**	0.99996	**For loads 0 to -300N	
		compression 0-4500N	77.60/mV* (compression)	0.1N	±.1N*	1.00000	*For loads 0 to 140N Beyond this error will increase to -1%	Stress path Cell 2 ld cell regauged April 1986
		tension -4500-0N	85.03mV** (tension)	0.1N	±.6N**	0.99992	**For loads 0 to -300N	
Radial strain belt LVDT	RDP Electronics D5/40W	±3mm	270mm/mV* average for linear portion	.0002mm	±.006mm (from curve)	0.99900	*3rd order polynomial used over whole range	
Plane strain lateral displ. LVDT	RDP Electronics	±3mm	234.33mm/mV	.0002mm	±.003mm	0.99996		

Plane Strain cell calibrations February 1987

Transducer	Model	Range	Sensitivity	Resolution	Mean error from best st. line	Coefft.of correlation of best st. line	Remarks
Back Pressure	Shape SP1020	0-1000kPa	27.05kPa/mV	.01kPa	±1.2kPa	0.99998	
Pore Pressure	Druck PDCR81* No. 3209	0-1400kPa	17.17kPa/mV	.01kPa	±.5kPa	1.00000	*Used previously with stress path cell 1
Disp Transducer	HPE	0-25mm	0.747mm/mV	.005mm	±.01mm	1.00000	
Vol Gauge	IC	0-50ml	1.355ml/mV**	.002ml	±.03ml	1.00000	**Against a back pressure
Load Cell (Vertical load)	IC	compression 0-4500N	79.30N/mV (compression)	0.1N	±.02*	0.99999	*To 140N. At higher loads error will be about +1%
		tension -4500-0	81.72N/mV (tension)		±1.4N**	0.99992	**-900N to 0N
Load Cell (Horizontal load)	IC	compression 0-4500N	91.80N/mV*	0.1N	±0.5N*	0.99961	*For loads up to 160N
			100.92N/mV**		±11.0N**	0.99985	**For high load range up to 3500N
		tension -4500-0N	100.25N/mV***	0.1N	±1.1N***	0.99993	***-900N to 0N
Cell Pressure	Shape SP108	0-1000kPa	19.72N/mV	.01kPa	±0.9kPa	1.00000	
Ram Pressure	Bell & Howell	0-700kPa	29.38N/mV	.01kPa	±1.7kPa	0.99996	

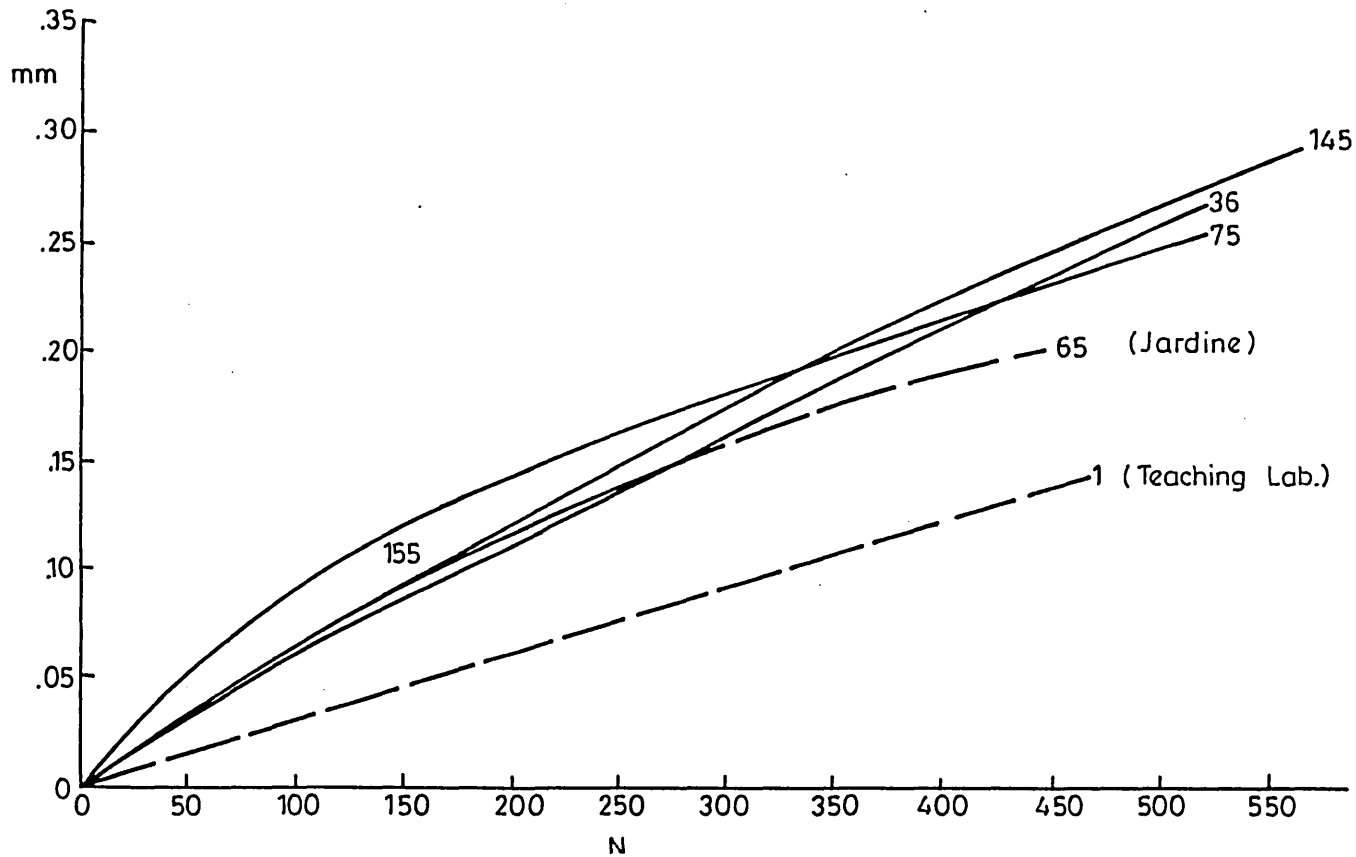


Figure A1.1. Load cell deflection/bedding calibrations: compression.

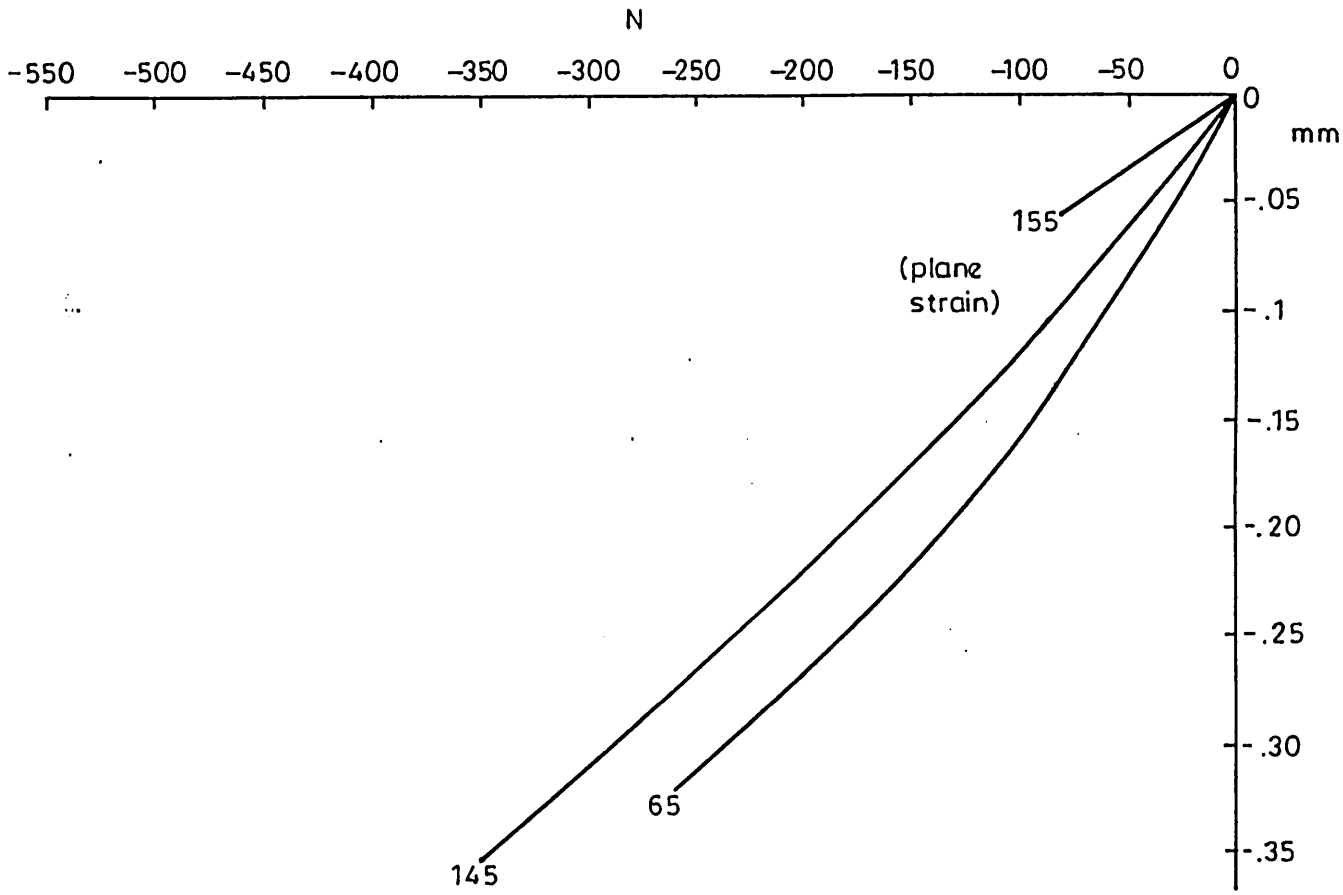


Figure A1.2. Load cell deflection/bedding calibrations: tension.

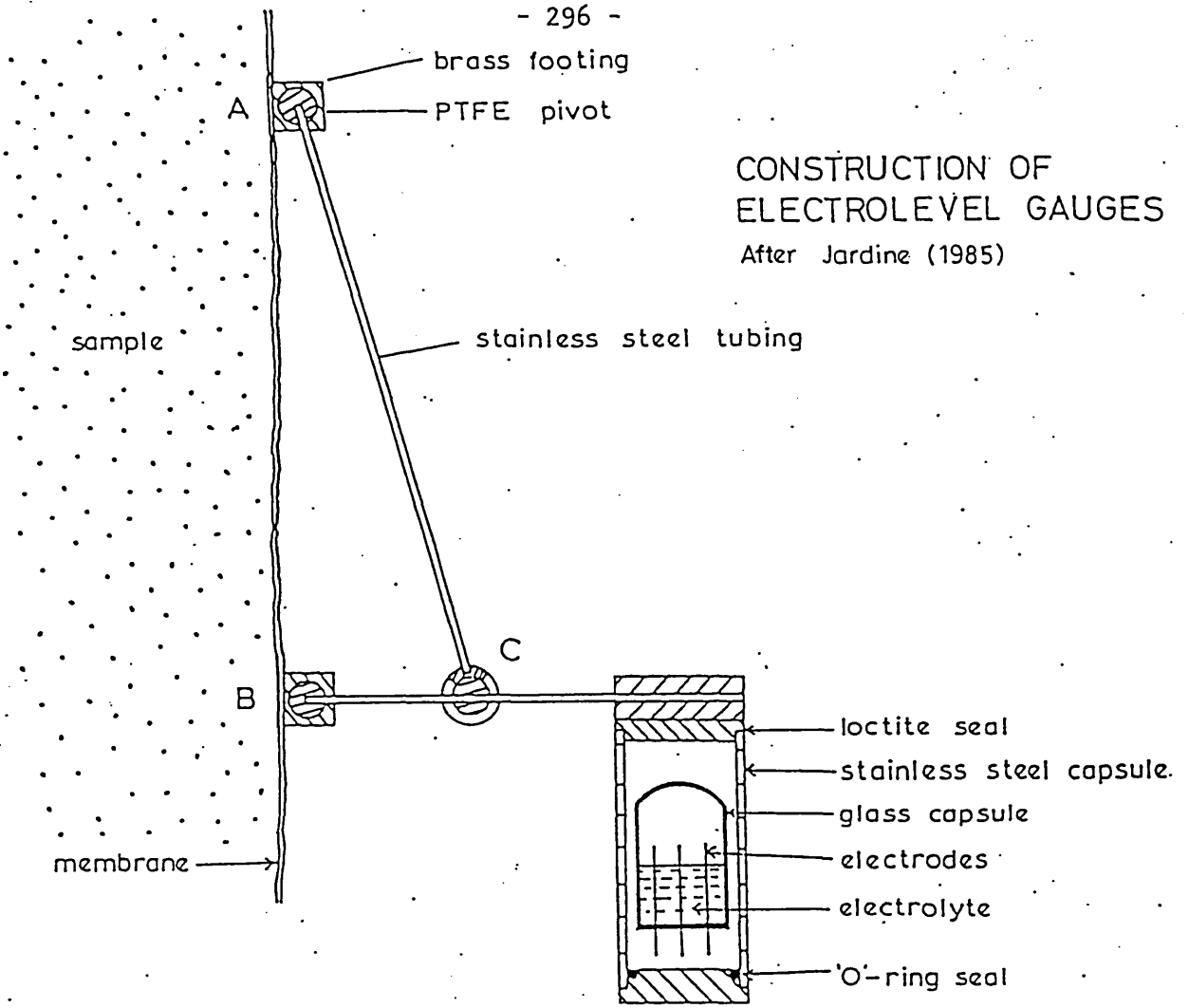
APPENDIX A2

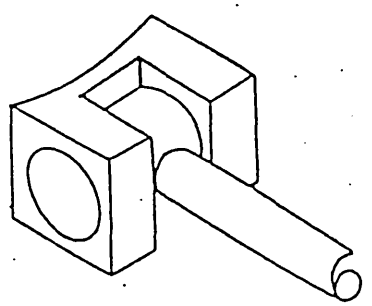
TABLE AND FIGURES

Table A2.1

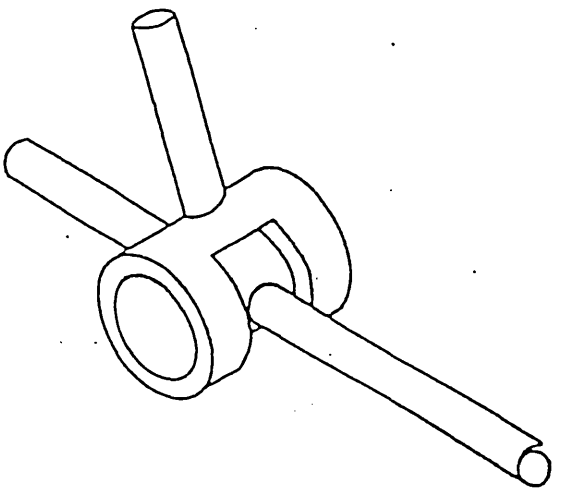
Theoretical Errors in local strain device reading due to rotation of support pads

Gauge configuration	Initial gap (mm)	Theoretical error (%) at axial strain .002%	1%	5%	Distance of hinge from side of sample (mm)
Old	50	6	6	7	3
Old	40	15	14	13	3
New	40	6	6	7	3
New	40	1			0.5
Old	40	3			0.5





HINGES A and B



HINGE C

Figure A2.1. Construction of electrolevel gauges.

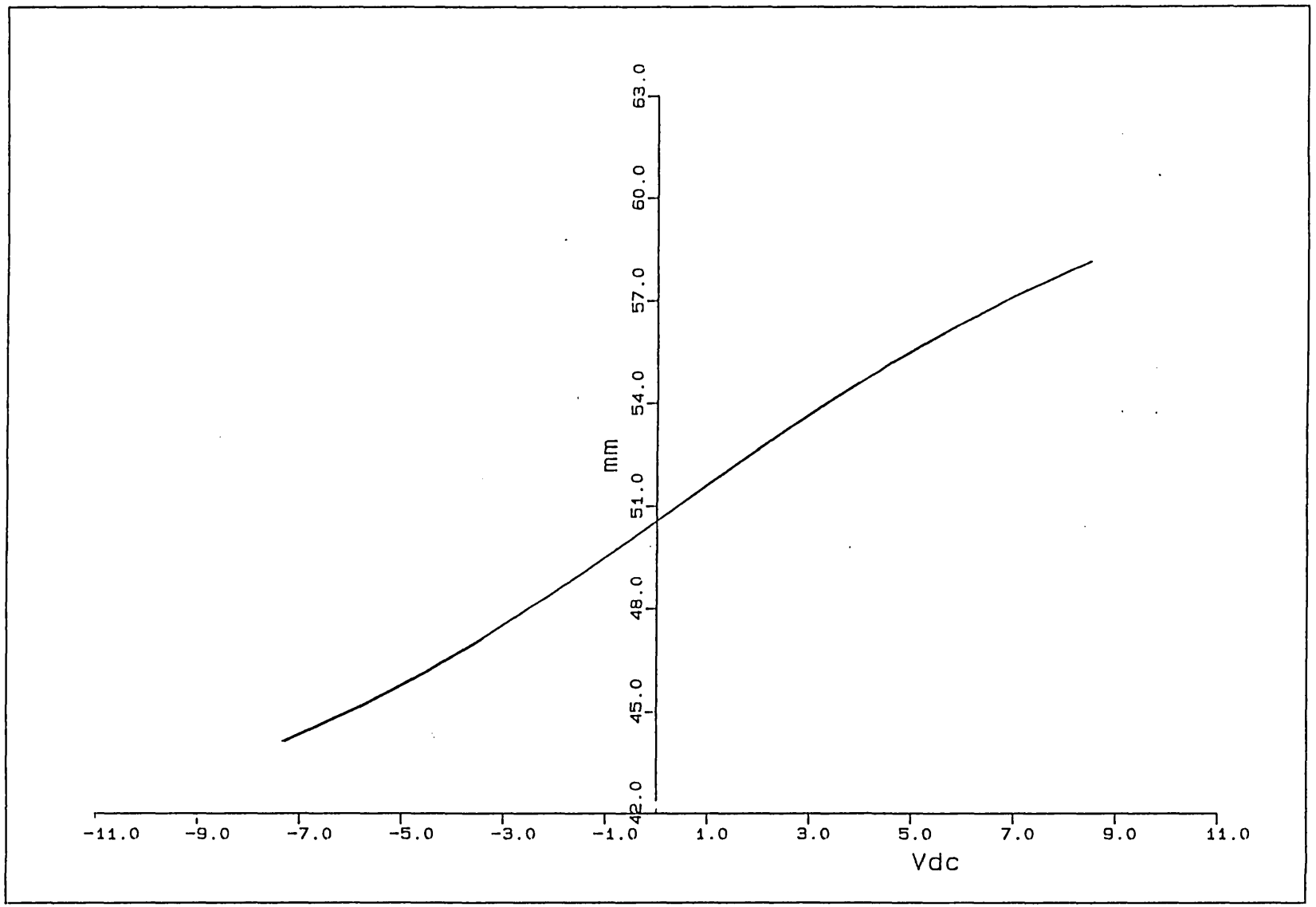


Figure A2.2. Typical calibration of electrolevel gauge.

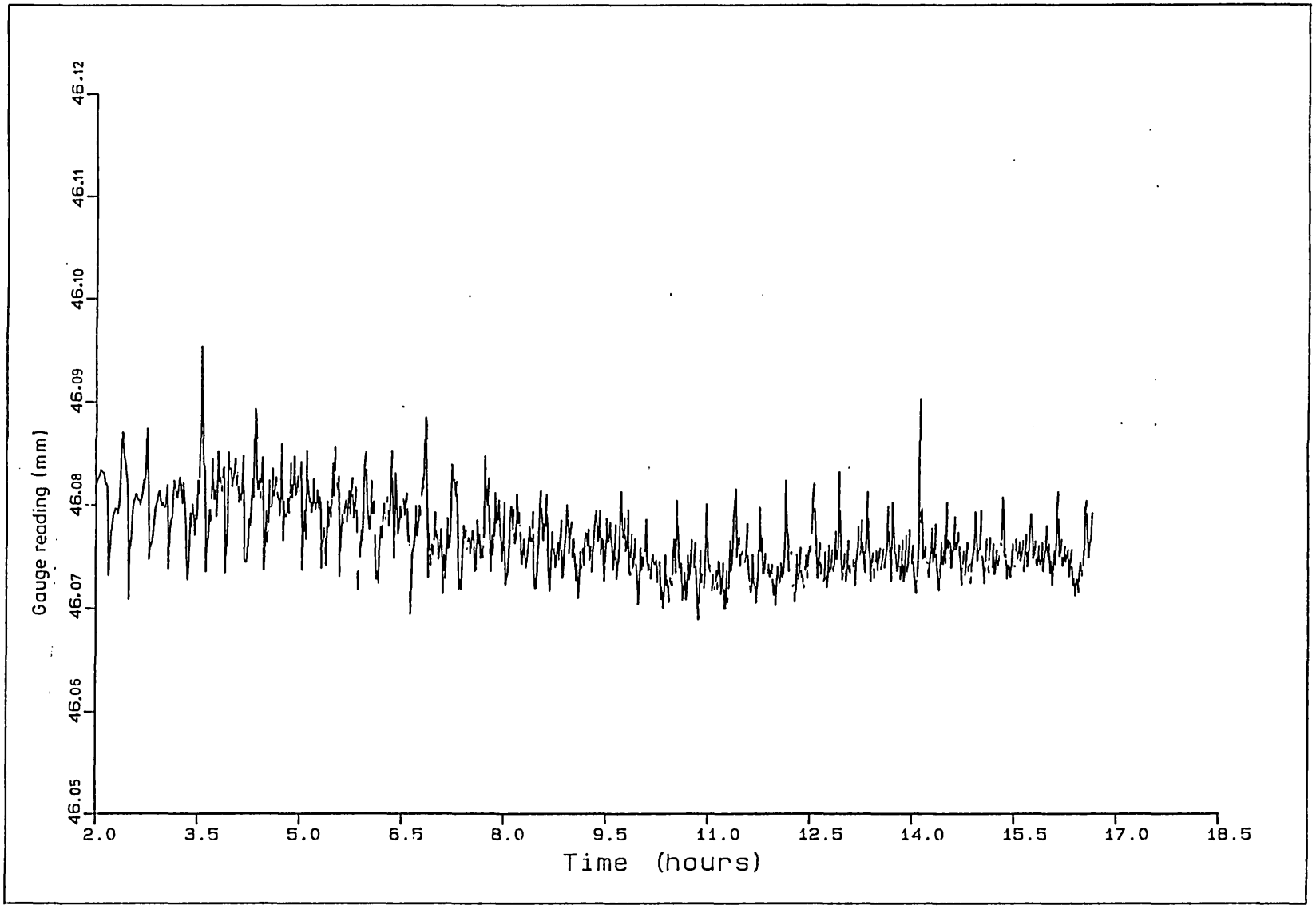


Figure A2.3. Stability check of typical electrolevel gauge.

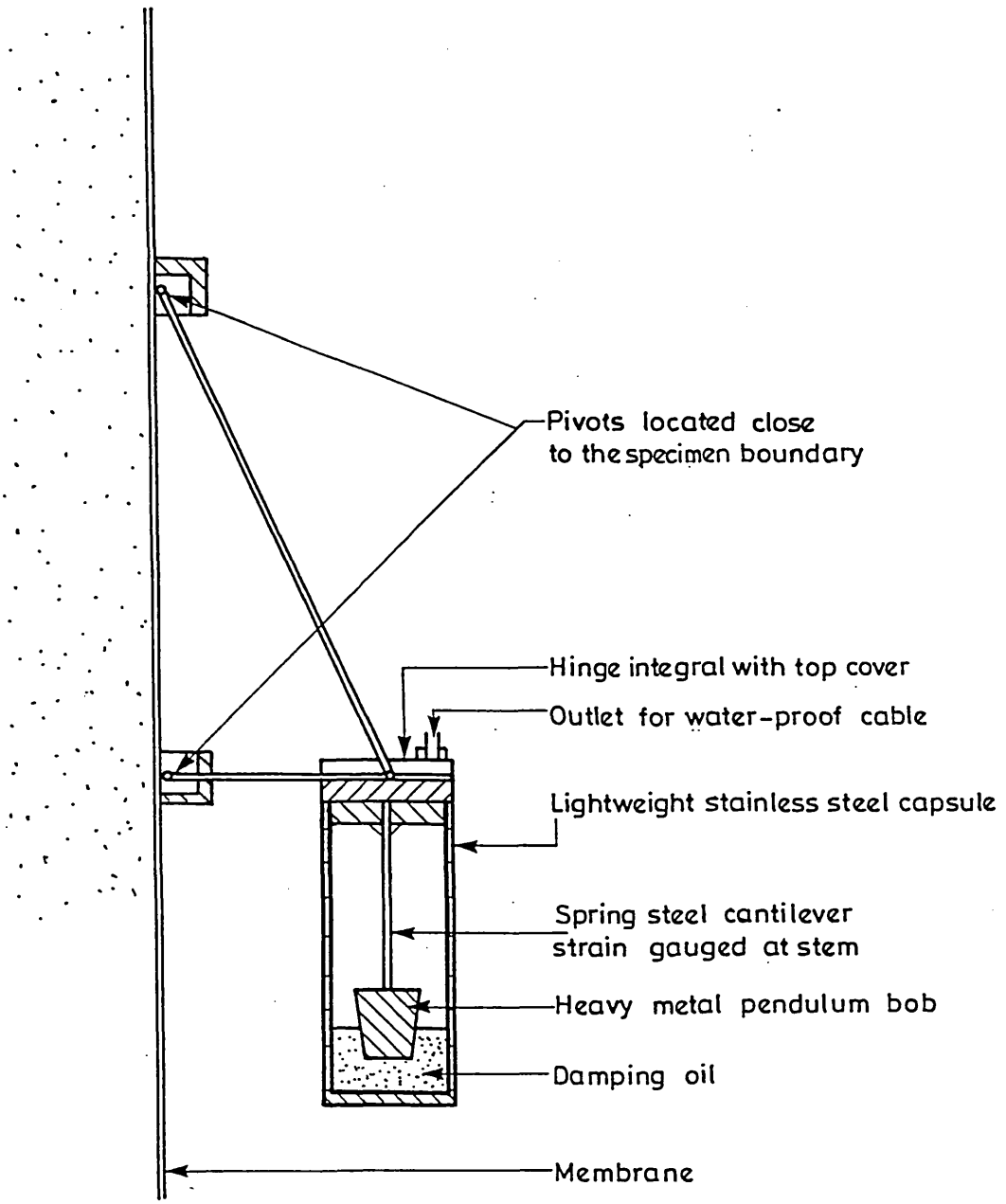
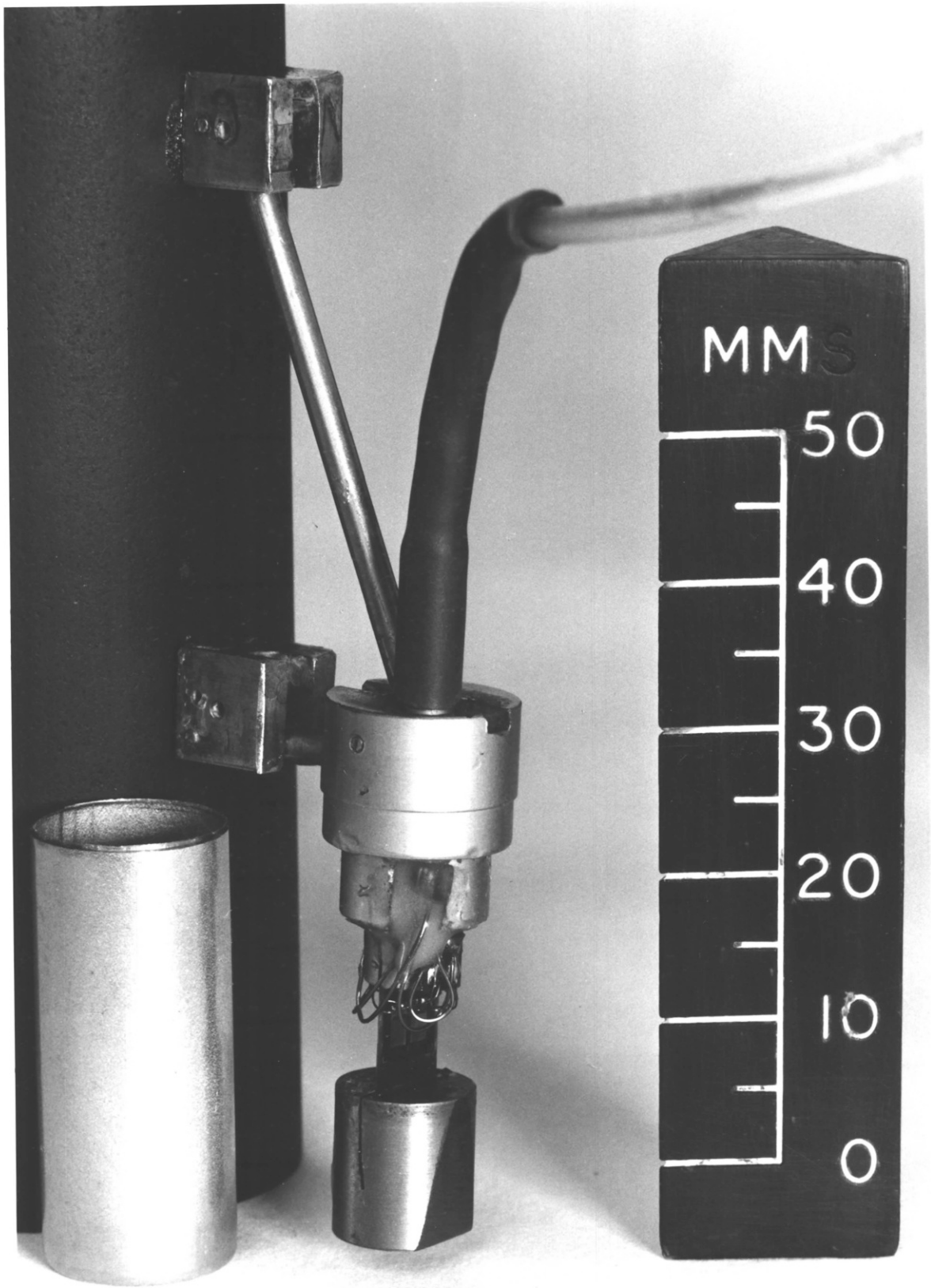


Figure A2.4. The new pendulum local strain device.

Figure A2.5

Photograph of a dismantled pendulum local strain device.


MMS
50
40
30
20
10
0

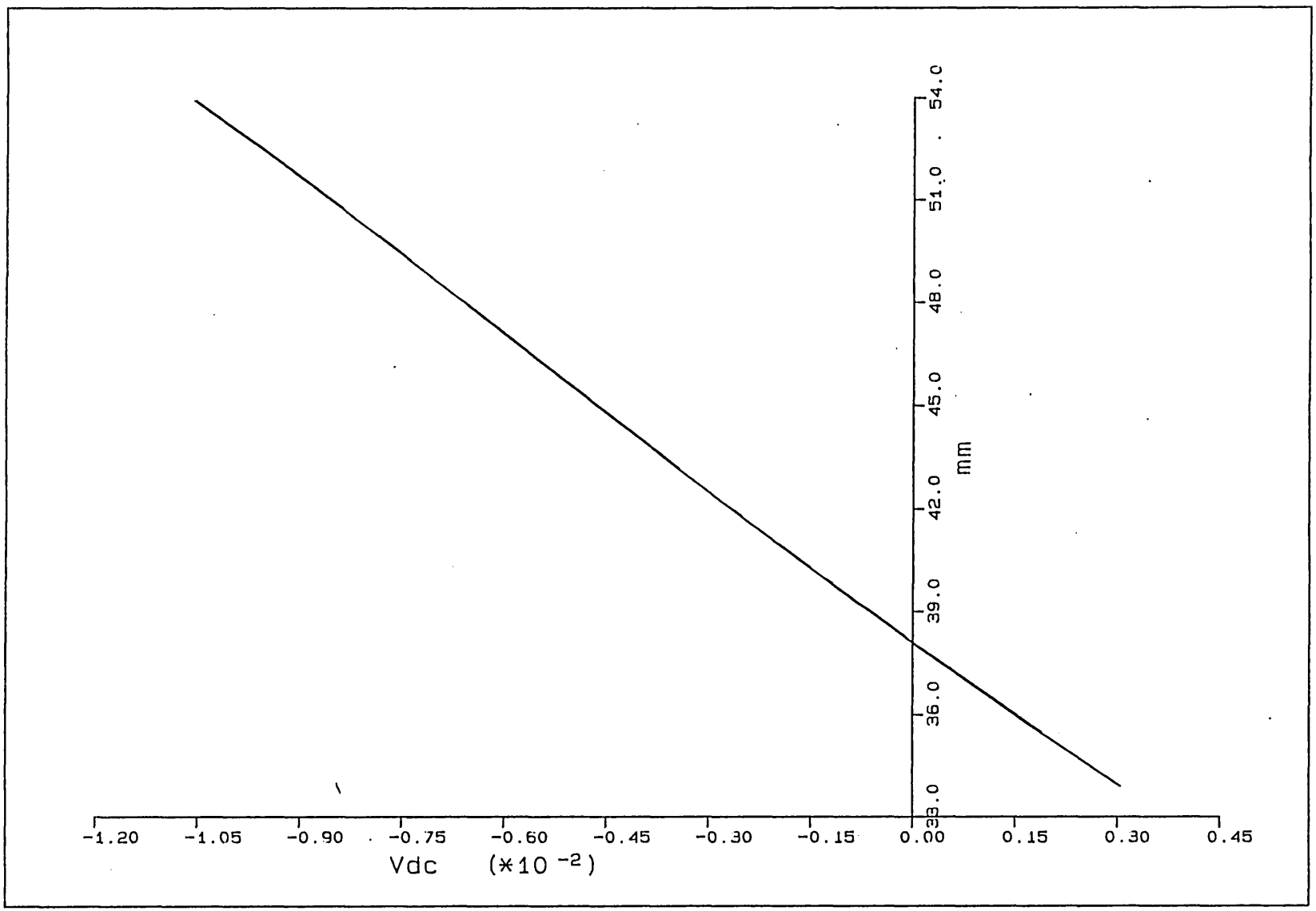


Figure A2.6. Typical calibration of pendulum device.

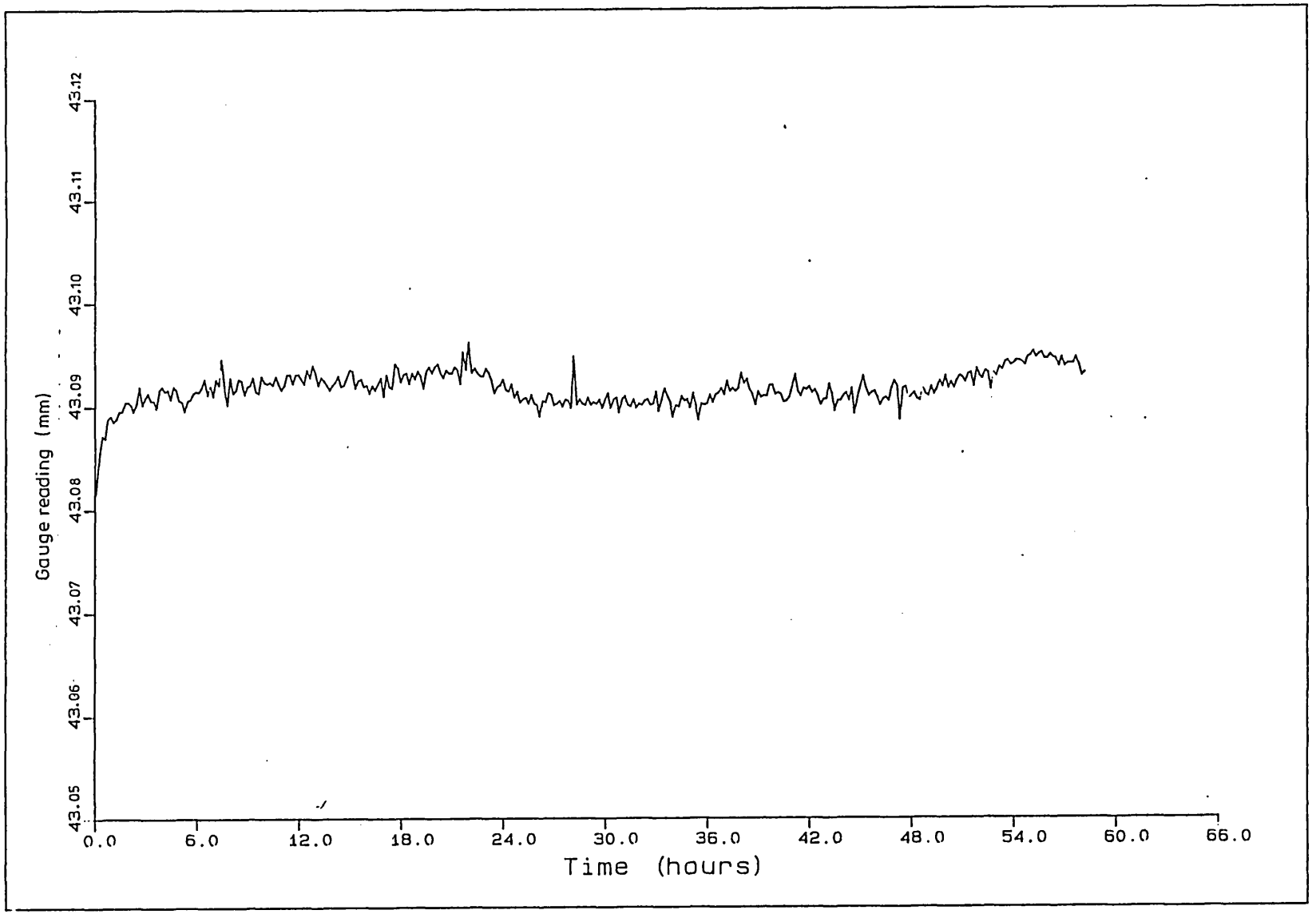


Figure A2.7. Stability check of new pendulum device.

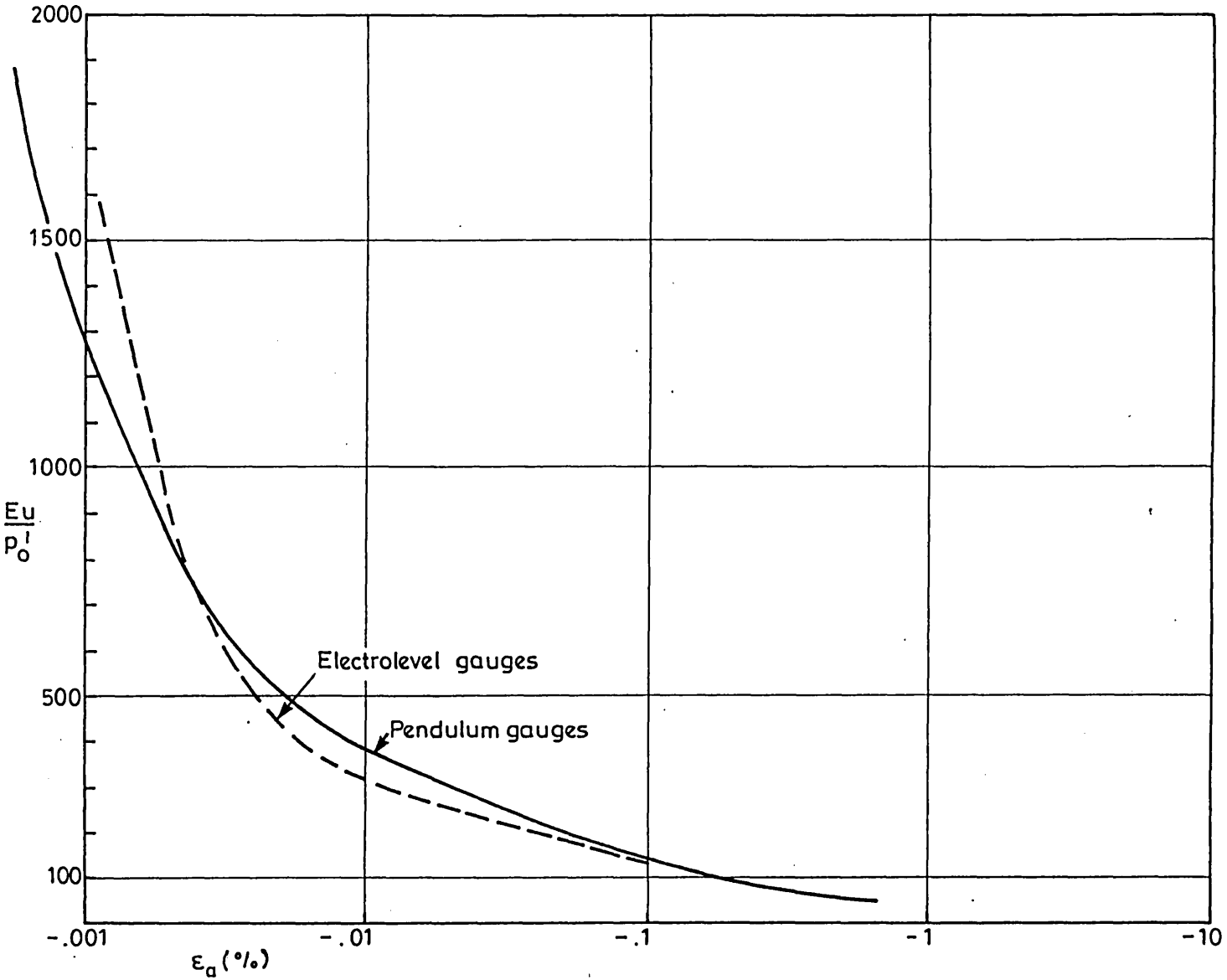


Figure A2.8. Comparison of stiffnesses from electrolevel and pendulum gauges for London clay extension test TLUU3.

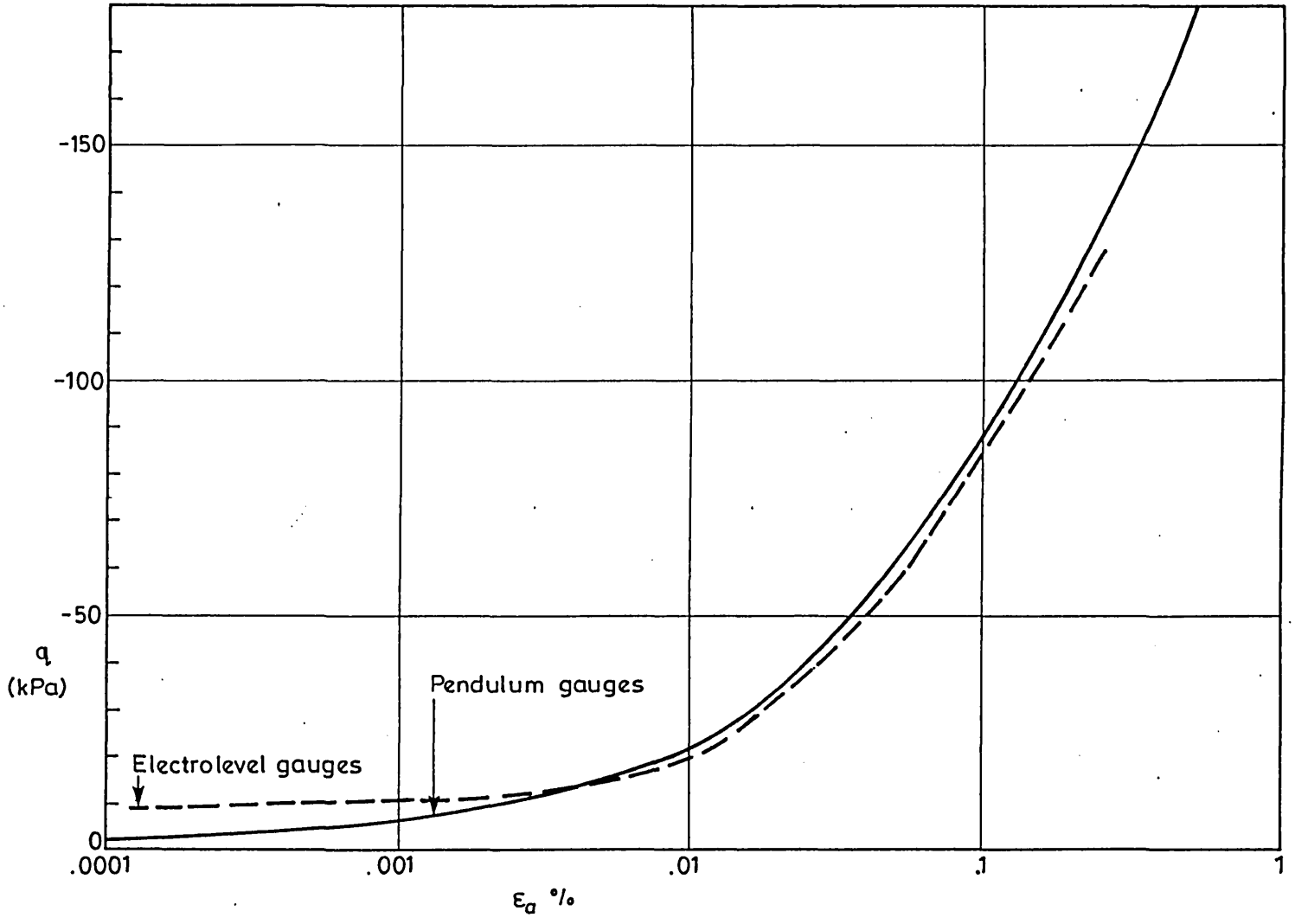


Figure A2.9. Stress-strain curves for London clay extension test TLUU3 from electrolevel and pendulum gauge readings.

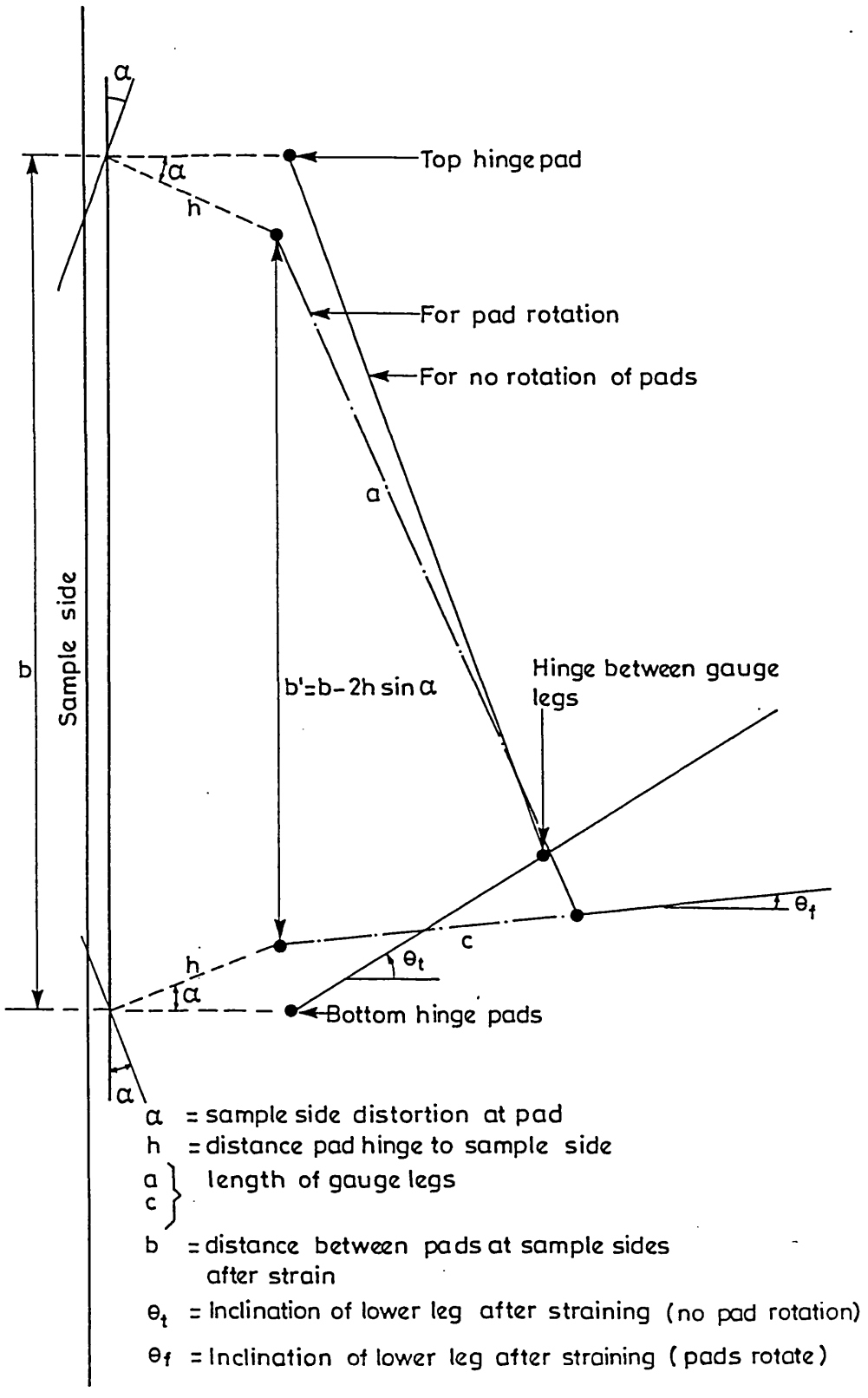


Figure A2.10. Diagrammatic representation of local strain device: effect of footing pad rotation.

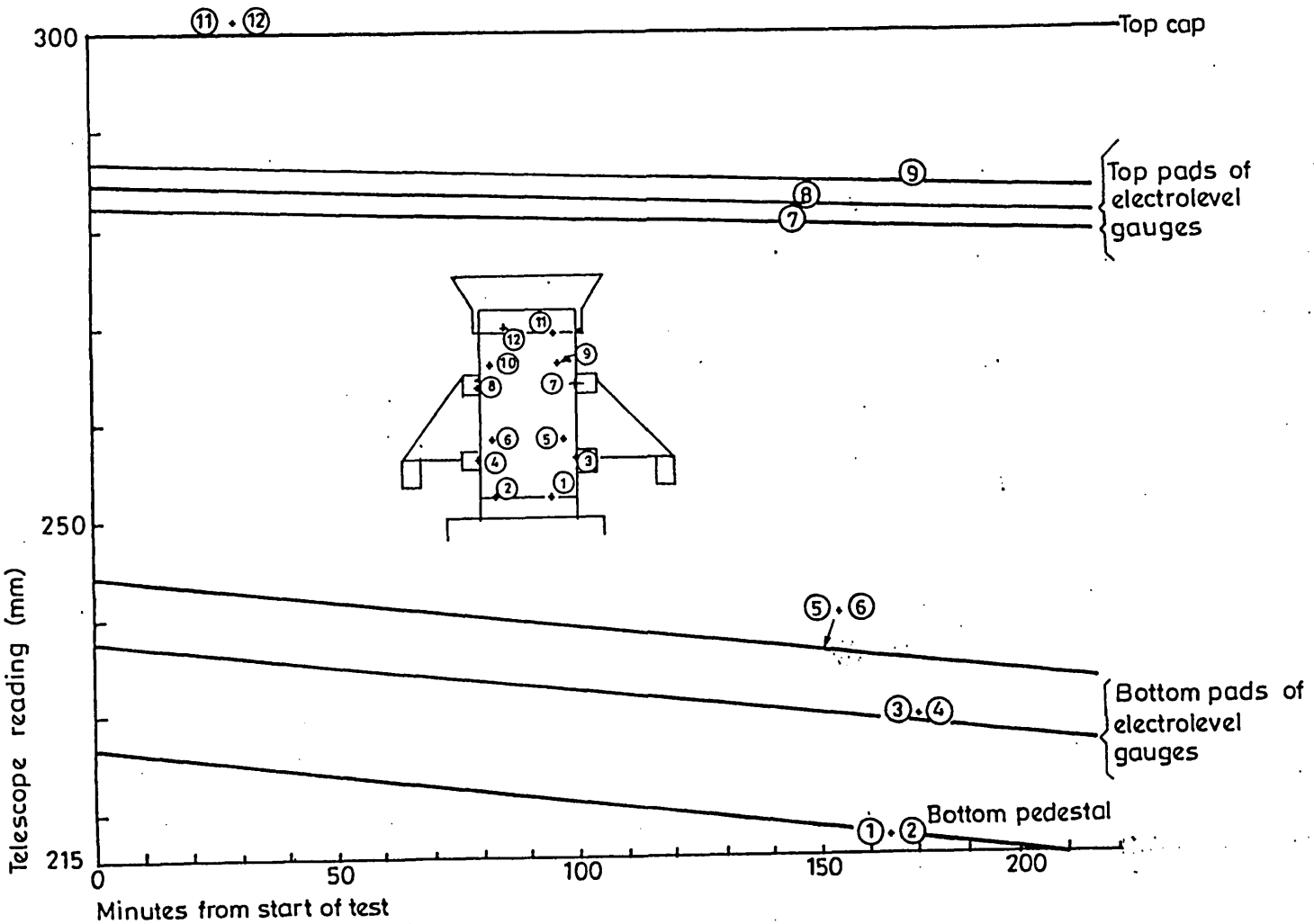


Figure A2.11. Local strain measurements through Vernier telescope for passive stress relief test SPS6.

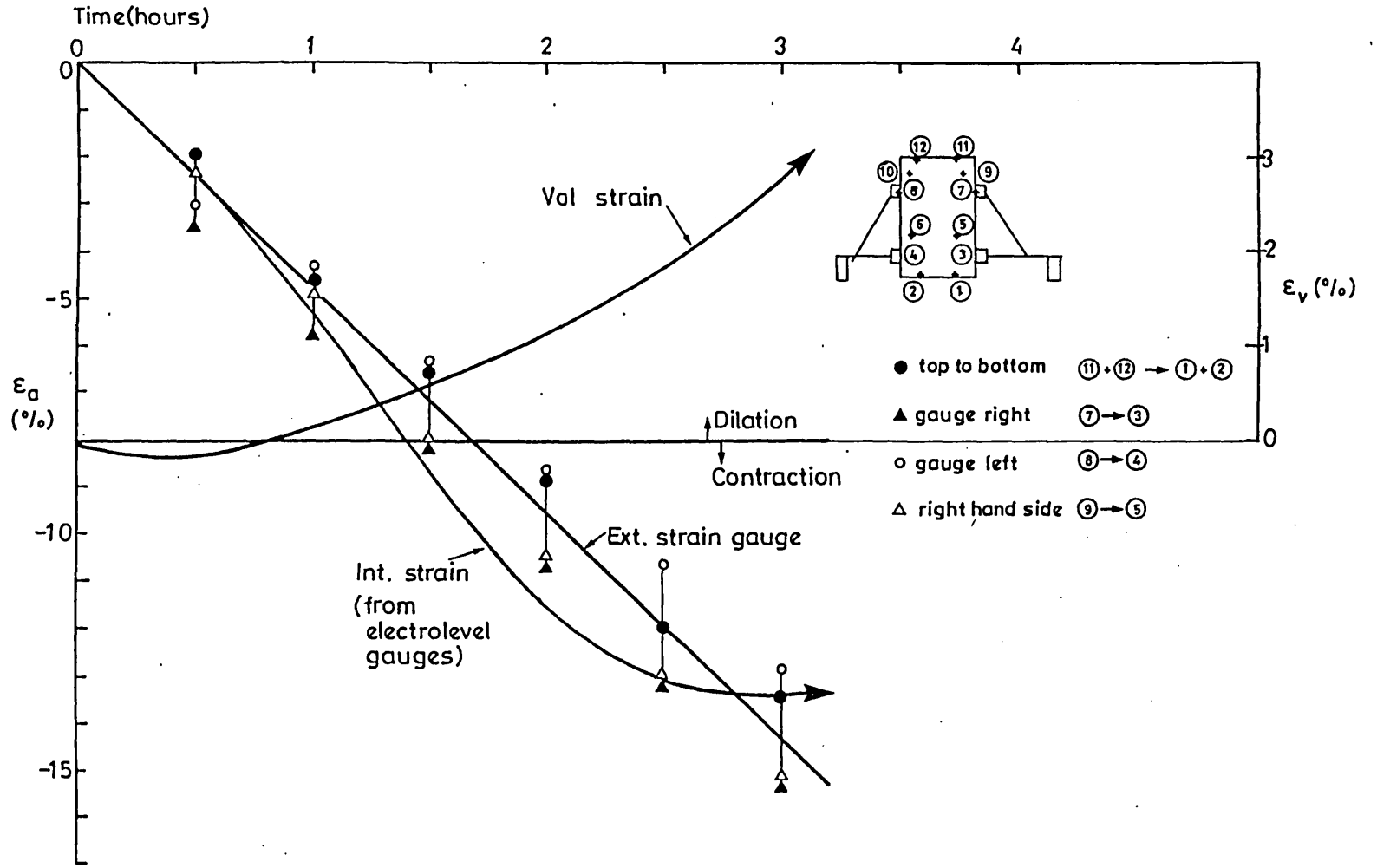
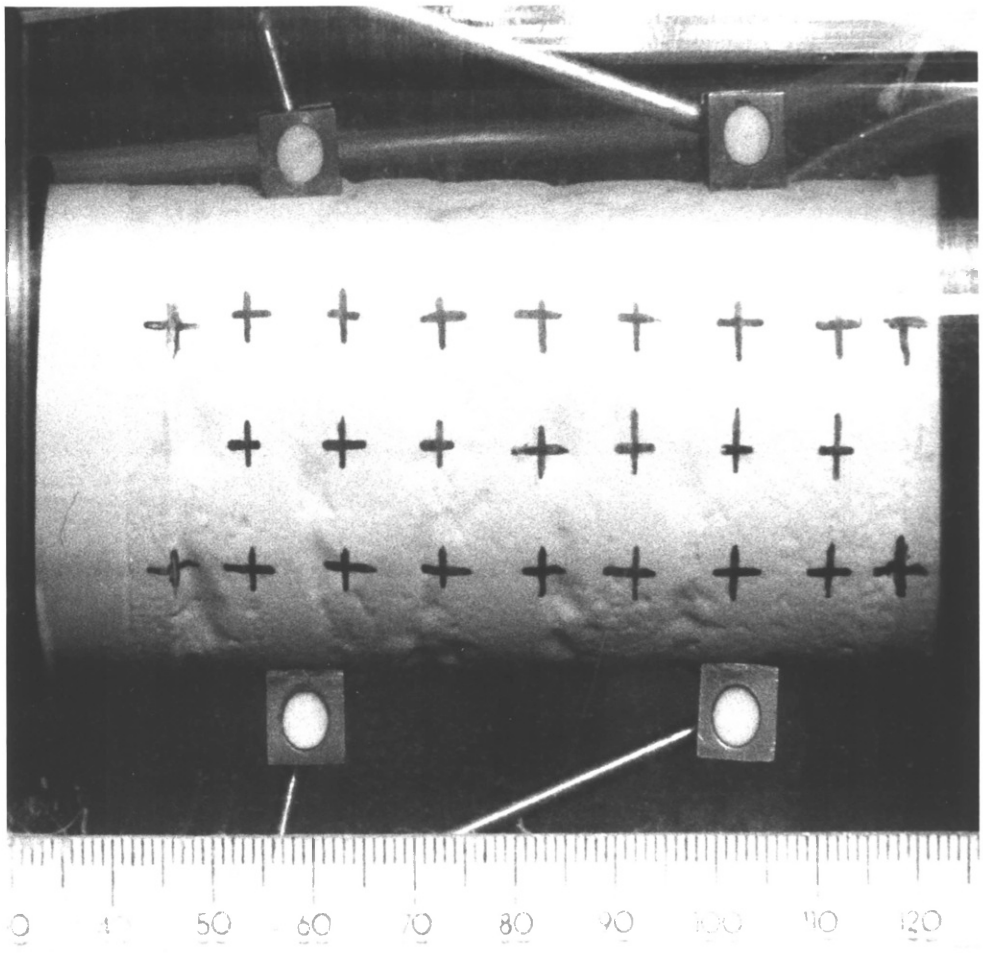
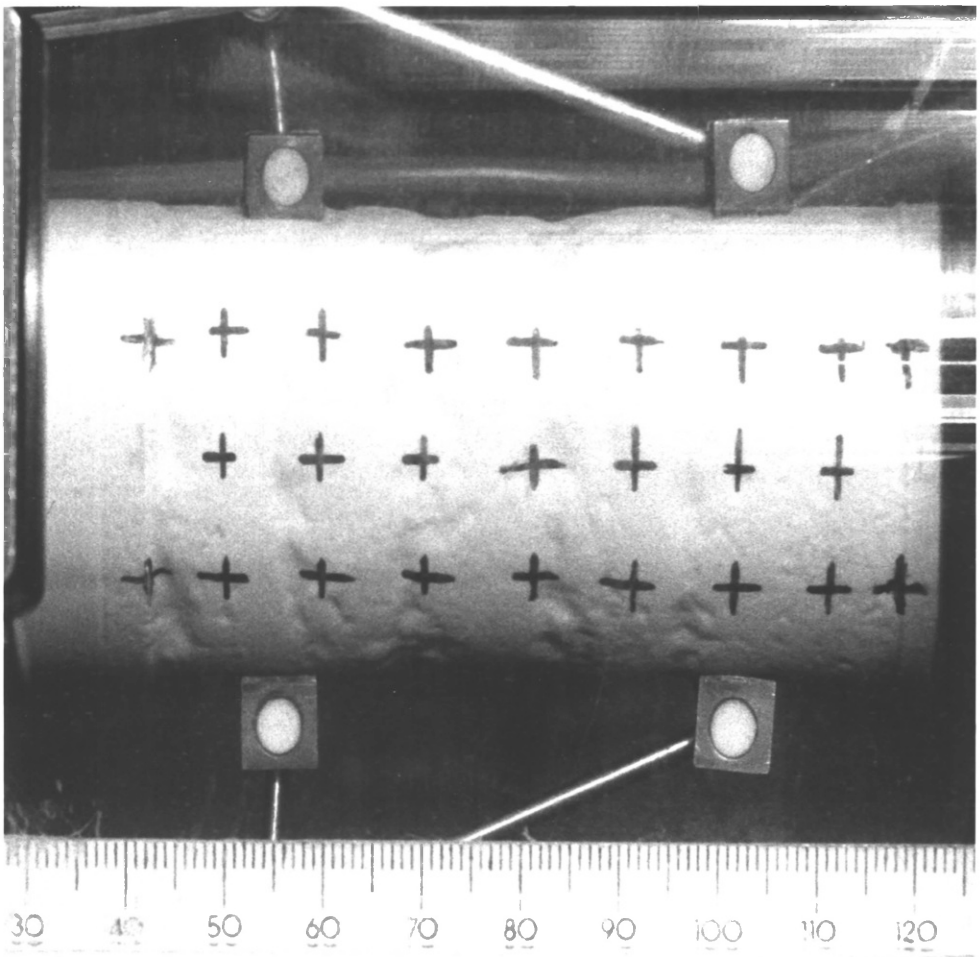


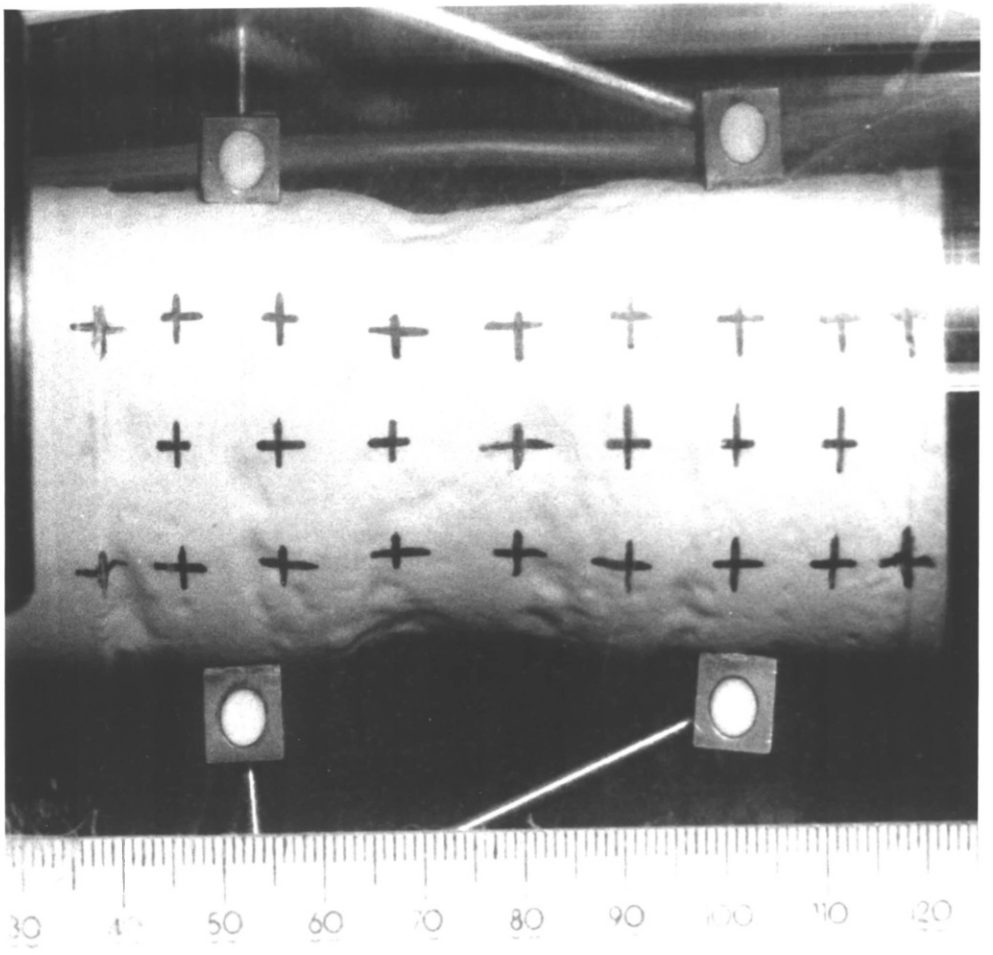
Figure A2.12. Comparison of local and external strain measurement for passive stress relief sand test SPS6.

Figure A2.13

Photographs of passive stress relief sand specimen SPS7 during testing.
Sheet 1: left-at 12.48 hrs., right-at 14.10 hrs.
Sheet 2: left-at 15.20 hrs., right-at 16.30 hrs.


50
60
70
80
90
110
120


30
50
60
70
80
90
100
110
120


30
50
60
70
80
90
110

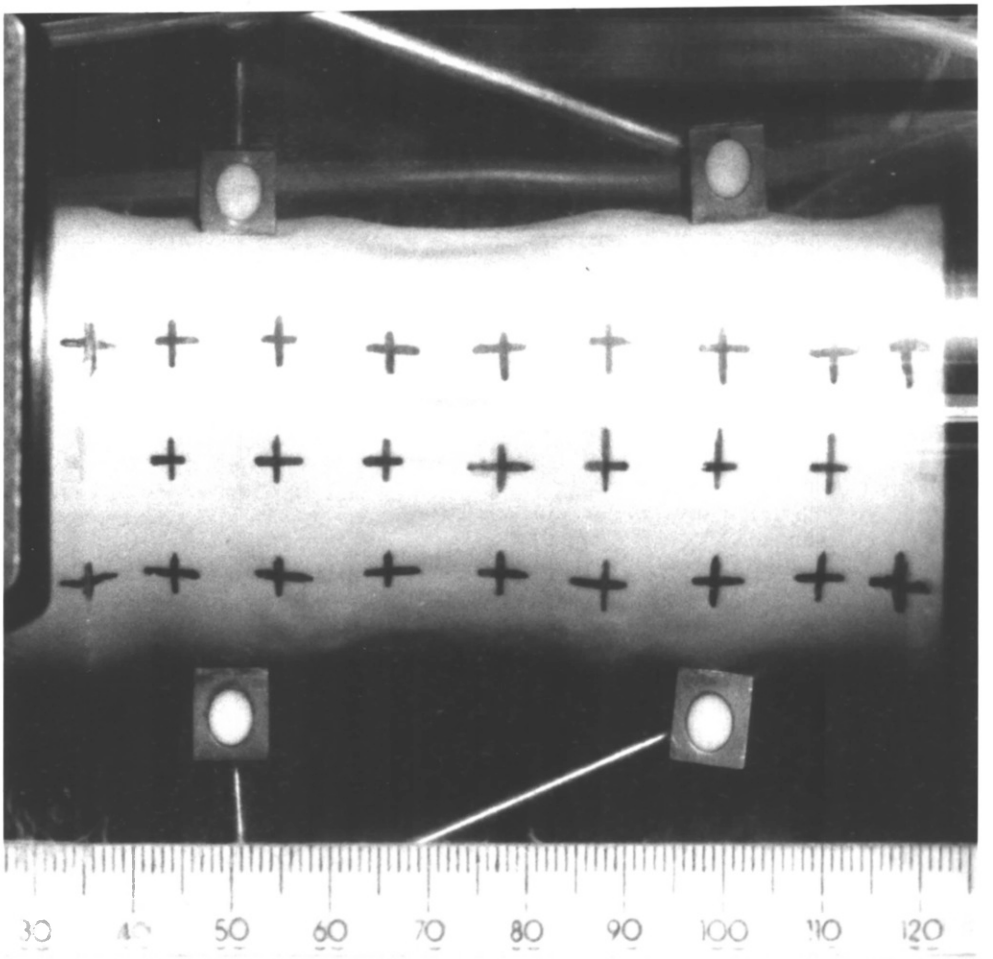
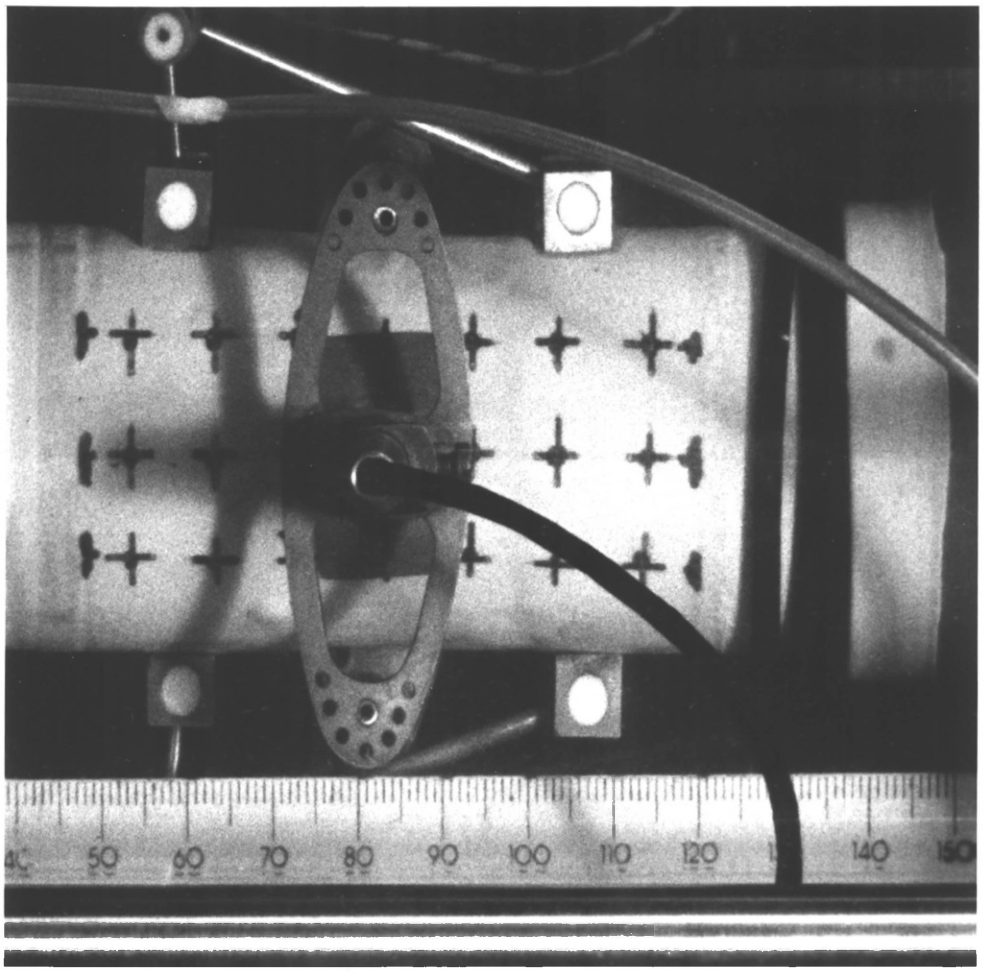

30
50
60
70
80
90
100
110
120

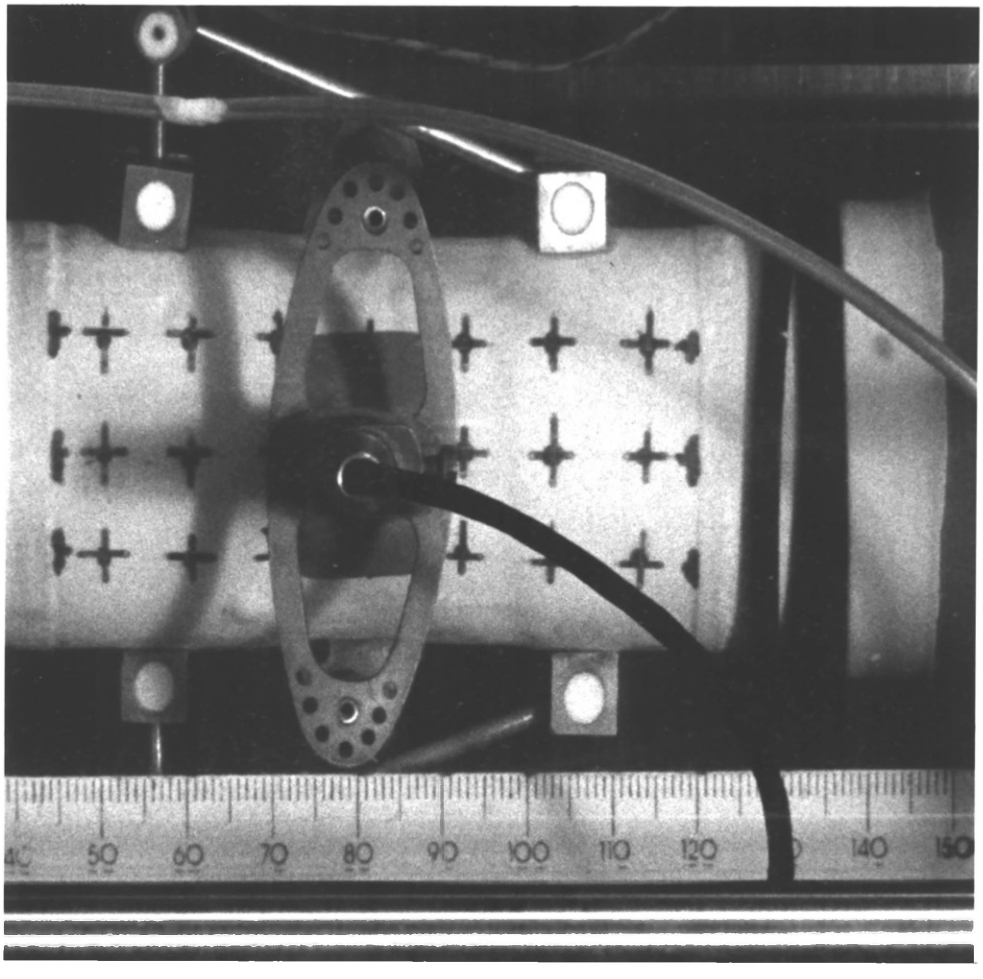
Figure A2.14

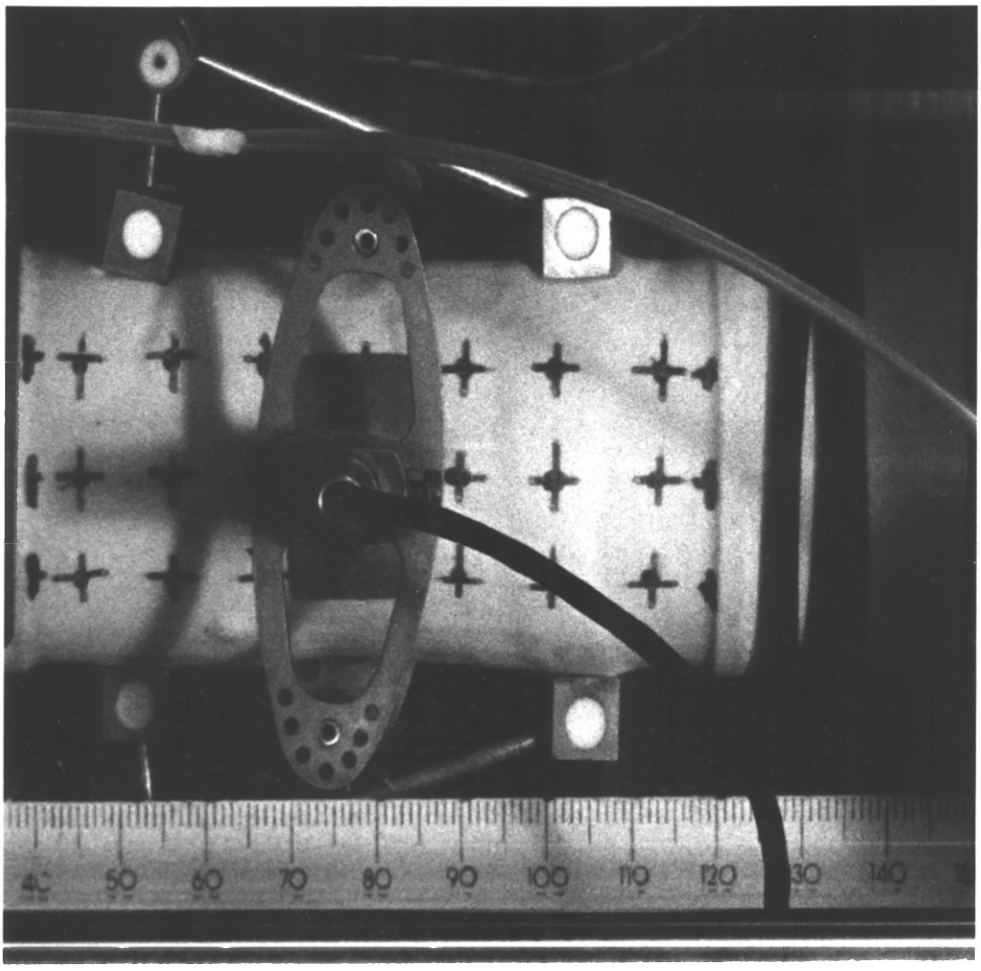
Photographs of passive stress relief sand specimen SPS/A/6 during testing.

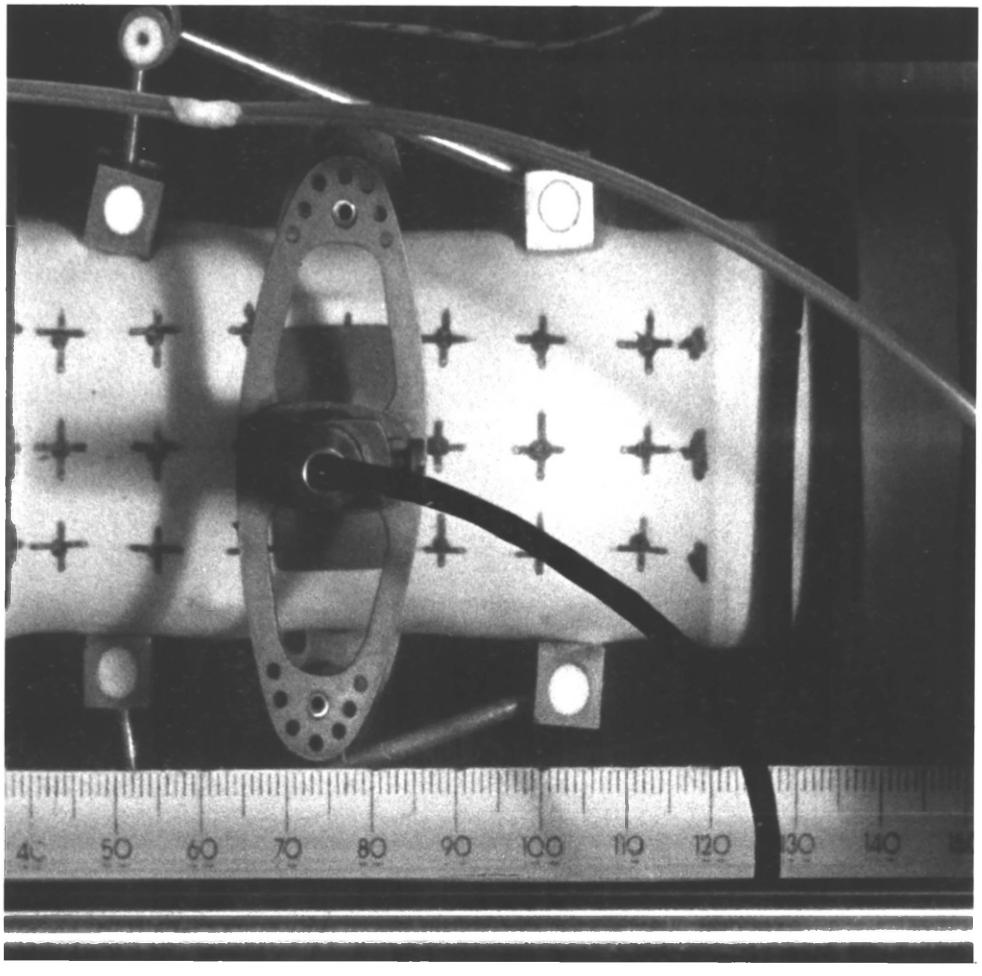
Sheet 1: left - at 13.09 hrs., right - at 14.14 hrs.

Sheet 2: left - at 15.33 hrs., right - at 16.30 hrs.


50
60
70
80
90
100
110
120
140
150


50
60
70
80
90
100
110
120
140
150


40
50
60
70
80
90
100
110
120
130
140


40
50
60
70
80
90
100
110
120
130
140

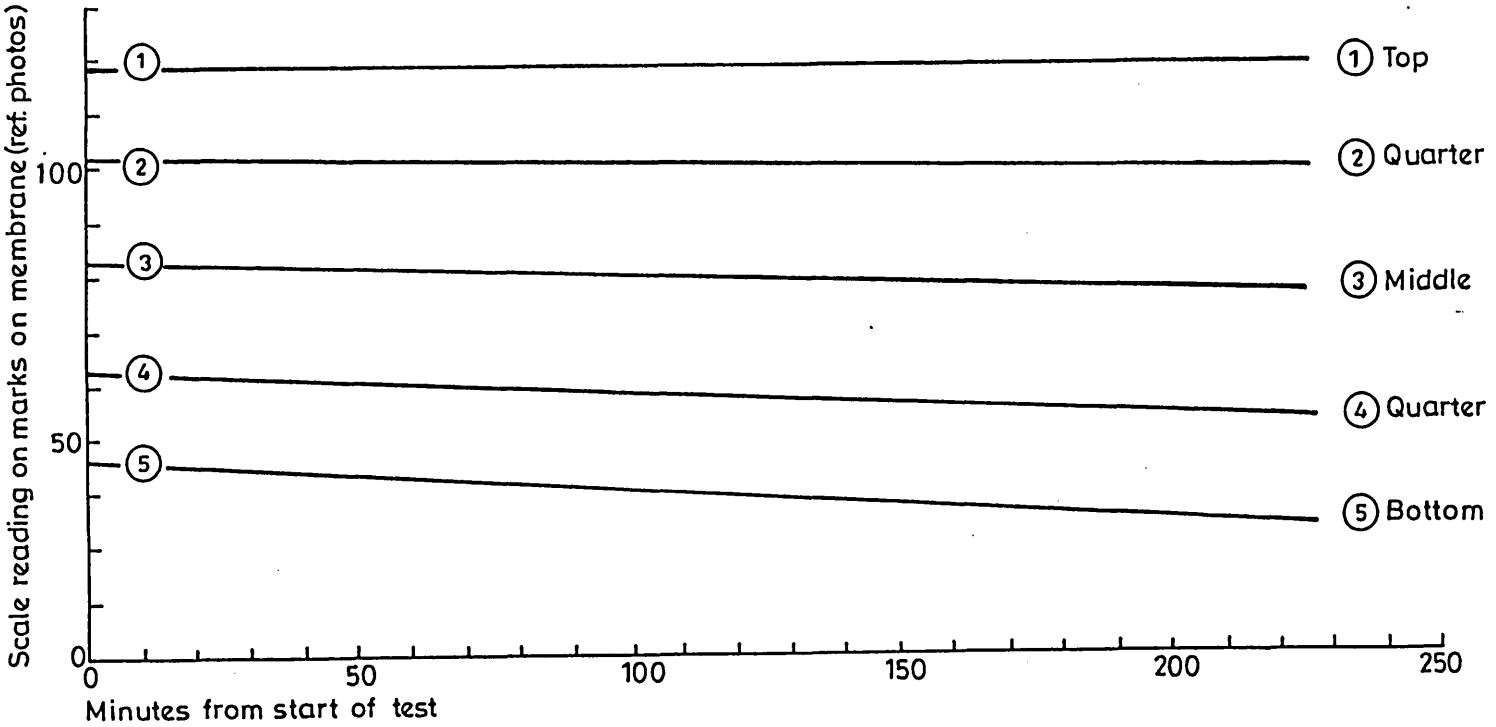


Figure A2.15. Local strains from photographs of specimen in passive stress relief sand test SPS7: scaling off marks on membrane on right hand side of specimen (ref. photographs Fig. A2.13).

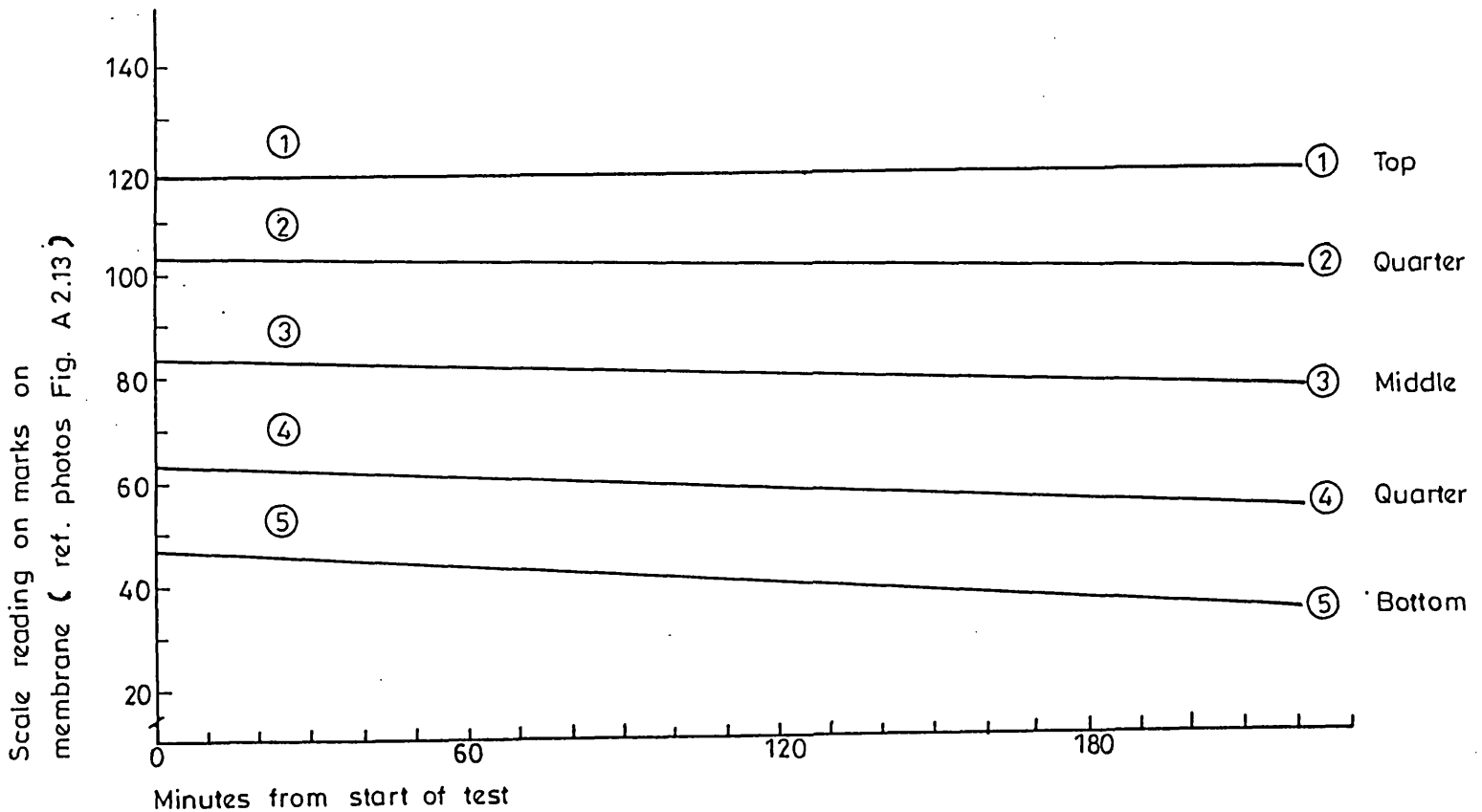


Figure A2.16. Local strains from photographs of specimen in passive stress relief sand test SPS7: scaling off marks on membrane on left hand side of specimen (ref. photographs Fig. A2.13).

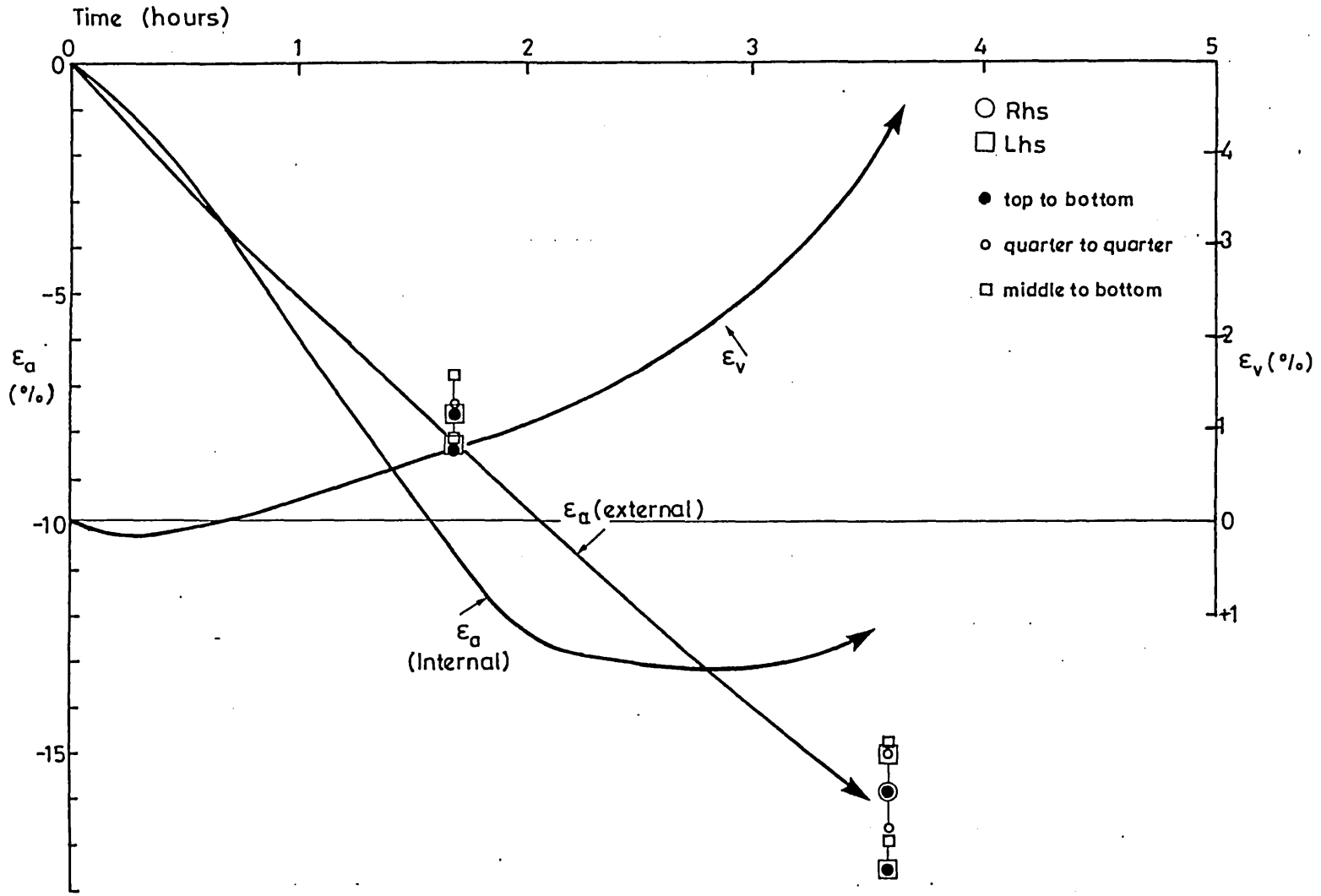


Figure A2.17. Comparison of local and external strain measurement: passive stress relief sand test SPS7.

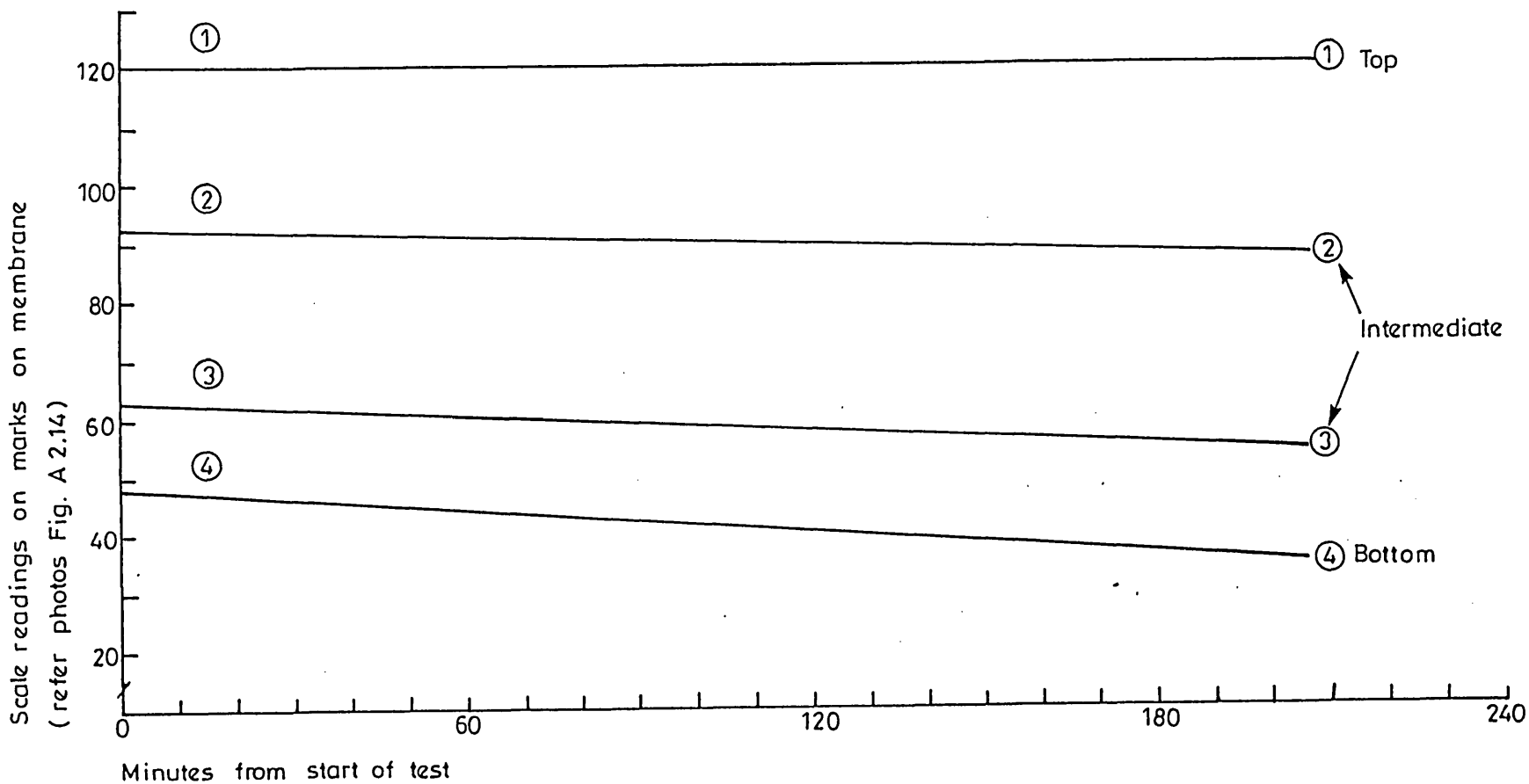


Figure A2.18. Local strains from photographs of specimen in passive stress relief sand test SPS/A/6: scaling off marks on membrane on right hand side of specimen (ref. photographs Fig. A2.14).

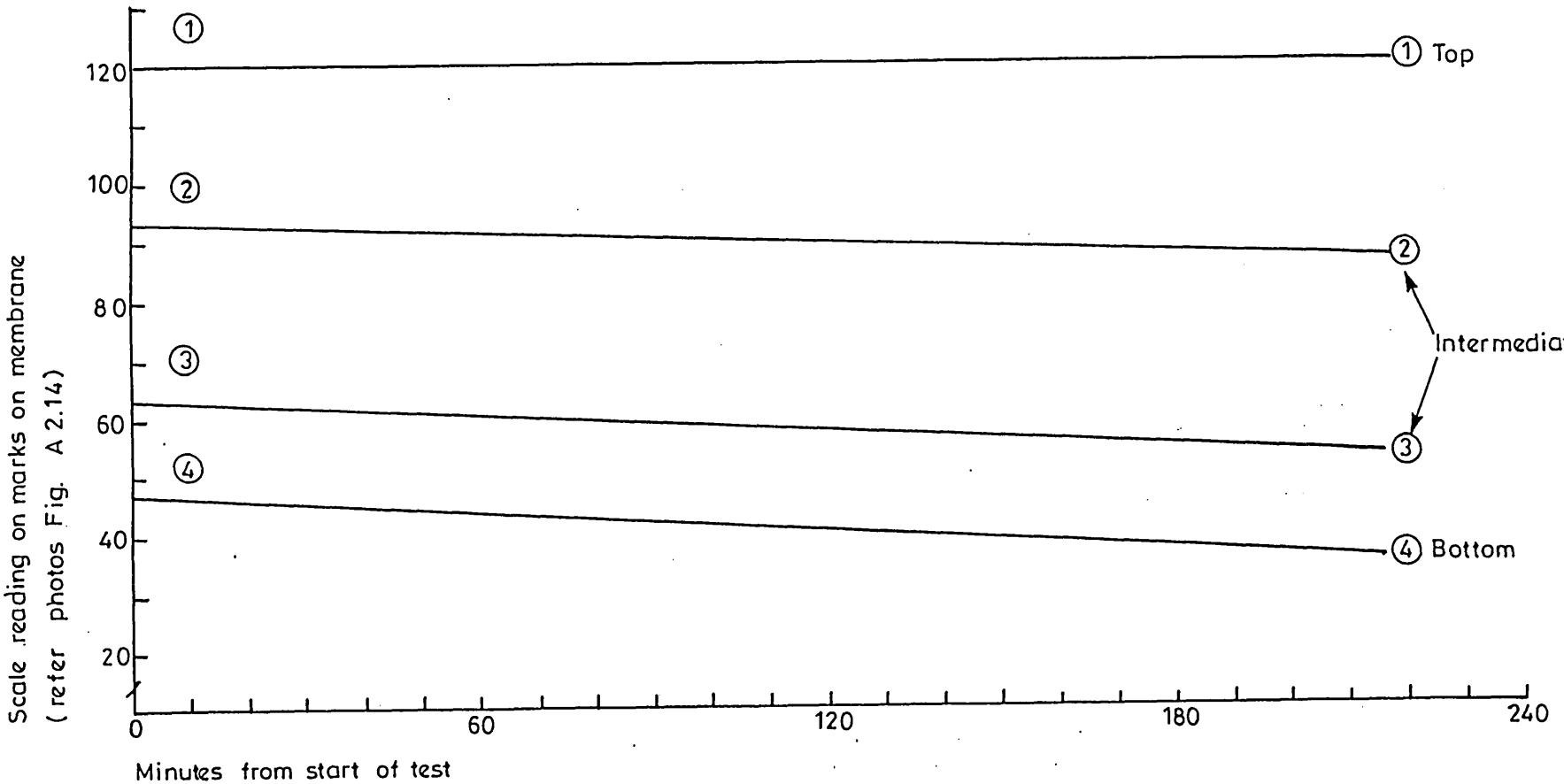


Figure A2.19. Local strains from photographs of specimen in passive stress relief sand test SPS/A/6: scaling off marks on membrane on left hand side of specimen (ref. photographs Fig. A2.14).

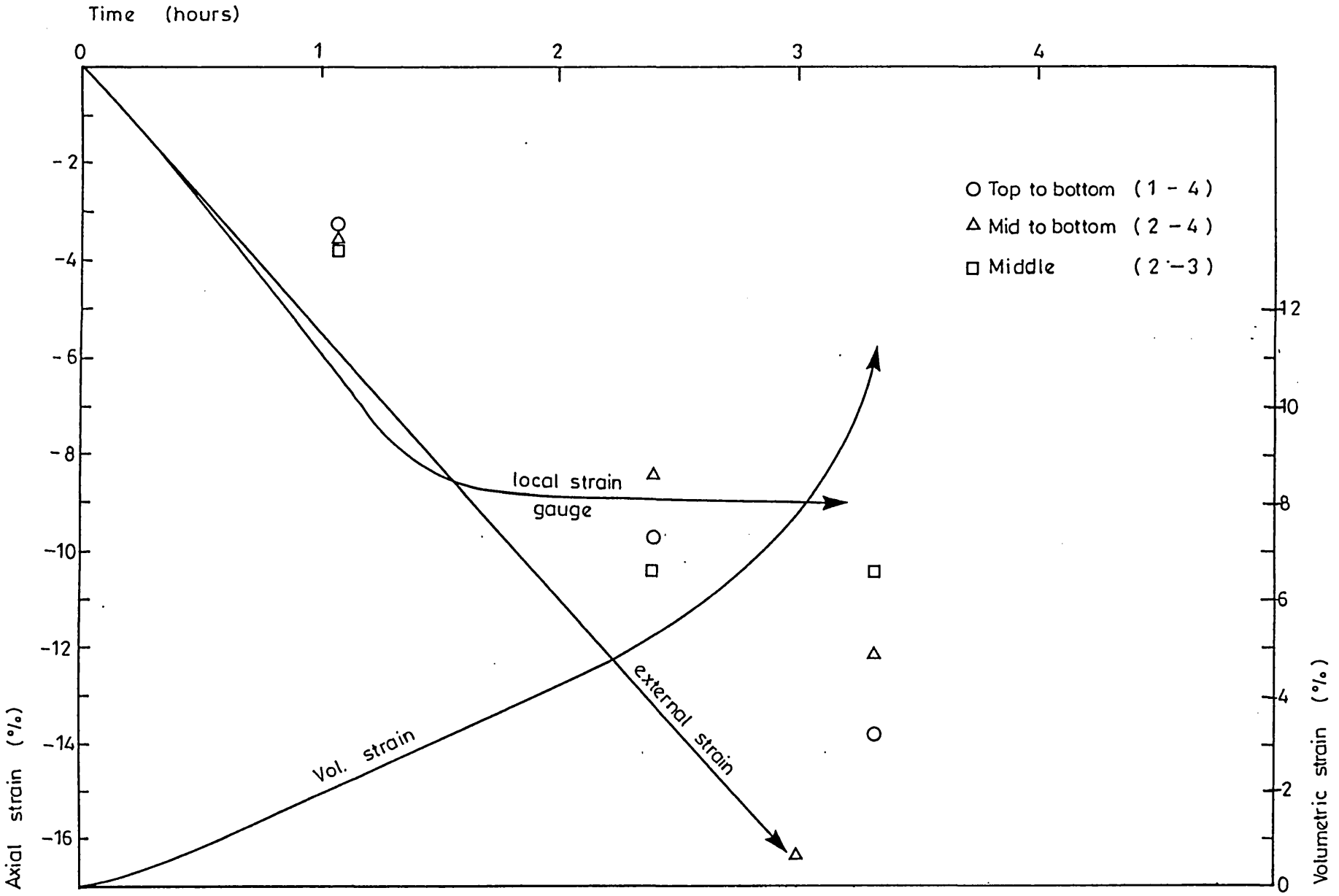
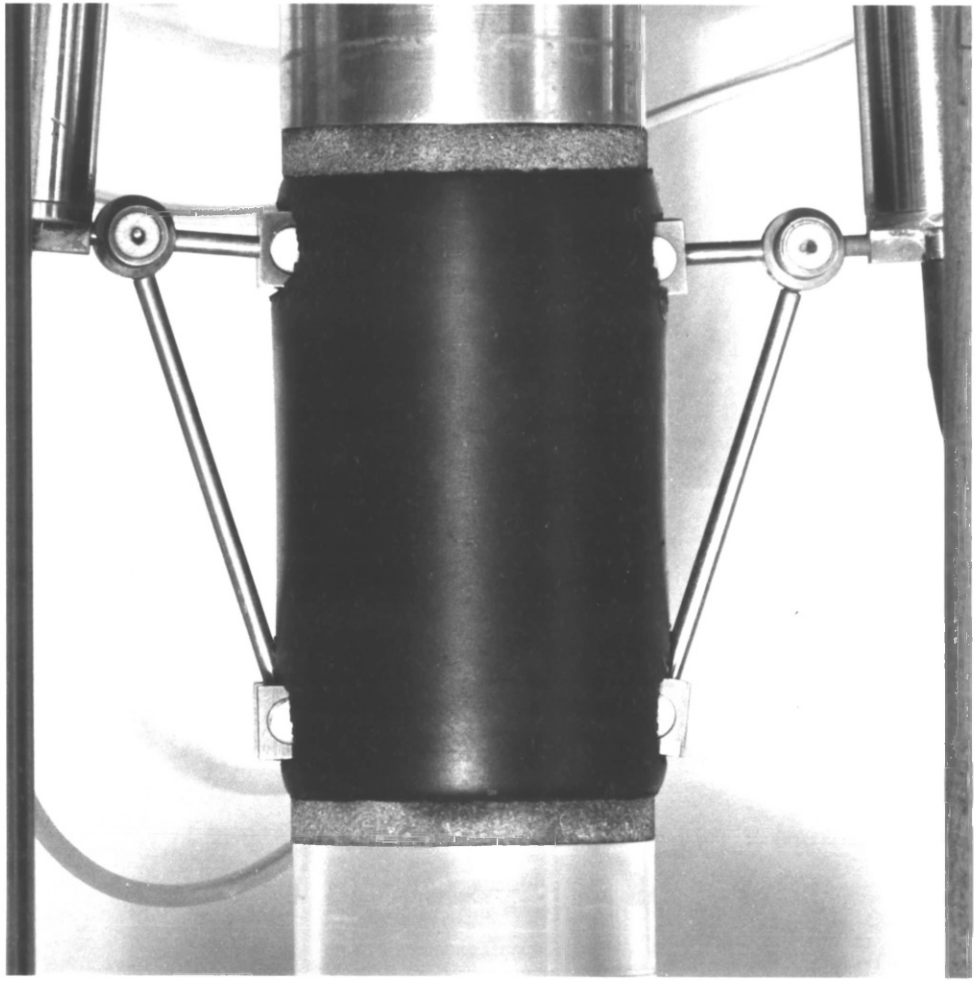
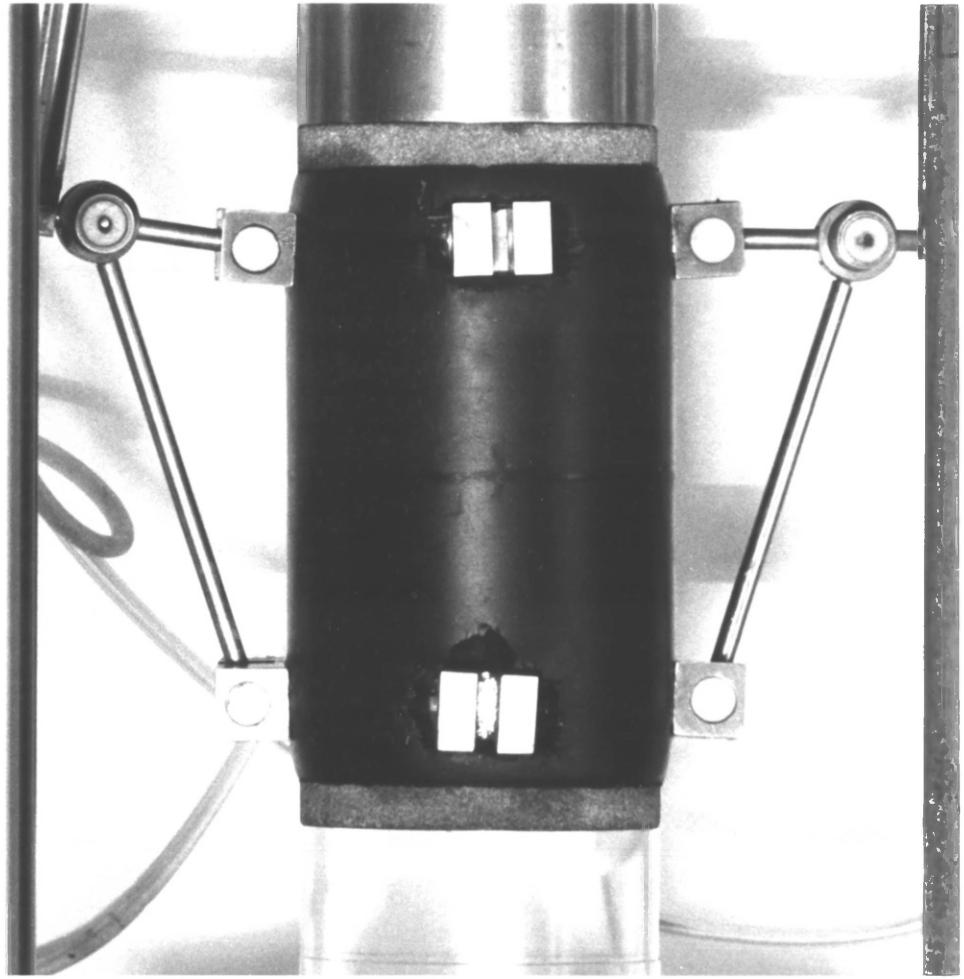


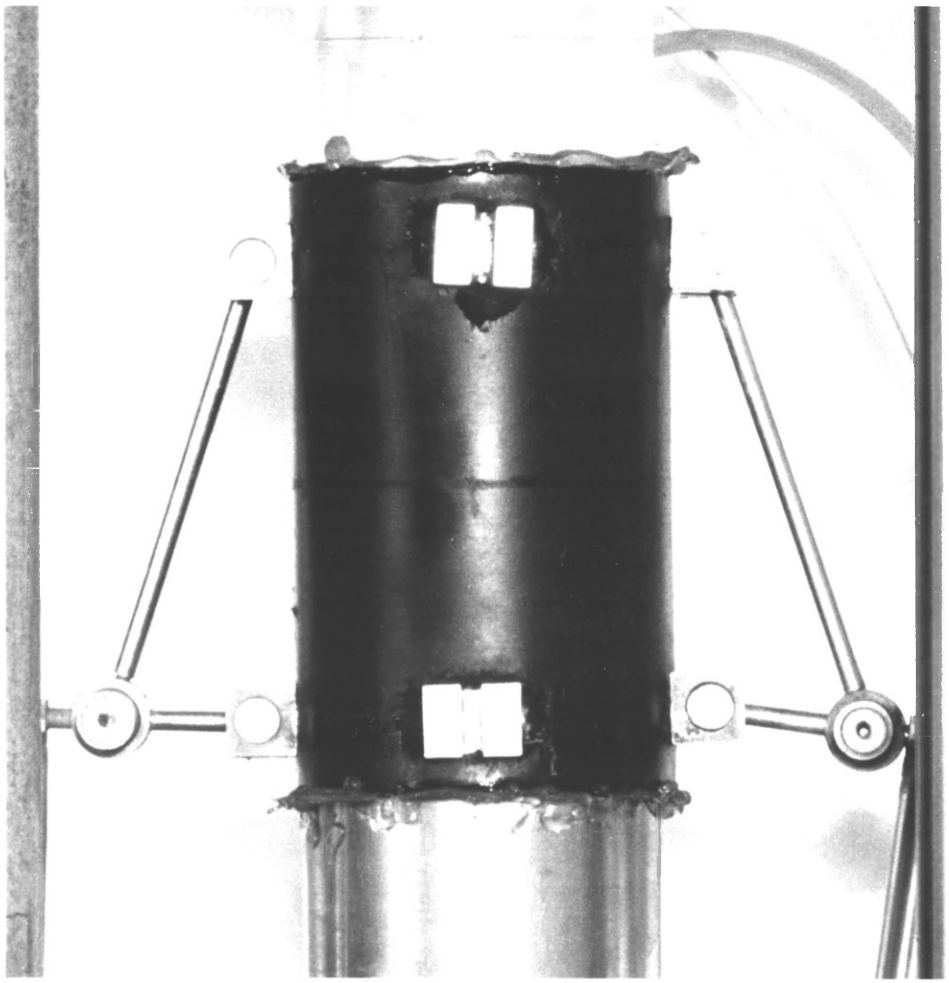
Figure A2.20. Comparison of local and external strain measurement: passive stress relief sand test SPS/A/6.

Figure A2.21

Unconfined compression tests on a rubber specimen - electrolevel gauge pads set on sides as usual (left) and also inset into the sides for comparison (right). Sheet 1 for rough ends and Sheet 2 for greased ends.









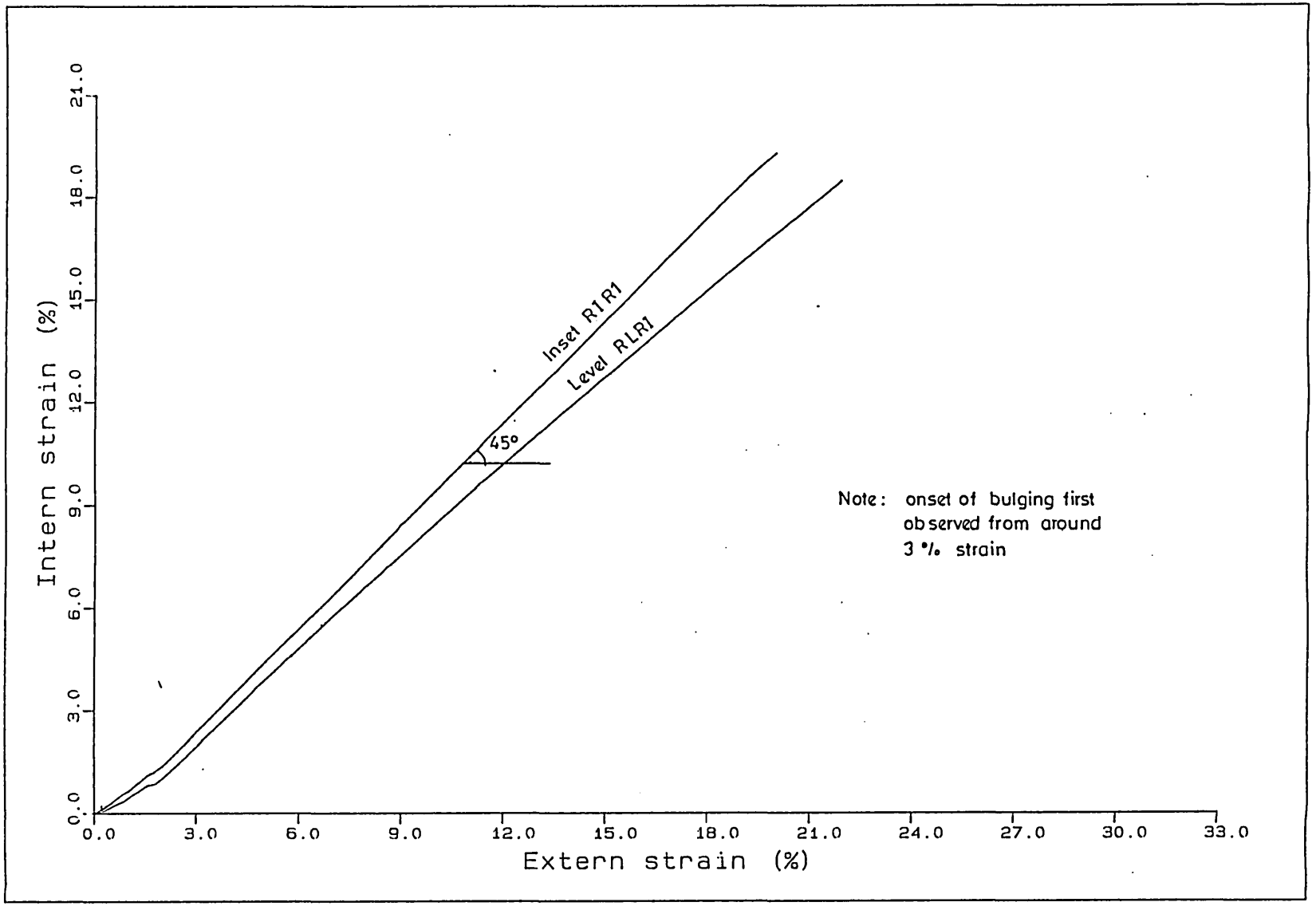


Figure A2.22. Compression tests on rubber specimen with rough ends: local strain measurement by electrolevel device with footing pads either set level on side of, or inset into, specimen.

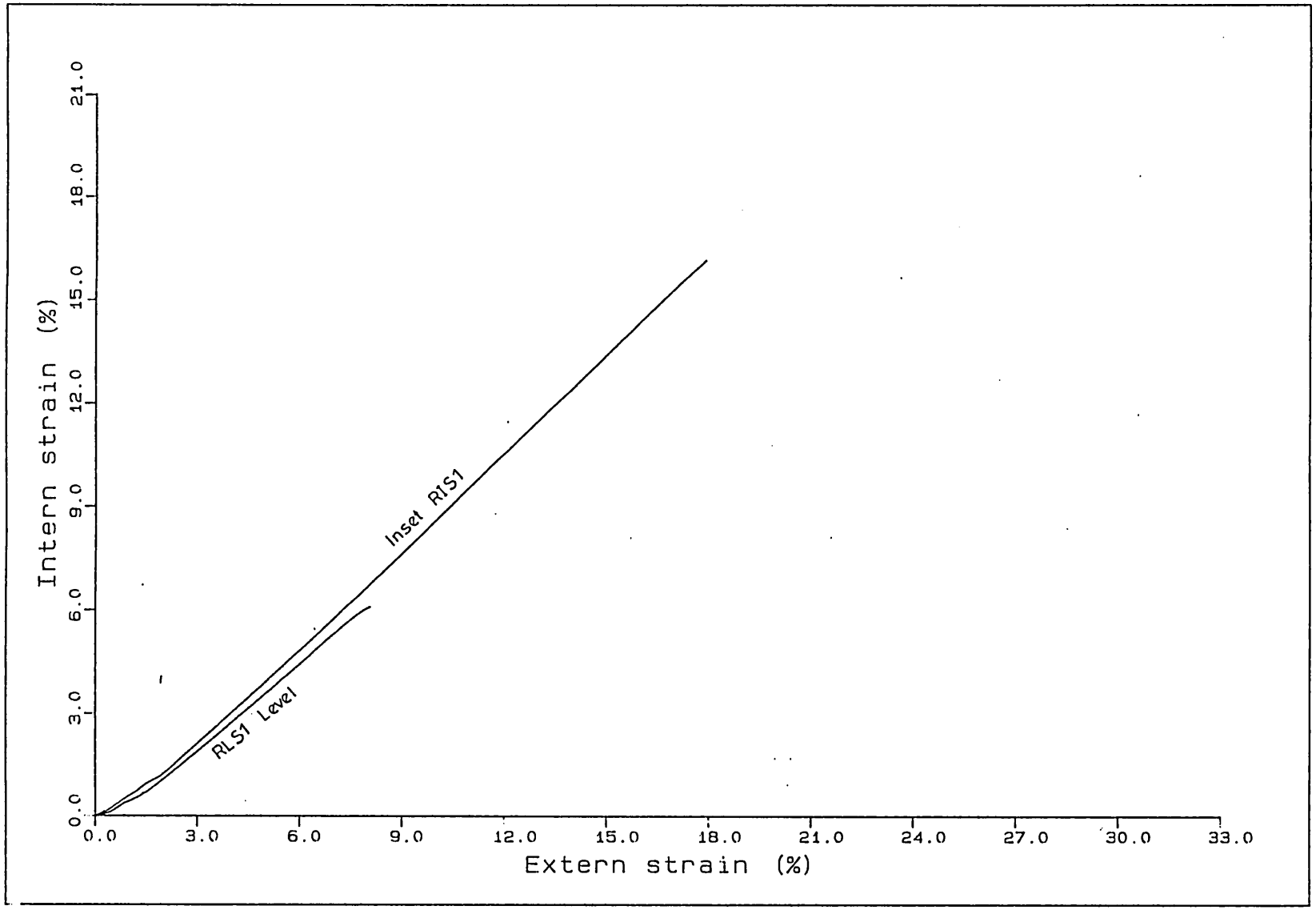
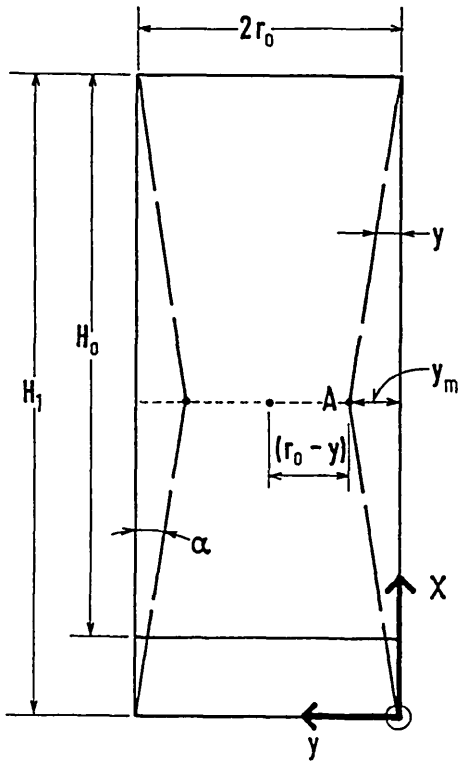


Figure A2.23. Compression tests on rubber specimen with greased ends: local strain measurement by electrolevel device with footing pads either set level on side of, or inset into, specimen.

Figure A2.24

Estimate of angle of rotation of a local strain gauge pad for an undrained extension test



Equating volumes of whole and deformed half cylinders:

$$\pi r_o^2 \frac{H_o}{2} = \int_0^{H_1/2} \pi (r_o - y)^2 \, dx$$

But $y = \frac{2y_m x}{H_1}$

So $r_o^2 \frac{H}{2} = \int_0^{H_1/2} \left[r_o - \frac{2y_m x}{H_1} \right]^2 dx$

ie $r_o^2 \frac{H}{2} = \left[r_o^2 x - \frac{2r_o y_m x^2}{H_1} + \frac{4}{3} \frac{y_m^2 x^3}{H_1^2} \right]_0^{H_1/2}$

$= r_o^2 \frac{H_1}{2} - \frac{2r_o y_m H_1^2}{H_1 \cdot 4} + \frac{4}{3} \frac{y_m^2}{H_1^2} \frac{H_1^3}{8}$

therefore, $\frac{r_o^2}{2} (H_o - H_1) = y_m H_1 \left[-\frac{r_o}{2} + \frac{y_m}{6} \right]$

and $y_m = \frac{r_o^2 \left[H_o - H_1 \right]}{2H_1 \left[-\frac{r_o}{2} + \frac{y_m}{6} \right]}$

But $\sin\alpha \approx \tan\alpha = \frac{2y_m}{H_1}$

/over

$$\text{So } \sin\alpha \approx 2r_o \left[\frac{H_1 - H_o}{H_1^2} \right]$$

$$\left(\text{neglecting } \frac{y_m}{6} \ll r_o/2\right)$$

$$\text{Say } \epsilon_a = \frac{H_o - H_1}{H_o}$$

$$1 - \epsilon_a = \frac{H_1}{H_o}$$

$$\text{then } \frac{\epsilon_a}{(1 - \epsilon_a)^2} = H_o \cdot \frac{H_o - H_1}{H_1^2}$$

$$\text{or } \sin\alpha = \frac{2r_o}{H_o} \cdot \frac{\epsilon_a}{(1 - \epsilon_a)^2}$$

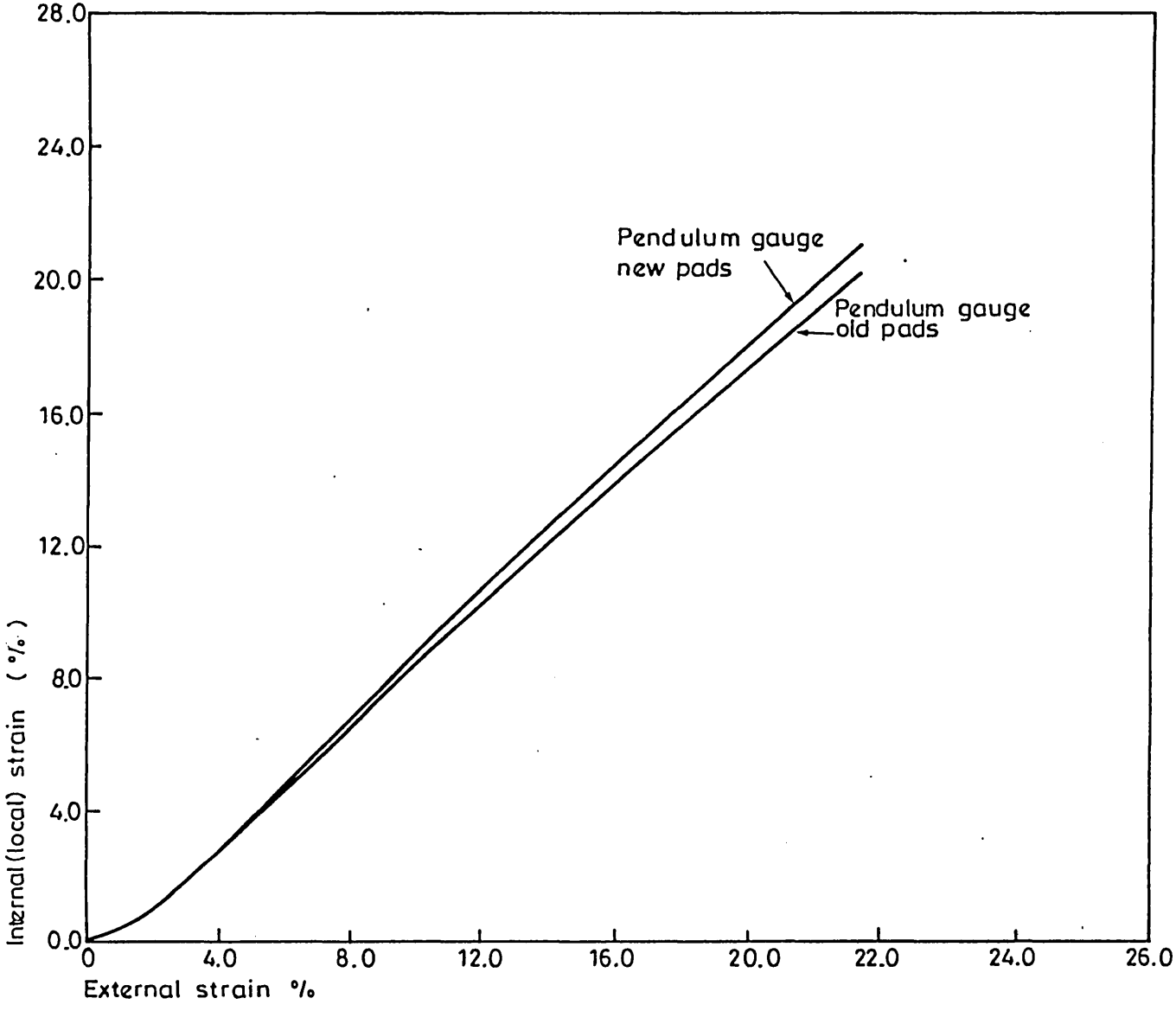


Figure A2.25. Compression tests on rubber specimen with rough ends: comparison of local strain measurement from pendulum gauge with new type support pads and with the gauge with old type pads.

APPENDIX A3

TABLE AND FIGURES

Table A3.1

Parameters used for the finite element membrane analyses

Run no	E_1	E_2	ν_1	ν_2	Load Type
1	10000	5000	0.5	0.5	compressive, point 0.227
2	10000	20000	0.5	0.5	compressive, point 0.227
3	10000	1250	0.5	0.5	compressive, point 0.227
4	10000	5000	0.3	0.5	compressive, point 0.227
5	10000	5000	0.5	0.5	compressive, uniformly distributed
6	10000	5000	0.5	0.5	tensile, point 0.227
8	10000	1	0.5	0.5	compressive, point 0.227
9	10000	10000	0.5	0.5	compressive, point 0.227
10	10000	100000	0.5	0.5	compressive, point 0.227

$E = 1 \times 10^9$ used for top cap

note: subscript 1 denotes sample
subscript 2 denotes membrane
E is Young's Modulus
ν is Poisson's Ratio.

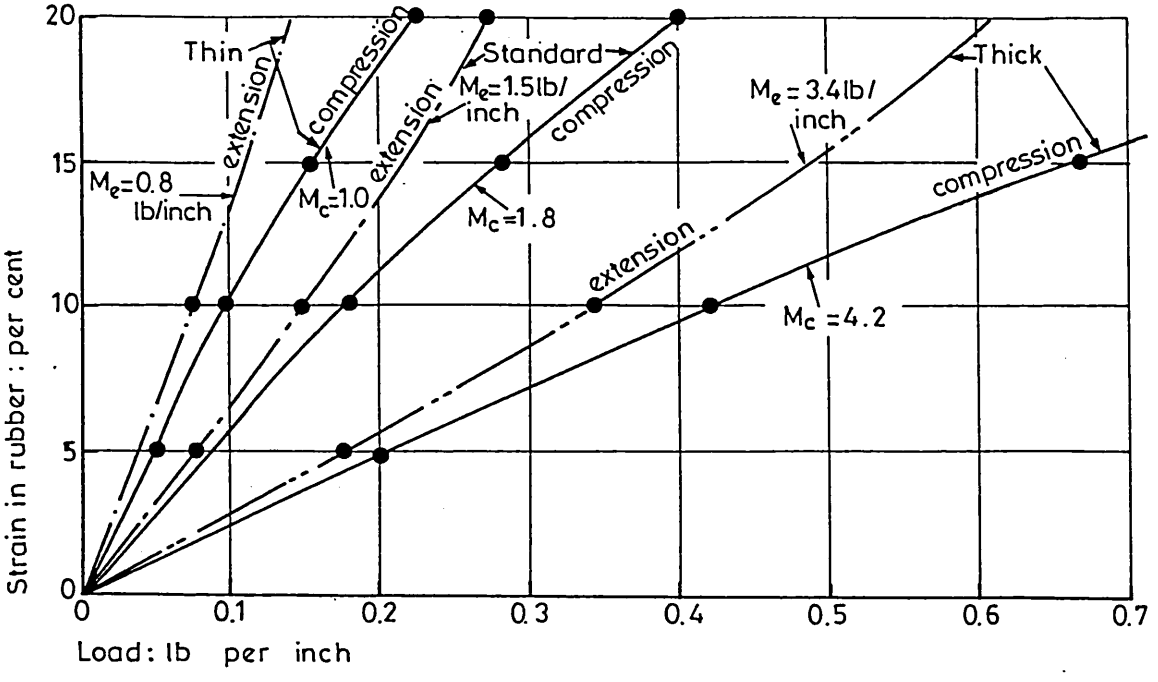


Figure A3.1. Loud/Strains curves for three rubber membranes.

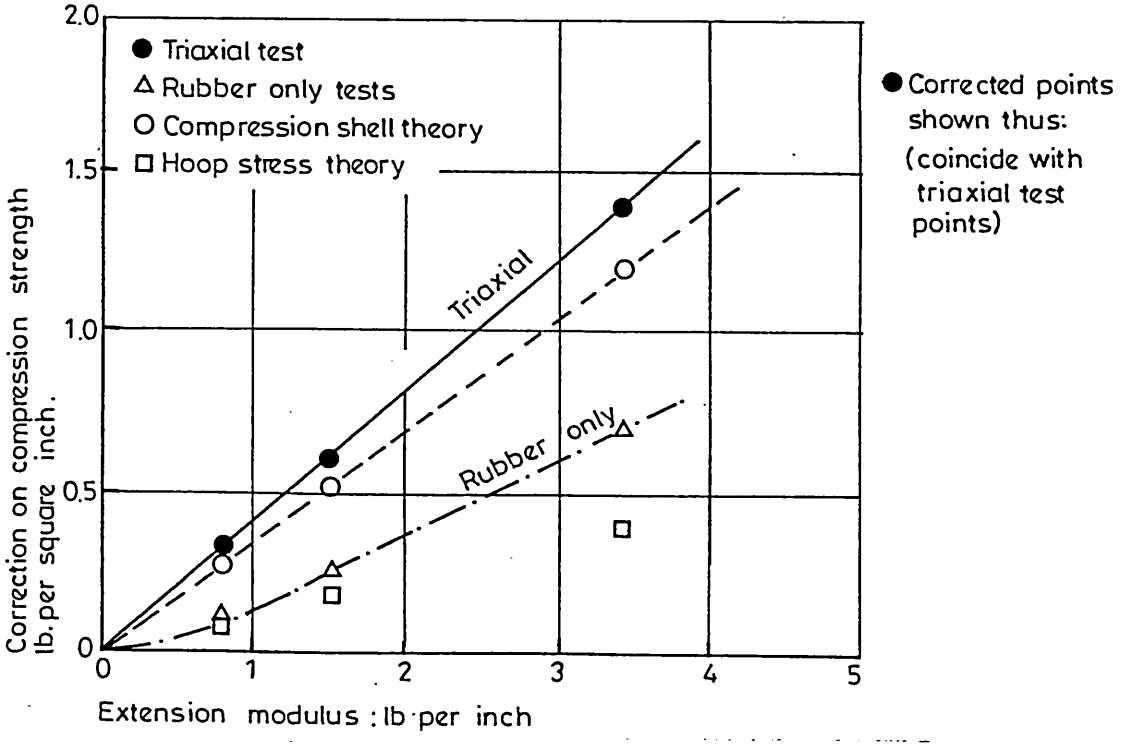
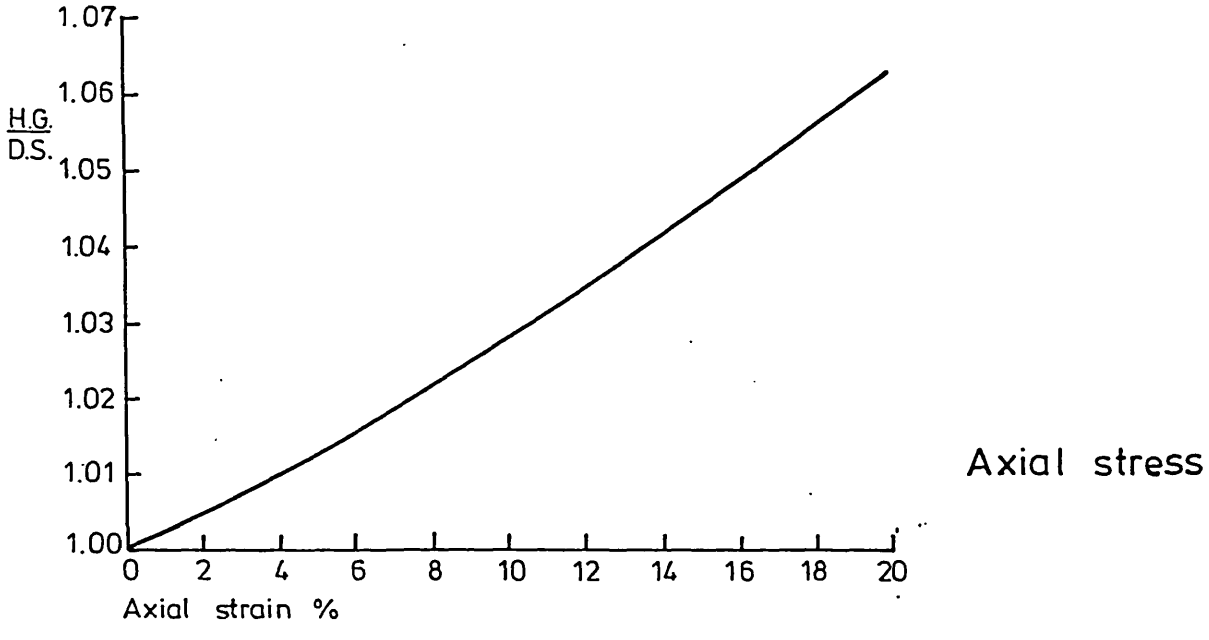


Figure A3.2. Rubber Correction for 15 percent failure strain (Henkel and Gilbert's, 1952, method).



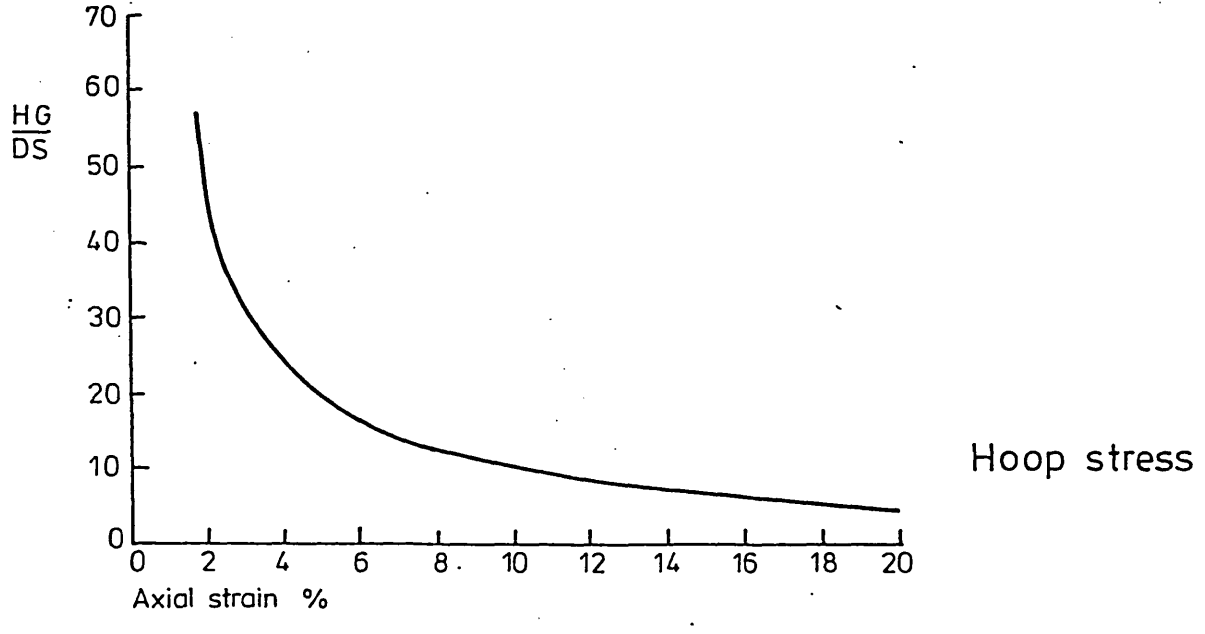


Figure A3.3a. Comparison of Henkel and Gilbert (HG) and Duncan and Seed (DS) methods for stresses on a specimen due to a membrane: undrained compression test.

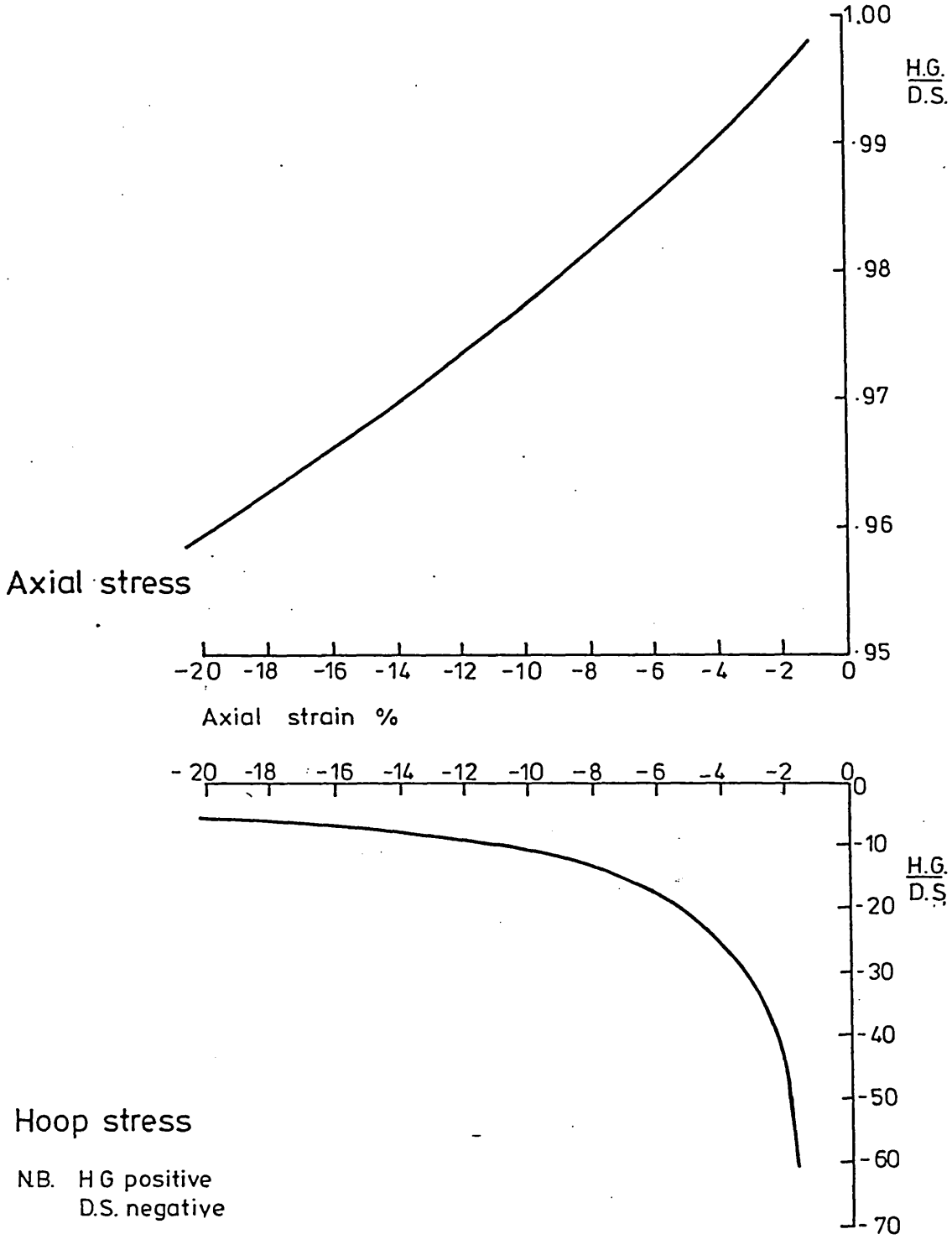
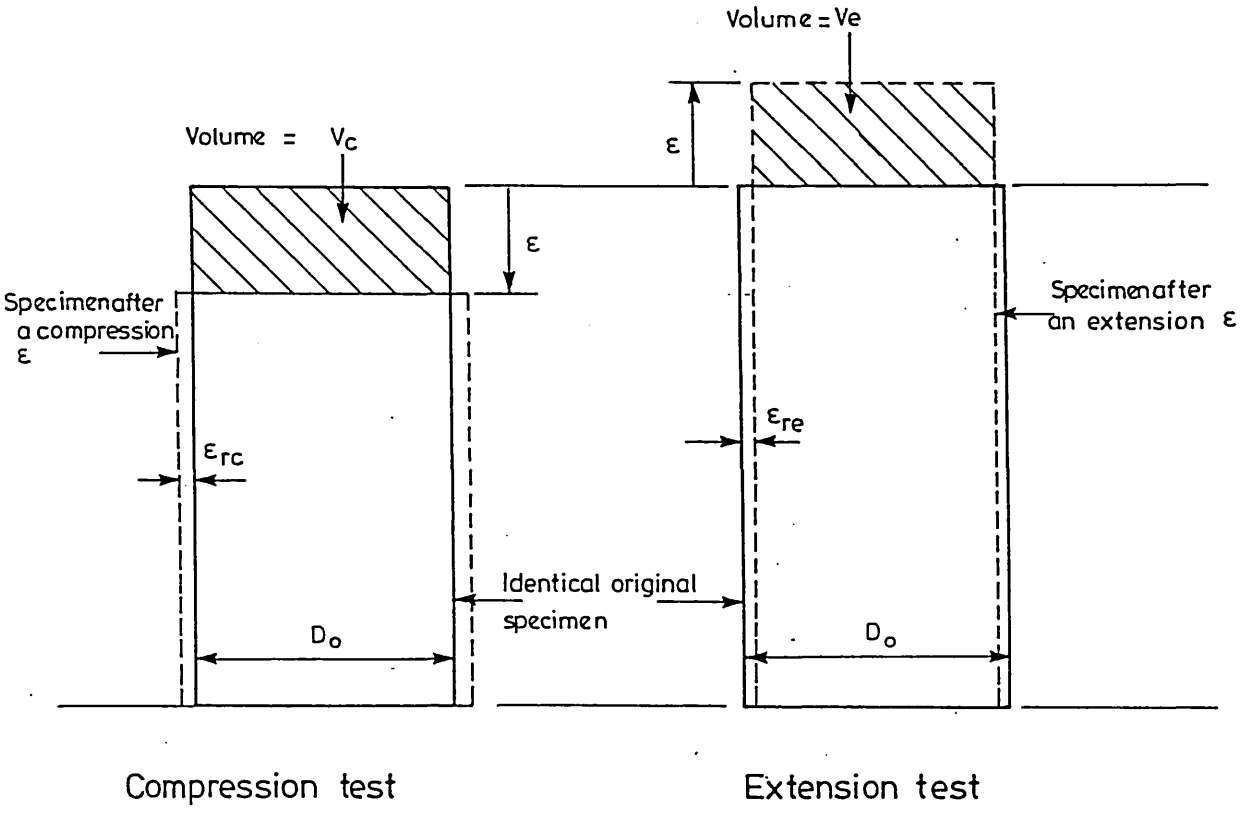


Figure A3.3b. Comparison of Henkel and Gilbert (HG) and Duncan and Seed (DS) methods for stresses on a specimen due to a membrane: undrained extension test.



Although the magnitude of ε is the same in both cases V_c is greater than V_e, so ε_{rc} is greater than ε_{re}

Figure A3.3c. Illustration of reason for obtaining different radial strains in compression and extension specimens for equal but opposite axial strains.

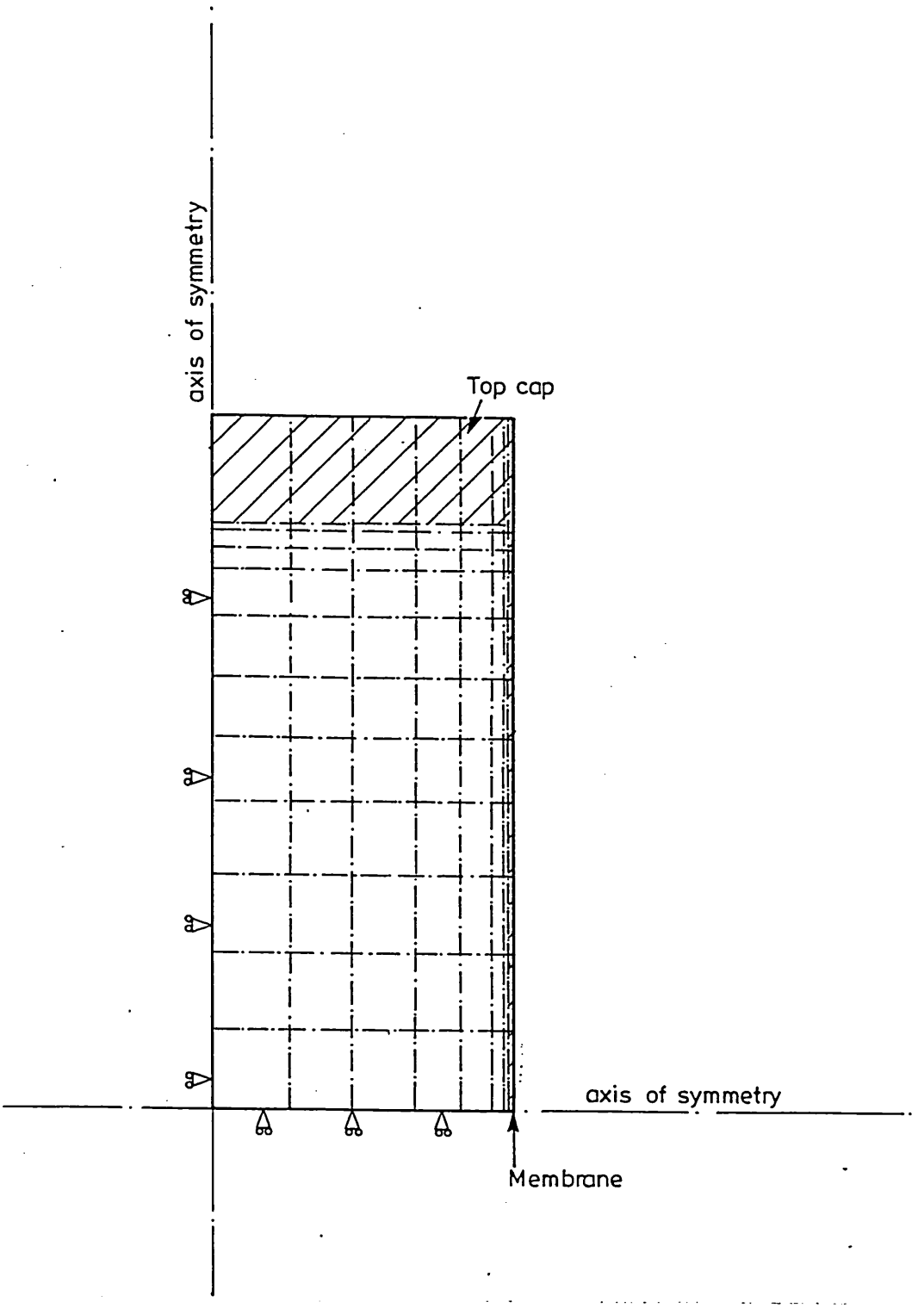


Figure A3.4. Finite element analysis for quarter of a triaxial specimen-subdivision of elements.

Figure A3.5 to A3.13

Vertical and lateral deformations down the side of a specimen in the finite element model (Note: subscript '1' refers to specimen and '2' to membrane; all cases for compression from a point load except run 5 which has a uniformly distributed load and run 6 which has a tensile point load - see Table A3.1).

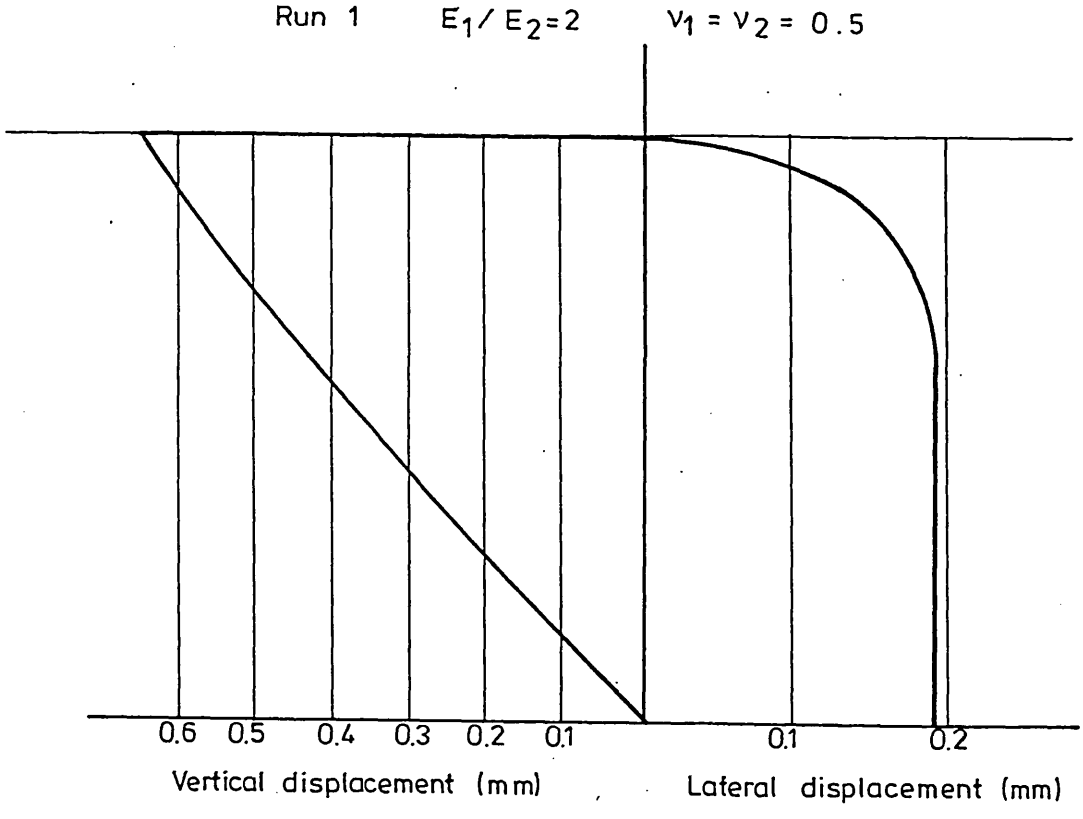


Figure A3.5.

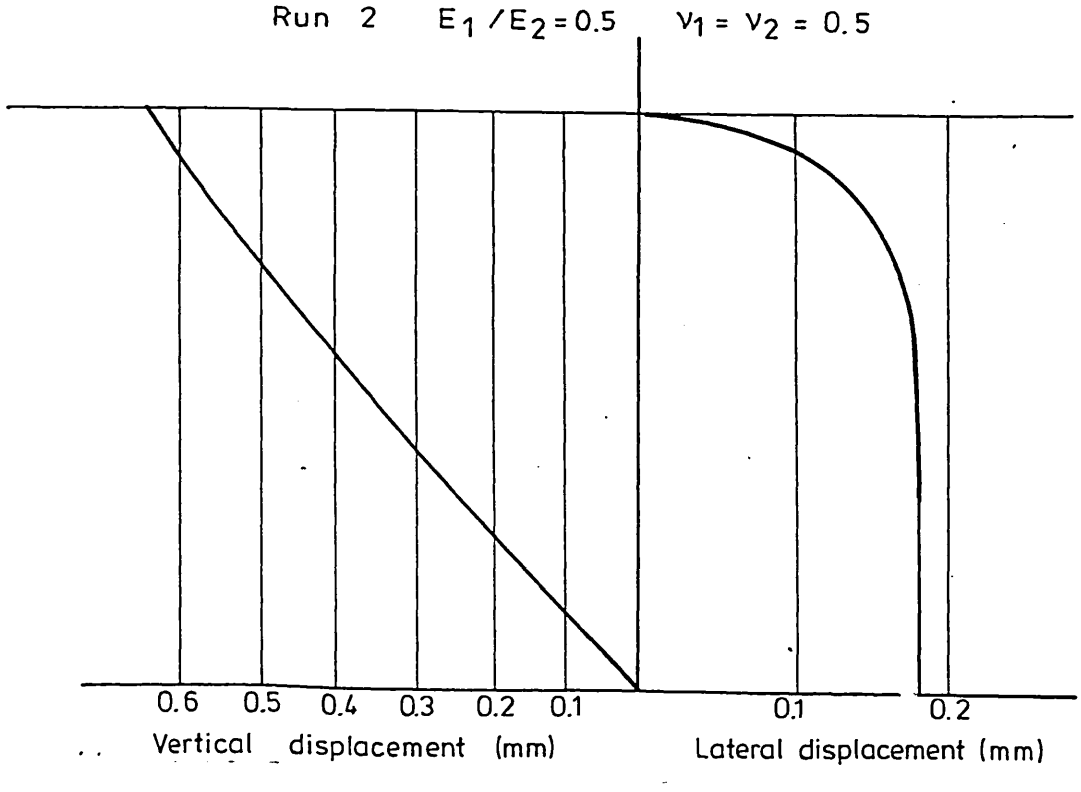


Figure A3.6.

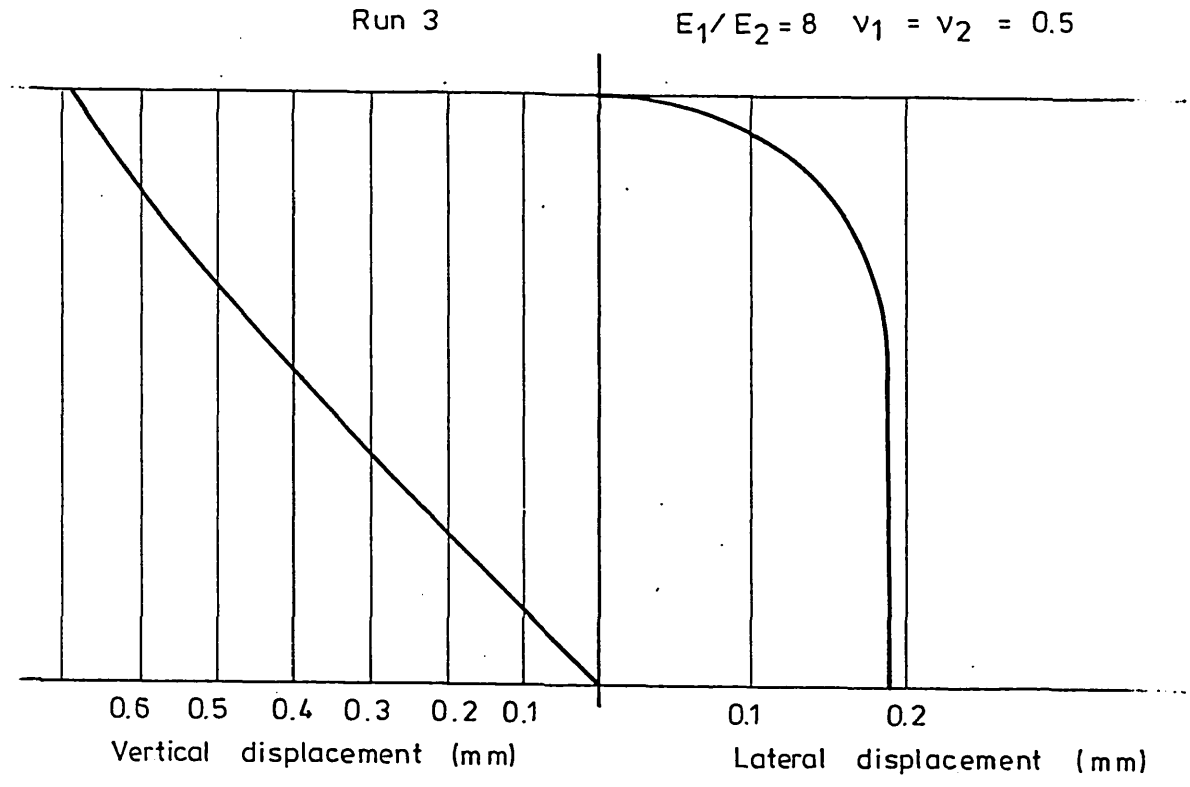


Figure A3.7.

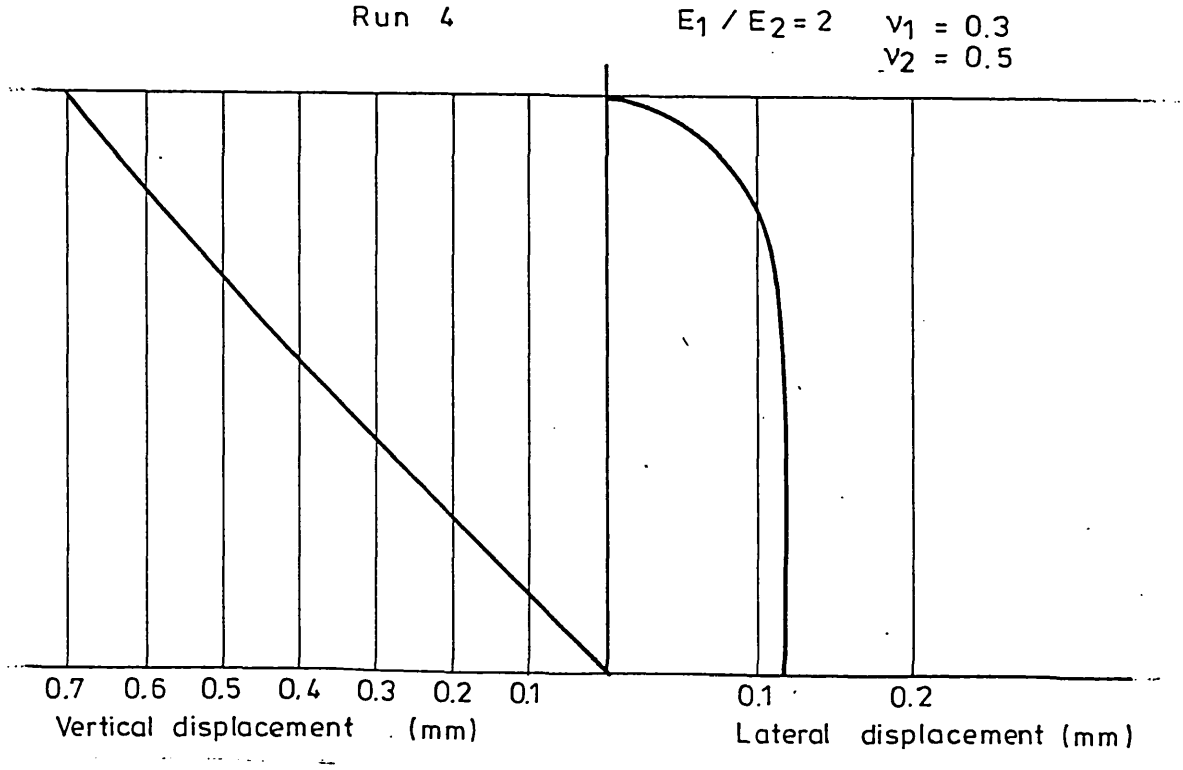


Figure A3.8.

Run 5

(Uniform load)

$E_1 / E_2 = 2 \quad \nu_1 = \nu_2 = 0.5$

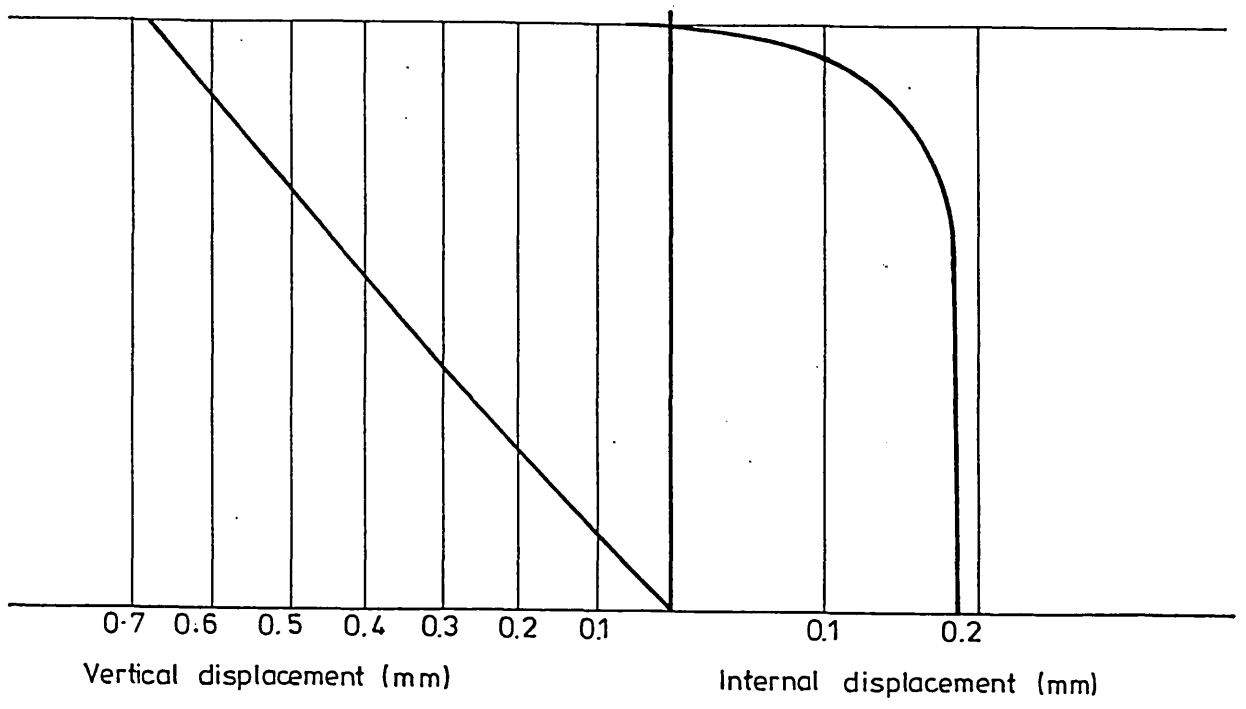


Figure A3.9.

Run 6

(extension)

$E_1 / E_2 = 2 \quad \nu_1 = \nu_2 = 0.5$

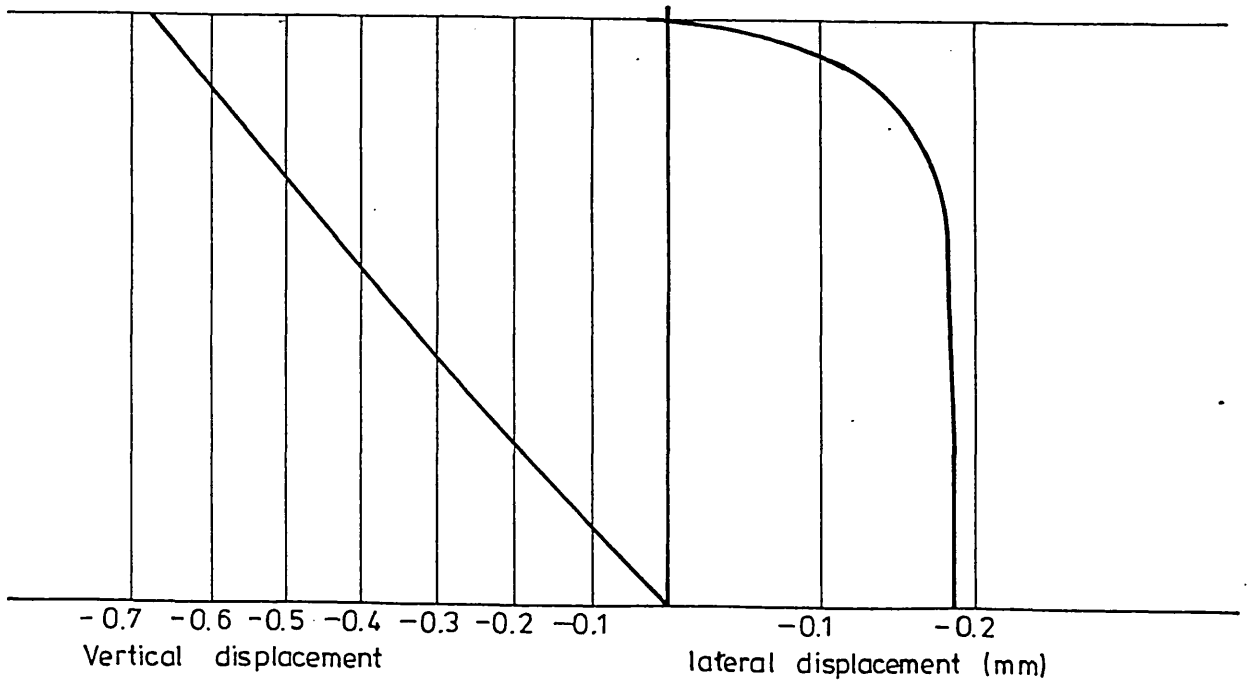


Figure A3.10.

Run 8 $E_1/E_2 = 10000$ $\nu_1 / \nu_2 = 0.5$

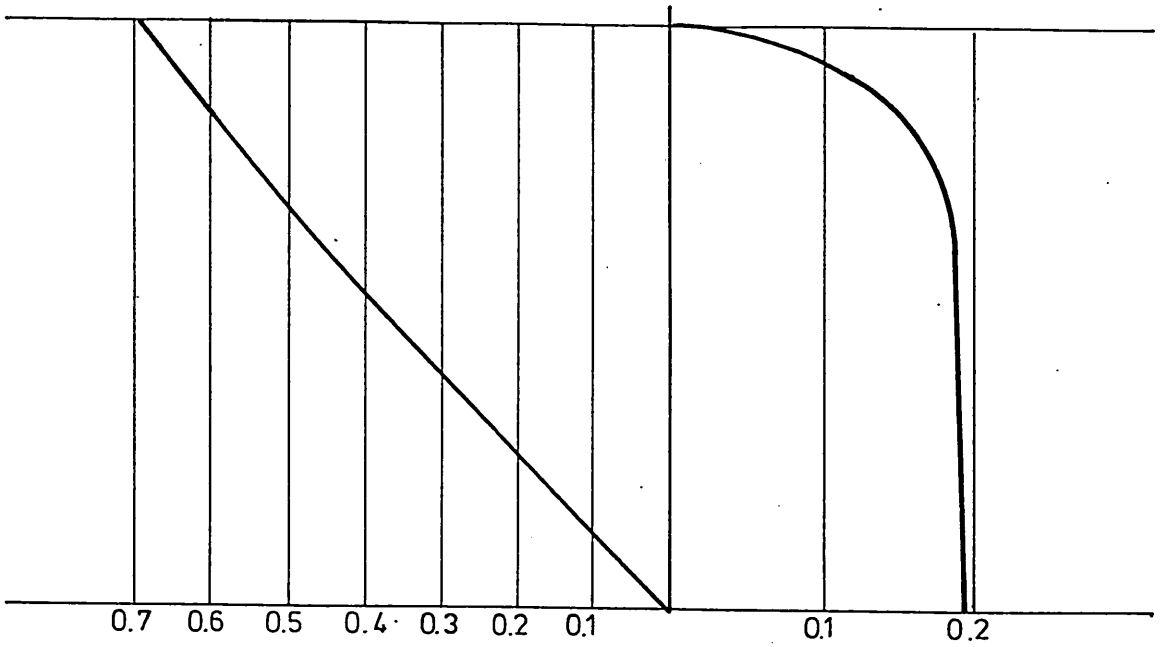


Figure A3.11.

Run 9 $E_1 = E_2$ $\nu_1 = \nu_2 = 0.5$

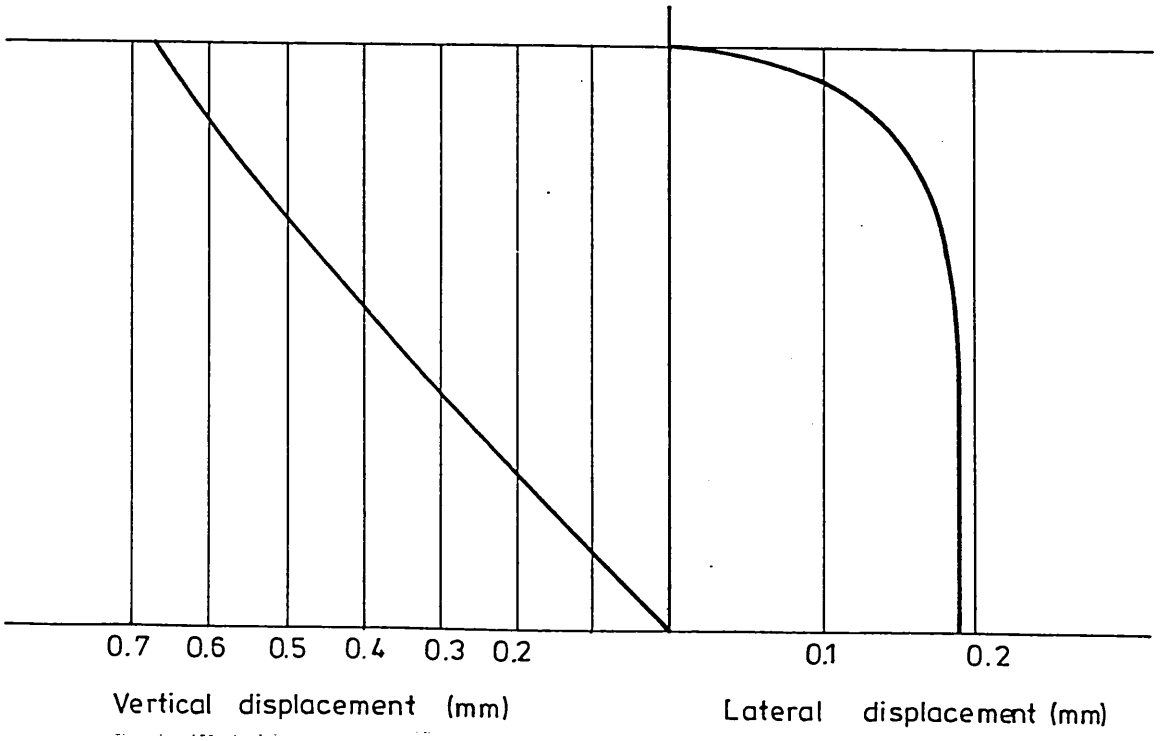


Figure A3.12.

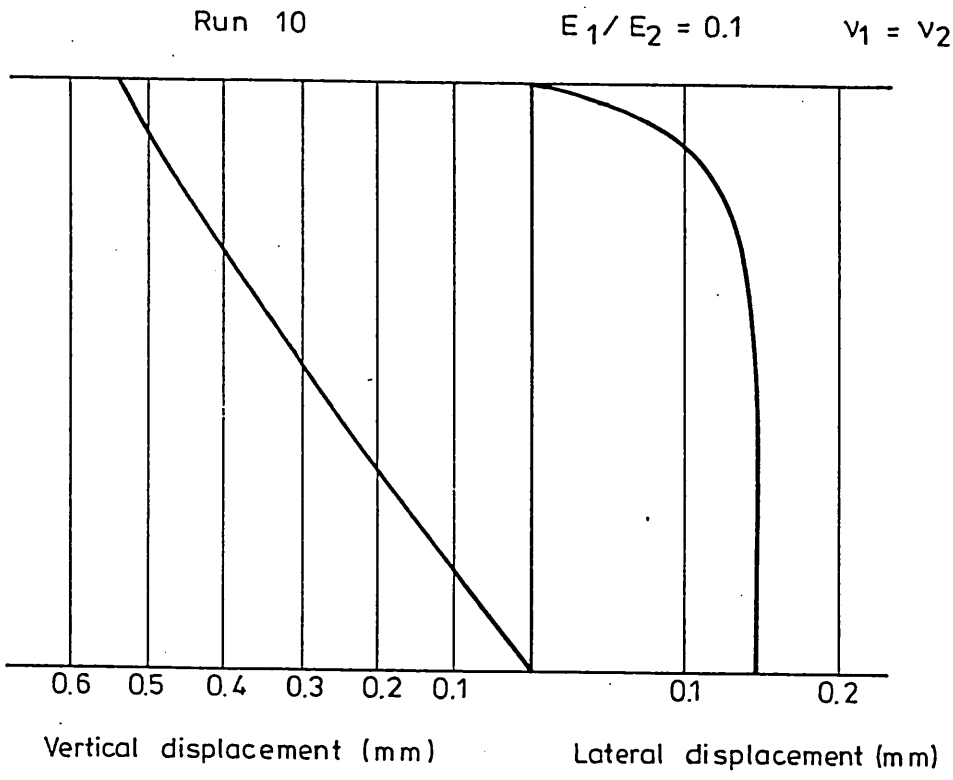

Run 10
$E_1 / E_2 = 0.1$
$\nu_1 = \nu_2 = 0.5$
0.6
0.5
0.4
0.3
0.2
0.1
0.1
0.2
Vertical displacement (mm)
Lateral displacement (mm)

Figure A3.13.

Figure A3.14 to A3.19

Vertical stresses in the membrane around the specimen in the finite element model. (Note HG refers to the Henkel and Gilbert method and DS to the Duncan and Seed method). Refer to Table A3.1 for description of parameters.

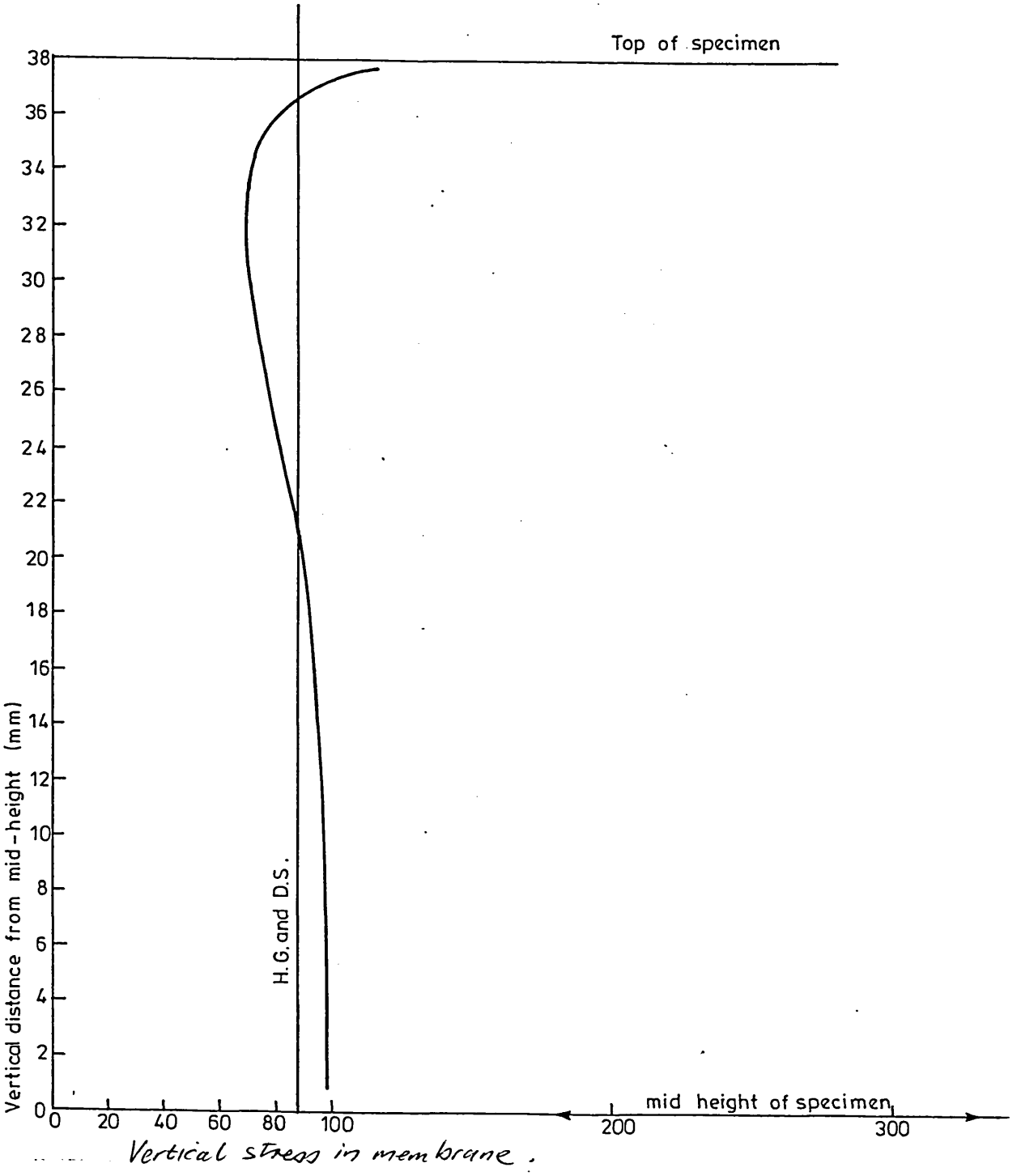

Run 1 $E_1/E_2 = 2$ $\nu_1 = \nu_2 = 0.5$
Top of specimen
38
36
34
32
30
28
26
24
22
20
18
16
14
12
10
8
6
4
2
0
Vertical distance from mid-height (mm)
H.G. and D.S.
0
20
40
60
80
100
200
300
mid height of specimen
Vertical stress in membrane.

Figure A3.14.

Run 2 $E_1 / E_2 = 0.5$ $\nu_1 = \nu_2 = 0.5$

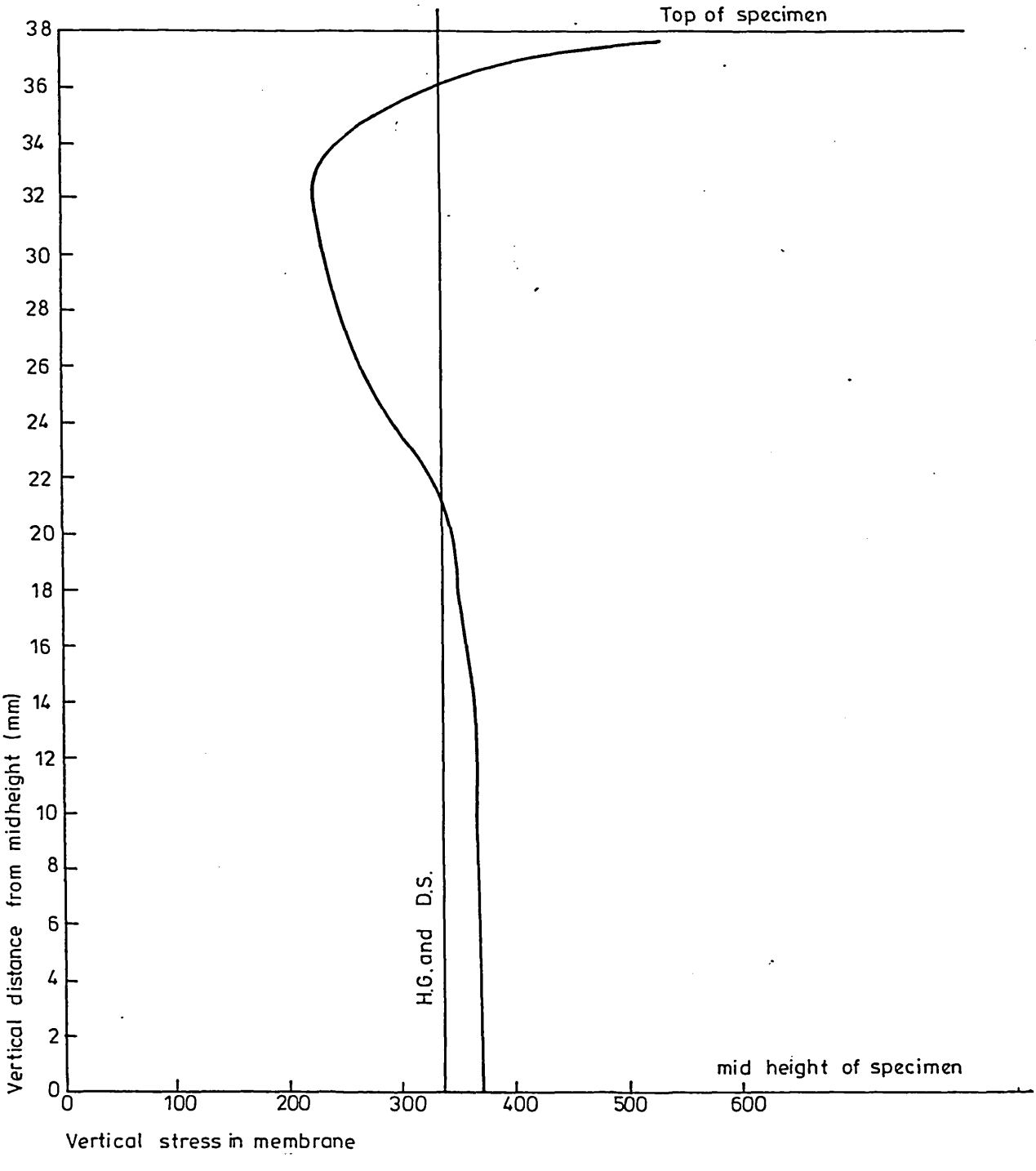


Figure A3.15.

Run 3 $E_1 / E_2 = 8$ $\nu_1 = \nu_2 = 0.5$

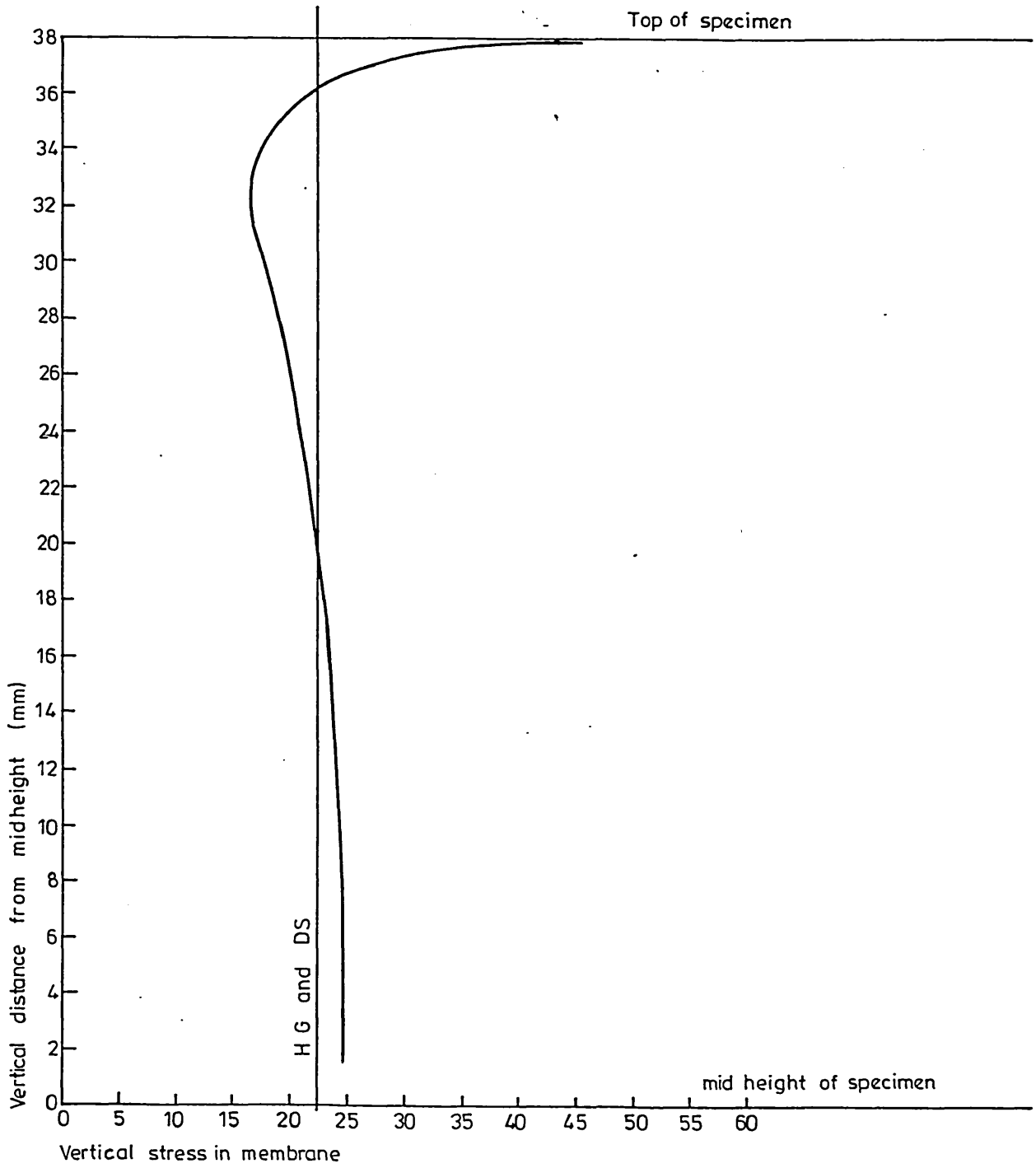


Figure A3.16.

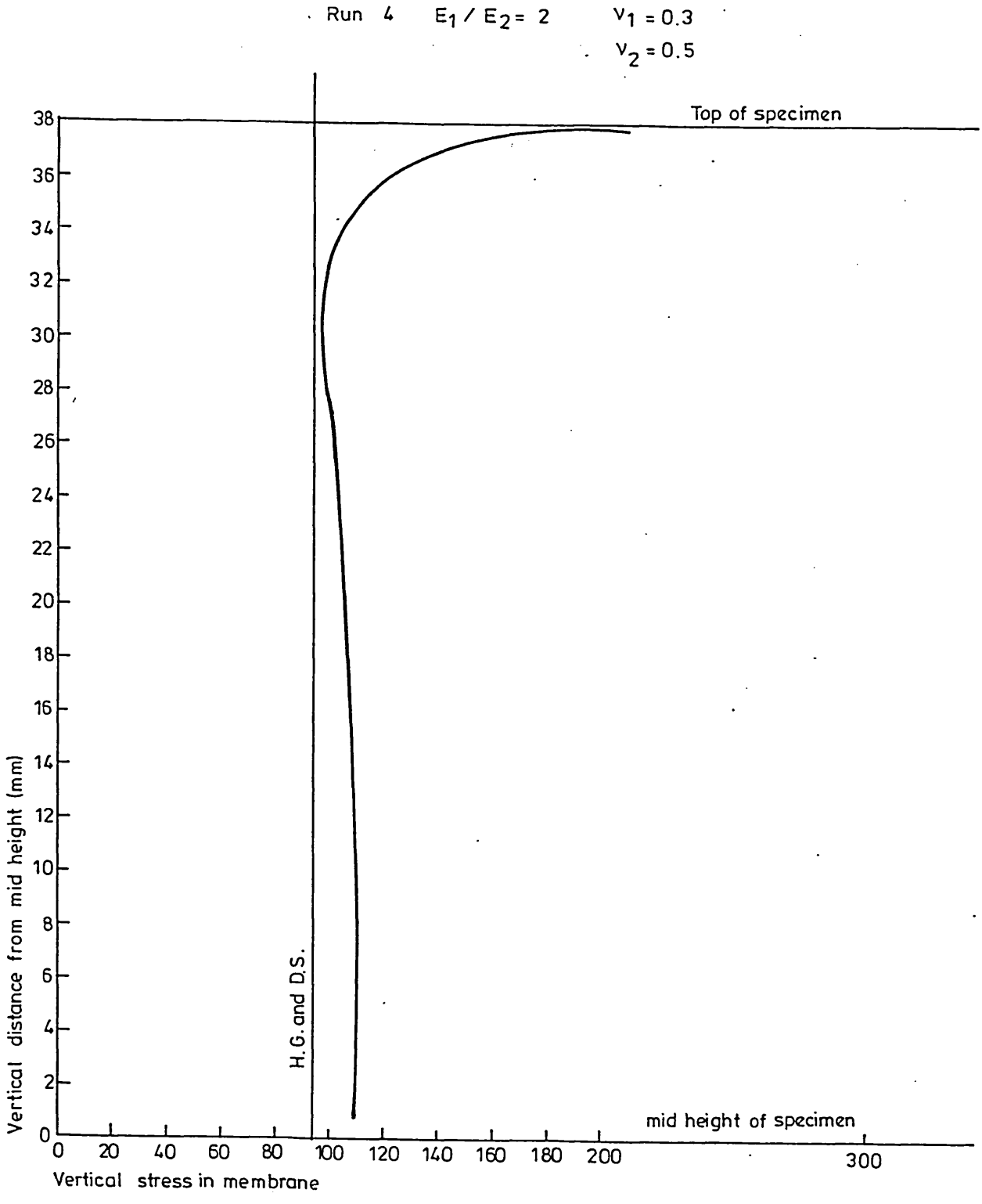

Run 4 $E_1 / E_2 = 2$ $\nu_1 = 0.3$ $\nu_2 = 0.5$
Top of specimen
mid height of specimen
H.G. and D.S.
Vertical distance from mid height (mm)
Vertical stress in membrane
0
2
4
6
8
10
12
14
16
18
20
22
24
26
28
30
32
34
36
38
0
20
40
60
80
100
120
140
160
180
200
300

Figure A3.17.

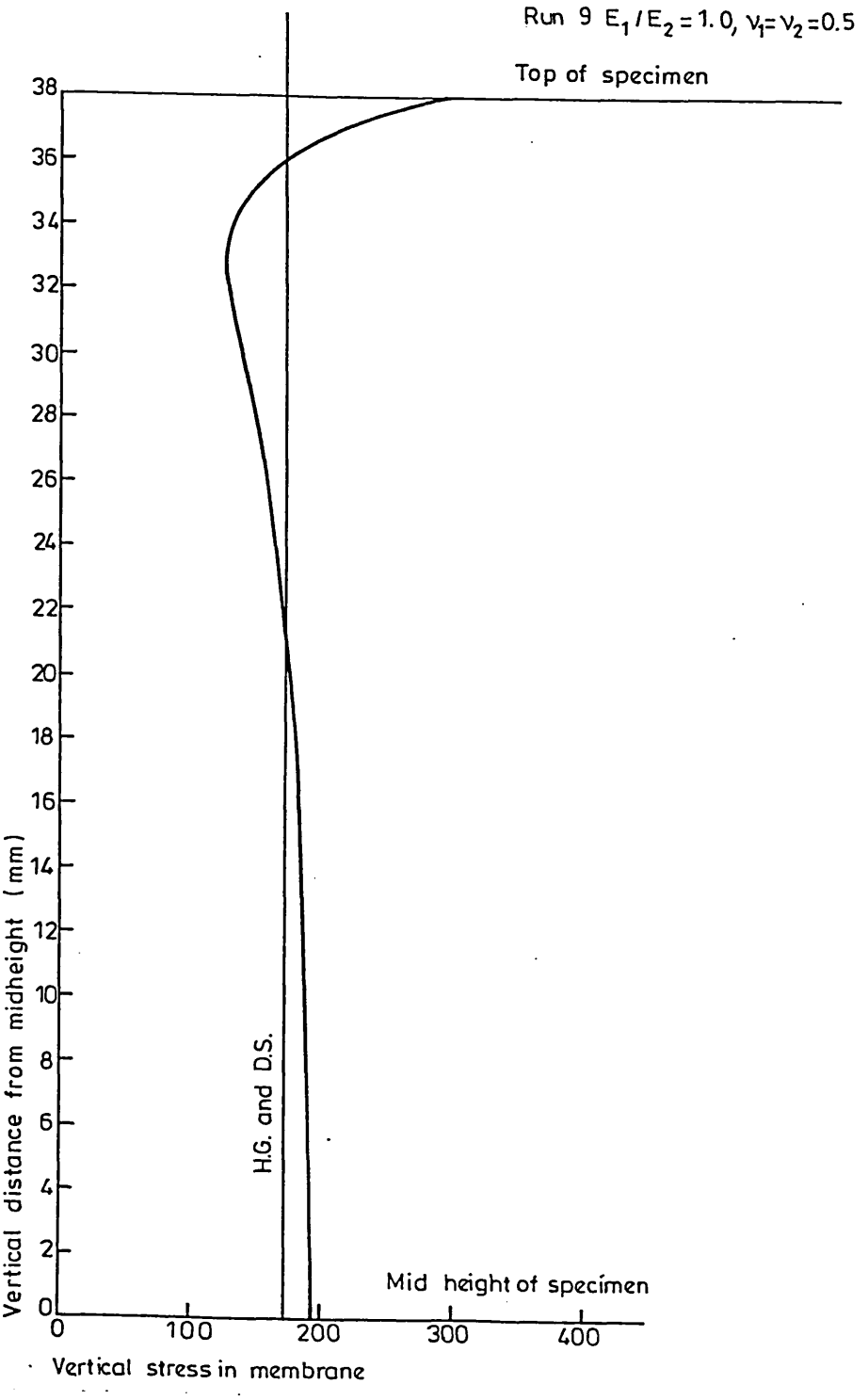

Run 9 $E_1/E_2 = 1.0$, $\nu_1 = \nu_2 = 0.5$
Top of specimen
38
36
34
32
30
28
26
24
22
20
18
16
14
12
10
8
6
4
2
0
Vertical distance from midheight (mm)
H.G. and D.S.
Mid height of specimen
0
100
200
300
400
Vertical stress in membrane

Figure A3.18.

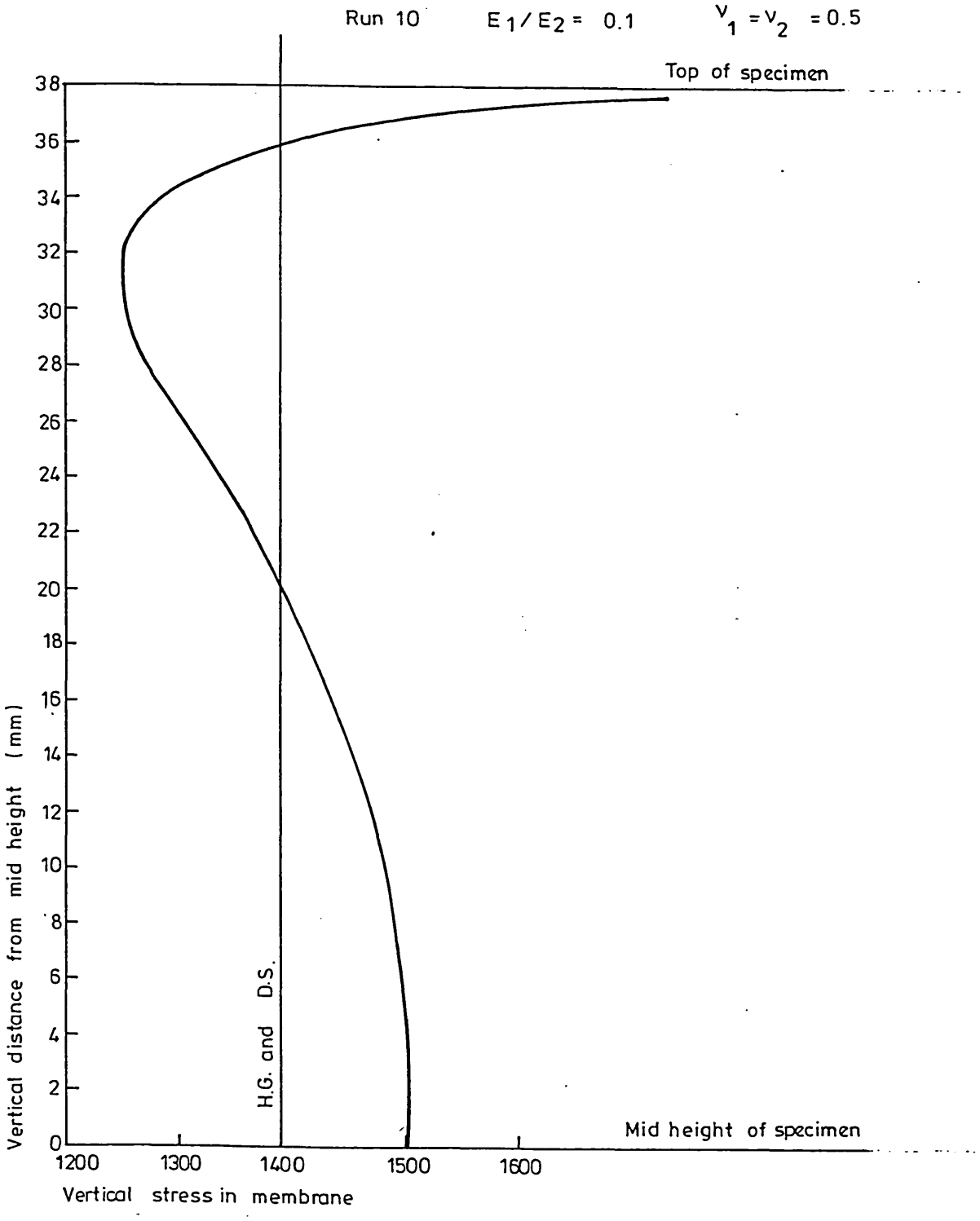

Run 10
E_1/E_2 = 0.1
$\nu_1 = \nu_2$ = 0.5
Top of specimen
Mid height of specimen
H.G. and D.S.
Vertical distance from mid height (mm)
38
36
34
32
30
28
26
24
22
20
18
16
14
12
10
8
6
4
2
0
1200
1300
1400
1500
1600
Vertical stress in membrane

Figure A3.19.

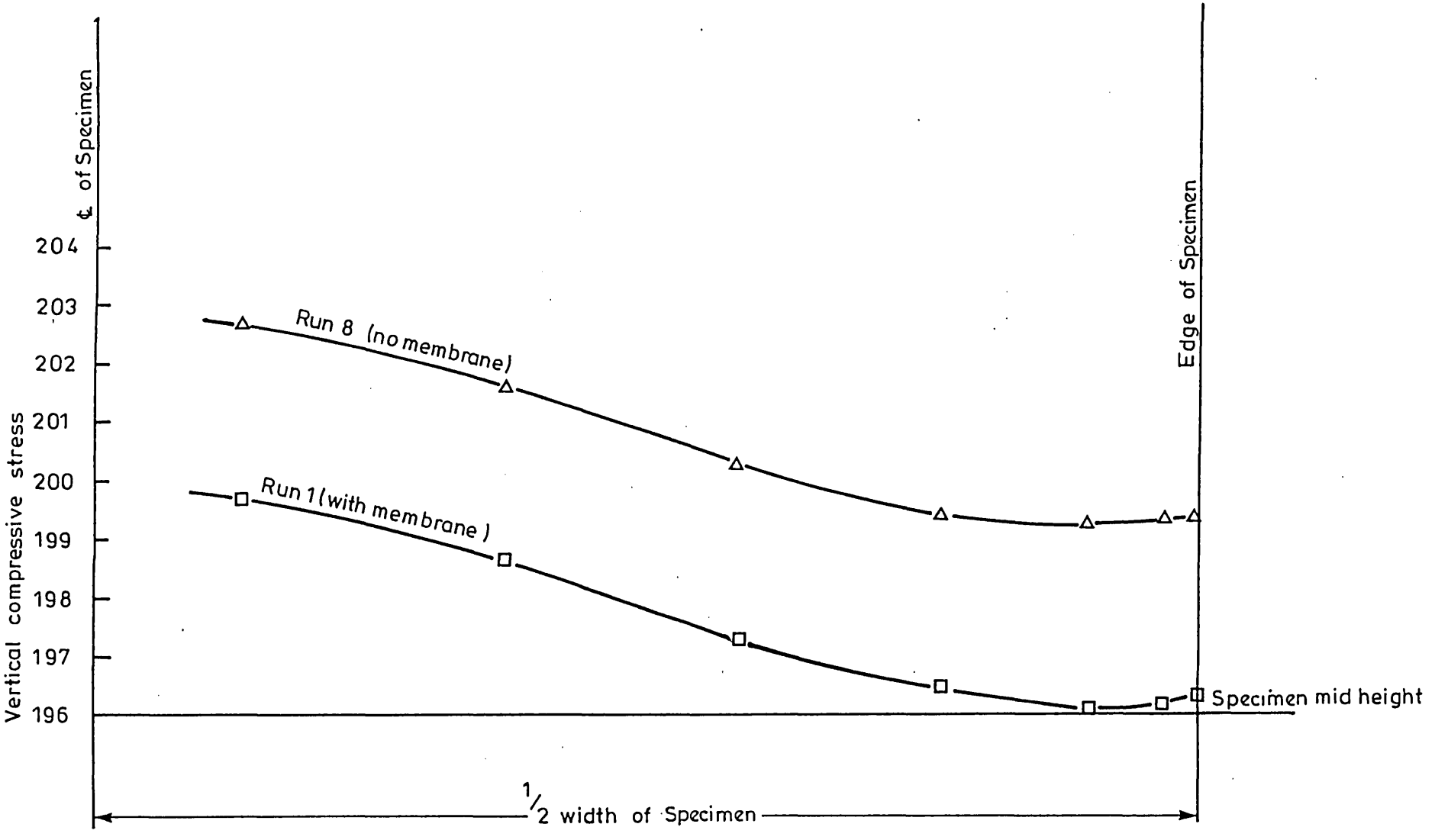


Figure A3.20. Finite element analysis of specimen with membrane: vertical compressive stress along horizontal line through mid height of specimen analyses with and without a membrane.

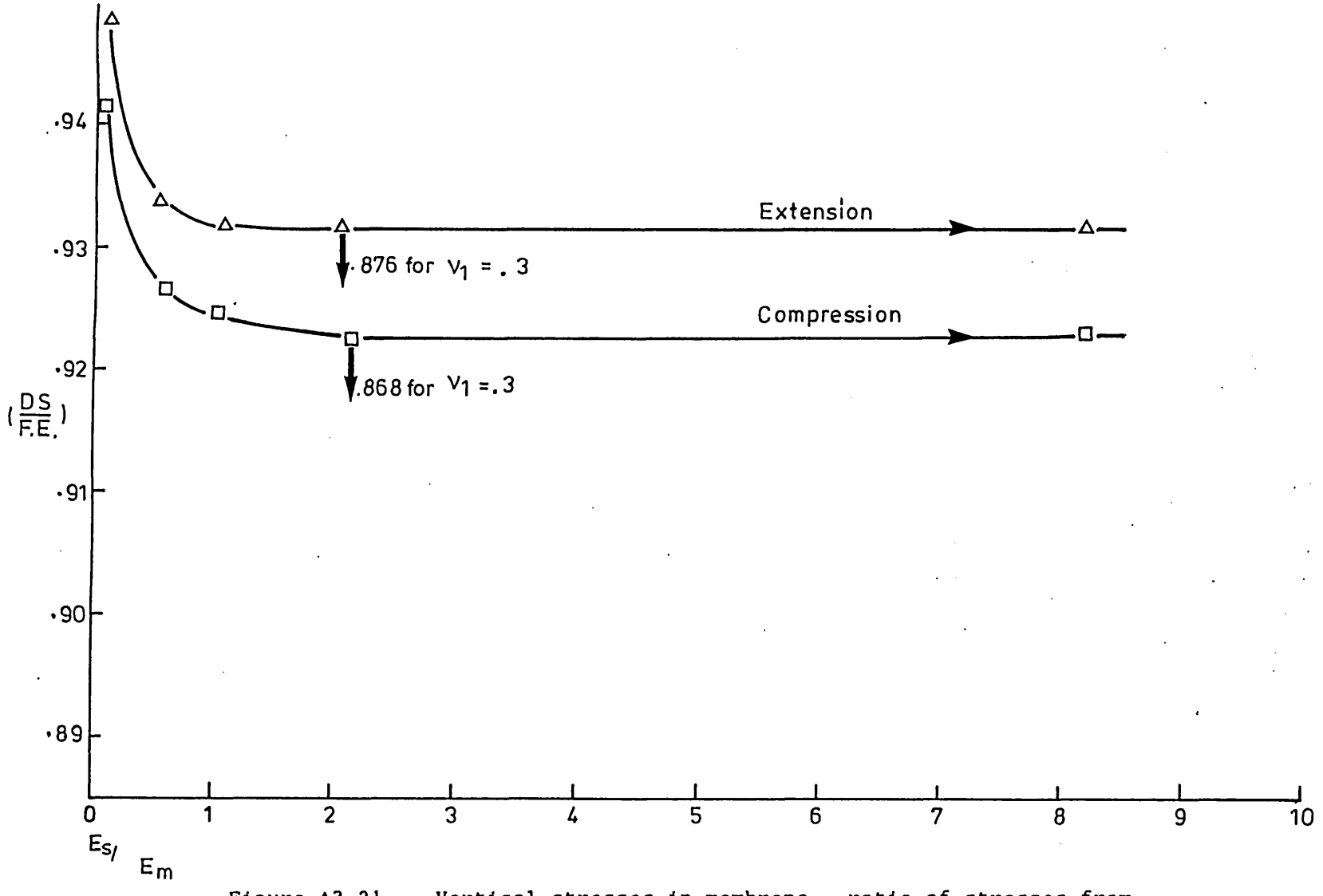


Figure A3.21. Vertical stresses in membrane - ratio of stresses from Duncan and Seed method (DS) to stresses from finite element (FE) method plotted against specimen to membrane stiffness ratio ($\nu_1 = \nu_2 = 0.5$).

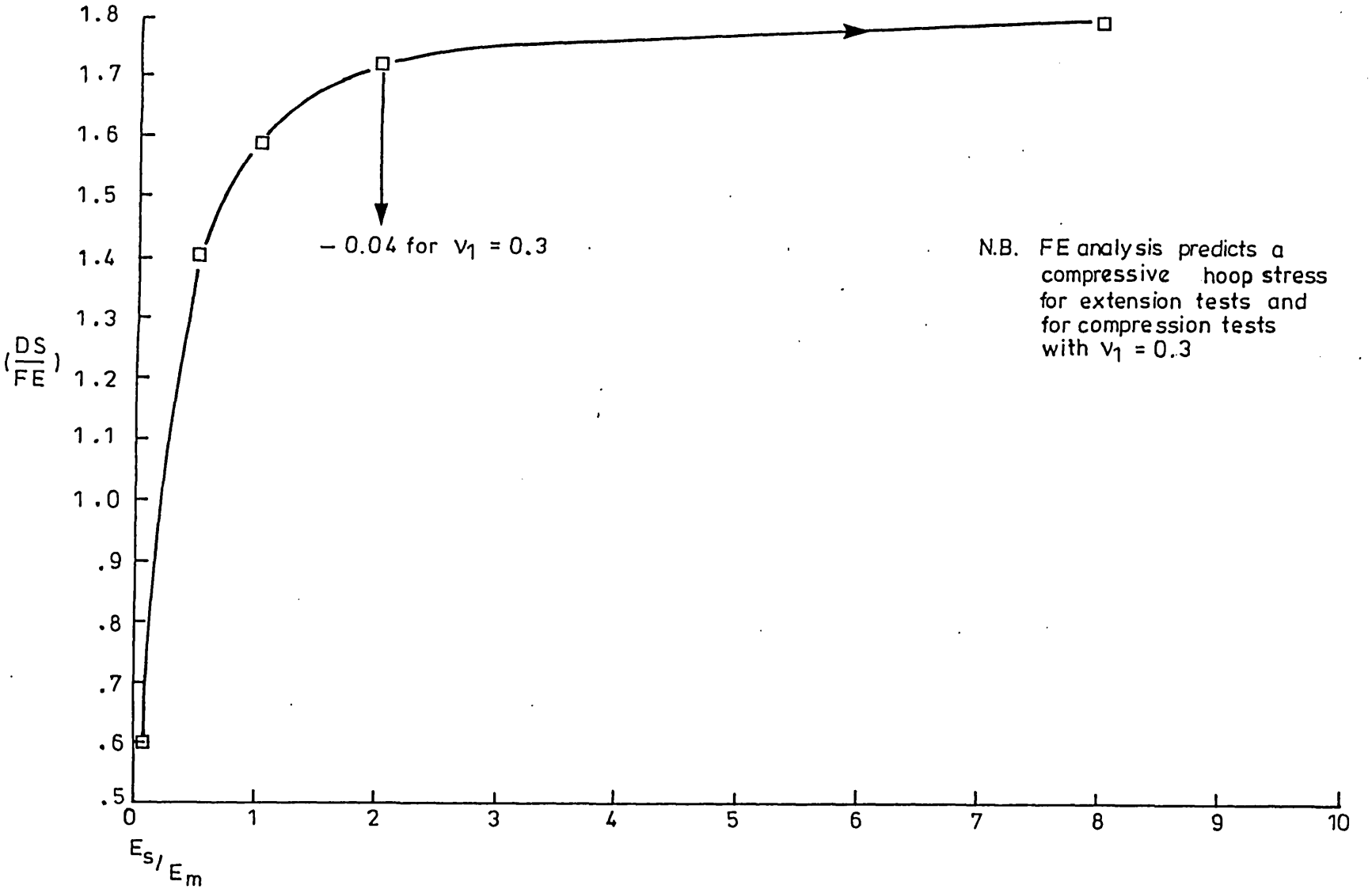


Figure A3.22. Hoop stress in membrane-ratio of stresses from Duncan and Seed method (DS) to stresses from finite element (FE) method plotted against specimen to membrane stiffness ratio for compression tests ($\nu_1 = \nu_2 = 0.5$).

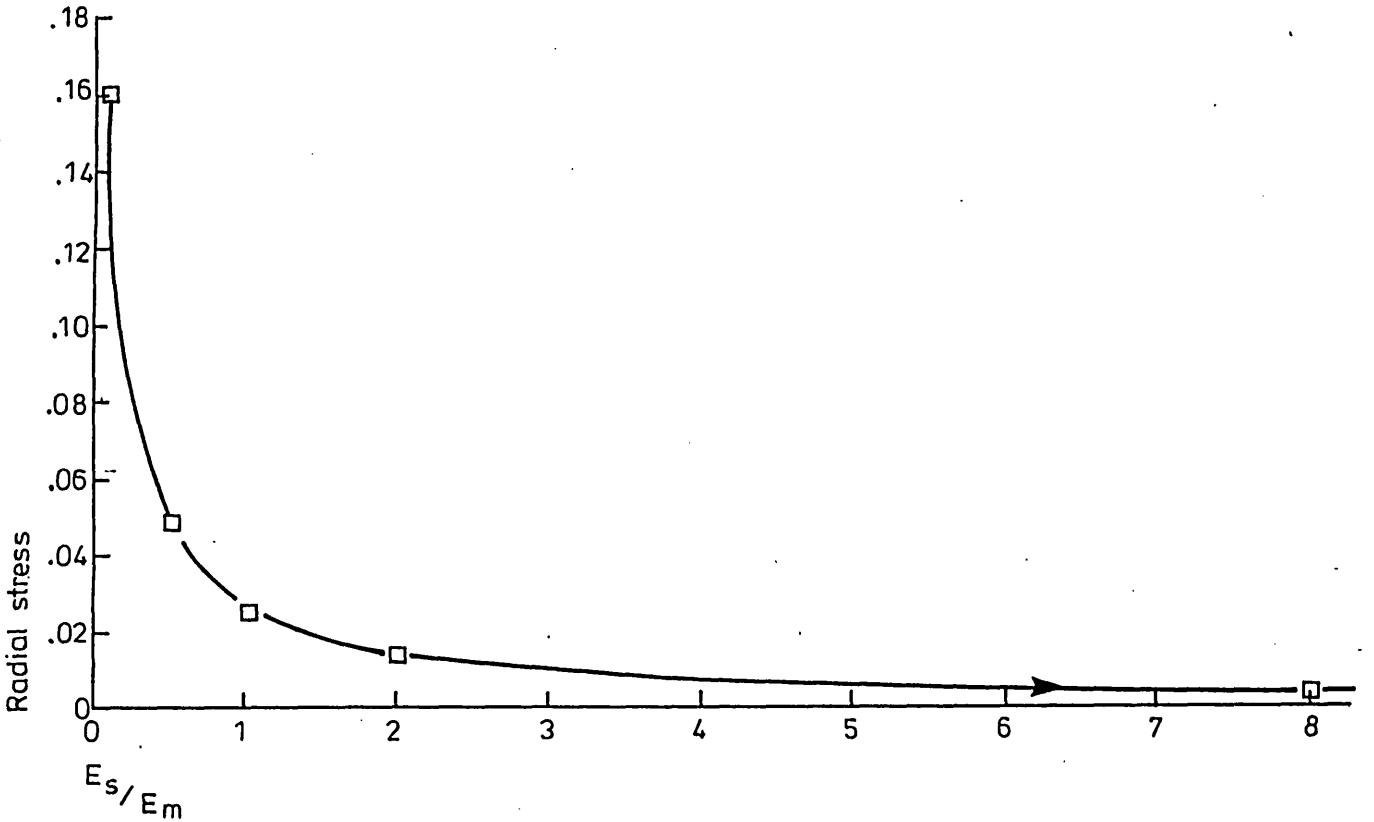
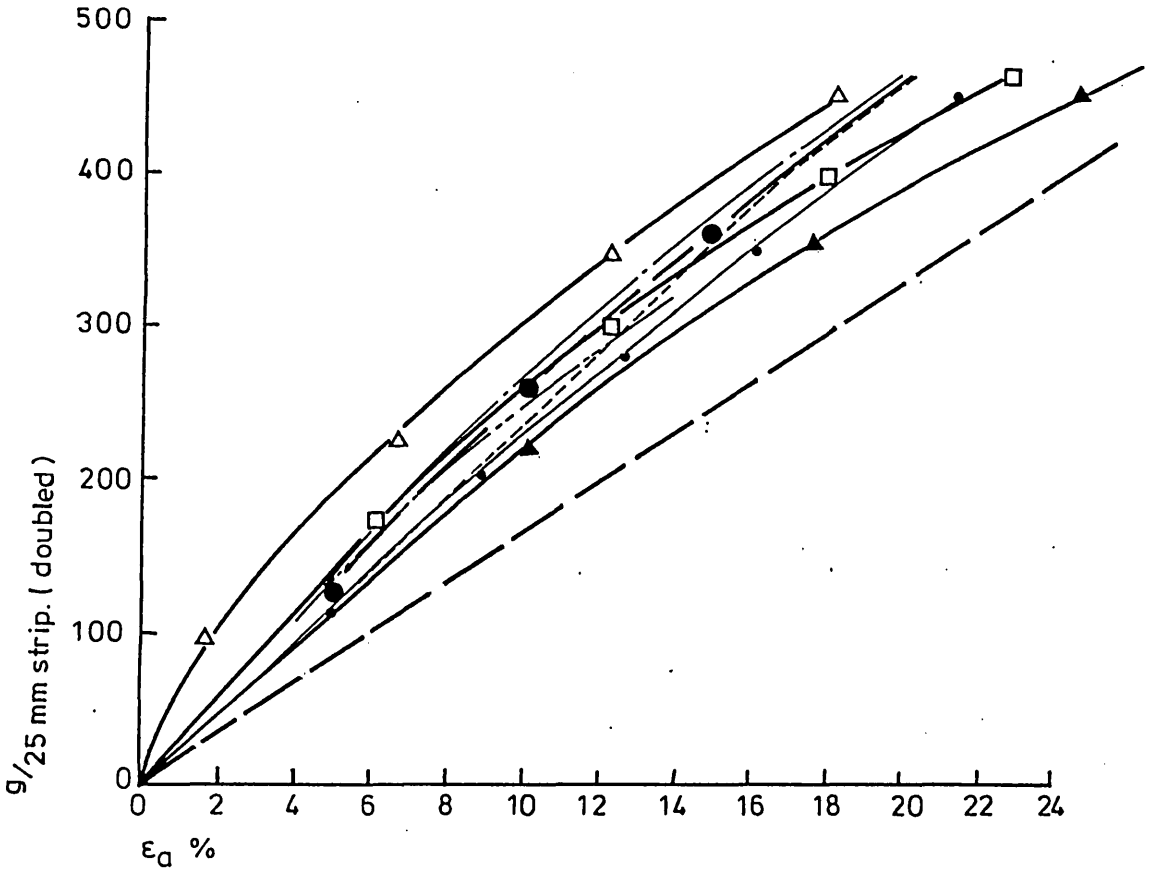


Figure A3.23. Radial stress between specimen and membrane versus ratio of specimen to membrane stiffness as predicted by the Duncan and Seed method.



t_o

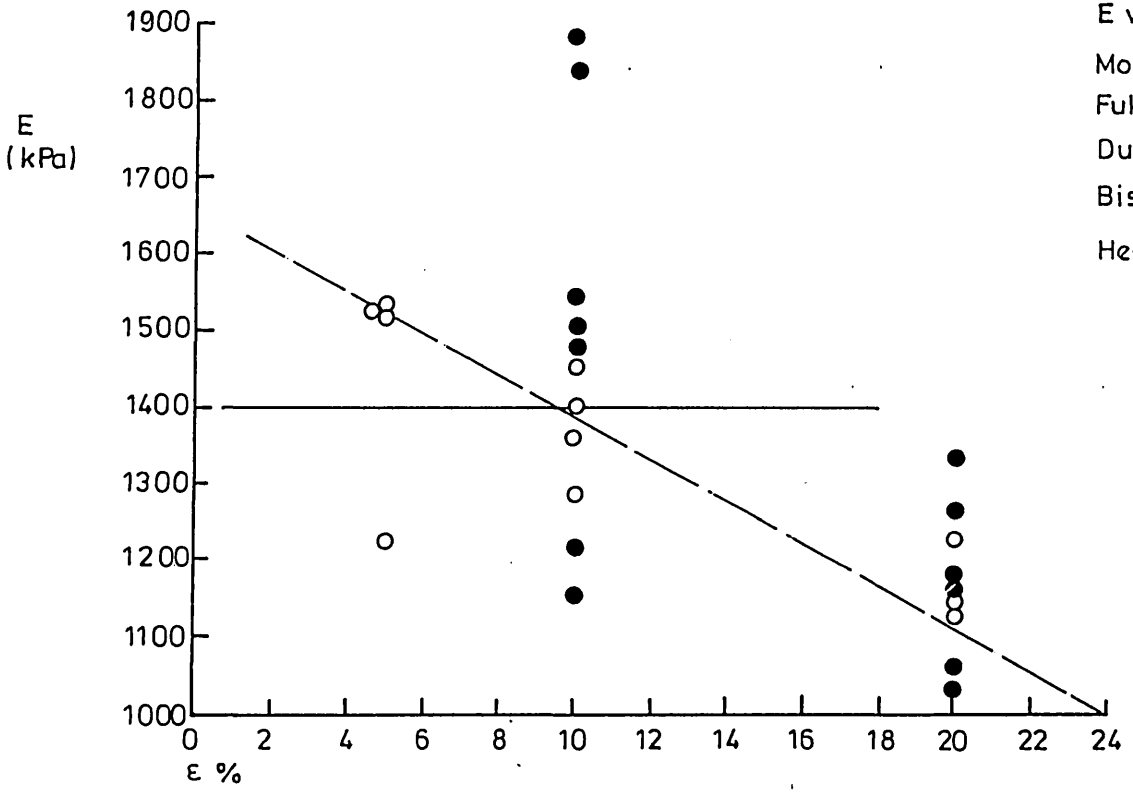
.33 mm (TLDRULI)
.26 mm (TLUU1)
.30 mm (TLPS3)
.29 mm (TLDRUL 2)
.255 mm (TLPS2)
.33 mm M1
.33 mm M2
.34 mm M3
.33 M5

t_o is initial membrane thickness

T - series are strips from membranes from these tests ( )

M - series are entire membranes tested.

Figure A3.24. Results of tests to establish the extension modulus of a fresh latex rubber membrane (a) by the Henkel and Gilbert method with membrane strips and (b) by performing extension tests on entire membranes (M1 to M5). Load on membrane strip plotted against strain.



o Whole membrane in stress path cell

● Strip of membrane as per Gilbert & Henkel, & Head

E values quoted by:

Molenkamp + Luger	(1981)	1300 kPa
Fukushima et al	(1984)	1490 "
Duncan + Seed	(1965)	1373 "
Bishop + Henkel	(1962)	1300-1500 kPa
Head	(1982)	1200-1300
	Average	1350 kPa

Figure A3.25. Young's Modulus for fresh latex rubber membranes plotted against strain (E values deduced from Fig. A3.24.).

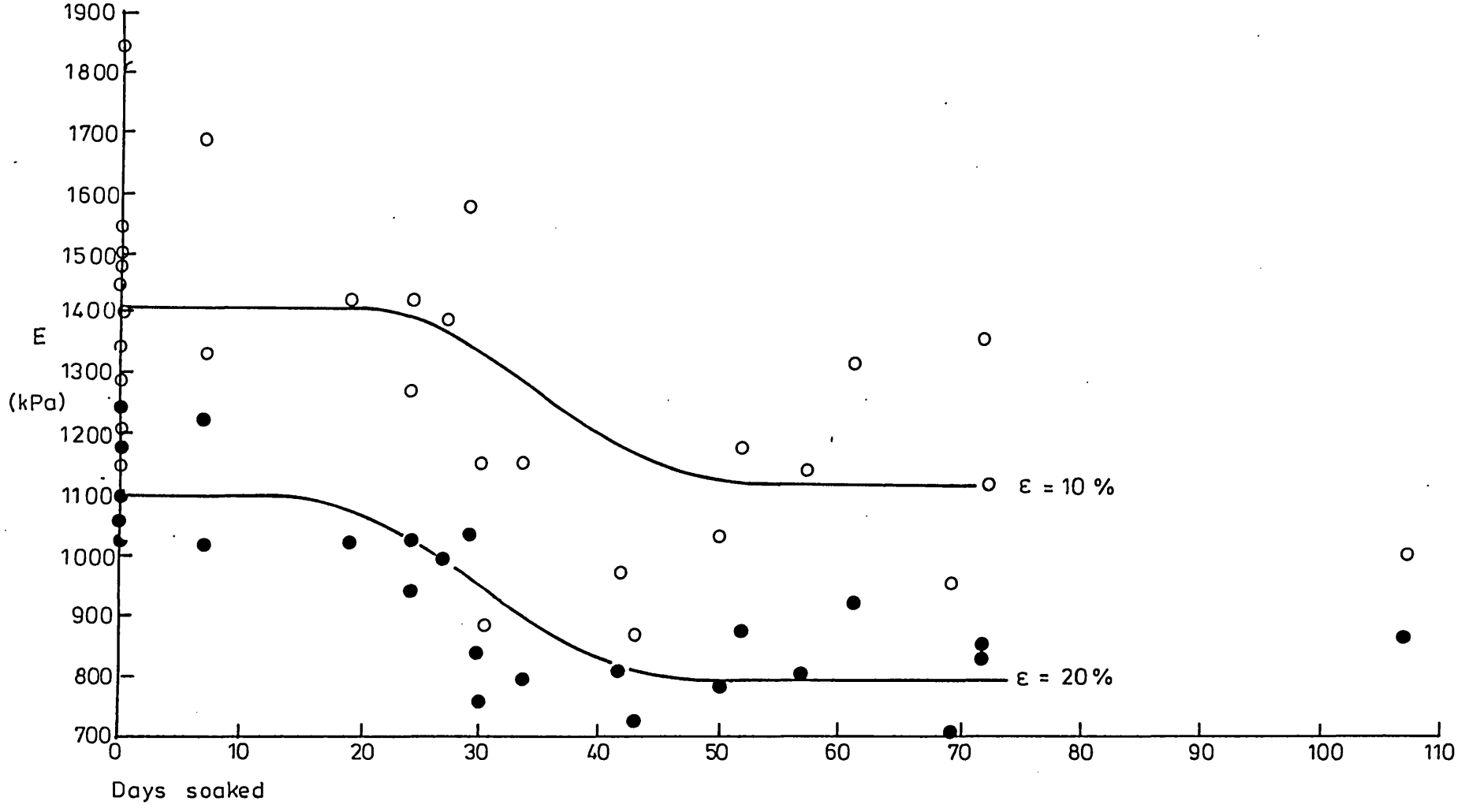


Figure A3.26. Young's Modulus for latex rubber membrane plotted against duration of soaking.

Figure A3.27 - A3.59

Plots of results of compression and extension tests on 'Hard' and 'Soft' rubber specimens (Note t_o, D_o denote initial thickness of membrane and initial specimen diameter respectively).

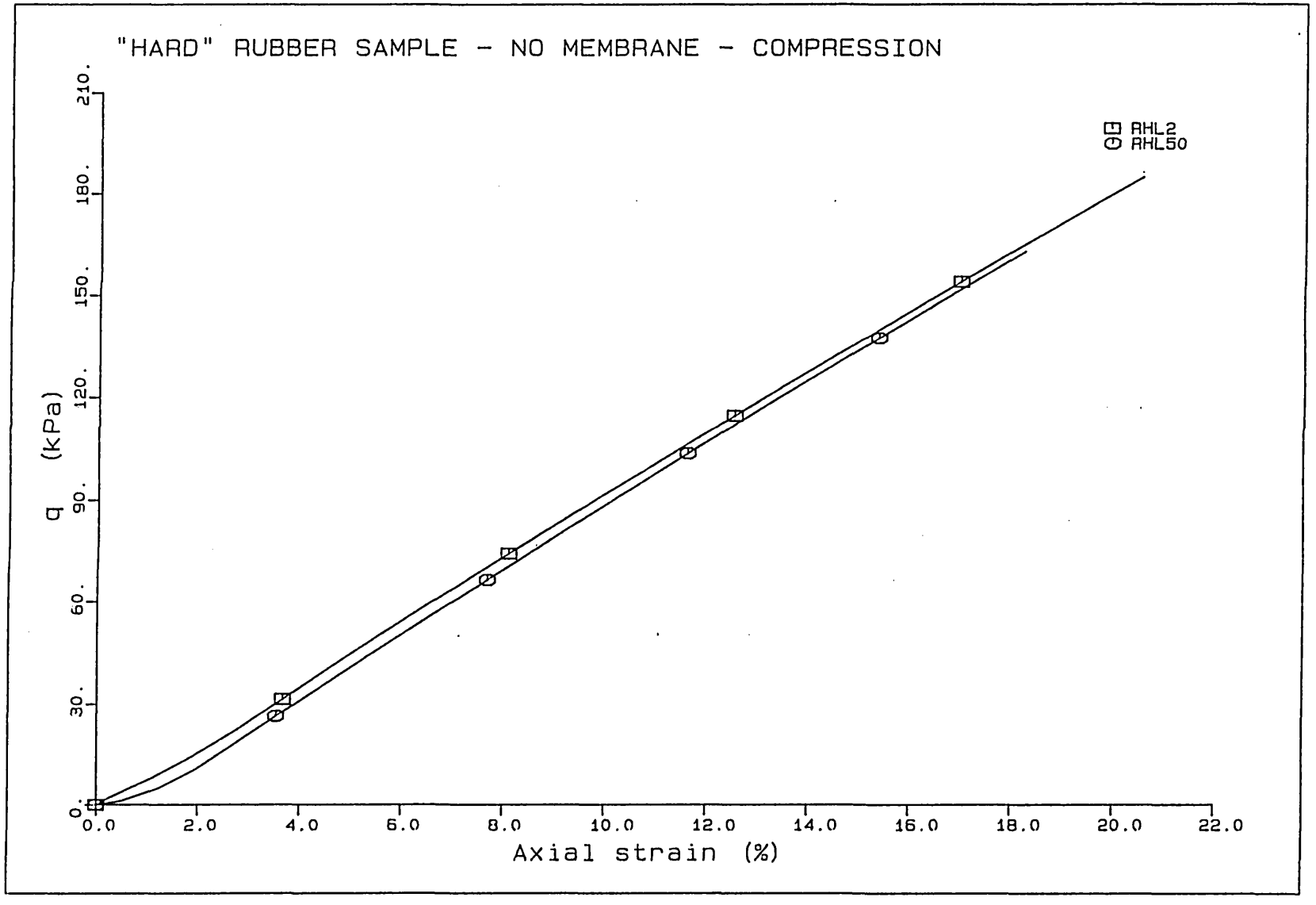

"HARD" RUBBER SAMPLE - NO MEMBRANE - COMPRESSION
AHL2
AHL50
q (kPa)
0.
30.
60.
90.
120.
150.
180.
210.
0.0
2.0
4.0
6.0
8.0
10.0
12.0
14.0
16.0
18.0
20.0
22.0
Axial strain (%)

Figure A3.27

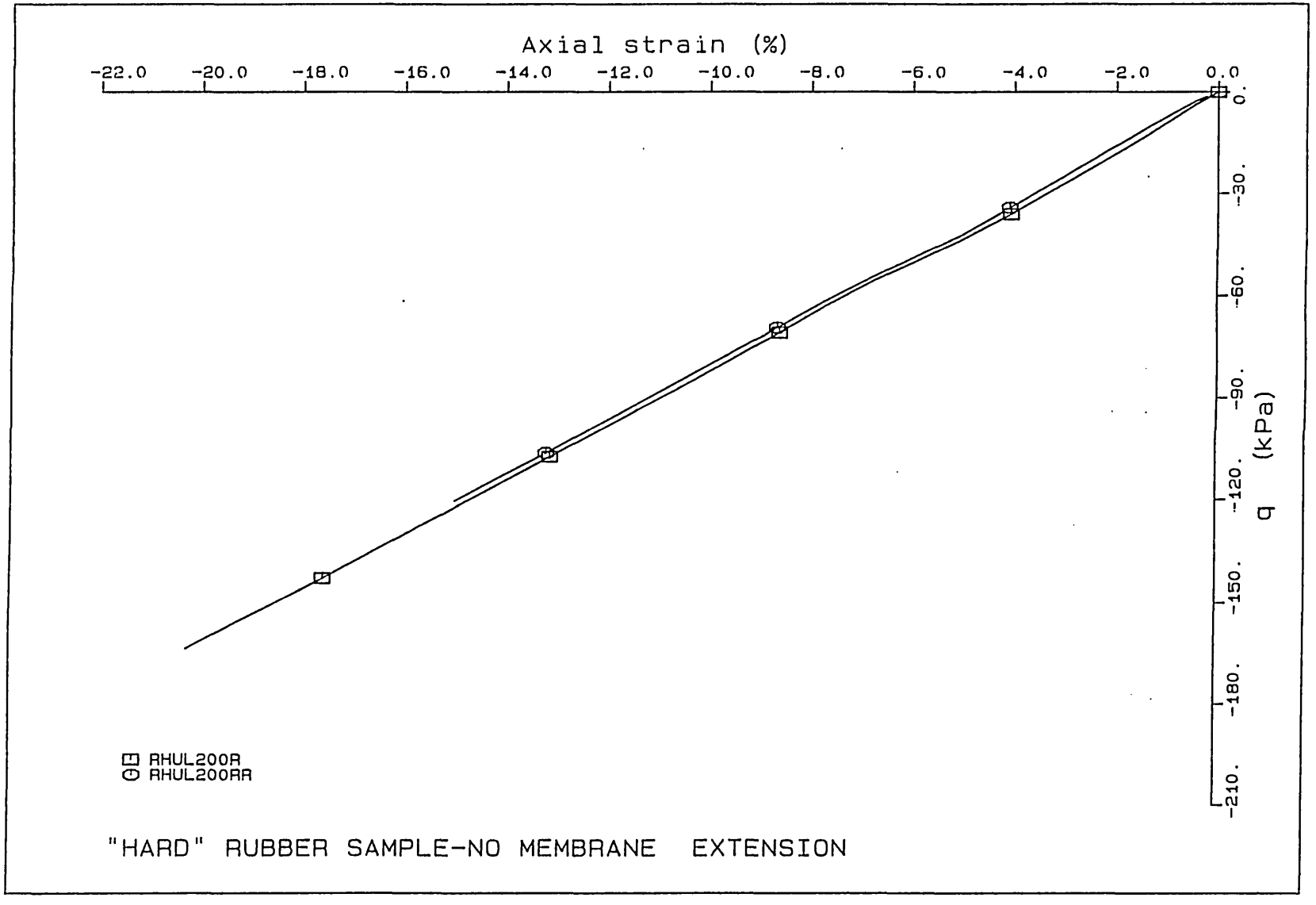

Axial strain (%)
-22.0
-20.0
-18.0
-16.0
-14.0
-12.0
-10.0
-8.0
-6.0
-4.0
-2.0
0.0
0.
-30.
-60.
-90.
-120.
-150.
-180.
-210.
q (kPa)
RHUL200R
RHUL200RR
"HARD" RUBBER SAMPLE-NO MEMBRANE EXTENSION

Figure A3.28

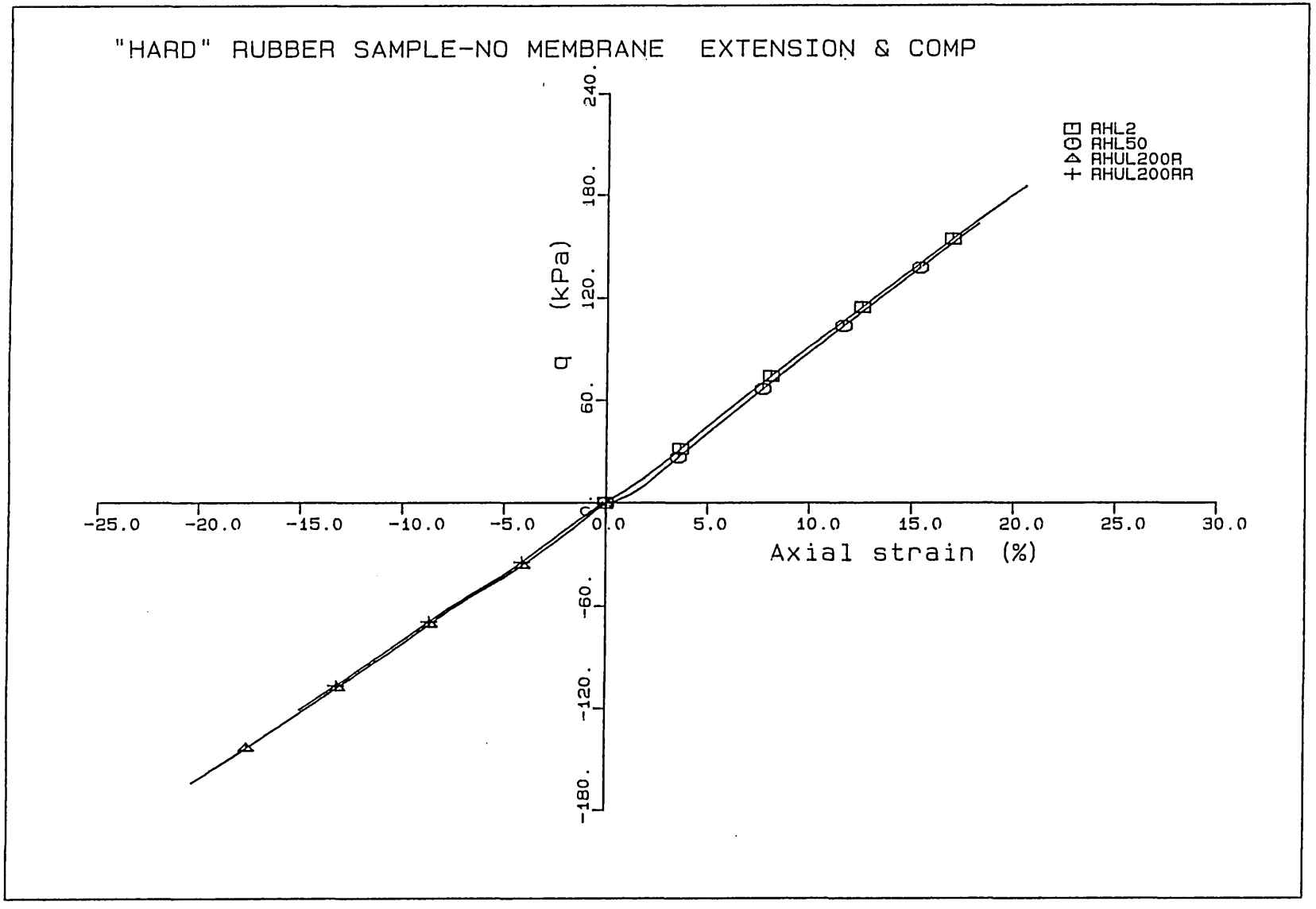

"HARD" RUBBER SAMPLE-NO MEMBRANE EXTENSION & COMP
AHL2
AHL50
AHUL200A
AHUL200AA
q (kPa)
240.
180.
120.
60.
0.
-60.
-120.
-180.
-25.0
-20.0
-15.0
-10.0
-5.0
0.0
5.0
10.0
15.0
20.0
25.0
30.0
Axial strain (%)

Figure A3.29

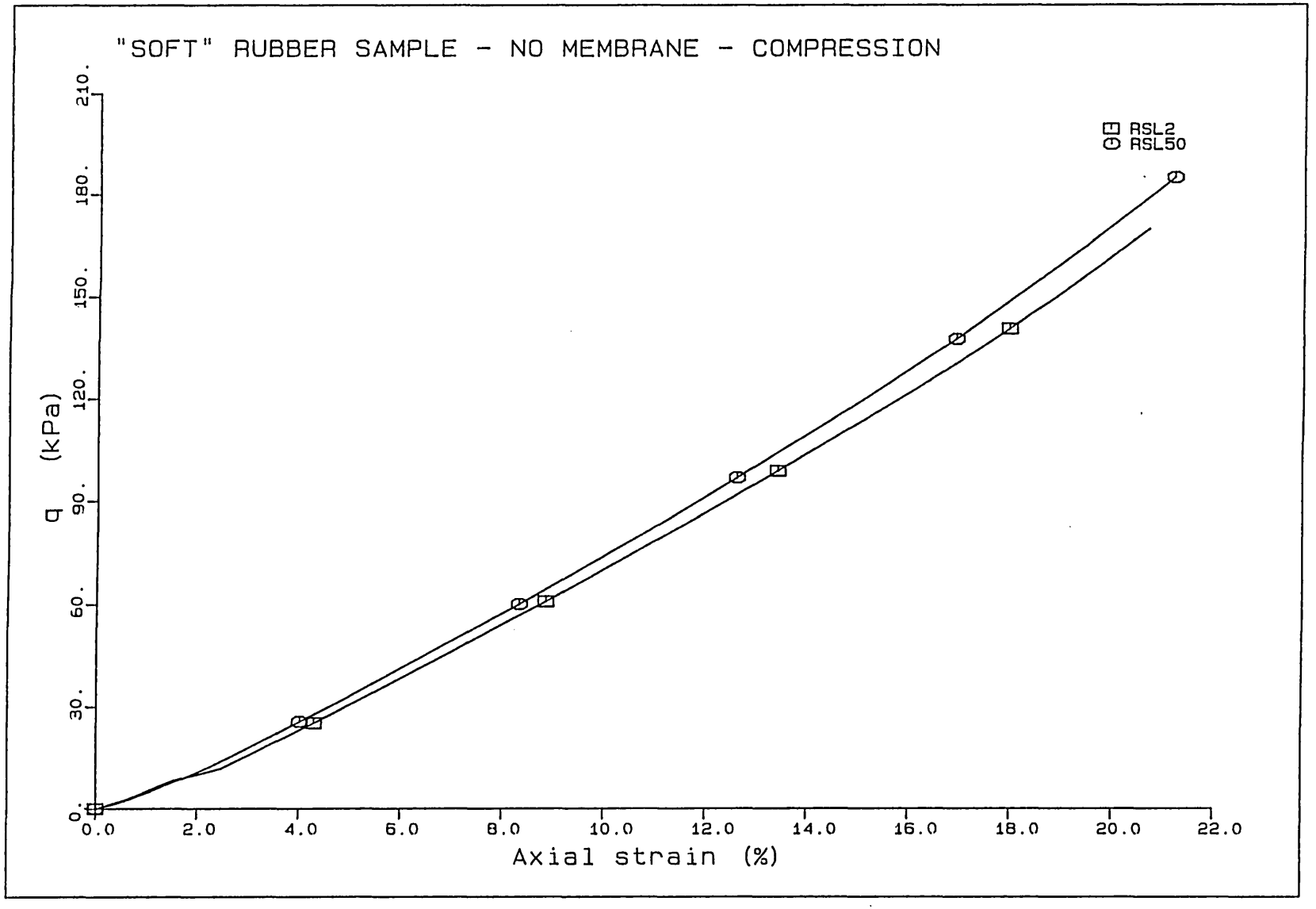

"SOFT" RUBBER SAMPLE - NO MEMBRANE - COMPRESSION
RSL2
RSL50
q (kPa)
0.
30.
60.
90.
120.
150.
180.
210.
0.0
2.0
4.0
6.0
8.0
10.0
12.0
14.0
16.0
18.0
20.0
22.0
Axial strain (%)

Figure A3.30

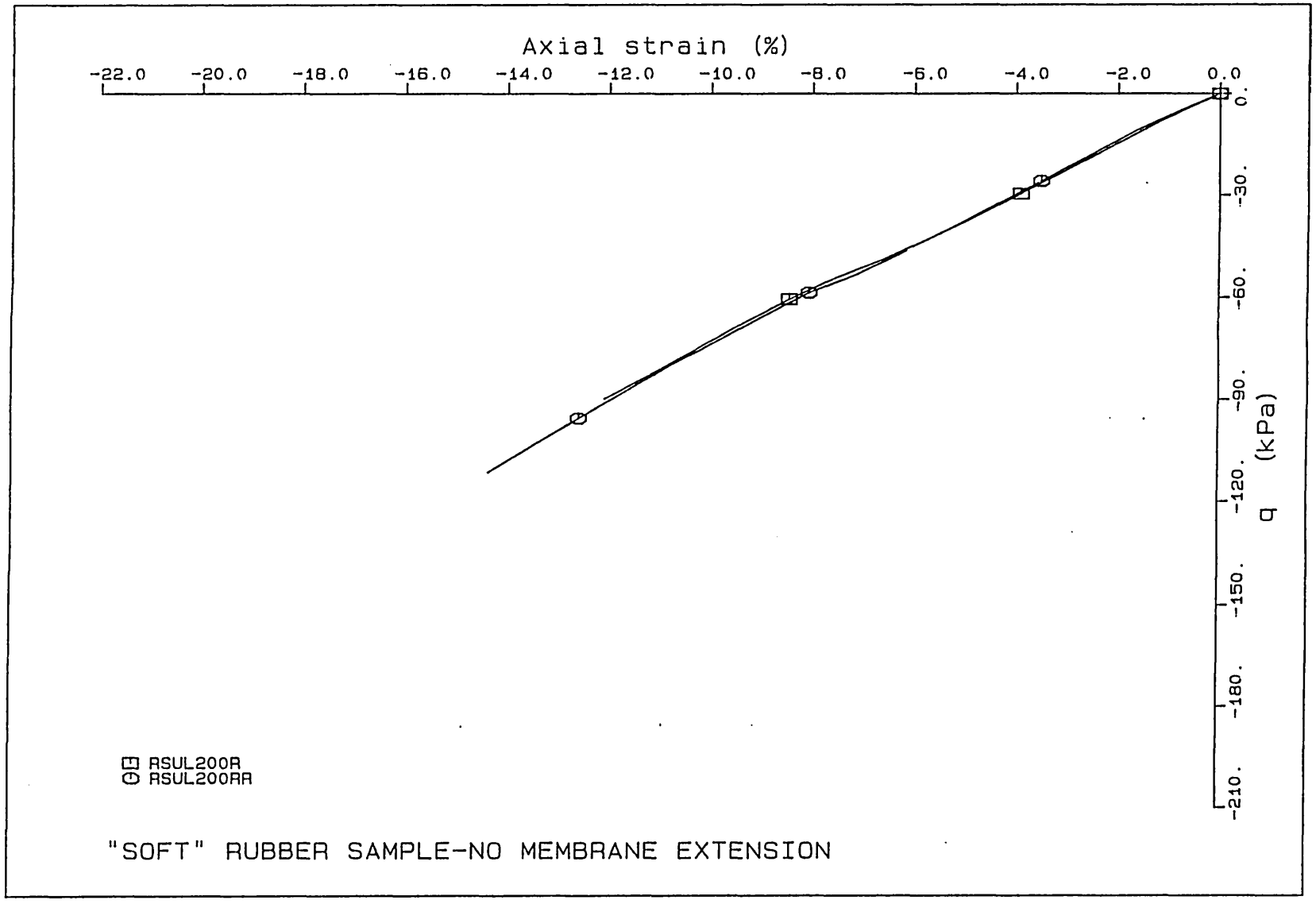

Axial strain (%)
-22.0
-20.0
-18.0
-16.0
-14.0
-12.0
-10.0
-8.0
-6.0
-4.0
-2.0
0.0
0.
-30.
-60.
-90.
-120.
-150.
-180.
-210.
q (kPa)
RSUL200R
RSUL200RR
"SOFT" RUBBER SAMPLE-NO MEMBRANE EXTENSION

Figure A3.31

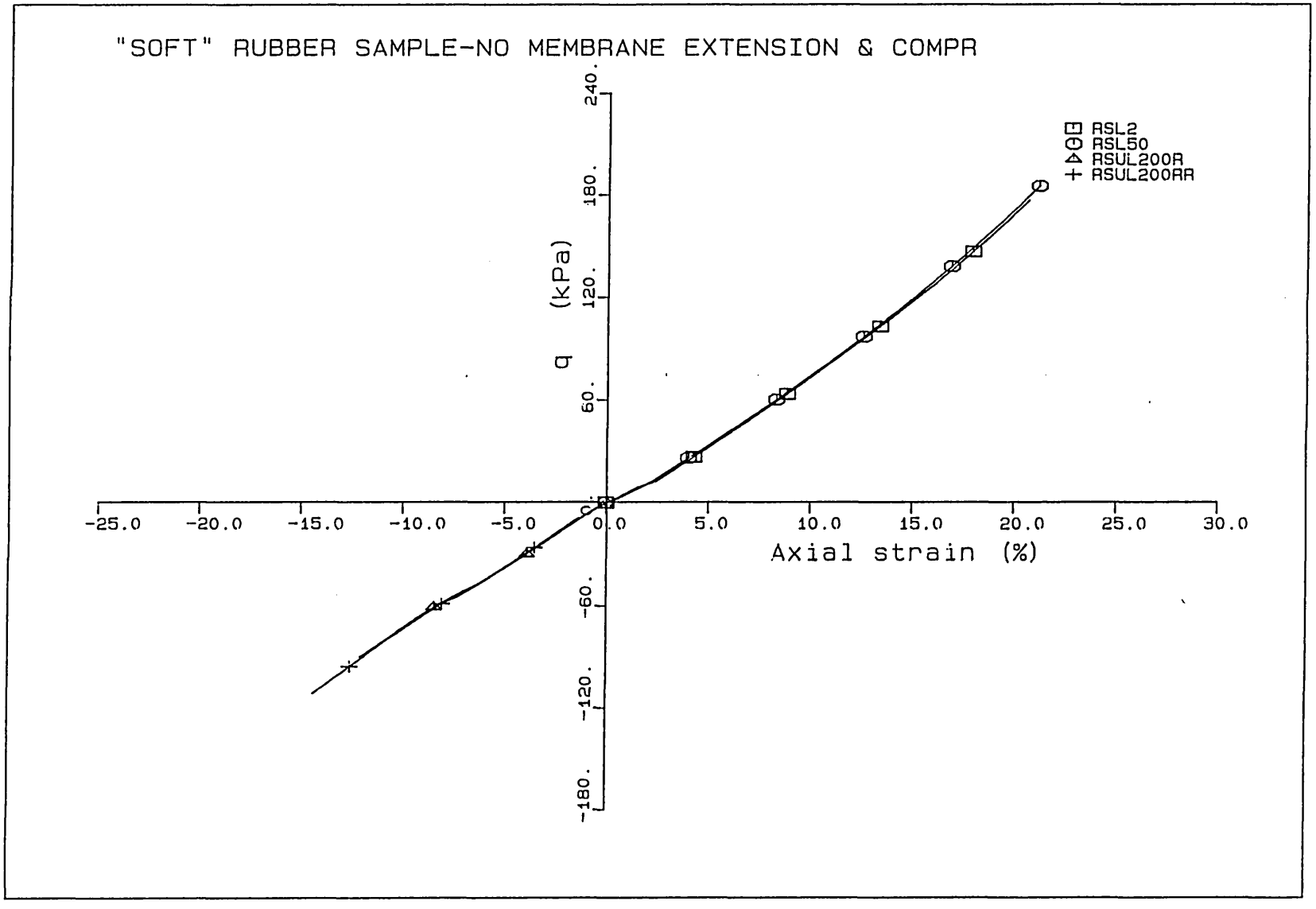

"SOFT" RUBBER SAMPLE-NO MEMBRANE EXTENSION & COMPR
RSL2
RSL50
RSUL200R
RSUL200RR
q (kPa)
240.
180.
120.
60.
0.
-60.
-120.
-180.
-25.0
-20.0
-15.0
-10.0
-5.0
0.0
5.0
10.0
15.0
20.0
25.0
30.0
Axial strain (%)

Figure A3.32

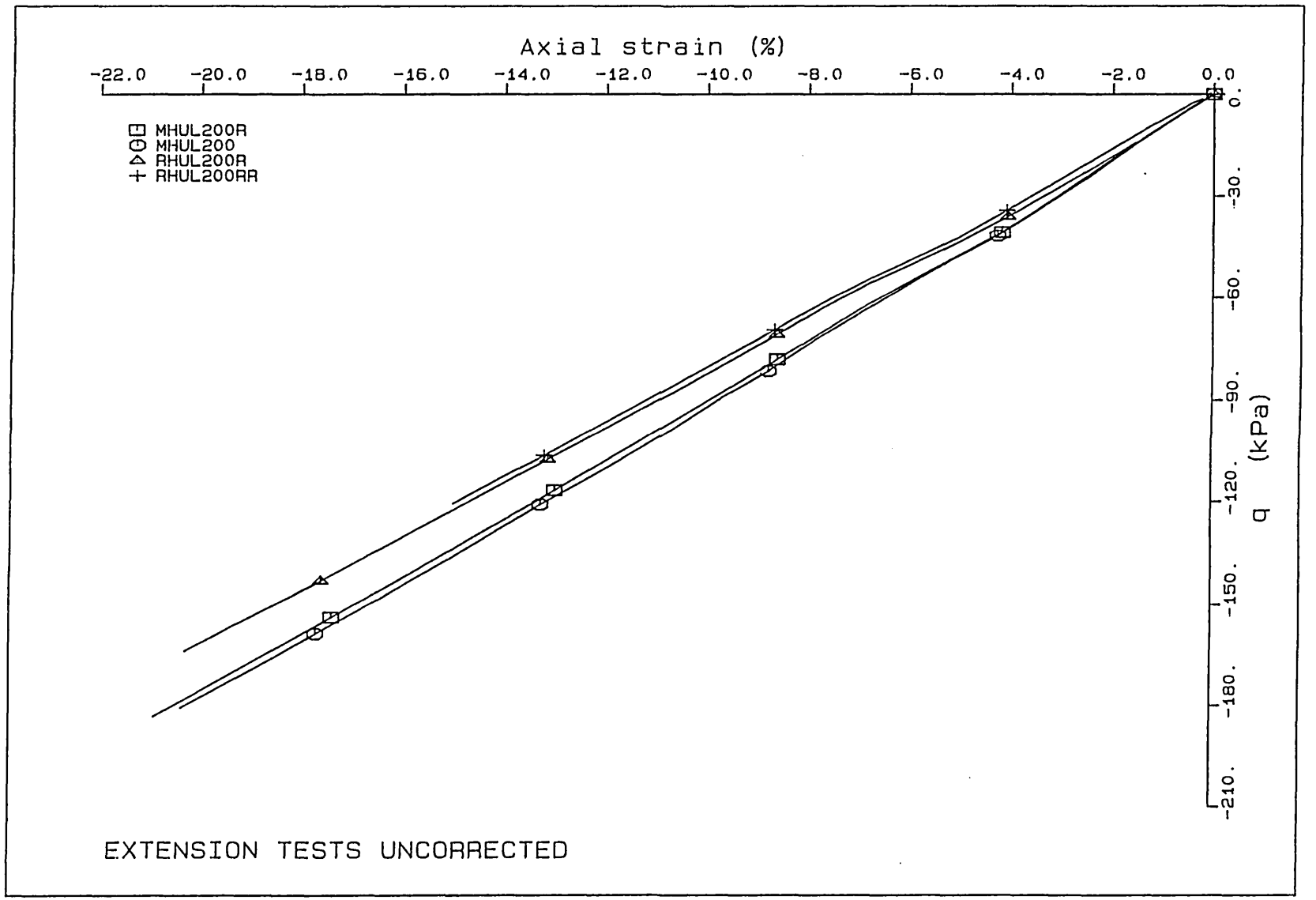

Axial strain (%)
-22.0
-20.0
-18.0
-16.0
-14.0
-12.0
-10.0
-8.0
-6.0
-4.0
-2.0
0.0
MHUL200R
MHUL200
RHUL200R
RHUL200RR
0.
-30.
-60.
-90.
-120.
-150.
-180.
-210.
q (kPa)
EXTENSION TESTS UNCORRECTED

Figure A3.33

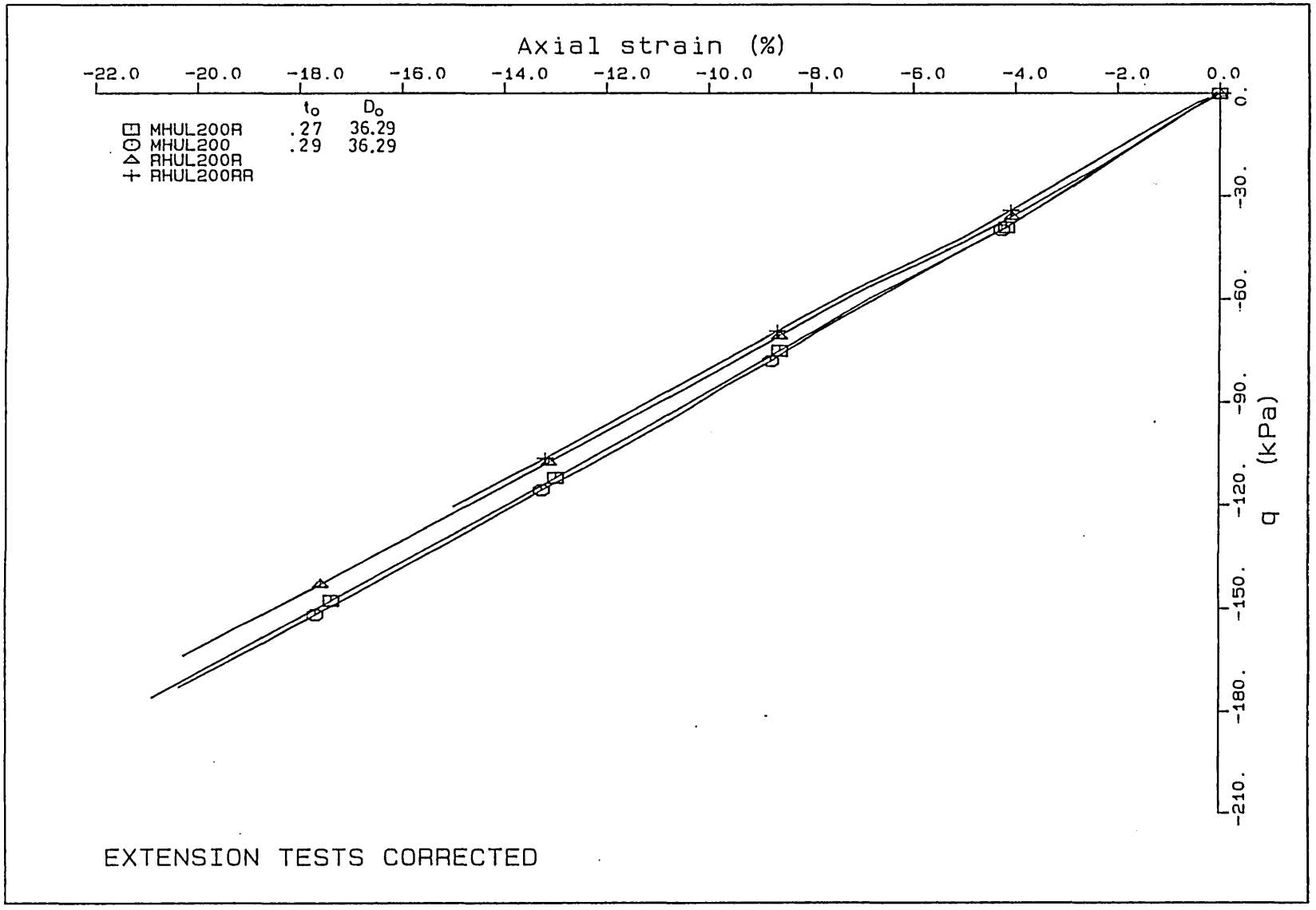

Axial strain (%)
-22.0
-20.0
-18.0
-16.0
-14.0
-12.0
-10.0
-8.0
-6.0
-4.0
-2.0
0.0
t_o
D_o
MHUL200R .27 36.29
MHUL200 .29 36.29
AHUL200R
AHUL200RR
0.
-30.
-60.
-90.
-120.
-150.
-180.
-210.
q (kPa)
EXTENSION TESTS CORRECTED

Figure A3.34

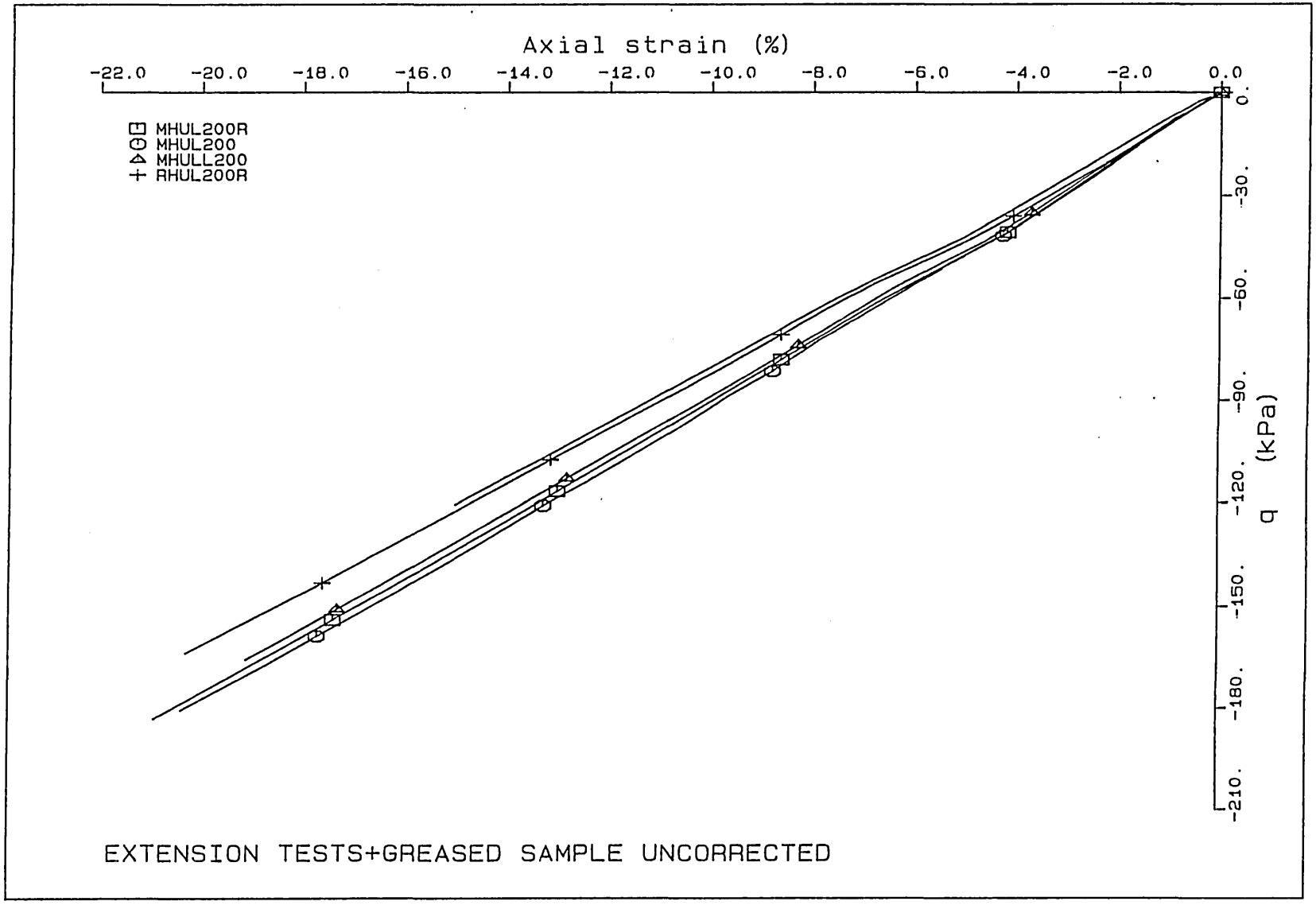

Axial strain (%)
-22.0
-20.0
-18.0
-16.0
-14.0
-12.0
-10.0
-8.0
-6.0
-4.0
-2.0
0.0
MHUL200R
MHUL200
MHULL200
RHUL200R
0.
-30.
-60.
-90.
-120.
-150.
-180.
-210.
q (kPa)
EXTENSION TESTS+GREASED SAMPLE UNCORRECTED

Figure A3.35

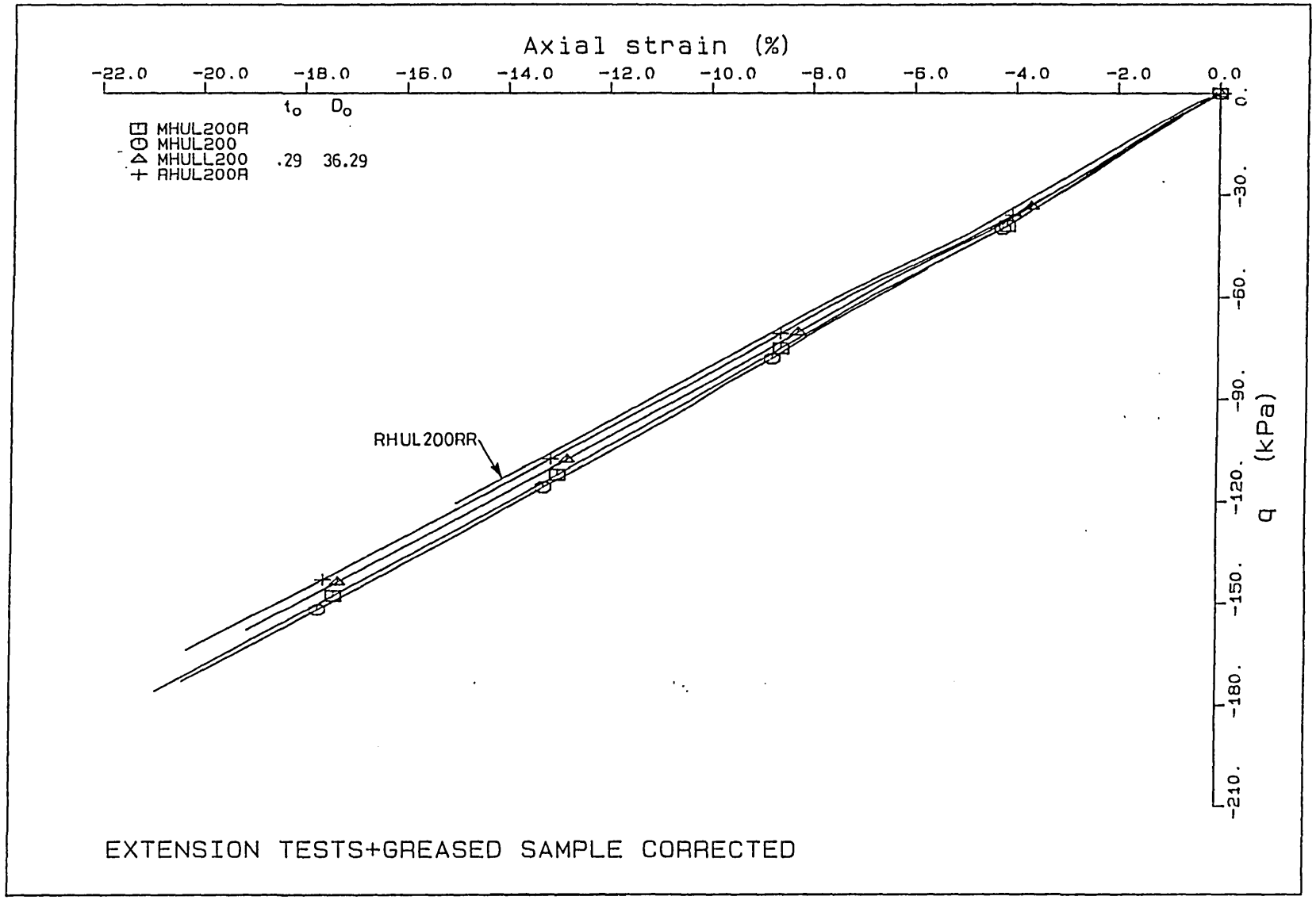

Axial strain (%)
-22.0
-20.0
-18.0
-16.0
-14.0
-12.0
-10.0
-8.0
-6.0
-4.0
-2.0
0.0
t_o D_o
MHUL200R
MHUL200
MHULL200 .29 36.29
RHUL200R
RHUL200RR
0.
-30.
-60.
-90.
-120.
-150.
-180.
-210.
q (kPa)
EXTENSION TESTS+GREASED SAMPLE CORRECTED

Figure A3.36

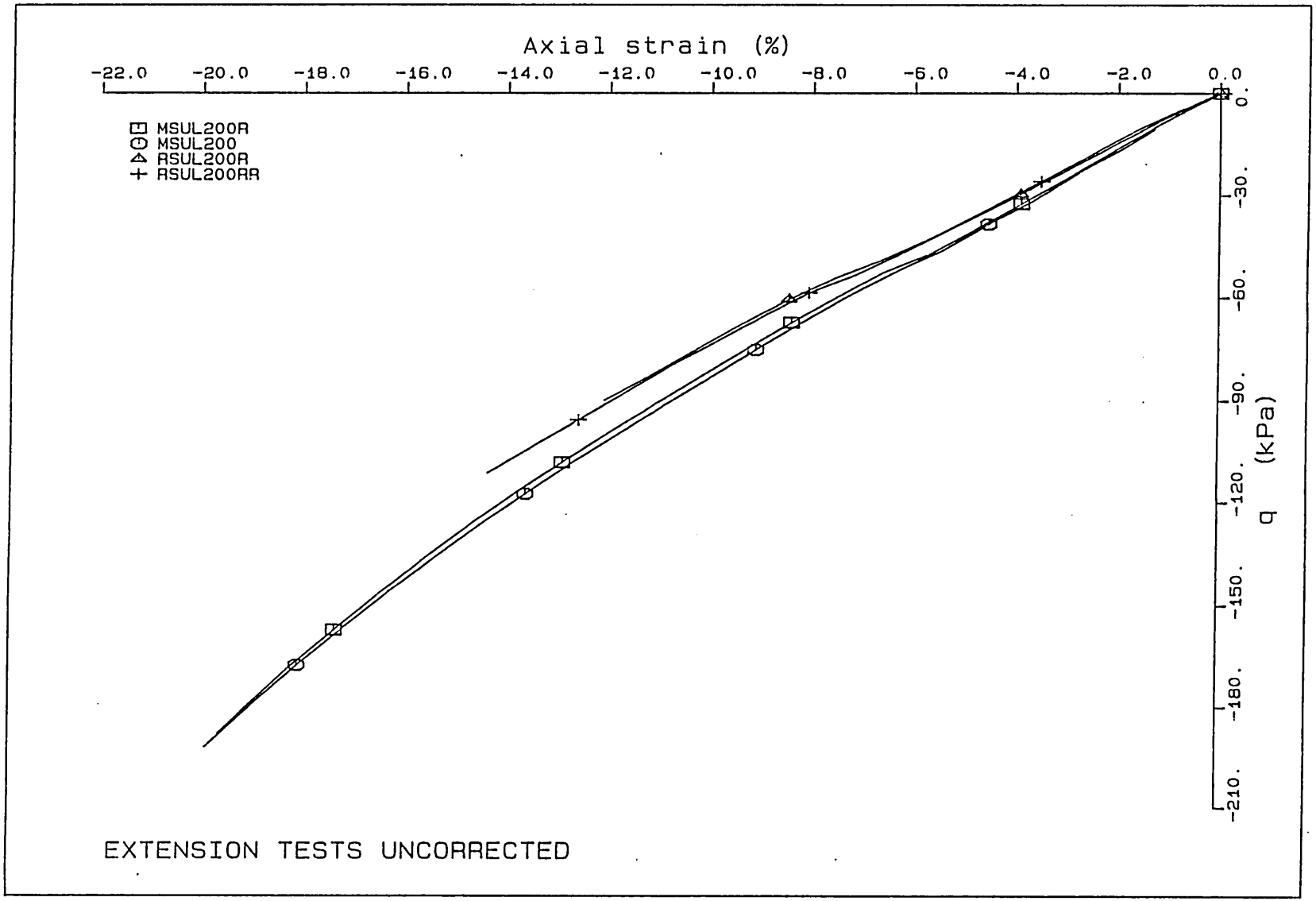

Axial strain (%)
-22.0
-20.0
-18.0
-16.0
-14.0
-12.0
-10.0
-8.0
-6.0
-4.0
-2.0
0.0
MSUL200R
MSUL200
RSUL200R
RSUL200RR
0.
-30.
-60.
-90.
-120.
-150.
-180.
-210.
q (kPa)
EXTENSION TESTS UNCORRECTED

Figure A3.37

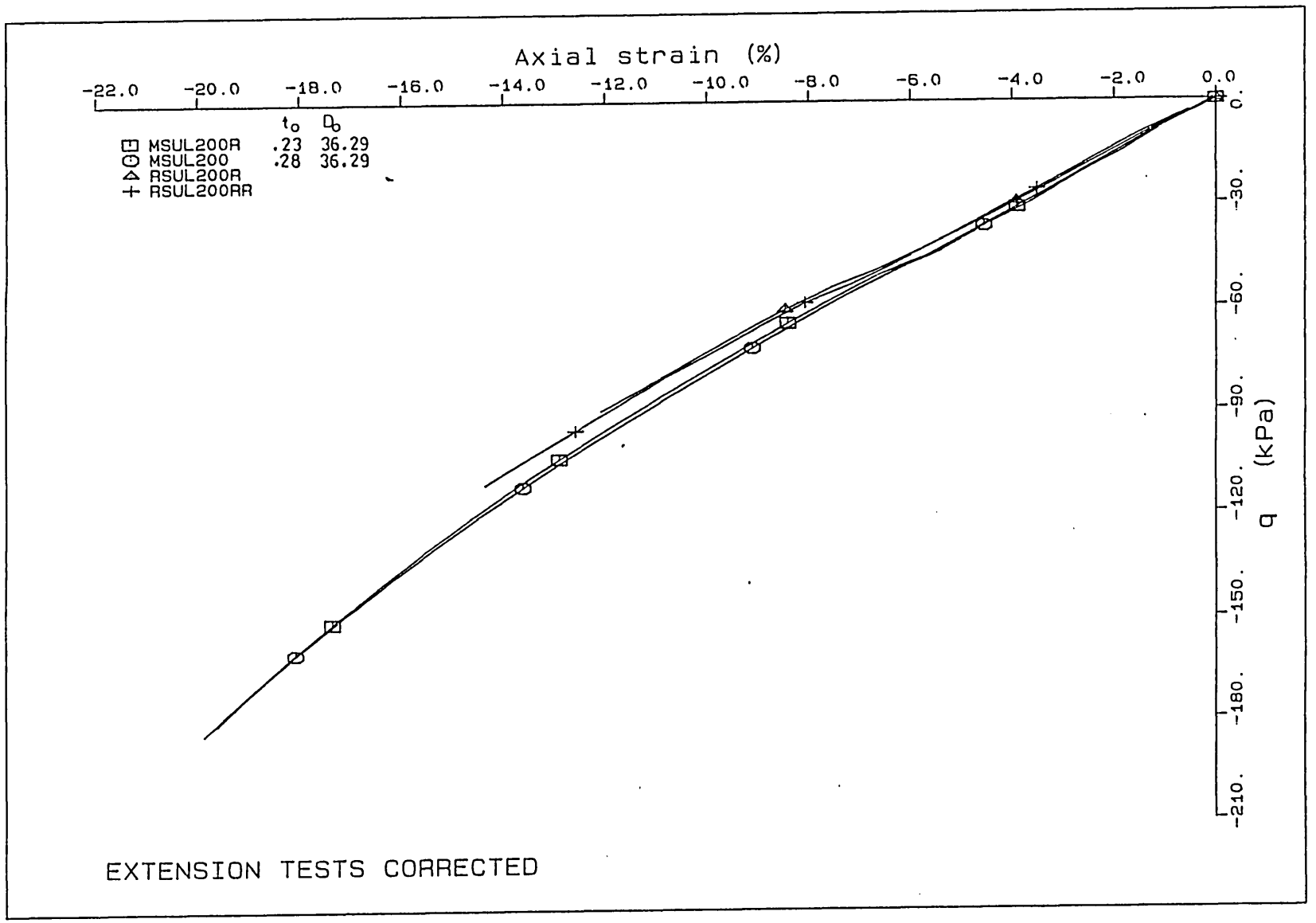

Axial strain (%)
-22.0
-20.0
-18.0
-16.0
-14.0
-12.0
-10.0
-8.0
-6.0
-4.0
-2.0
0.0
t_o D_o
MSUL200R .23 36.29
MSUL200 .28 36.29
RSUL200R
RSUL200RR
0.
-30.
-60.
-90.
-120.
-150.
-180.
-210.
q (kPa)
EXTENSION TESTS CORRECTED

Figure A3.38

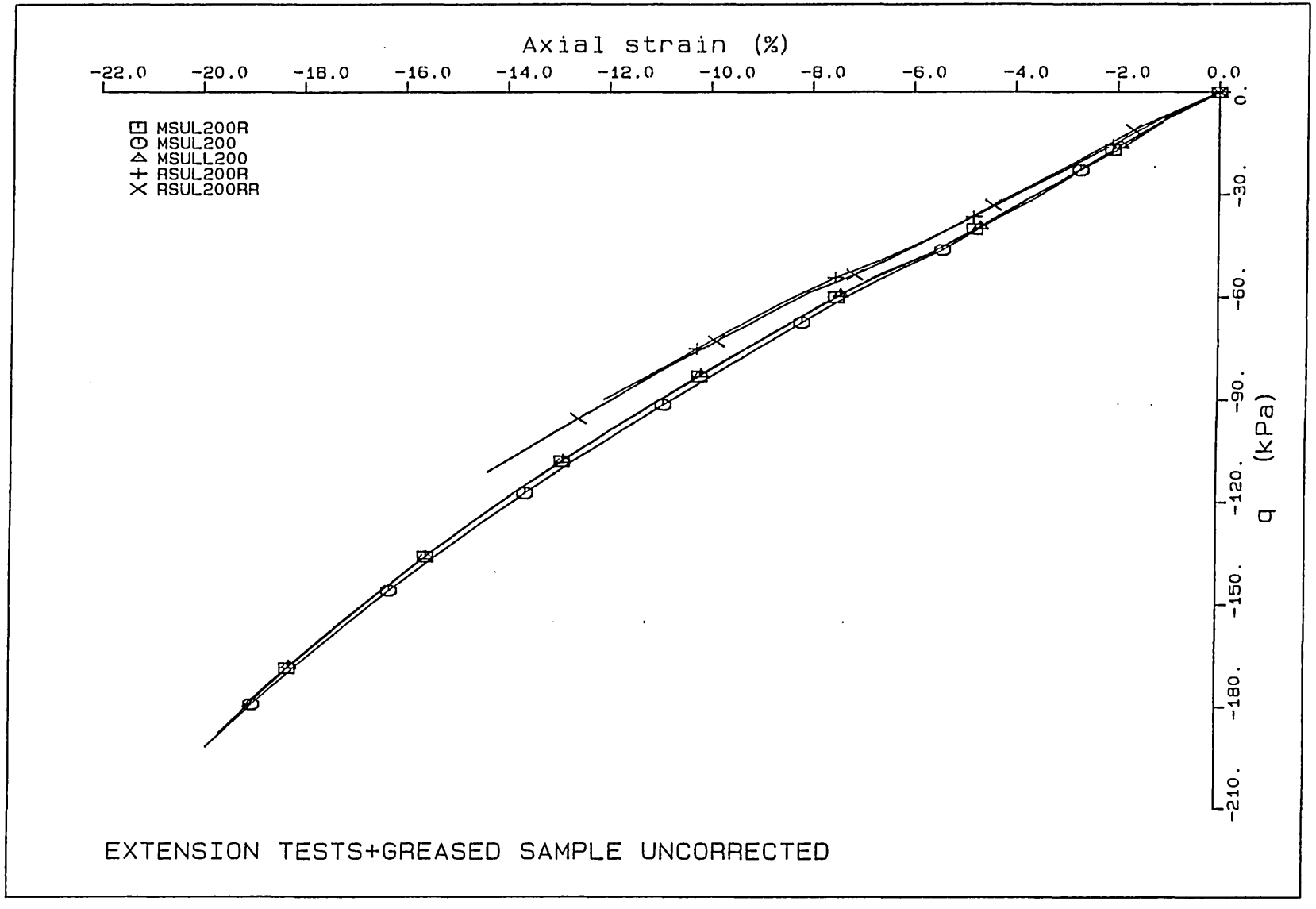

Axial strain (%)
-22.0
-20.0
-18.0
-16.0
-14.0
-12.0
-10.0
-8.0
-6.0
-4.0
-2.0
0.0
0.
-30.
-60.
-90.
-120.
-150.
-180.
-210.
q (kPa)
MSUL200R
MSUL200
MSULL200
RSUL200R
RSUL200RR
EXTENSION TESTS+GREASED SAMPLE UNCORRECTED

Figure A3.39

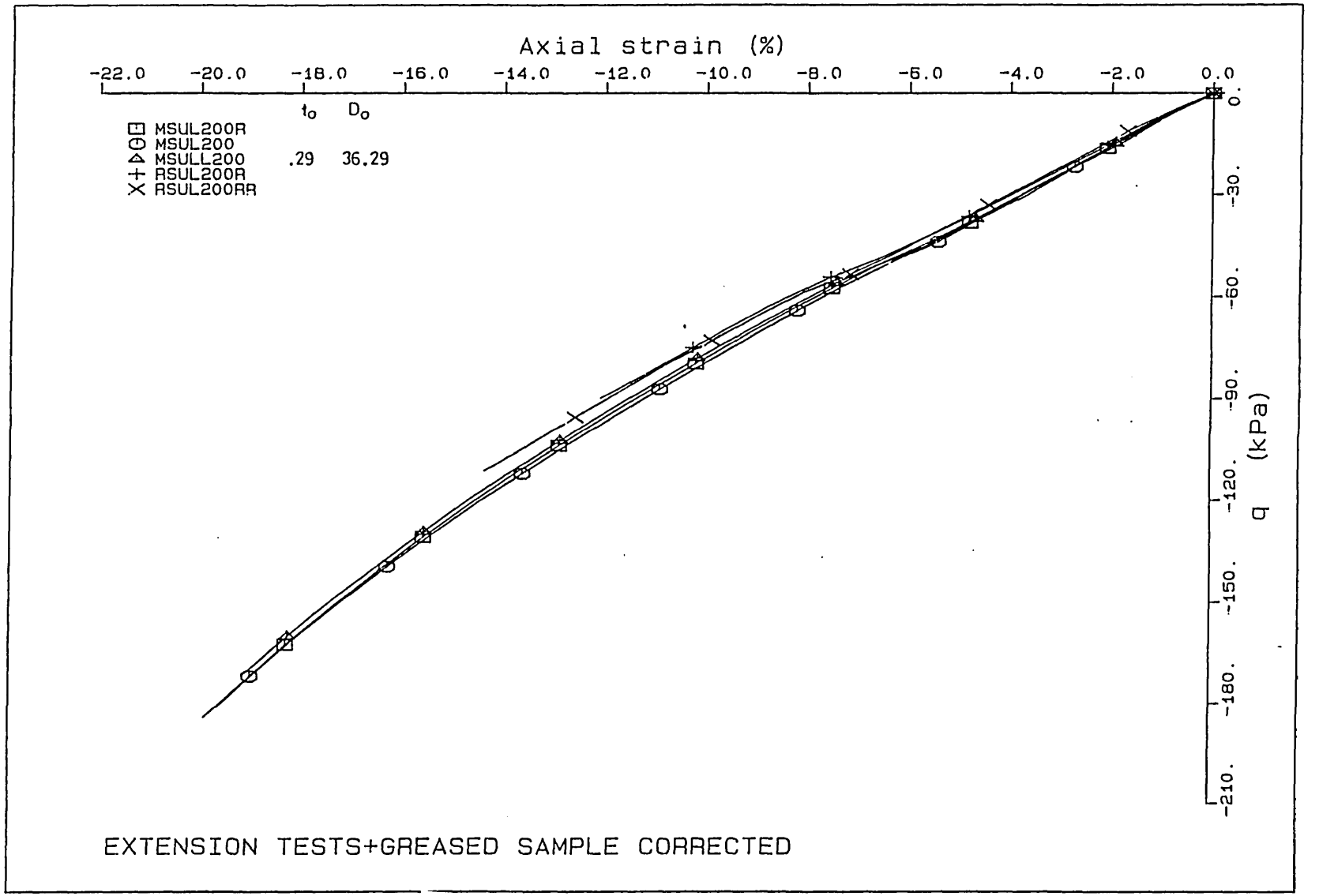

Axial strain (%)
-22.0
-20.0
-18.0
-16.0
-14.0
-12.0
-10.0
-8.0
-6.0
-4.0
-2.0
0.0
t_o
D_o
MSUL200R
MSUL200
MSULL200
RSUL200R
RSUL200RR
.29
36.29
0.
-30.
-60.
-90.
-120.
-150.
-180.
-210.
q (kPa)
EXTENSION TESTS+GREASED SAMPLE CORRECTED

Figure A3.40

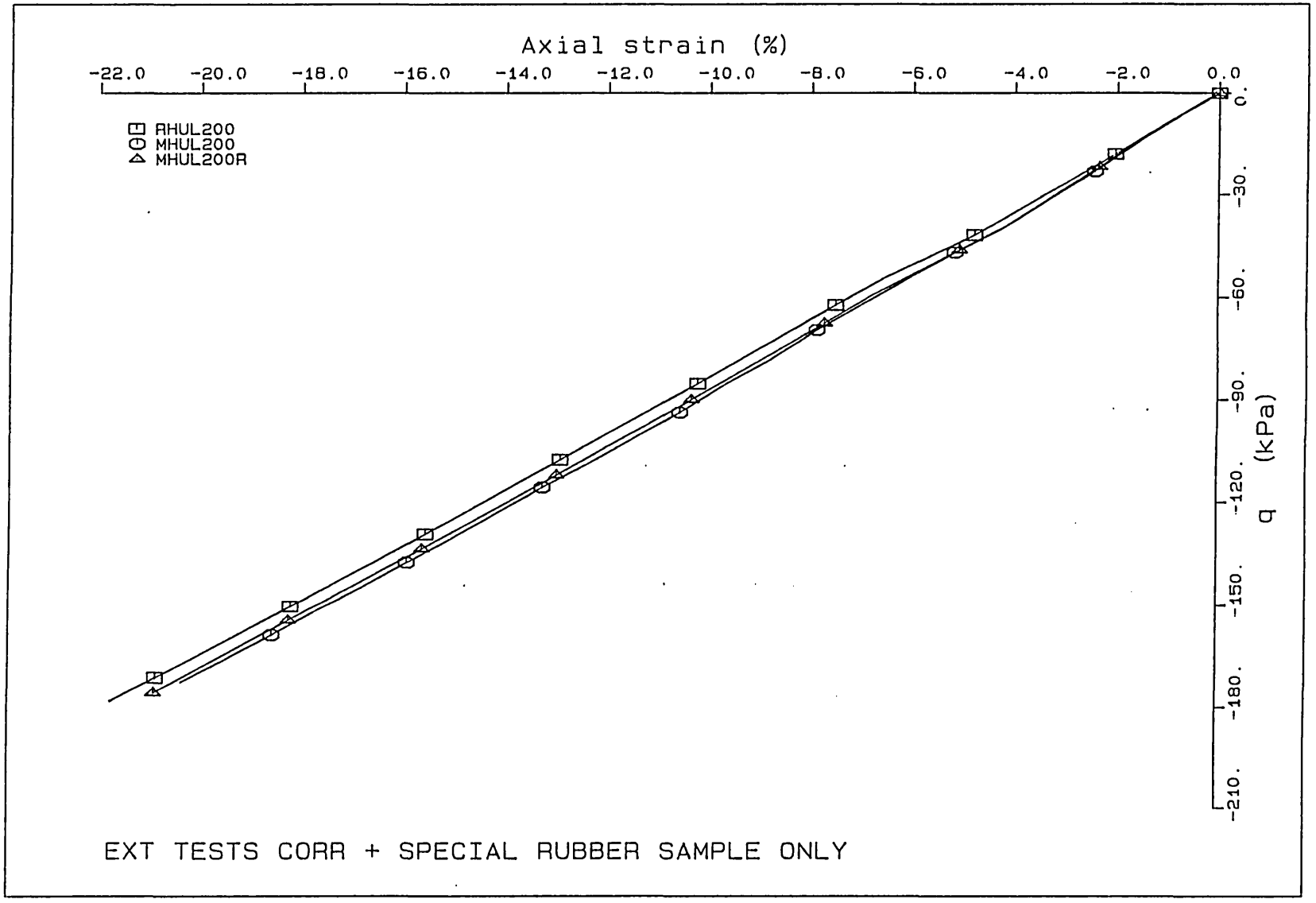

Axial strain (%)
-22.0
-20.0
-18.0
-16.0
-14.0
-12.0
-10.0
-8.0
-6.0
-4.0
-2.0
0.0
0.
-30.
-60.
-90.
-120.
-150.
-180.
-210.
q (kPa)
AHUL200
MHUL200
MHUL200R
EXT TESTS CORR + SPECIAL RUBBER SAMPLE ONLY

Figure A3.41

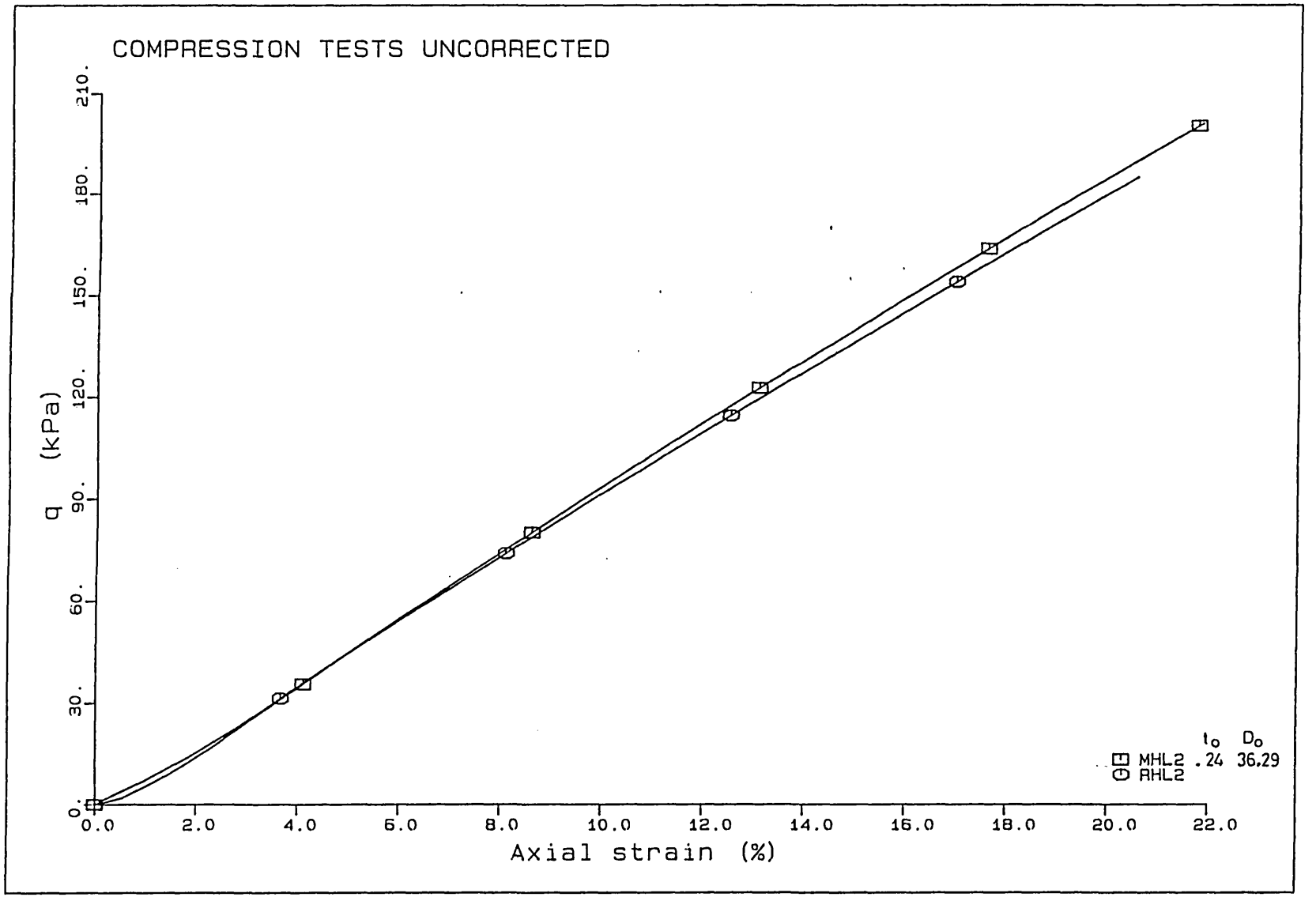

COMPRESSION TESTS UNCORRECTED
q (kPa)
0.
30.
60.
90.
120.
150.
180.
210.
0.0
2.0
4.0
6.0
8.0
10.0
12.0
14.0
16.0
18.0
20.0
22.0
Axial strain (%)
t_o D_o
MHL2 .24 36.29
RHL2

Figure A3.42

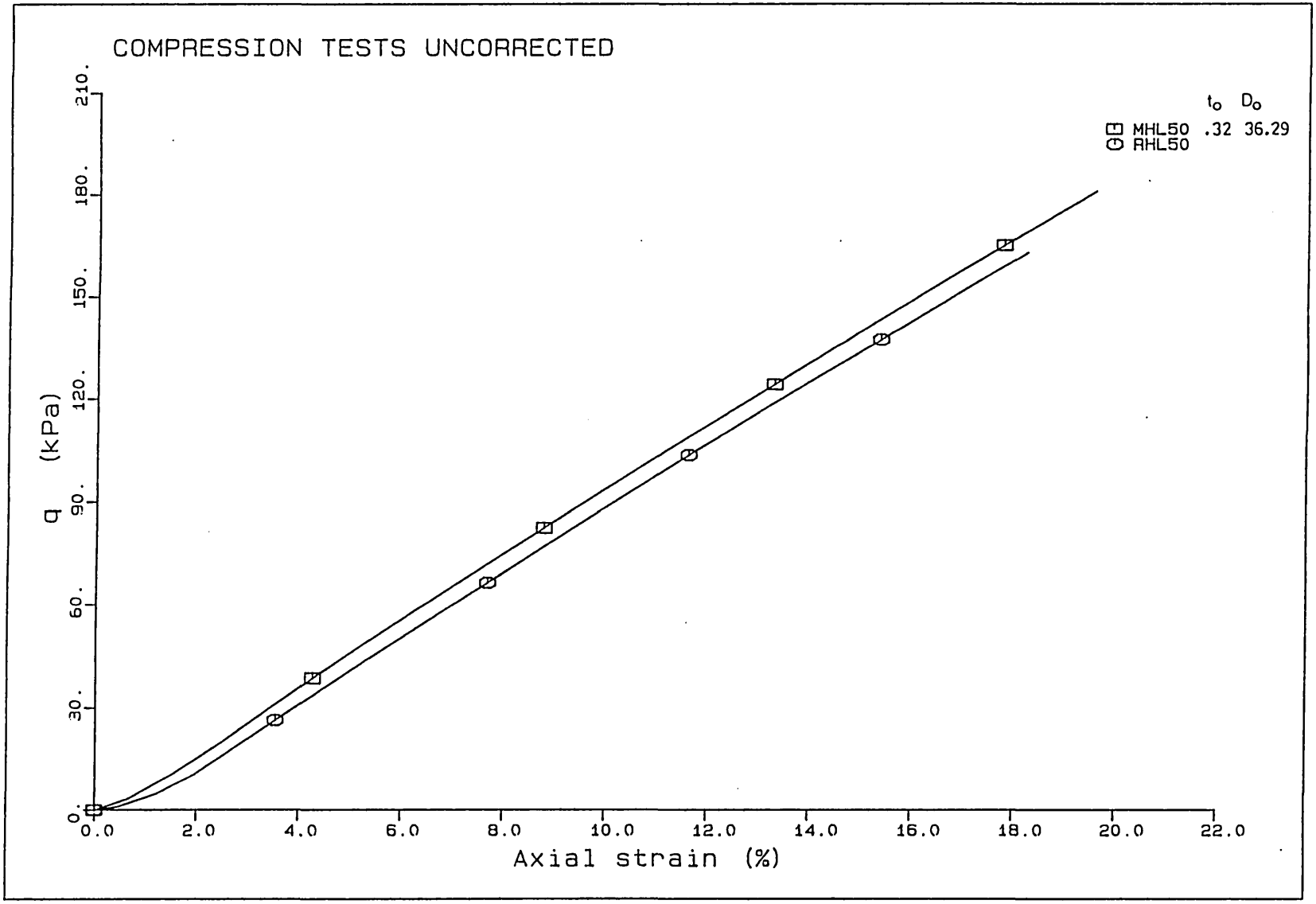

COMPRESSION TESTS UNCORRECTED
t_o D_o
MHL50 .32 36.29
RHL50
q (kPa)
0.
30.
60.
90.
120.
150.
180.
210.
0.0
2.0
4.0
6.0
8.0
10.0
12.0
14.0
16.0
18.0
20.0
22.0
Axial strain (%)

Figure A3.43

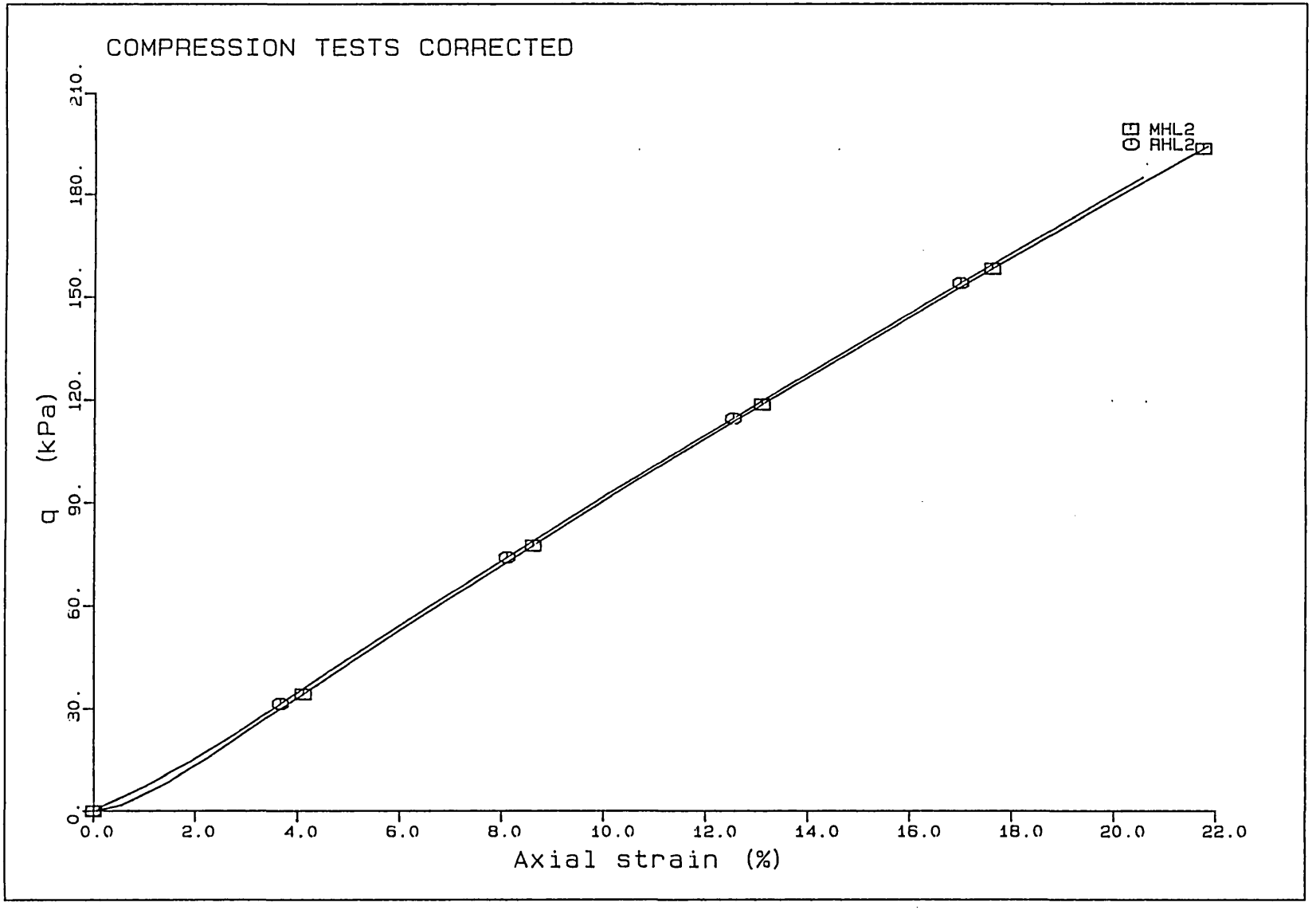

COMPRESSION TESTS CORRECTED
MHL2
AHL2
q (kPa)
0.
30.
60.
90.
120.
150.
180.
210.
0.0
2.0
4.0
6.0
8.0
10.0
12.0
14.0
16.0
18.0
20.0
22.0
Axial strain (%)

Figure A3.44

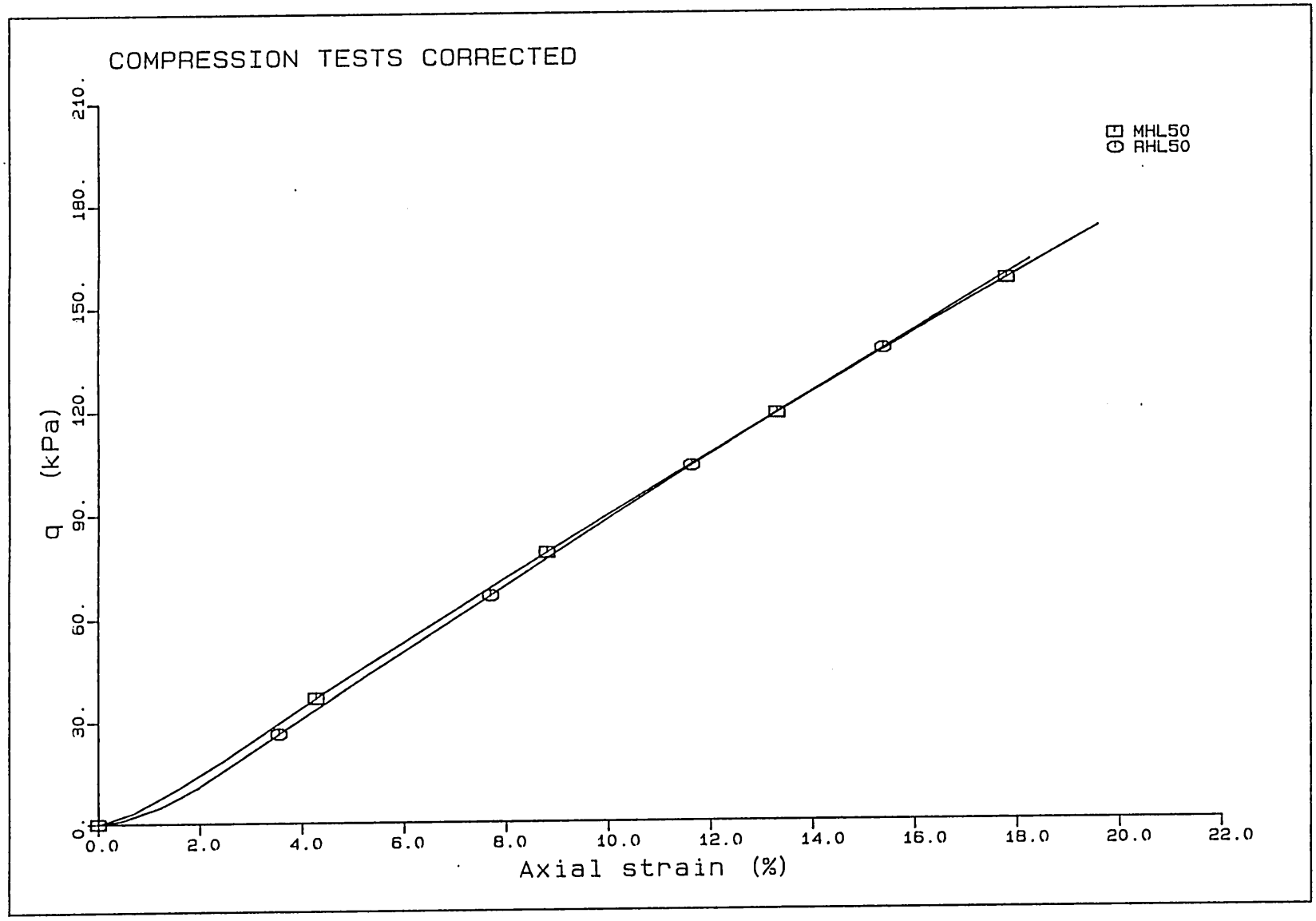

COMPRESSION TESTS CORRECTED
MHL50
RHL50
q (kPa)
0.
30.
60.
90.
120.
150.
180.
210.
0.0
2.0
4.0
6.0
8.0
10.0
12.0
14.0
16.0
18.0
20.0
22.0
Axial strain (%)

Figure A3.45

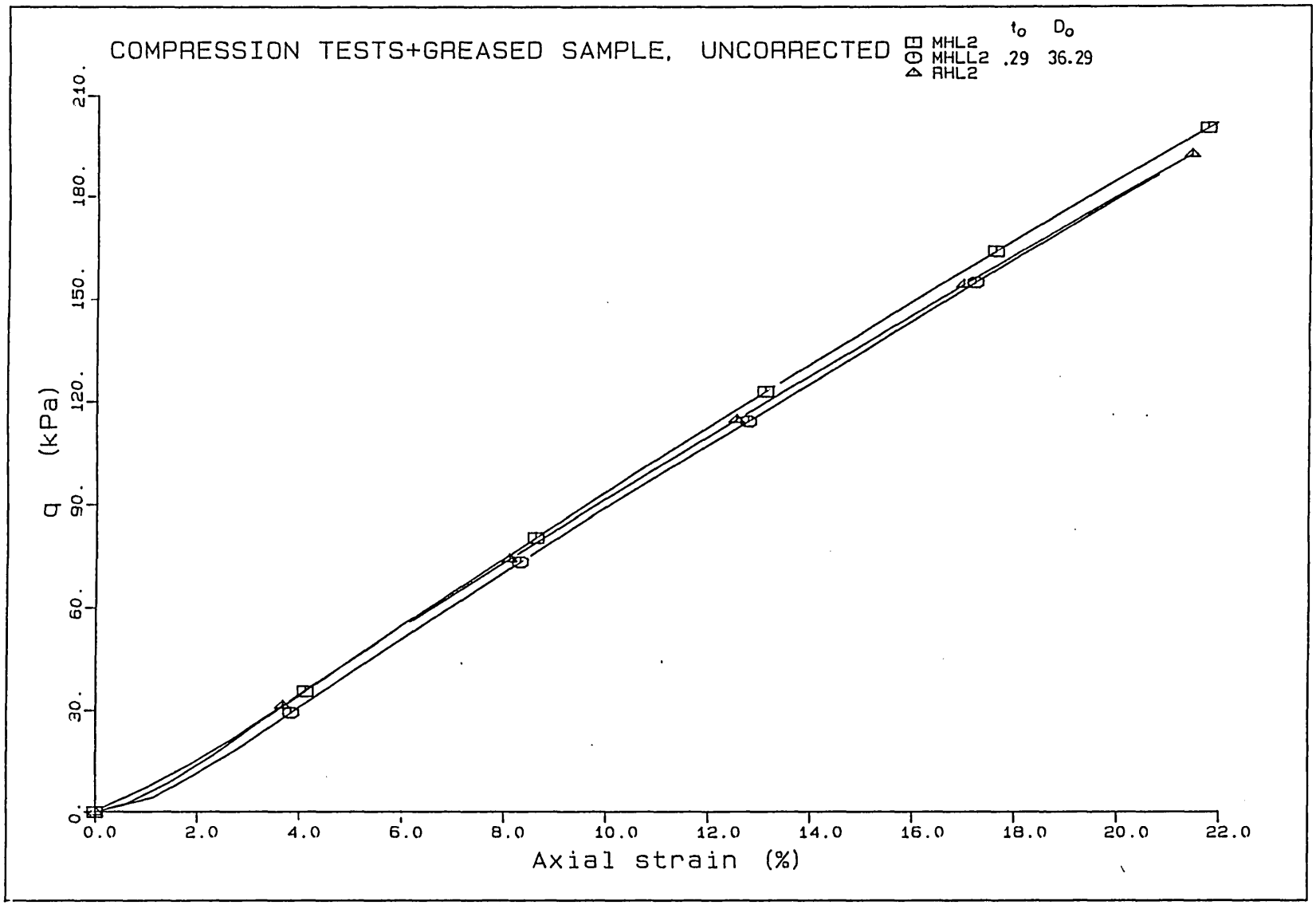

COMPRESSION TESTS+GREASED SAMPLE, UNCORRECTED
to Do
MHL2
MHLL2 .29 36.29
RHL2
q (kPa)
0.
30.
60.
90.
120.
150.
180.
210.
0.0
2.0
4.0
6.0
8.0
10.0
12.0
14.0
16.0
18.0
20.0
22.0
Axial strain (%)

Figure A3.46

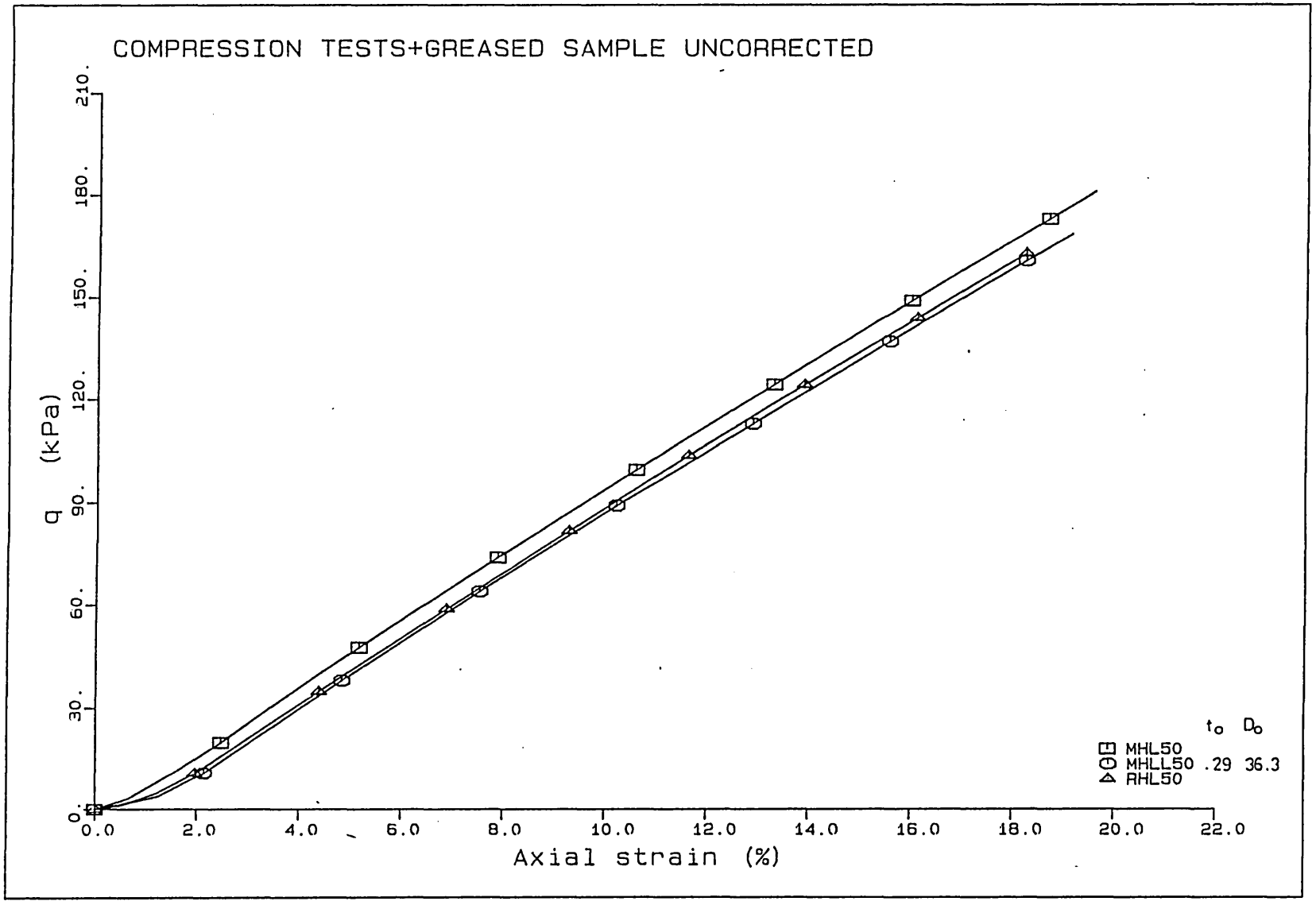

COMPRESSION TESTS+GREASED SAMPLE UNCORRECTED
q (kPa)
0.
30.
60.
90.
120.
150.
180.
210.
0.0
2.0
4.0
6.0
8.0
10.0
12.0
14.0
16.0
18.0
20.0
22.0
Axial strain (%)
to Do
MHL50
MHLL50 .29 36.3
RHL50

Figure A3.47

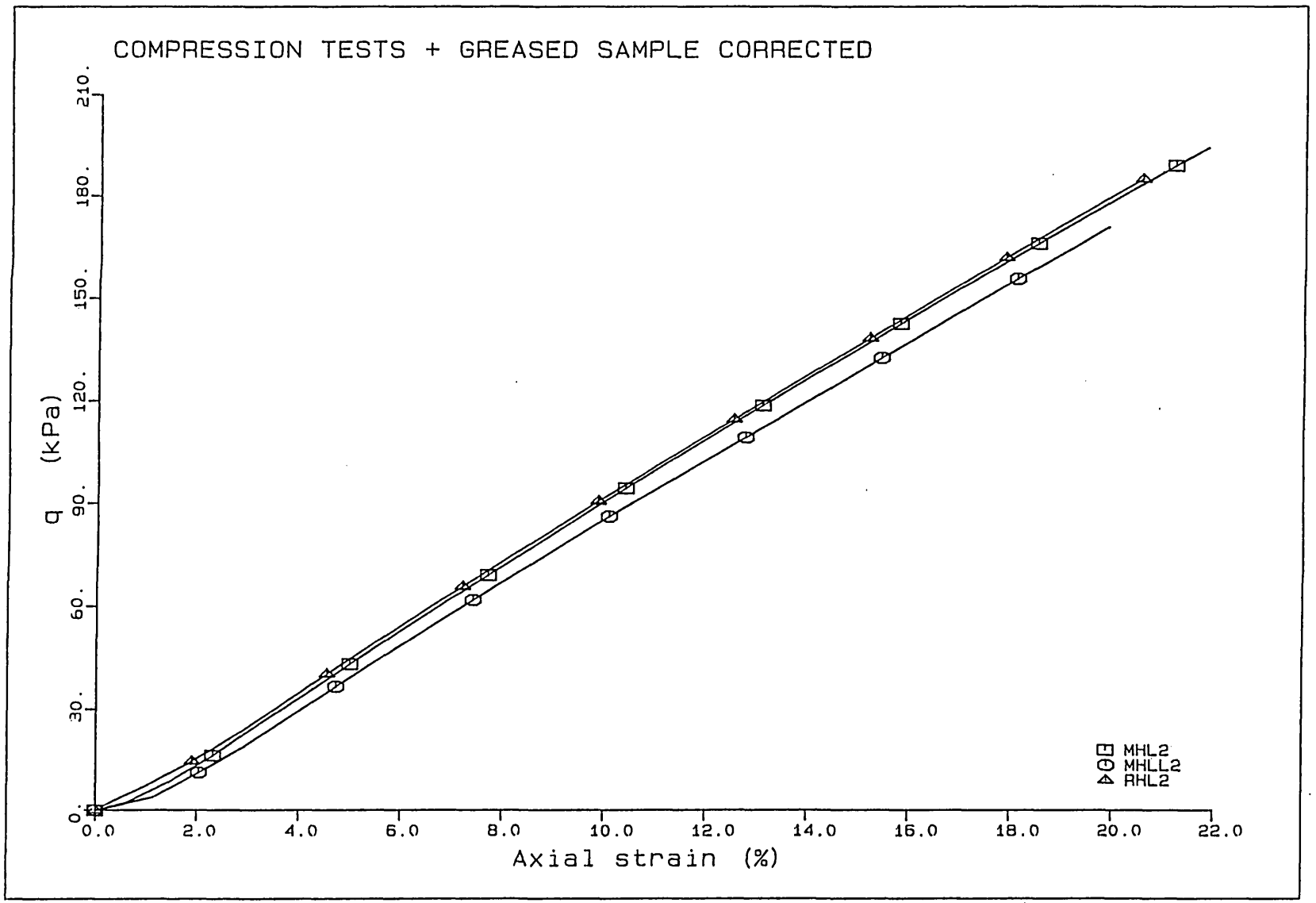

COMPRESSION TESTS + GREASED SAMPLE CORRECTED
q (kPa)
0.
30.
60.
90.
120.
150.
180.
210.
0.0
2.0
4.0
6.0
8.0
10.0
12.0
14.0
16.0
18.0
20.0
22.0
Axial strain (%)
MHL2
MHLL2
RHL2

Figure A3.48

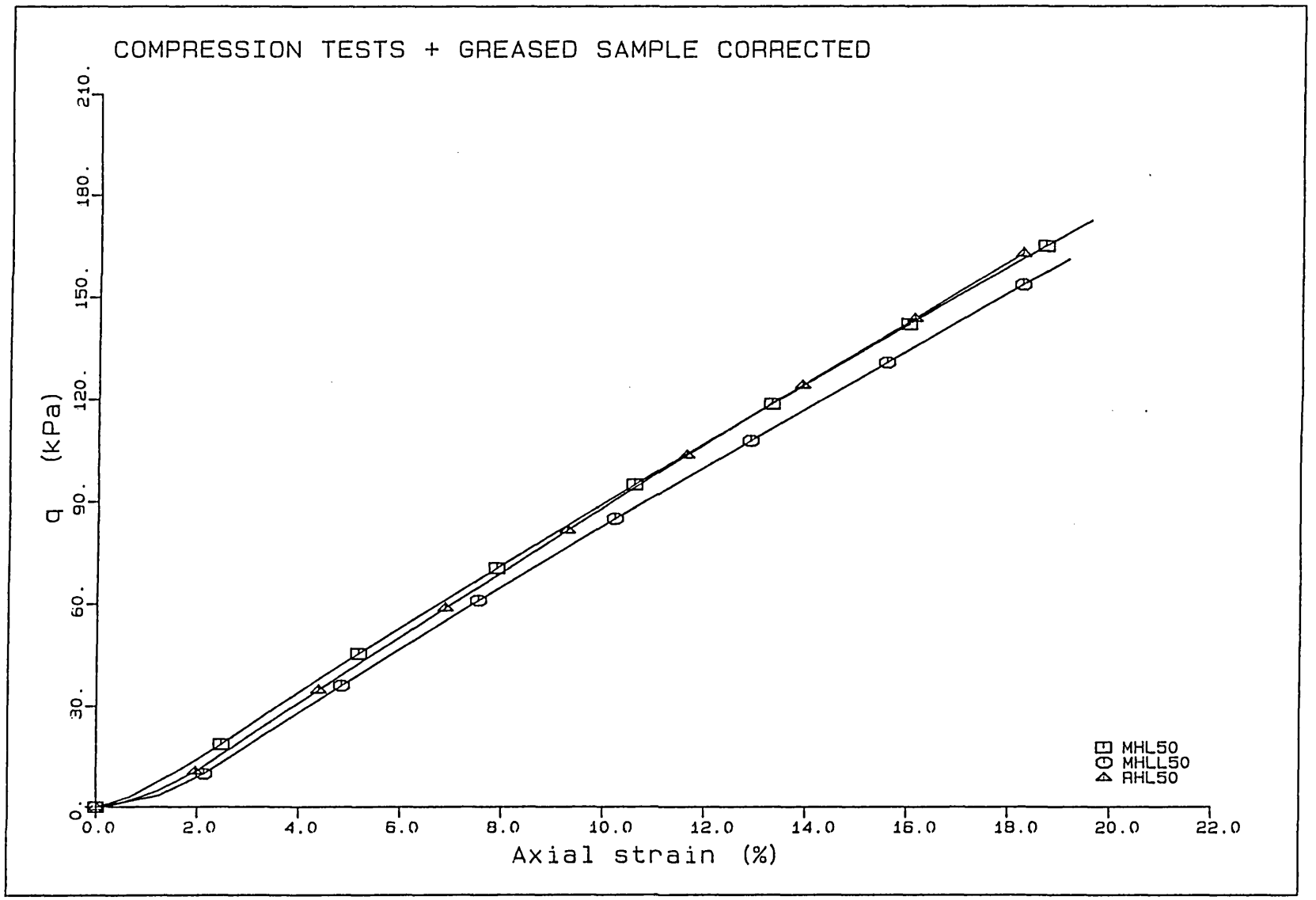

COMPRESSION TESTS + GREASED SAMPLE CORRECTED
q (kPa)
0.
30.
60.
90.
120.
150.
180.
210.
0.0
2.0
4.0
6.0
8.0
10.0
12.0
14.0
16.0
18.0
20.0
22.0
Axial strain (%)
MHL50
MHLL50
RHL50

Figure A3.49

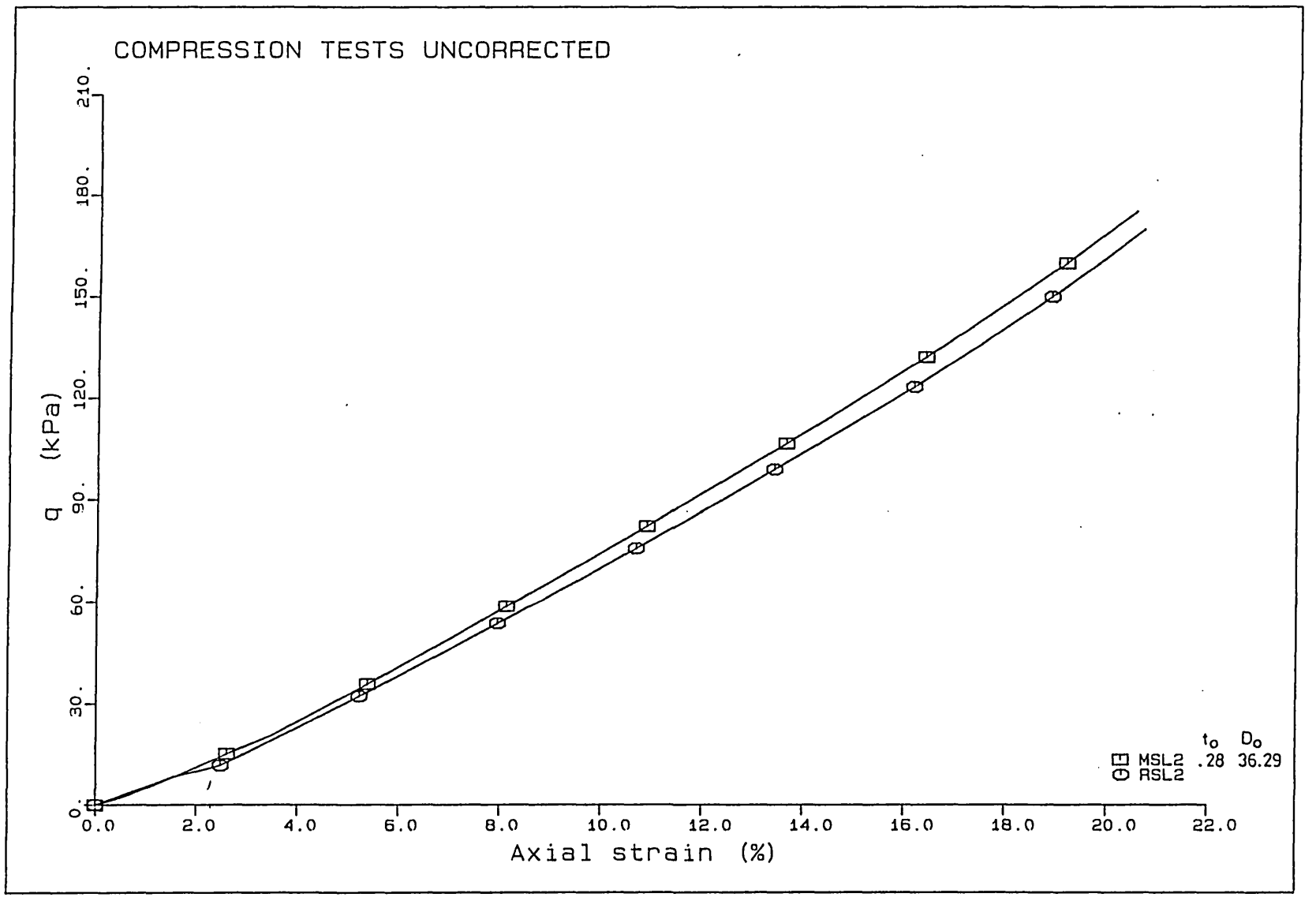

COMPRESSION TESTS UNCORRECTED
q (kPa)
0.
30.
60.
90.
120.
150.
180.
210.
0.0
2.0
4.0
6.0
8.0
10.0
12.0
14.0
16.0
18.0
20.0
22.0
Axial strain (%)
to Do
MSL2 .28 36.29
RSL2

Figure A3.50

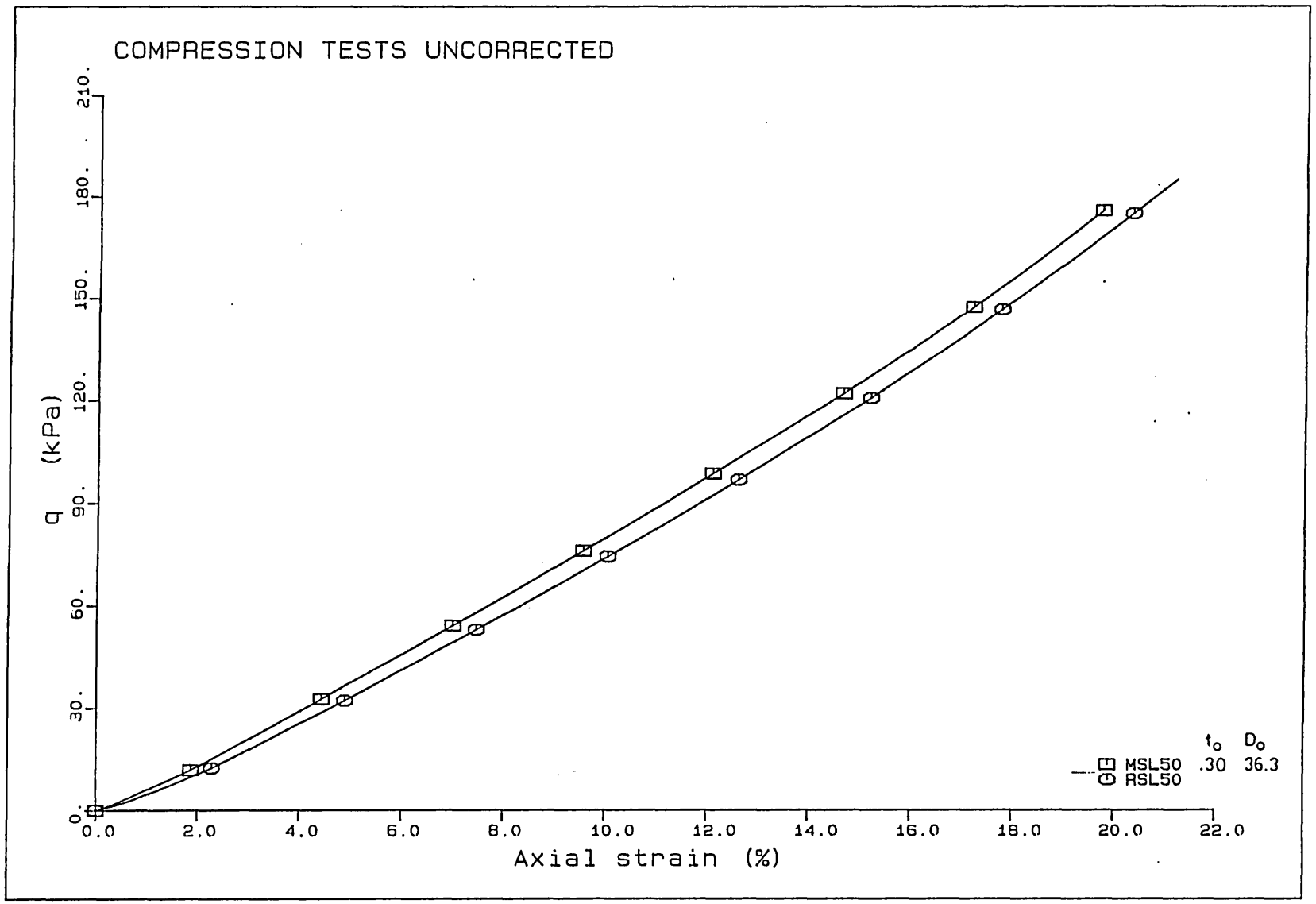

COMPRESSION TESTS UNCORRECTED
q (kPa)
0.
30.
60.
90.
120.
150.
180.
210.
0.0
2.0
4.0
6.0
8.0
10.0
12.0
14.0
16.0
18.0
20.0
22.0
Axial strain (%)
to Do
MSL50 .30 36.3
RSL50

Figure A3.51

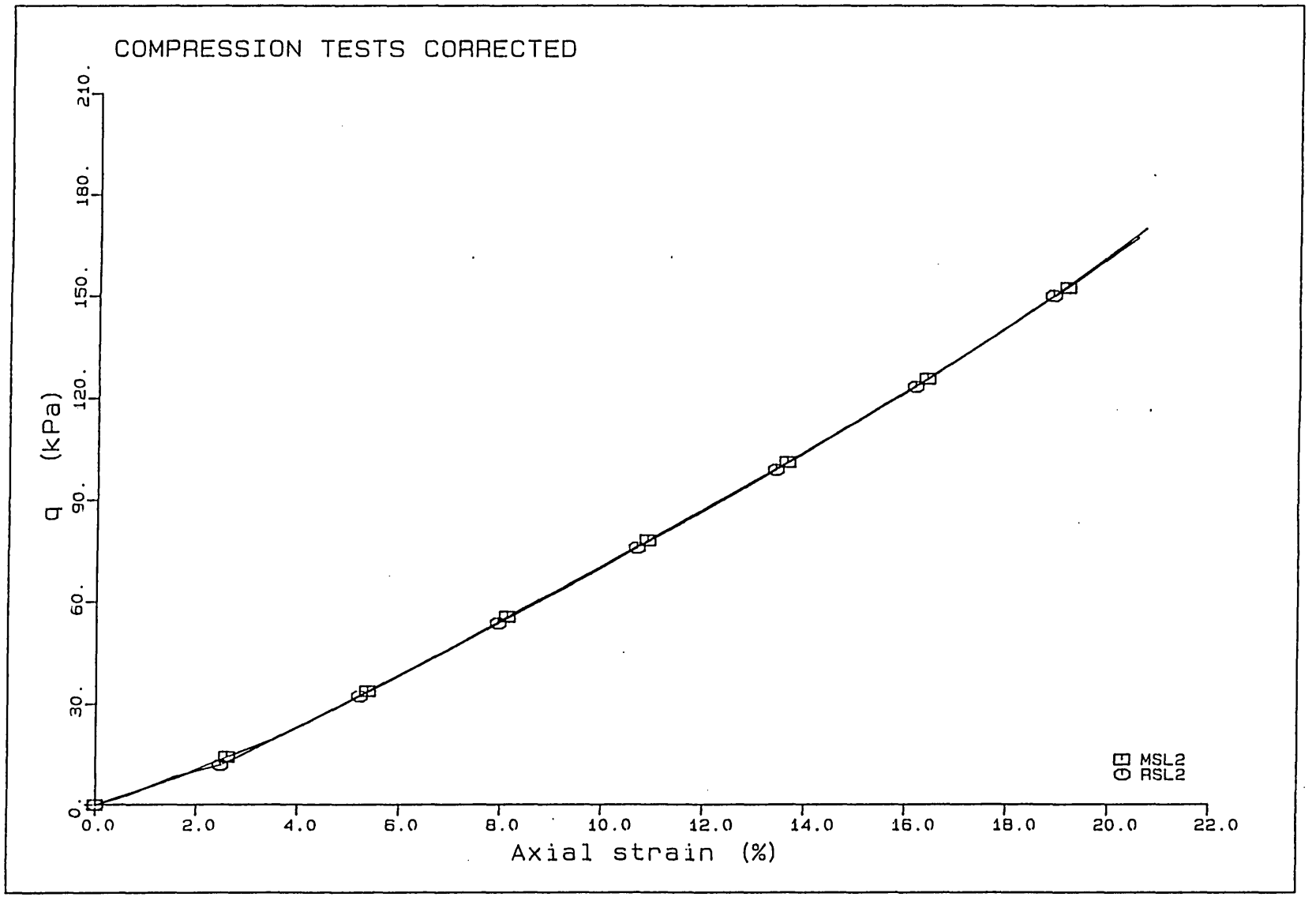

COMPRESSION TESTS CORRECTED
q (kPa)
0.
30.
60.
90.
120.
150.
180.
210.
0.0
2.0
4.0
6.0
8.0
10.0
12.0
14.0
16.0
18.0
20.0
22.0
Axial strain (%)
MSL2
RSL2

Figure A3.52

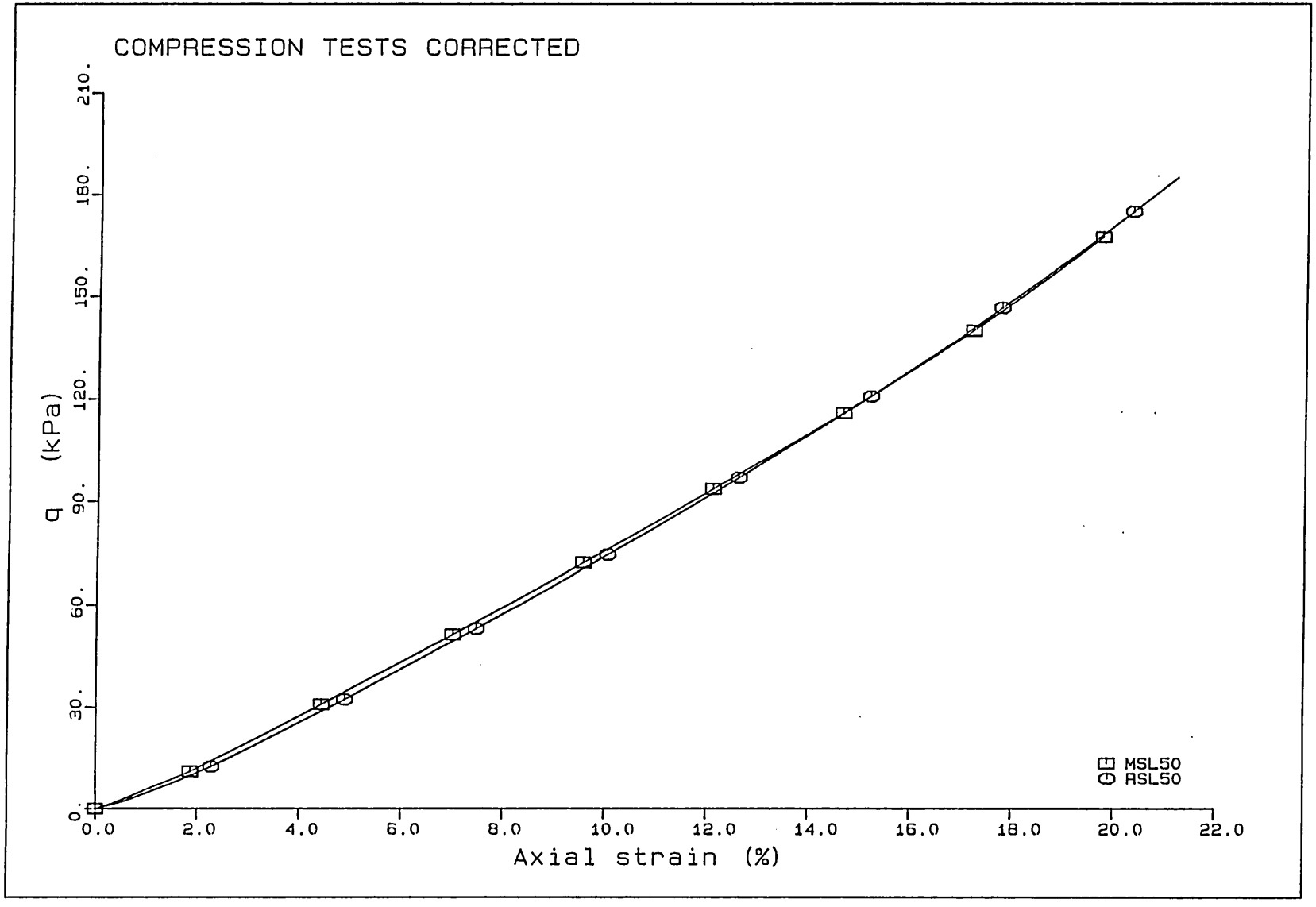

COMPRESSION TESTS CORRECTED
q (kPa)
0.
30.
60.
90.
120.
150.
180.
210.
0.0
2.0
4.0
6.0
8.0
10.0
12.0
14.0
16.0
18.0
20.0
22.0
Axial strain (%)
MSL50
RSL50

Figure A3.53

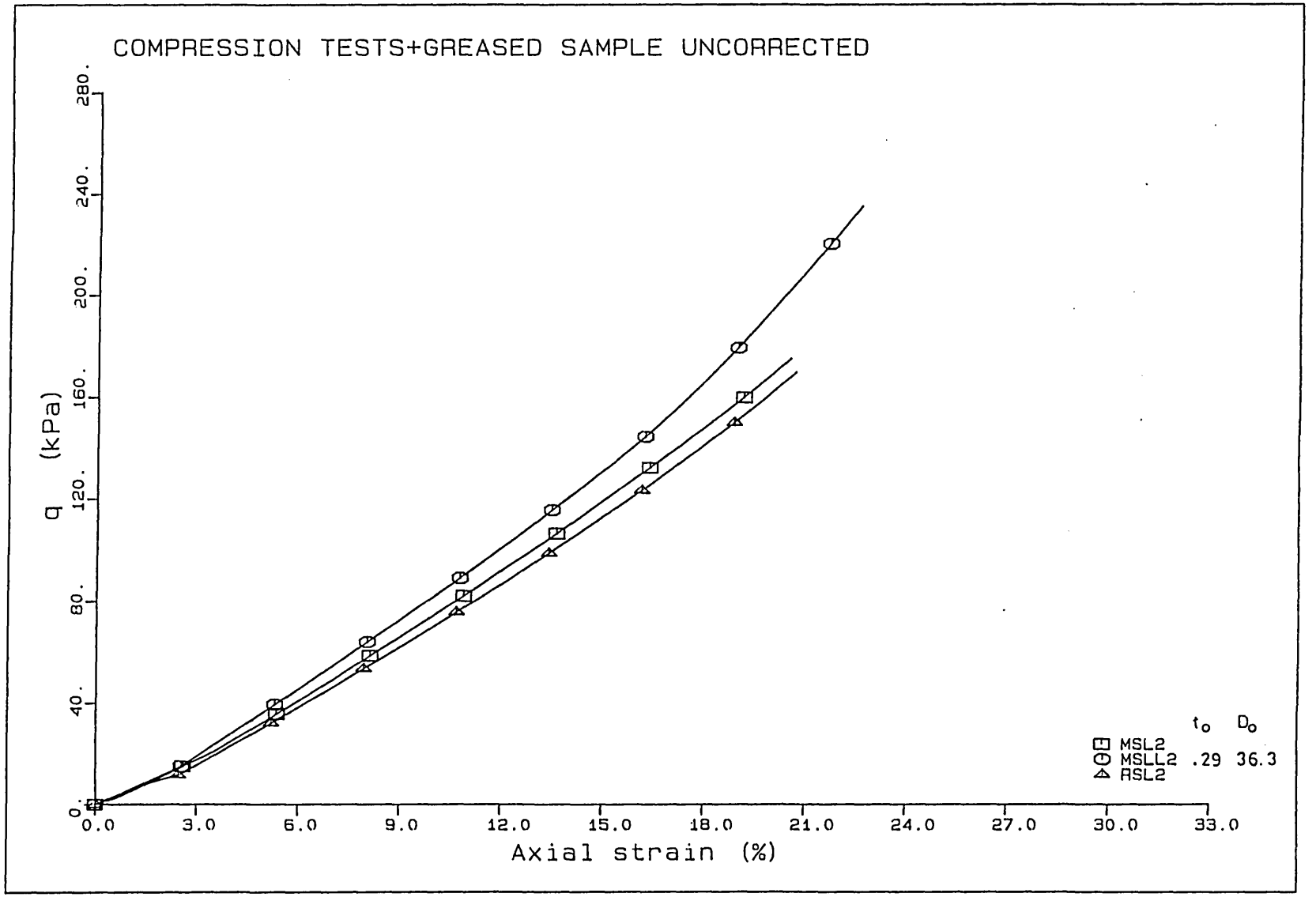

COMPRESSION TESTS+GREASED SAMPLE UNCORRECTED
q (kPa)
0.
40.
80.
120.
160.
200.
240.
280.
0.0
3.0
6.0
9.0
12.0
15.0
18.0
21.0
24.0
27.0
30.0
33.0
Axial strain (%)
to Do
MSL2
MSLL2 .29 36.3
RSL2

Figure A3.54

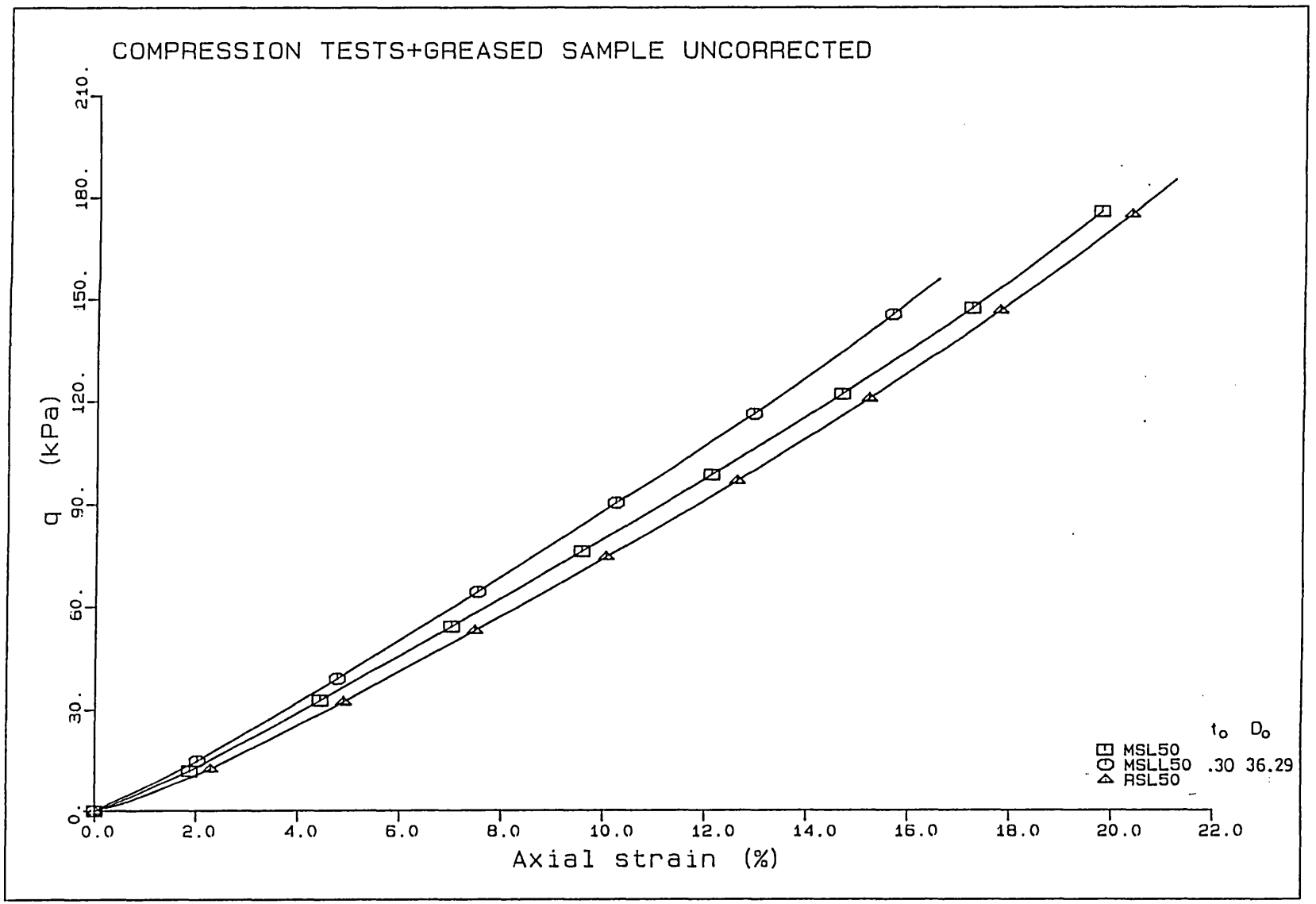

COMPRESSION TESTS+GREASED SAMPLE UNCORRECTED
q (kPa)
0.
30.
60.
90.
120.
150.
180.
210.
0.0
2.0
4.0
6.0
8.0
10.0
12.0
14.0
16.0
18.0
20.0
22.0
Axial strain (%)
to Do
MSL50
MSLL50 .30 36.29
RSL50

Figure A3.55

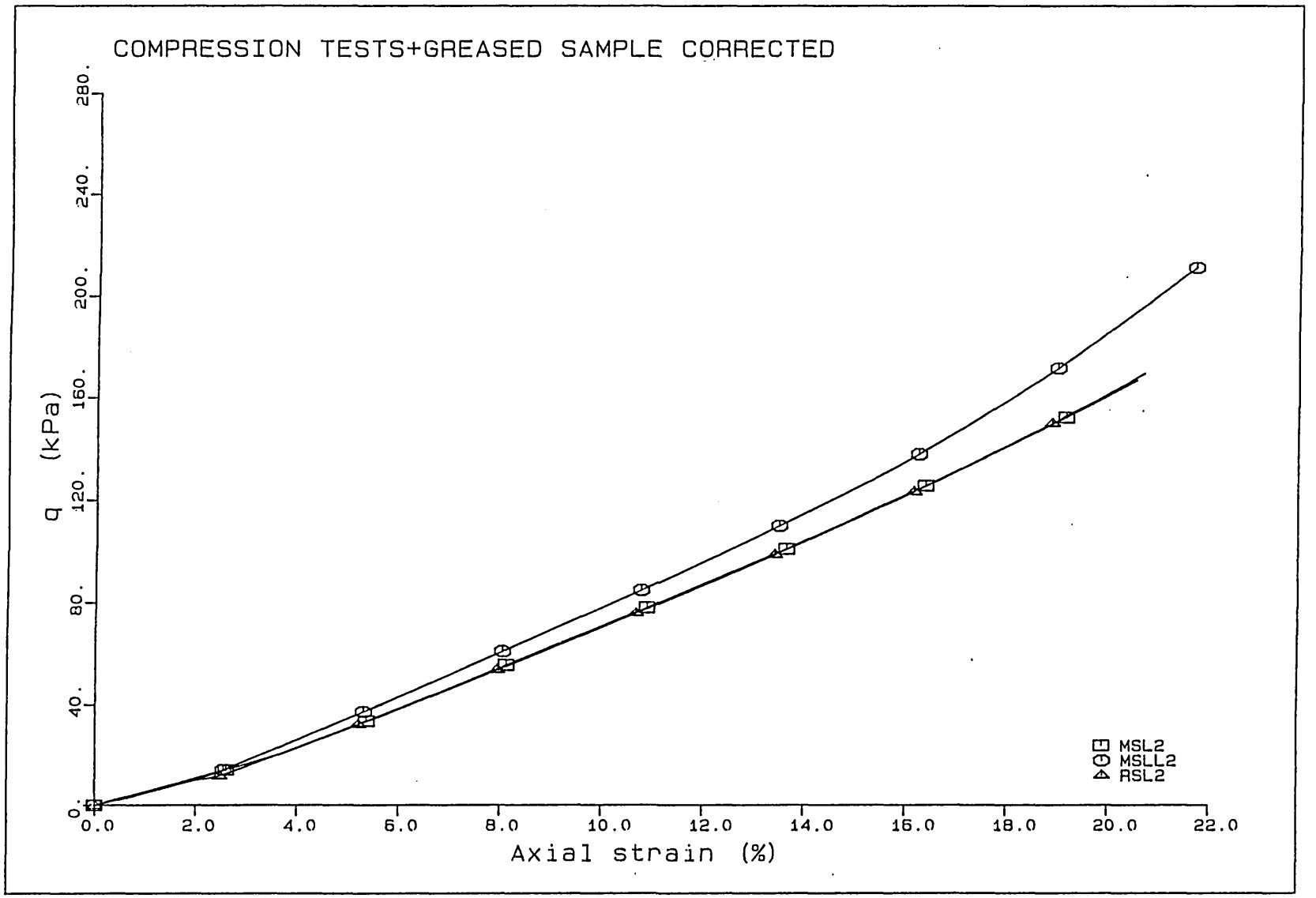

COMPRESSION TESTS+GREASED SAMPLE CORRECTED
q (kPa)
0.
40.
80.
120.
160.
200.
240.
280.
0.0
2.0
4.0
6.0
8.0
10.0
12.0
14.0
16.0
18.0
20.0
22.0
Axial strain (%)
MSL2
MSLL2
RSL2

Figure A3.56

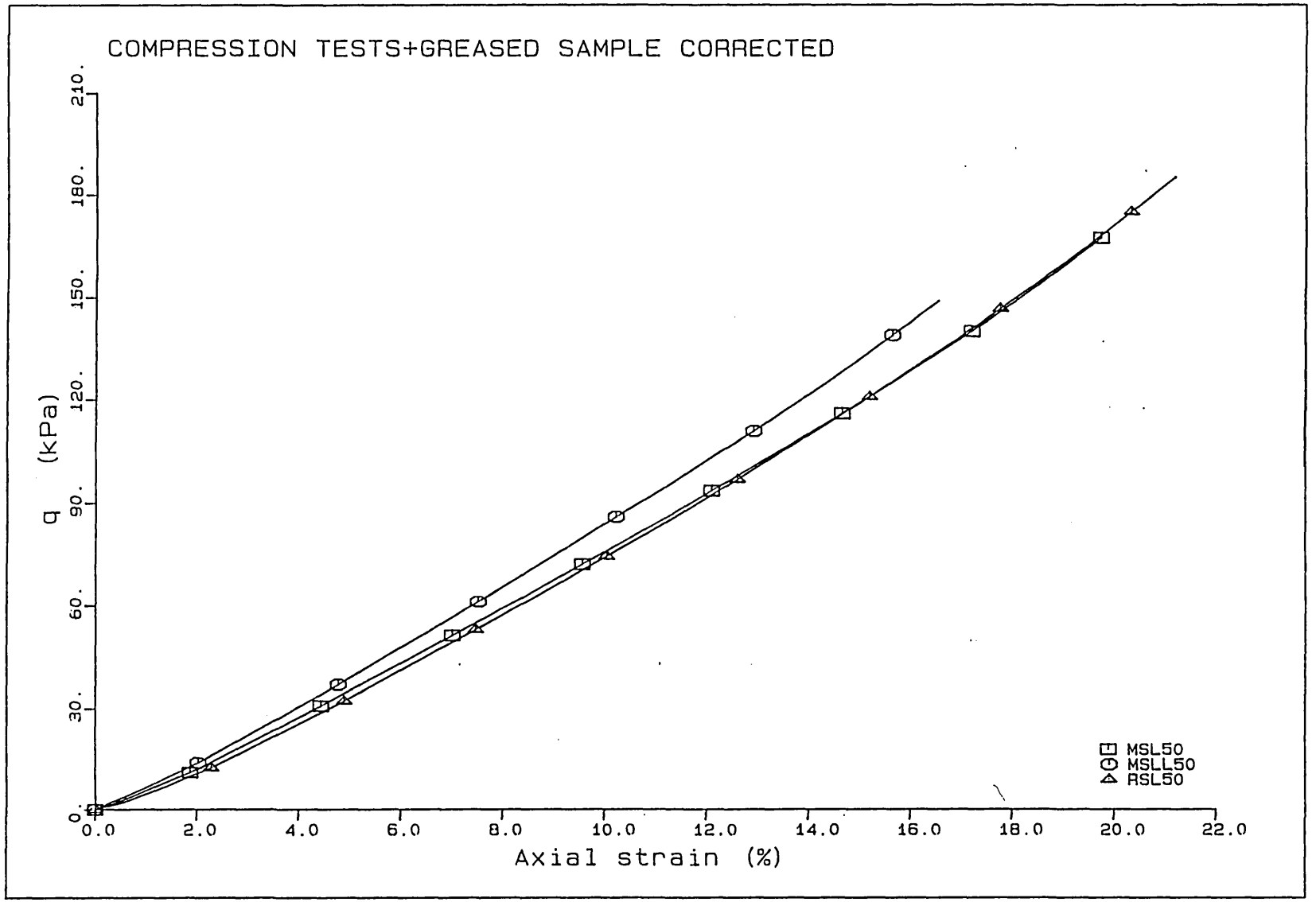

COMPRESSION TESTS+GREASED SAMPLE CORRECTED
q (kPa)
0.
30.
60.
90.
120.
150.
180.
210.
0.0
2.0
4.0
6.0
8.0
10.0
12.0
14.0
16.0
18.0
20.0
22.0
Axial strain (%)
MSL50
MSLL50
RSL50

Figure A3.57

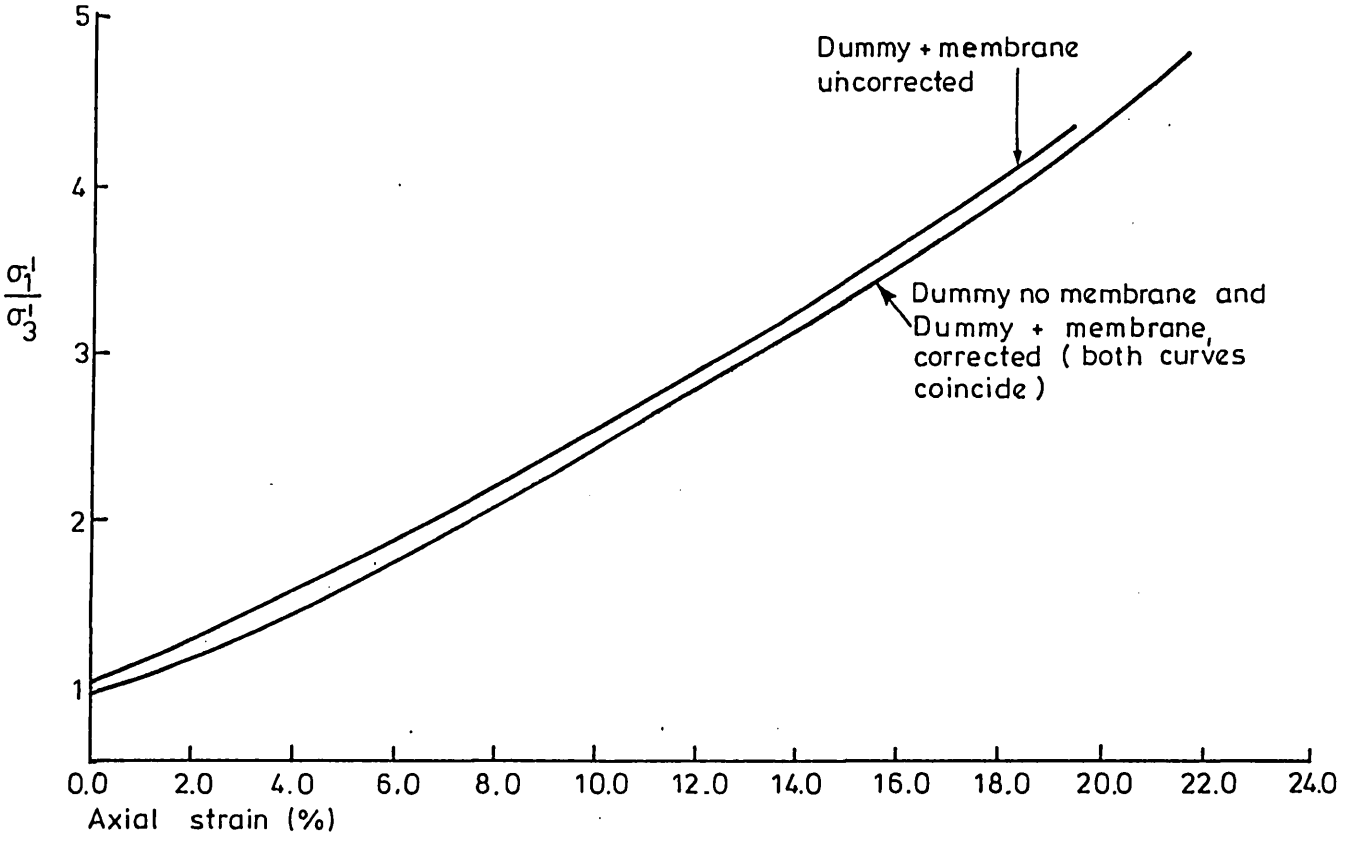


Figure A3.58 Principal stress ratios for tests on a soft rubber dummy specimen enclosed by a membrane: corrected and uncorrected for membrane effects.

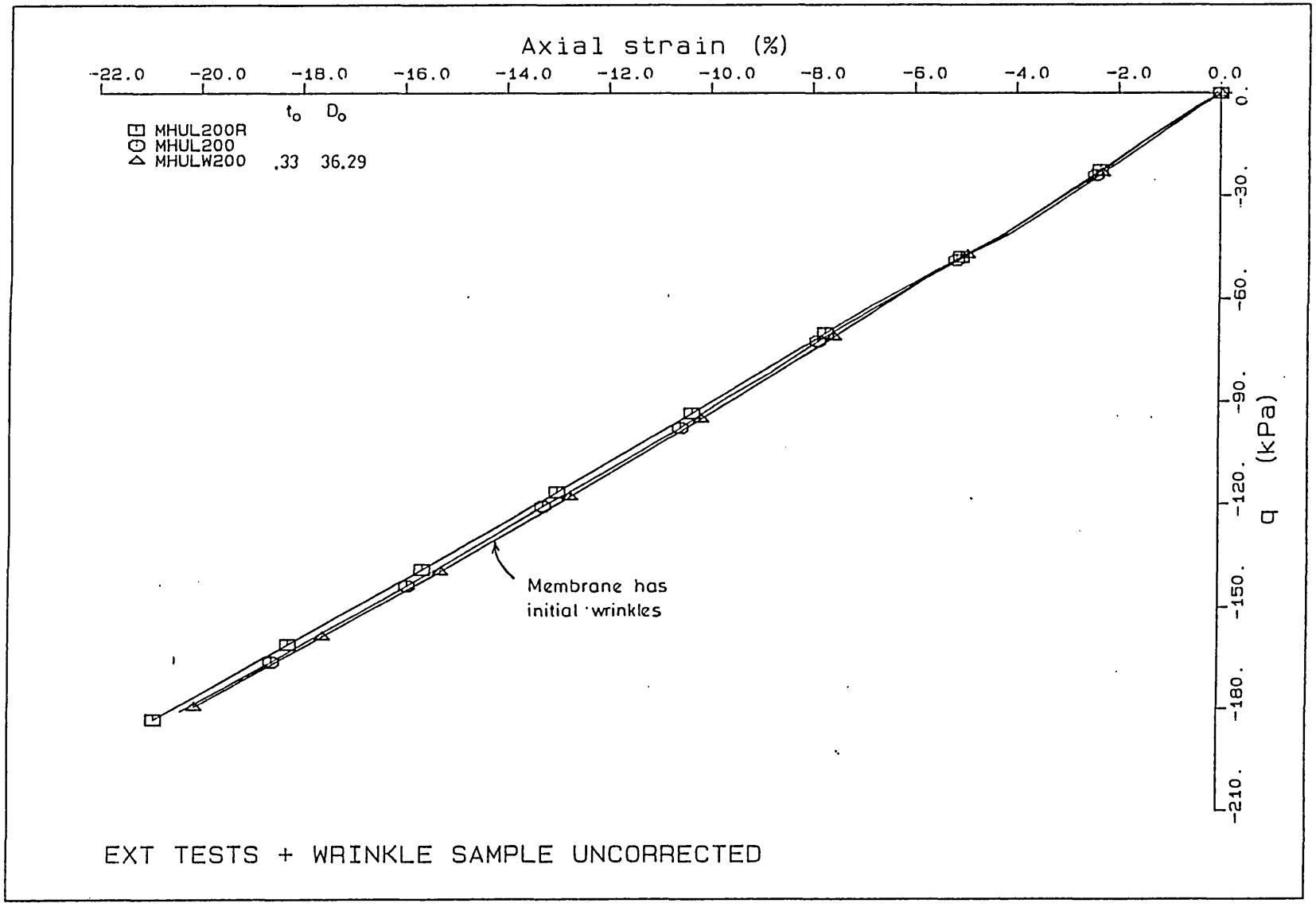


Figure A3.59. **Shear stress versus axial strain for extension tests on a hard rubber specimen for membrane with and without initial wrinkles.**

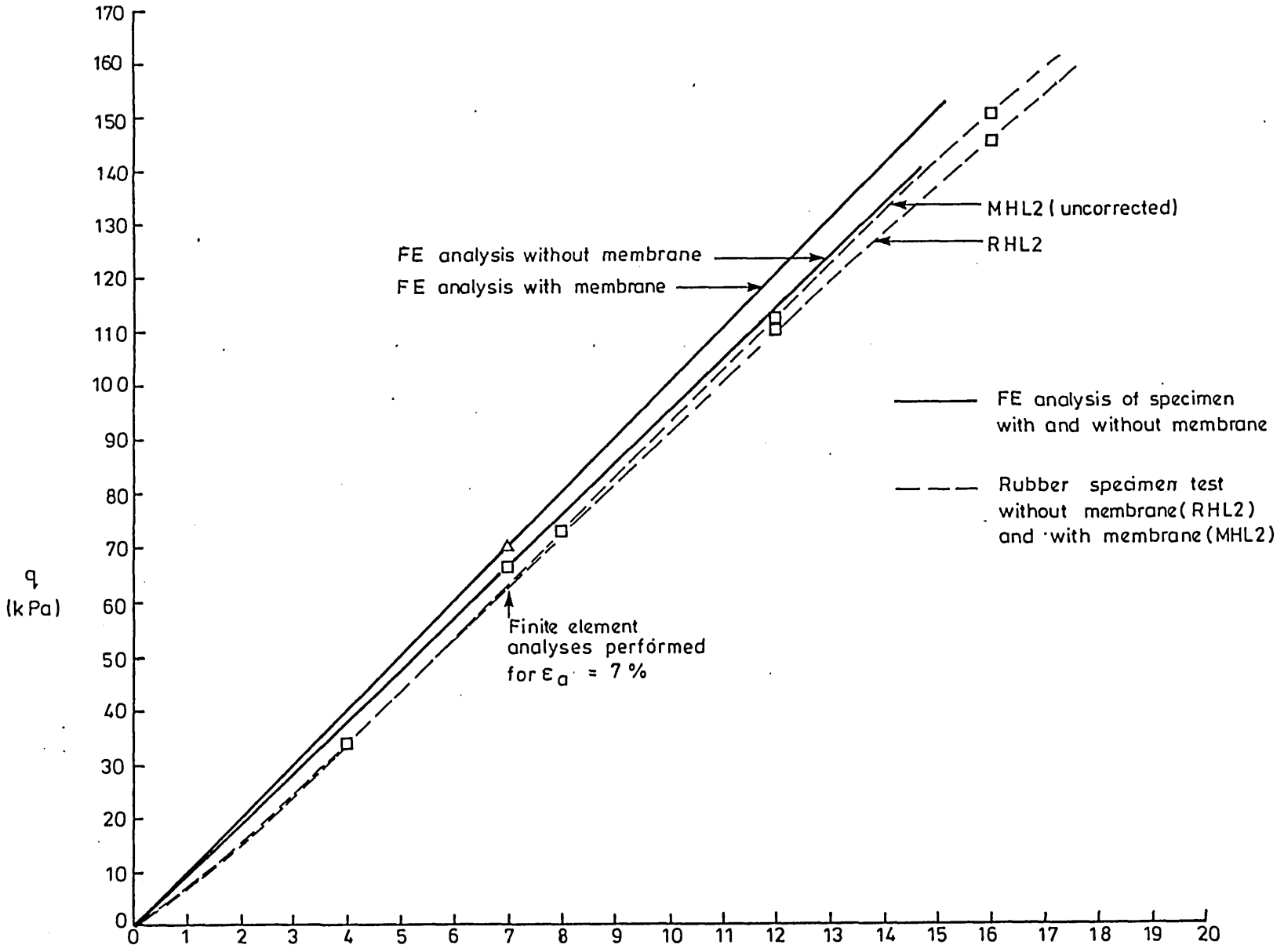


Figure A3.60. Compression tests on a hard rubber dummy with and without membrane: comparison of finite element analysis with actual test results.

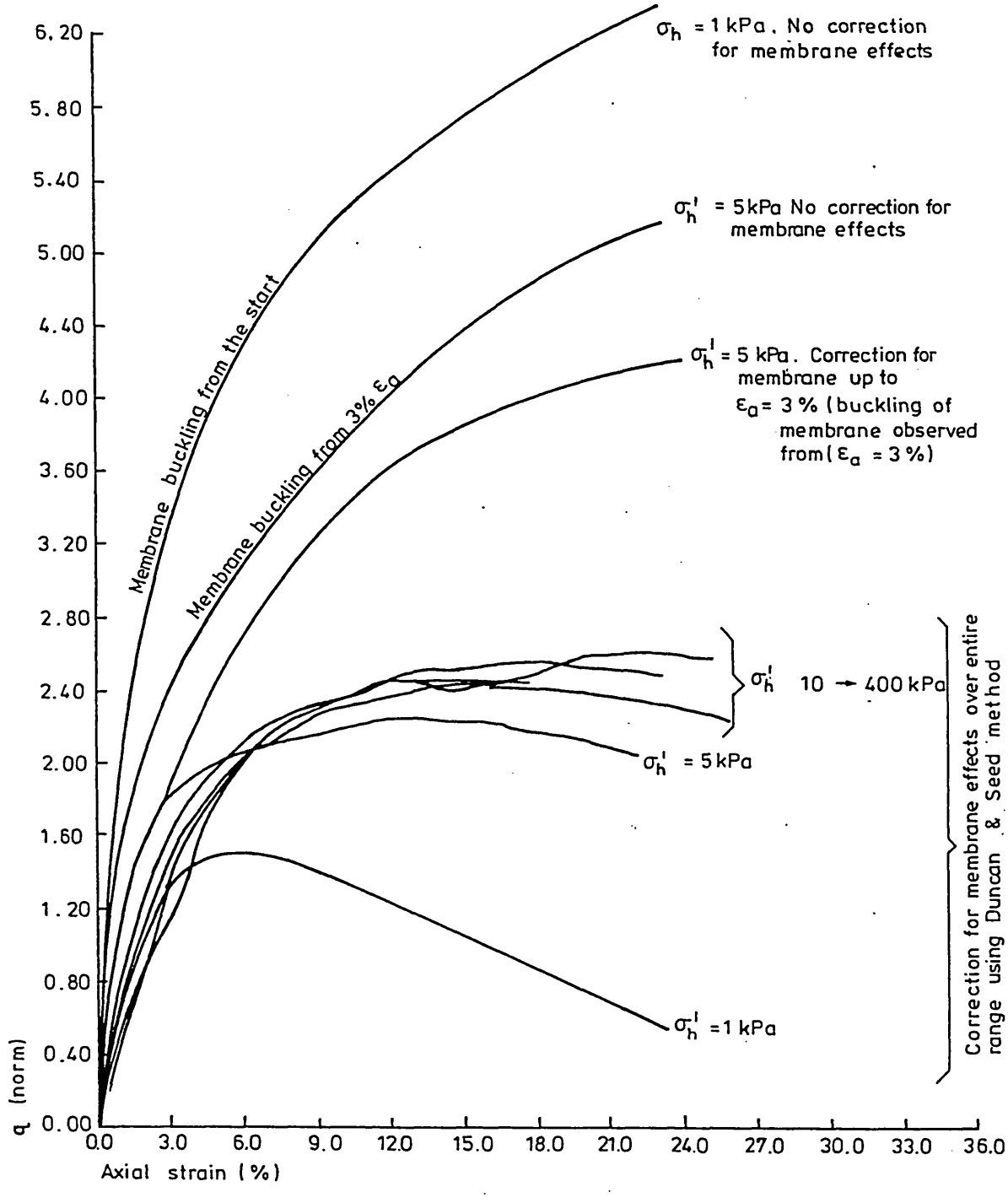


Figure A3.61. Deviator stress (normalised with effective horizontal stress) versus axial strain for drained triaxial compression tests on a very loose silty sand. All results corrected for membrane restraint except where indicated otherwise (Duncan and Seed theory).

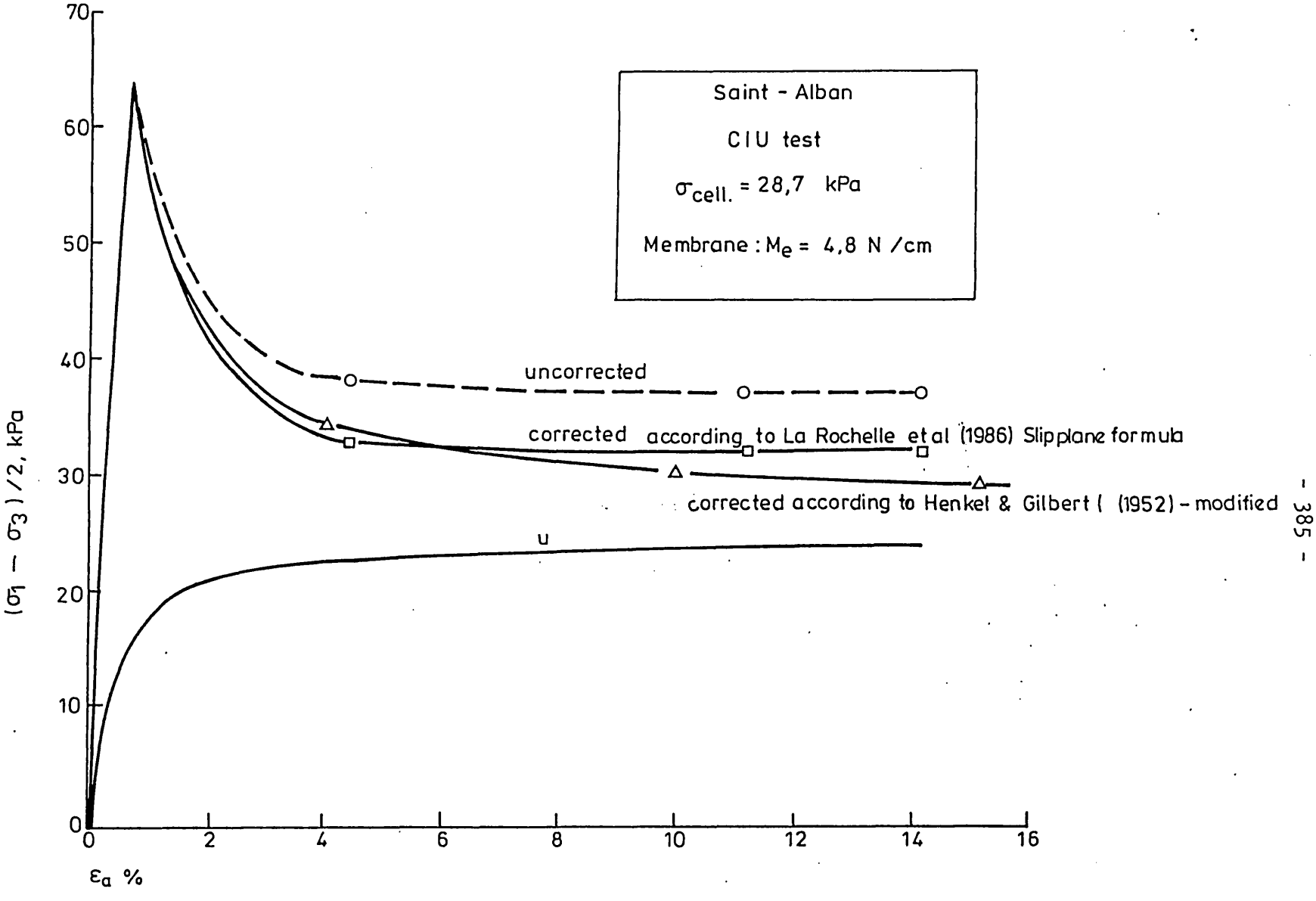


Figure A3.62. Triaxial compression test on Saint-Alban clay (La Rochelle, et al., 1986). Comparison of La Rochelle's slip plane correction for membrane restraint with the modifed Henkel and Gilbert correction.

APPENDIX A4

TABLE AND FIGURES

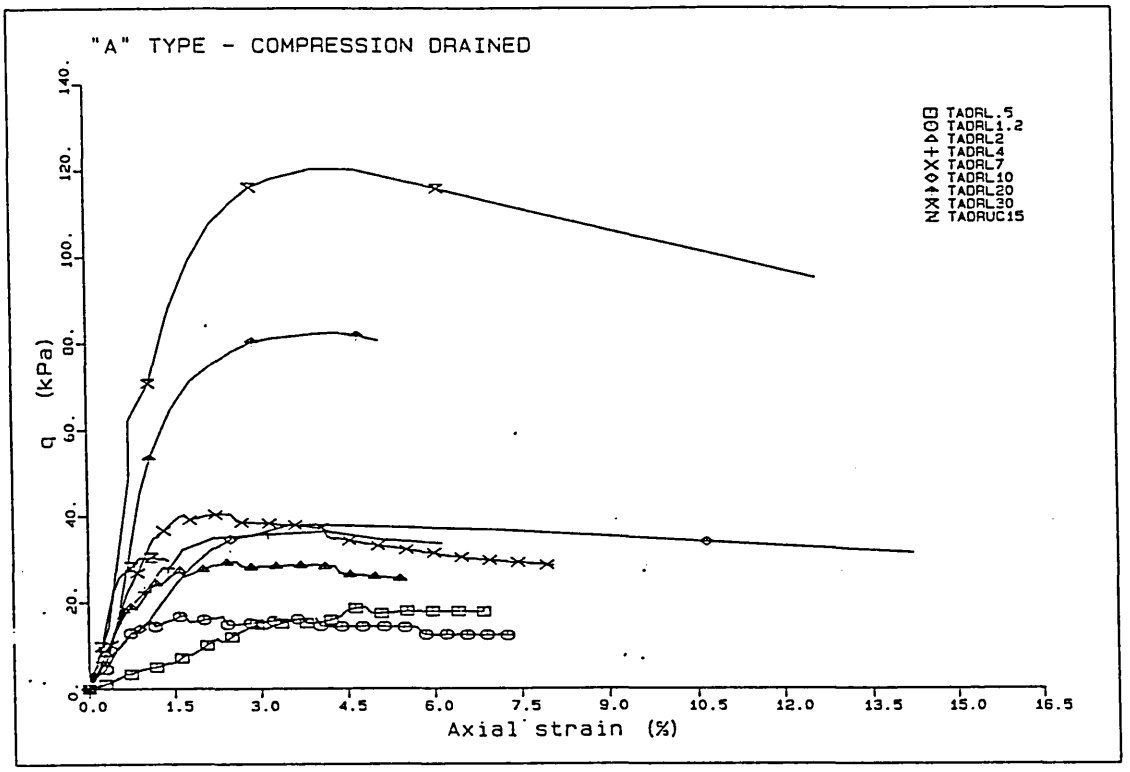
TABLE A4.1

Schedule of Sand tests

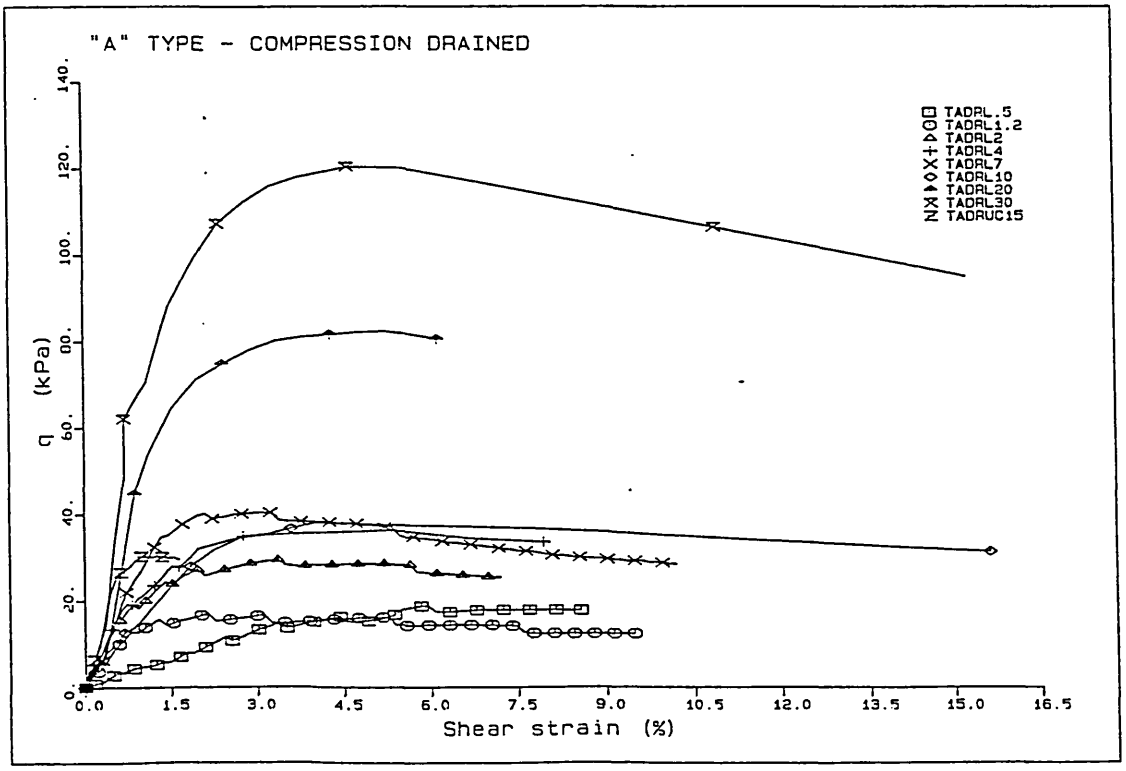
Label	Test Type	Initial relative density range % (equivalent e shown bracketed)	Appendix Number
TADRL.5 to 30 and TADRUC15	Compression , drained	79(.63) - 88(.60)	A4.A
TBDRL1 to 400	" "	56(.72) - 71(.66)	A4.B
TCDRL1 to 400 and TCDRUC5 to 35	" "	42(.77) - 61(.70)	A4.C
TDDRL1 to 400	" "	6(.86) - 30(.81)	A4.D
TAUNL1 to 400	Compression, undrained	83(.62) - 90(.60)	A4.E
TBUNL1 to 400	" "	63(.69) - 80(.63)	A4.F
TCUNL0.5 to 400	" "	45(.76) - 59(.71)	A4.G
TDUNL1 to 400	" "	10(.89) - 23(.84)	A4.4
TADRUL15 to 550	Extension, drained	79(.64) - 97(.57)	A4.I
TBDRUL10 to 40	" "	69(.67) - 78(.64)	A4.J
TCDRUL15 to 465	" "	45(.76) - 62(.70)	A4.K
TDDRUL15 to 40	" "	3(.91) - 25(.83)	A4.L

TABLE A4.1 (CONTINUED)

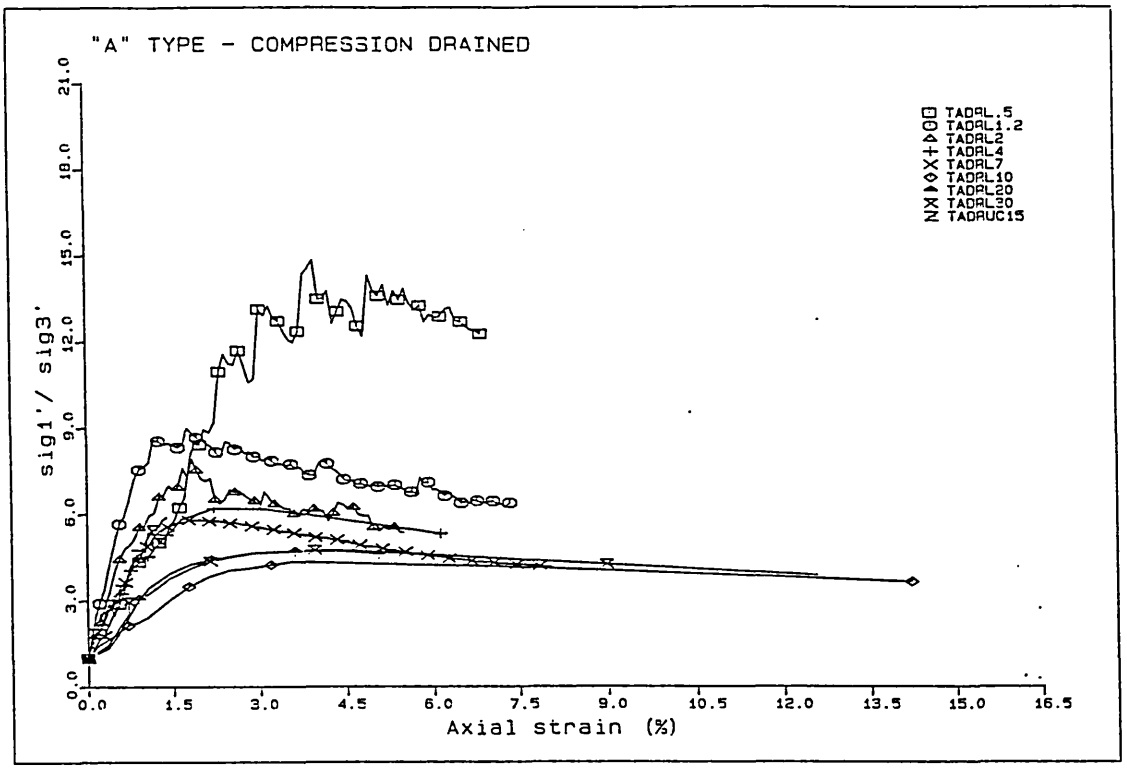
Label	Test type	Initial relative density range % (equivalent e shown bracketed)	Appendix Number
TAUNUL05 to 300	Extension, undrained	81(.63) - 90(.60)	A4.M
TBUNUL1 to 300	" "	55(.72) - 78(.64)	A4.N
TCUNUL35	" "	46(.76)	A4.O
TDUNUL0.9 - 375	" "	22(.84) - 37(.79)	A4.P
SPS1 - 7	Passive stress relief	22(.84) - 70(.70)	A4.Q
SPS/A/1 to 8 and SPS/B/1	" "	71(.66) - 90(.60)	A4.R
SASI1 to 3	Active stress increase	28(.82) - 43(.77)	A4.5


"A" TYPE - COMPRESSION DRAINED
TADRL.5
TADRL1.2
TADRL2
TADRL4
TADRL7
TADRL10
TADRL20
TADRL30
TADRUC15
q (kPa)
0.
20.
40.
60.
80.
100.
120.
140.
0.0
1.5
3.0
4.5
6.0
7.5
9.0
10.5
12.0
13.5
15.0
16.5
Axial strain (%)

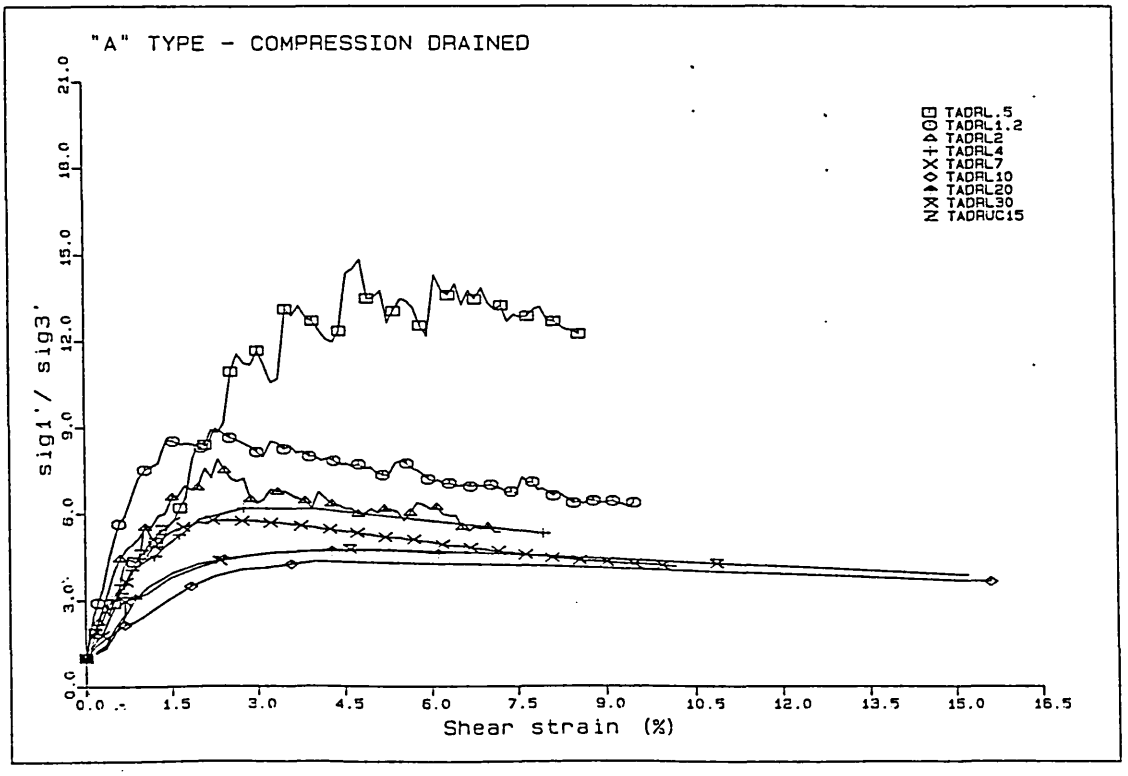
A4.A1


"A" TYPE - COMPRESSION DRAINED
TADRL.5
TADRL1.2
TADRL2
TADRL4
TADRL7
TADRL10
TADRL20
TADRL30
TADRUC15
q (kPa)
0.
20.
40.
60.
80.
100.
120.
140.
0.0
1.5
3.0
4.5
6.0
7.5
9.0
10.5
12.0
13.5
15.0
16.5
Shear strain (%)

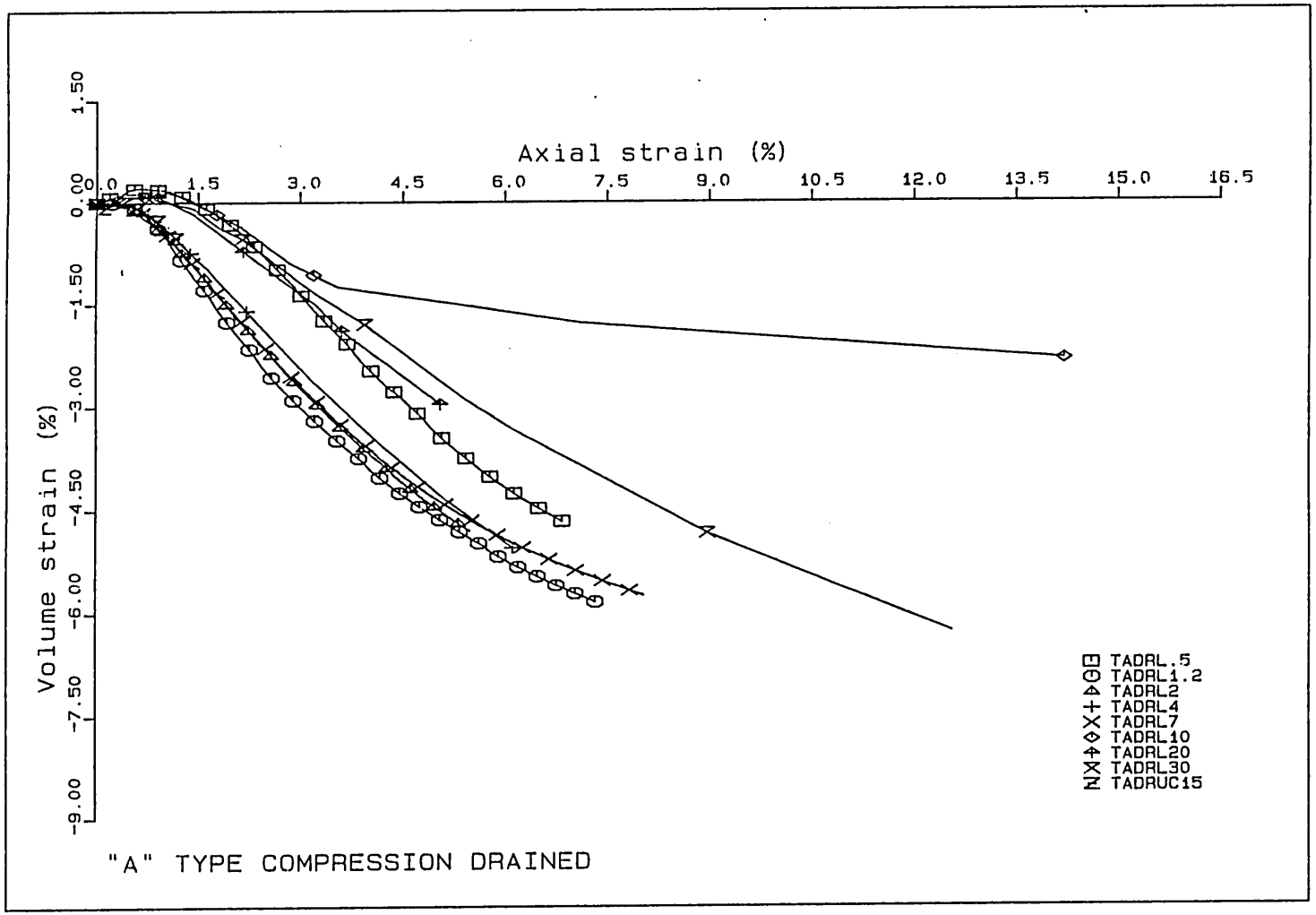
A4.A2


"A" TYPE - COMPRESSION DRAINED
sig1' / sig3'
Axial strain (%)
TADRL.5
TADRL1.2
TADRL2
TADRL4
TADRL7
TADRL10
TADRL20
TADRL30
TADRUC15

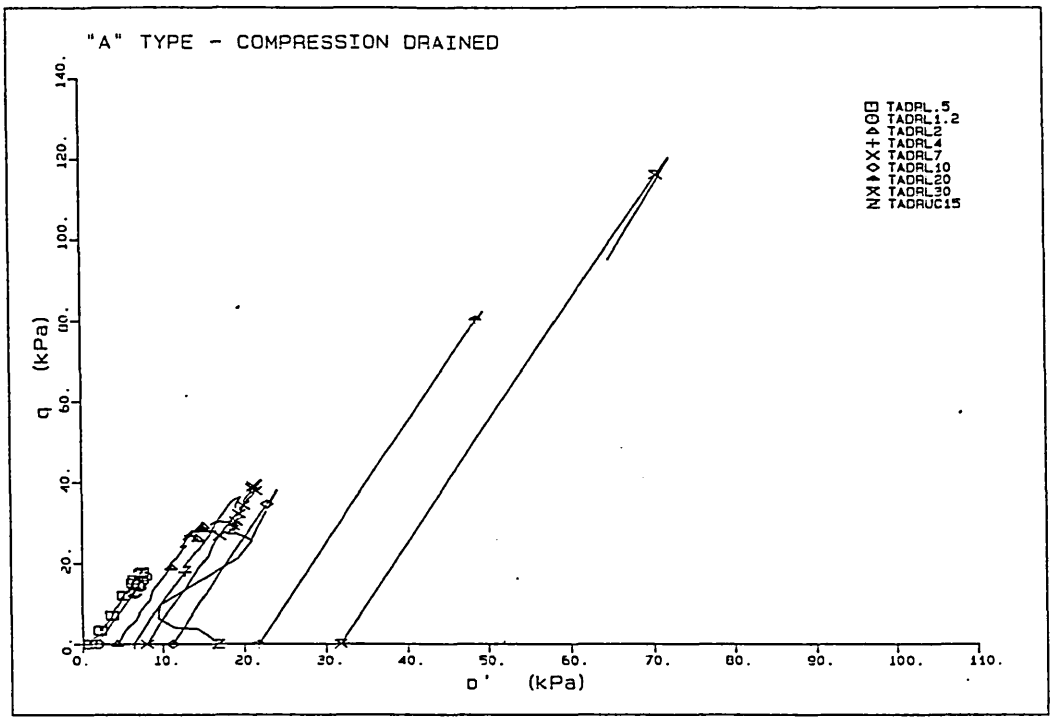
A4.A3


"A" TYPE - COMPRESSION DRAINED
sig1' / sig3'
Shear strain (%)
TADRL.5
TADRL1.2
TADRL2
TADRL4
TADRL7
TADRL10
TADRL20
TADRL30
TADRUC15

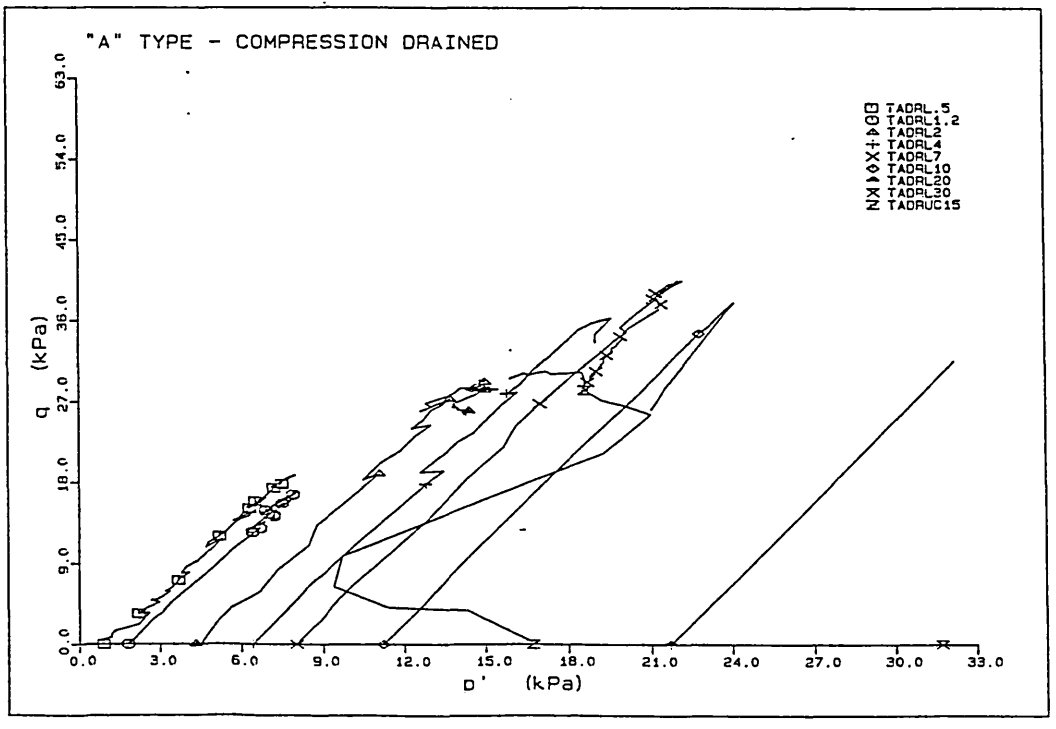
A4.A4


Axial strain (%)
0.0
1.5
3.0
4.5
6.0
7.5
9.0
10.5
12.0
13.5
15.0
16.5
Volume strain (%)
1.50
0.00
-1.50
-3.00
-4.50
-6.00
-7.50
-9.00
TADRL.5
TADRL1.2
TADRL2
TADRL4
TADRL7
TADRL10
TADRL20
TADRL30
TADRUC15
"A" TYPE COMPRESSION DRAINED

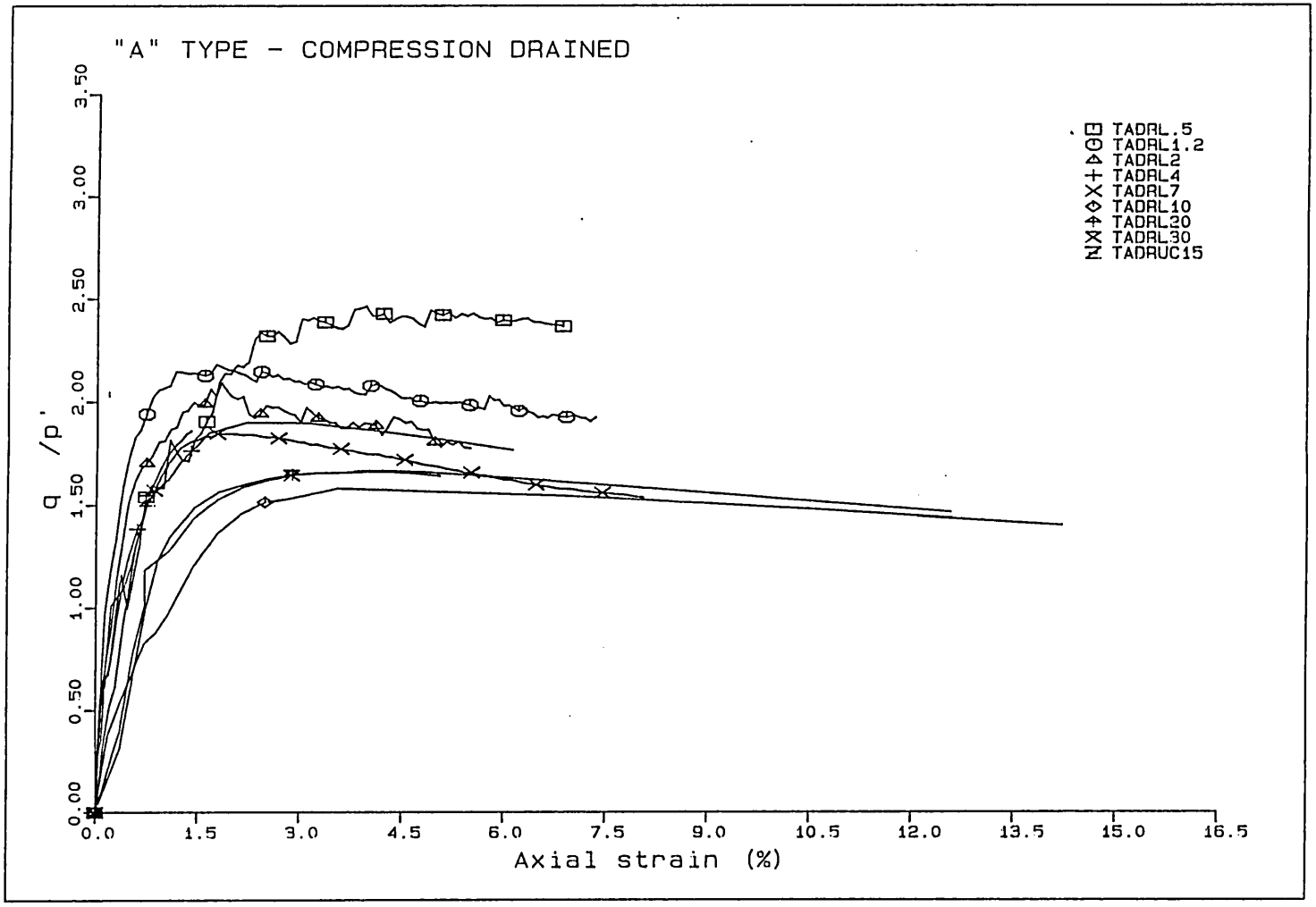
A4.A5


"A" TYPE - COMPRESSION DRAINED
TADRL.5
TADRL1.2
TADRL2
TADRL4
TADRL7
TADRL10
TADRL20
TADRL30
TADRUC15
q (kPa)
p' (kPa)
0.
20.
40.
60.
80.
100.
120.
140.
10.
30.
50.
70.
90.
110.

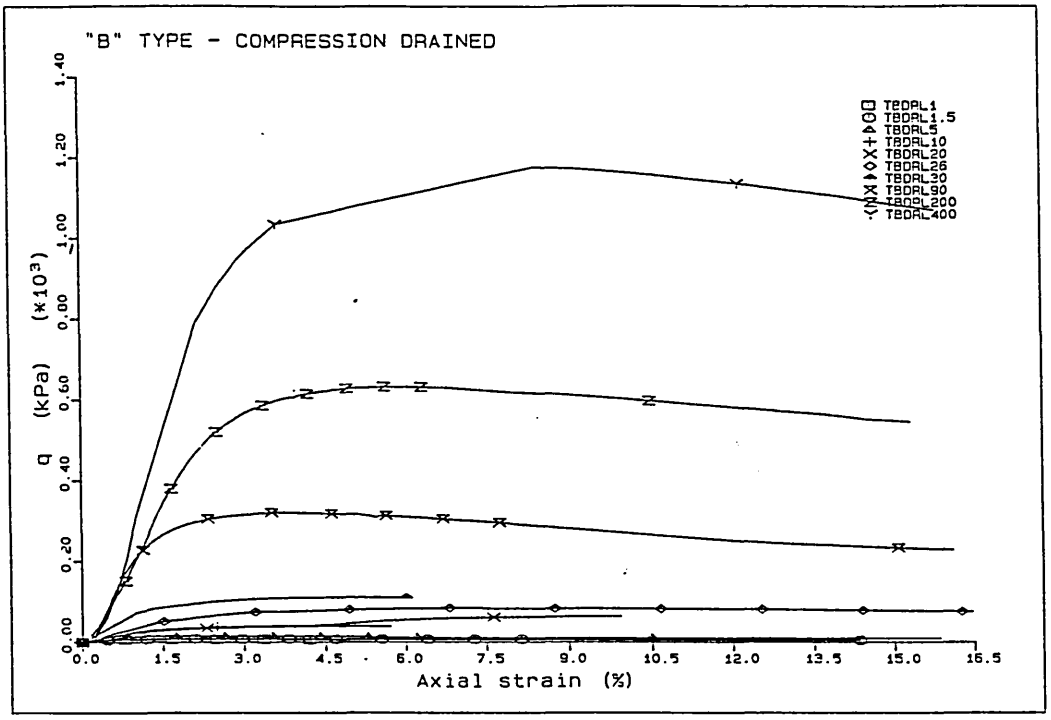
A4.A6


"A" TYPE - COMPRESSION DRAINED
TADRL.5
TADRL1.2
TADRL2
TADRL4
TADRL7
TADRL10
TADRL20
TADRL30
TADRUC15
q (kPa)
p' (kPa)
0.0
9.0
18.0
27.0
36.0
45.0
54.0
63.0
3.0
6.0
12.0
15.0
21.0
24.0
27.0
30.0
33.0

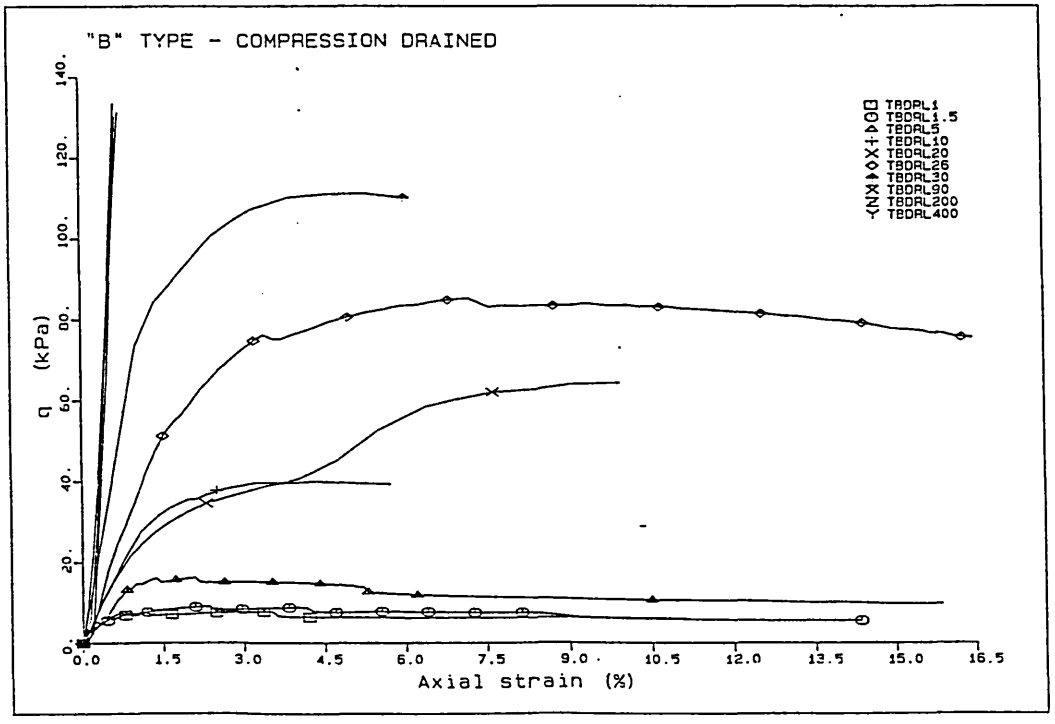
A4.A7


"A" TYPE - COMPRESSION DRAINED
TADRL.5
TADRL1.2
TADRL2
TADRL4
TADRL7
TADRL10
TADRL20
TADRL30
TADRUC15
q /p'
0.00
0.50
1.00
1.50
2.00
2.50
3.00
3.50
0.0
1.5
3.0
4.5
6.0
7.5
9.0
10.5
12.0
13.5
15.0
16.5
Axial strain (%)

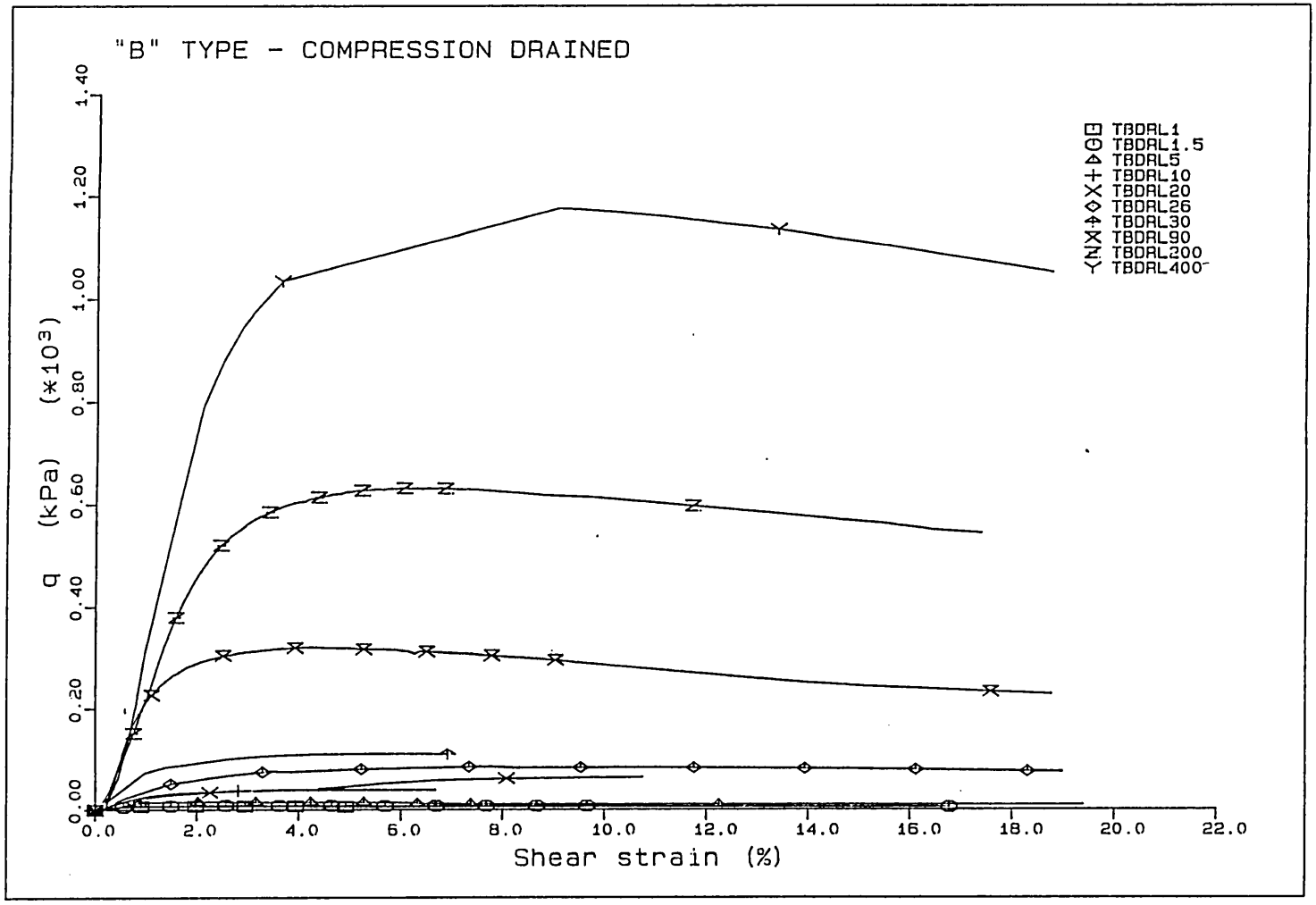
A4.A8


"B" TYPE - COMPRESSION DRAINED
q (kPa) (*10³)
Axial strain (%)
TBDRL1
TBDRL1.5
TBDRL5
TBDRL10
TBDRL20
TBDRL26
TBDRL30
TBDRL90
TBDRL200
TBDRL400

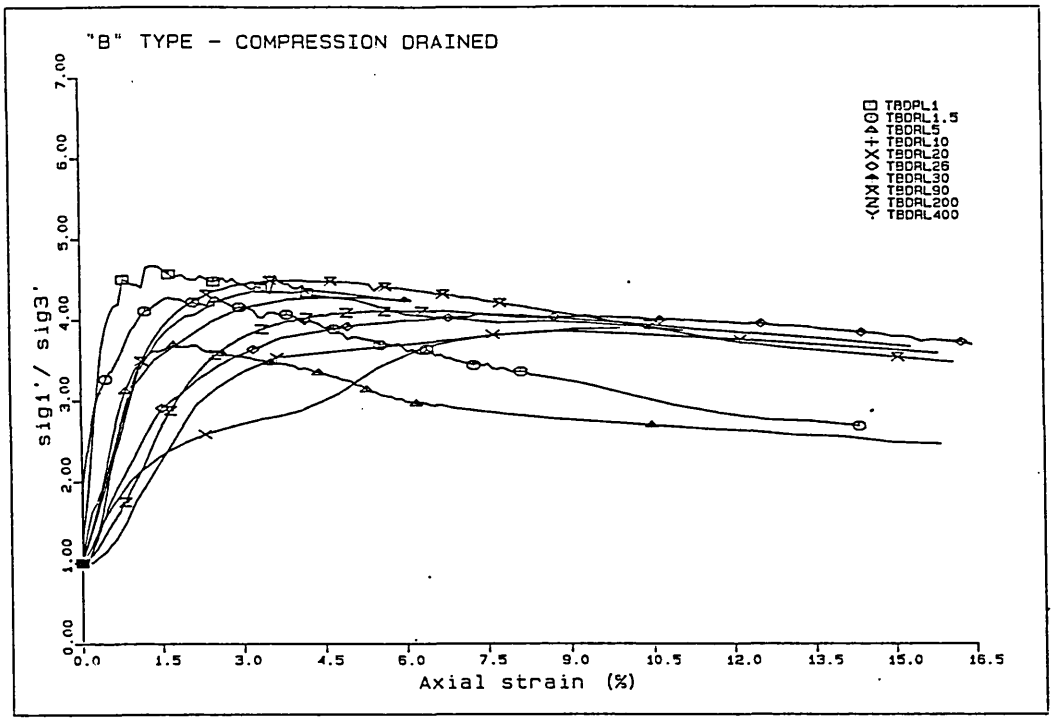
A4.B1


"B" TYPE - COMPRESSION DRAINED
q (kPa)
Axial strain (%)
TBDRL1
TBDRL1.5
TBDRL5
TBDRL10
TBDRL20
TBDRL26
TBDRL30
TBDRL90
TBDRL200
TBDRL400

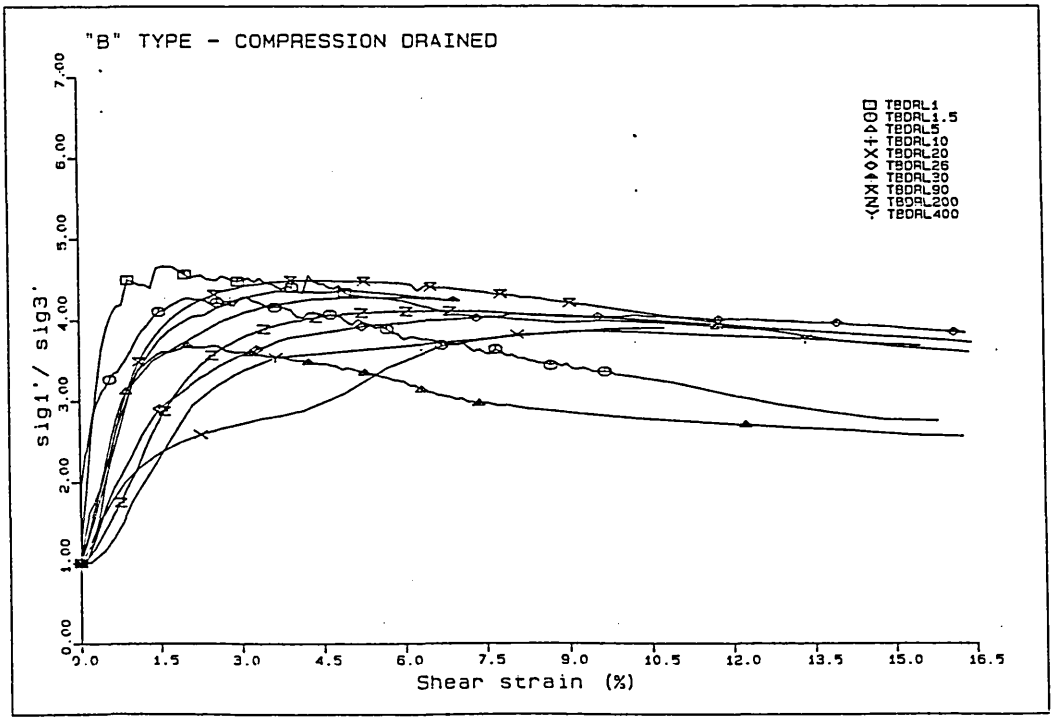
A4.B2


"B" TYPE - COMPRESSION DRAINED
q (kPa) (*10³)
0.00
0.20
0.40
0.60
0.80
1.00
1.20
1.40
0.0
2.0
4.0
6.0
8.0
10.0
12.0
14.0
16.0
18.0
20.0
22.0
Shear strain (%)
TBDRL1
TBDRL1.5
TBDRL5
TBDRL10
TBDRL20
TBDRL26
TBDRL30
TBDRL90
TBDRL200
TBDRL400

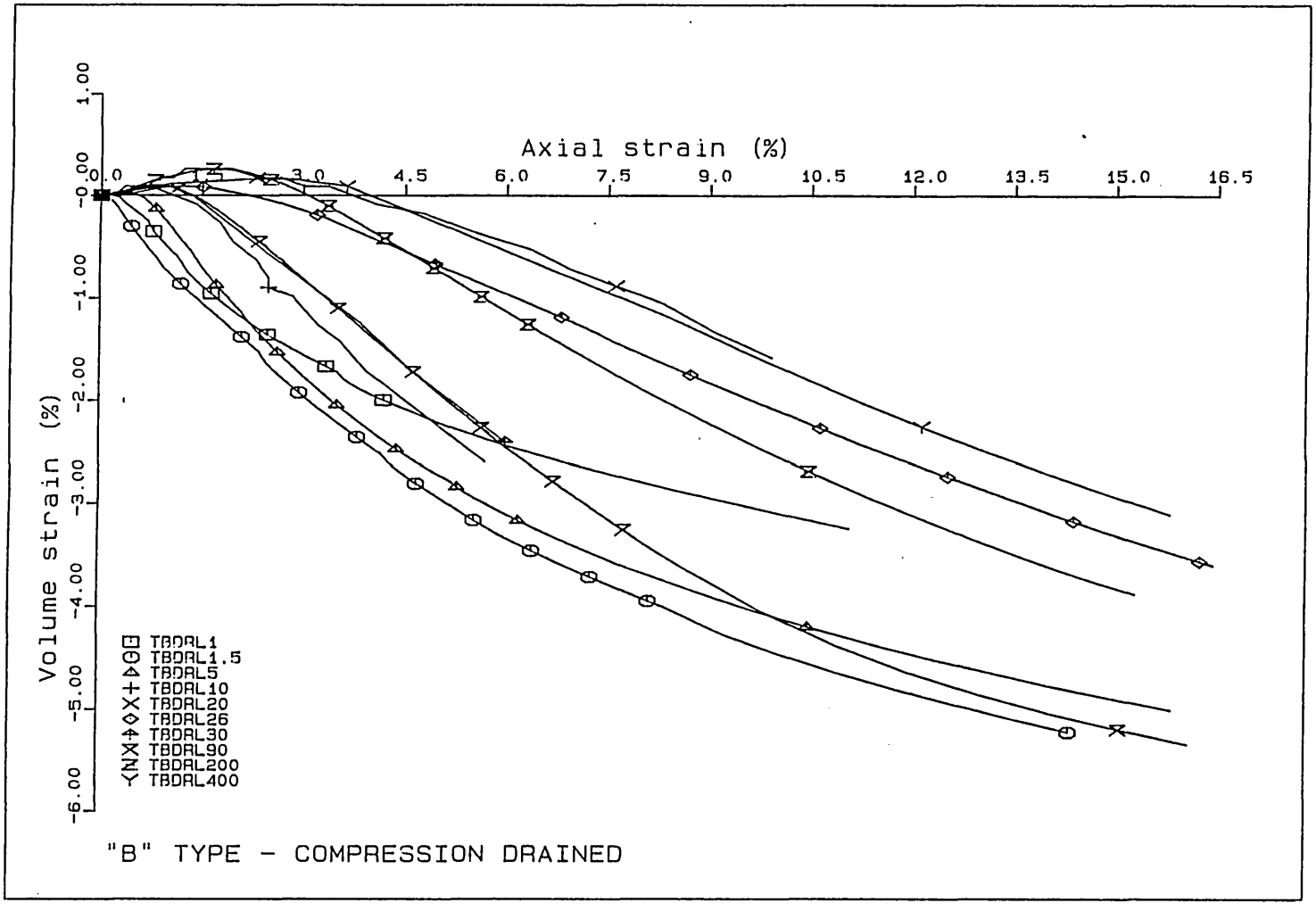
A4.B3


"B" TYPE - COMPRESSION DRAINED
TBDRL1
TBDRL1.5
TBDRL5
TBDRL10
TBDRL20
TBDRL26
TBDRL30
TBDRL90
TBDRL200
TBDRL400
sig1'/ sig3'
0.00
1.00
2.00
3.00
4.00
5.00
6.00
7.00
0.0
1.5
3.0
4.5
6.0
7.5
9.0
10.5
12.0
13.5
15.0
16.5
Axial strain (%)

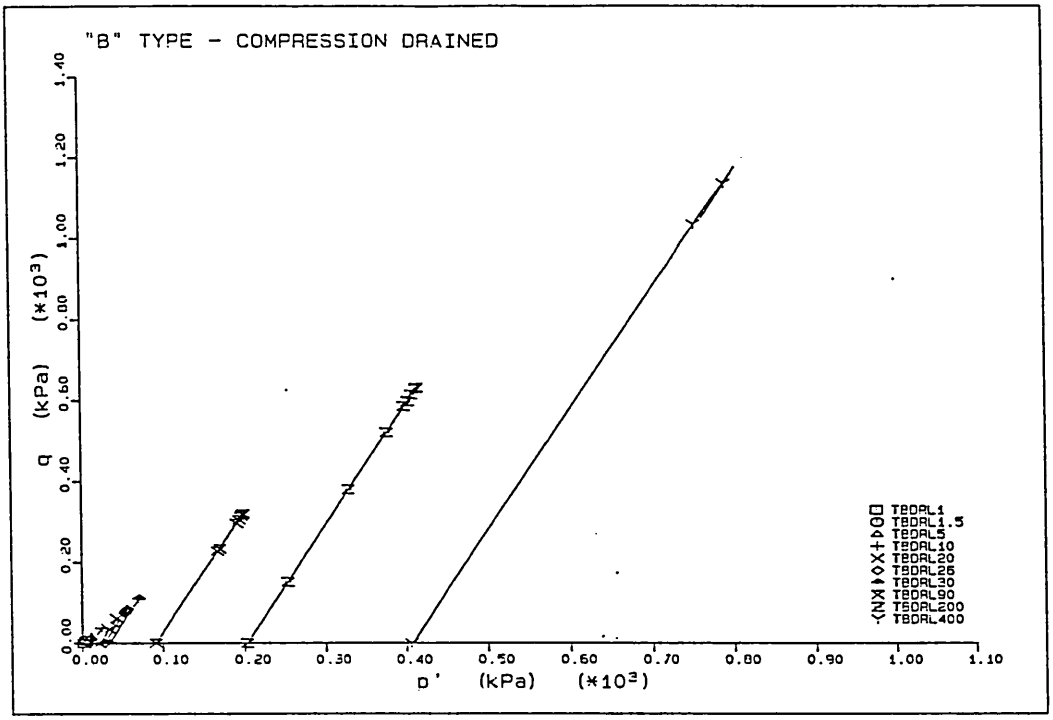
A4.B4


"B" TYPE - COMPRESSION DRAINED
TBDRL1
TBDRL1.5
TBDRL5
TBDRL10
TBDRL20
TBDRL26
TBDRL30
TBDRL90
TBDRL200
TBDRL400
sig1'/ sig3'
0.00
1.00
2.00
3.00
4.00
5.00
6.00
7.00
0.0
1.5
3.0
4.5
6.0
7.5
9.0
10.5
12.0
13.5
15.0
16.5
Shear strain (%)

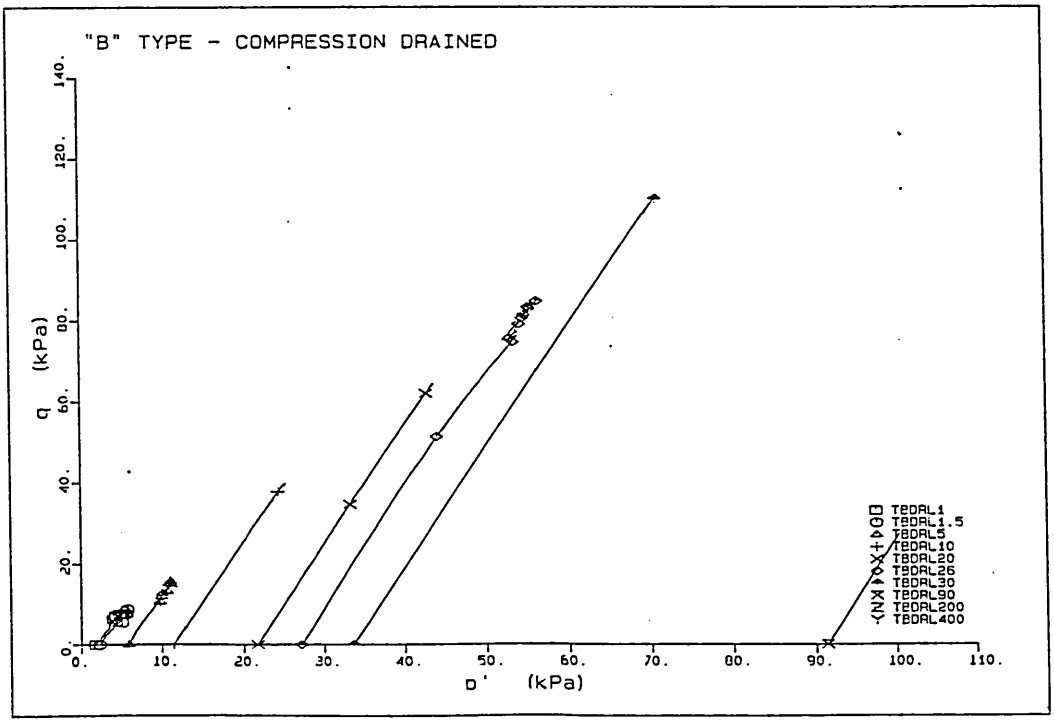
A4.B5


Axial strain (%)
0.0
3.0
4.5
6.0
7.5
9.0
10.5
12.0
13.5
15.0
16.5
Volume strain (%)
1.00
-0.00
-1.00
-2.00
-3.00
-4.00
-5.00
-6.00
TBDRL1
TBDRL1.5
TBDRL5
TBDRL10
TBDRL20
TBDRL26
TBDRL30
TBDRL90
TBDRL200
TBDRL400
"B" TYPE - COMPRESSION DRAINED

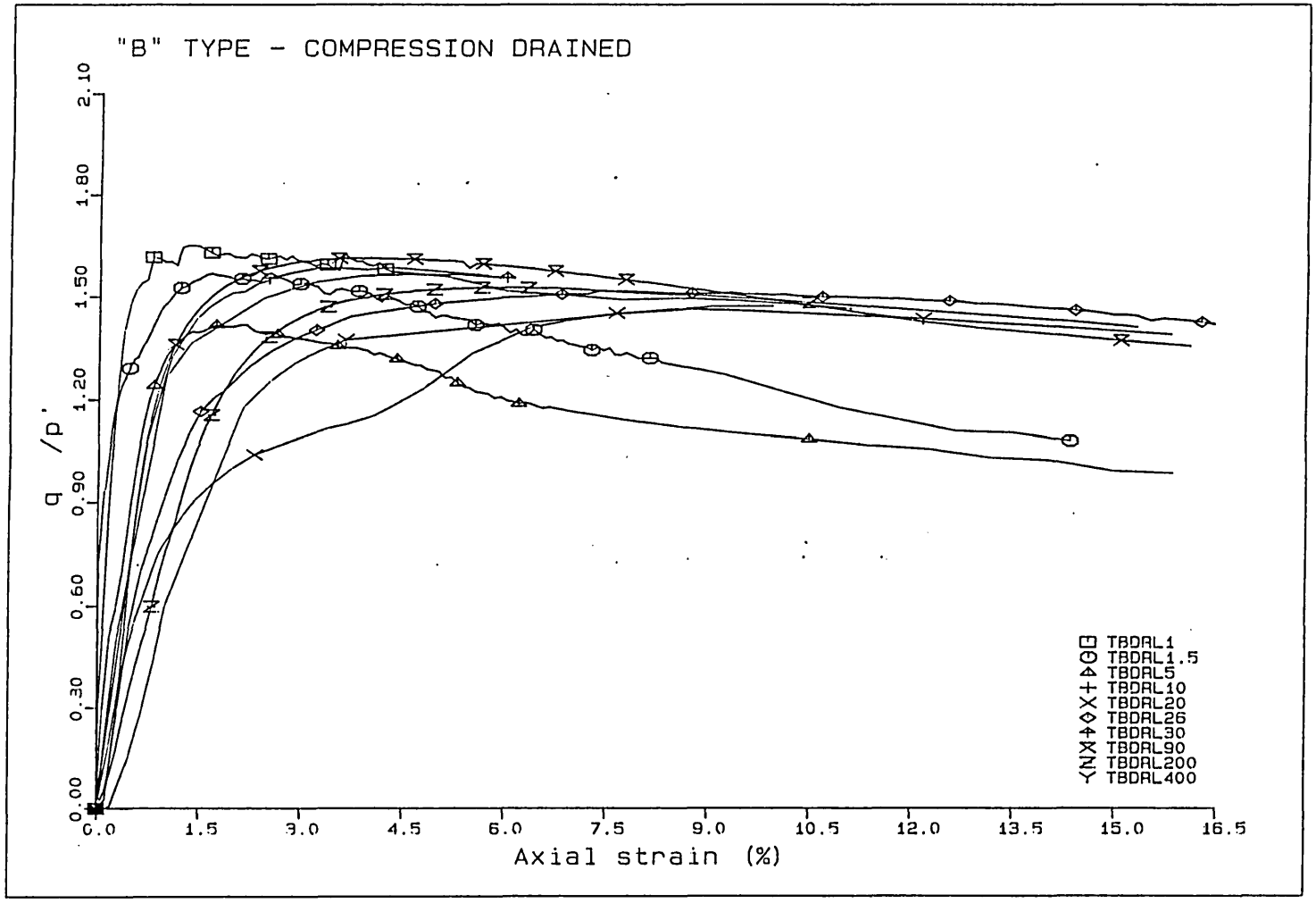
A4.B6


"B" TYPE - COMPRESSION DRAINED
q (kPa) (*10³)
p' (kPa) (*10³)
TBDRL1
TBDRL1.5
TBDRL5
TBDRL10
TBDRL20
TBDRL26
TBDRL30
TBDRL90
TBDRL200
TBDRL400

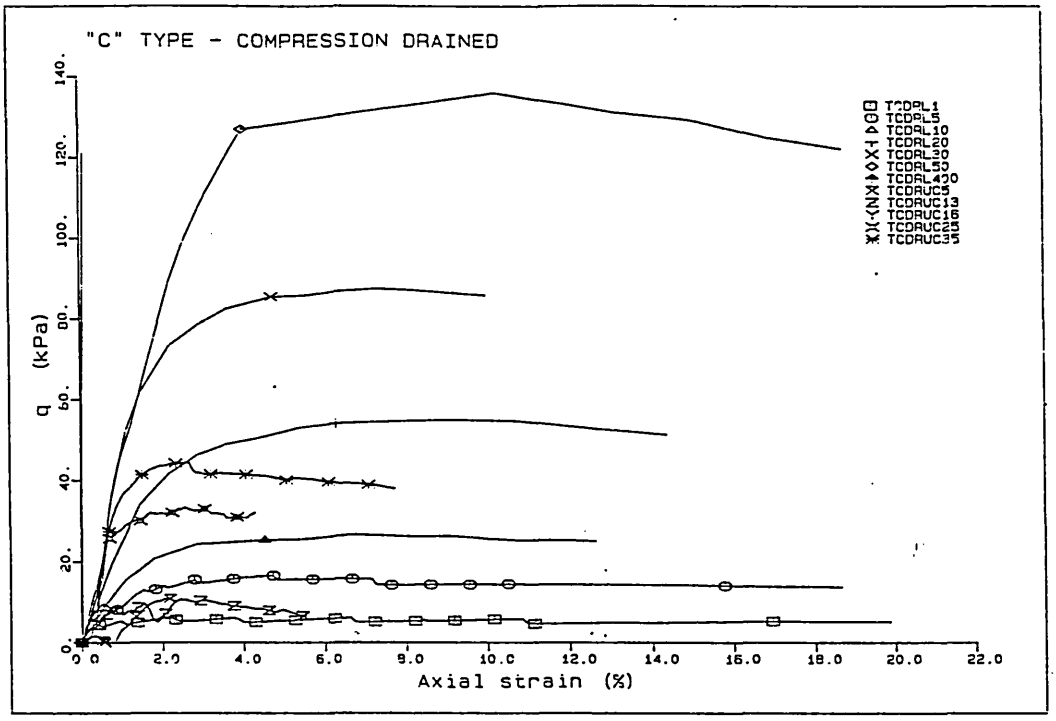
A4.B7


"B" TYPE - COMPRESSION DRAINED
q (kPa)
p' (kPa)
TBDRL1
TBDRL1.5
TBDRL5
TBDRL10
TBDRL20
TBDRL26
TBDRL30
TBDRL90
TBDRL200
TBDRL400

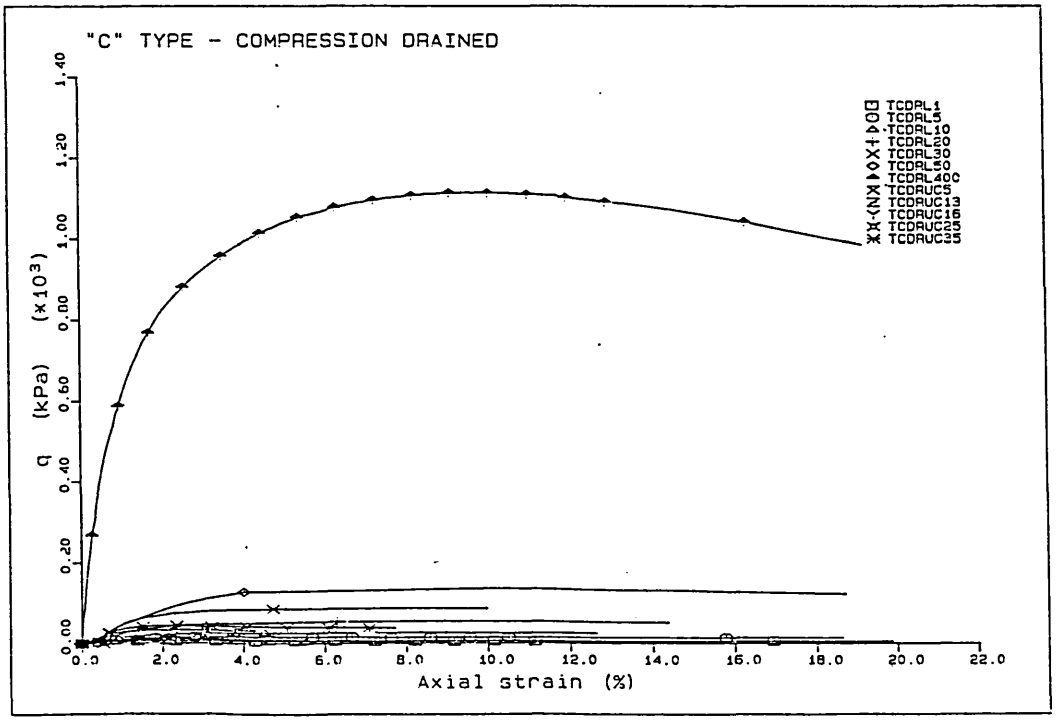
A4.B8


"B" TYPE - COMPRESSION DRAINED
q /p'
0.00
0.30
0.60
0.90
1.20
1.50
1.80
2.10
0.0
1.5
3.0
4.5
6.0
7.5
9.0
10.5
12.0
13.5
15.0
16.5
Axial strain (%)
TBDRL1
TBDRL1.5
TBDRL5
TBDRL10
TBDRL20
TBDRL26
TBDRL30
TBDRL90
TBDRL200
TBDRL400

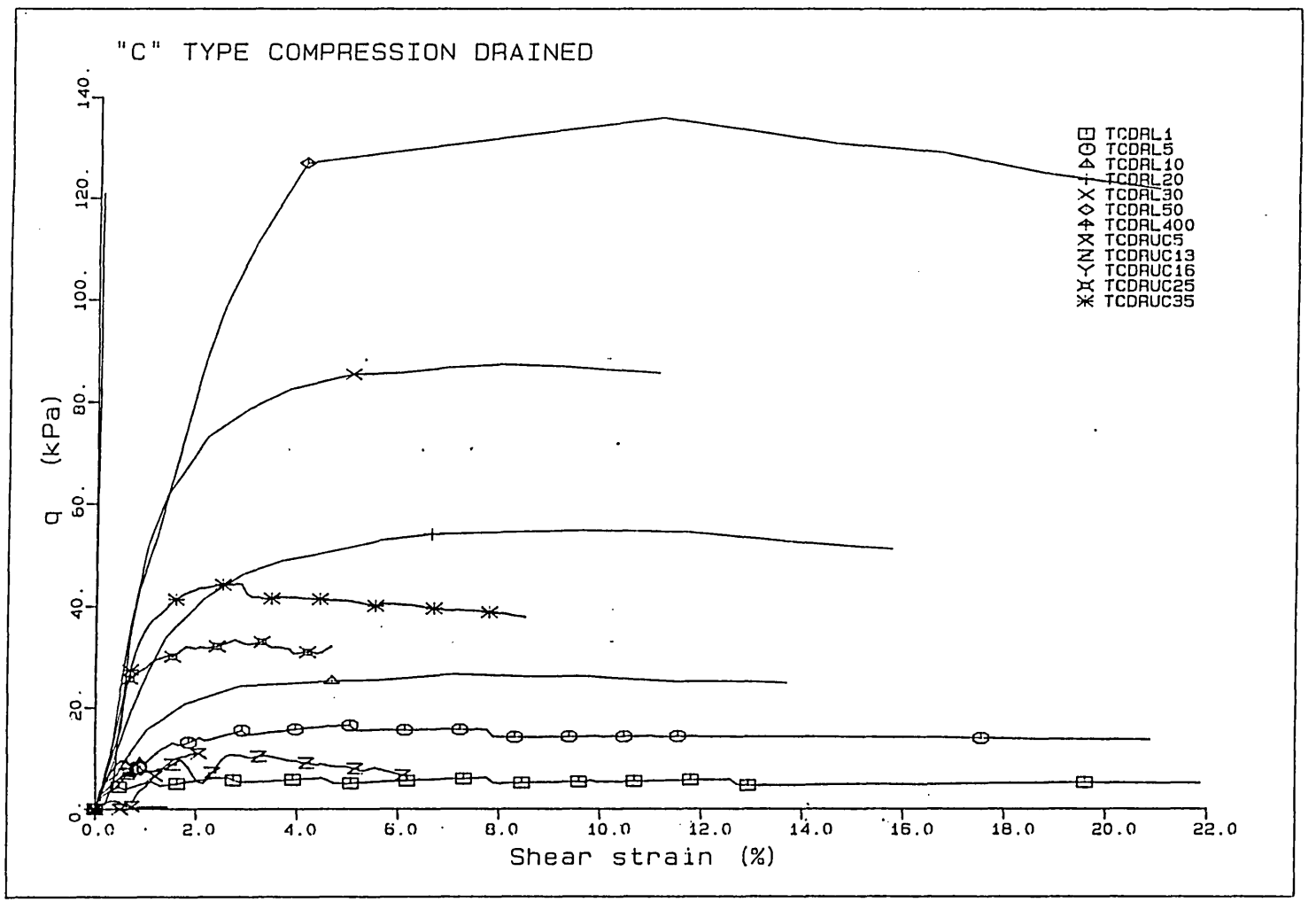
A4.B9


"C" TYPE - COMPRESSION DRAINED
q (kPa)
Axial strain (%)
TCDRL1
TCDRL5
TCDRL10
TCDRL20
TCDRL30
TCDRL50
TCDRL400
TCDRUC5
TCDRUC13
TCDRUC16
TCDRUC25
TCDRUC35

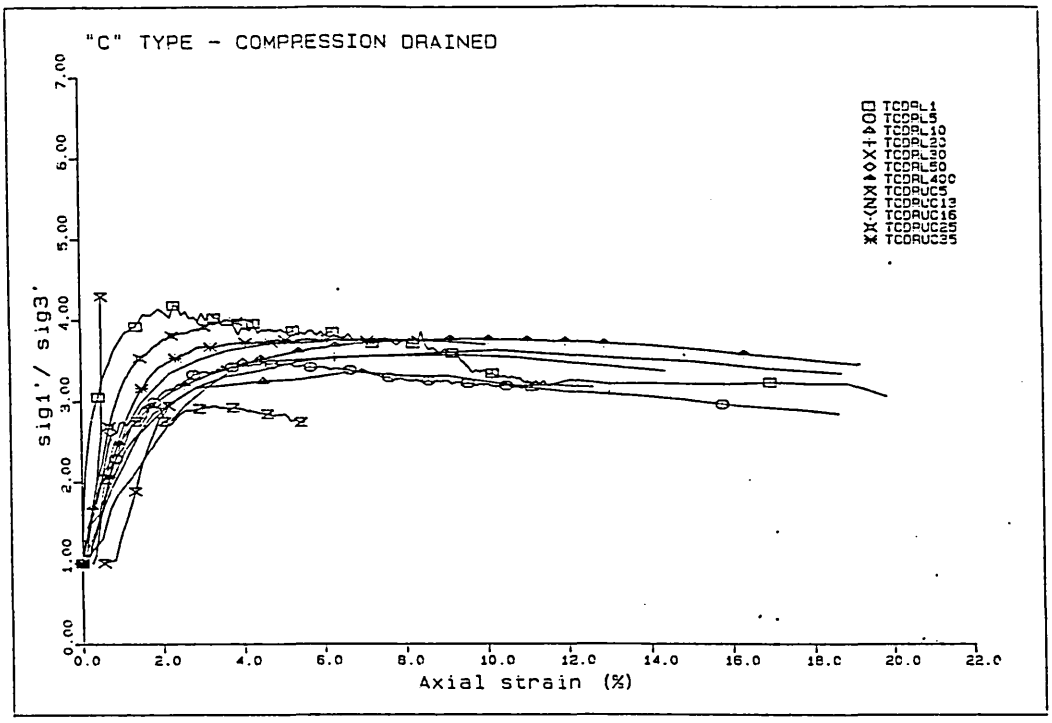
A4.C1


"C" TYPE - COMPRESSION DRAINED
q (kPa) (x10³)
Axial strain (%)
TCDRL1
TCDRL5
TCDRL10
TCDRL20
TCDRL30
TCDRL50
TCDRL400
TCDRUC5
TCDRUC13
TCDRUC16
TCDRUC25
TCDRUC35

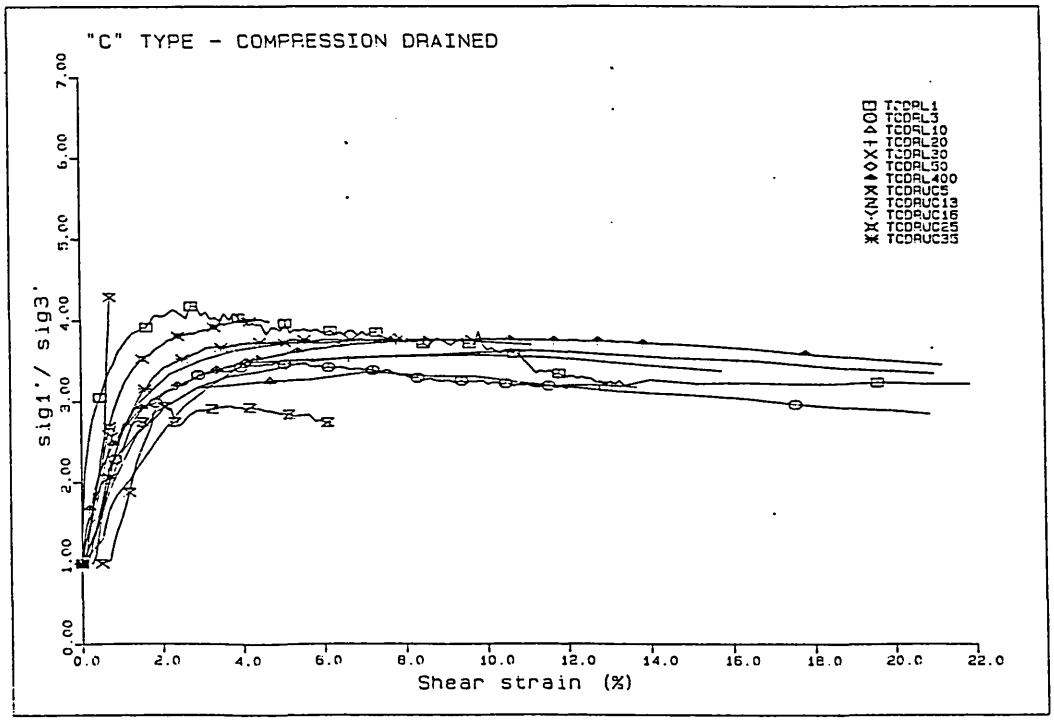
A4.C2


"C" TYPE COMPRESSION DRAINED
q (kPa)
0.
20.
40.
60.
80.
100.
120.
140.
0.0
2.0
4.0
6.0
8.0
10.0
12.0
14.0
16.0
18.0
20.0
22.0
Shear strain (%)
TCDAL1
TCDAL5
TCDAL10
TCDAL20
TCDAL30
TCDAL50
TCDAL400
TCDAUC5
TCDAUC13
TCDAUC16
TCDAUC25
TCDAUC35

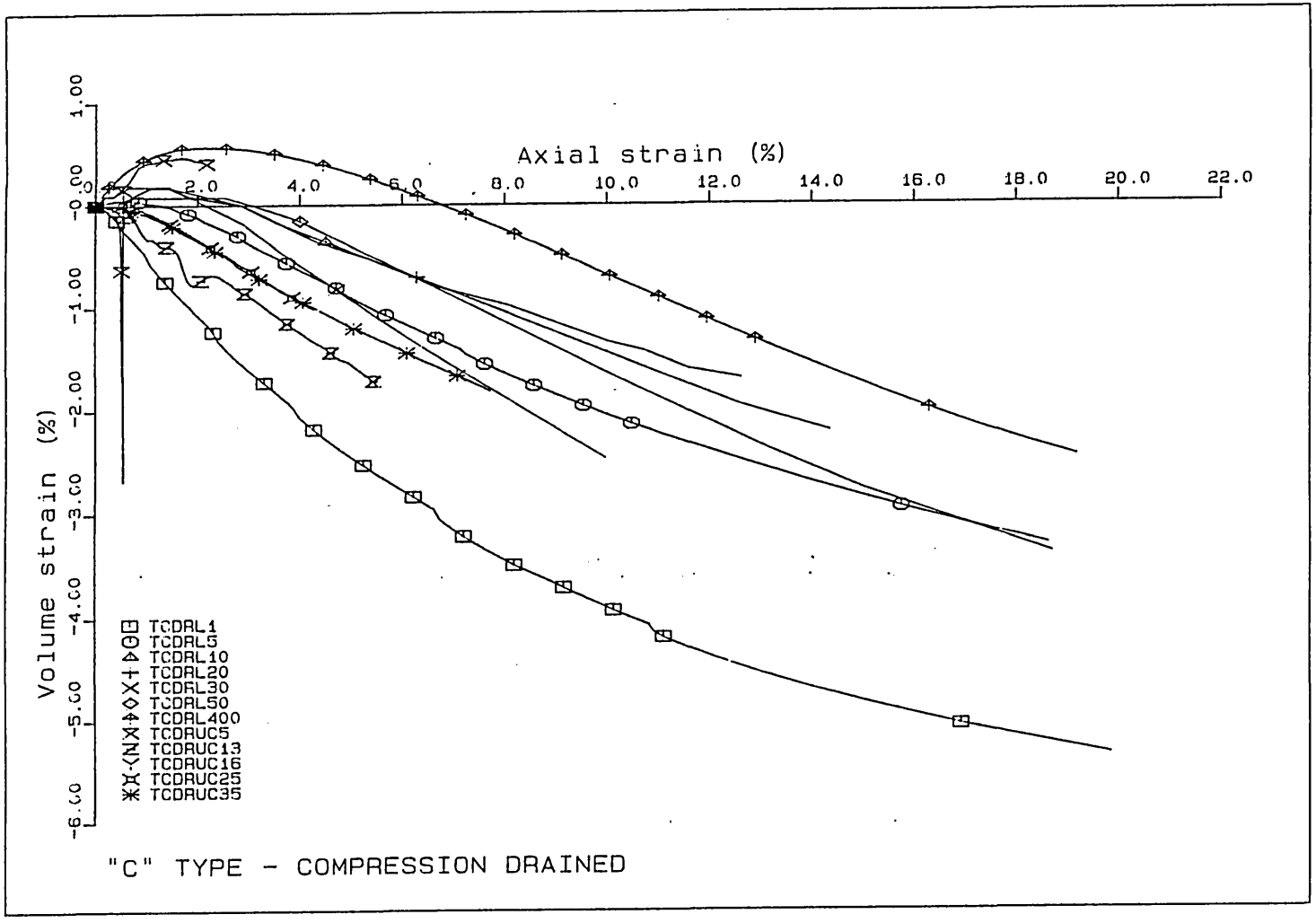
A4.C3


"C" TYPE - COMPRESSION DRAINED
sig1' / sig3'
Axial strain (%)
0.00
1.00
2.00
3.00
4.00
5.00
6.00
7.00
0.0
2.0
4.0
6.0
8.0
10.0
12.0
14.0
16.0
18.0
20.0
22.0

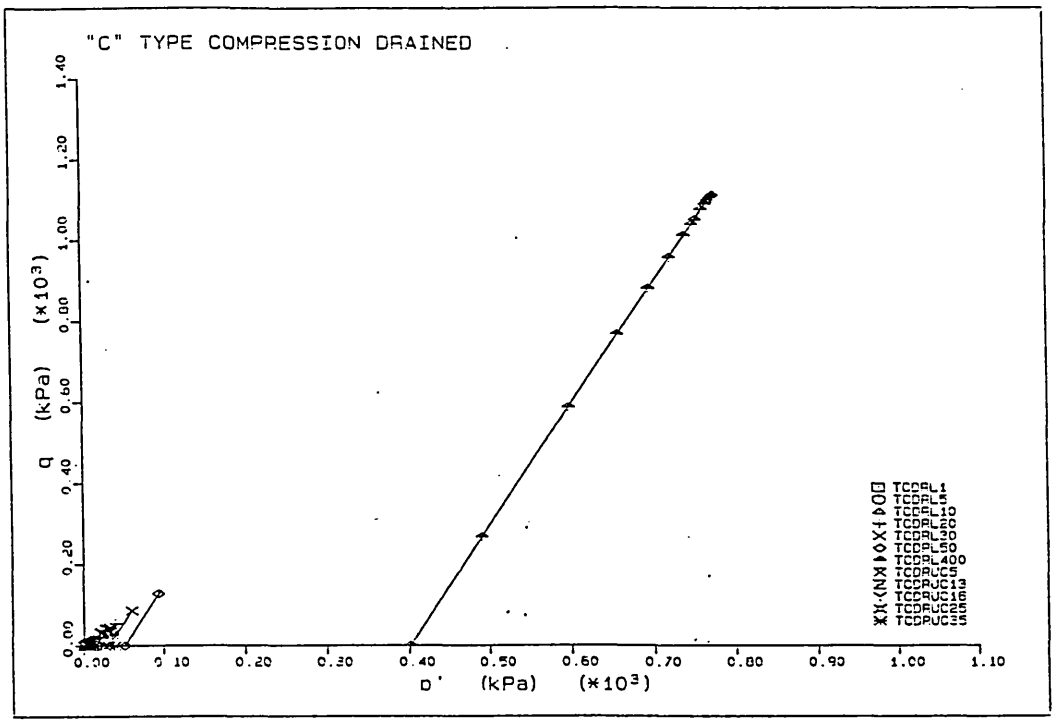
A4.C4


"C" TYPE - COMPRESSION DRAINED
sig1' / sig3'
Shear strain (%)
0.00
1.00
2.00
3.00
4.00
5.00
6.00
7.00
0.0
2.0
4.0
6.0
8.0
10.0
12.0
14.0
16.0
18.0
20.0
22.0

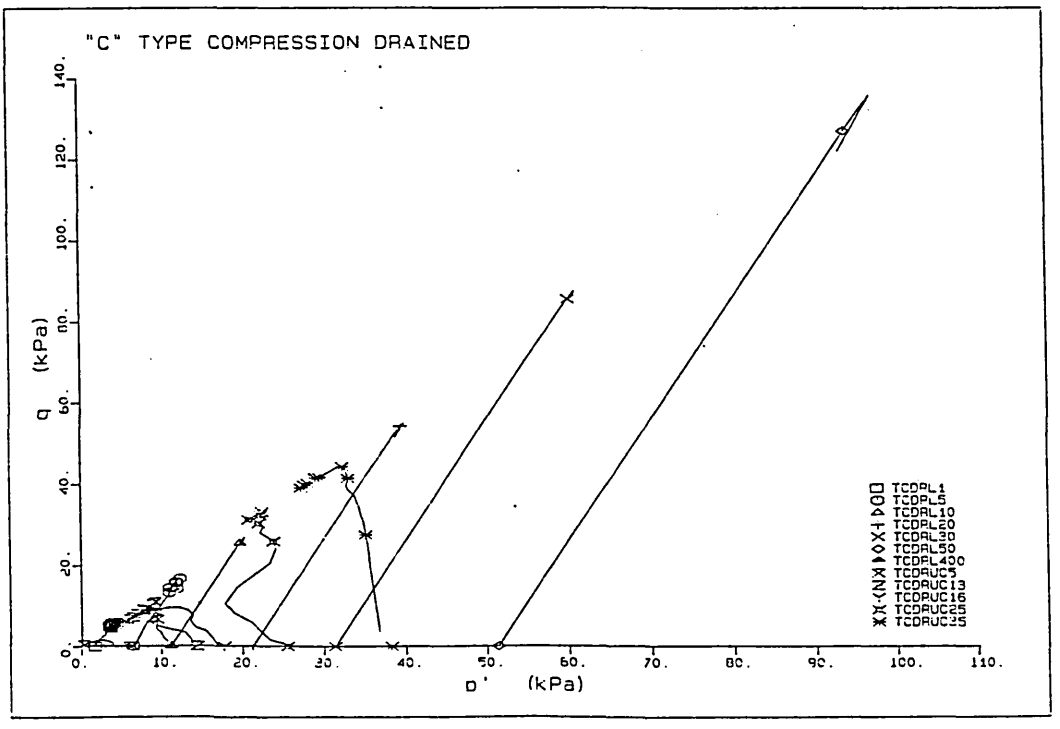
A4.C5


Axial strain (%)
2.0
4.0
6.0
8.0
10.0
12.0
14.0
16.0
18.0
20.0
22.0
Volume strain (%)
1.00
-0.00
-1.00
-2.00
-3.00
-4.00
-5.00
-6.00
TCDRL1
TCDRL5
TCDRL10
TCDRL20
TCDRL30
TCDRL50
TCDRL400
TCDRUC5
TCDRUC13
TCDRUC16
TCDRUC25
TCDRUC35
"C" TYPE - COMPRESSION DRAINED

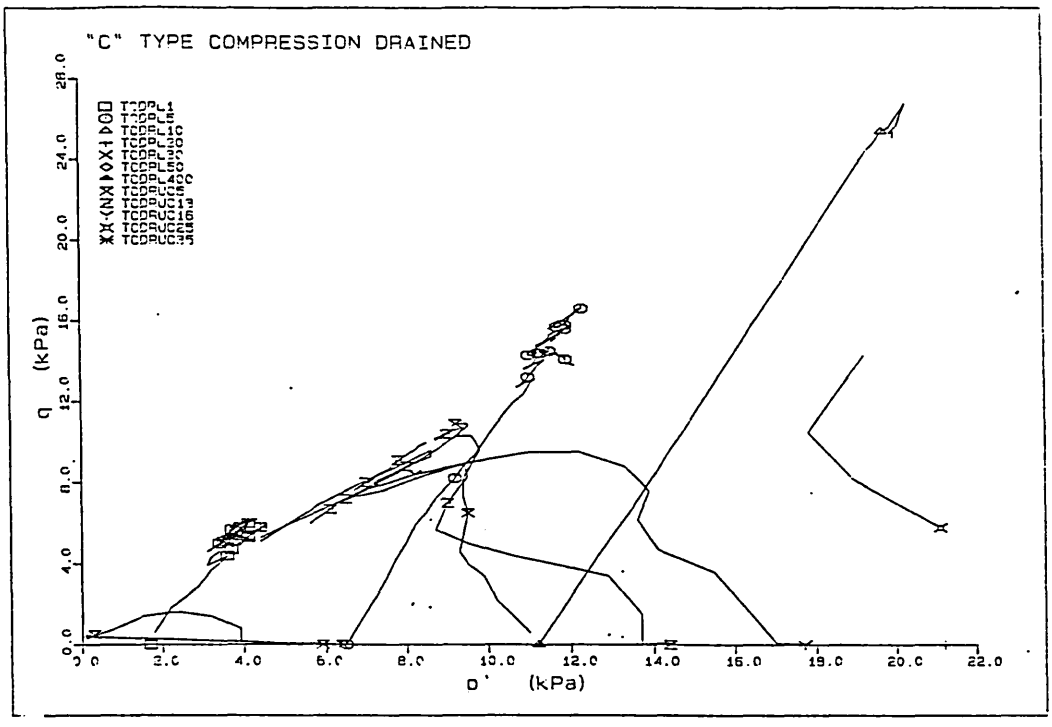
A4.C6


"C" TYPE COMPRESSION DRAINED
q (kPa) (*10³)
p' (kPa) (*10³)
TCDPL1
TCDPL5
TCDPL10
TCDPL20
TCDPL30
TCDPL50
TCDPL400
TCDPUC5
TCDPUC13
TCDPUC16
TCDPUC25
TCDPUC35

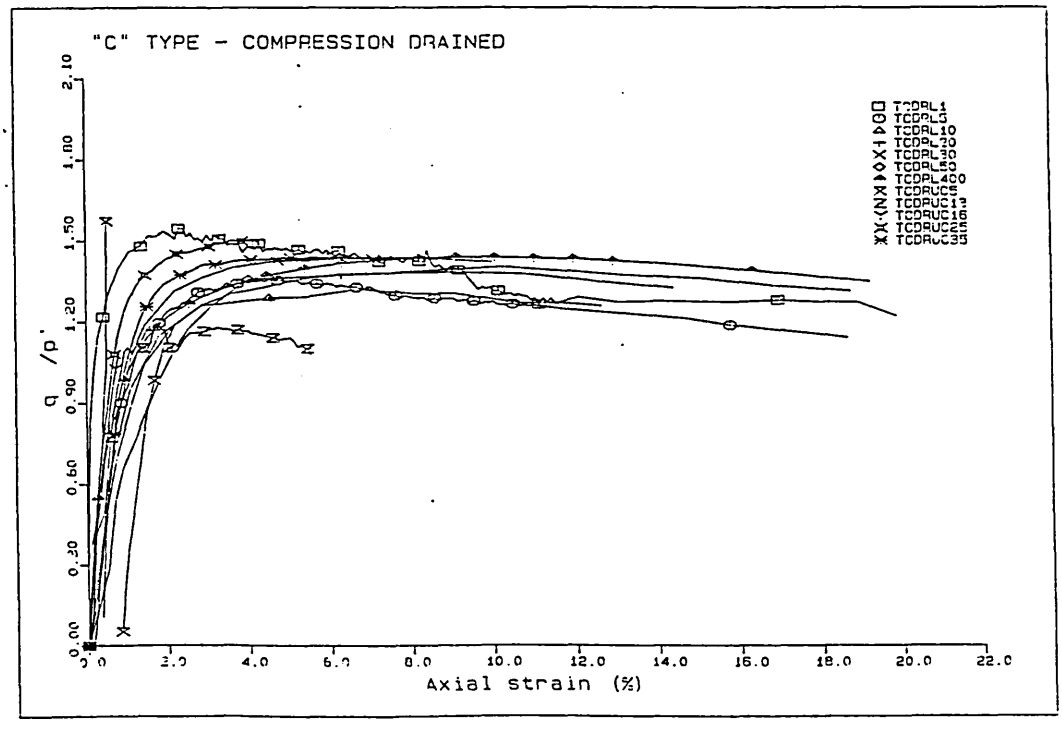
A4.C7


"C" TYPE COMPRESSION DRAINED
q (kPa)
p' (kPa)
TCDPL1
TCDPL5
TCDPL10
TCDPL20
TCDPL30
TCDPL50
TCDPL400
TCDPUC5
TCDPUC13
TCDPUC16
TCDPUC25
TCDPUC35

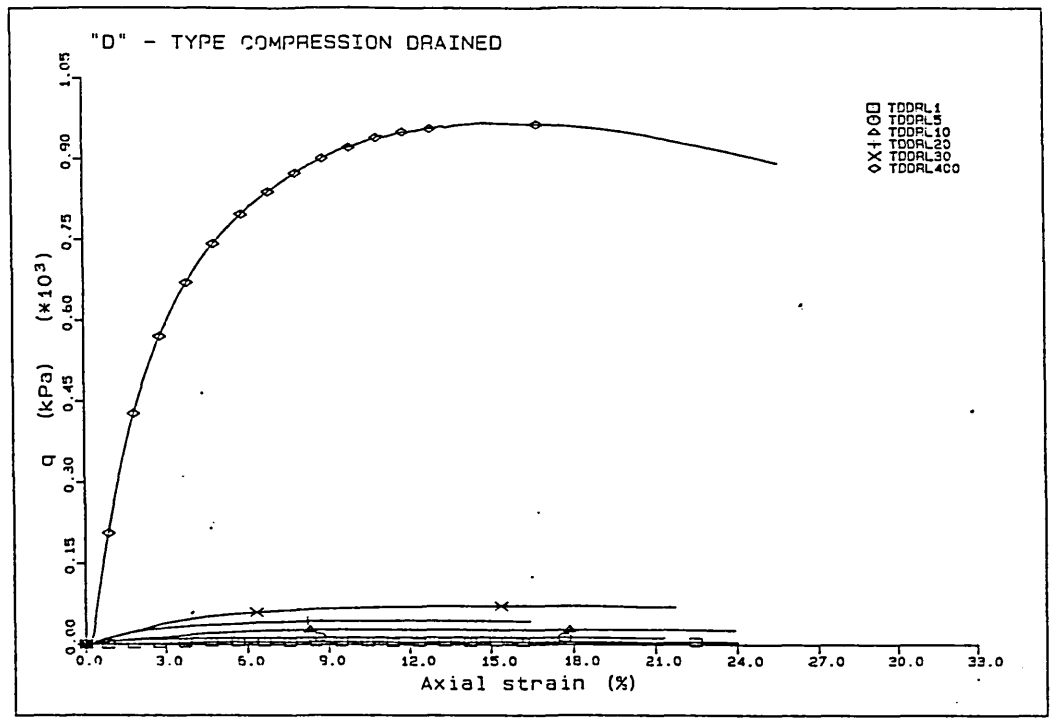
A4.C8


"C" TYPE COMPRESSION DRAINED
q (kPa)
p' (kPa)

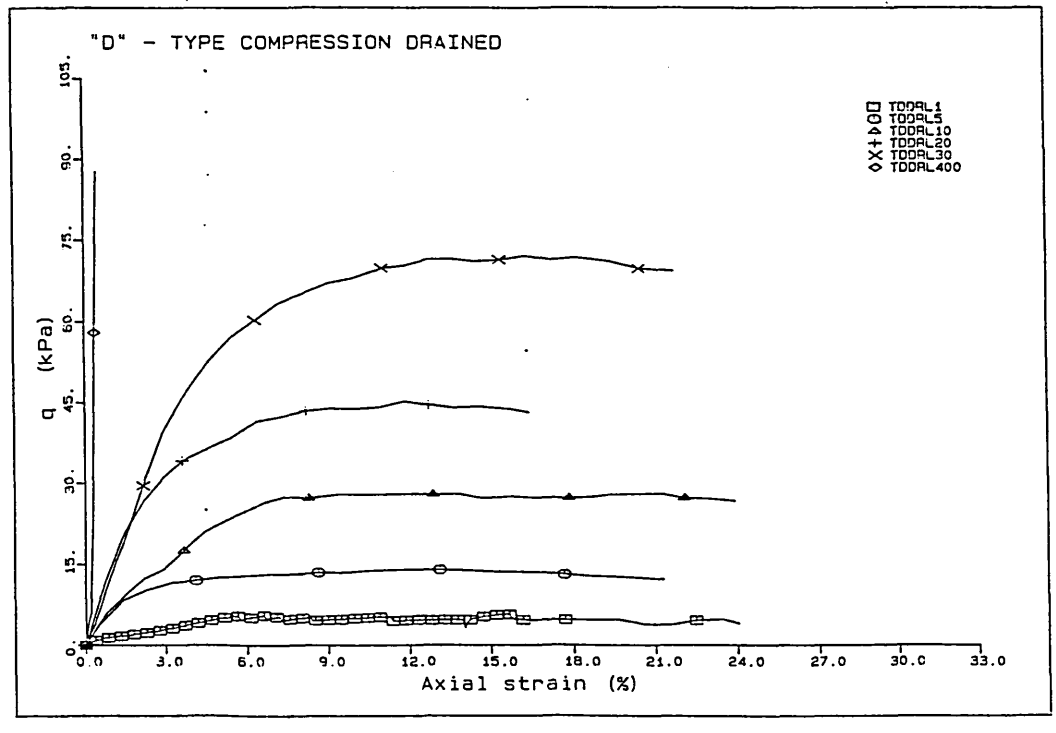
A4.C9


"C" TYPE - COMPRESSION DRAINED
q /p'
Axial strain (%)

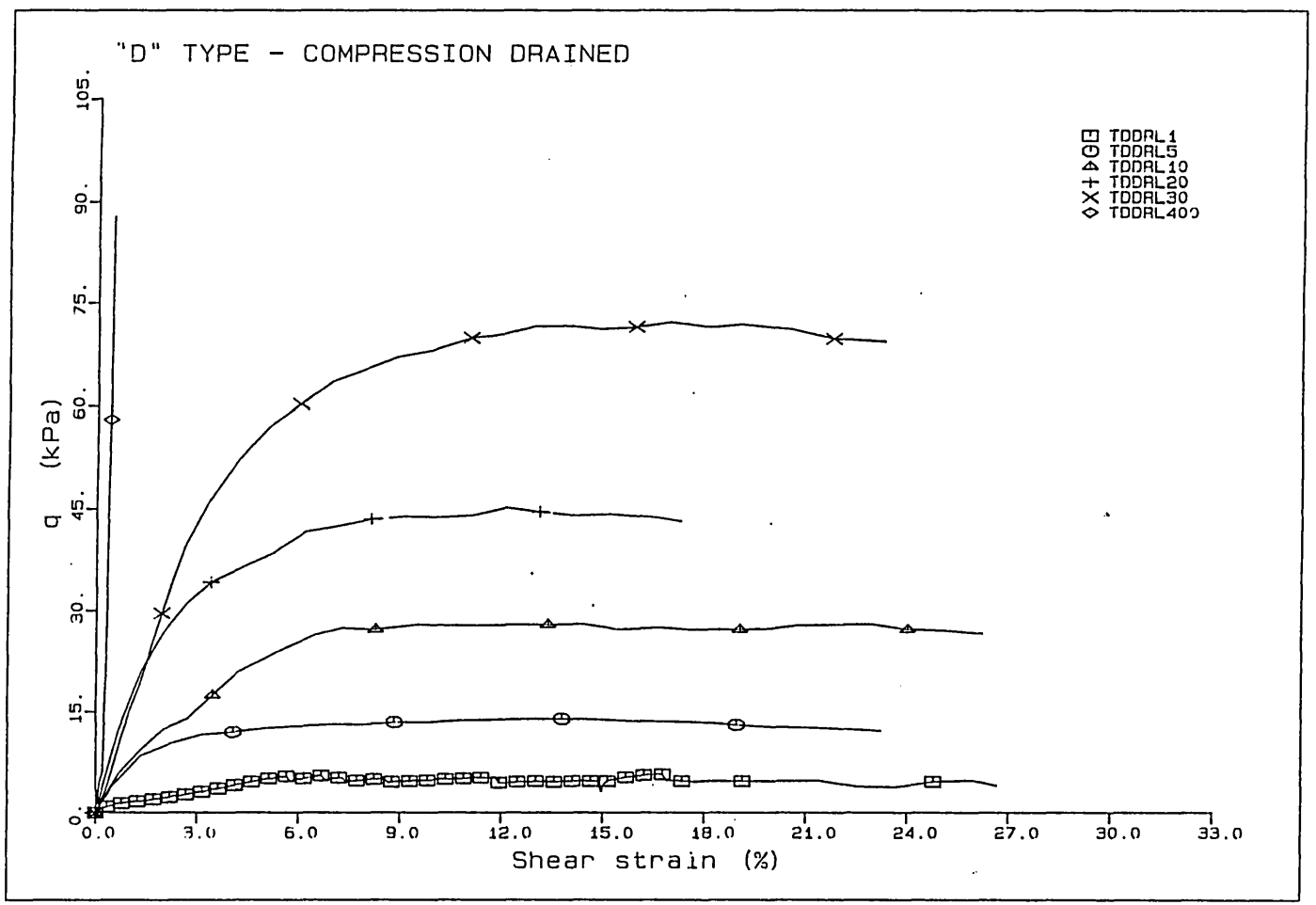
A4.C10


"D" - TYPE COMPRESSION DRAINED
q (kPa) (*10³)
0.00
0.15
0.30
0.45
0.60
0.75
0.90
1.05
0.0
3.0
6.0
9.0
12.0
15.0
18.0
21.0
24.0
27.0
30.0
33.0
Axial strain (%)
TDDRL1
TDDRL5
TDDRL10
TDDRL20
TDDRL30
TDDRL400

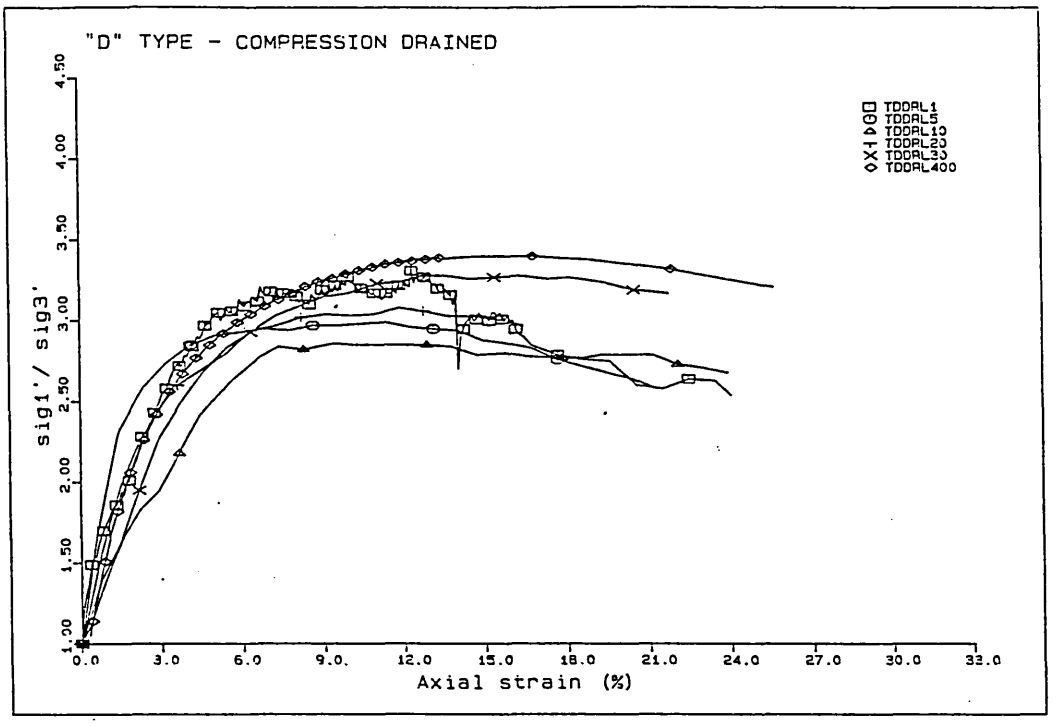
A4.D1


"D" - TYPE COMPRESSION DRAINED
q (kPa)
0.
15.
30.
45.
60.
75.
90.
105.
0.0
3.0
6.0
9.0
12.0
15.0
18.0
21.0
24.0
27.0
30.0
33.0
Axial strain (%)
TDDRL1
TDDRL5
TDDRL10
TDDRL20
TDDRL30
TDDRL400

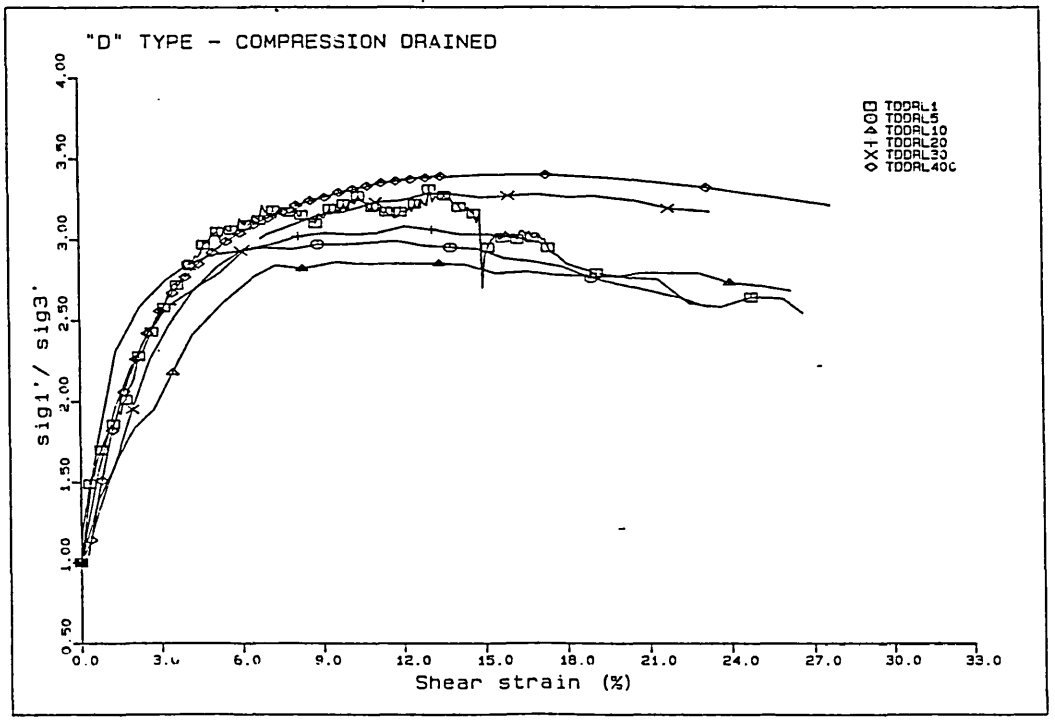
A4.D2


"D" TYPE - COMPRESSION DRAINED
TDDRL1
TDDRL5
TDDRL10
TDDRL20
TDDRL30
TDDRL40
q (kPa)
0.
15.
30.
45.
60.
75.
90.
105.
0.0
3.0
6.0
9.0
12.0
15.0
18.0
21.0
24.0
27.0
30.0
33.0
Shear strain (%)

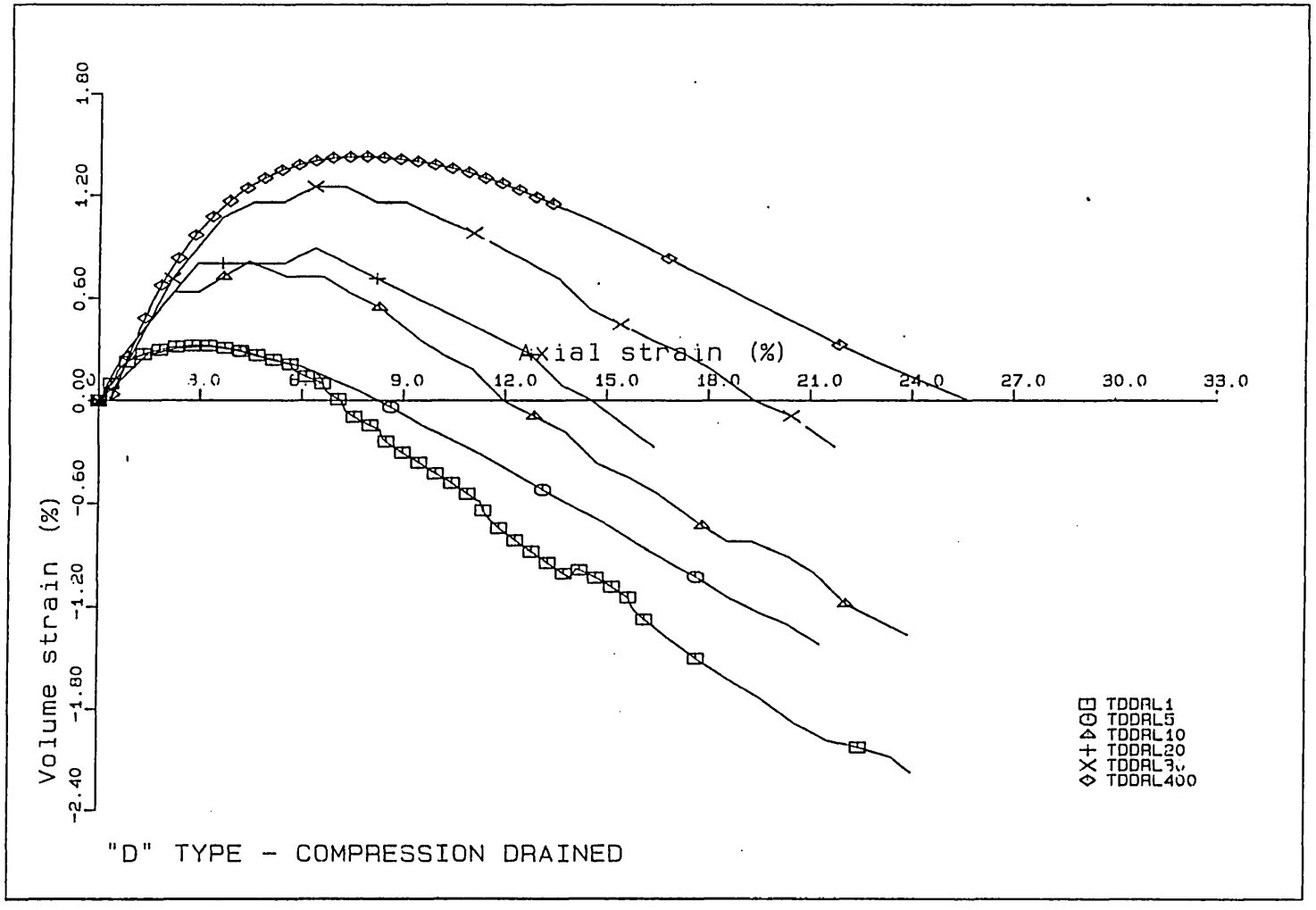
A4.D3


"D" TYPE - COMPRESSION DRAINED
TDDRL1
TDDRL5
TDDRL10
TDDRL20
TDDRL30
TDDRL400
sig1'/ sig3'
1.00
1.50
2.00
2.50
3.00
3.50
4.00
4.50
0.0
3.0
6.0
9.0
12.0
15.0
18.0
21.0
24.0
27.0
30.0
33.0
Axial strain (%)

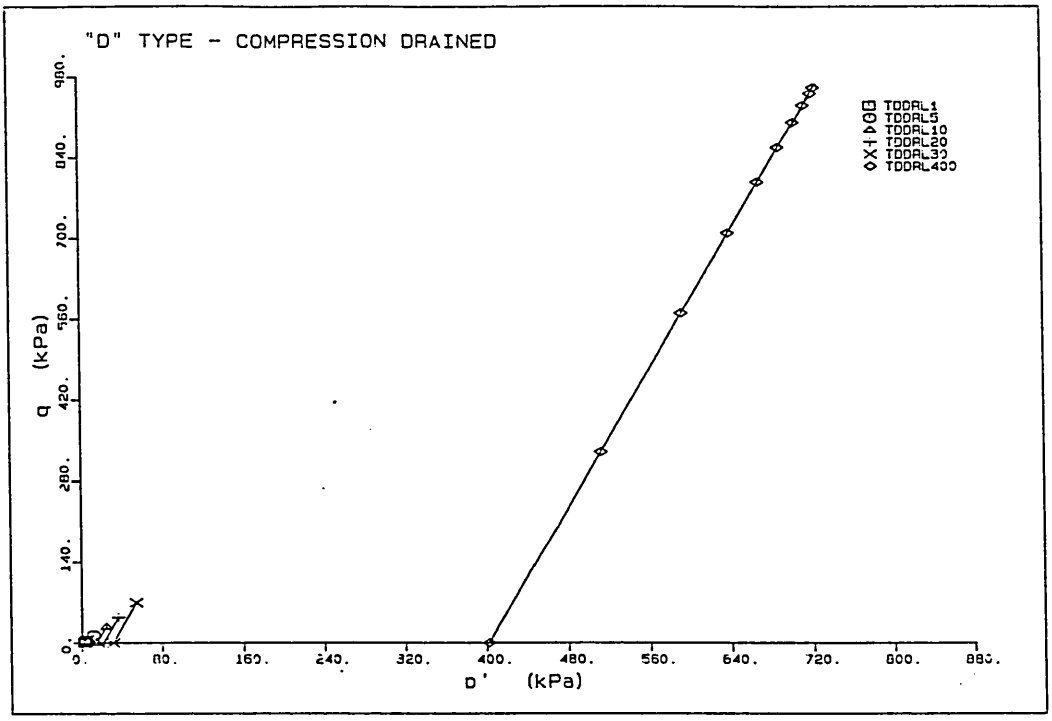
A4.D4


"D" TYPE - COMPRESSION DRAINED
TDDRL1
TDDRL5
TDDRL10
TDDRL20
TDDRL30
TDDRL400
sig1'/ sig3'
0.50
1.00
1.50
2.00
2.50
3.00
3.50
4.00
0.0
6.0
9.0
12.0
15.0
18.0
21.0
24.0
27.0
30.0
33.0
Shear strain (%)

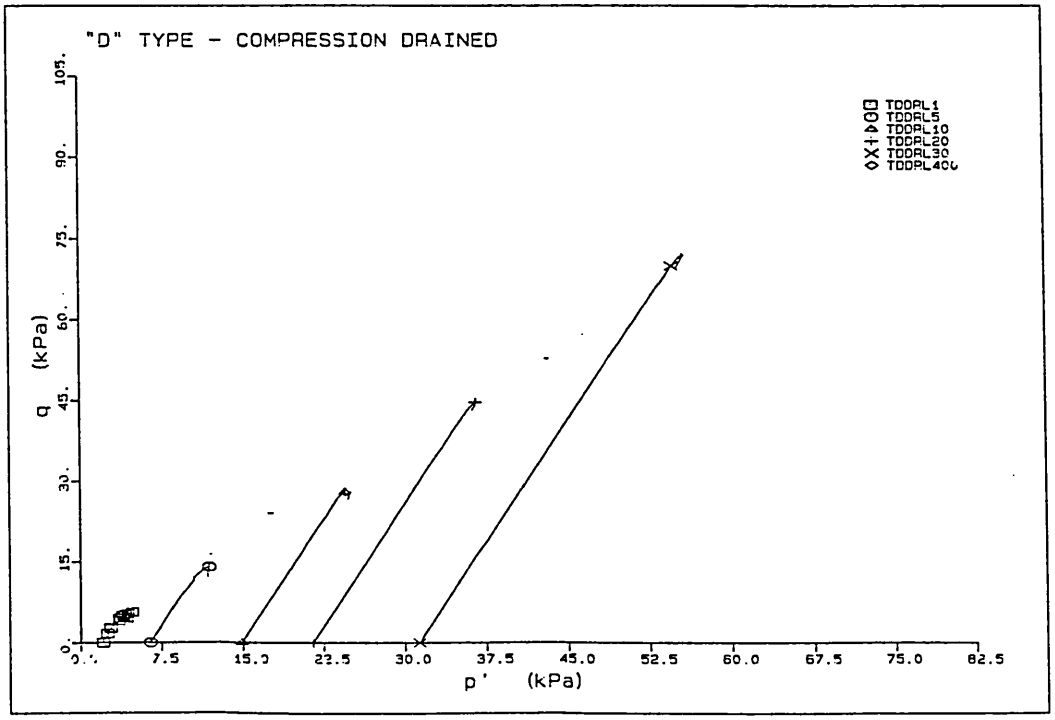
A4.D5


Axial strain (%)
3.0
6.0
9.0
12.0
15.0
18.0
21.0
24.0
27.0
30.0
33.0
Volume strain (%)
1.80
1.20
0.60
0.00
-0.60
-1.20
-1.80
-2.40
TDDRL1
TDDRL5
TDDRL10
TDDRL20
TDDRL400
"D" TYPE - COMPRESSION DRAINED

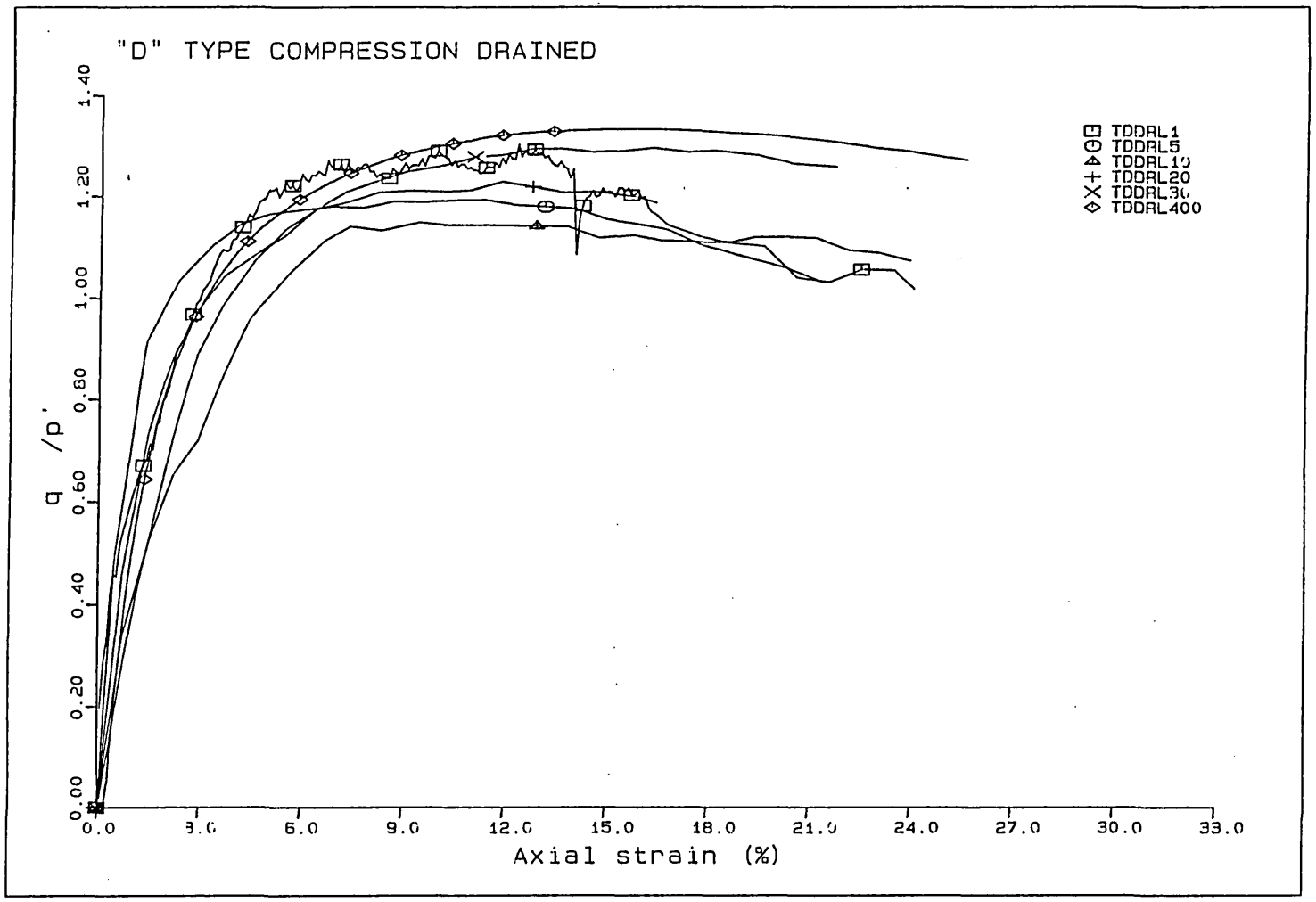
A4.D6


"D" TYPE - COMPRESSION DRAINED
TDDRL1
TDDRL5
TDDRL10
TDDRL20
TDDRL30
TDDRL400
q (kPa)
p' (kPa)

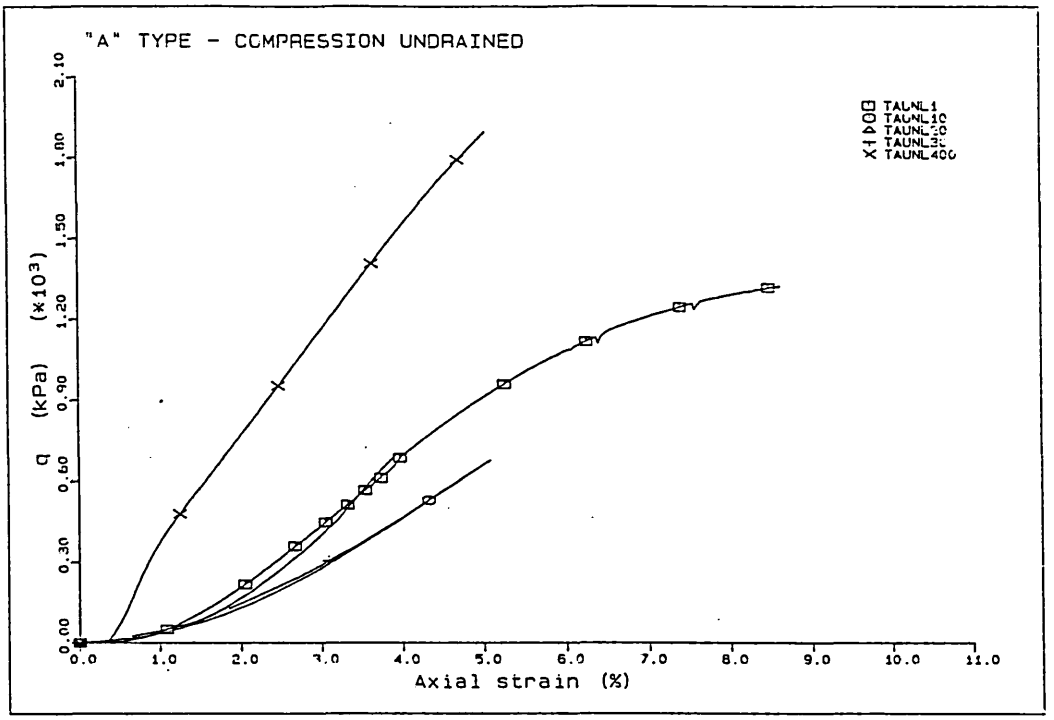
A4.D7


"D" TYPE - COMPRESSION DRAINED
TDDRL1
TDDRL5
TDDRL10
TDDRL20
TDDRL30
TDDRL400
q (kPa)
p' (kPa)

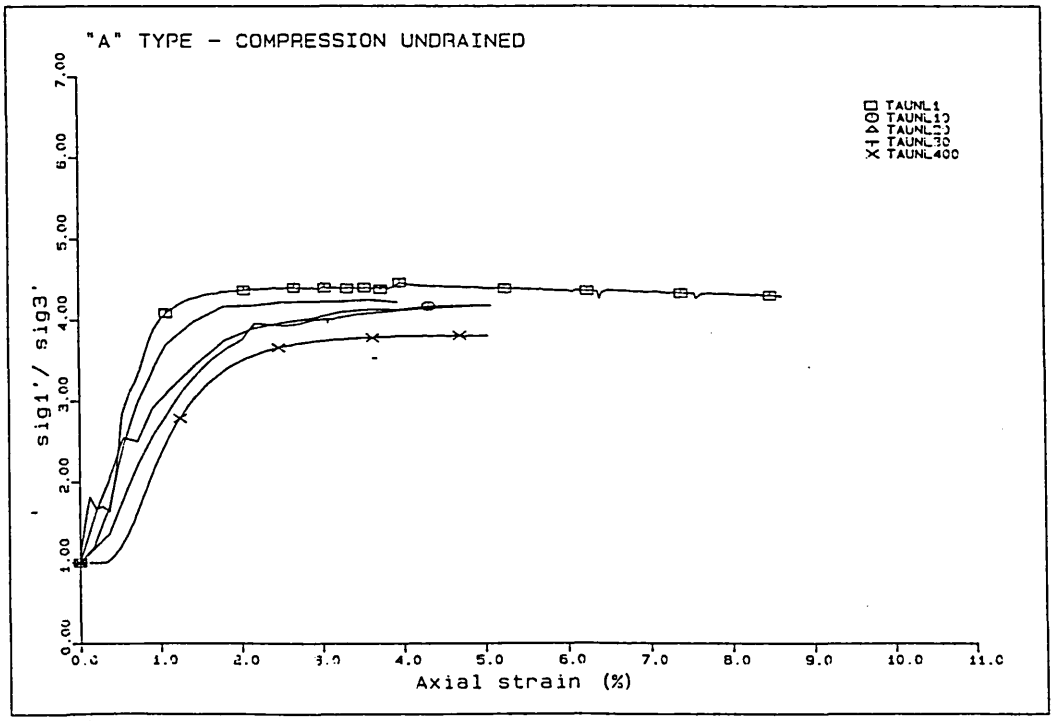
A4.D8


"D" TYPE COMPRESSION DRAINED
q /p'
0.00
0.20
0.40
0.60
0.80
1.00
1.20
1.40
0.0
3.0
6.0
9.0
12.0
15.0
18.0
21.0
24.0
27.0
30.0
33.0
Axial strain (%)
TDDRL1
TDDRL5
TDDRL10
TDDRL20
TDDRL30
TDDRL400

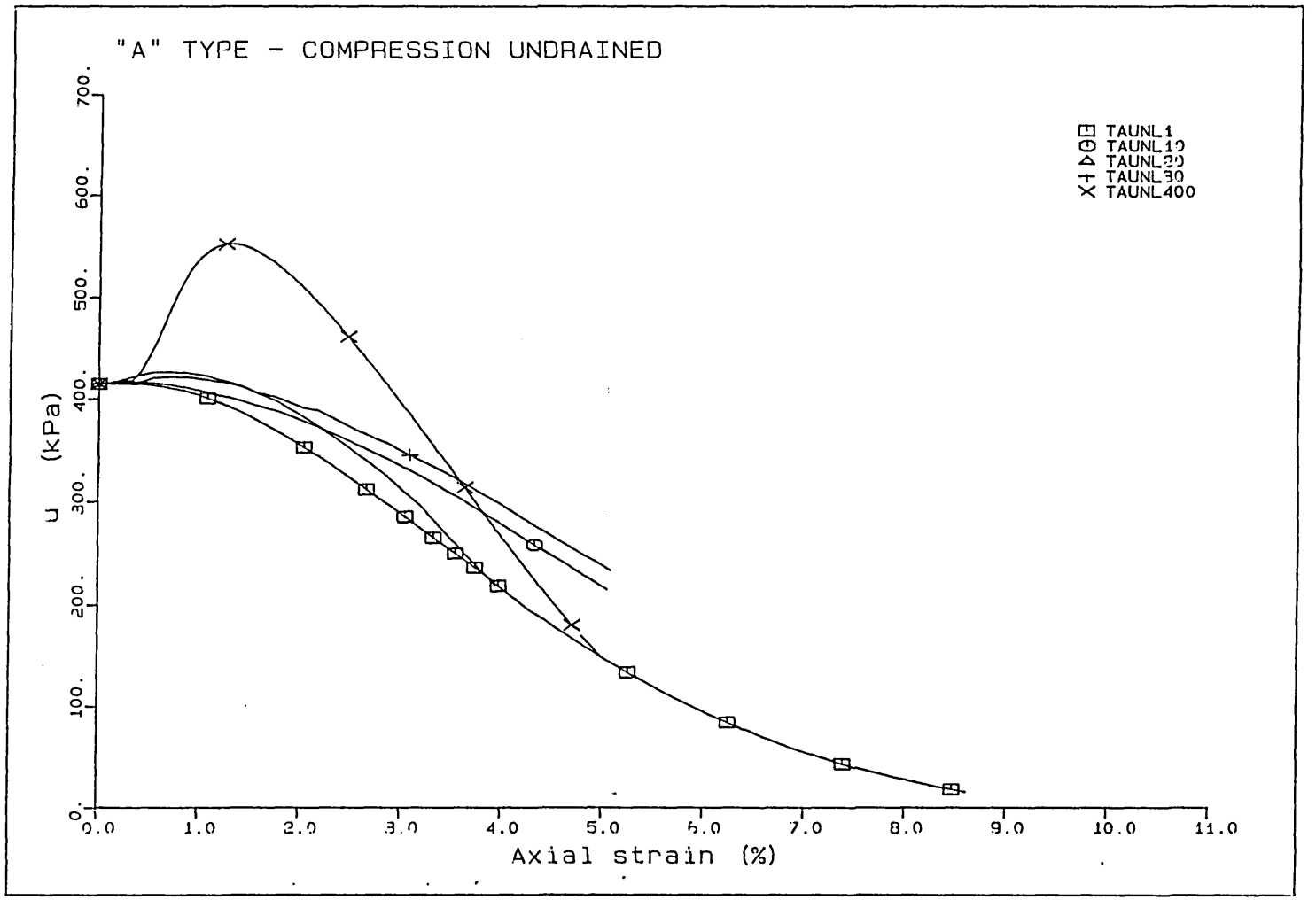
A4.D9


"A" TYPE - COMPRESSION UNDRAINED
q (kPa) (*10³)
Axial strain (%)
TAUNL1
TAUNL10
TAUNL30
TAUNL400

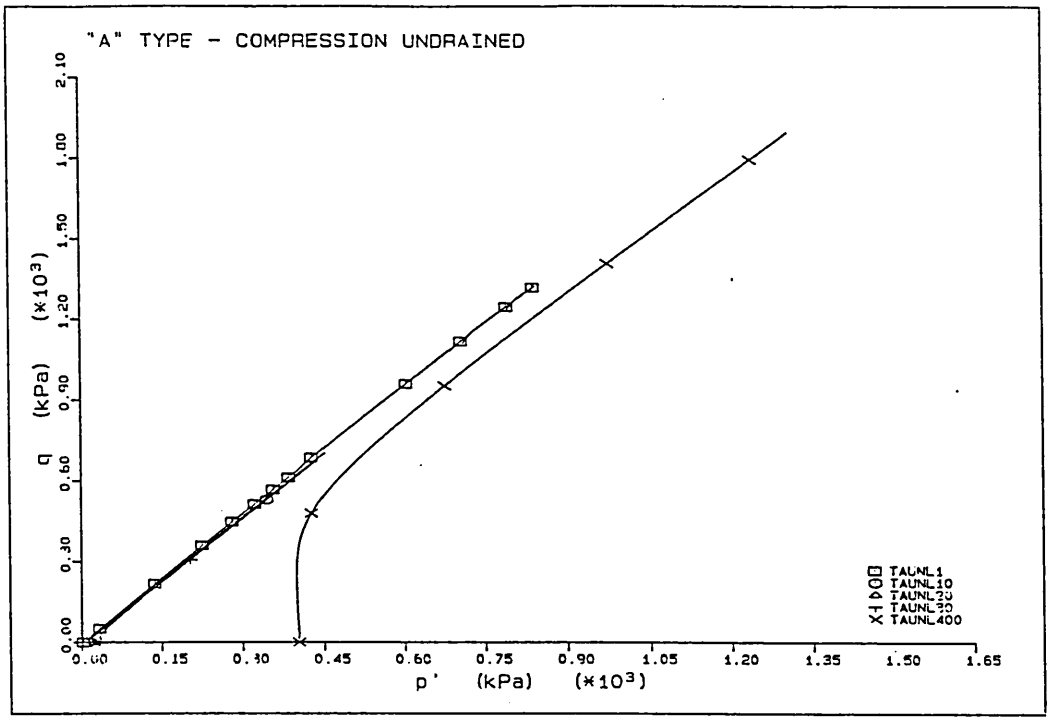
A4.E1


"A" TYPE - COMPRESSION UNDRAINED
sig1'/ sig3'
Axial strain (%)
TAUNL1
TAUNL10
TAUNL30
TAUNL400

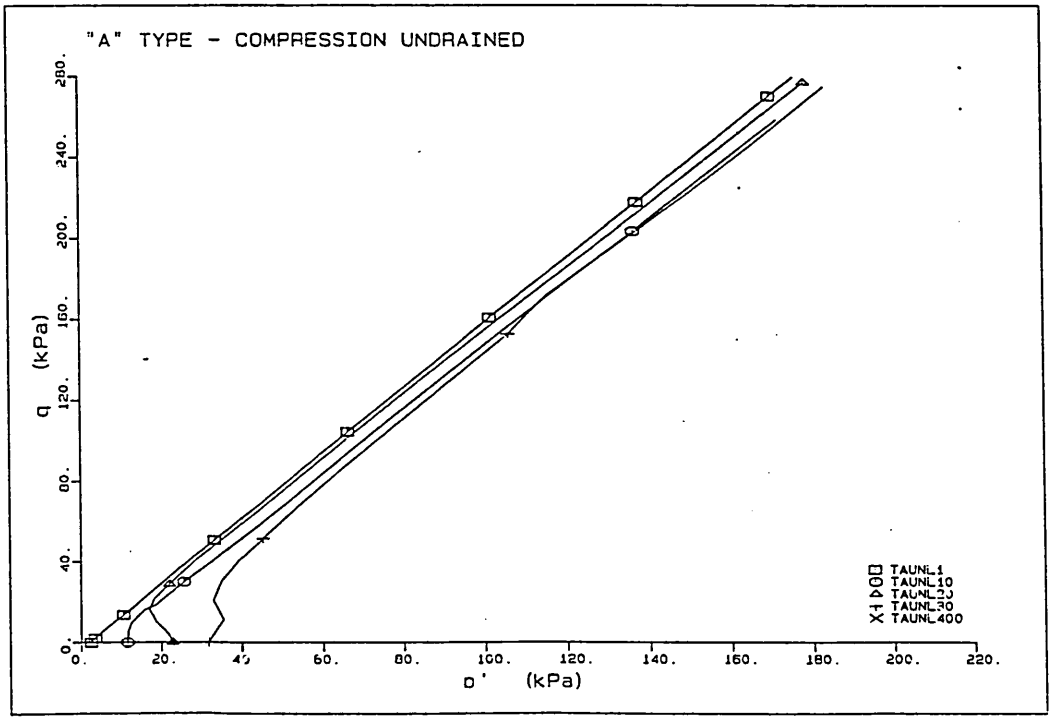
A4.E2


"A" TYPE - COMPRESSION UNDRAINED
TAUNL1
TAUNL10
TAUNL20
TAUNL30
TAUNL400
u (kPa)
0.
100.
200.
300.
400.
500.
600.
700.
0.0
1.0
2.0
3.0
4.0
5.0
6.0
7.0
8.0
9.0
10.0
11.0
Axial strain (%)

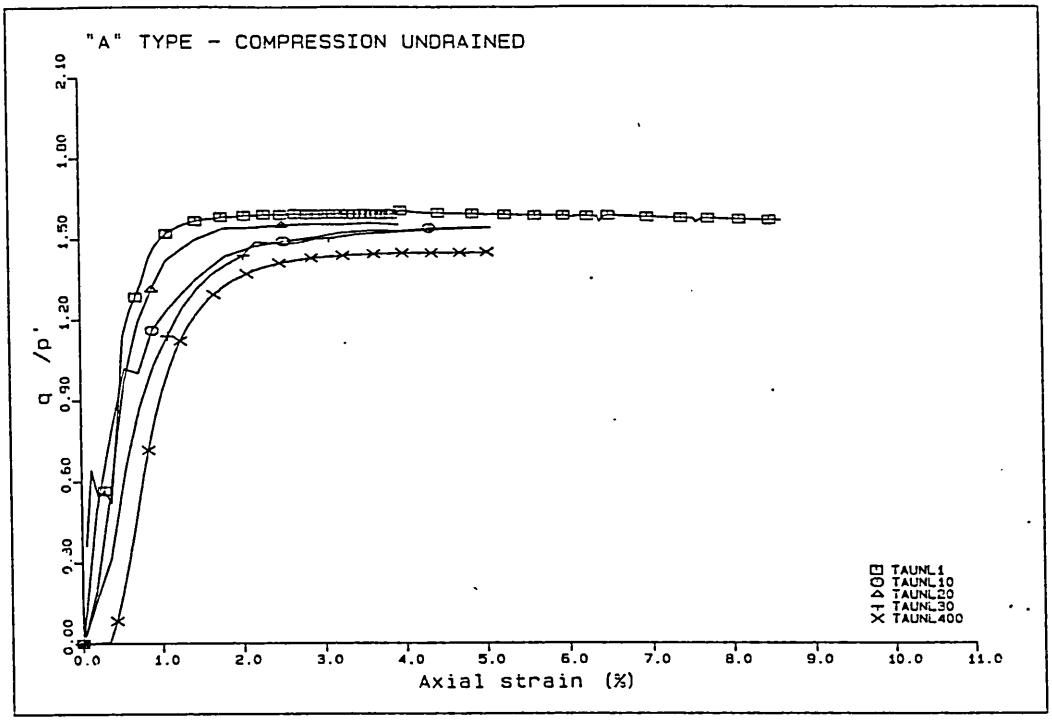
A4.E3


"A" TYPE - COMPRESSION UNDRAINED
q (kPa) (*10³)
p' (kPa) (*10³)
TAUNL1
TAUNL10
TAUNL20
TAUNL30
TAUNL400

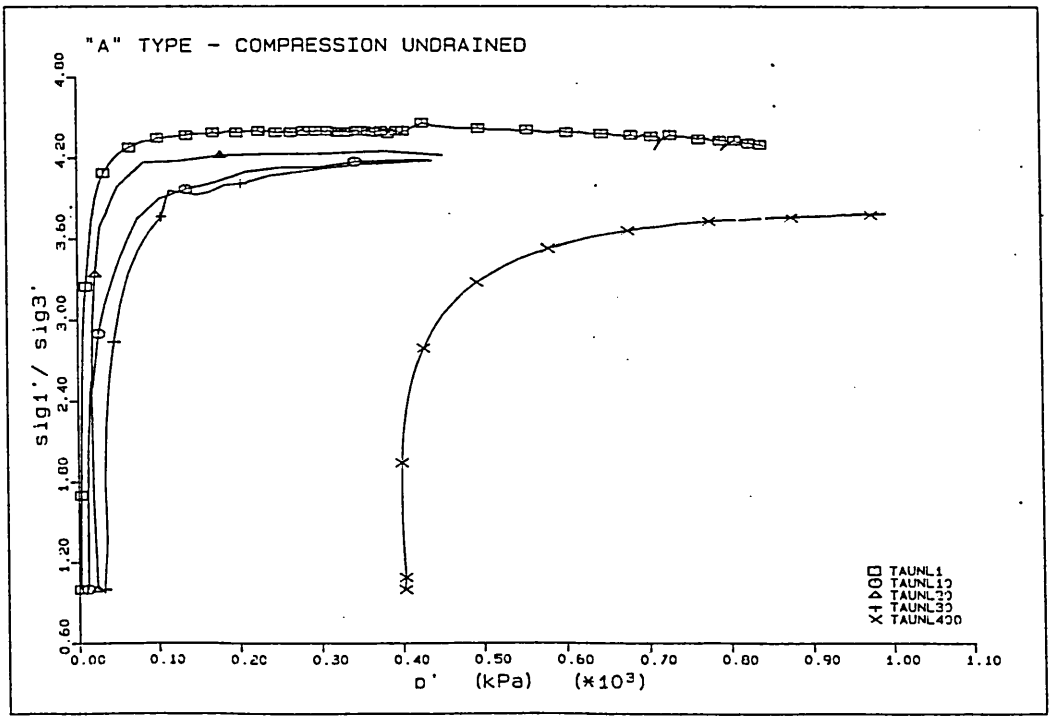
A4.E4


"A" TYPE - COMPRESSION UNDRAINED
q (kPa)
p' (kPa)
TAUNL1
TAUNL10
TAUNL20
TAUNL30
TAUNL400

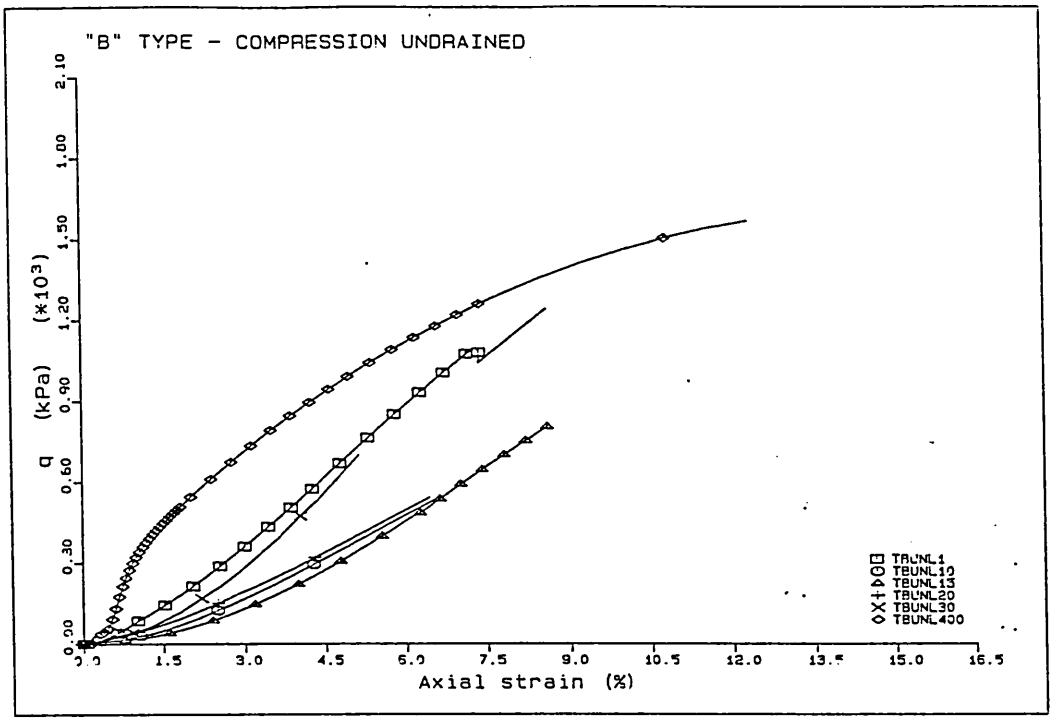
A4.E5


"A" TYPE - COMPRESSION UNDRAINED
q /p'
Axial strain (%)
TAUNL1
TAUNL10
TAUNL20
TAUNL30
TAUNL400

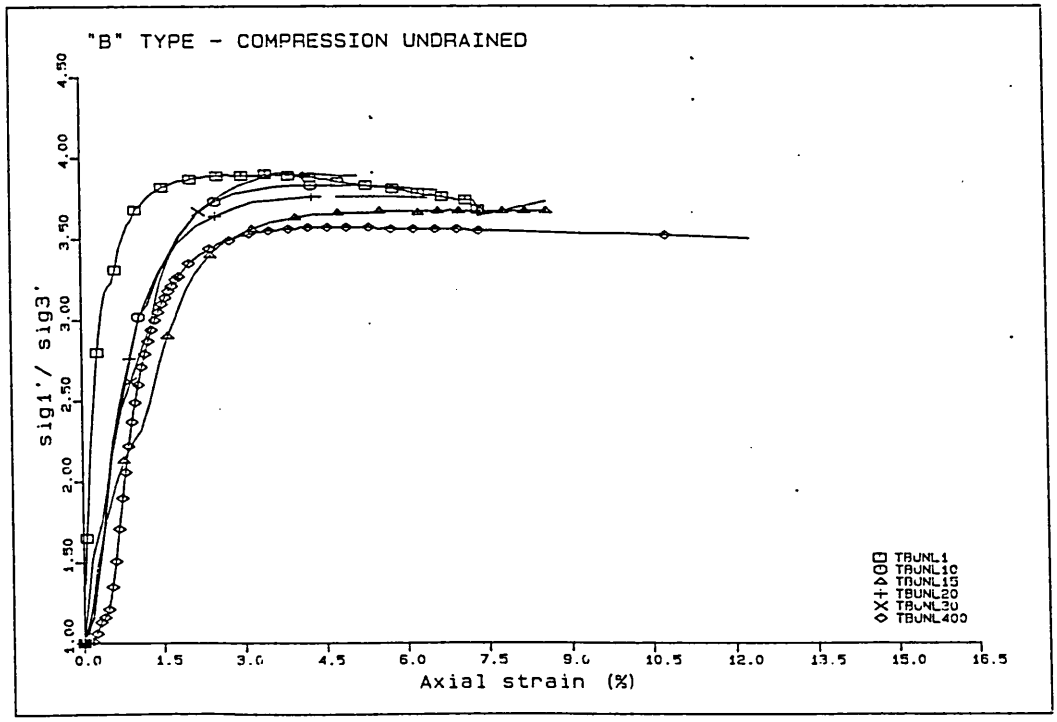
A4.E6


"A" TYPE - COMPRESSION UNDRAINED
sig1'/ sig3'
p' (kPa) (*10³)
TAUNL1
TAUNL10
TAUNL20
TAUNL30
TAUNL400

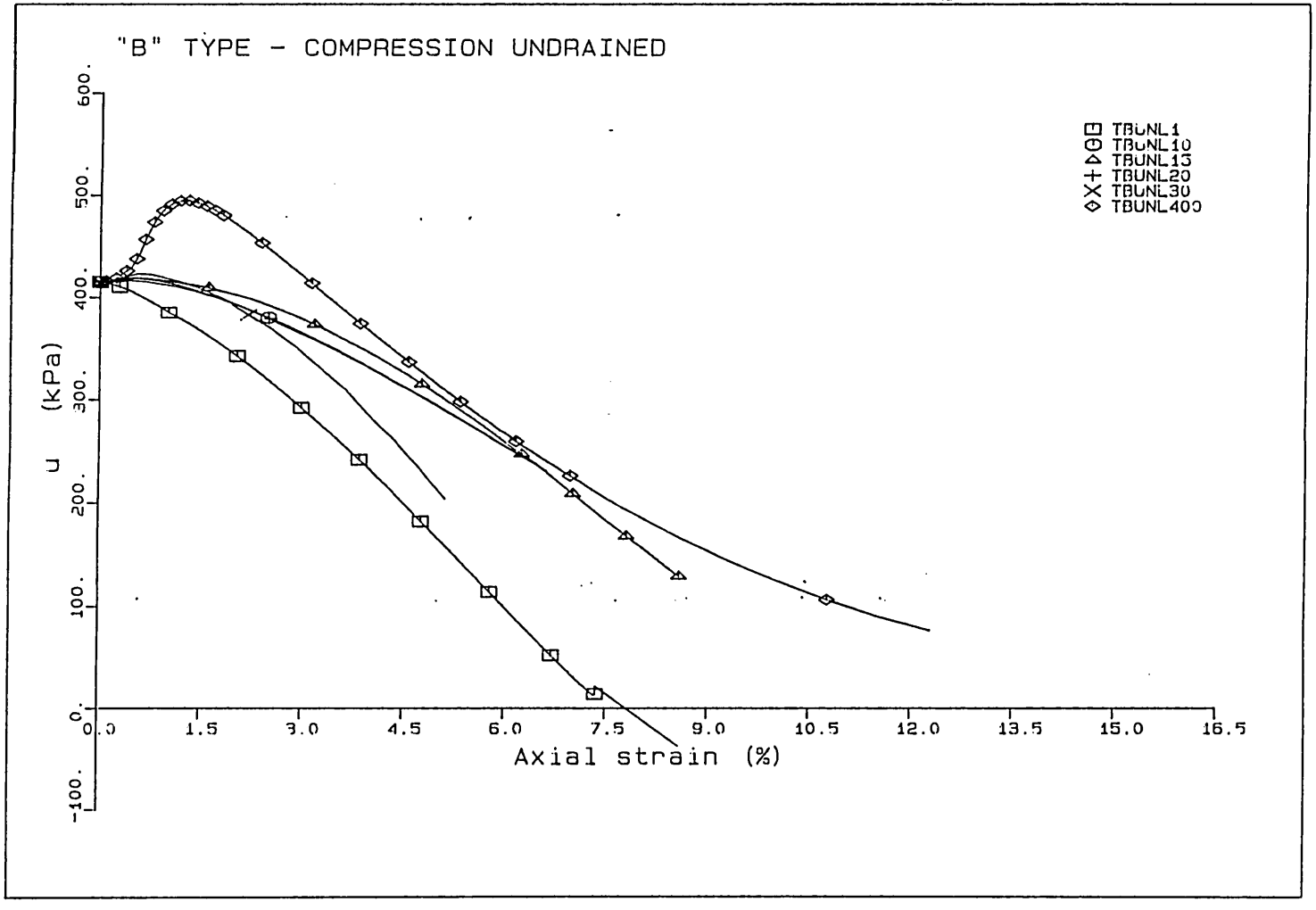
A4.E7


"B" TYPE - COMPRESSION UNDRAINED
q (kPa) (*10³)
0.00
0.30
0.60
0.90
1.20
1.50
1.80
2.10
0.0
1.5
3.0
4.5
6.0
7.5
9.0
10.5
12.0
13.5
15.0
16.5
Axial strain (%)
TBUNL1
TBUNL10
TBUNL15
TBUNL20
TBUNL30
TBUNL400

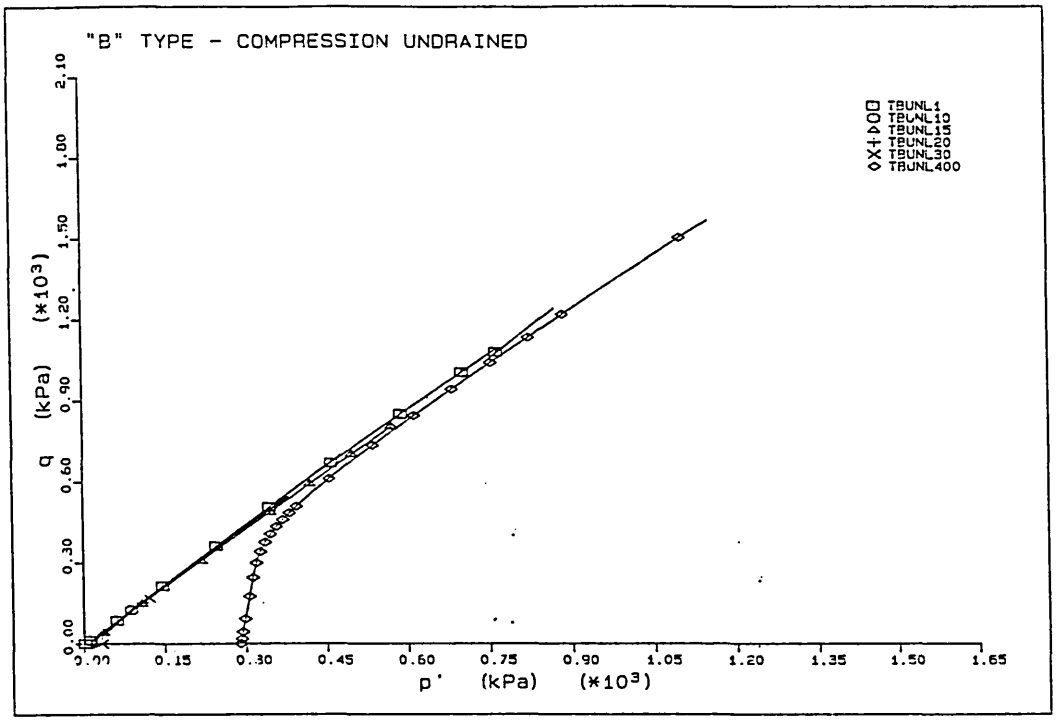
A4.F1


"B" TYPE - COMPRESSION UNDRAINED
sig1'/ sig3'
1.00
1.50
2.00
2.50
3.00
3.50
4.00
4.50
0.0
1.5
3.0
4.5
6.0
7.5
9.0
10.5
12.0
13.5
15.0
16.5
Axial strain (%)
TBUNL1
TBUNL10
TBUNL15
TBUNL20
TBUNL30
TBUNL400

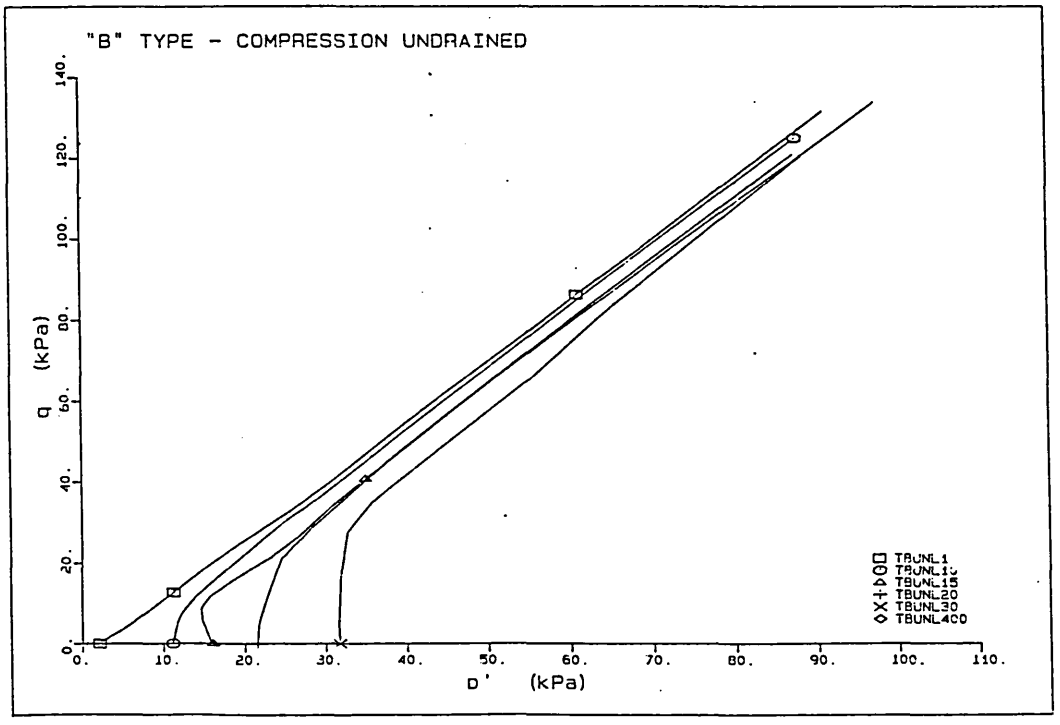
A4.F2


"B" TYPE - COMPRESSION UNDRAINED
TBUNL1
TBUNL10
TBUNL13
TBUNL20
TBUNL30
TBUNL400
u (kPa)
600.
500.
400.
300.
200.
100.
0.
-100.
0.0
1.5
3.0
4.5
6.0
7.5
9.0
10.5
12.0
13.5
15.0
16.5
Axial strain (%)

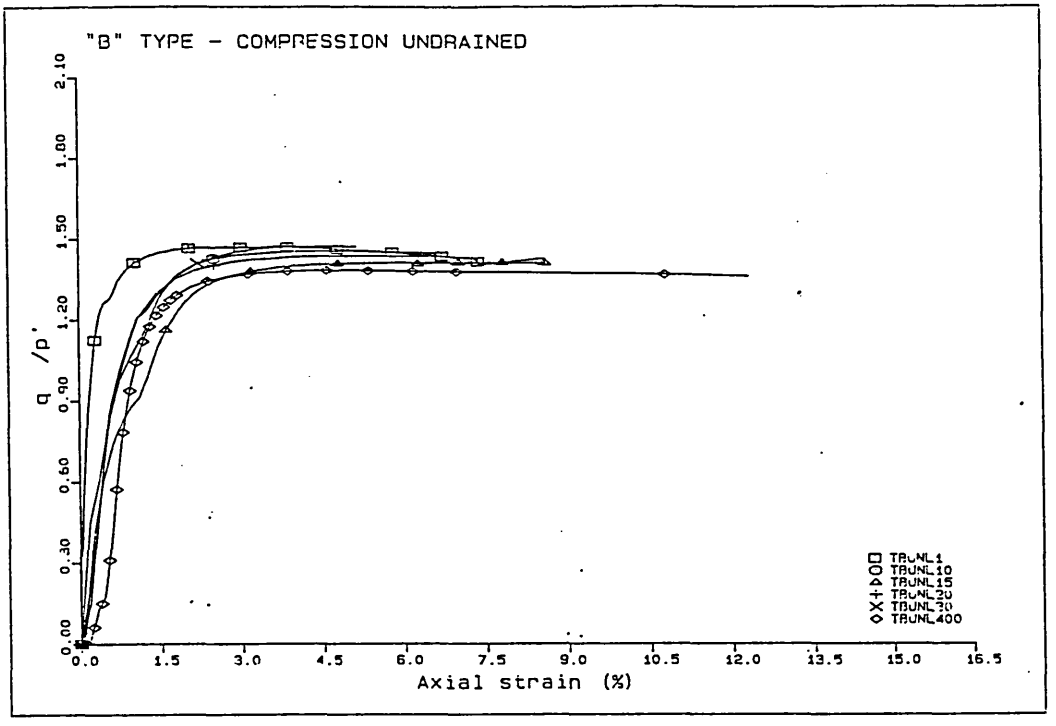
A4.F3


"B" TYPE - COMPRESSION UNDRAINED
TBUNL1
TBUNL10
TBUNL15
TBUNL20
TBUNL30
TBUNL400
q (kPa) (*10³)
p' (kPa) (*10³)
0.00
0.30
0.60
0.90
1.20
1.50
2.10
0.15
0.30
0.45
0.60
0.75
0.90
1.05
1.20
1.35
1.50
1.65

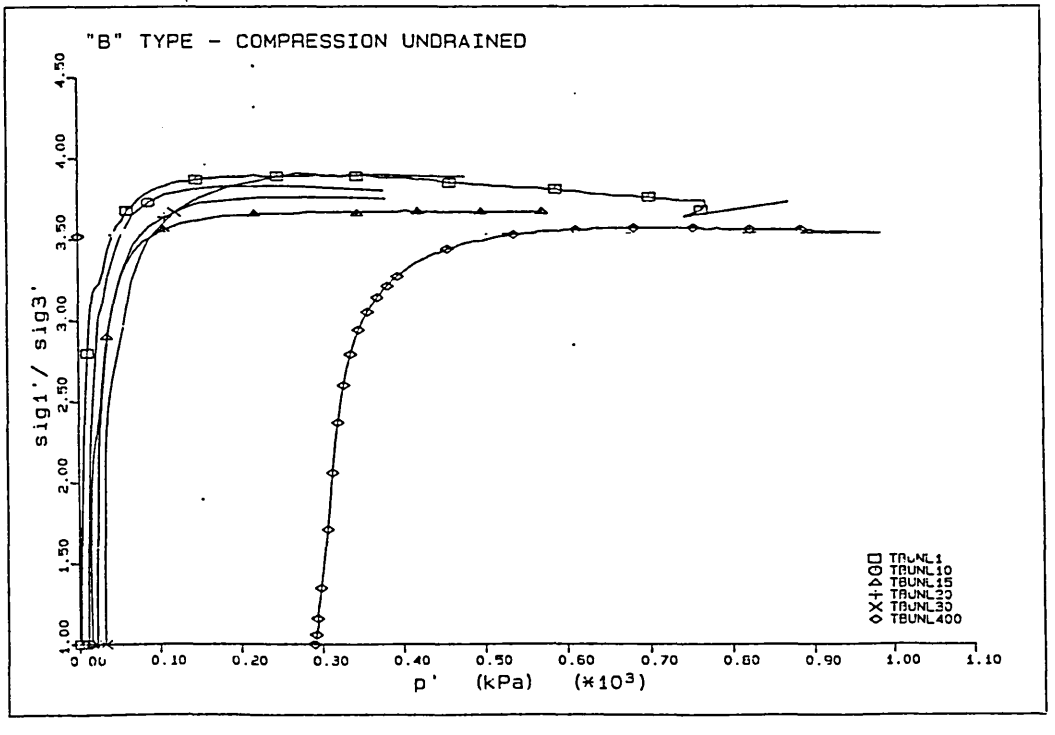
A4.F4


"B" TYPE - COMPRESSION UNDRAINED
TBUNL1
TBUNL10
TBUNL15
TBUNL20
TBUNL30
TBUNL400
q (kPa)
p' (kPa)
0.
20.
40.
60.
80.
100.
120.
140.
10.
20.
30.
40.
50.
60.
70.
80.
90.
100.
110.

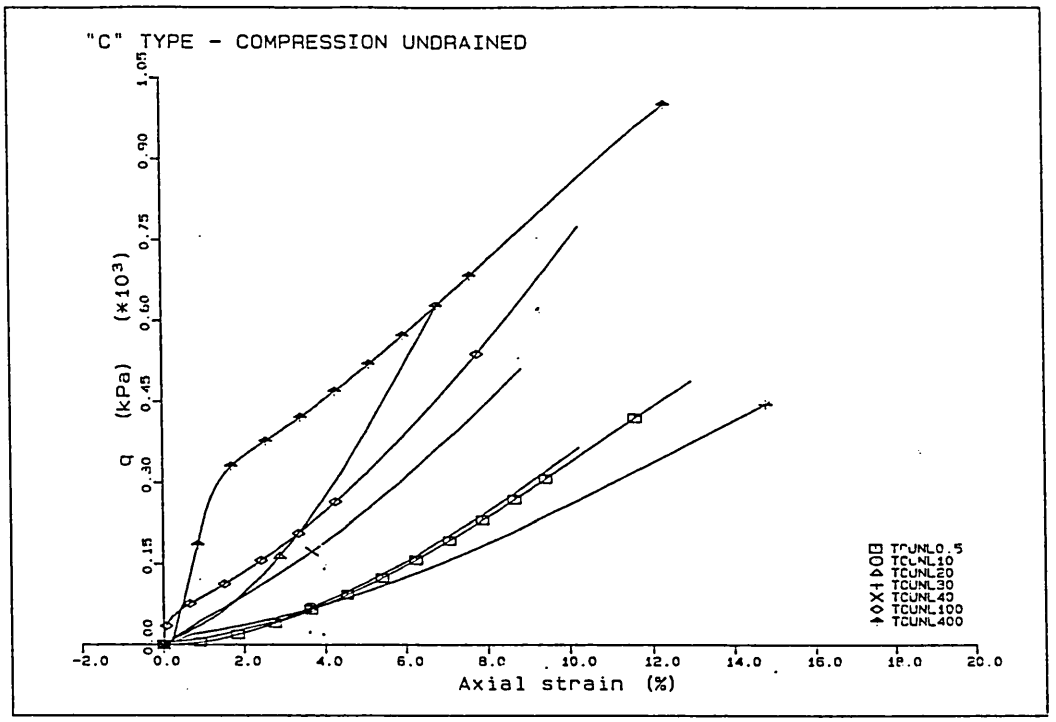
A4.F5


"B" TYPE - COMPRESSION UNDRAINED
q /p'
Axial strain (%)
TBUNL1
TBUNL10
TBUNL15
TBUNL20
TBUNL30
TBUNL400

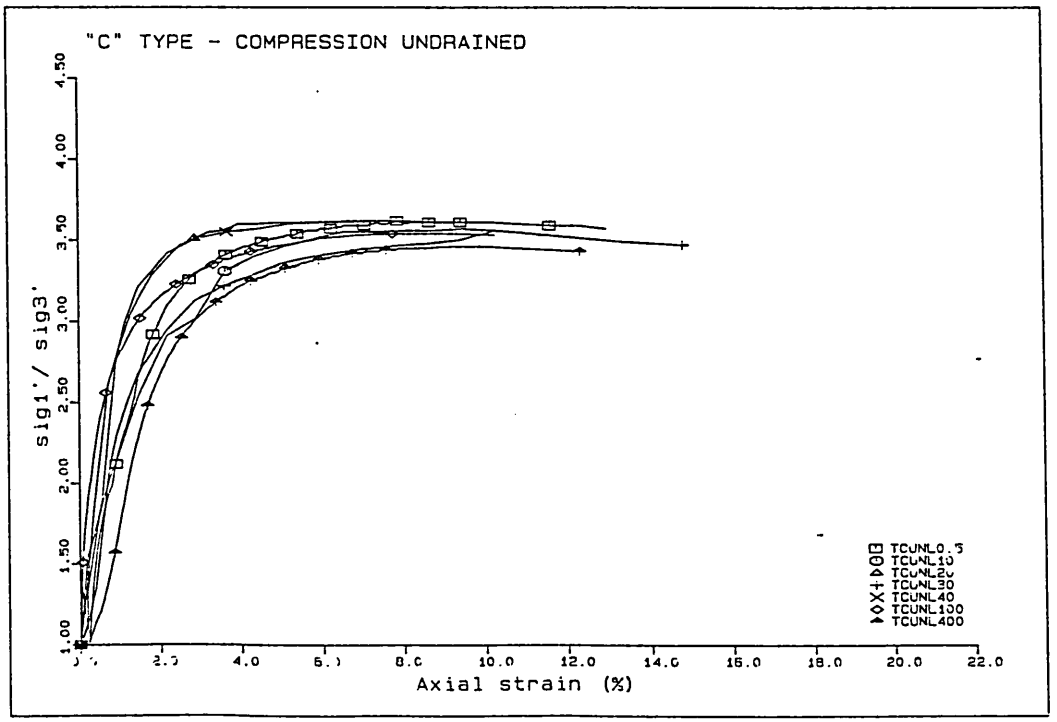
A4.F6


"B" TYPE - COMPRESSION UNDRAINED
sig1' / sig3'
p' (kPa) (*10³)
TBUNL1
TBUNL10
TBUNL15
TBUNL20
TBUNL30
TBUNL400

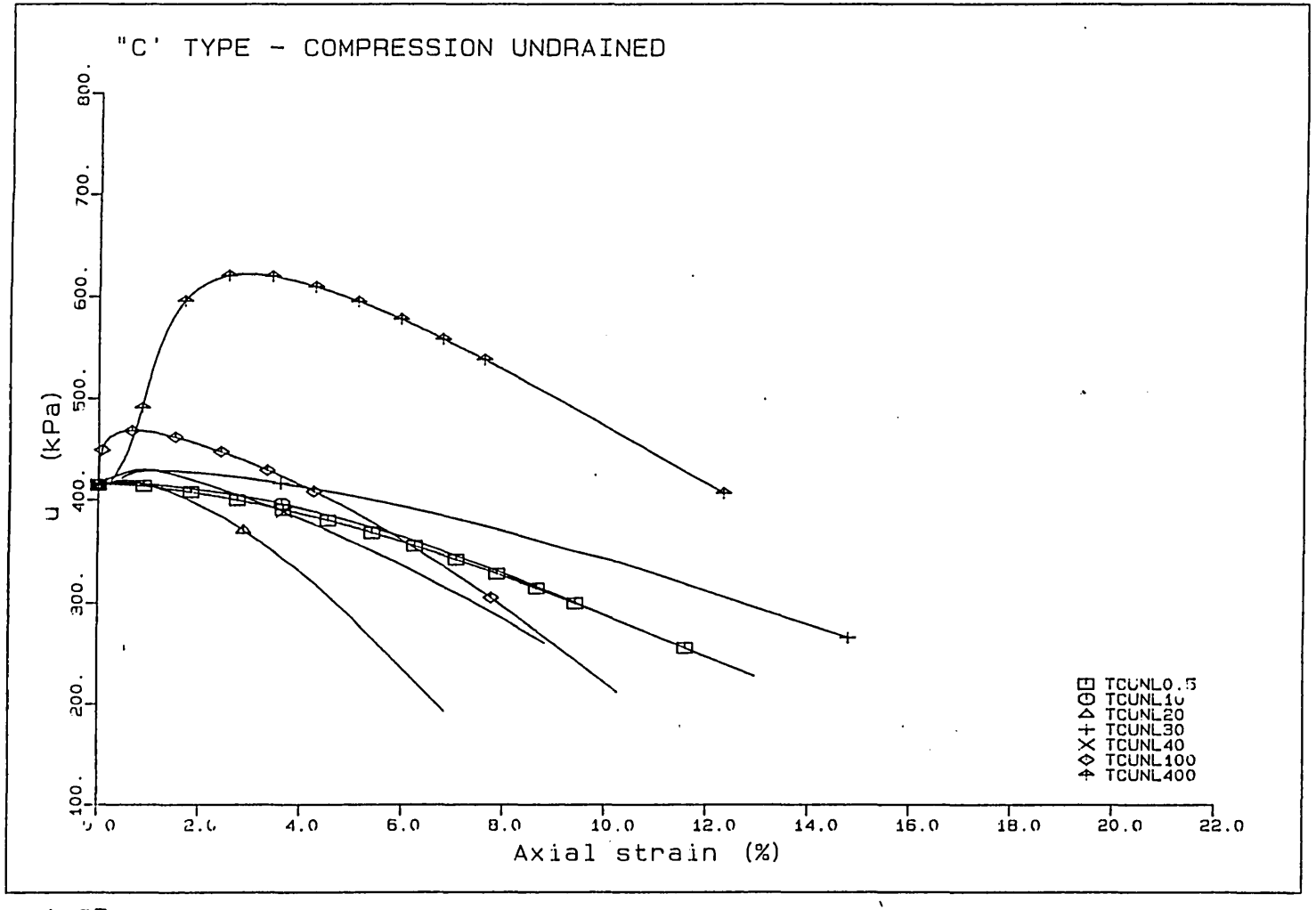
A4.F7


"C" TYPE - COMPRESSION UNDRAINED
q (kPa) (*10³)
Axial strain (%)
TCUNL0.5
TCUNL10
TCUNL20
TCUNL30
TCUNL40
TCUNL100
TCUNL400

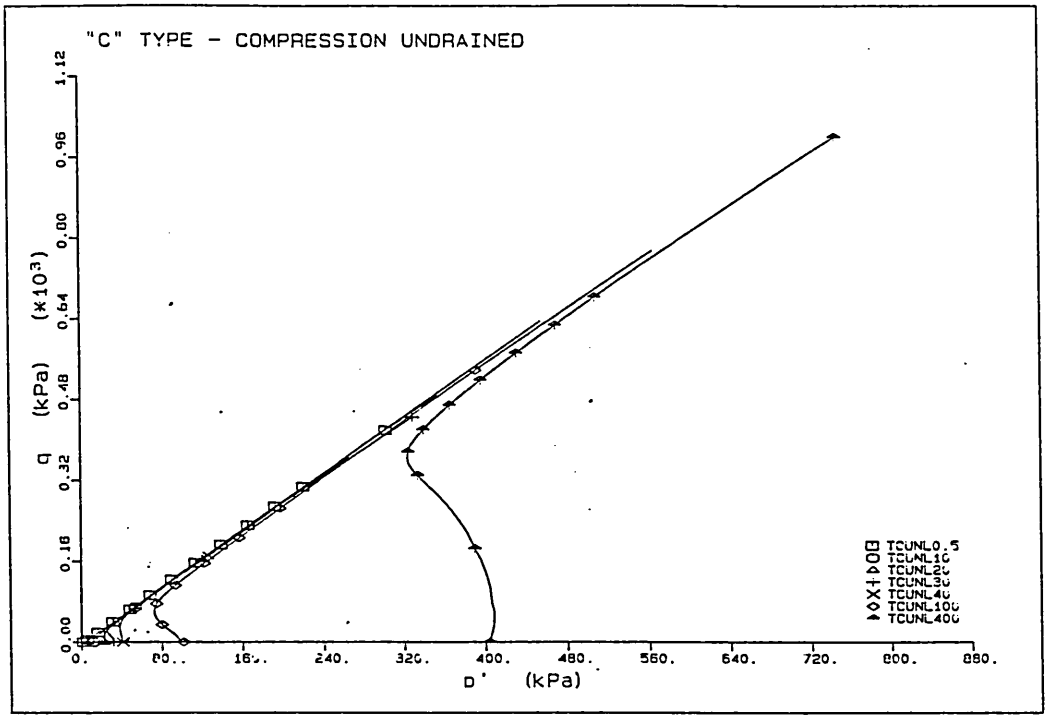
A4.G1


"C" TYPE - COMPRESSION UNDRAINED
sig1'/ sig3'
Axial strain (%)
TCUNL0.5
TCUNL10
TCUNL20
TCUNL30
TCUNL40
TCUNL100
TCUNL400

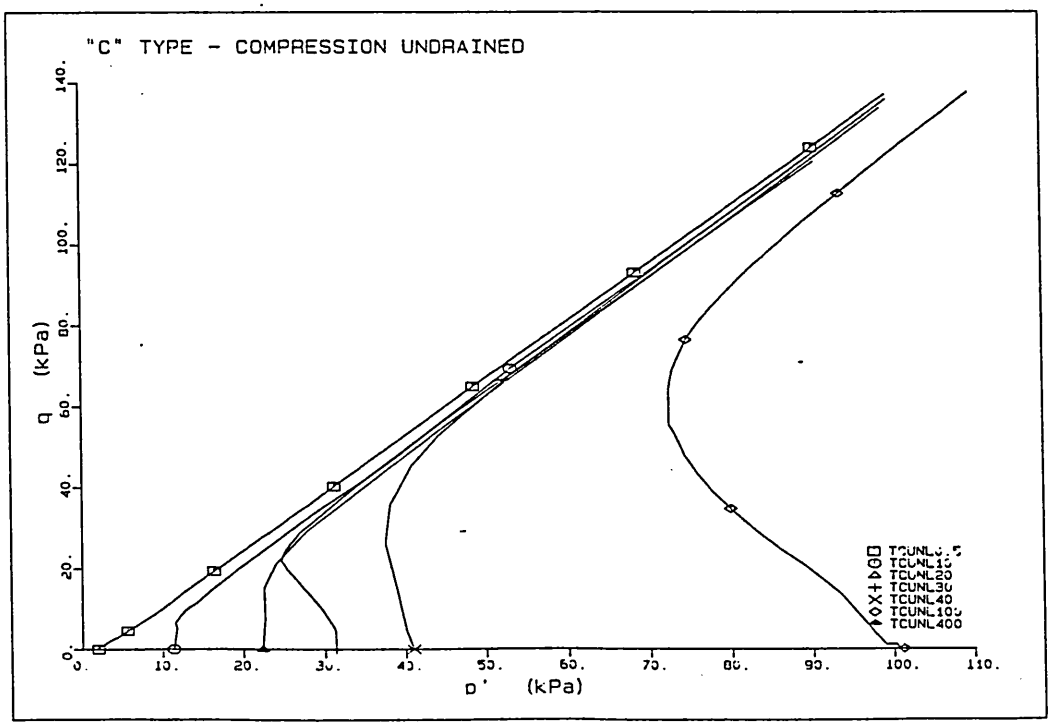
A4.G2


"C' TYPE - COMPRESSION UNDRAINED
u (kPa)
800.
700.
600.
500.
400.
300.
200.
100.
0.0
2.0
4.0
6.0
8.0
10.0
12.0
14.0
16.0
18.0
20.0
22.0
Axial strain (%)
TCUNL0.5
TCUNL10
TCUNL20
TCUNL30
TCUNL40
TCUNL100
TCUNL400

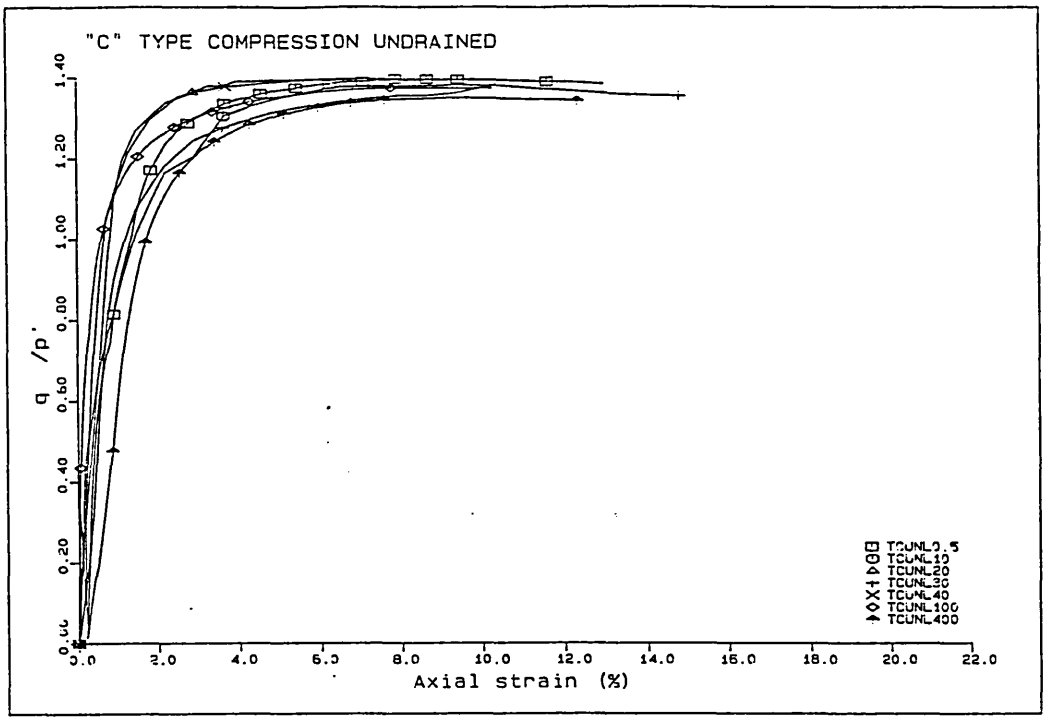
A4.G3


"C" TYPE - COMPRESSION UNDRAINED
q (kPa) (*10³)
0.00
0.16
0.32
0.48
0.64
0.80
0.96
1.12
0.
80.
160.
240.
320.
400.
480.
560.
640.
720.
800.
880.
p' (kPa)
TCUNL0.5
TCUNL10
TCUNL20
TCUNL30
TCUNL40
TCUNL100
TCUNL400

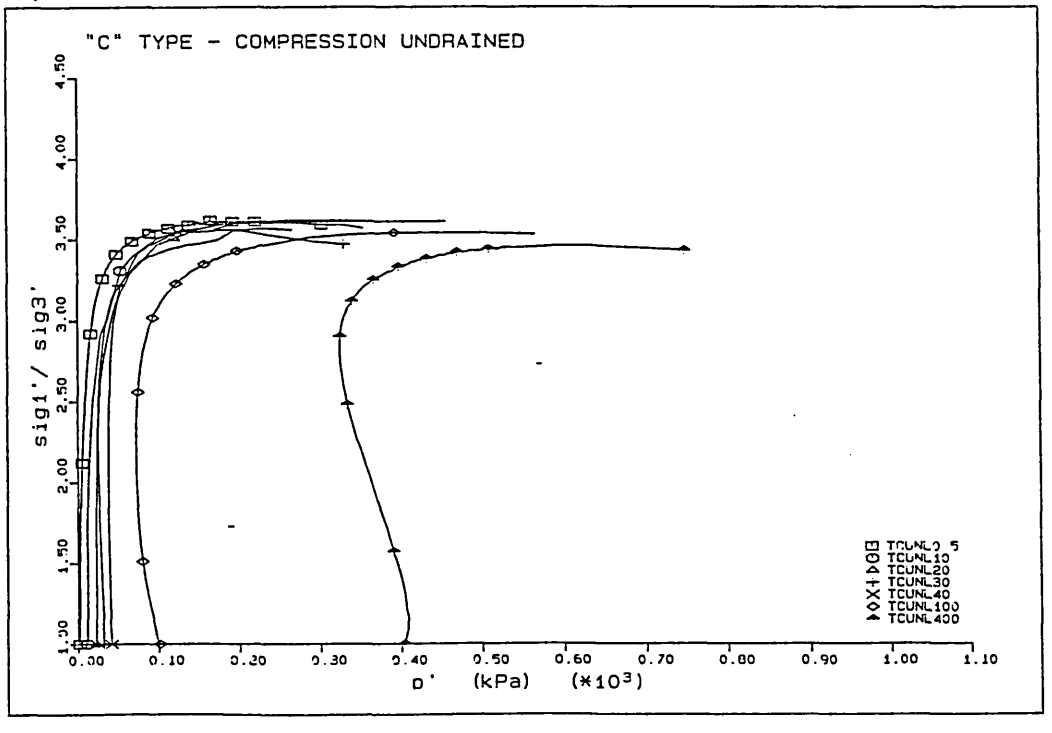
A4.G4


"C" TYPE - COMPRESSION UNDRAINED
q (kPa)
0.
20.
40.
60.
80.
100.
120.
140.
0.
10.
20.
30.
40.
50.
60.
70.
80.
90.
100.
110.
p' (kPa)
TCUNL0.5
TCUNL10
TCUNL20
TCUNL30
TCUNL40
TCUNL100
TCUNL400

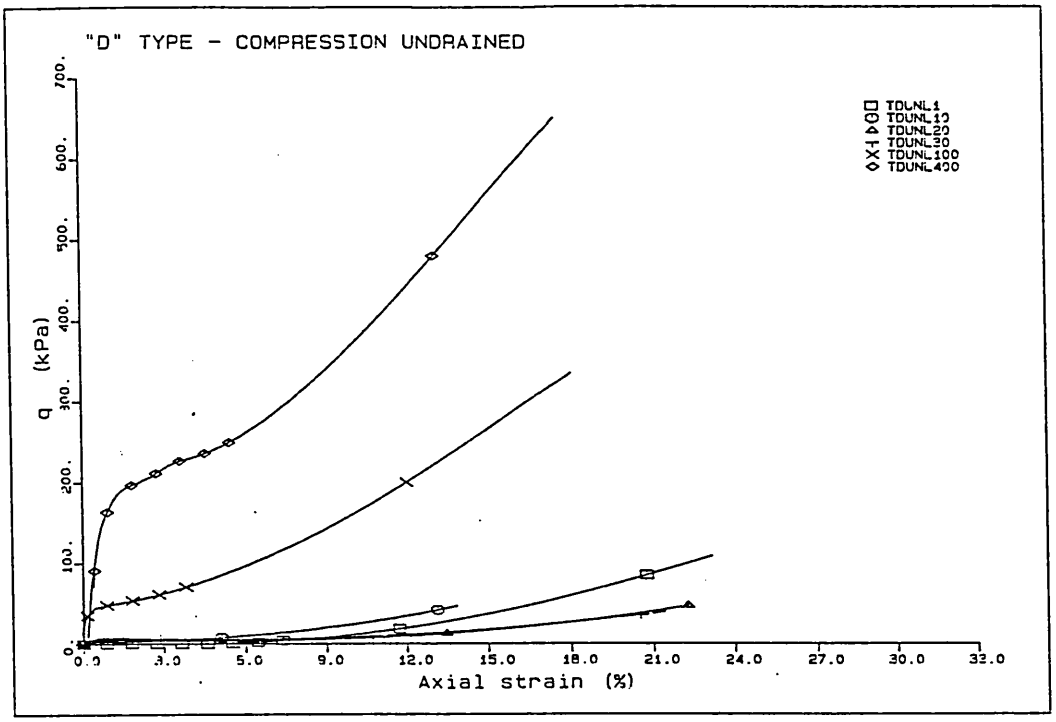
A4.G5


"C" TYPE COMPRESSION UNDRAINED
q /p'
Axial strain (%)
TCUNL0.5
TCUNL10
TCUNL20
TCUNL30
TCUNL40
TCUNL100
TCUNL400

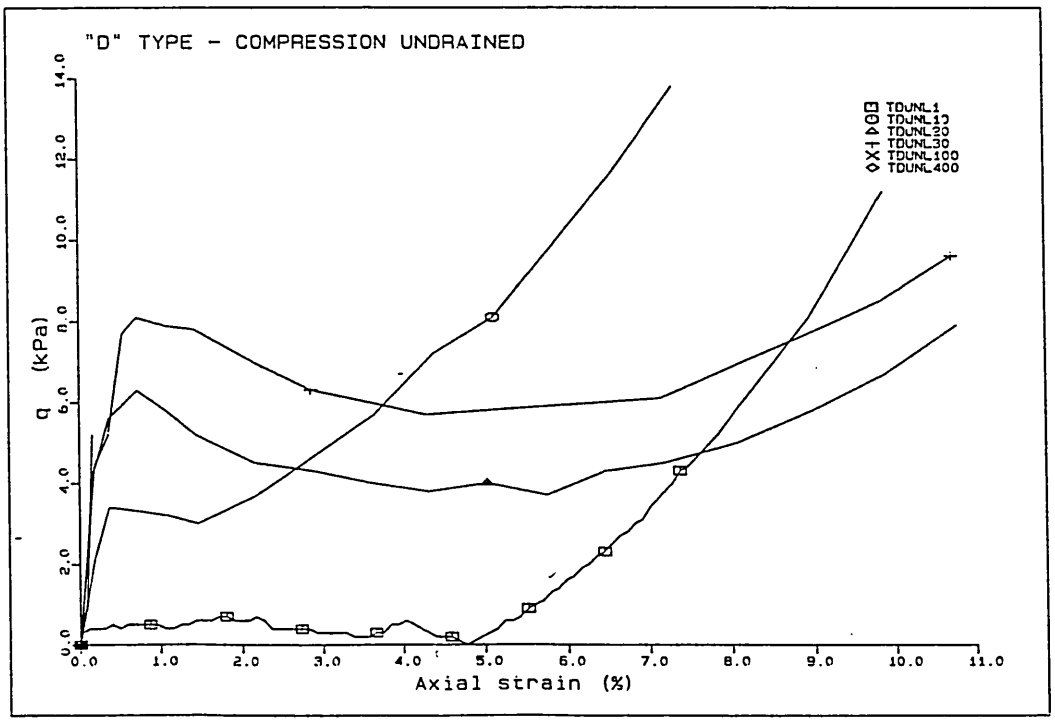
A4.G6


"C" TYPE - COMPRESSION UNDRAINED
sig1'/ sig3'
p' (kPa) (*10³)
TCUNL0.5
TCUNL10
TCUNL20
TCUNL30
TCUNL40
TCUNL100
TCUNL400

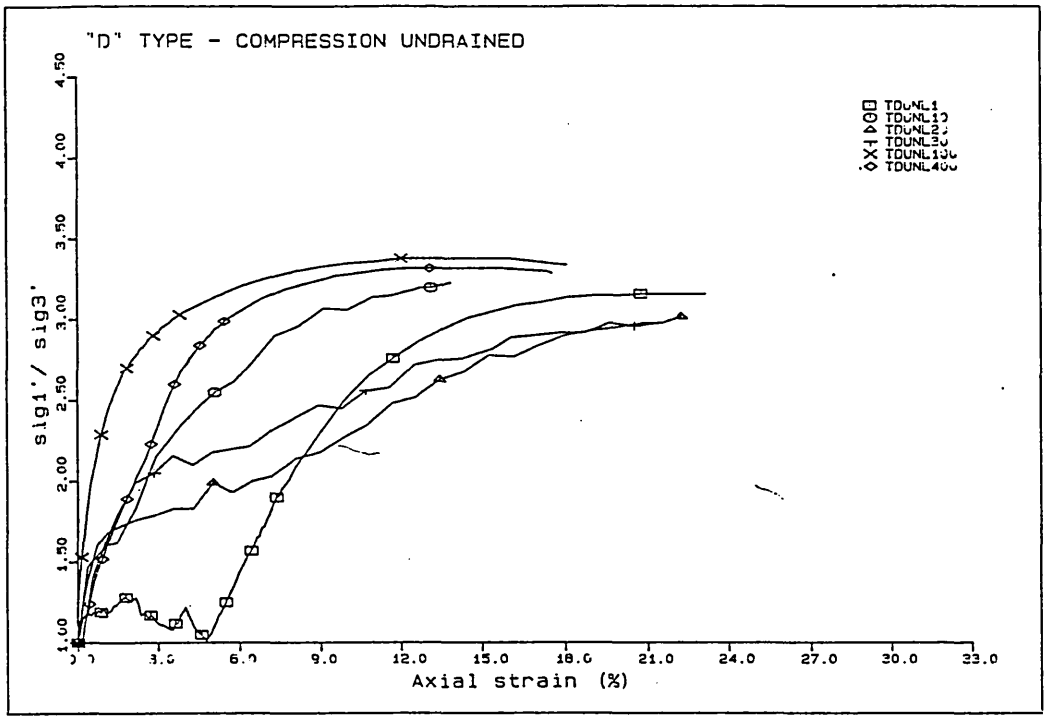
A4.G7


"D" TYPE - COMPRESSION UNDRAINED
q (kPa)
Axial strain (%)
TDUNL1
TDUNL10
TDUNL20
TDUNL30
TDUNL100
TDUNL400

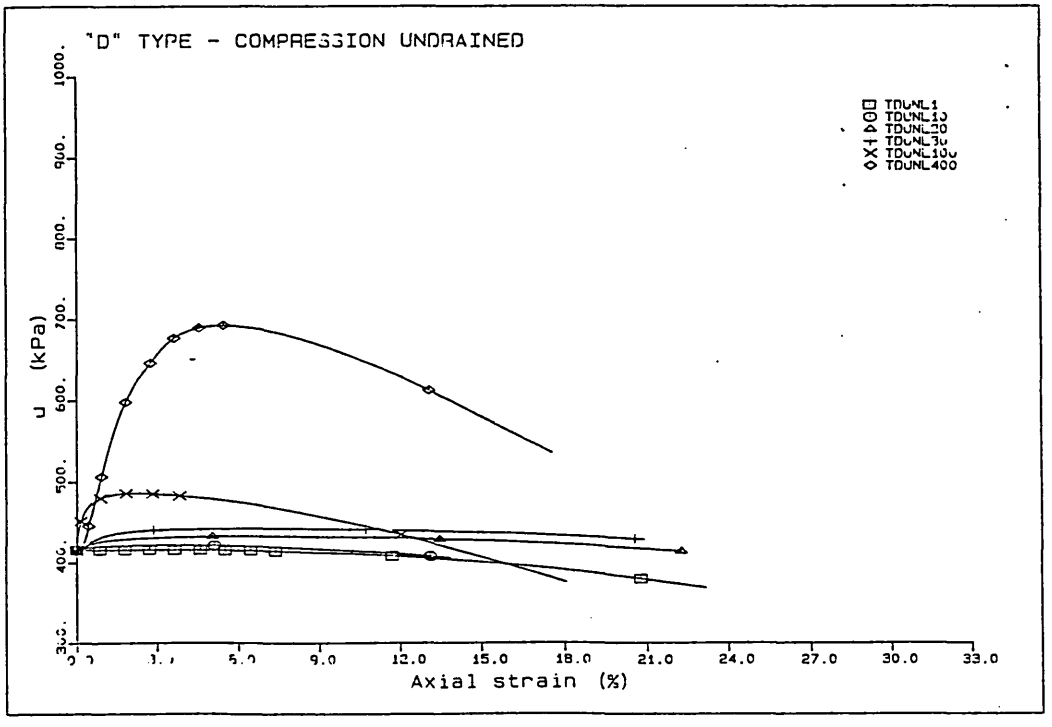
A4.H1


"D" TYPE - COMPRESSION UNDRAINED
q (kPa)
Axial strain (%)
TDUNL1
TDUNL10
TDUNL20
TDUNL30
TDUNL100
TDUNL400

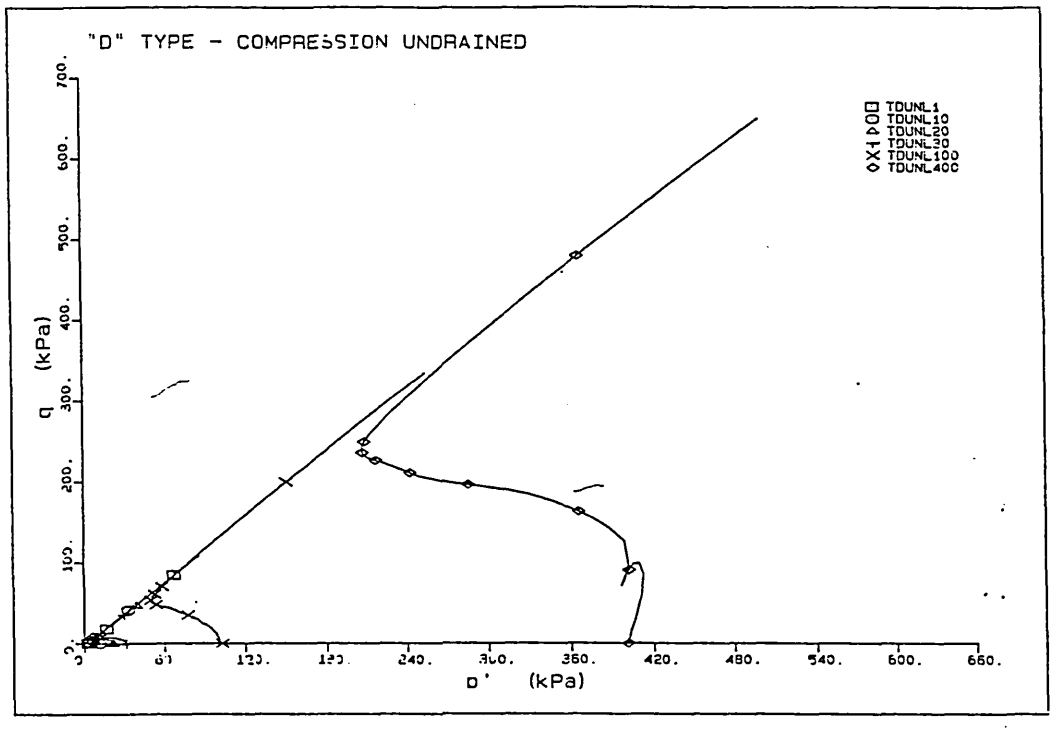
A4.H2


"D" TYPE - COMPRESSION UNDRAINED
sig1' / sig3'
Axial strain (%)
TDUNL1
TDUNL10
TDUNL30
TDUNL100
TDUNL400

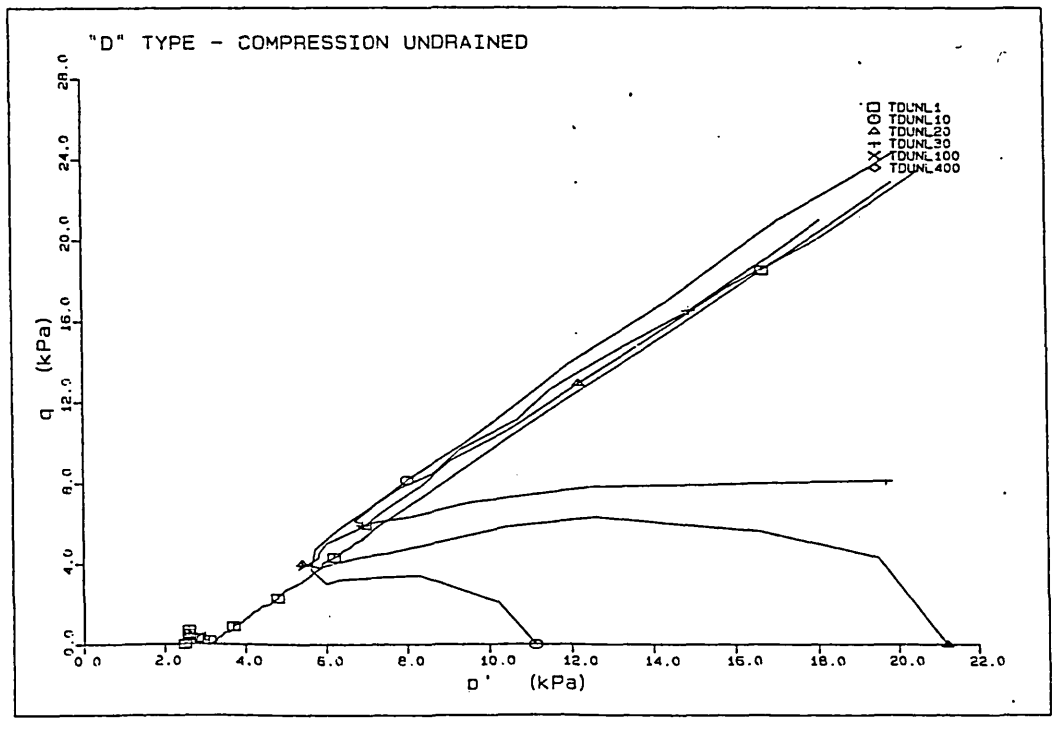
A4.H3


"D" TYPE - COMPRESSION UNDRAINED
u (kPa)
Axial strain (%)
TDUNL1
TDUNL10
TDUNL30
TDUNL100
TDUNL400

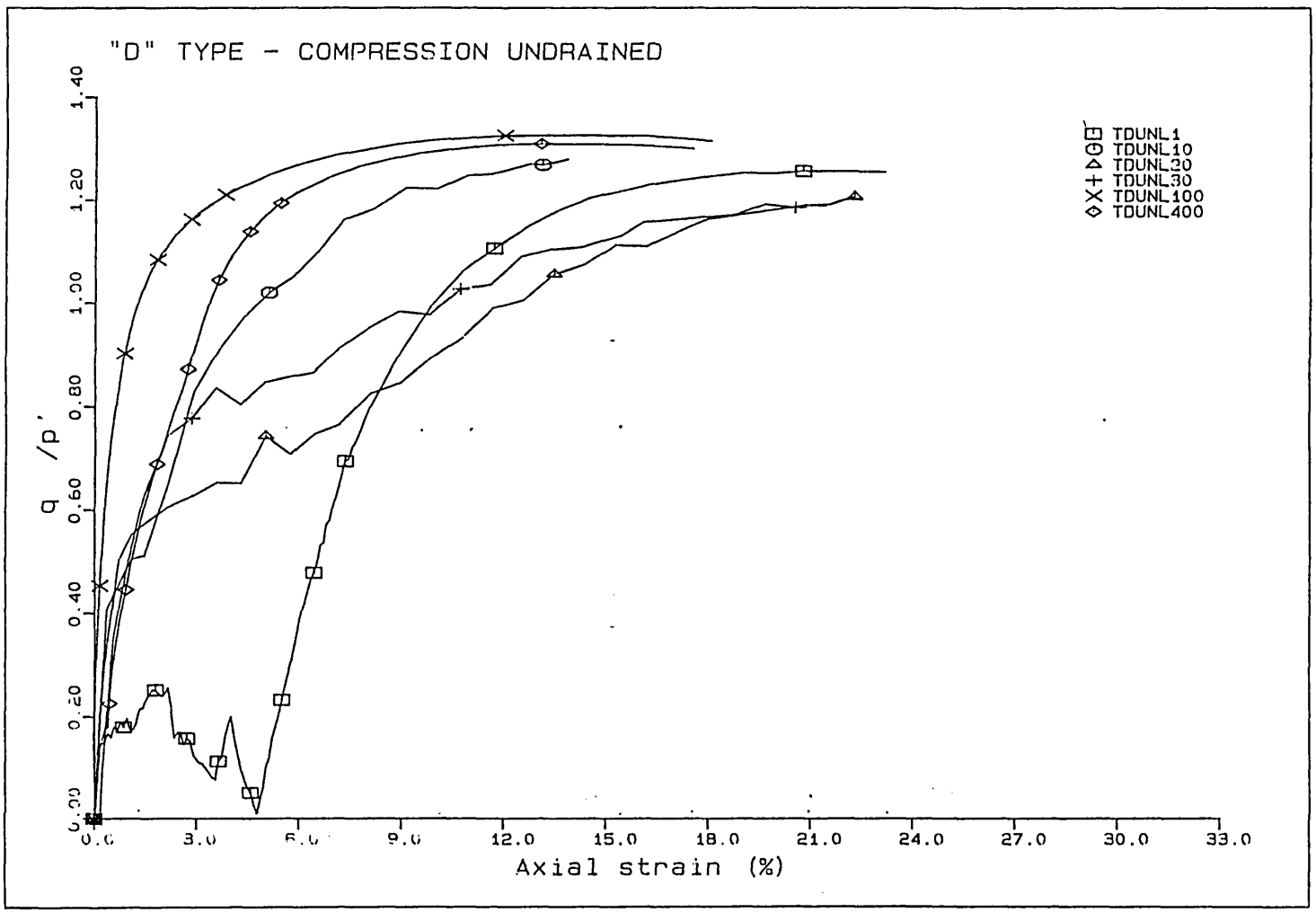
A4.H4


"D" TYPE - COMPRESSION UNDRAINED
TDUNL1
TDUNL10
TDUNL20
TDUNL30
TDUNL100
TDUNL400
q (kPa)
p' (kPa)

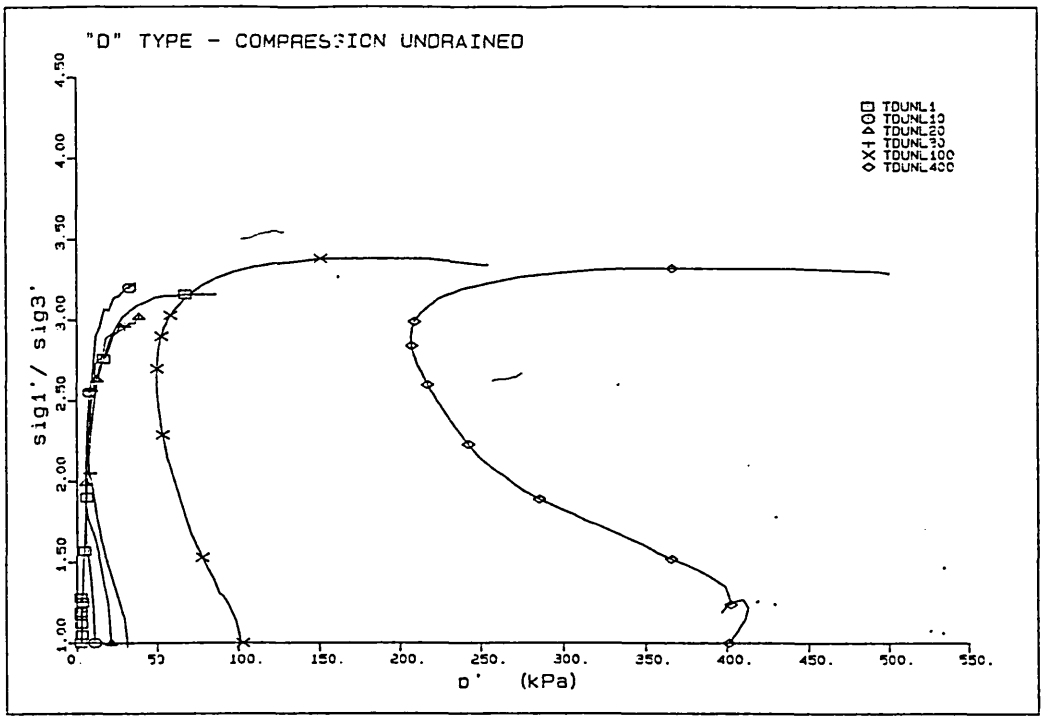
A4.H5


"D" TYPE - COMPRESSION UNDRAINED
TDUNL1
TDUNL10
TDUNL20
TDUNL30
TDUNL100
TDUNL400
q (kPa)
p' (kPa)

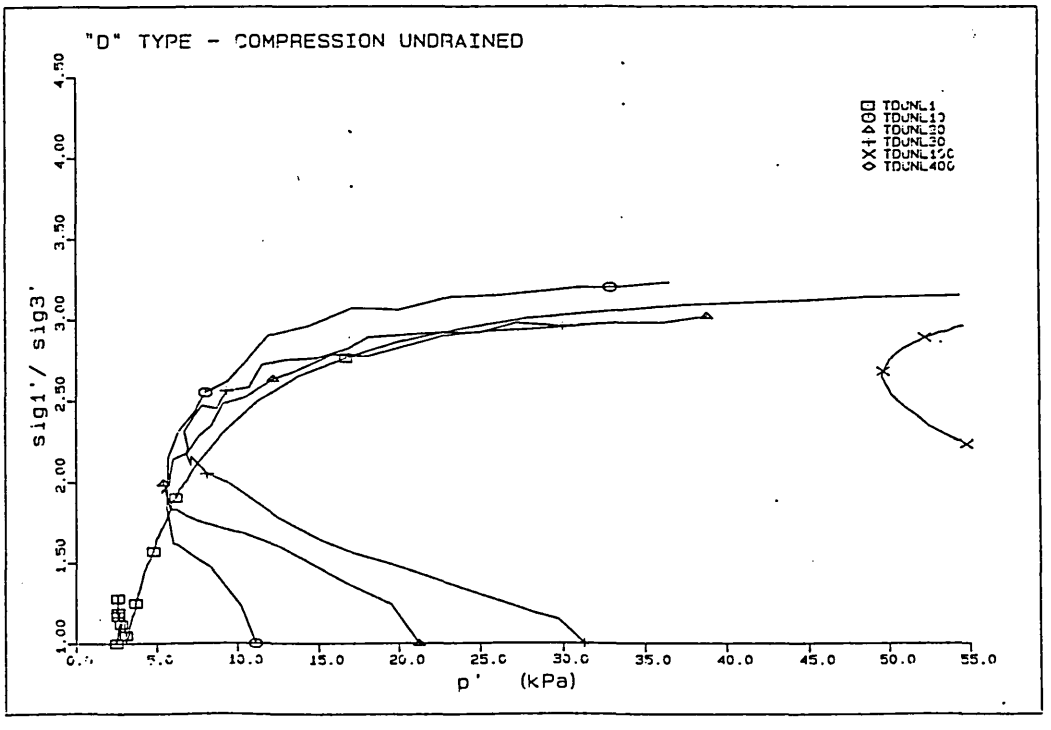
A4.H6


"D" TYPE - COMPRESSION UNDRAINED
q /p'
Axial strain (%)
TDUNL1
TDUNL10
TDUNL20
TDUNL30
TDUNL100
TDUNL400
0.00
0.20
0.40
0.60
0.80
1.00
1.20
1.40
0.0
3.0
6.0
9.0
12.0
15.0
18.0
21.0
24.0
27.0
30.0
33.0

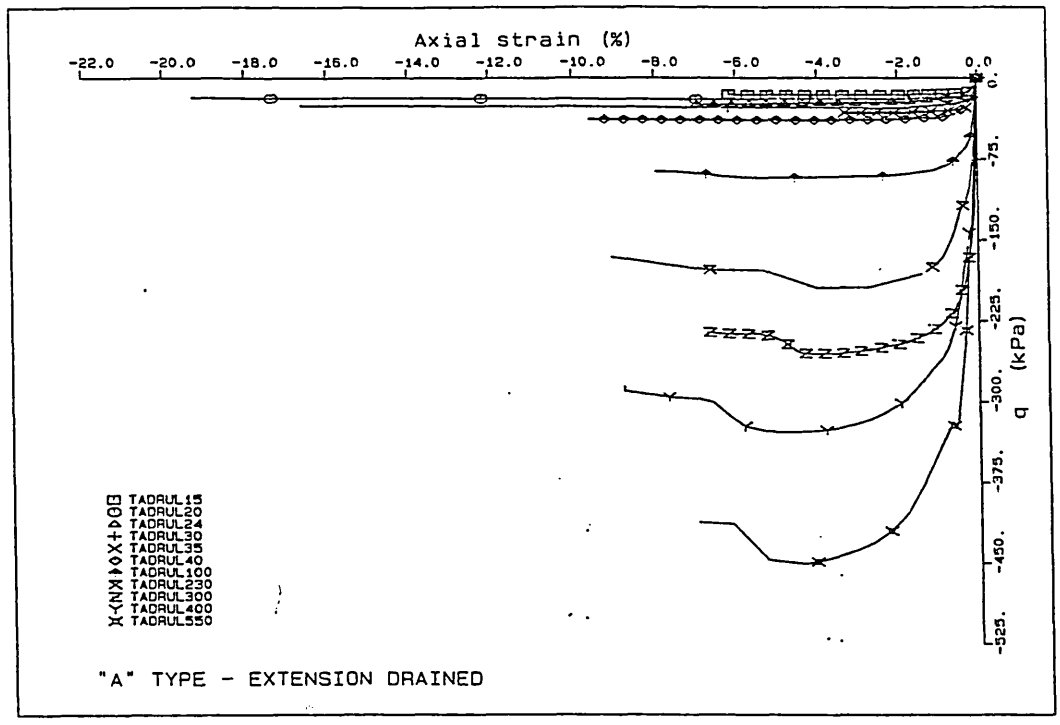
A4.H7


"D" TYPE - COMPRESSION UNDRAINED
TDUNL1
TDUNL10
TDUNL20
TDUNL30
TDUNL100
TDUNL400
sig1'/ sig3'
p' (kPa)

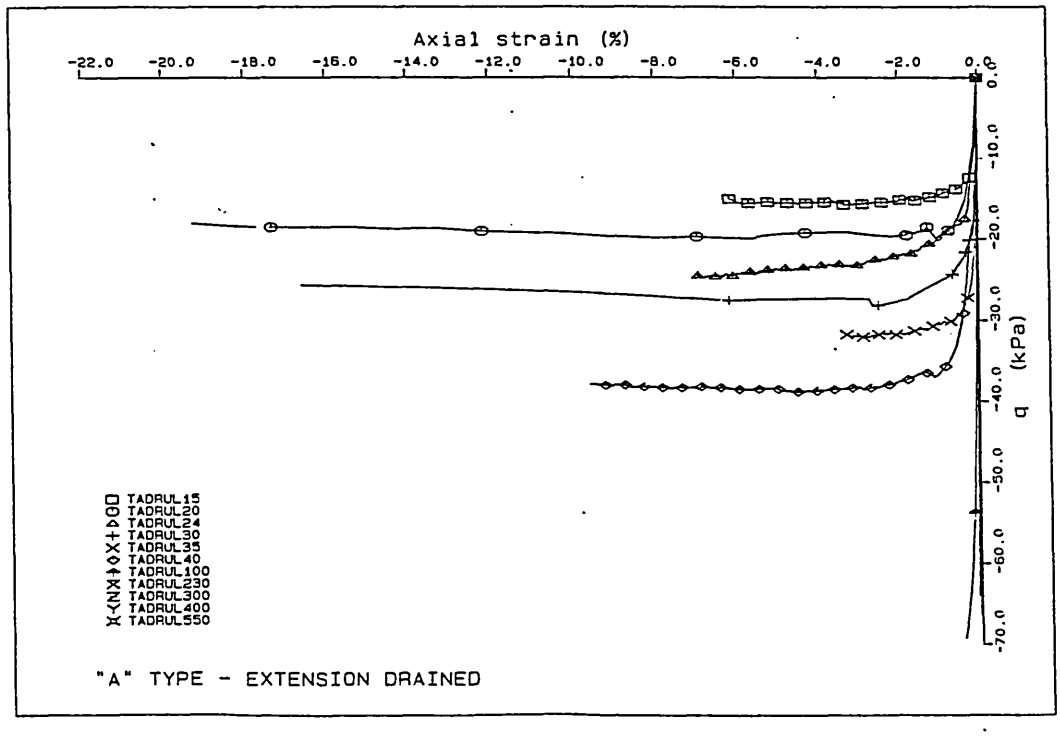
A4.H8


"D" TYPE - COMPRESSION UNDRAINED
TDUNL1
TDUNL10
TDUNL20
TDUNL30
TDUNL100
TDUNL400
sig1'/ sig3'
p' (kPa)

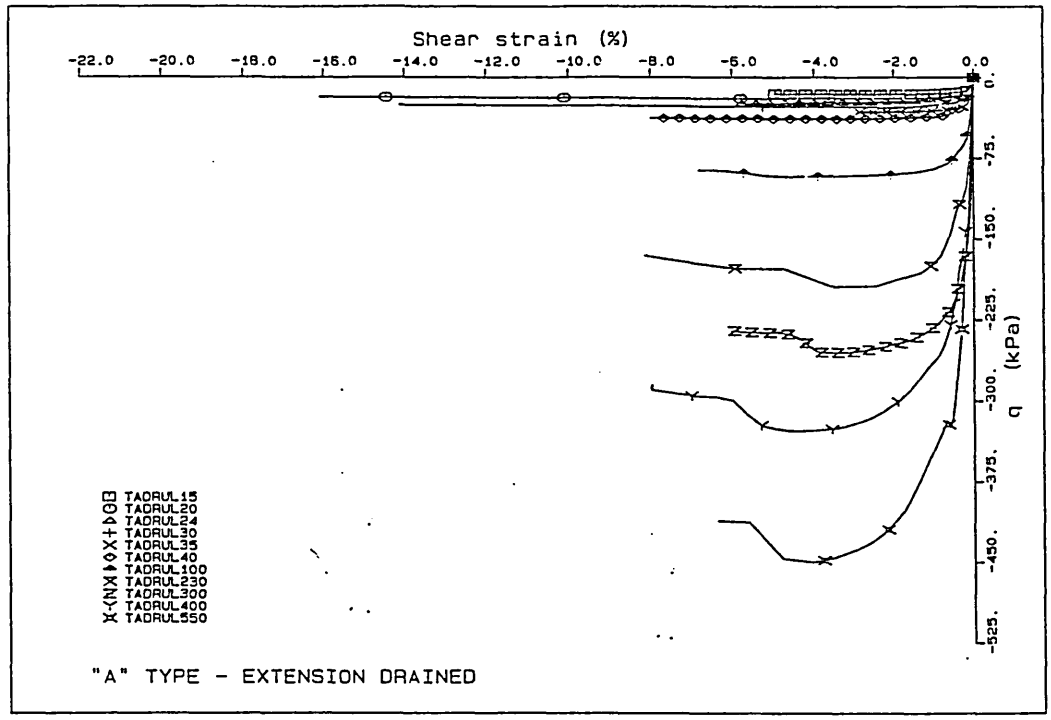
A4.H9


Axial strain (%)
-22.0 -20.0 -18.0 -16.0 -14.0 -12.0 -10.0 -8.0 -6.0 -4.0 -2.0 0.0
0. -75. -150. -225. -300. -375. -450. -525.
q (kPa)
TADRUL15
TADRUL20
TADRUL24
TADRUL30
TADRUL35
TADRUL40
TADRUL100
TADRUL230
TADRUL300
TADRUL400
TADRUL550
"A" TYPE - EXTENSION DRAINED

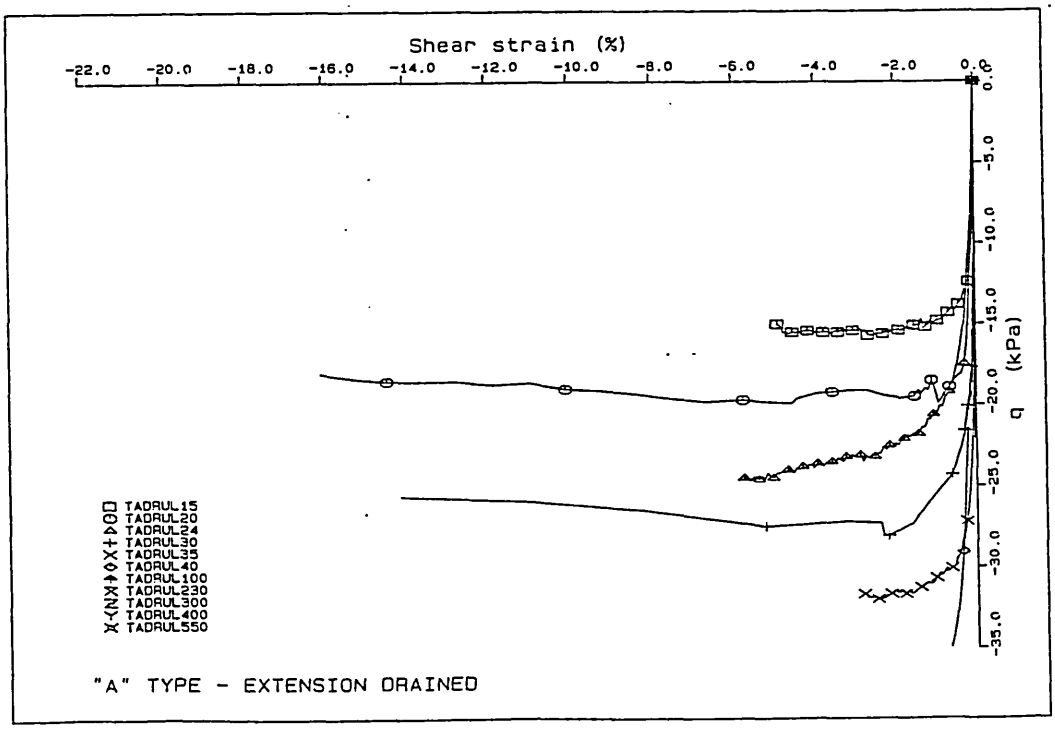
A4.I1


Axial strain (%)
-22.0 -20.0 -18.0 -16.0 -14.0 -12.0 -10.0 -8.0 -6.0 -4.0 -2.0 0.0
0.0 -10.0 -20.0 -30.0 -40.0 -50.0 -60.0 -70.0
q (kPa)
TADRUL15
TADRUL20
TADRUL24
TADRUL30
TADRUL35
TADRUL40
TADRUL100
TADRUL230
TADRUL300
TADRUL400
TADRUL550
"A" TYPE - EXTENSION DRAINED

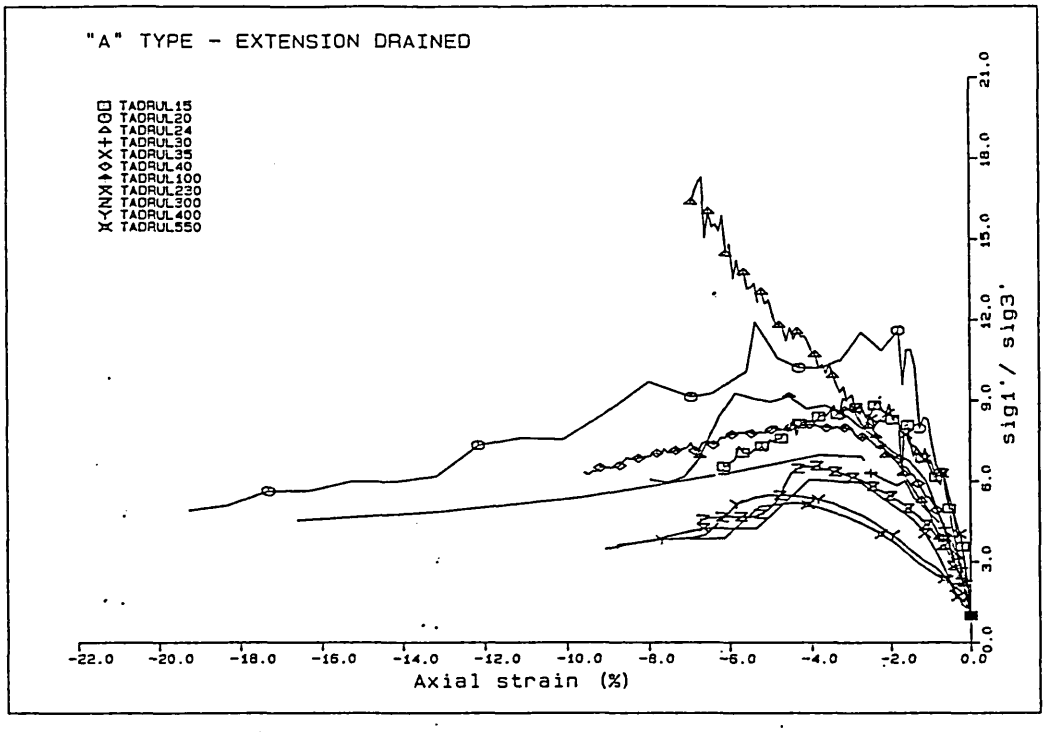
A4.I2


Shear strain (%)
-22.0 -20.0 -18.0 -16.0 -14.0 -12.0 -10.0 -8.0 -5.0 -4.0 -2.0 0.0
0. -75. -150. -225. -300. -375. -450. -525.
q (kPa)
TADRUL15
TADRUL20
TADRUL24
TADRUL30
TADRUL35
TADRUL40
TADRUL100
TADRUL230
TADRUL300
TADRUL400
TADRUL550
"A" TYPE - EXTENSION DRAINED

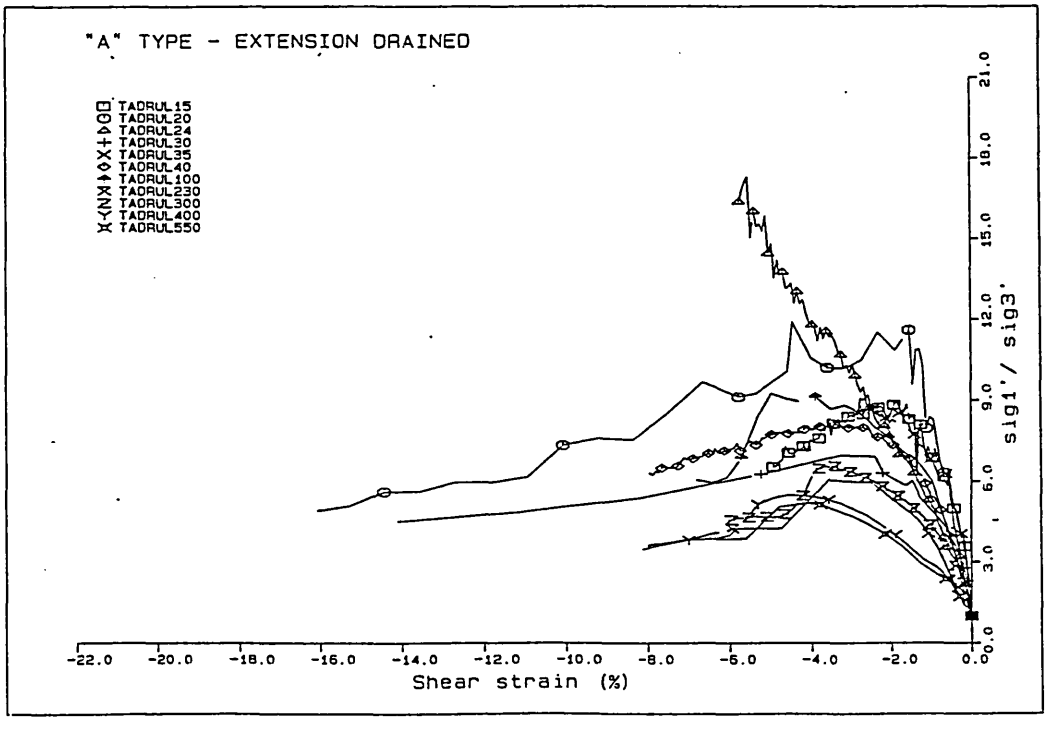
A4.I3


Shear strain (%)
-22.0 -20.0 -18.0 -16.0 -14.0 -12.0 -10.0 -8.0 -6.0 -4.0 -2.0 0.0
0. -5.0 -10.0 -15.0 -20.0 -25.0 -30.0 -35.0
q (kPa)
TADRUL15
TADRUL20
TADRUL24
TADRUL30
TADRUL35
TADRUL40
TADRUL100
TADRUL230
TADRUL300
TADRUL400
TADRUL550
"A" TYPE - EXTENSION DRAINED

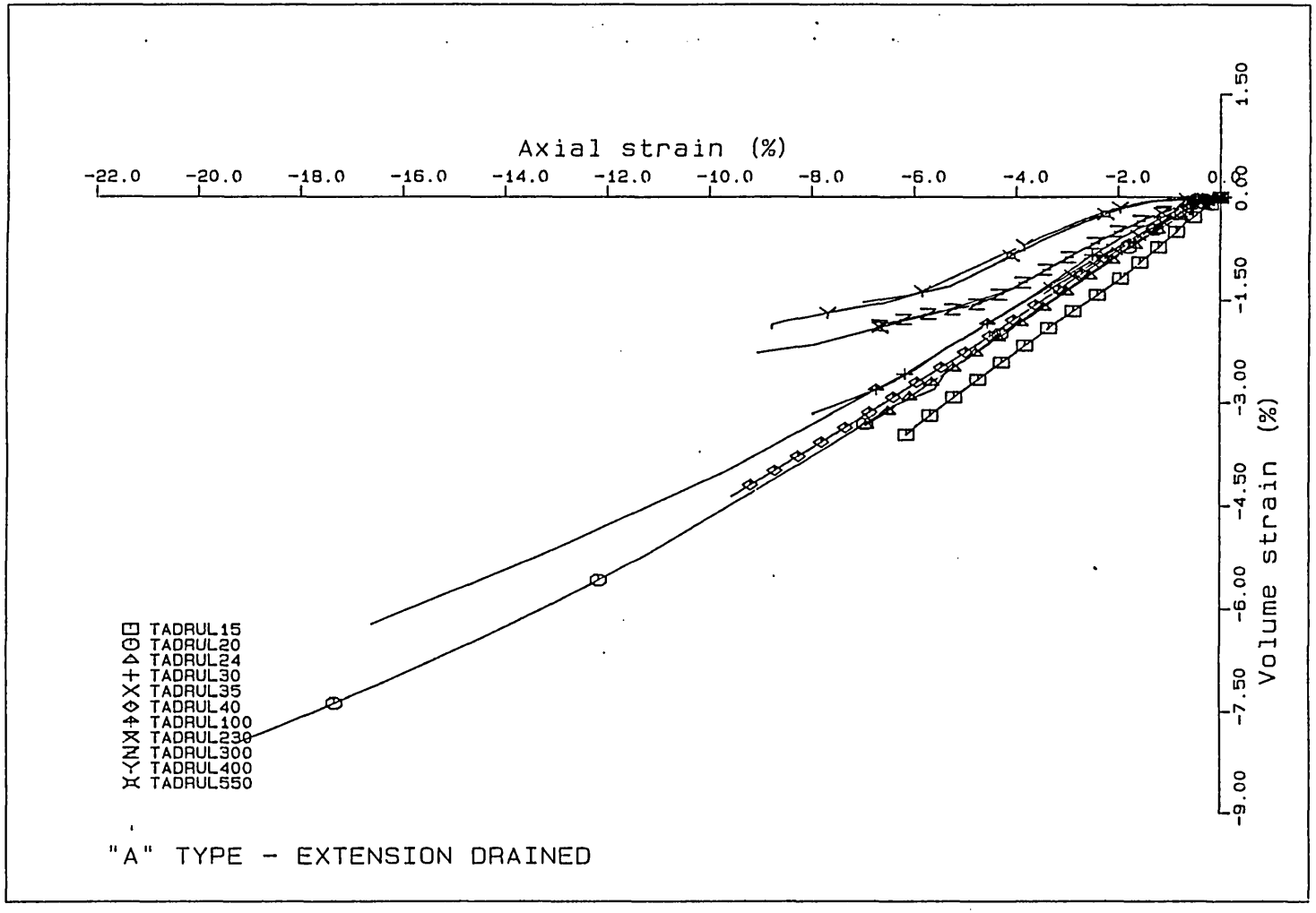
A4.I4


"A" TYPE - EXTENSION DRAINED
TADRUL15
TADRUL20
TADRUL24
TADRUL30
TADRUL35
TADRUL40
TADRUL100
TADRUL230
TADRUL300
TADRUL400
TADRUL550
sig1' / sig3'
Axial strain (%)

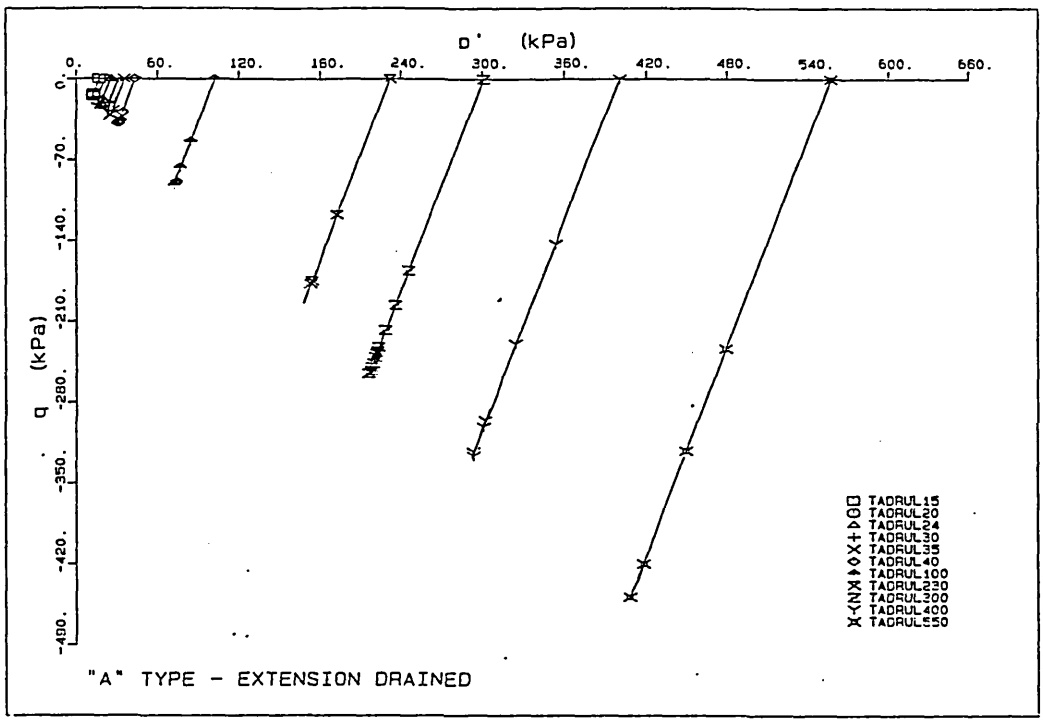
A4.I5


"A" TYPE - EXTENSION DRAINED
TADRUL15
TADRUL20
TADRUL24
TADRUL30
TADRUL35
TADRUL40
TADRUL100
TADRUL230
TADRUL300
TADRUL400
TADRUL550
sig1' / sig3'
Shear strain (%)

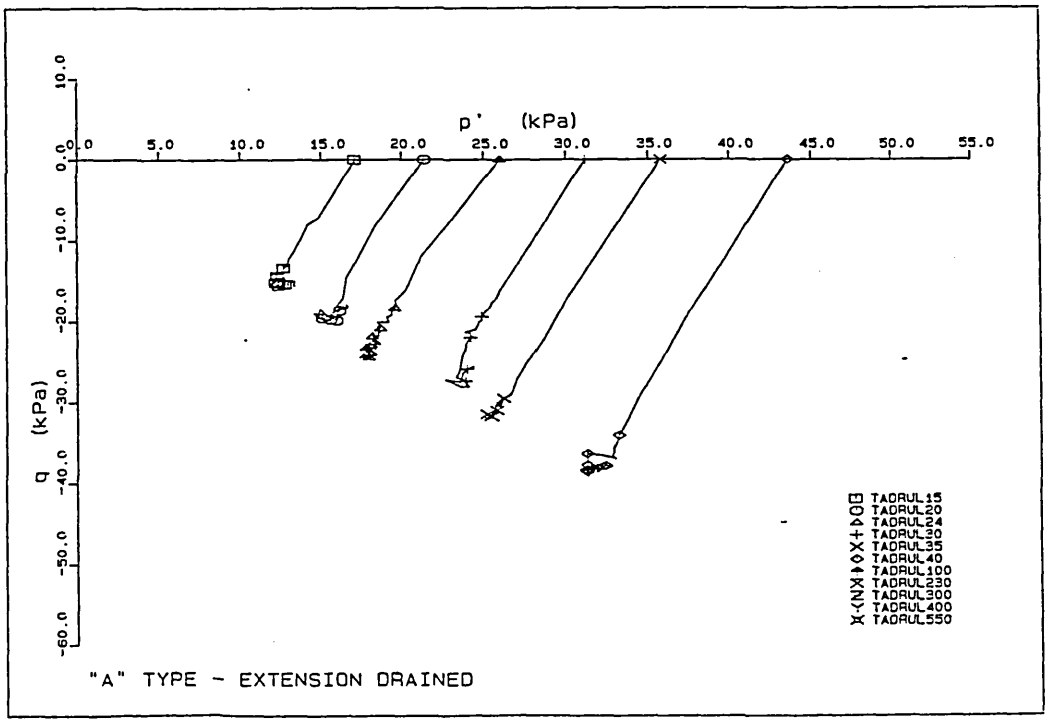
A4.I6


Axial strain (%)
-22.0
-20.0
-18.0
-16.0
-14.0
-12.0
-10.0
-8.0
-6.0
-4.0
-2.0
0.00
1.50
-1.50
-3.00
-4.50
-6.00
-7.50
-9.00
Volume strain (%)
TADRUL15
TADRUL20
TADRUL24
TADRUL30
TADRUL35
TADRUL40
TADRUL100
TADRUL230
TADRUL300
TADRUL400
TADRUL550
"A" TYPE - EXTENSION DRAINED

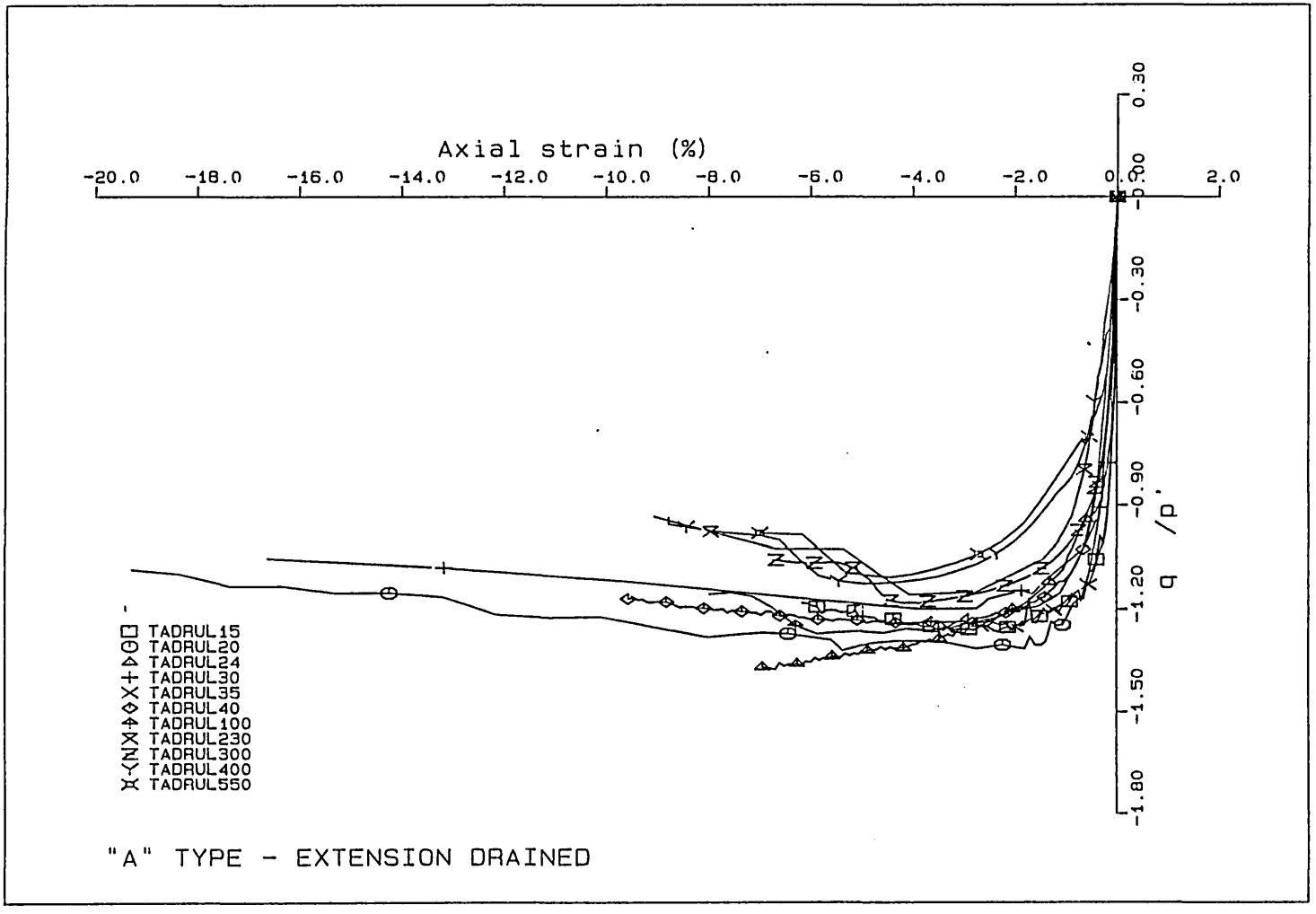
A4.I7


p' (kPa)
0. 60. 120. 180. 240. 300. 360. 420. 480. 540. 600. 660.
q (kPa)
0. -70. -140. -210. -280. -350. -420. -490.
TADRUL15
TADRUL20
TADRUL24
TADRUL30
TADRUL35
TADRUL40
TADRUL100
TADRUL230
TADRUL300
TADRUL400
TADRUL550
"A" TYPE - EXTENSION DRAINED

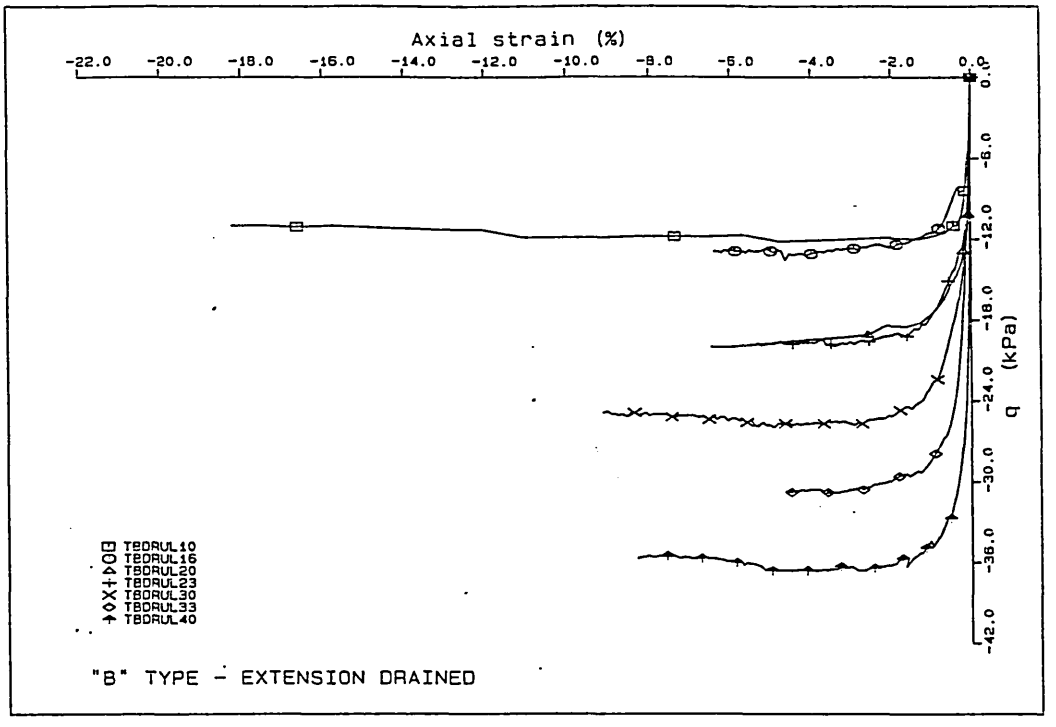
A4.I8


p' (kPa)
0.0 5.0 10.0 15.0 20.0 25.0 30.0 35.0 40.0 45.0 50.0 55.0
q (kPa)
10.0 0.0 -10.0 -20.0 -30.0 -40.0 -50.0 -60.0
TADRUL15
TADRUL20
TADRUL24
TADRUL30
TADRUL35
TADRUL40
TADRUL100
TADRUL230
TADRUL300
TADRUL400
TADRUL550
"A" TYPE - EXTENSION DRAINED

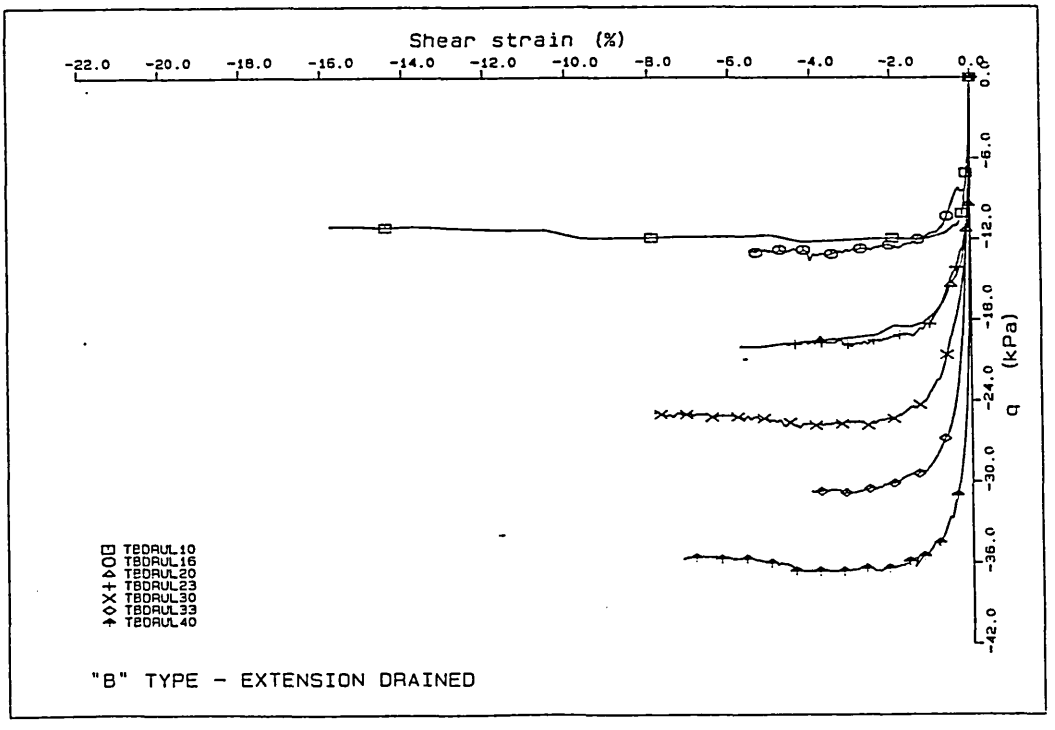
A4.I9


Axial strain (%)
-20.0
-18.0
-16.0
-14.0
-12.0
-10.0
-8.0
-6.0
-4.0
-2.0
0.0
2.0
0.30
0.00
-0.30
-0.60
-0.90
-1.20
-1.50
-1.80
q /p'
TADRUL15
TADRUL20
TADRUL24
TADRUL30
TADRUL35
TADRUL40
TADRUL100
TADRUL230
TADRUL300
TADRUL400
TADRUL550
"A" TYPE - EXTENSION DRAINED

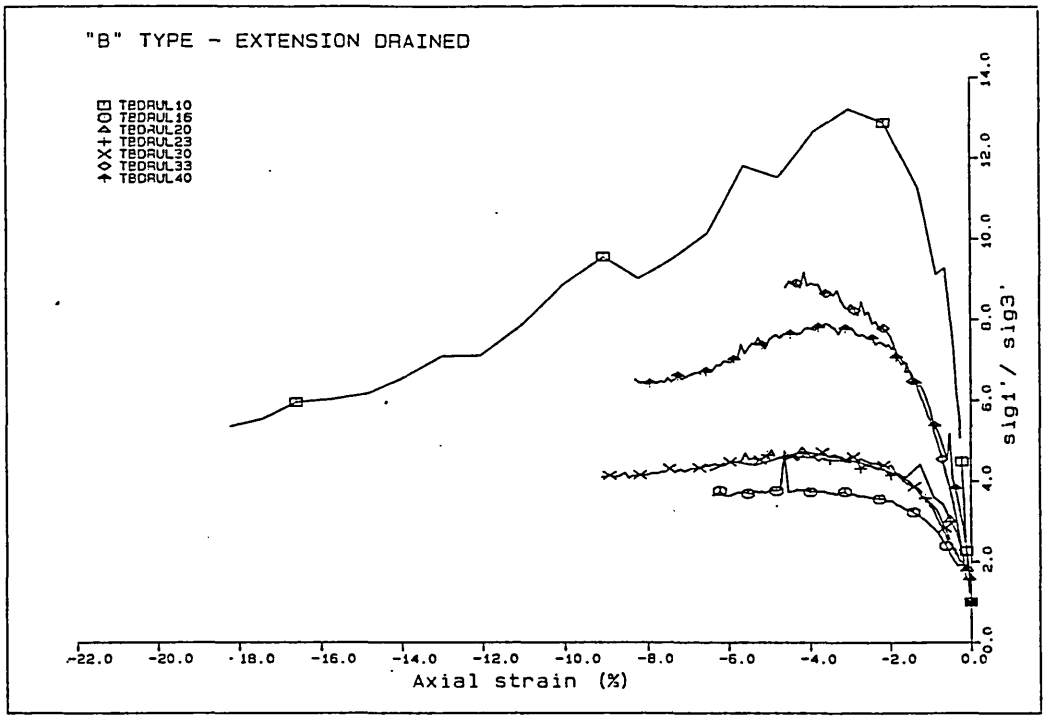
A4.I10


Axial strain (%)
-22.0
-20.0
-18.0
-16.0
-14.0
-12.0
-10.0
-8.0
-6.0
-4.0
-2.0
0.0
-6.0
-12.0
-18.0
-24.0
-30.0
-36.0
-42.0
q (kPa)
TBDRUL10
TBDRUL16
TBDRUL20
TBDRUL23
TBDRUL30
TBDRUL33
TBDRUL40
"B" TYPE - EXTENSION DRAINED

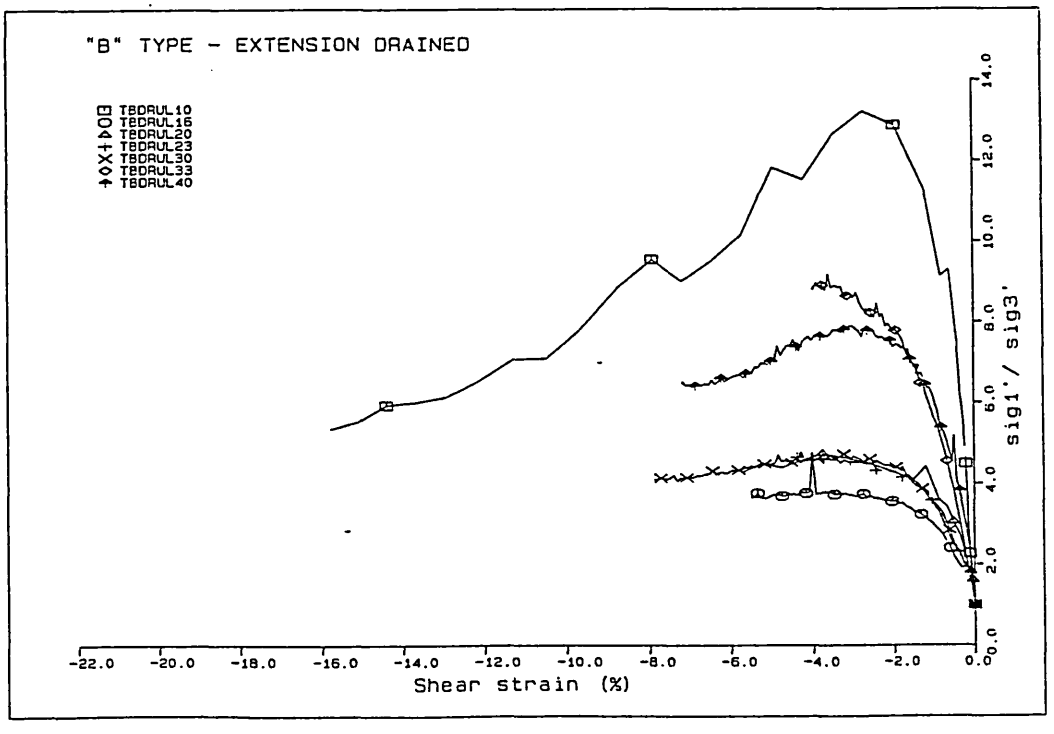
A4.J1


Shear strain (%)
-22.0
-20.0
-18.0
-16.0
-14.0
-12.0
-10.0
-8.0
-6.0
-4.0
-2.0
0.0
-6.0
-12.0
-18.0
-24.0
-30.0
-36.0
-42.0
q (kPa)
TBDRUL10
TBDRUL16
TBDRUL20
TBDRUL23
TBDRUL30
TBDRUL33
TBDRUL40
"B" TYPE - EXTENSION DRAINED

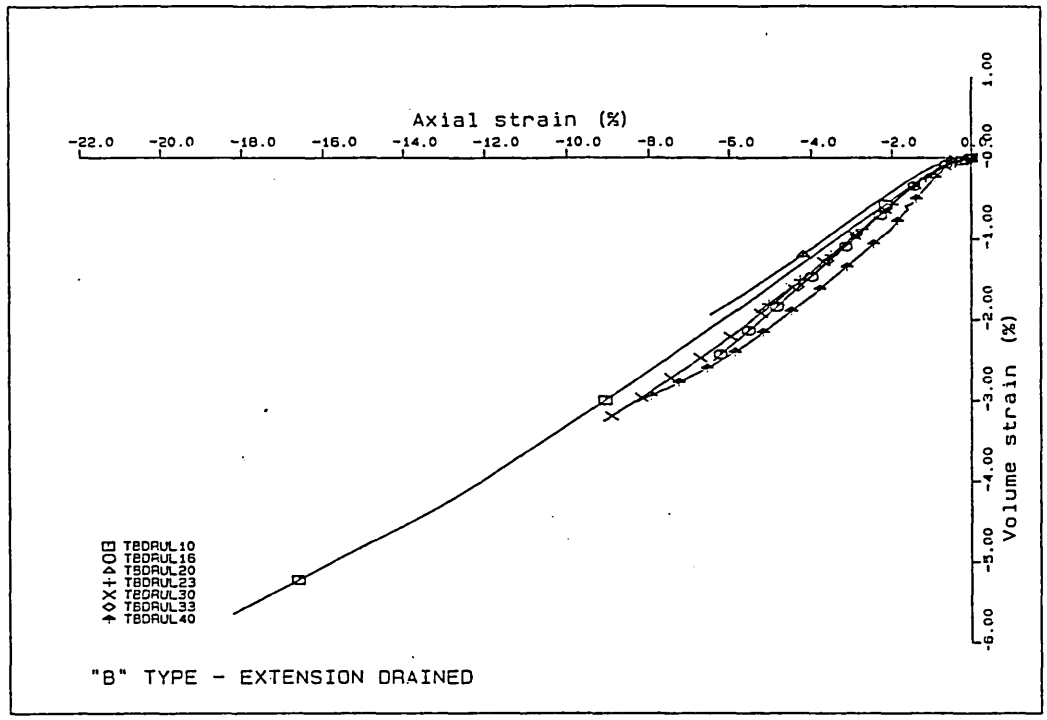
A4.J2


"B" TYPE - EXTENSION DRAINED
TBDRUL10
TBDRUL15
TBDRUL20
TBDRUL23
TBDRUL30
TBDRUL33
TBDRUL40
sig1' / sig3'
Axial strain (%)

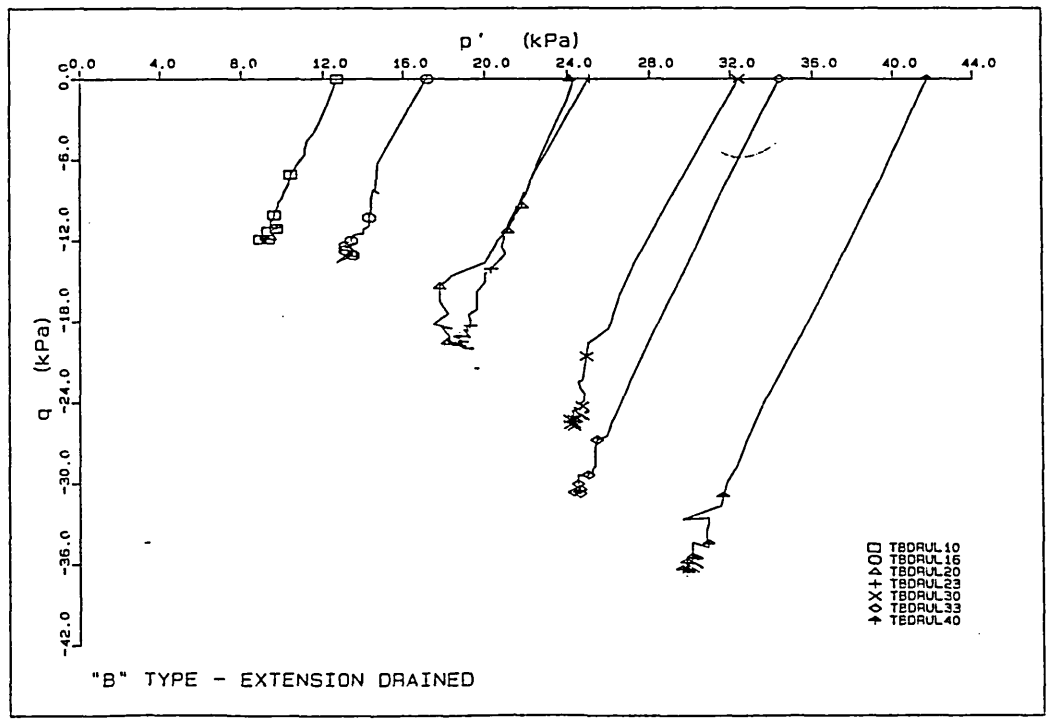
A4.J3


"B" TYPE - EXTENSION DRAINED
TBDRUL10
TBDRUL15
TBDRUL20
TBDRUL23
TBDRUL30
TBDRUL33
TBDRUL40
sig1' / sig3'
Shear strain (%)

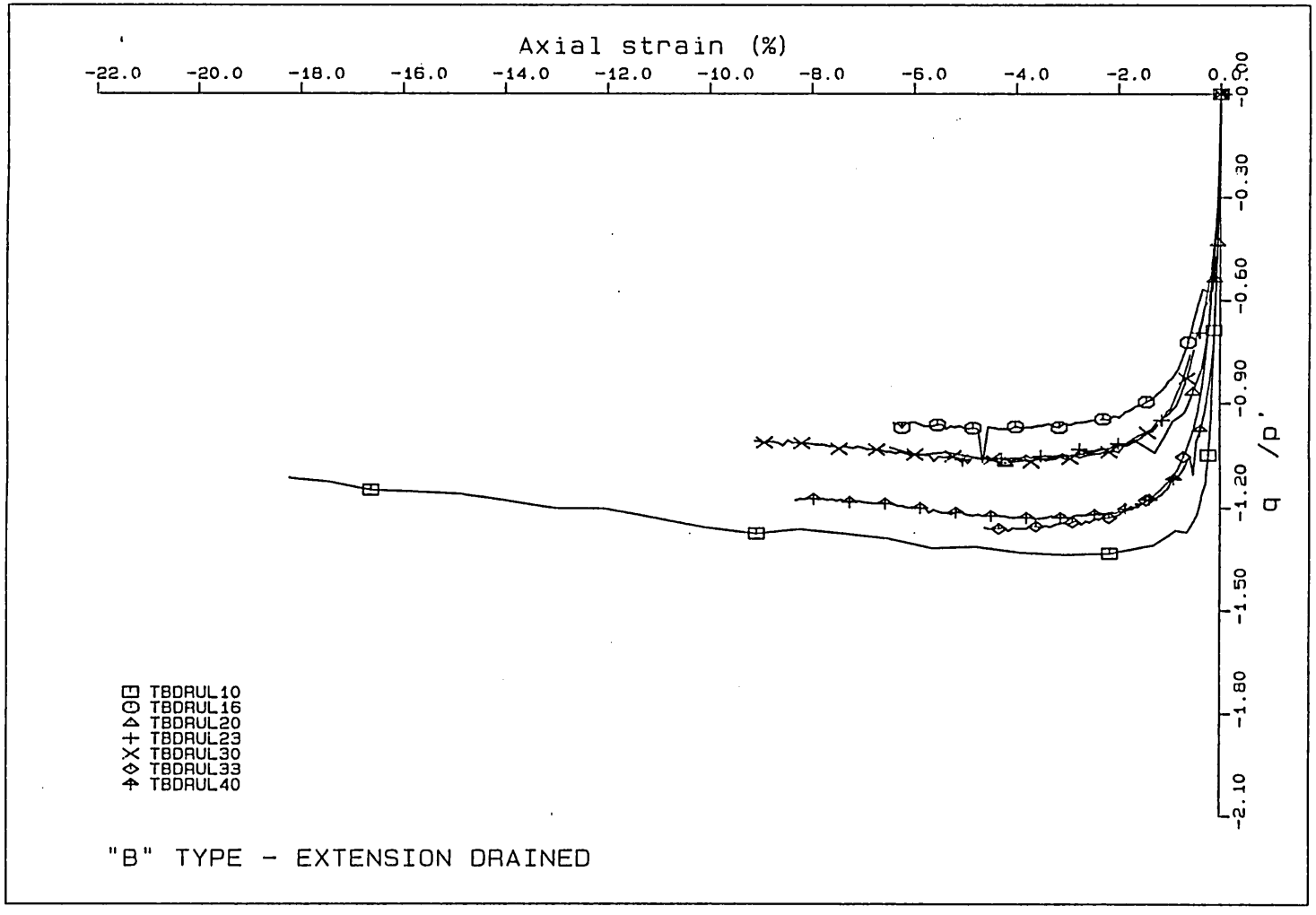
A4.J4


Axial strain (%)
-22.0 -20.0 -18.0 -16.0 -14.0 -12.0 -10.0 -8.0 -6.0 -4.0 -2.0 0.0
1.00 -0.00 -1.00 -2.00 -3.00 -4.00 -5.00 -6.00
Volume strain (%)
TBDAVL10
TBDAVL16
TBDAVL20
TBDAVL23
TBDAVL30
TBDAVL33
TBDAVL40
"B" TYPE - EXTENSION DRAINED

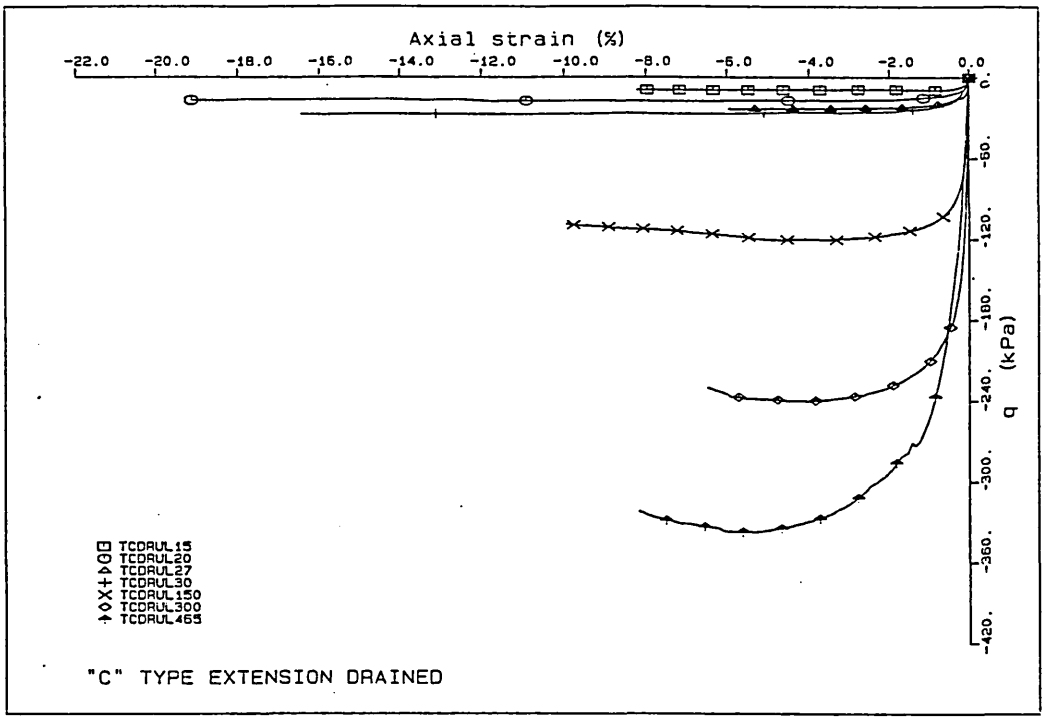
A4.J5


p' (kPa)
0.0 4.0 8.0 12.0 16.0 20.0 24.0 28.0 32.0 36.0 40.0 44.0
0.0 -6.0 -12.0 -18.0 -24.0 -30.0 -36.0 -42.0
q (kPa)
TBDAVL10
TBDAVL16
TBDAVL20
TBDAVL23
TBDAVL30
TBDAVL33
TBDAVL40
"B" TYPE - EXTENSION DRAINED

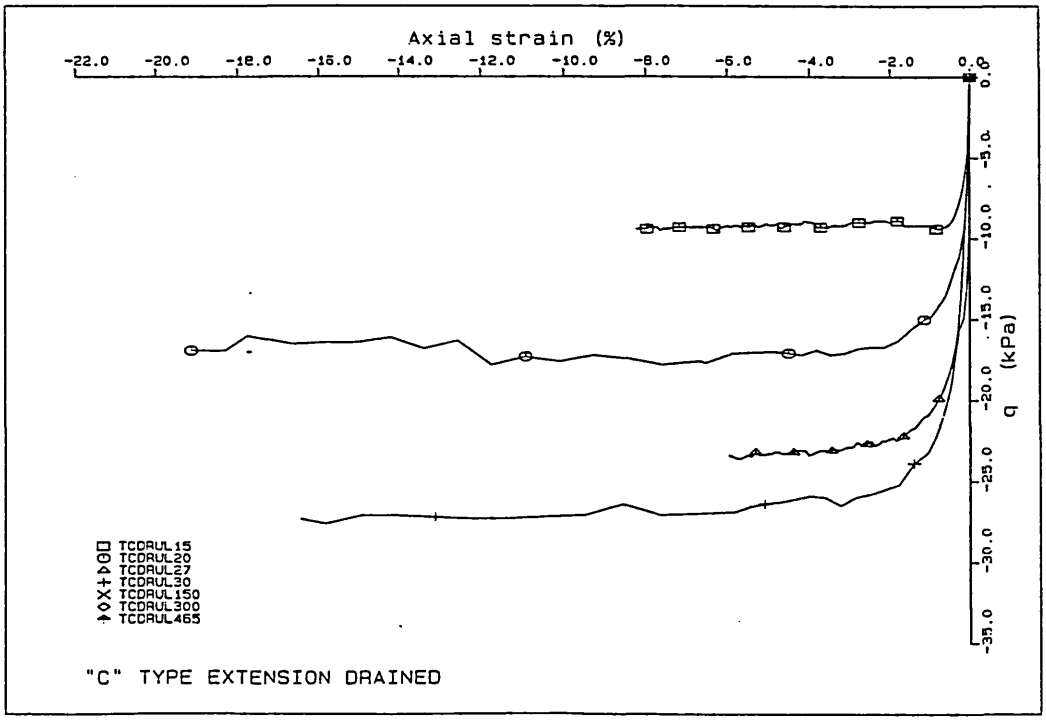
A4.J6


Axial strain (%)
-22.0
-20.0
-18.0
-16.0
-14.0
-12.0
-10.0
-8.0
-6.0
-4.0
-2.0
0.00
-0.30
-0.60
-0.90
-1.20
-1.50
-1.80
-2.10
q /p'
TBDRUL10
TBDRUL16
TBDRUL20
TBDRUL23
TBDRUL30
TBDRUL33
TBDRUL40
"B" TYPE - EXTENSION DRAINED

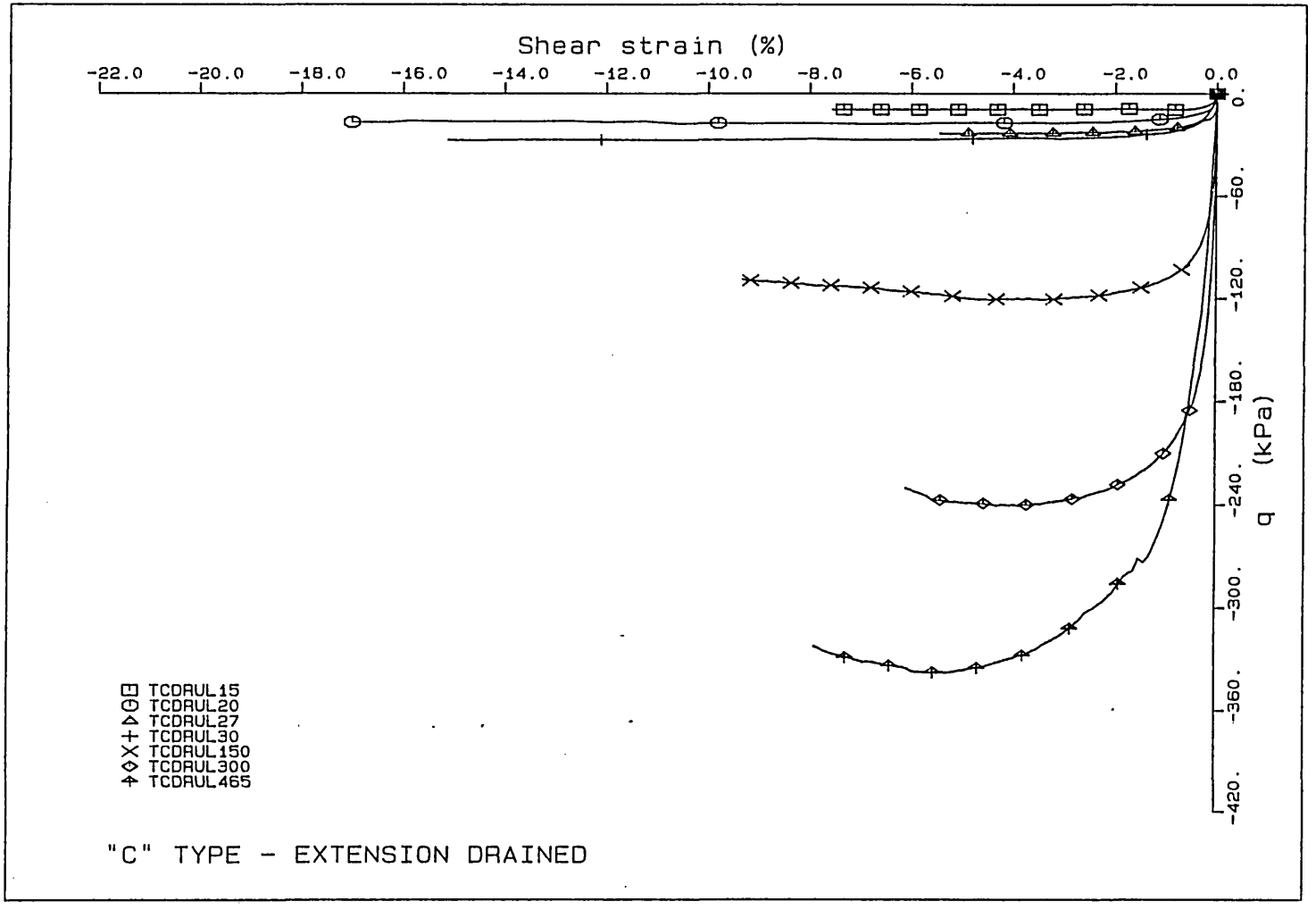
A4.J7


Axial strain (%)
-22.0 -20.0 -18.0 -16.0 -14.0 -12.0 -10.0 -8.0 -6.0 -4.0 -2.0 0.0
0. -60. -120. -180. -240. -300. -360. -420.
q (kPa)
TCDAUL15
TCDAUL20
TCDAUL27
TCDAUL30
TCDAUL150
TCDAUL300
TCDAUL465
"C" TYPE EXTENSION DRAINED

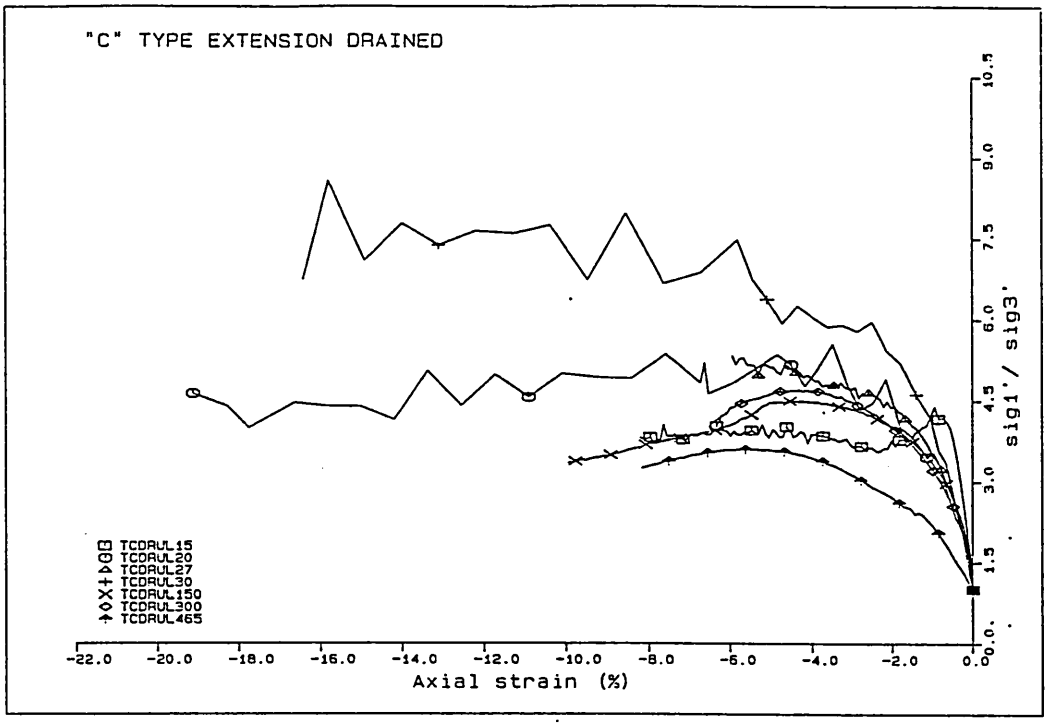
A4.K1


Axial strain (%)
-22.0 -20.0 -18.0 -16.0 -14.0 -12.0 -10.0 -8.0 -6.0 -4.0 -2.0 0.0
0.0 -5.0 -10.0 -15.0 -20.0 -25.0 -30.0 -35.0
q (kPa)
TCDAUL15
TCDAUL20
TCDAUL27
TCDAUL30
TCDAUL150
TCDAUL300
TCDAUL465
"C" TYPE EXTENSION DRAINED

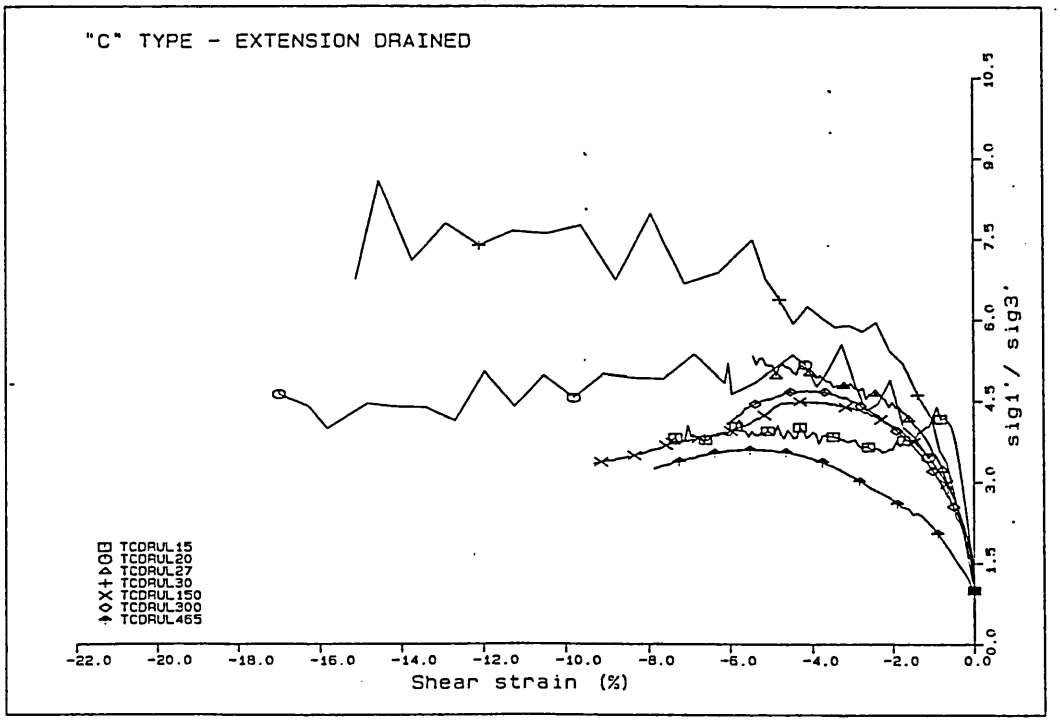
A4.K2


Shear strain (%)
-22.0
-20.0
-18.0
-16.0
-14.0
-12.0
-10.0
-8.0
-6.0
-4.0
-2.0
0.0
0.
-60.
-120.
-180.
-240.
-300.
-360.
-420.
q (kPa)
TCDAUL15
TCDAUL20
TCDAUL27
TCDAUL30
TCDAUL150
TCDAUL300
TCDAUL465
"C" TYPE - EXTENSION DRAINED

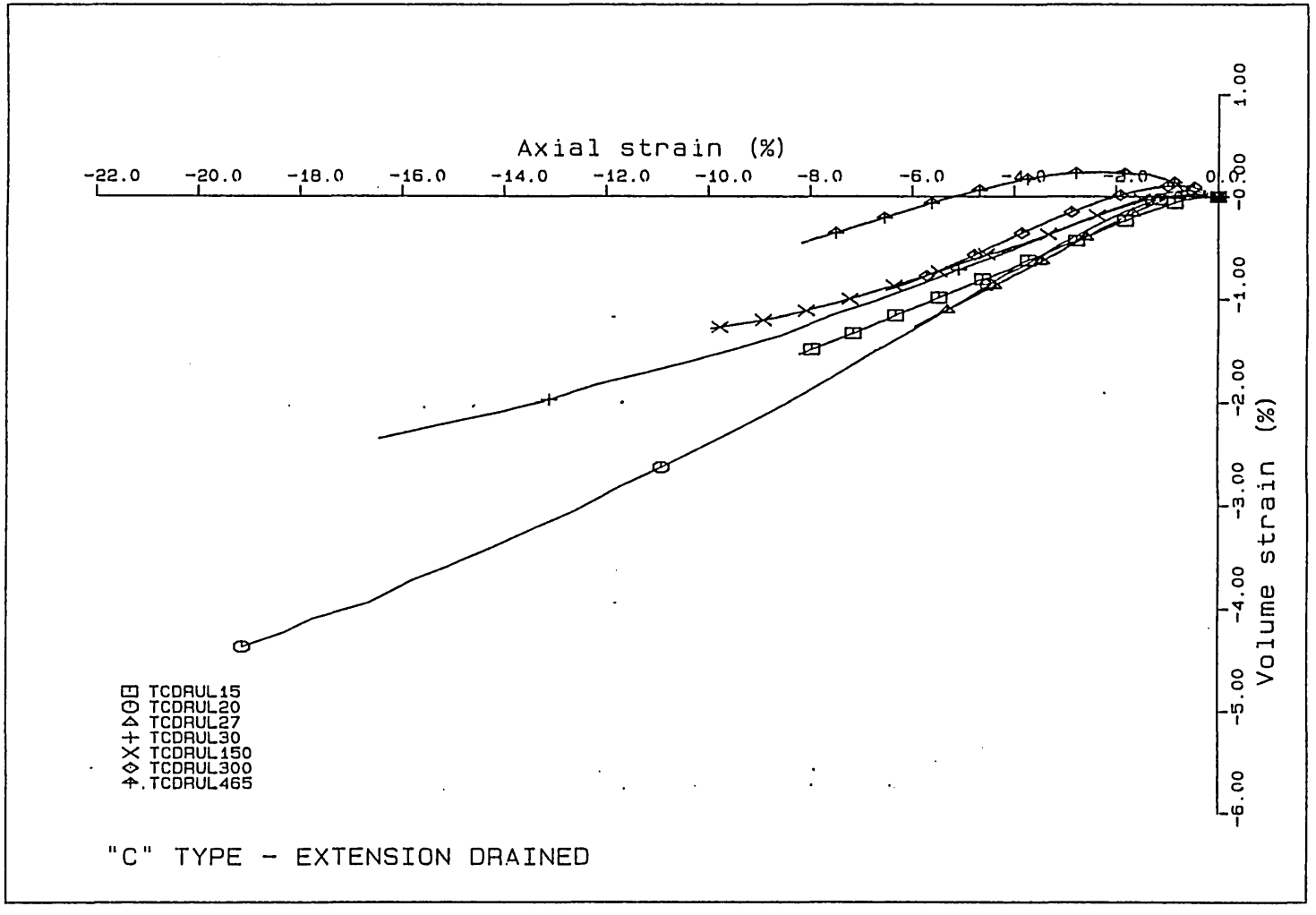
A4.K3


"C" TYPE EXTENSION DRAINED
TCDRUL15
TCDRUL20
TCDRUL27
TCDRUL30
TCDRUL150
TCDRUL300
TCDRUL465
-22.0 -20.0 -18.0 -16.0 -14.0 -12.0 -10.0 -8.0 -6.0 -4.0 -2.0 0.0
Axial strain (%)
0.0 1.5 3.0 4.5 6.0 7.5 9.0 10.5
sig1' / sig3'

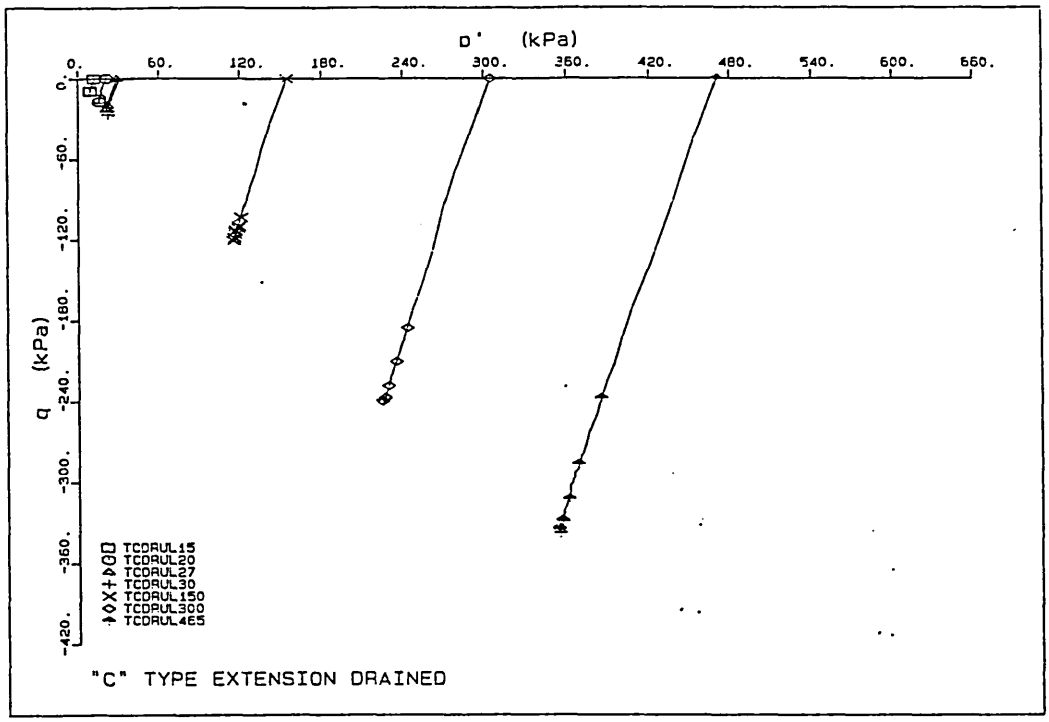
A4.K4


"C" TYPE - EXTENSION DRAINED
TCDRUL15
TCDRUL20
TCDRUL27
TCDRUL30
TCDRUL150
TCDRUL300
TCDRUL465
-22.0 -20.0 -18.0 -16.0 -14.0 -12.0 -10.0 -8.0 -6.0 -4.0 -2.0 0.0
Shear strain (%)
0.0 1.5 3.0 4.5 6.0 7.5 9.0 10.5
sig1' / sig3'

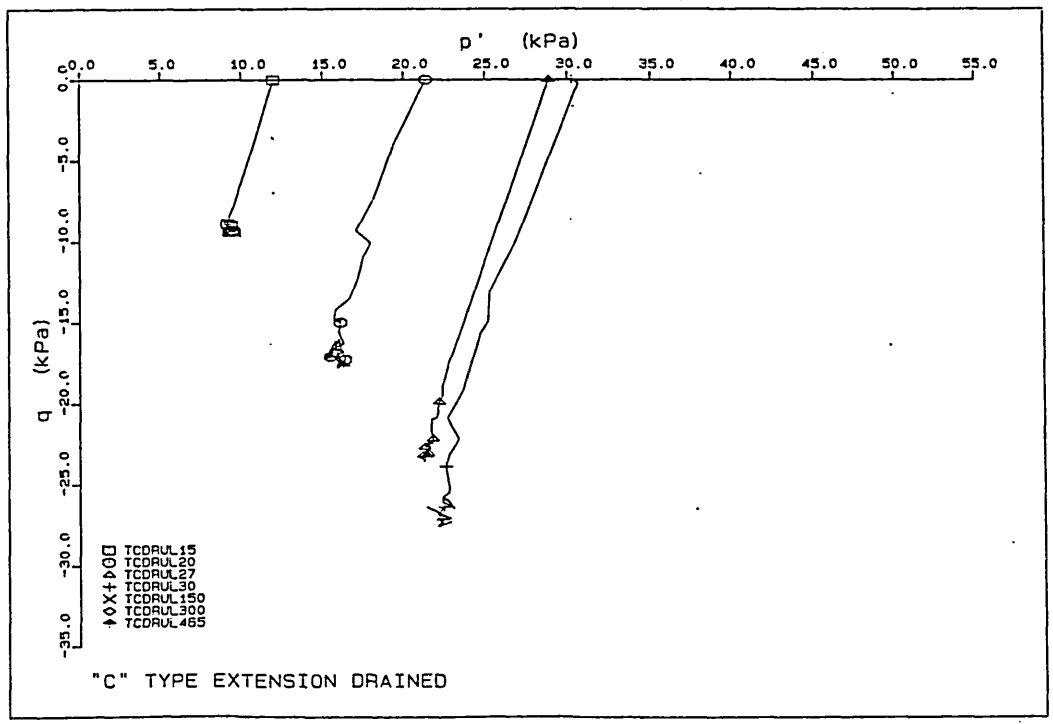
A4.K5


Axial strain (%)
-22.0
-20.0
-18.0
-16.0
-14.0
-12.0
-10.0
-8.0
-6.0
-4.0
-2.0
0.0
1.00
-0.00
-1.00
-2.00
-3.00
-4.00
-5.00
-6.00
Volume strain (%)
TCDRUL15
TCDRUL20
TCDRUL27
TCDRUL30
TCDRUL150
TCDRUL300
TCDRUL465
"C" TYPE - EXTENSION DRAINED

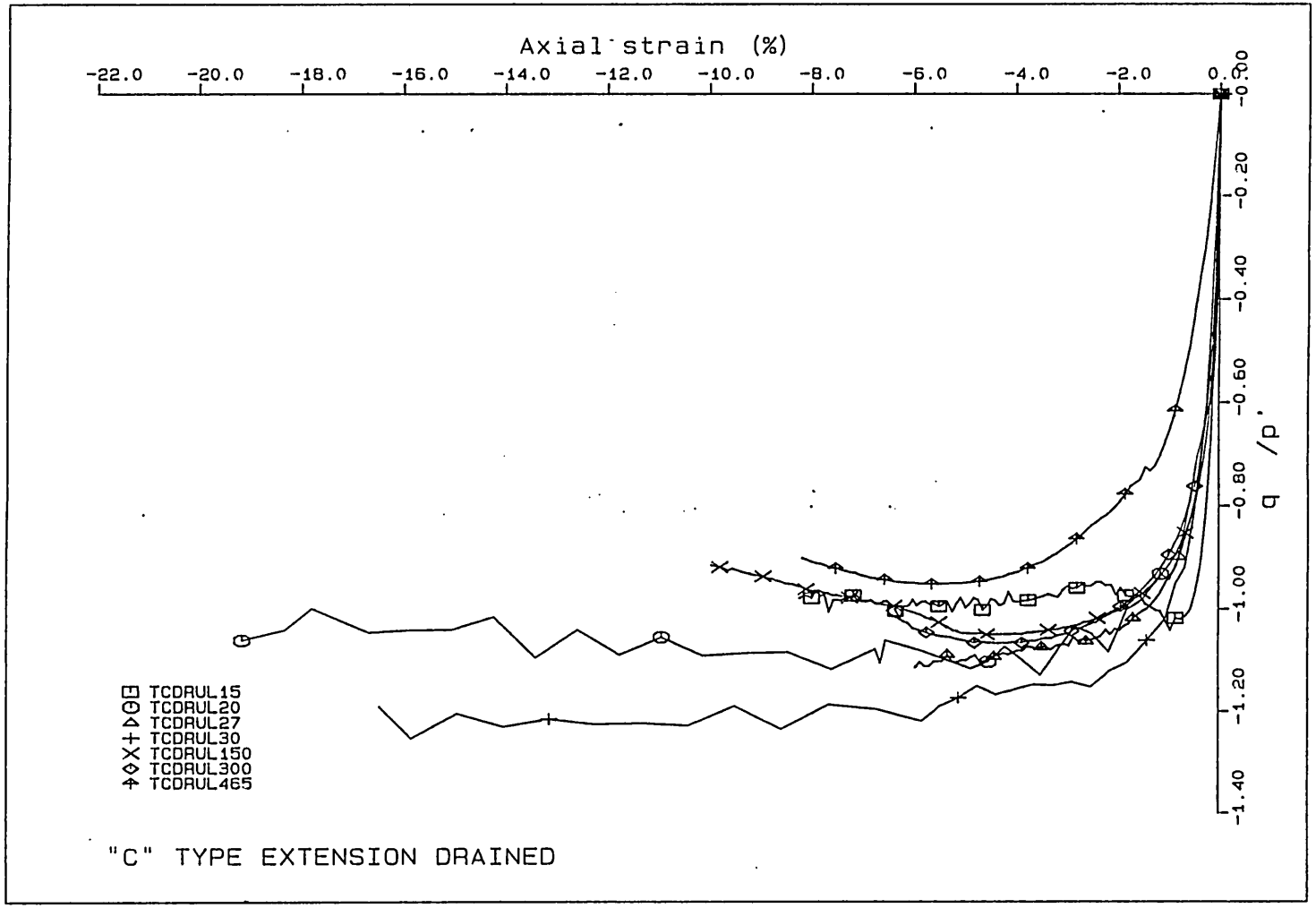
A4.K6


p' (kPa)
0. 60. 120. 180. 240. 300. 360. 420. 480. 540. 600. 660.
q (kPa)
0. -60. -120. -180. -240. -300. -360. -420.
TCDRUL15
TCDRUL20
TCDRUL27
TCDRUL30
TCDRUL150
TCDRUL300
TCDRUL465
"C" TYPE EXTENSION DRAINED

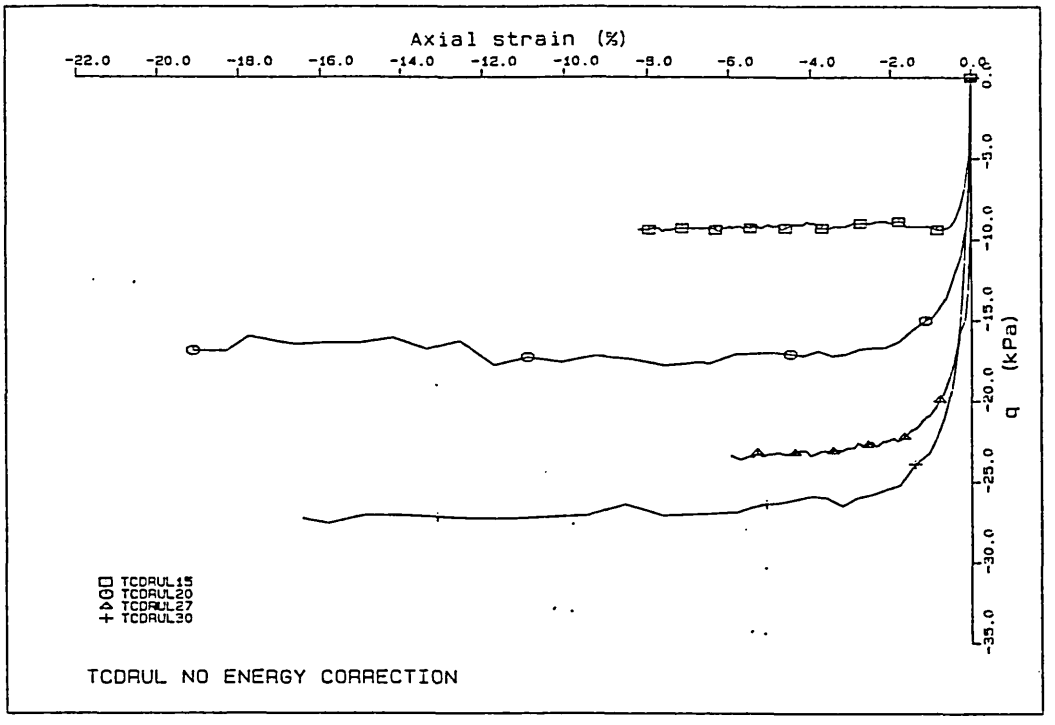
A4.K7


p' (kPa)
0.0 5.0 10.0 15.0 20.0 25.0 30.0 35.0 40.0 45.0 50.0 55.0
q (kPa)
0.0 -5.0 -10.0 -15.0 -20.0 -25.0 -30.0 -35.0
TCDRUL15
TCDRUL20
TCDRUL27
TCDRUL30
TCDRUL150
TCDRUL300
TCDRUL465
"C" TYPE EXTENSION DRAINED

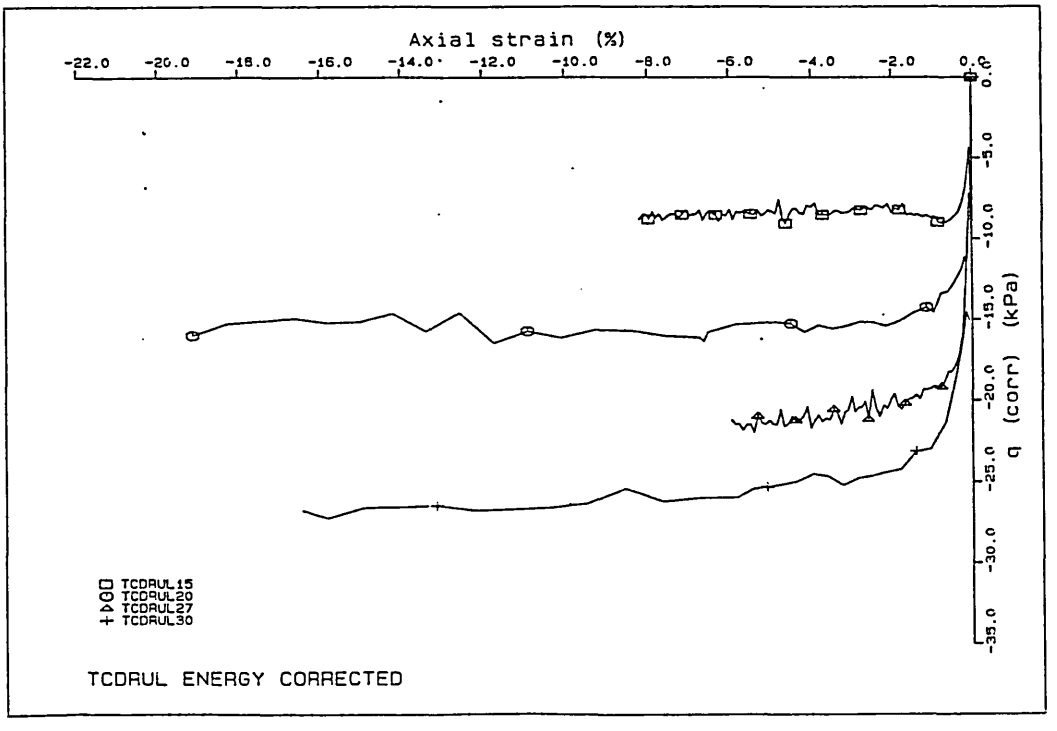
A4.K8


Axial strain (%)
-22.0
-20.0
-18.0
-16.0
-14.0
-12.0
-10.0
-8.0
-6.0
-4.0
-2.0
0.00
-0.20
-0.40
-0.60
-0.80
-1.00
-1.20
-1.40
q /p'
TCDRUL15
TCDRUL20
TCDRUL27
TCDRUL30
TCDRUL150
TCDRUL300
TCDRUL465
"C" TYPE EXTENSION DRAINED

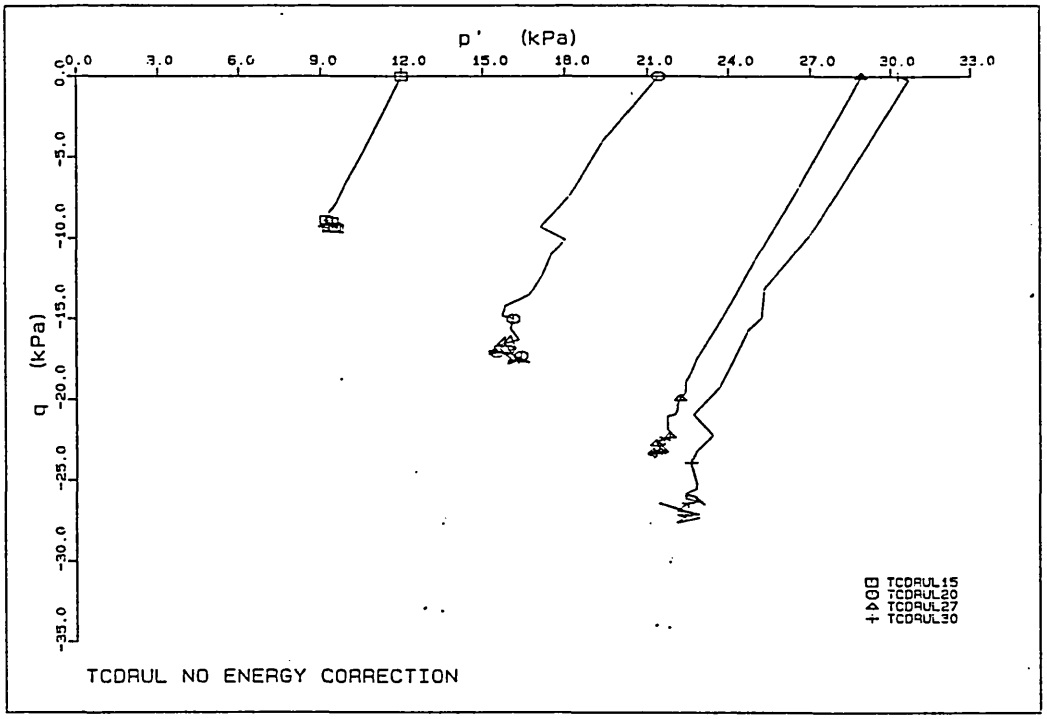
A4.K9


Axial strain (%)
-22.0 -20.0 -18.0 -16.0 -14.0 -12.0 -10.0 -8.0 -6.0 -4.0 -2.0 0.0
-5.0 -10.0 -15.0 -20.0 -25.0 -30.0 -35.0
q (kPa)
TCDRUL15
TCDRUL20
TCDRUL27
TCDRUL30
TCDRUL NO ENERGY CORRECTION

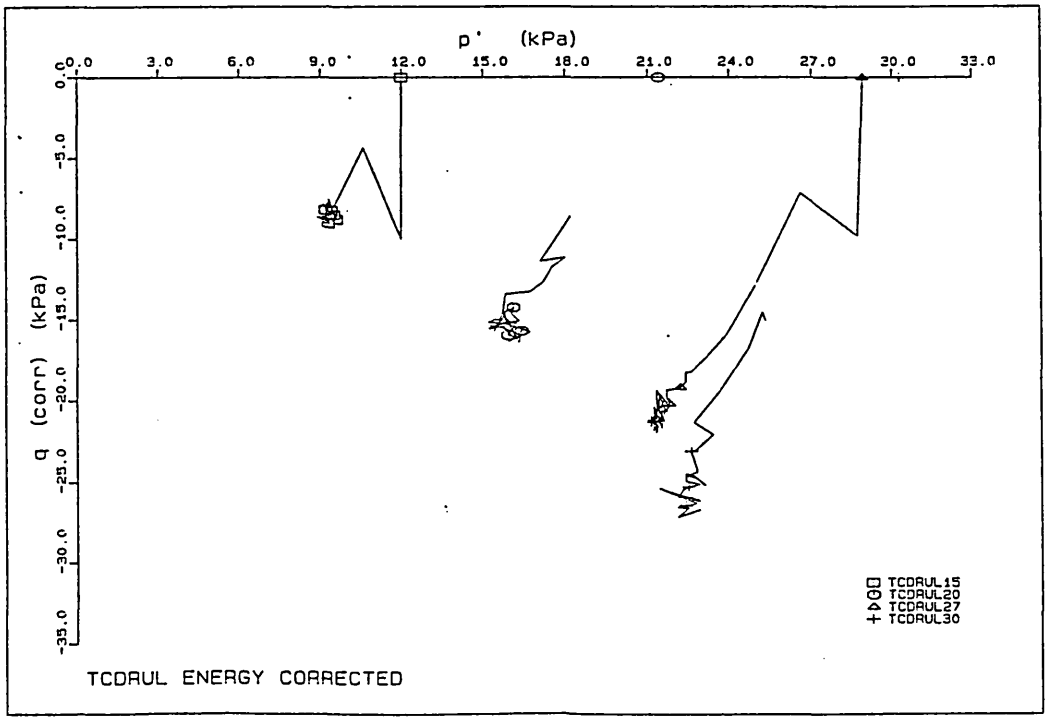
A4.K10


Axial strain (%)
-22.0 -20.0 -18.0 -16.0 -14.0 -12.0 -10.0 -8.0 -6.0 -4.0 -2.0 0.0
-5.0 -10.0 -15.0 -20.0 -25.0 -30.0 -35.0
q (corr) (kPa)
TCDRUL15
TCDRUL20
TCDRUL27
TCDRUL30
TCDRUL ENERGY CORRECTED

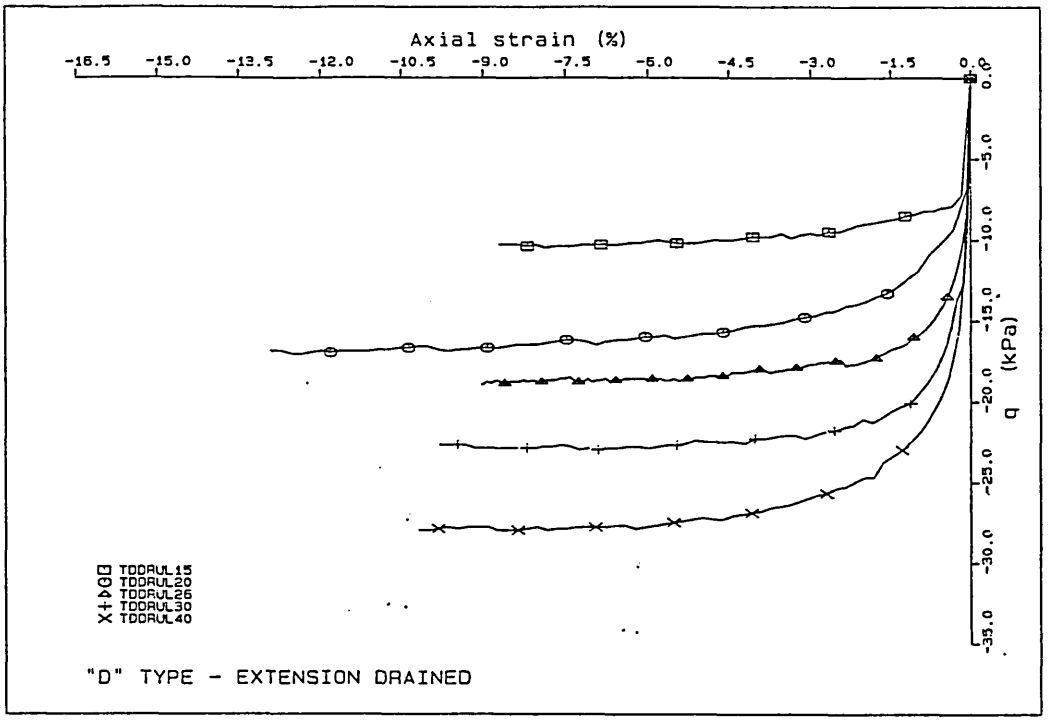
A4.K11


p' (kPa)
0.0
3.0
6.0
9.0
12.0
15.0
18.0
21.0
24.0
27.0
30.0
33.0
q (kPa)
-5.0
-10.0
-15.0
-20.0
-25.0
-30.0
-35.0
TCDAUL15
TCDAUL20
TCDAUL27
TCDAUL30
TCDAUL NO ENERGY CORRECTION

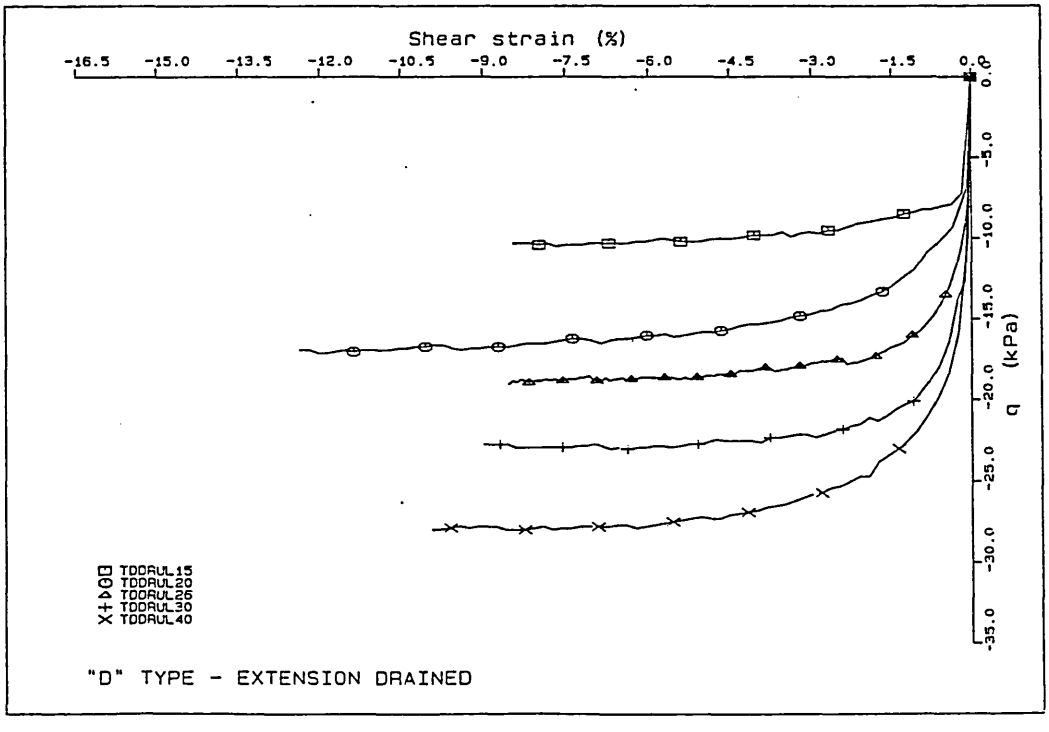
A4.K12


p' (kPa)
0.0
3.0
6.0
9.0
12.0
15.0
18.0
21.0
24.0
27.0
30.0
33.0
q (corr) (kPa)
-5.0
-10.0
-15.0
-20.0
-25.0
-30.0
-35.0
TCDAUL15
TCDAUL20
TCDAUL27
TCDAUL30
TCDAUL ENERGY CORRECTED

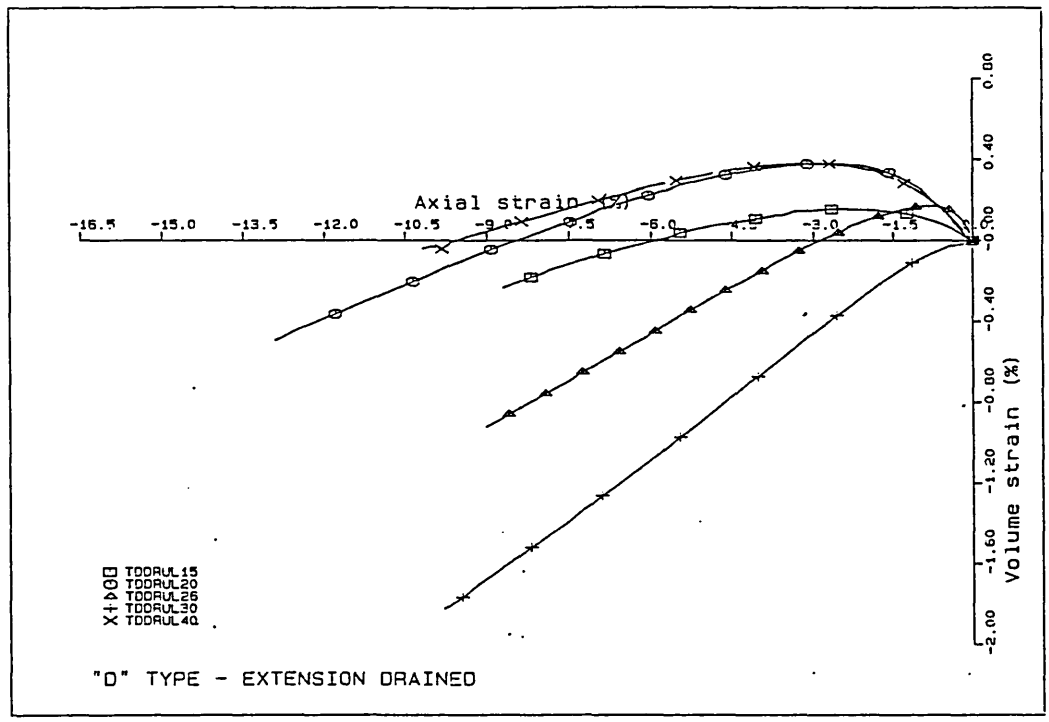
A4.K13


Axial strain (%)
-16.5 -15.0 -13.5 -12.0 -10.5 -9.0 -7.5 -6.0 -4.5 -3.0 -1.5 0.0
0.0 -5.0 -10.0 -15.0 -20.0 -25.0 -30.0 -35.0
q (kPa)
TDDAVL15
TDDAVL20
TDDAVL25
TDDAVL30
TDDAVL40
"D" TYPE - EXTENSION DRAINED

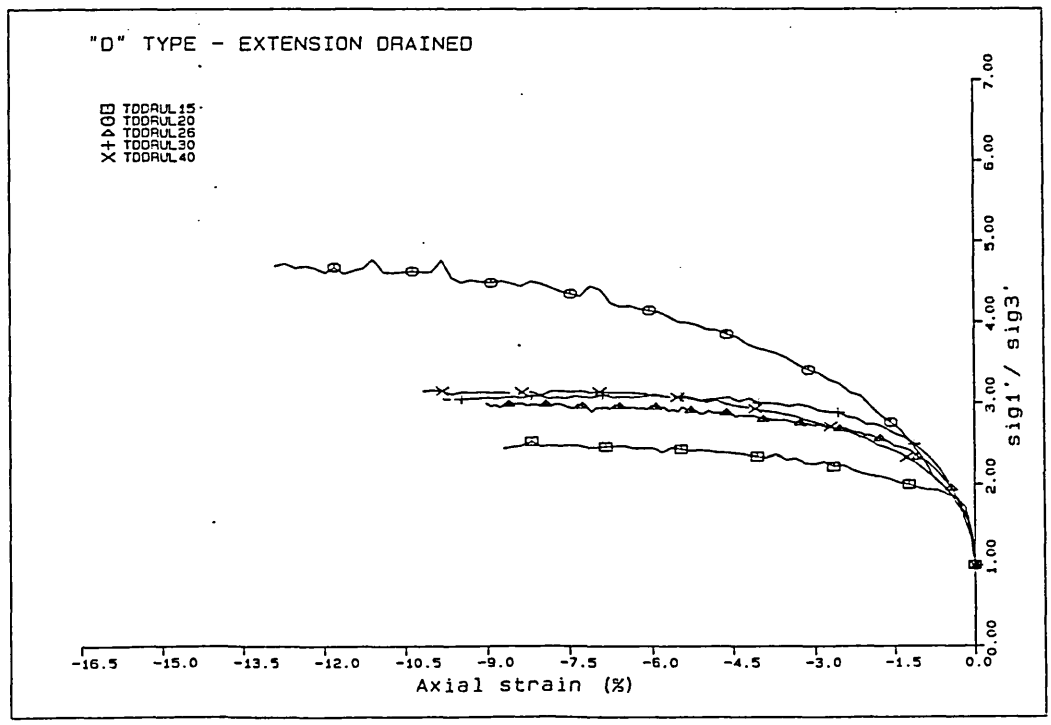
A4.L1


Shear strain (%)
-16.5 -15.0 -13.5 -12.0 -10.5 -9.0 -7.5 -6.0 -4.5 -3.0 -1.5 0.0
0.0 -5.0 -10.0 -15.0 -20.0 -25.0 -30.0 -35.0
q (kPa)
TDDAVL15
TDDAVL20
TDDAVL25
TDDAVL30
TDDAVL40
"D" TYPE - EXTENSION DRAINED

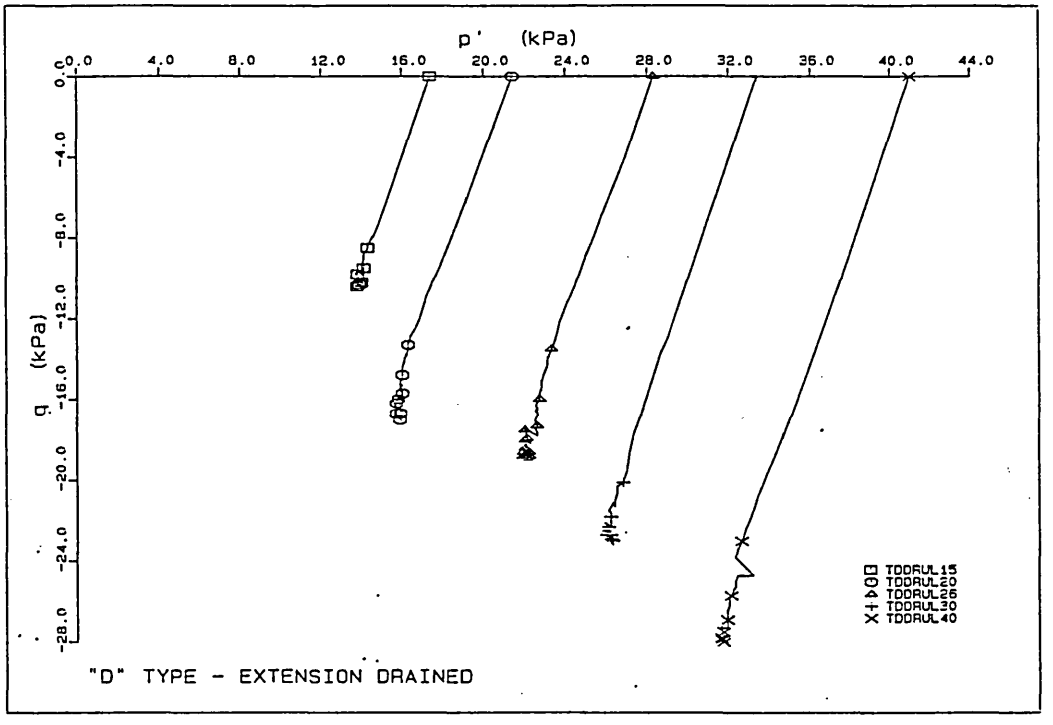
A4.L2


Axial strain (%)
-16.5
-15.0
-13.5
-12.0
-10.5
-9.0
-7.5
-6.0
-4.5
-3.0
-1.5
0.00
0.40
-0.00
-0.40
-0.80
-1.20
-1.60
-2.00
Volume strain (%)
TDDAUL15
TDDAUL20
TDDAUL26
TDDAUL30
TDDAUL40
"D" TYPE - EXTENSION DRAINED

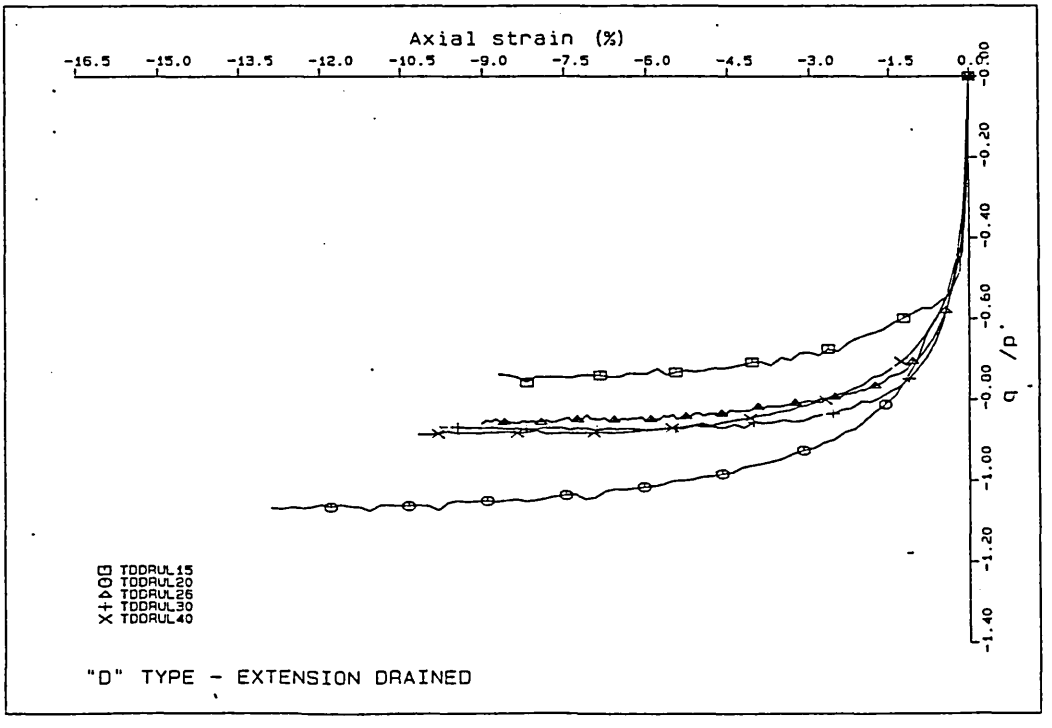
A4.L3


"D" TYPE - EXTENSION DRAINED
TDDAUL15
TDDAUL20
TDDAUL26
TDDAUL30
TDDAUL40
7.00
6.00
5.00
4.00
3.00
2.00
1.00
0.00
sig1'/ sig3'
-16.5
-15.0
-13.5
-12.0
-10.5
-9.0
-7.5
-6.0
-4.5
-3.0
-1.5
0.0
Axial strain (%)

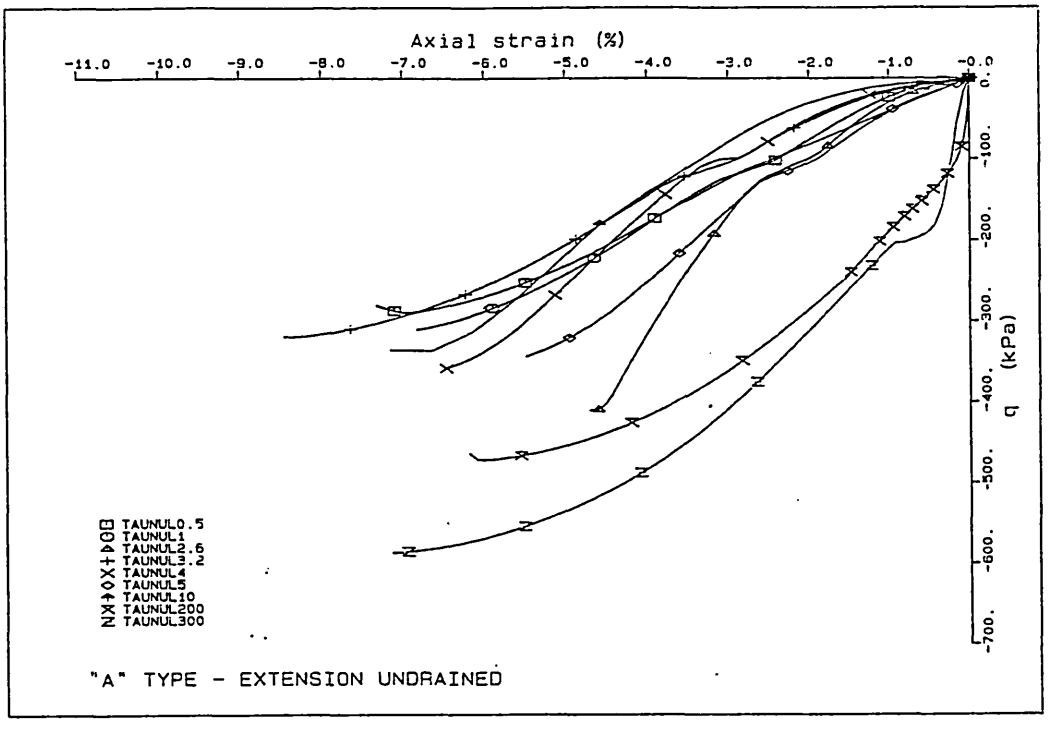
A4.L4


p' (kPa)
0.0
4.0
8.0
12.0
16.0
20.0
24.0
28.0
32.0
36.0
40.0
44.0
q (kPa)
0.
-4.0
-8.0
-12.0
-16.0
-20.0
-24.0
-28.0
TDDRUL15
TDDRUL20
TDDRUL25
TDDRUL30
TDDRUL40
"D" TYPE - EXTENSION DRAINED

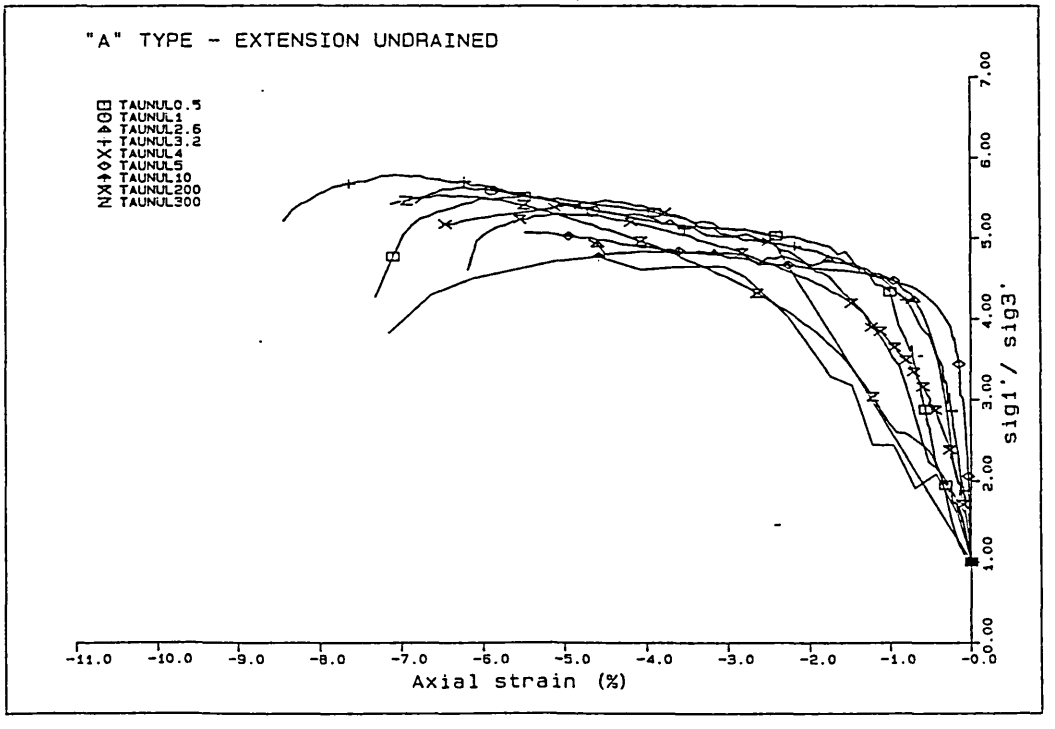
A4.L5


Axial strain (%)
-16.5
-15.0
-13.5
-12.0
-10.5
-9.0
-7.5
-6.0
-4.5
-3.0
-1.5
0.0
q /p'
0.00
-0.20
-0.40
-0.60
-0.80
-1.00
-1.20
-1.40
TDDRUL15
TDDRUL20
TDDRUL25
TDDRUL30
TDDRUL40
"D" TYPE - EXTENSION DRAINED

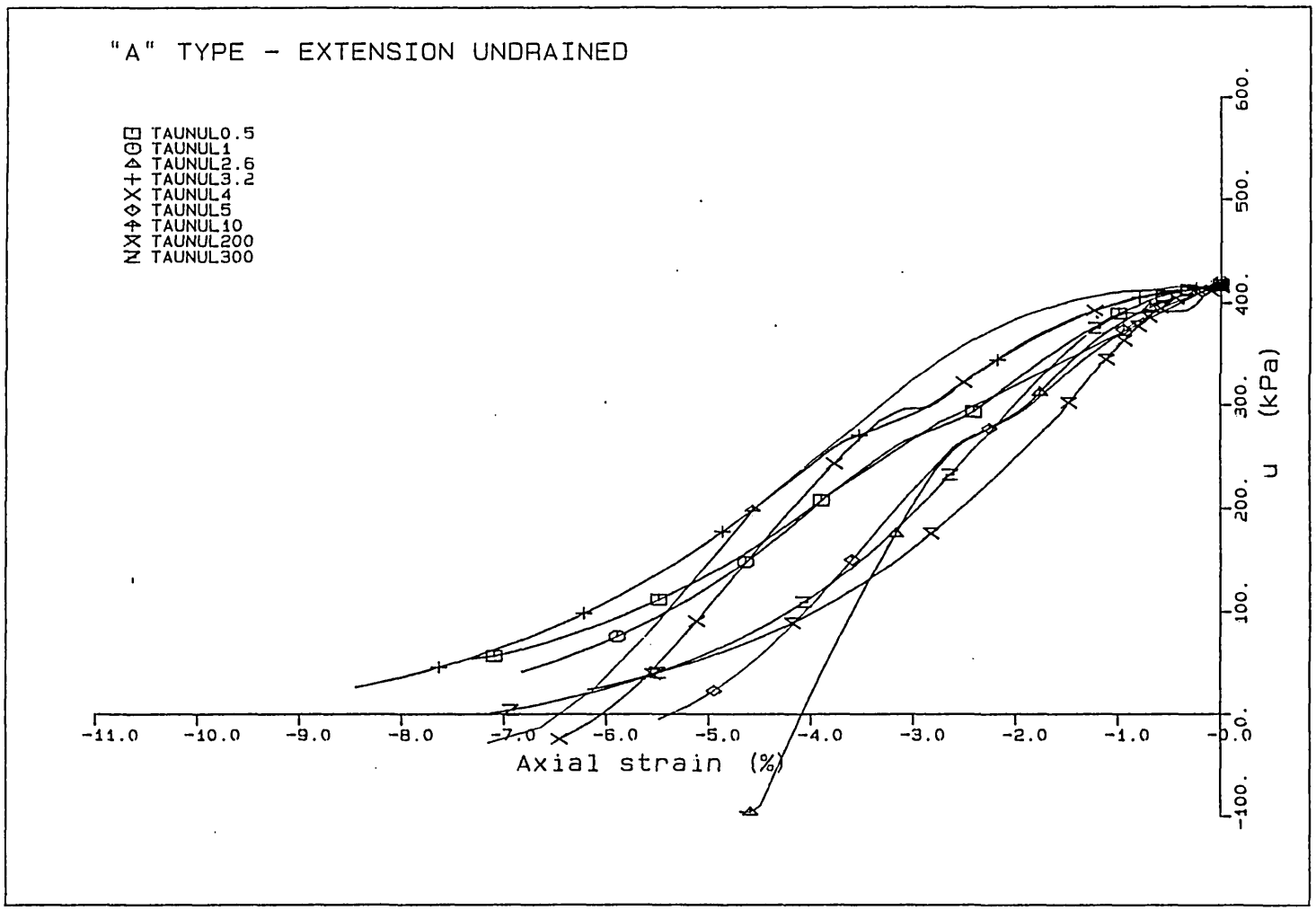
A4.L6


Axial strain (%)
-11.0 -10.0 -9.0 -8.0 -7.0 -6.0 -5.0 -4.0 -3.0 -2.0 -1.0 -0.0
-100. -200. -300. -400. -500. -600. -700.
q (kPa)
TAUNUL0.5
TAUNUL1
TAUNUL2.6
TAUNUL3.2
TAUNUL4
TAUNUL5
TAUNUL10
TAUNUL200
TAUNUL300
"A" TYPE - EXTENSION UNDRAINED

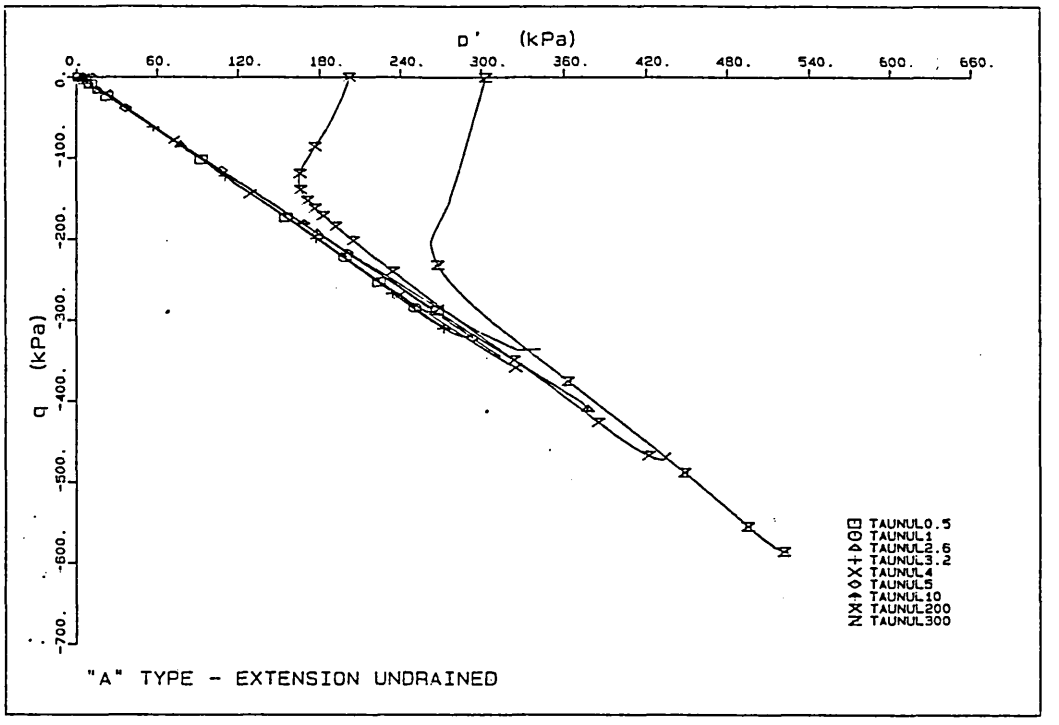
A4.M1


"A" TYPE - EXTENSION UNDRAINED
TAUNUL0.5
TAUNUL1
TAUNUL2.6
TAUNUL3.2
TAUNUL4
TAUNUL5
TAUNUL10
TAUNUL200
TAUNUL300
7.00 6.00 5.00 4.00 3.00 2.00 1.00 0.00
sig1'/ sig3'
-11.0 -10.0 -9.0 -8.0 -7.0 -6.0 -5.0 -4.0 -3.0 -2.0 -1.0 -0.0
Axial strain (%)

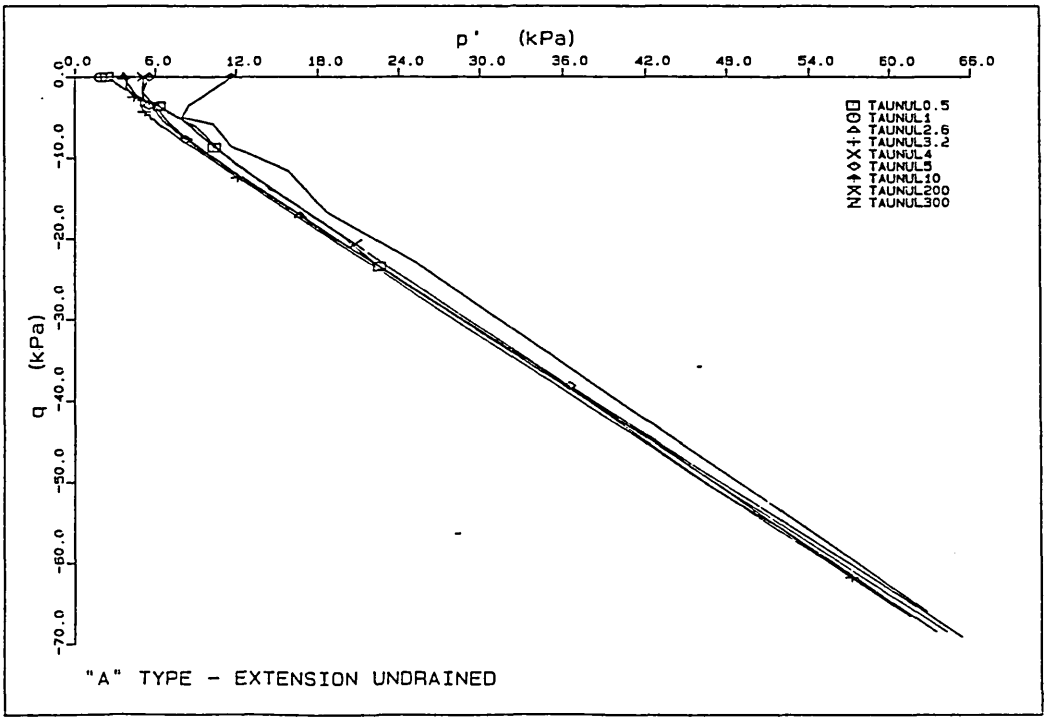
A4.M2


"A" TYPE - EXTENSION UNDRAINED
TAUNUL0.5
TAUNUL1
TAUNUL2.6
TAUNUL3.2
TAUNUL4
TAUNUL5
TAUNUL10
TAUNUL200
TAUNUL300
600.
500.
400.
300.
200.
100.
0.
-100.
u (kPa)
-11.0
-10.0
-9.0
-8.0
-7.0
-6.0
-5.0
-4.0
-3.0
-2.0
-1.0
-0.0
Axial strain (%)

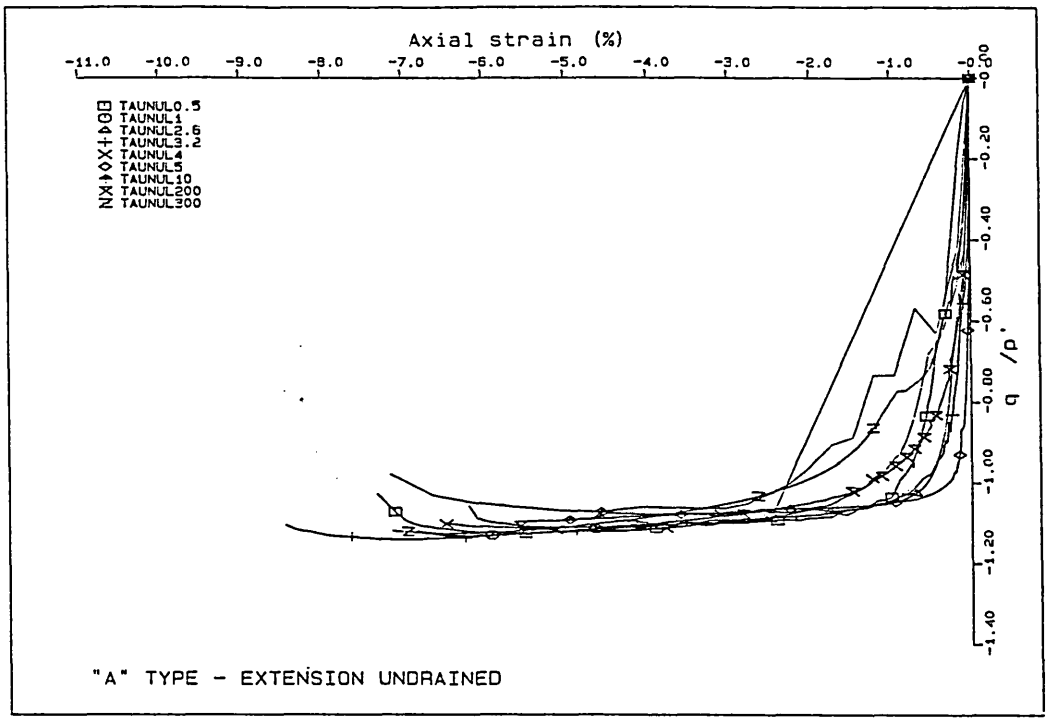
A4.M3


p' (kPa)
0. 60. 120. 180. 240. 300. 360. 420. 480. 540. 600. 660.
q (kPa)
0. -100. -200. -300. -400. -500. -600. -700.
TAUNUL0.5
TAUNUL1
TAUNUL2.6
TAUNUL3.2
TAUNUL4
TAUNUL5
TAUNUL10
TAUNUL200
TAUNUL300
"A" TYPE - EXTENSION UNDRAINED

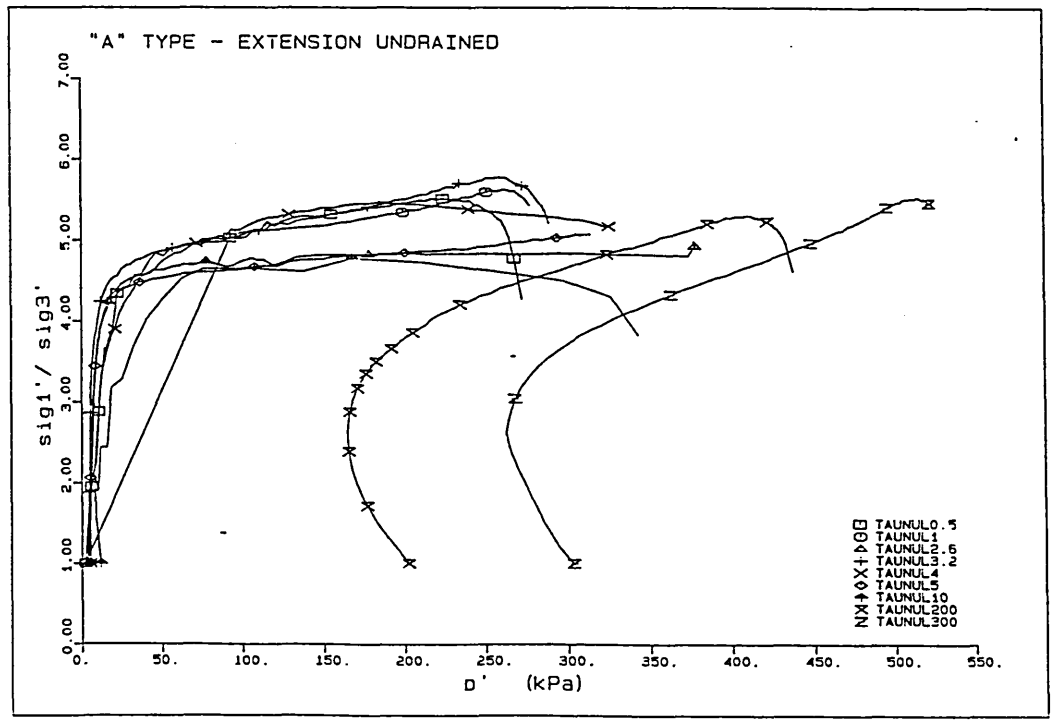
A4.M4


p' (kPa)
0.0 6.0 12.0 18.0 24.0 30.0 36.0 42.0 48.0 54.0 60.0 66.0
q (kPa)
0. -10.0 -20.0 -30.0 -40.0 -50.0 -60.0 -70.0
TAUNUL0.5
TAUNUL1
TAUNUL2.6
TAUNUL3.2
TAUNUL4
TAUNUL5
TAUNUL10
TAUNUL200
TAUNUL300
"A" TYPE - EXTENSION UNDRAINED

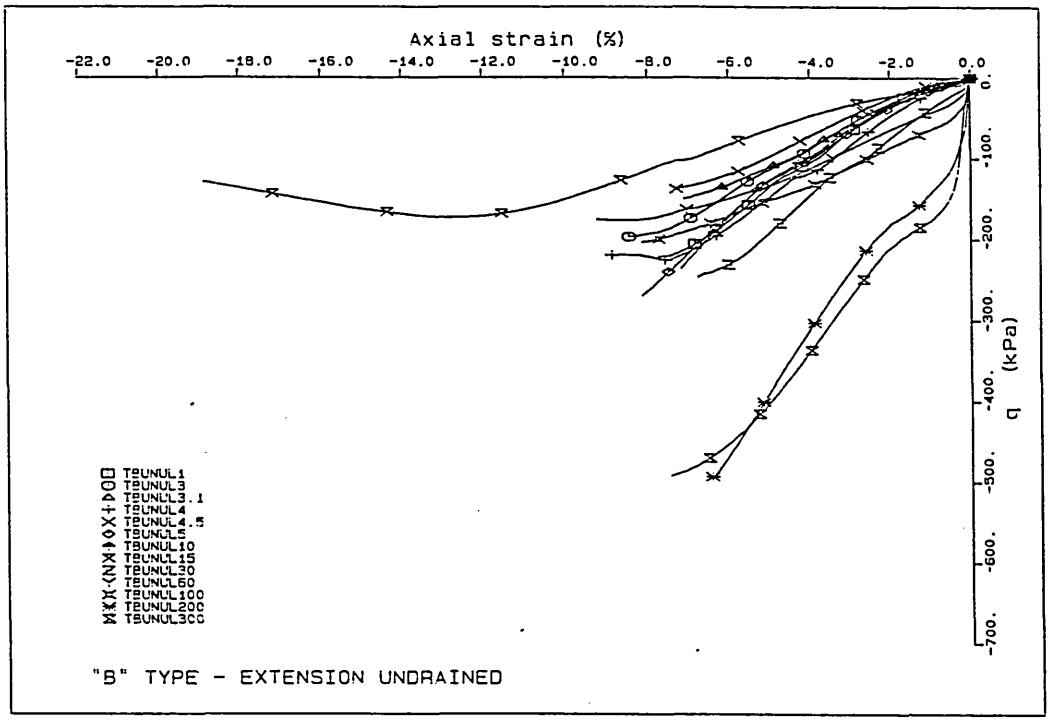
A4.M5


Axial strain (%)
-11.0 -10.0 -9.0 -8.0 -7.0 -6.0 -5.0 -4.0 -3.0 -2.0 -1.0 -0.0
TAUNUL0.5
TAUNUL1
TAUNUL2.6
TAUNUL3.2
TAUNUL4
TAUNUL5
TAUNUL10
TAUNUL200
TAUNUL300
-0.00 -0.20 -0.40 -0.60 -0.80 -1.00 -1.20 -1.40
q /p'
"A" TYPE - EXTENSION UNDRAINED

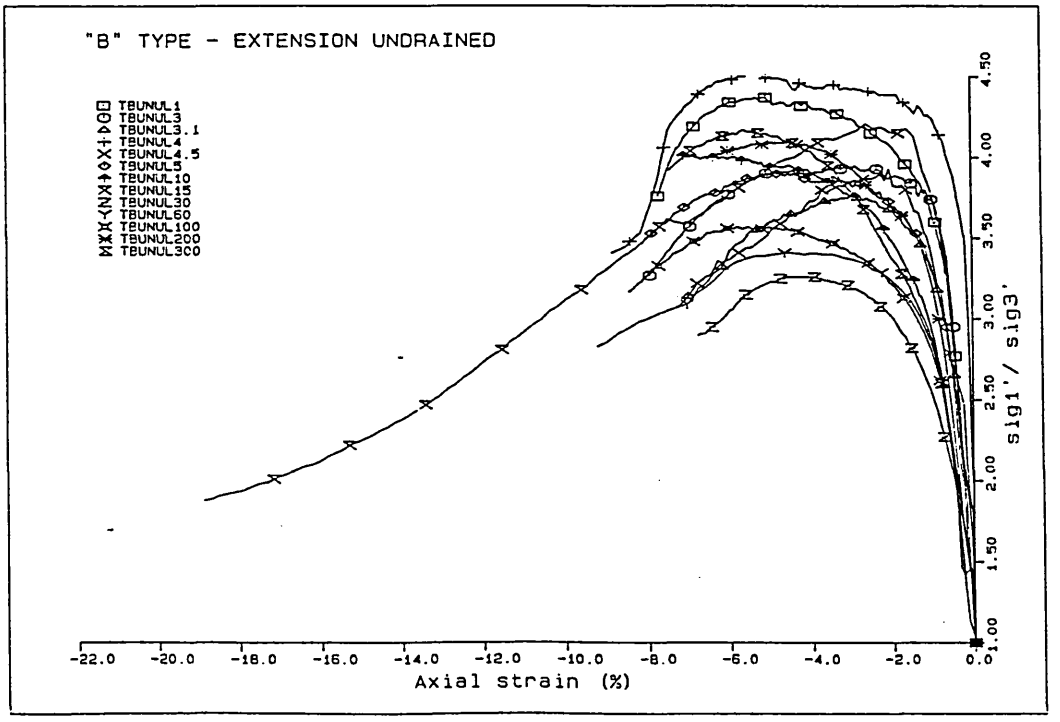
A4.M6


"A" TYPE - EXTENSION UNDRAINED
sig1'/ sig3'
0.00 1.00 2.00 3.00 4.00 5.00 6.00 7.00
0. 50. 100. 150. 200. 250. 300. 350. 400. 450. 500. 550.
p' (kPa)
TAUNUL0.5
TAUNUL1
TAUNUL2.6
TAUNUL3.2
TAUNUL4
TAUNUL5
TAUNUL10
TAUNUL200
TAUNUL300

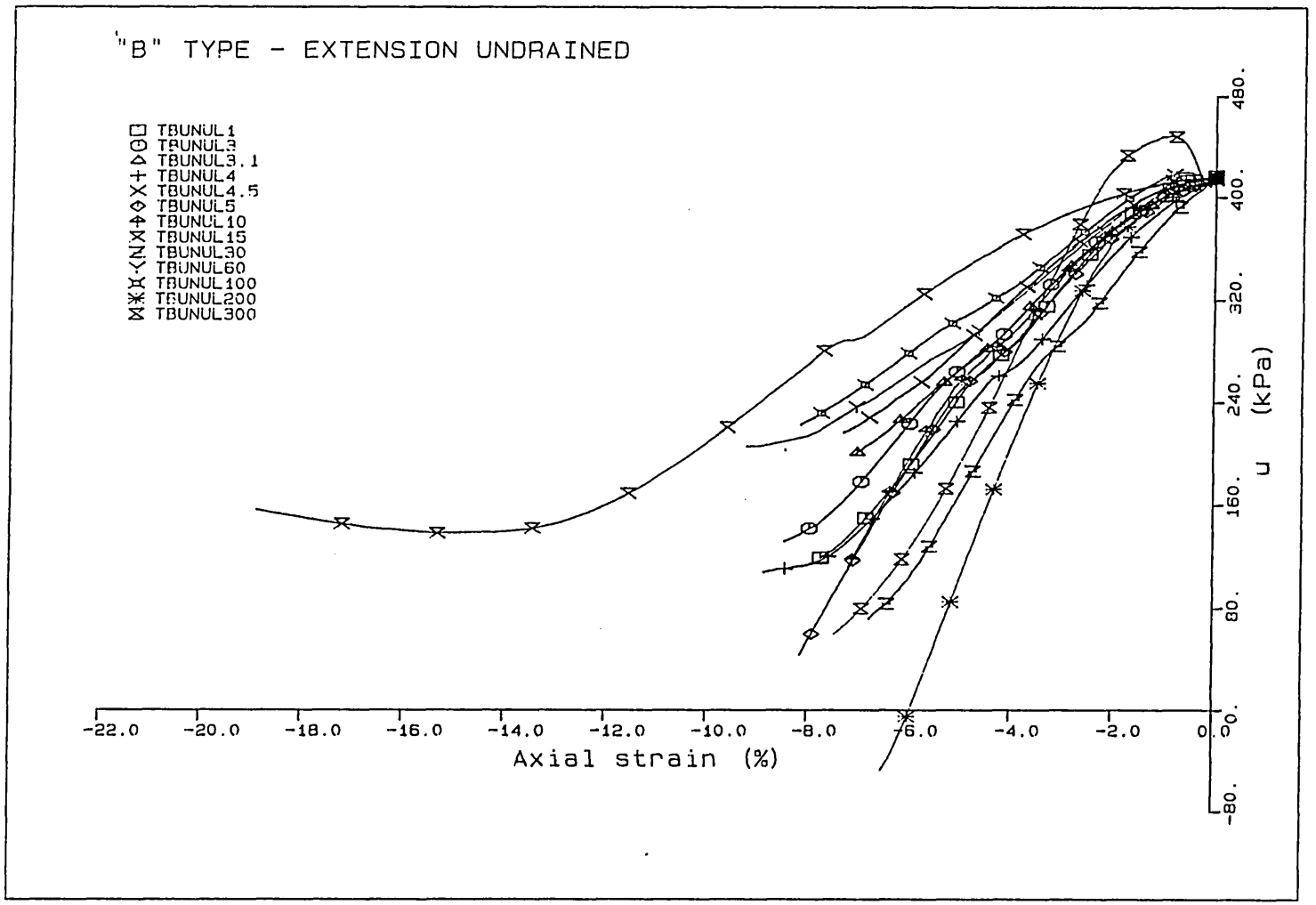
A4.M7


Axial strain (%)
-22.0 -20.0 -18.0 -16.0 -14.0 -12.0 -10.0 -8.0 -6.0 -4.0 -2.0 0.0
0. -100. -200. -300. -400. -500. -600. -700.
q (kPa)
TBUNUL1
TBUNUL3
TBUNUL3.1
TBUNUL4
TBUNUL4.5
TBUNUL5
TBUNUL10
TBUNUL15
TBUNUL30
TBUNUL60
TBUNUL100
TBUNUL200
TBUNUL300
"B" TYPE - EXTENSION UNDRAINED

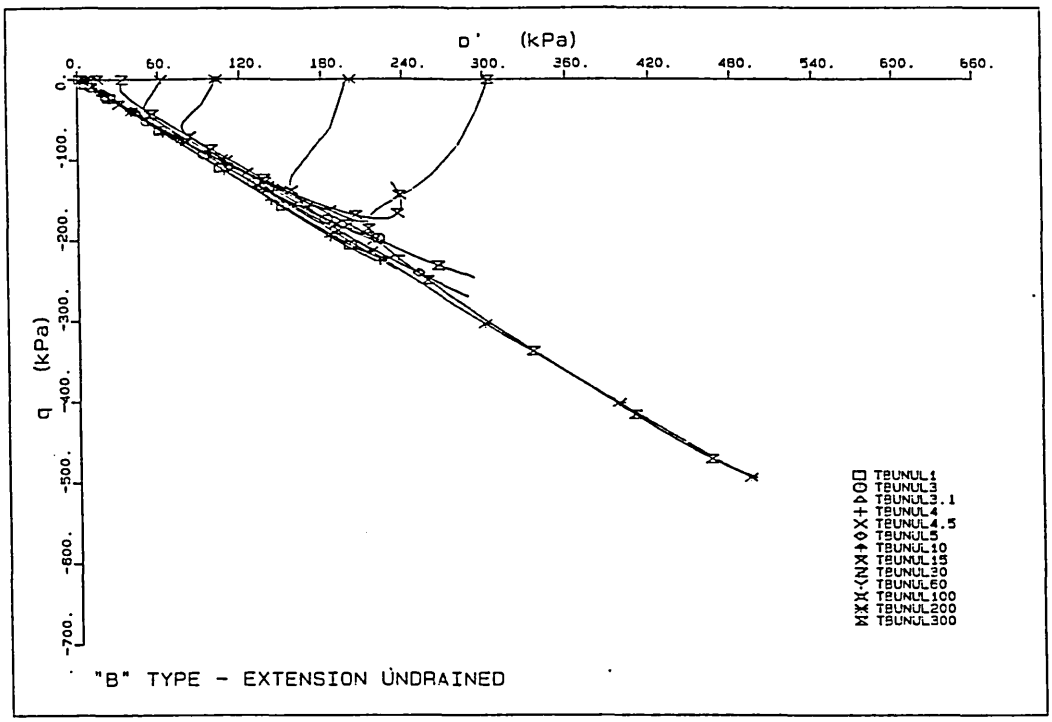
A4.N1


"B" TYPE - EXTENSION UNDRAINED
TBUNUL1
TBUNUL3
TBUNUL3.1
TBUNUL4
TBUNUL4.5
TBUNUL5
TBUNUL10
TBUNUL15
TBUNUL30
TBUNUL60
TBUNUL100
TBUNUL200
TBUNUL300
1.00 1.50 2.00 2.50 3.00 3.50 4.00 4.50
sig1' / sig3'
-22.0 -20.0 -18.0 -16.0 -14.0 -12.0 -10.0 -8.0 -6.0 -4.0 -2.0 0.0
Axial strain (%)

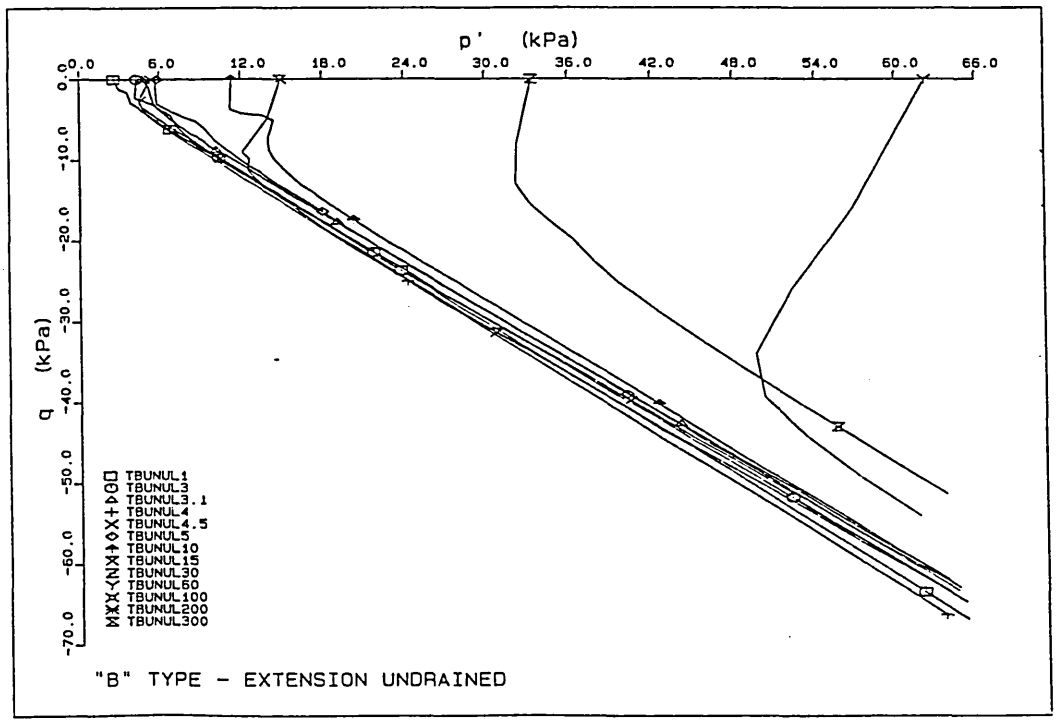
A4.N2


"B" TYPE - EXTENSION UNDRAINED
TBUNUL1
TBUNUL3
TBUNUL3.1
TBUNUL4
TBUNUL4.5
TBUNUL5
TBUNUL10
TBUNUL15
TBUNUL30
TBUNUL60
TBUNUL100
TBUNUL200
TBUNUL300
480.
400.
320.
240.
160.
80.
0.
-80.
u (kPa)
-22.0
-20.0
-18.0
-16.0
-14.0
-12.0
-10.0
-8.0
-6.0
-4.0
-2.0
0.0
Axial strain (%)

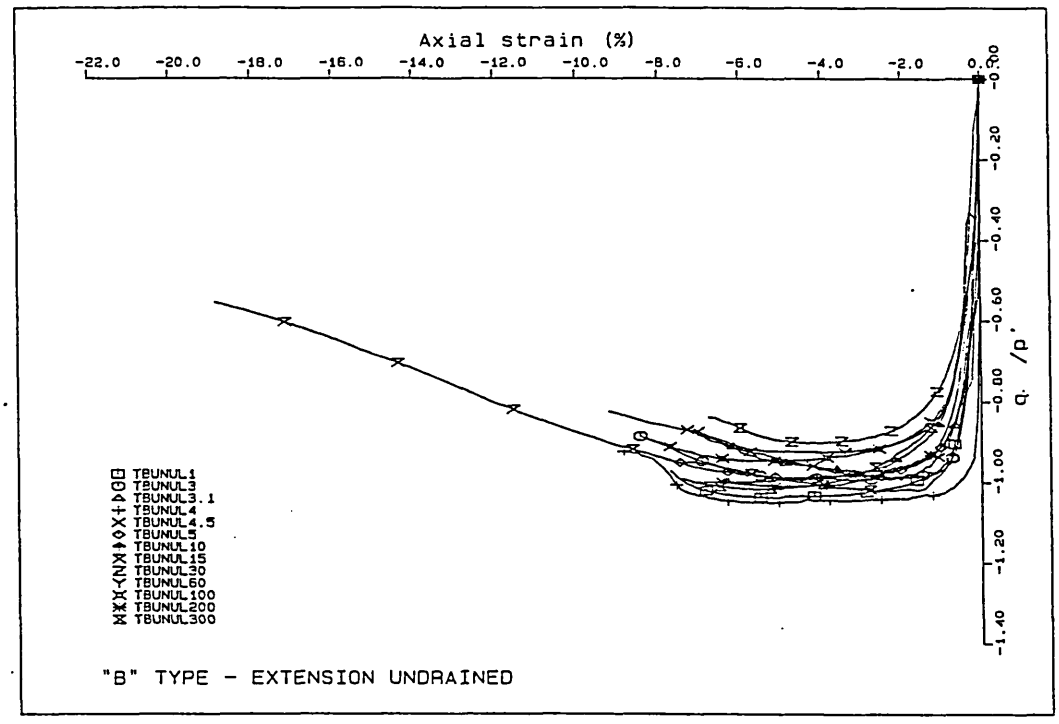
A4.N3


p' (kPa)
0. 60. 120. 180. 240. 300. 360. 420. 480. 540. 600. 660.
q (kPa)
0. -100. -200. -300. -400. -500. -600. -700.
TBUNUL1
TBUNUL3
TBUNUL3.1
TBUNUL4
TBUNUL4.5
TBUNUL5
TBUNUL10
TBUNUL15
TBUNUL30
TBUNUL60
TBUNUL100
TBUNUL200
TBUNUL300
"B" TYPE - EXTENSION UNDRAINED

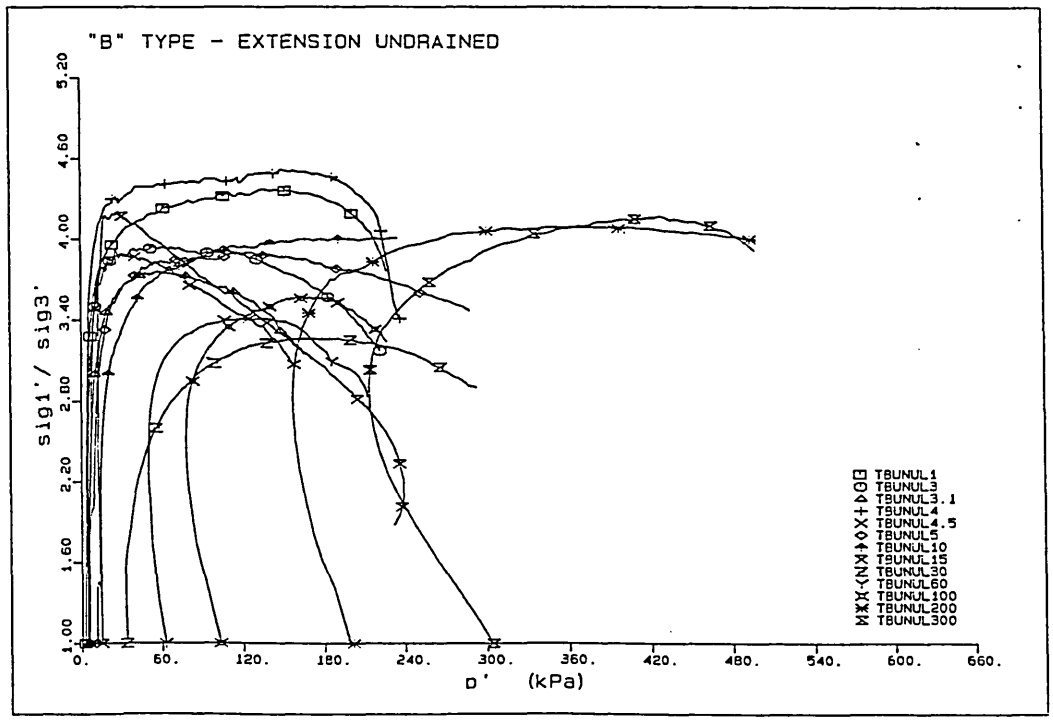
A4.N4


p' (kPa)
0.0 6.0 12.0 18.0 24.0 30.0 36.0 42.0 48.0 54.0 60.0 66.0
q (kPa)
0.0 -10.0 -20.0 -30.0 -40.0 -50.0 -60.0 -70.0
TBUNUL1
TBUNUL3
TBUNUL3.1
TBUNUL4
TBUNUL4.5
TBUNUL5
TBUNUL10
TBUNUL15
TBUNUL30
TBUNUL60
TBUNUL100
TBUNUL200
TBUNUL300
"B" TYPE - EXTENSION UNDRAINED

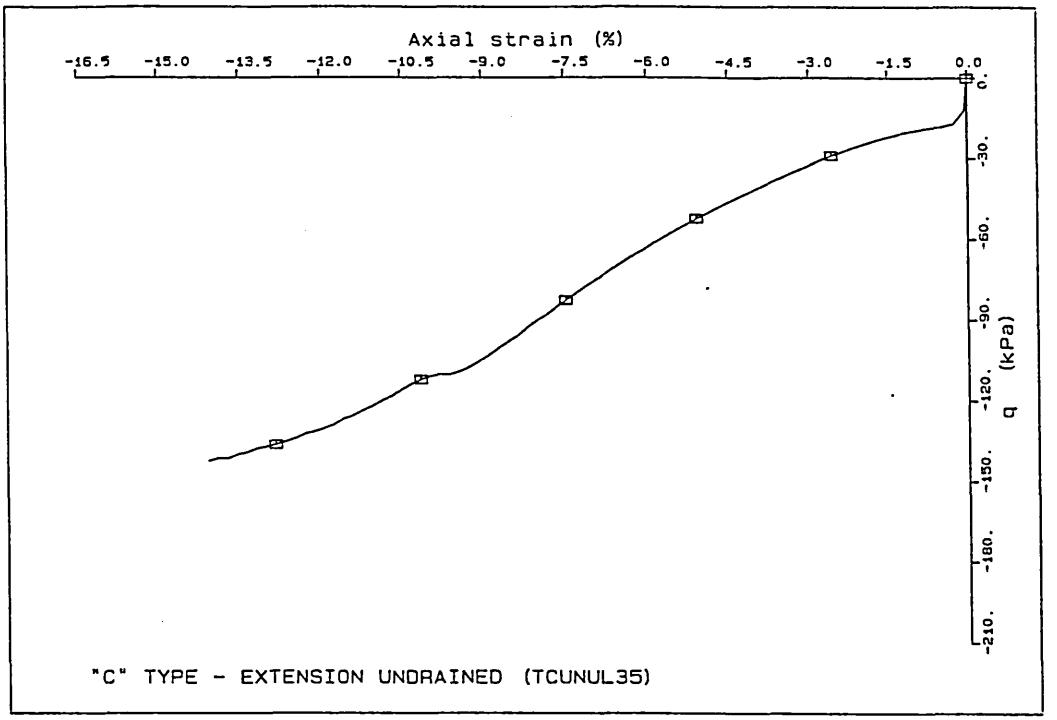
A4.N5


Axial strain (%)
-22.0
-20.0
-18.0
-16.0
-14.0
-12.0
-10.0
-8.0
-6.0
-4.0
-2.0
0.00
-0.20
-0.40
-0.60
-0.80
-1.00
-1.20
-1.40
q. /p'
TBUNUL1
TBUNUL3
TBUNUL3.1
TBUNUL4
TBUNUL4.5
TBUNUL5
TBUNUL10
TBUNUL15
TBUNUL30
TBUNUL60
TBUNUL100
TBUNUL200
TBUNUL300
"B" TYPE - EXTENSION UNDRAINED

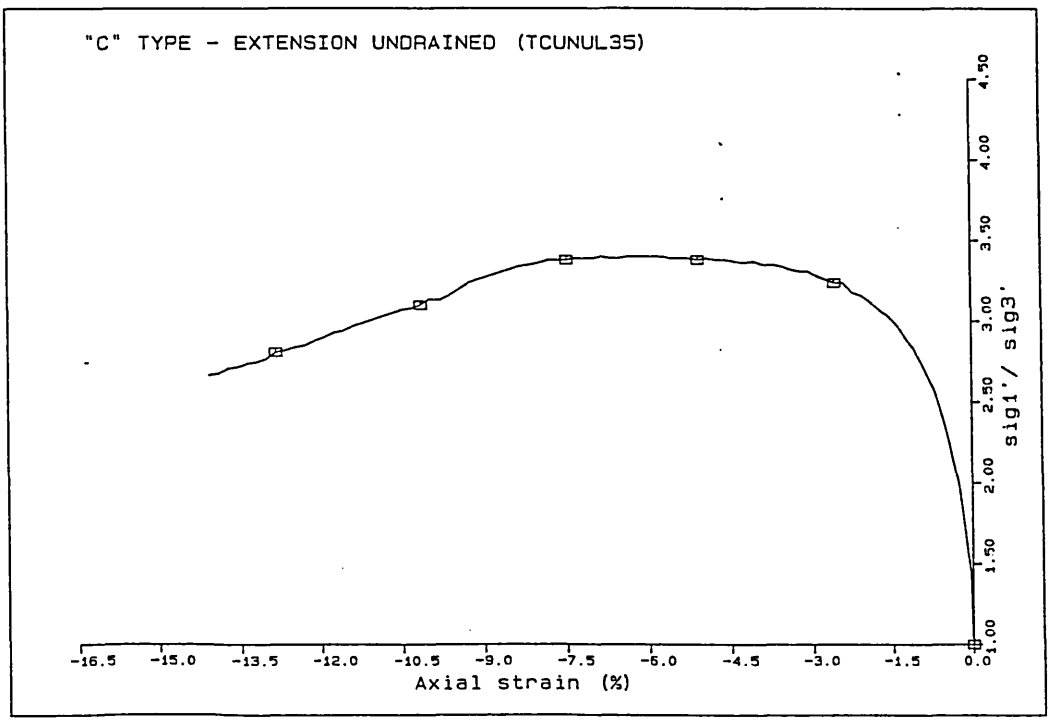
A4.N6


"B" TYPE - EXTENSION UNDRAINED
sig1' / sig3'
1.00
1.60
2.20
2.80
3.40
4.00
4.60
5.20
0.
60.
120.
180.
240.
300.
360.
420.
480.
540.
600.
660.
p' (kPa)
TBUNUL1
TBUNUL3
TBUNUL3.1
TBUNUL4
TBUNUL4.5
TBUNUL5
TBUNUL10
TBUNUL15
TBUNUL30
TBUNUL60
TBUNUL100
TBUNUL200
TBUNUL300

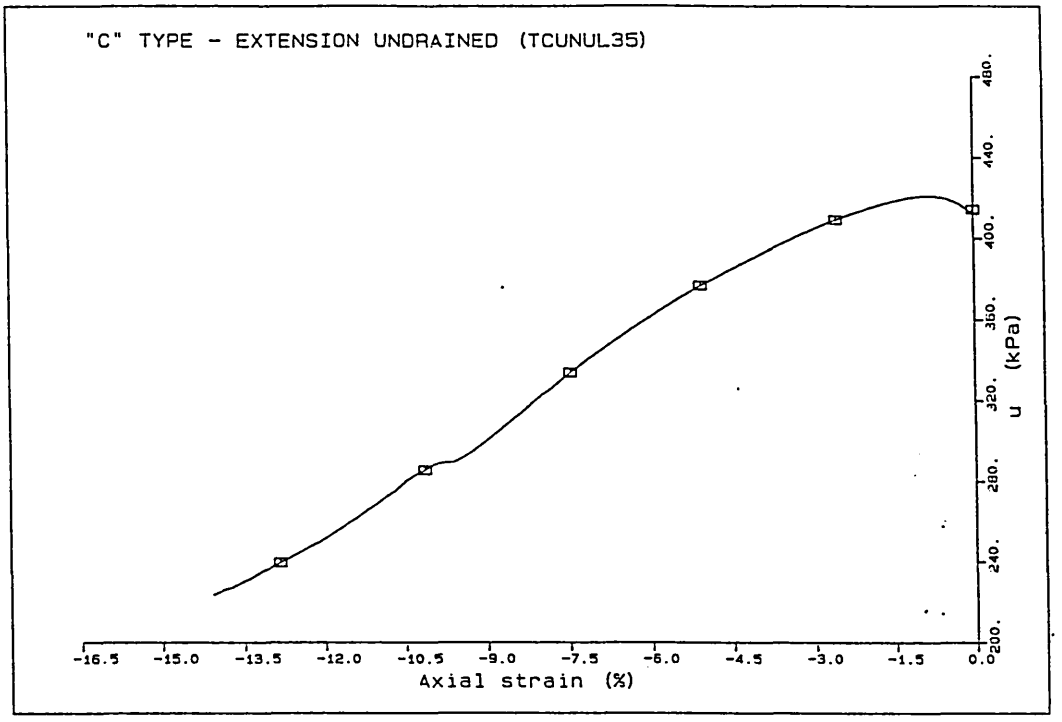
A4.N7


Axial strain (%)
-16.5 -15.0 -13.5 -12.0 -10.5 -9.0 -7.5 -6.0 -4.5 -3.0 -1.5 0.0
0. -30. -60. -90. -120. -150. -180. -210.
q (kPa)
"C" TYPE - EXTENSION UNDRAINED (TCUNUL35)

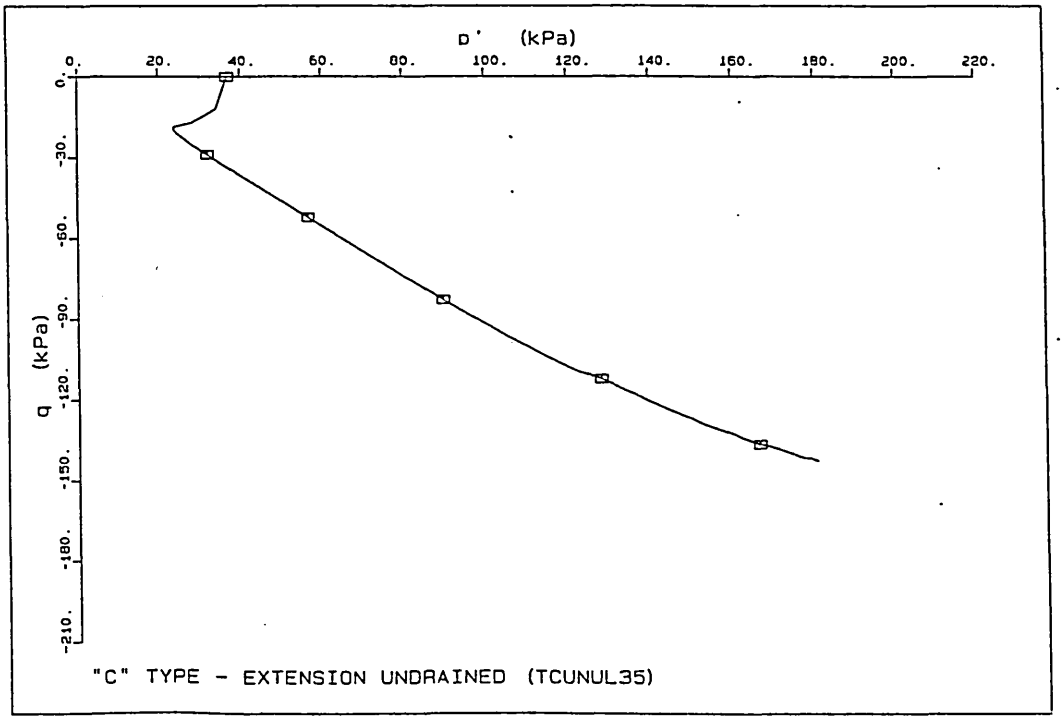
A4.01


"C" TYPE - EXTENSION UNDRAINED (TCUNUL35)
1.00 1.50 2.00 2.50 3.00 3.50 4.00 4.50
sig1'/ sig3'
-16.5 -15.0 -13.5 -12.0 -10.5 -9.0 -7.5 -6.0 -4.5 -3.0 -1.5 0.0
Axial strain (%)

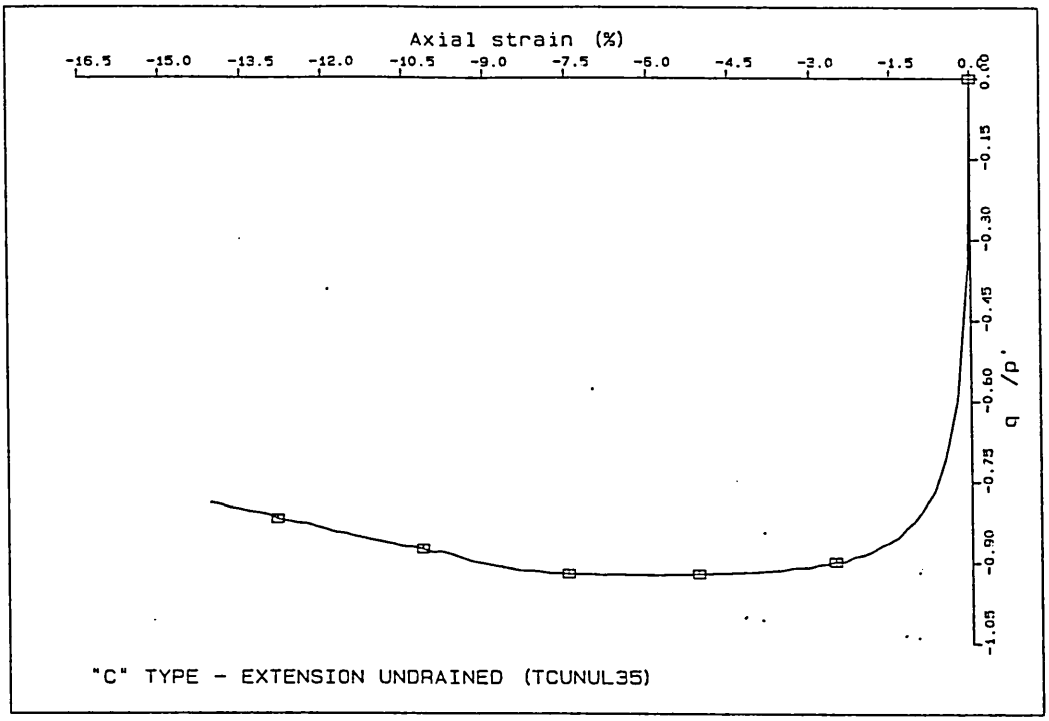
A4.02


"C" TYPE - EXTENSION UNDRAINED (TCUNUL35)
480.
440.
400.
360.
320.
280.
240.
200.
u (kPa)
-16.5
-15.0
-13.5
-12.0
-10.5
-9.0
-7.5
-6.0
-4.5
-3.0
-1.5
0.0
Axial strain (%)

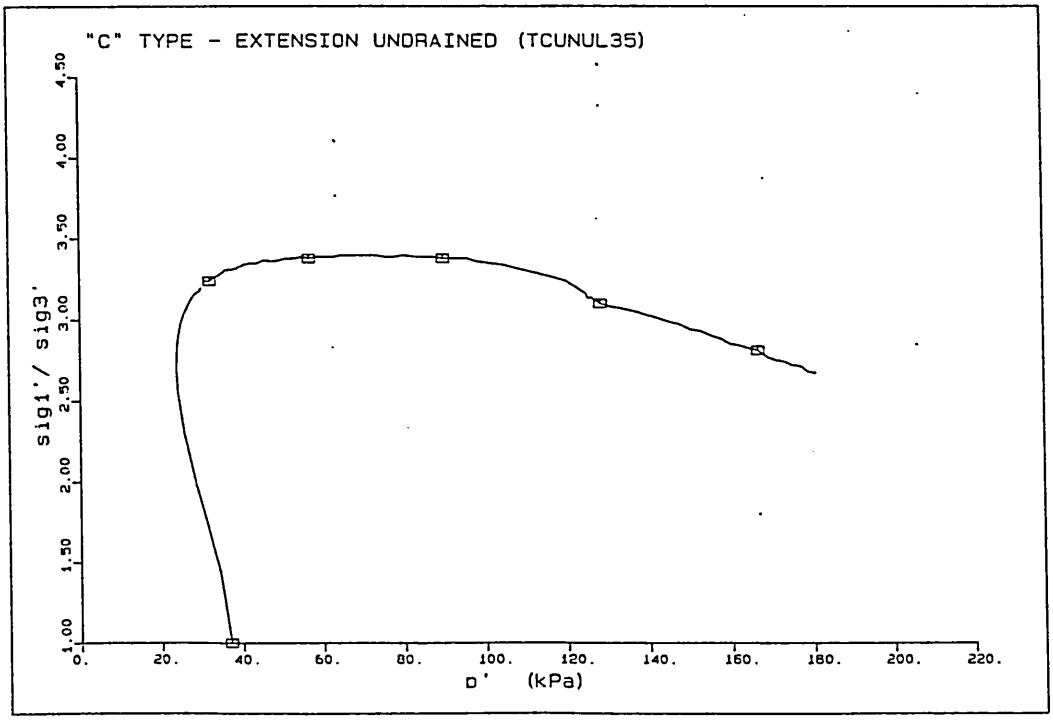
A4.03


p' (kPa)
0.
20.
40.
60.
80.
100.
120.
140.
160.
180.
200.
220.
0.
-30.
-60.
-90.
-120.
-150.
-180.
-210.
q (kPa)
"C" TYPE - EXTENSION UNDRAINED (TCUNUL35)

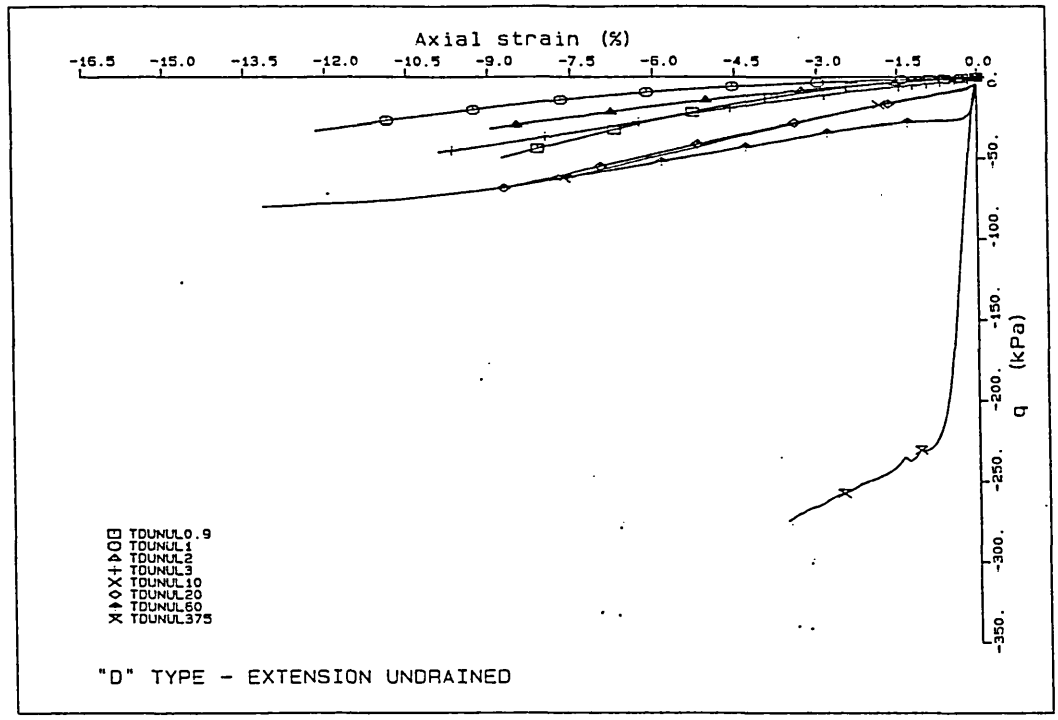
A4.04


Axial strain (%)
-16.5
-15.0
-13.5
-12.0
-10.5
-9.0
-7.5
-6.0
-4.5
-3.0
-1.5
0.0
0.00
-0.15
-0.30
-0.45
-0.60
-0.75
-0.90
-1.05
q /p'
"C" TYPE - EXTENSION UNDRAINED (TCUNUL35)

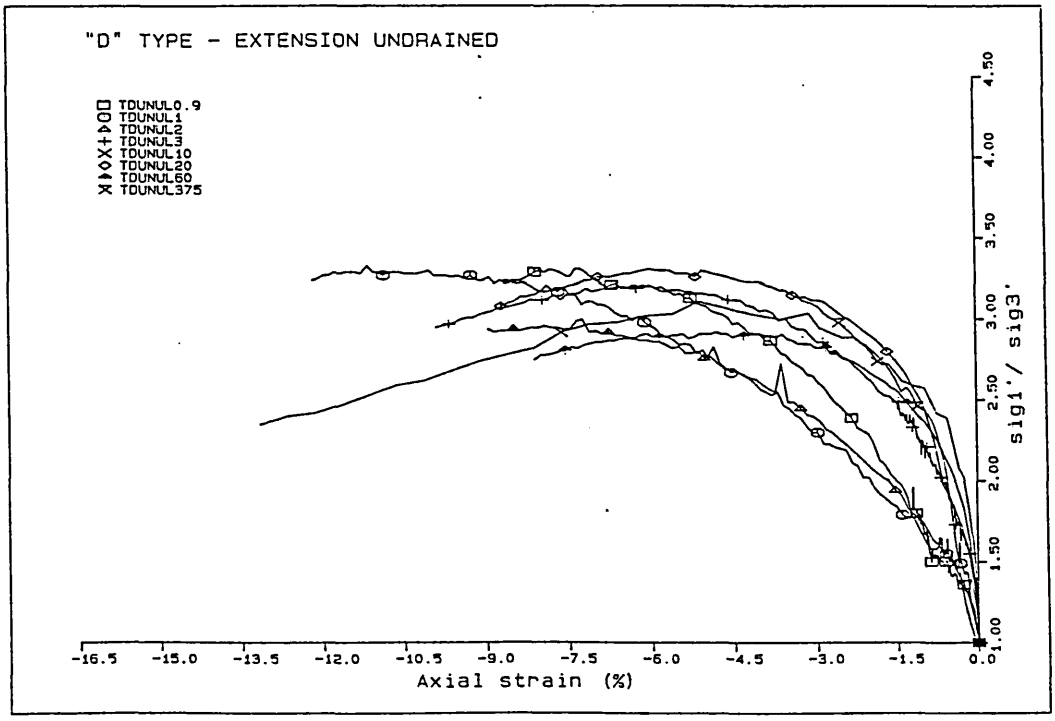
A4.05


"C" TYPE - EXTENSION UNDRAINED (TCUNUL35)
sig1' / sig3'
4.50
4.00
3.50
3.00
2.50
2.00
1.50
1.00
0.
20.
40.
60.
80.
100.
120.
140.
160.
180.
200.
220.
p' (kPa)

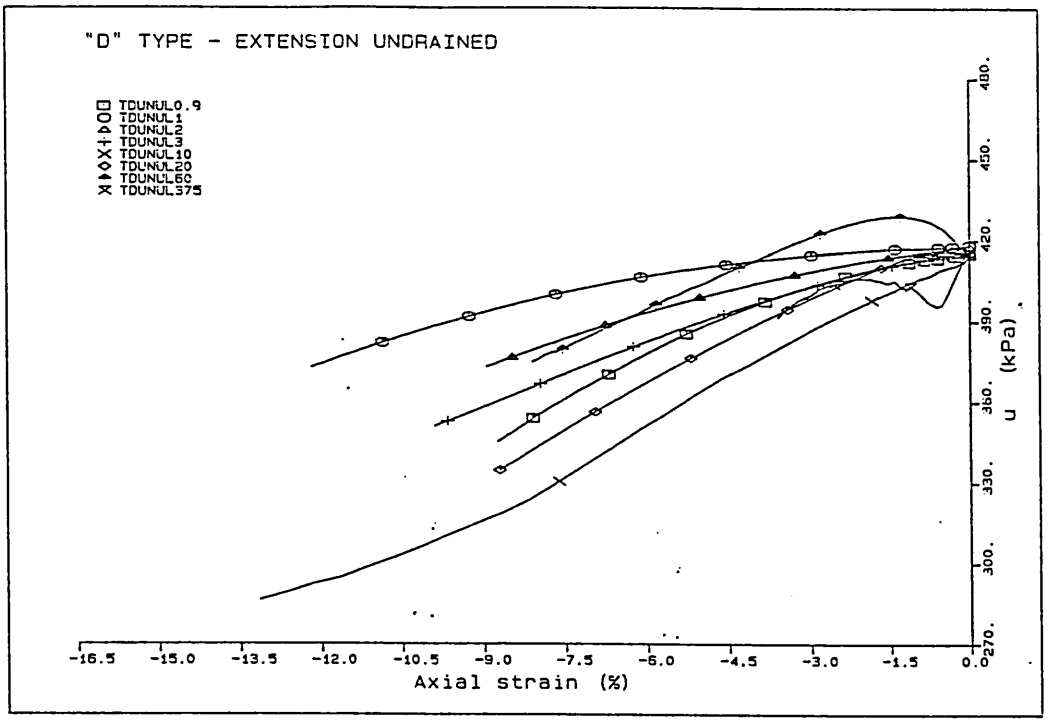
A4.06


Axial strain (%)
-16.5 -15.0 -13.5 -12.0 -10.5 -9.0 -7.5 -6.0 -4.5 -3.0 -1.5 0.0
0. -50. -100. -150. -200. -250. -300. -350.
q (kPa)
TDUNUL0.9
TDUNUL1
TDUNUL2
TDUNUL3
TDUNUL10
TDUNUL20
TDUNUL60
TDUNUL375
"D" TYPE - EXTENSION UNDRAINED

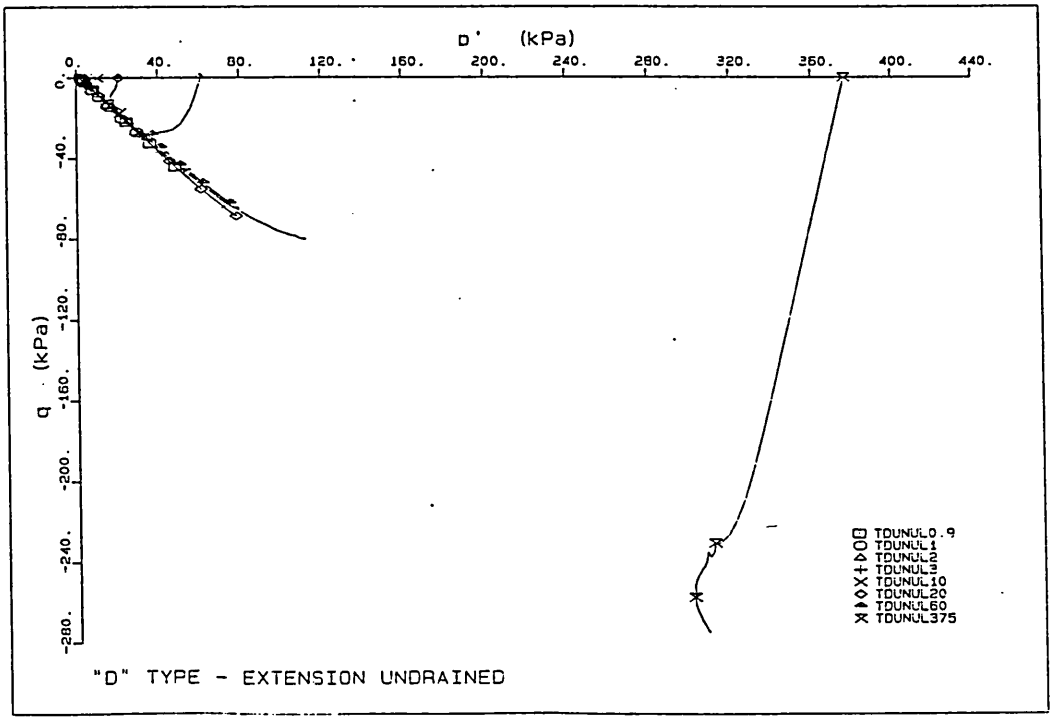
A4.P1


"D" TYPE - EXTENSION UNDRAINED
TDUNUL0.9
TDUNUL1
TDUNUL2
TDUNUL3
TDUNUL10
TDUNUL20
TDUNUL60
TDUNUL375
1.00 1.50 2.00 2.50 3.00 3.50 4.00 4.50
sig1' / sig3'
-16.5 -15.0 -13.5 -12.0 -10.5 -9.0 -7.5 -6.0 -4.5 -3.0 -1.5 0.0
Axial strain (%)

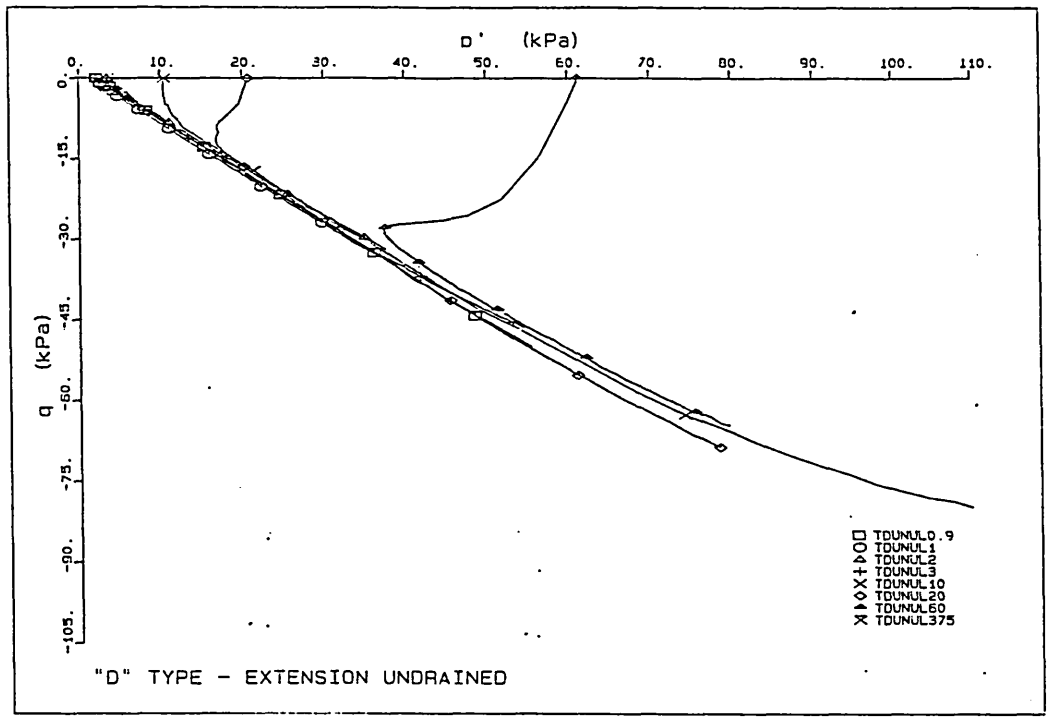
A4.P2


"D" TYPE - EXTENSION UNDRAINED
TDUNUL0.9
TDUNUL1
TDUNUL2
TDUNUL3
TDUNUL10
TDUNUL20
TDUNUL60
TDUNUL375
480.
450.
420.
390.
360.
330.
300.
270.
u (kPa)
-16.5
-15.0
-13.5
-12.0
-10.5
-9.0
-7.5
-6.0
-4.5
-3.0
-1.5
0.0
Axial strain (%)

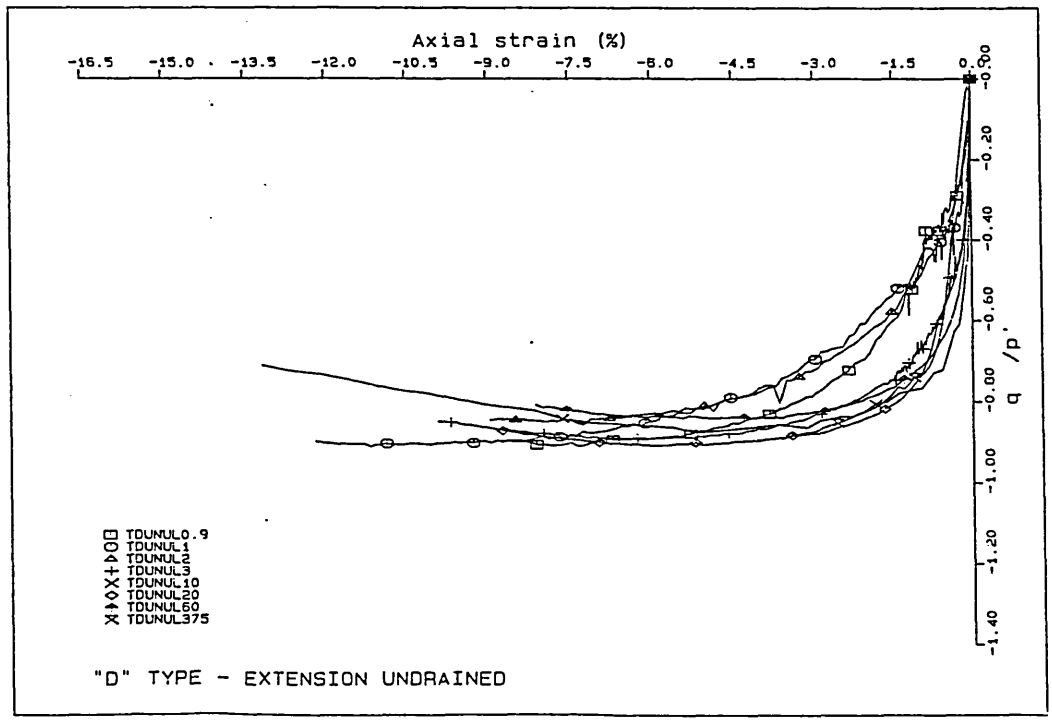
A4.P3


p' (kPa)
0.
40.
80.
120.
160.
200.
240.
280.
320.
360.
400.
440.
0.
-40.
-80.
-120.
-160.
-200.
-240.
-280.
q (kPa)
TDUNUL0.9
TDUNUL1
TDUNUL2
TDUNUL3
TDUNUL10
TDUNUL20
TDUNUL60
TDUNUL375
"D" TYPE - EXTENSION UNDRAINED

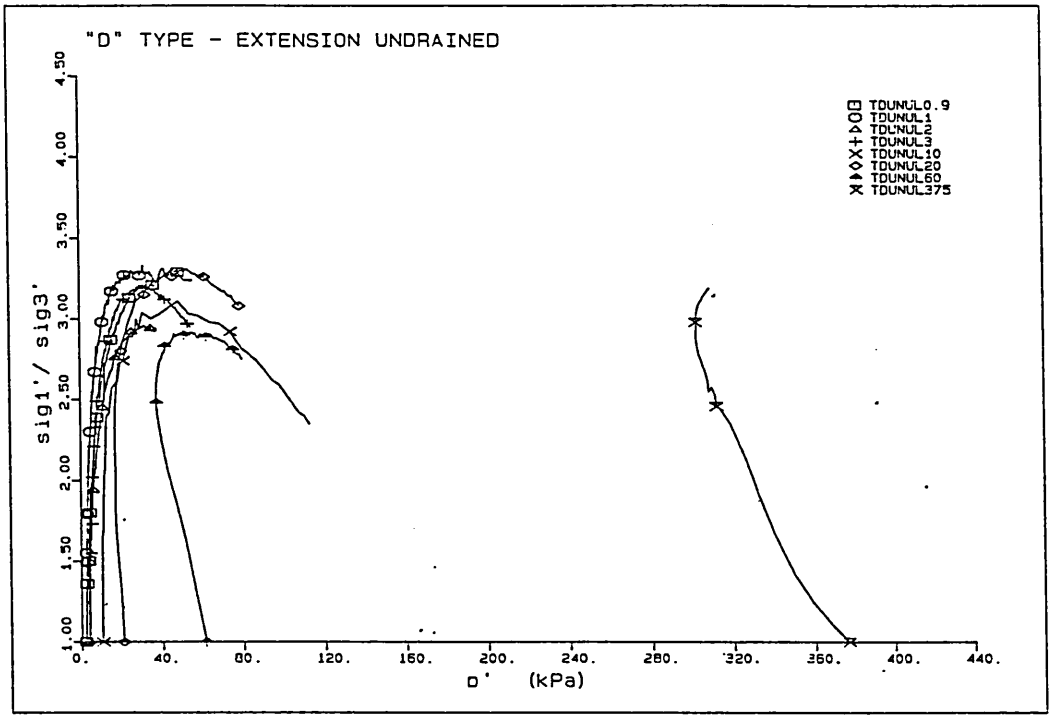
A4.P4


p' (kPa)
0. 10. 20. 30. 40. 50. 60. 70. 80. 90. 100. 110.
q (kPa)
0. -15. -30. -45. -60. -75. -90. -105.
TDUNUL0.9
TDUNUL1
TDUNUL2
TDUNUL3
TDUNUL10
TDUNUL20
TDUNUL60
TDUNUL375
"D" TYPE - EXTENSION UNDRAINED

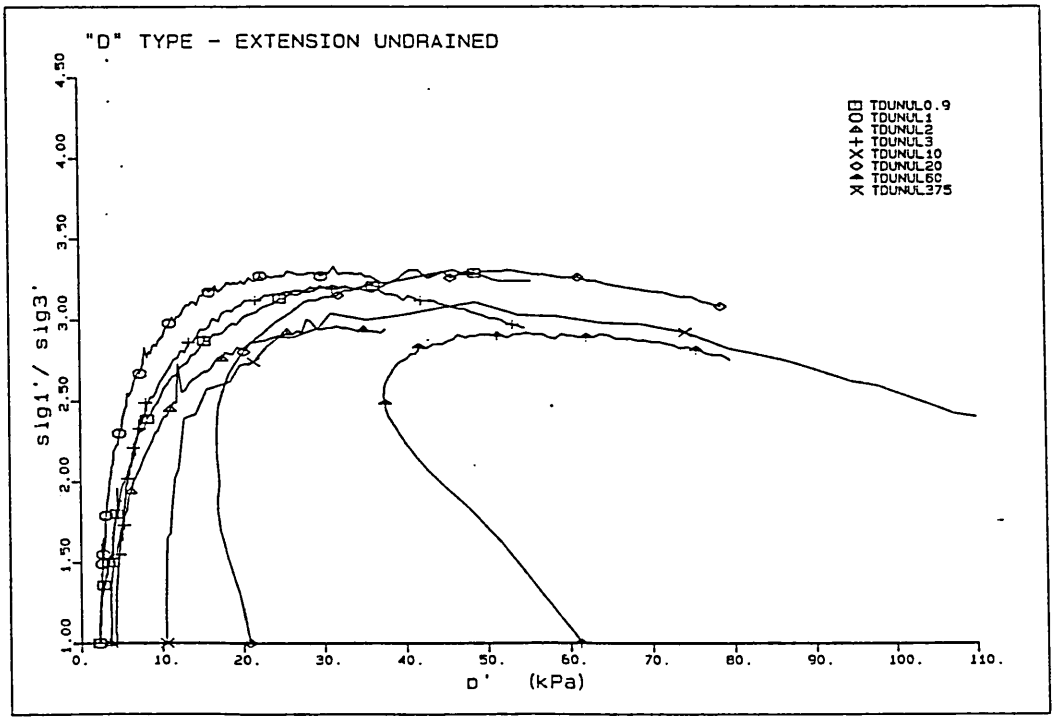
A4.P5


Axial strain (%)
-16.5 -15.0 -13.5 -12.0 -10.5 -9.0 -7.5 -6.0 -4.5 -3.0 -1.5 0.
q /p'
0.00 -0.20 -0.40 -0.60 -0.80 -1.00 -1.20 -1.40
TDUNUL0.9
TDUNUL1
TDUNUL2
TDUNUL3
TDUNUL10
TDUNUL20
TDUNUL60
TDUNUL375
"D" TYPE - EXTENSION UNDRAINED

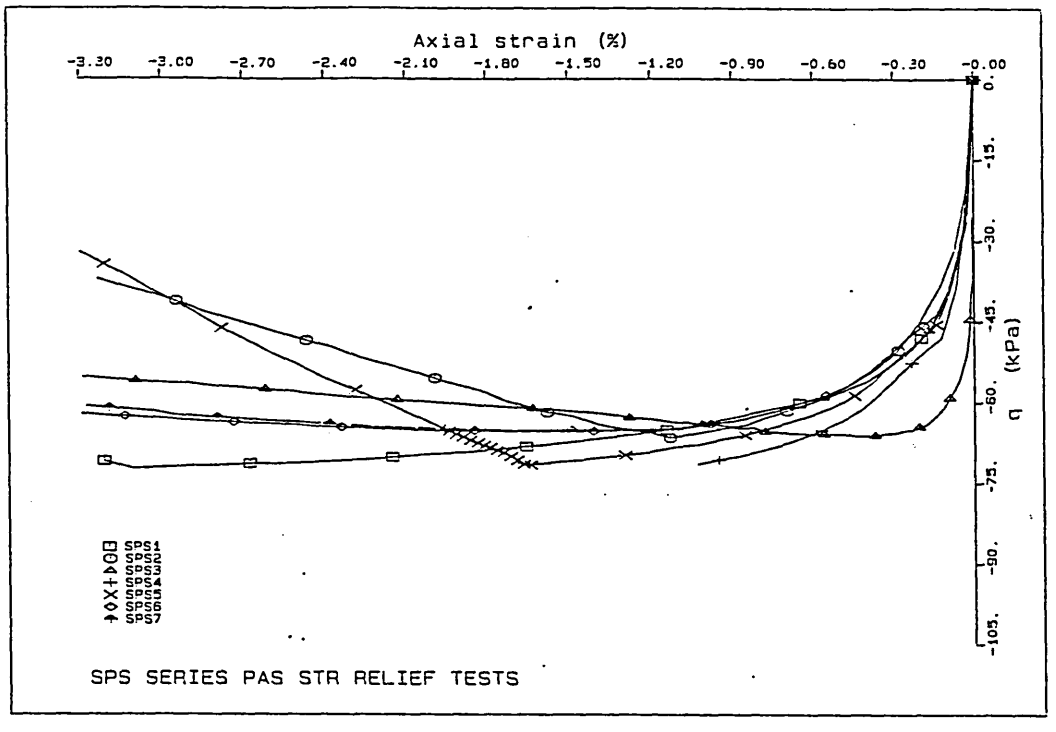
A4.P6


"D" TYPE - EXTENSION UNDRAINED
TDUNUL0.9
TDUNUL1
TDUNUL2
TDUNUL3
TDUNUL10
TDUNUL20
TDUNUL60
TDUNUL375
sig1' / sig3'
1.00
1.50
2.00
2.50
3.00
3.50
4.00
4.50
0.
40.
80.
120.
160.
200.
240.
280.
320.
360.
400.
440.
D' (kPa)

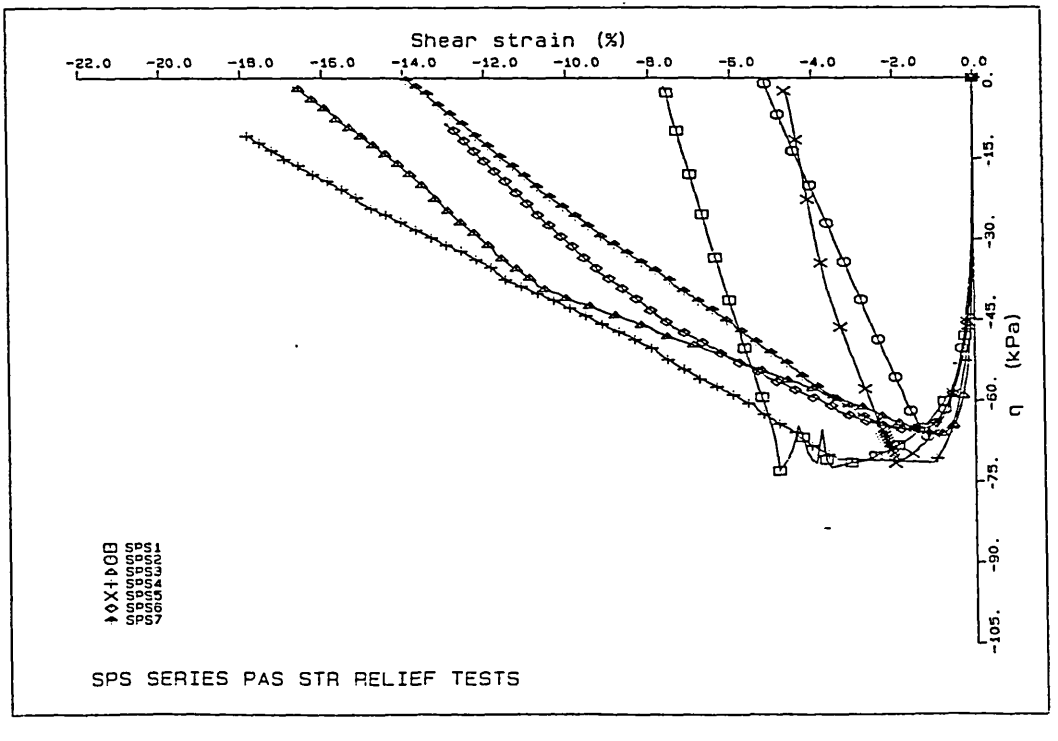
A4.P7


"D" TYPE - EXTENSION UNDRAINED
TDUNUL0.9
TDUNUL1
TDUNUL2
TDUNUL3
TDUNUL10
TDUNUL20
TDUNUL60
TDUNUL375
sig1' / sig3'
1.00
1.50
2.00
2.50
3.00
3.50
4.00
4.50
0.
10.
20.
30.
40.
50.
60.
70.
80.
90.
100.
110.
D' (kPa)

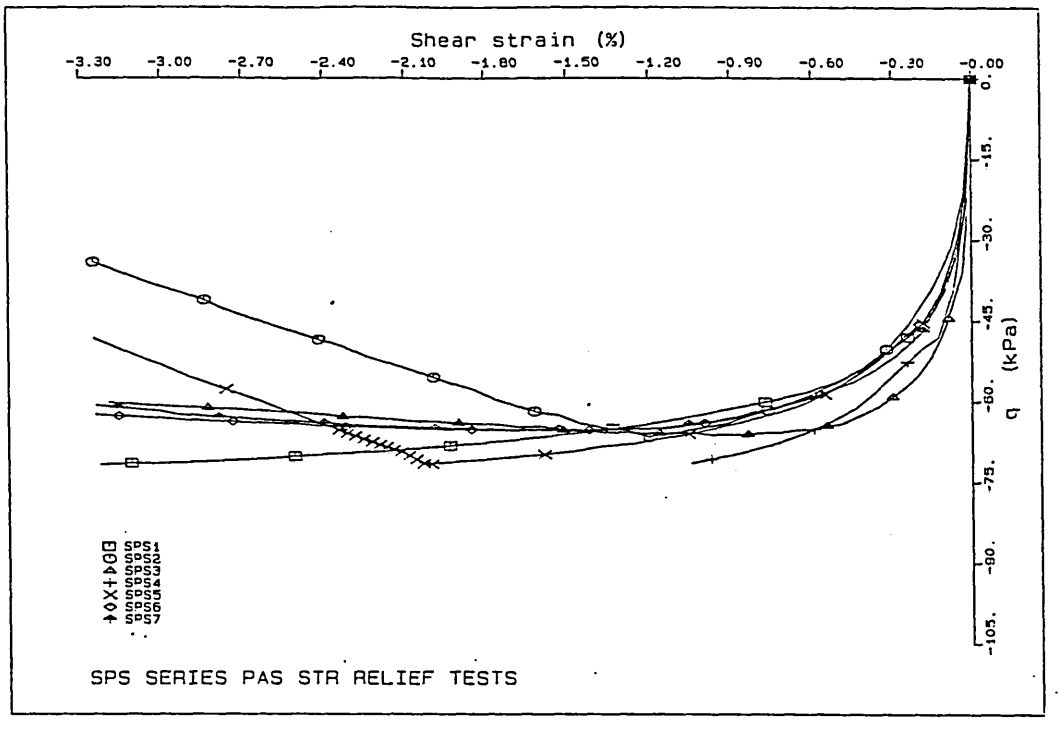
A4.P8


Axial strain (%)
-3.30 -3.00 -2.70 -2.40 -2.10 -1.80 -1.50 -1.20 -0.90 -0.60 -0.30 -0.00
0. -15. -30. -45. -60. -75. -90. -105.
q (kPa)
SPS1
SPS2
SPS3
SPS4
SPS5
SPS6
SPS7
SPS SERIES PAS STR RELIEF TESTS

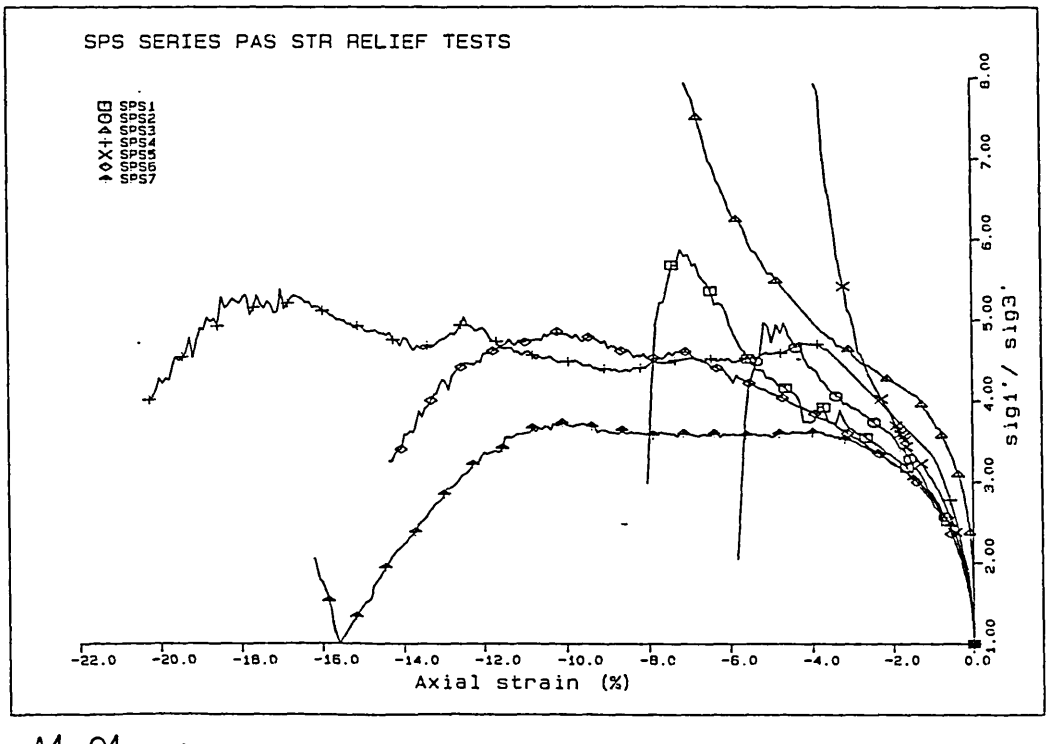
A4.Q1


Shear strain (%)
-22.0 -20.0 -18.0 -16.0 -14.0 -12.0 -10.0 -8.0 -6.0 -4.0 -2.0 0.0
0. -15. -30. -45. -60. -75. -90. -105.
q (kPa)
SPS1
SPS2
SPS3
SPS4
SPS5
SPS6
SPS7
SPS SERIES PAS STR RELIEF TESTS

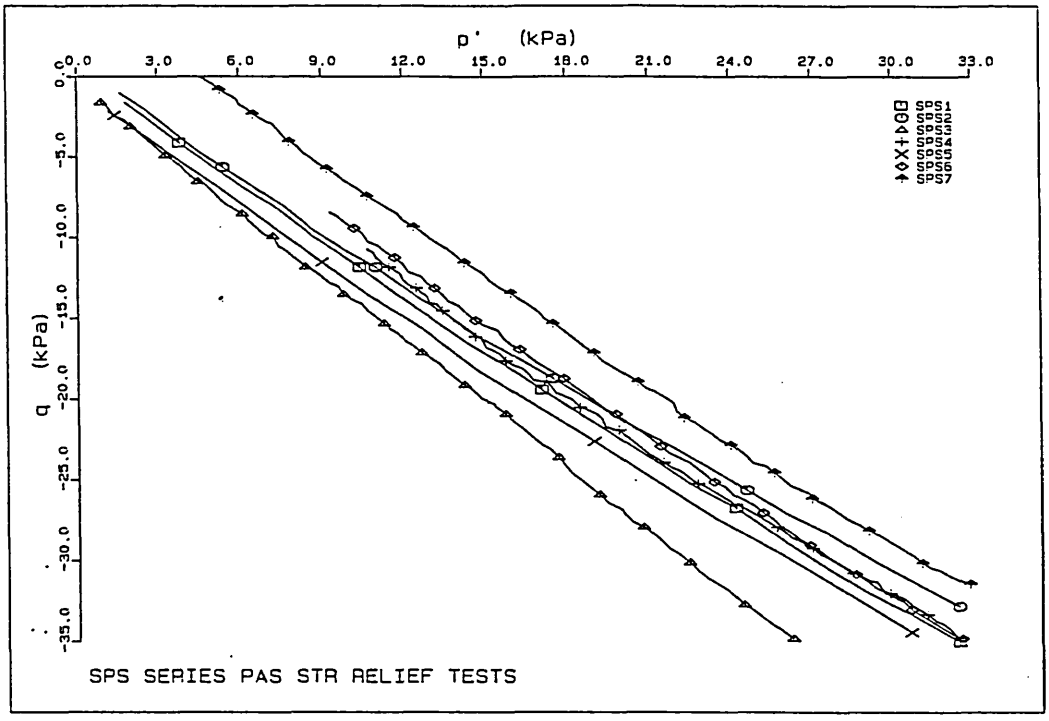
A4.Q2


Shear strain (%)
-3.30 -3.00 -2.70 -2.40 -2.10 -1.80 -1.50 -1.20 -0.90 -0.60 -0.30 -0.00
0. -15. -30. -45. -60. -75. -90. -105.
q (kPa)
SPS1
SPS2
SPS3
SPS4
SPS5
SPS6
SPS7
SPS SERIES PAS STR RELIEF TESTS

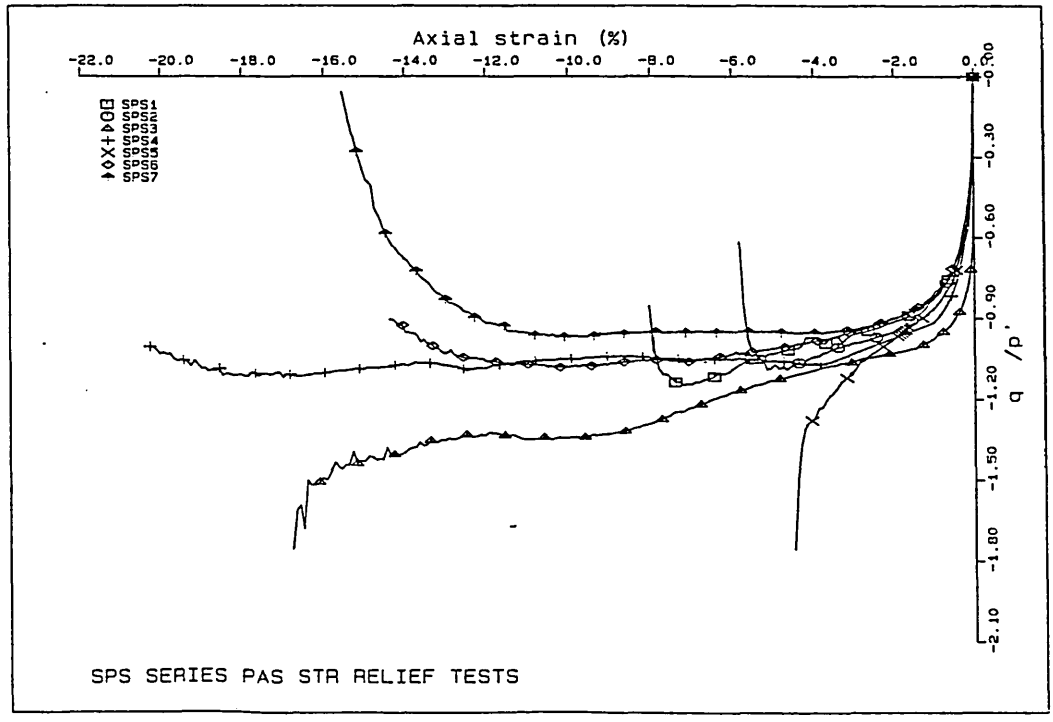
A4.Q3


SPS SERIES PAS STR RELIEF TESTS
SPS1
SPS2
SPS3
SPS4
SPS5
SPS6
SPS7
8.00 7.00 6.00 5.00 4.00 3.00 2.00 1.00
sig1'/ sig3'
-22.0 -20.0 -18.0 -16.0 -14.0 -12.0 -10.0 -8.0 -6.0 -4.0 -2.0 0.0
Axial strain (%)

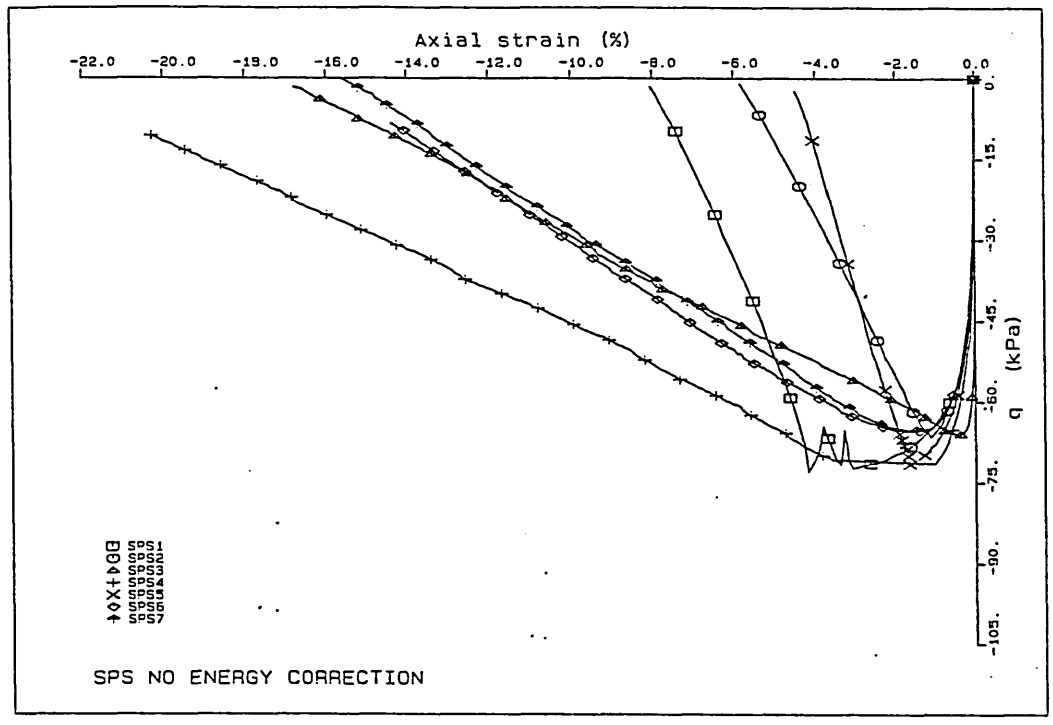
A4.Q4


p' (kPa)
0.0
3.0
6.0
9.0
12.0
15.0
18.0
21.0
24.0
27.0
30.0
33.0
q (kPa)
0.0
-5.0
-10.0
-15.0
-20.0
-25.0
-30.0
-35.0
SPS1
SPS2
SPS3
SPS4
SPS5
SPS6
SPS7
SPS SERIES PAS STR RELIEF TESTS

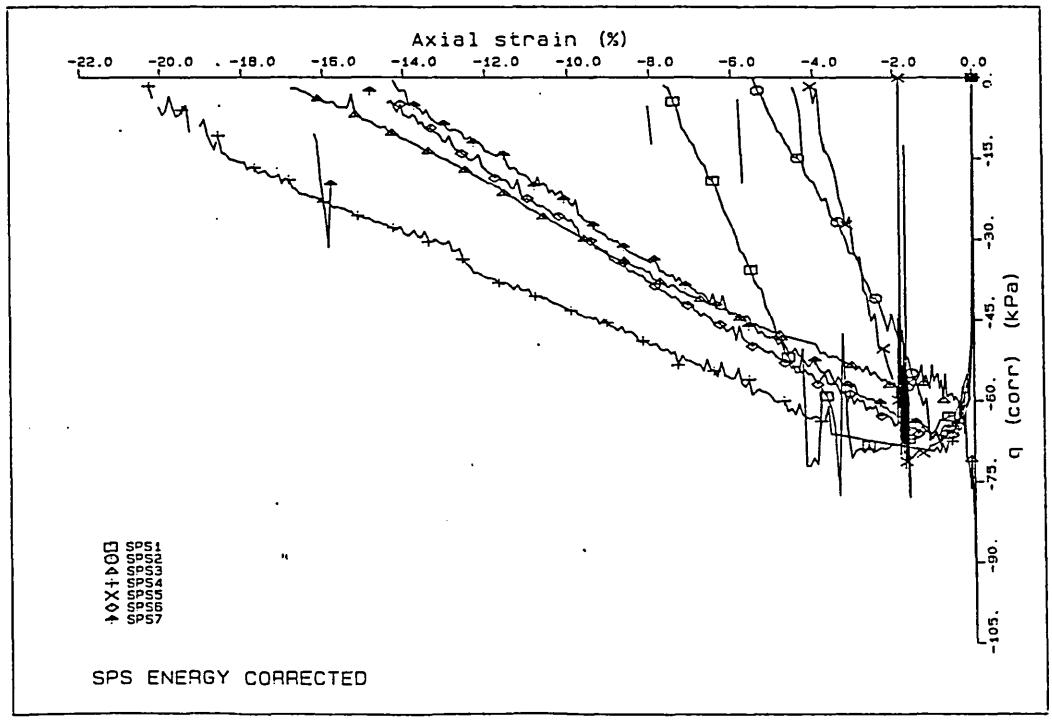
A4.Q5


Axial strain (%)
-22.0
-20.0
-18.0
-16.0
-14.0
-12.0
-10.0
-8.0
-6.0
-4.0
-2.0
0.0
q /p'
-0.00
-0.30
-0.60
-0.90
-1.20
-1.50
-1.80
-2.10
SPS1
SPS2
SPS3
SPS4
SPS5
SPS6
SPS7
SPS SERIES PAS STR RELIEF TESTS

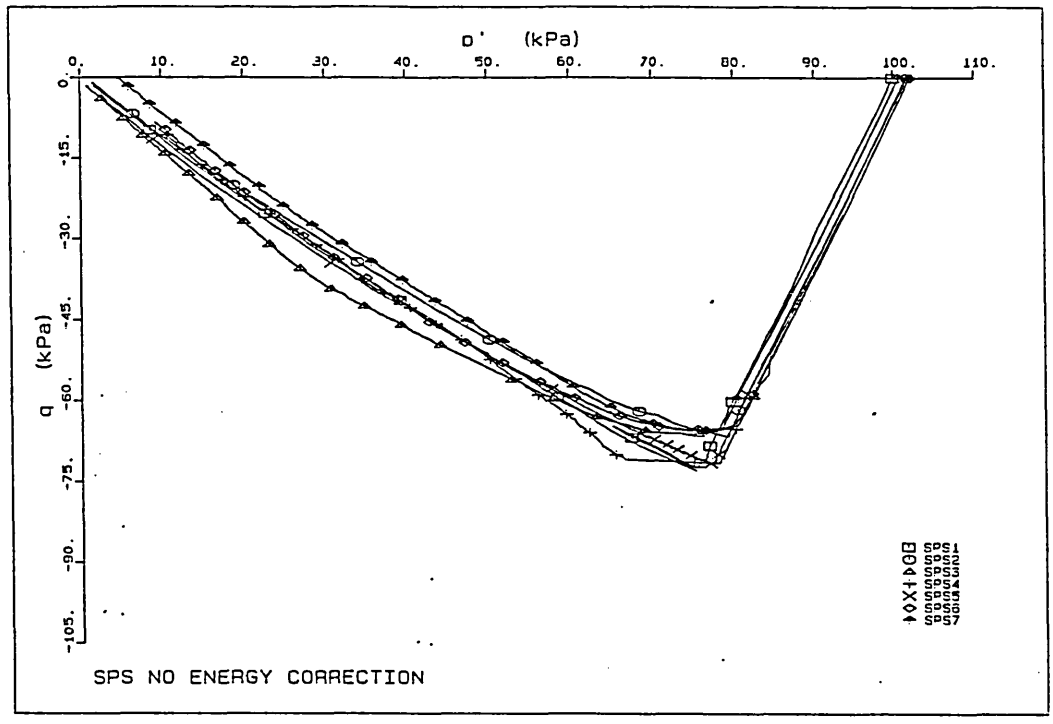
A4.Q6


Axial strain (%)
-22.0 -20.0 -18.0 -16.0 -14.0 -12.0 -10.0 -8.0 -6.0 -4.0 -2.0 0.0
0. -15. -30. -45. -60. -75. -90. -105.
q (kPa)
SPS1
SPS2
SPS3
SPS4
SPS5
SPS6
SPS7
SPS NO ENERGY CORRECTION

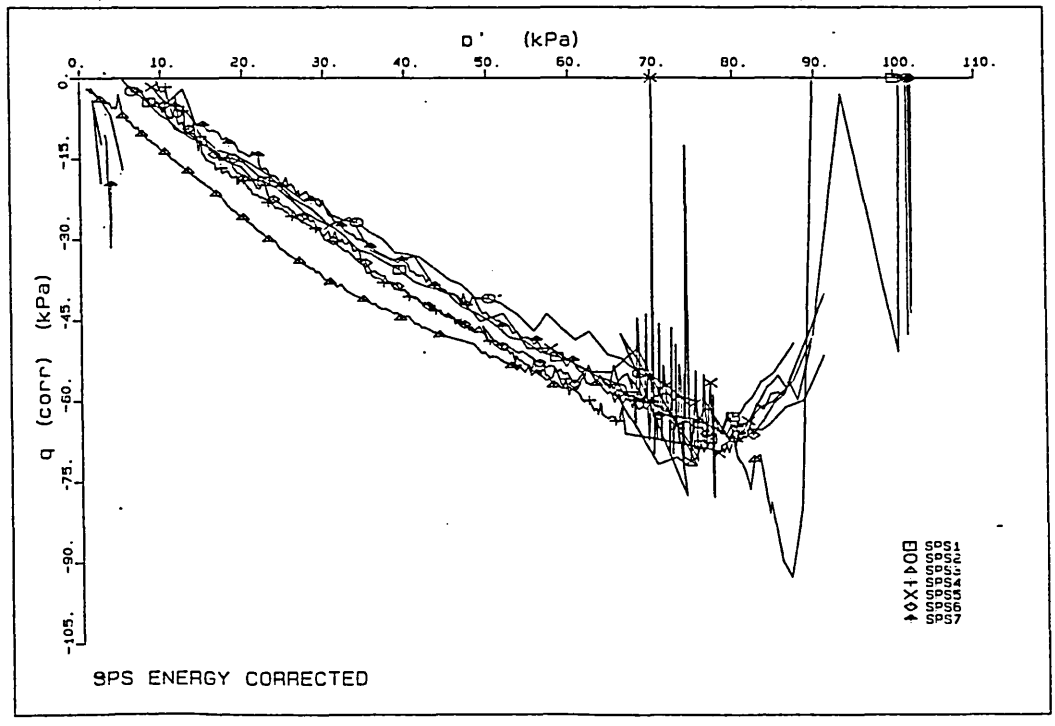
A4.Q7


Axial strain (%)
-22.0 -20.0 -18.0 -16.0 -14.0 -12.0 -10.0 -8.0 -6.0 -4.0 -2.0 0.0
0. -15. -30. -45. -60. -75. -90. -105.
q (corr) (kPa)
SPS1
SPS2
SPS3
SPS4
SPS5
SPS6
SPS7
SPS ENERGY CORRECTED

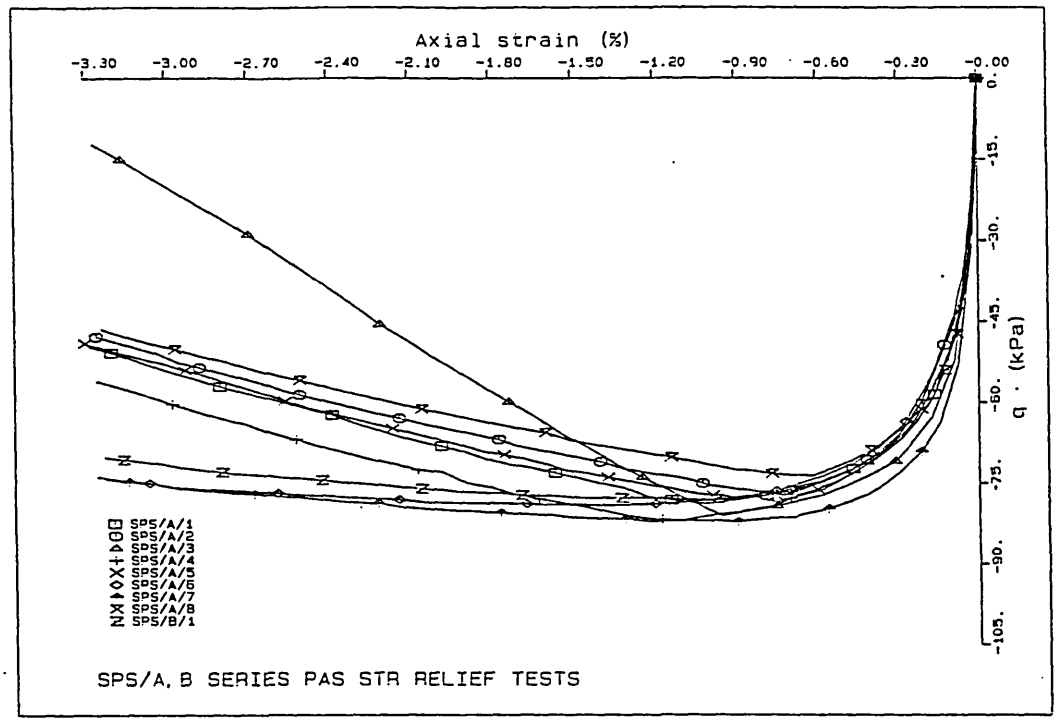
A4.Q8


p' (kPa)
0. 10. 20. 30. 40. 50. 60. 70. 80. 90. 100. 110.
0. -15. -30. -45. -60. -75. -90. -105.
q (kPa)
SPS NO ENERGY CORRECTION
SPS1
SPS2
SPS3
SPS4
SPS5
SPS6
SPS7

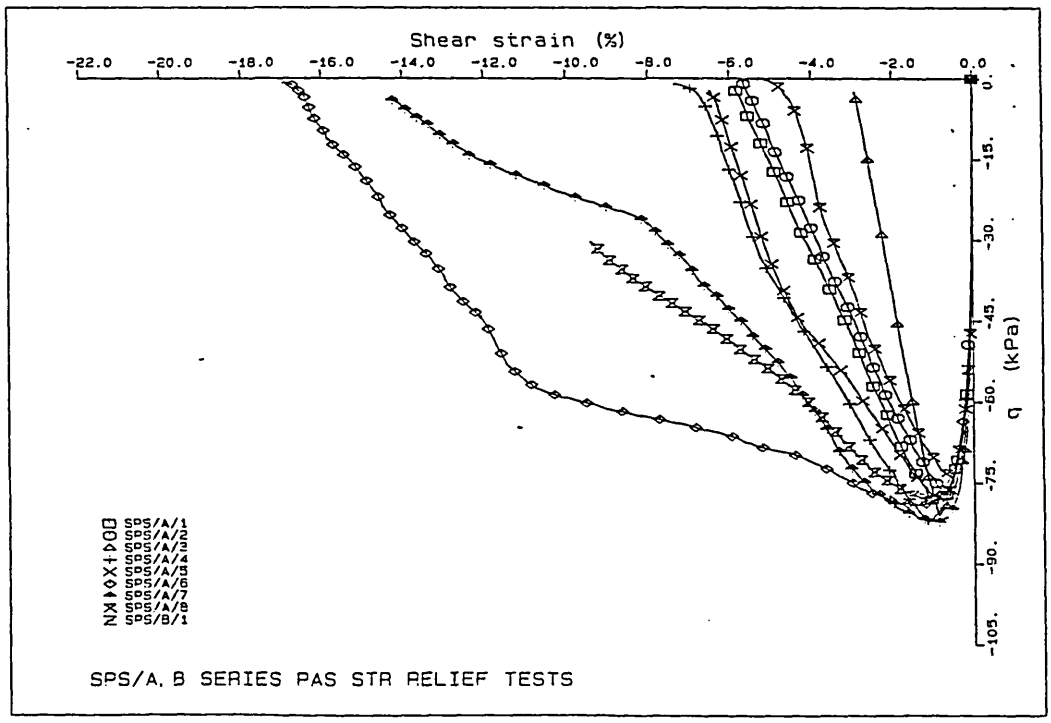
A4.Q9


p' (kPa)
0. 10. 20. 30. 40. 50. 60. 70. 80. 90. 100. 110.
0. -15. -30. -45. -60. -75. -90. -105.
q (corr) (kPa)
SPS ENERGY CORRECTED
SPS1
SPS2
SPS3
SPS4
SPS5
SPS6
SPS7

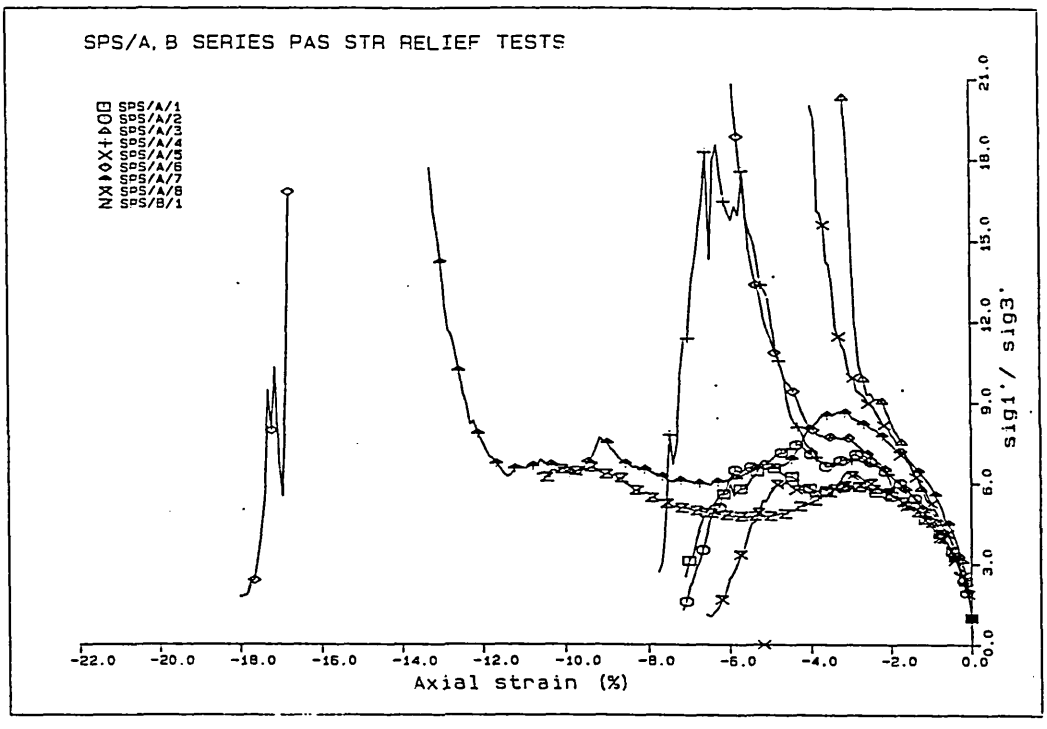
A4.Q10


Axial strain (%)
-3.30 -3.00 -2.70 -2.40 -2.10 -1.80 -1.50 -1.20 -0.90 -0.60 -0.30 -0.00
0. -15. -30. -45. -60. -75. -90. -105.
q (kPa)
SPS/A/1
SPS/A/2
SPS/A/3
SPS/A/4
SPS/A/5
SPS/A/6
SPS/A/7
SPS/A/8
SPS/B/1
SPS/A, B SERIES PAS STR RELIEF TESTS

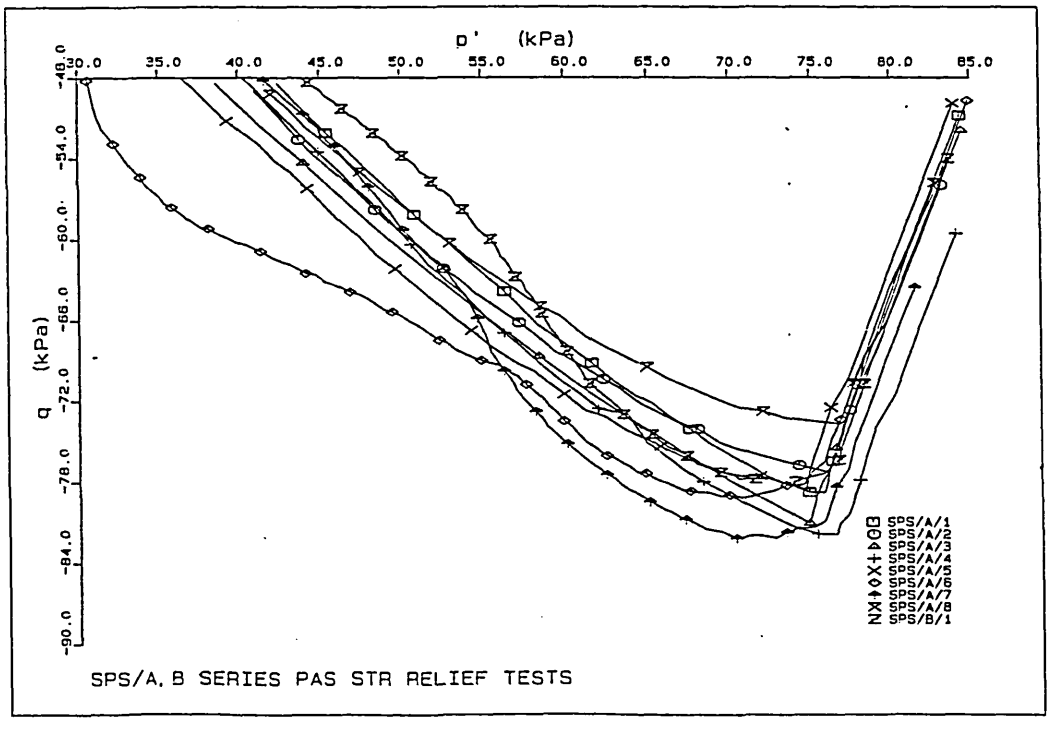
A4.R1


Shear strain (%)
-22.0 -20.0 -18.0 -16.0 -14.0 -12.0 -10.0 -8.0 -6.0 -4.0 -2.0 0.0
0. -15. -30. -45. -60. -75. -90. -105.
q (kPa)
SPS/A/1
SPS/A/2
SPS/A/3
SPS/A/4
SPS/A/5
SPS/A/6
SPS/A/7
SPS/A/8
SPS/B/1
SPS/A, B SERIES PAS STR RELIEF TESTS

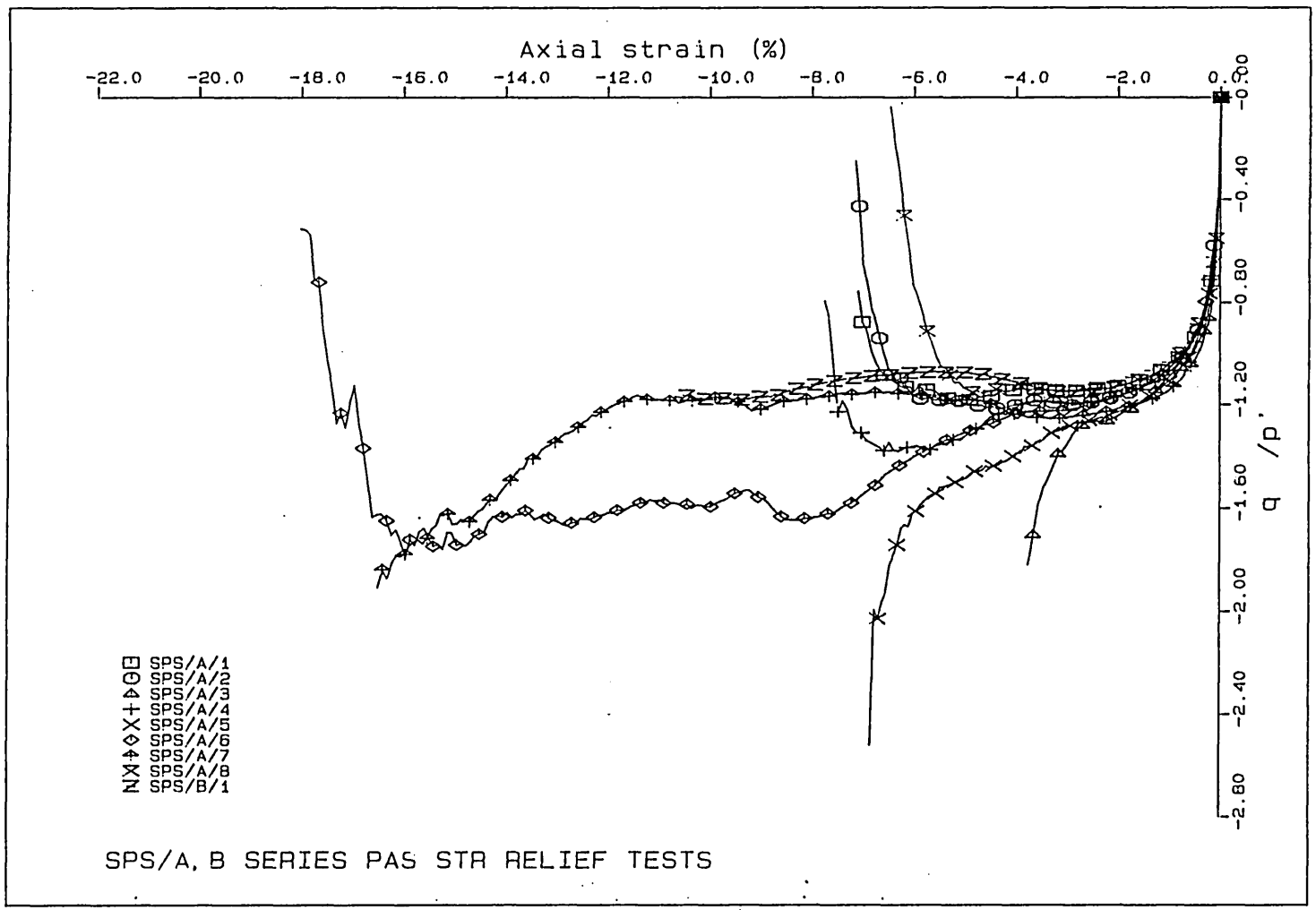
A4.R2


SPS/A, B SERIES PAS STR RELIEF TESTS
SPS/A/1
SPS/A/2
SPS/A/3
SPS/A/4
SPS/A/5
SPS/A/6
SPS/A/7
SPS/A/8
SPS/B/1
sig1' / sig3'
Axial strain (%)

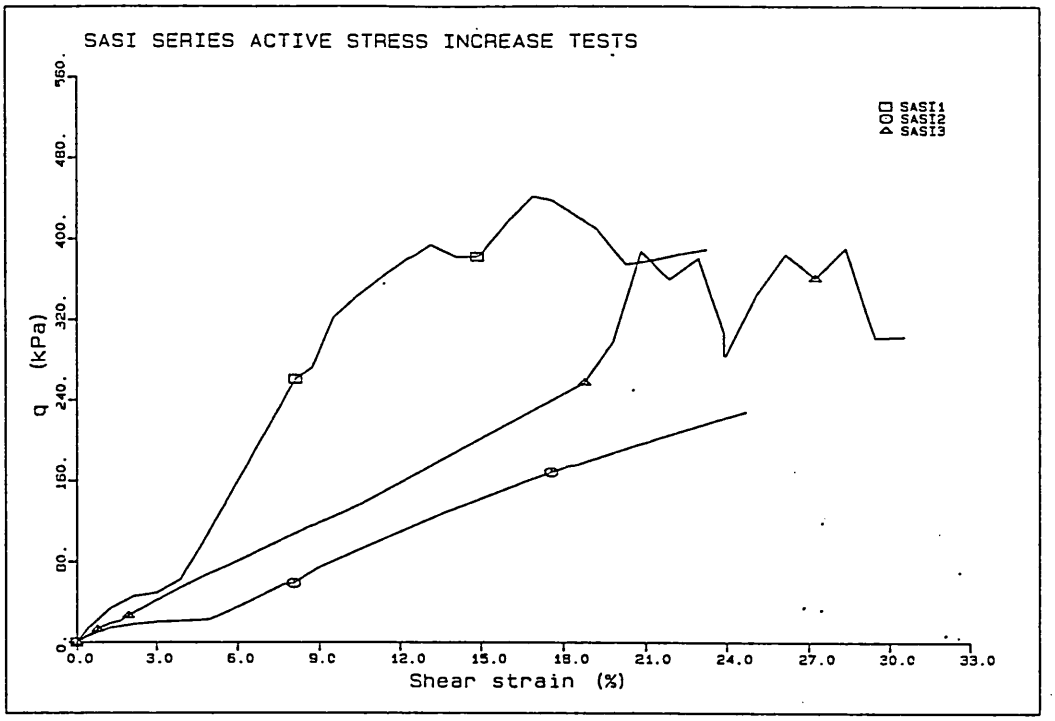
A4.R3


p' (kPa)
q (kPa)
SPS/A, B SERIES PAS STR RELIEF TESTS
SPS/A/1
SPS/A/2
SPS/A/3
SPS/A/4
SPS/A/5
SPS/A/6
SPS/A/7
SPS/A/8
SPS/B/1

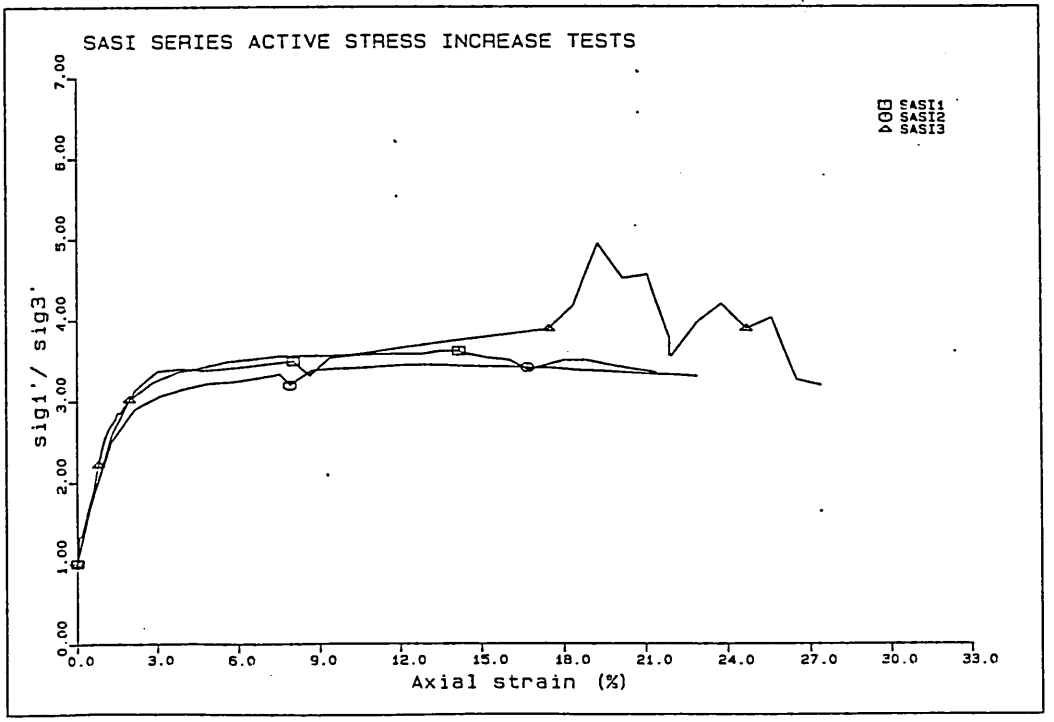
A4.R4


Axial strain (%)
-22.0
-20.0
-18.0
-16.0
-14.0
-12.0
-10.0
-8.0
-6.0
-4.0
-2.0
0.0
-0.00
-0.40
-0.80
-1.20
-1.60
-2.00
-2.40
-2.80
q /p'
SPS/A/1
SPS/A/2
SPS/A/3
SPS/A/4
SPS/A/5
SPS/A/6
SPS/A/7
SPS/A/8
SPS/B/1
SPS/A, B SERIES PAS STR RELIEF TESTS

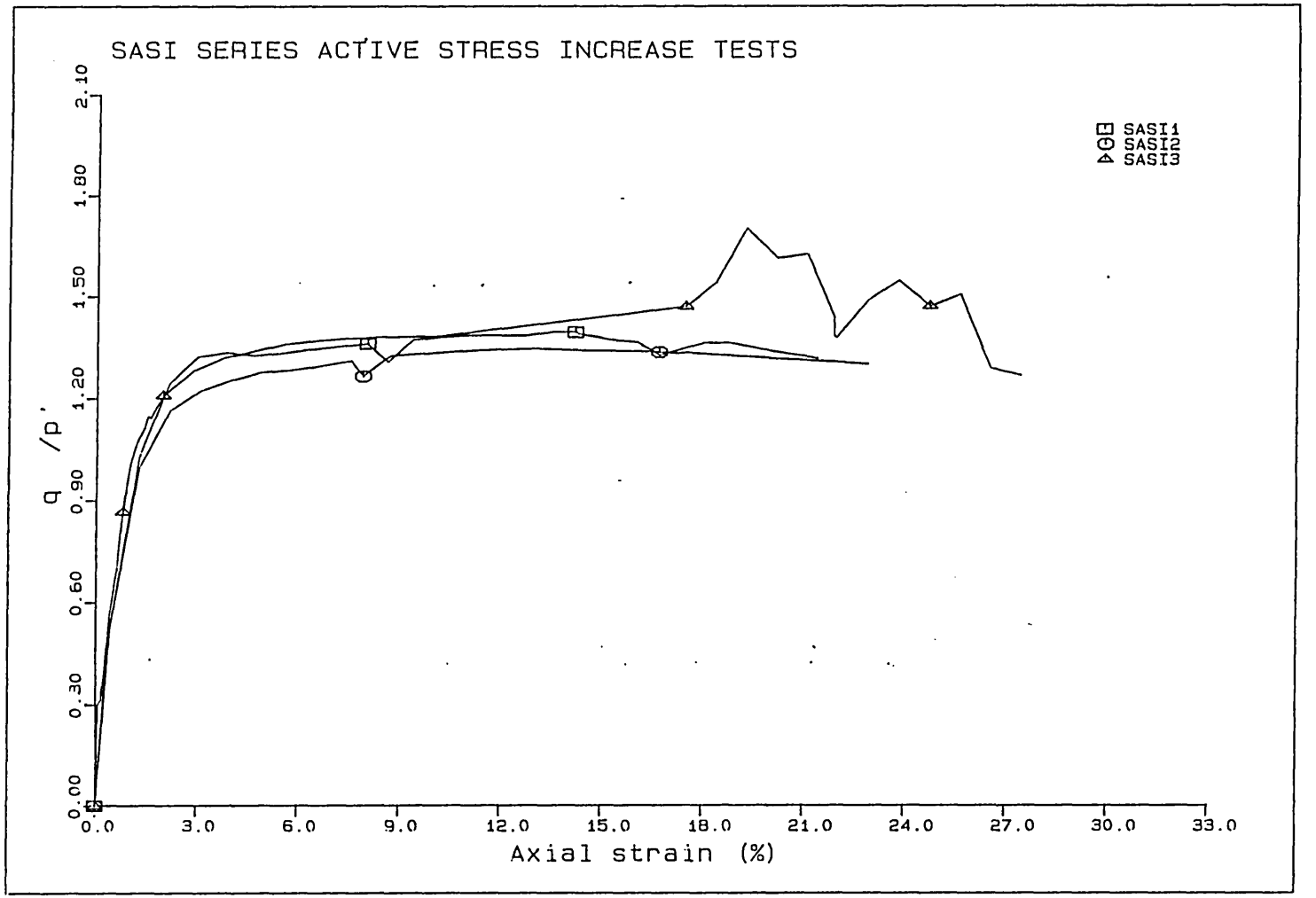
A4.R5


SASI SERIES ACTIVE STRESS INCREASE TESTS
SASI1
SASI2
SASI3
q (kPa)
0.
80.
160.
240.
320.
400.
480.
560.
0.0
3.0
6.0
9.0
12.0
15.0
18.0
21.0
24.0
27.0
30.0
33.0
Shear strain (%)

A4.S1


SASI SERIES ACTIVE STRESS INCREASE TESTS
SASI1
SASI2
SASI3
sig1'/ sig3'
0.00
1.00
2.00
3.00
4.00
5.00
6.00
7.00
0.0
3.0
6.0
9.0
12.0
15.0
18.0
21.0
24.0
27.0
30.0
33.0
Axial strain (%)

A4.S2


SASI SERIES ACTIVE STRESS INCREASE TESTS
SASI1
SASI2
SASI3
q /p'
0.00
0.30
0.60
0.90
1.20
1.50
1.80
2.10
0.0
3.0
6.0
9.0
12.0
15.0
18.0
21.0
24.0
27.0
30.0
33.0
Axial strain (%)

A4.S3

APPENDIX A5

TABLE AND FIGURES

Table A5.1

Schedule of triaxial tests and plane strain tests on specimens of Claygate beds and London clay. (All tests are extension unless otherwise noted).

Label	Depth (m) (plasticity index)	Description of testing procedure	Initial p'	p' after isotropic swell consolidation	K_o Stresses p'	K_o Stresses q	Stress after partial shear stage p'	Stress after partial shear stage q	Appendix
TCUU1	1.9 (26)	Undrained shear to failure from isotropic stress	19	42					A5.A1
TLUU1	14.2 (28)	" " " "	326	356					A5.A2
TLUU2	15.3 (35)	" " " "	371	380					A5.A3
TLUU3	18.9 (47)	" " " "	520	598					A5.A4
TLUU4	10.6 (39)	" " " "	310	303					A5.A5
TLUU5	13.0 (37)	" " " "	652	787					A5.A6
TLSU1	17.5 (42)	Swell to K_o. Undrained shear to failure.	340	331	251	- 33			A5.B1
TLSU2	9.4 (31)	" " " "	250	280	206	- 76			A5.B2
TLCU1	11.4 (37)	Swell to low p'. Undrained shear to failure.	371	105					A5.C1
TLCU2	11.6 (37)	" " " "	388	55					A5.C2
TCPS1	2.2 (27)	Swell to K_o. Undrained shear. Passive stress relief.	193	44	44	- 0	65	-57	A5.D1
TLPS1	14.8 (26)	" " " "	220	338	232	- 66	232	-132	A5.D2
TLPS2	13.4 (22)	Swell to K_o. Drained shear. Passive stress relief.	576	401	223	- 69	205	-125	A5.D3
TLPS3	20.4 (37)	Swell to K_o. Undrained shear. Passive stress relief.	300	350	280	- 37	312	-163	A5.D4
TLPS4	16.3 (39)	Swell to K_o. Undrained shear. Passive stress relief (computer control).	246	267	242	- 45	288	-182	A5.D5
TLPS5	10.3 (39)	Swell to K_o. Undrained shear. Passive stress relief (computer control).	223	247	204	- 85	213	-112	A5.D6
TLPS6	20.5 (37)	Swell to K_o. Undrained shear. Passive stress relief (Lubricated ends).	350	353	283	- 46	331	-153	A5.D7
TLDRUL1	13.8 (30)	K_o swell from high initial p'.	380	409					A5.E1
TLDRUL2	13.6 (26)	" " " "	620	400					A5.E2
TLD1	17.1 (39)	Isotropic swell. Undrained/ drained shear. (Incomplete pore water pressure dissipation during early part of test).	620	81					A5.F1
TLSUD1A	18.5 (43)	Swell to K_o. Undrained shear. Swell with q const.	289	317	259	-46	314	-183	A5.G1
TLSUD2B	10.7 (39)	" " " "	543	264	246	-42	231	-126	A5.G2
TCUA1	2.5 (26)	Undrained compression σ_v constant, σ_h decreasing.	512	50	50	-0			A5.H1
TLUA1	19.9 (31)	Swell to K_o. Undrained compression σ_v constant, σ_h decreasing.	586	350	280	-41			A5.I1
TLA1	15.2 (33)	Swell to K_o. Drained compression σ_v constant, σ_h decreasing.	300	338	223	-39			A5.J1
TLA2A	9.8 (36)	" " " "	310	245	197	-77			A5.J2
PLPS1	17.9 (49)	Swell to K_o. Drained shear. Passive stress relief.	390	269	250	-45	217	-111	A5.K1

Note to Appendix A5 Figures

In the following figures, where only a portion of the test is reproduced, the particular phase is referred to as follows:

UNISO undrained extension from isotropic

UNAN undrained extension from K_o

ANISO anisotropic swell to K_o

PS passive stress relief

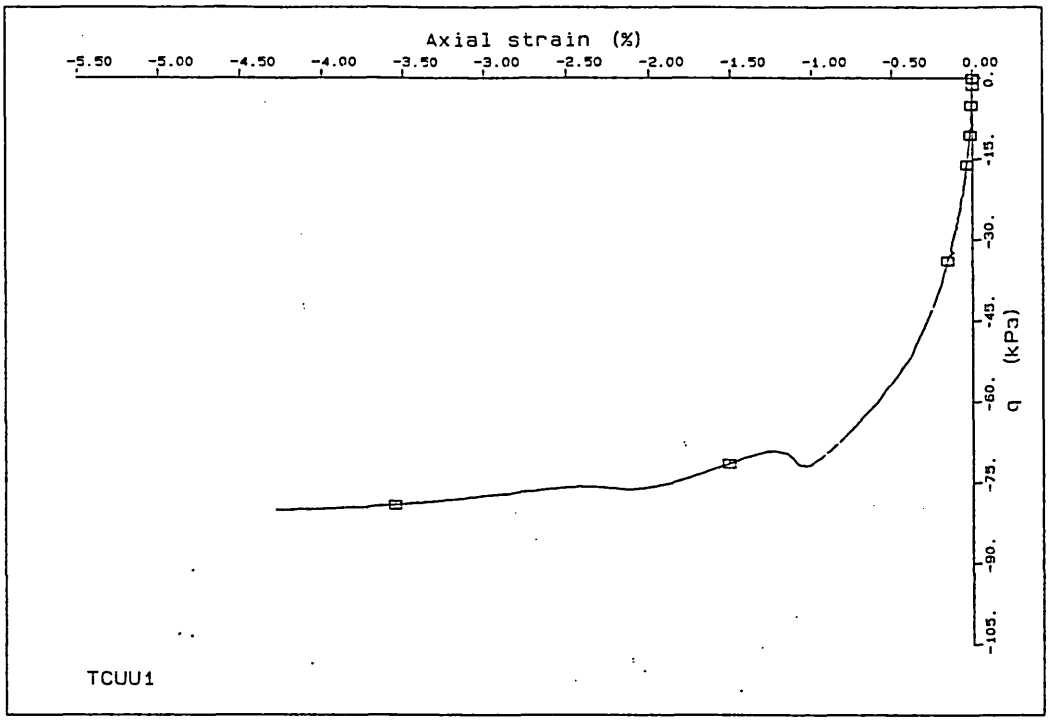
DRAN drained extension from K_o

DR drained extension from isotropic

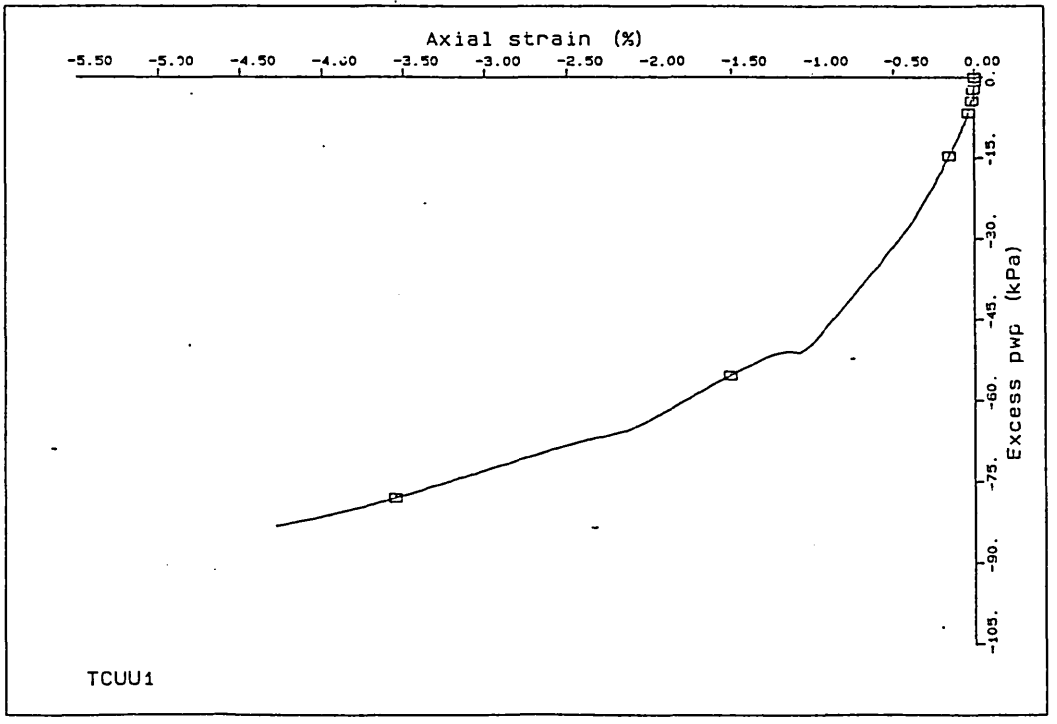
UNISOC undrained compression from isotropic

UNANC undrained compression from K_o

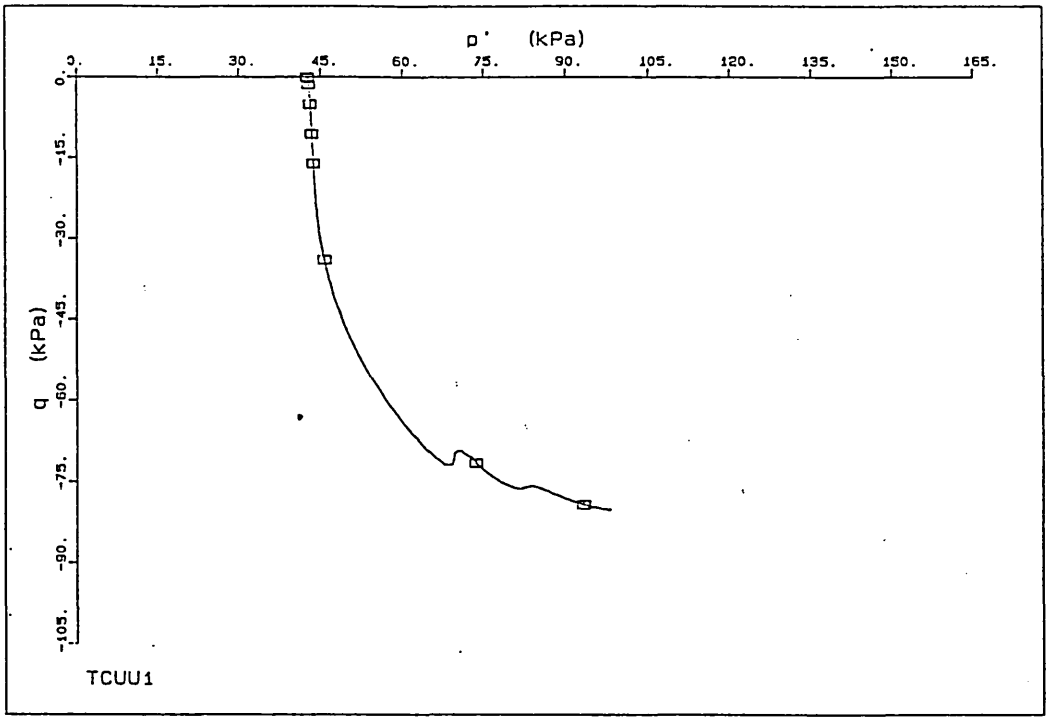
DRANC drained compression from K_o


Axial strain (%)
-5.50 -5.00 -4.50 -4.00 -3.50 -3.00 -2.50 -2.00 -1.50 -1.00 -0.50 0.00
0. -15. -30. -45. -60. -75. -90. -105.
q (kPa)
TCUU1

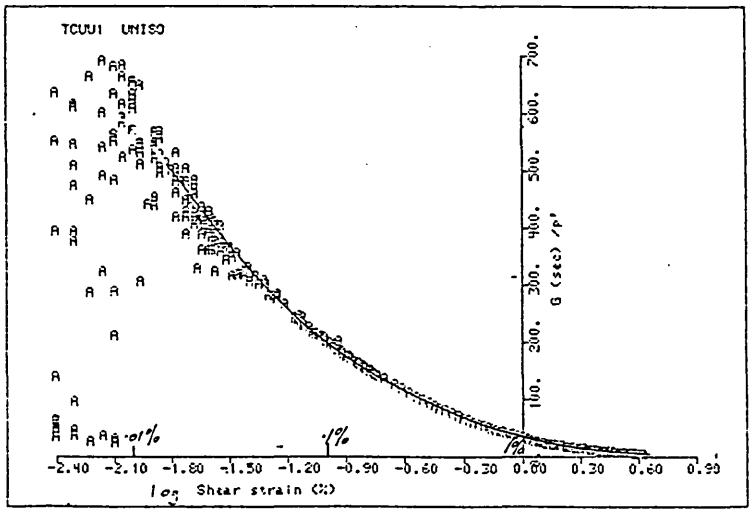
A5.A1.1


Axial strain (%)
-5.50 -5.00 -4.50 -4.00 -3.50 -3.00 -2.50 -2.00 -1.50 -1.00 -0.50 0.00
0. -15. -30. -45. -60. -75. -90. -105.
Excess pwp (kPa)
TCUU1

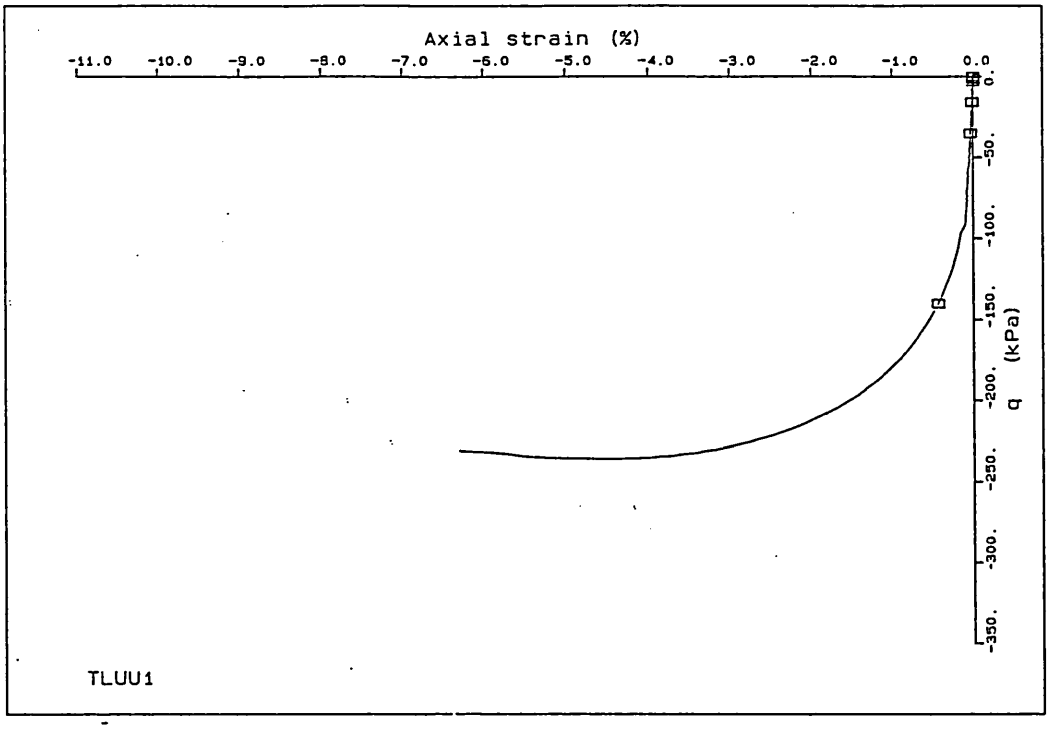
A5.A1.2


p' (kPa)
0. 15. 30. 45. 60. 75. 90. 105. 120. 135. 150. 165.
0. -15. -30. -45. -60. -75. -90. -105.
q (kPa)
TCUU1

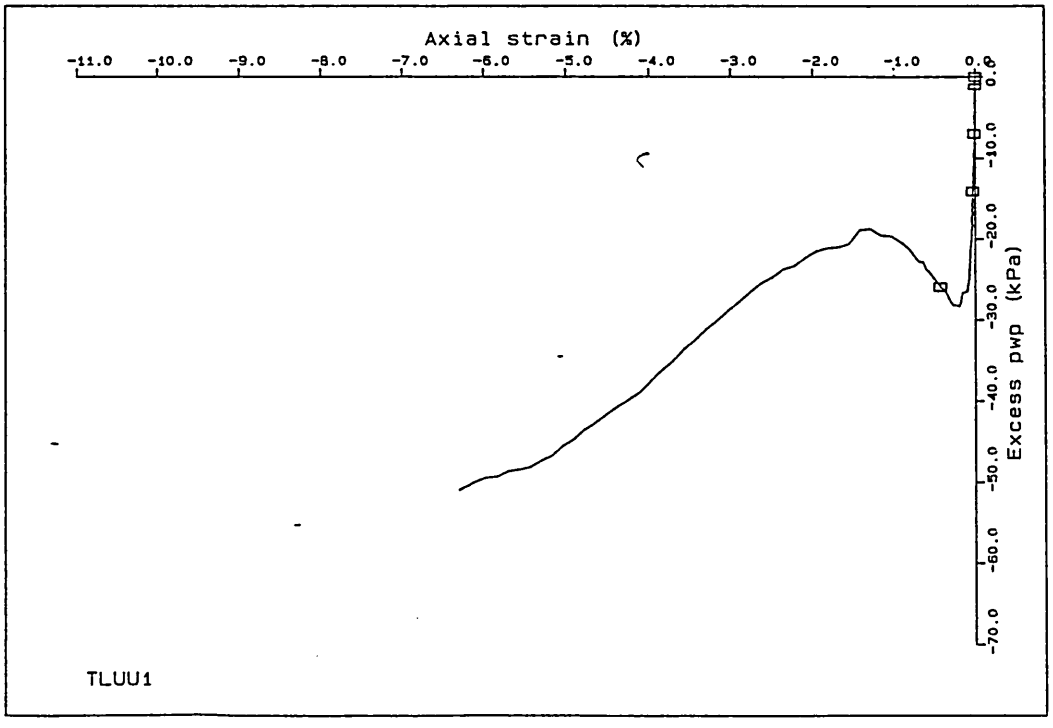
A5.A1.3


TCUU1 UNISO
-2.40 -2.10 -1.80 -1.50 -1.20 -0.90 -0.60 -0.30 0.00 0.30 0.60 0.90
Log Shear strain (%)
G (sec) /p'

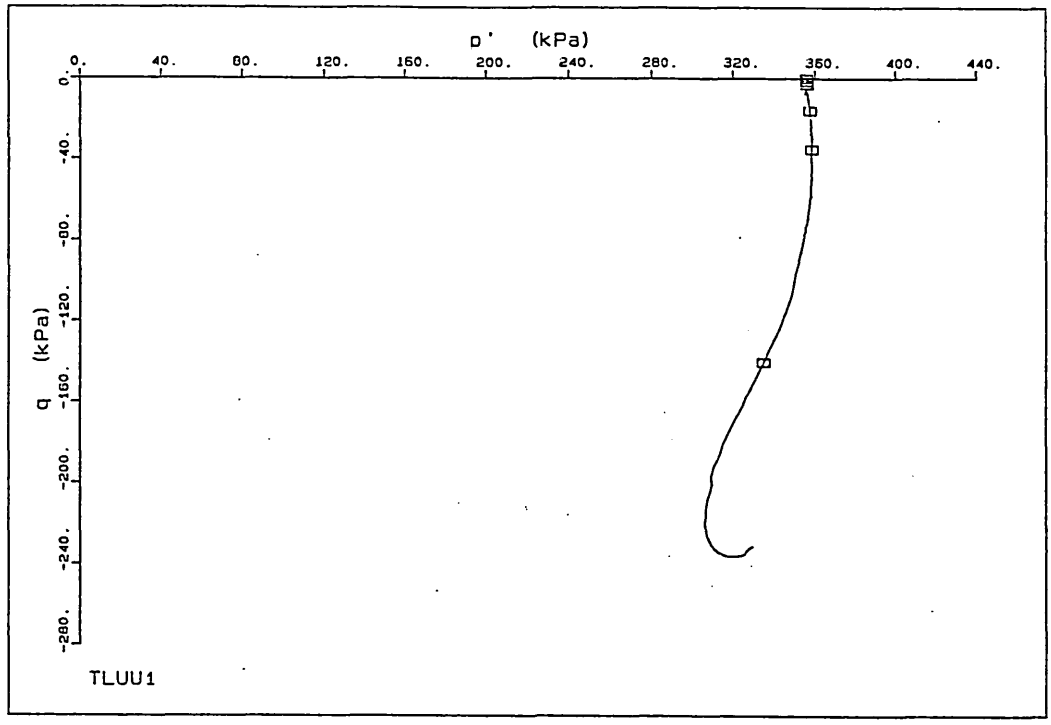
A5.A1.4


Axial strain (%)
-11.0
-10.0
-9.0
-8.0
-7.0
-6.0
-5.0
-4.0
-3.0
-2.0
-1.0
0.0
0.
-50.
-100.
-150.
-200.
-250.
-300.
-350.
q (kPa)
TLUU1

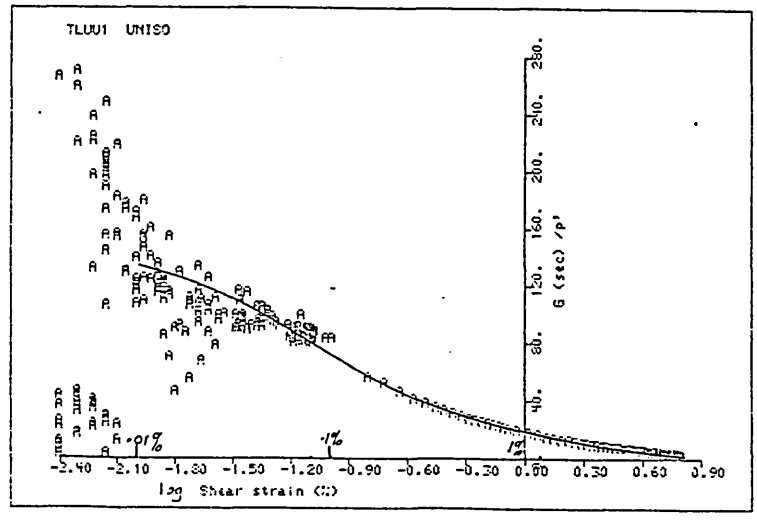
A5.A2.1


Axial strain (%)
-11.0
-10.0
-9.0
-8.0
-7.0
-6.0
-5.0
-4.0
-3.0
-2.0
-1.0
0.0
0.0
-10.0
-20.0
-30.0
-40.0
-50.0
-60.0
-70.0
Excess pwp (kPa)
TLUU1

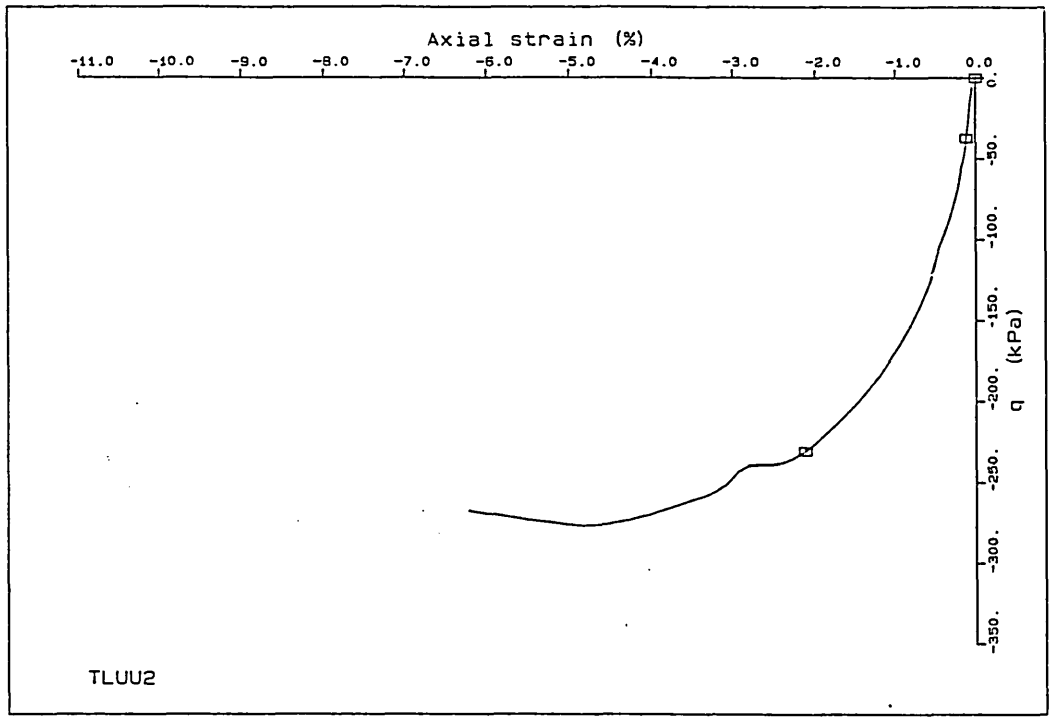
A5.A2.2


p' (kPa)
0. 40. 80. 120. 160. 200. 240. 280. 320. 360. 400. 440.
q (kPa)
0. -40. -80. -120. -160. -200. -240. -280.
TLUU1

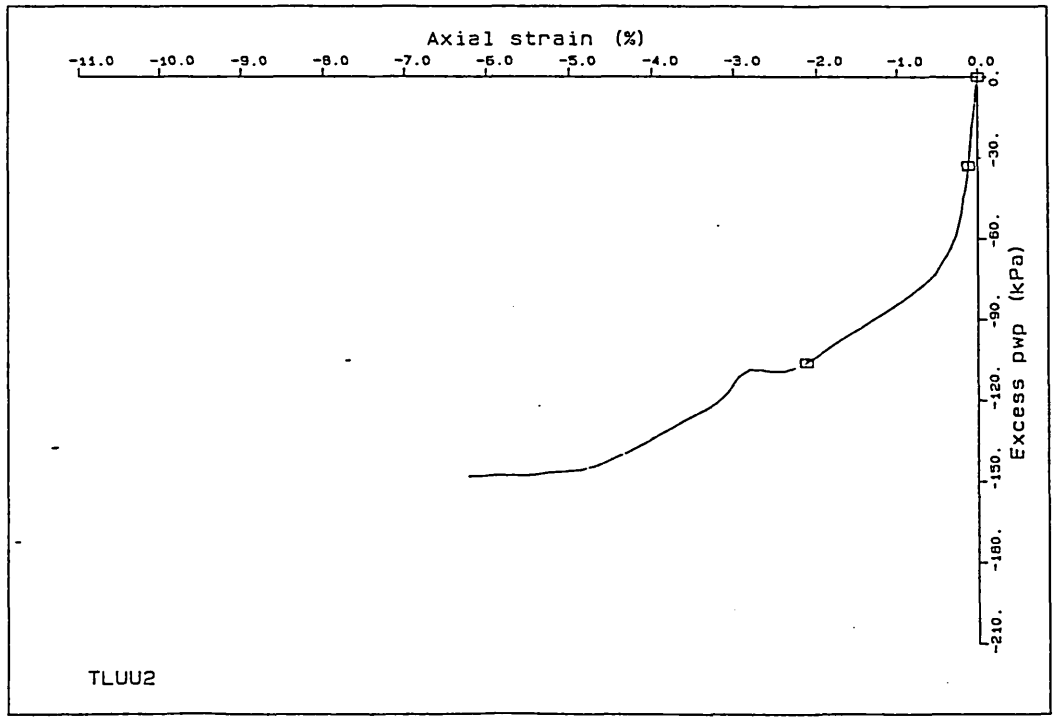
A5.A2.3


TLUU1 UNISO
G (sec) /p'
40. 80. 120. 160. 200. 240. 280.
.01%
.1%
1%
-2.40 -2.10 -1.80 -1.50 -1.20 -0.90 -0.60 -0.30 0.00 0.30 0.60 0.90
log Shear strain (%)

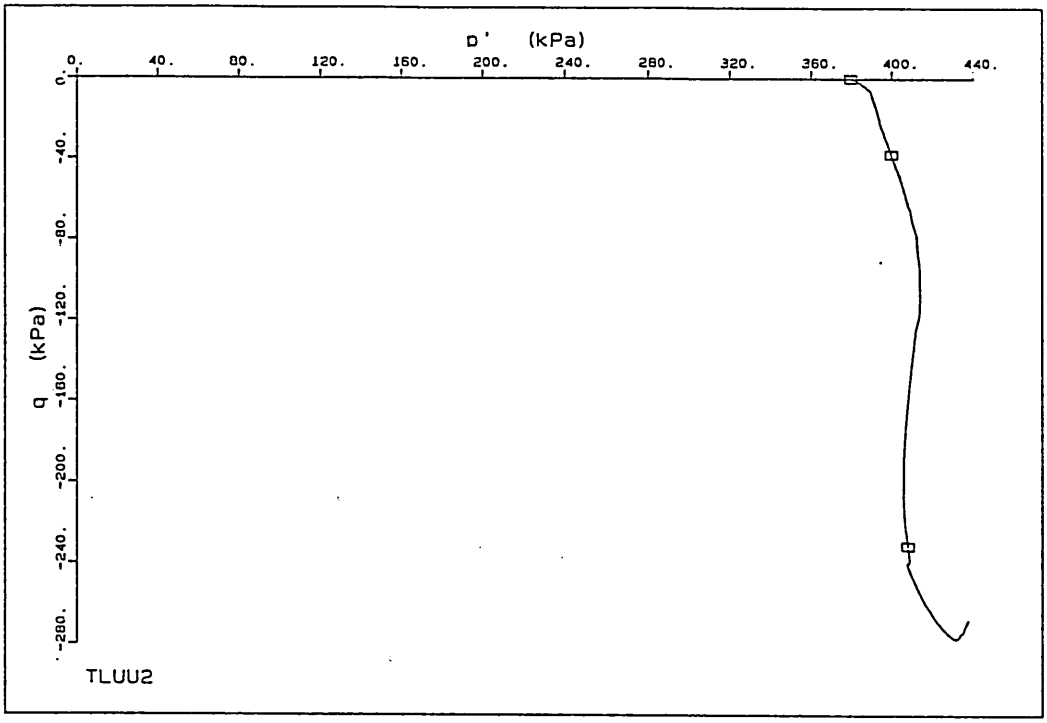
A5.A2.4


Axial strain (%)
-11.0
-10.0
-9.0
-8.0
-7.0
-6.0
-5.0
-4.0
-3.0
-2.0
-1.0
0.0
0.
-50.
-100.
-150.
-200.
-250.
-300.
-350.
q (kPa)
TLUU2

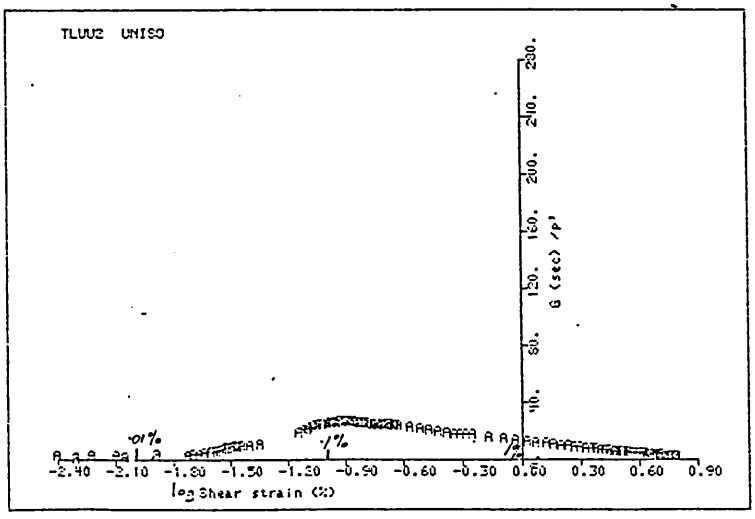
A5.A3.1


Axial strain (%)
-11.0
-10.0
-9.0
-8.0
-7.0
-6.0
-5.0
-4.0
-3.0
-2.0
-1.0
0.0
0.
-30.
-60.
-90.
-120.
-150.
-180.
-210.
Excess pwp (kPa)
TLUU2

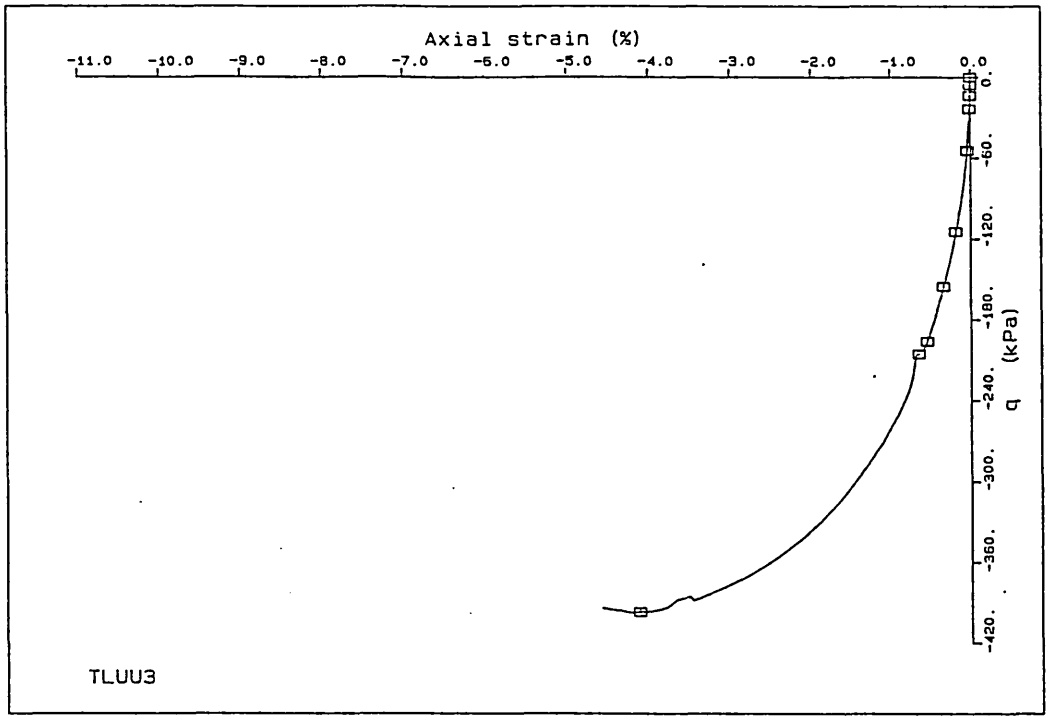
A5.A3.2


p' (kPa)
0. 40. 80. 120. 160. 200. 240. 280. 320. 360. 400. 440.
q (kPa)
0. -40. -80. -120. -160. -200. -240. -280.
TLUU2

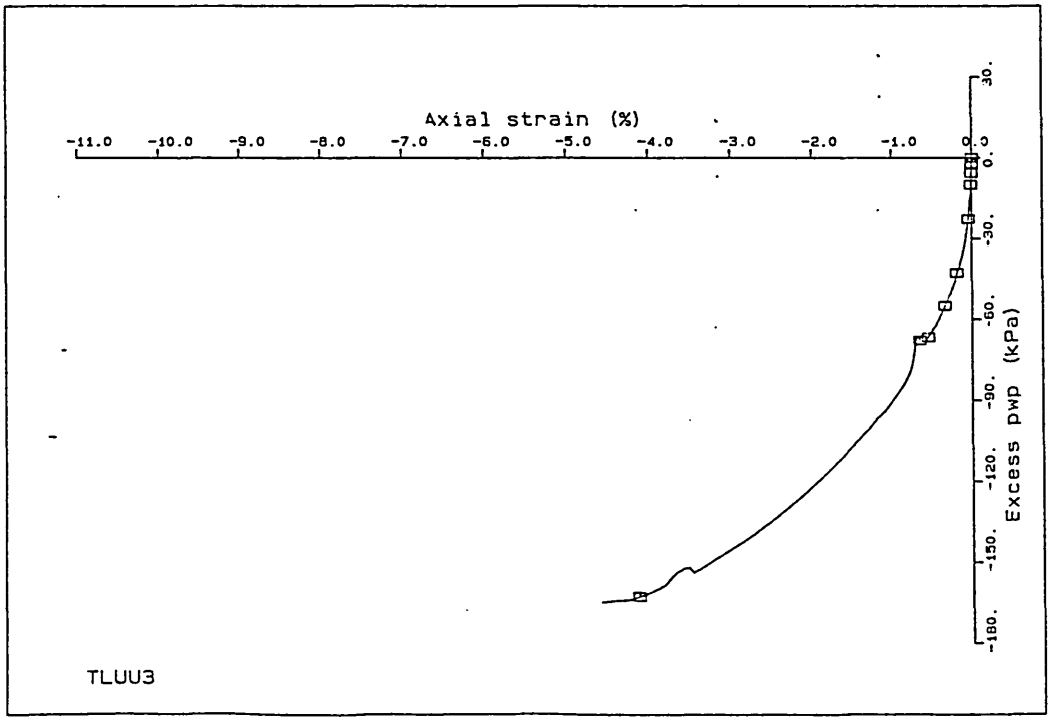
A5.A3.3


TLUU2 UNISO
G (sec) /p'
10. 50. 90. 130. 170. 210. 230.
-2.40 -2.10 -1.80 -1.50 -1.20 -0.90 -0.60 -0.30 0.00 0.30 0.60 0.90
log Shear strain (%)

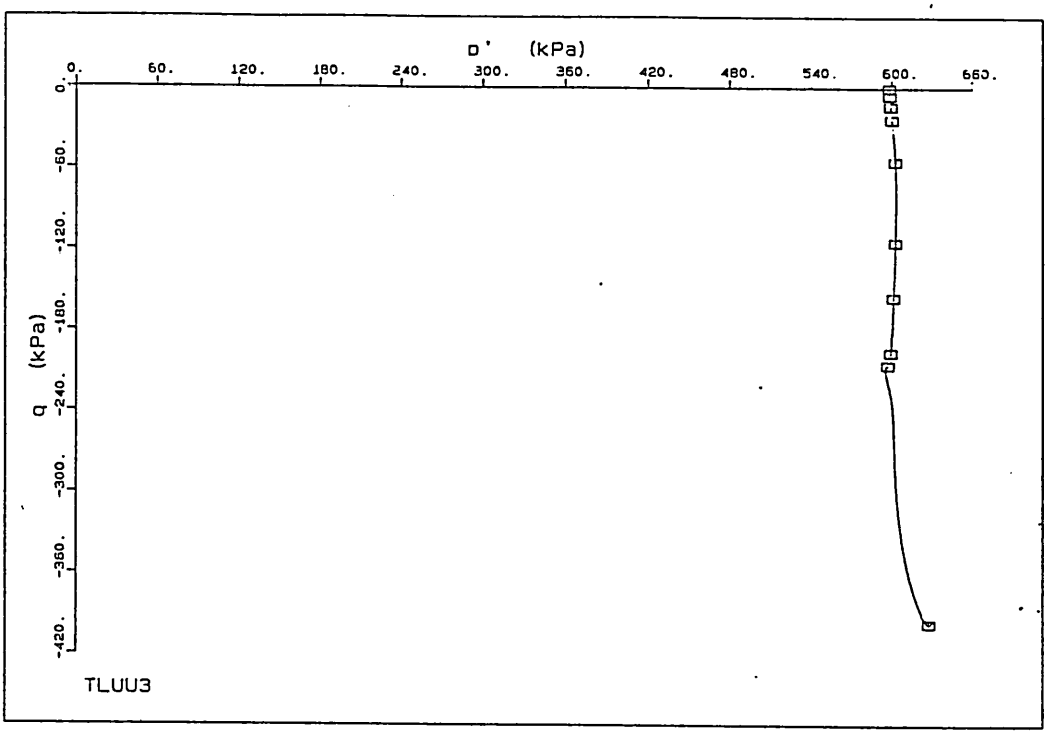
A5.A3.4


Axial strain (%)
-11.0
-10.0
-9.0
-8.0
-7.0
-6.0
-5.0
-4.0
-3.0
-2.0
-1.0
0.0
0.
-60.
-120.
-180.
-240.
-300.
-360.
-420.
q (kPa)
TLUU3

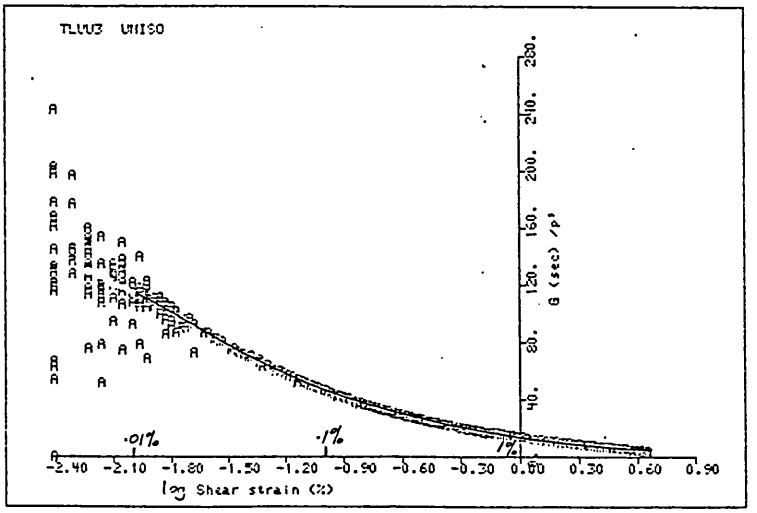
A5.A4.1


Axial strain (%)
-11.0
-10.0
-9.0
-8.0
-7.0
-6.0
-5.0
-4.0
-3.0
-2.0
-1.0
0.0
30.
0.
-30.
-60.
-90.
-120.
-150.
-180.
Excess pwp (kPa)
TLUU3

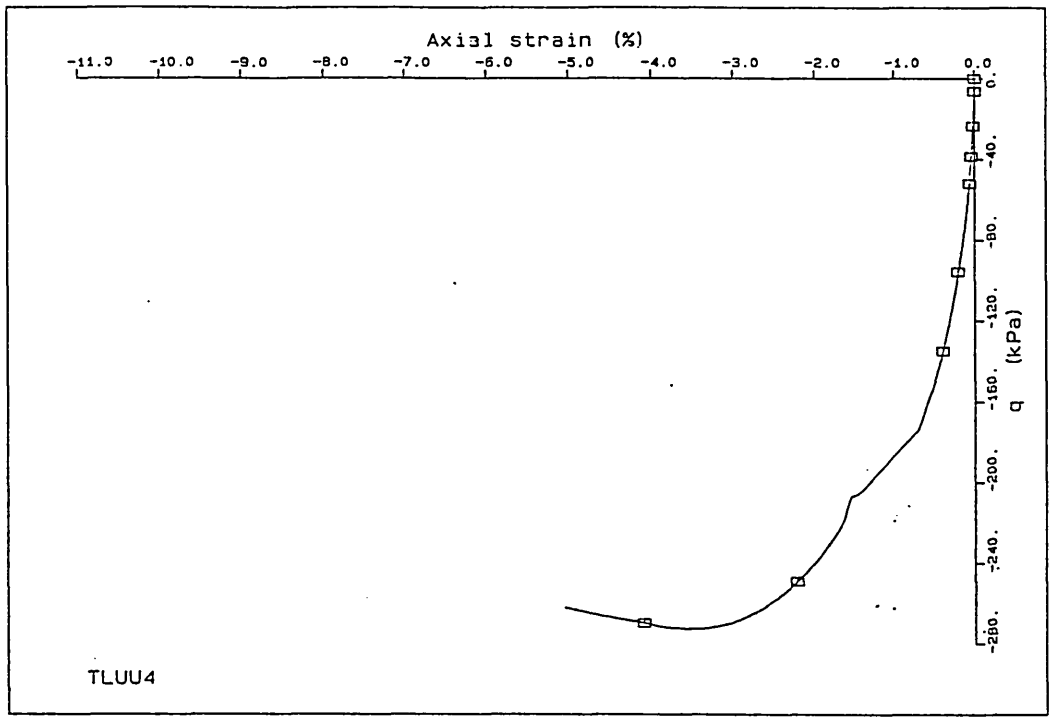
A5.A4.2


p' (kPa)
0. 60. 120. 180. 240. 300. 360. 420. 480. 540. 600. 660.
q (kPa)
0. -60. -120. -180. -240. -300. -360. -420.
TLUU3

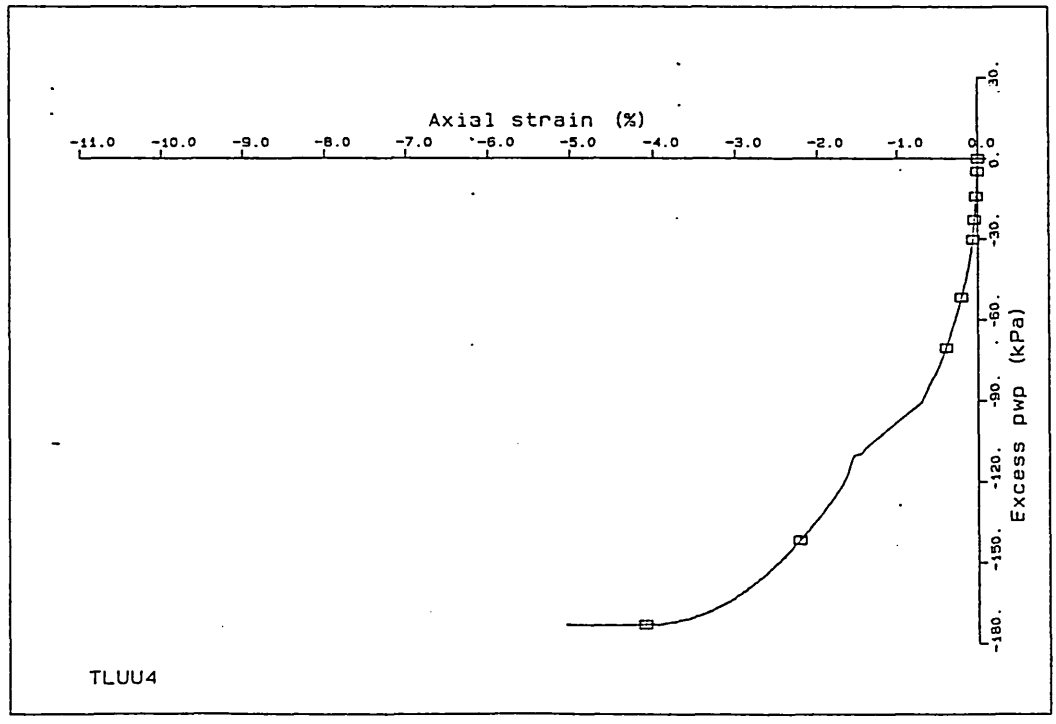
A5.A4.3


TLUU3 UNISO
G (sec) /p'
40. 80. 120. 160. 200. 240. 280.
·01%
·1%
1%
-2.40 -2.10 -1.80 -1.50 -1.20 -0.90 -0.60 -0.30 0.00 0.30 0.60 0.90
log Shear strain (%)

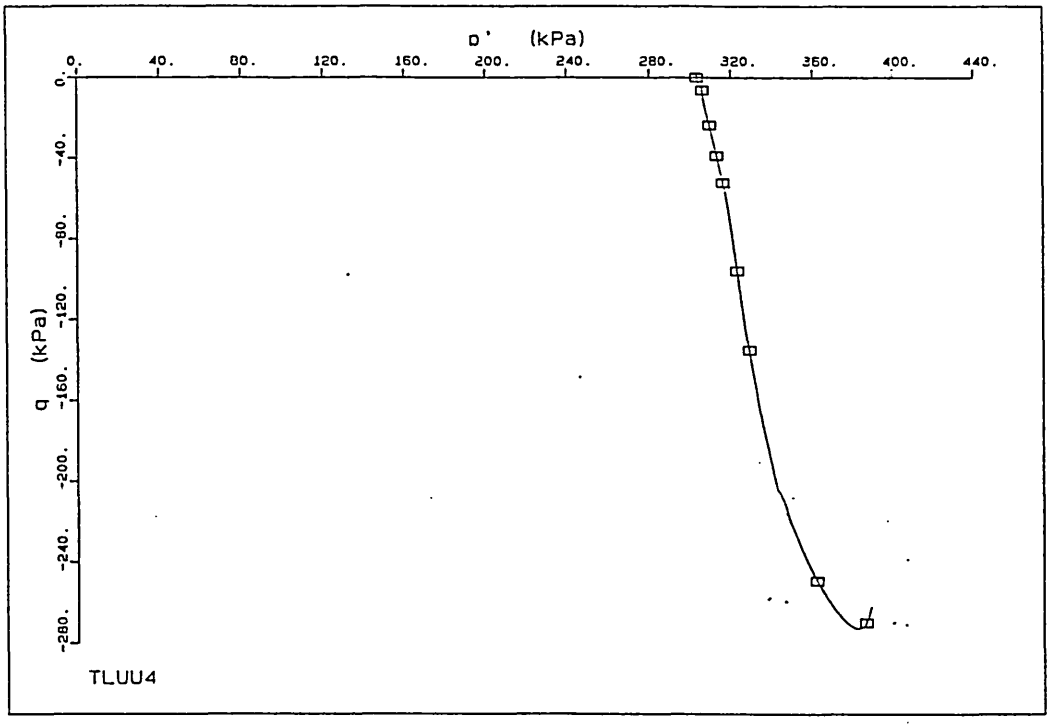
A5.A4.4


Axial strain (%)
-11.0
-10.0
-9.0
-8.0
-7.0
-6.0
-5.0
-4.0
-3.0
-2.0
-1.0
0.0
0.
-40.
-80.
-120.
-160.
-200.
-240.
-280.
q (kPa)
TLUU4

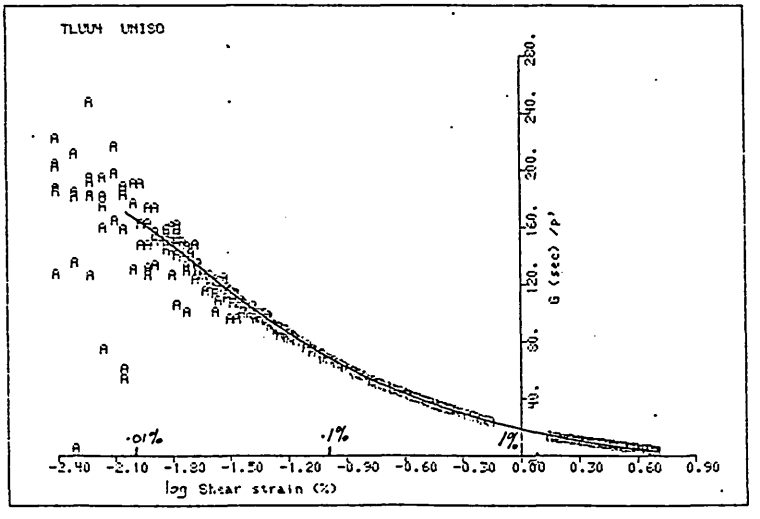
A5.A5.1


Axial strain (%)
-11.0
-10.0
-9.0
-8.0
-7.0
-6.0
-5.0
-4.0
-3.0
-2.0
-1.0
0.0
30.
0.
-30.
-60.
-90.
-120.
-150.
-180.
Excess pwp (kPa)
TLUU4

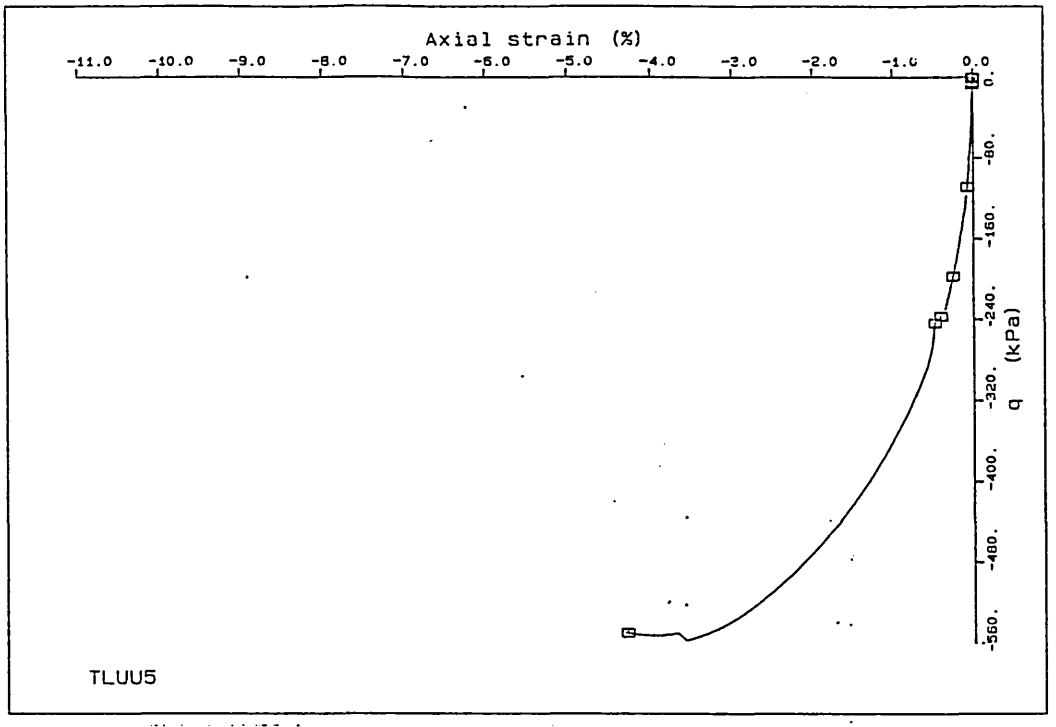
A5.A5.2


p' (kPa)
0. 40. 80. 120. 160. 200. 240. 280. 320. 360. 400. 440.
q (kPa)
0. -40. -80. -120. -160. -200. -240. -280.
TLUU4

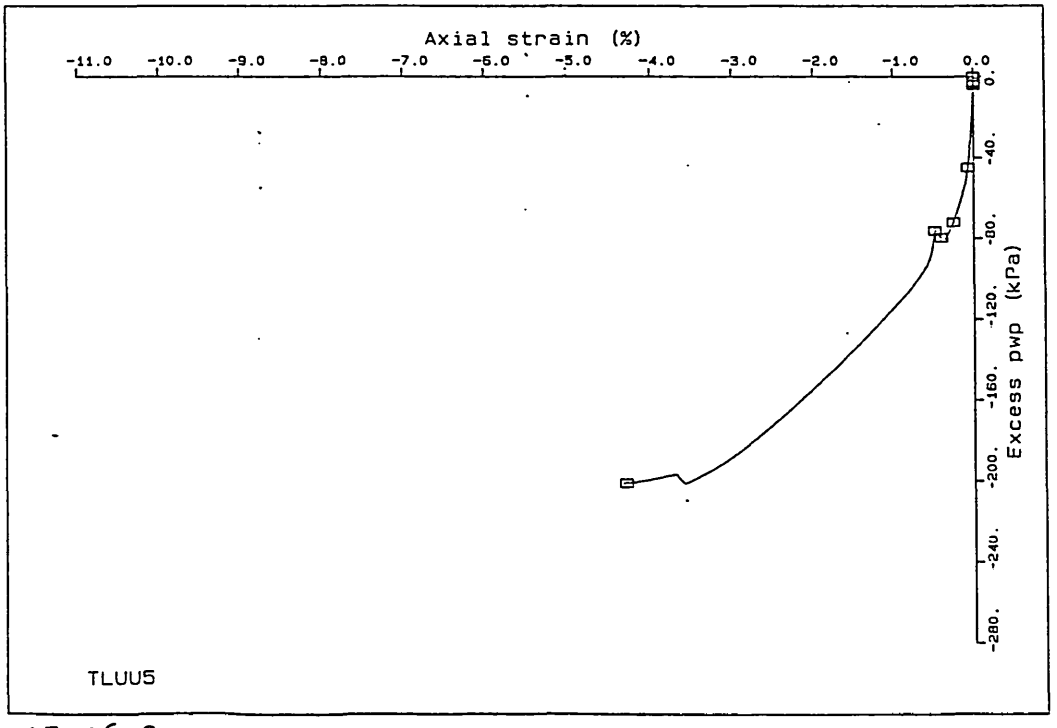
A5.A5.3


TLUU4 UNISO
G (sec) /p'
40. 80. 120. 160. 200. 240. 280.
.01% .1% 1%
-2.40 -2.10 -1.80 -1.50 -1.20 -0.90 -0.60 -0.30 0.00 0.30 0.60 0.90
log Shear strain (%)

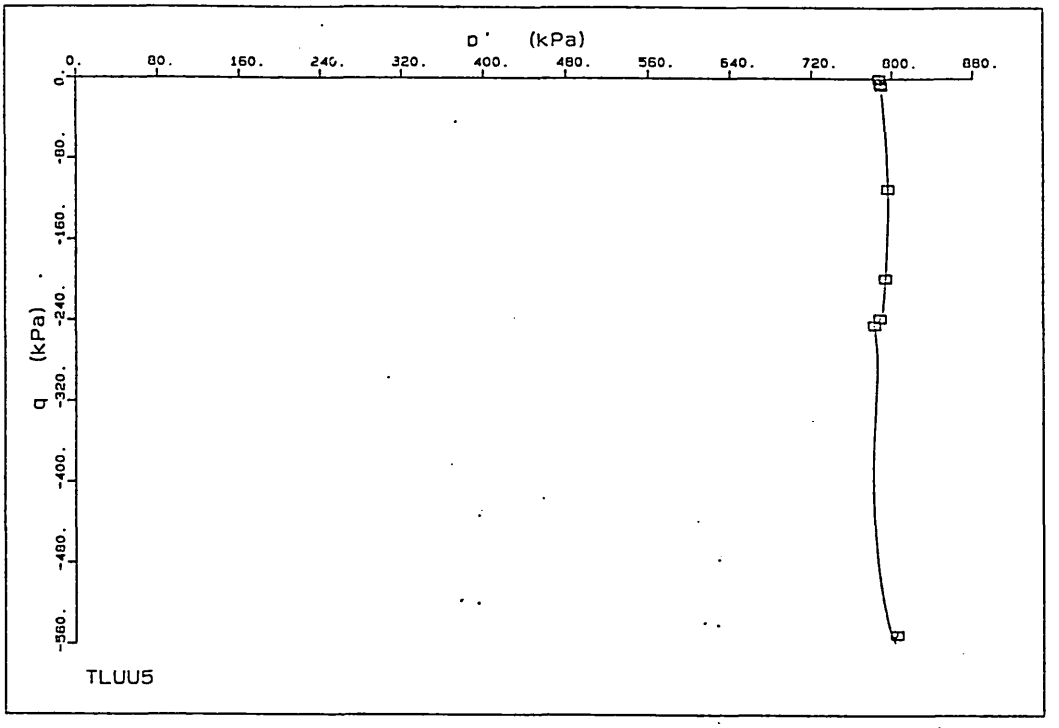
A5.A5.4


Axial strain (%)
-11.0
-10.0
-9.0
-8.0
-7.0
-6.0
-5.0
-4.0
-3.0
-2.0
-1.0
0.0
0.
-80.
-160.
-240.
-320.
-400.
-480.
-560.
q (kPa)
TLUU5

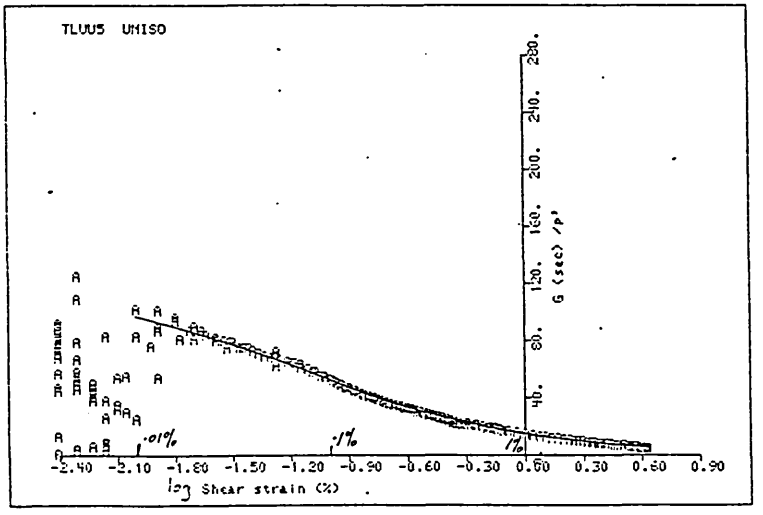
A5.A6.1


Axial strain (%)
-11.0
-10.0
-9.0
-8.0
-7.0
-6.0
-5.0
-4.0
-3.0
-2.0
-1.0
0.0
0.
-40.
-80.
-120.
-160.
-200.
-240.
-280.
Excess pwp (kPa)
TLUU5

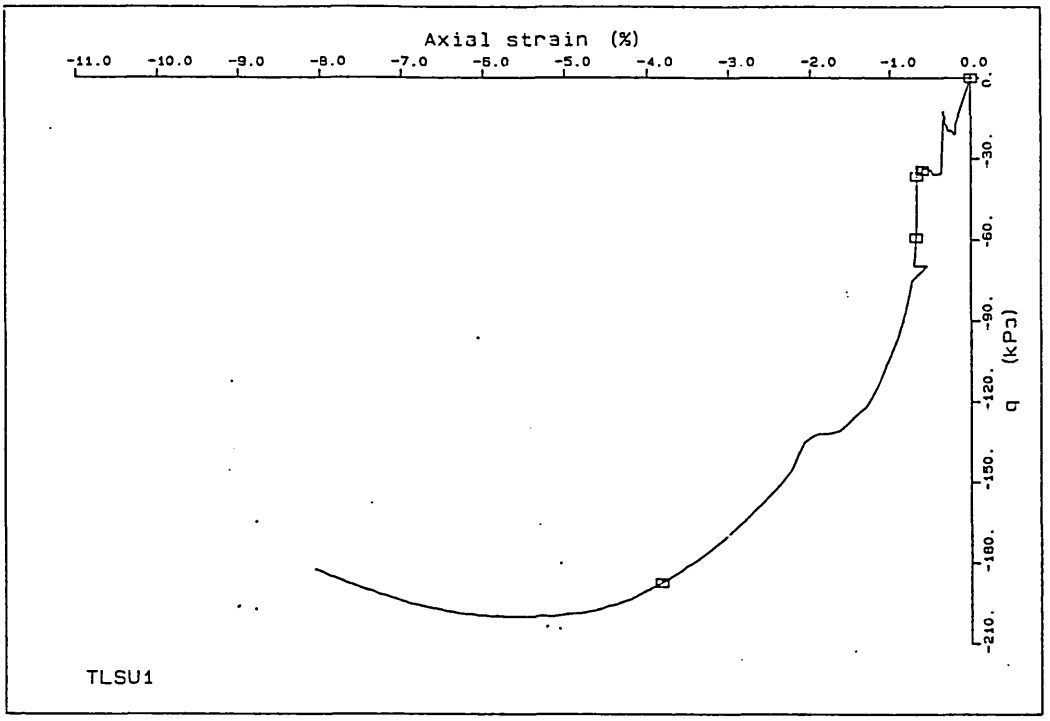
A5.A6.2


p' (kPa)
0. 80. 160. 240. 320. 400. 480. 560. 640. 720. 800. 880.
q (kPa)
0. -80. -160. -240. -320. -400. -480. -560.
TLUU5

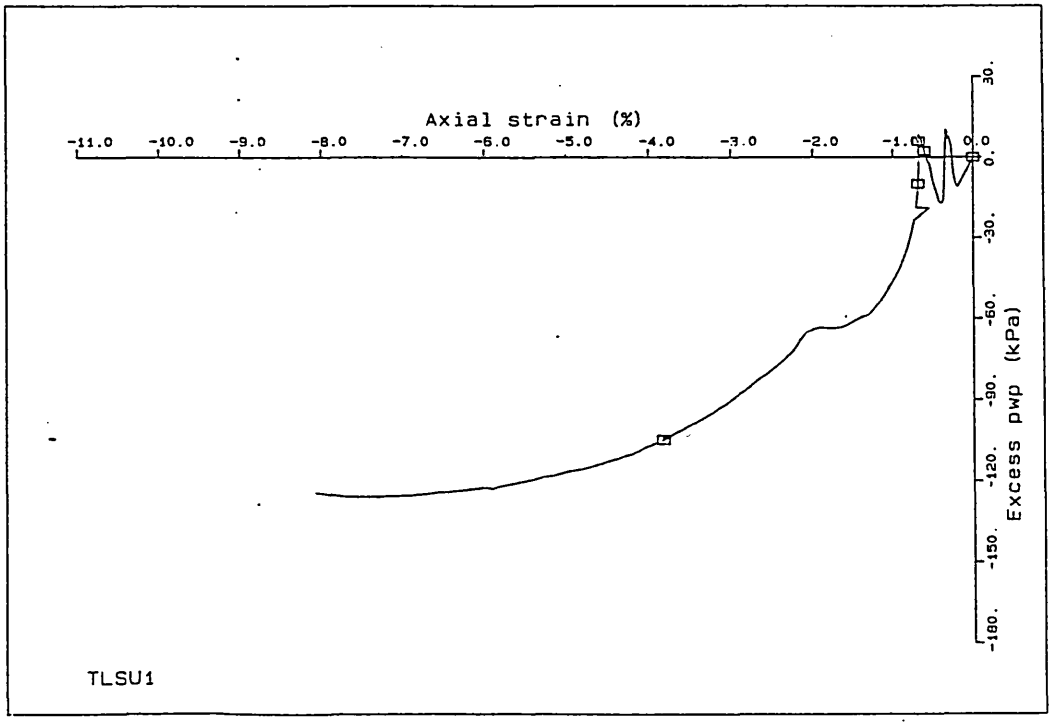
A5.A6.3


TLUU5 UNISO
G (sec) / p'
log Shear strain (%)
-2.40 -2.10 -1.80 -1.50 -1.20 -0.90 -0.60 -0.30 0.00 0.30 0.60 0.90
.01%
.1%
1%

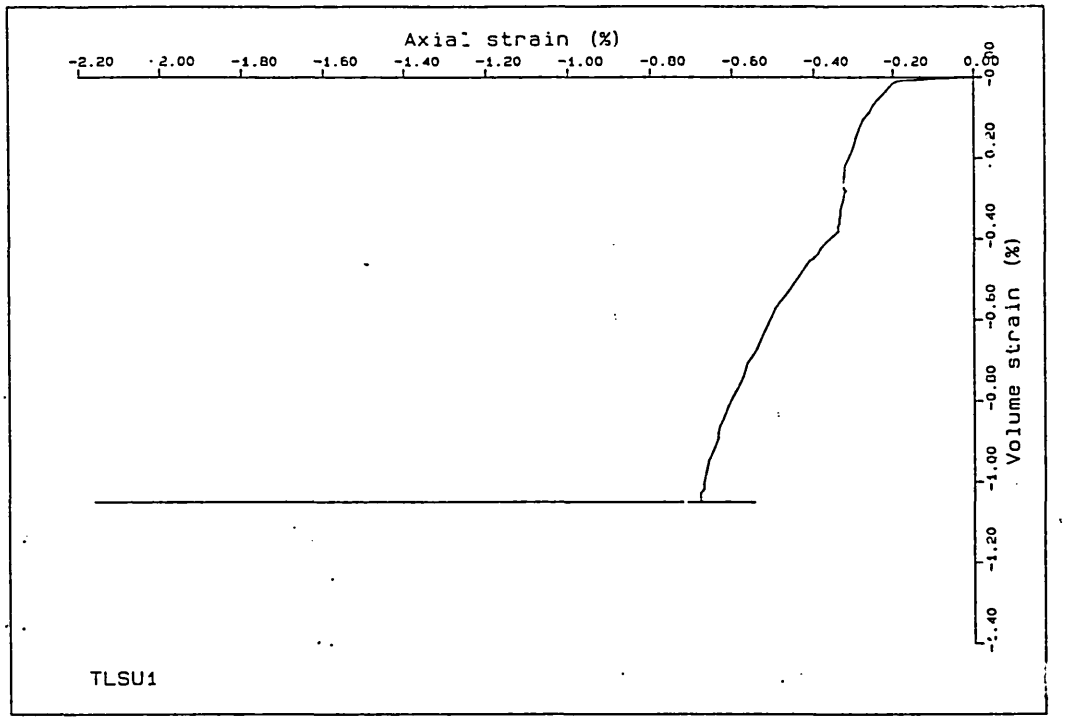
A5.A6.4


Axial strain (%)
-11.0
-10.0
-9.0
-8.0
-7.0
-6.0
-5.0
-4.0
-3.0
-2.0
-1.0
0.0
0.
-30.
-60.
-90.
-120.
-150.
-180.
-210.
q (kPa)
TLSU1

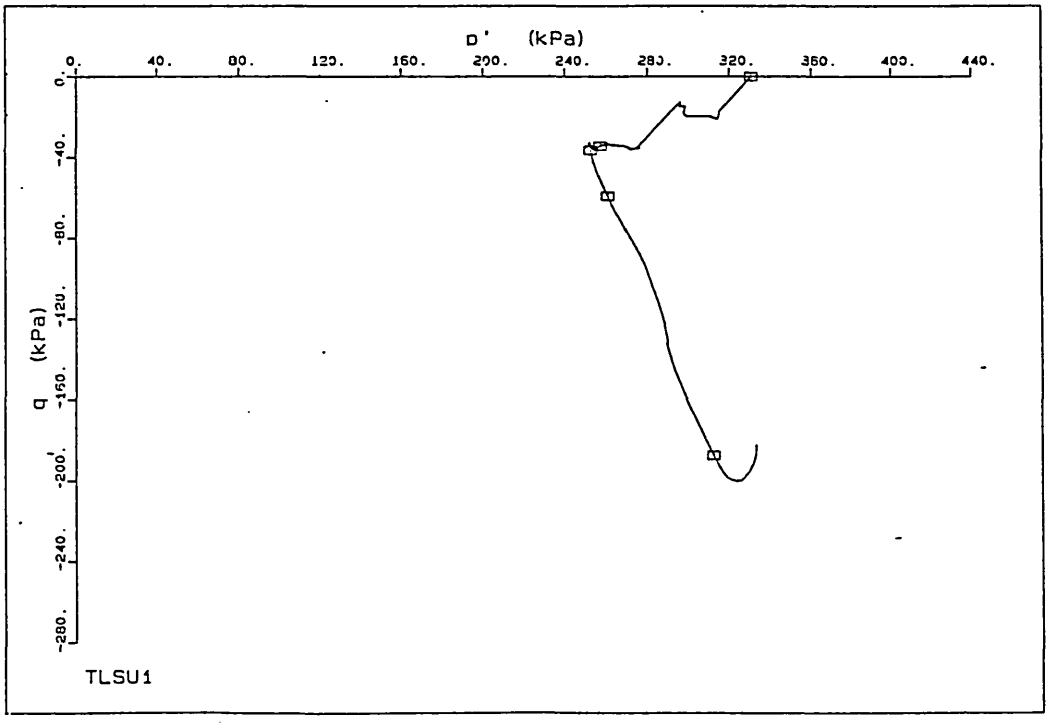
A5.B1.1


Axial strain (%)
-11.0
-10.0
-9.0
-8.0
-7.0
-6.0
-5.0
-4.0
-3.0
-2.0
-1.0
0.0
30.
0.
-30.
-60.
-90.
-120.
-150.
-180.
Excess pwp (kPa)
TLSU1

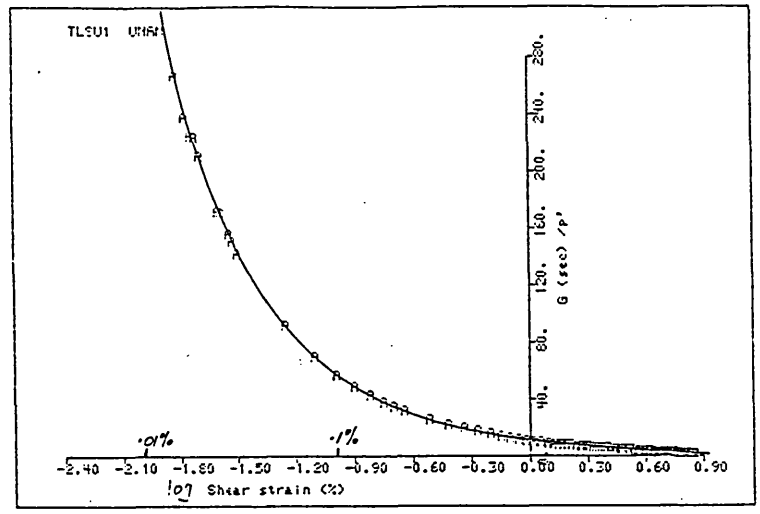
A5.B1.2


Axial strain (%)
-2.20
-2.00
-1.80
-1.60
-1.40
-1.20
-1.00
-0.80
-0.60
-0.40
-0.20
0.00
Volume strain (%)
-0.20
-0.40
-0.60
-0.80
-1.00
-1.20
-1.40
TLSU1

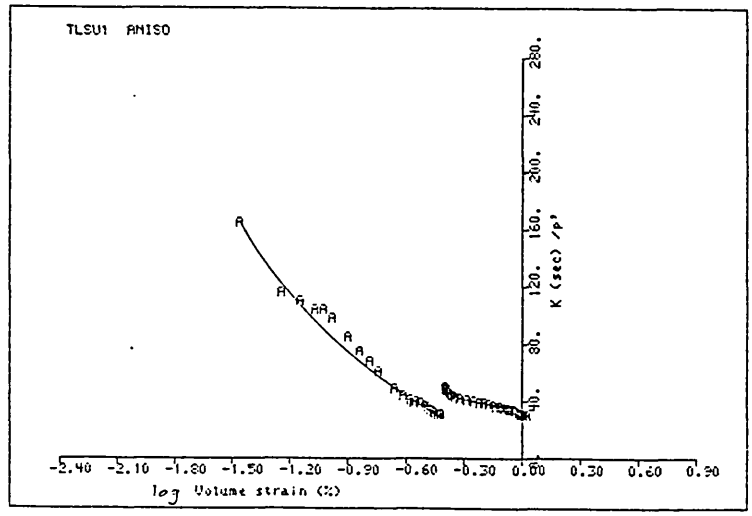
A5.B1.3


p' (kPa)
0.
40.
80.
120.
160.
200.
240.
280.
320.
360.
400.
440.
q (kPa)
0.
-40.
-80.
-120.
-160.
-200.
-240.
-280.
TLSU1

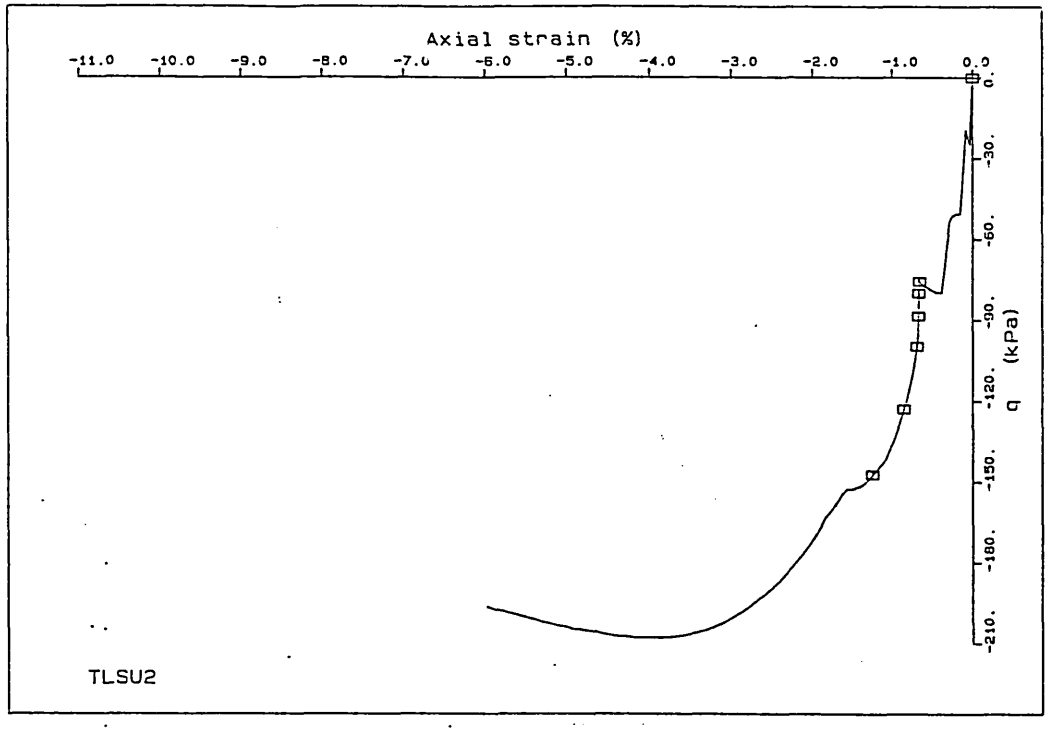
A5.B1.4


TLSU1 UNAN
G (sec) /p'
·01%
·1%
log Shear strain (%)

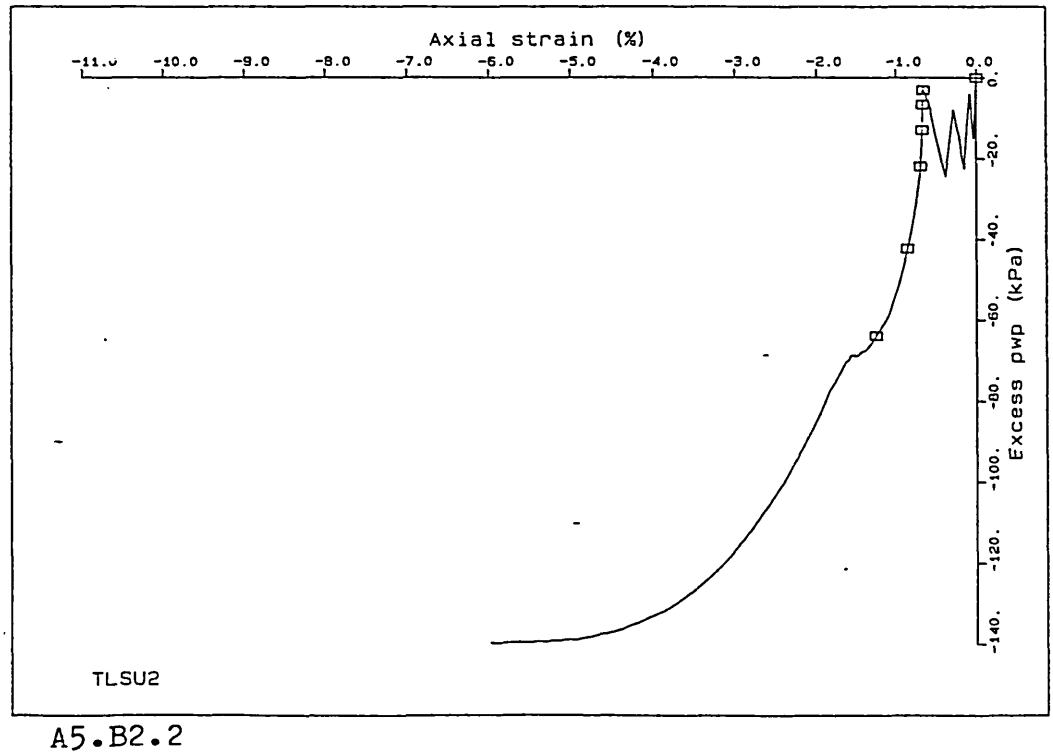
A5.B1.5


TLSU1 ANISO
K (sec) /p'
log Volume strain (%)

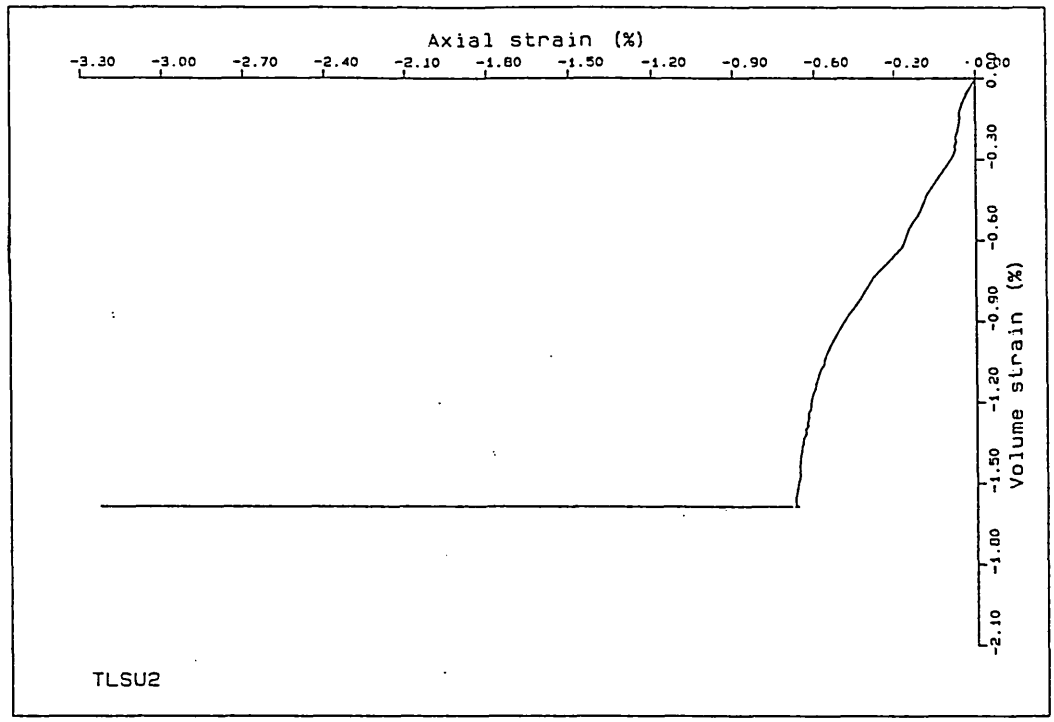
A5.B1.6


Axial strain (%)
-11.0
-10.0
-9.0
-8.0
-7.0
-6.0
-5.0
-4.0
-3.0
-2.0
-1.0
0.0
0.
-30.
-60.
-90.
-120.
-150.
-180.
-210.
q (kPa)
TLSU2

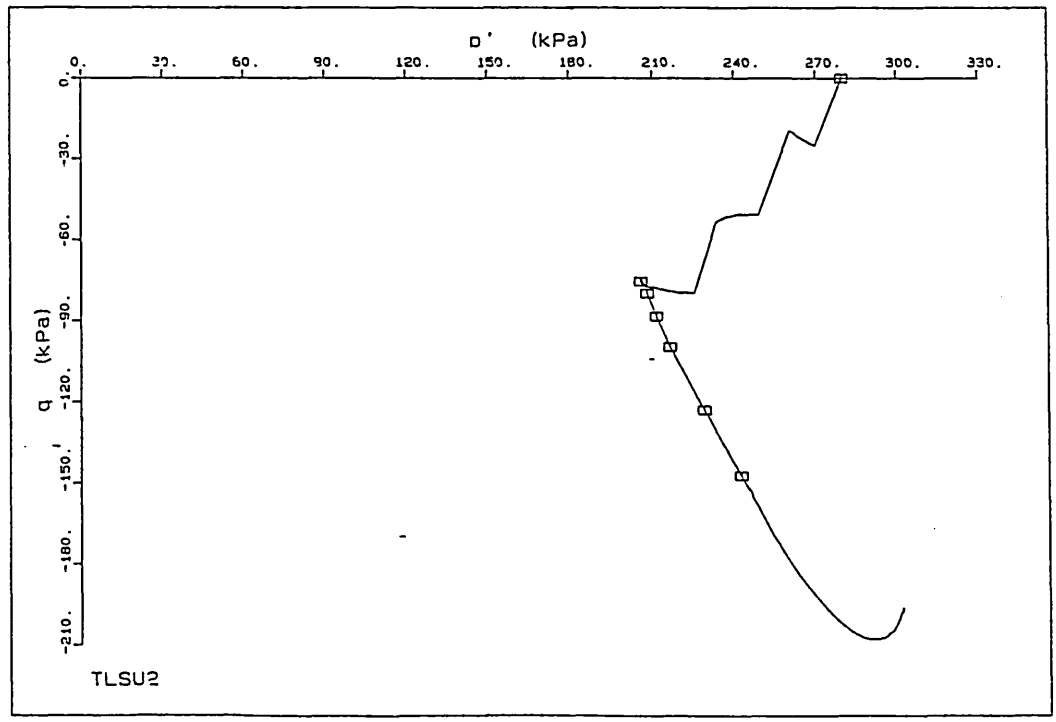
A5.B2.1


Axial strain (%)
-11.0
-10.0
-9.0
-8.0
-7.0
-6.0
-5.0
-4.0
-3.0
-2.0
-1.0
0.0
0.
-20.
-40.
-60.
-80.
-100.
-120.
-140.
Excess pwp (kPa)
TLSU2

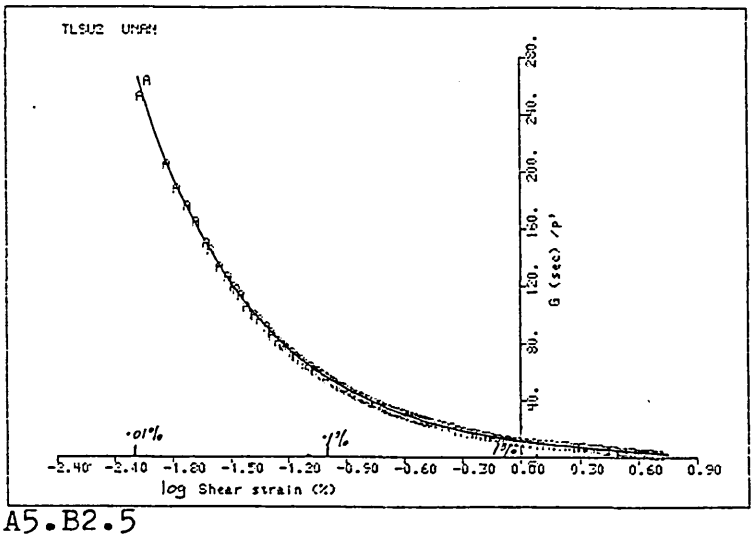
A5.B2.2


Axial strain (%)
-3.30
-3.00
-2.70
-2.40
-2.10
-1.80
-1.50
-1.20
-0.90
-0.60
-0.30
0.00
Volume strain (%)
0.00
-0.30
-0.60
-0.90
-1.20
-1.50
-1.80
-2.10
TLSU2

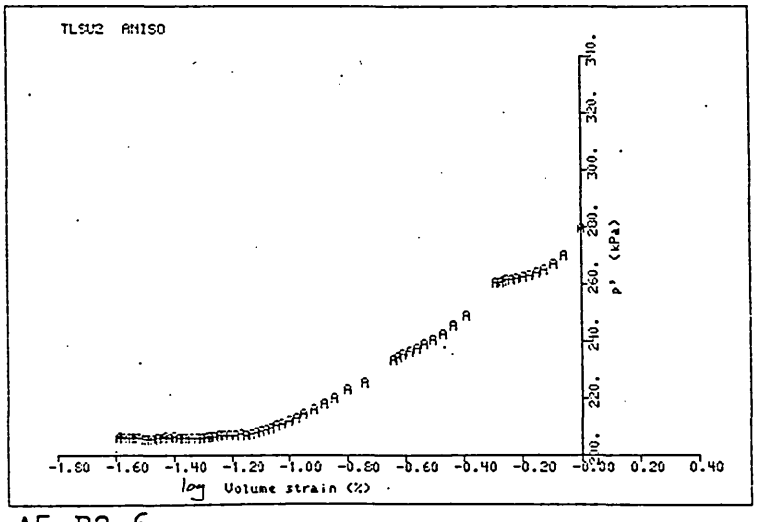
A5.B2.3


p' (kPa)
0.
30.
60.
90.
120.
150.
180.
210.
240.
270.
300.
330.
q (kPa)
0.
-30.
-60.
-90.
-120.
-150.
-180.
-210.
TLSU2

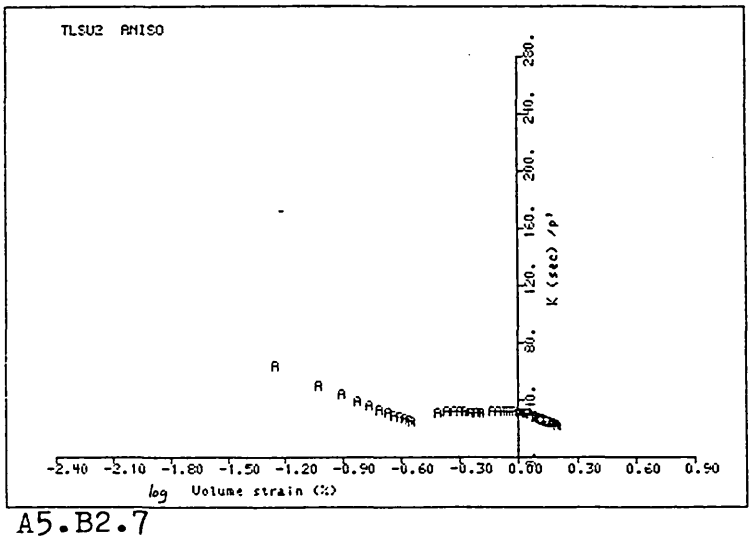
A5.B2.4



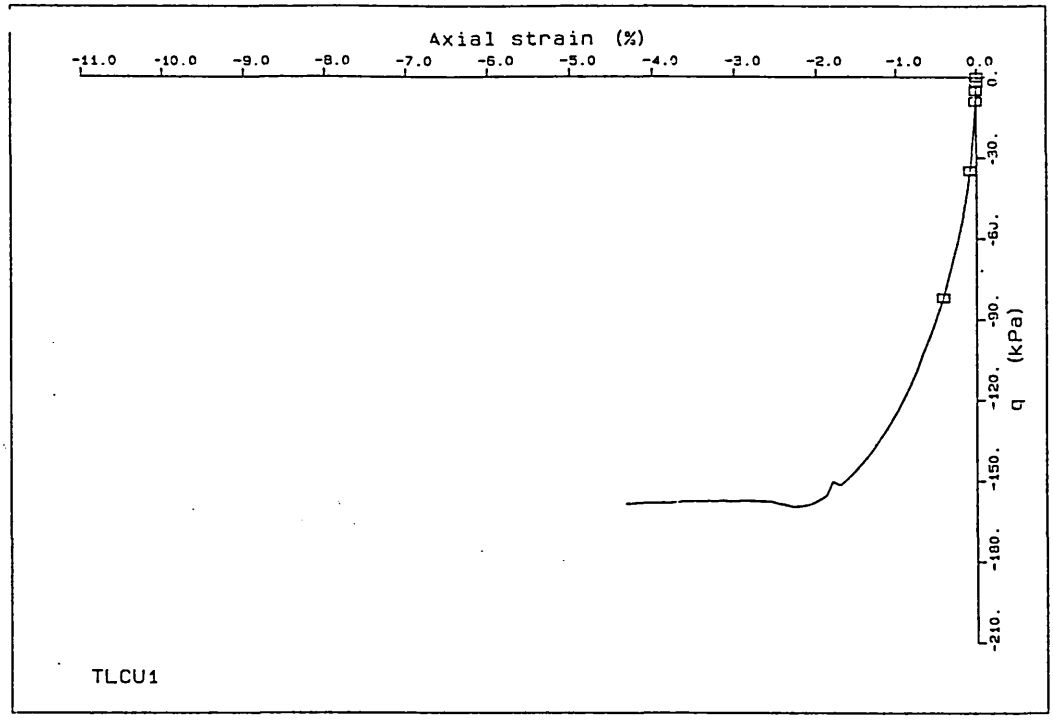
A5.B2.5



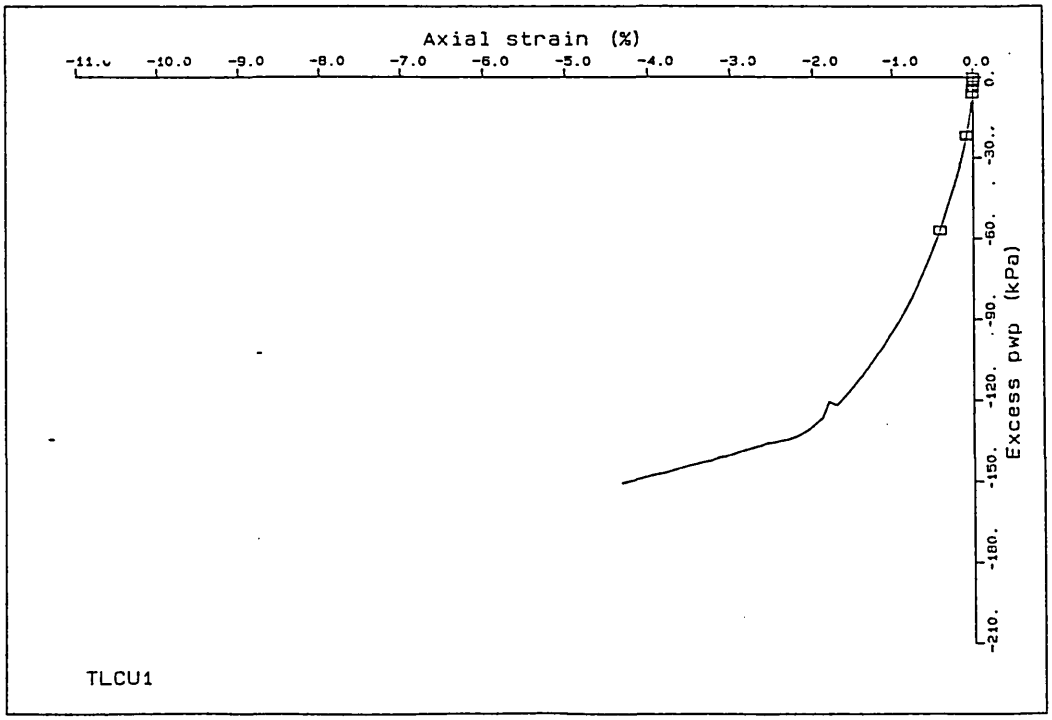
A5.B2.6



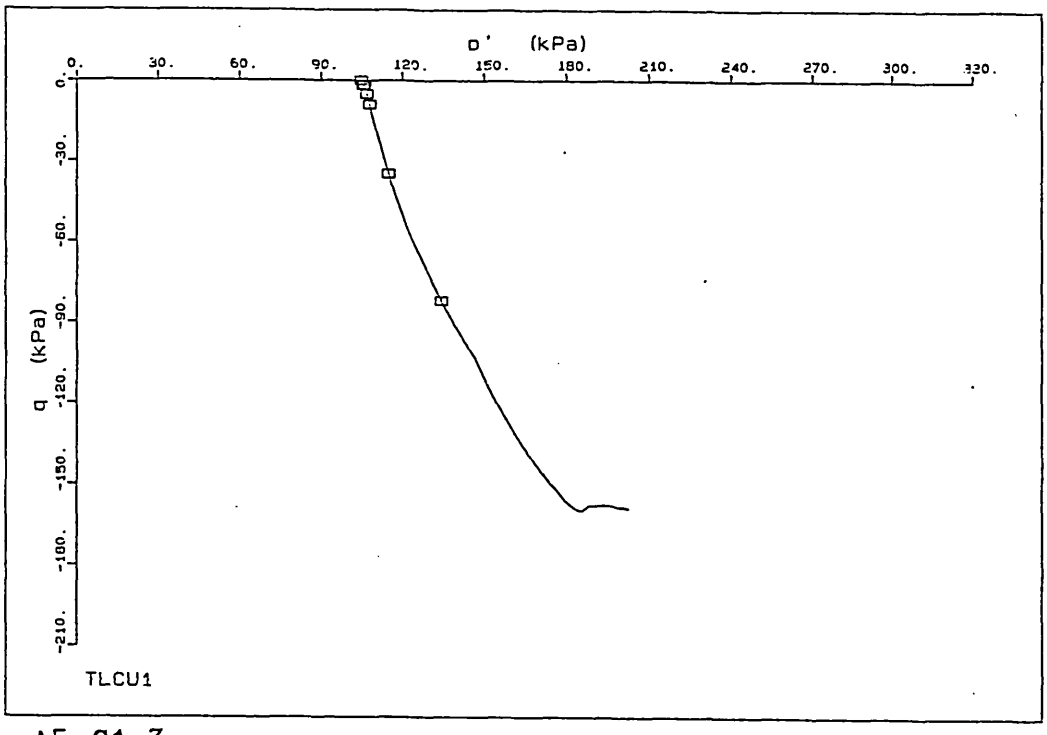
A5.B2.7


Axial strain (%)
-11.0
-10.0
-9.0
-8.0
-7.0
-6.0
-5.0
-4.0
-3.0
-2.0
-1.0
0.0
0.
-30.
-60.
-90.
-120.
-150.
-180.
-210.
q (kPa)
TLCU1

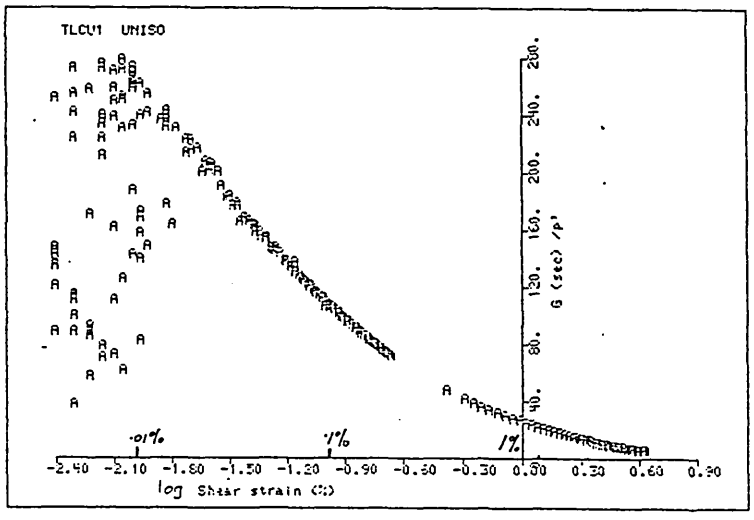
A5.C1.1


Axial strain (%)
-11.0
-10.0
-9.0
-8.0
-7.0
-6.0
-5.0
-4.0
-3.0
-2.0
-1.0
0.0
0.
-30.
-60.
-90.
-120.
-150.
-180.
-210.
Excess pwp (kPa)
TLCU1

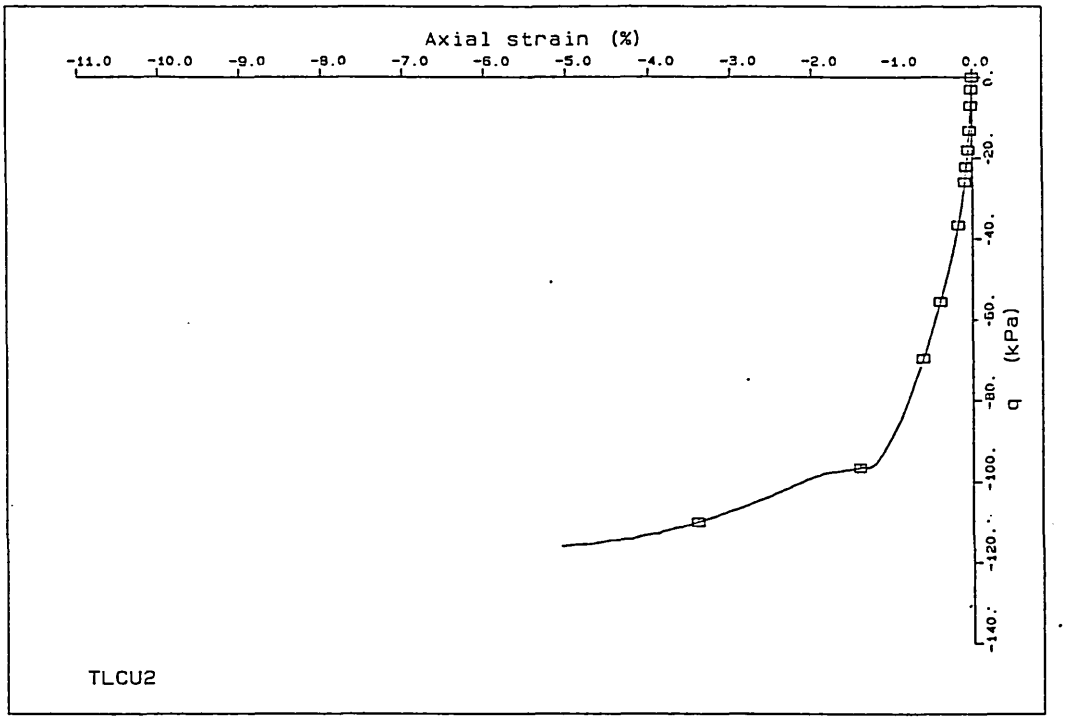
A5.C1.2


p' (kPa)
0. 30. 60. 90. 120. 150. 180. 210. 240. 270. 300. 330.
0.
-30.
-60.
-90.
-120.
-150.
-180.
-210.
q (kPa)
TLCU1

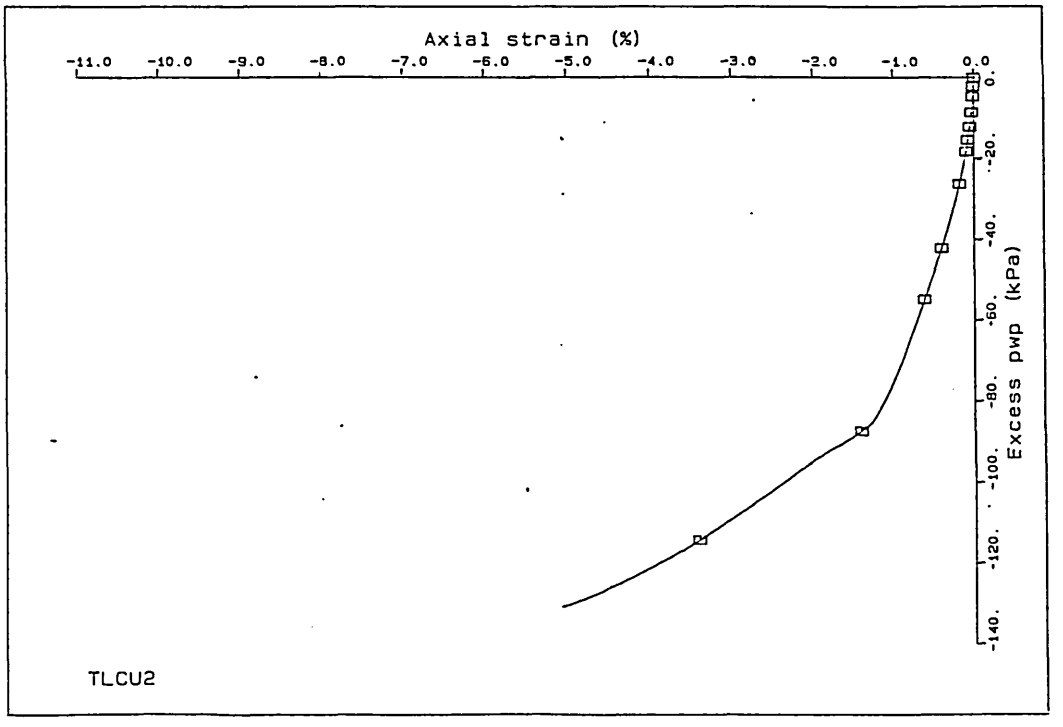
A5.C1.3


TLCU1 UNISO
200.
240.
200.
160.
120.
80.
40.
G (sec) /p'
.01%
.1%
1%
-2.40 -2.10 -1.80 -1.50 -1.20 -0.90 -0.60 -0.30 0.00 0.30 0.60 0.90
log Shear strain (%)

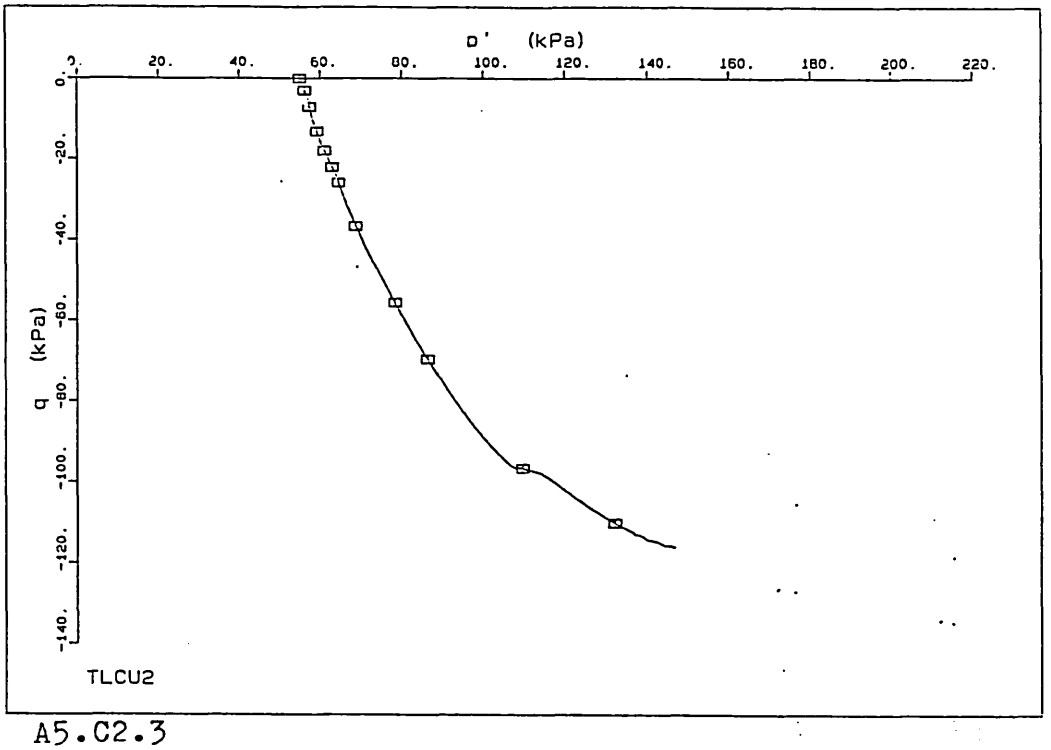
A5.C1.4


Axial strain (%)
-11.0
-10.0
-9.0
-8.0
-7.0
-6.0
-5.0
-4.0
-3.0
-2.0
-1.0
0.0
0.
-20.
-40.
-60.
-80.
-100.
-120.
-140.
q (kPa)
TLCU2

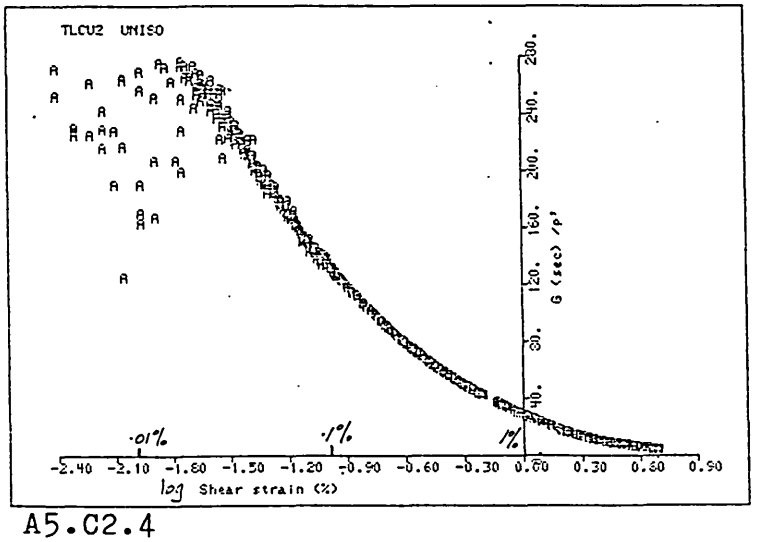
A5.C2.1


Axial strain (%)
-11.0
-10.0
-9.0
-8.0
-7.0
-6.0
-5.0
-4.0
-3.0
-2.0
-1.0
0.0
0.
-20.
-40.
-60.
-80.
-100.
-120.
-140.
Excess pwp (kPa)
TLCU2

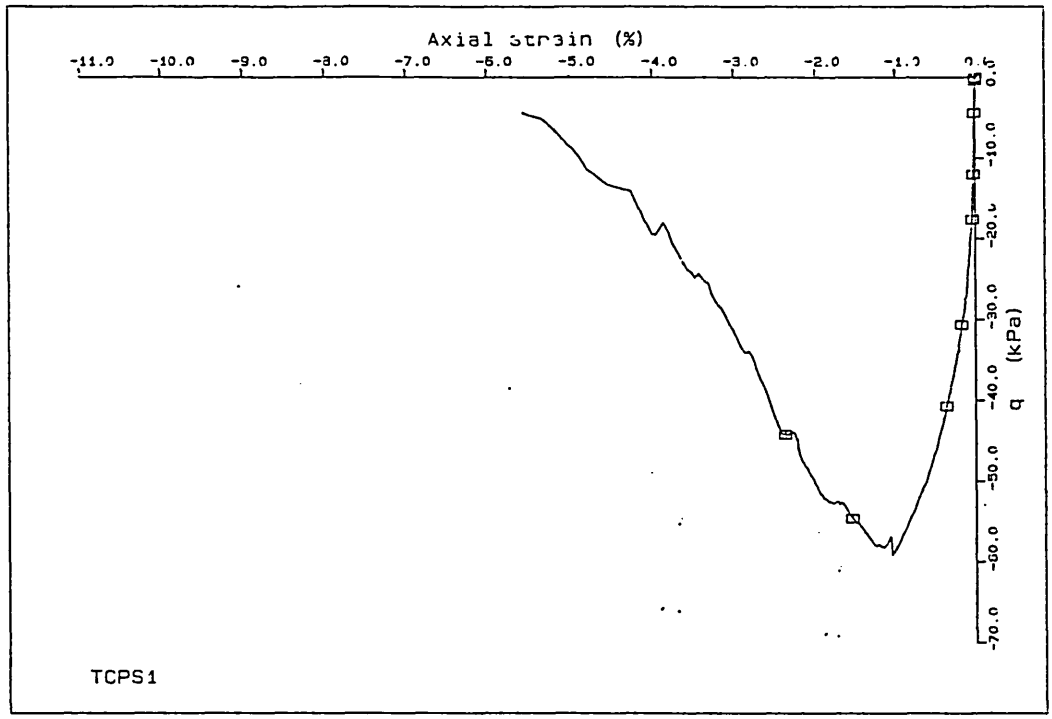
A5.C2.2


p' (kPa)
0.
20.
40.
60.
80.
100.
120.
140.
160.
180.
200.
220.
q (kPa)
0.
-20.
-40.
-60.
-80.
-100.
-120.
-140.
TLCU2

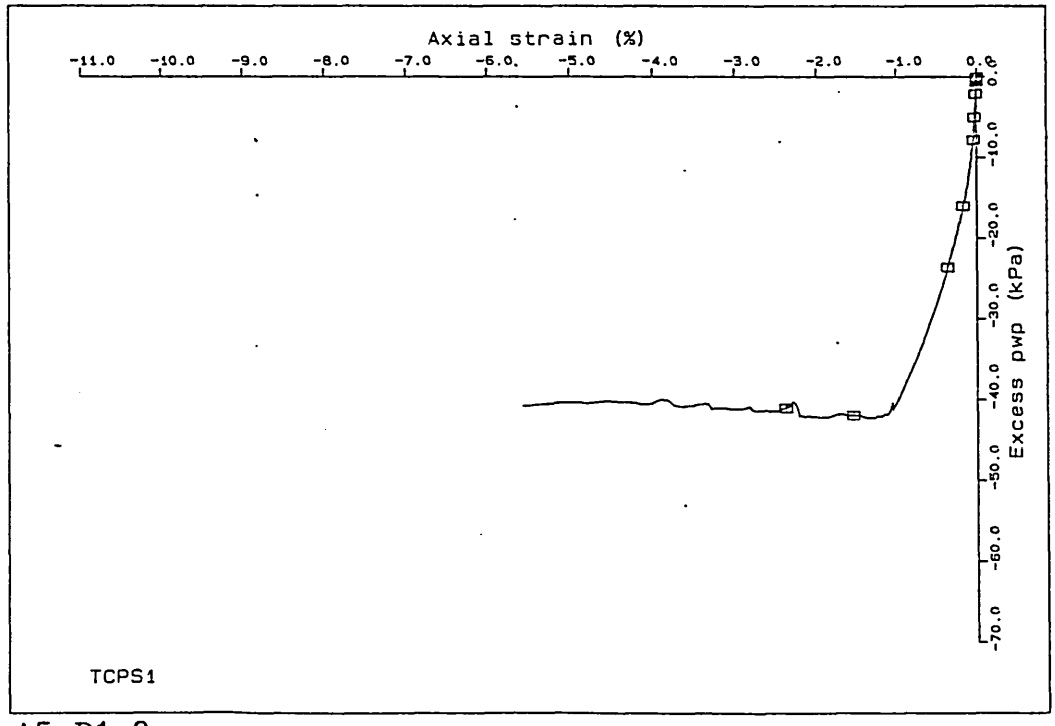
A5.C2.3


TLCU2 UNISO
G (sec) /p'
200.
240.
200.
160.
120.
80.
40.
·01%
·1%
1%
-2.40 -2.10 -1.80 -1.50 -1.20 -0.90 -0.60 -0.30 0.00 0.30 0.60 0.90
log Shear strain (%)

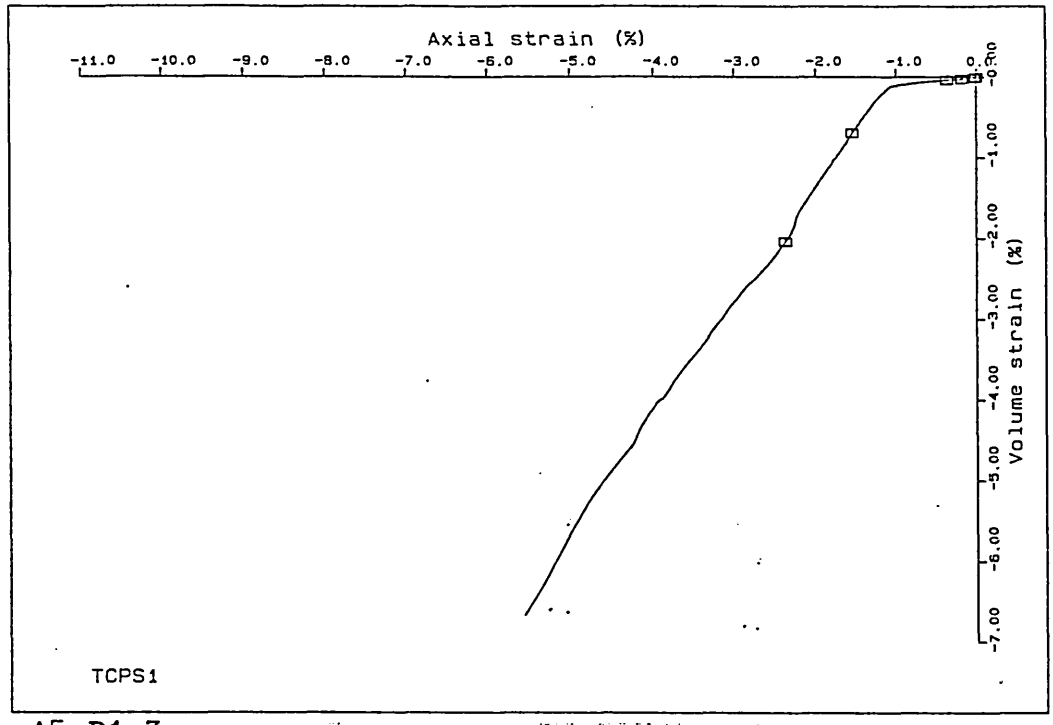
A5.C2.4


Axial strain (%)
-11.0 -10.0 -9.0 -8.0 -7.0 -6.0 -5.0 -4.0 -3.0 -2.0 -1.0 0.0
0.0 -10.0 -20.0 -30.0 -40.0 -50.0 -60.0 -70.0
q (kPa)
TCPS1

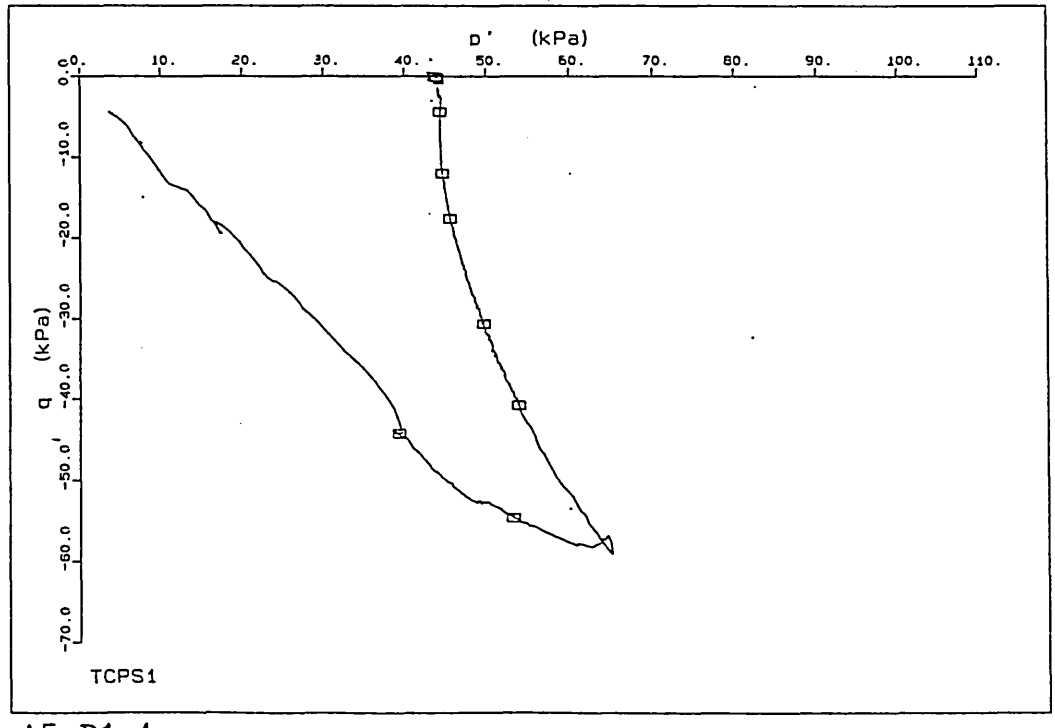
A5.D1.1


Axial strain (%)
-11.0 -10.0 -9.0 -8.0 -7.0 -6.0 -5.0 -4.0 -3.0 -2.0 -1.0 0.0
0.0 -10.0 -20.0 -30.0 -40.0 -50.0 -60.0 -70.0
Excess pwp (kPa)
TCPS1

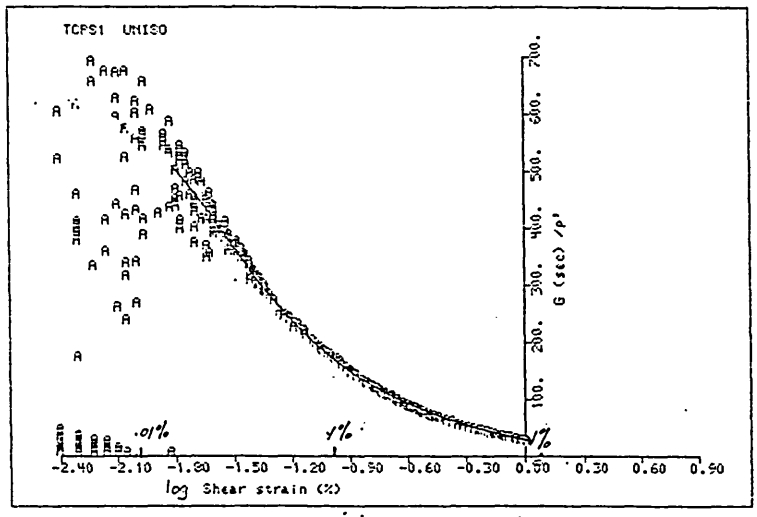
A5.D1.2


Axial strain (%)
-11.0
-10.0
-9.0
-8.0
-7.0
-6.0
-5.0
-4.0
-3.0
-2.0
-1.0
0.00
-1.00
-2.00
-3.00
-4.00
-5.00
-6.00
-7.00
Volume strain (%)
TCPS1

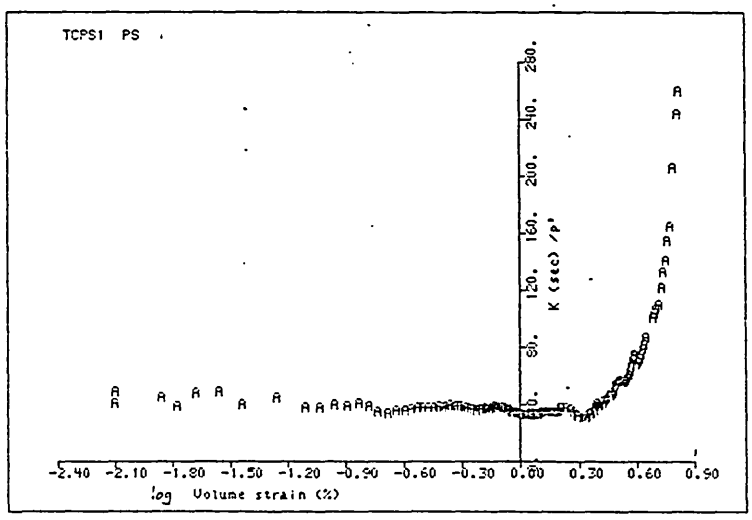
A5.D1.3


p' (kPa)
0.
10.
20.
30.
40.
50.
60.
70.
80.
90.
100.
110.
-10.0
-20.0
-30.0
-40.0
-50.0
-60.0
-70.0
q (kPa)
TCPS1

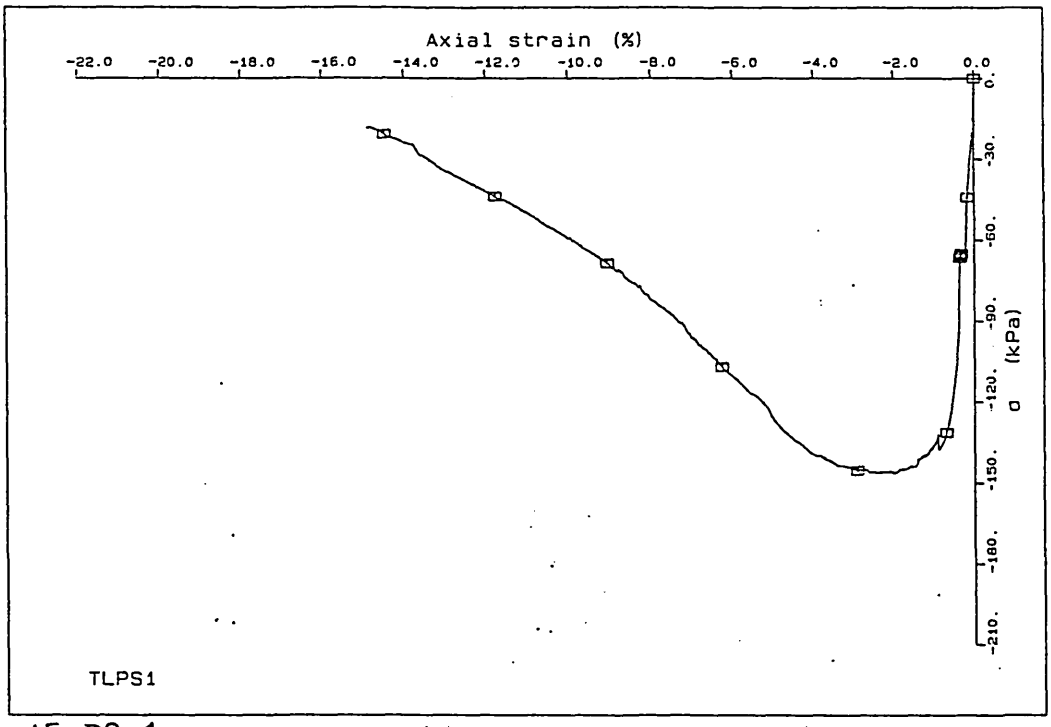
A5.D1.4


TCPS1 UNISO
700.
600.
500.
400.
300.
200.
100.
G (sec) /p'
.01%
1%
1%
-2.40 -2.10 -1.80 -1.50 -1.20 -0.90 -0.60 -0.30 0.00 0.30 0.60 0.90
log Shear strain (%)

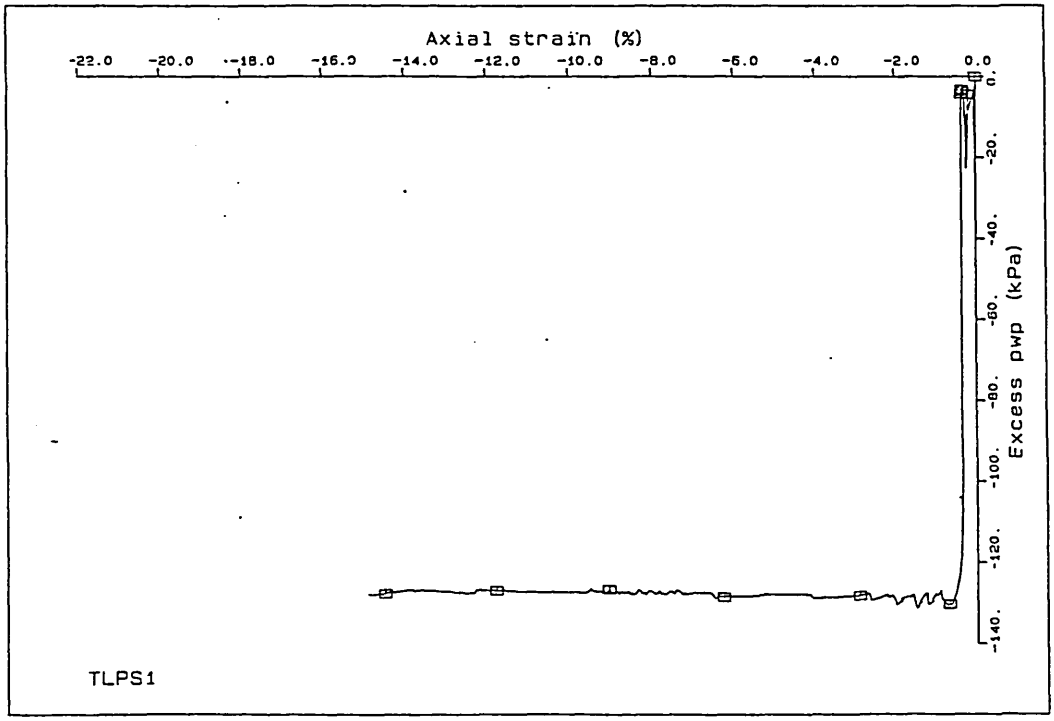
A5.D1.5


TCPS1 PS
280.
240.
200.
160.
120.
80.
0.
K (sec) /p'
-2.40 -2.10 -1.80 -1.50 -1.20 -0.90 -0.60 -0.30 0.00 0.30 0.60 0.90
log Volume strain (%)

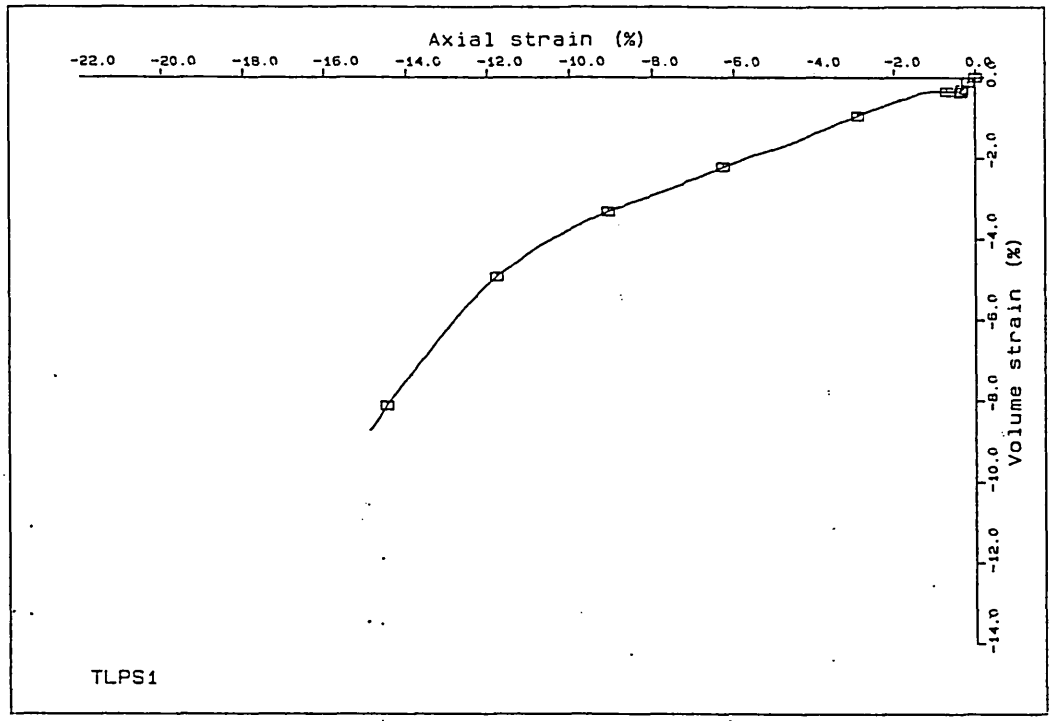
A5.D1.6


Axial strain (%)
-22.0
-20.0
-18.0
-16.0
-14.0
-12.0
-10.0
-8.0
-6.0
-4.0
-2.0
0.0
0.
-30.
-60.
-90.
-120.
-150.
-180.
-210.
σ (kPa)
TLPS1

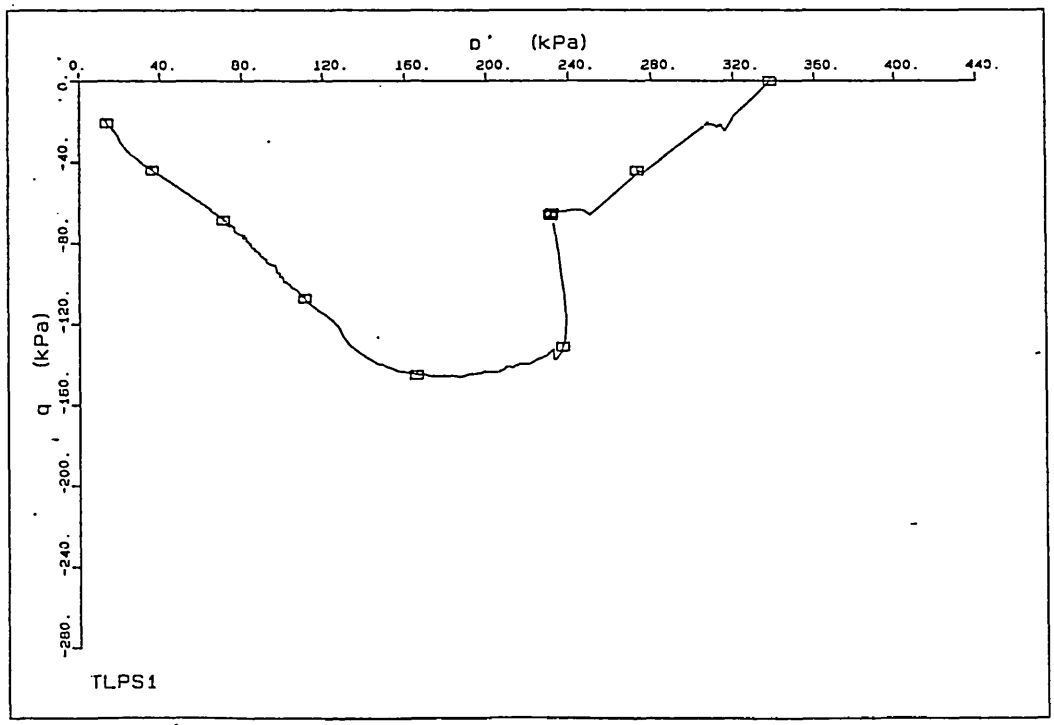
A5.D2.1


Axial strain (%)
-22.0
-20.0
-18.0
-16.0
-14.0
-12.0
-10.0
-8.0
-6.0
-4.0
-2.0
0.0
0.
-20.
-40.
-60.
-80.
-100.
-120.
-140.
Excess pwp (kPa)
TLPS1

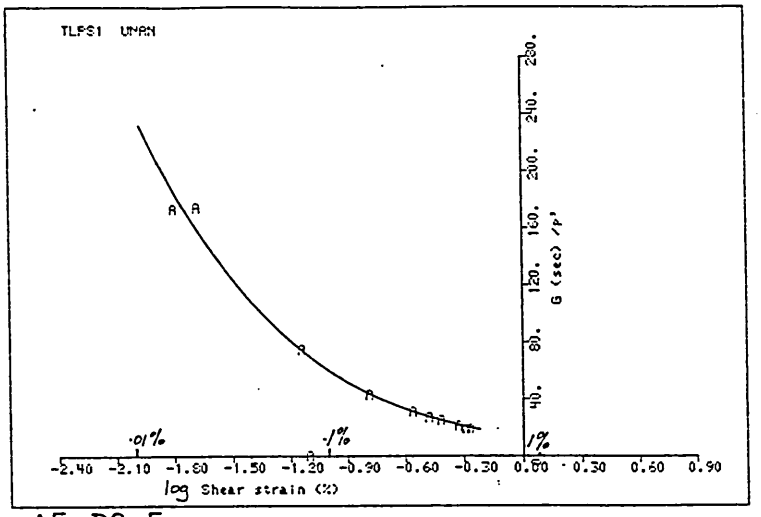
A5.D2.2


Axial strain (%)
-22.0
-20.0
-18.0
-16.0
-14.0
-12.0
-10.0
-8.0
-6.0
-4.0
-2.0
0.0
Volume strain (%)
-2.0
-4.0
-6.0
-8.0
-10.0
-12.0
-14.0
TLPS1

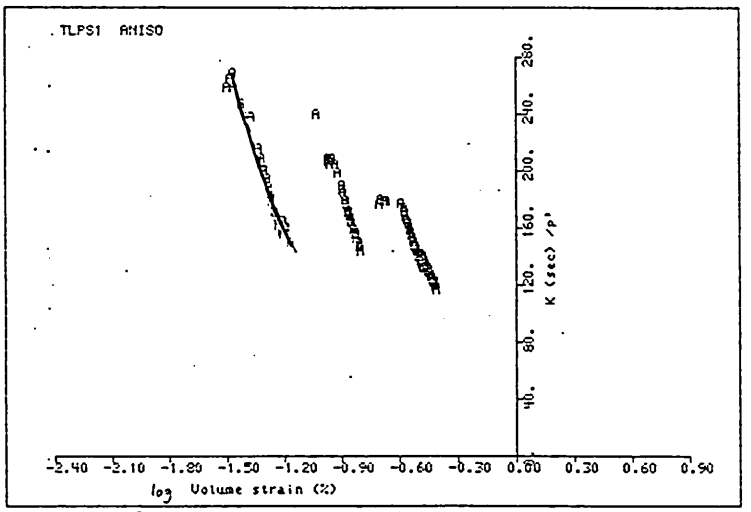
A5.D2.3


p' (kPa)
0.
40.
80.
120.
160.
200.
240.
280.
320.
360.
400.
440.
q (kPa)
-40.
-80.
-120.
-160.
-200.
-240.
-280.
TLPS1

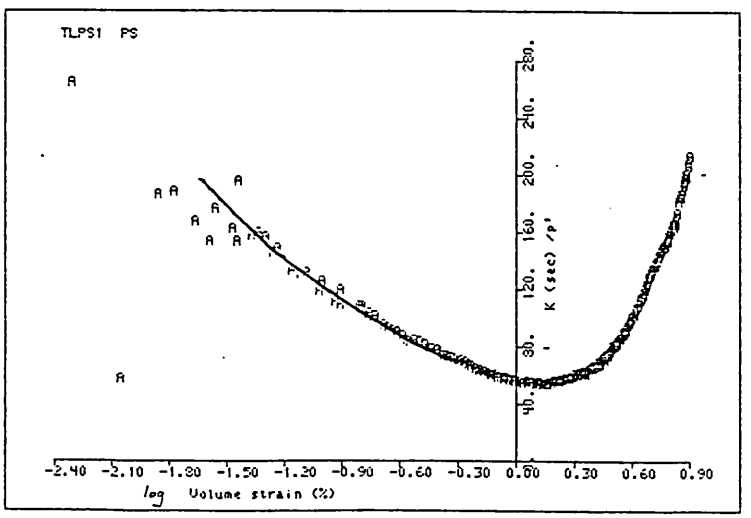
A5.D2.4



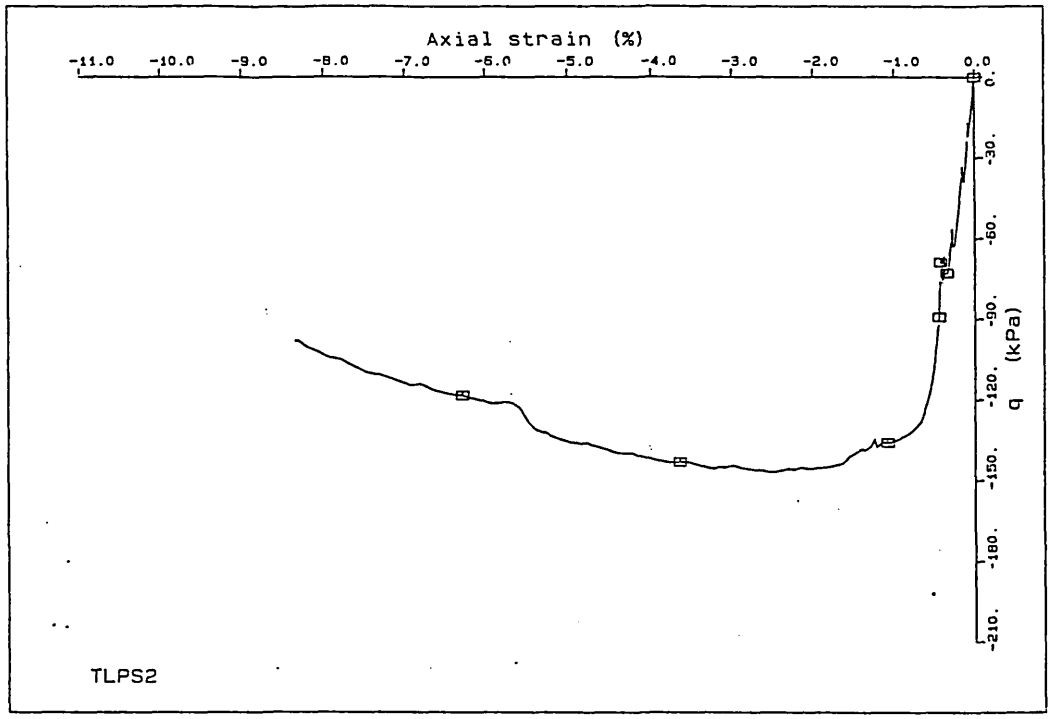
A5.D2.5



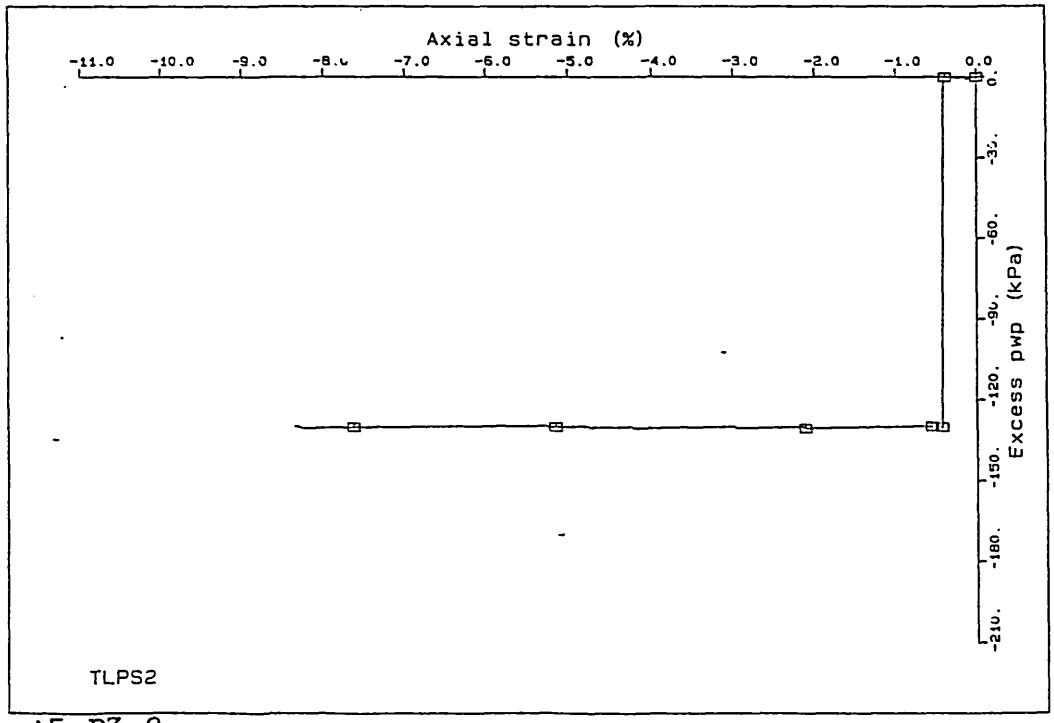
A5.D2.6



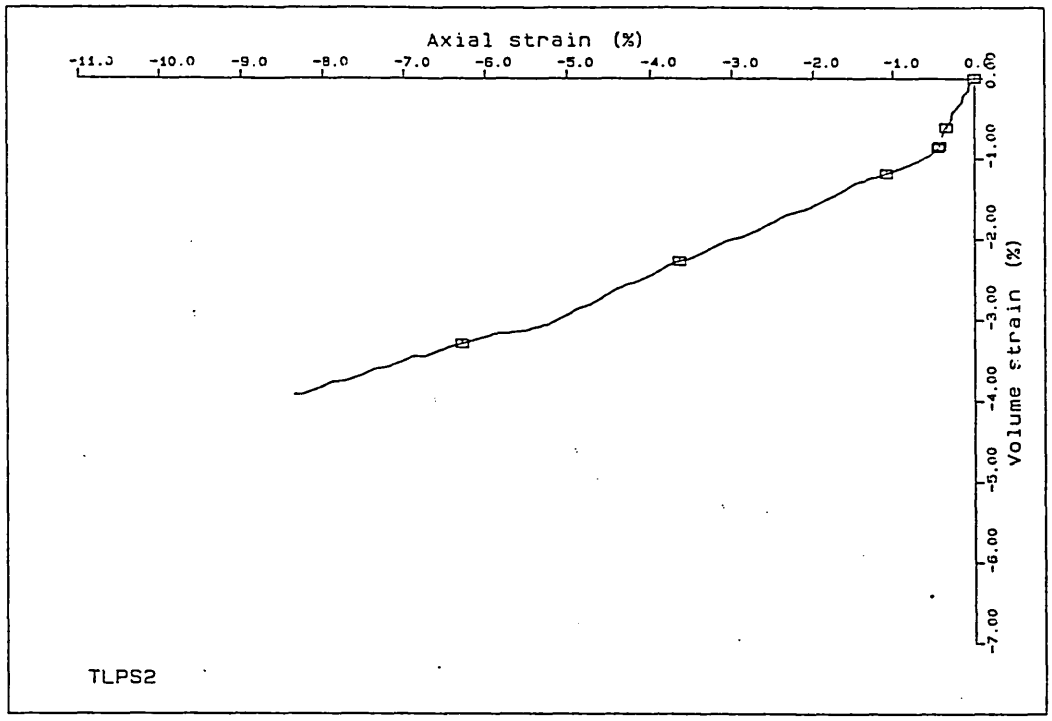
A5.D2.7


Axial strain (%)
-11.0
-10.0
-9.0
-8.0
-7.0
-6.0
-5.0
-4.0
-3.0
-2.0
-1.0
0.0
0.
-30.
-60.
-90.
-120.
-150.
-180.
-210.
q (kPa)
TLPS2

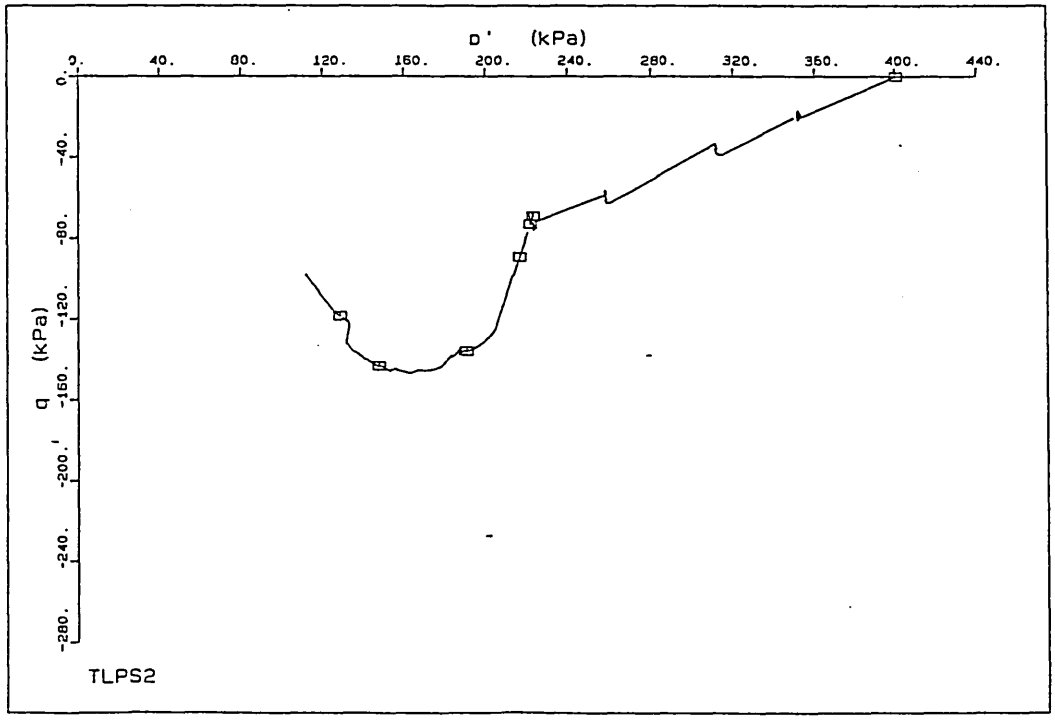
A5.D3.1


Axial strain (%)
-11.0
-10.0
-9.0
-7.0
-6.0
-5.0
-4.0
-3.0
-2.0
-1.0
0.0
0.
-60.
-120.
-150.
-180.
-210.
Excess pwp (kPa)
TLPS2

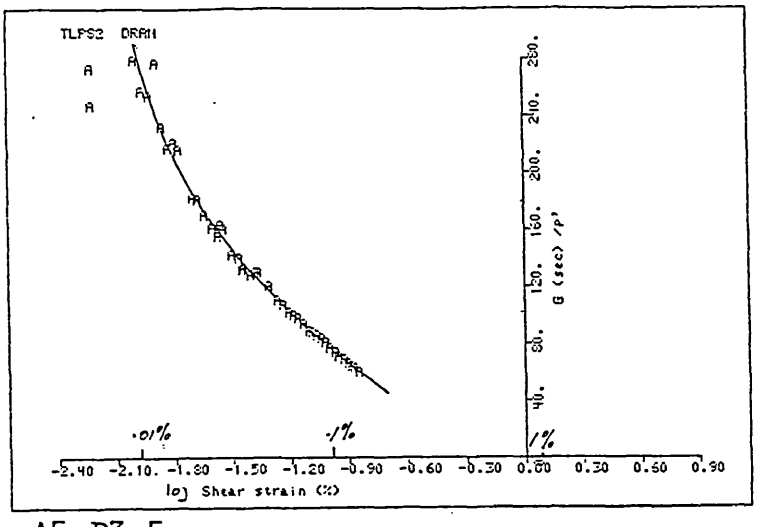
A5.D3.2


Axial strain (%)
-11.0
-10.0
-9.0
-8.0
-7.0
-6.0
-5.0
-4.0
-3.0
-2.0
-1.0
0.00
-1.00
-2.00
-3.00
-4.00
-5.00
-6.00
-7.00
Volume strain (%)
TLPS2

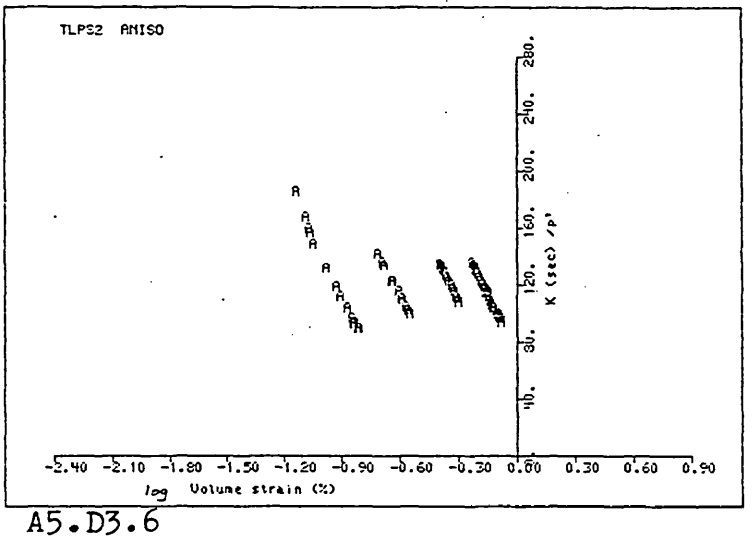
A5.D3.3


p' (kPa)
0.
40.
80.
120.
160.
200.
240.
280.
320.
360.
400.
440.
q (kPa)
-40.
-80.
-120.
-160.
-200.
-240.
-280.
TLPS2

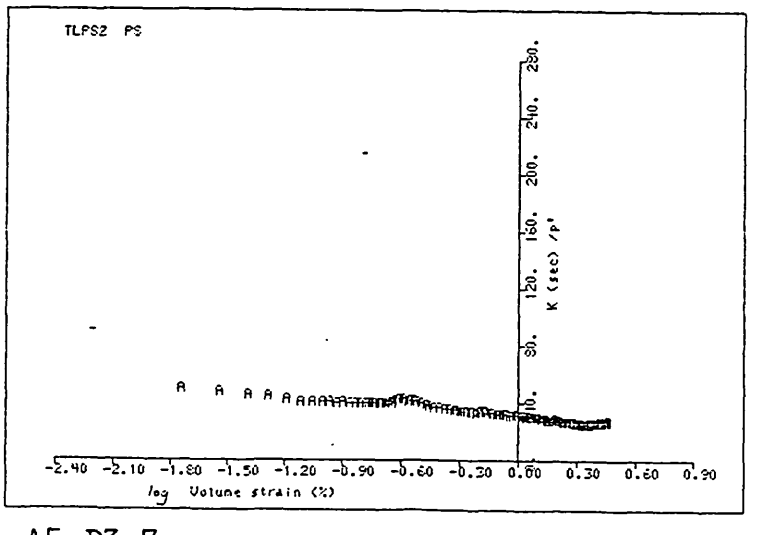
A5.D3.4



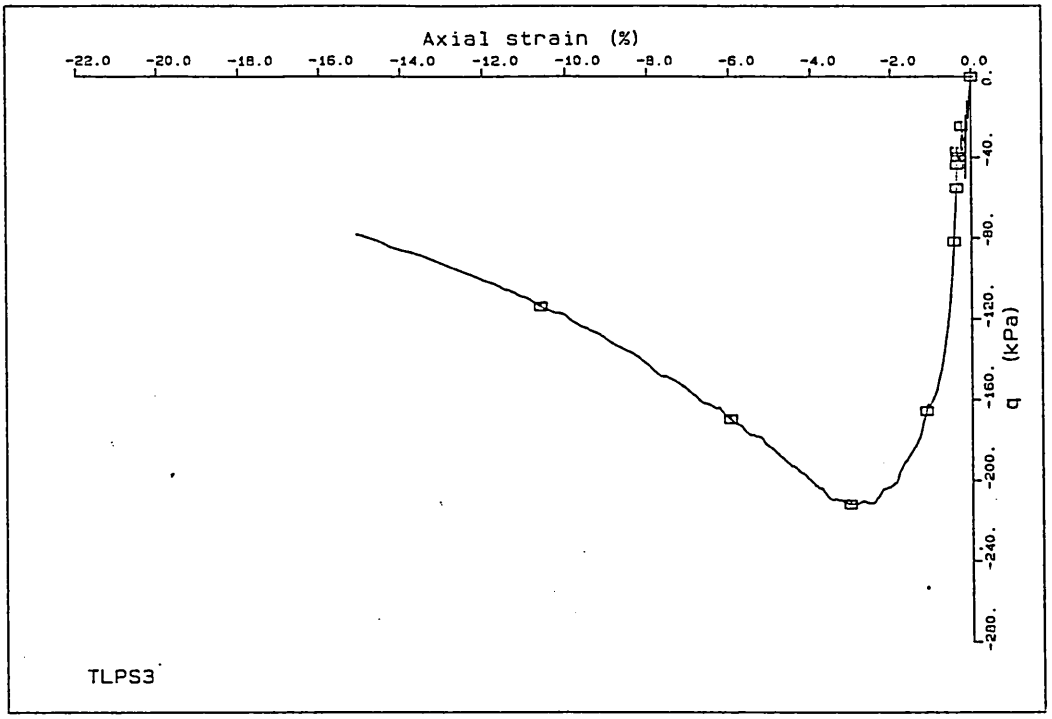
A5.D3.5



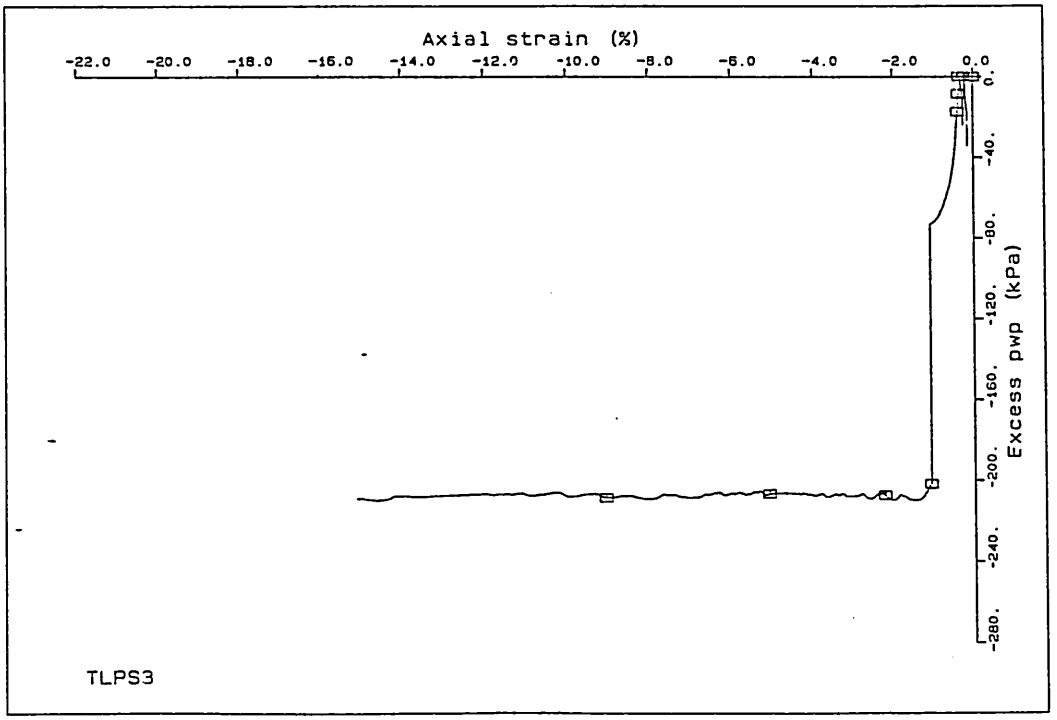
A5.D3.6



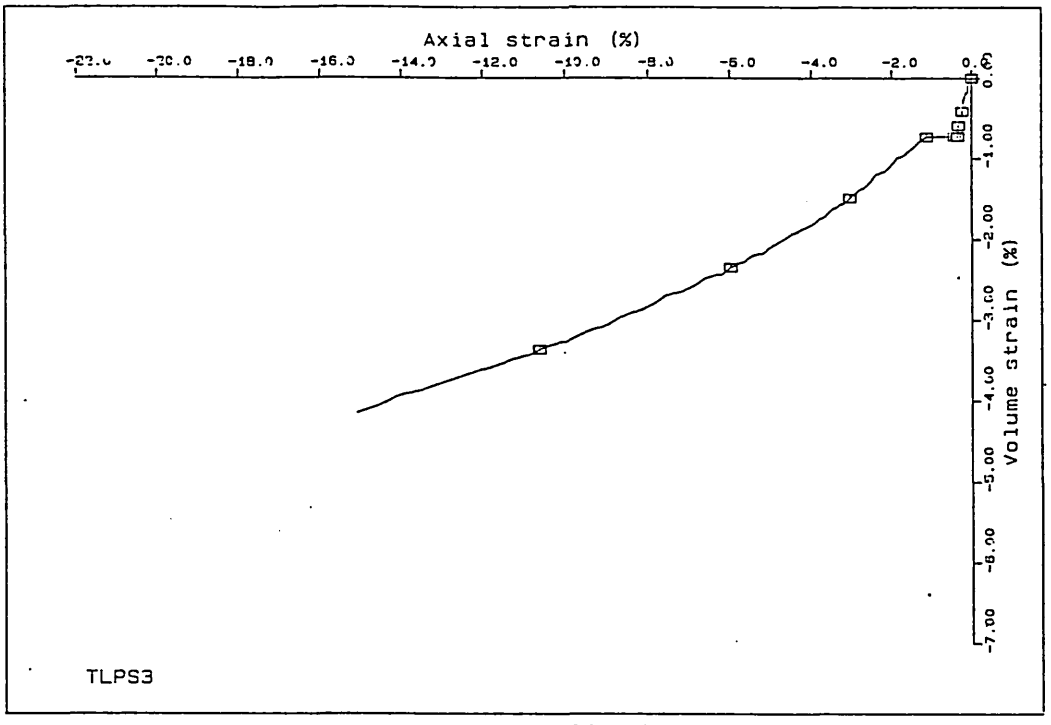
A5.D3.7


Axial strain (%)
-22.0 -20.0 -18.0 -16.0 -14.0 -12.0 -10.0 -8.0 -6.0 -4.0 -2.0 0.0
0. -40. -80. -120. -160. -200. -240. -280.
q (kPa)
TLPS3

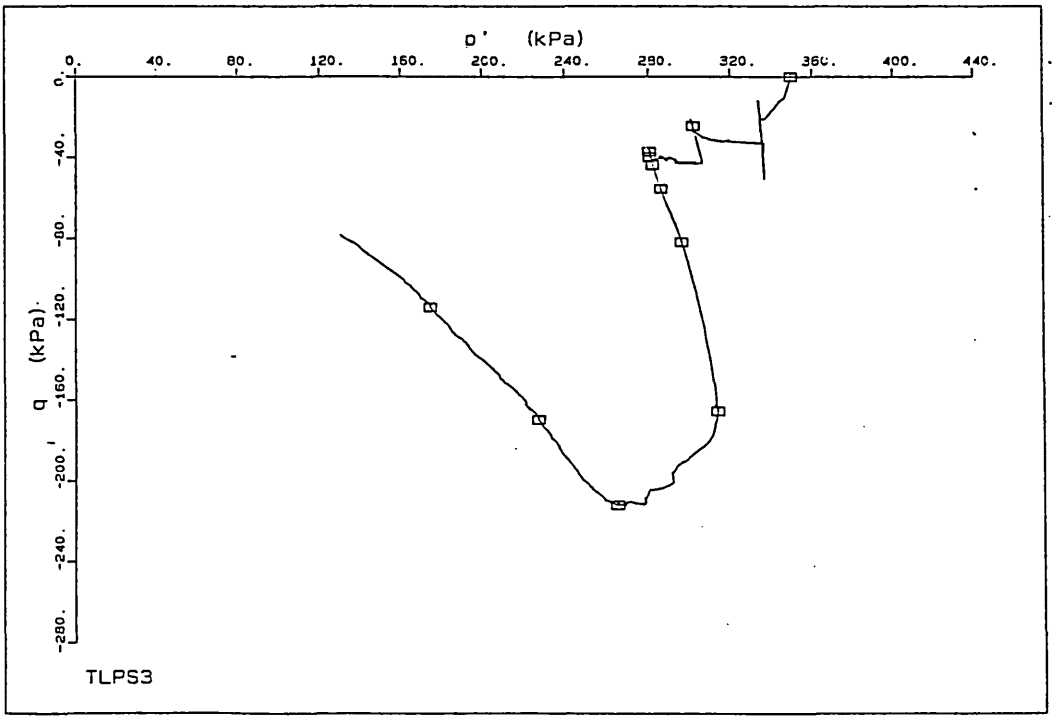
A5.D4.1


Axial strain (%)
-22.0 -20.0 -18.0 -16.0 -14.0 -12.0 -10.0 -8.0 -6.0 -4.0 -2.0 0.0
0. -40. -80. -120. -160. -200. -240. -280.
Excess pwp (kPa)
TLPS3

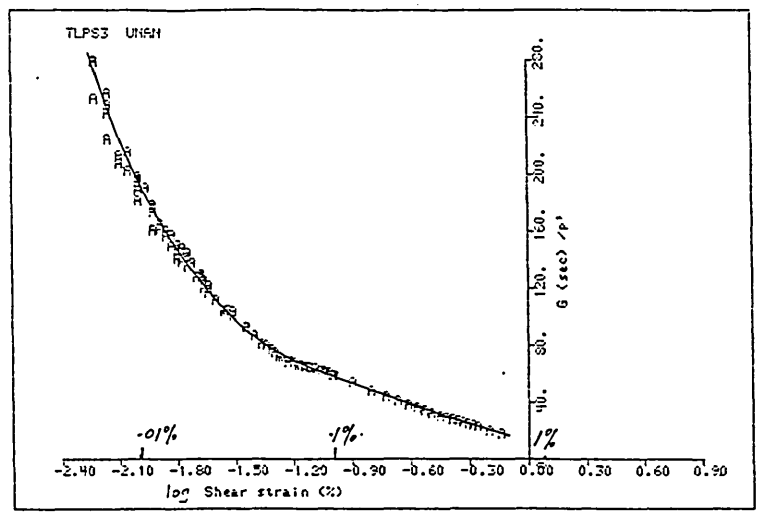
A5.D4.2


Axial strain (%)
-22.0
-20.0
-18.0
-16.0
-14.0
-12.0
-10.0
-8.0
-6.0
-4.0
-2.0
0.0
0.00
-1.00
-2.00
-3.00
-4.00
-5.00
-6.00
-7.00
Volume strain (%)
TLPS3

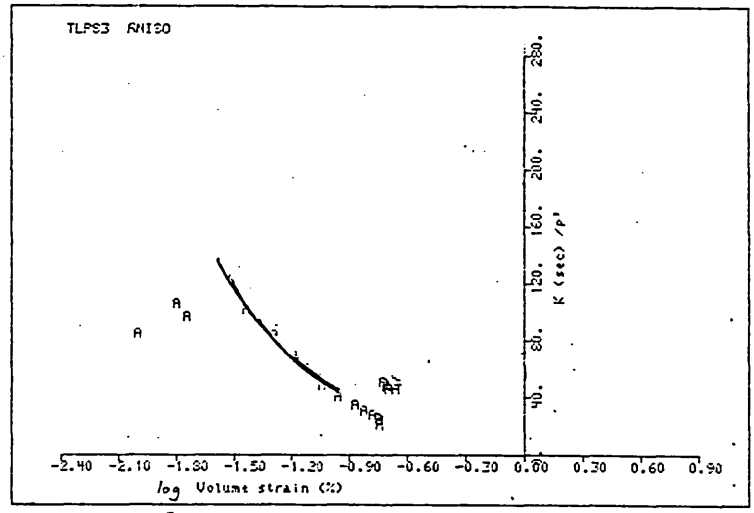
A5.D4.3


p' (kPa)
0.
40.
80.
120.
160.
200.
240.
280.
320.
360.
400.
440.
0.
-40.
-80.
-120.
-160.
-200.
-240.
-280.
q (kPa)
TLPS3

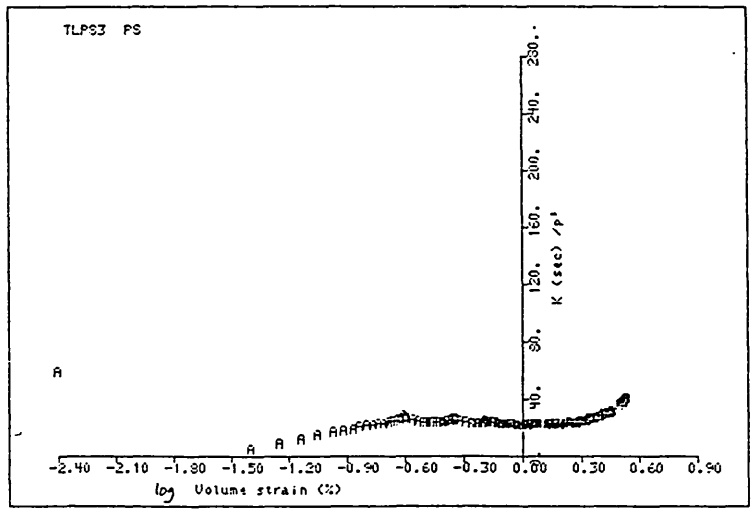
A5.D4.4



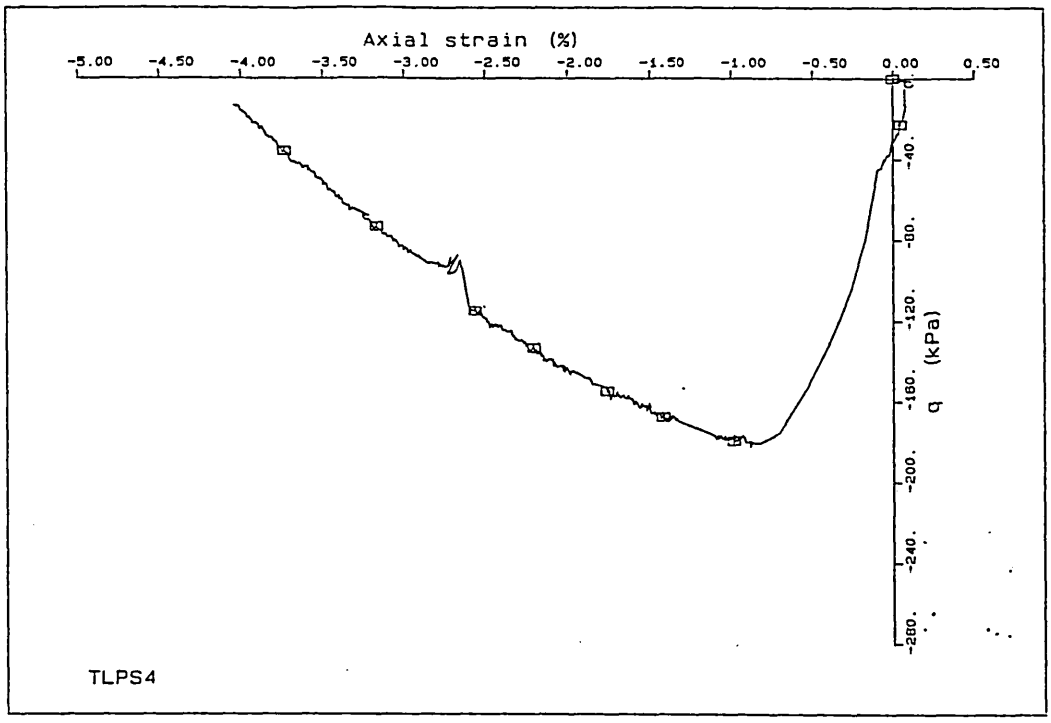
A5.D4.5



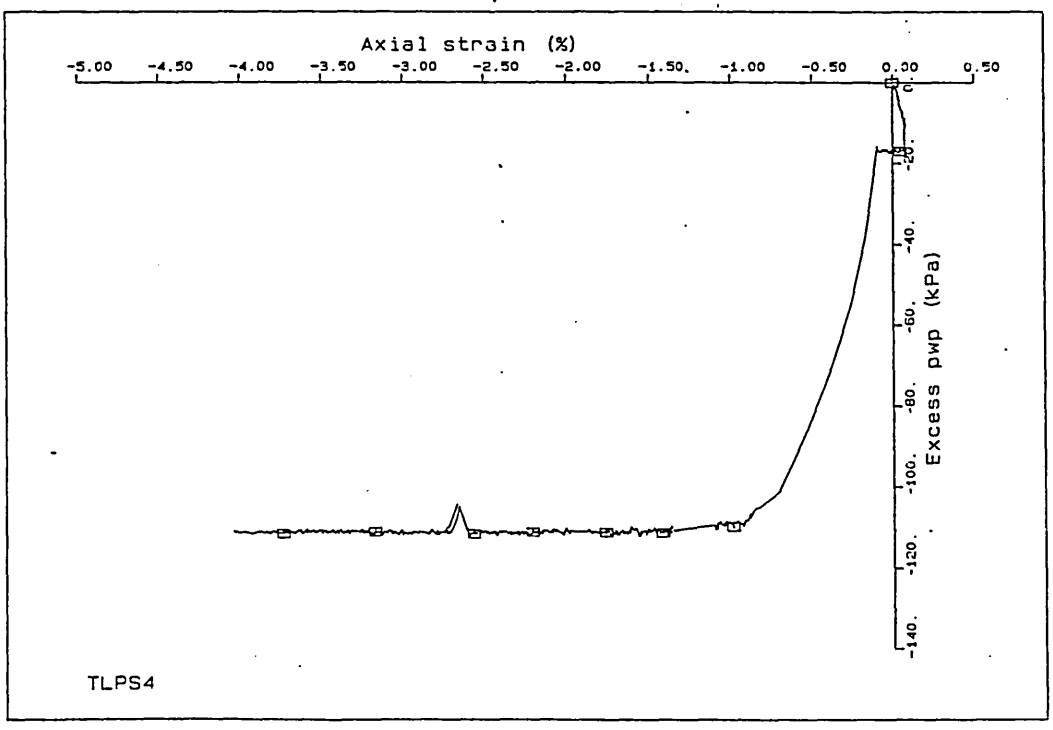
A5.D4.6



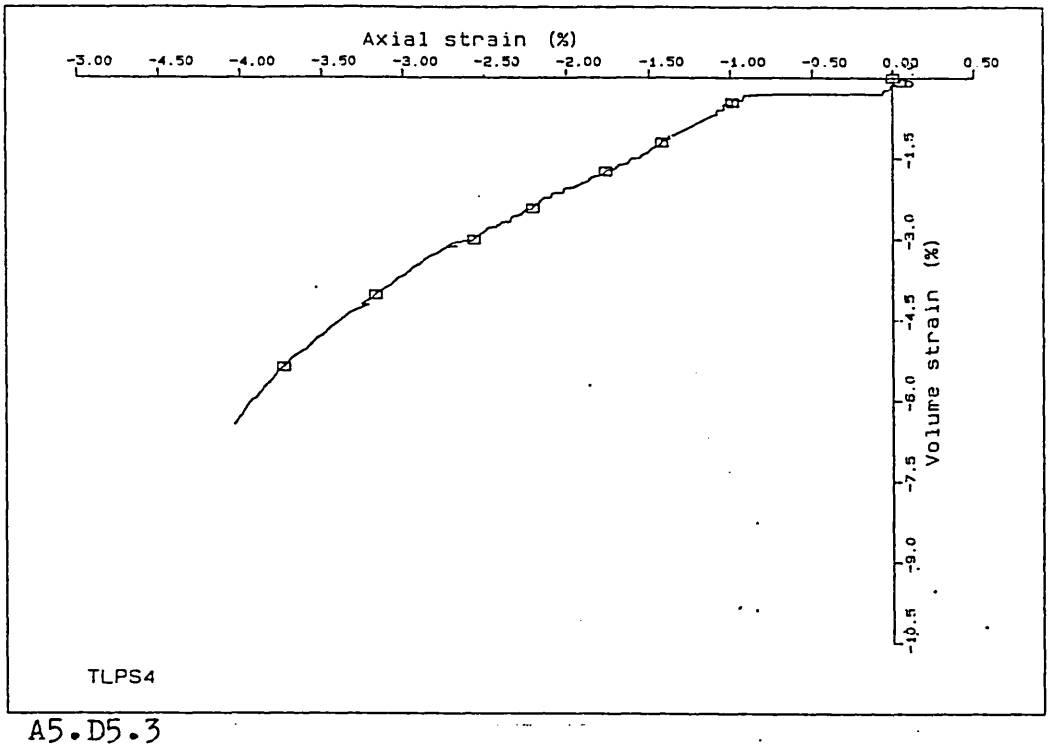
A5.D4.7


Axial strain (%)
-5.00 -4.50 -4.00 -3.50 -3.00 -2.50 -2.00 -1.50 -1.00 -0.50 0.00 0.50
0.
-40.
-80.
-120.
-160.
-200.
-240.
-280.
q (kPa)
TLPS4

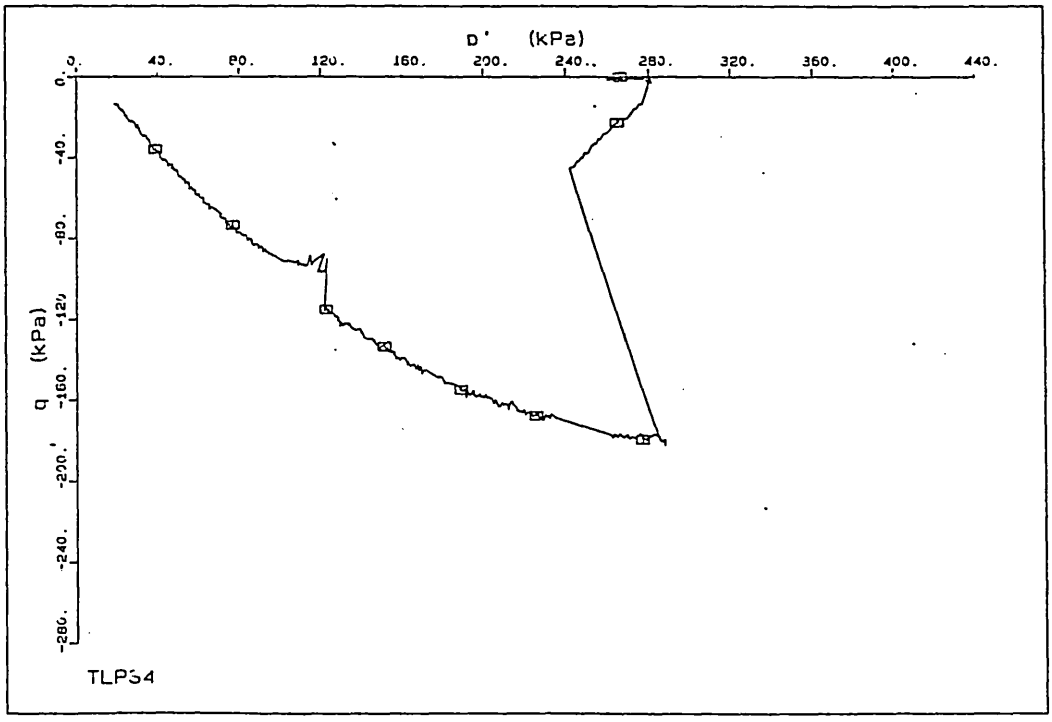
A5.D5.1


Axial strain (%)
-5.00 -4.50 -4.00 -3.50 -3.00 -2.50 -2.00 -1.50 -1.00 -0.50 0.00 0.50
0.
-20.
-40.
-60.
-80.
-100.
-120.
-140.
Excess pwp (kPa)
TLPS4

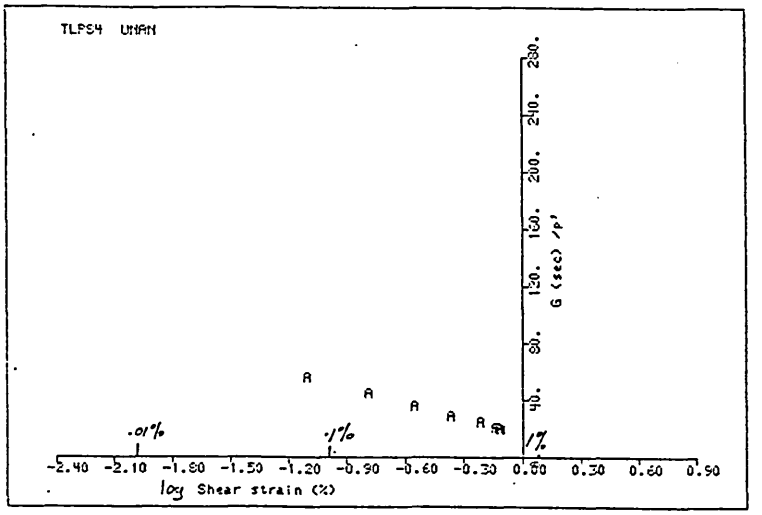
A5.D5.2


Axial strain (%)
-3.00 -4.50 -4.00 -3.50 -3.00 -2.50 -2.00 -1.50 -1.00 -0.50 0.00 0.50
Volume strain (%)
-1.5 -3.0 -4.5 -6.0 -7.5 -9.0 -10.5
TLPS4

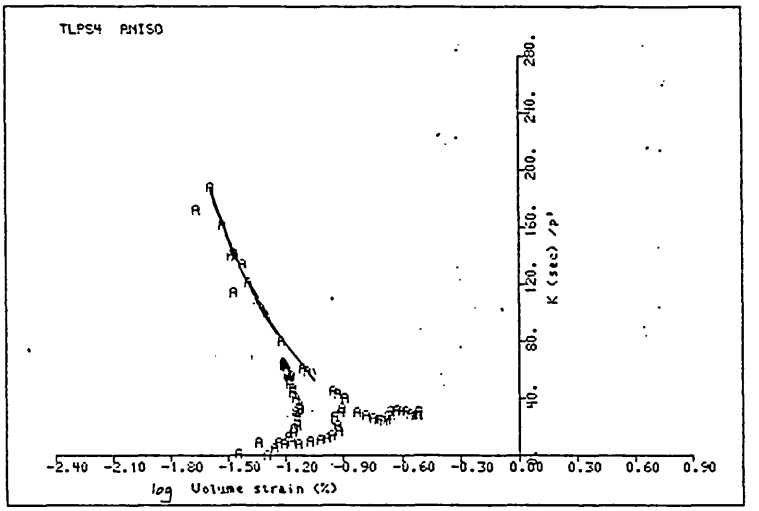
A5.D5.3


p' (kPa)
0. 40. 80. 120. 160. 200. 240. 280. 320. 360. 400. 440.
q (kPa)
0. -40. -80. -120. -160. -200. -240. -280.
TLPS4

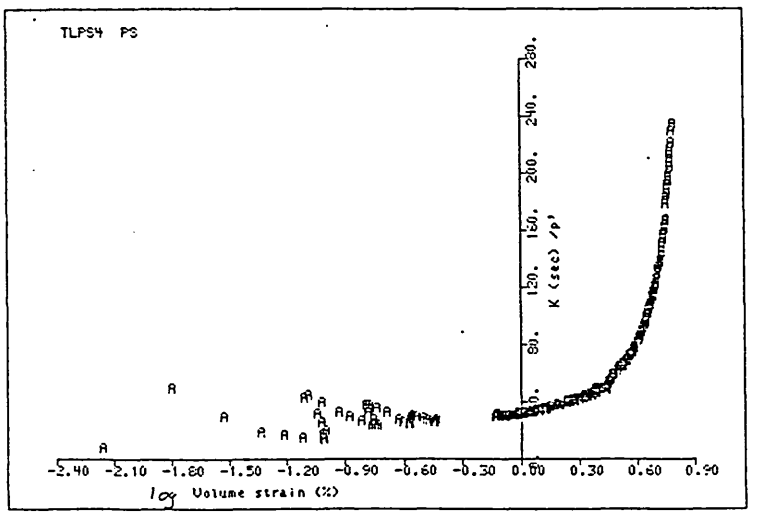
A5.D5.4



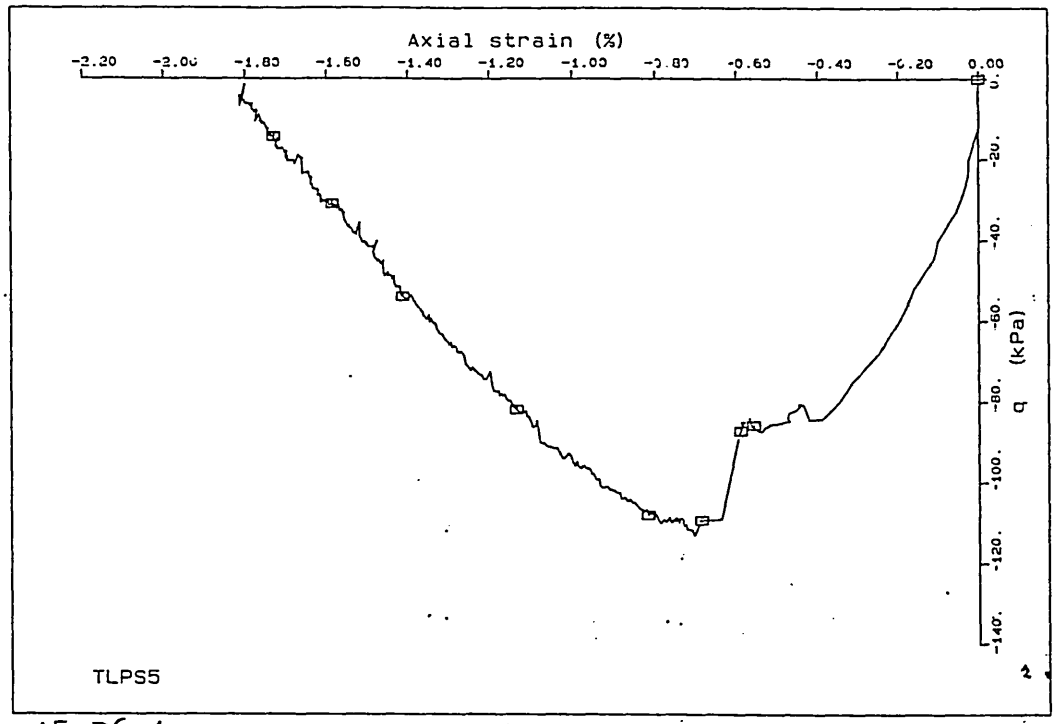
A5.D5.5



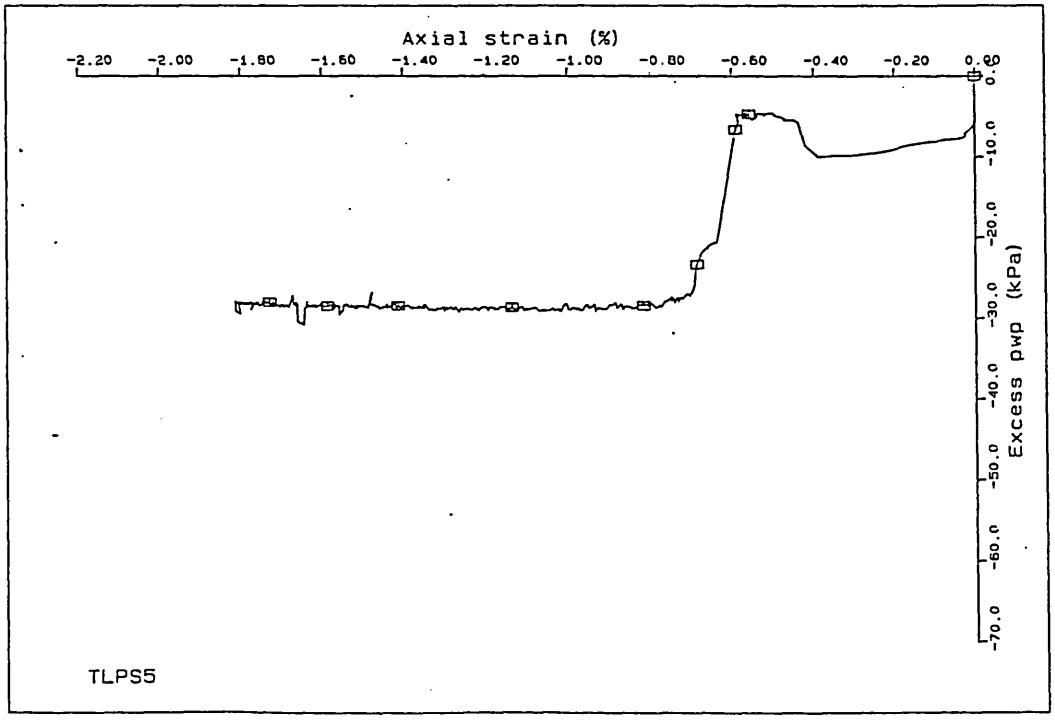
A5.D5.6



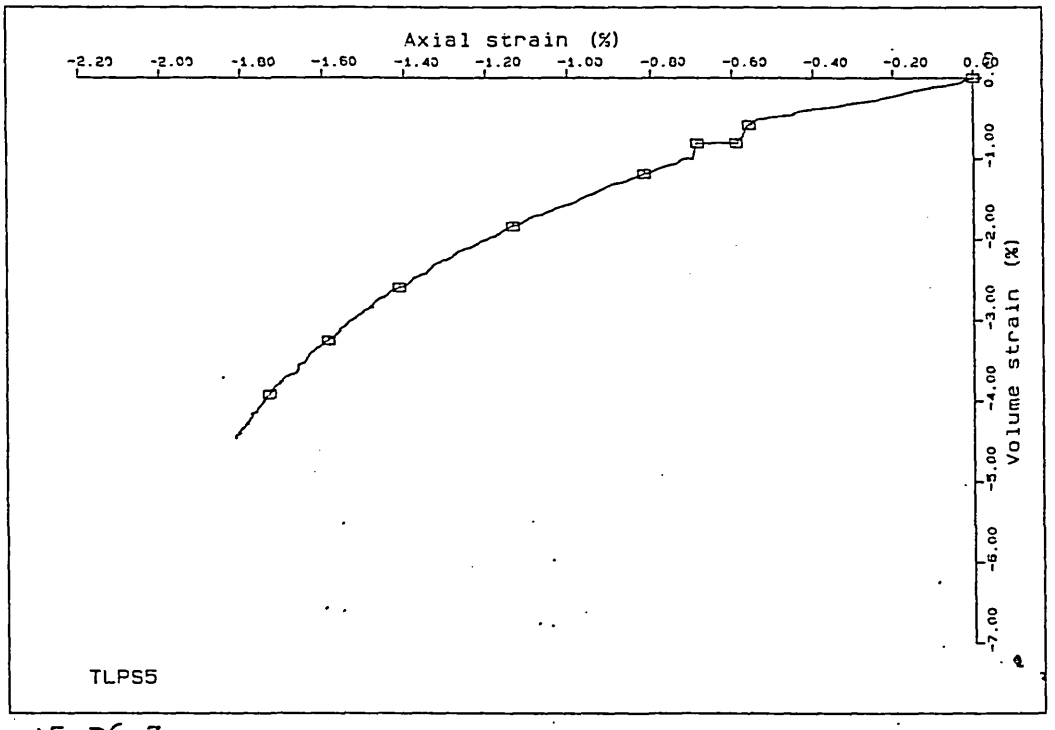
A5.D5.7


Axial strain (%)
-2.20
-2.00
-1.80
-1.60
-1.40
-1.20
-1.00
-0.80
-0.60
-0.40
-0.20
0.00
0.
-20.
-40.
-60.
-80.
-100.
-120.
-140.
q (kPa)
TLPS5

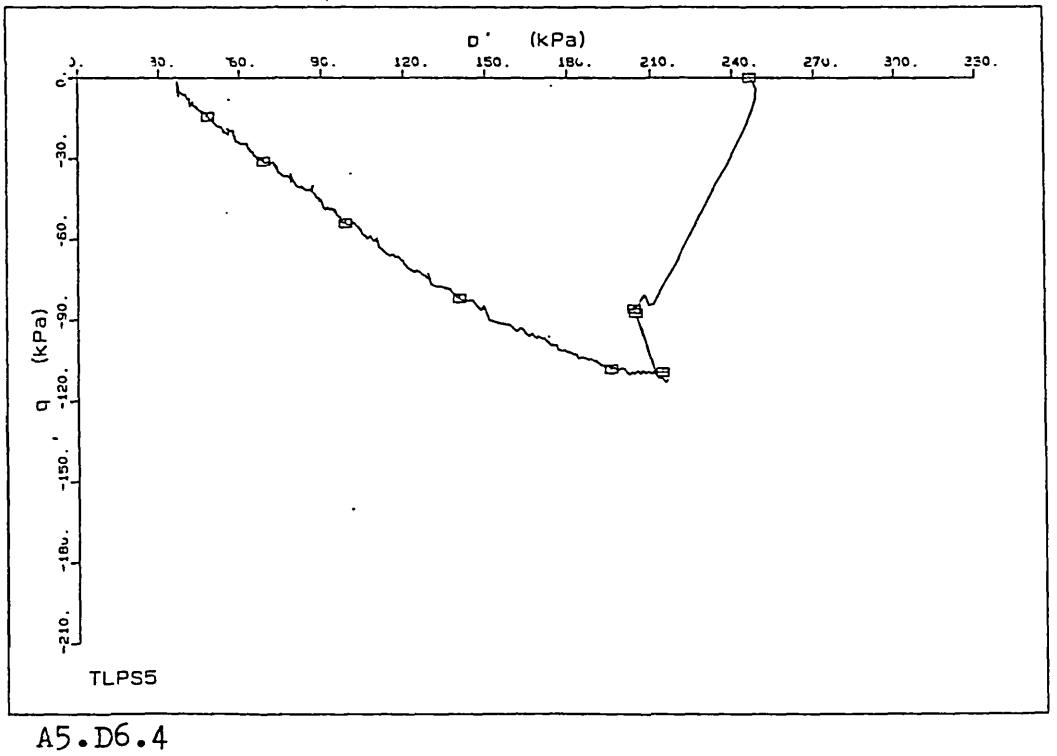
A5.D6.1


Axial strain (%)
-2.20
-2.00
-1.80
-1.60
-1.40
-1.20
-1.00
-0.80
-0.60
-0.40
-0.20
0.0
-10.0
-20.0
-30.0
-40.0
-50.0
-60.0
-70.0
Excess pwp (kPa)
TLPS5

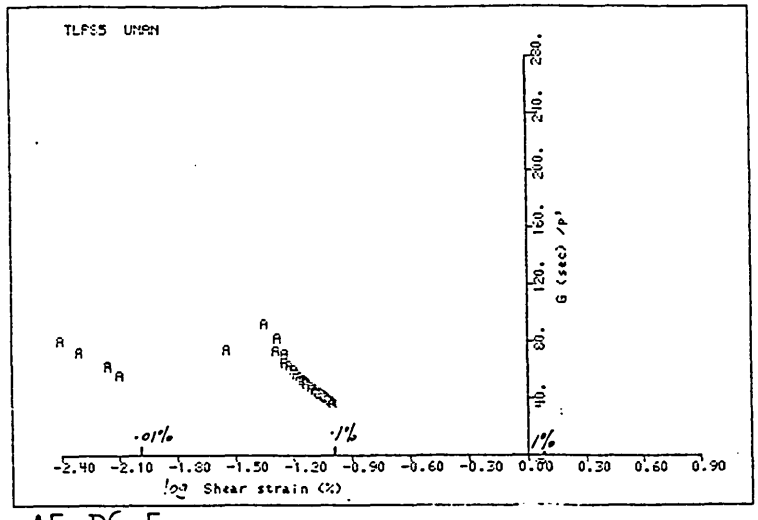
A5.D6.2


Axial strain (%)
-2.20
-2.00
-1.80
-1.60
-1.40
-1.20
-1.00
-0.80
-0.60
-0.40
-0.20
0.00
0.00
-1.00
-2.00
-3.00
-4.00
-5.00
-6.00
-7.00
Volume strain (%)
TLPS5

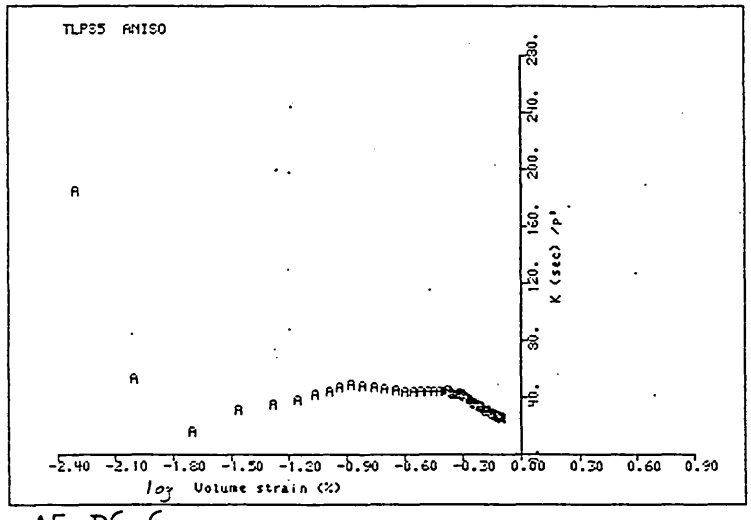
A5.D6.3


p' (kPa)
0.
30.
60.
90.
120.
150.
180.
210.
240.
270.
300.
330.
0.
-30.
-60.
-90.
-120.
-150.
-180.
-210.
q (kPa)
TLPS5

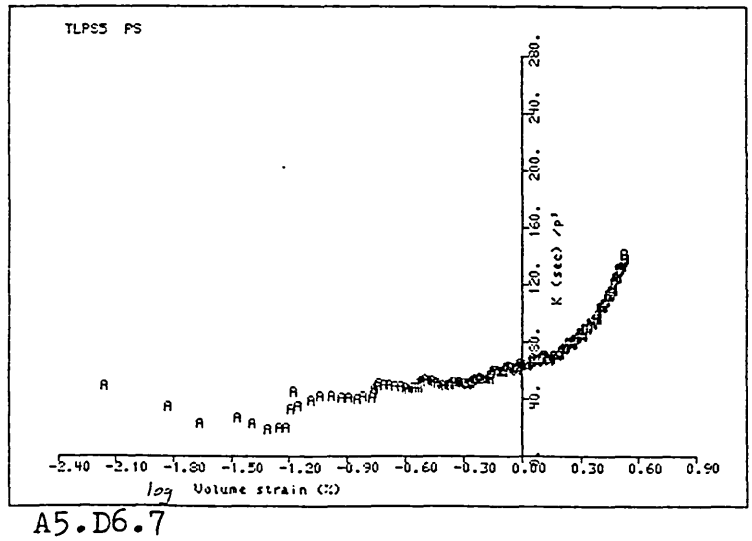
A5.D6.4



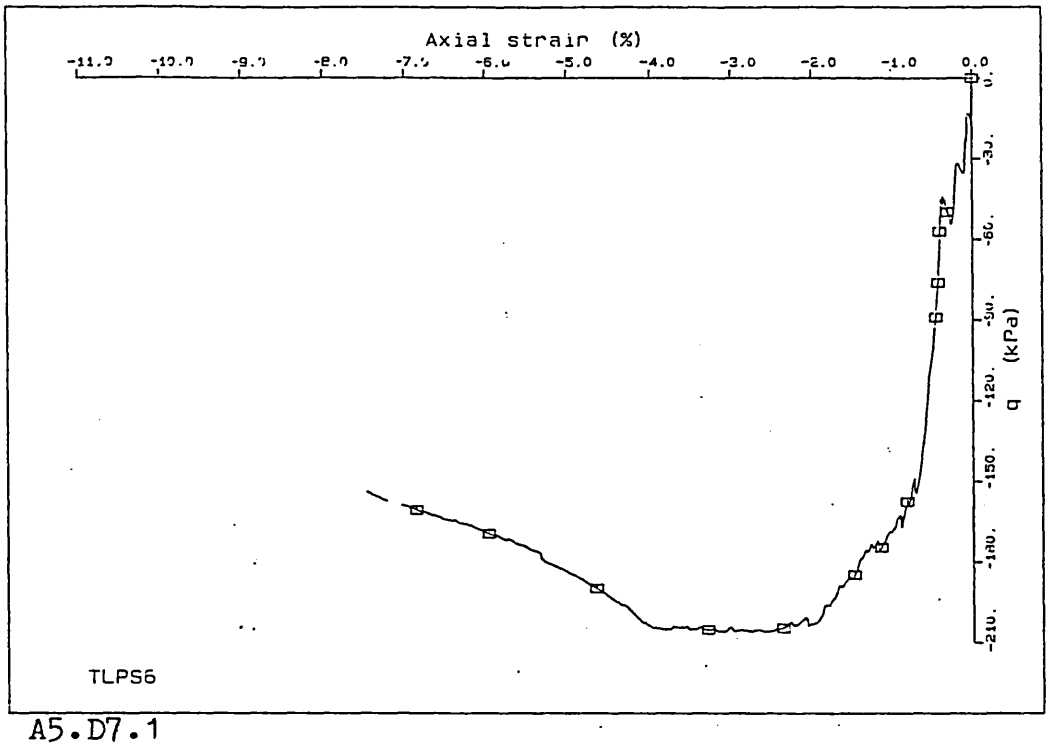
A5.D6.5



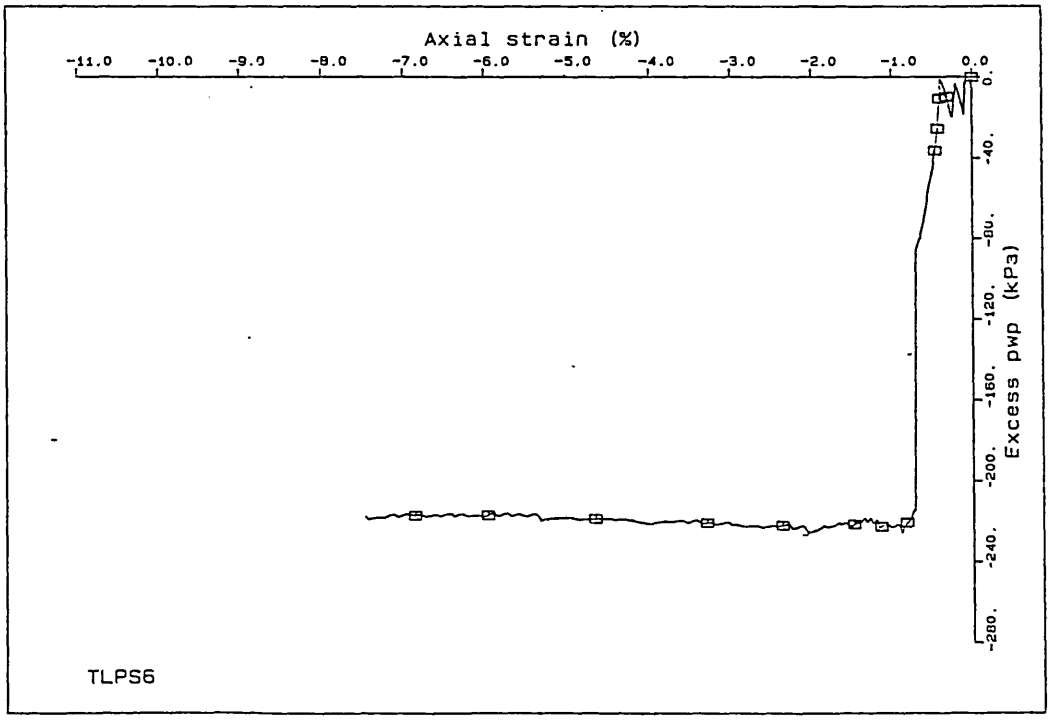
A5.D6.6



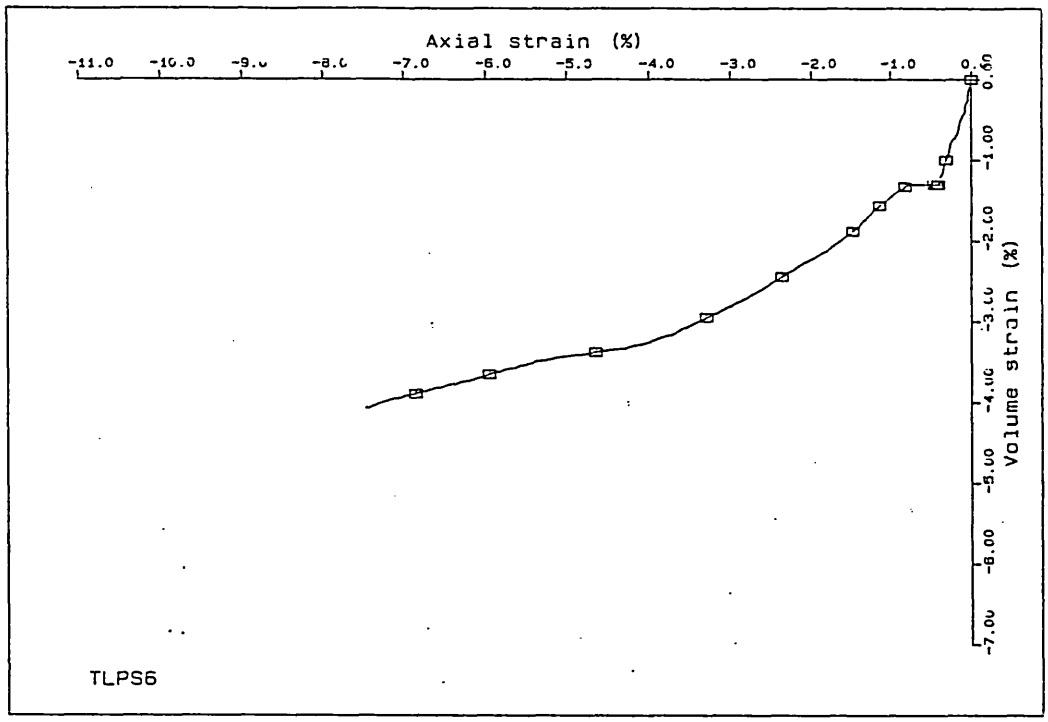
A5.D6.7


Axial strain (%)
-11.0
-10.0
-9.0
-8.0
-7.0
-6.0
-5.0
-4.0
-3.0
-2.0
-1.0
0.0
0.
-30.
-60.
-90.
-120.
-150.
-180.
-210.
q (kPa)
TLPS6

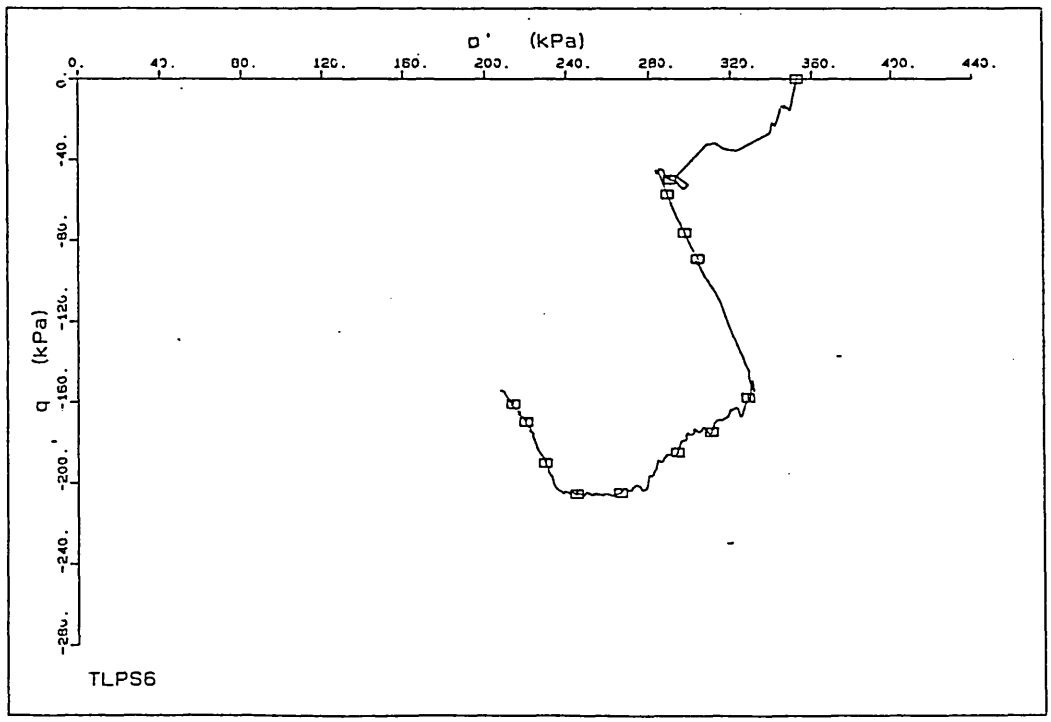
A5.D7.1


Axial strain (%)
-11.0
-10.0
-9.0
-8.0
-7.0
-6.0
-5.0
-4.0
-3.0
-2.0
-1.0
0.0
0.
-40.
-80.
-120.
-160.
-200.
-240.
-280.
Excess pwp (kPa)
TLPS6

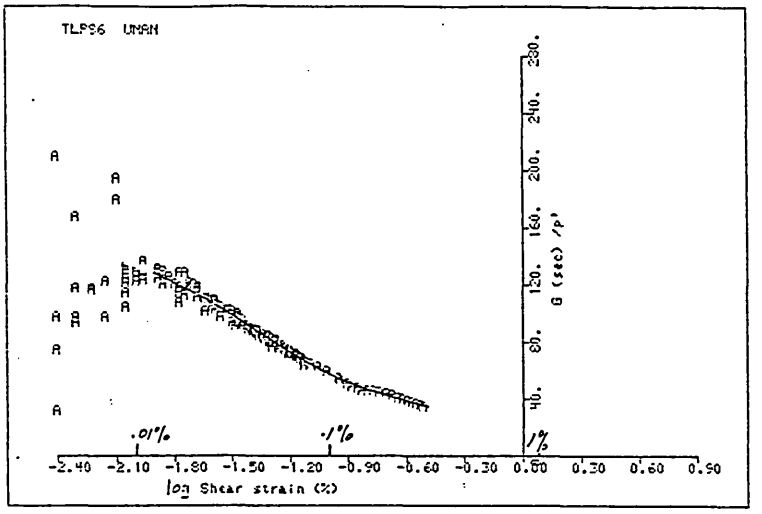
A5.D7.2


Axial strain (%)
-11.0
-10.0
-9.0
-8.0
-7.0
-6.0
-5.0
-4.0
-3.0
-2.0
-1.0
0.00
-1.00
-2.00
-3.00
-4.00
-5.00
-6.00
-7.00
Volume strain (%)
TLPS6

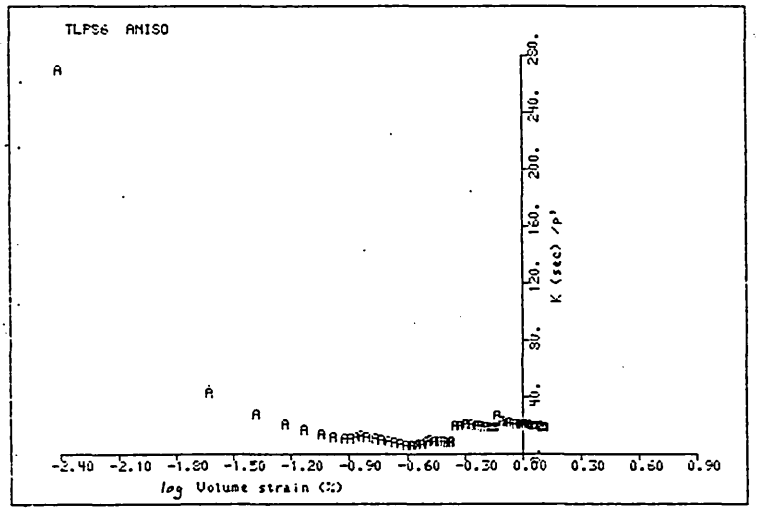
A5.D7.3


p' (kPa)
0.
40.
80.
120.
160.
200.
240.
280.
320.
360.
400.
440.
q (kPa)
-40.
-80.
-120.
-160.
-200.
-240.
-280.
TLPS6

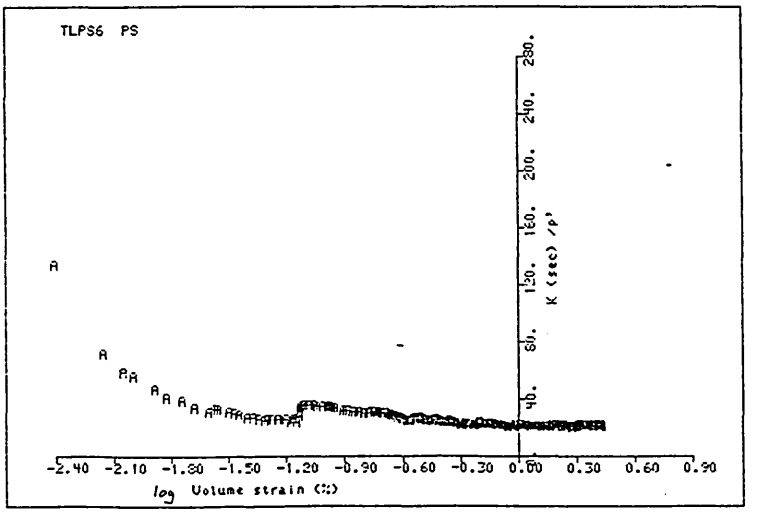
A5.D7.4



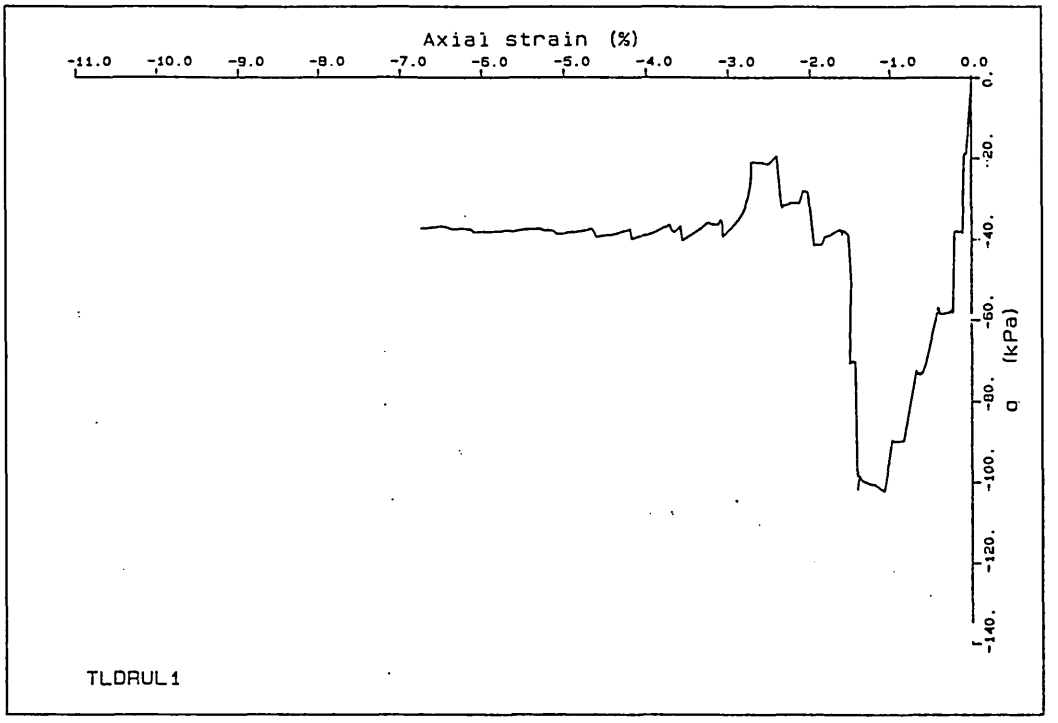
A5.D7.5



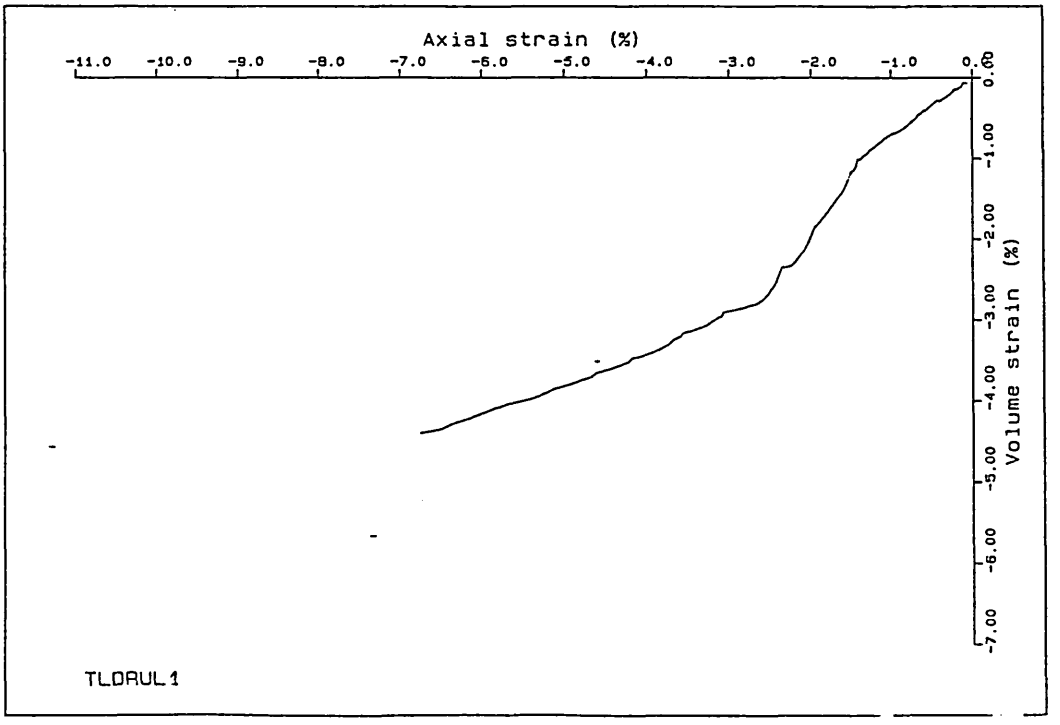
A5.D7.6



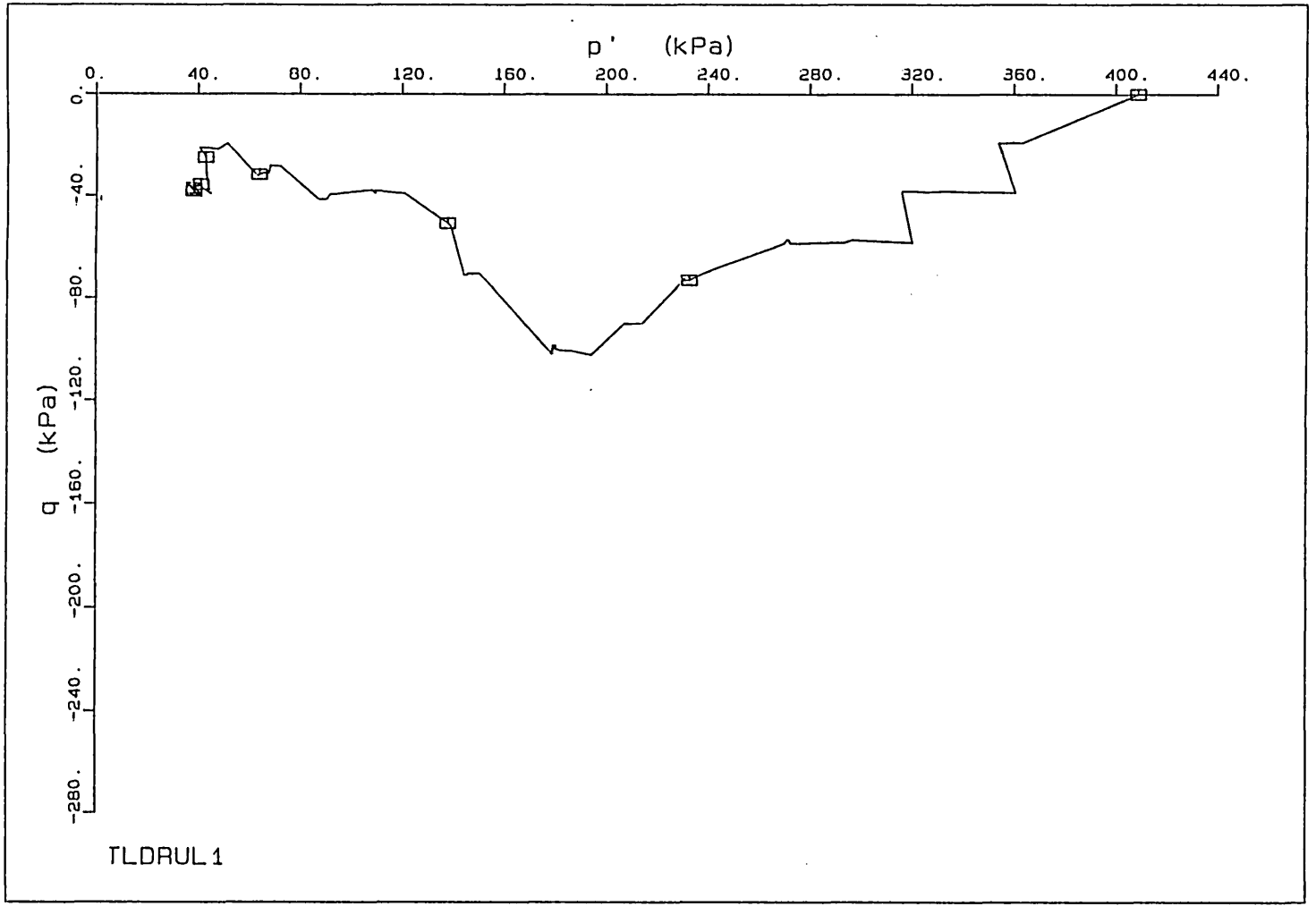
A5.D7.7


Axial strain (%)
-11.0
-10.0
-9.0
-8.0
-7.0
-6.0
-5.0
-4.0
-3.0
-2.0
-1.0
0.0
0.
-20.
-40.
-60.
-80.
-100.
-120.
-140.
σ (kPa)
TLDRUL1

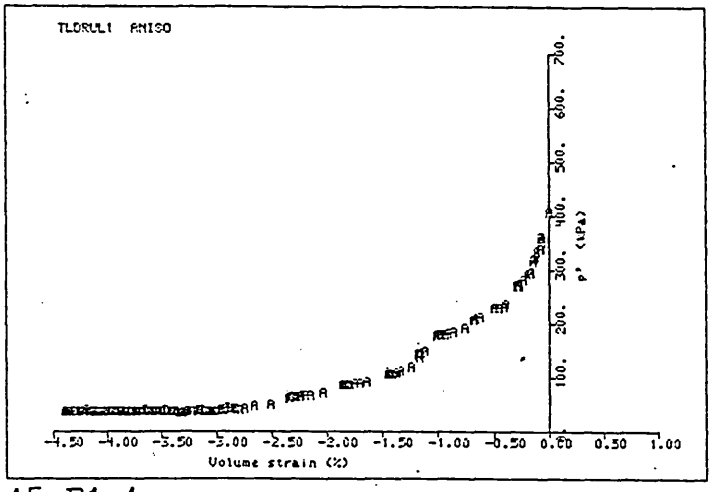
A5.E1.1


Axial strain (%)
-11.0
-10.0
-9.0
-8.0
-7.0
-6.0
-5.0
-4.0
-3.0
-2.0
-1.0
0.00
-1.00
-2.00
-3.00
-4.00
-5.00
-6.00
-7.00
Volume strain (%)
TLDRUL1

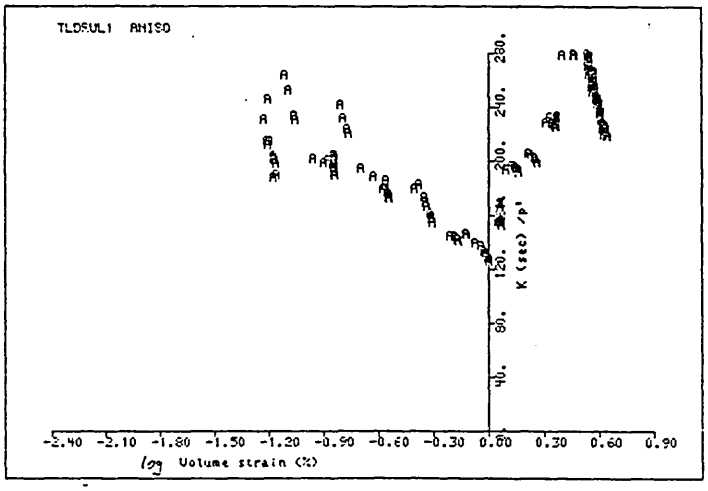
A5.E1.2


p' (kPa)
0.
40.
80.
120.
160.
200.
240.
280.
320.
360.
400.
440.
q (kPa)
0.
-40.
-80.
-120.
-160.
-200.
-240.
-280.
TLDRUL1

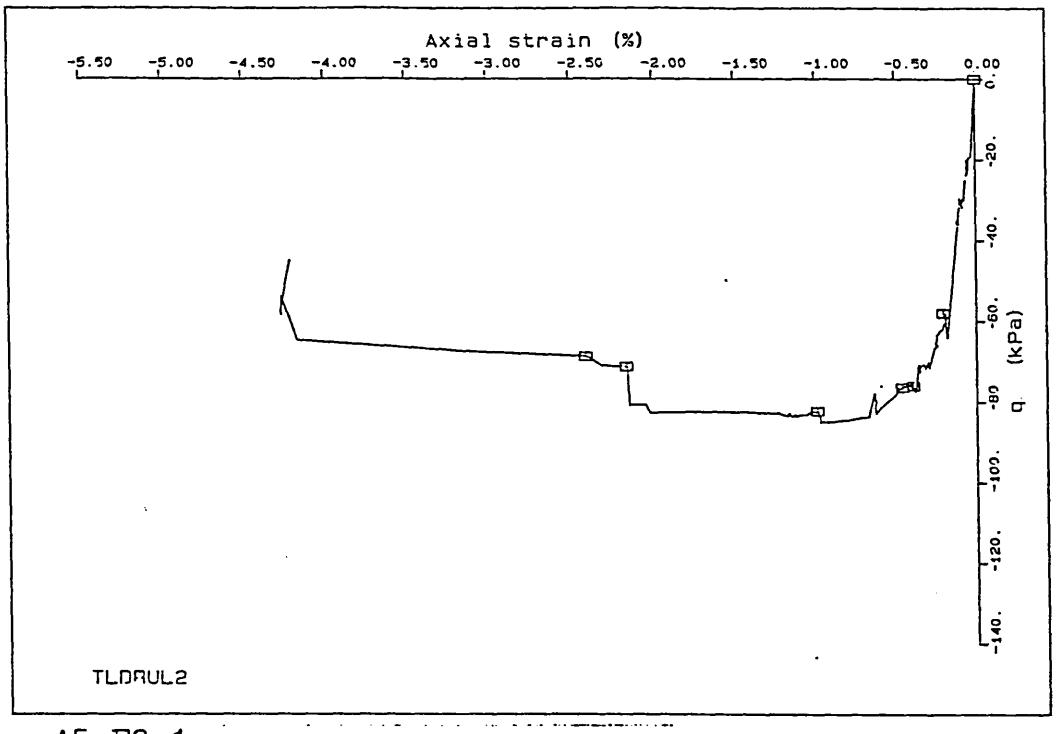
A5.E1.3


TLDRUL1 ANISO
700.
600.
500.
400.
300.
200.
100.
p' (kPa)
-4.50 -4.00 -3.50 -3.00 -2.50 -2.00 -1.50 -1.00 -0.50 0.00 0.50 1.00
Volume strain (%)

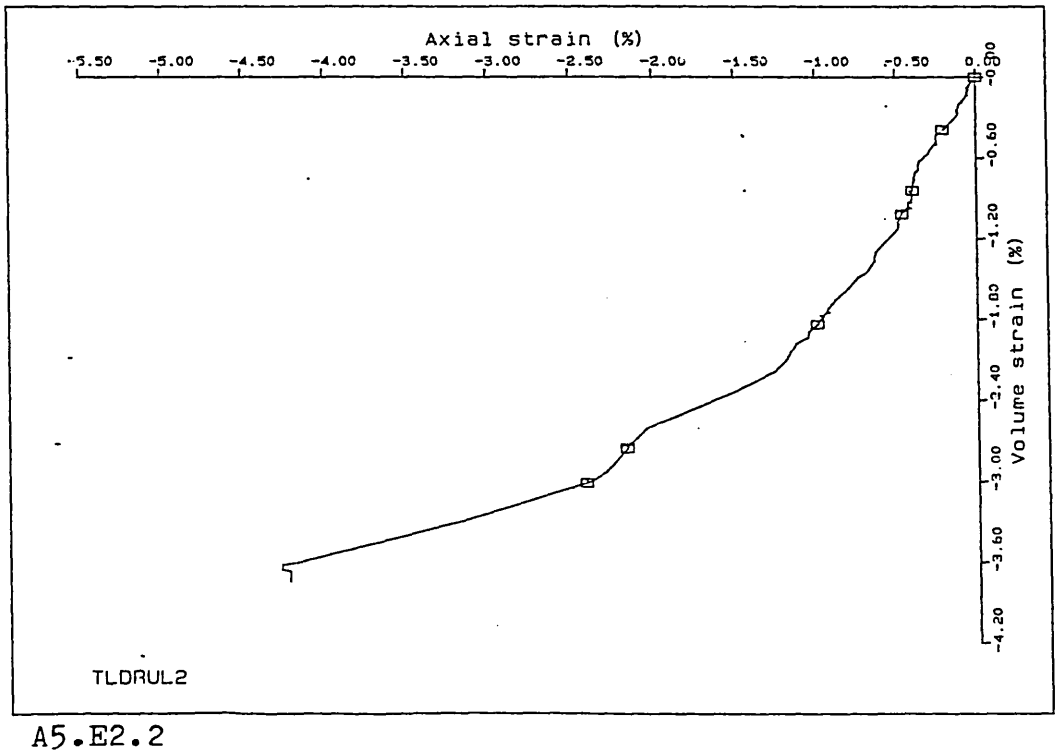
A5.E1.4


TLDRUL1 ANISO
280.
240.
200.
160.
120.
80.
40.
K (sec) /p'
-2.40 -2.10 -1.80 -1.50 -1.20 -0.90 -0.60 -0.30 0.00 0.30 0.60 0.90
log Volume strain (%)

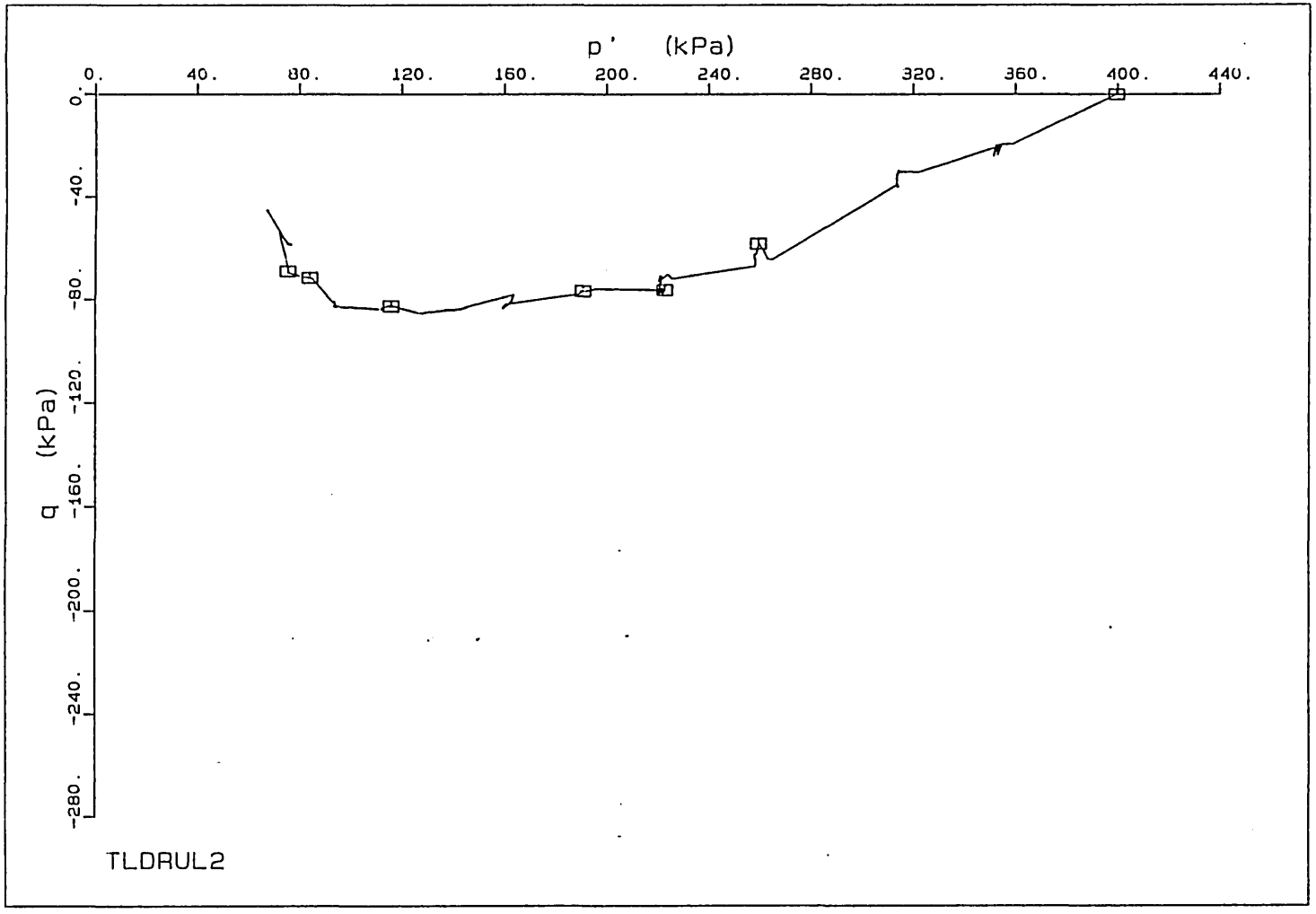
A5.E1.5


Axial strain (%)
-5.50 -5.00 -4.50 -4.00 -3.50 -3.00 -2.50 -2.00 -1.50 -1.00 -0.50 0.00
0.
-20.
-40.
-60.
-80.
-100.
-120.
-140.
q (kPa)
TLDRUL2

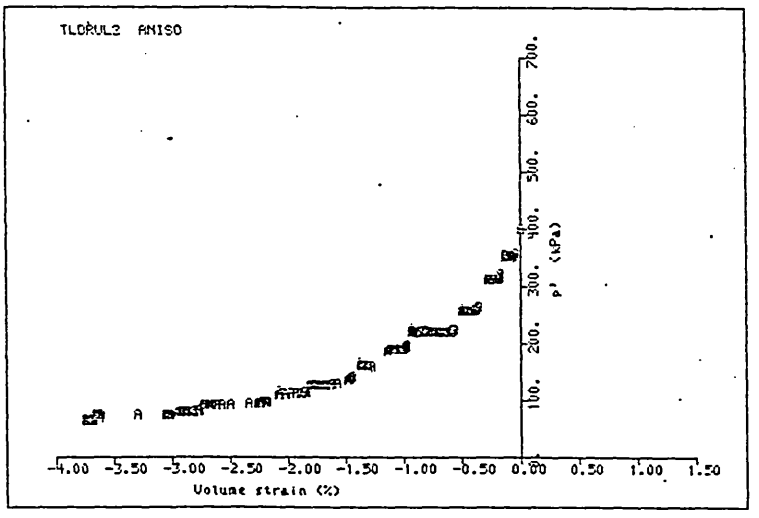
A5.E2.1


Axial strain (%)
-5.50 -5.00 -4.50 -4.00 -3.50 -3.00 -2.50 -2.00 -1.50 -1.00 -0.50 0.00
-0.00
-0.60
-1.20
-1.80
-2.40
-3.00
-3.60
-4.20
Volume strain (%)
TLDRUL2

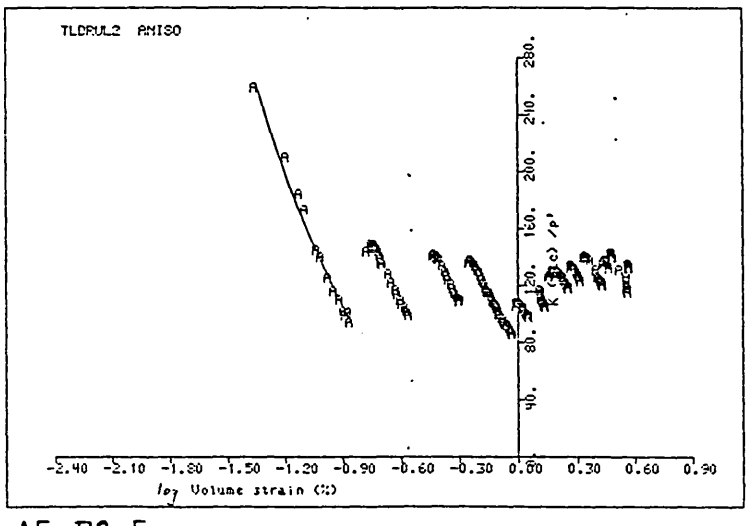
A5.E2.2


p' (kPa)
0.
40.
80.
120.
160.
200.
240.
280.
320.
360.
400.
440.
q (kPa)
0.
-40.
-80.
-120.
-160.
-200.
-240.
-280.
TLDRUL2

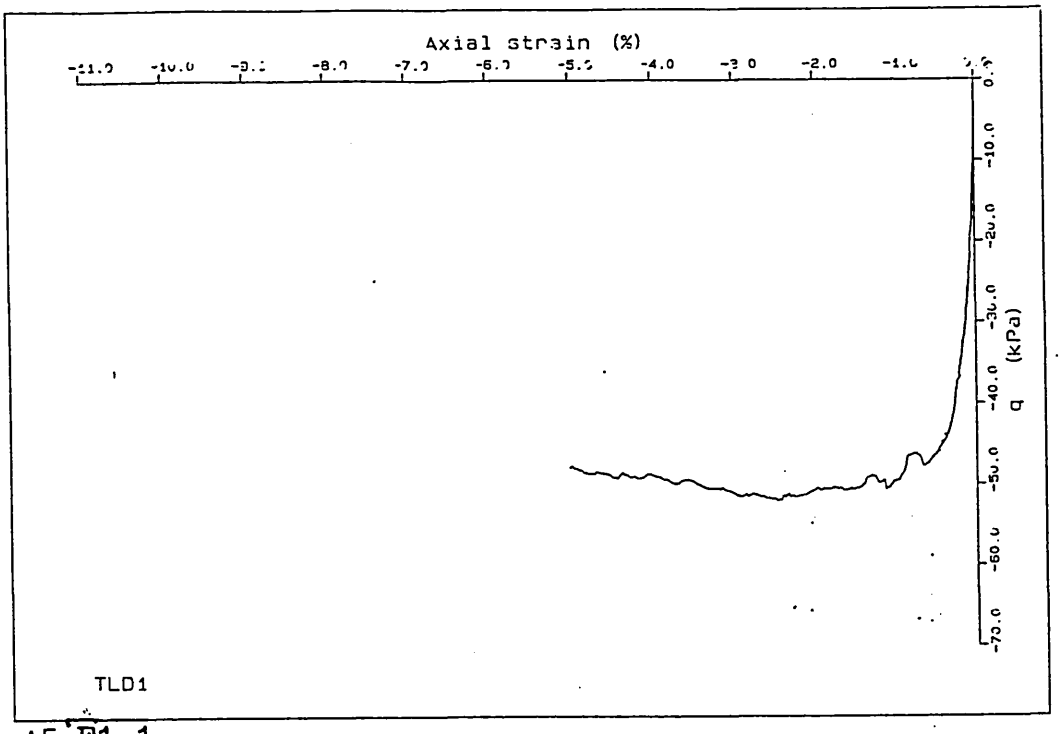
A5.E2.3


TLDRUL2 ANISO
700.
600.
500.
400.
300.
200.
100.
p' (kPa)
-4.00 -3.50 -3.00 -2.50 -2.00 -1.50 -1.00 -0.50 0.00 0.50 1.00 1.50
Volume strain (%)

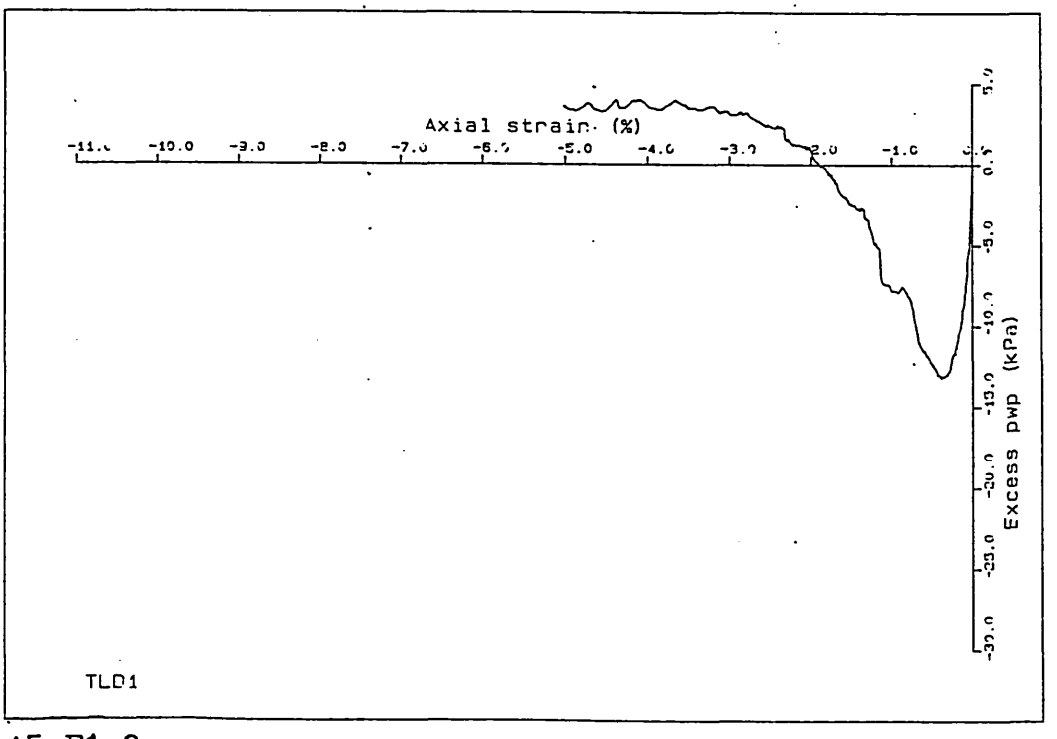
A5.E2.4


TLDRUL2 ANISO
280.
240.
200.
160.
120.
80.
40.
-2.40 -2.10 -1.80 -1.50 -1.20 -0.90 -0.60 -0.30 0.00 0.30 0.60 0.90
Volume strain (%)

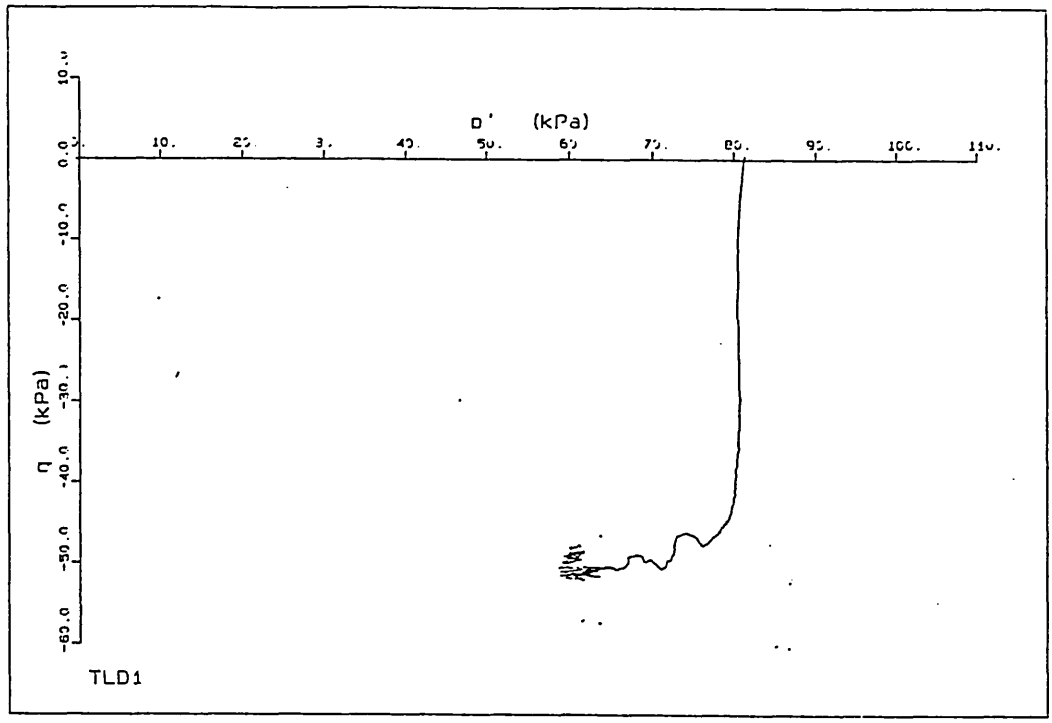
A5.E2.5


Axial strain (%)
-11.0
-10.0
-9.0
-8.0
-7.0
-6.0
-5.0
-4.0
-3.0
-2.0
-1.0
0.0
-10.0
-20.0
-30.0
-40.0
-50.0
-60.0
-70.0
q (kPa)
TLD1

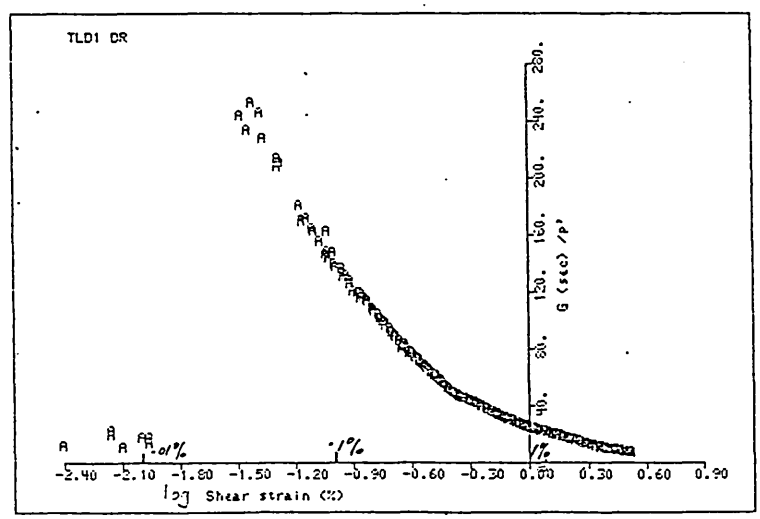
A5.F1.1


Axial strain (%)
-11.0
-10.0
-9.0
-8.0
-7.0
-6.0
-5.0
-4.0
-3.0
-2.0
-1.0
0.0
5.0
-5.0
-10.0
-15.0
-20.0
-25.0
-30.0
Excess pwp (kPa)
TLD1

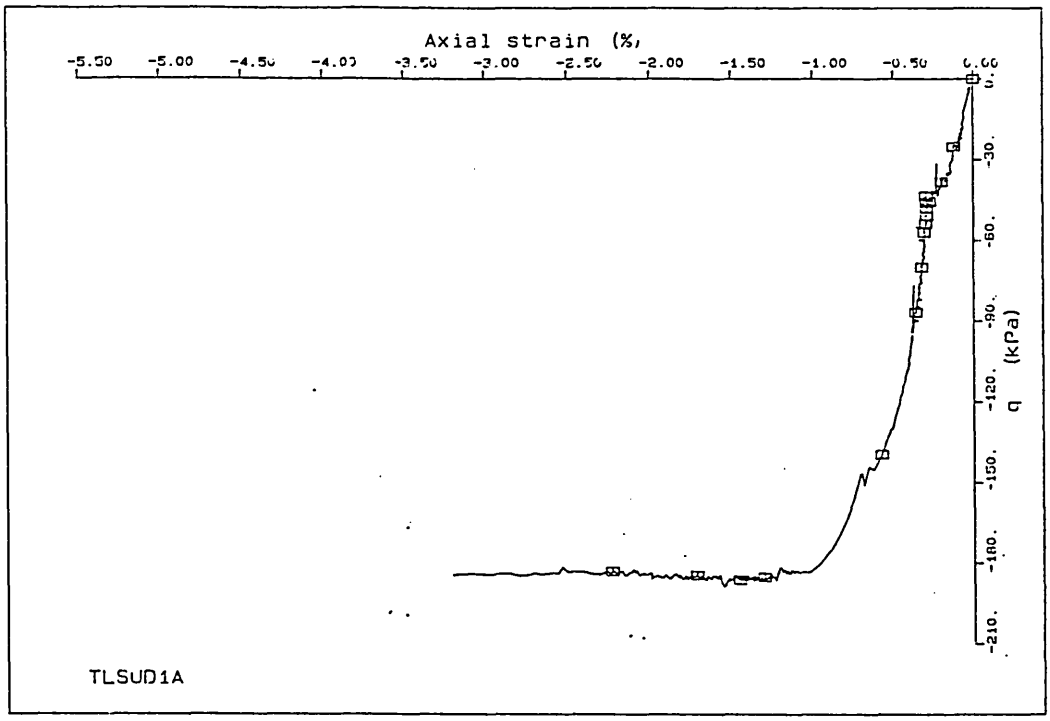
A5.F1.2


p' (kPa)
10.
20.
30.
40.
50.
60.
70.
80.
90.
100.
110.
0.0
-10.0
-20.0
-30.0
-40.0
-50.0
-60.0
q (kPa)
TLD1

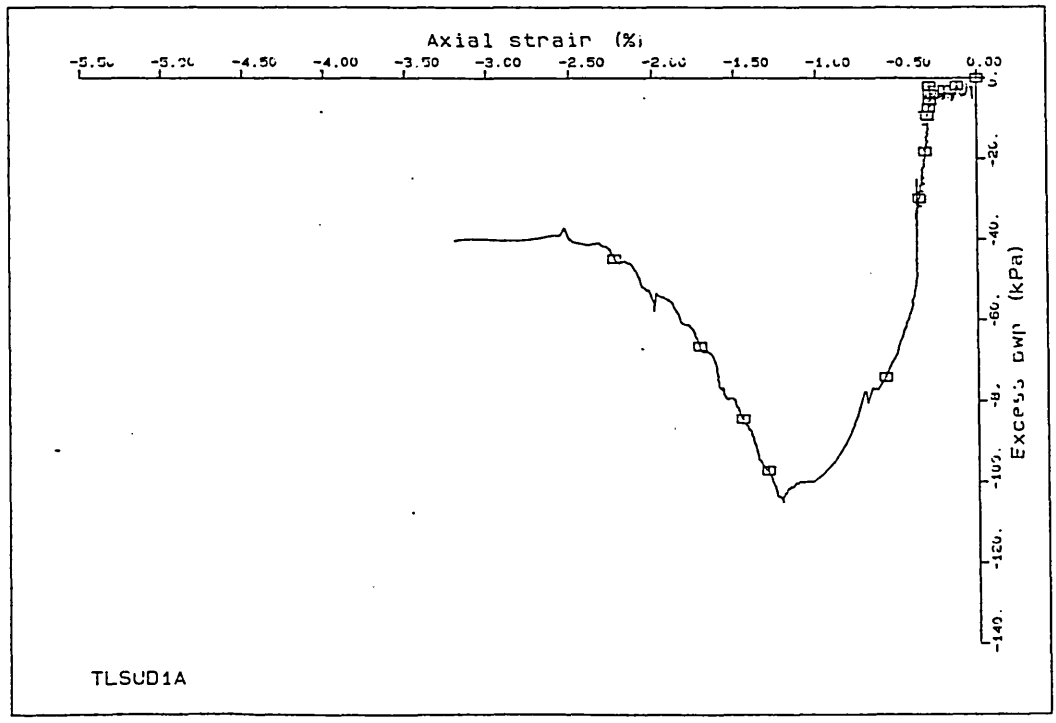
A5.F1.3


TLD1 DR
280.
240.
200.
160.
120.
80.
40.
G (sec) /p'
.01%
.1%
1%
-2.40
-2.10
-1.80
-1.50
-1.20
-0.90
-0.60
-0.30
0.00
0.30
0.60
0.90
log Shear strain (%)

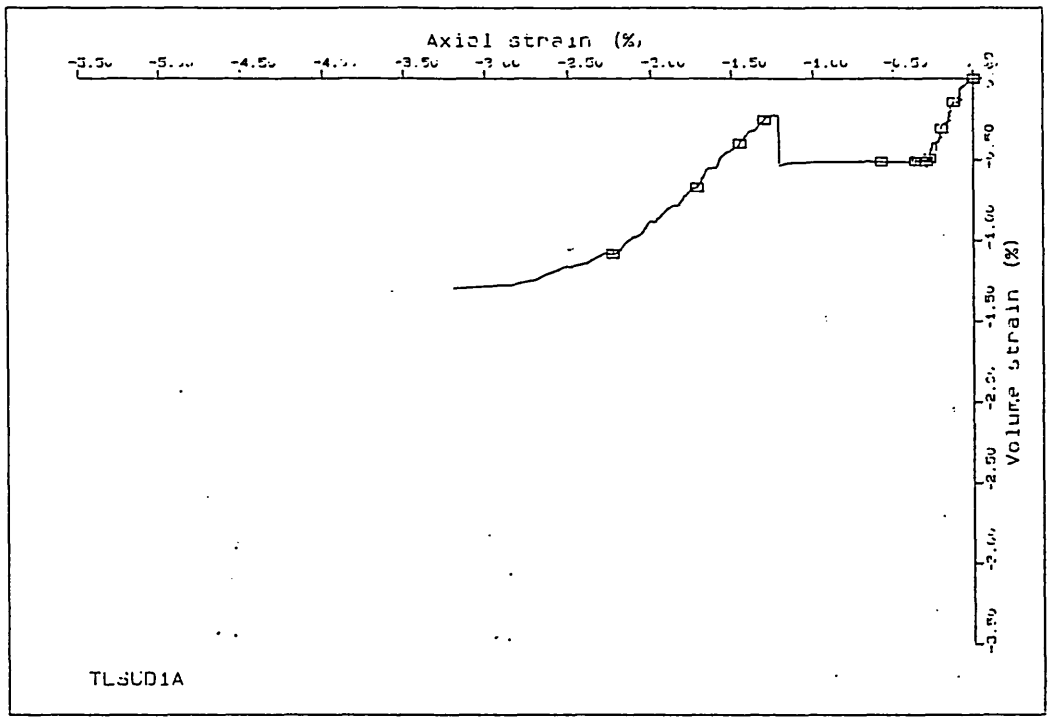
A5.F1.4


Axial strain (%)
-5.50
-5.00
-4.50
-4.00
-3.50
-3.00
-2.50
-2.00
-1.50
-1.00
-0.50
0.00
-30.
-60.
-90.
-120.
-150.
-180.
-210.
q (kPa)
TLSUD1A

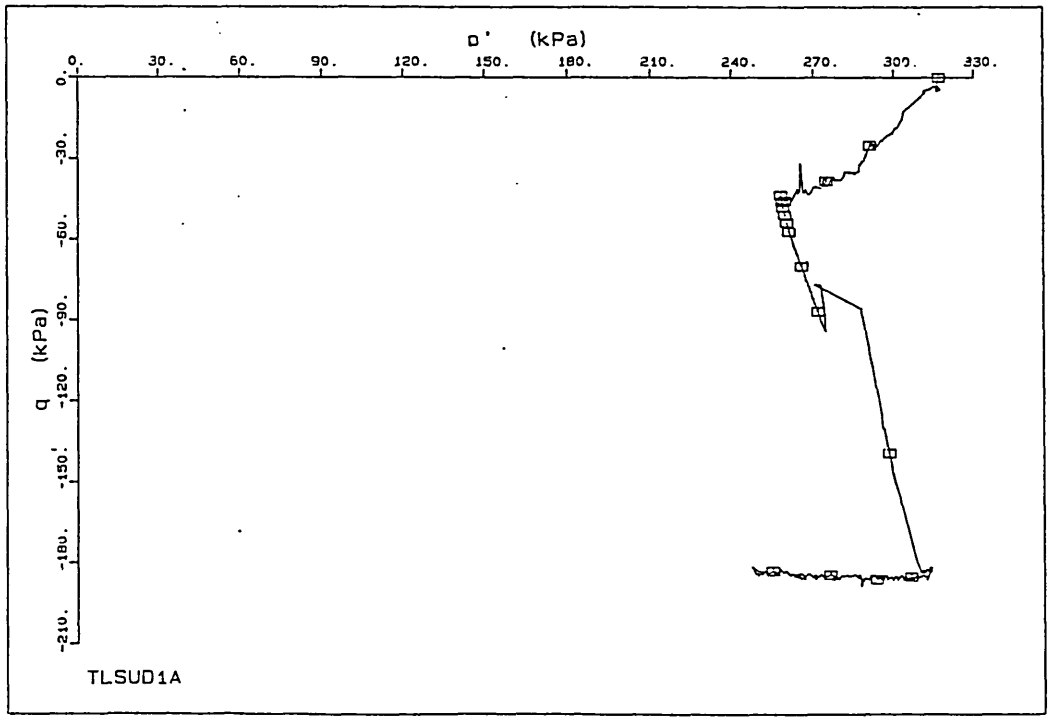
A5.G1.1


Axial strain (%)
-5.50
-5.00
-4.50
-4.00
-3.50
-3.00
-2.50
-2.00
-1.50
-1.00
-0.50
0.00
-20.
-40.
-60.
-80.
-100.
-120.
-140.
Excess pwp (kPa)
TLSUD1A

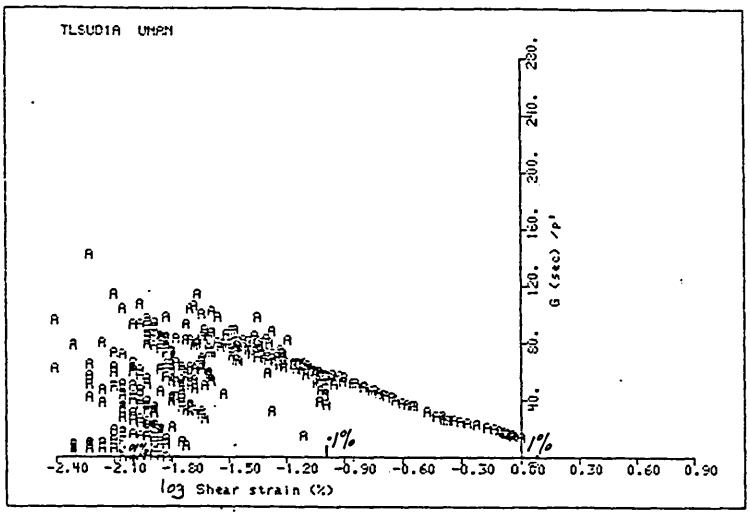
A5.G1.2


Axial strain (%)
Volume strain (%)
TLSUD1A

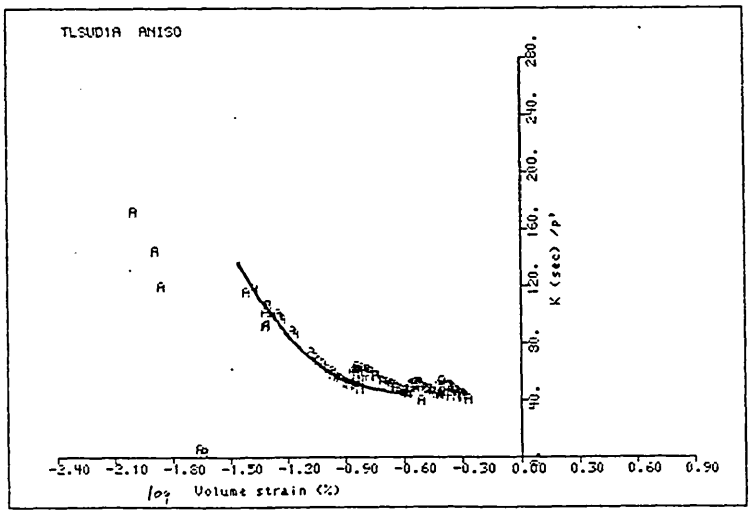
A5.G1.3


p' (kPa)
0.
30.
60.
90.
120.
150.
180.
210.
240.
270.
300.
330.
q (kPa)
-30.
-60.
-90.
-120.
-150.
-180.
-210.
TLSUD1A

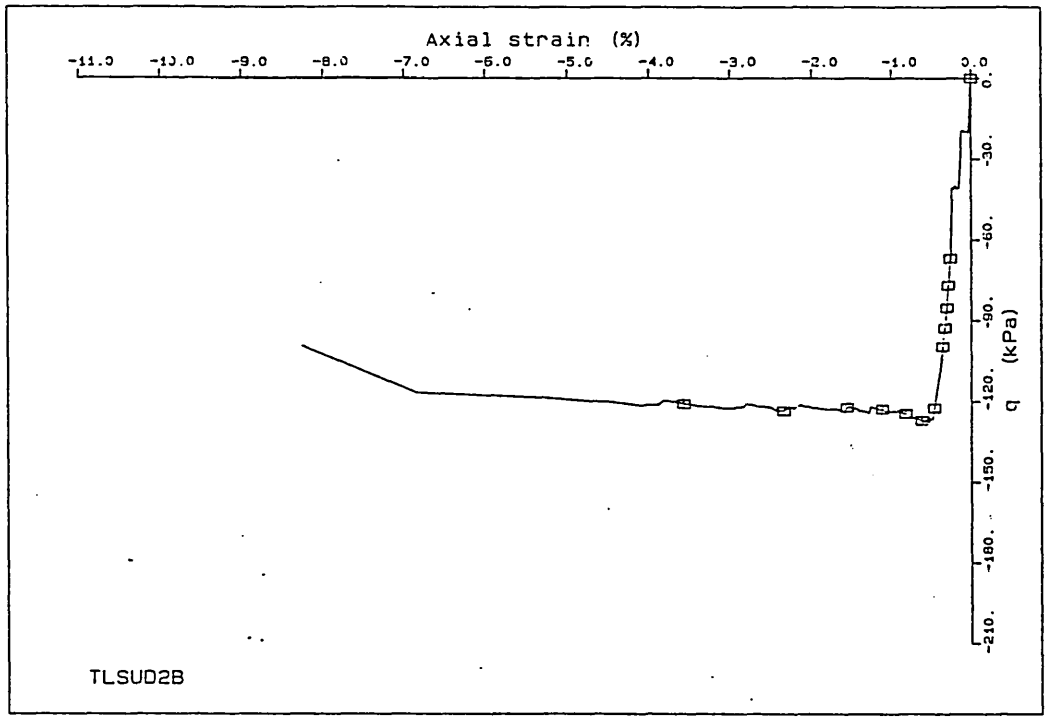
A5.G1.4


TLSUD1A UHAN
G (sec) /p'
log Shear strain (%)
-2.40 -2.10 -1.80 -1.50 -1.20 -0.90 -0.60 -0.30 0.00 0.30 0.60 0.90
40. 80. 120. 160. 200. 240. 280.
.1%
1%

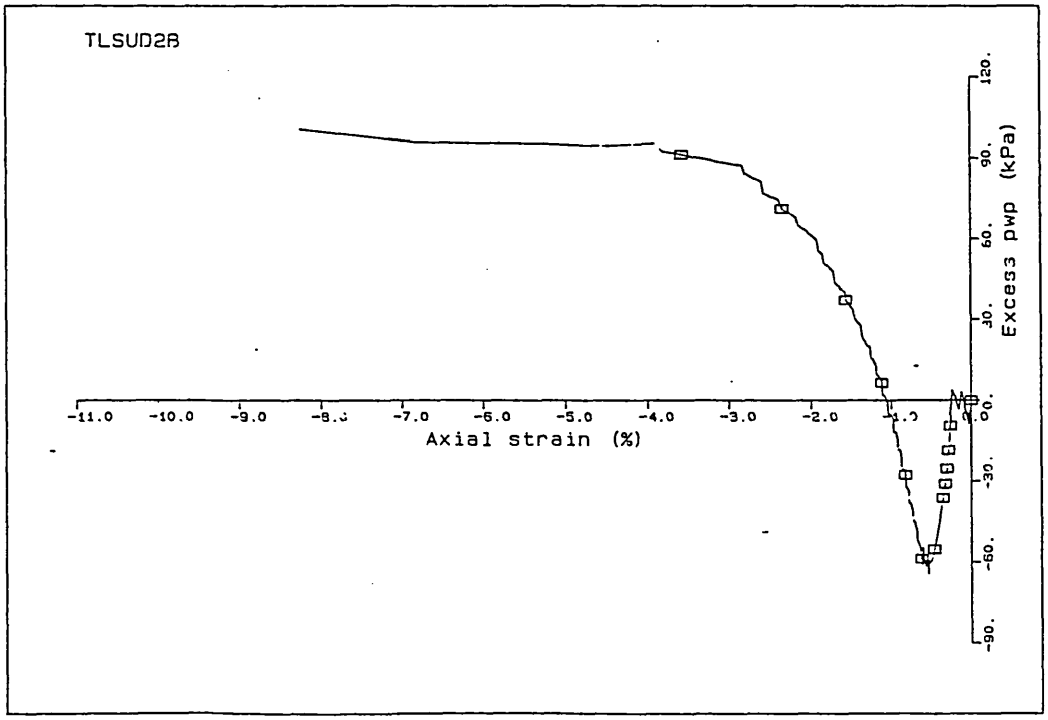
A5.G1.5


TLSUD1A ANISO
K (sec) /p'
log Volume strain (%)
-2.40 -2.10 -1.80 -1.50 -1.20 -0.90 -0.60 -0.30 0.00 0.30 0.60 0.90
40. 80. 120. 160. 200. 240. 280.

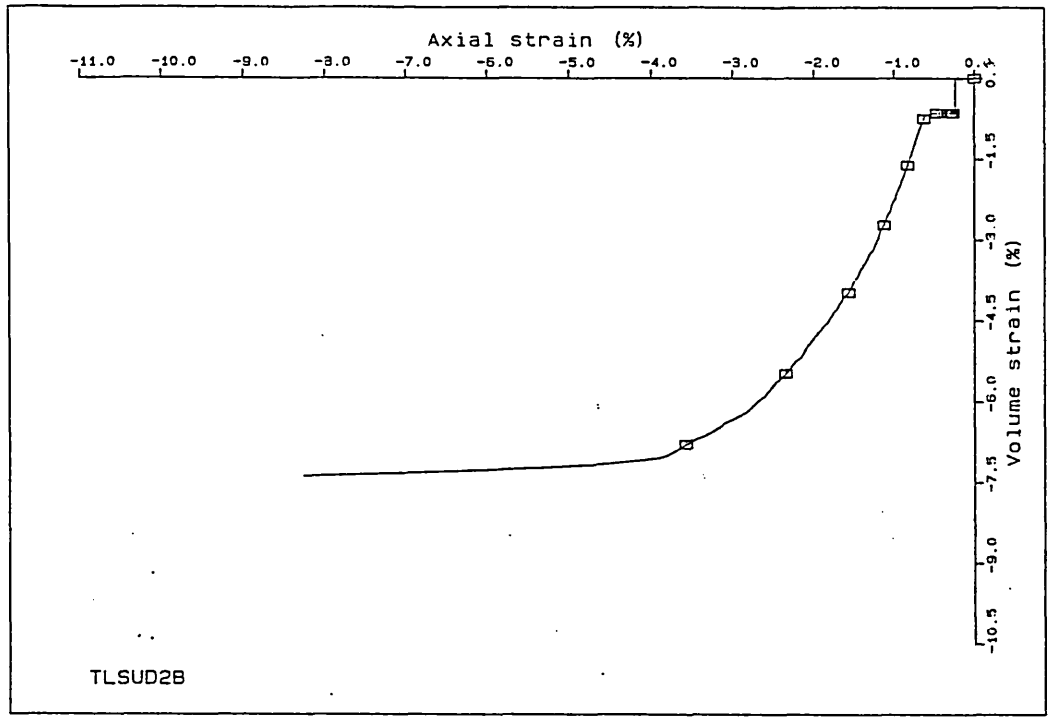
A5.G1.6


Axial strain (%)
-11.0
-10.0
-9.0
-8.0
-7.0
-6.0
-5.0
-4.0
-3.0
-2.0
-1.0
0.0
0.
-30.
-60.
-90.
-120.
-150.
-180.
-210.
q (kPa)
TLSUD2B

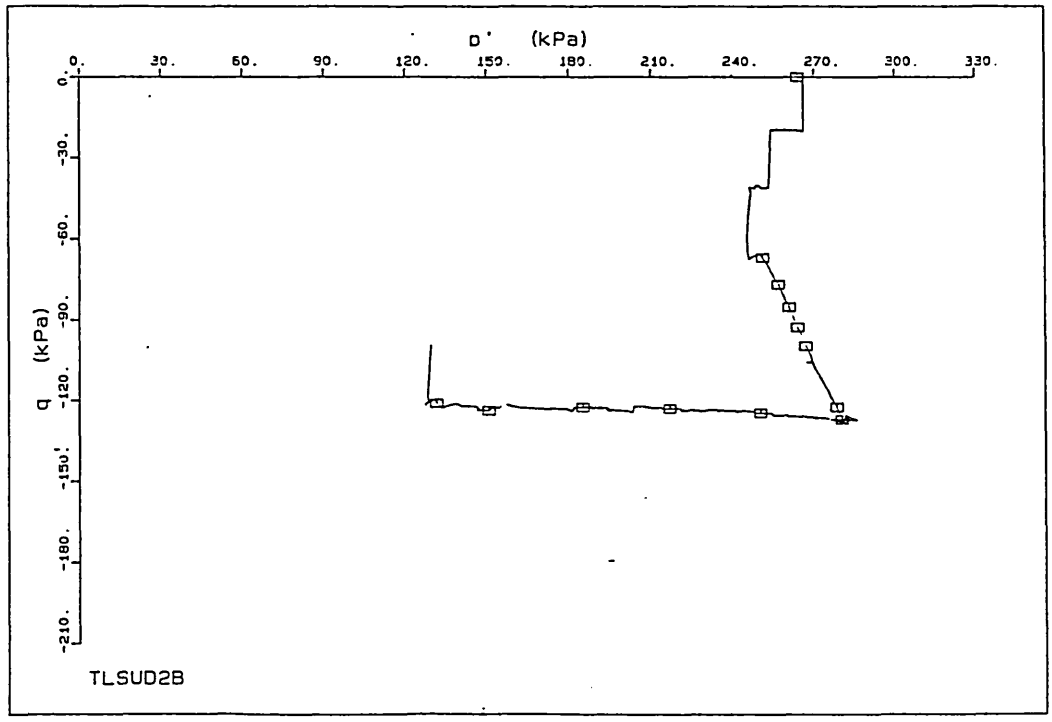
A5.G2.1


TLSUD2B
120.
90.
60.
30.
0.
-30.
-60.
-90.
Excess pwp (kPa)
-11.0
-10.0
-9.0
-7.0
-6.0
-5.0
-4.0
-3.0
-2.0
Axial strain (%)

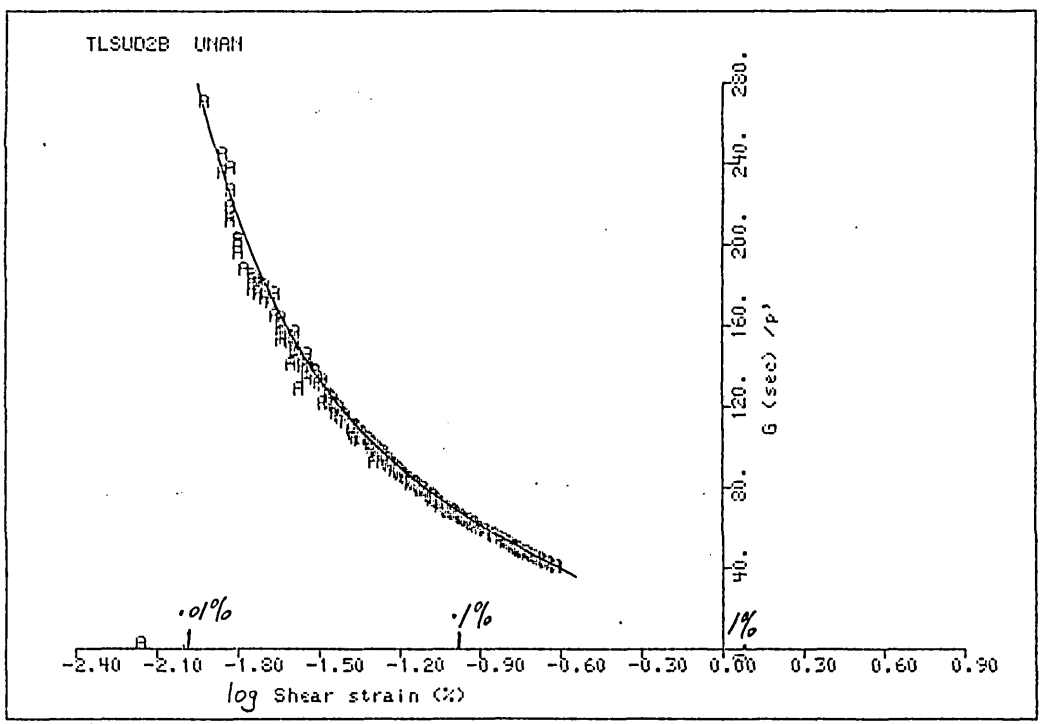
A5.G2.2


Axial strain (%)
-11.0
-10.0
-9.0
-8.0
-7.0
-6.0
-5.0
-4.0
-3.0
-2.0
-1.0
0.
0.
-1.5
-3.0
-4.5
-6.0
-7.5
-9.0
-10.5
Volume strain (%)
TLSUD2B

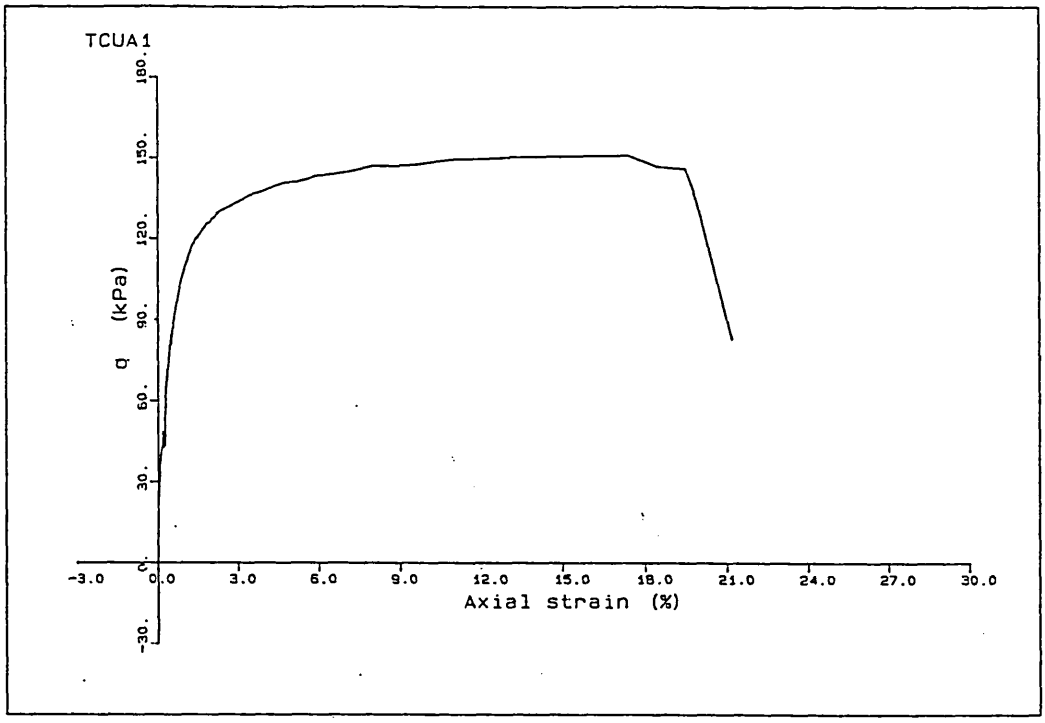
A5.G2.3


p' (kPa)
0.
30.
60.
90.
120.
150.
180.
210.
240.
270.
300.
330.
0.
-30.
-60.
-90.
-120.
-150.
-180.
-210.
q (kPa)
TLSUD2B

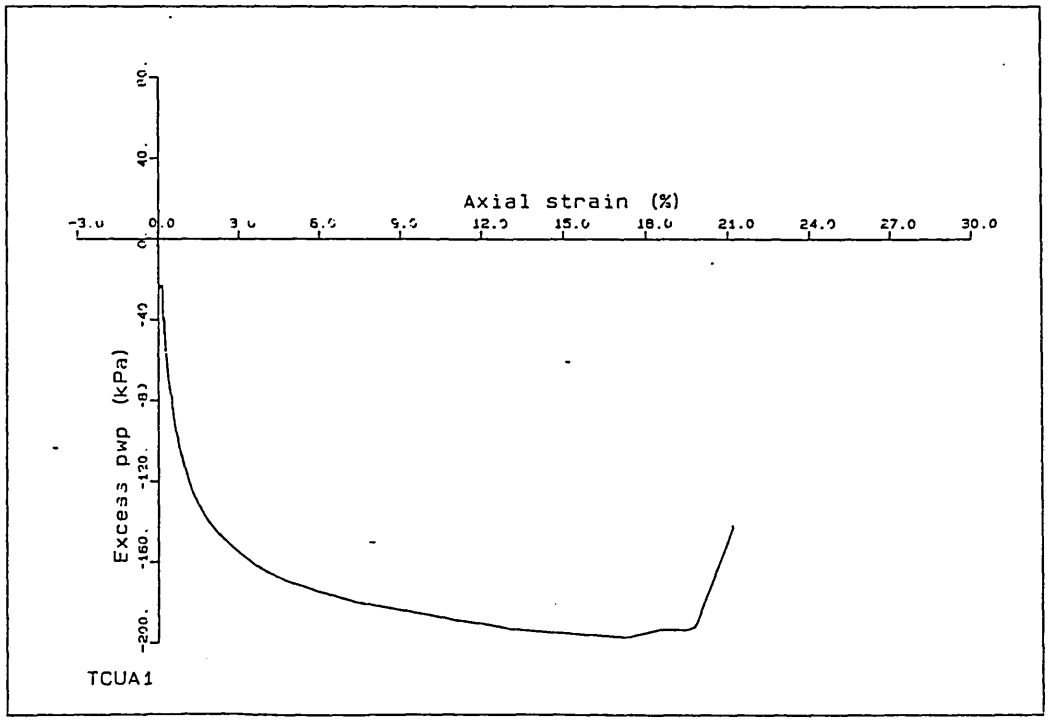
A5.G2.4


TLSUD2B UNAN
G (sec) /p'
40.
80.
120.
160.
200.
240.
280.
.01%
.1%
1%
-2.40 -2.10 -1.80 -1.50 -1.20 -0.90 -0.60 -0.30 0.00 0.30 0.60 0.90
log Shear strain (%)

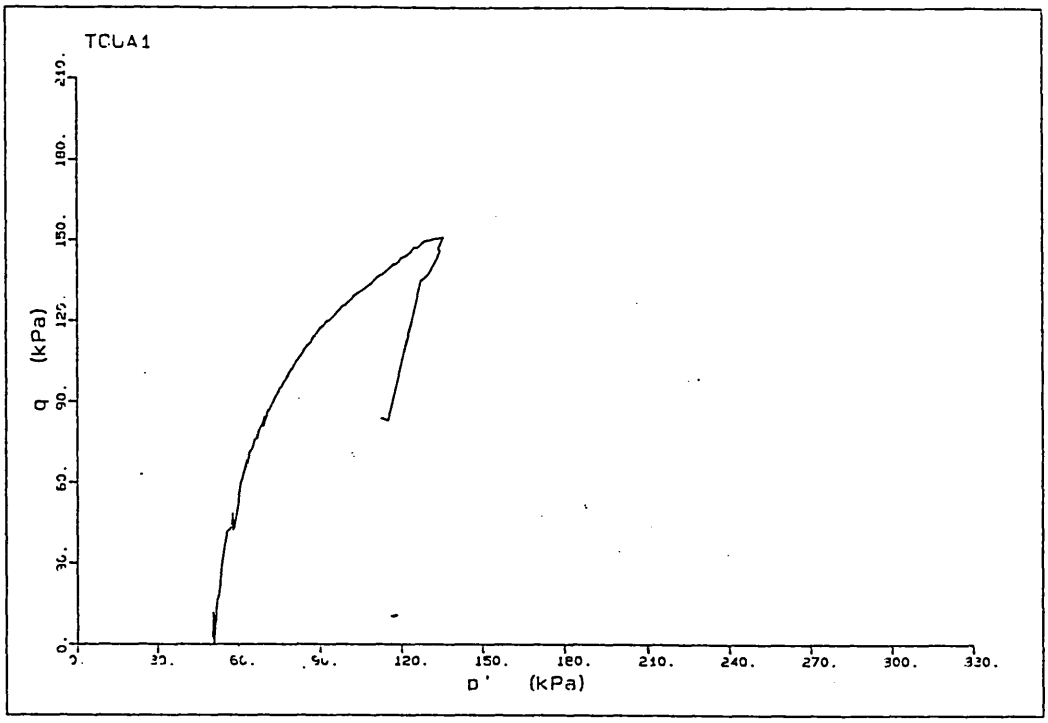
A5.G2.5


TCUA1
q (kPa)
180.
150.
120.
90.
60.
30.
0.
-30.
-3.0
0.0
3.0
6.0
9.0
12.0
15.0
18.0
21.0
24.0
27.0
30.0
Axial strain (%)

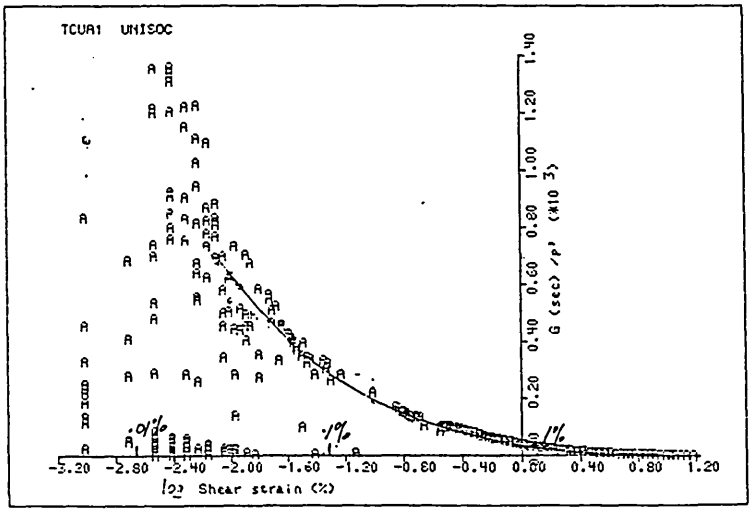
A5.H1.1


Axial strain (%)
Excess pwp (kPa)
40.
-40
-80
-120.
-160.
-200.
TCUA1

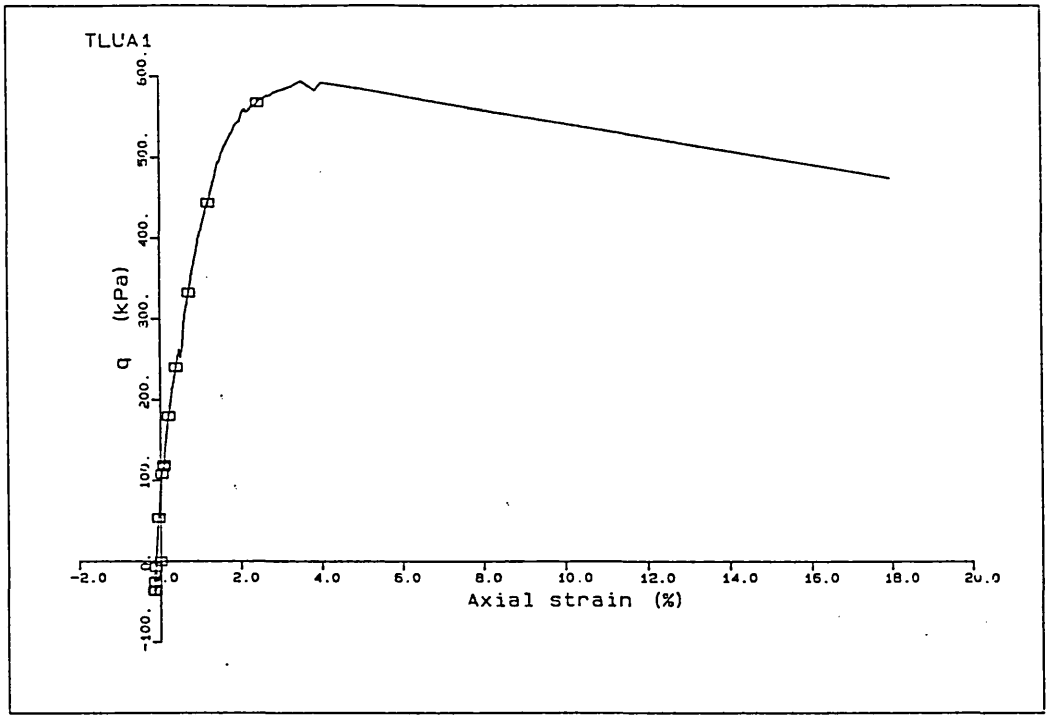
A5.H1.2



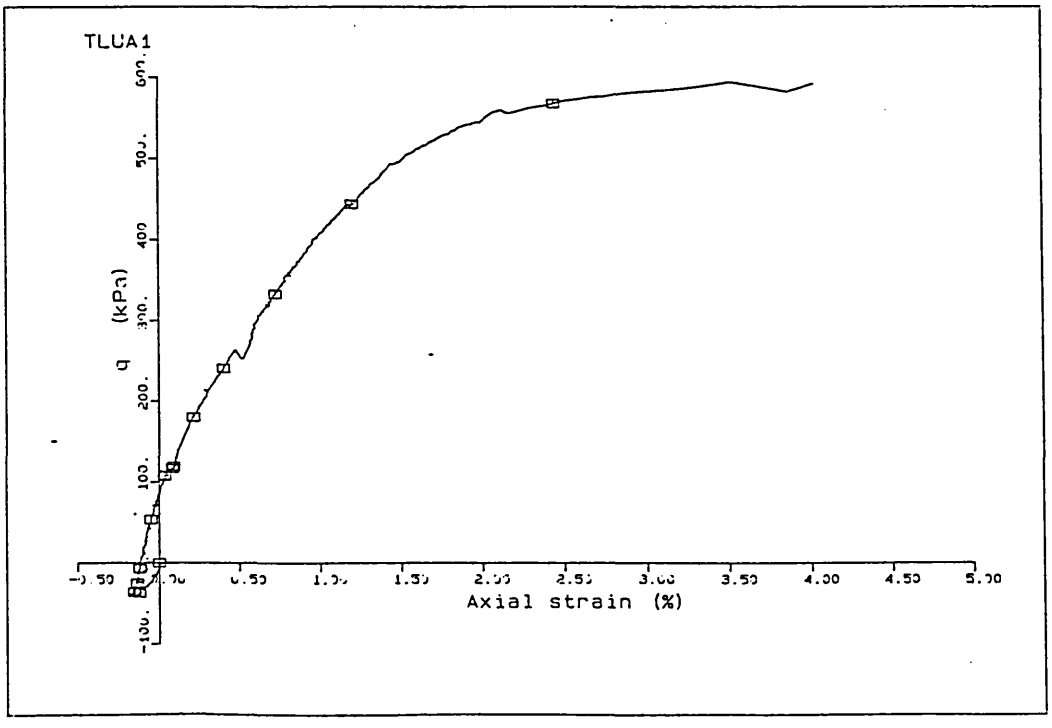
A5.H1.3



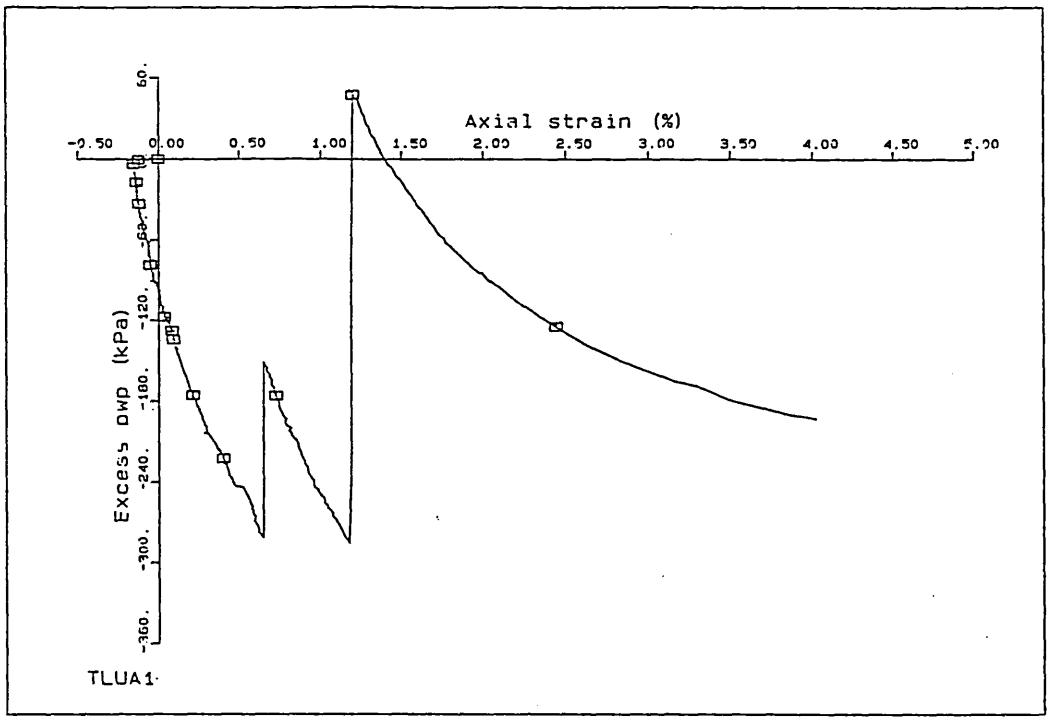
A5.H1.4



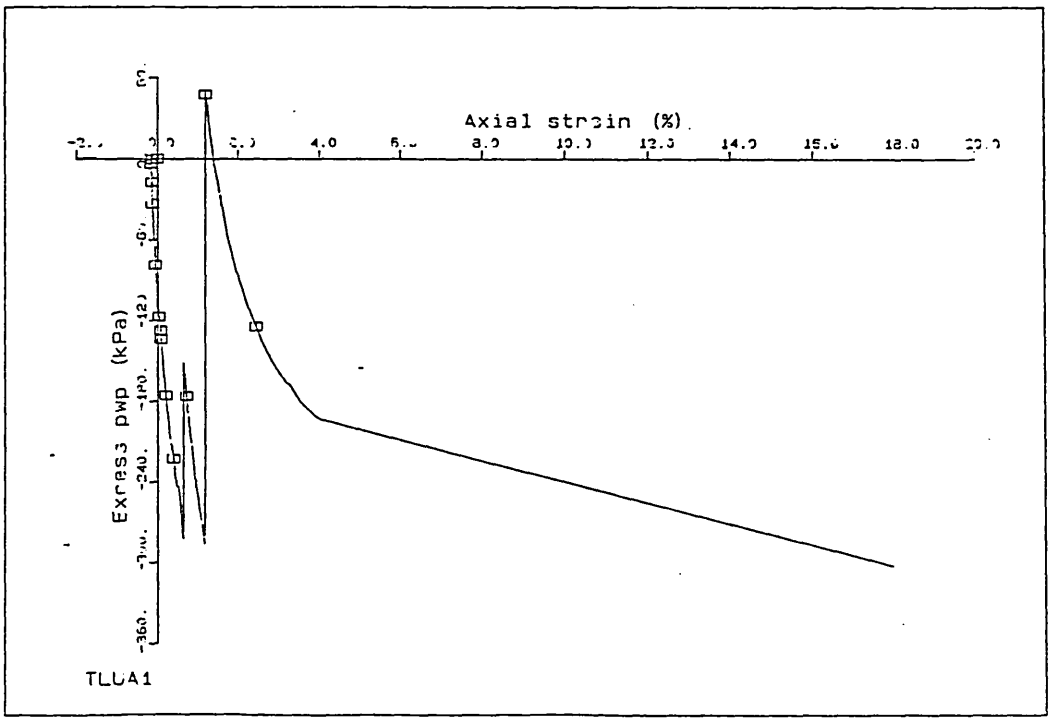
A5.I1.1



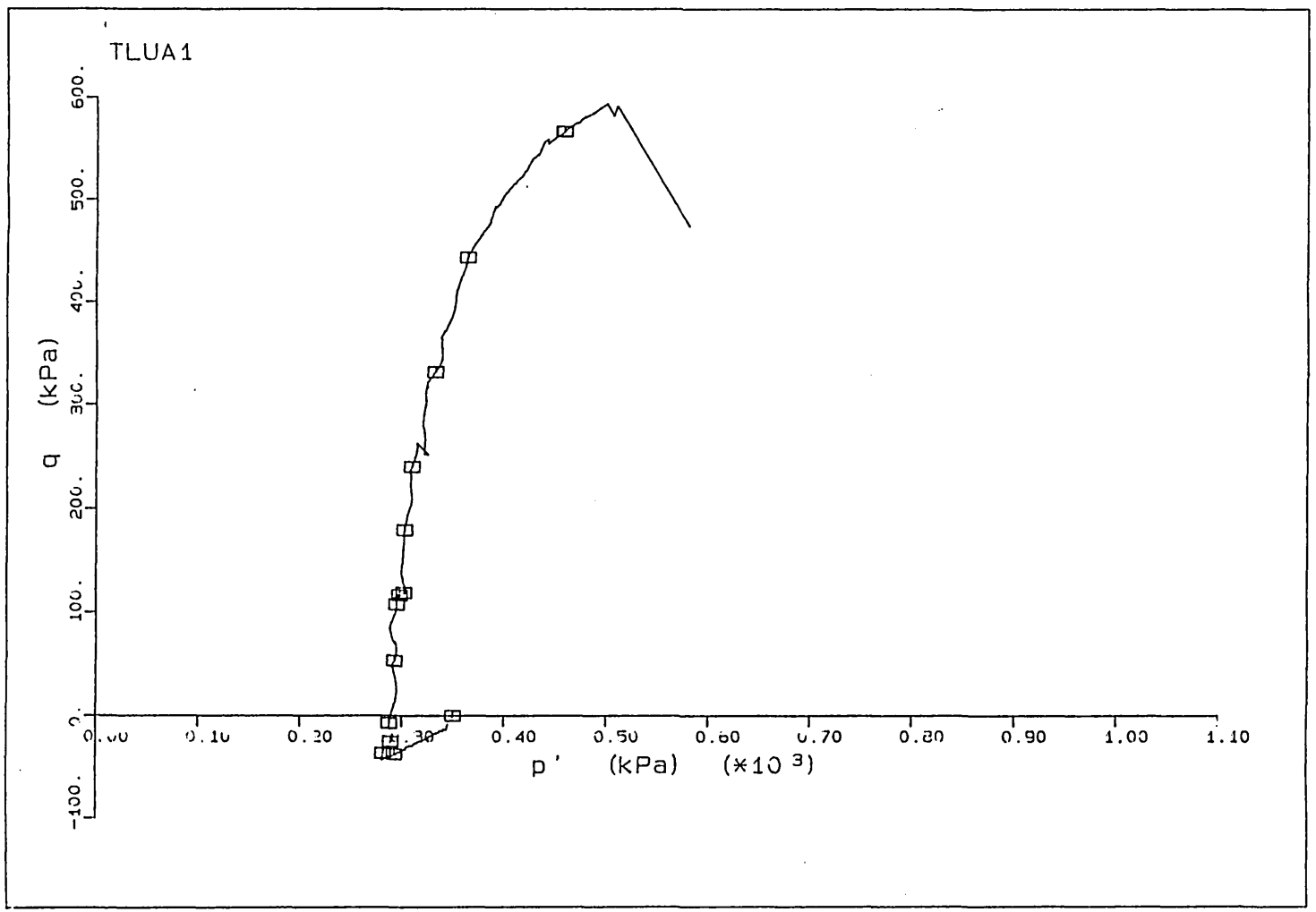
A5.I1.2


Axial strain (%)
-0.50
0.00
0.50
1.00
1.50
2.00
2.50
3.00
3.50
4.00
4.50
5.00
Excess pwp (kPa)
50.
-60.
-120.
-180.
-240.
-300.
-360.
TLUA1

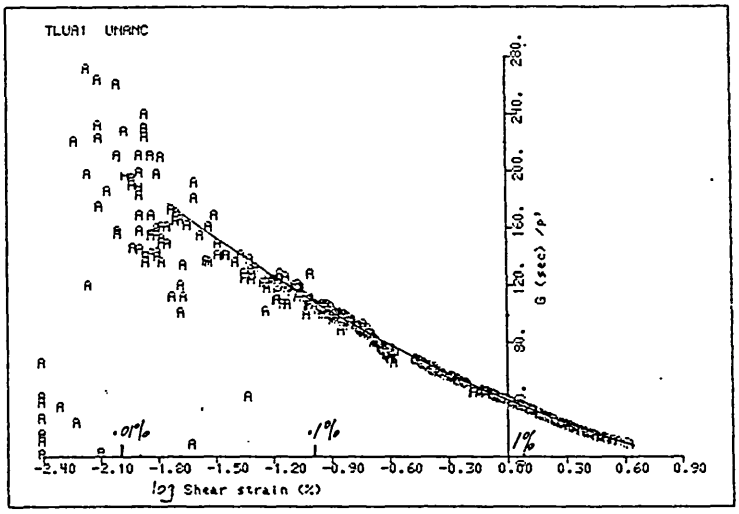
A5.I1.3


Axial strain (%)
4.0
8.0
12.0
14.0
16.0
18.0
Excess pwp (kPa)
-360.
TLUA1

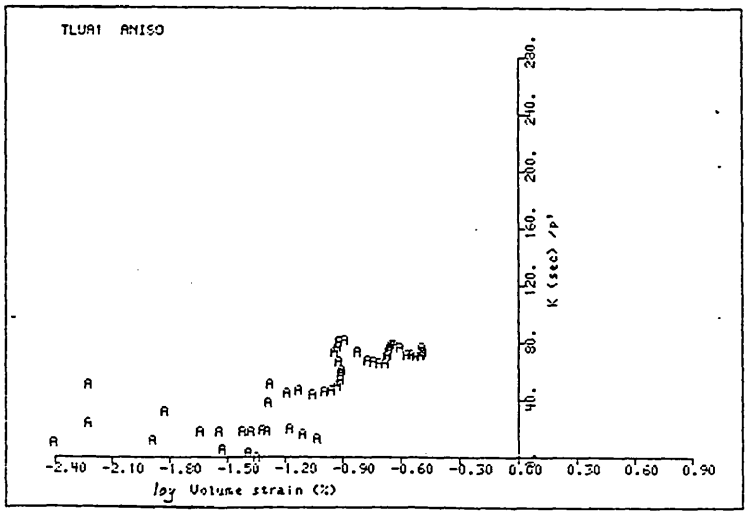
A5.I1.4


TLUA1
600.
500.
400.
300.
200.
100.
0.
-100.
q (kPa)
0.00
0.10
0.20
0.30
0.40
0.50
0.60
0.70
0.80
0.90
1.00
1.10
p' (kPa) (*10 3)

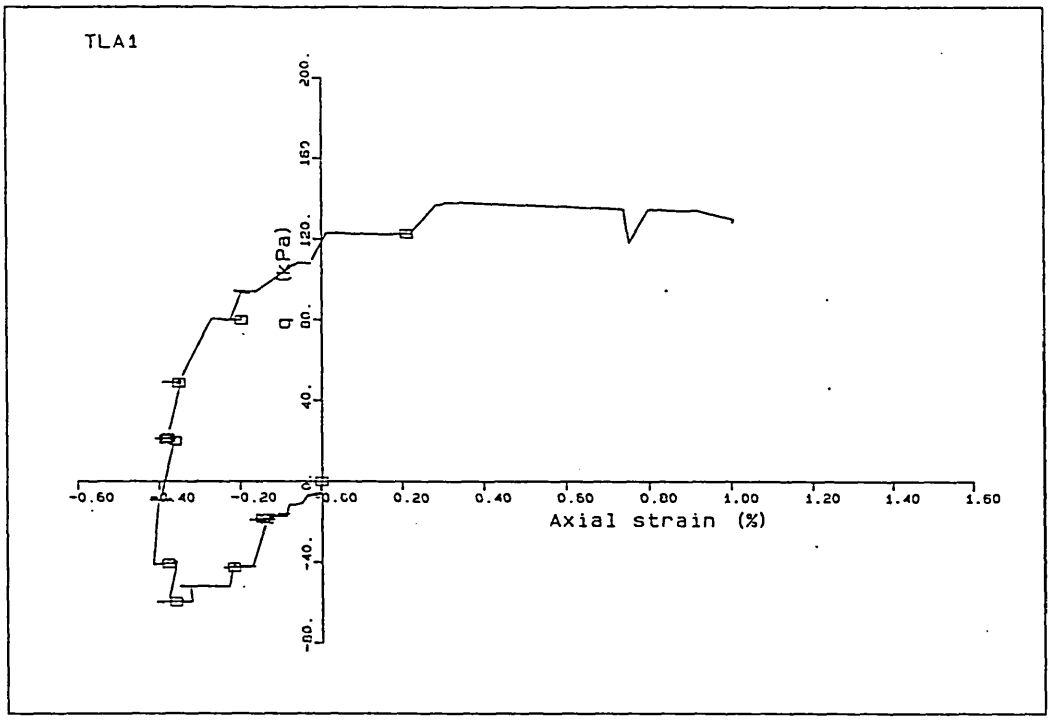
A5.I1.5


TLUA1 UNANC
280.
240.
200.
160.
120.
80.
G (sec) /p'
.01%
.1%
1%
-2.40 -2.10 -1.80 -1.50 -1.20 -0.90 -0.60 -0.30 0.00 0.30 0.60 0.90
log Shear strain (%)

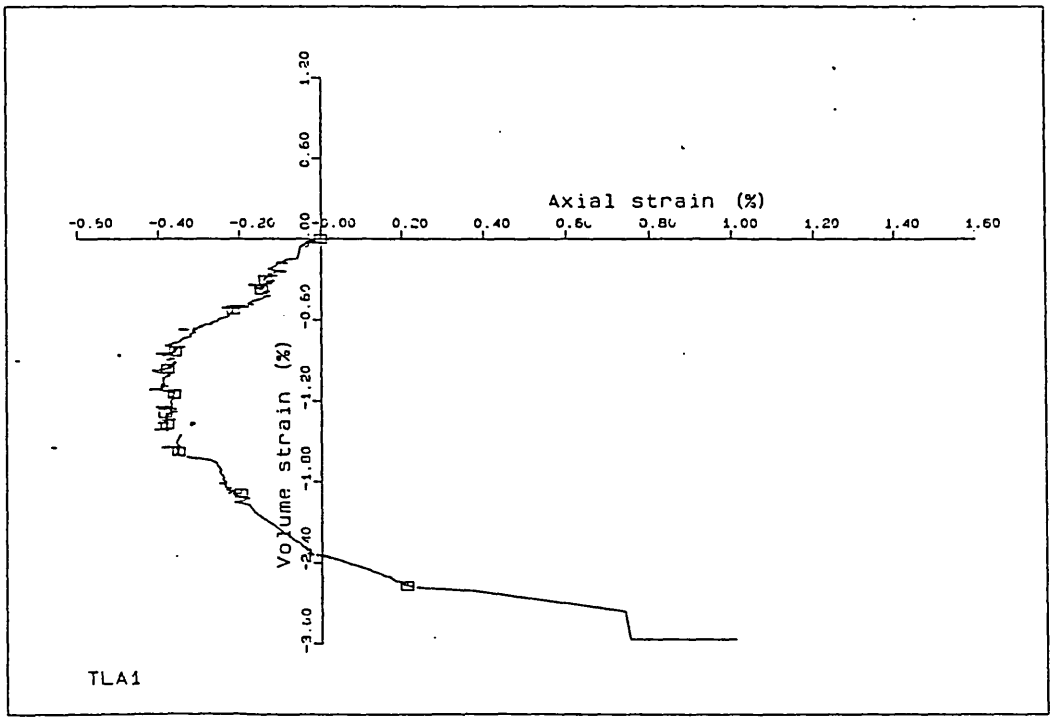
A5.I1.6


TLUA1 ANISO
280.
240.
200.
160.
120.
80.
40.
K (sec) /p'
-2.40 -2.10 -1.80 -1.50 -1.20 -0.90 -0.60 -0.30 0.00 0.30 0.60 0.90
log Volume strain (%)

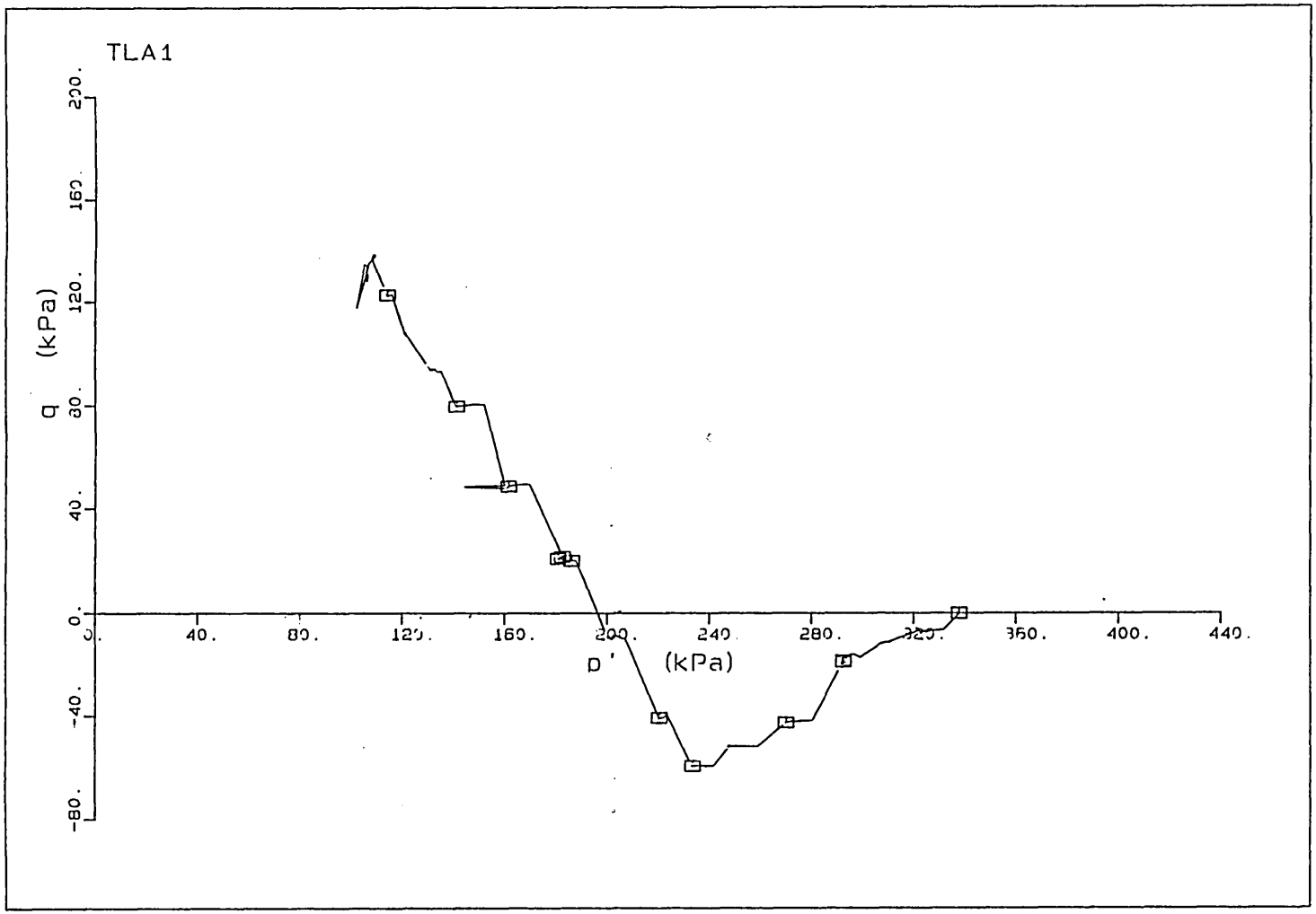
A5.I1.7



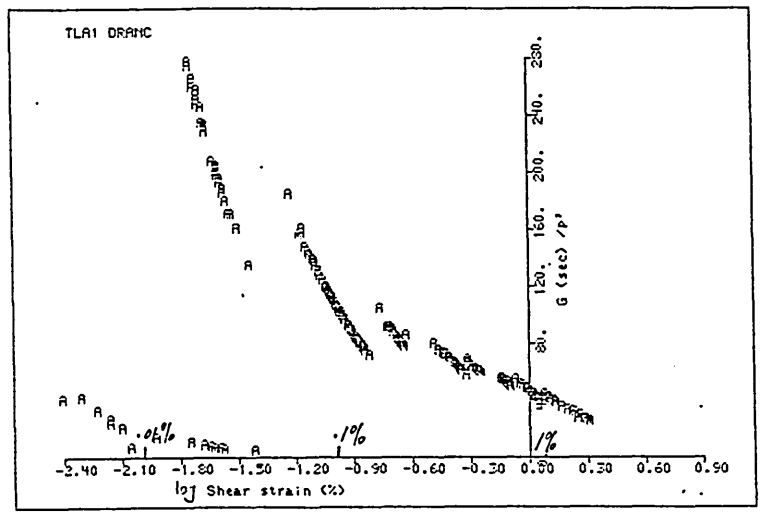
A5.J1.1



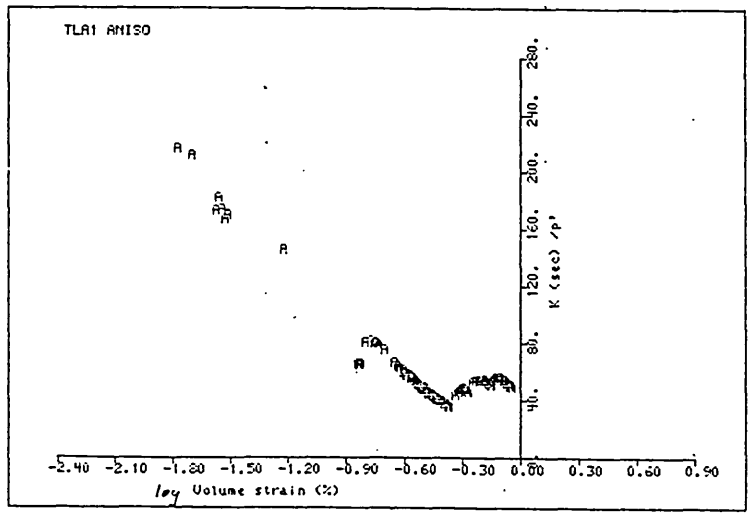
A5.J1.2


TLA1
q (kPa)
200.
160.
120.
80.
40.
0.
-40.
-80.
40.
80.
120.
160.
200.
240.
280.
320.
360.
400.
440.
p' (kPa)

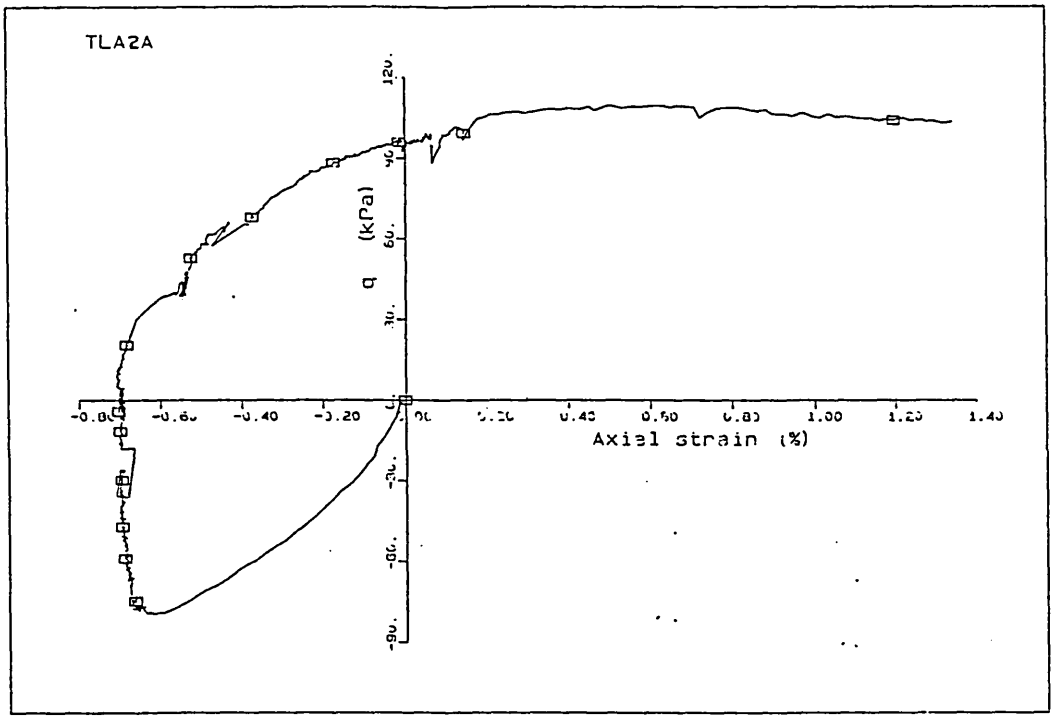
A5.J1.3


TLA1 DRAINC
G (sec) /p'
log Shear strain (%)
.01%
.1%
1%

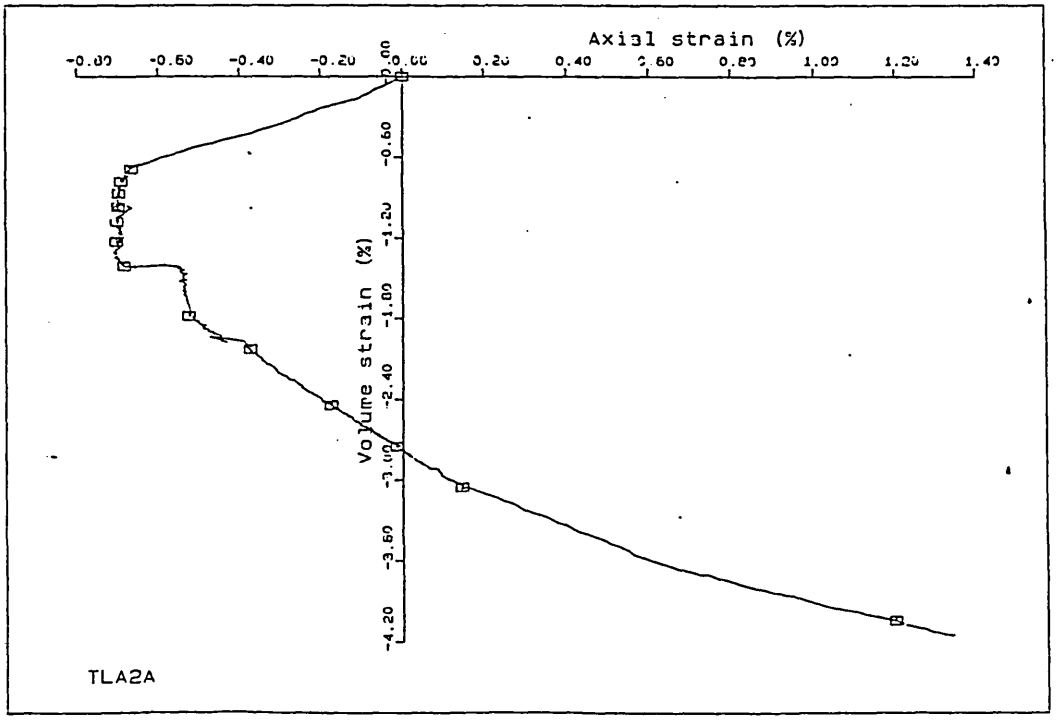
A5.J1.4


TLA1 ANISO
K (sec) /p'
log Volume strain (%)

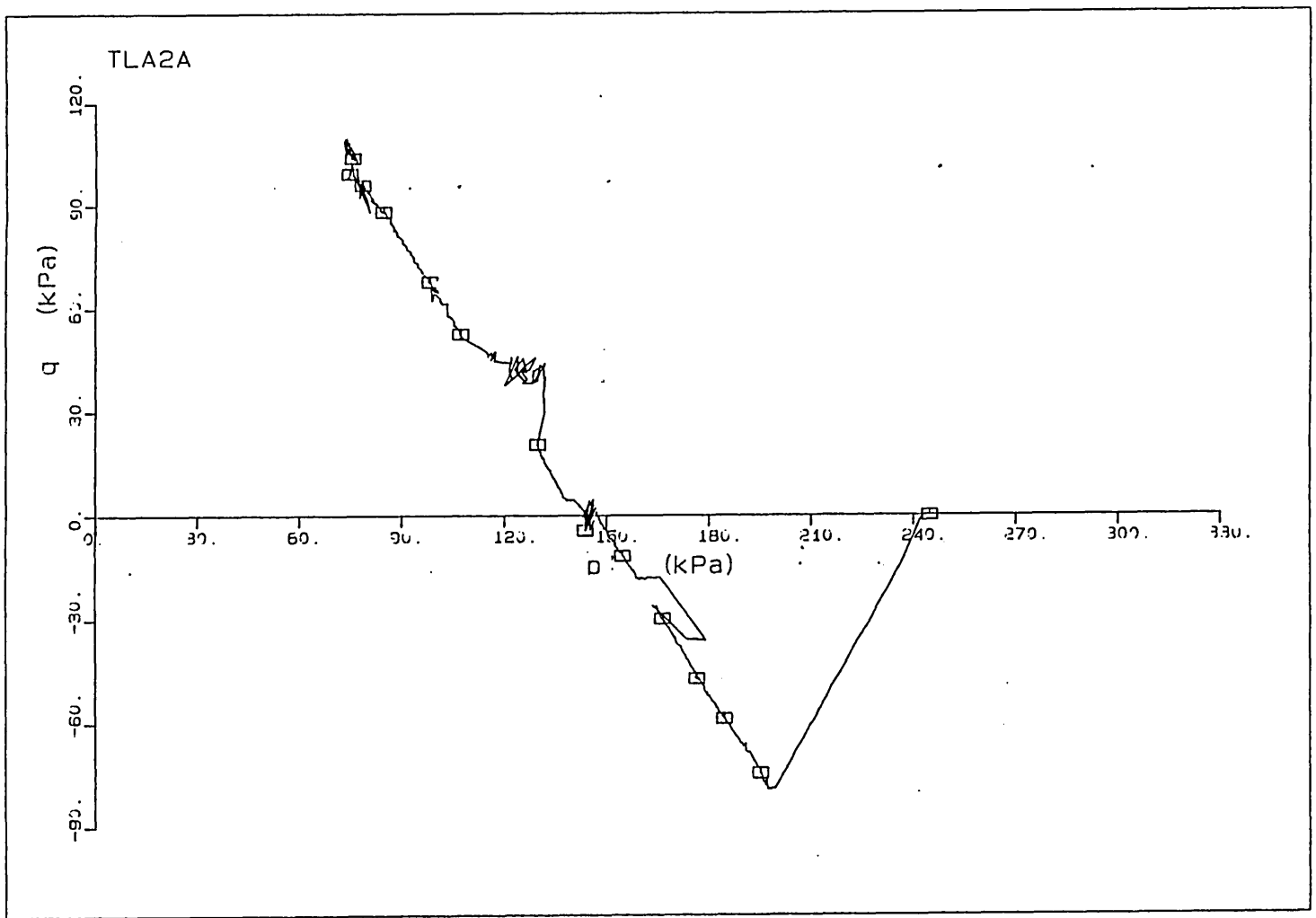
A5.J1.5



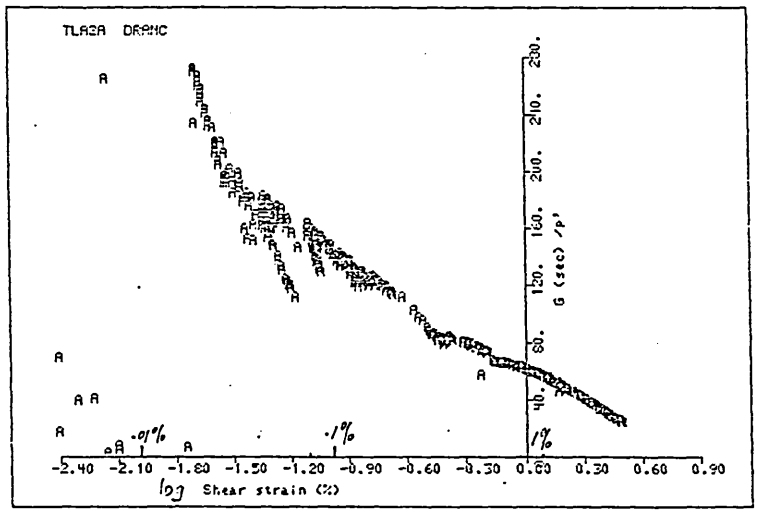
A5.J2.1



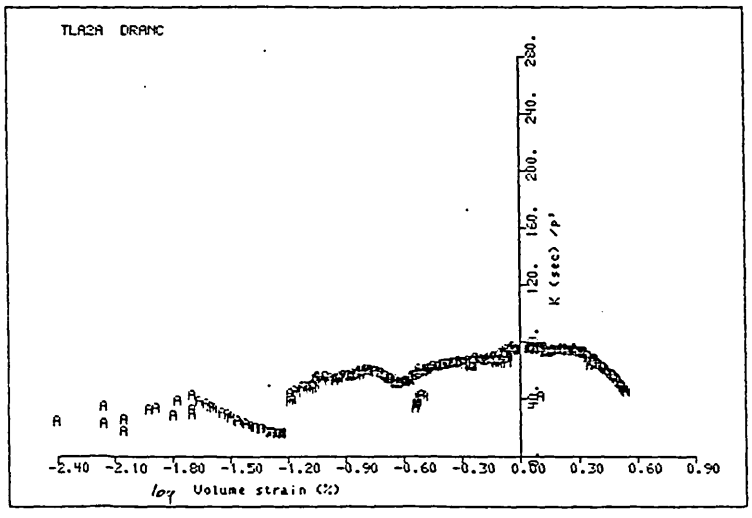
A5.J2.2


TLA2A
q (kPa)
120.
90.
30.
0.
-30.
-60.
-90.
0.
30.
60.
90.
120.
150.
180.
210.
240.
270.
300.
330.
p (kPa)

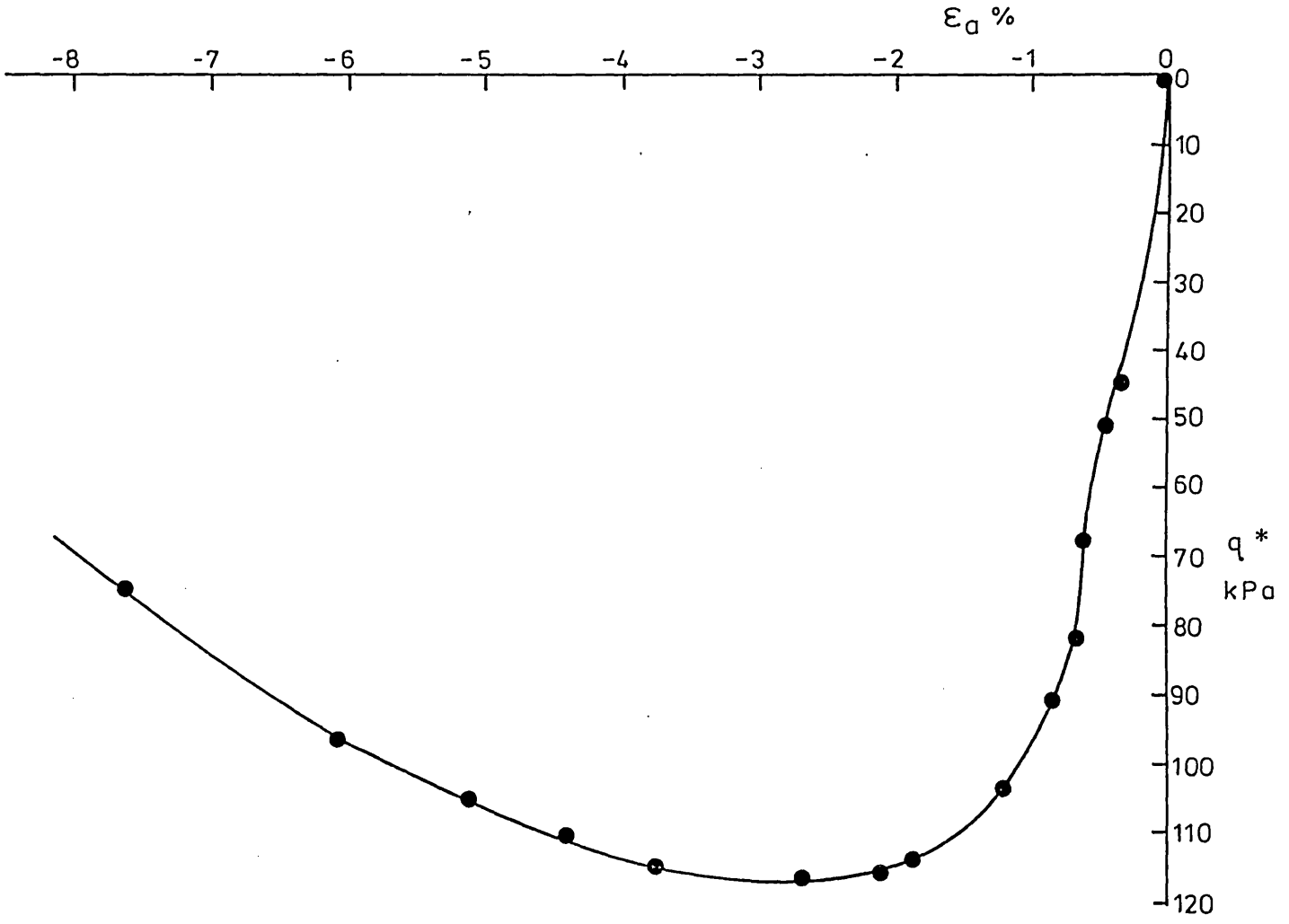
A5.J2.3


TLA2A DRANC
G (sec) /p'
log Shear strain (%)
-2.40 -2.10 -1.80 -1.50 -1.20 -0.90 -0.60 -0.30 0.00 0.30 0.60 0.90

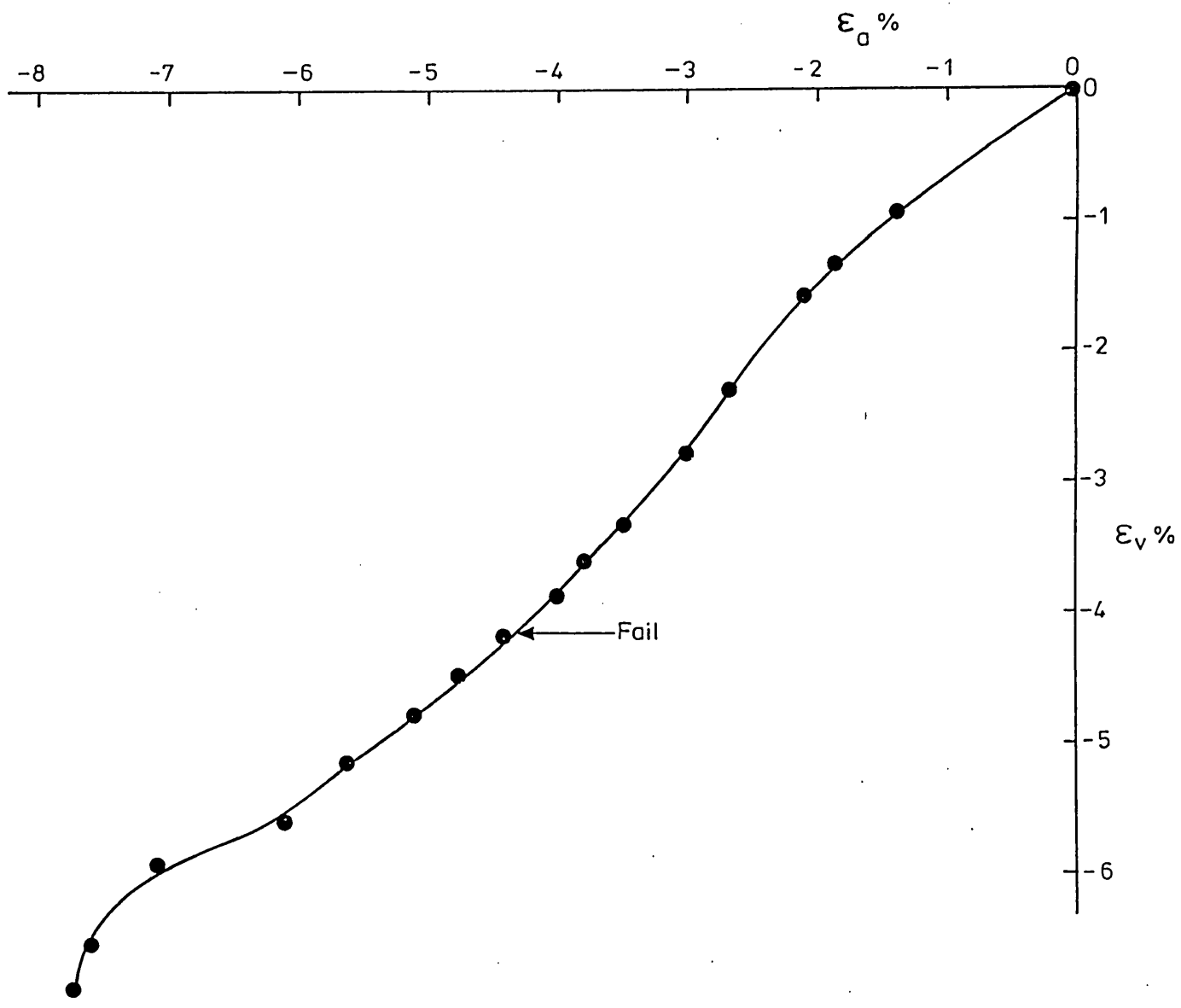
A5.J2.4


TLA2A DRANC
K (sec) /p'
log Volume strain (%)
-2.40 -2.10 -1.80 -1.50 -1.20 -0.90 -0.60 -0.30 0.00 0.30 0.60 0.90

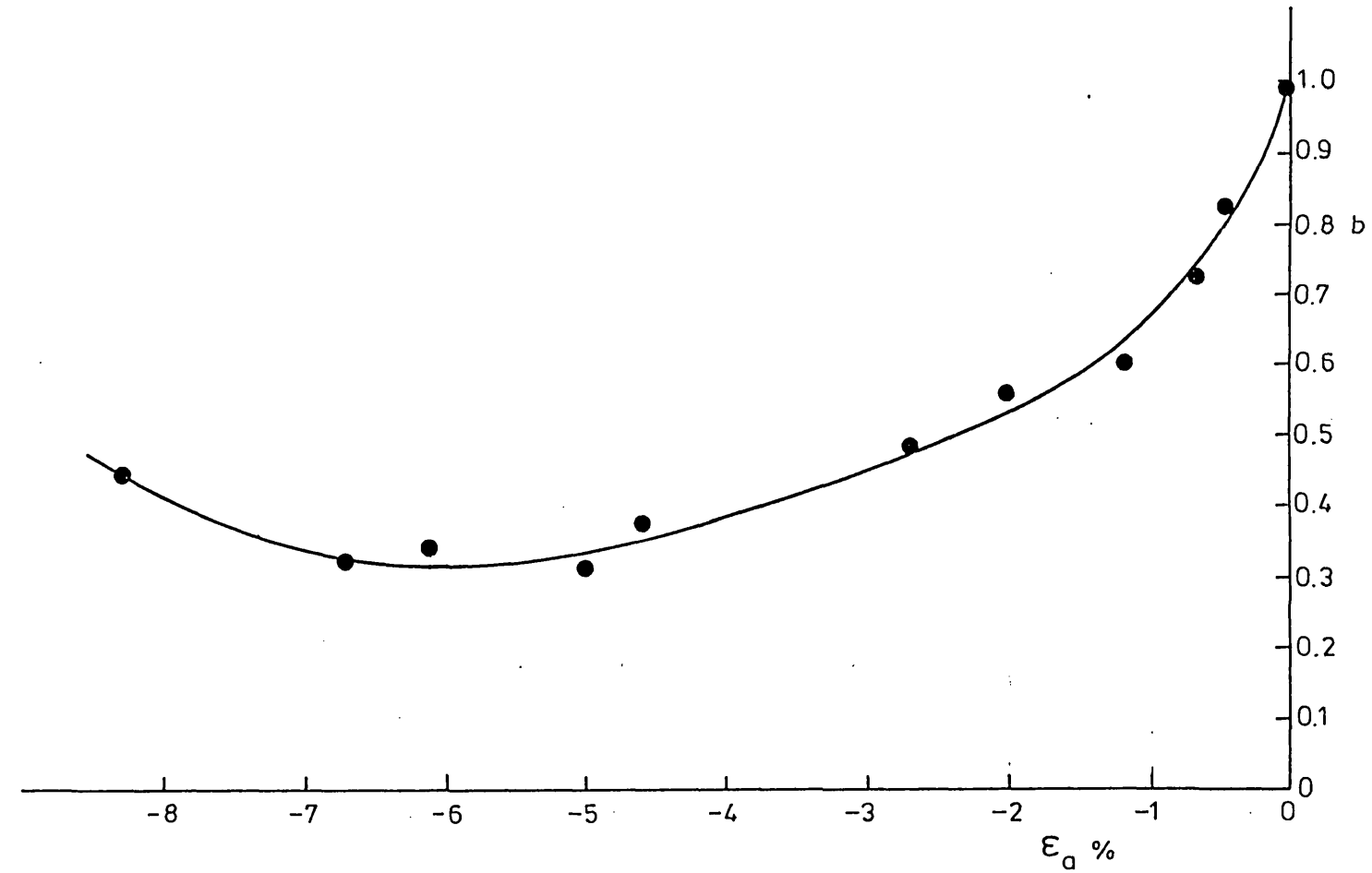
A5.J2.5


ε_a %
-8
-7
-6
-5
-4
-3
-2
-1
0
0
10
20
30
40
50
60
70
80
90
100
110
120
q *
kPa

A5.K1.1



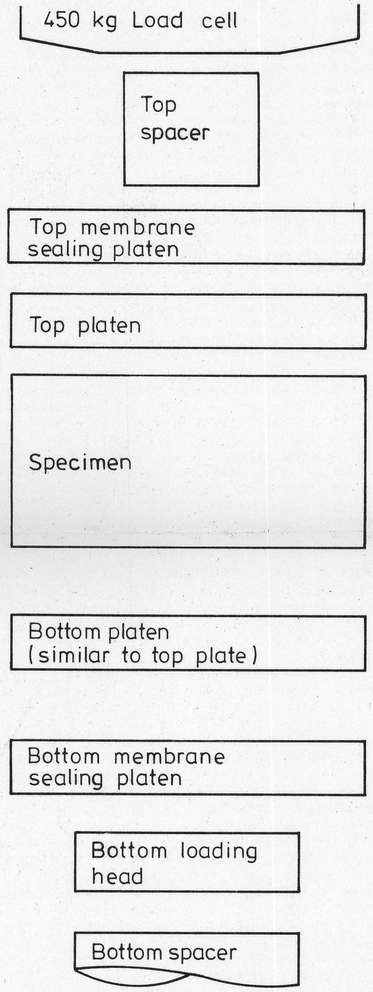
A5.K1.2



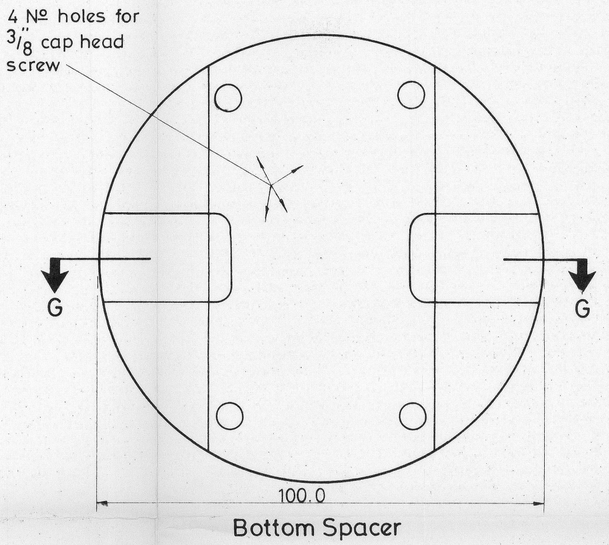
A5.K1.3

APPENDIX A6

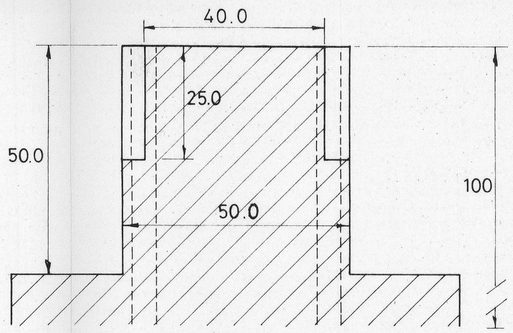
CONSTRUCTION DRAWINGS FOR NEW PLANE STRAIN DEVICE



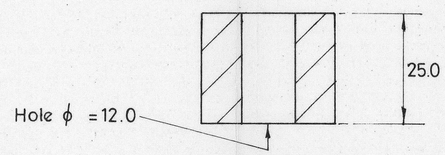
Diagrammatic Set-up of Vertical Loading Assembly



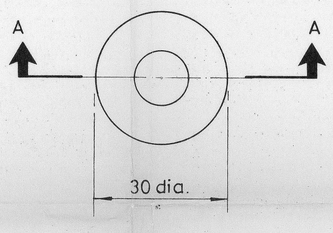
Bottom Spacer



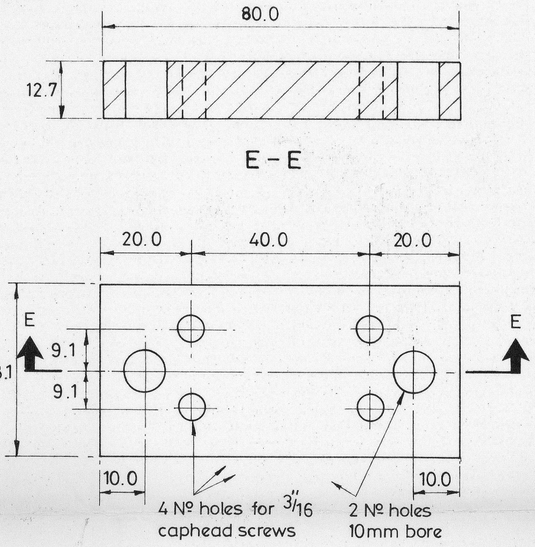
Section G-G



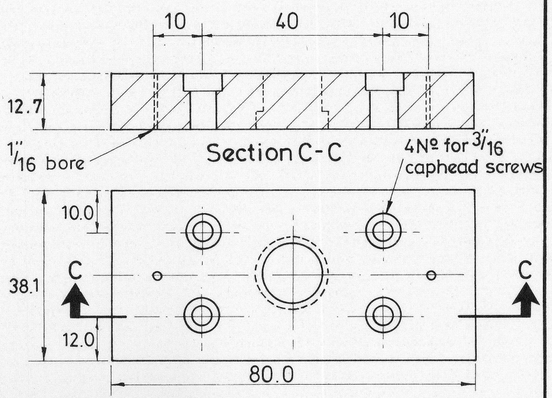
Section A-A



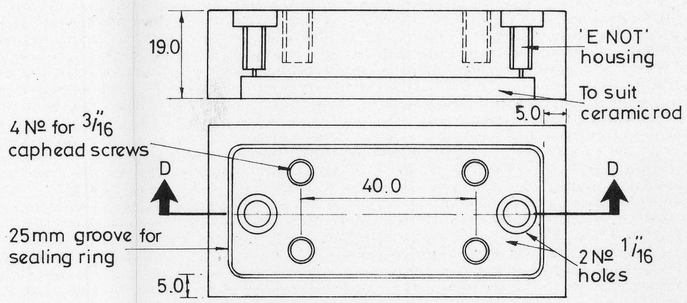
Top Spacer



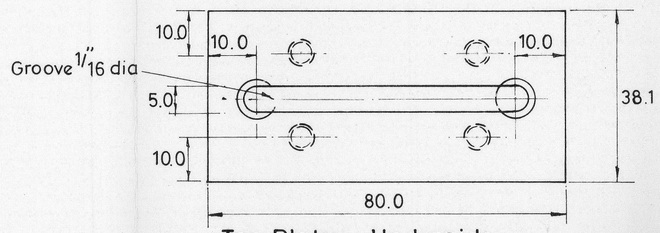
Bottom Membrane Sealing Platen



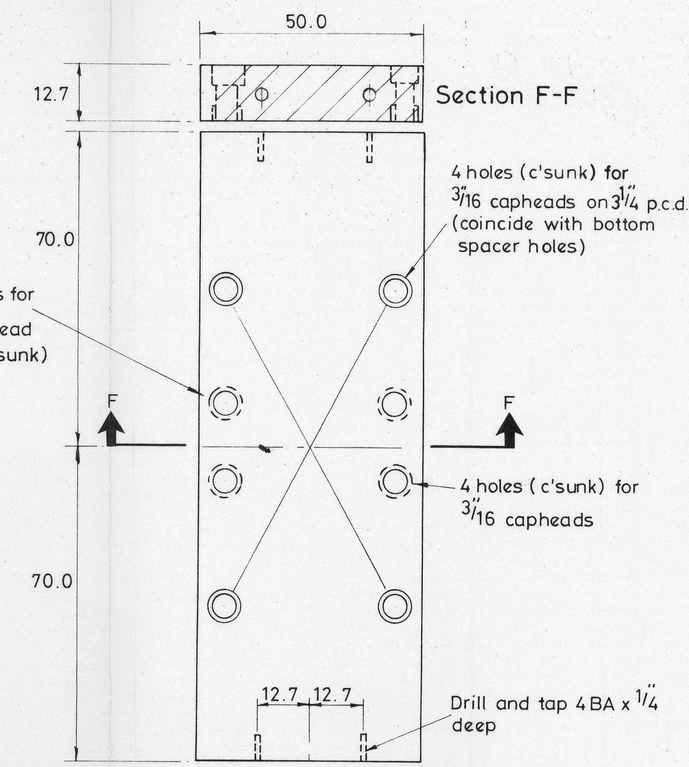
Top Membrane Sealing Platen



Top Platen-Top Side

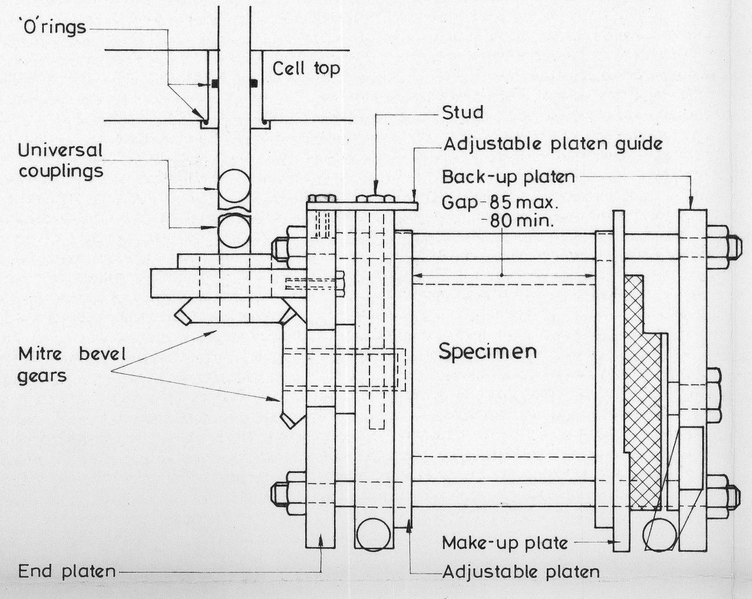


Top Platen - Underside



Bottom Loading Head

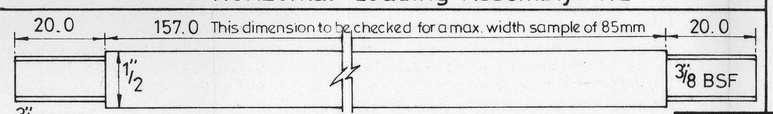
New Plane Strain Apparatus Imperial College			
October 1986	Scale: mm unless shown otherwise	J. E. Hellings	P/1



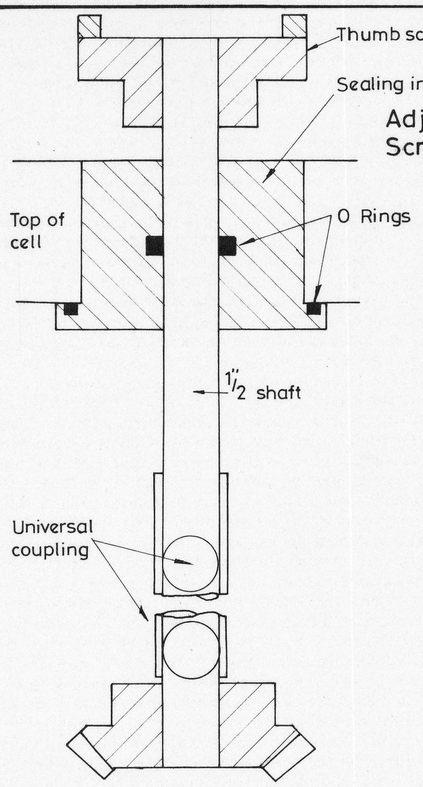
Existing end load cell

All of brass, except tie rods, Make-up platen, Adj. Platen in EN57 Stainless steel

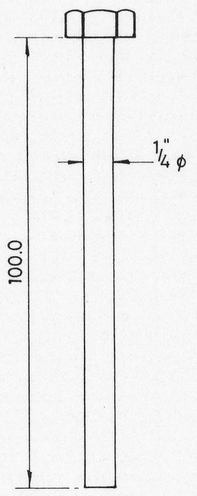
Horizontal Loading Assembly 1:2



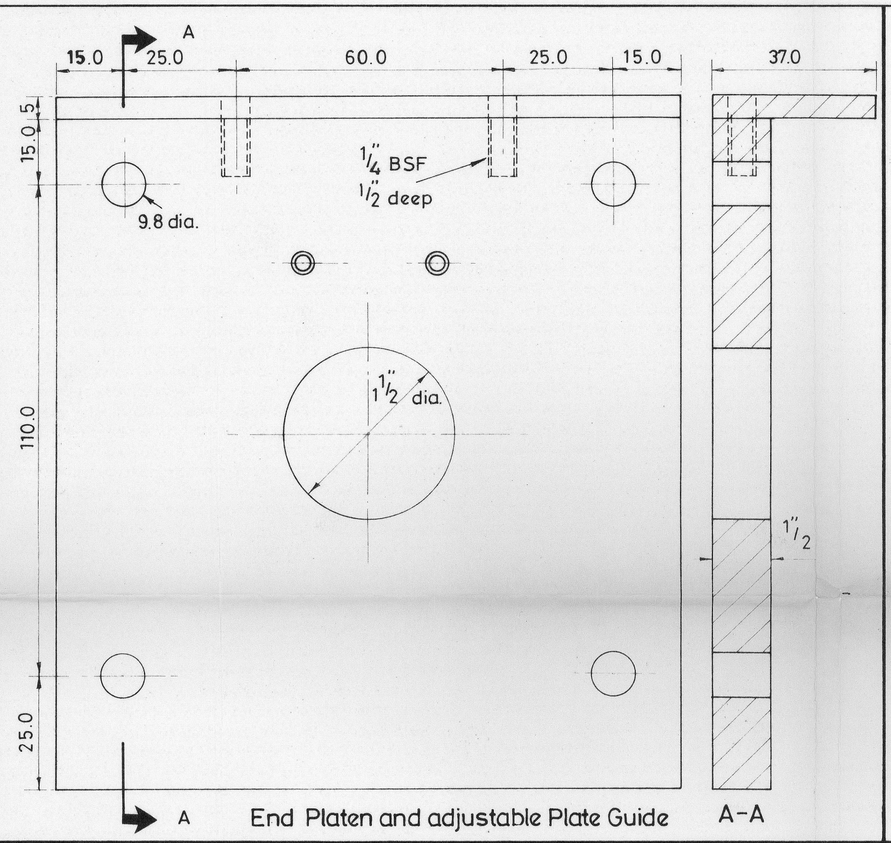
End Platen - Tie Rods (4)



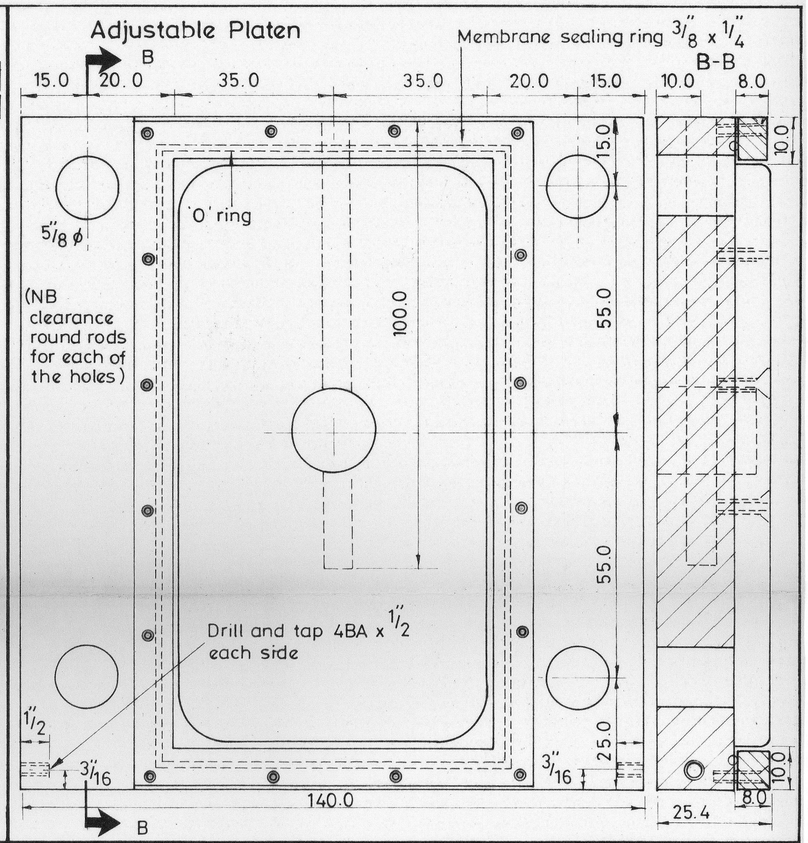
Adjustable Plate Screw Control Rod

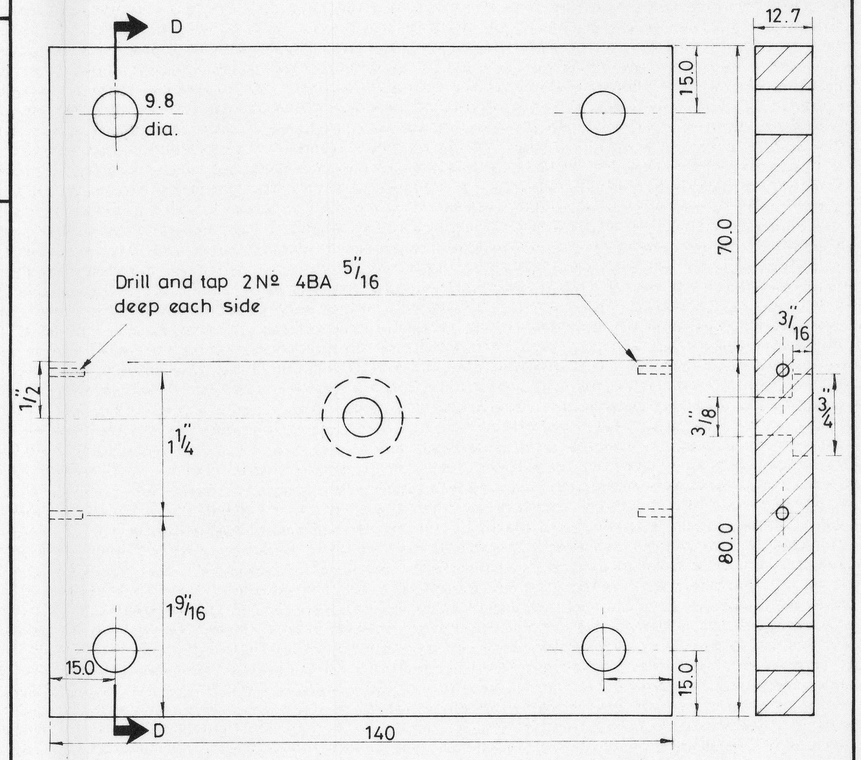


Stud



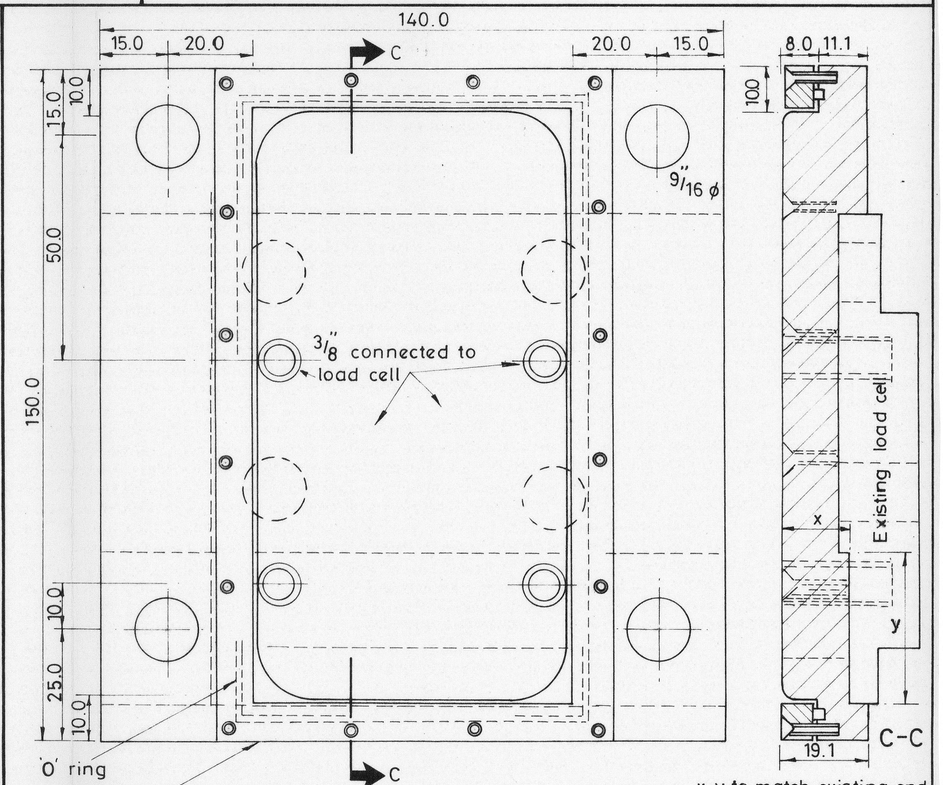
End Platen and adjustable Plate Guide





Back-up Platen

D-D

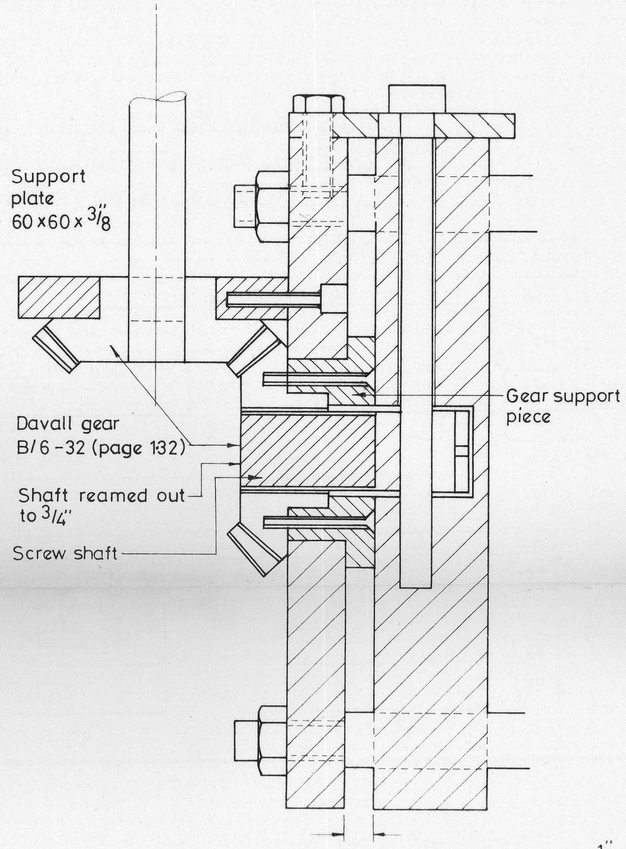


Make up Platen

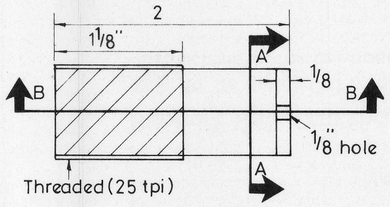
x,y to match existing end platen load cell face

New Plane Strain Apparatus Imperial College

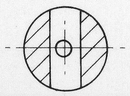
October 1986	Scale: mm unless shown otherwise	J.E Hellings	P/2



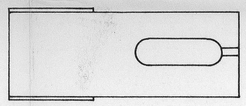
End Gear Assembly



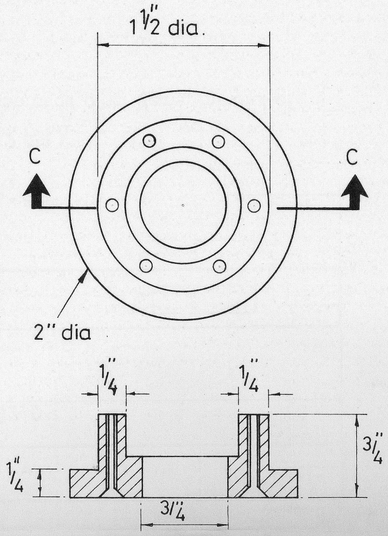
Screw Shaft



A-A

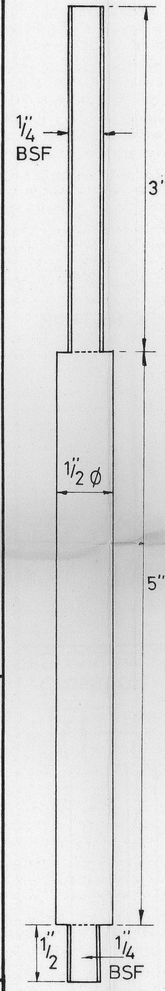


B-B

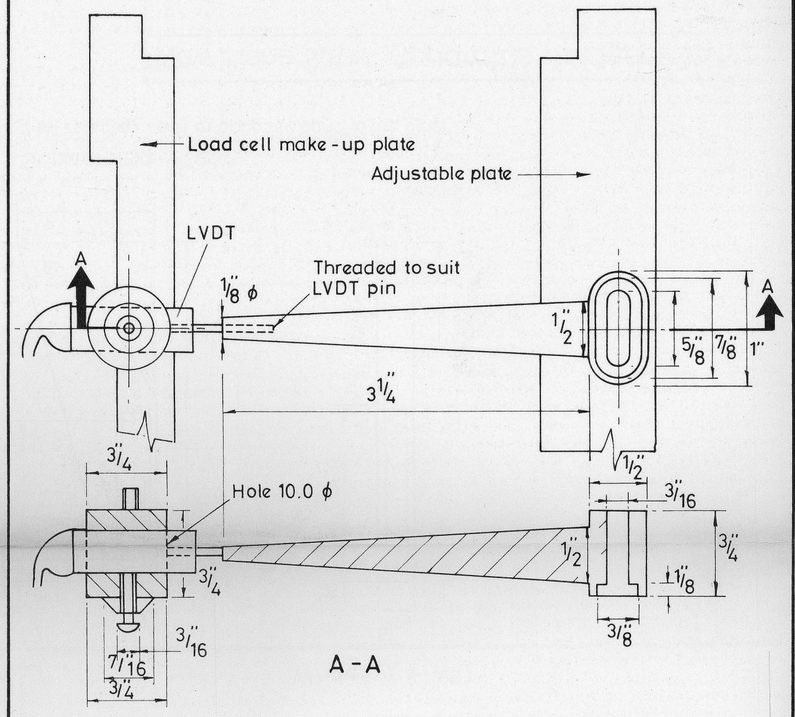


C - C
Gear Support Piece

ALL ITEMS ON THIS SHEET IN BRASS

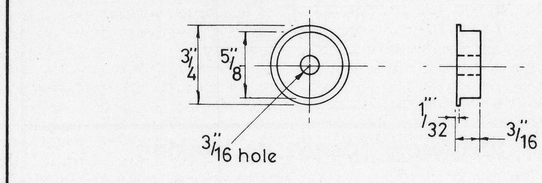


Crossbar Supports

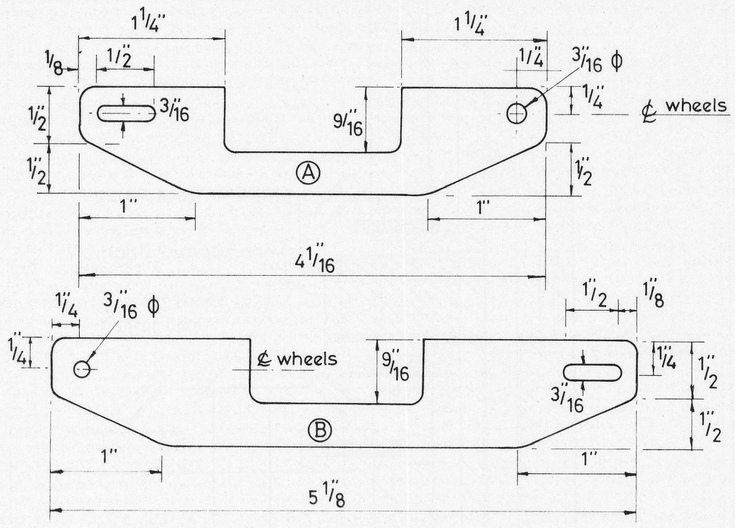


A - A

Support for Lateral Movement LVDT



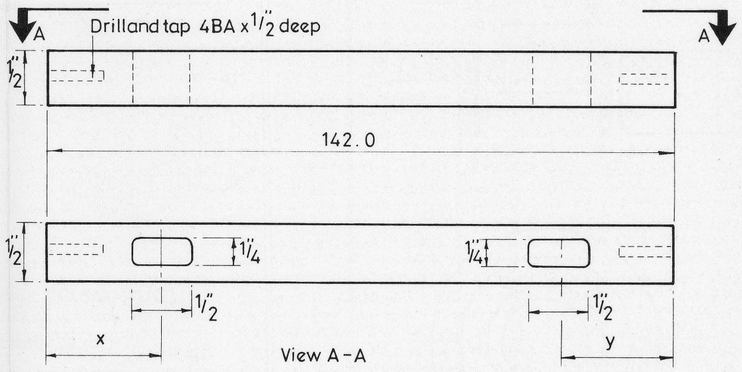
Wheels (4 Nº)



Support Rails (1/8" thick)

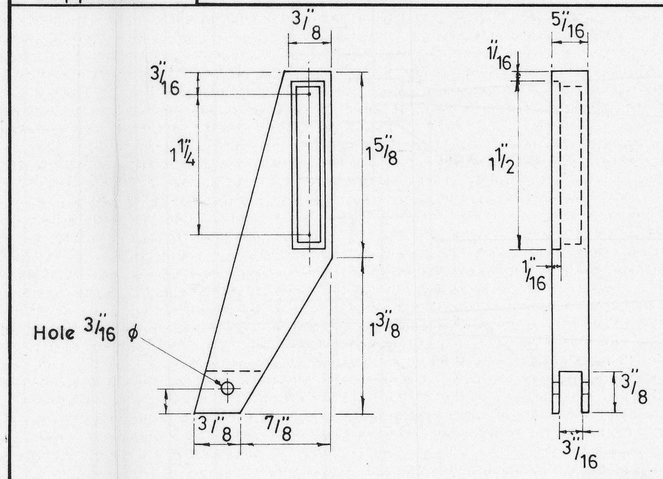
Ⓐ Attached to adjustable plate (2 Nº)

Ⓑ Attached to a back up plate (2 Nº)



Support Rail Crossbars (2 Nº)

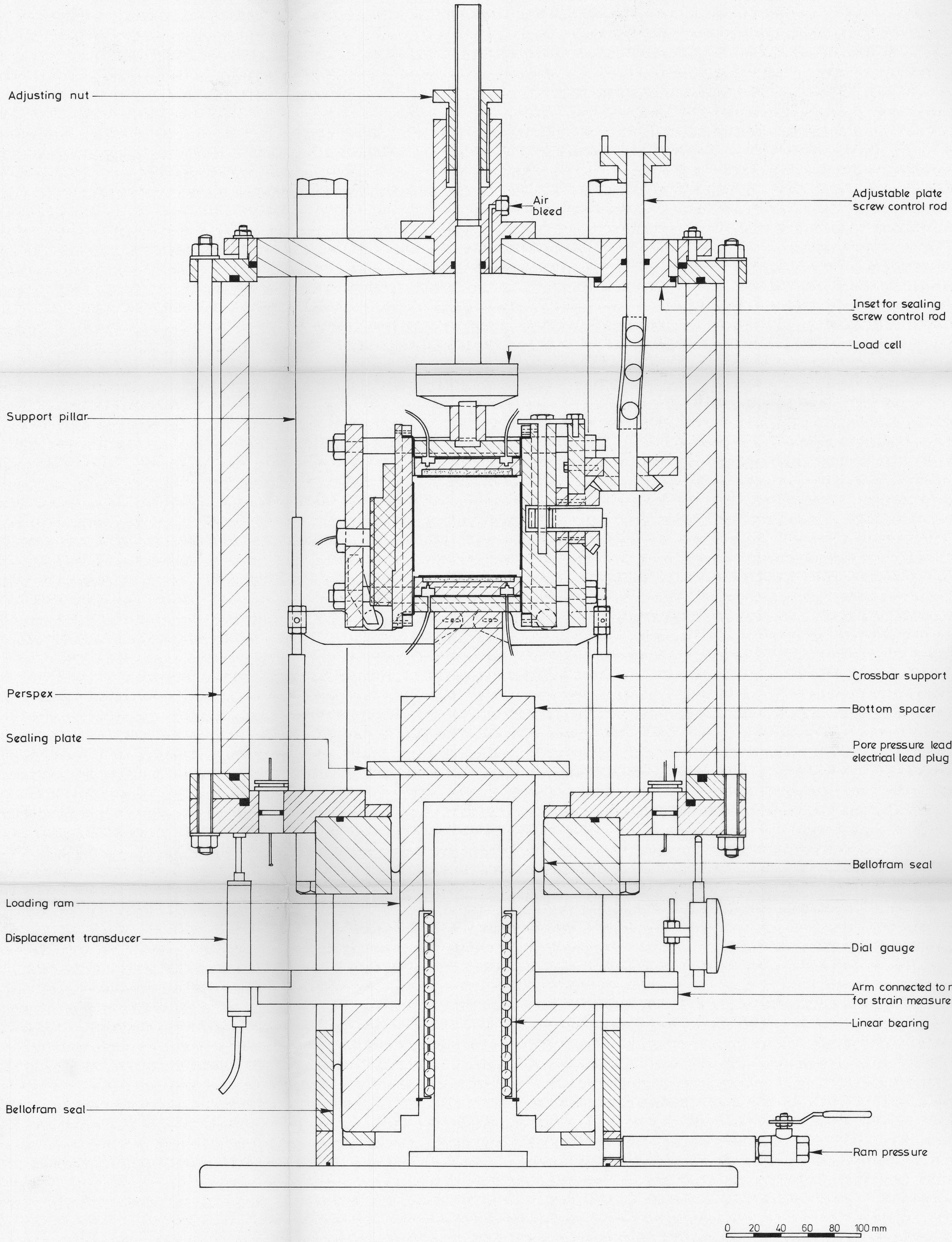
x, y to be decided at completion of all other items, mindful of obstructions at the cell base



Supporting Plate

2 Nº required each of opposite hand to the other

New Plane Strain Apparatus Imperial College			
			P/3
October 1986	Scale: F.S. unless shown otherwise	J. E. Hellings	



New Plane Strain Apparatus - Imperial College			
Apparatus in stress path cell			P/4
October 1986	Scale: Half full size	J.E. Hellings	